ICMIEE-PI-140101

Simulation of a workpiece in CNC milling machine on the basis of G and M code based NC programming

*Rakib Hasan *, Sakib Shahazad Ali, Dr. Tarapada Bhowmick*
Department of Mechanical Engineering, Khulna University of Engineering & Technology, Khulna-9203, BANGLADESH

ABSTRACT
The assisting technology of CNC milling machine is inaugurating the virtual machining platform, correcting NC program and process simulation and optimization, which can fabricate the efficient machine technology come true. The paper represents the G and M code based numerical control (NC) programming and real time 3D virtual simulation of workpiece in CNC milling machine (DENFORD MICROMILL, 2000), by using machine simulator. Machine simulators namely Denford Virtual Reality CNC milling.micromill and CncSimulator Pro. are used. The workpiece is designed through the MasterCAM (QuickCam) software (CAD/CAM Family) which reflects a milling process, setting all the movement trajectory of cutting tool over that workpiece using polynomial interpolation. Intelligent CAD/CAM generates NC program for a particular case along with a G and M code based NC program is also developed for a separate workpiece. The simulators used enable development of complex machine troubleshooting scenarios that are not feasible on real equipment.

Keywords: G and M code, Simulation, CNC Milling machine, MasterCAM, CncSimulator Pro.

1. Introduction

Modern manufacturing system and industrial robots are advanced automation systems that utilized computers as an intelligent division of their control, where an innovative organization of intelligent CAD/CAM (CAD – Computer Aided Design / CAM – Computer Aided Manufacturing) is implied, which can able to design the contours of workpiece, can easily be transferred it to the machine software for real time simulation, then manufacturing.

There exist many commercial software for NC machining simulation and verification in the market and verity of CAD/CAM software, which methodologies are mainly underlying either object-based, image-based or solid-based method and object-based simulation often adopt Z-Map method, which is most commonly used in machining simulation. There were many successful attempts for machine simulation and troubleshooting analysis. Ding [1] simulated the machining of flat-end and ball-end mill. For a 5-axis solid milling simulation Du et al. [2] used the envelope theory and swept volume generation method. Based on Z-Map method, Yun et al [3, 4] predicted cutting force for the initial transient toolpath and the stable middle toolpath of flat-end milling tool, which deals with the feature of machining simulation integrated with cutting force estimation. With the help of machine software Heidenhain iTNC 530, Gjelaj A. [5] shows the spline interpolation for simulation of workpiece.

This paper focused on the G and M code based programming for a workpiece simulation, individually for Denford Micromill-2000, along with the virtual milling environment analysis of a workpiece with the help of CncSimulator Pro. software. Programming command used for various geometric interpolation approach such as linier interpolation, circular interpolation, spline interpolation, which represents exactly in the simulated environment, for the tools trajectory.

Denford Micromill-2000 is a classic CNC milling machine, quite an accurate one, which working environments is simulated through Denford Virtual Reality CNC milling software. CncSimulator Pro. is another efficient CNC simulation software.

2. Mathematical Model of Geometric Interpolation for Programming Command

To fulfill the requirements of NC-machining, in a workpart dimensioning all coordinates should be specified that are necessary in conformity with G-code (DIN 66025 used in Germany) for programming the terminal point of a straight course or a circular arc, or of the circle center [6]. As a matter of fact, workshop drawings of workpart often lack some of the requisite dimensions. This can lead to extensive mathematical calculation in establishing the coordinates. In such cases the programming can be much facilitated by using the so-called programming of contour strings (also known as segment contour programming).

Different address code used for different interpolation.
G01 Linear Interpolation (for Contour String Programming G71)
G02 Circular Interpolation: Clockwise (for Contour String Programming G72)
G03 Circular Interpolation: Counterclockwise (for Contour String Programming G73) [8].

* Corresponding author. Tel.: +88-01742050053
E-mail address: rakibhasan.kuet@gmail.com

The following combinations are possible:

1. line – line
2. line – arc
3. arc – line
4. arc – arc

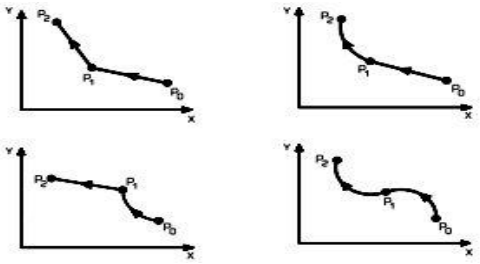

Figure 1. Three-Point-Strings

There is a spline interpolation function with a third degree polynomial, where manufacturing can be accomplished with two, three, four or five axes of the machine. Simulation processes have Spline interpolation sentences after third degree polynomial.

Therefore, the general mathematical model is given:

$$\begin{aligned} X(t) &= K_3X.t^3 + K_2X.t^2 + K_1X.t + X \\ Y(t) &= K_3Y.t^3 + K_2Y.t^2 + K_1Y.t + Y \\ Z(t) &= K_3Z.t^3 + K_2Z.t^2 + K_1Z.t + Z \\ I(t) &= K_3I.t^3 + K_2I.t^2 + K_1I.t + I \\ J(t) &= K_3J.t^3 + K_2J.t^2 + K_1J.t + J \end{aligned} \qquad (1)$$

Each detail of the coordinates in last command should be programmed as Spline interpolation parameter - K3 to K1. t is depended on feed rate and varies from 0 to 1 [6,5].

NC-Block G01 [X...] [Y...] [Z...] [F...] [S...]
[T...] [M...]
NC-Block G02 [X...] [Y...] [Z...] [I...] [J...]
[F...] [S...] [T...] [M...]
NC-Block G03 [X...] [Y...] [Z...] [I...] [J...]
[F...] [S...] [T...] [M...]

Optional Addresses

X	X-Coordinate of the target point
Y	Y-Coordinate of the target point
Z	Z-Coordinate of the target point
I	Circle Centre Incremental (distance between the starting position and the circle Centre in the X-direction).
J	Circle Centre Incremental (distance between the starting position and the circle Centre in the Y-direction).

When I or J (as defined above) are not programmed, the respective Centre coordinate is set to zero.

F	Feed rate (mm/min)
S	Spindle Speed (RPM)
T	Tool Change
M	Additional Function

3. Programming and simulation of workpiece

As an advanced simulation software for CNC milling, can be used to verify the collision, interference, over-cut, owse-cutting, and unreasonable cutting parameters which may arise in programs, and has been widely used the companies which using multi-axis CNC machining. The programming and simulation are analyzed by using the DENFORD MICROMILL, 2000, where master CAM (QuickCAM, CAD/CAM family) is used to make a design which produced the NC programming code by synchronizing with the Denford Virtual Reality CNC milling.micromill [7]. Intelligent CAD/CAM system have similar efficacy and functions based on common logarithms, but it lacks features for machining feed, speed and efficacy. MasterCAM can generate almost same NC code for a particular workpiece, along with MasterCAM generated code, required specific NC codes can be plugged to the CncSimulator Pro. (Ver: 1.0.5.2 beta) which gives an accurate real time simulated environment for particular workpiece.

So the machining simulation environment is completed by transferring G and M code based NC program, loading the control system, setting the machine parameters and structural variables, and by customizing special instructions.

3.1 Simulation approach with the Denford Virtual Reality CNC milling.micromill:

Dimension and design of the workpiece are made by using the QuickCam, which helps to realize the workpiece.

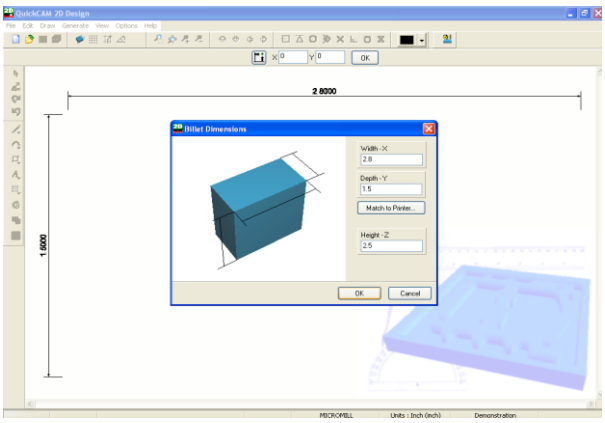

Figure 2. Dimensions of the workpiece

Machine simulators, Denford Virtual Reality CNC milling.micromill compiles with the MasterCAM designs and generates required G and M codes for the workpiece, which shows the real time machining of workpiece in a virtual environment. The design of the workpiece can be changed according to the observations.

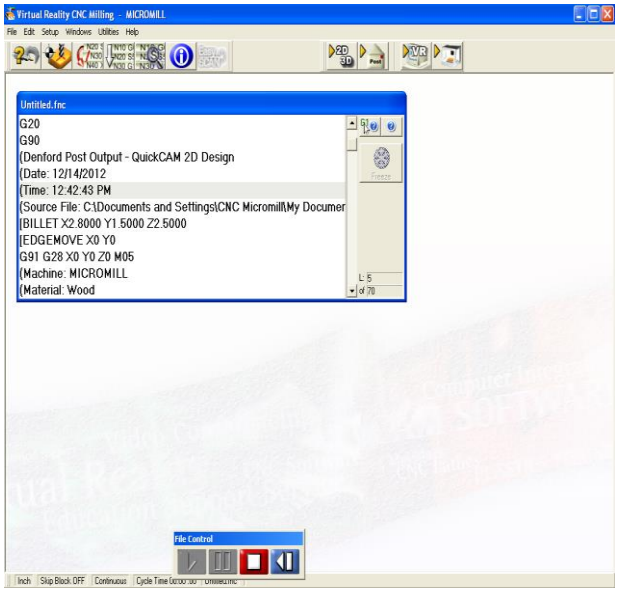

Figure 3. Generated NC program

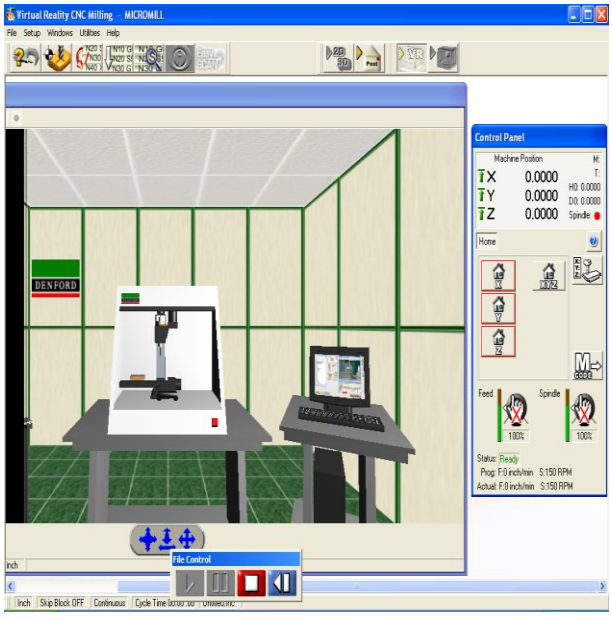

Figure 4. Machine Simulated environment

Simulated environment of the milling process of the workpiece, enables the operators to analyze the total process including the feed rate analysis, cutting speed and process and others which indicate the forecast for the real time troubleshooting.

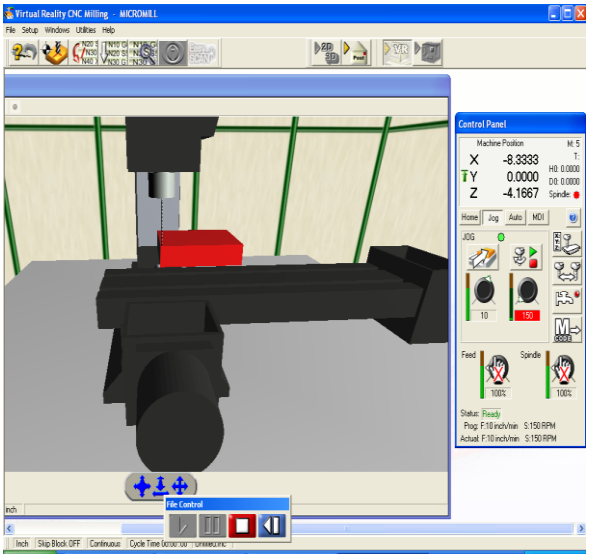

Figure 5. State of a virtual milling

3.2 Programming and simulation of workpiece in CNC milling machine with the help of CncSimulator Pro. (Ver: 1.0.5.2beta):

CncSimulator Pro. is an efficient machine simulator, which deals with DIN 66025 types machine language(G & M code) [8].

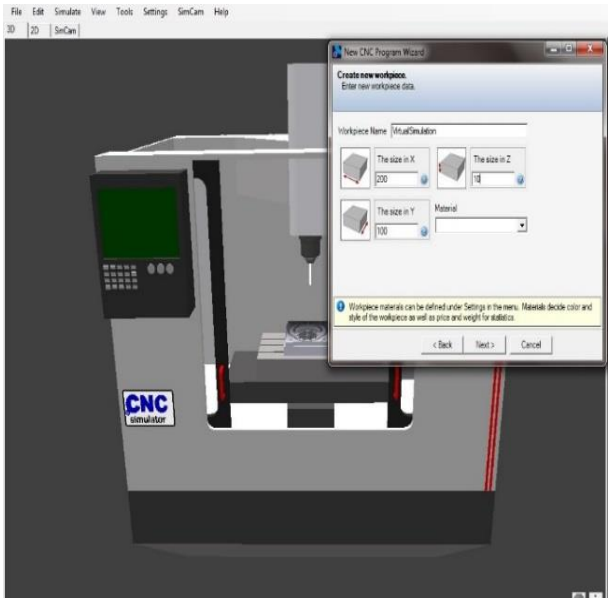

Figure 6. Virtual job setup

Software like CncSimulator Pro. is quit efficient one, used for 3D simulation, certainly helps for manufacturing forecast and for reducing errors. The process of the job setup and tool setup can be visualized in a virtual environment, this feature deals with the proper tool selection process for making a workpiece.

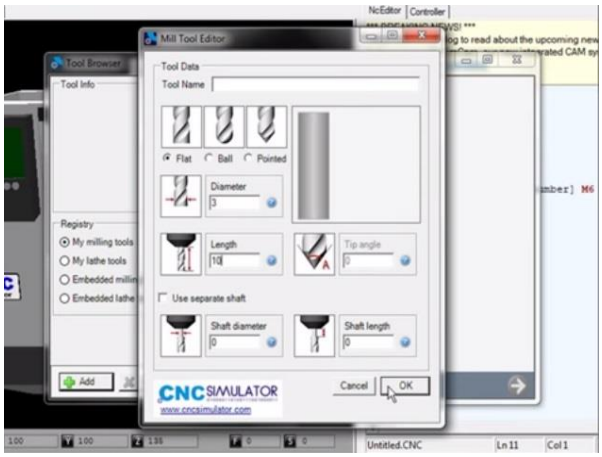

Figure 7. Virtual tool setup.

A G and M code based machine programming for a workpiece can be plugged in externally for checking the error in the code by observing the virtual simulation of workpiece.

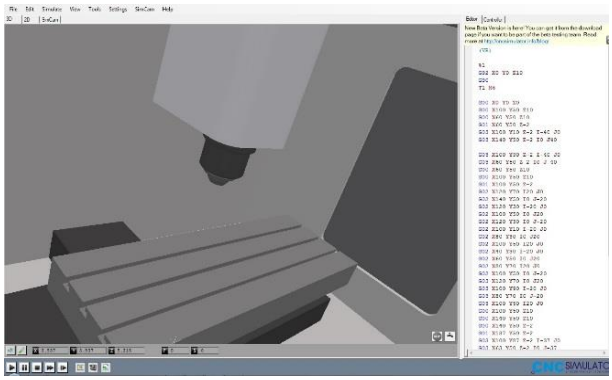

Figure 8. Plugging NC program code with the CncSimulator Pro.

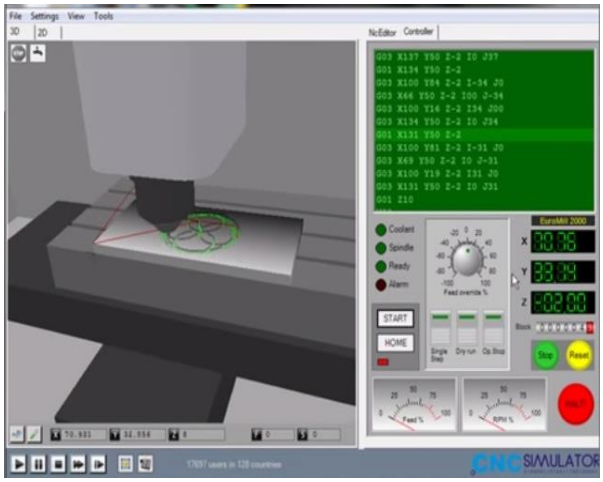

Figure 9. Simulation of cutting process

By utilizing real time virtual simulation of the machining process, engineers drastically can reduce the number of production errors which may be advised in case of settlement of tolerance. With this software we have slimmed down production costs and save material from errors during the fabrication operation.

3.3 The G and M code that using for the simulation of a workpiece with CncSimulator Pro. (Ver: 1.0.5.2 beta) is given below [8]:

G92 X0 Y0 Z10
G90
T1 M6

G00 X0 Y0 Z0
G00 X100 Y50 Z10
G00 X60 Y50 Z10
G01 X60 Y50 Z-2
G03 X100 Y10 Z-2 I-40 J0
G03 X140 Y50 Z-2 I0 J40

G03 X100 Y90 Z-2 I-40 J0
G03 X60 Y50 Z-2 I0 J-40
G00 X60 Y50 Z10
G00 X100 Y50 Z10
G01 X100 Y50 Z-2
G02 X120 Y70 I20 J0
G02 X140 Y50 I0 J-20
G02 X120 Y30 I-20 J0
G02 X100 Y50 I0 J20
G02 X120 Y30 I0 J-20
G02 X100 Y10 I-20 J0
G02 X80 Y30 I0 J20
G02 X100 Y50 I20 J0
G02 X40 Y30 I-20 J0
G02 X60 Y50 I0 J20
G02 X80 Y70 I20 J0
G02 X100 Y50 I0 J-20
G03 X120 Y70 I0 J20
G03 X100 Y90 I-20 J0
G03 X80 Y70 I0 J-20
G03 X100 Y50 I20 J0
G00 X100 Y50 Z10
G00 X140 Y50 Z10
G00 X140 Y50 Z-2
G01 X137 Y50 Z-2
G03 X100 Y87 Z-2 I-37 J0
G03 X63 Y50 Z-2 I0 J-37
G03 X100 Y13 Z-2 I37 J0
G03 X137 Y50 Z-2 I0 J37
G01 X134 Y50 Z-2
G03 X100 Y84 Z-2 I-34 J0
G03 X166 Y50 Z-2 I00 J-34

G03 X100 Y16 Z-2 I34 J00
G03 X134 Y50 Z-2 I0 J34
G01 X131 Y50 Z-2
G03 X100 Y81 Z-2 I-31 J0
G03 X69 Y50 Z-2 I0 J-31
G03 X100 Y19 Z-2 I31 J0
G03 X131 Y50 Z-2 I0 J-31
G01 Z10

M30

4. Conclusion:

An important direction to elevate the performance and efficiency of a CNC milling machine is to install a virtual machining system. By using MasterCAM (CAD/CAM system) the processing and manufacturing of a workpiece can be understood easily by comparison to the manual approach. Simulators can compile with MasterCAM, generates requisite NC programs of workpiece, in some extent, this is a frugal approach which saves time. A written NC program code of a workpiece can be tested accurately through the real time virtual simulation, consequently, improved efficiency, flexibility, productivity and manufacturing process are achieved, along with complex machine trouble shooting become feasible.

REFERENCES

[1] C. Y. Ding, "NC machining simulation under high-speed milling," master's thesis, Department of Mechanical Engineering, National Chung Cheng University, Chiayi, (2001).

[2] S. Du, T. Surmann, O. Webber, and K. Weinert, "Formulating swept profiles for five-axis tool motions," International Journal of Machine Tools & Manufacture, vol. 45, pp. 849–861, 2005

[3] Yun, W.-S.,Ko, J.H., Lee, H.U., et al.; Development of a virtual machining system, part3: cutting process simulation in transient cut. International Journal of Machine Tools & Manufacture 42, 1617-1626(2002).

[4] Won-Soo Yun, Jeong Hoon Ko, Han UI Lee, Kornel F. Enmann, "Development of a virtual machining system, Part 1:approximation of the size effect for cutting force prediction, International Journal of Machine Tools & Manufacture, vol. 42, pp. 1595-1605, 2002.

[5] Gjelaj A., Dr. sc.Bunjaku A.; "Pogramming and simulation of workpiece in cnc milling machine". 14th International Research/Expert Conference "Trends in the Development of Machinery and Associated Technology" TMT 2010, Mediterranean Cruise, pp11-18, September 2010

[6] Hans B. Kief &Helmut A. Roschiwal "NC/CNC Handbuch 2007/2008" CNC, DNC, CAD, CAM, CIM, FFS, SPS, RPD, LAN,NC-MAschinen,NC-Roboter, Antriebe, Simulation, Fach- und Stichwortverzeichnis.

[7] "G and M Programming for CNC Milling Machines", Denford Limited Birds Royd Brighous West Yorkshire England.

[8] "Programmer's Guide CNC-Simulator for Milling", MTS Mathematisch Technische Software-Entwicklung GmbH Kaiserin-Augusta-Allee 101 • D-10553 Berlin, May 1995ofp, May 1998 akss, ofp.

ICMIEE-PI-140102

Effect of Prandtl Number on 3D Heat Transfer through a Solar Collector

Rehena Nasrin, Salma Parvin and M.A. Alim*

Department of Mathematics, Bangladesh University of Engineering and Technology
Dhaka-1000, Bangladesh

ABSTRACT

Solar water heating systems are useful most likely to be cost effective for facilities with water heating systems that are expensive to operate or with operations such as laundries or kitchens that require large quantities of hot water. While solar collectors are most cost-effective in sunny, temperate areas, they can be cost effective virtually anywhere in the country so should be considered. Solar energy is one of the best sources of renewable energy with minimal environmental impact. The forced convection in solar collector continues to be a very active area of research during the past few decades. Commercial applications of solar collectors include swimming pool, space heating, car washes, military laundry facilities and eating establishments. A 3D heat transfer model is developed in which direct sunlight is incident on transparent glass cover of a flat plate solar collector (FPSC). Water/copper nanofluid is considered as heat transfer medium through the flat plate solar collector. The governing partial differential equations are solved using finite element method with Galerkin's weighted residual technique. In order to evaluate the temperature profile within the collector, the mass and momentum balance equations and heat transport equations for solid and fluid are solved numerically. Effect of Prandtl number is shown graphically in terms of streamlines pattern, rate of heat transfer (Nu), average temperature (θ_{av}), percentage of collector efficiency (η), outlet temperature (T) for water-Cu nanofluid and base fluid (clear water) through the collector. It is observed that at the highest value of Prandtl number the water based nanofluid is more effective than base fluid for the enhancement of heat transfer rate and collector efficiency.

Keywords: 3D heat transfer, flat plate solar collector, finite element method, Prandtl number, forced convection.

1. Introduction

Solar flat plate collectors are commonly used for domestic and industrial purposes and have the largest commercial application amongst the various solar collectors. This is mainly due to simple design as well as low maintenance cost. Solar radiation is radiant energy emitted by the sun. It is particularly electromagnetic energy. Solar irradiance (I) is the combination of bright light and radiant heat. Heat transfer due to emission of electromagnetic waves is known as thermal radiation. The heat transfer rate per unit area as thermal radiation is called radiative heat flux.

The fluids with solid-sized nanoparticles suspended in them are called "nanofluids". Applications of nanoparticles in thermal field are to augment warmth transport from solar collectors to luggage compartment tanks, to pick up proficiency of coolants in transformers.

The absorptance of the collector surface for shortwave solar radiation depends on the nature and colour of the coating and on the incident angle. Usually black colour is used. Various colour coatings had been proposed by Wazwaz et al. [1] mainly for aesthetic reasons. A low-cost mechanically manufactured selective solar absorber surface method had been proposed by Konttinen et al. [2]. A numerical experiment is performed for inclined solar collectors by Varol and Oztop [3]. Results indicated that heat transfer was increased with increasing Rayleigh number and aspect ratio, and was decreased with increasing wavelength.

There are so many methods introduced to increase the efficiency of the solar water heater of Xiaowu and Hua [4] and Hussain [5]. Hwang et al. [6] performed stability and thermal conductivity characteristics of nanofluids. In this study, they concluded that the thermal conductivity of ethylene glycol was increased by 30%.

Karanth et al. [7] numerically simulated a solar flat plate collector using Discrete Transfer Radiation Model. A 3D model of the collector involving the water pipe, absorber plate, the glass top and the air gap in-between the absorber plate and the glass top was modeled to provide for conduction, convection and radiation in their analysis. Bég et al. [8] performed non-similar mixed convection heat and species transfer along an inclined solar energy collector surface with cross diffusion effects, where the resulting governing equations were transformed and then solved numerically using the local nonsimilarity method and Runge-Kutta shooting quadrature. Manjunath et al. [9] analyzed three

* Corresponding author. Tel.: +88-01766924295
E-mail address: rehena@math.buet.ac.bd

dimensional conjugate heat transfers through unglazed solar flat plate collector. They used finned tubes and the heat transfer simulation due to solar irradiation to the fluid medium, increased with an increase in the mass flow rate. Vestlund [10] studied gas-filled flat plate solar collector. The gases examined were argon, krypton and xenon in his thesis paper.

Manjunath et al. [11] studied comparatively solar dimple plate collector with flat plate collector to augment the thermal performance. Their result described that the average exit water temperature showed a marked improvement of about 5.5^0C for a dimple solar collector as compared to that of a flat plate solar collector. CFD analysis of solar flat plate collector was conducted by Ingle et al. [12]. His work attempted to present numerical simulation of solar collector developed exclusively for grape drying. CFD analysis of triangular absorber tube of a solar flat plate collector was performed by Basavanna and Shashishekar [13] where the numerical results obtained using the experimentally measured temperatures are compared to the temperatures determined by the CFD model. Tagliafico et al. [14] reviewed dynamic thermal models and CFD analysis for flat-plate thermal solar collectors. A review of solar collector models was presented, including a proper classification and a description of main characteristics and performances in their study. Nasrin and Alim [15] developed a semi-empirical relation for forced convective analysis through a solar collector. A new correlation was derived from their obtained results and it was easy to use heat transfer purposes.

From the above literature review it is mentioned that a very few 3D numerical studies have been completed using traditional fluid that is water, gas, air etc. Thus there is a large scope to work 3D numerical investigation of heat transfer through a flat plate solar collector using nanofluid.

2. Problem Formulation

A schematic diagram of the system in three dimensional as well as cross sectional view considered in the present study is shown in Fig. 1. The system consists of a flat plate solar collector. The working fluid in the collector is water-based nanofluid containing Cu nanoparticles. The nanoparticles are generally spherical shaped and diameter is taken as 5 nm. The nanofluid is considered as single phase flow and surfactant analysis is neglected. The solar collector is a metal box with highly transparent and anti-reflected glass cover (called the glazing) on top and a dark colored copper absorber plate on the bottom. Length, width and thickness of the absorber plate are 1m, 0.15m and 0.0008m respectively. The riser pipe has inner diameter 0.01 m and thickness 0.0005m. Coefficients of heat absorption and emmision of copper absorber are 95% and 5% respectively. A trapezium shaped bonding conductance is located from middle one-third part of width of the absorber plate. It covers the three-fourth part of the riser pipe. It is as long as the absorber plate and tube. The bonding conductance is made of copper metal. The computation domain is the copper absorber plate containing a fluid passing copper riser pipe with bonding conductance. The riser pipe is generally ultrasonically welded to the absorber plate.

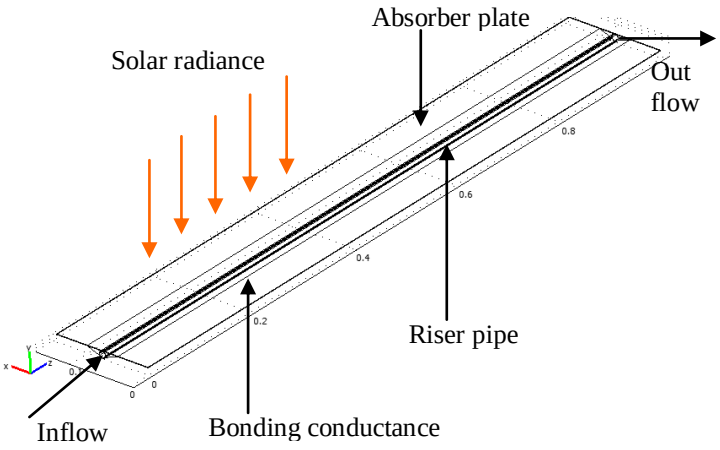

Fig. 1: Schematic diagram of the flat plate solar collector

3. Mathematical Formulation

In the present problem, it can be considered that the flow is three-dimensional and there is no viscous dissipation. The nanofluid is assumed incompressible and the flow is considered to be laminar. It is taken that water and nanoparticles are in thermal equilibrium and no slip occurs between them. Only steady state case is considered. The 3D governing equations in dimensional form are as follows

$$\frac{\partial u}{\partial x}+\frac{\partial v}{\partial y}+\frac{\partial w}{\partial z}=0$$

$$\rho_{nf}\left(u\frac{\partial u}{\partial x}+v\frac{\partial u}{\partial y}+w\frac{\partial u}{\partial z}\right)=-\frac{\partial p}{\partial x}+\mu_{nf}\left(\frac{\partial^2 u}{\partial x^2}+\frac{\partial^2 u}{\partial y^2}+\frac{\partial^2 u}{\partial z^2}\right)$$

$$\rho_{nf}\left(u\frac{\partial v}{\partial x}+v\frac{\partial v}{\partial y}+w\frac{\partial v}{\partial z}\right)=-\frac{\partial p}{\partial y}+\mu_{nf}\left(\frac{\partial^2 v}{\partial x^2}+\frac{\partial^2 v}{\partial y^2}+\frac{\partial^2 v}{\partial z^2}\right)$$

$$\rho_{nf}\left(u\frac{\partial w}{\partial x}+v\frac{\partial w}{\partial y}+w\frac{\partial w}{\partial z}\right)=-\frac{\partial p}{\partial z}+\mu_{nf}\left(\frac{\partial^2 w}{\partial x^2}+\frac{\partial^2 w}{\partial y^2}+\frac{\partial^2 w}{\partial z^2}\right)$$

$$u\frac{\partial T}{\partial x}+v\frac{\partial T}{\partial y}+w\frac{\partial T}{\partial z}=\alpha_{nf}\left(\frac{\partial^2 T}{\partial x^2}+\frac{\partial^2 T}{\partial y^2}+\frac{\partial^2 T}{\partial z^2}\right)$$

$$\frac{k_a}{\rho C_p}\left(\frac{\partial^2 T_a}{\partial x^2}+\frac{\partial^2 T_a}{\partial y^2}+\frac{\partial^2 T_a}{\partial z^2}\right)=0$$

where, $\alpha_{nf}=k_{nf}/\left(\rho C_p\right)_{nf}$ is the thermal diffusivity, $\rho_{nf}=(1-\phi)\rho_f+\phi\rho_s$ is the density, $\left(\rho C_p\right)_{nf}=(1-\phi)\left(\rho C_p\right)_f+\phi\left(\rho C_p\right)_s$ is the heat capacitance, $\mu_{nf}=\dfrac{\mu_f}{(1-\varphi)^{2.5}}$ is the viscosity of

Brinkman Model [16], the thermal conductivity of Maxwell Garnett (MG) model [17] is

$$k_{nf} = k_f \frac{k_s + 2k_f - 2\phi\left(k_f - k_s\right)}{k_s + 2k_f + \phi\left(k_f - k_s\right)}$$

The boundary conditions of the computation domain are:

at all solid boundaries of the riser pipe: $u = v = w = 0$

at the solid-fluid interface: $k_f\left(\frac{\partial T}{\partial n}\right)_{fluid} = k_a\left(\frac{\partial T}{\partial n}\right)_{solid}$

at the inlet boundary of the riser pipe: $T = T_{in}$, $w = W_{in}$

at the outlet boundary: convective boundary condition $p = 0$

at the top surface of the absorber: heat flux $-k_a \frac{\partial T_a}{\partial z} = q = I\tau\kappa - U_L\left(T_{in} - T_{amb}\right)$

at the other surfaces of absorber plate: $\frac{\partial T_a}{\partial n} = 0$

at the outer boundary of riser pipe: $\frac{\partial T}{\partial n} = 0$

at the outer boundary of bonding conductance: $\frac{\partial T_a}{\partial n} = 0$

The governing equations are non-dimensionalized by using the following dimensionless quantities

$$X = \frac{x}{D},\ Y = \frac{y}{D},\ Z = \frac{z}{D},\ U = \frac{u}{W_{in}},\ V = \frac{v}{W_{in}},\ W = \frac{w}{W_{in}},$$

$$P = \frac{p}{\rho_f {U_{in}}^2},\ \theta = \frac{\left(T - T_{in}\right)k_f}{qL},\ \ \theta_a = \frac{\left(T_a - T_{in}\right)k_a}{qL}$$

and $Pr = \frac{\nu_f}{\alpha_f}$ is the Prandtl number, $K = \frac{k_a}{k_f}$ is thermal conductivity ratio, $Re = \frac{W_{in} D}{\nu_f}$ is the Reynolds number, n and N is the dimensional and non-dimensional distances either along x or y or z directions acting normal to the surface respectively.

The average heat transfer rate of the collector can be written as

$$Nu = \frac{\iint_S \overline{Nu}\, ds}{\iint_s dS} = -\frac{1}{\pi DL}\frac{k_{nf}}{k_f}\iint_S \sqrt{\frac{\partial^2\theta}{\partial X^2} + \frac{\partial^2\theta}{\partial Y^2} + \frac{\partial^2\theta}{\partial Z^2}}\, ds$$

where L is the height of absorber tube.

The mean bulk temperature and average sub domain velocity of the fluid inside the collector may be written as $\theta_{av} = \frac{\iiint_v \theta d\mathrm{V}}{\iiint_v d\mathrm{V}} = \frac{4}{\pi D^2 L}\iiint_v \theta d\mathrm{V}$ and

$$\overline{\mathrm{V}}_{av} = \frac{\iiint_v \overline{\mathrm{V}} d\mathrm{V}}{\iiint_v d\mathrm{V}} = \frac{4}{\pi D^2 L}\iiint_v \overline{\mathrm{V}}\, d\mathrm{V} \quad , \text{ where V is the volume the absorber tube.} \qquad (17)$$

A measure of a flat plate collector performance is the collector efficiency (η) defined as the ratio of the useful energy gain (Q_{usfl}) to the incident solar energy. The instantaneous thermal efficiency of the collector is:

$$\eta = \frac{\text{useful gain}}{\text{available energy}} = \frac{Q_{\text{usfl}}}{AI} = \frac{F_R A\left[I\left(\tau\kappa\right) - U_L\left(T_{in} - T_{amb}\right)\right]}{AI}$$

$$= F_R\left(\tau\kappa\right) - F_R U_L \frac{\left(T_{in} - T_{amb}\right)}{I}$$

4. Numerical Formulation

The Galerkin finite element method Taylor and Hood [18] and Dechaumphai [19] is used to solve the non-dimensional governing equations along with boundary conditions for the considered problem. Conservation equations are solved for the finite element method to yield the velocity and temperature fields for the water flow in the absorber tube and the temperature fields for the absorber plate. The equation of continuity has been used as a constraint due to mass conservation and this restriction may be used to find the pressure distribution. The penalty finite element method is used to solve the governing equations, where the pressure P is eliminated by a penalty constraint. The continuity equation is automatically fulfilled for large values of this penalty constraint. Then the velocity components (U, V, W) and temperatures (θ, θ_a) are expanded using a basis set. The Galerkin finite element technique yields the subsequent nonlinear residual equations. Gaussian quadrature technique is used to evaluate the integrals in these equations. The non-linear residual equations are solved using Newton–Raphson method to determine the coefficients of the expansions. The convergence of solutions is assumed when the relative error for each variable between consecutive iterations is recorded below the convergence criterion such that $\left|\psi^{n+1} - \psi^n\right| \le 1.0\text{e}^{-6}$, where n is the number of iteration and Ψ is a function of U, V, W, θ and θ_a.

4.1 Mesh Generation

In finite element method, the mesh generation is the technique to subdivide a domain into a set of sub-domains, called finite elements, control volume etc. The discrete locations are defined by the numerical grid, at which the variables are to be calculated. It is basically a discrete representation of the geometric domain on which the problem is to be solved. The computational domains with irregular geometries by a collection of finite elements make the method a valuable practical tool for the solution of boundary value problems arising in various fields of engineering. Fig. 2 displays the 3D finite element mesh of the present physical domain. Fine mesh size is chosen for this geometry. The thermo-

physical properties of water and nanoparticles are taken from Ogut [20] and given in Table 1.

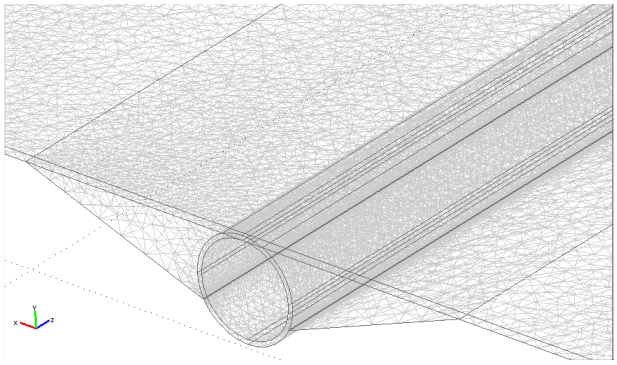

Fig. 2: Mesh generation of the collector

Table 1: Thermo-physical properties of water and Cu nanoparticles at 295K

Physical Properties	Fluid phase (water)	Cu
C_p(J/kgK)	4181	385
ρ (kg/m^3)	998.0	8933
k (W/mK)	0.606	400
$\alpha\times10^7$ (m^2/s)	1.47	1163.1
$\mu\times10^6$ (Ns/ m^2)	959	-

4.2. Grid Independent Test

The arrangement of discrete points throughout the domain is simply called a grid. The determination of a proper grid for the flow through a given geometric shape is important. The way that such a grid is determined is called grid generation. The grid generation is a significant consideration in CFD. Finite element method can be applied to unstructured grids. This is because the governing equations in this method are written in integral form and numerical integration can be carried out directly on the unstructured grid domain in which no coordinate transformation is required. The three dimensional computational domain is modeled using finite element mesh as shown in Fig. 2. The complete domain consists of 14,20,465 elements which include the riser tube and absorber plate. The mesh is composed of tetrahedron element type with ten nodes. The grid independence test is performed to check validity of the quality of mesh on the solution. The influence of further refinement does not change the result by more than 1.25 % which is taken here as the appropriate mesh quality for computation.

5. Results and Discussion

Finite element simulation is applied to perform the analysis of laminar forced convection temperature and fluid flow through a riser pipe of a flat plate solar collector filled with water/copper nanofluid. Effect of the Prandtl number (Pr) on heat transfer and collector efficiency of solar collector has been studied. The values of Prandtl number are taken as 4.2, 5.2, 6.6 and 7.6. All values chosen for the Prandtl number represent water at different temperature. Solid volume fraction (ϕ) is assumed to be fixed at 2%.

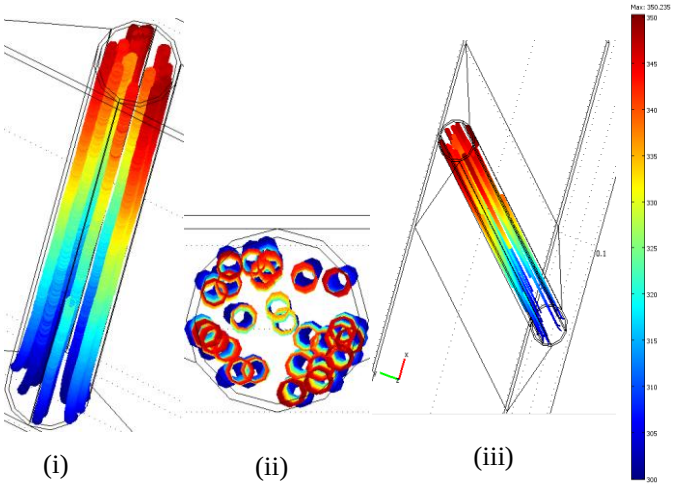

(i) (ii) (iii)

Fig. 3: Streamline plot with color expression for temperature (i) front view, (ii) slide view and (iii) back view

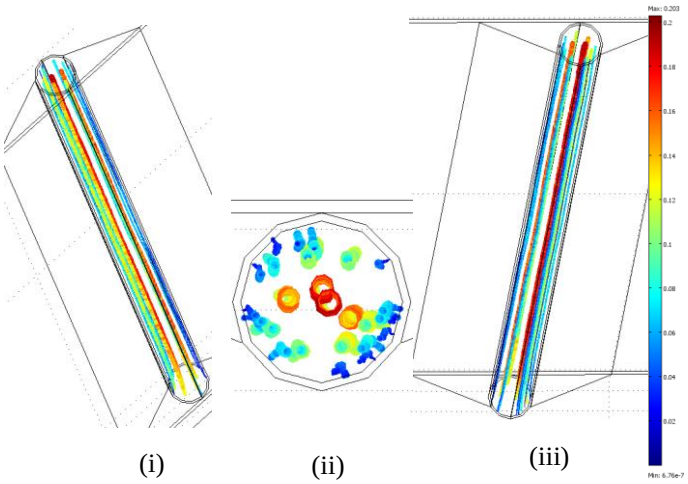

(i) (ii) (iii)

Fig. 4: Streamline plots with color expression for velocity (i) Front view, (ii) slide view and (iii) back view

Fig. 3(i-iii) represents the streamlines plot with color expression for temperature at Re = 1000, Pr = 6.6 and ϕ = 2%. The different colours indicate different temperature of streamlines. Streamlines plot are shown as front view, slide view and back view of a collector for water-copper nanofluid. The streamlines occupying the whole riser pipe of the flat plate solar collector. In all views of streamlines it is observed that the flow is laminar and the streamlines are parallel to each other. The temperature of the streamlines which are closer to the solid pipe is higher than the lines at the middle of the pipe.

On the other hand the streamlines plot with color expression for velocity field is shown in Fig. 4(i-iii). The strength of the streamlines which are closer to the solid pipe is lower than the lines at the middle of the pipe. That is the practical phenomena of the solar collector are satisfied by this simulation.

The average Nusselt number (*Nu*), average temperature (θ_{av}), collector efficiency (η), outlet mean temperature (dimensional) of nanofluid, subdomain mean velocity along with the various Prandtl number (*Pr*) are displayed in Fig. 5 (i)-(v). *Nu* enhances sharply with growing *Pr*. The rate of heat transfer for water-copper nanofluid is found to be more effective than the clear water due to higher thermal conductivity of solid nanoparticles. For growing viscous force from 4.2 to 7.6 rate of heat transfer rises 29% and 20% using water/Cu nanofluid and water respectively.

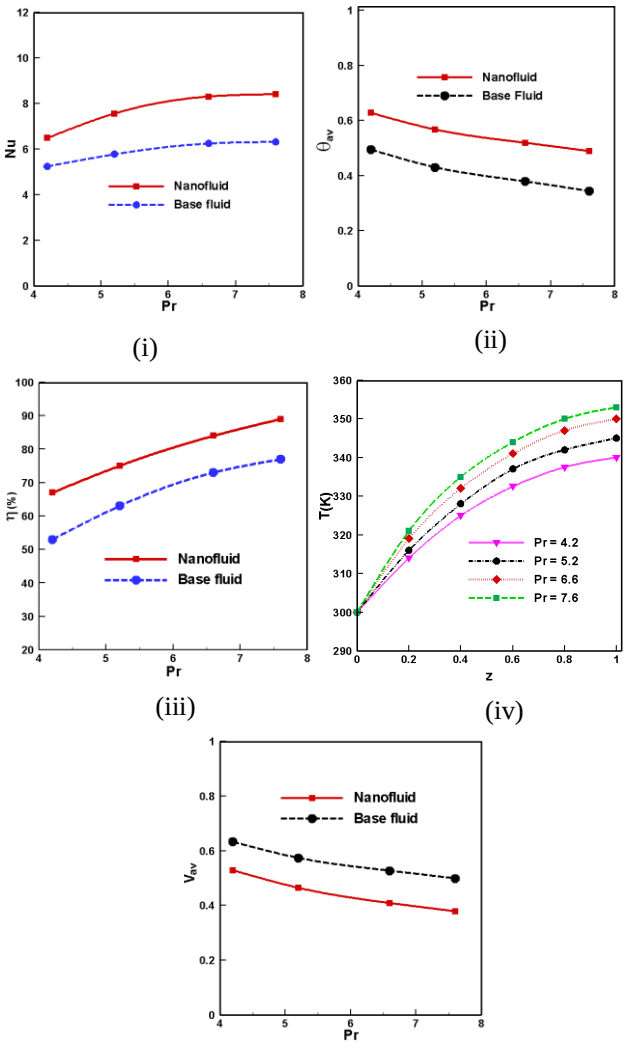

Fig. 5: Effect of *Pr* on (i) *Nu*, (ii) θ_{av}, (iii) η, (iv) *T* and (v) V

Mean temperature of fluids devalues gradually along with the increasing Prandtl numbers. It is well known that higher values of *Pr* indicate lower temperature of fluids. Here base fluid has lower mean temperature than the water-Cu nanofluid.

From Fig. 5(iii) it is observed that decreasing *Pr* devalues the percentage of collector efficiency (η) because greater *Pr* represents low tempered water which is found in winter season. Temperature of output water becomes high in summer season. Thermal efficiency enhances from 67%-89% for nanofluid and 53%-77% for water.

The inlet temperature of water-Cu nanofluid is maintained at 300K and then it increases gradually with the contact of heated solid surfaces of the riser pipe. And finally the output mean temperature of nanofluid becomes 340K, 345K, 350K and 353K for *Pr* = 4.2, 5.2, 6.6 and 7.6 respectively.

Magnitude of mean velocity (V_{av}) has notable changes with different values of viscous forces. It is well known that velocity of higher viscous fluid is less than that of lower viscous fluid. Clear water moves freely than solid concentrated nanofluid. Falling viscous force enhance the mean velocity of the fluids through the riser pipe of the flat plate solar collector.

6. Conclusion

Following conclusions have been drawn from the results of the numerical analysis:

- The configuration of the streamlines plot of heat and flow fields of the solar flat plate collector is found to significantly depend upon *Pr*.
- The water-Cu nanofluid with the highest *Pr* is established to be most effective in enhancing performance of heat transfer rate.
- Mean temperature devalues for both fluids with growing values of *Pr*.
- Collector efficiency is obtained higher for the highest Prandtl number.
- Outlet temperature of nanofluid rises due to escalating *Pr*.

NOMENCLATURE

A	Surface area of solar flat plate collector (m^2)
C_p	Specific heat at constant pressure (J kg^{-1} K^{-1})
I	Intensity of solar radiation (W m^{-2})
k	Thermal conductivity (W m^{-1} K^{-1})
L	Length of the solar collector (m)
m	Mass flow rate (Kg s^{-1})
Nu	Nusselt number,
Pr	Prandtl number,
Re	Reynolds number
T	Dimensional temperature (K)
T_{in}	Input temperature of nanofluid (K)
T_{out}	Output temperature of fluid (K)
u, v, w	Dimensional *x, y* and *z* components of velocity (m s^{-1})
U_l	Local heat transfer coefficient (W m^{-2} K^{-1})
U_i	Input velocity of fluid (ms^{-1})
U, V, W	Non dimensional velocities
V	Volume of the absorber tube (m^3)
X, Y, Z	Non dimensional co-ordinates

x, y, z Dimensional co-ordinates (m)

Greek Symbols

α Fluid thermal diffusivity ($m^2\ s^{-1}$)

β Thermal expansion coefficient (K^{-1})

ϕ Nanoparticles volume fraction

ν Kinematic viscosity ($m^2\ s^{-1}$)

η Collector efficiency,

θ Dimensionless temperature,

ρ Density ($kg\ m^{-3}$)

μ Dynamic viscosity ($N\ s\ m^{-2}$)

Subscripts

a absorber

av mean

f fluid

nf nanofluid

s solid particle

usfl useful

REFERENCES

[1] J. Wazwaz, H. Salmi, R. Hallak, Solar thermal performance of a nickel-pigmented aluminium oxide selective absorber, *Renewable Energy*, Vol. 27, pp. 277–292, 2002.

[2] P. Konttinen, PD. Lund, RJ. Kilpi, Mechanically manufactured selective solar absorber surfaces, *Solar Energy Mater Solar Cells*, Vol. 79, No. 3, pp. 273–283, 2003.

[3] Y. Varol and HF. Oztop, Buoyancy induced heat transfer and fluid flow inside a tilled wavy solar collector, *Building Environment*, Vol. 42, pp. 2062-2071, 2007.

[4] W. Xiaowu, B. Hua, Energy analysis of domestic-scale solar water heaters, *Renew. Sustain Energy Rev.*, Vol. 9, No. 6, pp. 638–645, 2005.

[5] A. Hussain, The performance of a cylindrical solar water heater, *Renew. Energy*, Vol. 31, No. 11, pp. 1751–1763, 2006.

[6] Y. Hwang, JK. Lee, CH. Lee, YM. Jung, SI. Cheong, CG. Lee, BC. Ku, SP. Jang, Stability and thermal conductivity characteristics of nanofluids, *Thermochimica Acta*, Vol. 455, No. 1–2, pp. 70–74, 2007.

[7] K.V. Karanth, M.S. Manjunath, N.Y. Sharma, Numerical simulation of a solar flat plate collector using discrete transfer radiation model (DTRM) – a CFD approach, Proc. of the World Cong. on Engg., London, U.K., III, 2011.

[8] OA. Bég, A. Bakier, R. Prasad, SK. Ghosh, Numerical modelling of non-similar mixed convection heat and species transfer along an inclined solar energy collector surface with cross diffusion effects, *World J. of Mech.*, Vol. 1, pp. 185-196, 2011.

[9] M.S, Manjunath, K.V. Karanth, N.Y. Sharma, Three dimensional numerical analysis of conjugate heat transfer for enhancement of thermal performance using finned tubes in an economical unglazed solar flat plate collector, *Proc. of the World Cong. on Engg.*, London, U.K., III, 2011.

[10] J. Vestlund, Gas-filled, flat plate solar collector, Ph. D. Thesis, Building Services Engg., Dept. of Energy and Environ., Chalmers University of Technology, Gothenburg, Sweden, 2012.

[11] M.S, Manjunath, K.V. Karanth, N.Y. Sharma, A comparative CFD study on solar dimple plate collector with flat plate collector to augment the thermal performance, *World Academy of Sci., Engg. and Tech.*, Vol. 6, pp. 10-21, 2012.

[12] P.W. Ingle, A.A. Pawar, B.D. Deshmukh, K.C. Bhosale, CFD analysis of solar flat plate collector, *Int. J. of Emerg. Techn. and Adv. Engg.*, Vol. 3, No. 4, pp. 337-342, 2013.

[13] S., Basavanna and K.S. Shashishekar, CFD analysis of triangular absorber tube of a solar flat plate collector, *Int. J. Mech. Eng. & Rob. Res.*, Vol. 2, No. 1, pp. 19-24, 2013.

[14] I.A. Tagliafico, F. Scarpa, M.D. Rosa, Dynamic thermal models and CFD analysis for flat-plate thermal solar collectors –a review, *Renew. and Sust. Energy Rev.*, Vol. 2, No. 30, pp. 526-537, 2014.

[15] R. Nasrin and M.A. Alim, Semi-empirical relation for forced convective analysis through a solar collector, *Solar Energy*, Vol. 105, pp. 455-467, 2014.

[16] H.C. Brinkman, The viscosity of concentrated suspensions and solution, *Journal Chem. Physics*, Vol. 20, pp. 571–581, 1952.

[17] JC. Maxwell-Garnett, Colours in metal glasses and in metallic films, *Philos. Trans. Roy. Soc. A*, Vol. 203, pp. 385–420, 1904.

[18] C. Taylor, P. Hood, A numerical solution of the Navier-Stokes equations using finite element technique, *Computer and Fluids*, Vol. 1, pp. 73–89, 1973.

[19] P. Dechaumphai, Finite Element Method in Engineering, 2nd ed., *Chulalongkorn University Press, Bangkok*, 1999.

[20] EB. Ogut, Natural convection of water-based nanofluids in an inclined enclosure with a heat source, *Int. J. of Thermal Sciences*, Vol. 48, No. 11, pp. 2063-2073, 2009.

ICMIEE-PI-140103

Performance Investigation of a Wet Counter flow Type cooling Tower with Corrugated Film Fill

Rifat-E-Nur Hossain[*1], Md. Nawsher Ali Moral* [1] , *Muzahidul Islam*[1]
[1] Department of Mechanical Engineering, Khulna University of Engineering & Technology, Khulna-9203, BANGLADESH

ABSTRACT

Cooling towers are one of the biggest heat and mass transfer devices that are in widespread use. The paper comprises designing of counter flow type induced draft cooling tower applying Merkel's theory. Performance investigation was carried out of a wet counter flow induced draft type cooling tower with corrugated film fill. The fill packing was 0.93m high, made of 21 galvanized metal sheets having a sinusoidal form. Mass flow rate of water was changed to investigate other important parameters such as range, approach, effectiveness, capacity etc. Effectiveness decreases with increase of water flow rate as is also observed in other types of cooling tower. For the fulfillment of the thesis a relevant study has been accomplished, cooling tower heat load was estimated, design calculations of the water cooling tower showing different geometrical parameters and dimensions are performed, material selection, fabrication of the different components and assembly of the cooling tower was also completed.

Keywords: Counter flow, Range, Approach.

1. Introduction

Cooling towers are heat removal devices used to transfer process waste heat to the atmosphere. Now a day's large numbers of industrial applications are using cooling tower to remove the process heat especially in power generating, refrigeration and air conditioning, chemicals, petrochemicals and petroleum industries. Wherever water is used as a cooling medium or process fluid cooling towers are used extensively.

Cooling towers are able to lower the water temperatures more than devices that use only air to reject heat, like the radiator in a car, and are therefore more cost-effective and energy efficient. In most industrial locations, cooled fresh water is scanty therefore, continuous reuse and re cooling of the limited fresh water with the help of cooling tower is more common and economical. Another strong motivation for the increased use of cooling towers is the environmental protection provided through the reduction of water withdrawals and minimizing of thermal discharge.

Many types of cooling towers have been developed for use at such varied levels of technological sophistication and sizes. Although cooling towers can be classified several ways, the primary classification is into dry towers, wet towers and some hybrid wet-dry combinations exist. Classification also exists according to the air water flow characteristics.

2. Wet Counter Flow Type Cooling Tower

Wet cooling tower operates based on evaporation principle. The working fluid and the evaporated fluid (usually water) are one and the same. It cools water by contacting it with the air and evaporating some of the water whereby some of the water is evaporated into a moving air stream and subsequently discharged into the atmosphere. As a result, the remainder of the water is cooled down significantly. In a wet cooling tower, the warm water can be cooled to a temperature lower than the ambient air dry-bulb temperature, if the air is relatively dry. In counter flow design the air flow is directly opposite to the water flow. Air is being sucked from the lower part of the cooling tower and rises upwards in this induced draft type design, it gets warmer and when it reaches the top, it is hottest at that point. Since the water is flowing in the downward direction, it is the hottest at the top. Now as the hottest of air meets the hottest of water, evaporation is more, and thus, the cooling is more. The water is sprayed through pressurized nozzles and flows downward through the fill, opposite to the air flow. Cooling towers employ fills to facilitate heat transfer by maximizing water and air contact. Performance of a counter flow type tower is greatly influenced by film type fill. The principle of operation of cooling tower fill is to put as much water surface area in contact with as much air as possible, for the longest amount of time possible. Film fills allow the water to form thin flowing sheets to expose as much water surface area as possible to the interacting flow.

2.1 Related parameters of cooling tower

Range: This is the difference between the cooling tower water inlet and outlet temperature. [3]

Approach: This is the difference between the cooling tower outlet cold water temperature and ambient wet bulb temperature.

* Corresponding author. Tel.: +88-01676110457
E-mail address: rifatenur08@gmail.com

Liquid/Gas (L/G) ratio: The L/G ratio of a cooling tower is the ratio between the water and the air mass flow rates. Theoretically:
L/G = (h2 – h1) / (Tw1 – Tw2)

Effectiveness: This is the ratio between the range and the ideal range (in percentage), i.e. difference between cooling water inlet temperature and ambient wet bulb temperature, or in other words it is = Range / (Range + Approach).

Cooling capacity: This is the heat rejected in kCal/hr or TR, given as product of mass flow rate of water, specific heat and temperature difference.
Cooling capacity = $m_w \times Cp_w \times (T_{wi}-T_{wo})$

3. Markel's theory for cooling tower design
The analysis combines [2] the sensible and latent heat transfer into an over-all process based on enthalpy potential as the driving force. The two processes are combined, ingeniously, into a single equation:

$$dQ = Ka\ dV(h_w - h_a) = Gdh_a \qquad (1)$$

which gives by integration

$$KaV/L = C_p \int_{tw2}^{tw1} \frac{dt}{(hw - ha)} \qquad (2)$$

Where,

Q= Heat transfer rate, watt
L = mass water rate, kg/sec
G = air flow rate, kg dry air /sec
t_{w1} = bulk water temperature at inlet (hot water), °C
t_{w2} = bulk water temperature at outlet (cold water), °C
h_w = enthalpy of air-water vapor mixture at the bulk water temperature, kJ/kg dry air
h_a = enthalpy of air-water vapor mixture at the wet bulb temperature, kJ/kg dry air
h_{a1}=enthalpy of entering air, kJ/kg
h_{a2}=enthalpy of leaving air, kJ/kg
KaV/L = Tower demand, kg air/ kg H_2O
Ka = Volumetric air mass transfer constant, kg H_2O/(sec m^3)
C_p= Specific heat of water, J/kg °C

V = Fill volume, m^3
For the evaluation of KaV/L,

$$KaV/L = C_p \int_{tw1}^{tw2} \frac{dt}{(hw - ha)}$$
$$= C_p x(t_{w2}-t_{w1}) x[1/Dh_1+1/Dh_2+1/Dh_3+1/Dh_4]/4 \qquad (3)$$

Where, Dh_1=value of (h_w - h_a) at a temperature of CWT + 0.1 x Range
Dh_2=value of (h_w - h_a) at a temperature of CWT + 0.4 x Range
Dh_3=value of (h_w - h_a) at a temperature of CWT + 0.6 x Range
Dh_4=value of (h_w - h_a) at a temperature of CWT + 0.9 x Range

Equation for enthalpy of leaving air:
$h_{a2} = h_{a1} + L/G * Range$
Equation for determining Ka:
$Ka = C \times [L]^m * [G]^n$
Where,
C, m and n are constants, which depend on the tower fill. These both factors are determined through fill test.

4. Design of the wet counter flow type cooling tower

4.1 Assumptions:
Inlet temperature of hot water entering tower, T1=50℃
Outlet temperature of cold water leaving tower, T2=35.6℃
Dry bulb temperature of air entering tower, T_{dbt}=35℃
Wet bulb temperature of air entering tower, T_{wbt}=24℃

4.2 Design data
Mass flow rate of hot water, mw=0.0334 kg/sec
Exhaust fan area, A_e=0.0929 m^2
Tower height, H=1.2192 m
Exhaust fan discharge velocity, V_d=3.3 m/sec
Exhaust fan suction velocity, V_s=0.99 m/sec (3% of discharge velocity)
Humidity ratio for inlet air, ω_{ai}= 0.0141
Enthalpy for inlet air, h_{ai}=72.4 kJ/kg dry air

4.3 Design
Design of cooling tower consists of calculation of basic parameters, determination of tower demand/tower characteristic KaV/L, tower dimension, capacity and makeup water requirement. Also calculation for dimensions and capacity of other related parts of the experimental setup such as collection basin and heater tank is carried out.
Basic parameters calculated are -
Mass flow rate of air, ma = 0.1043kg/sec
Liquid Gas ratio, L/G = 0.32
Range, R = 14.4℃
Approach, A = 11.6℃
Calculation for tower demand/ tower characteristic is presented in **Table 1**. Calculation for water side involve evaluation of bulk water temperature (t_w) at Δ intervals where Δ= 0.1, 0.4, 0.6, 0.9 within the cooling range using following expression –

$$t_w = T_2 + \Delta * R \qquad (4)$$

where, T_2= 35.5℃= Outlet temperature of cold water leaving tower
And for air side enthalpy (h_a) are found using following equations-

$$h_a = ha_1 + L/G * Range \qquad (5)$$

where, ha1= enthalpy of entering air at wet bulb temperature T_{wbt}=24℃

4.4 Summary of design
KaV/L = 0.58
Tower dimension =0.56m x 0.56 m x 1.2192m
Design effectiveness, ϵ =55.38%
Design cooling capacity, Q =2 kW
Makeup water, V_{makeup} =1.3 liters
Dimension of collection basin =0.56m x 0.56m x 0.11 m
Design capacity of collection basin =34 liters
Heater tank dimension =0.33 m x 0.33 m x 0.33 m
Design capacity of heater tank = 35.9 liters

5 Construction of the cooling tower

The constructed cooling tower unit consist of - hot water tank, hot water supply pump, cooling tower frame, exhaust fan, Ceiling shower, fill, sump, galvanized iron pipe, thermocouple. Water is heated up to 50℃ in the hot water tank (capacity 35.9liters) with help of electric heater and supplied to the tower through pump. Made of G.I. sheet and well insulated. A centrifugal pump of 0.5 hp supplies the hot water to the tower at a velocity 0.0659 m/sec at a height of 2.24 m. A wooden frame (0.56m x 0.56m x 1.2192m) holds exhaust fan (1400rpm) to suck ambient air from bottom of tower, 2 Ceiling showers (dia-0.127m) to spray hot water and film fill. Dimension of fill: 0.5461m x 1.0287m. Gap between each sheet=0.0254m. The experimental set up is shown in Fig.1and Fig 2 which is an autocad drawing of the setup.

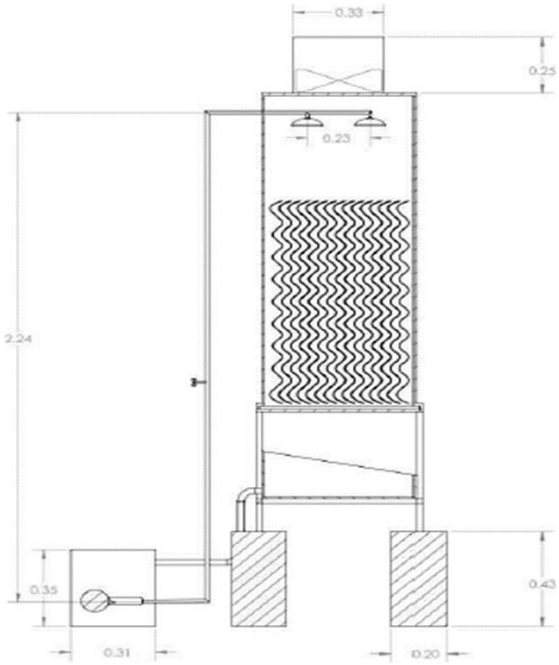

Fig.1 Schematic diagram of the experimental setup

Table.1 Calculation of tower demand in tabular form

Water side			Air side		Enthalpy diff.	
Descriptions	t_w (℃)	h_w (kJ/kg)	Descriptions	h_a (kJ/kg)	h_w-h_a	1/ (h_w-h_a)
35.6+14.4*0.1	37	154.86	72.5+0.32*14.4*0.1	72.96	81.9	0.0122
35.6+14.4*0.4	41.4	173.0	72.5+0.32*14.4*0.4	74.34	98.66	0.0101
35.6+14.4*0.6	44.2	185.12	72.5+0.32*14.4*0.6	75.26	109.89	0.0091
35.6+14.4*0.9	48.6	203.18	72.5+0.32*14.4*0.9	76.65	126.53	0.0079
Sum of 1/ h_w-h_a =0.0393						

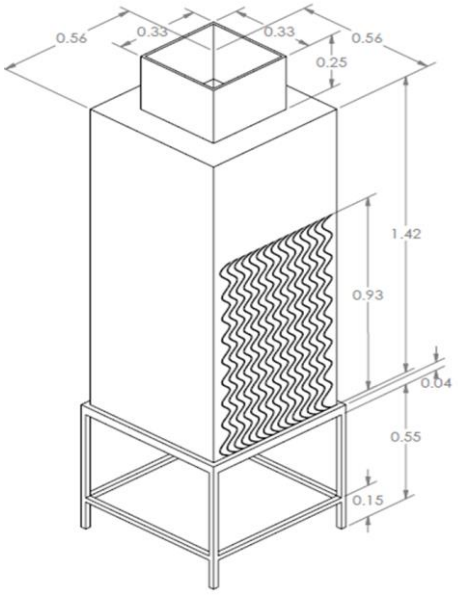

Fig.2 Isometric view of the experimental set up

6 Performance Test

The performance of cooling towers is evaluated to assess present levels of approach and range against their design values. During the performance evaluation, portable monitoring instruments are used to measure the following parameters: wet bulb temperature of air, dry bulb temperature of air, cooling tower inlet water temperature, cooling tower outlet water temperature,

Exhaust air humidity, water flow rate. These measured parameters are then used to determine the cooling tower performance in several ways such as:

- Range
- Approach
- Effectiveness
- Cooling capacity
- L/G ratio

7 Result and Discussion

Results are presented in tabular form in **Table 2.**

Experiments were conducted to investigate the effects of mass flow rate of water on range, cooling capacity, approach, and effectiveness. The water inlet temperature and air flow rate were maintained constants to 50℃ and 0.1043kg/sec respectively for all the experiments. Mass flow rate was varied from 0.0333kg/sec to 0.333kg/sec. It was observed that with the increase of water mass flow rate, range was decreased and cooling capacity was increased which is shown in **Fig 3**. An increased amount of water mass flow rate was responsible for decreasing heat transfer as it reduce the heat transfer time and disturbs the proper film formation. The wet bulb temperature of ambient air was found to vary between 27.5 ℃ and 29℃. The decrease of inlet humidity ratio and increase of water flow rate results in an increase of the percentage of water mass vaporized inside the cooling tower. While calculating the evaporation rate the highest evaporation rate 1.12x10-3kg/sec was found in the 9th observation, where water flow rate was the highest which is 0.333kg/sec and wet bulb temperature was found lowest of all the observations which was 27.5℃. Evaporation rates did not change uniformly due to variation of atmospheric conditions. From Fig 17 it is observed that the approach increases with increase of mass flow rate of water which is due to the increase of outlet water temperature. Effectiveness decreases with water mass flow rate to 44%. Though effectiveness was found highest at the lowest value of mass flow rate, we can't appreciate the lowest mass flow as it decreases the cooling capacity greatly. So it is recommended it to run the cooling tower at a medium water mass flow rate such as 0.125kg/sec so that one can achieve a good range and effectiveness with corresponding cooling capacity and approach.

Table.2 Presentation of result in tabular form

No of obs	Mass flow rate of hot water m_w (kg/sec)	L/G	Range R (℃)	Approach A (℃)	Effectiveness ϵ	Cooling capacity Q (kW)
1.	0.0333	0.319	19	2	0.905	2.64
2.	0.0417	0.399	18	4	0.818	3.13
3.	0.0625	0.599	18	4	0.818	4.70
4.	0.0833	0.798	17	5.5	0.756	5.92
5.	0.100	0.958	17	4.5	0.790	7.10
6.	0.125	1.19	16	6	0.727	8.35
7.	0.143	1.37	13	8	0.619	7.76
8.	0.200	1.92	11	11	0.500	9.19
9.	0.333	3.19	10	12.5	0.440	13.9

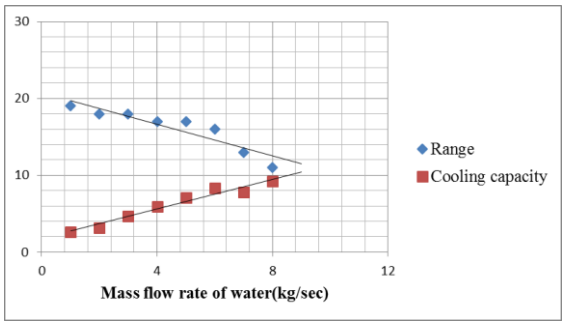

Fig.3 Effect of mass flow rate of water on range and cooling capacity

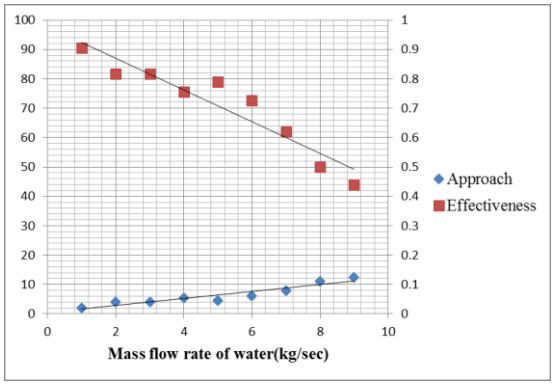

Fig.4 Effect of mass flow rate of water on effectiveness and approach

8 Conclusion

Performance of cooling tower found satisfactory throughout the test. The design wet bulb temperature was taken approximately average of year round wet bulb temperature of Bangladesh. In this study rectangular shaped cooling tower is designed with corrugated film fill. Which is different than conventional cooling towers with cylindrical tower body and PVC film fill. One of the major advantage of this design with rectangular shape and corrugated fill is cost effectiveness and ease of construction. As both the construction of cylindrical tower and fabrication of PVC fill is comparatively difficult.

Within the range of experiments following observations were found,

a) The cooling capacity was found to increase from 2.64 kW to 13.9 kW with the increase of water flow rate from 0.0333kg/sec to 0.333kg/sec.
b) With the increase of mass flow of water from 0.0333kg/sec 0.333kg/sec the approach was found to increase from 2 ℃ to 12.5 ℃ respectively.
c) The effectiveness was found to decrease from 90% to 44% with the increase of mass flow rate of water from 0.0333kg/sec to 0.333kg/sec.
d) The range was found to be decreased from 19 ℃ to 10℃ with the increase of mass flow rate of water from 0.0333kg/sec to 0.333kg/sec respectively.
e) During comparison between two arrangements a fair deviation of range and effectiveness after a water flow rate of 0.0625kg/sec was observed.
f) The overall performance of the cooling tower designed, constructed and tested was found satisfactory.

NOMENCLATURE

T_1 : Inlet hot water temperature, ℃
T_2 : Outlet cold water temperature, ℃
m_{evap} : Rate of evaporation, kg/sec
m_{da} : Mass flow rate of dry air, kg/sec
ω_{ao} : Humidity ratio of cooling tower outlet air
ω_{ai} : Humidity ratio of cooling tower inlet air
m_w : Cooling water mass flow rate, kg/sec
Cp : Specific heat of water, J/kg ℃
h_2 : Enthalpy of air-water vapor mixture at exhaust wet-bulb temperature, kJ/kg
h_1 : Enthalpy of air-water vapor mixture at inlet wet-bulb temperature, kJ/kg
L/G : Water air flow rate ratio
KaV/L : Tower characteristic, kg air/kg H2O
Ka : Volumetric air mass transfer constant
V : Fill volume, m^3
D : Diameter of pipe, m
H : Tower height, m
R : Range, ℃
T_{wbt} : Ambient air wet bulb temperature, ℃
Q : Cooling capacity, kW

REFERENCES

[1] S. V. Bedekar, P. Nithiarasu and K. N. Seerharanu, Experimental investigation of the performance of a counter-flow, packed-bed mechanical cooling tower, *Energy*, Vol. 23, pp 943-947 (1998)

[2] Don W. Green, Robert H. Perry, Evaporative cooling, *Perry's Chemical Engineers' Handbook*, Eighth Edition, Vol 12, pp 1214-1223(1999)

[3] Goshayshi HR, Missenden JF, Tozer R, Cooling tower an energy conservation resource, *Applied Thermal Engineering*, Vol 19, pp 1223-1235 (1999)

ICMIEE-PI-140105

Characteristics of flow over three side-by-side square prisms

Qinmin Zheng[1], *Md. Mahbub Alam*[1,2,*], *Yu Zhou*[1]
[1]Institute for Turbulence-Noise-Vibration Interaction and Control, Shenzhen Graduate School
Harbin Institute of Technology, Shenzhen, China
[2]Key Kab of Advanced Manufacturing and Technology, Shenzhen Graduate School
Harbin Institute of Technology, Shenzhen, China

ABSTRACT
A low-Reynolds number (Re = 150) flow over three side-by-side square prisms placed normal to the oncoming flow is simulated systematically at L/W = 1.2 ~ 8.0, using finite volume method, where L is the prism center-to-center spacing and W is the prism width. Six distinct flow structures and their ranges are identified, viz., single-bluff-body flow (L/W < 1.5), flip-flopping flow (1.5 ≤ L/W < 2.0), symmetrically-biased coupled flow (2.0 ≤ L/W ≤ 2.5), transition flow (2.5 < L/W < 3.0), non-biased coupled flow (3.0 ≤ L/W ≤ 7.0) and non-biased weakly coupled flow (L/W > 7.0). Physical aspects of each flow regime, such as vortex structures, gap flow deflections, shedding frequencies are discussed in detail. A secondary frequency other than the Strouhal number (primary frequency) is identified in symmetrically biased and non-biased coupled flow regimes. The origin and effect of the secondary frequency on lift forces are unearthed. These results, most of which have been obtained for the first time, are of fundamental significance.

Keywords: flow-structure interactions, three side-by-side square prisms, vortex streets, secondary frequency

1. Introduction

The square prism is the representative model of bluff bodies with sharp corners, characterized by a fixed flow separation point. However, in spite of its great importance to engineering, the flow around multiple square prisms has received much less attention than that of circular cylinders.

Alam *et al.*[1] at $Re = 4.7\times10^4$ performed systematic measurements of the flow field, Strouhal number St, and time-averaged and fluctuating forces for two side-by-side square prisms at L/W = 1.02 ~ 6.00. Four distinct flow regimes, namely (i) single-body regime (1.0 < L/W < 1.3), (ii) two-frequency regime (1.3 ≤ L/W ≤ 2.2), (iii) transition regime (2.2 < L/W < 3.0), and (iv) coupled vortex street regime (L/W ≥ 3.0) are identified. Besides, the interference between shear layers, the gap flow deflection and changeover, flow entrainment, recirculation bubble, vortex interactions and formation lengths for each regime, are studied in detail and connected to the characteristics of the time-averaged and fluctuating fluid forces. At much smaller Re = 300, Alam & Zhou [2] observed qualitatively similar results in flow visualization experiments.

Kumar *et al.* [3] simulated the flow around a row of nine square prisms at Re = 80 for L/W = 1.3 ~ 13.0, using lattice-Boltzmann method. Three flow regimes are recognized based on vorticity fields and drag coefficient signals: synchronized flow, quasi-periodic flow and chaotic flow. No significant interaction between the wakes is observed at L/W > 7.

In the present work, we focus on detailed physics of the flow over three side-by-side square prisms. Simulations are performed at Re = 150 for L/W = 1.2 ~ 8.0 covering all possible flow regimes. Vorticity fields, shedding frequencies along with the time series of lift force are analyzed to explicitly delineate the resultant flow structures.

2. Numerical methods

2.1. Computational models and boundary conditions

The dimensionless 2-D N-S equations governing the flow of a Newtonian fluid can be written in vector form as

$$\left.\begin{aligned}\frac{\partial\vec{U}}{\partial t}+\left(\vec{U}\cdot\nabla\right)\vec{U}&=-\nabla P+\frac{1}{Re}\nabla^2\vec{U}\\ \nabla\cdot\vec{U}&=0\end{aligned}\right\} \qquad (1)$$

where Re is the Reynolds number based on free-stream velocity U_∞ and prism width W. Re is kept constant at 150. In solving the governing equations, the different physical quantities are normalized by U_∞ and/or W. The finite volume method is applied on structured meshes. The pressure-velocity coupling is handled with the semi-implicit pressure linked equations (SIMPLE) scheme. Discretization of the convective terms in the conservation equations is accomplished through a second-order accurate upwind differencing scheme. Second-order implicit forward discretization is adopted for the time derivative term in order to accelerate the convergence process.

Fig. 1 shows a schematic diagram of the computational domain and grid distribution around a quadrant of a prism. As presented in Fig. 1(a), the computational domain is chosen to be $(30W + 3L) \times (40W + L)$ with

*Corresponding author.
Email address: alamm28@yahoo.com; alam@hitsz.edu.cn

the upstream and downstream boundaries located at $12W + 0.5L$ and $28W + 0.5L$, respectively, from the coordinate origin at the center of the middle prism. The lateral surfaces are located at $15W + 1.5L$ each from the origin. At the inlet, a uniform velocity profile ($u = 1, v = 0$) is imposed, while the stress vector is set to zero at the outlet boundary. On the upper and lower boundaries, the component of the velocity normal to, and the component of the stress vector along the boundaries are prescribed a zero value. No-slip boundary condition ($u = v = 0$) is employed on the surfaces of the square prisms. In the computation domain, the initial flow velocities (at $t = 0$) are given as $u = U_\infty$, $v = 0$.

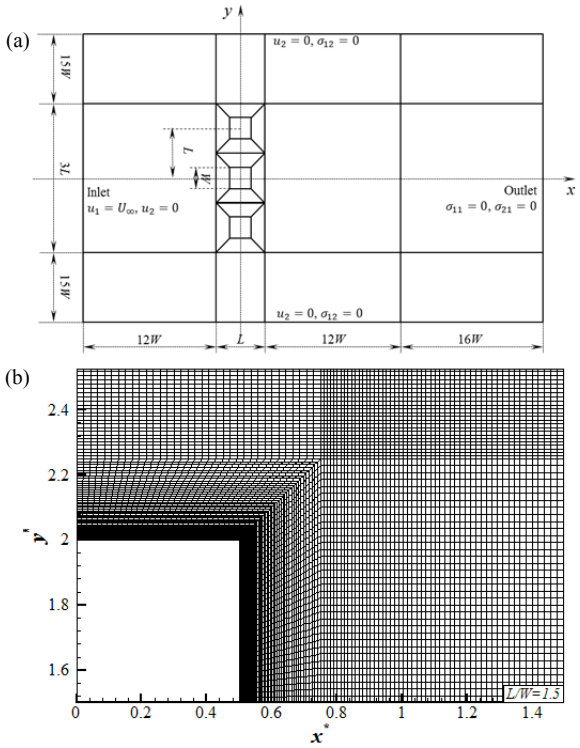

Fig. 1 (a) Sketch of the computational domain and boundary conditions, and (b) grid distribution around a quadrant of a prism.

2.2. Grid independence test and result validation

Grid independence test for the flow around a single square prism was carried out before the extensive simulations, where the computational domain and grid distribution of the prism are made similar to those of three side-by-side square prisms. Table 1 compares C_L', $\overline{C_D}$, C_D', and St obtained from the present and previous simulations for a single square prism at $Re = 150$.

Table 1 Grid independence test for single prism at $Re = 150$

Case	C_L'	$\overline{C_D}$	C_D'	St
Present	0.2721	1.4799	0.0167	0.1576
Saha *et al.*[4]	0.2740	-	0.0170	-
Sohankar *et al.* [5]	0.2300	1.4400	-	0.1650
Kumar *et al.* [3]	-	1.5200	-	0.1570
Sharma *et al.* [6]	-	1.4700	-	0.1560

Overall, C_L', $\overline{C_D}$, C_D', and St results display a good accordance with those in the literatures.

3. Flow structure

$L/W = 1.2$ was simulated first and increased successively to 8.0. The prisms at $L/W = 8.0$ behaved almost independently and a weak interaction was observed between the adjacent wakes. So less attention will be paid to the results at this L/W. The wakes interact each other in a complicated manner at $L/W \leq 7.0$, resulting in six distinct flow structures: (A) single-bluff-body flow ($L/W < 1.5$), (B) flip-flopping flow ($1.5 \leq L/W < 2.0$), (C) symmetrically-biased coupled flow ($2.0 \leq L/W \leq 2.5$), (D) transition flow ($2.5 < L/W < 3.0$), (E) non-biased coupled flow ($3.0 \leq L/W \leq 7.0$) and (F) non-biased weakly coupled flow ($L/W > 7.0$). Each regime has distinct intrinsic features associated vortex structures, shear layer behaviors, gap flow deflections, shedding frequencies and force characteristics.

Fig. 2 shows the contours of non-dimensional instantaneous vorticity patterns at different regimes. The single-bluff-body flow (regime A) prevails at $L/W < 1.5$, where vortex shedding occurs essentially from the outer shear layers of the outer prisms (Fig. 2a); a single vortex street, thus, forms behind the three prisms, similarly to that of a single bluff body. Although weak, flows through the two gaps are apparent and are prone to bias toward the growing vortex. When the vortex from the lower side grows, both gap flows swerve to the lower side. In the next half cycle of the vortex shedding, the upper vortex will grow and pull the gap flows toward the upper side.

When L/W is increased to regime B ($1.5 \leq L/W < 2.0$), a greater amount of flow can pass through the gaps and can split the wake into three immediately downstream of the prisms. Appreciable vortices from the gap sides form around the prisms. The vortices merge with the outer vortices shed from the outer prisms. The gap flow now can flip-flop randomly at different fashions to be biased upward (Fig. $2b_1$), downward (Fig. $2b_2$), inward (Fig. $2b_3$) and outward (Fig. $2b_4$), generating four different flow structures.

The symmetrically-biased coupled flow occurring at $2.0 \leq L/W \leq 2.5$ (regime C) is characterized by the gap flow biased/diverged outward symmetrically (Fig. 2c). A substantial wide wake thus accompanies the middle prism and a narrow wake complements each outer prism. This flow structure is very similar to that in Fig. $2(b_4)$, implying that the flow structure change from regimes B to C is continuous. The vortices shedding from the outer prisms are found to be perfectly coupled with a constant phase lag $\phi = 180°$ (antiphase). Note that here coupling means the coupling between the vortices from the outer prisms only, as the middle prism shedding frequency is always different from the outer prisms. It was found that the mean base-pressure of the outer prisms was identical and much smaller than that of the middle prism. Since

the gap width is now large enough, the narrow wake associated with low base pressure can pull only the nearest shear layer of the middle prism. The gap flows are thus stably biased outward, not prone to switch.

In the non-biased coupled flow regime ($3.0 \le L/W \le 7.0$, regime E), the gap flows are no longer biased. Unlike other flow regimes A-D, a single vortex street, qualitatively similar to that behind an isolated prism, persists behind each prism. Again the vortex sheddings from the outer prisms occurring at the same frequency are coupled with a fixed ϕ. The vortex shedding frequency of the middle prism is however different, slightly higher than that of the outer prisms. The instantaneous phase relationship between the vortex sheddings from the middle and outer prisms thus changes periodically from anti-phase (Fig. $2d_1$) to in-phase (Fig. $2d_2$), and vice versa, which has a great impact on the time histories of lift forces of the prisms. It is noted that the phase lag between the vortex sheddings from outer prisms depends on L/W; ϕ decaying from 110° to 0° between $L/W = 3.0$ and 3.5 remains 0° at $3.5 \le L/W \le 4.0$ before increasing gradually to 80° at $L/W = 7.0$. In the latter L/W range, the interaction between the wakes weakens, leading to the change in the phase lag.

Regime D ($2.5 < L/W < 3.0$) is the transition between regimes C and E, where the modification of the flow from symmetrically-biased to non-biased is discontinuous; both flow modes perhaps appear intermittently in this regime. Alam *et al.*[1] for two side-by-side square prisms observed similar transition regime where biased and coupled flows switched from one to the other.

At $L/W > 7.0$, the coupling between the outer wakes is weak and each prism tends to behave like a single prism with difference in frequencies between the middle and outer prisms getting smaller. This regime, hence, can be regarded as weak-interaction or non-biased weakly coupled flow regime.

4. Shedding frequency

The power spectra of fluctuating lifts of the three prisms at different regimes are shown in Fig. 3. Here prisms 1, 2 and 3 refer to the upper, middle and lower prisms, respectively. For single-bluff-body flow, identical $St = 0.068$ is observed for the three prisms (Fig. 3a), implying that vortices are separated at the same frequency from the freestream sides of the prisms and generate a single Karman vortex street behind the three prisms. $St = 0.0821$ may be associated with the influence of the gap flow. The remaining peaks are the harmonic and linear combinations of these two frequencies.

In the flip-flopping flow, though the gap flows are biased and flip-flop, a single combined wake dominantly forms behind the three prisms. The flows through the gaps acting as base bleeds postpone the vortex formation from the free stream sides, *St* thus jumps to 0.1504 (Fig. 3b). The peaks corresponding to the *St* are relatively wider than those in the other regimes, because of the random switch of the gap flows.

The narrow wakes behind the outer prisms in the symmetrically-biased coupled flow are connected to a *St* of 0.1896 (Fig. 3c), while the wide wake behind the middle prism is associated with a smaller and higher $St = 0.1505$ and 0.2288. The $St = 0.1505$ is due to a tendency of shedding corresponding to the wide wake, while $St = 0.2288$ results from a strong alternate coupling of vortices in the two gaps. Different from the single-bluff-body and flip-flopping flows, a very low frequency ($St = 0.0390$) with a tiny peak (see the insets) is found in this regime. It is referred to as a secondary frequency hereafter. Indeed, $St = 0.0390$ is the difference between $St = 0.1896$ and 0.1505. The secondary frequency has a great influence to make a beat-like variation in the time histories of lift forces of the prisms. The origin of the secondary frequency and its effect will be discussed more detailed later. The secondary frequency will be more obvious in the non-biased coupled flow.

When the gap flows are not biased (non-biased coupled flow), the low *St* of the middle prism jumps and the high *St* disappears. The difference in *St* between the middle and outer prisms becomes smaller (Fig. 3d). Here the middle prism *St* is larger than that of the outer prisms, resulted from the higher mean velocity in the shear layers of the middle prism. The peak at $St = 0.0116$ is again associated with the secondary frequency.

5. Physics of the secondary frequency

As mentioned above, the shedding frequencies of the outer prisms are identical, but higher at symmetrically -biased coupled flow and smaller at non-biased coupled flow than that of the middle prism. It would be interesting to see how the flow classification is connected to *St*. Variations in *St* of the three prisms are shown in Fig. 4(a). While *St*(s) of the all three prisms are identical and very small in regime A, they remaining identical jumps to a higher value in regime B. The middle and outer prisms have however different *St* in regime C, smaller for the middle prism. *St* again jumps in the transition regime D, before tapering off slowly with L/W in the regime E where *St* is larger for the middle prism than outer prisms. The difference in *St* between the middle and outer prisms is small in regime F. The difference in the frequencies between the middle and outer prisms in regimes C, D, E and F may be connected to difference in velocities between the gaps and outer sides. Therefore, the average of time-mean streamwise velocities at the two sides (see the inset) of each prism, U_{avg}, is estimated and plotted concurrently in Fig. 4(a). What is interesting here is that U_{avg} follows the *St* behavior, being smaller for the middle prism in regime C

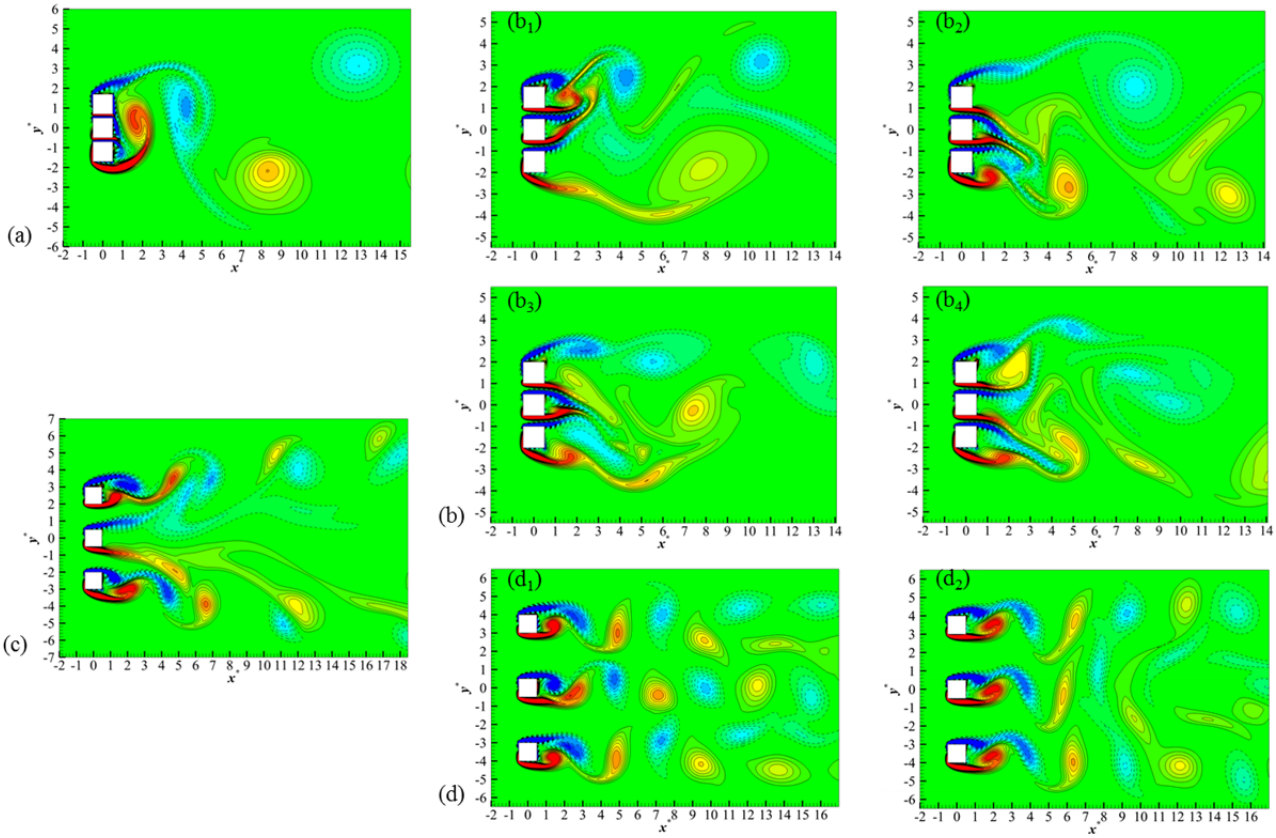

Fig. 2 Contours of vorticity at (a) $L/W = 1.2$ (single bluff body flow, regime A, $L/W < 1.5$); (b) $L/W = 1.5$ (flip-flopping flow, regime B, $1.5 \le L/W < 2.0$): the gap flows biased (b_1) upward, (b_2) downward, (b_3) inward, (b_4) outward; (c) $L/W = 2.5$ (symmetrically-biased coupled flow, regime C, $2.0 \le L/W \le 2.5$); (d) $L/W = 3.5$ (non-biased coupled flow, regime E, $3.0 \le L/W \le 7.0$): the middle prism shedding (d_1) anti-phase and (d_2) in-phase with the others. Transition flow (regime D, $2.5 < L/W < 3.0$) and non-biased weakly coupled flow (regime F, $L/W > 7$) are not shown here.

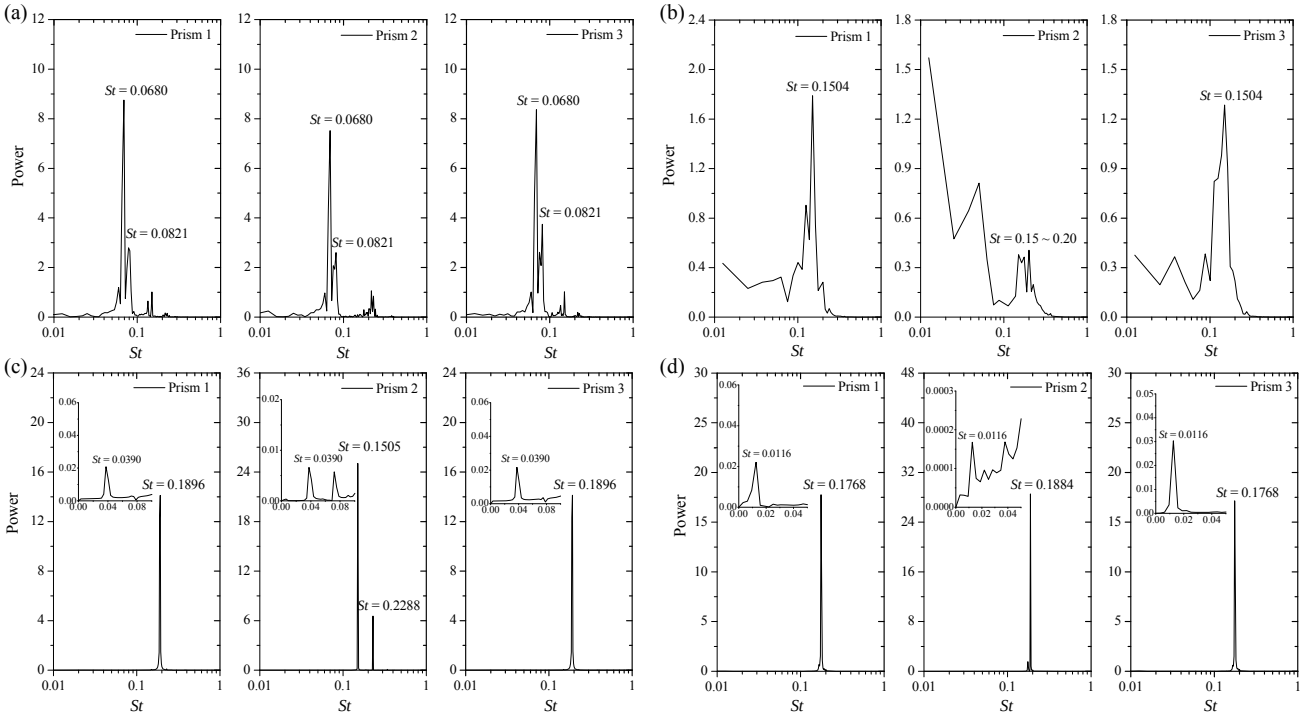

Fig. 3 Power spectra of fluctuating lift at (a) $L/W = 1.2$ (regime A, $L/W < 1.5$), (b) $L/W = 1.5$, (regime B, $1.5 \le L/W < 2.0$), (c) $L/W = 2.5$ (regime C, $2.0 \le L/W \le 2.5$), (d) $L/W = 3.5$, (regime E, $3.0 \le L/W \le 7.0$). Power is in arbitrary units.

where *St* is smaller, and greater in regime E where *St* is larger, all compared to those of the counterpart outer prisms.

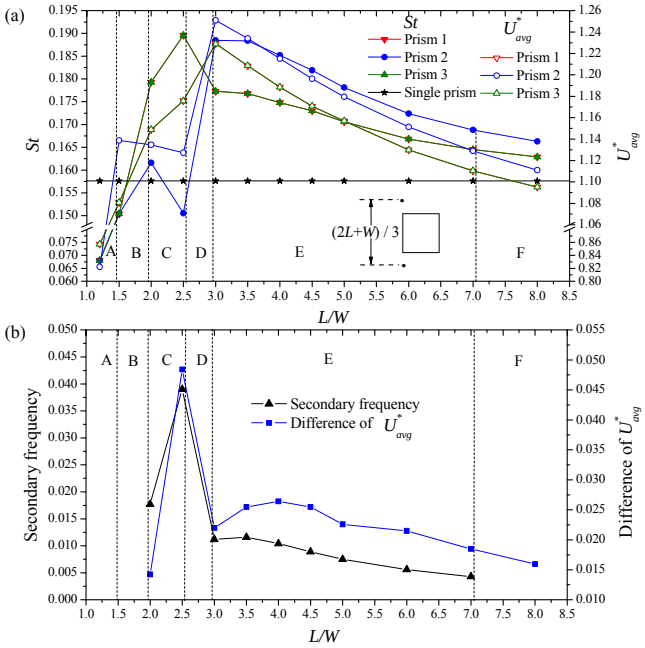

Fig. 4 (a)Variation of shedding frequency (*St*) and U^*_{avg} with *L/W*. (b) Variation of the secondary frequency and difference of U^*_{avg} between the outer and middle prisms with *L/W*. $U^*_{avg} = U_{avg}/U_\infty$.

Table 2 Variation in Strouhal number (middle prism) based on U_∞ and U_{gap} as a function of *L/W*.

L/W	fW/U_∞	U_{gap}/U_∞	fW/U_{gap}
2.0	0.1616	1.1346	0.1424
2.5	0.1505	1.1273	0.1335
3.0	0.1885	1.2509	0.1507
3.5	0.1884	1.2340	0.1527
4.0	0.1852	1.2151	0.1524
4.5	0.1819	1.1963	0.1521
5.0	0.1781	1.1795	0.1510
6.0	0.1724	1.1513	0.1497
7.0	0.1688	1.1289	0.1495
8.0	0.1663	1.1111	0.1497

To check the argument about the effect of U_{avg} on *St*, modified *St* based on U_{gap} (= U_{avg}) is calculated for the middle prism as presented in Table 2. While *St* based on U_∞ varies from 0.1505 to 0.1885, the modified *St* based on U_{gap} collapses to about ≈ 0.15, with a small departure at *L/W* = 2.0 and 2.5. The departure may be due to fact that since the gap flow is highly biased outward, the U_{gap} measurement location lies in the shear layer. In overall, it can be concluded that *St* of the middle prism is primarily influenced by the flow velocity around the prism and is proportional to U_{gap}.

Figure 4(b) displays the secondary frequency and difference in U_{avg} between the middle and outer prisms. They both follow the same trend, confirming that the secondary frequency is somehow associated with the difference in *St* or U_{avg} in turn between the middle and outer prisms.

6. The origin of the secondary frequency and its effect on C_L

From the power spectrum results, it has been observed that C_L signals at the symmetrically-biased and non-biased flow regimes have a short (Strouhal or primary frequency,) and long (secondary frequency) periods. The amplitude associated with the long period is small compared to that with the short period. Fig. 5 shows time histories of lifts of the three prisms at *L/W* = 3.5. The short period is easily understood, while a beat-like change in C_L amplitude is also obvious, with maximum, minimum and again maximum amplitudes around time *t* = 114.2, 118.0 and 122.9 seconds, respectively. This beat period is therefore about 8.7 seconds, corresponding to *St* = 0.0118, very close to the secondary *St* = 0.0116 obtained in the power spectrum (Fig. 3d). It thus proves that the beat phenomenon is associated with the secondary frequency. As we know from sound/light interference, a beat occurs when two sound/light waves of two different frequencies interact each other and the beat frequency is equal to the difference of the two frequencies. Here we observed the same phenomenon; the secondary/beat frequency is the difference in the shedding frequencies of the middle and outer prisms. It may be interesting to view representative flow structures at maximum and minimum amplitudes (associated with the secondary frequency) of C_L. Indeed the flow structures presented in Figs. 2(d_1) and (d_2) correspond to the maximum and minimum amplitude of C_L (*t* = 114.2 and 118.0 seconds, respectively) associated with the secondary frequency and at the same time both flow structures correspond to a maximum C_L associated with the primary frequency of the middle prism, as indicated by vertical lines. Interestingly, maximum C_L associated with the secondary frequency occurs when an in-phase shedding occurs from the two sides of a gap (Fig. 2d_1). On the other hand, an anti-phase shedding from the two sides of a gap results in a minimum C_L associated with the secondary frequency (Fig. 2d_2). Fortuitously, both gaps have the in-phase shedding (Fig. 2d_1) and antiphase shedding (Fig. 2d_2) at this *L/W*, as the shedding phase lag between the outer prisms was a constant of ≈ 0°. C_L(s) of the three prisms, associated with the secondary frequency, are thus reaching maximum or minimum simultaneously. When the phase lag between the outer prisms is ≠ 0°, maximum or minimum C_L of the three prisms does not occur simultaneously. So the beat/secondary frequency results from a continuous change in the phase lag between the sheddings from the two sides of a gap, from in-phase to

anti-phase, anti-phase to in-phase, and so on. Due to the different shedding frequencies from the two sides of a gap, the phase lag changes in every primary period. It should not be confused that when the shedding frequencies are different, how can the phase lag be obtained? Here the phase lag means the phase of the longer period shedding with respect to that of the shorter period shedding, i.e., considering the shorter period as a reference complete cycle period.

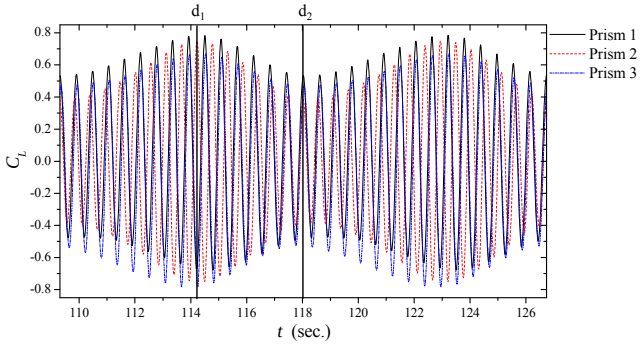

Fig. 5 The time histories of lift signals of the three prisms at $L/W = 3.5$. Note that the vertical lines d_1 and d_2 correspond to the wake structure presented in Fig. 1(d_1) and (d_2), respectively.

7. Conclusions

Based on vortex structure, fluid force and shedding frequencies, six distinct flow regimes have been identified. (i) Single-bluff-body flow (regime A) identified at $L/W < 1.5$ is characterized by vortex shedding from the freestream sides only, forming a single Karman vortex street with an identical *St*. (ii) Flip-flopping flow (regime B) appears at $1.5 \leq L/W < 2.0$ where the gap flows gain adequate strength to split the wake into three immediately downstream, but the three wakes merge into one shortly. Again a single *St* persists in the wake. The two gap flows flip-flop, both to be biased upward, downward, inward, and outward. (iii) Symmetrically-biased coupled flow (regime C, $2.0 \leq L/W \leq 2.5$) features with the two gap flows deflecting outward symmetrically, forming one wide wake of smaller *St* behind the middle prism and two narrow wakes of a larger *St* behind the two outer prisms. (iv) Transition flow ($2.5 < L/W < 3.0$, regime D) occurring between regimes C and E displays a remarkable jump in *St* of the middle prism and drop in *St* of outer prisms associated with a discontinuous change in the flow between regimes C and E. (v) The non-biased coupled flow (regime E) taking place at $3.0 \leq L/W \leq 7.0$ is exemplified by the fact that the gap flows are not biased anymore; the wake behind each prism is similar to that of an isolated prism. The sheddings from the outer prisms are coupled with a constant phase lag and identical *St*. The *St* of the middle prism is however different, higher than that of the outer prisms, both *St* decreasing with an increase in *L/W*. (vi) Non-biased weakly coupled flow (regime F, $L/W > 7.0$), where the difference in *St* between the middle and outer prisms is smaller and the interaction between the adjacent wake is weak.

A secondary frequency is observed in the symmetrically -biased and non-biased coupled flows, equal to the difference in shedding frequencies of the middle and outer prisms. The flow in the gap receives an interaction of the two frequencies, resulting in the secondary frequency. The secondary frequency has a great impact on the time series of the lift force to have a beat-like change, where the lift force associated with the beat is maximum when the sheddings from the two sides of a gap are inphase, and reaches a minimum when they are antiphase.

Acknowledgments

Alam wishes to acknowledge supports given to him from the Research Grant Council of Shenzhen Government through grants JCYJ20120613145300404 and JCYJ20130402100505796.

REFERENCES

[1] M. M. Alam, Y. Zhou, X. W. Wang, The wake of two side-by-side square cylinders, *Journal of Fluid Mechanics*, Vol. 669, pp 432-471, (2011).

[2] M. M. Alam and Y. Zhou, Intrinsic features of flow around two side-by-side square cylinders, *Physics of Fluids*, Vol. 25, pp 085106-1-21, (2013).

[3] S. R. Kumar, A. Sharma and A. Agrawal, Simulation of flow around a row of square cylinders, *Journal of Fluid Mechanics*, Vol. 606, pp 369-397, (2008).

[4] A. K. Saha, G. Biswas, K. Muralidhar, Three-dimensional study of flow past a square cylinder at low Reynolds numbers, *International Journal of Heat and Fluid Flow*, Vol. 24, pp 54-66, (2003).

[5] Sohankar, C. Norberg, and L. Davidson, Simulation of three-dimensional flow around a square cylinder at moderate Reynolds numbers, *Physics of Fluids*, Vol. 11, pp 288-306, (1999).

[6] Sharma and V. Eswaran, Heat and fluid flow across a square cylinder in the two-dimensional laminar flow regime, *Numerical Heat Transfer, Part A: Applications*, Vol. 45, pp 247-269, (2004).

ICMIEE-PI-140107

DESIGN & ANALYSIS OF A MODEL COMBUSTION CHAMBER OF GAS TURBINE

Samsul Arfin Mahmood[1], Mahabub Hasan[2], Md. Siddiqur Rahman[3]*
Department of Mechanical Engineering, Khulna University of Engineering & Technology, Khulna-9203, BANGLADESH

ABSTRACT
Development of a country is assessed by it's power consumed per capital. Gas turbine is highly dependable power generating source in every country. As a developing country Bangladesh needs a huge amount of power. To keep pace with the other developed countries and their technologies, it is customary to have a great amount of power generating sources. Gas turbine can easily serve this purpose. For fulfilling this purpose our present effort is to design & analysis of a combustion chamber which is a vital part of gas turbine. This paper summarizes the design and analysis of gas turbine combustion chamber.3D model of the combustion chamber is generated & finite element method is used for meshing and applying boundary conditions for static and thermal analysis. Here we have done the study on different materials which are suitable for improvement of combustion chamber. This paper also validates the design using available alloys. Any development regarding this project will be accepted based on it's validity.

Keywords: Design ; Combustion chamber ; Analysis ; F.E method.

1.0 Introduction

A combustion chamber is an enclosure in which combustion takes place just like burning of fuel & oxidant. It is the 2nd subsequent part of a gas turbine. It is also known as burner, flame holder or combustor. High pressure air or gas comes from compression system and enter into the combustion chamber. The combustion chamber then heats this air at constant pressure. After heating, air passes from the combustion chamber through the nozzle guide vanes to the turbine. At constant pressure, a high temperature is produce which is sustained by combustor wall. So it is necessary to design a combustion chamber with appropriate temperature sustainable metal.

In spite of having different available metal, it is difficult to find out proper one. The ability to heat consume depends on the yield strength of metal. This property changes metal to metal according to their molecular arrangement, impurities or other containing ingredient. But it is not possible to find out these properties one by one in real life. For this reason there arise the topics of simulation for different metal which will be used to construct a combustor.

There are different methods of analysis of metal properties. From all of those finite element method is considered as perfect and less time consuming method. It is a numerical method for finding approximate solution of boundary value problems. For a combustion chamber, inlet pressure, temperature are known value just like initial condition and there also exist a boundary condition. So applying this conditions and other affecting parameter, the internal heat generating environment and condition of combustor wall are easily determined by the iteration of F.E.M.

According to design criteria and simulation result, some metals are selected. Among them, most reliable and financially less consuming metal is find out to use as a combustor outer wall & components.

All recent research allow the procedure of construct a combustion chamber in this systematic way. But metal by metal analysis is uniqueness of this procedure which application can be more popular than before.

2.0 Finite Element Method

The finite element method (FEM) rapidly grew as the most useful numerical analysis tool for engineers and applied mathematicians because of it natural benefits over prior approaches. The main advantages are that it can be applied to arbitrary shapes in any no of dimensions. The shape can be made of any number of materials. The material properties can be non-homogeneous. (depends on location) and/or anisotropic (depend on direction). The way that the shape is supported (also called fixtures or restraints) can be quite general, as can the applied sources (forces, pressures, heat flux, etc.). The FEM provides a standard process for converting governing energy principles or governing differential equations in to a system of matrix equations to be solved for an approximate solution. For linear problems such solutions can be very accurate and quickly obtained. Having obtained an approximate solution, the FEM provides additional standard procedures for fol -low up calculations (post-processing), such as determining the integral of the solution or its derivatives at various points in the shape .The post-processing also yields impressive color displays, or graphs, of the solution and it's related information. Today, a second post-processing of the recovered derivatives can yield error estimates that show where the study needs improvement. Indeed, adaptive procedure allowed

* Corresponding author. Tel.: +88-01747890428
E-mail address: mahabub.me.kuet@gmail.com

automatic corrections & resolutions to reach a user specified level of accuracy. However, very accurate & pretty solutions of models that are based on errors or incorrect assumptions are still wrong. When the FEM is applied to a specified field of analysis (like stress analysis, thermal analysis, or vibration analysis) it is often referred to as finite element analysis(FEA) . FEA is the most common tool for stress and structural analysis . Various field of study are often related. For example, distributions of non-uniform temperatures induce non obvious loading conditions on solid structural members .Thus it is common to conduct a thermal FEA to obtain temperature results that in turn become input data for a stress FEA.

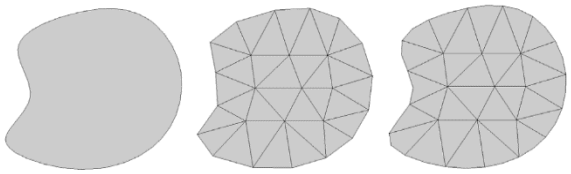

Fig.1 An area meshed with linear and quadratic triangles.

The sum the areas of the individual triangles:

$$A = \sum_{k=1}^{n} A^k.$$

About assigning a linear material to each part, modern FEA systems have a material library containing the "linear" mechanical, thermal, and/or fluid properties of most standardized materials. They also allow the user to define custom properties.

3.0 Types of Combustion Chamber

There are usually 4 types of combustion chamber .These are:

- can type
- can-annular type
- annular type
- reverse flow type

3.1 Can type

Can combustors are self contained cylindrical combustion chambers. Each can get an air source from individual opening .For the same air flow, it is longer , since the individual can diameter must be held to a minimum. The individual can are wasteful of the available space, since they use the individual cross-sectional area inefficiently.

3.2 Can-annular type

Like the can type combustor, can annular combustors have discrete combustion zones contained in separate lines with their own fuel injectors. Unlike the can combustor, all the combustion zones share a common air casing. Each can has primary air admitted near the fuel nozzle & is perforated so that secondary cooling air may be admitted downstream of the primary zones. There usually is a flame tube that joints the cans enabling the flame to pass from can to can during starting.

3.3 Annular type

Annular combustors do away with the separate combustion zones and simply have a continuous liner and casing in a ring (the annulus). It consists of one or two continuous shrouds. The fuel is introduced through nozzles at the inlet to the shroud, with secondary air entering though holes. This secondary air keeps the flame away from the shroud & the dilutes the combustion chamber gases to the desired turbine inlet temperature.

3.4 Reverse flow type

Reverse flow combustion chamber, especially known as reverse flow ring combustion chamber, for gas turbine propulsion units. Which have at least one flame tube wall with film-cooling arrangement. It includes an annular chamber enclosed between flame tube wall sections to which cooling air is so supplied from an outer annular channel acted upon with secondary air opposite the main flow direction in the flame tube in such a manner that the cooling air that it is blown out in the opposite flow direction film-like against an adjoining flame tube wall.

4.0 Simulation setup & grid generation:

For the simulation at first what is need, is a CAD model. So a cad model of is used in the analysis. The CAD model was of arbitrary dimensions & was modeled in SolidWorks. Though it has an arbitrary dimensions, the shape has quite similarities with the actual combustion chamber that is used now–a-days.

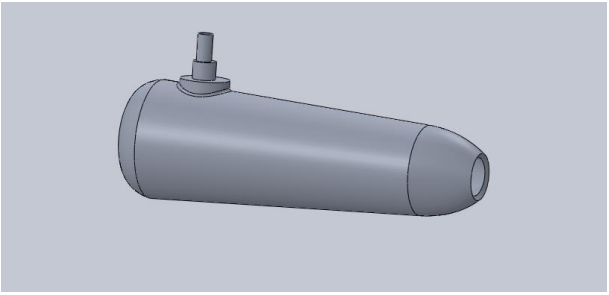

Fig.2 Integrated CAD part of a Combustion Chamber.

The sction view of the combustion chamber is also attached here for better understanding of the internal views.

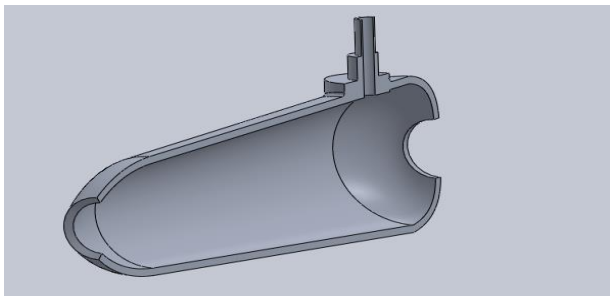

Fig.3 Section view of the generated CAD model.

There are three preview window is used of the software during analysis.

FEA editor window: Initial conditions and boundary conditions are given here. Grid generation was also done in this setup.
Results generation window (heat analysis): In this window steady state heat analysis has been done.
Results generation window (linear stress analysis):In this window a linear stress analysis has been done. To deal with the thermal stress analysis of the materials, results from steady state heat transfer analysis has been used in the linear stress analysis.

(a)

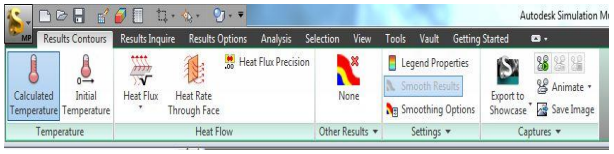

(b)

(c)

Fig.4 (a) Grid generation window.
(b) Heat transfer window.
(c) Linear stress analysis window.

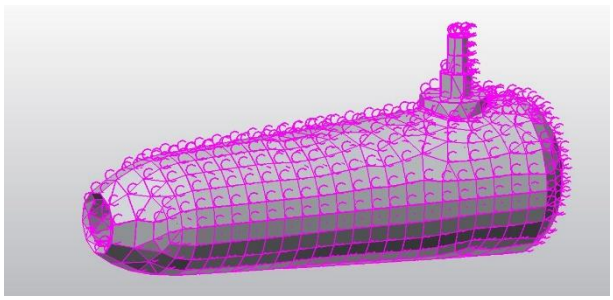

Fig.5 CAD model with grids after meshing.

The primary simulation setup and grid generation is completed. Now the CAD model is ready for simulation and result extraction.

5.0 Model generated in solidworks

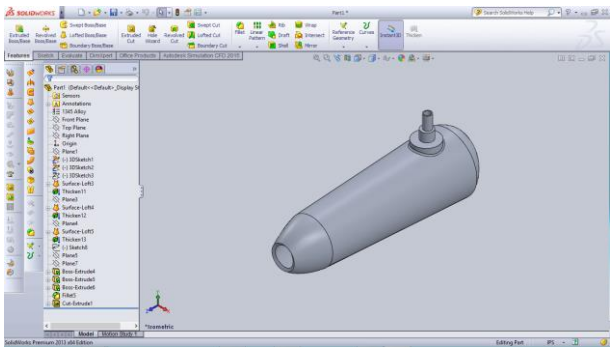

Fig.6 Arbitrary model of combustion chamber.

6.0 Structural analysis

In this analysis calculated maximum temperature, generated heat through faces, heat flux, static stress & static strain are the required criteria.

6.1.0 Thermal analysis for Aluminium alloy 1345

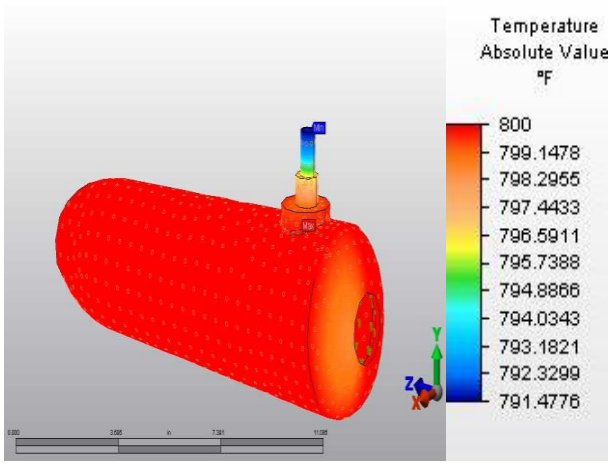

Fig.7 Calculated maximum temperature.

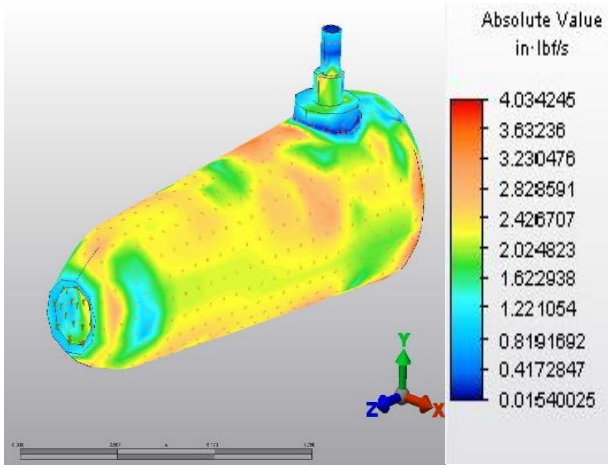

Fig.8 Generated heat.

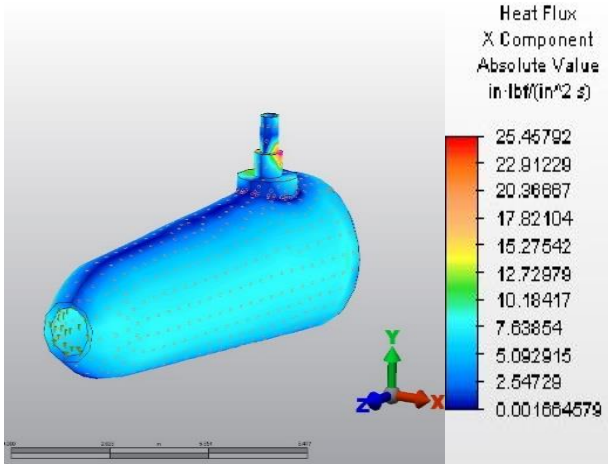

Fig.9 Heat flux along X axis.

6.1.1 Linear static analysis for Aluminium alloy 1345

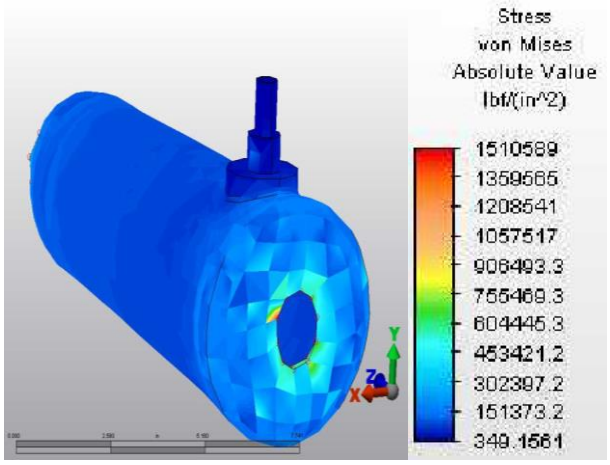

Fig.10 Static stress analysis.

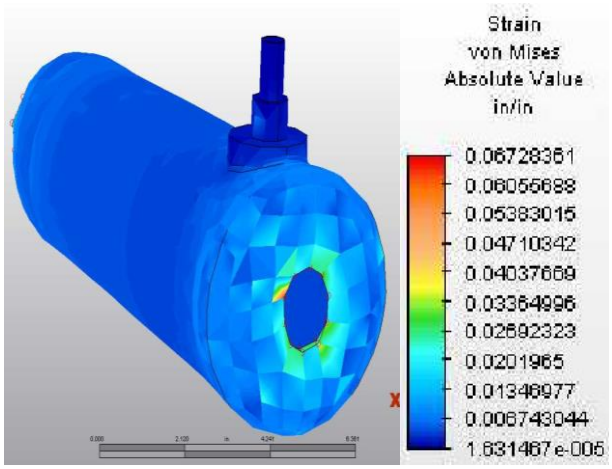

Fig.11 Static strain analysis.

6.2.0 Thermal analysis for Aluminium Alloy 5005-H18

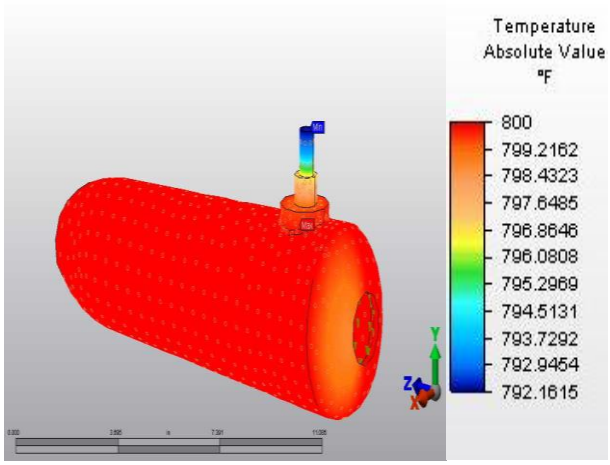

Fig.12 Calculated maximum temperature.

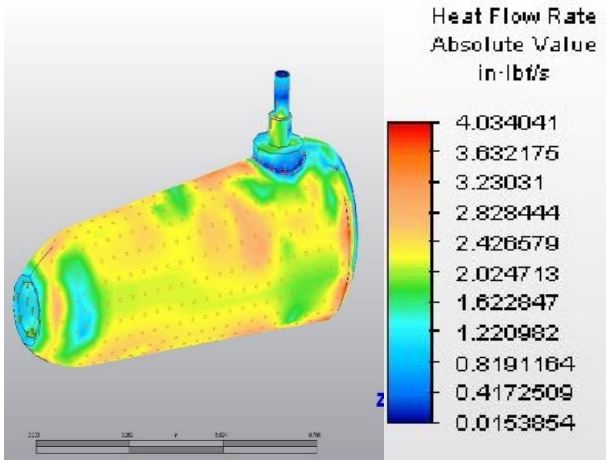

Fig.13 Generated heat.

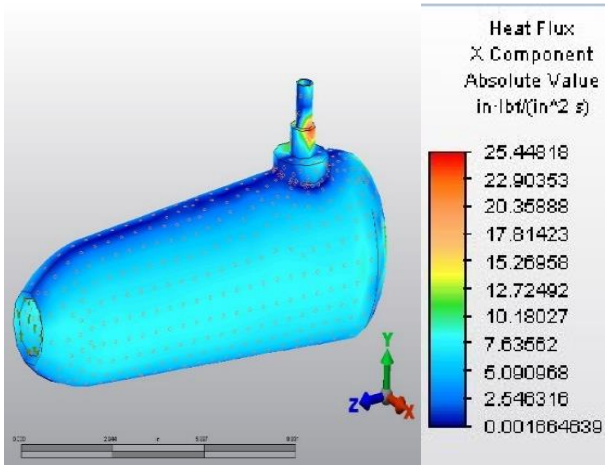

Fig.14 Heat flux along X axis.

6.2.1 Linear static analysis for Aluminium Alloy 5005-H18

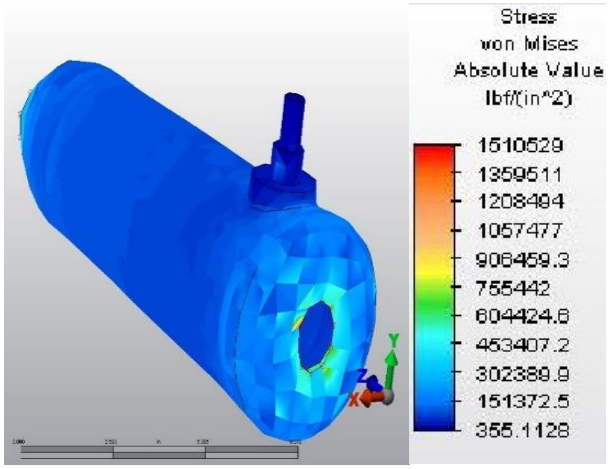

Fig.15 Static stress analysis.

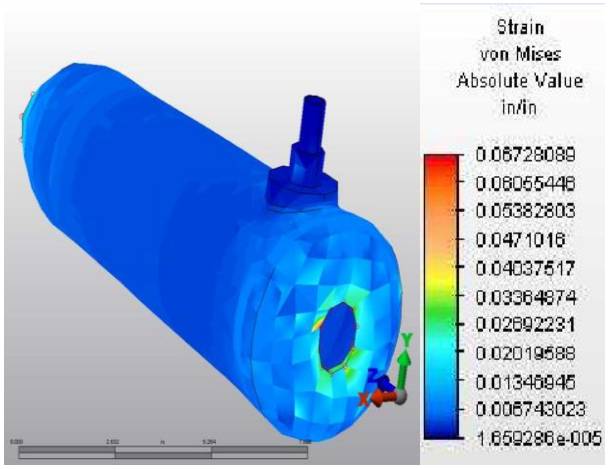

Fig.16 Static strain analysis.

6.3.0 Thermal analysis for Ceram Tec Grade 950Toughned Alumina (Al2o3)

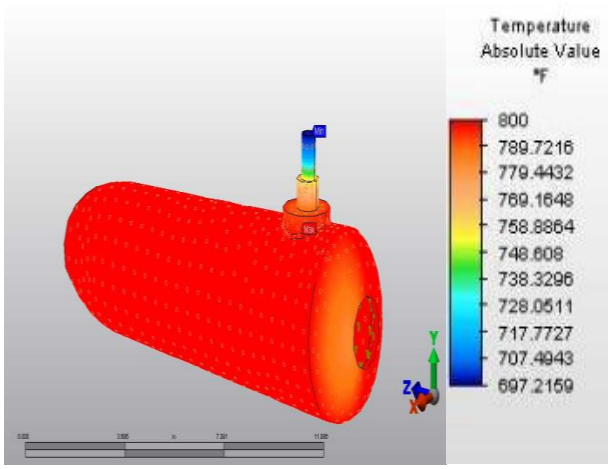

Fig.17 Calculated maximum temperature.

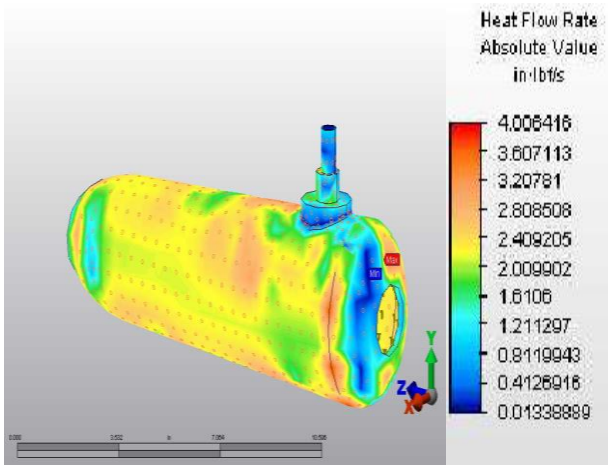

Fig.18 Generated heat.

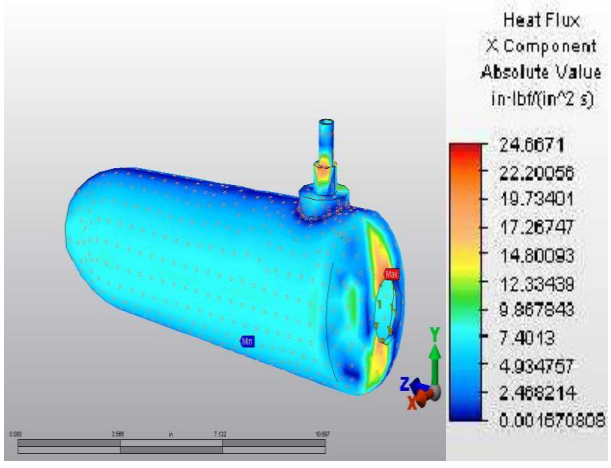

Fig.19 Heat flux along X axis.

6.3.1 Linear static analysis for Ceram Tec Grade 950Toughned Alumina (Al2o3)

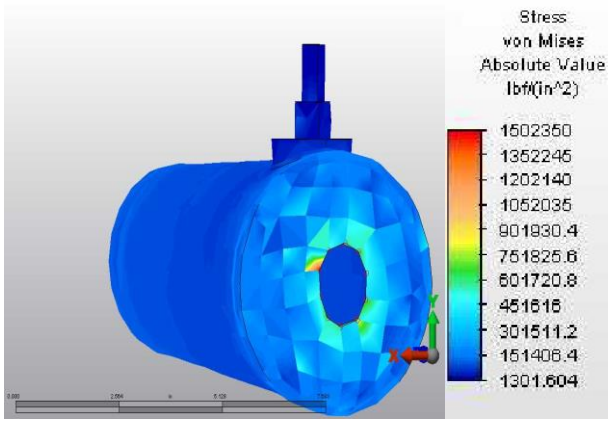

Fig.20 Static stress analysis.

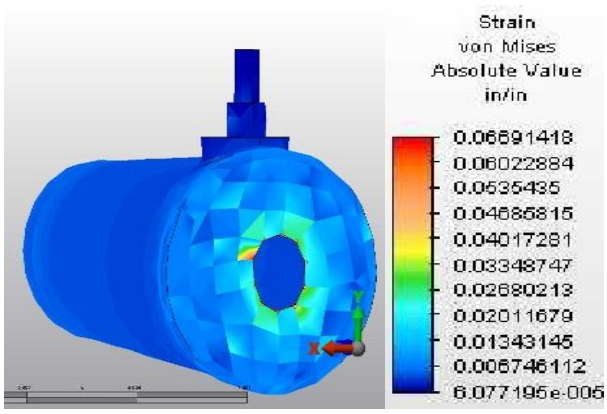

Fig.21 Static strain analysis.

7.0 Results in tabular form

Material	Aluminium alloy 1345	Aluminium Alloy 5005-H18	Ceram Tec Grade 950Toughned Alumina (Al_2O_3)
Material properties			
Mass density	0.00027362	0.00025362	4.1E-04
Thermal conductivity	27.2	25	1.8734078 5962217
Structural analysis			
Stress (in/in^2)	1510589	1510529	1502350
Strain (in/in)	0.06728361	0.08728089	0.0669142
Displacement (in)	0.03879156	0.03879078	0.0386875
Thermal analysis			
Temperature (°F)	800	800	800
Generated heat (in-lbf/s)	4.034245	4.034041	4.006416
Heat flux (in-lb/in^2 s)	25.75892	25.44818	24.6671

8.0 Conclusion

In this paper we have analyzed previous designs and generals of combustion chamber for gas turbine to do further optimization, Finite element results for free standing combustion chamber give a complete picture of structural characteristics, which can utilized for the improvement in the design and optimization of the operating conditions.

In the first step we have designed a combustion chamber using arbitrary dimensions.

In the second step we have done the study on different materials which are suitable for the improvement of turbine combustor.

In the third step we have validated our design using existing materials.

In the next step we have applied different materials for combustion chamber to suggest best material.

From the above results we can conclude that , using of Ceram Tec Grade 950Toughned Alumina (Al_2O_3) is more efficient and satisfactory among all those materials that has been analyzed , due to low stress displacement, good thermal strength and easy to manufacture.

9.0 REFERENCES

[1] William W. Bathie, Fundamentals of Gas Turbines, John Wiley & Sons, Inc., Second Edition, pp. 70-86, 1996.

[2] Meherwan P. Boyce, Gas Turbine Engineering Handbook, Gulf Professional Publishing, Second Edition, pp. 370-405, 2002.

[3] I. G. Rice, "Thermodynamic Evaluation of Gas Turbine Cogeneration Cycles: Part 1-Heat Balance Method Analysis," Journal of Engineering for Gas Turbines and Power, Vol. 109, No. 1, 1987, pp. 1-7. doi:10.1115/1.3240001

[4] G.Boudier, L.Y.M.Gicquel and T. J. Poinsot, Effect of mesh resolution on LES of reacting flows in complex geometry combustor, Combustion and Flame, 155, pp. 196-214, 2008.

[5] H Cohen. GFC Rogers HIH Saravanamutto, Gas Turbine Theory, Longman Group Limited, 4th Edition, pp. 233-242, 1996.

ICMIEE-PI-140110

Design and Simulation of a Robot-Farmer for Gripping and Cutting Crops

Md. Hafizur Rahman[1], *Md.Helal-An-Nahiyan*[1], *Md. Mahabubur Rahman*[1]
[1] Department of Mechanical Engineering,
Khulna University of Engineering & Technology, Khulna-9203, BANGLADESH

ABSTRACT
Now-a-days every field is heading towards automation, whereas agricultural field is still an exception. Current scenario says many countries do not have enough farmer to cultivate lands and even in Bangladesh there are lots of families that are lacking an able member to toil during harvesting period. To overcome this problem, a robot farmer is the optimum solution. The objective of this research is to design a robot farmer which can work in the crop-fields for automatically cutting and placing crops aside with a pre-installed embedded system. It will reduce the necessity of man-operated machineries. The total design of this robot farmer consists of 7 motors, a distance measuring sensor, and an Arduino board. This research work will be helpful for the researchers who are interested to introduce automation in the agricultural sector and who want to perform any smooth cutting operation which requires holding of an object before cutting.

Keywords: Robot farmer, Distance measurement sensor, Robotic manipulator, Gear based gripping mechanism.

1. Introduction

Modern machineries of the crop field are used mostly for cutting a huge range of crops and those machineries are very expensive which costs around BDT 2 lakh per machine except its operating and maintenance cost. In recent time, few machines are available for rent in some areas of tamilnadu, India by 2000 rupees per hour which is somehow fulfilling few farmers' need. Moreover due to uncertainty of rain and unavailability of laborer, the harvesting remains challenging for rural farmers who cannot afford the money. In fact, in many parts of the world those costly machineries are not even available. To minimize these problems our proposed robot farmer will fulfill the need of the farmers with its structural durability and ease of operation. As a result of these consequences farmer robot can start a new era of farming for individual land owners by helping them to cut their crops quickly and without the physical involvement of human being.

2. Background Research

Fig.1.1 Currently available man operated small machines

Fig.1.2 Currently available costly Crop cutting vehicle

The concept of this farmer robot came from the worldwide implementation of robotic manipulator in industrial fields. So far, only a few studies of introducing autonomous agricultural field machinery have been published. Goense (2003) [1] compared autonomous equipment with conventional equipments and showed that even if the autonomous equipment is utilized 23 hours a day, it would be economically feasible. Later in 2005 S.M. Pedersen [2] showed three scenarios with field scouting in cereals; robotic weeding in sugar beet, and autonomous grass cutting in golf courses. For first two cases he used an autonomous research platform (API). The third analysis was based on real data from the operational costs for grass cutting on golf courses. He therefore have estimated the cost of building an autonomous grass cutting vehicle to replace the existing human-driven vehicles and proved a robotic wedding machine can give 12.2% economic benefit than a man operated grass cutter. But the study resulted in a very costly machine (20834 euro) which is equivalent to 21 lakhs in BDT.

At present, few small man operated cutting machines are available (fig.1.1) in south Asia which are being used but the necessity of carrying the machine makes it tough for a person and the cut crops are also not kept in sequence. For these reasons a huge amount of paddy is wasted. Besides, the machine is run with diesel engine which is not so positive towards the environment and cost. Due to these reasons a better solution in the crop field has become mandatory.

All these things forced our research work to introduce an autonomous crop cutting machine specially for paddy harvesting. In this research, we are showing the model of such an autonomous machine which can be manufactured by locally available materials. This research work actually comprises the basics of a robotic manipulator, an obstacle detector car that detects obstacle with distance measuring sensor, and a rotating cutter. Later in this research, through simulation analysis we have proved its sustainability by using simulation platform solid works which has now got popularity in simulation analysis field. In 2013, V. Kaundal used this platform for his research work [3]. In

* Corresponding author. Tel.: +88-01911208438
E-mail addresses: nahiyan.me@gmail.com

our research work, the electrical circuit and the program algorithm of the robot farmer is provided and eventually the cost is estimated and a comparison is provided between our farmer robot and the currently available man operated machineries of the crop field.

3. Methodology and Design

The robot farmer, designed in this research work consists of three major parts involving a 4 wheeled car, a cutter and a robotic manipulator with 2 degree of freedom. The mechanism involves a distance measuring

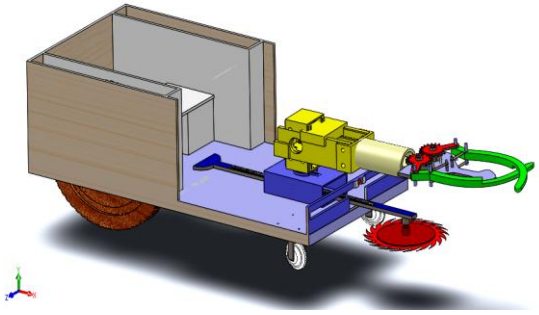

Fig.2 Structure of our proposed robot farmer

sensor which is mounted at the front side of the car body (fig 3) to identify the exact location of the nearest crop. After that, two motors drive two rear wheels and lead the robot to take its position near the crop. Then, end effector of the manipulator grabs the crop using a servo controlled gripping mechanism (fig.6 and fig.7) and the cutter comes out of a gear box using rack and pinion mechanism to cut the crop at 6 cm above the ground. Finally, the manipulator arm puts the cut crop aside by the help of 2 revolute joints situated at the bottom and at the wrist. 2 revolute joints of the manipulator are controlled with 2 servo motors.

4. Mechanical Structure

Mechanical structure of the model of our robot farmer can be divided into 3 individual parts. Each of these parts is subdivided into few more parts. Here is a brief description of the mechanical structure part by part.

4.1 Part 1: Car

Car has three parts. Rear wheels, front wheels and chassis.

(1) Chassis

Aluminum 2014 t-6 sheet metal is used to build the car chassis in virtual environment. The base has a thickness of 10 mm. For upper portions 5 mm thick sheet is used as it is mentioned in figure 3. The model is designed involving the rear wheels inside boxes to ensure the minimum required place for moving of the robot inside a paddy field. It is found by field investigation in the paddy fields of manikgonj and khulna of Bangladesh that, the paddy are planted with 5-6 inch gap between each row. So the chesis is designed with 12 inch width

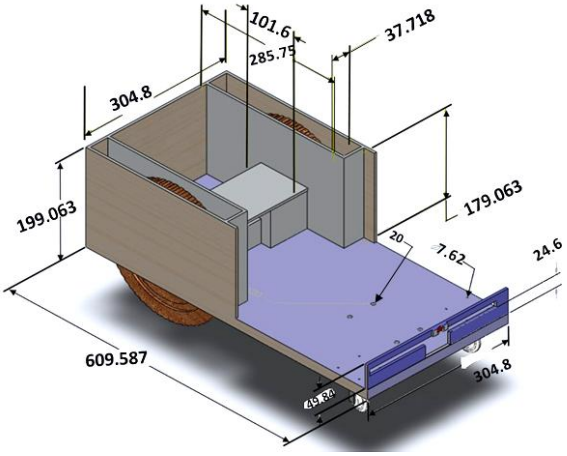

Fig.3 Car chesis of the robot (dimensions in mm)

and 10 inch height and 24 inch length so that it can easily move into the field without hampering the crops. As the arm is screw fastened over this chesis, the chessis has to endure axial stress. So, for the reason of stability, Aluminium 2014-6 is used. It's cost is also relatively low (table 3) and it has resonable mechanical properties (table 1).

Table 1 Mechanical properties of Aluminum 2014 t-6.

Properties	Unit(SI)	Scale
Brinwell Hardness	135	AA; load 500 g; 10 mm ball
UTS	483 MPa	AA; Typical
Modulus of Elasticity	72.4 GPa	In Tension
Compressive Modulus	73.8 GPa	
Ultimate Bearing Strength	889 MPa	Edge distance/pin dia = 2.0
Bearing Yield Strength	662 MPa	Edge distance/pin dia = 2.0
Fatigue Strength	124 MPa	AA; 500,000,000 cycles; reversed stress
Machinability	70 %	0-100 Scale of Aluminum Alloys
Shear Strength	290 MPa	AA; Typical

(2) Rear wheels

The rear wheels are chosen to be wooden and highly available mehogany wood is chosen for rear wheel material. Mehogony wood is chosen due to its eco friendly attitude and durability against corrosion and availability in rural areas. These rear wheels are replacable and negociable with any type of metal that posses the similar properties. It is designed with 10 inch diameter and 1 inch thickness.

(3) Front wheels
Front wheels need to rotate freely for movement of the robot. So, these parts are designed with 2 inch diameter moving plastic wheels.

4.2 Part 2: Cutter
Aluminium 2014-6 is assigned to it to ensure necessary strength to the cutter (table 1). Cutter consists of a cutting blade, a blade holder datum and a gear box.

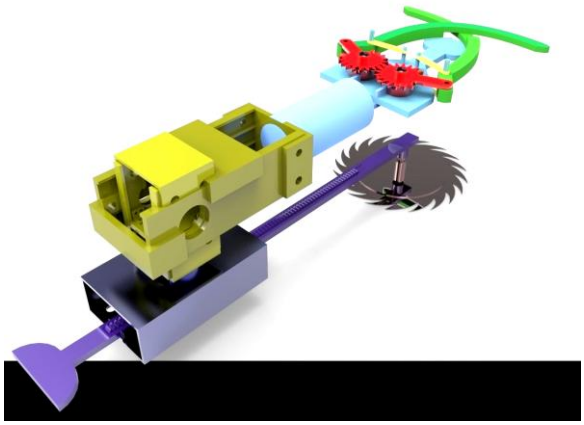

Fig.4 Robotic arm and cutter

(1) Cutting blade
It's a 6 inch diameter, circular blade. This type of blade is currently used in hand operated paddy cutter machines in India. In the cutting operation, a DC motor will guide this part with a rotation of 1500 rpm for smooth cutting action.

(a) Cutter (idle time) (b) Cutter (coming out)

Fig.5 Cutter positions

(2) Blade holder datum
Blade holder datum contains the rack type portion of rack and pinion mechanism. There is a pinion gear mounted inside the box (fig 7) guided with a DC motor. It helps the cutter to go forward linearly during cutting operation and helps to come back after the operation.

(3) Gear box
A rack and pinion comprises a pair of gears which convert rotational motion into linear motion. A circular gear called "the pinion" engages teeth on a linear "gear" bar called "the rack"; rotational motion applied to the pinion causes the rack to move, thereby translating the rotational motion of the pinion into the linear motion of the rack. The gear box of our farmer robot contains a pinion gear and the rack mentioned earlier. The pinion is driven with a servo motor. The gear ratio[4] of rack and pinion will be 1:1

4.3 Part 3: Robotic Arm
This part consists of 4 sub-parts-

- Arm base with bearings (fig.8)
- Arm elbow (fig.9)
- Arm wrist with piping (fig.6,7,10)
- End effector or gripper

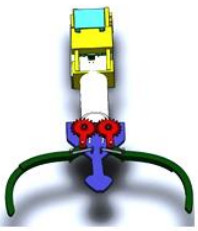

Fig.6 Arm (grip opened)

Fig.7 Arm (grip closed)

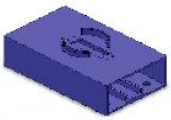

Fig 8 Arm base with bearings (gear box)

Fig 9 Arm (elbow)

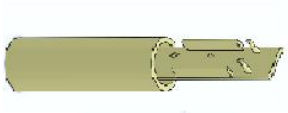

Fig.10 Arm (wrist)

5. Gripping mechanism with end effector
Our proposed model cuts crops like a human farmer. so it is designed with an arm having gripping ability in the end effector. This arm is origined from the upper portion of the gear box with a ball bearing based revolute joint. It will ensure its circular rotation using a servo motor. Another ball bearing based revolute joint is at the starting of the wrist part (white part in the figures 6) which will allow the cut crop to be put aside. This part is also of aluminum 2014 t-6 whereas for the finger plates and base plate of gripper there will be an additional portion of EPDM 70 durometer (70A) rubber material for ensuring a better frictional surface for gripping. EPDM is used for its environment friendly attitude, it works against abrasion.
The gripping model of arm is shown in figure 11 and 12. While searching for a tree, the grip will be opened and the open fingers will surround 10 inch portion.

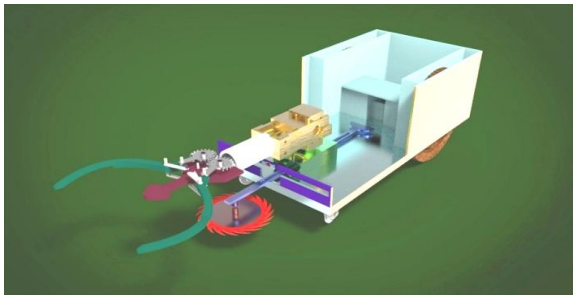

Fig.11 Farmer robot searching for crop in the crop field

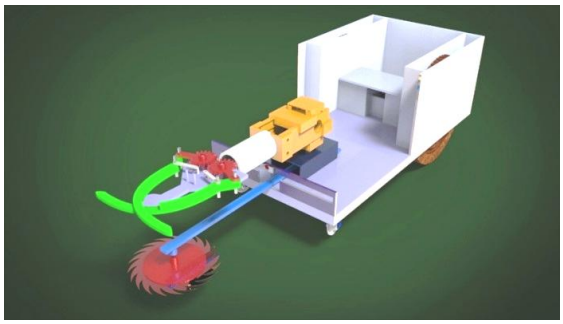

Fig.12 Robot farmer found crop and grip got closed and cutter comes

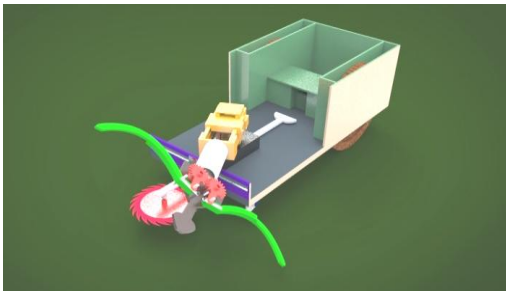

Fig.13 The manipulator turns left and opens grip to put the tree aside (Cutter is not rotating then)

When it senses a tree inside range, it will close its paw and with the help of an extended plate the grip will hold the cutting object tightly. The mechanism is run by 2 gears with a gear ratio 1:1

6. Electrical Parts

This part involves 4 DC and 3 servo motors, a distance measuring sensor, an arduino board, and electrical wires.

6.1 Motors

There are two motors at the rear wheels which drive the left and right wheels independently. The motor power ranges from 150W to 200 W. The torque of the motor is ranging from 50kg-cm to 80kg-cm. The higher torque rating enables the motors to drive the wheel at a higher efficiency. For DC motor, a motor driver IC (L293D) is used in the circuit diagram (Fig.16).

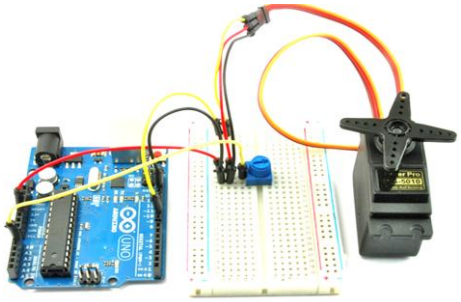

Fig.14 driving servo motor using Arduino board

DC Motor specifications:
1. Holding torque: 19N.m
2. Rated speed: 1500rpm

6.2 Distance measuring sensor:

For advanced measurement techniques distance Measuring Sensors are being used in robotics field. A distance measuring sensor measures where the nearest object is. Here we designed our robot with sharp distance measuring sensor. Unlike to a conventional sensor, it does not depend on color. It gives higher precision. Utilizing a focused beam, it indicates where an object is, or whether the object is in range.

Sensor specification:
Family: GP2Y0D02YK0F
Functionality: Digital
Range: 80 cm
Response Time: 39 ms

Fig.15 Distance measuring sensor

6.3 Arduino board

For controlling the system, an Arduino MEGA board is used. Arduino is a single-board microcontroller, intended to make the application of interactive objects or environments more accessible. The hardware consists of an open-source hardware board designed around an Atmega 2650 microcontroller. Current models consists of a USB interface, 6 analog input pins, as well as 14 digital I/O pins which allow the user to attach various extension boards.

7.0 Circuit Layout:

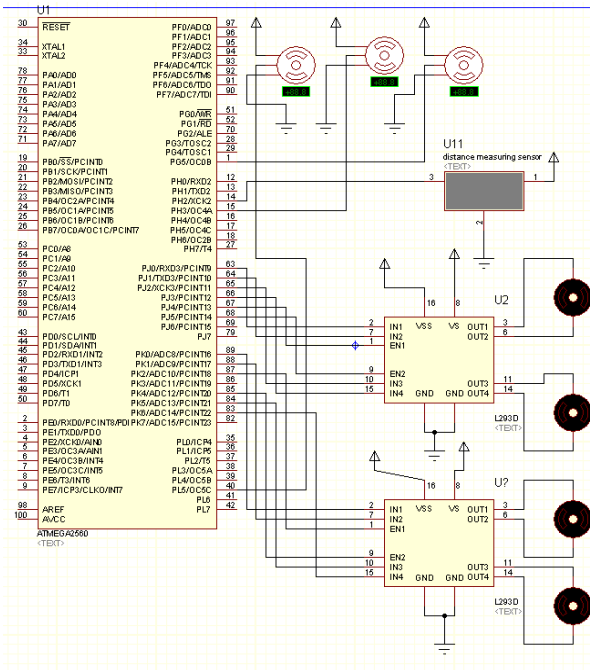

Fig.16 Circuit diagram of the system

The circuit is designed for Atmega 2560 microcontroller which is used in Arduino mega.

8.0 Program Algorithm (Control Loop)
Initialize sensor
Start left wheel motor clockwise and right rear wheel motor anti-clockwise (car moves forward)
If
Sensor detects obstacle, move up to limit (11 inches apart) and stop both motors
Else
Start both motors clockwise (car tends to turns right)
If
Sensor detects obstacle, stop motors and start left wheel motor clockwise and right wheel motor anti-clockwise up to limit (car moves forward) and then stop both
While
Both wheel motors stop (crop is inside gripper fingers)
Do
Start gripper motor on counter clockwise up to limit and stop (grip closed)
While
Gripper motor stops
Do
Turn pinion motor on up to limit and stop and start cutter blade motor on
While
Pinion motor turns off
Do
Turn revolute joint motor 1 (at base) counter clockwise on up to limit and stop (arm rotates in left direction)
While
Revolute joint motor 1 stops
Do
Turn revolute joint motor 2 (at elbow) clockwise on up to limit and stop (crop tends to get parallel to ground)
While
Revolute joint motor 2 stops
Do
Turn gripper motor on clockwise (crop is stored at the left side) and stop up to limit
While
Gripper motor stops,
Do
Wait 5 seconds and turn gripper motor counter clockwise on up to limit and stop and turn revolute joint motor 1 clockwise up to limit and stop and turn revolute joint motor 2 on counter clockwise up to limit and stop (arm is at initial position)
Start from the first again
If
no signal is found in 1 minuet
Then Stop

9. Design analysis and Simulation
Design analysis is studied and analyzed in solid works 2010 simulation platform.

9.1 Terminologies used in simulation
(1) Meshing
It is a very crucial step in design analysis. The automatic mesher in the software generates a mesh based on the global element size, tolerance, and local

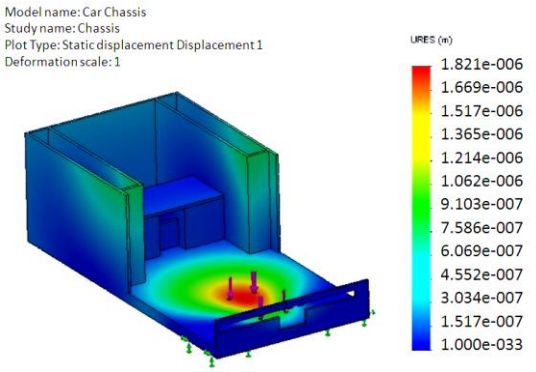

Fig.17 Static Displacement analysis (m)

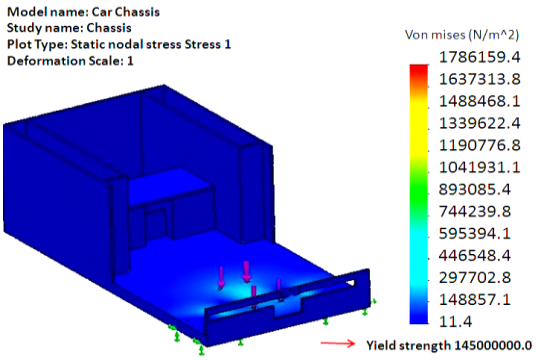

Fig.18 Von mises stress analysis

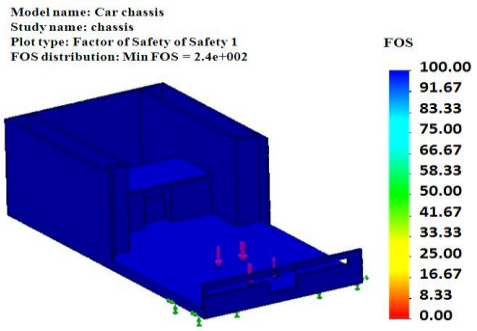

Fig.19 Factor of Safety (FOS)

mesh control specifications. Mesh control helps us to specify different sizes of elements for components, faces, edges, and vertices. A mesh consists of one type of elements unless the mixed mesh type is specified. Solid elements are naturally suitable for bulky models. Shell elements are naturally suitable for modeling thin parts (sheet metals), and beams and trusses are suitable for modeling structural members.

(2) Von Mises Stress
The von Mises yield criterion suggests that the yielding of materials begins when the second deviatory stress invariant reaches a critical value. For this reason, it is sometimes named as the -plasticity or flow theory. It is part of a plasticity theory that applies best to ductile materials, such as metals.

(3) Factor of Safety (FOS)
FOS is the ultimate strength of a given material divided by an arbitrary factor of safety, dependent on material and the use to which it is to be put, gives the allowable stress.[5]

$$FS = \frac{S_{al}}{\sigma_{ap}}$$

Where,
S_{al} = Allowable strength
σ_{ap} = Applied stress (Allowable stress)
FS = Factor of Safety

10. Result and Discussion

The simulation analysis shows that the material selection allows a factor of safety of 240 for the different parts of the robot chassis which will carry the other parts. The displacement is nearly negligible and the maximum displacement is analyzed as 1.821 micro meter. The basic forces acting on the robot are mainly the weight force as the external force added by a paddy tree is very small. Through stress and strain analysis the model is simulated after meshing and no alarming deformation or excess stress is identified with the given material properties. So the design can be considered as stable. Yet, more analysis is required to produce this robot industrially depending on the environment, materials available, and crop type. On the basis of stated mechanism and material in our model we calculated that the total farmer robot will cost BDT 15,290 only.

Table 2 Material cost:

Sr. no	material	Amount	price	Final Price (BDT)
1	Aluminum 2014 t-6	17 kg	240 BDT/kg	4080
2	mahogany	.137 x10^-3	320 BDT/ Sq. meter	10
3	EPDM70 udometer	1/4 roll	12000/roll	3000
4	DC Motors	4	200 BDT/piece	800
5	Servo motors	3	800 BDT/ pc	2400
6.	Miscellaneous (machining, production)	-	5000	5000
			Total:	15,290

Table 3 Advantage over Traditional vehicles:

Sr. no.	Topic	Traditional vehicle	Robot farmer
1.	Power source	Diesel/gasoline engine	Runs with rechargeable battery
2.	Approximate cost	200000 BDT or more	15,290 BDT
3.	Physical involvement	At least 2 persons needed to operate	No physical involvement needed, Just monitoring is needed

11. Conclusion

In this paper, through utilizing new materials and mechanism we have integrated the advantages of a robotic manipulator, and an automated cutter to serve a single specific purpose of cutting operation in the field as a farmer robot. This design is compared with the traditional man operated vehicles and it is found that this is more cost effective and affordable for most of the farmers. Further research is required to improve it for serving the purpose of the farmers and to increase the production rate of the crops like paddy.

REFERENCES

[1] Goense, The economics of autonomous vehicles. - Proceedings of the VDI-MEG, *Conference on Agricultural Engineering in Hanover*, pp 283-290 (2003).

[2] S. M. Pedersen, S. Fountas, H. Have and B.S. Blackmore, Agricultural robots: an economic feasibility study, *Precision Agriculture*, PP 589-583 (2005)

[3] V. Kaundal, R. Singh, Low Cost Robotic Wheel Chair for Disabled People in Developing Countries, *Conference on Advances in Communication and Control Systems*, pp 277-583 (2013)

[4] R.S. Khurmi & J.K. Gupta, Theory of Machines, *Eurasia Publishing House* , pp 382-414 (2005)

[5] D. G. Ullman, The Mechanical Design Process, *McGraw-Hill publishers*, pp 403-406 (2009)

ICMIEE-PI-140111

Design and Simulation of an Automated Wheelchair with Vertically Adjustable Seat

Kazi Ehsanul Karim[1], **Helal-An-Nahiyan*[1], *Hasnayen Ahmed*[1]
[1]Department of Mechanical Engineering, Khulna University of Engineering & Technology, Khulna-9203, BANGLADESH

ABSTRACT
The motivation of this research work is to design an automated wheelchair for the physically disabled people of both developed and developing countries. This design also facilitates the users to adjust the wheelchair seat vertically according to their needs. Though many designs of automatic wheelchairs are published in different research works, those are not so available in present market that common people can buy and use it for their personal purpose. Beside this, the high price restricts most of the disabled people of developing countries like Bangladesh from using the automated wheelchair for their maneuvering. For this reason, A microcontroller based embedded system is designed to control the wheelchair motion comfortably along with the vertical movements of the seat. On the contrary, the price of the wheelchair will not exceed the economic range of general people. The feasibility of this design is also verified through simulation works.

Keywords: Automatic Wheelchair, Embedded system, vertically adjustable seat, Belt and pulley

1. Introduction
The number of physically impaired people is increasing rapidly in recent years. Recent statistics shows that around 15% people (700 million) of total world population are physically and mentally disabled. Among them 100 million people are physically challenged. One study presents that the number of physically challenged people in Bangladesh is around 5.6% (8.4 million) of total population (Fig.1) [1], whereas, the actual scenario is much more acute. The majority of physically challenged persons of countries like Bangladesh either use crutches or manual wheelchairs for their maneuvering. Because of physical weakness, many wheelchair users cannot control the wheelchairs properly by using their hands. Moreover automated wheelchairs are not available everywhere in developing countries and the cost is high with respect to the economic status of the common people.

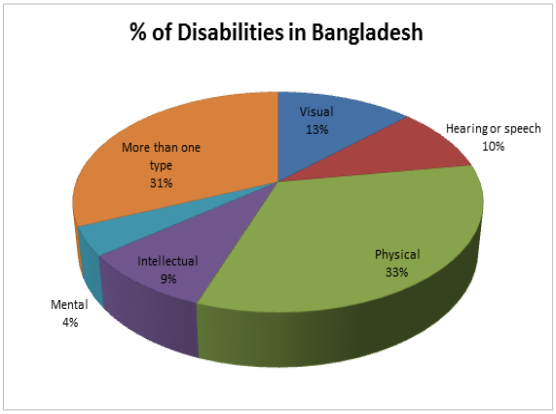

Fig.1 Percentage of disable people in Bangladesh

User uses the traditional automatic wheelchairs need help from others and cannot move the wheelchair seat for their necessary purposes (shown in Fig.2). Moreover physically weak users also face problems to grip joystick for moving the automated wheelchairs. In this circumstance, this research aims to design an automatic wheelchair with a vertically moveable seat to enhance its facilities for the users.

Fig.2 Hindrance of Wheelchair users during work

2. Background
The main purpose of scientific research is to facilitate every human being through the scientific inventions. Though automated wheelchair is the gift of modern science, most of the common people of developing countries do not have its access because of its high price and less availability. From the last decades of 19th century, researchers had been working on this purpose. In 1994, MITRE Corporation published their research on low cost automated wheelchair which was a theoretical modification of manual wheelchair [6]. Their practical implementation was found in 1995 [12]. Later, in the research of Taslima reza, 2012 [4], EMG signal was used for controlling the wheelchair, but its practical implementation is still a long way to go. The smart wheelchair showed by Trivedi (2013) [5] is a laptop assembled wheelchair and such kinds of wheelchair is too expensive for the common people of developing countries. NavChair and other joystick controlled wheelchairs [10, 13] are difficult for those users having wrist weakness. Vision based EOG system for wheelchair [7], voice operated wheelchair [8], voice enabled device [9], and gesture recognition based

* Corresponding author. Tel.: +88-01911208438
E-mail address: nahiyan.me@gmail.com

wheelchair [11] are not feasible yet for the application in developing countries. The signal processing system of these wheelchairs are still in research level and the user interaction of these wheelchairs are not easy to adapt. The design and implementation of wheelchair by Humaira salmin [2] is as same as "Tin man" by MITRE Corporation [12]. As the manual wheelchair is disassembled and then converted into automated wheelchair, it is nothing but a power car and there is no option for adjusting the seat height. From above analysis it is seen that no one still feel the necessity of vertical movement of wheelchair seat for facilitating users need. Because of these technical limitations and economic perspective of developing countries, we present a new design of automatic wheelchair.

3. Mechanical Design

The design of the wheelchair is done by using Solidworks 2013 software and the outlook view is generated with Keyshot4 software. Solidworks 2013 software is further used for stress and displacement analysis. AISI 1020 steel is used as material for simulation purposes. The material properties of AISI 1020 are given at Table 1.

Table 1 Material property of AISI 1020

Property	Value	Units
Elastic Modulus	2e+011	N/m^2
Poisson Ratio	0.29	N/A
Shear Modulus	7.7e+010	N/m^2
Density	7900	Kg/m^3
Tensile Strength	420507000	N/m^2
Specific Heat	420	J/(Kg.K)
Yield Strength	351571000	N/m^2
Thermal Expansion Coefficient	1.5e-005	/k
Thermal Conductivity	47	W/(m.K)

The design of the wheelchair is done by considering the maximum weight of the person is 100kg. So, the structure of the wheelchair has to be capable of carrying 980N load. Von Mises stress analysis and URES displacements indicate the validation of structure strength, using AISI 1020 steel under 980N load. Designed structure of the wheelchair is given below

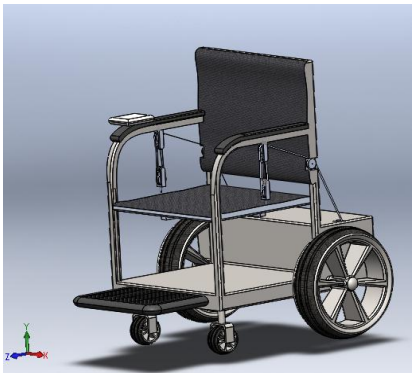

Fig.3 Isometric view of designed wheelchair

3.1 Von Mises stress analysis

Von Mises stress analysis is used to find the yielding criteria of isotropic or ductile materials under complex load. According to Von Mises yield criterion, it is independent of first stress invariant. But the ductile materials will exceed yield point when the second deviatory stress invariant will reach a critical value. The stress analysis of wheelchair frame, seat and pulley are given in the Fig.4, Fig.5 and Fig.6 respectively.

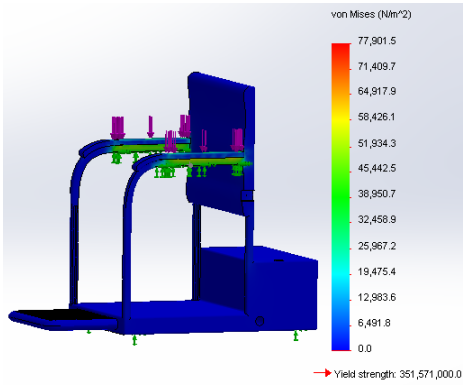

Fig.4 Von Mises stress analysis of frame

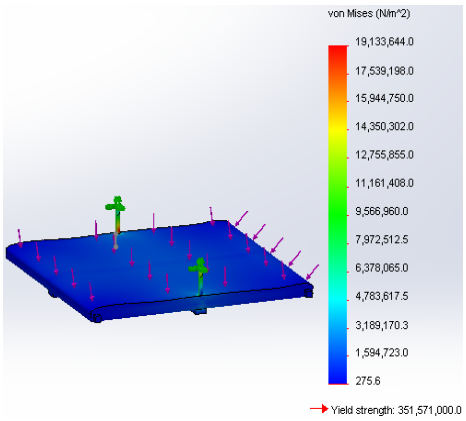

Fig.5 Von Mises stress analysis of seat

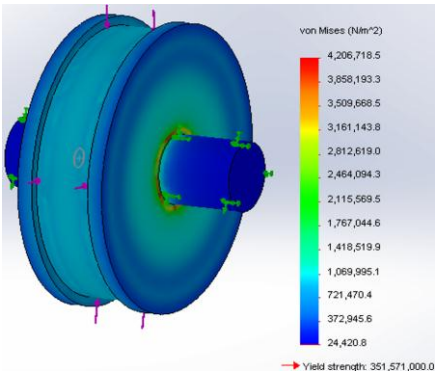

Fig.6 Von Mises stress analysis of pulley

From the stress analysis of the wheelchair frame, seat and pulley, it is found that the structures will sustain under the applied load.

3.2 Resultant displacement

The resultant URES displacement of Solidwork shows the average displacement of the wheelchair structure. It includes the resultant deformation in X, Y, and Z direction. It is found from the analysis that the highest deformation of the wheelchair frame is 0.00000815mm under the applied load. The URES displacement of the wheelchair frame, seat and pulley are shown in Fig.7, Fig.8, and Fig.9 respectively.

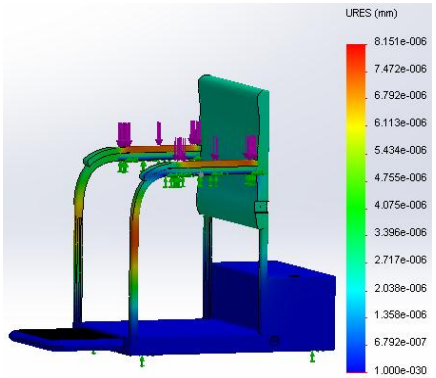

Fig.7 URES displacement of wheelchair frame

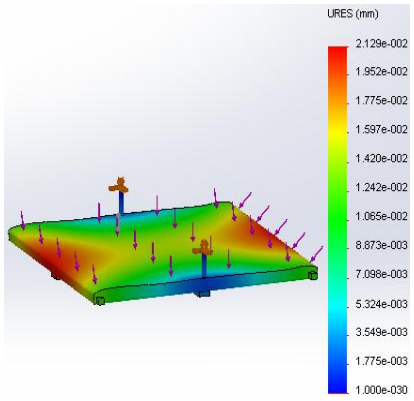

Fig.8 URES displacement of wheelchair seat

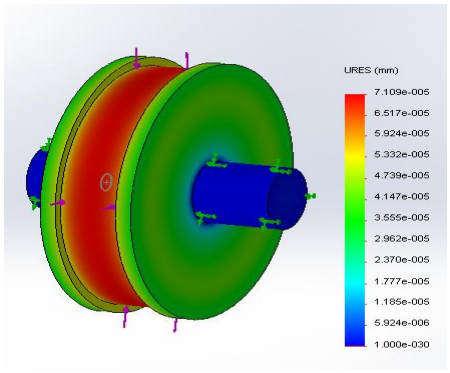

Fig.9 URES displacement of wheelchair pulley

3.3 Suitable wire for load

To hold 980N, 3/8 inches (9.5mm) diameter steel wire is well enough which is justified by Engineering Toolbox-wire-rope-strength table [4].

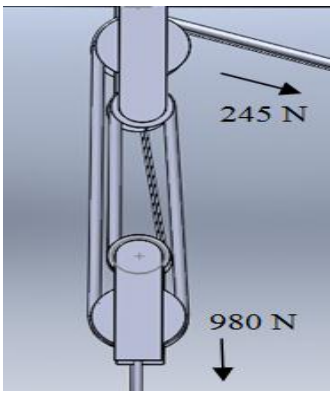

Fig.10 Wire rope and pulley

The safe load of this wire is 10.9 KN. So the maximum safe mass, M for 3/8 inches wire, can be calculated as

$$M = F/g \quad (1)$$

The maximum weight limit of the wire is 1111kg. So the factor of safety of our design is more than 10.

4. Electrical Components

In order to drive and control the wheelchair two DC motors, one DC gear motor, rechargeable battery, ATMEGA 32 micro- controller, and L293D motor driver are used as the electrical components.

4.1 DC motors

Two DC motors are used for independent rotation of rear wheels. The output power, torque and voltage of this DC motor are 200W, 20Nm and 24V respectively. High torque of DC motor ensures the smooth movement of the wheelchair. The torque of DC gear motor is 50Kg-cm which is used to pull 980N load of a wheelchair user smoothly.

Fig.11 DC Motor for rear wheel and DC gear Motor for lifting seat

4.2 Wheelchair Battery

NiMH battery is a kind of rechargeable battery. The specific energy of large NiMH cells is about 270 KJ/Kg. This battery is very robust and shows the current charge status by pressing a button. It's charging time is 2 hours and volumetric energy density is 1,080 MJ/m^3. The voltage and current of one set of battery is 24V and 2200mAh.

Fig.12 Rechargeable NiMH Battery

4.3 ATMEGA 32 microcontroller

This microcontroller have 32 Kbytes self - programmable Flash program memory, 1024 Bytes EEPROM, 2 Kbytes internal SRAM, 8 channel-10 bit ADC and 32 programmable I/O lines. Operating voltage of this microcontroller ranges between 4.5V-5.5V. This is helpful for multifunctional automated system with low cost and low power consumption.

Fig.13 ATMEGA 32 microcontroller

4.4 L293D motor driver

L293D is quadruple high-current half-H drivers. It provides bidirectional drive currents up to 600mA at voltages from 4.5 V to 36 V. It is designed to drive inductive, high current/high voltage loads such as relays, solenoids, DC motors etc. in positive supply applications.

Fig.14 L293D motor driver

5. Control Algorithm

Functions of wheelchair motor are controlled by ATMEGA32 microcontroller, L293D motor driver by using PWM (Pulse Width Modulation) and measuring duty cycle of motor. When the PWM is initialized, motors are individually rotated according to the user's purposes. If the user desires to move forward or backward, then the both rear wheel motors will rotate in forward or backward direction. This command is sent to the register of microcontroller by switch1 and switch2 respectively. Similarly, the wheelchair will turn left when the right motor will rotate in forward direction and left motor will be in reverse direction by pressing switch4. On the other hand, switch3 will set signal to microcontroller register to enable the rotation of wheelchair to turn right. The DC gear motor is controlled by pressing switch6 or switch7 to move the seat vertically up and down. The flowchart of control algorithm and the circuit diagram are given in Fig.15 and Fig.16 respectively.

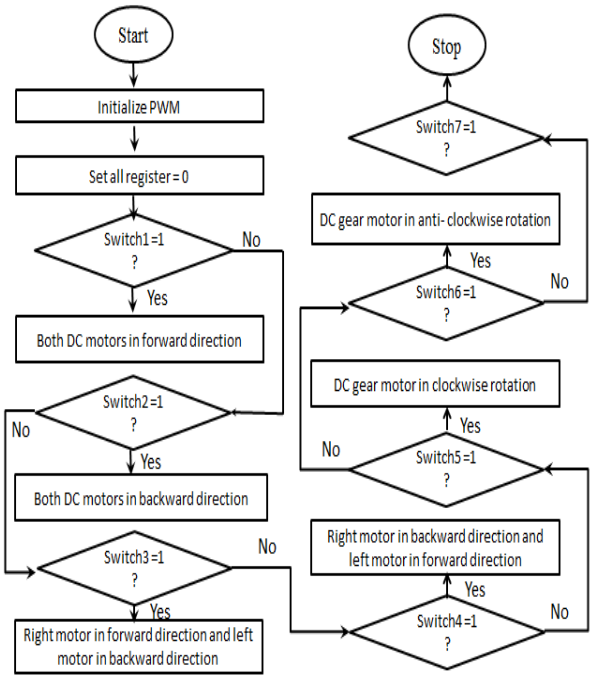

Fig.15 Flowchart of control mechanism

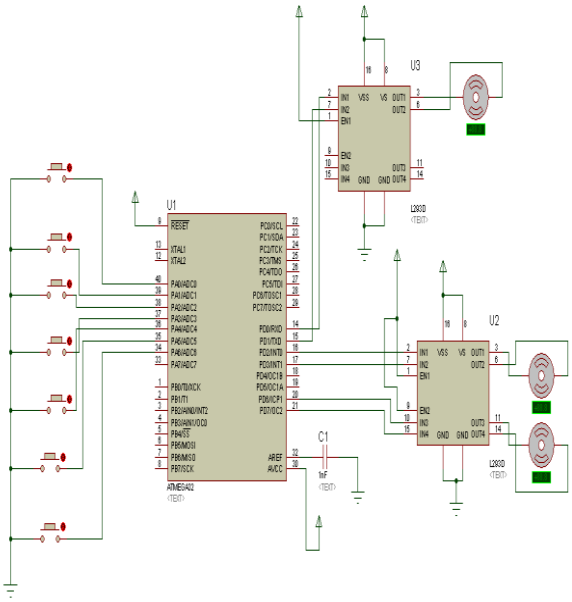

Fig.16 Circuit arrangement by Proteus software

Wheelchair seat movements are shown in the Fig.17

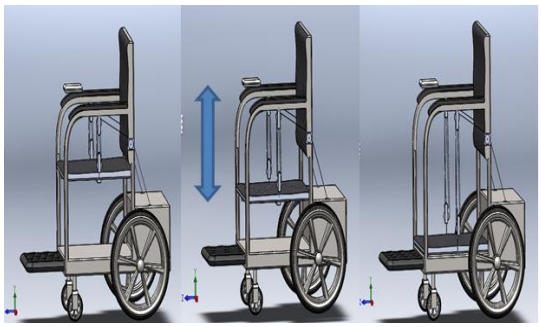

Fig.17 Downward motion of wheelchair seat

6. Final rendering of wheelchair

The final rendering is presented by Keyshot4 software.

Fig.18 Final design

6. Economic analysis

The necessary components of the proposed wheelchair are available in the electronics market of Bangladesh, TechshopBD and eBay. From the market price of these components, the estimated price of this wheelchair is given in Table 2.

Table 2 Estimated price of Wheelchair

Parts name	Price in BDT	Price in $
Wheelchair frame	10,000	128.2
Electrical component(microcontroller chip, mosfet, buttons)	1200	15.38
Dc wheel motor	4988	62.35
Dc gear motor	2494	31.18
Mechanical equipment	3000	37.5
Battery	6392	79.9
Total -	28,074	354.51

7. Result and Discussion

The main focus of this research work is to design an automatic wheelchair with vertically adjustable under the economic production feasibility. The load carrying capacity of the seat depends on the structure and the material stability of related parts of the wheelchair. After designing the wheelchair structure, stress and displacements analysis of the wheelchair frame, seat and pulley are justified. The results of simulation work show the sustainability of the mentioned parts under applied load (980 N). Thus the stability of wheelchair structure is verified. The rope and pulley system is used to minimize the load on DC gear motor. The suggested DC wheel motors and gear motor are able to make the motion and to carry the mentioned load. Thus the structure can bear the load, and the motor can operate synchronously. So the designed structure has passed all the necessary safety criteria. The cost analysis also represents that it is going to be the cheapest wheelchair model with vertically adjustable seat.

8. Conclusion

The recent research works of automated wheelchairs are mostly concerned about control mechanisms. Though some low cost wheelchair projects are done, no new design is proposed for low production cost and multiple function facilities. This research work presents a new multifunctional wheelchair which will diminish the inaccessibility of automated wheelchair for the common people of developing countries. This project develops a new design of wheelchair which can be accessible to every people and a unique concept of wheelchair seat movement is developed with practical feasibility through simulation software. The future work of this research can focus on engaging more sensors and developing sophisticated control system that will add more freedom for the disabled user.

NOMENENCLATURE

M : mass , Kg
F : Force , N
G : Gravitational acceleration , m/
EPW : Electrical Powered Wheelchair
NiMH: Nickel Metal Hydride.

REFERENCES

[1] P. Norek, M. Ahmed, et al, Livelihood Challenges for Extremely Poor Disabled People in the Southwest Costal Region of Bangladesh, Shiree working paper 12, January 2013.

[2] Salmin, H. Rakibul, et al, Design and Implementation of an Electric Wheel-Chair to Economize it with Respect to Bangladesh, *International Journal of multidisciplinary Science and Engineering*, vol. 5, NO. 2, FEB. 2014.

[3] V. Kaundal, R. Singh, Low Cost Robotic Wheel Chair for Disabled People in Developing Countries, *Conference on Advances in Communication and Control Systems*, 2013.

[4] T. Reza, S.M.Ferdous, et al, A Low Cost Surface Electromyogram (sEMG) Signal Guided Automated Wheel Chair for the Disabled, *International Journal of Scientific & Engineering Research*, Volume 3, Issue 2, Feb., 2012.

[5] A. R. Trivedi, A. K. S. K. Singh, et al, Design and Implementation of a Smart Wheelchair, *Conf. on Advances in robotics*, pp. 1-6, 2013.

[6] D. P. Miller and M. G. Slack, Increasing Access with a Low-Cost Robotic Wheelchair, *IEEE Int. conf.*, vol. 3, pp. 1663-1667, Sept. 1994.

[7] R. Barea, L. Boquete, M. Mazo and E. Lopze, Wheelchair Guidance Strategies Using EOG, *Journal of Intelligent and Robotic Systems*: 279–299, 2002. 279 © 2002 Kluwer Academic Publishers.

[8] J. K. Kokate, A. M. Agarkar, Voice Operated Wheel Chair, *International Journal of Research in Engineering and Technology*.

[9] B. R. Reddy, J. V. Sharma, Movement based and Voice enabled Device Switching for basic needs of Physically Challenged Persons *International Journal of Science and Research (IJSR*), India Online ISSN: 2319-7064.

[10] S. P. Levine, D. A. Bell, L. A. Jaros, et al, The NavChair Assistive Wheelchair Navigation System, *IEEE Trans. on Rehab. Eng*., vol. 7, NO. 4, DEC. 1999

[11] R. A. Kalantri, D.K. Chitre, Automatic Wheelchair using Gesture Recognition *International Journal of Engineering and Advanced Technology (IJEAT*), ISSN: 2249 –8958, Volume-2, Issue-6, August 2013.

[12] D. P. Miller and M. G. Slack, Design and Testing of a Low-Cost Robotic Wheelchair Prototype, 1995 *Kluwer Academic Publishers, Boston*.

[13] T. Rofer, C.Mandel, T. Laue, Controlling an Automated Wheelchair via Joystick/Head-Joystick Supported by Smart Driving Assistance, IEEE 11th *International Conference on Rehabilitation Robotics Kyoto International Conference Center, Japan*, June 23-26, 2009.

.

ICMIEE-PI-140115

Numerical Analysis of Laminar Natural Convection from Heated Vertical Plate and Horizontal Cylinder

Md. Navid Unjum [1]*, *Md. Fazlay Rabbi* [1], *Nawsher Ali Moral*[1]
[1] Department of Mechanical Engineering, Khulna University of Engineering & Technology, Khulna-9203, BANGLADESH

ABSTRACT
The study aims to investigate the fluid flow and heat transfer characteristics around the vertical plate and horizontal cylinder. In this study, the constant temperature boundary condition is applied .The two dimensional mathematical models consisting the systems of partial differential equations such as Continuity equation, Navier-Stokes equation and Energy equation are used here. The solution was obtained using a commercial CFD code. Further grid independence test was undertaken to justify the value of numerical solutions. Results were basically obtained for a Prandtl number of 0.7; this being approximately the value of air. Numerical results are obtained in terms of Nusselt and Rayleigh Numbers. After comparing the numerically simulated figure and conventional figure found in literature, it is seen that the trend lines are similar for each and every cases. And finally, the numerical values are compared with the established empirical relation of Churchill and Chu, Merk and Prins, Morgan, McAdams etc.

Keywords: Natural convection, Heat Transfer, Numerical Analysis, Vertical Plate, Horizontal Cylinder.

1. Introduction

Natural convection heat transfer from a vertical plate and horizontal cylinder has been studied experimentally for more than fifty years. It is reported by the researchers that the obtained results show high levels of deviation among each other due to various reasons such as under sized test cabin, faulty temperature measurement system etc. This is why natural convective heat transfer from vertical plate and horizontal cylinder in laminar flow regions has been numerically studied to get better accuracy.

The problem of boundary layer free convection flow past a vertical plate and horizontal cylinder under different conditions was studied by many researchers. Several techniques and process of solution had been developed for the qualitative and quantitative analysis of convection, amongst which, one may make reference to experimental techniques, pure theoretical analysis and numerical simulation. Empirical approaches based on scaling analysis and finished by experimental information, and most recently, numerical simulations techniques, arisen to the computational advances, have been used in the study of natural convection.

Here heated objects are placed on the atmospheric condition and the flow phenomena are observed. Five different diameters are used for horizontal cylinder while a single plate is used for vertical plate. The GAMBIT mesh generator associated with FLUENT has been used to plot and mesh the 2D model of the vertical plate and cylinder. Grids are used according to the specific requirement for both cases. For cylinder, the grids are clustered close to the small cylinder while for grid adjacent to the wall is finer compared to that in the central region.

Natural Convection Heat Transfer from vertical plate involves in number of practical situations involving electrical and electronic equipment such as printed circuit boards, chips, conductors, solar cells, measurement systems etc. The size and inclination angle affect heat transfer from vertical plate and thus play a vital role in thermal design and manufacture of electronic equipment.

Free convective heat transfer from cylinders having circular and square cross sections has significant practical importance and is relevant to numbers of applications in the cooling of electrical and electronic components such as square pin fin heat sinks, resistors, capacitors, conductors, transformers, diodes, thyristors etc.

2. Physical Model of the Computational Domain

The height of the plate = 0.2 m

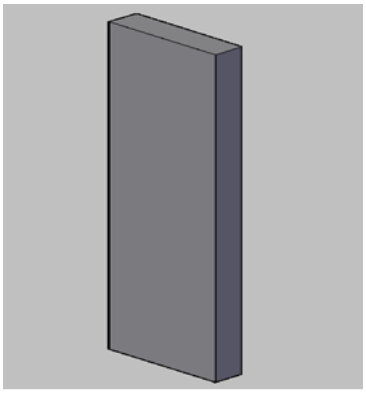

Fig.1 Vertical plate

The diameters of the cylinders are 0.05 m, 0.07 m, 0.1 m, 0.12 m and 0.15 m

* Corresponding author. Tel.: +88-01917177345
E-mail address: navid450@yahoo.com

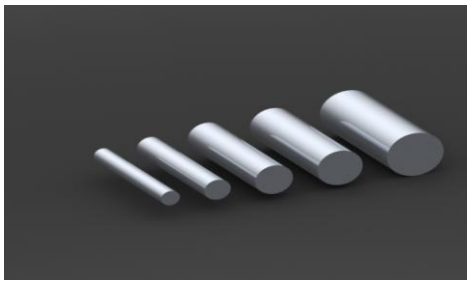

Fig.2 Horizontal Cylinder of various diameters

3. Boundary Conditions

The Physical boundary conditions for the problem include zero velocity components at the wall surface, no axial velocity outside the boundary layer, temperatures T_s at the wall and T_∞outside the boundary layer. These boundary conditions are stated as follows:

At y=0 (wall)
i)U=0
ii)V=0
iii) T=T_s
At y→∞ (or outside boundary layer)
i)U=0
ii) T=T_∞

Boundary conditions used for vertical plate and horizontal cylinder is shown graphically in the Figure 6 and Figure 7

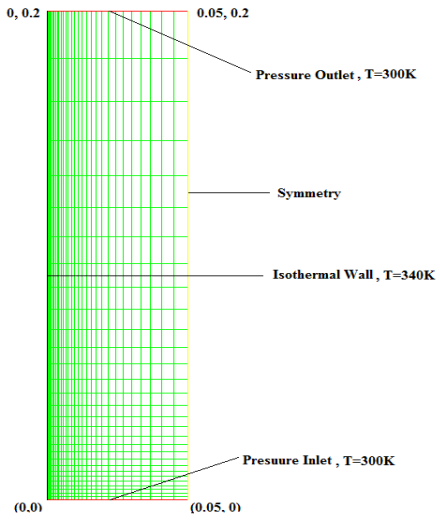

Fig.3 Computational Domain with boundary conditions for vertical plate

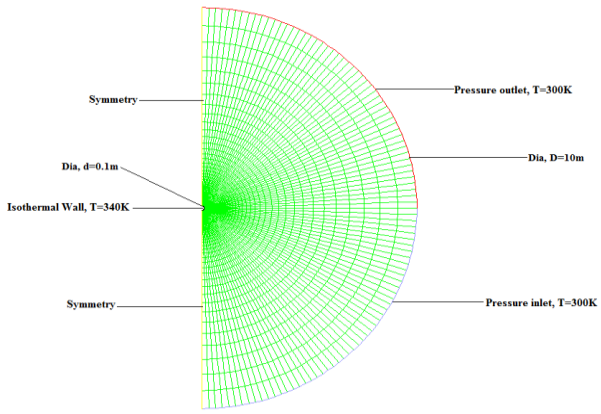

Fig.4 Computational Domain with boundary conditions for horizontal cylinder

5. Initial Conditions:

Material: Aluminum
Fluid: Air
Temperature of the wall, T_s = 340 k
Bulk temperature of the fluid, T_∞= =300 k

6. Solution Methods

Here the two problems are investigated using FLUENT as a 2D steady laminar flow problem. The heat transfer module of the FLUENT solver was enabled. The operating pressure of the domain was specified as 101325 Pa. At the heated wall, an isothermal boundary condition was used. At the bottom and top of the domain, a pressure inlet and outlet condition was specified. A symmetry boundary condition was imposed on the right end of the domain (Vertical plate) and on the left end of the domain (Horizontal Cylinder). Both the flow and energy equations were solved using the SIMPLE algorithm for pressure-velocity coupling. The PRESTO Scheme was used to discretize the pressure equations, and the momentum as well as the energy equations used a second order upwind scheme for spatial discretization. For this discretization, gradient is evaluated using a Least Squares Cell Based Method. The Under- Relaxation Factors used for pressure, density, body forces, momentum and energy is set to 0.3, 1, 1, 0.7 and 1 respectively. Boussinesq approximation was used for density evaluation. The Boussinesq approximation neglects the effect of fluid-density dependence on pressure of the air phase, but includes the density dependence on temperature. It enables the flow to be treated as incompressible flow but still accounts for density variation locally in the momentum and energy equations. As the Rayleigh number of the flow will be less than the critical value, no turbulence models were used in the solution. Here the convergence criteria for mass, momentums and energy equations have been set at 1E-6

7. Equations

Continuity equation

$$\frac{\partial u}{\partial x}+\frac{\partial v}{\partial y}=0 \qquad (1)$$

Navier- Stokes equation

$$u\frac{\partial u}{\partial x}+v\frac{\partial u}{\partial y}=-\frac{1}{\rho}\frac{\partial p}{\partial x}+\vartheta\left(\frac{\partial^2 u}{\partial x^2}+\frac{\partial^2 u}{\partial y^2}\right) \qquad (2)$$

Energy equation

$$u\frac{\partial T}{\partial x}+v\frac{\partial T}{\partial y}=\frac{k}{\rho c_p}\left(\frac{\partial^2 T}{\partial x^2}+\frac{\partial^2 T}{\partial y^2}\right) \qquad (3)$$

Equations for Nusselt number, heat transfer co-efficient and boundary layer thickness calculation:

1. $Nu=Q_p{*}X_p$ or $D/(T-T_b)*K$ [3]

2. $Nu_x = 0.508 * Ra_x^{1/4} * \left(\frac{Pr}{0.952+Pr}\right)^{1/4}$ [3]

3. $Ra_x = Gr_x * Pr$ [3]

4. $Nu_m = 0.68 + \frac{0.67*Ra^{1/4}}{[1+(0.492/Pr)^{\frac{9}{16}}]^{4/9}}$ [8]

5. $h_x = 0.508* Pr^{1/2} * \frac{Gr^{1/4}}{(0.952+Pr)^{1/4}} * \frac{k}{x}$ [1]

6. $\delta = 3.93* X *\left[\frac{0.952+Pr}{Pr^2*Gr}\right]^{1/4}$ [1]

7. $Nu_m^{1/2} = 0.60 + \frac{0.387*Ra^{1/6}}{[1+(0.559/Pr)^{\frac{9}{16}}]^{8/27}}$ [5]

8. $Nu= C* Ra^{1/4}$ [4]

9. $Nu= C* Ra^{n}$ [7]

8. Results

After solving the models in FLUENT, the result from the numerical analysis is checked for mesh independence. Also the numerical result is validated using available experimental data. After successful validation, the result is post-processed using FLUENT for visualizing the flow behavior & heat transfer characteristics.

8.1 Comparison with Standard Results

For the test results to be accepted, the computed flow field should qualitatively agree with the general understanding of the flow physics expected for natural convection flows along heated vertical plate and horizontal cylinder. A comparison between conventional figure and figure from the result of numerical solution is done in order to validate the test results.

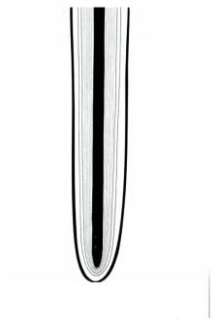

Fig.5 Interferometer photograph showing lines of constant temperatures around a heated vertical plate in natural convection [1]

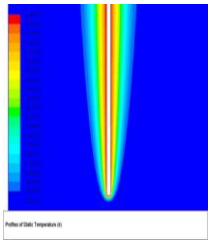

Fig.6 Color contours of constant temperatures around a heated vertical plate from the problem investigated

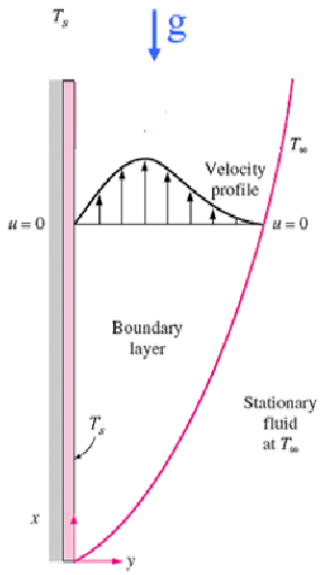

Fig.7 Velocity profiles for free convection from a hot vertical plate [1]

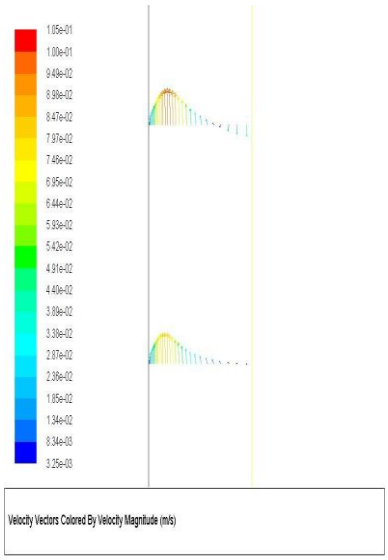

Fig.8 Velocity profiles for free convection from the hot vertical plate of the problem investigated

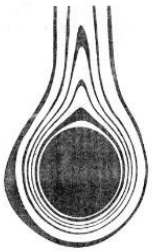

Fig.9 Interferometer photograph showing lines of constant temperatures around a heated horizontal cylinder in natural convection [1]

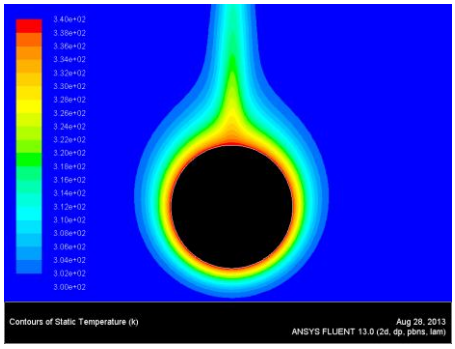

Fig.10 Color contours of constant temperatures around a heated horizontal cylinder (.1 dia) from the problem investigated

8.2 Validation of Numerical Result

In general, there is a higher degree of uncertainty between various experimental results. So it becomes troublesome to match the numerical values with the experimental value. Hence matching the numerical values within $\pm$ 5 percent [2] could be considered sufficient acceptance condition.

For Vertical Plate:

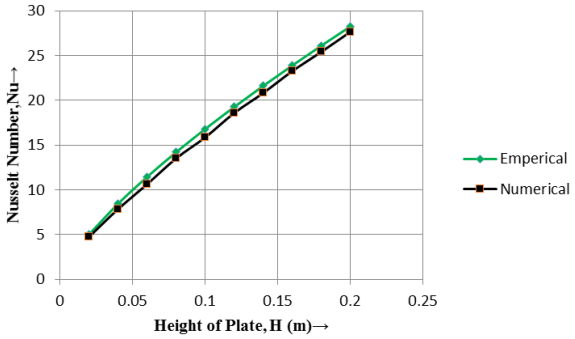

Fig.11 Comparison of Empirical and Numerical values of Nusselt Number along the vertical length of the heated plate

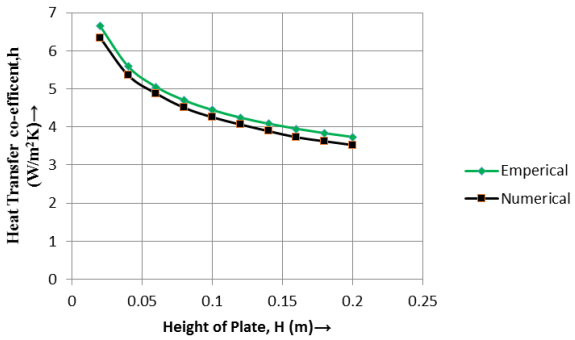

Fig.12 Comparison of Empirical and Numerical values of Heat Transfer Co-efficient along the vertical length of the heated plate

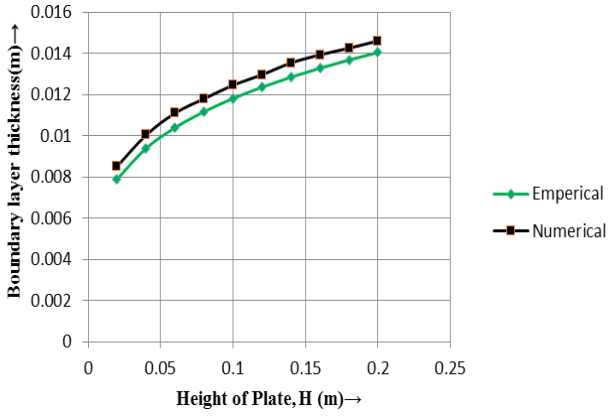

Fig.13 Comparison of Empirical and Numerical values of boundary layer thickness at various points on the heated vertical plate

For Horizontal Cylinder:
Nusselt number derived from various correlations is compared with the numerical value. From the figure 14, 15 and 16 it can be seen that the empirical and numerical values fall in ±5percent to ±7percent band respectively.

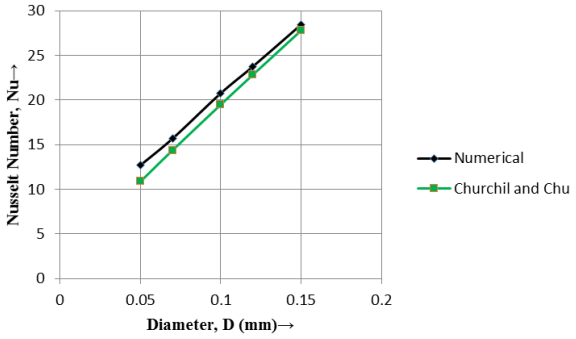

Fig.14 Comparison of Empirical [5] and Numerical values of Nusselt Number for heated horizontal cylinder of various diameters

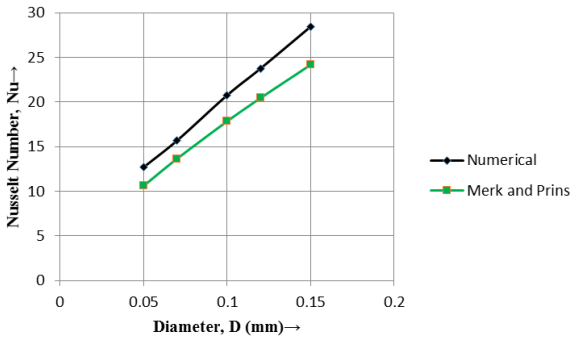

Fig.15 Comparison of Empirical [6] and Numerical values of Nusselt Number for heated horizontal cylinder of various diameters

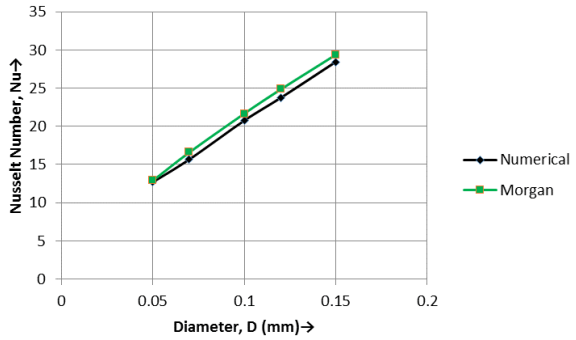

Fig.16 Comparison of Empirical [7] and Numerical values of Nusselt Number for heated horizontal cylinder of various diameters

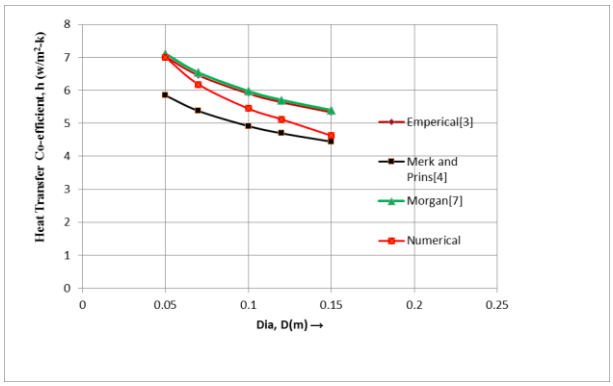

Fig.17 Comparison of Empirical [3], [4],[7] and Numerical values of heat transfer co-efficient for heated horizontal cylinder of various diameters

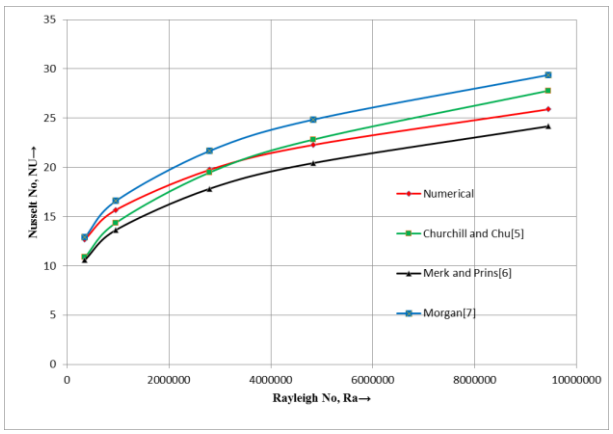

Fig.18 Comparison of Empirical [5], [6],[7] and Numerical values of Nusselt Number for various Rayleigh Number

9. Conclusion

1. For the vertical heated plate, both hydrodynamic and thermal boundary layer increases as the flow moves vertically upward. This is consistent with analytical solution [1].
2. The pattern of the boundary layers for heated horizontal cylinder satisfies the criteria of overall goodness and established understanding of the physical phenomena.
3. Comparison of numerical and analytical results for heat transfer coefficient for various diameter of horizontal cylinder was seen to fall into ±20% band.
4. Nusselt number increases with the increase of vertical length along the plate. So along the length of the vertical plate, convection becomes dominant than conduction.
5. Heat transfer co-efficient is inversely proportional to the distance along vertical plate while the boundary layer thickness increases with the increase of the distance.
6. Nusselt numbers obtained from these studies are compared with the correlations of Churchill and Chu [33], Merk and Prins [34], Morgan [35] according to the

different test cylinders. In addition to this, majority of data belong to other correlations were seen to fall into the 20% deviation line.

7. Nusselt number increases with increasing Rayleigh number in this study.

NOMENCLATURE:

K: Thermal conductivity, $W \cdot m^{-1} \cdot K^{-1}$
Nu: Nusselt number
Ra: Rayleigh number
Gr: Grashof number
Pr: Prandtl number
C_p: Specific heat at constant pressure, $J \cdot kg^{-1} \cdot K^{-1}$
T: Constant temperature of the walls, K
T_b : Fluid temperature, K
Q: Heat Flux, $W \cdot m^{-3}$
X: Location along the vertical plate, m
D: Diameter of the cylinder, m
x, y: Cartesian co-ordinates
ρ: Density of fluid, $Kg \cdot m^{-3}$
ϑ: Kinematic viscosity of fluid, $Kg \cdot m^{-1} \cdot s^{-1}$
ψ : Stream function, $Kg \cdot s^{-1}$
λ: Relaxation factor
μ: Dynamic viscosity of fluid, $Kg \cdot m^{-1} \cdot s^{-1}$
α: Thermal diffusivity, $m^2 \cdot s\text{-}1$
β Thermal expansion co-effiecient, $1 \cdot k^{-1}$
u, *v*: Velocity components, $m \cdot s^{-1}$
g: Gravitational acceleration, $m \cdot s^{-2}$
h: Heat Transfer Co-efficient, $W \cdot m^{-2} \cdot k^{-1}$

REFERENCES:

[1] Nag, P. K., *"Heat and Mass Transfer",* 2nd Edition, Page-425-441

[2] Ş. Özgür Atayılmaz & İsmail Teke, "Experimental and Numerical Study of the Natural Convection from A Heated Horizontal Cylinder", *International Communications in Heat and Mass Transfer 36* (2009) 731–738

[3] Ozisik, M. Necati, *Heat Transfer – A Basic Approach*, McGraw-Hill Book Company, International Edition, 1985, page-427- 431

[4] Merk, H.J., and Prins, J.A. 1953, Thermal Convection Laminar Boundary Layer I, *Applied Scientific Research*, Vol. A4, pp. 11-24

[5] Churchill, S.W. and H.H.S. Chu, "Correlating Equations for Laminar and Turbulent Free Convection from a Horizontal Cylinder", *Int. J. Heat Mass Transfer*, 18: 1049-1053 (1975)

[6] Merk, H.J. and Prins, J.A., 1953, Thermal Convection Laminar Boundary Layer I, *Applied Scientific Research*, Vol. A4, pp. 11-24

[7] Morgan, V. T., "The Overall Convective Heat Transfer from Smooth Circular Cylinders", in T.F. Irvine and J.P> Hartnett (eds), *Advances in Heat Transfer*, vol.16 Academic, New York, 1975, pp. 199-264

[8] Churchill, S.W. and H.H.S. Chu, "Correlating Equations for Laminar and Turbulent Free Convection from a Vertical Plate", *Int. J. Heat Mass Transfer*, 18: 1323 (1975)

ICMIEE-PI-140116

Development of new perlite/sodium silicate composites

Md Arifuzzaman[1,2,] and Ho Sung Kim [1]*
[1]Mechanical Engineering, School of Engineering, Faculty of Engineering and Built Environment,
The University of Newcastle, Callaghan, NSW 2308, AUSTRALIA
[2]Department of Mechanical Engineering, Khulna University of Engineering & Technology (KUET),
Khulna 9203, BANGLADESH

ABSTRACT
A novel mechanical behaviour of perlite/sodium silicate composites is studied. The objective was to develop new perlite composites. The flotation method was adopted for expanded perlite consolidation. For the composites development, sodium silicate dehydration behaviour was characterised with phases formed during dehydration i.e. liquid, gel, and solid phases. The water loss-time curve for dehydration was found to have three distinctive parts - linear part at an early stage for liquid phase, followed by non-linear part during a period between commencements of gel and hydrated solid phase formations, and then another linear part for hydrated solid phase. Foams as composites were manufactured with diluted sodium silicate binder for a density range of 0.2 - 0.5 g/cm^3. Compressive strengths and foam densities were obtained for optimum performance as functions of two independent variables i.e. compaction ratio and binder content. One of practical milestones observed was a density of 0.3 g/cm^3 at a compressive strength of 1MPa without reinforcement.

Keywords: Expanded Perlite, Sodium Silicate, Foam, Density, Compressive Strength.

1. Introduction

Perlite is a glassy volcanic rock of rhyolitic composition [1], which can be processed into an expanded form for cellular structure formation [2,3]. The expansion takes place due to the presence of water in perlite when heated to about 649-816^{o}C [4]. The expanded perlite particles are light, environmentally friendly [5], and possess good acoustic [6] and insulation properties [7]. They have been used as additives or main components for composites, e.g. Portland cement/perlite composites for blocks [8-10], perlite/sodium silicate boards [11], roof insulation panels made of perlite/fibers/bituminous material [12], fibre reinforced perlite/cement composites [13], building boards made of fiber/asphalt coated perlite [14] or urea–formaldehyde resin/mineral fibers/gypsum/glass fibers [15], fibre reinforced sodium silicate/perlite composite [16], moisture resistant gypsum boards modified with perlite/starch/boric acid/vinyl acetate [5], gypsum/perlite composites [17], and light weight concrete [18]. However, their applications as the main constituent of composites have been limited due to relatively poor mechanical properties. One of the reasons is that the expanded perlite particles are fragile and hence easily damaged during the process of mixing with binder, resulting in a high ratio of density to strength. At the same time, the study on mechanical performance of perlite composites compatible with gypsum boards [19,20] has not much been available in the literature. It is only recently that Shastri and Kim [21,22] studied some selected properties for mechanical behavior of expanded perlite consolidated with starch for demonstration of a new manufacturing process based on the principle of flotation [23-28]. The new process appears to be capable of extending the limitation of perlite applications, allowing us to manufacture samples for exploring novel mechanical behavior of consolidated expanded perlite particles.

In the development of perlite composites, selection of binder is another consideration along with manufacturing process. Sodium silicate may be one of candidate binders, which is an inorganic colloidal system. It has been used as foundry sand binder, fire-retardants, adhesives, and deflocculants among other applications [29]. Also, it is non-combustible, water-resistant and sufficiently inexpensive for developing building materials. This paper focuses on the novel mechanical behavior of expanded perlite/sodium silicate composites developed using the new manufacturing process developed by Shastri and Kim [22].

2. Constituent materials and characteristics

2.1 Expanded perlite

Commercial grades of expanded perlite particles were obtained from Australian Perlite Pty Limited. Expanded perlite particles were sieved using a vibratory sieve shaker (Analysette 3 SPARTAN) into three different particle size ranges i.e. sizes between1 and 2 mm, 2 and 2.8 mm, and 2.8 and 4 mm, which will be referred to as Size 1-2, Size 2-3, and Size 3-4 respectively.

Four different types of perlite densities were measured and listed in Table 1. For bulk density, an initial volume of 100 cm^3 of expanded perlite particles was poured into a glass measuring cylinder with a 28 mm diameter fitted to a manual tapper with a tapping stroke height of 5 mm, and then tapping was conducted for 300 times.

* Corresponding author. Mobile: +61 04 7068 9925; fax: +61 02 4921 6946
E-mail addresses: md.arifuzzaman@uon.edu.au

For envelope density (terminology from ASTM D 3766-08), a volume of about 4 cm^3 of expanded perlite particles was poured into molten paraffin wax in an aluminium container (37 mm in diameter and 13 mm height), ensuring it was fully submerged and each particle was fully wetted before wax solidification. The enveloped volume of perlite was determined by the difference in wax volume before and after submersion of perlite. The calculated envelope density is given in Table 1.

Table 1 Densities of expanded perlite particles.

Perlite particle size	Bulk density (g/cm^3)	Particle envelope density (g/cm^3)	Particle skeletal density (g/cm^3)	Material density (g/cm^3)
Size 1-2	0.089	0.140	1.466	2.46
Size 2-3	0.091	0.160	1.309	2.46
Size 3-4	0.100	0.152	1.207	2.46

Particle skeletal and material/true densities were measured using a gas pycnometer (AccuPyc 1330). For the material density sample preparation, expanded perlite particles were crushed into fine powder using a ball mill (8000D Mixer/Mill SPEX) for at least 5 minutes to remove the closed pores before volume was measured in pycnometer. It was confirmed using an optical microscope (Olympus SZ-CTV) that the closed pores were removed. Various types of porosities were obtained and listed in Table 2.

Table 2 Various porosities, fractions of open pores and closed pores of perlite particles.

Perlite particle size	Total porosity in bulk volume (υ_{total}), %	Fraction of open pores in perlite particles (υ_{opore})	Fraction of closed pores in perlite particles (υ_{cpore})	Particle porosity (υ_{pp}), %	Inter-particle Porosity in bulk volume (υ_{ipp}), %
Size 1-2	96.37	0.9045	0.0386	94.31	36.43
Size 2-3	96.31	0.8778	0.0572	93.50	43.13
Size 3-4	95.92	0.8741	0.0641	93.82	34.21

2.2 Sodium silicate solution and dehydration behaviour

Sodium silicate solution (ChemSupply) with a density range of 1.37-1.40 gm/cm^3, a solid content range of 37.10 - 38.00% (by mass), and a weight ratio of silica to sodium oxide (SiO_2/Na_2O) range of 3.16-3.22 was used as binder. Sodium silicate solution was dehydrated at 80°C to obtain a solid sample, and then was ball-milled (8000D Mixer/Mill, SPEX) for 30 minutes into powder for density measurement. The density was measured using a gas pycnometer (AccuPyc 1330) and found to be 2.17 g/cm^3.

To characterise the dehydration behaviour, sodium silicate solution (SSS) was diluted with water as specified in Table 3. The diluted samples were kept inside an electric fan forced air oven (Lebec Oven BTC-9090) at 65°C and mass loss was recorded every 10 minutes. Three dehydration phases were identified from diluted sodium silicate solution as dehydration progresses. The first phase was made of liquid, the second made of gel, and the third made of solid. (The gel is a cohesive substance consisting of colloidal particles [29]). The commencement and completion points of the gel formation and other phases are indicated in Fig. 1 and water contents at different stages are listed in Table 4.

Table 3 Samples of sodium silicate solution (SSS) used for dehydration behaviour.

Samples	Mass of SSS (g)	Mass of diluted SSS, (g)	Water content after dilution with water (%)
Sample 1 (control)	13.85	13.85	62.45[a]
Sample 2	6.93	11.93	78.21
Sample 3	4.61	11.28	84.66
Sample 4	3.46	10.96	88.14

[a] Provided by the manufacturer (ChemSupply)

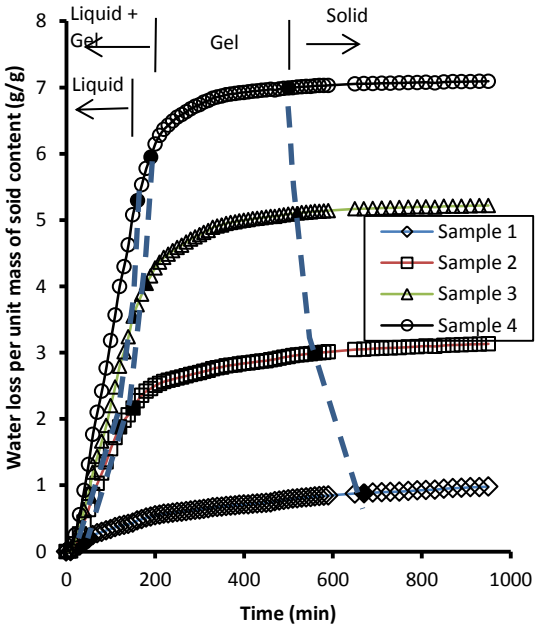

Fig.1 Water loss during dehydration at 65°C.

Some phase transitional points appear to be practically distinguishable on the water loss - time curve (Fig. 1). The first linear portion of the curve corresponds to liquid phase, non-linear portion corresponds to a stage where gel phase started to form from liquid phase until the two phases (liquid and gel) becomes fully gel prior to solidification, and the other linear part corresponds to hydrated solid phase.

It is noted that water contents at the completion of gel formation from (gel+liquid) are approximately constant at high dilution levels (Table 4). Further drying of the gel leads to the hydrated solid phase. However, the water contents in hydrated solid phase are not as much constant as those at the gel completion point. Even some trend is noticeable – the more water content at dilution the less water content at the solid phase.

Table 4 Water contents at different stages for dehydration at 65℃.

Samples	Water content at commencement of gel (%)	Water content at gel completion (%)	Water content at hydrated solid formation (%)
Sample 1 (control)	61.12	59.44	43.92
Sample 2	63.06	58.71	37.14
Sample 3	66.31	59.58	29.12
Sample 4	68.12	59.73	30.76

3. Manufacturing process of samples and mechanical tests

The process consists of different stages: dilution of sodium silicate binder, mixing of binder and perlite in a container, flotation of wet-mix, moulding and compaction, demoulding and drying as detailed elsewhere [21]. The dilution of sodium silicate was made in drinkable tap water. The perlite was poured into a mixing container containing the prepared binder, followed by stirring/tumbling of the mixture for phase separation consisting of top phase of perlite and binder, and bottom phase of binder. The mixing container was left until perlite particles float to the surface, forming two phases i.e. top phase made of perlite and binder and bottom phase made of just binder. The top phase was formed immediately and transferred into a mould for compaction. The compaction was conducted at a crosshead speed of 10 mm/minute on a universal testing machine (Shimadzu 5000).

Compression tests of manufactured foam specimens were conducted on a universal testing machine (Shimadzu 5000) at a crosshead speed of 5.0 mm/min and at an ambient temperature range 16°-21°C. A Hounsfield compression cage was used, in which the platens were lubricated (engine oil SAE 15-40) to minimize the friction between test samples and platens. Samples of 35mm high and 35mm in diameter were compressed 10-15 % of the initial height of the test sample, which was sufficient to obtain the results for characteristic stages of stress-strain curve. Compressive strength was calculated using the original cross-sectional area and compressive modulus was calculated from the tangent to the inflection point of the stress-strain curve.

4. Results and discussion

Data points obtained for dry foam density (of perlite-sodium silicate) versus applied compaction pressure are shown in Fig. 2.

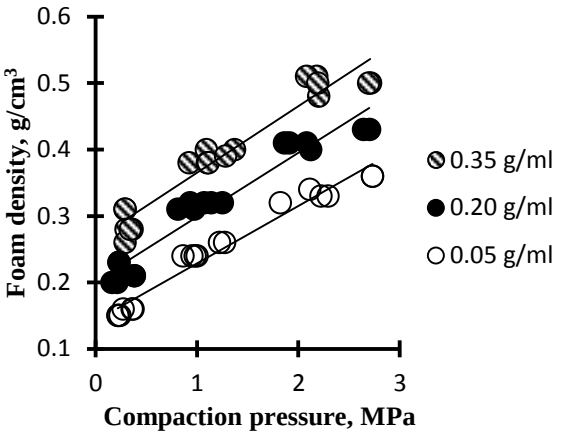

Fig. 2 Foam dry density versus applied compaction pressure for various binder contents - pure binder mass per unit diluted binder volume (g/ml).

For any given binder content, foam density tends to increase linearly with increasing compaction pressure for all the particle sizes (not shown). The Pearson correlation coefficients (r) for the combined plots in Fig. 2 were found to be 0.968, 0.967, and 0.983 for sodium silicate contents, 0.35 g/ml, 0.2 g/ml, and 0.05 g/ml respectively, indicating foam densities are not sensitive to particle size although there was a weak tendency that the smaller particle size the higher foam density, and a little higher compaction pressure is required for larger particle sizes to achieve a certain density. Also, it is found that a higher compaction pressure is required for a certain foam density as the binder content gets lower as expected. On the other hand, a reason why the initially smaller particles tend to have higher foam densities may be due to a higher binder retention for a higher volume of voids for smaller particles, as will be discussed below (Fig. 3), when there is not much difference in fraction of open pores between different particle sizes as indicated in Table 2.

Various volume fractions of perlite foams at a compaction ratio of 3.55-3.66 are plotted in Fig. 3 as a function of volume fraction of sodium silicate in diluted binder (VFSSB). The volume fraction of perlite in foam (VFPF) [Fig. 3 (a)] appears to be not sensitive to VFSSB but the larger particle size tends to have a higher VFPF probably because the fragmentation of larger particles during compaction did not leave much space for inter-particle voids.

Also, as expected, the volume fraction of voids in foam (VFSSF) [Fig. 3 (b)] decreases as VFSSB increases but without much sensitivity of particle size effect. On the

other hand, the volume fraction of SS in foam (VFSSF) [Fig. 3 (c)] is found to be highly proportional to VFSSB. The Pearson correlation coefficients (r) with a forced intercept at zero were found to be 0.987, 0.985, and 0.989 for Size 1-2, Size 2-3, and Size 3-4 respectively. The VFSSF displays some dependency on particle sizes as the VFSSB increases - the smaller particles size the higher VFSSF probably because of more void spaces for smaller particles.

Compressive strength and specific compressive strength of perlite-silicate foams are plotted as a function of dry foam density in Fig. 4. It is seen that they increase with increasing foam density as expected for all the different contents of sodium silicate in diluted binder. The least square lines and Pearson correlation coefficients (r) for compressive strength were found to be y = 8.3871x - 1.6972 with r = 0.982, y = 5.3022x - 0.7358 with r = 0.9409, and y = 3.0676x - 0.3445 with r = 0.9821 for respective sodium silicate contents of 0.35, 0.20, and 0.05 g/ml. Also, for specific compressive strength, y = 12.198x - 0.9403 with r = 0.952, y = 8.0803x + 0.2482 with r = 0.8485, and y = 6.3112x - 0.0268 with r = 0.9821 for respective sodium silicate contents of 0.35, 0.20, and 0.05 g/ml were found. Each data set for each least square line includes three different particle size ranges (Sizes 1-2, 2-3, and 3-4) appearing in a small cluster for similar foam density values in Fig. 4.

The high correlation coefficients indicate that the particle size effect on the compressive strength is insignificant. The slope of the least square line increases with increasing sodium silicate content. The foam density increases for each sodium silicate content is due to the increase of compaction ratio from 1.5 up to 3.5. Thus, the compressive strength is a function of two independent variables. Accordingly, an optimum combination of two independent variables may be necessary for practical manufacturing purposes. If we choose a value of 1 MPa for compressive strength with a density of 0.3 g/cm^3, there may be two different choices i.e. sodium silicate contents, 0.35 g/ml with a compaction ratio of about 1.5 (not shown on graph), and 0.20 g/ml with a compaction ratio of 2.5(not shown on graph). A gypsum compressive strength of 1MPa with a density of 0.87 g/cm^3 by Colak [19] may be a reference for comparison. Also, a specific compressive strength range of 0.8-5.37 MPa/(g/cm^3) in Fig. 4(b) may be compared with a range of 0.62 – 2.03 MPa/(g/cm^3) for gypsum by Colak [19], a range of 1.1- 3.1 MPa/(g/cm^3) for foam gypsum by Skujans et al [20] or 1-3.86 MPa/(g/cm^3) for gypsum/perlite composites by Vimmrova et al[17].

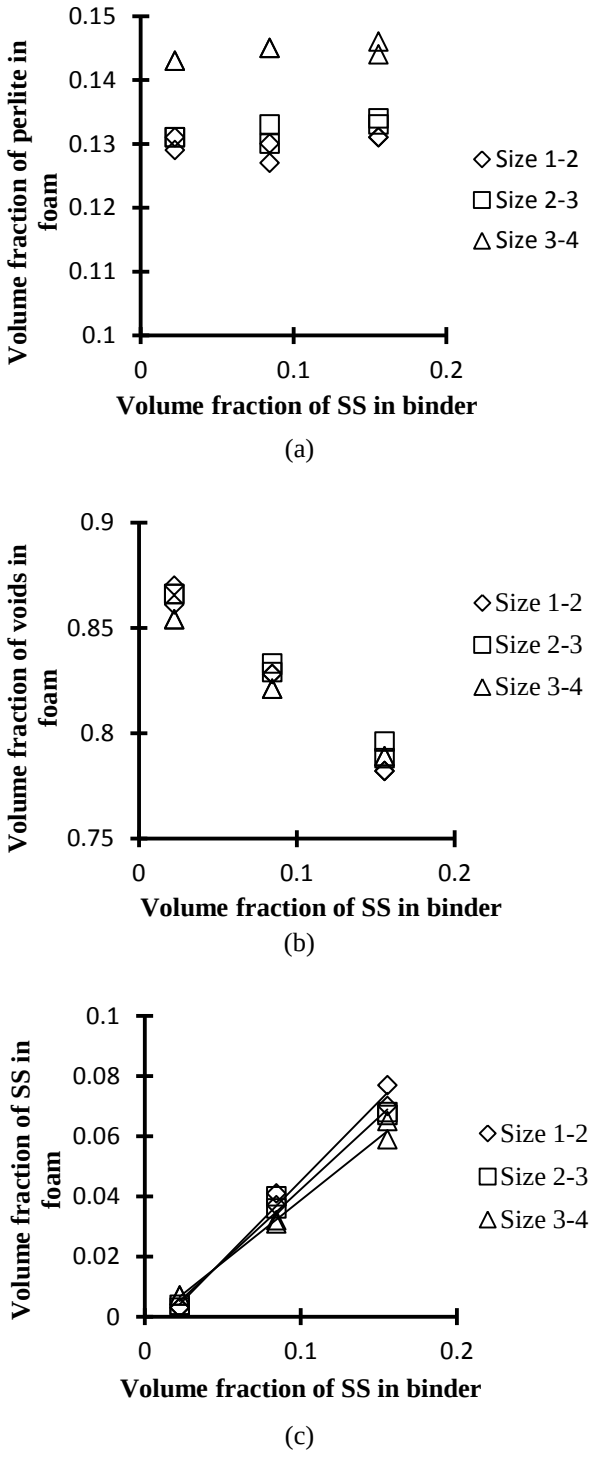

Fig. 3 Volume fractions of perlite-sodium silicate foam as a function of volume fraction of sodium silicate in diluted binder for compaction ratio c = 3.55-3.66: (a) volume fraction of perlite material excluding pores in foam; (b) volume fraction of voids in foam; and (c) volume fraction of sodium silicate in foam (Person correlation coefficients *r* with forced intercept at zero for 1-2 mm = 0.987, 2-2.8mm = 0.985, and 2.8 – 4 mm = 0.989.

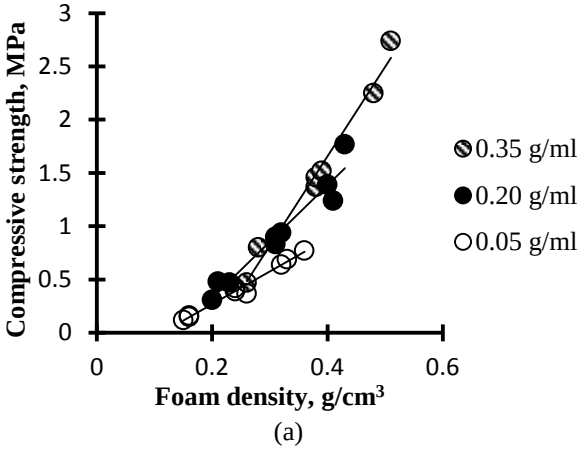

(a)

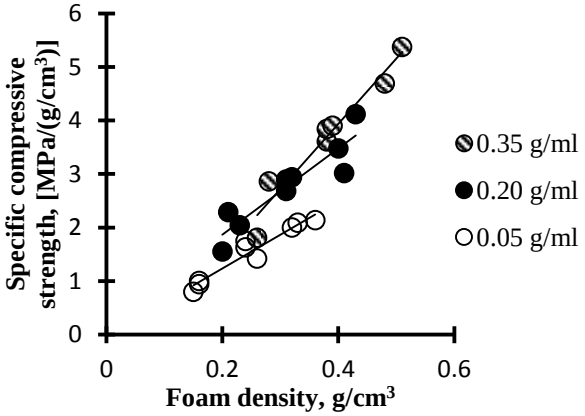

(b)

Fig. 4 (a) Compressive strength as a function of foam density for various sodium silicate contents. (b) Specific compressive strength as a function of foam density for various sodium silicate contents. [Compaction ratio was varied within a range of 1.5 -3.5 for all the sodium silicate conctents.]

Compressive modulus and specific compressive modulus for various binder contents (but without distinguishing particle sizes) are given in Fig. 5. As expected, they increase with increasing foam density, and more rapidly increase with increasing binder content despite relatively high scatters compared with compressive strengths.

5. Conclusion

Sodium silicate as binder has been characterised for developing perlite foams. Perlite foams have been manufactured with sodium silicate as new composites for a foam density range of 0.2 - 0.5 g/cm^3. Compressive strengths and foam densities can be optimized with two independent variables i.e. compaction ratio and binder content. One of practical milestones achieved appears to be a density of 0.3 g/cm^3 at a compressive strength of 1MPa without reinforcement.

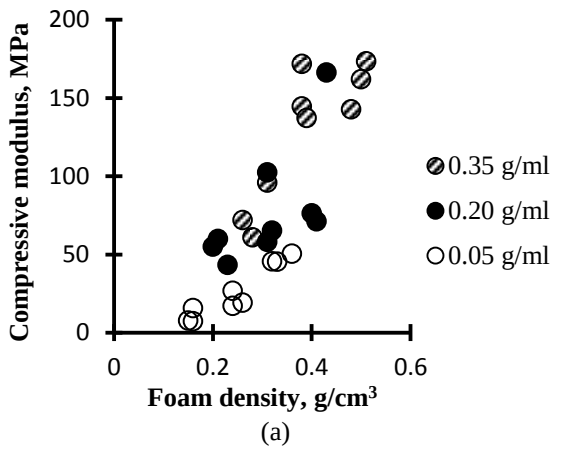

(a)

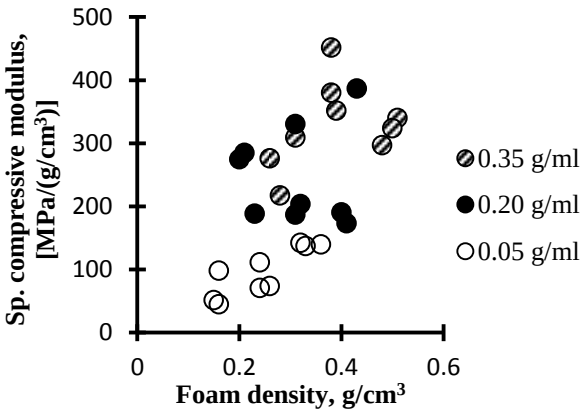

(b)

Fig. 5 (a) Compressive modulus and (b) specific compressive modulus as function of foam density.

Acknowledgments

The authors gratefully acknowledge the Newcastle University International Postgraduate Research Scholarship (NUIPRS) and The University of Newcastle Research Scholarship (UNRSC 50:50) provided for one of authors (MA).

REFERENCES

[1] Le Maitre RW, Streckeisen A, Zanettin B, Le Bas BM, Bonin B, Bateman P, Bellieni G, Dudek A, Efremova S, Keller J, J. Lamere, Sabine PA, Schmid R, Sorensen H, Woolley AR. Igneous Rocks: A Classification and Glossary of Terms, Recommendations of the International Union of Geological Sciences, *Subcommission of the Systematics of Igneous Rocks*. 2nd ed. West Nyack, NY: Cambridge University Press; 2002.

[2] M. Singh, M. Garg, Perlite-based building materials – a review of current applications, *Construction & Building Materials*, 5:75-81, 1991.

[3] N. Burriesci, A Carmelo, P. Antonucci, Physico-chemical characterization of perlite of various origins, *Materials Letters*, 3 (3): 103-110, 1985.

[4] SJ Johnstone, MG Johnstone, Minerals for the chemical and allied industries. 2nd ed. London: Chapman and Hall; 1961.

[5] J. S. Luongo, Strengthened, lightweight wallboard and method and apparatus for making the same, *US Patent No 6,251,979 B1*, 2001.
[6] S. Yilmazer, MB. Ozdeniz, The effect of moisture content on sound absorption of expanded perlite plates, *Building and Environment*; 40:311-318, 2005.
[7] W. P. Dube, L. L. Sparks, A. J. Slifka, Thermal conductivity of evacuated perlite at low temperatures as a function of load and load history. *Cryogenics*, 31: 3-6, 1991.
[8] T. Kendall, No sign of the bubble bursting – perlite uses and markets, *Industrial Minerals*, 51-59, June 2000.
[9] B. Rodsky, Building Material, *US Patent No 2,858,227*, 1958.
[10] B. Gray, Building material. *US Patent No. 4,042,406*, August 1977.
[11] P. B. Shepherd, R. L. Dolin, Lightweight building material board, *US Patent No. 5,256,222*, October 1993.
[12] J. H. Hill, Perlitic insulation board, *US Patent No. 4,126,512*, November 1978.
[13] H. Aglan, M. Morsy, A. Allie, F. Fouad, Evaluation of fiber reinforced nanostructured perlite-cementitious surface compounds for building skin applications, *Constr. Build. Mater.*, 23:138–45, 2009.
[14] J. Miscall, C. E. Rahr, Building board of fiber and asphalt coated perlite, *US Patent No 2,626,864*, 1953.
[15] N. Sherman, J. H. Cameron, Method of manufacturing improved mineral board, *US Patent No 4,297,311*, 1981.
[16] H. G. Seybold, Wallboard composition and method of making same, *US Patent No 2,705,198*, 1955.
[17] A. Vimmrova, M. Keppert, L. Svoboda, R. Cerny, Lightweight gypsum composites: Design strategies for multi-functionality, *Cement and Concrete Composites*, 33:84-89, 2011.
[18] I. B. Topcu, B. Isikdag, Effect of expanded perlite aggregate on the properties of lightweight concrete, *Journal of Materials Processing Technology*, 204: 34-38, 2008.
[19] A. Colak, Density and strength characteristics of foamed gypsum, *Cement and Concrete Composites*, 22:193-200, 2000.
[20] J. Skujans, A. Vulans, I. Uldis, A. Aboltins, Measurements of heat transfer of multi-layered wall construction with foam gypsum, *Applied Thermal Engineering*, 27: 1219–1224, 2007.
[21] D. Shastri, H. S. Kim, A new consolidation process for expanded perlite particles, *Construction and Building Materials,* 60:1-7, 2014.
[22] H. S. Kim, Method of forming syntactic foams, US Patent No 2014/0033953 A1, Feb 6, 2014.
[23] H. S. Kim, M. M. Islam, Syntactic foams as building materials consisting of inorganic hollow microspheres and starch binder, In: Cornejo DC, Haro JL, editors. *Building materials: properties and performance and applications*, Nova Publishers, p. 1–56 [chapter 1] 2009.
[24] H. S. Kim, P. Plubrai, Manufacturing and failure mechanisms of syntactic foam under compression. *Compos. A: Appl. Sci. Manuf.* , 35:1009–15, 2004.
[25] M. M. Islam, H. S. Kim, Novel syntactic foams made of ceramic hollow microspheres and starch – theory, structure and properties. *J. Mater. Sci.* 42:6123–32, 2007.
[26] M. M. Islam, H. S. Kim, Manufacture of syntactic foams: pre-mold processing. *Mater. Manuf. Processes*, 22:28–36, 2007.
[27] M. M. Islam, H. S. Kim, Manufacture of syntactic foams using starch as binder: post-mold processing, Mater. Manuf. Processes, 23:884–92, 2008.
[28] M. M. Islam, H. S. Kim, Pre-mould processing technique for syntactic foams: generalised modelling, theory and experiment, J. Mater. Process Technol., 211:708–16, 2011.
[29] Y. A. Owusu, Physical-chemical study of sodium silicate as a foundry sand binder, *Advances in Colloid and Interface Science*, 18: 57-91, 1982.

ICMIEE-PI-140119

Implementation of a waste-heat driven vapor absorption-based car air conditioning system

Md. Hasib Hossen [1,*], *Md. Towhidur Rahman* [2]
[1] B.Sc. in Mechanical Engineering, Khulna University of Engineering & Technology, Khulna-9203, BANGLADESH
[2] B.Sc. in Mechanical Engineering, Khulna University of Engineering & Technology, Khulna-9203, BANGLADESH

ABSTRACT
Waste-heat driven air conditioning system eliminates compressor and introduces absorber, pump, and generator. Thus, the consumption of electricity is reduced and waste-heat of exhaust gas is used as energy input. The most common refrigerant-absorbent pair in vapor absorption system is NH_3-water due to its availability, low cost, and high refrigerating effect. The drawback of using NH_3 as refrigerant is its toxicity, corrosiveness, and explosiveness. A small capacity vapor absorption system is first analyzed for its implementation in car air conditioning unit. Components are designed based on capacity 2 kW. The appropriate equations describing the working properties are specified. The cooling load, COP of the unit, variation of absorption rate with NH_3 weight percentage, variation of evaporator outlet temperature are examined. The experimentally obtained COP is 0.24 which is less than the designed COP 0.58. Absorber heat rejection increases with increasing absorber temperature.

Keywords: Vapor absorption system; Automobile air conditioning; Waste heat; COP.

1. Introduction

With the development of modern technology, the engineers have become more concerned with the further technological development of the existing systems and eliminate the drawbacks of those systems. This includes improvisation of performance and efficiency, reduction in cost, precision, energy savings, usage of renewable energy, and many more. In this context, some alternative systems of car air conditioning have been developed.

Today, almost all car air-conditioning systems are charged with R-134a. However, alternatives with lower GWP than R-134a are desirable. Some new systems are being developed in order to revitalize the use of ecologically safe refrigerants. For example, a system for car air-conditioning using CO_2 as the refrigerant has been developed by Lorentzen and Pettersen (1993). The testing of a laboratory prototype has shown that CO_2 is an acceptable refrigerant for car air-conditioners.

Due to the international attempt to find alternative energies, absorption refrigeration has become a prime system for many cooling applications. Where thermal energy is available the absorption refrigerator can very well substitute the vapor compression system. It is a well-known fact that a large amount of heat energy associated with the exhaust gases from an engine is wasted. A rough energy balance of the available energy in the combustion of fuel in a motor car engine shows that one third is converted into shaft work, one third is lost at the radiator and one third is wasted as heat at the exhaust system (Greene and Lucas, 1969). Even for a relative small car-engine, such as for the Nissan1400, 15 kW of heat energy can be utilized from the exhaust gas (Wang, 1997). This heat is enough to power an absorption refrigeration system to produce a refrigeration capacity of 5 kW.

* Corresponding author. Tel.: +88-01917303028
E-mail address: avro.hasib@gmail.com

This project is based on the construction of a car cooling system by using the heat of exhaust gas. Here, the prime vision is to use the waste energy of exhaust gas and to construct a cooling system by giving the heat input in the refrigeration cycle from that exhaust gas.

In the conventional cooling system of a car, usually vapor compression refrigeration cycle is used. Here, a certain amount of energy from engine crank shaft is used to run the compressor. On the other hand, a huge amount of heat energy is released to environment as waste heat. If that heat is used as energy input of cooling process, it is possible to save a huge amount of energy. Moreover, the use of vapor absorption refrigeration system instead of vapor compression system eliminates the compressor. As a result, load on engine decreases and efficiency of engine increases.

2. Working Procedure of a Single Effect Aqua-Ammonia Air Conditioning System of a Car

The Working principle is shown in fig.1

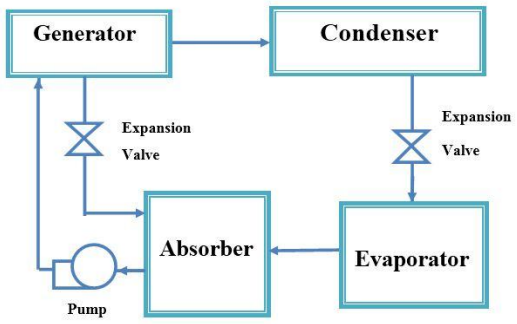

Fig.1.a) Block Diagram of Simplified Single-effect Aqua-Ammonia Absorption System

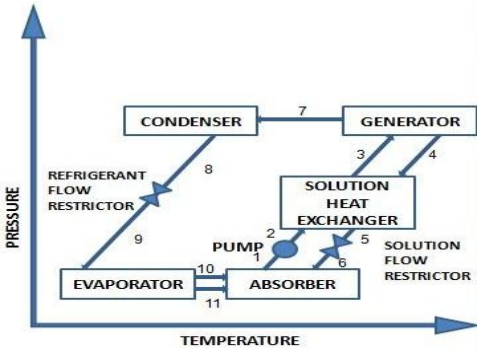

Fig.1.b) P-T diagram of Aqua-ammonia absorption cooling cycle.

A simple vapor absorption cycle eliminates compression. It uses absorber, pump, generator, analyzer, and reflux condensed in combined form as a replacement of compressor. Here, we will use aqua-ammonia system, where ammonia is used as refrigerant and water is used as absorber.

The low pressure refrigerant from the evaporator is absorbed by the liquid solution in the absorber. The pump receives low pressure liquid from the absorber and elevates the pressure. After that, the high pressure liquid solution is delivered to the generator. In the generator, heat from a high temperature source drives off the vapor that had been absorbed by the solution. The vapor refrigerant then enters the condenser. Remaining liquid solution returns to the absorber through a throttling valve whose purpose is to provide a pressure drop to maintain the pressure difference between the generator and absorber. In condenser, the vapor is cooled and condensed. There the heat is rejected in the atmosphere. After that the condensed refrigerant is passed through the expansion valve where the pressure is released. Then the low pressure refrigerant enters the evaporator. In evaporator, the refrigerant is evaporated by using the heat extracted from the refrigerated space. Thus, the space to be refrigerated gets cooled at a temperature lower than atmospheric temperature.

The main concern is to work with the function of a generator in vapor absorption refrigeration system. We have previously discussed that generator needs work input in the form of heat energy to separate refrigerant by evaporating it from the liquid absorbent solution. We are going to provide this heat input from the exhaust gas of car engine. From the exhaust pipe, it is possible to get an average temperature of 300◦c to 400◦c. By using an air to water heat exchanger, this heat can be extracted from exhaust gas and delivered to the generator. Thus, a huge amount of waste heat from the exhaust gas can be utilized in useful purpose.

3. Design of Air Conditioning System of a Car

Cooling load was calculated for a passenger car and according to cooling load calculation, the other portions of an air conditioning system are designed.

3.1 Calculation of cooling load of a Compact Car

Overall heat transfer coefficient: [1]

$$U_{glass} = \frac{1}{(\frac{1}{h_A} + \frac{dx_w}{k} + \frac{1}{h_B})}$$

Heat transfer through glass: (conduction)

$$Q_{glass} = A_{glass} \times U_{glass} \times ETD_{glass}$$

Heat transfer through body: (conduction)

$$Q_{body} = A_{body} \times U_{body} \times ETD_{body}$$

Heat transfer due to solar radiation: [1]

$$Q_{glass} = A_{glass} \times SHGF$$

Total sensible heat= Sum of all Sensible heats

Effective sensible heat=Sum of total sensible heat and heat gain due to occupancy

Heat gain due to infiltration: [1]

$$Q_{s,inf} = m_{inf} \times C_p \times (T_0 - T_i)$$

Effective latent heat=Sum of all latent heat, heat gain due to infiltration and heat gain due to occupancy

Grand total Heat, Q= Sum of Effective sensible heat and Effective Latent Heat

Obtained cooling load using the equations stated above is 4.393 KW.

If air locks are used in doors & windows, we can minimize filtration & by pass air considerably.

By using heat non-conducting leather or Rexene cover inside the body & seats, this heat can be considerably reduced. So, we will consider the cooling capacity of 2 KW.

3.2 Basic Assumptions and Design Parameters

To perform designing of equipment size and performance evaluation of a single-effect Aqua-ammonia absorption cooler basic assumptions are made. The basic assumptions are:

1. The steady state refrigerant is pure water.
2. There are no pressure changes except through the flow restrictors and the pump.
3. At points 1, 4, 8 and 11, there is only saturated liquid.
4. At point 10 there is only saturated vapor.
5. The pump is isentropic.
6. There are no jacket heat losses.
7. The capacity of the system is 2kW.

Some design parameters have been set up as per design requirement. They are stated below:

Parameter	Symbol	Value
Capacity	Q_e	2 kW
Generator solution exit temperature	T_4	90 ^{0}C
Weak solution mass fraction	X_1	55% NH_3
Strong solution mass fraction	X_4	60% NH_3
Generator vapor exit temperature	T_7	85 ^{0}C

3.3 Evaporator analysis

Since, in the evaporator, the refrigerant is saturated water vapor and temperature (T_{10}) is assumed 10 ^{0}C, the saturation pressure and enthalpy are calculated from curve fits [5].

Pressure and Enthalpy are determined by using these equations: [6]

$$P = 0.000000000002T^6 - 0.000000003T^5 + 0.0000002T^4 + 0.00003T^3 + 0.0014T^2 + 0.0444T$$

$$h = -0.00125397T^2 + 1.88060937T + 2500.559$$

Aqua-ammonia solution and refrigerant pressure and temperatures are obtained from these equations: [6]

$$LogP = C + \frac{D}{(T_{ref} + 273)} + \frac{E}{(T_{ref} + 273)^2}$$

$$T_{sol} = T_{ref}\Sigma A + \Sigma B$$

Now, ΣA and ΣB are obtained from following equations:

$$\Sigma A = A_0 X^0 + A_1 X^1 + A_2 X^2 + A_3 X^3$$
$$\Sigma B = B_0 X^0 + B_1 X^1 + B_2 X^2 + B_3 X^3$$

For range 45% < X < 70% NH_3
(Mass fraction, X = 60%)
A_0 = - 2.00755; A_1 = 0.16976;
A_2 = - 0.003133362; A_3 = 0.0000197668
B_0 = 124.937; B_1 = - 7.71649;
B_2 = 0.152286; B_3 = -0.0007959

Enthalpy of NH_3-water solution is obtained from following solution: [7]

$$h = \Sigma A + T\Sigma B + T^2\Sigma C$$

Now, ΣA ΣB, and ΣC are obtained from following equations:

$$\Sigma A = A_0 X^0 + A_1 X^1 + A_2 X^2 + A_3 X^3 + A_4 X^4$$
$$\Sigma B = B_0 X^0 + B_1 X^1 + B_2 X^2 + B_3 X^3 + B_4 X^4$$
$$\Sigma C = C_1 X^1 + C_2 X^2 + C_3 X^3 + C_4 X^4$$

Where, these values are obtained for specific range of mass fraction:

A_0 = - 2024.33; A_1 = 163.309;
A_2 = -4.88161; A_3 = 0.06302948;
A_4 = -0.0002913704.
B_0 = 18.2829; B_1 = -1.1691757; B_2 = 0.03248041;
B_3 = - 0.0004034184, B_4 = 0.0000018520569.
C_0 = -0.037008214; C_1 = 0.03248041;
C_2 = -0.000081313015; C_3 = 0.00000099116628;
C_4 = -0.0000000044441207

Mass balance on evaporator is as follows:
$m_9 = m_{10} + m_{11}$

Energy balance on evaporator is as follows:

$Q_e = m_{10} h_{10} + m_{11}h_{11} - m_9h_9$

From these two equations the value of m_9, m_{10}, and m_{11} can be obtained.

3.4 Absorber analysis

Since the values of m_{10}, m_{11} are known, mass balance around the absorber can be stated as bellows:

$$m_1 = m_{10} + m_{11} + m_6$$
$$x_1m_1 = x_6m_6$$

From these two equations the value of m_1 and m_6 can be obtained.

The temperature and pressure around the absorber can be calculated by using the following equations:

$$LogP = C + \frac{D}{(T_{ref} + 273)} + \frac{E}{(T_{ref} + 273)^2}$$
$$T_{sol} = T_{ref}\Sigma A + \Sigma B$$

Here,
$\Sigma A = A_0 X^0 + A_1 X^1 + A_2 X^2 + A_3 X^3$
$\Sigma B = B_0 X^0 + B_1 X^1 + B_2 X^2 + B_3 X^3$
A_0 = - 2.00755; A_1 = 0.16976;
A_2 = - 0.003133362; A_3 = 0.0000197668
B_0 = 124.937; B_1 = - 7.71649;
B_2 = 0.152286; B_3 = - 0.0007959
C = 7.05; D = -1596.49; E = -104095.5

The equation of enthalpy is as bellows:

$$h = \Sigma A + T\Sigma B + T^2\Sigma C$$

Here,
$\Sigma A = A_0 X^0 + A_1 X^1 + A_2 X^2 + A_3 X^3 + A_4 X^4$
$\Sigma B = B_0 X^0 + B_1 X^1 + B_2 X^2 + B_3 X^3 + B_4 X^4$
$\Sigma C = C_1 X^1 + C_2 X^2 + C_3 X^3 + C_4 X^4$
A_0 = - 2024.33; A_1 = 163.309;
A_2 = -4.88161; A_3 = 0.06302948; A_4 = -0.0002913704.

B_0 = 18.2829; B_1 = -1.1691757;
B_2 = 0.03248041; B_3 = - 0.0004034184;
B_4 = 0.0000018520569.
C_0 = -0.037008214; C_1 = 0.03248041;
C_2 = -0.000081313015; C_3 = 0.00000099116628,
C_4 = -0.0000000044441207.

The enthalpy at point 5 is not known but can be determined from the energy balance.

$$m_2 h_2 + m_4 h_4 = m_3 h_3 + m_5 h_5$$

For, T = 34.9 ^{0}C, X_0 = 55/100 = 0.55, Density of NH_3 solution is obtained as: [7]

$$\rho = 1145.36 + 470.84X_0 + 1374.79X_0^2 - (0.333393 + 0.571749X_0)(273 + T)$$

Since, all variables are known, the pump power can be calculated as:

$$w = m_1 v_1 (p_2 - p_1)$$

Energy balance on the absorber is stated by the following equation:

$$Q_a = m_{10} h_{10} + m_{11} h_{11} + m_6 h_6 - m_1 h_1$$

3.5 Generator analysis
The heat input to the generator is determined from energy balance equations:

$$Q_g = m_4 h_4 + m_7 h_7 - m_3 h_3$$

$$m_7 = m_3 - m_4$$

3.6 Condenser analysis
The condenser heat can be determined from an energy balance equation given below:

$$Q_c = m_7 (h_7 - h_8)$$

3.7 Coefficient of performance
The COP is defined as follows:

$$COP = \frac{Q_e}{Q_g} = \frac{2}{3.45} = 0.58$$

According to the previous calculations Energy flows at various component of the system are shown in table below:

Description	Symbol	kW
Capacity	Q_e	2
Pump work	W	0.067
Absorber heat rejected	Q_a	2.8
Heat input to the generator	Q_g	3.45
Condenser heat rejected	Q_c	2.62

4. Design of Heat Exchangers
In single-pass heat exchangers, the temperature difference ΔT between the hot and the cold fluids is not constant but it varies with distance along the heat exchanger. In the heat transfer analysis, it is convenient to establish a mean temperature difference (ΔT_m) between the hot and cold fluids such that the total heat transfer rate Q between the fluids can be determined from the following expression: [3]

$$Q = AU\Delta T_m$$

Mean temperature difference is calculated by using the equation stated below:

$$\Delta T_m = F\Delta T_{ln} = F\left(\frac{\Delta T_0 - \Delta T_L}{\ln(\Delta T_0 / \Delta T_L)}\right)$$

The overall heat transfer coefficient (U) based on the outside surface of the tube is defined as [3]

$$U = \frac{1}{(D_0/D_i)(1/h_i) + (D_0/D_i)F_i + (1/2k)D_0 ln\,(D_0/D_i) + F_0 + 1/h_0}$$

For the design of the heat exchangers, the cooling water inlet and outlet temperatures are assumed. The cooling water inlet temperature depends exclusively on the available source of water, which may be a cooling tower or a well.

4.1 Absorber Design
For this design, the solution film can flow downward either on horizontal or on vertical tubes. The design of the horizontal tubes for the absorber, although theoretically well studied, presents a great problem with the shell tightness because of the large length of welds. In the case of this study the water vapor produced in the evaporator is absorbed in the flow of the NH_3-water solution and is condensing on the heat exchanger tubes. The design of the heat exchanger therefore requires values for heat and mass transfer coefficients.

The fig.2 shows a model of absorber that has been used in car air conditioning unit.

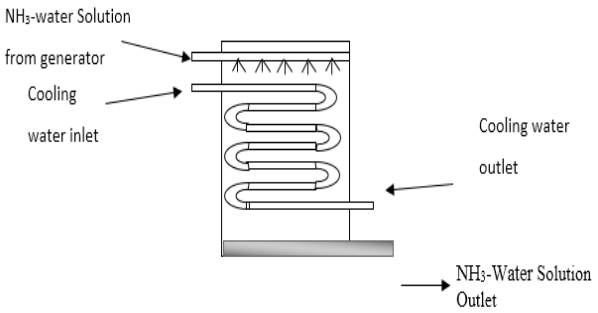

Fig.2: Schematic representation of an absorber

Design parameters of an absorber are stated in table below:

Parameter	Value
Tube dimension	Tube outside diameter D_o = 12.7 mm and inside diameter D_i =11.7 mm
Cooling water inlet temperature	25°C
Cooling water outlet temperature	26°C
Mass flow rate of cooling water (m)	0.21 kg/s
Absorber load *(Q_a)*	2.8kW
Solution cooling	From 44.6°C to 34.9°C
Absorber pressure	1.227kPa
Inlet solution mass flow rate	0.0117975 kg/s

The independent variables, which affect the problem, are solution mass flow rate, solution inlet concentration, and absorber pressure and wall temperature. The data are correlated with the introduction of the "absorption percentage (A_p), defined as:

$$A_p = \frac{C_{in} - C_{out}}{C_{in} - C_{eq}} \times 100$$

Determination of the equilibrium concentration, C_{eq} requires the solution of the following set of expressions:

$$A = -2.00755 + 0.16976\,X - 3.133362 \times .001\,X^2 + 1.97668 \times 0.00001\,X^3$$

$$B = 321.128 - 19.322\,X + 0.374382\,X^2 - 2.0637 \times .001\,X^3$$

C = 6.21147
D = -2886.373

$$T' = (-2\,E / [D + (D^2 - 4\,E\,(C - \log(P / 6894.8))]^{.5}) - 459.72$$

$$T_W = (5 / 9) * (AT' + B - 32)$$

E = -337269.46

The above set of expressions requires an iterative type of solution to find C_{eq}, given T_W and P. In the case of this study T_W=31 °C and P=1227 Pa, therefore C_{eq}= 0.52 and from Eq. stated above, A_P=62.5. A_P is correlated to the length of plate (L) by the expression:

$$L = am^b$$

Where, $a = -132\left(\frac{\ln(100 - A_p)}{86}\right)$, b = 1.33

An iterative solution gives, m=0.0292 kg/m-s corresponding to the area of 5.4 m length pipe.
The next step is to check the area of pipes needed to cool the solution to the required level.
Patnaik *et al.* (1993), suggest that Wilke's correlation, valid for constant heat flux wall with progressively decreasing difference from isothermal wall outside the entrance region, can be used for the falling film.
It is assumed that the flow is fully developed in a wavy, laminar regime and that the bulk solution temperature profile is linear with respect to the transverse coordinate (Patnaik *et al.,* 1993). Wilke's correlation is:

$$h_s = \frac{k_s}{\delta}(0.29(Re_s)^{0.53} Pr_s^{0.344})$$

The film thickness δ is given by:

$$\delta = \left(\frac{3\mu\Gamma}{\rho^2 g}\right)^{1/3}$$

And the solution Reynolds number (Re_s) for the tube *is:*

$Re_s = 4\Gamma/\mu$

4.2 Generator Design

The generator provides sensible heat and latent heat of vaporization. The sensible heat raises the inlet stream temperature up to the saturation temperature. This amount of heat, typical in practice, is 13% of the total heat required [6]. The heat of vaporization consists of the heat of vaporization of pure water and the latent heat of mixing of the liquid solution.

Design parameters for generator design are stated in table below:

Parameter	Value
Tube dimension	Tube outside diameter D_o = 9.53 mm and inside diameter D_i =8.5 mm
Generator pressure	9.66kPa
Generator solution	Entering: 60% NH_3 at 65°C Leaving: 55% NH_3 at 90°C
Generator water vapor mass flow rate (m)	0.00107 kg/s
Generator load *(Q_g)*	3.45kW

5. Construction

After designing all components, the construction is done according to the figure below. Stainless Steel tubes and galvanized iron plates are used for constructing these components.

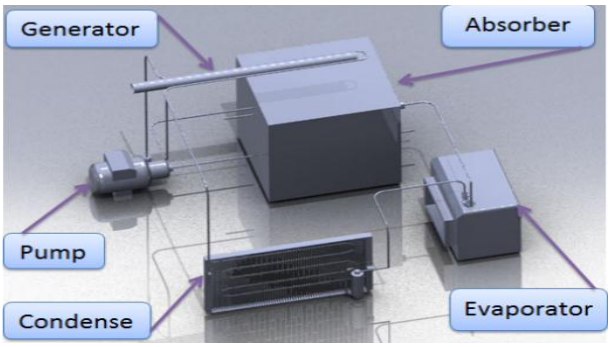

Fig.3: Schemetic Diagram of Vapor Absorption based Cooling System of a Car

6. Result and Conclusion

6.1 Inlet outlet temperature of various components

Heat Exchangers	Cooling/Heating water temperature (°C)	
	Entering	Leaving
Generator	-	59
Condenser	-	44
Evaporator	30	25
Absorber	25	26

6.2 COP analysis

The equation for COP calculation is: [1]

$$COP = \frac{Q_e}{Q_g}$$

$$Q_e = mC_p\Delta T = 0.84\ kW$$

$$Q_g = 3.45\ kW$$

So, COP= 0.24 which is less than the COP obtained in design before. The actual overall heat transfer coefficient of stainless steel tubes are less than the ideal heat transfer coefficient. This is because of rust on the upper surface of tubes. Another reason is the less concentration of ammonia in absorber than designed concentration.

6.3 Conclusion

1. A car cooling system which uses exhaust gas as heating source is designed based on some correlations and formulas involving vapor absorption cycle.
2. Each component is constructed with locally available materials.
3. COP of the cooling unit is measured and compared with design COP.
4. The COP lower than the designed COP.
5. Some performance test is done to evaluate performance of the system.
6. Cooling unit offers a better environment.
7. A Fair amount of waste energy is used for their operation.

NOMENCLATURE

Q_e	:	Capacity
$SHGF$	:	Solar Heat Gain Factor
ETD	:	Effective Temperature Difference
T_{10}	:	Evaporator temperature, °C
T_4	:	Generator solution exit temperature, °C
X_1	:	Weak solution mass fraction
X_4	:	Strong solution mass fraction
T_3	:	Heat exchanger exit temperature, °C
$T7$	:	Generator vapor exit temperature, °C
ρ	:	Density, kg/m^3
m_{11}	:	Liquid carryover from evaporator
P	:	Saturation pressure, kPa
h	:	Enthalpy
W	:	Pump work, kJ
Q_a	:	Absorber heat rejected, kJ
Q_g	:	Heat input to the generator, kJ
Q	:	Heat transfer rate, kJ/sec
ΔTm	:	Mean temperature difference
A	:	Total heat transfer area, m^2
U	:	Overall heat transfer coefficient, W/m^2-°C
ΔT_{ln}	:	Logarithmic mean temperature difference
Re	:	Reynolds number
Pr	:	Prandtl number
δ	:	Film thickness
F	:	Correction Factor for Heat Exchanger

REFERENCES

[1] C. P. Arora, “Refrigeration and Air Conditioning”, McGraw-Hill Publishing Company Limited, 2000, 1981.

[2] “ASHRAE, Handbook of Fundamentals”, Atlanta, 1997.

[3] Ozisik, M., “Heat Transfer-A Basic Approach”, McGraw-Hill Book Company, 1985. ISBN 0- 07-066460-9

[4] Herold, K.E. and Klein, S.A.; “Absorption Chillers and Heat Pumps”, CRC Press, Inc. USA, 1996: ISBN 0-8493-9427-9.

[5] Park Y.M, Sonntag R.E., “Thermodynamic properties of ammonia-water mixtures: a generalized equation of state approach”, ASHRAE Trans 1990; 96: 150–9.

[6] Fatouh M, Murthy SS., “Comparison of R22-absorbent pairs for vapor absorption heat transformers based on P-T-X-H data”, Heat Recovery Systems and CHP, 1993; 13(1):33–48.

[7] Kang Y.T., Christensen R.N., “Transient analysis and design model of LiBr-H2O absorber with rotating drums”, ASHRAE Trans 1995; 101: 1163–74.

ICMIEE-PI-140120

EFFECTS OF WELDING PARAMETERS ON BEAD GEOMETRY OF STAINLESS STEEL WELDING BY MIG

Lipika Nath [1*], *Md.Fazlay Rabbi* [1], *Naseem Ahmed* [1]

[1] Department of Mechanical Engineering, Khulna University of Engineering & Technology, Khulna-9203, BANGLADESH

ABSTRACT

Welding is a process of joining two materials. It is more economical and is much faster process compared to both casting and riveting. Nowadays Gas Metal Arc welding process (GMAW) has become the most commonly used welding technique throughout the industrial world. In this study the effect of MIG welding parameters on the weld bead geometry of stainless steel specimen of dimension 127:25:25 mm has been investigated. In this present investigation AWS E6013 with diameter of 1.0 mm was used as electrodes. Argon was employed for shielding purposes. The welding current, welding speed, gas flow rate were taken as welding parameters. The bead height, bead width, depth of penetration and HAZ were measured for each specimen after the etching operation. All the data included in this work gave a graphical representation which showed that a variation in the welding parameters varied with the weld characteristics such as bead width, bead height, HAZ etc.

Keywords: Metal Inert Gas Welding (MIG), Heat Affected Zone (HAZ), Welding parameter, Bead geometry

1. Introduction

Welding may be defined as the process of joining two pieces of metal so that bonding accompanied by appropriate inter atomic penetration takes place at their original boundary surfaces. Welding is carried out by the use of heat or pressure or both and with or without added metal.Welding joins metal by melting and fusing (i) The base metals being joined and ii) the filler metal applied. Most welding involves ferrous based metals such as steel and stainless steel. Welding covers a temp range of 1500^0-3000^0 F (800^0 C- 1635^0 C) weld joints are usually stronger or as strong as the base metal being joined.Various welding methods are: Shielded Metal Arc Welding (SMAW),Tungsten Inert Gas Welding (TIG),Plasma Arc Welding (PAW),Gas Metal Arc Welding (GMAW),Electro Slag Welding (ESW),Submerged Arc Welding etc. Nowadays Gas Metal Arc welding process (GMAW) has been the most commonly used welding technique throughout the industrial world. Gas metal arc welding (GMAW) is formerly known as MIG (Metal Inert Gas) welding, where the arc is maintained between the work piece and an automatically fed bare wire electrode. GMAW uses a welding torch, a electric power source, shielding gas & a wire pool with wire drive control. The welding process is very simple. GMAW process can be used to weld thicker metal plates with high productivity. The shielding gas is used to protect the weld pool from oxidation. The shielding gas used is either inert gas or carbon dioxide. There is no frequent change of electrodes as with the shielded metal arc process. No flux is required and no slag forms over the weld. Thus multi pass welds can be made without the need for intermediate cleaning. The process can be readily automated. A reverse polarity dc arc is generally used because if it's deep penetration, spray transfer and ability to produce smooth welds with good profile.

The quality of weld is determined by the weld bead geometry characteristics (also referred as physical parameters in this study); i.e the weld bead width, weld bead penetration, weld reinforcement height, weld left leg length , weld right leg length. This weld bead geometry characteristics is a function of input variables (also referred as control parameters in this study) which are welding current, welding voltage, welding speed, wire tip distance, weld joint position, wire diameter, shielding gas composition, gas flow rate, material composition and material thickness. These control parameters affect the quality of the weld.

Stainless steel is not a single specific material, but the name given to a group of corrosion-resistant steels. Stainless steels are those steels that have a chromium content of at least 11%. Varying additions of nickel, molybdenum, nitrogen, copper, manganese, wolfram, titanium, niobium, cerium and other elements may also be present. Interest in nitrogen as an alloying element is growing and many stainless steel grades, both austenitic and duplex, containing relatively large amounts of nitrogen, have come onto the market during the last 10 years. It is well established that nitrogen, in combination with molybdenum, greatly improves resistance to pitting corrosion. Nitrogen also increases the yield strength by solution hardening on the austenite. Since mechanical properties and behavior in service of each type of stainless steel depend upon its composition and microstructure, it is vital to consider the various properties of each grade before selecting one for a particular application.

* Corresponding author. Tel.: +88-01961176429
E-mail address: lipikanath029@gmail.com

2. Selection Of material:

Austenitic is the most widely used type of stainless steel. It has a nickel content of at least of 7%, which makes the steel structure fully austenitic and gives it ductility, a large scale of service temperature, non-magnetic properties and good weld ability. Austenitic grades are those alloys which are commonly in use for stainless applications. The austenitic grades are not magnetic. The most common austenitic alloys are iron-chromium-nickel steels and are widely known as the 300 series. The austenitic stainless steels, because of their high chromium and nickel content, are the most corrosion resistant of the stainless group providing unusually fine mechanical properties. They cannot be hardened by heat treatment, but can be hardened significantly by cold-working.

Table 1:Material Composition of Austenitic Stainless Steel

Component	W%
C	Max 0.8
Cr	18-20
Fe	66.345-74
Mn	Max 2
Ni	8-10.5
P	Max .045
Si	Max 1

As the stainless steel is classified in different categories like austenitic, ferritic, martens tic etc., from this we have chosen austenitic stainless steel (304) because of its low cost, easy availability in the market.

3. Experimental Details

3.1 Experimental Procedure:

Firstly,High Strength Low Alloy Steel (HSLA Steel) of grade type :IS 304 is taken as the base material.The dimension of each specimen are 127mm × 25 mm× 25 mm Welding electrode confirming to AWS E6013 with diameter 1.0 mm is used to lay down the weld beads.Argon+.08% Carbon Dioxide is used for shielding purposes in this welding process. The primary purpose of shielding gas is to prevent exposure of the molten weld pool to oxygen, nitrogen and hydrogen contained in the air atmosphere. The reaction of these elements with the weld pool can create a variety of problems, including porosity (holes within the weld bead) and excessive spatter.Argon +.08% Carbon Dioxide can further stabilize the arc,improve the fluidity and also improve the quality the weld deposit.A step down transformer is used as power source with current capacity 150-350 A and 20-80 volt.The plates are cleaned chemically to remove the oxide layer and any other source of hydrogen before welding.before igniting the arc gas and water flow is checked .Welding is done in random manner to avoid systematic error.Welding is done for 4 passes with respect to welding current,welding speed and gas flow rate.After completing the welding on the plates,they are allowed to cool.Then the welded plates are divided into several parts by using power saw for various inspection and testings.All the divided welded plates are grinded by a grinding machine. The surfaces of the plates are filed smoothly with the help of a file. Then the surfaces are more polished by using three sets of emery paper-first 220 grade, then 320 grade and finally 400 grade. The welded plates are further polished in the polishing machine which gives a mirror like polished surface. Next the region of the welded metal is etched by using eacng reagent.Two types of eachants are used. The composition of the eachants are given below,

Type 1 Eachant-
1.Ferric Chloride-8.5 gm
2.Cupric Chloride-2.4 gm
3.alcohol-122 ml
4.Hydro Chloric Acid-122 ml
5.Nitric Acid-225 ml.

Type 2 Eachant-
1.Cupric Chloride-1.2 gm
2.Hydro Chloric Acid-20ml
3.Alcohol-225 ml

Fig 1:Specimen after MIG welding.

Within a minute or more a contour was formed on the welded metal surface which gives the weld bead.Then the bead height, bead width, depth of penetration was measured with the help of digital slide calipers.

3.2 Conduct of the Experiment

The experiment is done on High Strength Low Alloy Steel of grade type:IS 304 and the dimension of each specimen is 127mm × 25 mm× 25 mm

Serial No	Welding current	Bead width (mm)	Bead height (mm)	Depth of penetration (mm)	Depth of HAZ (mm)
01	220	9.0	3.5	2.2	1.2
02	240	9.1	4.0	2.3	1.5
03	260	10	4.2	2.4	1.7
04	280	10	4.8	2.4	1.8

Table 1: Measured experimental data when welding current is taken as variable

Serial no	Gas Flow Rate (lpm)	Bead width (mm)	Bead height (mm)	Depth of penetration (mm)	Depth of HAZ (mm)
9	12	10.5	4.6	1.2	1.0
10	14	10.2	4.7	1.2	1.0
11	16	10.0	4.8	1.2	1.0
12	18	9.5	5.0	1.2	1.0

Table 2: Measured experimental data when gas flow is taken as variable

Serial no	Travel Speed (mm/min)	Bead width (mm)	Bead height (mm)	Depth of penetration (mm)	Depth of HAZ (mm)
05	140	10	4.5	2.6	1.3
06	142	9.6	3.7	2.5	1.2
07	145	9.5	3.5	2.5	1.2
08	150	9.0	3.4	2.5	1.1

Table 3: Measured experimental data when welding speed is taken as variable

4. Results and Discussion:

Effect of welding current

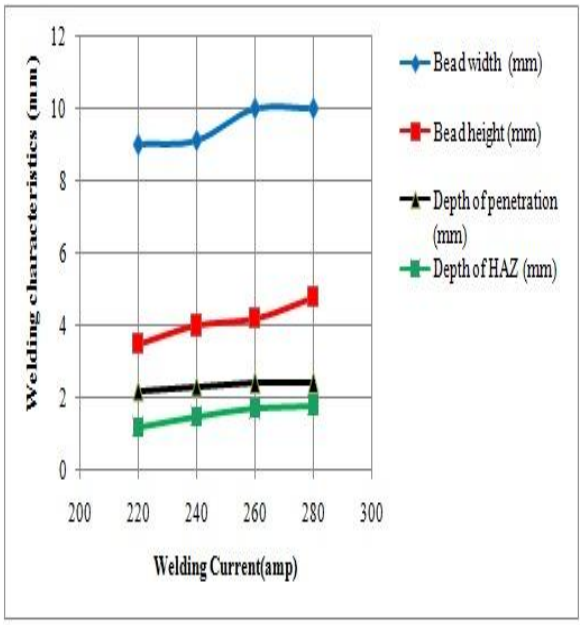

Fig 2:Welding current vs Welding characteristics

Bead width, depth of penetration and HAZ increase gradually, but bead height decreases gradually with the increase of welding current.

From the relation $H=I^2RT$: it is seen that current is proportional to the heat input. Thus a variation in the current makes a variation in the heat input of the welding process. The graph is shown above states the changes in various welding parameters with the current as well as the heat input.

Increase in current give rise to enhanced line power per unit length of weld bead and higher current density,causing larger volume of base material to melt and hence deeper penetration. As current increases the temperature,the heat content of the droplet also increases,which results in more heat being transferred to the base material.Increase in current also increases the momentum of droplets,which on striking the weld pool causes a deeper penetration.

Effect of welding speed

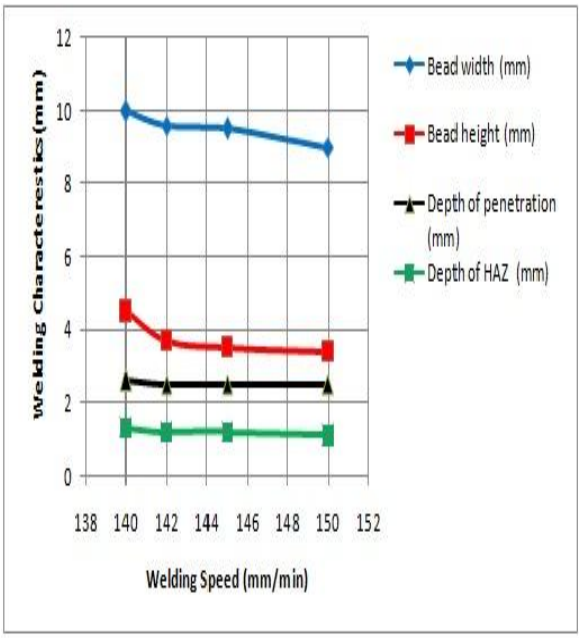

Fig 3:Welding speed vs Welding characteristics

Bead width and bead height decreases gradually but depth of penetration remains almost constant with increase of welding speed. Welding speed is not showing any significant effect on penetration. At any current, bead width is inversely proportional to the welding speed . With high welding speed, the excess weld metal builds up due to rapid cooling of the weld pool edges and results in increase of height and simultaneously width decreases. Decrease in height could be due to the fact that weld pool size is affected by cooling rate, which decreases with increasing the welding current or by decreasing the travel speed. Thus at higher welding speed, size of the weld pool and metal deposition rate will decrease i.e. width, and height will decrease.

Effect of Gas flow rate

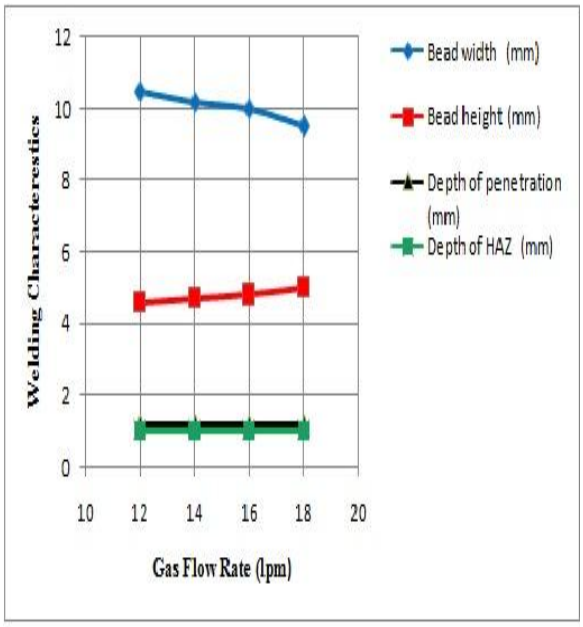

Fig 4:Gas flow rate vs Welding characteristics

Bead width decreases whereas bead height increases gradually. But depth of penetration remains constant.
Gas flow rate shows no significant effect on both penetrations. The bead height is increasing, which may be due to the reason that the increased flow rate is providing space to increase. As the velocity of gas is increasing it is imparting low pressure on the bead, resulting in increase of height.

5. Conclusions:

From the above investigation on stainless steel of dimension 127×25×25 mm ,the following conclusions have been drawn :

1. When welding current is increased, bead width and depth of penetration increase gradually,but bead height decreases gradually.HAZ also increases with the increase of current.

2. When travel speed is increased, bead width and height decrease gradually but depth of penetration remains almost constant.

3. When gas flow rate is increased, bead width decreases where as bead height increases gradually. But depth of penetration remains constant.

REFERENCES

[1] Black J.T. "*Materials & processes in Manufacturing*"**,** 8th edition, Prentice, Hall of India, New Delhi-11001

[2] Jain,R.K, "*Production Technology*", 5th edition, Khanna Publishers, Delhi.

[3] Schmid,S.R, *"Manufacturing Engineering & Technology",*4th , Pearson Education

[4] Narang,G.B.S *"Materials and Metallurgy",* 6th edition, Khanna Publishers, Delhi-110006

[5] Avner,S.H, "*Introduction to Physical Metallurgy",*2nd edition, Tata Mcgraw-hill

[6] Bonollo F, Tiziani A, Tovo T, Volpone LM, "*Super austenitic stainless steel: the microstructure and fatigue strength a welded joint*",*Welding International*, Vol. 18, No. 1, 2004, pp. 24-30.

[7] Arka Sen1, Dr.Sudip Mukherjee, **"***An Experimental Study to Predict Optimum Weld Bead Geometry through Effect of Control Parameters for Gas Metal Arc Welding Process in Low Caron Mild Steel"***,** International Journal of Modern Engineering Research (IJMER), Vol. 3, Issue. 4, Jul - Aug. 2013 pp-2572-2576.

[8] P.Sathiya, S.Aravindan, P.M. Ajith, B.Arivazhagan,A. Noorul Ha, "*Microstructural characteristics on bead on plate welding of AISI 904 L super austenitic stainless steel using Gas metal arc welding process"*, International Journal of Engineering, Science and Technology Vol. 2, No. 6, 2010, pp. 189-199.

ICMIEE-PI-140123

Numerical Investigation of fluid flow Over a Lid-driven Square Cavity

Mohammad A.Hossain [1], Mominul Huq [2]

[1] Department of Mechanical Engineering, The University of Texas at El Paso, El Paso, TX, USA
[2] Department of Mechanical and Production Engineering, Ahsanullah University of Science and Technology, Dhaka, BANGLADESH

ABSTRACT
This work is focused on numeric investigation of fluid flow over a lid-driven cavity. A square cavity is chosen to do the simulation. The simulation is done for both laminar, transient and turbulent flow for both 2D and 3D case. Reynolds number is considered between $1 < Re < 7500$. First the mesh independence test is done by different mesh size. Five different quadratic mesh configuration is used for mesh independence test. Finally a 200*200 cell elements are used for the final simulation. Commercial software ANSYS Fluent is used for the simulation. A pressured based solver is used with QUICK solution schema to find the horizontal velocity components at different Reynolds number. The results are compared with available published data. There are significant agreement with the experimental data. Streamlines at different Reynolds number, position of the primary and secondary vortex are compared with the experimental data and presented.

Keywords: lid driven cavity, vortex, CFD

1. Introduction

Flow through a lid driven cavity is one of the classic fluid mechanics problem used for validation and verification of fluid flow models. Due to the simplicity of the geometry and complex flow field, this problem has been used for verification of 2D Navier Stokes equation as it is very difficult to capture the flow phenomena near the singular points near the corner of the cavity [1-2]. The cavity analysis is used for material process, metal casting, designing journal bearing and many more.

Many researcher have done significant amount of work on cavity flow. Ghia el al [3] have done the detail analysis of cavity flow. N.A.C Sidik et al [4] considered the cubic interpolated pseudo particle method validate their results with shear driven flow in shallow cavity. There have been some works devoted to the issue of heat transfer in the shear driven cavity. Manca et al [5] presented a numerical analysis of laminar mixed convection in an open cavity with a heated wall bounded by a horizontally insulated plate. Results were reported for Reynolds numbers from 100 to 1000 and aspect ratio in the ranges from 0.1 to 1.5. They presented that the maximum decrease in temperature was occurred at higher Reynolds. The effect of the ratio of channel height to the cavity height was found to be played a significant role on streamlines and isotherm patterns for different heating configurations. The investigation also indicates that opposing forced flow configuration has the highest thermal performance, in terms of both maximum temperature and average Nusselt number. Numerical simulation of unsteady mixed convection in a driven cavity using an externally excited sliding lid is conducted by Khanafer et al [6]. They observed that, *Re* and *Gr* would either enhance or retard the energy transport process and drag force behavior depending on the conduct of the velocity cycle.

Ch.-H. Bruneau and M. Saad [7] have pointed out that, driven cavity flows exhibit almost all the phenomena that can possibly occur in incompressible flows: eddies, secondary flows, complex three-dimensional patterns, chaotic particle motions, instability, and turbulence. Thus, these broad spectra of features make the cavity flows overwhelmingly attractive for examining the computational schemes.

2. Objective

The purpose of the study is to investigate the flow behavior through the lid-driven cavity and to calculate flow separation and recirculation zone at different Re. In order to validate the result, the simulated data would have to compare with the experimental data [1].

3. Theory

The simulation is done by solving 2D Navier-Stoke equation for constant density flow. The continuity and momentum equation for a steady state 2D constant density flow are given as follows-
Continuity Equation,

$$\frac{\partial}{\partial x}(\rho u) + \frac{\partial}{\partial y}(\rho v) = 0$$

For Constant density,

$$\frac{\partial u}{\partial x} + \frac{\partial v}{\partial y} = 0$$

* Mominul Huq. Tel.: +88-01673729672
E-mail addresses: mhpurab@gmail.com

Momentum Equation,

X-Momentum:

$$u\frac{\partial u}{\partial x} + v\frac{\partial u}{\partial y} = -\frac{1}{\rho}\frac{\partial p}{\partial x} + \vartheta\left[\frac{\partial^2 u}{\partial x^2} + \frac{\partial^2 u}{\partial y^2}\right]$$

Y-Momentum:

$$u\frac{\partial v}{\partial x} + v\frac{\partial v}{\partial y} = -\frac{1}{\rho}\frac{\partial p}{\partial y} + \vartheta\left[\frac{\partial^2 v}{\partial x^2} + \frac{\partial^2 v}{\partial y^2}\right]$$

Vorticity:

$$\vec{\omega} = \vec{\nabla} \times \vec{u}$$

Here u, v are the horizontal and vertical velocity component of the flow. The boundary conditions are assumed as-

$$@\ wall : u = v = 0\ (no\ slip)$$

$$@\ lid - velocity : u = Based\ on\ Re,\ \ v = 0$$

$$@\ outlet : \frac{\partial u}{\partial x} = 0; \qquad \frac{\partial v}{\partial y} = 0$$

4. Numerical modeling

4.1 Geometry

The geometry is developed based on the cavity size. A square cavity of height L is assumed during the development of geometry. Other parameters are assumed as a function of L. Figure 1 shows the schematic of the geometry of a square cavity. The depth of the cavity L is assumed as 100mm.

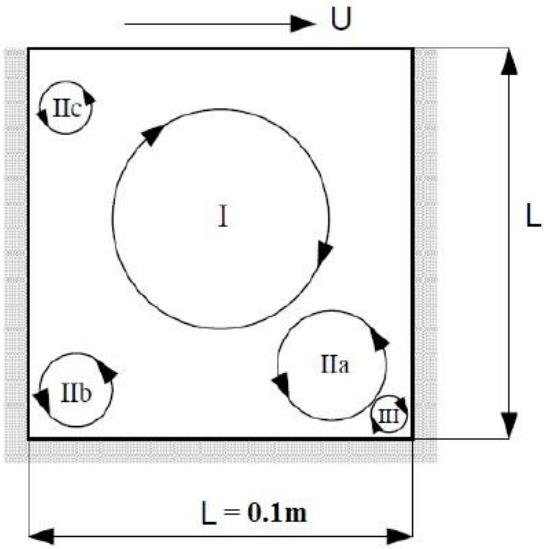

Figure 1. Schematic of the square cavity

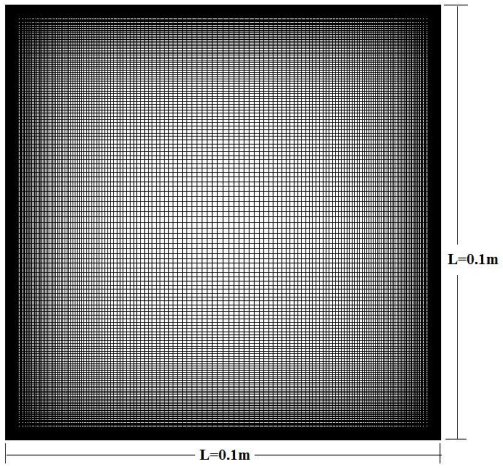

Figure 2. Mesh generation of the model

4.2 Mesh Generation

Around 40,000 structured quadrilateral mesh is used within the entire domain having 200 * 200 cells. The mesh elements were clustered near the wall boundary (figure 2) in order to resolve the boundary layer. Maximum face size of the mesh is assumed as 0.5mm. The orthogonal quality of the mesh remains 0.98 and maximum aspect ratio is 1.8. A mesh independence test was done based on u-velocity at x = 0.5L at Re = 400. Different mesh configurations were used to check mesh independence.

Figure 3 shows the mesh dependency on u-velocity. 3 different cases are checked for this, keeping Re = 400. From the table it's clearly shown that the problem become mesh independent at mesh size of 100 * 100. To find more accurate result the final mesh is done with 200 * 200 cells.

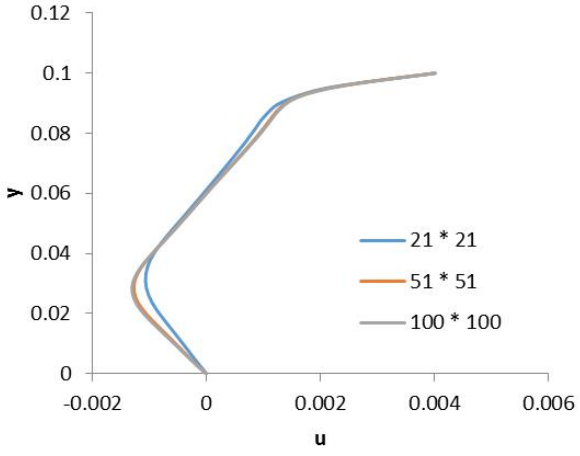

Figure 3. Mesh independence test for different cell number

5. Case setup and Solution

A 2D planner pressure based solver is used for the simulation. Water is considered as a working fluid. Inlet

boundary condition is determined based on Re. For Re calculation the characteristic length is assumed as L, where L is the depth.

$$Re = \frac{\rho v L}{\mu}$$

Standard least square discretization technique is used. A second order upwind solution method with QUICK solver is used. Re is set from 1 to 5000 as inlet condition. For convergence, the residue for continuity and velocity is set as 1e-10. Each solution is allowed to run 10,000 iteration to meet the minimum convergence criteria. To validate the CFD model, u-velocity is at x=0.5L and Re = 400 is compared with the published data. Figure 4 shows the comparison of CFD results which have a good agreement with experimental data.

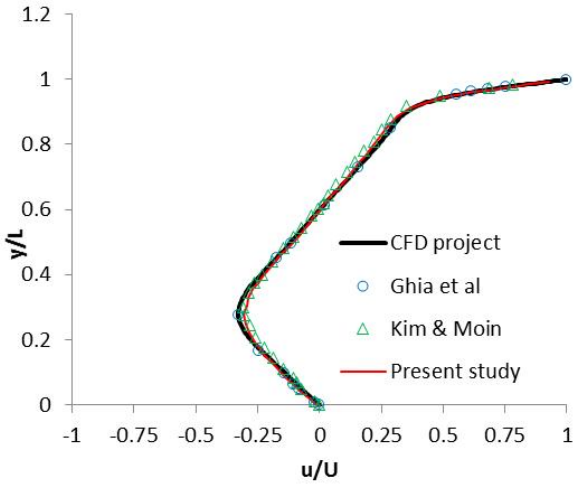

Figure 4. Validation of result at x =0.5L and Re=400

6. Results and Discussion

Horizontal velocity have been calculated for different Re ranging from 100 to 5000 in order to observe the flow behavior in Laminar, transition and turbulent regimes. The primary vortex form initially and as Re increases the vortex change its position. Figure 5 shows a typical streamline to demonstrate the formation of primary, secondary and tertiary vortex. Table 1 shows the center position of the primary vortex at different Re. It also shows the published data. The results are significantly close enough. Figure 6 shows the x-y coordinates of the primary vortex. It also shows the deviation from the published result. It is observed that, the center of the primary vortex become close to the center of the cavity as Re increases.

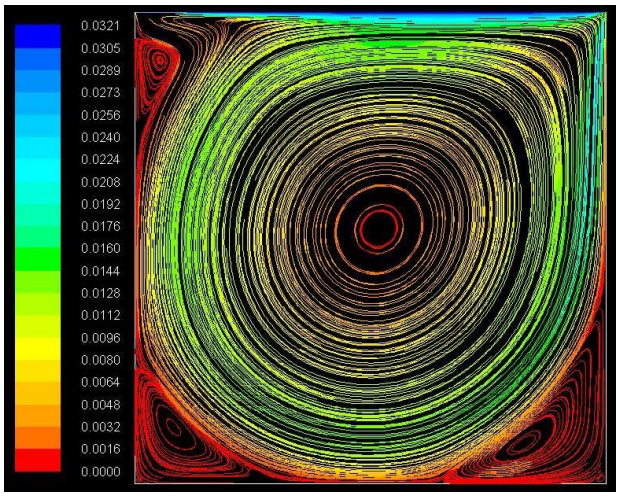

Figure 5. Different vortex formation at Re = 5000

Table 1. Position of the center of the primary vortex

Re	100	400	1000	3200	5000
Present	(0.619,0.742) 21 * 21	(0.560, 0.607) 31 * 31	(0.532, 0.564) 41 * 41	(0.518, 0.540) 61 * 61	(0.502, 0.514) 61 * 61
Ghia 82	(0.617, 0.734) 129 * 129	(0.555, 0.606) 257 * 257	(0.537, x) 257 * 257	(x , 0.547) 257 * 257	(0.512, 0.535) 257 * 257
CFD Project	(0.614, 0.734) 250 * 250	(0.553, 0.606) 250 * 250	(0.532, 0.562) 250 * 250	(0.540, 0.518) 250 * 250	(0.535, 0.502) 250 * 250

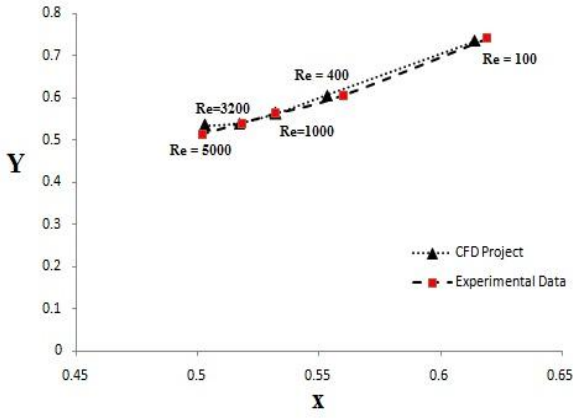

Figure 6. Coordinate of primary vortex at different Re

Figure 7(a) and 7(b) also show the change of position of the primary vortex in X and Y coordinate. The results are also compared with the published data and the deviation is significantly low. Figure 8(a) - 8(g) shows the streamlines at different Re. The primary and the secondary vortices are clearly visible there. The simulation successfully resolved the tertiary vortex at the corner of the cavity at Re = 5000 showed in figure 8(g).

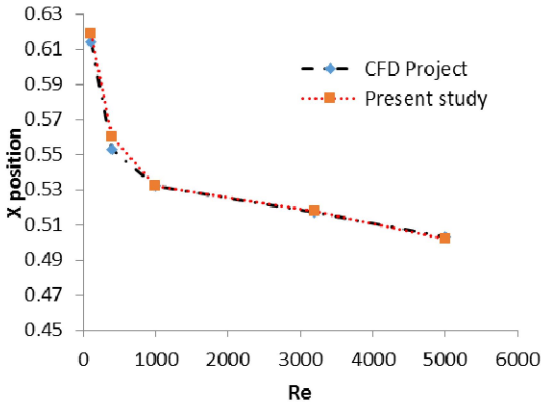

7(a)

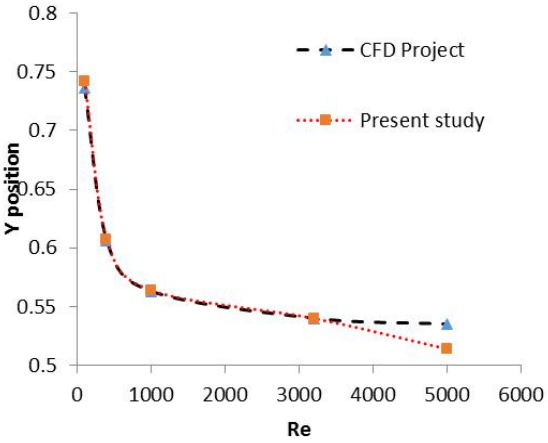

7(b)

Figure 7. Position of the primary vortex at different Re. (a) X-coordinate, (b) Y - coordinate

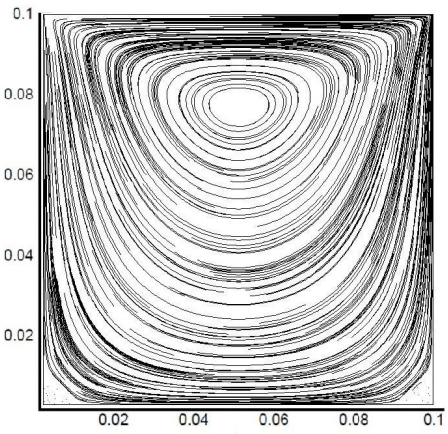

8(a) Re = 1

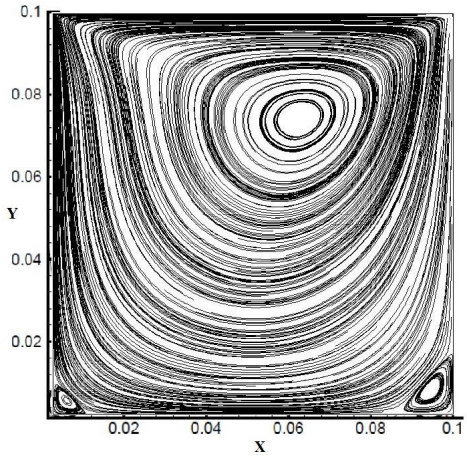

8(b) Re = 100

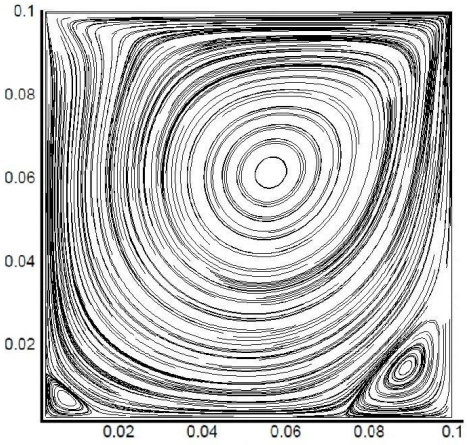

8(c) R = 400

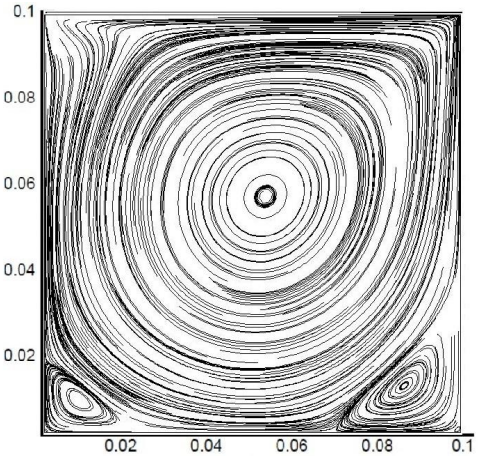

8(d) Re = 1000

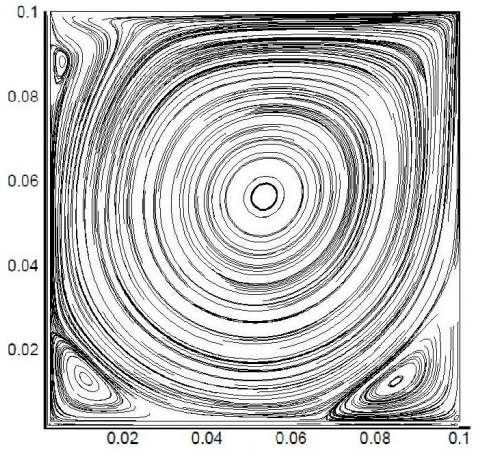

8(e) Re = 2000

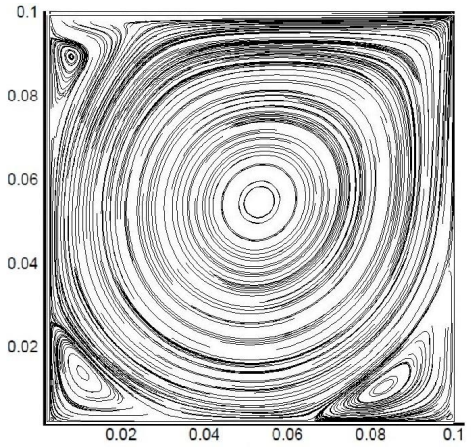

8(f) Re = 3200

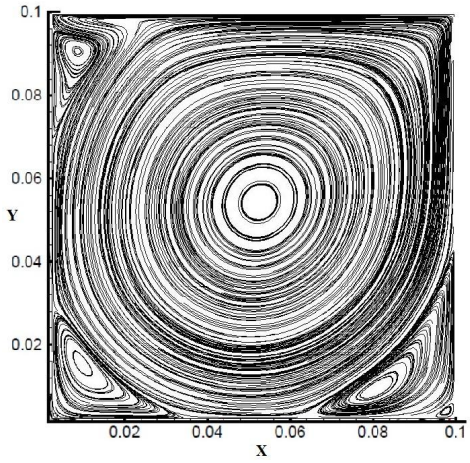

8(f) Re = 5000

A 3D flow simulation is also done for the cavity. Figure 9 shows the velocity contour at the center of the cavity. Figure 10 shows the volumetric streamline for the cavity. The streamline is showed with particle form.

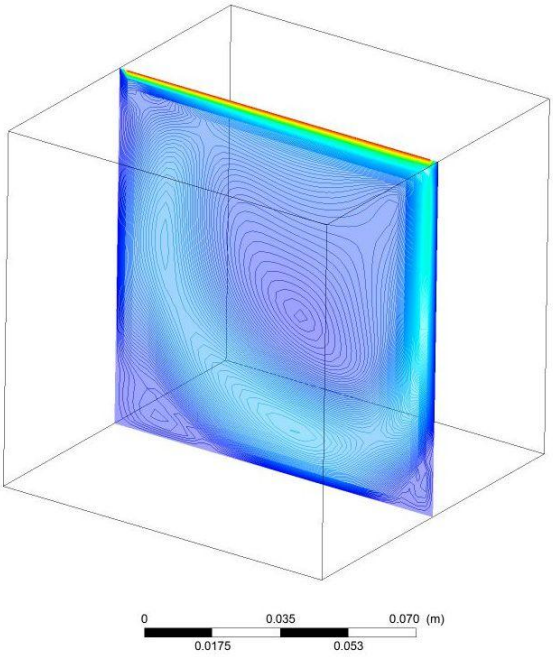

Figure 9. Velocity contour at the center plane of the cavity at Re = 400

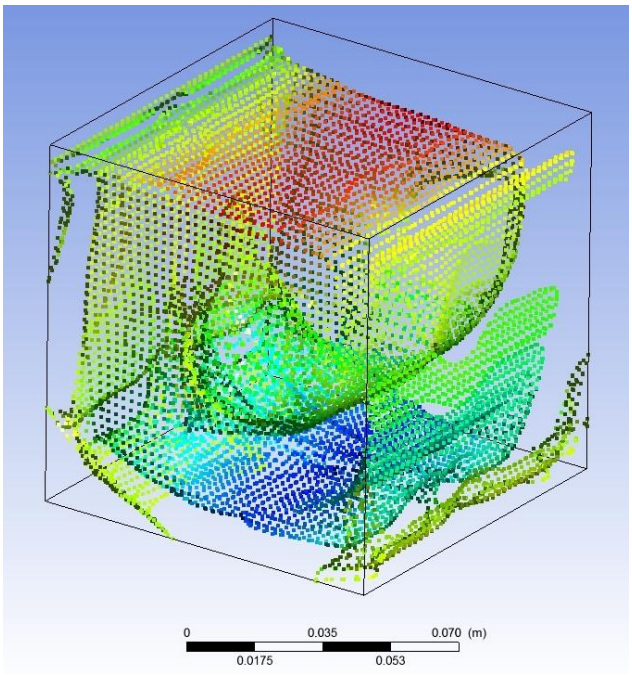

Figure 10. Streamline in particle form at Re = 400

7. Conclusion

The flow through a square cavity is simulated for both 2D and 3D case for different Re and the position of the vortices are presented. Mesh dependency is done for different cell number. The results are compared with the published data and it shows good agreement with published work.

NOMENCLATURE

$u = Horizontal\ velocity\ component$
$v = Vertical\ velocity\ component$
$Re = Reynold's\ Number$
$I = Primary\ Vortex$
$IIa, IIb, IIc = Secondary\ Vortex$
$III = Tersiary\ Vortex$
$\omega = vorticity$
$L = cavity\ height$
$\mu = Dynamic\ viscosity$
$\rho = Density$
$U = Maximum\ velocity$

REFERENCE

[1] Chen S, A large-eddy-based lattice Boltzmann Model for turbulent flow simulation. Applied Mathematics and Computation, 215, 591–595.

[2] S.L. Li, Y.C. Chen, and C.A. Lin. Multi relaxation time lattice Boltzmann simulations of deep lid driven cavity flows at different aspect ratios. Comput. & Fluids, 2011, 45(1): 233-240

[3] U Ghai et al, High-Re solution for incompressible flow using the Navier stokes equation and using a multi grid method, J of computational physics, 48, 387-411(1982)

[4] N. A. C. Sidik and S. M. R. Attarzadeh, An accurate numerical prediction of solid particle fluid flow in a lid-driven cavity. Intl. J. Mech. 2011, 5(3): 123-128.

[5] O. Manca, S. Nardini, K. Khanafer and K. Vafai, Effect of Heated Wall Position on Mixed Convection in a Channel with an Open Cavity, *Numer. Heat Transfer, Part A*, vol. 43, pp.259–282, 2003

[6] K.M. Khanafer, A.M. Al-Amiri and I. Pop, Numerical simulation of unsteady mixed convection in a driven cavity using an externally excited sliding lid, *European J. Mechanics B/Fluids*, vol. 26, pp.669-687, 2007.

[7] Ch.-H. Bruneau, M. Saad, The 2D lid-driven cavity problem revisited, Computers & Fluids35 (3), 2006.

ICMIEE-PI-140125

A Review on the Investigation of the Causes of Bullwhip Effect in Supply Chain Management

Md. Habibur Rahman, Md. Nawazish Ali, Md. Monirujjaman munna, Md. Rafiquzzaman
Department of Industrial Engineering and Management, Khulna University of Engineering & Technology, Khulna-9203, BANGLADESH.

ABSTRACT
In this study the review on the investigation of the causes of Bullwhip effect (BWE) associated with supply chain management is presented. It refers to a trend of large and larger swing in inventory in response to changes in customer demand swings in demand due to changes in customer demand throughout the whole process from supplier to customer. Supply chain management consists from raw material suppliers to customers. There are several stages in this chain. In this paper presents a details classified study of the overall research studied on the effect of both the operational and behavioral factors on bullwhip effect. Step taken by the various industries in order to tackle the bullwhip effect is also discussed in this paper. Finally the various scopes for further researches and instructions of the present and newer companies are also provided in this paper.

Key Words**:** Bullwhip effect, Collaboration, Operational causes, Behavioral causes.

1. Introduction

"Bullwhip effect" is one of the major obstacle in supply chain management. Due to incoordination the manufacturer can't forecast the actual demand of the customer. Actual demand is fluctuated among the stages. This demand fluctuation and the demand information distortion phenomenon is called "Bullwhip effect" [1]. The retailer is not interested to know the reason for the sudden demand of the products or services. They think that the demand has increased more than the previous time so the retailer demands more products to the distributor. By this way it reaches to the suppliers in an extensive demanded form which is many times than the actual demand of the customer [2]. The demand is oscillated within the stages of the supply chain. This oscillation of demand amplifies the demand along the supply chain. There are many studies to identify the causes of the Bullwhip effect. However the most "real world" supply chains are not easy to access [3]. The supply chain process is consists of several stages. So it is difficult to identify the actual reason for BWE.

BWE is a forecast driven problem. Bullwhip effect is a dynamic phenomenon and is the reason of the tendency of the variability of the order rates. Bullwhip creates unstable production schedules are the cause of a range of unnecessary costs in supply chains. Companies have to invest in extra capacity to meet the high variable demand. This capacity is then under-utilized when demand drops [4]. In the previous period many studies had described different modelling and causes of Bullwhip effect [1-52]. The Bullwhip effect can be described by different modelling. Analytical, agent-based and simulation modeling have been discussed in [8-16]. One the major problem in supply chain management is Bullwhip effect that associated numerous reasons for it related to information distortion, demand fluctuation, price variations and other reasons. These reasons have been discussed in different way [1-52]. The lead time variability, local optimization within functions or stages, demand forecasting error, large lead time for information shearing, lack of supply chain coordination and other causes have been interpreted by investigation [38-52]. Therefore, in this paper presents a details classified study of the overall research studied on the effect of both the operational and behavioral factors on bullwhip effect. Step taken by the various industries in order to tackle the bullwhip effect is also discussed in this paper. Finally identified the various scopes of the further research for the future researchers and instructions of the present and newer companies are also provided in this paper. The bullwhip effect can be explained with a quadratic equation [52] by the amplification of the order rate from customer to manufacturer.

Bullwhip effect

Bullwhip effect is a problem which is related with the supply chain management. Supply chain management is related from the customer to raw material suppliers. The bullwhip effect is an observed phenomenon and forecast driven. The Bullwhip effect is mainly the fluctuation of the demand of product. When the information of demand order is distorted from stage to stage in the supply chain management, the demand order is fluctuated along the supply chain. Bullwhip effect is a trend of large and larger swing in inventory in response to changes in customer demand. The concept of Bullwhip effect was first appeared in *Industrial Dynamics* (1961) by "Jay Forrester".

1. Supply Chain Modelling

1.1 Analytical Modelling

The characteristics of the BWE can be derived by different mathematical theories such as probability,

* Corresponding author. Tel.: +88-01790847464, +88-01724178388
E-mail address: rafiqbitr@yahoo.com, habibur091@gmail.com

calculus, or linear algebra [2]. These theories derived the Bullwhip effect from the different angles. Since there are numerous causes of Bullwhip effect, stochastic variables and capacity constraints, it is difficult to derive the appropriate model of it. From [7] Kahn showed that a serially correlated demand results in the Bullwhip Effect. Lee et al. (1997a) used the same demand assumption in which orders, D_t, depend on the orders in the previous time interval, D_{t-1}, as:

$$D_t = \rho D_{t-1} + d + u_1 \quad (1)$$

There are two constants d and are ρ where d>0 and $-1 < \rho < 1$, and u_t is normally distributed with zero mean and variance, σ^2. (Negative demands are unlikely when $\sigma << d$.).

1.2 Agent-Based Modelling

The agent-based concepts has emerged in literature relevant to computer applications since 1990s [8]. Agent exhibits adaptability, mobility and rationality. It also exhibits autonomy, social ability and responsibility [9]. In order to advance in the artificial intelligence (AI) field it has to investigate the possible solutions of supply chain management problems in the form of multi agent systems [2]. Each agent is autonomous and achieving its system goal by coordination by independent computer program [10]. For the collaborative, autonomous and intelligence system the multi agent technology has many beneficial features in the distributed environment. Recent research literature acknowledges intelligent agents as the most appropriate technology for trading and auctioning in electronic markets [11]. Agents are able to track demand, eliminate the Bullwhip effect, discover the optimal policies (where they are known), and find good policies under complex scenarios where analytical solutions are not available [2].

1.3 Simulation modelling

In the supply chain management the analytical methods are impractical because the analytical problems are related to mathematical models relate to realistic cases. Usually too complex problems are solved by analytical methods. These complex methods are not possible to solve by physical experimentations because it is high cost related. For the large scale situations a modeling and simulation approach is the only practical recourse for exploring the performance. The simulation model where to be used depends on the problems of the supply chain [12]. Almost every aspect of manufacturing systems simulation has been successful in mimicking. Enterprises has discovered an environment through supply chain management that increased customer satisfactions. Due to stochastic properties in the supply chain there have been encountered difficulties in the large number of uncertain variables [13].For the theory development the simulation has become a significant methodology and strengthening the organizations [14-18]. As the primary method several influential efforts have used [19, 20]. For the research the simulation model software is important. The simulation model makes the supply chain simple.

2. VARIOUS CAUSES OF THE BULLWHIP EFFECT

Bullwhip effect is a problem for the supply chain management. There are many causes of BWE. Many papers have been published on the causes of BWE. From the research of previous literatures there all the cases of BWE have been gathers. Price fluctuations [2], demand forecasting error [21-24], order batching [21-25], Rationing and shortage gaming [22], Machine Breakdown [23], Number of echelons [21,26], Lead time of information and material as the primary reason for the bullwhip effect [28-32], Lead Time Variability [27-39], Workloads [40], Local optimization within functions or stages of a supply chain [41], Information-processing obstacles [42], Lack of information shearing [43], Demand information uncertainty [43,44], Demand information dynamic [43,44], Secondary reasons for the bullwhip effect: Planning and behavioral [45],Inventory policy [46,47], Exaggerated order quantity in case of delivery bottlenecks [48,49], variability of machine reliability and output [50,51], Replenishment policy [52] are the main causes of BWE.

3. Supply Chain Structure and Processes

There are the following causes of BWE under supply chain structure and processes.

3.1 Demand forecast updating

Demand forecasting is related with pricing decisions of the customers it may be used in making pricing decisions, in assessing future capacity requirements, or in making decisions on whether to enter a new market [21-24]. Since demand forecasting is related with pricing, product demand fluctuates with the fluctuation of the price. Shortage or surplus may arises due to lacking of updating of demand forecasting.

3.2 Order batching

Aggregating products through a short size order can be called “lumpy” order. Grabara and Patyk [21] and McBurney P et al. [25] also explained the “lumpy” order size. Order picking deals with the retrieval of articles from their storage locations in order to satisfy customer requests. The transformation and consolidation of customer orders into picking orders (batches) is pivotal for the performance of order picking systems. Typically, customer orders have to be completed by certain due dates in order to avoid delays in production or in the shipment to customers. Batching of orders minimizes unit ordering and production costs. However, it causes the distortion of demand information. From Alony and Aneiro [22] the supply chain upstream members receive periodical spikes in customer demand.

3.3 Rationing and shortage gaming

From [22] Rationing schemes that allocate production in proportion to orders places by retailers leads to a magnification of information distortion. This can occur when a high demand product is in short supply. HP, for example, has faces many situations in which a new product has demand for that fur exceed supply. In such situation manufacturers come up with a variety of mechanisms to ration the scarce supply of product among various distributors of product. Buyers' strategic ordering behavior as a possible cause of the bullwhip effect. They explain that in an environment where there is supply shortage, buyers tend to over-order to secure resources for themselves, and suppliers tend to correct this over ordering by rationing back to smaller quantities.

3.4 Price fluctuations

Chopra et al. [2] discussed that Trade promotions and others short term discounts offered by a manufacturers results in forward buying, by which a whole seller or retailer purchases large lots during the discount period to cover the demand for future periods. Forward buying results in large orders during the promotion period to cover demand during the promotions periods followed by very small orders. The promotions thus results in a variability in manufacturer shipments that is significantly higher than the variability in retailer sales.

4. Supply Variability

4.1 Machine Breakdown

In the supply chain management the whole process from supplier to customer is related with one another. Due to the breakage of any stage causes the whole process distortion. Breakdown is the loss of functional ability efficiently. When machine breakdown occurs at the top level of supply chain management then the product supply will be hampered in the downstream stages. The supplier will not be able to fulfill the demand of its following stages. There will create the shortage of the product. When the retailer will be unable to fulfill the customer demand arises bullwhip effect.

4.2 Capacity Limit

The capacity of a manufacturer means its production ability during a specific time period. The manufacturer supply goods or services to all its downstream stages. When it takes to produce more time the product or production delay increased, the downstream stages remains in the lack of product. From Chopra [2] and Talor [23]. Since the manufacturer takes more time to supply the products or services it causes erratic ordering by the downstream members and create a bullwhip effect. The distributor can't fulfill the retailer's demand, the retailer can't fulfill customer's demand. The demand becomes more erratic from stage to stage. However the capacity limit has a significant effect in the supply chain system and causes the Bullwhip effect.

4.3 Number of echelons

Grabara and Patyk [21] suggested that there should be minimum number of echelons appropriate to the goals of the supply chain. According to Alony I [26] more echelons need more time to process. In the supply chain system there are five or six echelons in some cases again two or three echelons in some cases. Where there are more echelons it takes more time to reach goods or services to the customers. Besides there creates a lack of information shearing due to having numerous echelons, there may be created misunderstanding and miss collaboration among them and that may not result in actual demand of customers.

4.4 Lead Time Variability

Lead time is the time between the placement of an order and delivery of a new product. Otherwise lead time is the latency between the initiation and execution of a process. When lead time is short the customer gets their goods or services soon. So there is not such impact of Bullwhip effect. Jörg Nienhaus [27] represented that the longer time of information or material have the strong effect on the Bullwhip effect. But when there is long lead time there is great impact of bullwhip effect. The BWE due to lead time variability has been discussed [27-39]. This long waiting exacerbates the customers, i.e. increases the effect of Bullwhip effect.

4.5 Workloads

Workload is the extra pressure of works that one or a group has to do within a certain time period. If the manufacturer has to perform numerous task within a short time then the firm cannot gain 100% accuracy. Akkermans and Vos [40] found that the more workloads the more Bullwhip effect. Besides the higher workload is the reason of rework and that product requires more time to repair. Workload is a cause of Bullwhip effect. Due to workload sometimes it is not possible to obtain the better efficiency. Workload is the cause of rework that means higher workloads. Sometimes in the supply chain management the Bullwhip effect is measured through by the measurement of backlogs instead of the measurement of finished work.

4.6 Lack of supply chain coordination

A lack of coordination occurs either because different stages of the supply chain have objectives that conflict or because information moving between stages is delayed and distorted. Different stages of the supply chain may have conflicting objectives if each stage has a different owner. As a result each stage tries to maximize its own profits, resulting in action that diminish total supply chain profits [2] and [22]. There is

missing the coordination among these stages. For that reason the owner of a stage is not interested to know another's stage owner. There creates a lack of information shearing that is the reason of the fluctuation of demand. Finally creates Bullwhip effect.

4.7 Local optimization within functions or stages of a supply chain

Incentives that focus only on the local impact of an action result in decisions that do not maximize total supply chain profits [41]. One stage namely transportation manager wishes to lower transportation system that ultimately requires more time for transportation that increases the profits of the transportation manager but not the total supply chain management. This creates the variability of the available product and cause Bullwhip effect. Other causes of BWE are discussed in Table 1.

Table 1 Other causes of BWE

Causes of BWE	Causes discussed by
Sales force incentives	Chopra, Meindl et al. [2], Moyaux T et al. [41]
Information-processing obstacles	Sohn SY, Lim M [42]
Forecasting based on orders not on customer demand	Sohn SY, Lim M [42]
Lack of information shearing	Sohn SY, Lim M [42]
Demand information uncertainty	David H. Taylor [43], Sohn SY et al [44]
Nonlinear delayed information	David H. Taylor [43], Sohn SY, Lim M [44]
Staggered timing of the node because of information game	David H. Taylor [43], Sohn SY, Lim M [44]
Planning and behavioral causes	Nienhaus J et al. [45]
Inventory policy	Chandra C, Grabis J [46], Aharon B-T et al. [47]
Exaggerated order quantity in case of delivery bottlenecks	Lee, L. H et al. [48-49]
Variability of machine reliability and output	Huang Lizhen Liu Yongping [50], Taylor DH [51].

5. Scope for the further research

Since BWE has a great influence on the supply chain system, further researches are required to eradicate BWE. There are some issues for further researches:

- It may be investigated the ways that minimizes the complexity of the supply chain.
- Finding out the ways that improve the collaboration among the stages of the supply chain.
- It may be surveyed that how many manufacturers are concern about all the causes of BWE.
- It may be researched that what will happen if one or more intermediate stages are eliminated of the supply chain.
- Investigation the gaps of the previous researches.

6. Instructions for the supply chain system

From the above discussion, many causes of BWE and the scope of further research were pointed out. Now this paper is providing some instructions for the present business firms and companies. First, the each stage of supply chain will be aware of the information sharing and there should have technology based way of information shearing. Second, avoid the as usual demand forecasting method and select a way that can investigate the actual customer demand. Third, the coordination must be improved among the different stages of the supply chain system to avoid disruption of information shearing. Forth, there will have a restriction against local optimization within functions or stages.

Conclusion:

The supply chain is a complex chain system that starts from the raw material suppliers to customers. Any type of disruption causes the BWE makes the supply chain complex. The all causes of BWE have been categorized into some categories (1) causes due to supply chain processes and structure (2) Causes due to material and information lead time (3) Causes due to supply variability (4) causes due to other causes. Although the modelling and causes of Bullwhip effect have been discussed extensively, there are also some limitations in the total system. Vast awareness and concentration is needed to overcome this problem. But for the most company in supply chain there are some limitations for this reason it becomes difficult to overcome this problem. From the literature review supply chain modelling and causes like long lead time, order batching, rational and shortage gaming etc. are discussed in this paper. Strong management policy and more concentration should take extensively to minimize the BWE. Often it becomes difficult to investigate the actual causes of Bullwhip effect. This review paper will help to find out the causes of BWE and provides the appropriate actions to tackle the BWE. Finally, this paper represents the scope of further research in the area

of BWE. Additionally, this paper provides a brief instruction against BWE to the manufacturer.

REFERENCES

[1] Chen, F., Drezner, Z., and et al, The Bullwhip Effect: Management insights on the impact of forecasting and information a variability in a supply chain, quantitative models for supply chain management." *Kluwer Academic Publishers*, Vol 17, pp 417-439, (2000).

[2] Sunil Chopra, Pater Meindl and D.V. Kalra, Supply Chain Management Strategy, Planning and Operation, Fourth Edition, pp 509-544.

[3] H. B. Hwarng, C. S. P. Chong, N. Xie, and T. F. Burgess, Modelling a complex supply chain: understanding the effect of simplified assumptions, *International Journal of Production Research*, vol. 43, pp. 2829, (2005).

[4] Hongchun Wang, Baizhou He, Research on the Reducing Measures of Bullwhip Effect, *IPCSIT* vol.9 (2011).

[5] D. R. Towill, Smoothing supply chain dynamics, *International Journal of Computer Integrated Manufacturing*, vol. 4, pp. 197-208, (1991).

[6] Svensson G, The bullwhip effect in intra-organisational echelons, *Int J Phys Distrib Logist Manag* 33(2):103–131, (2003).

[7] J. D. Sterman, Modeling Managerial Behavior: Misperceptions of Feedback In, *Management Science*, vol. 35, pp. 321, (1989).

[8] WanSup Um, Huitian Lu, Teresa J. K. Hall, A Study of Multi-Agent Based Supply Chain Modeling and Management, *iBusiness, 2010*, 2, 333-341, (2010).

[9] N. R. Jennings and M. Wooldridge, Applying Agent Technology, *Applied Artificial Intelligence*, Vol. 9, pp. 357-369, (1995).

[10] H. V. D. Parunak, R. Savit, and R. L. Riolo, Agent-based modeling vs. Equation-based modeling: A case study and users guide, *Presented at Proceedings of multi-agent systems and agent-based simulation (MABS'98)*, (1998).

[11] J. M. Swaminathan, Modeling Supply Chain Dynamics: A Multiagent Approach, *Decision Sciences*, Vol. 29, No. 3, pp. 607-632, (1997).

[12] Caroline Thierry, Gérard Bel, André Thomas, The Role of Modeling and Simulation in Supply Chain Management, *SCS M&S Magazine*, (2010).

[13] R. G. Ingalls, The value of simulation in modeling supply chain, *Presented at Proceedings of the 1998 Winter Simulation Conference, Washington D.C.*, (1998).

[14] R. Adner, When are technologies disruptive? A demand-based view of the emergence of competition, *Strategic Management Journal*, vol. 23, pp. 667-688, (2002).

[15] T. Lant and S. Menzias, Managing discontinuous change: A simulation study of organisational learning and entrepreneurship,*Strategic Management Journal*, vol. 11, pp. 147-179, (1990).

[16] N. Repenning, A simulation based approach to understanding the dynamics of innovation implementation, *Organization Science*, vol. 13, pp. 109-127, (2002).

[17] J. W. Rivkin and N. Sigglelkow, Balancing search and stability: Interdependencies among elements of organizational design, *Management Science*, vol. 49, pp. 290-311, (2003).

[18] C. Zott, Dynamic capabilities and the emergence of intra-industry differential firm performance: Insights from a simulation study, *Strategic Management Journal*, vol. 24, pp. 97-125, (2003).

[19] M. D. Cohen, J. March, and J. P. Olsen, A garbage can model of organizational choice, *Administrative Science Quarterly*, vol. 17, pp. 1-25, (1972).

[20] J. March, Exploration and exploitation in organisational learning, *Organization Science*, vol. 2, pp. 71-87, (1991).

[21] Janusz K. Grabara, Marta Starostka-Patyk, THE BULLWHIP EFFECTIN SUPPLY CHAIN, *Management Science*, vol. 46, pp. 436-443.

[22] Alony and Albert Munoz Aneiro, The Bullwhip effect in complex supply chains, pp 1355-1360, *International Symposium on Communications and Information Technologies ISCIT*, 17-19 Oct, (2007).

[23] Wright D, Yuan X, Mitigating the bullwhip effect by ordering policies and forecasting methods, *Int J Prod Econ*, 113 (2):587–597,(2008).

[24] Lee HL, Padmanabhan V, Seungjin W,The bullwhip effect in supply chains, *Sloan Manage Rev* 38(3):93–102 (1997).

[25] McBurney P, Parsons S, Green J, Forecasting market demand for new telecommunications services: an introduction, *Telematics Inform* 19(3):225–249 (2002).

[26] Alony I, Munoz A, The bullwhip effect in complex supply chains, *2007 International Symposium on Communications and Information Technologies Proceedings ,Darling Harbour, Sydney, Australia*, pp. 1355–1360,17–19 October, (2007).

[27] Jörg Nienhaus, What is the BullwhipEffect caused by?,*Supply Chain World Europe 2002*, 28-30 October, Amsterdam, (2002).

[28] Joerg Nienhaus, Arne Ziegenbein, Christoph Duijts, How human behaviour amplifies the bullwhip effect – a study based on the beer distribution game online, *Production Planning & Control: The Management of Operations*, Volume 17, Issue 6, (2006).

[29] Forrester, J. W, Industrial Dynamics-A major breakthrough for decision makers, *Harvard Business Review*, Vol 36, Num 4, pp. 37-66 (1958).

[30] Lee, L. H.; V. Padmanabhan, Whang S, The Bullwhip Effect in Supply Chains, *Sloan Management Review*, pp. 93-102 (1997).

[31] Lee, L. H, Padmanabhan, Whang, S.:" Information Distortion in a Supply Chain: The Bullwhip Effect," Management Science, 43 (1997) 4, pp. 546-558.

[32] Simchi-Levi, D. Kaminsky, Simchi-Levi, Designing and Managing the Supply Chain. Concepts, Strategies, and Case Studies, *Irwin McGraw-Hill*, (2000).

[33] Liao C-J, Shyu C-H, An analytical determination of lead time with normal demand, *Int J Oper Prod Manage*, 11(9):72–78, (1993).

[34] Bookbinder JH, Çakanyildirim M, Random lead times and expedited orders in (Q, r) inventory systems, *Eur J Oper Res*, 115 (2):300–313, (1999).

[35] Ben-Daya M, Raouf A, Inventory models involving lead time as a decision variable, *J Oper Res*, Soc 45(5):579–582, (1994).

[36] Ouyang L-Y, Yeh N-C, Wu K-S,Mixture inventory model with backorders and lost sales for variable lead time, *J Oper ResSoc* 47(6):829–832 (1996).

[37] Ryu SW, Lee KK, A stochastic inventory model of dual sourced supply chain with lead-time reduction, *Int J Prod Econ*, 81–82:513–524, (2003).

[38] Gaalman G, Bullwhip reduction for ARMA demand: the proportional order-up-to policy versus the full-state-feedbackb policy, *Automatica*, 42(8):1283–1290, (2006).

[39] Heydari Jafar, Kazemzadeh RB, SK Chaharsooghi, A study of lead time variation impact on supply chain performance, *Int J Adv Manuf Technol*, 40(11–12):1206–1215, (2009).

[40] H. Akkermans and B. Vos, Amplification in Service Supply Chains: An Exploratory Case Study from the Telecom Industry, *Production and Operations Management*, vol. 12, pp. 204–223, (2003).

[41] Moyaux T, Chaib-draa B, D'Amours S, Information sharing as a coordination mechanism for reducing the bullwhip effect in a supply chain, *IEEE Transactions on Systems, Man and Cybernetics Part C: Applications and Reviews*, 37(3): 396–40, (2007).

[42] Sohn SY, Lim M, The effect of forecasting and information sharing in SCM for multi-generation products, *Eur J Oper Res*, 186(1):276–287, (2008).

[43] David H. Taylor, Measurement and Analysis of Demand Amplification Across the Supply Chain, *International Journal of Logistics Management*, Vol. 10 Iss: 2, pp.55, (1999).

[44] Sohn SY, Lim M, The effect of forecasting and information sharing in SCM for multi-generation products, *Eur J Oper Res*, 186(1):276–287, (2008).

[45] Nienhaus J, Ziegenbein A, Schoensleben P, How human behaviour amplifies the bullwhip effect—a study based on the beer distribution game online, *Prod Plan Control*, 17(6):547–557, (2006).

[46] Chandra C, Grabis J, Application of multi-steps forecast-ing for restraining the bullwhip effect and improving inventory performance under autoregressive demand, *Eur J Oper Res*, 166 (2):337–350, (2005).

[47] Aharon B-T, Boaz G, Shimrit S, Robust multi-echelon multi-period inventory control, *Eur J Oper Res*, 199(3):922–935, (2009).

[48] Lee, L. H, Padmanabhan, V, Whang, S, The Bullwhip Effect in Supply Chains, *Sloan Management Review*, pp. 93-102, (1997).

[49] Hau L Lee, V Padmanabhan, Whang S, Information Distortion in a Supply Chain: The Bullwhip Effect, *Management Science*, Vol 43, Num 4, pp. 546-558, (2004).

[50] Huang Lizhen and Liu Yongping, Supply chain dynamics under the sustainable development, *2008 International Confer-ence on Wireless Communications, Networking and Mobile Computing, Dalian*, pp. 1-6, (2008).

[51] Taylor DH, Measurement and analysis of demand amplification across the supply chain, *Int J Logistics Management*, 10(2):55–70, (1991).

[52] Roger D. H. Warburton, Jonathan P. E. Hodgson, Yong K. Kim, An Analytical Investigation of the Bullwhip Effect NTC S03-MD13s.

ICMIEE-PI-140126

Design and Construction of a micro-controller based automated railway gate control system

Mohammad Shafiul Amin Bhuiyan *, *Rakib Hasan, Dr. Kutub Uddin*
Department of Mechanical Engineering, Khulna University of Engineering & Technology, Khulna-9203, BANGLADESH

ABSTRACT
This paper reflects on the automation of the control of railway gate using micro-controller. A complete prototype is designed and constructed that contained several sensors on both sides of the railway gate to provide necessary input data related to gate closure into micro-controller, which then sends signal into the gate control system for immediate opening or closing of railway gate. For input sensors Lasers are used on both sides combined with LDR. For all the data processing Arduino (UNO) is used for overall simplicity. This automated system can be used in faraway places where human recruitment for manual gate control is much problematic and unreliable.

Keywords: Automation, gate control, Lasers, LDR, Arduino (UNO).

1. Introduction

Bangladesh is a country which depends significantly on railway transport system. For this reason level crossing at the places of huge traffic density is not rare in our country. Even though the concept of implementing automated railway gate in faraway places is not new in foreign developed countries, it is still not considered as a solution of most of the level crossing related accidents. Railway gates are controlled by human operators depending on the information received from the stations.

This system can causes inevitable human error due to lack of responsibilities, bad weather or lack of good communication system. For these reasons in densely populated areas where drivers and pedestrians are not careful enough, the closure or opening of the gate cannot be done properly at the right moment, depending only on the guessing of the gate operator. This can cause traffic jam or accidents in many cases. Any level crossing accident causes heavy financial burden due to railway and road service obstruction and also for the damage to the railway and road properties. The objective here is to design and construct an automated system for railway gate and developing a program that determines the time of gate opening and closure and send signals accordingly. By using automated railway gate at level crossing the closing and opening of the gate can be determined by placing sensors placed at both sides of the gate, which will results in reduced time for road obstruction and also reduced human labor. This type of railway gate can also be implemented in faraway rather less populated areas where human recruitment and maintenance is difficult. As the whole system is completely automated, therefore any error due to manually operating the gate can be avoided. Using micro-controller also makes it also highly economical.

2. Gate Control System

To construct the controlling system of the railway gate using micro-controller, Arduino board is used for the overall simplicity of the system and its high reliability and effectiveness. Sensors are placed on both sides of the railway gate to provide the information of the arrival and departure of the train. Several pairs of laser light and LDR are used together at both sides of the gate for the high reliability of this sensing system and for the ability of working in any kind of environment. Using more than one sensor at one side makes it more reliable to determine the arrival or departure of the train. Servomotor is used for controlling the movement of the gate in clockwise and anticlockwise direction.

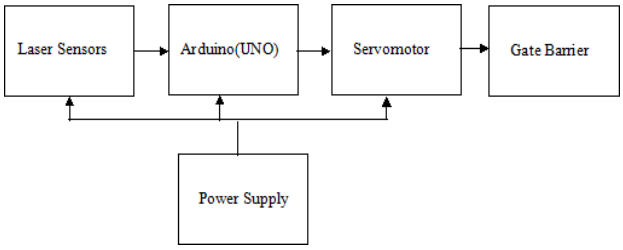

Fig.1 Block diagram for automated railway gate control system.

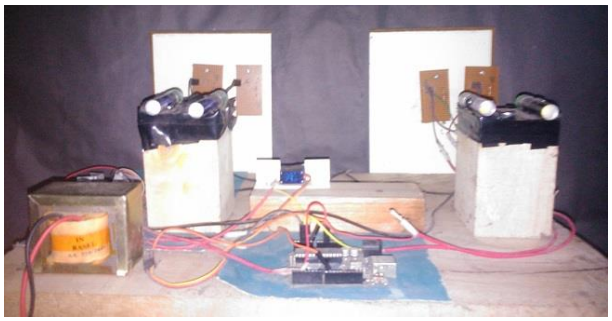

Fig.2 Constructed system with all the necessary equipment.

2.1 Arduino

The Arduino is an Atmel AVR micro-controller based computing platform [1]. The specific board used in this project is the uno board that is based on ATmega328. It has 14 digital input/output pins, thus creating enough options for using several lasers and LDR for input signals. The Arduino is used here as a processing unit.

* Corresponding author. Tel.: +88-01676057579
E-mail address: shafiulaminbhuiyan.kuet@gmail.com

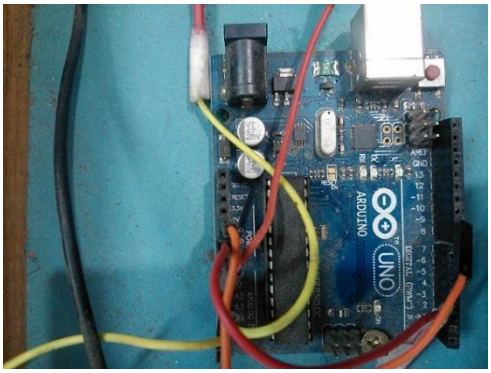

Fig.3 Arduino (UNO) used in the construction

2.2 Servo Motor

A servomotor is a rotary actuator that allows for precise control of angular position, velocity and acceleration [2]. It consists of a suitable motor coupled to a sensor for position feedback. The motor is connected with the Arduino which provide position and speed feedback. At the default position the motor keeps the gate at open position. After receiving signals coming from the Arduino the gate is closed or opened by the motor. This creates a loop for the gate control system. If any error occurs the gate is reset at its default position and kept there until new input signal comes from the sensors.

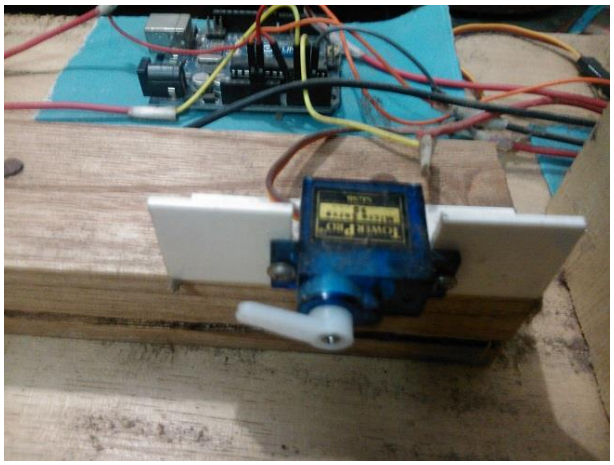

Fig.4 Servomotor connected with Arduino(UNO)

2.3 Light Dependent Resistor (LDR)

LDR or Light Dependent Resistor is a special kind of resistor whose resistance decreases with increasing incident light intensity [3]. The reason of using LDR coupled with Laser is the intensity of light incidence from the laser is quite which enables the LDR to create a quite high voltage resistance when there is any absence of light source. The laser light sources and LDR are placed on both sides of the railway track. Whenever a train crosses the light path of the laser, the resistance of the LDR increases immediately, which provide signals to the Arduino for immediate activation of the control system of the gate. As the laser light is not absorbed by air or water and goes in straight way, this system works in various environments as long as the light is not obstructed by any other unwanted object. If the sensors get activated without any train on the rail due to people or animal on the track the gate will close the road unnecessarily.

3. Avoiding unnecessary activation

One main disadvantage of using LDR and laser as sensor unit is the unnecessary activation of the gate control system without any train obstructing the light source. As the railway tracks are usually unprotected it is possible for the people or animals to obstruct the laser light source easily. This will cause the gate to close or open immediately. To avoid this occurrence several pairs of sensors consisting of a laser light source and a LDR are placed on each side of the gate. The minimum number of sensor should be at least two for each side and for further safety the number can be increased to four or six. The gate will close or open only when all of the sensors at one side of the gate activates at the same time.

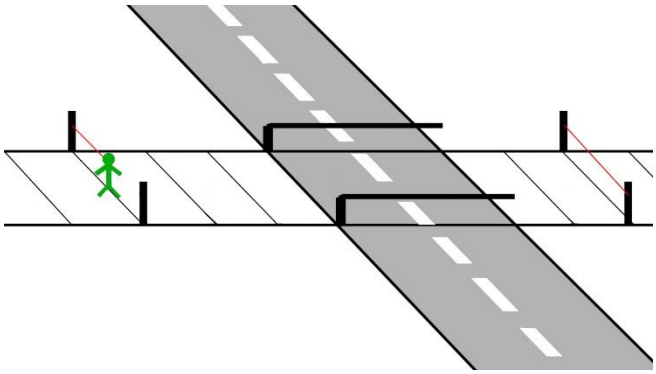

Fig.5 Gate getting closed for obstruction of laser light

Above figure explains the disadvantage of using only one sensor at each side of the gate. Any kind of object having the height to obstruct the laser light that goes towards the LDR may cause unwanted closure or opening of the gate resulting in road service termination or accidents.

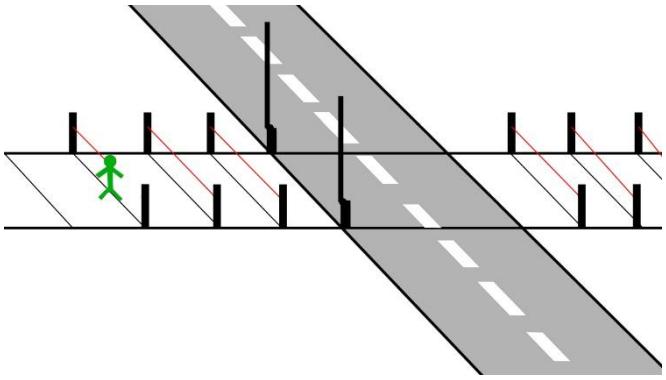

Fig.6 Gate is unaffected by people or any other object passing through the light path.

Above figure shows one simple way of solving the problem of unwanted activation of the automated gate

while using sensors to control the rotation of the gate. Several sensors are placed on either side of the gate and gate will start rotating only when all of the LDR has laser light incidence upon them or when there is no laser light incidence upon them.
There are other safety precautions can be taken such as placing the sensors at such a height that only anything as high as a train can affect it. This step can reduce the probability of unwanted activation of the gate. The sensors can also be placed in a restricted tunnel where the possibility of people or any animal or any other unwanted object intrusion is limited.

4. Program structure of the system

The program at first defines the default position of the gate at the open state. The program is designed for four sensors for the gate. The four sensors pins inputs are then defined which makes the Arduino processing system ready for deciding send signal at the servo output pin to control the servomotor depending on any information of the arrival or departure of the train. After all of the first two pairs of sensors send inputs in the Arduino the control part of the program activates enabling the servomotor to rotate 90 degrees to reach the close position. After that the gate remains closed until all the last two pairs of sensors on the other side of the gate send inputs to the Arduino to reset the system to default open position. The program works for trains coming in either way of the railway gate. The flow diagram here is the basis on which the control system was programmed.
The flow diagram of the system is given below.

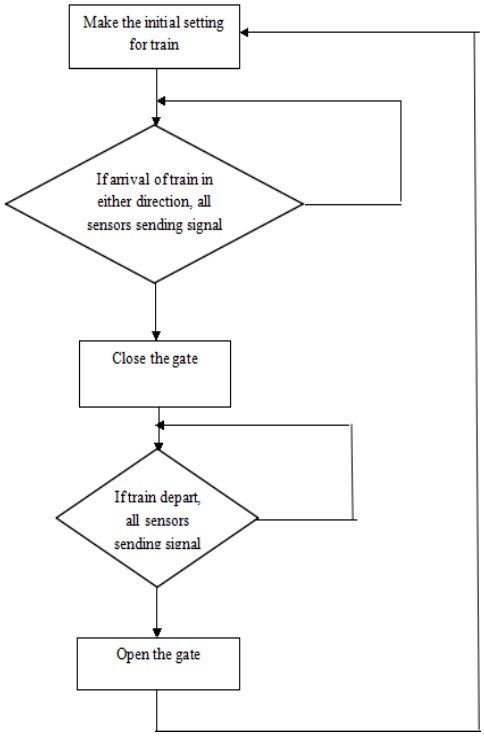

Fig.7 Flow diagram of the system

5. Circuit Diagram

Circuit diagram here is designed for four LDR which is connected with the Arduino at the input port. Necessary voltage regulator with heat sink and transformer with diodes are used to supply power to the servomotor and the Arduino. The lasers are common red light emitting lasers with enough light intensity to create enough high voltage with the LDR to activate the circuit. The program that is loaded in ATmega 328 only execute in laser light. The lasers are powered externally using batteries.

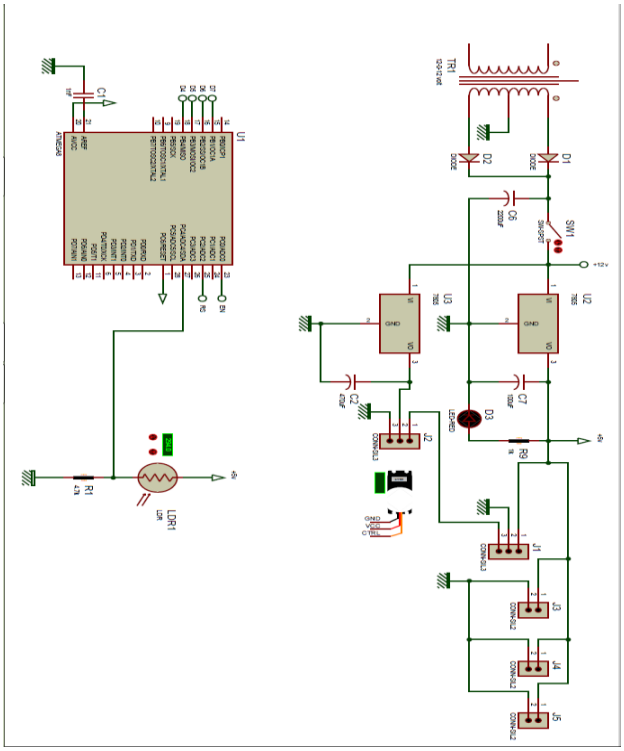

Fig. 8 Circuit Diagram of the system.

6. Discussion

An automated railway gate control system has three important factors that control the accuracy of the whole system. The accuracy of the sensors to fully determine the position of the train on the rail, swiftness of sending feedback to the control unit, in this case, micro-controller based Arduino(UNO) and swiftness of the motor activation to close or open the barrier. Any fault in any of these parts can result in fatal accident. For these reasons Lasers are used instead of infrared, sonar or pressure sensors. To avoid unwanted activation the easiest solution of using multiple sensors is followed. To reduce the closing and opening time and considering practical implementation of this system servomotor is used for the accurate control of motions. The whole system can also be designed by using Programmable Logic Controller (PLC) which is more costly in initial state. But micro-controller is more reliable than PLC and using Arduino makes the whole system simpler, while keeping an easier way of improvement.

7. Conclusion and future scope of work

This project completes the design and construction of an automated railway gate having more reliable sensor design that has the focus of avoiding unwanted activation of the gate control system. But the reliability of this system can be further increased by using global position system (GPS) to monitor the position of the train more accurately that will reduce the closure time of the gate even more. This will also reduce the possibilities of any level crossing related accidents. One major advantage of this system would be the facility of measuring the current speed of a moving train and comparing it the required speed that is needed for it reach destination within the schedule.

To complete this system another sensor system can be added to detect any traffic on the railway track before closing the gate and adjust the speed or direction of the motion of the gate.

To increase the safety measurement the gate can be made movable horizontally to create space for any traffic that is obstructed in the enclosed area after closing the gate to let it reach a safe zone, away from the railway track.

Implementing automated gate control system at the level crossing can be a huge challenge to take because the total cost for this would be quite high even though the designed system is economical in many senses. But on the other hand our country is hugely dependent on railroad transport system so any negligence in this sector will result in high financial loss in the long run. Finding a cost effective method to implement the system quickly without heavily affecting the transport system can be helpful for this regard. Automated railway gate system has already been implemented in several countries successfully. Even though regular maintenance for this system is required but interruption of the operations does not occur due to fatigue and negligence of the operator. That is why it is possible that the percentage of accident due to collision at level crossing will decrease greatly after implementing it.

REFERENCES

[1] http://arduino.cc (10 September, 2014)

[2] Hobby Servo Fundamentals by Darren Sawicz (8 September, 2014)

[3] diffenderfes, Robert (2005). Electronic devices: system and applications. New Delhi: delimar. p. 480. ISBN 978-1401835149.

ICMIEE-PI-140129

Comparative Analysis of AHP and Fuzzy-AHP in Supplier Selection: A Case Study on a Cement Industry

Mst.Nazma Sultana[1], S.M. Atikur Rahman[2], Mustafizur Rahman[3],Utpal kumar Dey[4]

[1, 2, 3] Department of Industrial Engineering and Management, Khulna University of Engineering & Technology, Khulna-9203, BANGLADESH
[4] Department of Computer Science and Engineering, Khulna University of Engineering & Technology, Khulna-9203, BANGLADESH

ABSTRACT
Now-a-days, supplier selection must be systematically considered from the decision makers is one of the most important issues for a company. That is why supplier selection process were evaluated by researchers experimentally and analytically for many years in various sectors using numerous method but every moment it's criteria's are changing according to consumers behavior's, technological development and there are needed to be considered them promisingly for real success in business sector. In this paper, supplier selection is considered as a multi-criteria decision problem by using conventional AHP and Fuzzy-AHP. A detailed step by step implementation method is presented in this paper for the proposed model.

Keywords: Supplier selection, Analytical Hierarchy Process, Fuzzy-AHP.

1. Introduction

Today, the competition between corporations grows fast. In this highly competitive environment companies which design and manage their supply chains best will be more profitable and hence stronger [1]. Decision making is one of the most important activities in business.

Managers need reliable and true forecasts for their decisions. Doing this they should consider scientific criteria. In general, a decision making problem is selecting the most appropriate alternative according to at least one goal or criteria from the alternatives cluster. This decision making involves the right selection of the raw material supplier in the supply chain. The selection of a supplier for partnership is the most important step in creating a successful alliance. The selection of an appropriate supplier is an important factor affecting eventual buyer–supplier relationship. If the process is done correctly, a higher quality, longer lasting relationship is more attainable [2].
A corporation which develops good relationships with its suppliers gain cost advantages through on-time and desired quality deliveries. Therefore supplier evaluation has a strategic importance for the corporations [1]. Actually there is various processes for supplier selection and evaluation such as AHP, Fuzzy-AHP, ANP, TOPSIS, MCDM, Goal programming, Supply chain networking etc. AHP is one of them and it only involves pair-wise comparison and it does not take into account all criterion of the supplier selection in practical.

In this paper the proposed model is to compare the AHP and Fuzzy-AHP method for supplier selection in a cement industry. We consider twenty-one criteria for supplier selection including both subjective and objective factors.

* Corresponding author. Tel.: +88-01941055289
E-mail address: nazma.kuet@yahoo.com

Dickson presented 23 supplier selection criteria, and assigned the rankings of these criteria. Some recent supplier evaluation and selection studies in various industries are, Baby Food Manufacturing Industry, Weber [3]; Wooden Furniture Industry, Yahya and .Kingsman (1999) [4]; Agricultural and Construction Equipment Industry, Liu et al. Telecommunications Industry, Narasimhan et al. [5]; Food Manufacturing Industry. We also consider the other various approach's for supplier selection in this paper such as Sugeno-Yasukawa approach, Takag Sugeno approach, Savic-Pedryze approach. Partovi & Burton applied the analytic hierarchy process (AHP) to inventory classification in order to include both quantitative and qualitative evaluation criteria.

Finally we compare between the two methods AHP vs. Fuzzy-AHP and also the determination of their relative importance in real case study in a cement industry from where the necessary data were collected. At first step the supplier is selected through AHP method and then it is in Fuzzy-AHP method.

2. Decision analysis model for supplier selection

2.1 Analytic Hierarchy Process

Since 1977, Saaty proposed AHP as a decision aid to help solve unstructured problems in economics, social and management sciences. AHP has been applied in a variety of contexts: from a simple everyday problem of selecting a school to the complex problems of designing alternative future outcomes of a developing country, evaluating political candidacy, allocating energy resources and so on. The AHP enables the decision makers to structure a complex problem in the form of a simple hierarchy and to evaluate quantitative and qualitative factors in the systematic manner under multiple criteria environment in confliction. The

application of the AHP to the complex problem usually involves four major steps:

1. To break down the complex problem into a number of small constituent elements and then structure the elements in a hierarchical form
2. To make a series of pair wise comparisons among the elements according to a ratio scale
3. To use the Eigen value method to estimate the relative weights of the elements
4. To aggregate these relative weights and synthesizes them for the final measurement of given decision alternatives.

Saaty proposed carrying out paired comparisons between the different elements because the human brain is perfectly designed to make comparisons between two elements, hence proposing the scale in Table 1.

Table 1 Fundamental scale for paired comparison

Definition Intensely of	**Intensely of Importance**
Equally important	1
Moderately more important	3
Strongly more important	5
Very strong more important	7
Extremely more important	9
Intermediate more important	2,4,6,8
If activity i has one of the above nonzero numbers assigned to it when compared with activity j, then j has the reciprocal value when compared with i.	Reciprocals of the above

2.2 Why Fuzzy-AHP IN STEAD OF AHP?

In the conventional AHP, the pair wise comparisons for each level with respect to the goal of the best alternative selection are conducted using a nine-point scale. So, the application of Saaty's AHP has some shortcomings as follows ;(1) The AHP method is mainly used in nearly crisp decision applications, (2) The AHP method creates and deals with a very unbalanced scale of judgment, (3) The AHP method does not take into account the uncertainty associated with the mapping of one's judgment to a number, (4) Ranking of the AHP method is rather imprecise, (5) The subjective judgment, selection and preference of decision-makers have great influence on the AHP results. In addition, a decision-makers requirements on evaluating alternatives always contain ambiguity and multiplicity of meaning. Furthermore, it is also recognized that human assessment on qualitative attributes is always subjective and thus imprecise. Therefore, conventional AHP seems inadequate to capture decision maker's Requirements explicitly. In order to model this kind of uncertainty in human preference, fuzzy sets could be incorporated with the pair wise comparison as an extension of AHP. A variant of AHP, called Fuzzy AHP, comes into implementation in order to overcome the compensatory approach and the inability of the AHP in handling linguistic variables. The fuzzy AHP approach allows a more accurate description of the decision making process.

2.3 Fuzzy Analytic Hierarchy Process

The fuzzy AHP technique can be viewed as an advanced analytical method developed from the traditional AHP. Generally, it is impossible to reflect the decision makers' uncertain preferences through crisp values. Therefore, FAHP is proposed to relieve the uncertainness of AHP method, where the fuzzy comparisons ratios are used. There are the several procedures to attain the priorities in FAHP. The fuzzy least square method based on the fuzzy modification of the LLSM, geometric mean method ,the direct fuzzification of the method of ,synthetic extend analysis ,Mikhailov's fuzzy preference programming and two-stage logarithmic programming are some of these methods.

Chang's extent analysis on fuzzy AHP depends on the degree of possibilities of each criterion. According to the responses on the question form, the corresponding triangular fuzzy values for the linguistic variables are placed and for a particular level on the hierarchy the pairwise comparison matrix is constructed. Sub totals are calculated for each row of the matrix and new (*l, m, u)* set is obtained, then in order to find the overall triangular fuzzy values for each criterion, *li/Σli, mi/Σmi, ui/Σui, (i=1,2,..., n)* values are found and used as the latest *Mi(li, mi, ui)* set for criterion *Mi* in the rest of the process. In the next step, membership functions are constructed for the each criterion and intersections are determined by comparing each couple. Fuzzy logic approach, for each comparison the intersection point is found, and then the membership values of the point correspond to the weight of that point. This membership value can also be defined as the degree of possibility of the value. For a particular criterion, the minimum degree of possibility of the situations, where the value is greater than the others, is also the weight of this criterion before normalization. After obtaining the weights for each criterion, they are normalized and called the final importance degrees or weights for the hierarchy level.

To apply the process depending on this hierarchy, according to the method of extent analysis, each criterion is taken and extent analysis for each criterion, gi; is performed on, respectively. Therefore, m extent analysis values for each criterion can be obtained by using following notation :

$$M_{gi}^{1}, M_{gi}^{2} \dots\dots\dots M_{gi}^{in}, i = 1,2,3 \dots\dots\dots\dots n$$

(1)

Where all the M_{gi}^{j} (j= 2,3….m) are TFNs

$$S_i = \sum_{j=1}^{m} M_{gi}^{j} * \left[\sum_{i=1}^{n}\sum_{j=1}^{m} M_{gi}^{j}\right]^{-1}$$

(2)

To obtain $\sum_{j=1}^{m} M_{gi}^{j}$, perform the fuzzy addition operation of *m* extent analysis values for a particular matrix such that

$$\sum_{j=1}^{m} M_{gi}^{j} = \left(\sum_{j=1}^{m} l_j, \sum_{j=1}^{m} m_j, \sum_{j=1}^{m} u_i\right) \quad (3)$$

And to obtain $\left(\sum_{i-1}^{n}\sum_{j-1}^{m} M_{gi}^{j}\right)^{-1}$, perform the fuzzy addition operation of M_{gi}^{j} (j= 1,2,……..m) values such that

$$\sum_{i=1}^{n}\sum_{j=1}^{m} M_{gi}^{j} = \left(\sum_{i=1}^{n} l_i, \sum_{i=1}^{n} m_i, \sum_{i=1}^{n} u_i\right) \quad (4)$$

And then compute the inverse of the vector in equation (4) such that

$$\left[\sum_{i=1}^{n}\sum_{j=1}^{m} M_{gi}^{j}\right]^{-1} = \left(\frac{1}{\sum_{i=1}^{n} l_i}, \frac{1}{\sum_{i=1}^{n} m_i}, \frac{1}{\sum_{i=1}^{n} u_i}\right) \quad (5)$$

(2) The degree of possibility of $M_2 = (l_2, m_2, u_2) \geq M_1 = (l_1, m_1, u_1)$ is defined as

$$V\ (M_2 \geq M_1) = \sup_{y \geq x} \left[min(\mu_{M_1}(x), \mu_{M_2}(y))\right] \quad (6)$$

And can be equivalently expressed as follows

$$V\ (M_2 \geq M_1) = hgt(M_1 \cap M_2) = \mu_{M_2}(d) \quad (7)$$

$$= \begin{cases} 1 & if\ m_2 \geq m_1, \\ 0 & if\ l_1 \geq u_2 \\ \frac{l_1 - u_2}{(m_2 - u_2) - (m_1 - l_1)} & otherwise \end{cases} \quad (8)$$

Where d is the ordinate of the highest intersection point D between μ_{M_1} and μ_{M_2} . In the figure (2) the intersection between M_1 and M_2 can be seen.

To compare M_1 and M_2, we need both the values of V ($M_1 \geq M_2$) and V ($M_2 \geq M_1$)

(3) the degree of possibility for a convex fuzzy number to be greater than k convex fuzzy numbers M_i (*i*=1,2….k) can be defined by

V ($M \geq M_1$, M_2 ….. M_k) = V ($M \geq M_1$) and V ($M \geq M_2$) … and V ($M \geq M_k$) = *min* V ($M \geq M_i$),(*i*= 1,2…..*k*) (9)

Assuming that d' (A_i) = *min* V ($S_i \geq S_k$) (10) For *k*= 1,2……..*n*

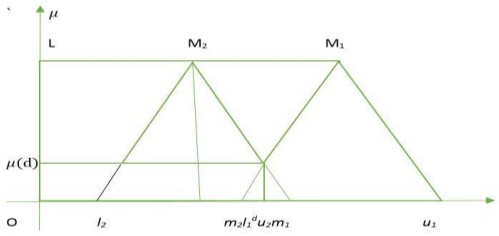

Fig. 2 The intersection between M_1 and M_2

$$W' = \{(d'(A_1), d'(A_2), \ldots\ldots d'(A_n)\}^T \quad (11)$$

Where A_i (*i*= 1,2……..*n*) are *n* elements

(4) Via normalization, the normalized weight vectors are

$$W = \{(d(A_1), d(A_2), \ldots\ldots d(A_n)\}^T \quad (12)$$

Where *W* is a non-fuzzy number. This gives the priority weights of one alternative over another.

3. Case Study

3.1. Problem statement

A reputed cement industry Holcim Bangladesh LTD faced many problems in their supplier selection. They call for a tender and then they investigate their profile then call two or three supplier and trial their raw materials to produce cement but this causes their profit or success at late. For finding solution we proposed a model of supplier selection. In this section the steps those should be followed in supplier selection are briefly described. These are the basic steps of our proposed method and can be used as a guideline for the selection of appropriate supplier with more or less modifications.

Step 1 Calling for public tender

This is the first step of the proposed process in selecting a new supplier from different available suppliers. In this step, companies are invited publicly to tender against the requirements of the company as in the traditional process. To make this process open for all, the company may publish their invitation in any mass media so that no supplier becomes uninformed. The demands of the company should be clearly stated in the advertisement so that the supplier may understand everything easily without any confusion. As the main target is to select the best supplier among different alternatives, the calling approach should be in such a way that only the better suppliers are encouraged to apply. Consequently, the initial screening will not be that much time-consuming and cumbersome. To ensure the fairness of the selection process, the applicants may also know the selection procedures and the steps included. They should conceive that if they want to compete, they have to be fit for the job. Every supplier will be given equal priority without being biased.

Step 2 Determination of key supplier selecting and evaluating indicators

As supplier selection is a vital process for every organization, it is very much important to define clearly the basis on which this selection process will be performed. To select a suitable supplier we have to first evaluate and then to decide which supplier will be selected. To perform this, we defined some evaluation criteria.In the application, the control hierarchy has been shown in Figure1.

To solve by AHP, we have defined the five main criteria as objective functions, which are used to find out the desired output. They are:

Objective 1 Price of supplied product (PR)
Objective 2 Quality System (QS) of the supplier
Objective 3 General and organizational profile (GS) of supplier
Objective 4 Service Facilities (SF)
Objective 5 Manufacturing capability (MC)

Step 3 By using AHP method compute weighted value of each suppliers

In this step, first by using AHP the weighted values of each sub-indicator are computed to measure the relative weight put the manufacturer against each sub-indicator, as shown in Table 2.

Table 2: Detailed data collected against each sub-criterion among available suppliers

No.	Evaluation Factors	Supplier A	Supplier B	Supplier C
1	Supply capacity	5000000 tons/yr	6200000 tons/yr	5800000 tons/yr
2	Production technology	Both auto and semi-auto	Both auto and semi-auto	Both auto and semi-auto
3	Material lead time	Approximately 15 days	Approximately 12 days	Approximately 10 days
4	Price	Medium	Medium	Medium
5	Facility Location	Approximately 28 km	Approximately 25 km	Approximately 30 km
6	Production Capacity	17000000 tons/yr	20000000 tons/yr	18000000 tons/yr
7	Communication system	Through EDI	Through EDI	Through EDI
8	Flexibility	15 days	20 days	22 days
9	Reputation	Good	Good	Good
10	Material appropriateness and Quality	Good	Moderate	Good
11	Warrantee	Good	-	-
12	Financial position	Good	Good	Good
13	R & D activities	Fair	Good	Moderate
14	Sales & Service network	Best	Good	-
15	Technological knowledge &Training	On the job & Off the job facility	On the job facility	On the job facility
16	Quality system certificate of the supplier	ISO 9001	ISO 9001	ISO 9001
17	Employees number	2500	1800	2200
18	Packaging & Carrying Capacity	Fair	Good	Good
19	Environmental impact(Green Purchasing)	Moderately Followed	Moderately Followed	Strictly Followed
20	Purchase transaction	Self-pick up	Self-pick up	Self-pick up
21	Management & Organization	Well structured & responsibilities are clearly defined	Well structured & responsibilities are clearly defined	Well structured & responsibilities are clearly defined

Now, using AHP we will determine the weights put by the manager against each key indicator. So, we begin by writing down a 5 × 5 matrix which is known as pair wise comparison matrix A. The entry in row i and column j of A (aij) indicates how much more important objective i is than objective j. Then, the matrix for five criteria is given below:

Table 3: Pair wise comparison for criteria attributes

		QS	GS	SF	PR	MC
	QS	1	3	5	7	9
	GS	0.333	1	2	4	7
A	SF	0.2	0.5	1	3	6
	PR	0.143	0.25	0.333	1	4
	MC	0.111	0.143	0.167	0.25	1
	SUM	1.787	4.893	8.5	15.25	27

Now, divide each entry in column i of A by the sum of the entries in column i. This yields a new matrix A norm (for normalized) in which the sum of the entries in each column is 1.Normalized form from the above calculation is given below according to the pair-wise comparison**:**

Table 4: Normalized form for the criteria attributes

		QS	GS	SF	PR	MC
	QS	0.56	0.613	0.588	0.459	0.333
	GS	0.186	0.204	0.235	0.262	0.259
A_{NORM}=	SF	0.112	0.102	0.118	0.197	0.222
	PR	0.08	0.57	0.039	0.066	0.148
	MC	0.062	0.29	0.0196	0.016	0.037
		QS	GS	SF	PR	MC

Now, estimate Wi as the average of the entries in row i of A_{NORM}. This yield:

W_{QS}= 0.5106; W_{GS}= 0.229; W_{SF}= 0.1502;
W_{PR}= 0.0768; W_{MC}= 0.033

We have checked the degree of consistency and found that the pair wise comparison matrix does not exhibit any serious inconsistencies. Now, we will find out the scores of each objective by making proper comparisons among the suppliers (A, B, C). For example, in SF the weighted values can be calculated as:

Finally we get,
$(\text{Supplier A})_{SF} = .259$
$(\text{Supplier B})_{SF} = .105$
$(\text{Supplier C})_{SF} = .634$

In the same way, we can calculate the weighted values of other key indicators and the results have been summarized in a Table 6 as shown below.

Table 5: The weight values of each supplier candidate for sub-indicators

QS	GS	SF	PR	MC
Supplier A = 0.539 Supplier B = 0.297 Supplier C = 0.164	Supplier A = 0.547 Supplier B = 0.151 Supplier C = 0.302	Supplier A = 0.259 Supplier B = 0.105 Supplier C = 0.634	Supplier A = 0.143 Supplier B = 0.286 Supplier C = 0.571	Supplier A = 0.27 Supplier B = 0.613 Supplier C = 0.118

The hierarchy of supplier selection process

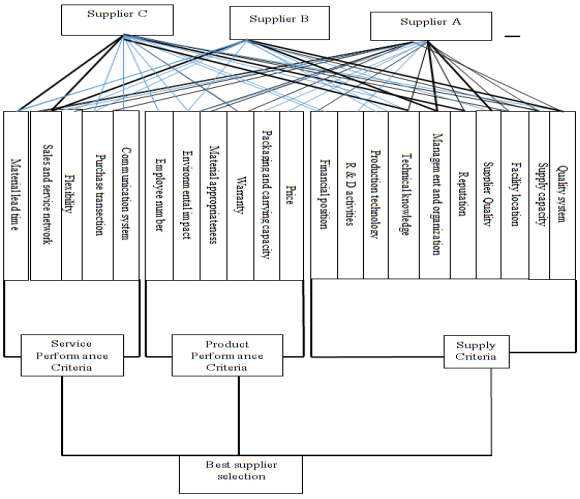

Step 4 *Validation of the result and finally select the best supplier*
As we have already solved the algorithm and all the results on hand, we can rate the suppliers as below.
From above calculation the over-all score is calculated as follows:

Table 6: Score calculation and determination of overall score

Supplier name	Score calculation	Overall score
Supplier A	(0.5106*0.539)+(0.229*0.547)+ (0.1502*0.259)+(0.768*0.143)+(0.033* 0.27)	0.459
Supplier B	(0.5106*0.297)+(0.229*0.157)+(0.1502 *0.105)+(0.0768*0.286)+(0.033*0.613)	0.244
Supplier C	(0.5106*0.164)+(0.229*0.302)+ (0.1502*0.634)+(0.0768*0.571)+(0.033* 0.118)	0.296

It is seen that the over-all score for supplier A is 0.459 is largest value. Hence our selected supplier in AHP method is supplier A and then the supplier B, supplier C.

Table 7: The linguistic variables and their corresponding fuzzy numbers:

Equally preferred (EP)	(1, 1, 1)
Weakly preferred (WP)	(2/3, 1, 3/2)
Fairly strongly preferred (FSP)	(3/2, 2, 5/2)
Very strongly preferred (VSP)	(5/2, 3, 7/2)
Absolutely preferred (AP)	(7/2, 4, 9/2)

Table 8: Priority vectors for the decision hierarchy

Variables in level 1	Level 1 Priorities	Variables in level 2	Level 2 Priorities	Variables in level 3	Level 3 Priorities
Supplier criteria	0.36	Quality system (QS)	0.1	Supplier A	0.13
				Supplier B	0.57
				Supplier C	0.29
		Supply capacity (SC)	0.09	Supplier A	0.99
				Supplier B	0
				Supplier C	0
		Facility location (FL)	0.1	Supplier A	0.29
				Supplier B	0.35
				Supplier C	0.35
		Quality system of the supplier (QSS)	0.1	Supplier A	0.67
				Supplier B	0.33
				Supplier C	0
		Reputation (R)	0.8	Supplier A	0.57
				Supplier B	0.29
				Supplier C	0.132
		Management and organization (MO)	0.1	Supplier A	0.99
				Supplier B	0
				Supplier C	0
		Technical knowledge (TK)	0.08	Supplier A	0.4
				Supplier B	0.18
				Supplier C	0.4
		Production technology (PT)	0.12	Supplier A	0.52
				Supplier B	0.09
				Supplier C	0.38
		R & D activities (RD)	0.1	Supplier A	0.67
				Supplier B	0.33
				Supplier C	0
		Financial position (FP)	0.1	Supplier A	0.57
				Supplier B	0.29
				Supplier C	0.132
Product performance	0.36	Price (P)	0.15	Supplier A	0.26
				Supplier B	0.36
				Supplier C	0.37
		Packaging and carrying capacity (PCC)	0.167	Supplier A	0.99
				Supplier B	0
				Supplier C	0
		Warranty (W)	0.22	Supplier A	0132
				Supplier B	0,57
				Supplier C	0.29
		Material appropriateness (MA)	0.2	Supplier A	0.67
				Supplier B	0.33
				Supplier C	0
		Environmental impact (EI)	0.2	Supplier A	0.29
				Supplier B	0.35
				Supplier C	0.35
		Employee number (EN)	0.06	Supplier A	0.4
				Supplier B	0.18
				Supplier C	0.4

Service Performance	0.26	Communication system (CS)	0.22	Supplier A	0.26
				Supplier B	0.36
				Supplier C	0.37
		Purchase Transaction (PT)	0.18	Supplier A	0.57
				Supplier B	0.29
				Supplier C	0.132
		Flexibility (F)	0.15	Supplier A	0.99
				Supplier B	0
				Supplier C	0
		Sales and service network (SS)	0.20	Supplier A	0.52
				Supplier B	0.09
				Supplier C	0.38
		Material lead time (ML)	0.23	Supplier A	0.26
				Supplier B	0.36
				Supplier C	0.37

The overall score of each supplier is given below: In Table 10, each column of the matrix was multiplied by the priority weight at the top of the column and then those values were added up for each row. At the end, the priority weights of the alternatives with respect to supplier attribute were calculated. The same calculations have been applied to the sub-attributes of product performance attribute and service performance attribute and the priority weights of the alternatives with respect to product performance and service performance attributes have been calculated.

Table 9: Main-attributes of the Goal

	Supplier Criteria	Product Performance	Service Performance	APW
WEIGHT	0.37	0.37	0.26	
Supplier A	0.58	0.45	0.50	0.51
Supplier B	0.25	0.33	0.23	0.27
Supplier C	0.18	0.22	0.27	0.22

The priority weights are shown in the table 13. The priority weights of each alternative with respect to the main attributes were combined and the priority weights of each alternative were determined.
To shorten the process of supplier selection, Code block programming software and Excel sheet is used extensively to facilitate the comparison of main attributes, sub-attribute's , alternatives. The priority weights of each alternative in this solution process are (0.51, 0.27 and 0.22). It is clear from the final scoring that the supplier A is most preferred and the supplier B is the next recognized supplier.

4. Conclusion

By using a common set of criteria or attributes, supplier selection is a broad comparison to identify the best supplier with the highest potential needs and at a reasonable price that meets firm's requirements consistently. Actually the selection of the best supplier not only reduces purchasing cost but also improves corporate competitiveness in modern comprehensive business sector. Hence, supplier selection is one of most important challenge in multi-criteria decision making process. In this paper, supplier selection has been done using both method AHP and Fuzzy-AHP process to assess the right supplier in the cement industry. In AHP method only some quantative analysis is used to select right supplier but it is not enough, there are also some other qualitative factors that needs to be taken into account. For this reason we also discussed Fuzzy-AHP approach that considers three main attributes and twenty one sub-attributes for supplier selection and the best supplier is selected by calculating the overall score of each supplier using Fuzzy-AHP approach.

In this paper the AHP calculations are done using Math-lab software but in case of Fuzzy-AHP code-block programming is used.MS-Excel sometimes used but very little. Here programming software is used to avoid hand-made error. Various information on suppliers such as delivery date, certification of the organization, quality system of the supplier can be collected from the database of ERP .This can reduce time consuming effort in the supplier selection process.

REFERENCES

[1] Mohammad Marufuzzaman and Kazi Badrul Ahsan*, Supplier selection and evaluation method using Analytical Hierarchy Process (AHP): a case study on an apparel manufacturing organization, *International Journal of Value Chain Management*, Vol.3, No.2, (2009).

[2] Lee, A.H.I., A fuzzy supplier selection model with the consideration of benefits, opportunities, costs and risks, Vol. 36 ,2009, pp. 2879–2893.

[3] WEBER, C. A., Data Envelopment Analysis Approach to Measuring Vendor Performance, *Journal of Supply Chain Management*, Vol.1, No.1, pp. 28-39, (1996).

[4] YAHYA, S. and KINGSMAN, S. ,Vendor Rating for an Entrepreneur Development Program A Case Study Using the Analytical Hierarchy Process Method., *Journal of Operational Research Society*, Vol. 50, No 9. pp. 916-930, (1999).

[5] NARASHIMAN, R., TALLURİ, S., and MENDEZ, D.,Supplier evaluation and rationalization via data envelopment analysis: an empirical examination. *Journal o f Supply Chain Management*, Vol. 37, No. 3, (2001) .

ICMIEE-PI-140135

A New Concept in Modern Industry Sector; "Virtual Industry Model"

Md. Badiuzzaman [1] *Dr. Md. Rafiquzzaman* [2]

[1, 2] Department of Industrial Engineering and Management, Khulna University of Engineering & Technology, Khulna-9203, BANGLADESH

ABSTRACT

In this paper we proposed a framework named "Virtual Industry Model" so that one can start an industrial business even with a little amount initial cost. Our goal is to setup an industry in virtual world which is an extension of virtual office to virtual industry. We arranged a structure of all working process of an industry trough internet, with others ICT tolls and contact with an industry for physical production. Total system is operated using online software that is communicate, synchronize among all segment of production process. Thus, entrepreneurs can fulfill their dream by establish an industry in very low cost, less paper works as well as they can make their product more versatile compare to the other traditional industry, because virtual industry can rent any possible industry for required product. Despite of some disadvantage like the system requires a sophisticated software and fulltime communication support, but our proposed "Virtual Industry" model reduce all of the initial high investment related limitations to setup an industry and our feasibility study says that the conceptual industry will perform better than traditional industry. Finally it can be concluded that our proposed model is a new concept in modern industrial sector.

Keywords: Virtual Industry, E-commerce, ICT, Traditional Industry

1. Introduction

In 21st century everything almost relates and working based on or with help of information and communication technology (ICT). In the Electronic Commerce or e-commerce, it is a new and most futuristic term called virtual office. The e-commerce industry is one of the most progressive sectors of the economy. Many people have good idea to setup an industry but they couldn't due to lack of sufficient resources such as high initial cost, insufficient information etc. Virtual industry model consist of some modern technology, tools and some new ideas [1-3]. It is an alternate solution for establishing an industry .

Our model refers a complete industry without owning a physical industry, land and other expensive infrastructure. Entrepreneur can fulfill their dream to establishing an industry using this model. Now a day we can see that freelancing, outsourcing is most popular working process in IT field where people can work for any industry situated at far away staying their home. Even outsourcing is on of most spread working method in Bangladesh. This "Virtual Industry Model" will be such kind of industry where people (designers, engineers, manager, and other employee) will be able to perform their task from their residence or any place using some modern technology like computers, mobile etc. So the industry based on our model doesn't require any big office space. Now the question is where will be the production? We know that there has a production method using rental or contractual industry. In our model, we will use such type industry for final production shown in Fig.1

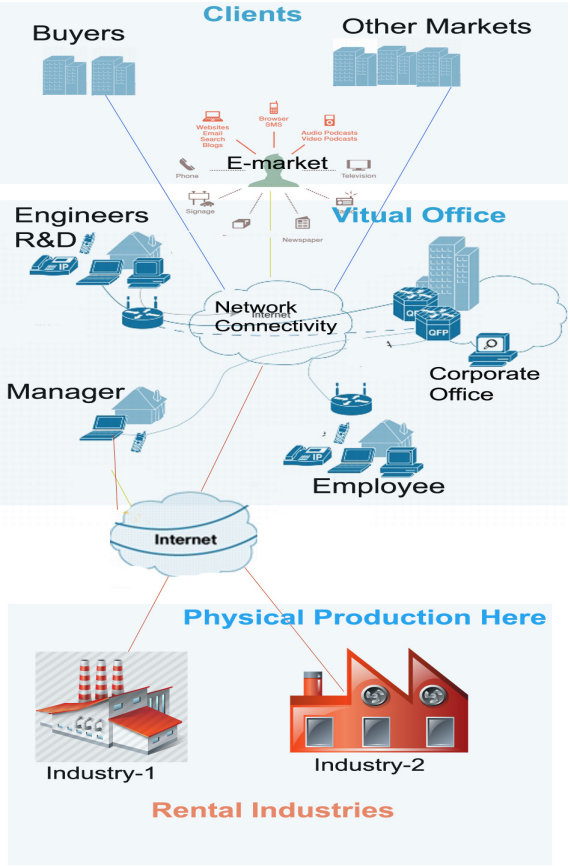

Fig.1: Virtual Industry Model

* Corresponding author. Tel.: +88-01911788766, 01790847464

E-mail address: bodiuzzaman116@gmail.com, rafiqbitr@yahoo.com

This will reduce a big fixed cost of setup an industry and variable cost to maintaining that industry. It is also costly to hire an expert fulltime for industrial research and development purpose to design and implement new product ideas. Otherwise we proposed to hire expertise as they can work for our industry from his/her place anytime for less remuneration as pert time worker. He needs to logon the system and fulfill his given task what will be explained later. The total system will work using software which will be named "Virtual Industry System". The software contains strong database system and other computing method as required for an industry. It is also interesting that using of software the total process will be automated and computerized what is a big deal in industrial process.

2. Virtual Industry Model Components

In Fig.1 we can see the model which has three different blocks as clients, virtual office, and rental industry. These three blocks has several components to perform and communicate to work as an industry. It is very important to make all the components synchronized for smooth operation of an industry using this model. Here we will know about the different blocks:

2.1 Clients

Clients are simply who will be the consumer of precuts. Or for whom we are going to produce something. For an industry most of case clients are buyer group/company, local or foreign market (export), and in our model online customers are a big market. Buyers will be able to access and order directly from their place via our "Virtual Industry System" software and the software will count, calculate the production plan from some given inputs from clients and mangers. It will be very easy to forecast about product's wants from the software. After that it will make automatically production plan, MRP, CRP, and BOM. And finally manger/admin will give approval to order about the production lot to pre contracted industry.

2.2 Virtual office

In our model it is the focal point and backbone to establish a virtual industry. Virtual office is a business location that exists only in cyberspace. A virtual office setup allows business owners and employees to work from any location by using technology such as laptop computers, cell phones and internet access. A virtual office can provide significant savings and flexibility compared to renting a traditional office space. Meetings can be conducted via teleconferencing and video conferencing, and documents can be transmitted electronically. Some companies even provide virtual office services to give virtual offices the prestige associated with physical offices, such as an important-sounding address, a professional phone-answering service and even occasional rental of office space and conference rooms. Everybody in this model are free to work from any place but they have to complete their tasks as per given time and deadline. So we will ensure our goal and outputs from the human resource. The figure showing that all the officials are working at their home via connecting a common network and software system that we developed in our model. Virtual office needs only a single room to setup some technical equipment. Mangers and owner of the industry can monitor the whole working process from anywhere around the world. We can say that this industry will be a global working environment.

2.2.1 Managers

Mangers are key person for an industry to manage the man, machine material in an industry. As our model skipped physical industry but also manager will play key role in our model. He will organize and synchronized among all part. We made it very easy for manger as he is going to perform any task, monitor the progress using software and other tools.

2.2.2 Engineers (R&D)

In this model we proposed part time such expertise who will perform research and development, making new product ideas. And due to part time work our industry will pay less than a fulltime such employee. As it will reduce cost also gives chance to hire several experts as entrepreneur wish. The model showing that this employee also connected via internet to total system. For renting other industries we doesn't need to recruit engineers for maintenance, operation and other purpose as a typical industry needs.

2.2.3 Employee

An industry needs different employees for different purpose as example accounts, marketing, advertising etc. All of such employee will also work through a network accessing the virtual industry software system and complete their job as they given. Interesting fact is that in this system, there has no opportunity to claiming wages without working exactly because of the software system.

2.2.4 Network Connectivity

Network connectivity means physical (wired or wireless) and logical (protocol) connection of a computer network or an individual device to a network, such as the Internet or a LAN. In web hosting this can be referring to how the company receives its bandwidth and how it is connected to the provider. In our proposed model it is first needs to have an fast network connectivity to connect all the functional blocks. We can use internet, mobile networks and other fast internet service for connecting remote human resources to login our software and work. To communicate with rental industry we can use internet, if the industry locate near our virtual office network area we can use LAN. Because it needs very high speed fulltime network to observe, communicate and monitor that industry's working progress due to virtual industry's order. In Fig.1 we can see the functional blocks are connected

through various network and network tools, technologies which are very important in our model.

3. Rental Industries

Hire, rent and lease are common term in industrial production system. Many companies use rental or leasing industries and factories for produce their product. Such as world famous brand "Nike" which has no own factory for produce their branded shoes. There have lot of companies who just use their brand but produce from different factories basis of contract. In our model we emphasized on rental factory. Since factory, machineries, land and other setup is the main cost that is obstacle for an entrepreneur to establish an industry. Also maintaining and operating is important for a physical industry but our model doesn't need it. We need to make a good connectivity on the virtual software system. At least we can fix an employee for physically conducting with the factory and he will inputs the update of production planning at software system from there. We have an advantage in virtual industry model that we could plan for producing several products as we wish, because we can make our production contact with any factories in local or foreign region. This gives "Virtual Industry" versatility of production thinking.

4. Tools & Technology for Implementation

Actually this model is a package of software and communication tools that will make an environment of an industry like traditional industry in virtual/cyber world. First of all it needs strong online database based software where all types of processing and input will be taken. Using technical tools like wireless or wired internet, IP camera, computers, laptop, and modem in this software we will make the environment that we are calling "Virtual Industry Model". So our main goal to develop a software system named "Virtual Industry System". We are using very familiar tools and technology that people can use the system frankly. And it will be a user-friendly feasible model. All user will use a graphical user interface and user login option for perform their task, the system will count how long they are working, what is the status of all tasks, progress of production, production status and statistics. This software has some sophisticated and expandable feature like we can sell, show our products via online marketing or e-commerce system. It will be a whole solution to operate the operation of an industry. Once it will be able to replace the typical industrial working system that the current era needs.

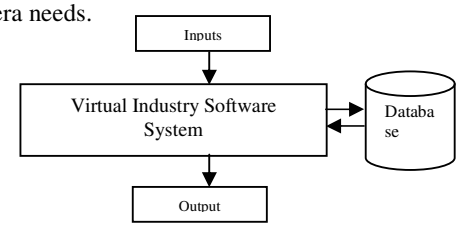

Fig.2: Basic Structure of virtual industry system software

4.1. Virtual industry Software

The "Virtual Industry Model" will work based on a software named "Virtual Industry System". The basic structure of virtual industry system software is shown in fig.2. This software is an online application what is able to perform a complete official and industrial working process through it. It takes some inputs from its users and processing that it gives desired outputs. The system will be customizable due to industry. Flowchart of virtual industry software is sown in fig.3.

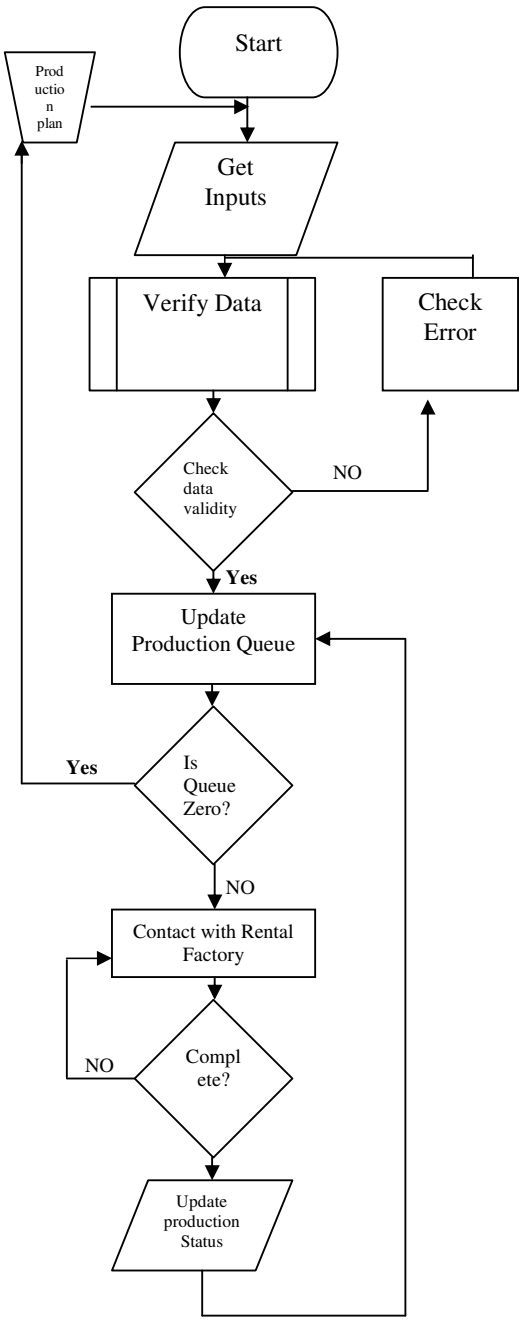

Fig.3: Flowchart of Virtual Industry software system

4.1.1. Inputs of Software

There could be several users to input data but the types of input will be production plan, market analysis data, research and development data, product order, statistical data of production. Capacity of this virtual industry will be also given into this software, to calculate wages of employees, monitoring and evaluating them the software needs employee information and his log data of working hours. As it is a computerized system, so it will be able to calculate and evaluate them. Sometime it may needs to input some video from IP cam to observe from remote place the rental factory if it satisfies the contracting policy. Then the manager or owner of industry will be able to watch product status, progress and also will be able to show that to his buyers.

4.1.2. Database

It is an important part of this online software system. All inputs will be accumulated and stored in this database for further needs and processing. Every single working process, single change will be stored in this database. This database is able to make a paperless office which is applied in some big companies like google or Grameenphone Ltd in Bangladesh. As our target to reduce industry setup cost and makes it affordable for all entrepreneur to touch their dream. Thus, this tool will help us robustly.

4.1.3. Outputs of Software

Output of this software not the desired product but the status of production. It will provide a transparent view of the industry in a single click which is impossible at a traditional industry. It will produce all type of report, analytical data, and payments of employees, company revenue, production order, and production queue status. From the production plan of and industry, production process, marketing, delivery status and capacity all data will be output of this software. As a results manger or administration will able to control easily everything which is tough in typical industry due to various limitation like CBA association, political hazard etc.

5. Key difference than traditional e-business

Now a day, we can find a lot of e-business, e-marketing and many more electronics based business [1-3]. Most common and known system is freelancing. A person who works as a writer, designer, performer, or the like, selling work or services by the hour, day, job, etc., rather than working on a regular salary basis for one employer is called freelancer. In IT based industry it is most used employment method all over the world. In fact various industries now hiring people basis on freelancing. It is one of most progressive way where IT professional earning in Bangladesh. All of this has its own small customized management system but not a common model. We are developing a common model for all of this e-business, e-markets, IT based freelancing. Our model proposes that any business can be performed using a common model. This model will be an instigated system where a single freelancer to a complete manufacturing system could be implemented. By connecting several part of a manufacturing system from various remote places we can structure any business even a heavy industry, for what we are calling our model “Virtual Industry Model”. Where the existing systems have no ideal model and one is not applicable for another. Rather our “Virtual Industry Model” is ideal model that will be applicable for any electronics based business system.

6. Conclusions

In this paper we proposed a framework named “Virtual Industry Model” so that one can start an industrial business even with a little amount initial cost. We developed a structure of all working process of an industry trough internet and others ICT tolls in where total system is operated using online software that is communicate, synchronize among all segment of production process. Thus, entrepreneurs can fulfill their dream by establish an industry in very low cost, less paper works as well as they can make their product more versatile compare to the other traditional industry. Additionally, those industries which have less production and marketing opportunity, they can be profited when they will conduct production with a “Virtual Industry”. Despite of some disadvantage like the system requires a sophisticated software and fulltime communication support, but our proposed “Virtual Industry” model reduce all of the initial high investment related limitations to setup an industry and our feasibility study says that the conceptual industry will perform better than traditional industry. Finally it can be concluded that our proposed model is a new concept in modern industrial sector.

REFERENCES

[1] Dev Chaffey, E-Business and E-commerce Management (Third Edition): pag. 3–145

[2 Ian Daniel, E-commerce get it right! (First Edition) pag. 1-20

[3] Dev Chaffey & Fiona Eillis-Chadwick, Digital Marketing (Fifth Edition): pag. 3-122

ICMIEE-PI-140136

A Review on Bamboo and Jute Fiber Reinforced Polymer composites

Joyeshree Biswas [1,*], *Dr.Md. Rafiquzzaman* [2]
[1, 2] Department of Industrial Engineering and Management, Khulna University of Engineering & Technology, Khulna-9203, BANGLADESH

ABSTRACT
Natural fiber reinforced polymer composite consist of polymer matrix reinforced with natural fiber. Traditional fibers such as glass, carbon, and synthetic fiber reinforced polymer composites have high strength, but it involves high processing cost and also it is not renewable and not environmental friendly. For these reason researchers are searching for low cost, environmental friendly and renewable material such as natural fiber based composite. Natural fibers have attracted the attention of many researchers due to their low cost, easy availability, light weight, ease of separation, recyclable properties, enhanced energy recovery, high toughness, noncorrosive nature and good thermal properties. Most common types of natural fiber are jute, coconut, hemp, kenaf, flax, banana, bamboo, rice, cotton, sisal etc. Natural fiber reinforced polymer composites are used in packaging, construction, automobile applications. This paper deals with review of bamboo and jute fiber reinforced polymer composite, especially their mechanical properties.

Keywords: Natural Fiber, Mechanical Properties, Polymer Composite.

1. Introduction

Composite materials have rapidly become a material of choice as an alternative to other traditional materials such as metals and have found applications in many sectors [1]. The term 'composite' has been used in material science refers to a material made up of a matrix containing reinforcing agent. Reinforcement provides strength and rigidity, helping to support structural load. The matrix or binder (organic or in-organic) maintains the position and orientation of the reinforcement [2]. A fiber reinforced polymer (FRP) is a composite material consisting of a polymer matrix imbedded with high-strength fibers. Generally, polymer can be classified into two classes, thermoplastics and thermosetting. The most commonly used thermoplastics for this purpose are polypropylene (PP), polyethylene, and poly vinyl chloride (PVC); while phenolic, epoxy and polyester resins are the most commonly used thermosetting matrices [3].Synthetic fibres like glass, carbon and aramid are widely used in polymer-based composites because of their high stiffness and strength properties. However, these fibres have serious drawbacks in terms of their biodegradability, initial processing costs, recyclability, energy consumption, machine abrasion, health hazards, etc. Despite these most significantly, adverse environmental impacts alter the attention from synthetic fibres to natural/renewable fibres [4]. Advantages of natural fibers over traditional reinforcing materials such as glass fibers, carbon fibers, etc. are their specific strength properties, easy availability, light weight, ease of separation, recyclable properties, and enhanced energy recovery, high toughness, noncorrosive nature, low density, low cost, good thermal properties, reduced tool wear during processing and less abrasion to processing equipment, less machine wear, easy with respect to polymer matrices, no health hazards [2]. S.V. Joshia and L.T. Drzal [5] have reported that natural fiber reinforced composites are likely to be environmentally superior to glass fiber reinforced composites in most applications also for the following reasons: (1) natural fiber production results in lower environmental impacts compared to glass fiber production, (2)NFR(Natural Fibre Reinforced) composites have higher fiber content for equivalent performance, which reduces the amount of more polluting base polymers,(3) lower weight of NFR composites improves fuel efficiency and reduces emissions during the use phase of the components, especially in auto applications and (4) end of life incineration of natural fibers results in energy and carbon credits. Applications of natural fiber composites are expanding in many engineering areas, from civil construction to automobile manufacturing, construction, aerospace, packaging etc. Uses of natural-fiber reinforcement have proven viable in a number of automotive parts [1]. The drawback that limits extensive uses of these fibres is hydrophilic nature of the fibres that lowers the compatibility with the hydrophobic matrix. This causes ineffective stress transfer throughout the interface of the composites to fiber. Chemical treatment is an essential processing parameter to reduce hydrophilic nature of the fibres and thus improves adhesion with the matrix. The chemical sources for the treatments include alkali, silane, acetylation, benzoylation, acrylation and acrylonitrile grafting, maleated coupling agents, permanganate, peroxide, isocyanate, stearic acid, sodium chlorite, triazine, fatty acid derivate (oleoyl chloride) and fungal [4]. Another drawback is degradation behavior of natural fibre that limits the processing temperature of composite. Natural fibre generally starts degrading at about 240ºC. Lignin starts degrading at a temperature around 200ºC and hemicelluloses and cellulosic constituents degraded at higher temperatures. The degradation of natural fibres needs to be considered in the development of composites in both manufacturing

* Corresponding author. Tel.: +88-01754467446
E-mail address: joyeshreebiswas@yahoo.com

and materials in service [4]. This paper will review bamboo and jute fibre reinforced polymer composite. Bamboo and jute fibres are widely available in Bangladesh and they can become an alternative source to synthetic fibres.

2. Classification of natural fiber

Natural fibre is a type of renewable sources and a new generation of reinforcements and supplements for polymer based materials. Classification of natural fibre based on their on their origin is shown in Fig. 1, [6].

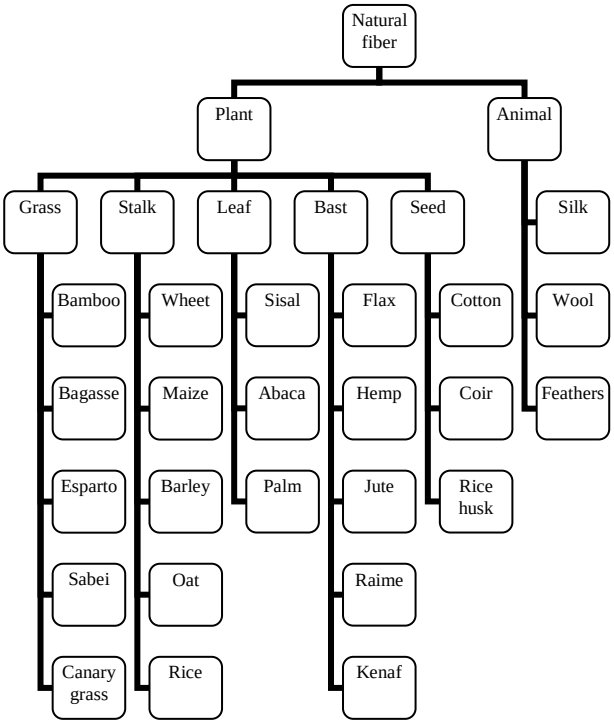

Fig.1 Classification of natural fibre [6]

3. Properties of natural fiber

Plant based natural fibres are lignocellulosic in nature and are composed of cellulose, hemicelluloses, lignin, pectin and waxy substances. The successful use of these fibres is dependent on their well-defined structural and mechanical properties. These properties are influenced by the locality in which they originate, climate conditions, age of the plants and the extraction methods that are used [4]. Table 1 summarizes the mechanical properties of natural and man-made fibres [6].

Table 1 Properties of natural and manmade fibers [6].

	Density (g/cm^3)	Elongation (%)	Tensile Strength (MPa)	Young's modulus
Cotton	1.5-1.6	7.0-8.0	287-597	5.5-12.6
Jute	1.3	1.5-1.8	393-773	26.5
Flax	1.5	2.7-3.2	345-1035	27.6
Hemp		1.6	690	
Ramie		3.6-3.8	400-938	61.4-128
Sisal	1.5	2.0-2.5	511-635	9.4-22.0
Coir	1.2	30.0	175	4.0-6.02
Kenaf		1.5	930	53
Abaca			430-760	
Oil palm	0.7-1.55	3.2	248	25
Pineapple		2.4	170-162.7	60-82
Banana		3	529-914	27-32
Wool		25-35	120-174	2.3-3.4
Spider silk		17-18	875-972	11-13
Tussah silk	1.32	33.48	248.77	5.79
Bamboo	1.4		500-740	30-50
E-glass	2.5	2.5	2000-3500	70.0
Aramid	1.4	3.3-3.7	3000-3150	63.0-67.0
Carbon	1.4	1.4-1.8	4000	230.0-240.0

4. Mechanical Properties of Bamboo Fiber Reinforced Polymer composite

The effect of fibre loading on the mechanical properties of bamboo fibre reinforced polymer composites are discussed in details as follows:

Tingju Lu and Shimeng Liu [7] investigated the mechanical properties of the bamboo cellulose fibers (BCF) Poly(lactic acid) Composites. With the addition of virgin BCFs, the Young's modulus was increased slightly because of the high stiffness of the BCF itself. While the ultimate tensile strength, the elongation at break as well as the impact toughness were decreased obviously. This was mainly attributed to the bad dispersion of BCFs and poor interfacial interaction between the filler and matrix. Three kinds of modifications, alkali soaking or silane coupling cellulose and maleic anhydride grafting poly (L-lactic acid) were applied in the preparation of cellulose/poly(L-lactic acid) composites to improve properties. The results demonstrated that the alkali soaking provided the composites with highest strength and Young's modulus, increased by 28.6% and 36.8% respectively than PLLA filled with untreated BCFs. The highest impact toughness and elongation were achieved by silane agent pretreatment, which were 115% and 62% higher than those of poly(L-lactic acid) reinforced with virgin bamboo cellulosic fibers. Maleic anhydride grafting had moderate effects on both the stiffness and ductility, exhibiting best over-all properties.

C.S. Verma and V.M. Chariar [8] developed layered bamboo–epoxy composite laminates and found their mechanical properties. Three samples were prepared with different lamina configurations/angles: Sample A (0º/0º/0º/0º/0º), Sample B (0º/45º/0º/45º/0º), Sample C(0º/90º/0º/90º/0º). Strength of sample A was greater than sample B and of sample B than sample C because in sample A, all fibers of laminas were in unidirectional and cross linking of the polymer was continuous where as in samples B and C, all fibers were not unidirectional and cross linking was not continuous. Thus it can be said that the tensile and compressive properties of layered laminated bamboo–epoxy composite decrease

with increase in lamina angle from 0º. Flexural strength of sample A was greater than sample C and of sample C was greater than sample B but sample B predicted more toughness compare to sample A and C.

K.J. Wonga and S. Zahi [9] studied fracture behavior of short bamboo fibre reinforced polyester composites. The matrix was reinforced with fibres ranging from 10 to 50, 30 to 50 and 30 to 60 vol.% at increments of 10 vol.% for bamboo fibres at 4, 7 and 10 mm lengths respectively. The results revealed that at 4 mm of fibre length, the increment in fibre content deteriorates the fracture toughness. As for 7 and 10 mm fibre lengths, positive effect of fibre reinforcement was observed. The optimum fibre content was found to be at 40 vol.% for 7 mm fibre and 50 vol.% for 10 mm fibre. The highest fracture toughness was achieved at 10 mm/50 vol. % fibre reinforced composite, with 340% of improvement compared to neat polyester. Tensile strength was improved only at 10 mm fibre length with increasing fibre content and highest was achieved with 25% improvement for 10 mm/40 vol.%. Young's modulus was deteriorated by fibre reinforcement except at 10 mm/40 vol.% of reinforcement.

Bamboo cellulose fibers were treated with NaOH aqueous solution and silane coupling agent, respectively, before they were applied into epoxy composites. Compared with the untreated cellulose filled epoxy composites, the NaOH solution treatment increased the tensile strength by 34% and elongation at break by 31%. While silane coupling agent treatment produced 71% enhancement in tensile strength and 53% increase in elongation at break [10].

Shah Huda and Narendra Reddy [11] investigated the properties of bamboo strips (BS)/polypropylene (PP) web composite and saw that flexural properties of BS–PP web decrease with increasing width of the strips. Increasing bamboo strip concentration up to 50% led to increase in flexural strength but the strength decreased at higher bamboo concentrations. Modulus of elasticity increased up to 60% and then decreased. However, the difference in modulus of elasticity between 60% and 70% bamboo concentration was not statistically significant. Offset yield load also increased up to 50% and then decreased. For similar weight and thickness, flexural strength, flexural modulus of elasticity, and offset yield load of bamboo Strips/polypropylene web composites were 3.8*, 1.7*, and 3.9* higher than that of jute/PP composites. For bidirectional BS–PP composites, the compared values were 5.8*, 2.9*, and 6.5*, respectively.

The influence of moisture absorption on the interfacial shear strength (IFSS) of bamboo/vinyl ester composite was studied. The IFSS decreased steadily with the increase of relative humidity at manufacture. The IFSS achieved at normal room conditions (20ºC, 60% RH) was only a half of what was achieved in the dry condition and almost zero at 90% RH. The IFSS decreased almost linearly with the increase of bamboo strip moisture content from 0% to about 12%. A further increase of 2% in bamboo moisture content caused a reduction of more than 80% in IFSS. Exposure of the bamboo/vinyl ester composite to water caused significant damage to the interfacial shear strength. The damage took place in the first 9 day, causing a 38% reduction in IFSS. Prolonged water immersion up until 100 day did not result in further reduction in IFSS [12].

R. Krishnaprasad, N. R. Veena [13] prepared composites based on polyhydroxybutyrate (PHB) and bamboo microfibrils with various microfibrils loading and evaluated mechanical properties. The mechanical properties showed that pure PHB exhibited tensile strength of 10.99 MPa and Youngs modulus of 1044 MPa. The tensile strength was found to be decreasing with addition of 5%wt of bamboo microfibrils. At lower loading (5%wt.) the microfibrils were insufficient for reinforcement of the PHB matrix and act as flaws or stress concentration points. With further increase in microfibril loading the tensile strength was found to be increasing and reached a maximum at fiber loading of 20% wt. Further increase in fiber loading (20–30%wt) resulted in a decrease in tensile strength. Young modulus increase with increasing fibre loading and reached maximum at 30% fibre loading to 2165 MPa. Pure PHB showed impact strength of 595 kg/m². The impact strength and elongation at break were found to be increasing with incorporation of microfibrils and reached a maximum value at 10 wt% of the fiber to 991 kg/m² and 2.25% respectively, then found to be decreasing with an increase in the filler loading.

Sandeep Kumar and Veena Choudhary [14] studied on the compatibility of unbleached and bleached bamboo fibers (UBF and BBF) with LLDPE matrix. The tensile strength, modulus and elongation of pure LLDPE were found to be 19 MPA, 128 MPA, and 1079(%), respectively. The overall tensile strength of both types of composites was lower when compared to pure LLDPE because of the poor interfacial adhesion due to hydrophilic BF and hydrophobic LLDPE. The tensile strength was dropped by 40–53% in UBF and 26–48% in BBF composites. Tensile modulus increased from 34 to 130% in UBF composites and 50 to 97% in BBF composites as a function of fiber content. Up to 30% fiber content, BBF composites gave higher modulus than UBF composites but on further increasing the fiber content UBF gave high modulus value when compared to BBF composites. The elongation decreased significantly upon incorporation of BF.

Chuanbao Wang and Sanjiu Ying [15] used a novel strategy to prepare the bamboo fiber (BF)/polypropylene (PP) composites which improved the distribution of BF so as to increase the mechanical properties. Both tensile and flexural properties of raw and alkali treated BF/PP composites were found to

increase with the increment of fiber content. The mechanical properties of the alkali treated BF/PP composites were found to be much higher than that of the composites of untreated BF. The water absorption of alkali treated BF/PP composites was observed to be lower than that of raw BF/PP composites with the whole BF contents. These may be attributed to the better distribution of BF in the matrix by the premixing of BF with PP fiber and stronger fiber-matrix interaction caused by alkali treatment of BF.

5. Mechanical Properties of Jute Fiber Reinforced Polymer composite

The effect of fibre loading and on the mechanical properties of jute fibre reinforced polymer composites are discussed in details as follows:

Bhanu K. Goriparthi and K.N.S. Suman [16] investigated effect of fiber surface treatments on tensile properties of PLA/ Jute fiber composites. To improve the adhesion of jute fiber with polylactide (PLA) surface of the jute fiber was modified by alkali, permanganate, peroxide and silane treatments. The fiber treatments significantly influenced the tensile strength and moduli of the composites. Increment of tensile properties followed the order: silane > peroxide > permanganate > alkalization > untreated. Treatment of jute fiber with silane (trimethoxy methyl silane) resulted in the maximum improvement of tensile strength and moduli by 35% and 38% respectively. Modification of fiber surface resulted in improvement of flexural strength and flexural modulus by 24% and 41% respectively in case of silane treated composite. Unlike to tensile and flexural properties izod impact strength of treated composites was quite lower than the untreated composite. Alkali, permanganate and peroxide treated composites exhibited lower thermal stability, whereas silane treated composites showed a higher thermal stability when compared to untreated composites.

Md. Rashnal Hossain and Md. Aminul Islam [17] prepared jute epoxy laminated composite at staking sequences (0/0/0/0), (0/+45°/-45°/0) and (0/90°/90°/0). For all cases, a total of 25% volume fraction of jute fiber was incorporated. In the case of (0/0/0/0) and (0/+45°/-45°/0) laminate, longitudinal tensile strength was higher than that of the transverse direction. However, for (0/90°/90°/0) laminate, tensile strength in both directions had been found to be very close to each other. In longitudinal direction, the tensile strength and stiffness of 0-0 laminate composites was higher compared to that of 0-45 or 0-90 laminate composites but the trends for bending strength were opposite. In transverse direction, both the tensile and bending strengths 0-0 laminate composites had been found to be lower compared to that of 0-45 or 0-90 laminate composites.

Bidirectional jute fiber reinforced epoxy composite was fabricated by hand lay-up technique and their physical and mechanical properties were evaluated. The presence of the voids may affect the mechanical properties of the composites. The void formations in the polymer composite occur due to air entrapment during the preparation of resin system and moisture absorption during material processing or storage. Pure epoxy had the minimum void content, with the addition of 12 wt. % fiber the void content increased instantly to 5.312 % but with increase from 12 wt. % to 48 wt.% fiber content, the void content of the specimens decreased. Surface hardness of pure epoxy is 40 HRB and increased by 77% with the incorporation of 12 wt. % fiber in the matrix. Hardness of the composite increased with increasing fibre loading and reached maximum at 48% fiber loading to 85.5 HRB .The tensile strength increased from 43MPa to 110 MPa and tensile modulus from 0.15 GPa to 4.45 GPa with the fiber content increase from 0 to 48 wt%. Flexural strength, flexural modulus and inter laminar shear strength decreased with fibre loading from 0-12% due increase in void formation, increased after 12% fiber loading and reached maximum at 48% fiber loading to 55.8 MPa, 3.02 GPa and 66.5 MPa respectively [18].

Abu Saleh Ahmed and Md. Saiful Islam [19] studied the effect of chemical treatment on physical and mechanical properties of jute fiber reinforced polypropylene (PP) biocomposites with different fiber loading (5, 10, 15, and 20 wt%). Before being manufactured jute fiber/PP composite, raw jute fiber was chemically treated with succinic anhydride for the chemical reaction with cellulose hydroxyl group of fiber and to increase adhesion and compatibility to the polymer matrix. The mechanical properties of jute/PP composite in terms of tensile strength and young's modulus was found to be increased with fiber loading up to 15 wt% with treated fibre and 10wt% with untreated fibre and decreased at 20 wt%. Conversely, flexural strength and flexural modulus of both composite increased with fiber loading up to 10 wt% and start decreasing at 15 wt%.The tensile strength of treated jute fiber/PP composites at 15 % loading exhibited higher improvement compared to raw one (i.e. treated composite-7.88 MPa and raw composite -6.1 MPa). For 10 % fiber loading, the flexural strength of raw and treated composite were 60.66 MPa and 67.72 MPa respectively. This indicated tensile strength and flexural strength of the treated composites increased by approximately 6-29% and 5-17 % respectively over the raw composites. The hardness and water absorption of both composite increased with increasing fibre loading. The treated jute/PP composite had higher hardness (Rockwell) and lower water absorption value compared to that of the untreated ones.

Mechanical properties of non-woven jute soy (NJS) and woven jute soy (WJS) composites shows that jute loading increased from 40 to 60 wt%, tensile strength and modulus of NJS increased from 24.8 to 37.1 MPa and 780 to 1040 MPa respectively. Similar trend

obtained in case of flexural properties as the flexural properties increased from 25.8 to 38.4MPa and the flexural modulus enhanced from 832 to 1120MPa with increase in jute loading from 40 to 60 wt %. Tensile and flexural strength of WJS composites increased from 22.4 to 35.6MPa and 21.9 to 33.5MPa respectively with increase in jute loading (40 to 60 wt%). Jute and soy resin are hydrophilic in nature showing contact angle values of 42.1◦ and 50.4◦ respectively, which correspond to water absorption values of 190% and 110.6% respectively after 24 h immersion in water. Due to high hydrophilic nature of soy resin, after 7 days of biodegradation, soy resin degraded most by 52% weight loss [20].

The physical characteristics and mechanical properties of cement mortar can be significantly improved by the jute fibre reinforcement. By optimizing the processing conditions and fibre loading, the cold crushing strength and flexural strength, flexural toughness and the toughness index of the mortar has significantly been increased [21].

Lifang Liu and Jianyong Yu [22] investigated the biodegradability of PBS/jute composites. The weight loss of PBS/jute composite after 180 days was 62.5%, 54.8% and 47.3%, respectively, in accordance with the fibre content of 10 wt.%, 20 wt.% and 30 wt.%. While the weight losses of pure PBS film and bulk jute fibre were 31.4% and 24.7% respectively, showing that compounding of jute fibre and PBS accelerates the biodegradation of either jute fibre or PBS. The weight loss was also observed to decrease with the increase of fibre content, and maximum at the fibre content of 10 wt.%. In the case of the effect of fibre diameter, the weight loss was found to decrease with decreasing fibre diameter. For the effect of fibre surface modification, the order of higher weight loss was PBS/untreated jute> PBS/alkali treated jute> PBS/coupling agent treated jute. Furthermore, the composite of PBS/woven fabric has the highest weight loss, followed by that of PBS/nonwoven fabric and PBS/bulk jute fibre respectively. Takian Fakhrul and M.A.Islam [23] found that the biodegradability of polypropylene is improved by blending it with small additions (5%) wood sawdust and wheat flour. The composite was exposed to open atmosphere, moist soil, water and brine solution for a period of 15weeks. The most pronounced degradation was observed in sample exposed to brine solution. PP-sawdust composite exhibited greater biodegradability than PP-wheat flour composite.

There are many other factors that can influence the performance of natural fiber reinforced composites. Apart from the effects of loading and chemical treatments the properties of the natural fiber reinforced composites can also be influenced by the manufacturing techniques and process parameters [3]. Natural fibre based thermoset composites can be successfully manufactured by several methods, including wet lay-up, resin transfer moulding (RTM) and vacuum assisted resin infusion[1] .By varying and controlling the process conditions (pressure, temperature, time) of the fabrication method mechanical properties of natural composite material can be improved [7]. Dirk E. Hebel and Alireza Javadian [24] studied the tensile strengths of the bamboo reinforced composites with the relationship of pressure, temperature and press/hold time. The tensile strengths of the composites for different pressures and temperatures of the hot press fabrication were analyzed. Highest tensile strengths were obtained when applying pressures of 20 MPa and 25 MPa at temperatures of 100ºC and 80ºC respectively. At a pressure of 25 MPa increasing the temperature above 100ºC favors the carbonization of the bamboo strip and decomposition of composite. At 140ºC the bamboo fibers started to carbonize already at a pressure of 15 MPa. At 15 MPa and 20 MPa, maximum tensile strength was found at 100 ºC. It is possible to tune the mechanical properties of the composite by either varying the temperature or the pressure within a specific range. Thereby, the maximum tensile strength holds not only for one single pressure/temperature combination but may be also obtained when lowering the temperature and simultaneously increasing the pressure or vice versa. The variation of the press/hold time between 5/5 min and 60/60 min appears to affect the tensile strength of the composites only in a time range below 30 min. The interactions formed between the bamboo fibers and the polymer in the 5/5-min press/hold composites were weaker as for 15/15 min samples which is reflected by the lower tensile strength. After 30 min processing time, no significant improvement of the tensile strength is achieved by elongating this time. It is possible to tune the press/hold time by varying the temperature. Increasing the temperature increases the energy amount per time delivered to the system.

6. Conclusion

In this study, the use of bamboo and jute fibre as reinforcement in polymer based composites were reviewed from viewpoints of status and future expectations of natural fibres. Natural fibers such as bamboo and jute fibers are using as an alternative to glass, carbon and other manmade fibers because of their low cost, easily availability, lightweight and apparently environmentally superior properties. Composites based on these fibres may have very good implications in the automotive and transportation industry. Since Bangladesh is one of the largest bamboo and jute fibre producing countries in the world, polymer composites based on these fiber and the subsequent applications would be very attractive from the economic point of view. From the above discussion, it became quite evident that newer composites using abundantly available bamboo and jute fibers are brings new trends in composite materials. However, suitable cost-effective design and fabrication techniques for manufacture should be developed. Finally it can be concluded that

with systematic and persistent research there will be a good scope and better future for bamboo and jute fibre-polymer composites in the near future.

REFERENCES

[1] Abdullah A. Kafi, Kevin Magniez, Effect of manufacturing process on the flexural, fracture toughness and thermo-mechanical properties of bio-composites, *Composites: Part A*, Vol. 42, pp 993–999 (2011).

[2] Shrikant M. Harle, The Performance of Natural Fiber Reinforced Polymer Composites: Review, *ISSN 2278-3652*, Vol. 5, pp 285-288 (2014).

[3] H. Ku, H. Wang, A review on the tensile properties of natural fiber reinforced polymer composites, *Composites: Part B*, Vol. 42, pp 856–873 (2011).

[4] M.M. Kabir, H. Wang, Chemical treatments on plant-based natural fibre reinforced polymer composites, An overview, *Composites: Part B*, Vol. 43, pp 2883–2892 (2012).

[5] S.V. Joshi, L.T. Drzal, Are natural fiber composites environmentally superior to glass fiber reinforced composites?, *Composites: Part A*, Vol. 35, pp 371–376 (2004).

[6] Mei-po Ho, Hao Wanga, Critical factors on manufacturing processes of natural fibre composites, *Composites: Part B*, Vol. 43, pp 3549–3562 (2012).

[7] Tingju Lu, Shimeng Liu, Effects of modifications of bamboo cellulose fibers on the improved mechanical properties of cellulose reinforced poly(lactic acid) composites, *Composites: Part B*, Vol. 62, pp 191–197 (2014).

[8] C.S. Verma, V.M. Chariar, Development of layered laminate bamboo composite and their mechanical properties, *Composites: Part B*, Vol. 43, pp 1063–1069 (2012).

[9] K.J. Wonga, S. Zahi, Fracture characterisation of short bamboo fibre reinforced polyester composites, *Materials and Design*, Vol. 31, pp 4147–4154 (2010).

[10] Tingju Lua, Man Jianga, Effect of surface modification of bamboo cellulose fibers on mechanical properties of cellulose/epoxy composites, *Composites: Part B*, Vol. 62, pp 191–197 (2014).

[11] Shah Huda, Narendra Reddy, Ultra-light-weight composites from bamboo strips and polypropylene web with exceptional flexural properties, *Composites: Part B*, Vol. 43, pp 1658–1664 (2012).

[12] Hongyan Chen, Menghe Miao, Influence of moisture absorption on the interfacial strength of bamboo/vinyl ester composites, *Composites: Part A*, Vol.40, pp 2013–2019 (2009).

[13] R. Krishnaprasad, N. R. Veena, Mechanical and Thermal Properties of Bamboo Microfibril Reinforced Polyhydroxybutyrate Biocomposites, *J Polym Environ*, Vol. 17, pp 109–114 (2009).

[14] Sandeep Kumar, Veena Choudhary, Study on the compatibility of unbleached and bleached bamboo-fiber with LLDPE matrix, *J Therm Anal Calorim*, Vol. 102, pp 751–76 (2010).

[15] Chuanbao Wang, Sanjiu Ying, A Novel Strategy for the Preparation of Bamboo Fiber Reinforced Polypropylene Composites, *Fibers and Polymers*, Vol. 15, pp 117-125 (2014).

[16] Bhanu K. Goriparthi, K.N.S. Suman, Effect of fiber surface treatments on mechanical and abrasive wear performance of polylactide/jute composites, *Composites: Part A*, Vol. 43, pp 1800–1808 (2012).

[17] Md. Rashnal Hossain, Md. Aminul Islama, Tensile behavior of environment friendly jute epoxy laminated Composite, *Procedia Engineering*, Vol. 56, pp 782 – 788 (2013).

[18] Vivek Mishra, Sandhyarani Biswas, Physical and Mechanical Properties of Bi-directional Jute Fiber epoxy Composites, *Procedia Engineering*, Vol. 51, pp 561 – 566 (2013).

[19] Abu Saleh Ahmed and Md. Saiful Islam, Impact of Succinic Anhydride on the Properties of Jute Fiber/Polypropylene Biocomposites, *Fibers and Polymers*, Vol. 15, pp 307-314 (2014).

[20] Ajaya Kumar Beheraa, Sridevi Avancha, Fabrication and characterizations of biodegradable jute reinforced soy based green composites, *Carbohydrate Polymers*, Vol. 88, pp 329–335 (2012).

[21] Sumit Chakraborty, Sarada Prasad Kundu, Improvement of the mechanical properties of jute fibre reinforced cement mortar: A statistical approach, *Construction and Building Materials* Vol. 38, pp 776–784 (2013).

[22] Lifang Liu, Jianyong Yu, Biodegradability of poly (butylene succinate) (PBS) composite reinforced with jute fibre, *Polymer Degradation and Stability*, Vol. 94, pp 90–94 (2009).

[23] Takian Fakhrul, M.A.Islam, Degradation behavior of natural fiber reinforced polymer composite, *Procedia Engineering*, Vol. 56, pp 795 – 800 (2013).

[24] Dirk E. Hebel, Alireza Javadian, Process-controlled optimization of the tensile strength of bamboo fiber composites for structural applications, *Composites: Part B*, Vol. 67, pp 125–131 (2014).

ICMIEE-PI-140137

Compressive Properties of Ceramic Microballoon Syntactic Foams

Zulzamri Salleh [1,2], *Md Mainul Islam* [2*] *and Jayantha Ananda Epaarachchi* [1]
[1]Centre of Excellence in Engineered Fibre Composites and School of Mechanical and Electrical Engineering,
Faculty of Health, Engineering and Sciences, University of Southern Queensland,
Toowoomba, Queensland 4350, AUSTRALIA
[2]Universiti Kuala Lumpur, Malaysian Institute of Marine Engineering Technology (MIMET),
32200, Lumut Perak, MALAYSIA

ABSTRACT
In this paper, fabrications of vinyl ester syntactic foams with different contents of ceramic microballoons or microspheres were prepared using the open mould method for compression specimens. The effects of the ceramic microballoons on the mechanical properties, particularly compressive properties were investigated. The results show that the syntactic foams with vinyl ester matrix possess strength behaviour varied with different contents of ceramic microballoons. Ceramic microballoons have an important effect on the stress-strain, mean plateau stress and strain energy absorption capacities of syntactic foams. The results also show that the content of ceramic microballoons in vinyl ester syntactic foams should be controlled in order to obtain a good combination of compressive strength and energy absorption capacities. The reasons are discussed here in details.

Keywords: Syntactic foams, ceramic microballoons, compressive properties, content.

1. Introduction

Ceramic microballoon or microspehere is defined as an inorganic nonmetallic polycrystal sphere or approximate sphere with the size of micron [1]. Ceramic microballoon is widely used in the medical industry, chemical and nuclear industry and also in the defence industry. From the literature review, ceramic microballoons are widely used combining with Aluminium matrix. It is not only limited use for aviation, but also used for civil industry and automotive industry [1]. This metallic foam is defined as metal-matrix syntactic foams (MMSFs) with the first production in 1990s [2]. The structural engineering is always desired for the better mechanical properties of material such the compressive behaviour of the products. For example stronger and lighter materials such as syntactic foams are better choice for both of the mechanical behaviours particularly for structural engineering. In the previous works, many researchers were interested on the properties of the foams particularly characteristic on the compressive strength and the absorbed energy. The investigation on the effects of the microballoon size on the compressive strength is very beneficial for future engineering [3]. From the research it was found that smaller microspheres ensure higher compressive strength because they contain fewer flaws in their microstructure than the larger ones. While Palmer et al. proved that larger microspheres contain more porosity in their walls and more flaws in their microstructure than the smaller ones [4]. From the literature review it was also found that the chemical reaction contributed detrimental effect on the load transfer during mechanical testing [5]. Balch et al. found that the microspheres have at least the same importance in the syntactic foams as the matrix material [6]. The fracture strength and the yield strength of the matrix determine the failure stress of the syntactic forms. Therefore, the investigation on mechanical properties, particularly compressive strength effect will be affected the quality of the microspheres and it is very important. Nevertheless, no report was published for ceramic microballoons mix with vinyl resin as matrix materials. In this study, the report will cover from the preparation of samples to the mechanical properties. The aim of this study is to investigate the distribution of the constituents in the ceramic microballoons with the different contents' effect on the vinyl ester resin as matrix material. All these information will be beneficial and acceptable for the production of ceramic microballoon of syntactic foams.

2. Materials and Methodology

Ceramic microballoons type SL75 is used in the difference weight percentages as 2.0wt.%, 4.0wt.%, 6.0wt%, 8.0wt.% and 10.0wt.% to fabricate these foams. E-spheres a ceramic bubble was supplied by Envirospheres Pty. Ltd (Australia) company are used in this study [7]. Their main parameters are provided by supplier is listed in Table 1.

Table 1 Properties of ceramic microballoon.

V	ρ	T	Compressive Strength	Chemical Composition
45	0.40	1600-1800	45MPa	SiO_2-60% $Al2O_3$-38% TiO_2-2%

Fig. 1 shows the SEM photo for ceramic microballoon provided by the supplier [7]. Vinyl ester resin, supplied by Norox Australia Company, is used as the matrix material. This is diglicidyl ether of bisphenol A-based resin. An amine-based MEKP is used as a hardener.

* Corresponding author. Tel.: +6174631 1338
E-mail address: Mainul.Islam@usq.edu.au

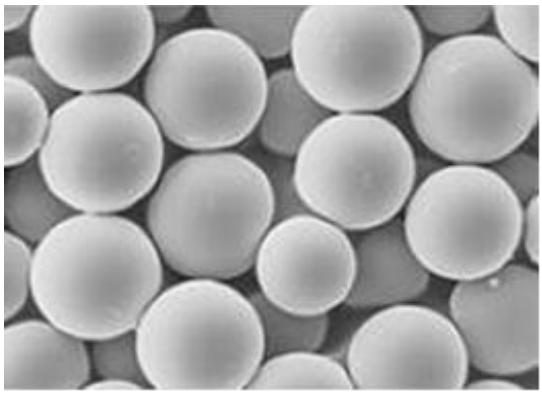

Fig.1 SEM photo for ceramic microballoons [7]

The synthesis method consists of mixing measured quantities of ceramic microballoons in the vinyl ester resin and mixing them until a slurry of uniform viscosity is obtained with the intermittent mixing approximately 4 ~ 5 minutes. The hardener is added to this slurry and gently mixed using a stir magnetic bar at stir machine until completely mixing also approximately 4 ~ 5 minutes. Fig. 2 shows that the slurry was mixed with stir magnetic bar during the process of syntactic foams.

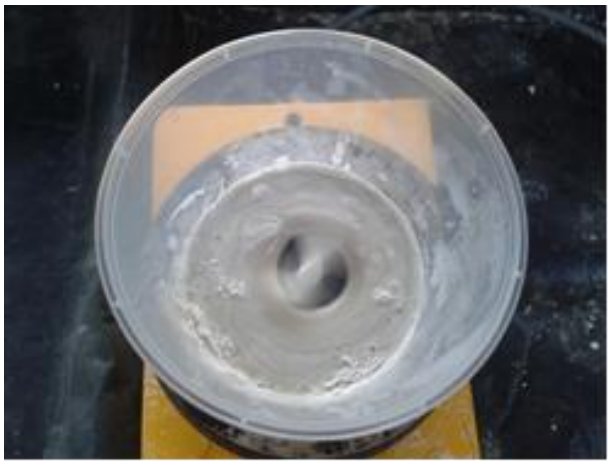

Fig.2 The magnetic stir bar for mixing process

The mixture is then cast in PVC pipe moulds with the diameter 19mm and length 42mm. The overview of one of the specimen photos shown at Fig. 3 after re-moulded process and next is sent to the curing process. This size is following the ASTM D-695 for compression test of syntactic foams [8]. The specimens cure in the mould for 24 h at room temperature and re-moulded on next day for post-cured at 80^{o}C for 4 h in the oven. After post cure all the specimens need to trim by using the grinder machine on the top and bottom surfaces. This process is done before proceeding to compression testing because both surfaces need the flatness surface in order to avoid the erosion phenomena which is will affect the compression values. The compression values also can be affected when the specimens were not located properly between upper jaw jig and lower jaw jig. Hence, the specimens must be centred on the lower jaw jig surface and make sure it is not too tight or too loose. Otherwise the starting point will have negative values, and then the graph will not start from the zero point. Selection for the data is important while plot the graph for stress versus strain during the data analysis process.

Fig.3 Overview one of specimen syntactic foam for compression test

Compression test is carried out using MTS test systems show at Fig. 4. The test is carried out at the constant deformation rate of 2 mm/min. The compression tests are carried out on specimens following the ASTM-D695 dimensions. Fig. 5 shows the enlarged photo for one of the specimen was tested during compression test at MTS machine. From the output result, there are two parameters has been selected for data analysis such as load and crosshead displacement to develop the stress–strain curves. Then for next step it is necessary to re-calculate the actual values of stress and strain by using the area formula for cylindrical shape of each sample. This is a very important procedure need to be taken because the raw data for the stress and strain from the machine sometime inaccurately.

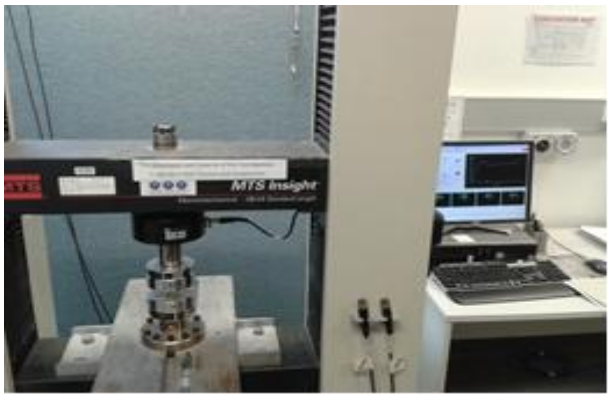

Fig.4 MTS Insight machine for compression testing

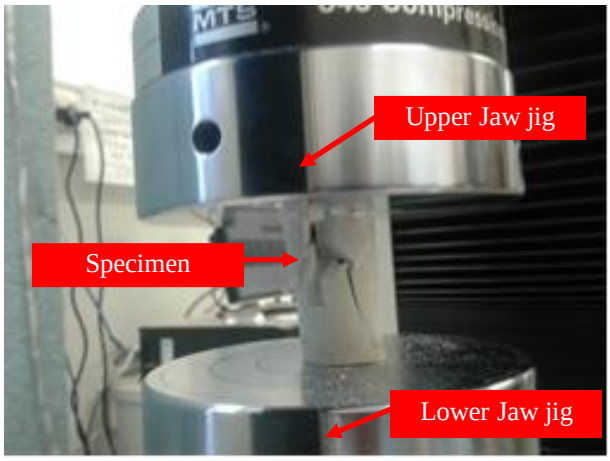

Fig.5 MTS Specimen in-progress for compression test

3. Results ad Discussion

The representative compressive engineering stress-engineering strain curve for all types of vinyl ester/ceramic microballoons are presented in Fig.6. From the stress–strain profiles both neat resin and syntactic foams show the same consisting of a linear elastic region followed by a strain softening region that is characterized by a slight drop in stress. When the compression is continued further, then the stress starts rising again. The increase in stress is faster and significantly higher in the case of neat resin, whereas for syntactic foams it depends on the type and volume fraction of microballoons [8]. The compressive modulus values are measured as the slope of the initial linear region of the stress–strain graphs and are presented in Fig. 6. This initial linear deformation region (I) is where stress, increased linearly to the first peak (from this gradient line it can be defined the yield strength or Young's Modulus), followed by a plastic plateau stage (II) where stress slightly increased as the strain increasing, then a densification stage (III) where stress raises sharply with strain increasing slightly. It can be observed that all syntactic foam compositions show a stress plateau, which is a typical feature of most types of syntactic foams[11].The compressive modulus values at stage (I) is measured as the slope of the initial linear region of the stress–strain graphs shown in Fig. 7. The results show that the compressive modulus of syntactic foams increases with increasing the contents of microballoons and only composition with 2wt% shows the lower modulus behaviour. It is also seen that the modulus decreases as the volume fraction of the same type of microballoons increases. Several syntactic foam compositions show compressive modulus values comparable to that of the neat resin, however, the specific moduli for most composites are 10–47% higher than the neat resin tested at the same compression rate, see Fig. 6. Hence, for compressive loading conditions, syntactic foams can lead to a significant advantage over the neat resin in terms of weight saving. Compressive strength of composites is defined as the first peak in the Engineering stress–Engineering strain curves at stage (I). Fig. 7 shows that the strength values for several foam compositions are comparable to each other's.

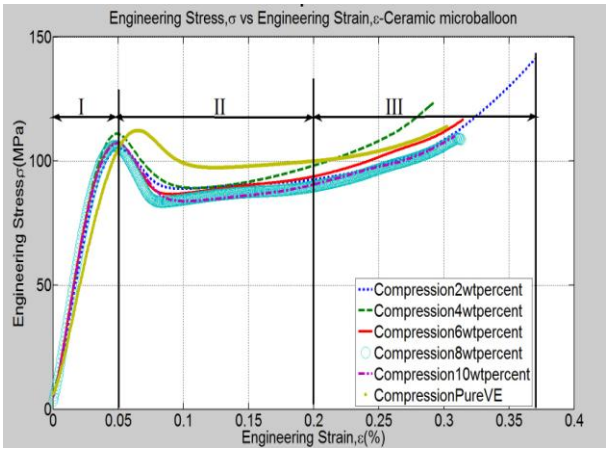

Fig.6 Engineering stress–Engineering strain curves.

The results also indicate that the compressive strength can be tailored over a wide range by selecting microballoons SL75 by using them in different weight percentages. The yield strengths of the foams with ceramic microballoon contents of 2.0wt.%, 4.0wt.%, 6.0wt.%, 8.0 wt.% and 10.0wt.% are about 102, 115, 105, 103 and 104 MPa, respectively.

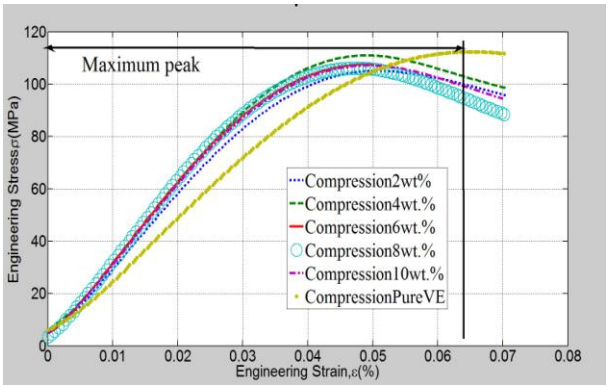

Fig.7 Graph for initial linear deformation region (I).

For the mean plateau stresses of these foams at stage (II) (shown in Fig. 8 are around 95, 124, 90, 87 and 89 MPa. This indicates that SL75 ceramic microballoons have a significant effect on the foams yield strength, mean plateau strength and densification stress under compression state. The yield strength for the specimen 4.0wt.% have the maximum stress is about 115MPa. Similar phenomenon appears on mean plateau stress of the foams as having the higher stress of 124MPa. All of these results could be effected on higher energy absorption capacity of the foams containing different contents of SL75 ceramic microballoon (as shown in Fig. 10) and the energy absorption capacity decreased with the strain increasing like other foams [7,12]. Therefore, for densification strain, SL75 ceramic microballoons enhance the densification strain of the foams. It is interesting that there is slightly reduction in

the energy while variety of the foams increased with different contents of SL75 ceramic microballoon.

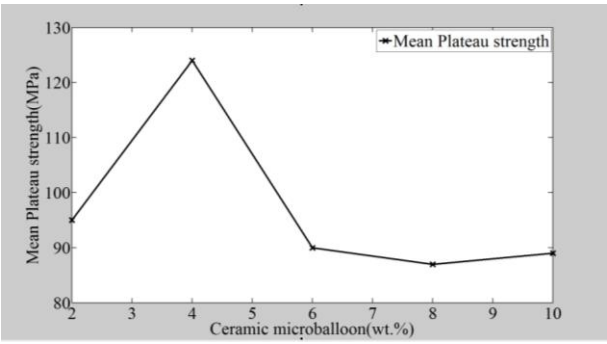

Fig.8 Graph for mean plateau region strength (II).

Fracture features of five types of syntactic foams are compared in Fig. 9. It is observed that the foam specimens containing 2wt.% microballoons deform with longer time to fracture as well as have higher stress behaviour at 141MPa compared other specimens. Although the specimens with 4wt.% have maximum compressive strength in the earlier stage (I) but it did not sustained at the end because it fractured around 124MPa compared with specimen 2wt.%. The failure features of these specimens are similar to those presented earlier [31], which include initiation of shear cracks in the specimen and formation of fragments from the side walls. Inclusion of higher weight percentage of stiff ceramic microballoons in relatively ductile matrix results in increased brittleness of the composite.

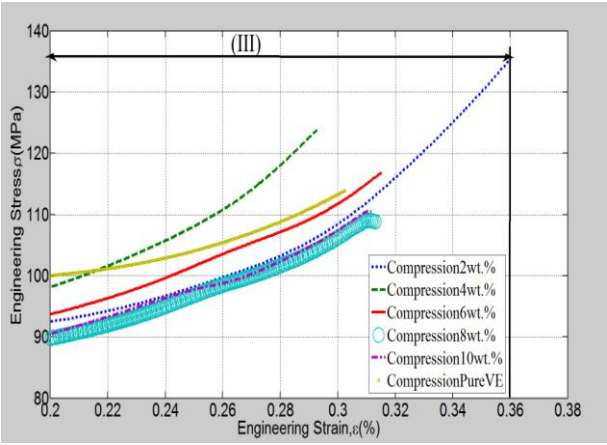

Fig.9 Graph for fractured feature region (III).

An area under the graph of the engineering stress-Engineering strain can be defined as energy absorption capacity [9]. Numerically it can also be determined by using the trapezoidal integration method and can be plotted by using the Matlab software. Energy absorption capacity (E) is an important aspect to evaluate the properties of metal foams. It is also known as energy absorption and can be calculated till the end of plateau region (II) i.e., where the stress value starts to increase again [10]. Fig. 10 shows the graph of energy absorption capacity vs microballoon contents. The energy absorption capacity (E) of closed-cell vinyl ester ceramic syntactic foams was calculated according to Eq. (1):

$$E = \int_0^{\varepsilon} \sigma d\varepsilon \qquad (1)$$

Where σ is called as engineering stress and ε is called as engineering strain which is varied from zero to maximum strain values. The energy shows decreases after adding more weight contents of ceramic microballoons starting with initial content of 2wt. %, initially starting from 40J then decrease slowly, almost four times to 32.3J. This trend was observed and reported that it was similar for all the ceramic material systems [11]. This result also supports that the ductility of the specimens is more, hence the internal structure become weak and has difficulty to combine with matrix vinyl ester resin.

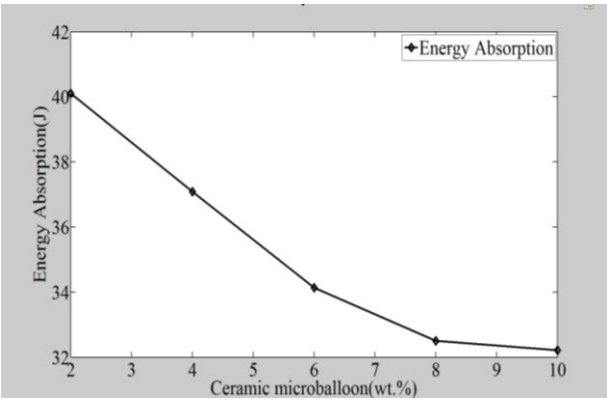

Fig.10 Graph for energy absorption capacity.

4. Conclusion

The effects of SL75 ceramic microballoons on the compressive properties of vinyl ester syntactic foams were studied and the results were summarised as follows:

- The distribution of ceramic microballoons particularly of 4wt.% possesses the highest compressive stress.
- The addition of ceramic microballoons prominently improved the mean plateau stress specifically, for specimens with 4 wt.% while for both behaviours of densification strain and energy absorption capacity was led by specimens with 2 wt.%.
- Hence, by using the small amount of ceramic microballoons it might also reduce the porosity contain in the specimens, and additional checking is needed to study on this matter.

It is clearly shown that to achieve the optimum stress value, the contents of ceramic microballoons in the syntactic foams also should be limited because to ensure that it is not difficult to mix with vinyl ester resin.

5. Acknowledgment
The authors wish to thank Universiti Kuala Lumpur Malaysia and MARA for providing scholarship to first author on doing this work.

NOMENCLATURE

∇ : Mean particle size, µm
ρ : Bulk density, g/m^3
T : Melting point, ^{o}C
σ : Engineering Stress, MPa
wt.% : Weight percentage
ASTM: American Standard Testing Method
E : Energy Absorption, kJ
PVC : Polyvinyl Chloride
SEM : Scanning Microscope Machine
ε : Engineering Strain, %

REFERENCES

[1] Cheng X., Liu P., LI X., Shui A., and Zeng L., Preparation of Beauxite Ceramic Microsphere, *Journal of Materials Science*, Vol. 42(13), pp 4047-4054, (2006).

[2] G.H. Wu. Z.Y. Dou, D.L. Sun, L.T. Jiang, B.S. Ding and B.F. He, Compression behaviours of cenosphere–pure aluminum syntactic foams, *Scripta Materialia*, Vol.56, pp 221–224, (2007).

[3] Imre N. O., and Kornél M, Microballoon of Metal-matrix composite reinforced by ceramic microballoon, *Physics of Fluids*, Vol. 16, pp 11180-1126, (2004).

[4] R. A. Palmer, K. Gao, T. M. Doan, L. Green and G. Cavallaro, Pressure infiltrated syntactic foams-Process development and mechanical properties, *Materials Science and Engineering A*, Vol.(464), pp 85–92, (2007).

[5] D. K. Balch and D. C. Dunand, Load partitioning in aluminum syntactic foams containing ceramic microspheres, *Acta Materialia* Vol.(54), pp 1501–1511, (2006).

[6] D.K. Balch, J. G. O'Dwyer, G. R. Davis, C. M. Cady, G. T. Gray III, and D. C. Dunand, Plasticity and damage in aluminum syntactic foams deformed under dynamic and quasi-static conditions, *Materials Science and Engineering A* Vol.(391), pp 408–417(2005).

[7] Product specification Envirospheres Pty. Ltd, view 14 Nov 2014, <http://www.envirospheres.com.au/products.asp>

[8] N.Gupta, R.Ye, M and Porfiri, Comparison of tensile and compressive characteristics of vinyl ester/glass microballoon syntactic foams, *Composites: Part B*, Vol.(41), pp 236–245, (2010).

[9] C. Swetha and R. Kumar, Quasi-static uni-axial compression behaviour of hollow glass microspheres/epoxy based syntactic foams, *Materials and Design*, Vol.(32), pp 4152–4163, (2011).

[10] Periasamy C,Jhaver R and Tippur HV., Quasi-static and dynamic compression response of a light weight interpenetrating phase composite foam. *Material Science Engineering A*, Vol.(527), pp 2845–56, (2010).

[11] Xing C.X, Xiaowei C., Zan Z., Xu C., Weimin Z., Bo L. and Boyoung H., Compressive properties of closed-cell aluminum foams with different contents of ceramic microspheres. *Materials and Design* Vol.(56), pp 353-358, (2014).

ICMIEE-PI-140138

Selection of Hemp Fabric as Reinforcement in Composite Materials

Mohd Iqbal Misnon [1, 2], Md Mainul Islam [1], Jayantha Ananda Epaarachchi [1], Kin-tak Lau [3]*
[1] Centre of Excellence in Engineered Fibre Composites and School of Mechanical and Electrical Engineering,
Faculty of Health, Engineering and Sciences, University of Southern Queensland,
Toowoomba, Queensland 4350, AUSTRALIA
[2] Faculty of Applied Sciences, Universiti Teknologi MARA,
40450, Shah Alam, Selangor, MALAYSIA
[3] Department of Mechanical Engineering, The Hong Kong Polytechnic University,
Hung Hom, Kowloon, HONG KONG

ABSTRACT
One of the main problems on utilising the plant fibres in composite materials is control of fibre orientation and distribution. This problem can be solved by converting the plant fibres into yarns or fabrics. Plant fibres in the form of fabric are the most convenient material for a reinforcement considering its good fibre distribution as well as easy to handle during composite fabrication. The selection of fabric criterion on top of fibre type is also essential to ensure its suitability as reinforcement. In this work, three types of fabrics were analysed for their characteristics. Fabrics were analysed in terms of their physical characteristics such as fabric density, weight, thickness, yarn size and yarn crimp. The analysis continued with the fibre density and cloth cover factor determination which are related with the resin penetration. Tensile property characterisation was also done on the fabric which is important to predict their contribution on the composite materials. Fabric characteristics are important to be determined as we need to decide which fabric is more suitable as reinforcement and could give desired composite properties.

Keywords: Hemp fabrics, fabric characterisation, cloth cover factor, tensile properties, composites.

1. Introduction

The growth of global awareness on the environmental issues leads for the developing, creating and innovating eco-friendly materials. One of the remedies for this situation is the utilisation of natural fibres from plant (either fibre crops or agricultural wastes) in composite materials which suit the global direction above [1-4]. As for natural fibres, these kinds of fibres have existed for quite sometimes and their utilisation in composite materials is not new including those in automotive and building industries [5-7]. This is mostly driven by lower price, global availability and complete data of natural fibres which seem promising to be used as raw materials [7, 8].

Natural fibres possess good mechanical properties; however, the main problem in utilising natural fibres is control of the fibre orientation and distribution. This is because the optimum mechanical properties will not efficiently utilised as reinforcement if the problem cannot be resolved [9]. A wide range of techniques have long existed to convert the natural fibres into yarn and then into fabric in the textile industry [10]. However, utilisation of yarn is quite difficult in terms of reinforcement handling in composite fabrication. Utilisation of traditional textile fabric (high performance fibres) is more convenient considering their advantages on high strength, good fibre orientation and fibre distribution and more importantly easy to handle during composite fabrication [11]. Nevertheless, in the case of natural woven fabric, there is less work reported on their utilization especially when considering the type of natural fabrics to be used as reinforcement in composite material [4].

Several fibres such as jute and hemp were established in woven fabric and they possess good properties as reinforcement in composite materials. However, they come in different qualities depend on the manufacturing parameters which could affect the composite properties at the end. Therefore, a study to characterize a different fabric batch is needed to assess how far the difference in their properties is as well as to decide on which fabric is suitable for reinforcement in composite materials. Therefore, in this work, two hemp fabrics in a similar quality but two different batches have been characterized with respect to; i) fabric physical properties, ii) fibre density, iii) fabric appearance structure, and iv) mechanical properties. Another fabric in different quality was also characterized, which follows the similar procedure in order to seek and decide the suitability of these fabrics as composite reinforcement.

2. Materials and Method

Commercial hemp woven fabrics in two (2) batches were bought with time interval of about three (3) months were investigated and supplied by Hemp Wholesale Australia. According to the supplier, the two fabrics were having equal nominal properties. The weight of fabrics is 271 g/m^2 and due to this, it can be categorized as 'heavy fabric' in textile term. These two fabrics will be denoted as Fabric A and Fabric B for this work. Another thicker and heavier woven hemp fabric (Fabric C) with the weight of 407 g/m2 supplied by similar supplier was also investigated in this work. The

* Corresponding author. Tel.: +61-746311338
E-mail address: mainul.islam@usq.edu.au

fabrics were produced by 100 % yarn hemp in both warp and weft. These yarns were then converted into fabric via weaving processes and the fabrics were woven by employing plain weave (taffeta) structure.

2.1 Fabric Characterisation

All fabric characterisations have been done employing several textile materials standard methods. These standard methods (Table 1) are commonly used in textile industry for characterization as well as product quality determination purposes.

Table 1 List of standard methods for fabric properties determination.

Properties	Testing	Standard Method
Fabric Density	Warp (end) and filling (pick) count of woven fabrics	ASTM D3775
Fabric Weight	Mass per unit area (weight) of fabric	ASTM D3776
Fabric Thickness	Thickness of Textile Materials	ASTM D1777
Yarn Size	Yarn number (linear density)	ASTM D1907
Yarn Crimp	Yarn crimp and yarn take-up in woven fabrics	ASTM D3883

2.2 Fibre Density

The density of the hemp fibres was determined by Multipycnometer MVP D160E using Helium gas as a displacement medium. The data reported are the average and standard deviation of 3 measurements.

2.3 Moisture Content

Moisture content of the fabric was determined by using Sartorius Moisture Analyser MA100/MA50. This instrument will heat up the sample up to 105 °C.

2.4 Tensile Properties

Tensile properties (ASTM D 5034) of hemp fabrics were characterized using universal testing machine MTS Alliance RT/10. Tensile tests were performed using a gauge length of 75 mm and a cross-head speed 2 mm/min. The cross-sectional area used to convert load into stress was calculated from the test specimen width and the thickness of fabric obtained from the fabric characterization [12, 13]. The initial response of the curve was nonlinear but then the slope increased slowly until finally becoming linear. Tensile moduli of the fabric were determined from the linear part of the curves.

3. Results and Discussion

3.1 Physical Properties of Hemp Fabric

Table 2 presents the determined physical properties of hemp fabrics. When observing all the fabrics, no defect was found along the fabric length for at least 5 meters. Therefore, it can be concluded all fabrics were manufactured in good loom (most probably shuttleless loom) and they are good-quality fabrics.

Table 2 Physical properties results of woven hemp fabric.

Fabric Types		Fabric A	Fabric B	Fabric C
Weave Structure		Plain	Plain	Plain
Fabric Density (per 2cm)	Warp	25	25	34
	Weft	23	23	26
Fabric Weight (Reading) (g/m^2)		231.410	228.520	410.720
Thickness (mm)		0.41	0.41	0.71
Yarn Size (Tex)	Warp	89.661	90.459	106.717
	Weft	92.896	92.970	123.600
Yarn Crimp (%)	Warp	5.4	6.0	27.4
	Weft	9.3	9.3	3.6

According to Table 2, fabric density for Fabric A and B was determined similar but lower in comparison with Fabric C indicates that Fabric C is more compact than Fabric A and B. In terms of fabric weight, Fabric A was found a slightly heavier than Fabric B and yet their weight was at least 17 % lesser than the specification given by the supplier (271 g/m^2). In comparison with Fabric C, they are recorded at least 77 % lower than Fabric A and B. All the weights reflected their measured thicknesses which were 0.41 mm for Fabric A and B and 0.71 mm for Fabric C. In terms of yarn size, the weft yarn for Fabric A and B were recorded similar which was 93 tex, yet their warps' sizes were recorded a little different which were 89.661 and 90.459 tex respectively. The sizes of warp and weft for Fabric C were determined even higher by at least 24 % than other two fabrics and this is the reason why it is heavier.

It is well known that yarn crimp in a woven fabric is an important parameter that affects most of its physical properties and that include the thickness and the weight of fabric [14]. Based on the results in Table 2, both fabrics have relatively similar warp and weft crimp percentage which is 5.4 and 9.3 % respectively. The slight different warp between fabric A and B was normally due to the different 'picking stroke' action in loom machine during fabric manufacturing. More importantly is the yarn crimp for Fabric C, which was measured to have very significant difference with other two fabrics for at least 78 % in warp and 158 % for weft yarns. This will relatively give a significant different between Fabric C and other two fabric in their mechanical properties responses.

3.2 Density of Fibre

The density of fibre for Fabric A and B determined by pycnometry are presented in Table 3. The results show

that for each series of measurements, the fibre density is higher for Fabric A than Fabric B with overall means of 1.512 and 1.473 g/cm^3 respectively. The determined density of the hemp fabric fibres is comparable and within the typically reported densities of hemp fibres varying between 1.4 and 1.5 g/cm^3 [4, 15]. Fibre density of Fabric C was determined a little higher than other two fabrics which is 1.526 g/cm^3.

Normally, the bulkiness of natural fibre makes it quite difficult to compress. Even with a good spinner and loom, the pressure given is unable to compact the fibre to make the density lower than 1.4 g/cm^3, due to fibre irregularities along the fibre length. The irregularities create higher cavities on the yarn as compared to the synthetic fibres [16]. In the case of hemp fabrics, Fabric C was determined to have higher fabric density in its both warp and weft direction as compared to Fabrics A and B (refer Table 2). The higher warp and weft that accommodate in fabric make the fabric more compact thus affects the fibre density of the fabric [17]. This is main the reason of the slight higher fibre density of Fabric C in comparison with other two fabrics.

Table 3 Density of fibre (g/cm^3) of the Fabrics A and B determined by 3 series of measurements.

Fabric Types	Series of measurement				
	I	II	III	Average	Stdv.
Fabric A	1.528	1.499	1.510	1.512	0.015
Fabric B	1.481	1.472	1.466	1.473	0.007
Fabric C	1.518	1.531	1.530	1.526	0.007

3.3 Fabric Appearance Structure

Fig. 1 shows the appearance structure of woven hemp fabrics. It was observed that all the fabrics were woven with the plain/taffeta weave structure. This is the most basic woven structure other than twill and satin and is usually utilised for technical purposes [18].

Yarns for all fabrics were observed to vary in cross-sectional dimensions, especially for Fabrics A and B. It can be shown in Fig. 1 that lots of thick and thin yarns found to be running in the warp and weft directions. The yarns' size determined for both fabrics are just the average values (refer Table 2). Since the fabrics used are made of natural fibres, this kind of irregularities and inconsistencies with the yarn were expected to happen [4]. The yarns for both fabrics were observed to have twists with a right-handed angle to the yarn axis (Z-twist). Yarns in Fabric C are also varied in cross-sectional; however, since it is more compact than other two fabrics, the variation was less appeared and a bit difficult to be seen. The weft yarn for this fabric was spun in Z-twist whilst the warp yarn was two plied-yarns in S-twist, and each ply yarn was spun in Z-twist. This twist value is received as specified by the supplier. More importantly, the properties related to the fabric appearance should be emphasized.

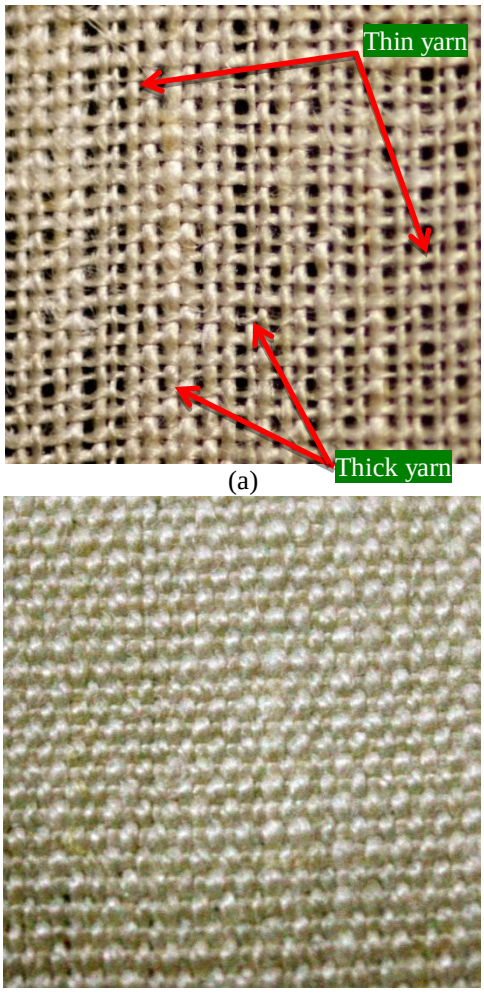

Fig. 1 The structure of woven hemp fabrics, (a) Fabric A and B, (b) Fabric C.

Fabric cover factor indicated the extent to which the area is covered by one set of yarns. For composite fabrication, this characteristic can tell how well the resin could penetrate into the fabric system. In order to determine the total fabric cover factor, a modified equation introduced by Chen and Leaf [19] was used and the K-value is the ratio on how big the area is covered by the yarns.

Table 4 Result of cover factor for both fabric used in this work.

Fabric Types	Fractional yarn cover		Total Fabric Cover
	Warp C1	Weft C2	K
Fabric A	0.435	0.406	0.664
Fabric B	0.433	0.405	0.663
Fabric C	0.642	0.529	0.832

The results tabulated in Table 4 clearly show that 66 % (0.66) of the fabric sheets are therefore covered by yarn for Fabrics A and B. From the textile point of view, these fabrics share identical cover factor quality and can be used in a similar batch of textile product for certain application. The total cover factor for Fabric C was determined higher than other two fabrics with 83 % of the yarn cover the fabric sheet and this is consistent with the fabric density it possesses (refer Table 2). From the K-values, it can be inferred that Fabrics A and B would have better resin penetration than Fabric C thus better adhesion is expected from these fabrics.

3.4 Mechanical Properties

Typical stress-strain curve of all woven hemp fabrics is shown in Fig. 2. In the initial phase, the curve rose with a low slope due to decrimping and crimp interchange. The decrimping and crimp interchange is internal interaction (crossover between warp and weft yarns) of a fabric that results to the initial curve. Second phase is shown in which the stress-strain curve increased sharply. From here, the yarns appear to become less flattened due to the consolidation into more circular cross-section. As the pressure builds up for the yarn in the direction of force, yarn extension now only accounts for a small portion as compared to the extension of yarn in the first phase. This situation continuously happens until it reaches the peak and then breaks.

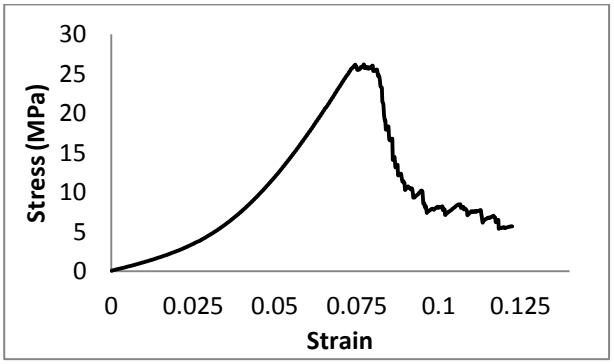

Fig. 2 Typical stress-strain response for all woven hemp fabrics used in this work.

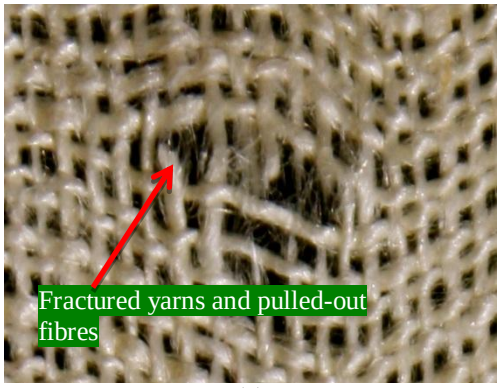

(a)

(b)

Fig. 3 Typical fabric fracture after subjected to tensile force for; (a) Fabric A and B, (b) Fabric C.

Fig. 3 shows magnified yarn fractures area on the fabrics. It was observed that the fractures were happened mainly at the area which has many thin yarns. There were many pulled-out fibres found at the fractured yarns which suggesting that the fibres were resisting the tensile force acting on them.

Table 5 Summary of average tensile properties for woven hemp fabrics.

Fabric Types		Peak Load (N)	Tensile Strength (MPa)	Tensile Strain	Tensile Modulus (GPa)
Fabric A	Warp	442.1 (±29)	23.392 (±1.52)	0.074 (±0.004)	0.540 (±0.023)
	Weft	497.5 (±56)	26.304 (±2.99)	0.121 (±0.008)	0.511 (±0.032)
Fabric B	Warp	415.3(±21)	21.975 (±1.11)	0.093 (±0.026)	0.530 (±0.041)
	Weft	469.3 (±38)	24.833 (±1.99)	0.112 (±0.006)	0.493 (±0.044)
Fabric C	Warp	1289.3 (±17.55)	33.777 (±3.85)	0.353 (±0.036)	0.175 (±0.019
	Weft	1249.3 (±123)	34.58 (±3.41)	0.065 (±0.009)	0.642 (±0.029)

*Figures in parentheses represent standard deviations

The results of tensile properties for both woven hemp fabric are shown in Table 7. The figures in the table are the average ± standard deviation for at least 9 specimens. Overall, it can be said that the tensile strength of Fabric A is higher than Fabric B. In warp direction, tensile strength of Fabric B was recorded 6 % lesser than Fabric A while the weft direction specimen with the tensile strength of Fabric B was determined 6.4 % lower than Fabric A. Tensile strength of Fabric C was determined at least 21 % higher than Fabric A and B due to higher fibre content (fabric weight) in the fabric. The lowest tensile modulus of all the hemp woven fabric was Fabric C in the warp direction which was determined as 0.175 GPa and this most probably due to

the higher crimp (refer Table 2) it possesses in warp direction.

4. Conclusions

The results suggest that Fabrics A and B are designed as it should be physically and mechanically balanced in warp and weft direction. The slight difference between these two fabric properties are due to variation on the yarn properties as well as in the process of fabric manufacturing. In terms of Fabric C, the fabric is not balanced in warp and weft direction in all characteristics, especially for their crimps. Even though the properties are different between warp and weft, it has higher fibre content and more compact than other two fabrics. This supposedly gives best mechanical properties for the composite material as compared to Fabrics A and B. However, the total cover factor for Fabric C is far higher than Fabrics A and B. With the 66 % of Fabric A and B are covered by yarns as compared to Fabric B which is 83 %, it is expected that the penetration of resin is far better for Fabric C. This also means a good adhesion between the resin and yarn for those two fabrics than Fabric C if it is used as reinforcement in composite material.

5. Acknowledgement

The authors would like to thank Ministry of Higher Education, Malaysia and Universiti Teknologi MARA, Malaysia for providing scholarship to first author on doing this work.

REFERENCES

[1] Nishino T, Hirao K, Kotera M, Nakamae K, Inagaki H. Kenaf reinforced biodegradable composite. Composites Science and Technology. 2003;63:1281-6.
[2] Mishra S, Tripathy SS, Misra M, Mohanty AK, Nayak SK. Novel Eco-Friendly Biocomposites: Biofiber Reinforced Biodegradable Polyester Amide Composites—Fabrication and Properties Evaluation. Journal of Reinforced Plastics and Composites. 2002;21:55-70.
[3] Misnon MI, Bahari SA, Wan Ahmad WY, Ab Kadir MI, Anuar M. Reinforcement of Textile Fabric in Agricultural Waste Particleboard. in Proceeding 87th Textile Institute World Conference 2010. 2011:408-52.
[4] Misnon MI, Islam MM, Epaarachchi JA, Lau K-t. Potentiality of utilising natural textile materials for engineering composites applications. Materials & Design. 2014;59:359-68.
[5] Chilton J, Velasco R. Applications of textile composites in the construction industry. In: Long AC, editor. Design and manufacture of textile composites. England: CRC Press, Woodhead Publishing Ltd, Cambridge; 2005. p. 424-35.
[6] Netravali AN, Huang X, Mizuta K. Advanced 'green' composites. Advanced Composite Materials. 2007;16:269-82.
[7] Faruk O, Bledzki AK, Fink H-P, Sain M. Biocomposites reinforced with natural fibers: 2000–2010. Progress in Polymer Science. 2012;37:1552-96.
[8] Satyanarayana KG, Arizaga GGC, Wypych F. Biodegradable composites based on lignocellulosic fibers—An overview. Progress in Polymer Science. 2009;34:982-1021.
[9] Madsen B, Hoffmeyer P, Thomsen AB, Lilholt H. Hemp yarn reinforced composites – I. Yarn characteristics. Composites Part A: Applied Science and Manufacturing. 2007;38:2194-203.
[10] Akovali G, Uyanik N. Introduction. In: Akovali G, editor. Handbook of Composite Fabrication. Shropshire, U.K: Rapra Technology Limited; 2001. p. 1-19.
[11] Scardino F. An Introduction to Textile Structures and their Behaviour. Textile Structural Composite. 1989;3:1-26.
[12] Yahya MF, Salleh J, Ahmad WYW. Uniaxial failure resistance of square-isotropic 3D woven fabric modelled with finite element analysis. Business, Engineering and Industrial Applications (ISBEIA), 2011 IEEE Symposium on2011. p. 16-21.
[13] Huang X, Netravali A. Characterization of flax fiber reinforced soy protein resin based green composites modified with nano-clay particles. Composites Science and Technology. 2007;67:2005-14.
[14] Süle G. Investigation of bending and drape properties of woven fabrics and the effects of fabric constructional parameters and warp tension on these properties. Textile Research Journal. 2012;82:810-9.
[15] Dittenber DB, GangaRao HVS. Critical review of recent publications on use of natural composites in infrastructure. Composites Part A: Applied Science and Manufacturing. 2012;43:1419-29.
[16] Kadolph SJ, Langford AL. Textiles. 9th ed. New Jersey:: Prentice Hall; 2001.
[17] Shahabi NE, Saharkhiz S, Varkiyani H, Mohammad S. Effect of Fabric Structure and Weft Density on the Poisson's Ratio of Worsted Fabric. Journal of Engineered Fabrics & Fibers (JEFF). 2013;8.
[18] Sondhelm WS. Technical fabric structures – 1. Woven fabrics. In: Horrocks AR, Anand SC, editors. Handbook of Technical Textiles. North and South America: Woodhead Publishing Limited & The Textile Institute; 2000.
[19] Chen X, Leaf GAV. Engineering Design of Woven Fabrics for Specific Properties. Textile Research Journal. 2000;70:437-42.

ICMIEE-PI-140101

Analysis of Stress Distribution between Interacting Planar Cracks

Md. Abdul Hasib [1,*], *Akihide Saimoto* [2]
[1] Department of Science and Technology, Nagasaki University, Nagasaki, JAPAN
[2] Mechanical Systems Engineering, Nagasaki University, Nagasaki, JAPAN

ABSTRACT
A hand-made numerical program based on Body Force Method (BFM) applicable to planar crack problems is developed. Numerical analysis is carried out for arbitrary shaped coplanar 3D cracks interacting each other in an infinite solid. As a fundamental solution, a stress field at an observation point induced by a body force doublet applied at a source point in an infinite elastic medium is employed. In the present analysis, a planar triangular element is used to cover the total crack surface. Special crack tip elements considering the stress singularity at a crack front are employed to the crack front element. The crack problem is formulated as hypersingular boundary integral equations with unknown distribution of the body force doublet. Finally, the unknown distribution of the body force doublet is solved by transforming the boundary integral equation into a set of simultaneous equations. In addition to the theoretical background of the present method, several numerical results are shown graphically.

Keywords: Body force method, Mixed-mode SIF, Crack interaction, Triangular element.

1. Introduction

A crack to crack interaction exhibits a major influence on behavior of crack growth. Multiple cracking is one of the most common problems in engineering structures and may caused catastrophic or structural failures in aircraft, ship, bridge, automotive components and machine parts. The interactions of crack change the SIF and stress distribution near the crack fronts. The SIF and stress distribution because of crack interaction not only depended on the number of cracks but also the size, shape, distance between cracks. The analysis of SIF and stress distribution due to crack interaction is very important and useful in evaluating the strength and safe life prediction of engineering materials structures. Several numerical methods have been applied for the SIF and stress distribution analysis of multiple cracks, such as finite element method [1], enriched meshless method [2], integral equation method [3], boundary element method [4], boundary collocation method [5], Lagrangian finite difference method [6], alternating iteration method [7] and body force method. Among these methods FEM and BEM are much more general than other methods. But the main problem in BEM and FEM is that, it is indispensable to divide a whole domain or surface into several segments. Furthermore, it is not convenient to simulate the crack propagation due to need for re-meshing near crack tips. In this paper body force method (BFM) has been used for the analyzing multiple cracks. Nisitani proposed BFM as a method of numerical stress analysis [8]. Compared with the FEM, the BFM has some advantages in solving elastic fracture problems. The reason is due to the fact that the BFM only contains the boundary discretization of the problem domain and a more accurate result could be obtained with a lesser effort. Nisitani et al. [9] first applied the body force method to investigate problems of an elliptical crack or a semi elliptical crack in an infinite plate under tension. After that Murakami et al. [10] applied BFM for the analysis of interaction between semi-elliptical surface cracks in an semi-infinite elastic body under tension and bending. Isida et al. [11] applied BFM for the first time to analyze two parallel elliptical cracks under mixed-mode stress state at the infinity. Isida et al. [12] again applied BFM for the analysis of multiple semi-elliptical surface cracks in semi-infinite solid under tension. Wang et al. [13] discussed numerical solutions using singular integral equation of the BFM for 3D rectangular crack problems. Later Noda et al. [14] applied singular integral equation method based on BFM for the calculation of SIF of interacting semi-elliptical surface cracks. In BFM, each research has been carried out by developing the special numerical program suitable for each problem. Therefore, a versatile stress analysis program applicable to arbitrary shaped 3D interacting cracks under mixed-mode loading has not been developed until today.

In this research a versatile numerical program has been developed for the analysis of mixed-mode planar crack. The 3D crack problem is formulated in terms of singular integral equations with singularity of the order of r^{-3}, where r is the distance between source and reference points. The stress field induced by a body force doublet in an infinite body is used as the fundamental solution. The unknown functions are approximated by the product of fundamental density function and weight function. The approximate solution is obtained easily by providing the triangular mesh data and boundary conditions. By using the developed program, the coplanar interactive surface cracks in an infinite solid

* Corresponding author. Tel.: +81958192493
E-mail address: s-aki@nagasaki-u.ac.jp

subjected to remote tension and bending loads are computed.

2. Fundamental principle of BFM

The body force method (BFM) is directly based on this principle of superposition. The essence of BFM is to transform a given elastic problem to an equivalent problem of an infinite domain in which body forces are embedded. BFM is classified as an indirect BEM since the stress and displacement at a reference point is expressed in terms of densities of body force. The fundamental concept of BFM is to express the elastic fields of a problem by means of the principle of superposition. A solution of an elastic problem should satisfy three conditions of i) equilibrium condition, ii) compatibility condition and iii) boundary condition. Since the elastic fields are superposable, in BFM the elastic field due to a point force under investigation can be expressed by superposing some specific known elastic fields. In the BFM the specific known elastic fields, which can be written in a closed form, are superposed with some unknown weight-magnitudes as follows

Elastic field under investigation	= ∑	Specific known solution of elastic field	×	Unknown weight-magnitudes	(1)

If a given boundary condition is satisfied by adjustment of the unknowns in Eq. (1), the superposed elastic field is the solution of the given problem, because the solution of elastic problem is unique. Finally Eq. (1) is transformed into summation of simultaneous equations and unknown weight magnitudes to be determined through boundary conditions. If the boundary condition is satisfied exactly, it means that an exact solution is derived by BFM.

Consider an infinite body having a penny-shaped crack on *x-y* plane which is subjected to uniform tension at infinity. According to the body force method this problem is transferred as a combination of two problems. One is an infinite solid with uniform stress distribution at the infinity and another is an imaginary crack in an infinite solid along which the unknown force doublets is acting continuously as shown in Fig. 1.

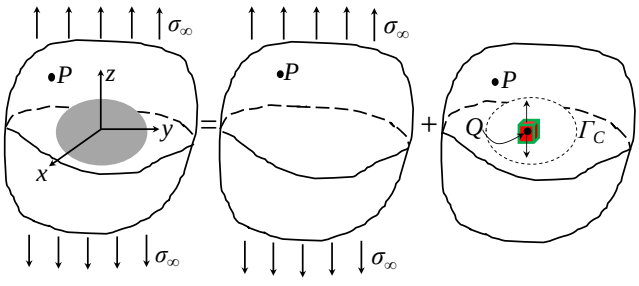

Fig.1 Uniaxial tension of an infinite solid with a single penny-shaped crack.

The stress component at an arbitrary point in an infinite solid with crack can be expressed as follows,

$$\sigma_{ij}(P) = \sigma_{ij}^{\infty}(P) + \iint_{\Omega_c} \sigma_{ij}^{kl}(P,Q)\rho_{kl}(Q)d\Omega_c(Q) \qquad (2)$$

Where $P(x,y,z)$ is a reference point, $Q(\xi,\eta,\zeta)$ is a source point, Ω_c is an imaginary crack surface, $\sigma_{ij}^{\infty}(P)$ represents the initial stress at the reference point, ρ_{kl} is the density of force doublet, $\sigma_{ij}^{kl}(P,Q)$ is the stress component at a reference point which is obtained by differentiation with respect to co-ordinate variable l $(l = \xi,\eta,\zeta)$ of the stress component σ_{ij} due to a unit magnitude of point force acting in the k $(k = x,y,z)$ direction at the source point [15]. In order to determine $\rho_{kl}(Q)$, it is required to approach P from the exterior of Γ to the surface of the crack. At the surface of the crack, the traction-free condition is applied. Thus Eq. (2) becomes the boundary integral equation for the determination of unknown density $\rho_{kl}(Q)$ in a complete infinite domain. Once the unknown density function $\rho_{kl}(Q)$ is obtained, the stress at an arbitrary point P can be obtained by putting the $\rho_{kl}(Q)$ in Eq. (2). In such a way, an arbitrary boundary value problem is transformed into a form of integral equations with unknown density through the principle of superposition of the known fundamental solution.

3. Theoretical Analysis

In BFM, solution of any elasticity problem is transformed into a problem of a complete infinite domain without any crack. That is, a boundary of given problem is replaced by an equivalent imaginary boundary along which body force or body force doublets are embedded. In BFM, an elastic boundary value problem is transformed into the form of a boundary integral equation. Consider an infinite body having a penny-shaped crack as shown in Fig. 2 which is subjected to mixed mode loading at infinity.

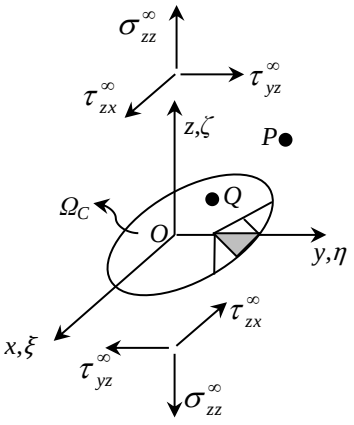

Fig.2 Crack in an infinite solid subjected to uniform stress at infinity.

Let σ_{zz}, τ_{zx} and τ_{yz} be the stress component due to the fundamental force doublets distributed over the crack surface and stress at the infinity. On the idea of the body force method, the problem is reduced to sets of integral equations in which the density of force doublets are unknowns to be determined. The stress components at any arbitrary point are as follows:

$$\sigma_{zz}(P) = \sigma_{zz}^{\infty}(P) + \iint_{\Omega_c} [\sigma_{zz}^{zz}(P,Q)\gamma_{zz}(Q) + \sigma_{zz}^{zx}(P,Q)\gamma_{zx}(Q) + \sigma_{zz}^{yz}(P,Q)\gamma_{yz}(Q)]d\Omega_c(Q) \quad (3)$$

$$\tau_{zx}(P) = \tau_{zx}^{\infty}(P) + \iint_{\Omega_c} [\tau_{zx}^{zz}(P,Q)\gamma_{zz}(Q) + \tau_{zx}^{zx}(P,Q)\gamma_{zx}(Q) + \tau_{zx}^{yz}(P,Q)\gamma_{yz}(Q)]d\Omega_c(Q) \quad (4)$$

$$\tau_{yz}(P) = \tau_{yz}^{\infty}(P) + \iint_{\Omega_c} [\tau_{yz}^{zz}(P,Q)\gamma_{zz}(Q) + \tau_{yz}^{zx}(P,Q)\gamma_{zx}(Q) + \tau_{yz}^{yz}(P,Q)\gamma_{yz}(Q)]d\Omega_c(Q) \quad (5)$$

Where *P*(*x*,*y*,z) is a reference point, *Q*(ξ, η, ζ) is a source point, Ω_c is an imaginary crack surface, γ_{zz}, γ_{zx} and γ_{yz} are the density of standard force doublets.
In above equations the fundamental solutions are calculated from the following expressions.

$$\sigma_{ij}^{zz}(P,Q) = \left.\frac{\partial \sigma_{ij}^{Z}}{\partial \zeta}\right|_{Z=1} + A\left\{\left.\frac{\partial \sigma_{ij}^{X}}{\partial \xi}\right|_{X=1} + \left.\frac{\partial \sigma_{ij}^{Y}}{\partial \eta}\right|_{Y=1}\right\} \quad (6)$$

$$\sigma_{ij}^{zx}(P,Q) = \left.\frac{\partial \sigma_{ij}^{X}}{\partial \zeta}\right|_{X=1} + \left.\frac{\partial \sigma_{ij}^{Z}}{\partial \xi}\right|_{Z=1} \quad (7)$$

$$\sigma_{ij}^{yz}(P,Q) = \left.\frac{\partial \sigma_{ij}^{Y}}{\partial \zeta}\right|_{Y=1} + \left.\frac{\partial \sigma_{ij}^{Z}}{\partial \eta}\right|_{Z=1} \quad (8)$$

$$i,j = x,y,z;\ A = \frac{\nu}{1-\nu}$$

Where, $\sigma_{zz}^{kl}, \sigma_{zx}^{kl}$ and σ_{yz}^{kl} be the stress components due to the fundamental force doublets distributed over the crack surface. $\sigma_{ij}^{X}, \sigma_{ij}^{Y}$ and σ_{ij}^{Z} are the known expressions of stress components at point *P*(*x*,*y*,z) due to concentrated forces acting at point *Q*(ξ, η, ζ) called Kelvin solution. The concrete from of fundamental solution are as follows:

$$\sigma_{zz}^{zz}(P,Q) = \frac{1-2\nu}{8\pi(1-\nu)^2}\left[\frac{1}{r^3} + 6\frac{{r_z}^2}{r^5} - 15\frac{{r_z}^4}{r^7}\right] \quad (9)$$

$$\sigma_{zz}^{zx}(P,Q) = \frac{3}{4\pi(1-\nu)} r_x r_z \left[\frac{1}{r^5} - 5\frac{{r_z}^2}{r^7}\right] \quad (10)$$

$$\sigma_{zz}^{yz}(P,Q) = \frac{3}{4\pi(1-\nu)} r_y r_z \left[\frac{1}{r^5} - 5\frac{{r_z}^2}{r^7}\right] \quad (11)$$

$$\tau_{zx}^{zz}(P,Q) = \frac{3(1-2\nu)}{8\pi(1-\nu)^2} r_x r_z \left[\frac{1}{r^5} - 5\frac{{r_z}^2}{r^7}\right] \quad (12)$$

$$\tau_{zx}^{zx}(P,Q) = \frac{1}{4\pi(1-\nu)}\left[\frac{E}{r^3} - \frac{3\nu {r_y}^2}{r^5} - \frac{15 {r_x}^2 {r_z}^2}{r^7}\right] \quad (13)$$

$$\tau_{zx}^{yz}(P,Q) = \frac{3}{4\pi(1-\nu)} r_x r_y \left[\frac{\nu}{r^5} - 5\frac{{r_z}^2}{r^7}\right] \quad (14)$$

$$\tau_{yz}^{zz}(P,Q) = \frac{3(1-2\nu)}{8\pi(1-\nu)^2} r_y r_z \left[\frac{1}{r^5} - 5\frac{{r_z}^2}{r^7}\right] \quad (15)$$

$$\tau_{yz}^{zx}(P,Q) = \frac{3}{4\pi(1-\nu)} r_x r_y \left[\frac{\nu}{r^5} - 5\frac{{r_z}^2}{r^7}\right] \quad (16)$$

$$\tau_{yz}^{yz}(P,Q) = \frac{1}{4\pi(1-\nu)}\left[\frac{E}{r^3} - \frac{3\nu {r_x}^2}{r^5} - \frac{15 {r_y}^2 {r_z}^2}{r^7}\right] \quad (17)$$

Where $r_x = x - \xi, r_y = y - \eta, r_z = z - \zeta, E = 1 + \nu$
$r^2 = {r_x}^2 + {r_y}^2 + {r_z}^2$ and ν is the poisson's ratio.

In this analysis, the surface of the crack is expressed by the aggregation of planar triangles and in each triangle the density of the force doublets is assumed at constant. The triangles which are placed at the crack front, the basic density function is considered as shown in Fig. 3. Density of standard force doublets γ_{zz}, γ_{zx} and γ_{yz} are expressed by the product of basic density function $\sqrt{h(\xi,\eta)}$ and weight functions $W_{zz}(\xi,\eta), W_{zx}(\xi,\eta)$ and $W_{yz}(\xi,\eta)$ respectively.

$$\gamma_{zz}(Q) = \sqrt{h(\xi,\eta)} W_{zz}(\xi,\eta) \quad (18)$$

$$\gamma_{zx}(Q) = \sqrt{h(\xi,\eta)} W_{zx}(\xi,\eta) \quad (19)$$

$$\gamma_{yz}(Q) = \sqrt{h(\xi,\eta)} W_{yz}(\xi,\eta) \quad (20)$$

$$h(\xi,\eta) = \frac{|x_2 y_1 - y_2 x_1 + y_{21}\xi - x_{21}\eta|}{\sqrt{{y_{21}}^2 + {x_{21}}^2}} \quad (21)$$

Where $y_{21} = y_2 - y_1$ and $x_{21} = x_2 - x_1$

When the crack is free of traction, σ_{zz}, τ_{zx} and τ_{yz} are zero at the same time, when $P \to P^{\Omega c}$.

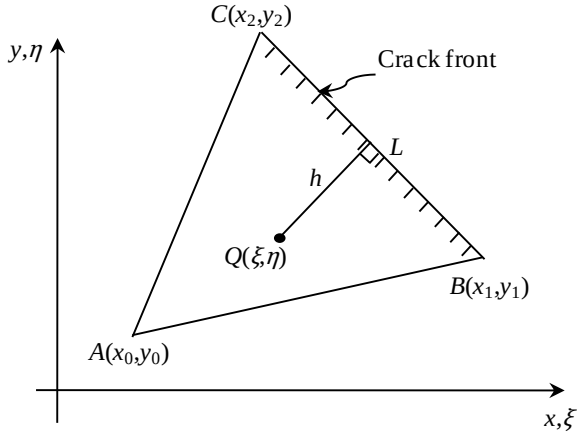

Fig. 3 Planar triangle surface element with force doublets (shaded triangle in Fig. 2).

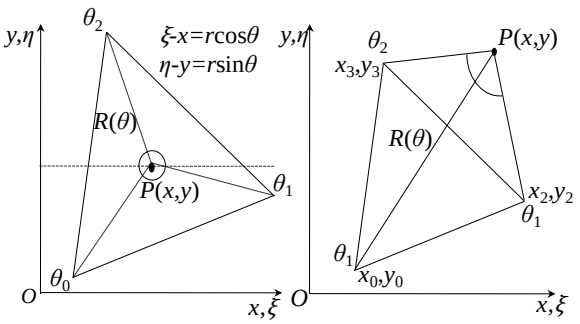

Fig. 4 Parameter transformation from cartesian to polar coordinates.

After solving the simultaneous equations expressing the boundary condition, the value of weight functions are obtained. Weight function $W_{zz}(\xi,\eta)$ is responsible for the mode-I SIF K_{I} and $W_{zx}(\xi,\eta), W_{yz}(\xi,\eta)$ are responsible for the K_{II} and K_{III} at crack front. Hyper singularity occurs, when observation point is on crack surface i.e. $x=\xi$ and $y=\eta$. In order to remove this singularity polar transformation has been used. For the calculation of integral equations numerically, integration limits varies depending on the position of observation points. We can calculate $\theta_0, \theta_1, \theta_2$ from the vertices of triangle and observation point. For θ_3 if the observation point is inside of triangle then $\theta_3 = \theta_0 + 2\pi$, if outside of triangle then $\theta_3 = \theta_0$ as shown in Fig. 4. Here, $R(\theta)$ means a distance between reference point $P(x,y)$ and a point on the prospective boundary of the triangle as shown in Fig. 4.

4. Numerical results and discussion

In order to employ the BFM to deduce the interaction effects of multiple cracks on their SIF values, it is necessary to correlate the SIF values of single crack predicted by BFM with published data. Initially, a single crack subjected to mixed-mode loading at infinity is considered to illustrate the effectiveness of the present analysis. The normalized SIF is compared with the literature solution. In this method desirable results can be obtained with relatively coarse pattern as the SIFs values are obtained by extrapolating the obtained results for different number of triangles NT. The accuracy of the SIF calculation was satisfactorily examined for rectangular, penny-shaped and elliptical planar cracks embedded in an infinite elastic body. Later the numerical results of stress distribution for the interference effects between two coplanar penny-shaped cracks, elliptical cracks, rectangular cracks, penny-shaped and elliptical cracks, penny-shaped and rectangular cracks, and elliptical and rectangular cracks has been carried out. The obtained numerical results shows that the numerical approach presented in the present study is simple, yet very user friendly for analyzing the interference effect of arbitrary shaped multiple cracks in plane elasticity. In order to verify the numerical accuracy, SIF calculation was examined for elliptical cracks with different aspect ratio embedded in an infinite elastic body. In this paper, for all cases the poisson's ratio was set at $\nu = 0.3$. In demonstrating the results of stress intensity factor SIFs, the following dimensionless F_{n} will be used.

$$F_{\mathrm{n},b} = \frac{(K_{\mathrm{n}})_b}{\sigma_{ij}^{\infty}\sqrt{\pi b}} \tag{22}$$

Where, $i,j = x,y,z$ and n=I,II,III.

The normalized SIFs of elliptical crack is calculated for different aspect ratio and plotted in Fig. 5. The normalized mode-I stress intensity factor F_{I} is compared with the exact solutions. It is found that the present solutions are almost coincides with the exact solution. In present research the surface of the corresponding crack was divided with regularly distributed number of triangles NT. In this method desirable results can be obtained with relatively coarse pattern as the SIFs values are obtained by extrapolating the obtained results for different number of triangles.

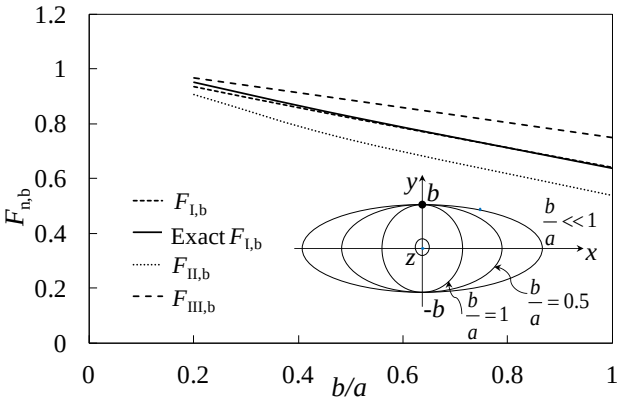

Fig. 5 Normalized mixed-mode SIF of a elliptical crack.

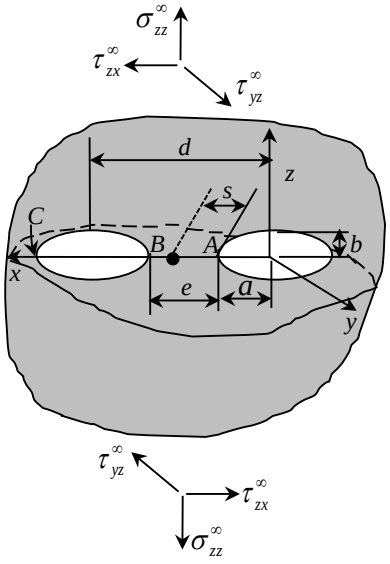

Fig. 6 Interference of two cracks under mixed-mode loading at infinity.

Fig. 6 shows the two coplanar cracks in an infinite elastic medium under remote loading at infinity along *zz*, *zx* and *yz* direction. The distance *e* between A and B can be varied. Both cracks surface is meshed in a same number of triangles NT. The ratio of minor and major axes of elliptical cracks are varied. When the radius of each crack is *a*=*b*=1.0, the normalized τ_{zx} distribution along *x*-axis for different values of *e* is shown in Fig. 7. It is found that the smaller the distance *e* between A and B, the greater the change of stress distribution along line AB. Near point C, the influence of the distance between A and B on the stress intensity factor is smaller. When *e*/*a*=0.5 and for the same radii of penny-shaped crack, the stress distribution is higher than stress distribution for other values of *e*/*a*. But as the ratio of *d*/*a* is increases the stress distribution is decreases. When the ratio of *e*/*a*=2.0, the stress distribution is same manner like the stress distribution of single penny-shaped crack as shown in Fig. 7. The interference analysis between elliptical cracks under mixed stress state at the infinity is also carried out. The normalized τ_{zx} distribution along *x*-axis between elliptical cracks for different values of *e* is shown in Fig. 8. The normalized stress distribution has the same trend like the normalized stress distribution between penny-shaped cracks.

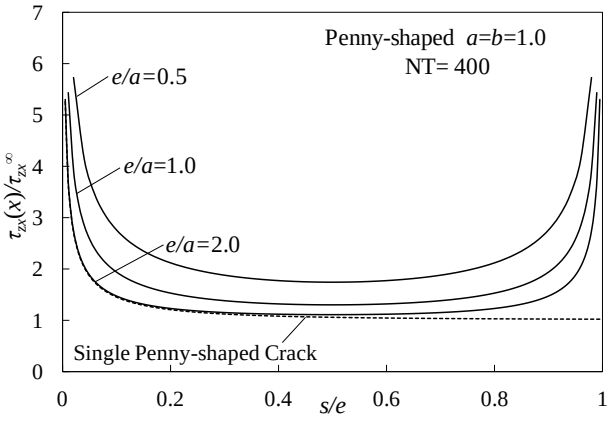

Fig. 7 Interference analysis between penny-shaped cracks.

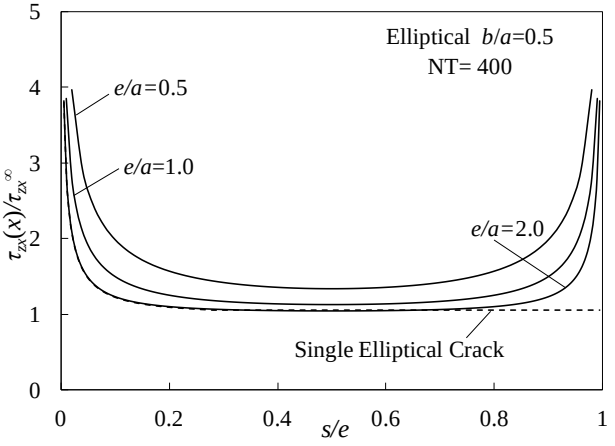

Fig. 8 Interference analysis between elliptical cracks.

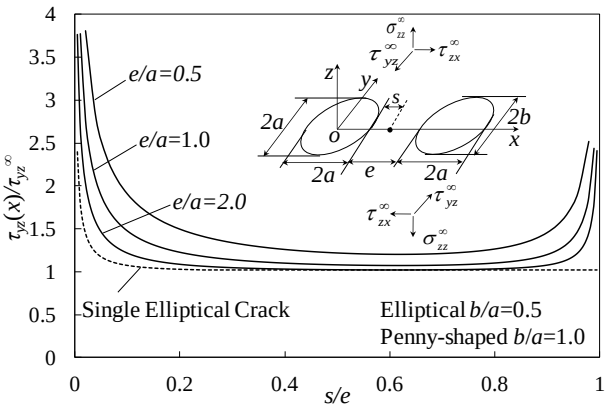

Fig. 9 Interference analysis between penny-shaped and elliptical cracks.

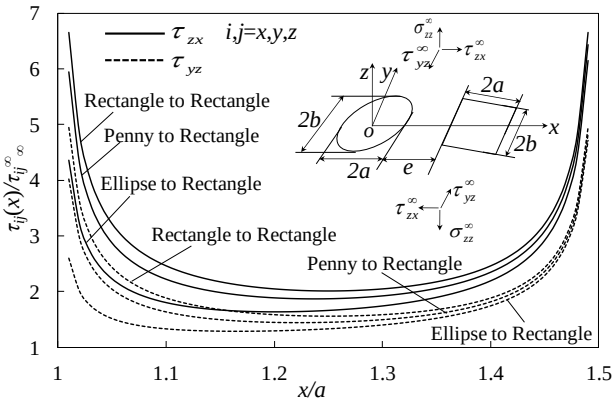

Fig. 10 τ_{ij} distribution between various shaped planar cracks (*e*/*a*=0.5).

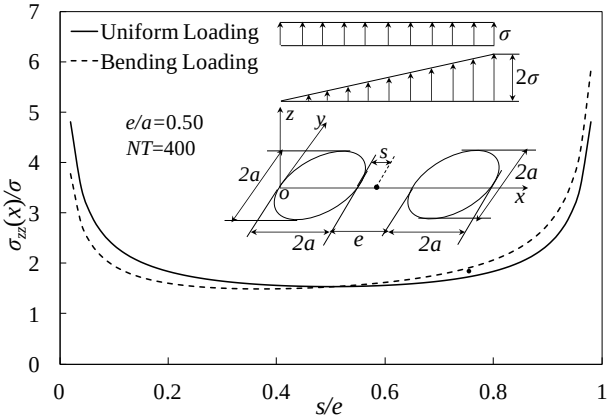

Fig. 11 Distribution of σ_{zz} along *x*-axis for uniform stress and bending loads.

Fig. 9 shows the interference effect between penny-shaped and elliptical cracks for different distance between center of cracks and fixed number of NT. Here aspect ratio *b*/*a* of the cracks are taken as 0.5. But any elliptical cracks with different aspect ratio can be analyzed. The crack tip difference *e* is varied from 0.5 to 2.0. For different values of *e*/*a*, as the distance between centers of cracks increases the magnitude of

stress distribution decreases. Fig. 10 shows the interference effect between different shaped cracks with fixed distance of *e/a*. The number of triangular elements for each crack was fixed at 400. Among compared for both cases, the rectangle to rectangle crack combination showed the largest interference effect. The interference analysis of cracks under bending load is also analyzed. Fig. 11 shows the interference between penny-shaped cracks under uniform stress and bending loads respectively for fixed distance between center of cracks and fixed NT.

5. Conclusion

The SIFs of cracks were evaluated using developed numerical program based on BFM. In this study, the effect of interaction between different shaped cracks on the SIFs and stress distribution was investigated. The problem was formulated as an integral equation on the idea of BFM. The unknown functions were approximated by the product of fundamental density function and weight function. The approximate solution is obtained easily by providing the triangular mesh data and boundary conditions. The interaction is influenced not only the relative position but also by the relative shape and length of crack. The interaction between two cracks becomes large as the distance between the cracks become small. If the crack length difference is greater than a certain level, there is no interaction effect on the stress distribution. From the obtained results it was found that the developed numerical program is applicable for analyzing interacting between arbitrary shaped planar cracks under any loading condition. Any kinds and any number of 3D planar cracks under any loading condition can be solved effectively only by providing input data.

NOMENCLATURE

P (x,y,z)	: Reference point
$Q(\xi,\eta,\zeta)$	: Source point
γ_{ij}	: Density of standard force doublets (i,j=x,y,z)
$\sqrt{h(\xi,\eta)}$	: Basic density function
$W_{ij}(\xi,\eta)$	: Weight functions (i,j=x,y,z)
$R(\theta)$	: Distance between reference point and a point on the prospective boundary
σ_{ij},τ_{ij}	: Stress components (i,j=x,y,z)
$\sigma_{ij}^{\infty},\tau_{ij}^{\infty}$	: Stress at the infinity (i,j=x,y,z)
a, b	: Major and minor axes of cracks respectively
K_{n}	: Stress intensity factor (n=I,II,III)
F_{n}	: Normalized stress intensity factor (n=I,II,III)
NT	: Number of triangles
s	: Distance from the crack surface along x-axis
e	: Distance between cracks surface

REFERENCES

[1] D. K. L. Tsang, S.O. Oyadiji, A.Y.T. Leung, Multiple penny-shaped cracks interaction in a finite body and their effect on stress intensity factor, *Engineering Fracture Mechanics*, Vol. 70, pp 2199-2214, (2003) .

[2] B. N. Rao, S. Rahman, An efficient meshless method for fracture analysis of cracks, *Computational Mechanics*, Vol. 26, pp 398-408, (2008).

[3] A. Roy, T.K. Saha, Interaction of a penny-shaped crack with an elliptic crack, *International Journal of Fracture*, Vol. 73 pp 51-65 (1995).

[4] M. Denda, Y. F. Dong, Complex variable approach to the BEM for multiple crack problems, *Computer methods in applied mechanics and engineering*, Vol. 141, pp 247-264, (1997).

[5] E. Madenci, B. Sergeev, S. Shkarayev, Boundary collocation method for multiple defect interactions in an anisotropic finite region, *International Journal of Fracture*, Vol. 94, pp 339-355, (1998).

[6] Y. M. Chen, Numerical computation of dynamic stress intensity factors by a Lagrangian finite-difference method (the HEMP code), *Engineering Fracture Mechanics*, Vol. 7, pp 653-660, (1975).

[7] J. H. Kuang, C. K. Chen, Alternating iteration method for interacting multiple crack problems, Fatigue & Fracture of Engineering Materials & Structures, Vol. 22, pp 743-752, (1999).

[8] H. Nisitani, The two-dimensional stress problem solved using an electric digital computer, *Bulletin of the Japan society of mechanical engineers*, Vol. 11, pp 14-23, (1968).

[9] H. Nisitani and Y. Murakami, Stress intensity factor of an elliptical crack and semi-elliptical crack in plates subjected to tension, *International Journal of Fracture*, Vol. 10, pp 353-368, (1974).

[10] Y. Murakami, S. Nemat-Nasser, Interacting dissimilar semi elliptical surface flaws under tension and bending, *Engineering Fracture Mechanics* , Vol. 16, pp 373–386, (1982).

[11] M. Isida, K. Hirota, H. Noguchi, T. Yoshida, Two parallel elliptical cracks in an infinite solid subjected to tension, *International Journal on Fracture*, Vol. 27, pp 31–48, (1985).

[12] M. Isida, T. Yoshida, H. Noguchi, Parallel array of semi-elliptical surface cracks in semi-infinite solid under tension, *Engineering Fracture Mechanics*, Vol 39, pp 845-850, (1991).

[13] Q. Wang, N. A. Noda, M. A. Honda, M. Chen, Variation of stress intensity factor along the front of a 3D rectangular crack by using a singular integral equation method, *International Journal of Fracture*, Vol. 108, pp119–131, (2001).

[14] N. A. Noda, K. Kobayashi, T. Oohashi, Variation of the Stress Intensity Factor Along the Crack Front of Interacting Semi-Elliptical Surface Cracks, *Archive of Applied Mechanics*, Vol. 71, pp 43-52, (2001).

[15] A. E. H. Love, A Treatise on Mathematical Theory of Elasticity, 4th edition, *New York Dover P*ublications, pp 183-185, (1944).

ICMIEE-140142

Defects Minimization through DMAIC Methodology of Six Sigma

Syed Misbah Uddin, Rashidul Hasan, Md. Saddam Hosen*
Department of Industrial & Production Engineering,
ShahJalal University of Science & Technology, Sylhet-3114, BANGLADESH

ABSTRACT
The demand for higher value at lower price is increasing and to survive, garment manufacturers need to improve their operations through producing "right first time" quality product. Minimization of defects is the prerequisite to the quality improvement. This paper presents how to minimize the defects rate by introducing and implementing the DMAIC Methodology of Six Sigma into a sewing section of a selected garment factory. This is a systematic approach towards defects minimization through five phases of DMAIC methodology named Define, Measure, Analyze, Improve and Control. Pareto chart was used to identify the top occurring defects. After identifying the major defects, brainstorming tool was used to identify the probable causes and then potential root causes were identified by online inspections and root cause analysis. The result found after implementation of the methodology was very significant. The defect percentage was reduced from 11.229 to 7.604 and the Sigma level was improved from 2.714 to 2.93.

Keywords: Defects, DMAIC, Pareto Chart, Cause & Effect Diagram, Sigma level.

1. Introduction

Ready-made garment (RMG) is the most important sector in Bangladesh in terms of employment, foreign exchange earnings and its contribution to Gross Domestic Product (GDP). It is the largest exporting industry in Bangladesh, which experienced phenomenal growth during the last 20 years. According to the annual financial report of BKMEA, in the financial year 2012-2013, 79.63% of Bangladesh's export earnings came from the garment industry and its contribution to the GDP was 8.07% [1]. The export-quota system and the availability of cheap labor are the two main reasons behind the success of this industry. But, the phase-out of the export-quota system from the beginning of 2005 has raised the competitiveness issue of the Bangladesh Readymade Garments industry as a top priority topic.

According to Tennant and Geoff, "A systematic continuous improvement process can largely minimize the defect percentage and increase the productivity" [2]. On the other hand, most of the garments factories in Bangladesh have not any particular quality management system. In order to minimize the defect rate, it is very important to follow a particular methodology in their quality management system. Considering the reasons above, this study makes an attempt to introduce and implement the DMAIC methodology of Six Sigma in a selected garment industry to minimize the defect percentage. DMAIC methodology of Six Sigma is a problem solving technique where process data is analyzed by different Six Sigma tools and identify the problems which cause the defects produce in the product.

Six Sigma is a quality improvement process of final product by reducing the defects, minimizing the variation and improving capability in the manufacturing process. A study by Antony et al. indicates Six Sigma as a more advanced level of quality, which will certainly implement those organizations that tend to business excellence after QMS certification per ISO 9000 series [3]. It is a set of techniques based on Statistical Process Control (SPC) which can help companies to achieve significant improvement in product quality and therefore increase competitiveness. The term Six Sigma originated from terminology associated with statistical modeling of manufacturing processes. By definition, Six Sigma is less than 3.4 Defect per Million Opportunities (DPMO) or parts per million (PPM). Six Sigma concept typically involves using process roadmaps and problem-solving tools. The Six Sigma DMAIC (Define, Measure, Analyze, Improve and Control) methodology helps to improve existing processes through incremental improvements.

2. Background of the Study

Defects play a vital role in the productivity of the garments factory. If a defect creates in one section of the production process and it is detected in the final inspection then defective garment has to travel a long distance before being identified. Money spent during the production process on a defective garment is a waste as the product cannot be exported. Even if it is made exportable with alterations, it is done so only by spending more money, which is of no value to a factory owner.

A study by Saroj Bala concluded that the demand for higher value at lower price is increasing and to survive, garments manufacturers need to improve their

* Corresponding author. Tel.: +88-01680304439
E-mail address: misbah-ipe@sust.edu

operations through producing right first time quality and waste reduction. The industry can gain higher productivity and profitability with improved quality product by minimizing the need for reworks. It also minimizes cost and improves internal throughout time [4].

In a garment factory, defects may originate from the fabric section, cutting section, sewing section or finishing section. Among those the sewing section is the largest and most complex in operation. A study by Kayaalp I. and Erdogan, M. showed that more than 75% garment defects were found in the final inspection coming from sewing section [5]. In this context, defect minimization in the sewing section of Readymade Garments factory is selected for this research work. The major defects occur from the sewing section are open seams, wrong stitching techniques, non matching threads, missing stitches, improper creasing of the garment, improper thread tension etc.

3. Methodology

The research methodology adopted for this study is done by the case study and brain storming. The case study conducted on a garment factory named "Vision Composite Knit Limited" located at Savar, Dhaka. At first preliminary investigation was carried out at cutting, sewing, washing, finishing and packing section to identify the area where most of the defects are occurred. It is found the sewing section is highly suffered from defect and rework problems. For this reason, we decided to work on sewing line to minimize the defect percentage by using DMAIC approach of Six Sigma methodology

We collected the secondary data of the sewing section which was provided by the management of the factory. The data was collected for Pant only. According to our observation and using the end line quality data provided by the management we identified some repetitive defects that occur in the sewing section

The information and data collected were arranged so that further study and analysis could be performed. Two mostly used Six Sigma tools namely Pareto Analysis and Cause-Effect Diagram were used in our analysis part

Pareto analysis was used to identify the top occurring defects. Brainstorming session was conducted to identify the probable causes and then potential root causes were identified by online inspections. Cause-Effect Diagrams were constructed for those defects. After identifying the major causes of the top occurring defects, we provided some respective suggestions to minimize the frequency of the defects. The suggestions were made based on the brain storming session which was arranged by the management of the factory. Experts of the factory from different areas were present on that session.

Due to time constraint, management could not be able to implement all of our suggestions. But they implemented some of our suggestions in short time-frame on their pilot line and found some improvement

4. Data Analysis and Result

4.1 Data Collection

Data sheets were collected from the management for pant only. The data had been taken by the end line quality inspectors from two production lines of sewing section. The combined 16 days data for the inspection of pants is given by the table 1.

Table 1: Inspection Report for Pants

Day	Checked Pieces	Defects found
1	610	60
2	888	106
3	989	107
4	861	88
5	992	97
6	857	92
7	761	83
8	805	78
9	851	79
10	176	23
11	800	91
12	749	93
13	808	87
14	731	98
15	476	70
16	143	39
Total	11497	1291

4.2 Application of Six Sigma DMAIC Methodology

4.2.1 Define Phase

Define is the first phase of the DMAIC methodology of Six Sigma. The purpose of this phase is to define the problem, goal of the project and the process that needs to be improved to get higher sigma level. There are different six sigma tools are available for define phase. This research has applied the tool called SIPOC.

Problem Statement: The garment industries are suffering from high rate of rejections of their products due to the defects.

Goal Statement: To reduce the defect percentage to minimum level and thereby improve the quality, reduce wastes and increase productivity.

SIPOC

This is a process map that includes Suppliers, Inputs, Process, Outputs and Customers. Quality is judged based on the output of a process. Table 2 shows the SIPOC flow of the selected factory.

Table 2: SIPOC Flow of Vision Composite Knit Ltd

Suppliers	Inputs	Processes	Outputs	Customers
-Altex Fabrics Ltd. -Fabian Group	Unstitched cloth Machinery Thread Needles Button Zipper Label	Cutting Sewing Washing Ironing Finishing Packaging	T-shirt Polo-shirt Pant	C & A Tesco Masko s

4.2.2 Measure Phase

At this phase, percentage of defects, existing DPMO (Defect per Million Opportunity) and Sigma Level of the selected factory were calculated which is indicated in table 3. The frequency of defects of the inspected pants was also calculated and recorded in table 4. Pareto Chart was used as a Six Sigma tool here.

Table 3: DPMO and Sigma Level of Existing Process

Total Checked	11497
No. of Defectives	1291
% Defectives	11.229
DPO	0.11229
DPMO	112290
Sigma level	2.714

Table 4: Frequency of Defects of the Inspected Pants

Defects	Total Occurrence	% of Occurrence
Over Stitch	87	6.739
Down Stitch	135	10.457
Skip Stitch	147	11.387
Raw Edge	152	11.774
Joint Stitch	249	19.287
Thread Tension	87	6.739
Uneven Stitch	85	6.584
Puckering	24	1.859
Fabric Fault	2	0.155
Bar tack Missing	27	2.091
Spot	39	3.021
Slanted Stitch	140	10.844
Others	117	9.063
Total	1291	100

4.2.2.1 Pareto Chart

Pareto Chart is used to graphically summarize and display the relative importance of the differences between groups of data. It is a bar graph. The lengths of the bars represent frequency and are arranged with longest bars on the left and the shortest to the right. In this way the chart visually depicts which areas are more significant.

In this research, the major causes or types of defects were identified through Pareto Chart. The chart was constructed by the MiniTab Software. From the Pareto Chart following major sewing defects were identified.

1. Joint Stitch
2. Raw edge
3. Skip Stitch
4. Slanted Stitch
5. Down Stitch
6. Over Stitch
7. Thread Tension
8. Uneven Stitch

Among all, only these 8 defects are responsible for 86.3% of total defects.

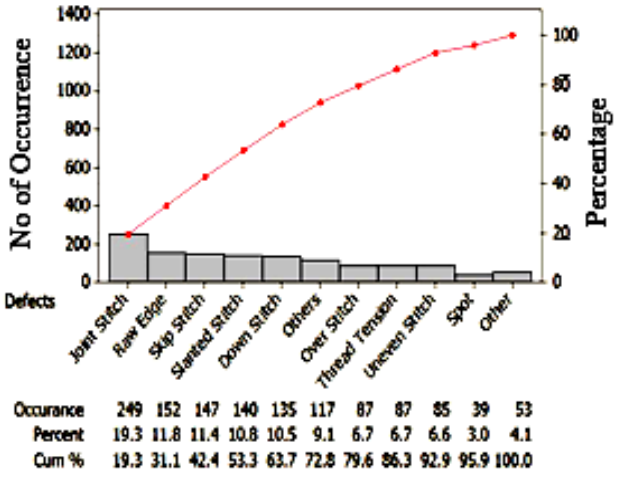

Figure 1: Pareto Chart for Identifying Major Defects

4.2.3 Analyze Phase

The purpose of the analyze phase is to target the improvement opportunities by taking a closer look at the data to determine the root causes of the process problems and inefficiencies. At the measure phase eight major types of defects were identified and the target of this phase is to find out all the potential causes of those defects. Two problem solving six sigma tools are used at Analyze Phase and these are: Brainstorming and Cause & Effect Diagram.

4.2.3.1 Brainstorming

Brainstorming is one of the most effective problem solving tools. The goal of this tool is to identify the issues, solutions and opportunities. In order to identify the probable causes of the defects and their respective solutions a Brainstorming session was arranged at the selected factory. The session was carried out by Round Robin method with the presence of factory manager, sewing floor manager, industrial engineer, end line quality inspector, line supervisor and sewing machine operator.

4.2.3.2 Cause & Effect Diagram

Cause & Effect diagram is a chart that identifies potential causes for particular quality problems. They are often called fishbone diagram. These causes could be related to the machines, workers, measurement, suppliers, materials, and many other aspects of the production process. This study has considered the causes related to 4 M's- Man, Machine, Method and Material. Cause & Effect diagrams are constructed based on the root causes identified by the online inspection. Total 470 pieces were inspected directly and 49 defects were found. The causes behind the defects were also identified immediately. There are some vital causes those have the highest frequency and mostly responsible for the defects. Table 5 shows the root causes sequentially according to their frequency of occurrence.

Table 5: Root Causes Analysis

Areas	Root Causes	No of Occurrences	Total
Man	Carelessness	9	17
	Unskilled operator	4	
	Margin not followed properly while stitching	2	
	Improper feeding	1	
	Lack of understanding about the whole operation	1	
Machine	Inappropriate thread tension	3	10
	Excessive pressure on pressure foot	2	
	Machine is threaded incorrectly	2	
	Dull sewing machine knives	2	
	Dull sewing machine needle or bent needle	1	
Method	Insufficient thread with respect to the length of the stitch	7	16
	The stitch is too long for the type of fabric in work	3	
	Machine speed is too high	2	
	Thread breaks during sewing	1	
	Improper folding	1	
	The stitch hole in the feed dog is too small or too large	1	
	Excessive abrasion or chemical degradation of the thread during the wash process	1	
Material	Poor quality thread	0	0
	Poor quality needle	0	

From table 5, it is observed that there were several man, machine and method related causes for the defects but no material related causes were found. Carelessness and lack of skills are two man related causes those have the highest frequency of occurrence (frequency: 13 of 17). Inappropriate thread tension or incorrect threading of the machines and excessive pressure on pressure foot are two major machine related causes (frequency: 7 of 10). On the other hand, insufficient thread and long stitch length are the major method related causes identified by the online inspection (frequency: 10 of 16). The identified causes are given in Cause & Effect diagram that is shown in figure 2.

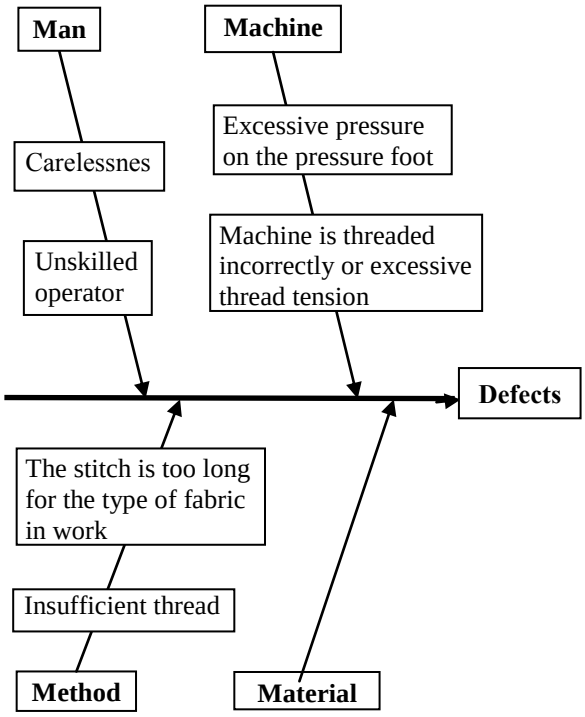

Figure 2: Cause & Effect Diagram for Major Defects

4.2.4 Improve Phase

The goal of the DMAIC Improve phase is to identify a solution to the problem that the project aims to address. This involves brainstorming potential solutions, selection of solutions to test and evaluating the results of the implemented solutions. Often a pilot implementation is conducted prior to a full-scale rollout of improvements.

4.2.4.1 Suggested Solutions

This study tried to suggest some potential solutions to minimize the causes of defects through brainstorming, direct observation and literature review. The solutions of the causes related to man, machine and method are given in table 6.

4.2.4.2 Implementation of the Solutions

This is the most difficult part for any research. Time constraint is one of the big reasons for the difficulty. Also, it is a big challenge for the research team to make an understanding to the management of an industry about the importance of the changes. This study also faced same difficulties and challenges. After a long discussion with the management, they agreed to implement some of the suggested solutions into one of their pilot sewing lines.

This study followed the Kaizen Improvement Technique that means continuous improvement. In order that the

solutions were divided into two categories: short term and long term. First, implement the short term solutions and then gradually go for the long term solutions.

Table 6: Suggested Solutions for Root Causes

Root Causes	Suggested Solutions
Man 1. Carelessness 2. Lack of skill of the operators	1. Improve supervision to make them careful 2. Provide adequate training to the operators to boost up their skill
Machine 1. Machine is threaded incorrectly or excessive thread tension 2. Excessive pressure on the presser foot 3. Dull or bent sewing machine needle and knife	1. Rethread the machine properly and make sure the thread goes through the tension discs. Ensure the stitch on the seam line is loose and be able to move if the needle hits it during a subsequent sewing operation. 2. Adjust the pressure on the presser foot. 3. Replace the needle and knife when it is dull or bent.
Method 1.Insufficient thread with respect to the length of the stitch 2. Long stitch for the type of fabric in work 3.Machine speed is too high	1. Make sure that the thread is sufficient to complete the whole length of stitch. 2. Reduce the length of the stitch by means of the stitch regulator, especially when sewing fine fabrics. 3. Start with lower speed then gradually increase the speed.

Short term solutions are:

- Replacement of dull or bent sewing machine needles and knives with new ones
- Insert the needles to the correct position
- Rethread the incorrectly threaded bobbins
- Always use good quality thread
- Use proper stitch length (as small as possible) during sewing
- Carefully follow the marked line during sewing

Long term solutions are:

- Provide adequate training to the operator
- Improve supervision
- Change faulty machine parts
- Develop a proper quality management system in order to quick detection and solution of the quality problems.

4.2.4.3 Result

Based on the solutions provided by this study, some corrective actions were taken. All short term solutions were implemented into one of their pilot sewing lines. Defects data were taken for eleven days after implementation of solutions that is recorded in table 7. The percentage of defectives, DPO, DPMO (Defect per Million Opportunity) and Sigma Level were calculated and reported on table 8.

Table 7: Number of Defects in Inspection of Pants after Improvement

Day	Checked Pieces	Defectives
1	720	45
2	839	75
3	752	53
4	690	41
5	805	64
6	731	45
7	163	12
8	792	61
9	827	67
10	878	88
11	470	32
Total	7667	583

Table 8: DPMO and Sigma Level after Improvement

Total Checked	7667
No. of Defectives	583
% Defectives	7.604
DPO	0.07604
DPMO	76040
Sigma level	2.93

4.2.5 Control Phase

After implementation of the solutions, the positive results were discussed with the management of the selected garment industry. The major defects were identified and partially reduced in amount. Now the real challenge is to sustain the improvements and make improving the process continuously. So, this research made a control plan in order to sustain the improvements and make the process improving.

4.2.5.1 Control Plan

The following are the mandatory actions that need to be taken by the management to sustain the results after Six Sigma implementation.

- The operators of garment industry must be given training on a continuous basis on the issue of quality.
- Always use good quality threads, needles and other garment accessories.
- The management should give incentives for high quality performance.
- The focus should be on preventing defects rather than correcting defects.
- Tight quality controls should be enforced.
- The organization should develop a proper Quality Management System.

5. Conclusion

Minimizing defect is very important for ensuring the quality of products. The importance of the garment industry in the economy of Bangladesh is very high. The explosive growth of the RMG industry in the country, however, has not been enough supported by the growth of backward linkage facilities. So manufacturing the quality product is mandatory to sustain in this global competitive market. Good Quality increases the value of a product or service, establishes brand name, and builds up good reputation for the garment exporter, which in turn results into consumer satisfaction, high sales and foreign exchange for the country.

From the Pareto Chart total eight defects (Joint Stitch, Raw edge, Skip Stitch, Slanted Stitch, Down Stitch, Over Stitch, Thread Tension, Uneven Stitch) were identified and those defects were responsible for near about 80% of total defects occurring in the sewing section of the garment factory for pant only. After finding the major defects, brainstorming tool was used to identify the probable causes and then potential root causes were identified by online inspections and root cause analysis.

This research found that the selected garment industry was operating at a defect percentage of 11.229. The rate was very high at this present business context. After implementing the DMAIC Methodology of Six Sigma the percentage of defect was reduced to 7.604. There was also found a significant improvement of the Sigma level of the industry. It was shift from 2.714 to 2.93. So, this methodology is very effective to the minimization of defects. As the minimization of defects is a continuous process further implementation of this methodology will help the company enjoying more reduction on defect rate and improvement on productivity.

Many medium scale garment industries in Bangladesh are not aware of the Six Sigma concepts and this study will trigger a positive wave across the garment industries and make them more competitive.

REFERENCES

[1] BKMEA (2014). Export Performance of RMG of Bangladesh for 2011-12 & 2012-13. *Annual Repot of Bangladesh Knitwear Manufacturers and Export Association*.

[2] Tennant and Geoff (2001). *SIX SIGMA: SPC and TQM in Manufacturing and Services*. Gower Publishing Ltd. p. 25.

[3] Antony J., Kumar M., Madu C. N. (2005). Six sigma in small and medium-sized UK manufacturing enterprises: Some empirical observations. *International Journal of Quality & Reliability Management*. Vol. 22(8). p. 860–874.

[4] Saroj Bala (2003). Factors Influencing Costing of Woven Fabrics. *The Indian Textile Journal*. Vol. 1(2). p. 57-68.

[5] Kayaalp, I. and Erdogan, M. (2009). Decreasing Sewing Defects by Using Statistical Process Control Methods in the Apparel Factory. *Tekstilve Konfeksiyon*. Vol. 19(1). p. 169-174.

ICMIEE-PI-140144

Evaluating the integrated performances of two CAD systems applied in garments manufacturing process

Lal Mohan Baral[1], *Ruhul Amin Khokon*[2]
[1]Ahsanullah University of Science and Technology, Dhaka, BANGLADESH
[2]"Sinha Knitting Ltd", Dhaka, BANGLADESH

ABSTRACT

The purpose of this paper is to identify the weak points of Gerber and Grafis CAD systems during practical application in a knit garments manufacturing process and also evaluate their integrated working performances for the same product. At first, the comparative working capability of both CAD systems has been investigated considering the elements like: i) Pattern development (ii) Pattern modification (iii) Pattern grading (iv) Marker development (v) Data transferring facility (vi) Advanced features and (vii) Purchasing cost. Afterward, both of those systems have been integrated only taking their strong elements and applied for the same product. Finally, the working performances of integrated systems have also been evaluated comparing with the individual performance of those CAD systems .The results revealed that the Grafis system has shown more effective performance than Gerber in respect of majority elements. Moreover, the results from integrated approach have expressed the significant advantages for all the selected elements. The results of our study suggested that the integration of Gerber with Grafis CAD systems would be one of the better solutions than individual for effective application.

Keywords: Garments CAD system, Garments manufacturing, Gerber, Grafis, Integrated performance.

1. Introduction

In the intensity and pace of today's cutthroat competitive business environment around the world, the garments manufacturers are using advanced computer technology extensively like other manufacturing areas for product designing, planning , manufacturing and marketing [1]. As an essential technology, the Computer Aided Design (CAD) has also been using for the garments manufacturing process, which provides support to the creative work in the design studio for pattern designing, pattern grading and marker making [1-3] . By using CAD systems in garments manufacturing, three main advantages would be achieved such as: production flexibility, productivity and storage capacity [2], which leads to benefits like reduction of lead times, lowering of direct cost and most importantly quick communication with customers and suppliers [3].In order to fulfill the increasing user's demands, a wide number of CAD systems namely Gerber, Lectra, Investronica, Bullmar, Optitex, Grafis, PAD and Assyst have been developed by the different companies, [3,4]. The available CAD systems developed for garments manufacturing have been featured with different working scopes according to the user's demands. All of those have some strong and weak points in respect of working flexibility and purchasing cost. Specially, the price of the CAD systems is one of the crucial factors for medium and small size garments manufacturers to invest. Due to higher investment cost, only large companies can able to purchase costly one, which have more operation flexibility [3]. Recently, some cheap garments CAD systems have also been developed with flexible working scopes. So, there is a need to analyze the working scopes and abilities of both costly and cheap CAD systems in order to find the possibility of combined application to fulfill the user's all requirements in a reasonable price.
In order to achieve that goal, in this research, two well known CAD systems Gerber (costly) and Grafis (cheap) have been analyzed through a practical application considering their working scopes, flexibilities and price in order to indentify the week and strong points. Then, an integrated application including both of those systems has also been investigated for the same product by taking positive features from both CAD systems.

2. Research methodology

In this research, at first, the comparative working capabilities of Gerber [5] and Grafis [6] CAD systems have been investigated through practical application on a knit garment manufacturing process considering the elements like: i) Pattern development (ii) Pattern modification (iii) Pattern grading (iv) Marker development (v) Data transferring facility (vi) Advanced features and (vii) Purchasing cost. Afterward, both of those systems have been integrated only taking their strong elements and applied for the same product. Finally, the working performances of integrated systems have also been evaluated comparing with the individual performance of those CAD systems by using qualitative and quantitative methods based on the elements characteristics.

* Corresponding author. Tel.: +40-0756365398
E-mail address: baraltex@aust.edu

3. Findings and Discussion

3.1 Pattern development

During developing the patterns of our product using Grafis, the following steps have been used sequentially: i) Call the basic pattern block from Grafis basic block storage ii) Adjust the basic block according to required measurements iii) Call the sleeve from Grafis basic block storage iv) Adjust the sleeve shape according to required measurements v) Call the collar from Grafis basic block storage and adjust it vi) Call the hood from Grafis basic block storage and adjust it vii) Finally all patterns have been completed. All Body measurements used in this drawing have been given input only in mm. There was no other option. On the other hand, for the same product, the patterns development steps were as follows while using the Gerber system: i) All basic blocks have been drawn manually by preparing a Rectangle for each pattern part ii) All individual patterns have been developed from the basic blocks and completed all patterns parts. In Gerber system, there were various options to input the body measurements such as mm, cm and inches.
To draw pattern curves using Grafis system, there was an adjustable curve containing two handles at both ends. It was very easy to adjust by using those handles. But in Gerber system, there was a moveable smooth line to adjust the curve that was time consuming function.

During dart drawing on pattern parts using Grafis system, there were adjustable darts within the basic blocks, which were very easy to modify and relocate. The shape of side seam was changed automatically with the changing of dirt amount. But in Gerber system, there was no adjustable dart without manual dart addition. The shape of side seam was changed manually with the changing of dart amount, which was also time consuming.

The finished measurements chart preparation during pattern construction was very easy while using Grafis system. In this system, it was needed to measure the body measurement for the basic pattern. In Gerber system, it was only possible to see the measurement by measuring body measurements.

After drawing the basic patterns for our selected product through applying the aforementioned operations, a comparison has been tabulated between both systems considering the different operations used for pattern development as shown in the table 1.

3.2 Pattern modification

Just after developing the basic patterns of our product, it was required to modify the pattern parts, which includes the following operations: shoulder forwarding, addition of seam allowance, developing mirror of the pattern, developing the hem shape, dart modification, modification of sleeve curve and addition of side vent.

Table 1: Comparison between Gerber and Grafis for pattern development operations

Element	Operations	CAD Systems		Leading System
		Gerber	Grafis	
Pattern Development	Initial drawing	Complicated (Requires more time)	Easy (Requires less time)	Grafis
	Input of Body measurement	Flexible (mm,cm, inch)	Not flexible (only mm)	Gerber
	Curve drawing	Complicated (Requires more time)	Easy (Requires less time)	Grafis
	Addition of dart	Complicated (Requires more time)	Easy (Requires less time)	Garfis
	Preparing finished measurements chart	Manual (Time consuming)	Automatic preparation	Grafis

During using Grafis for shoulder forwarding, it has been taken the interactive mode of shoulder part from the interactive option by clicking the right button of the mouse and given the input of required amount of shoulder forwarding. But in Gerber system, several steps have been used. At first, the parallel lines have been drawn by taking shoulder forward amount and then made the mirror of front neck curve, armhole curve and parallel line against the shoulder seam. Finally, got the shoulder forward of front and back parts using tracing from this block. Upon completing the shoulder forwarding, it has been experienced that the use of Grafis system for this operation was easy. On the other hand, it was difficult in Gerber system, where some extra works were required.

For addition of seam allowance in the pattern parts using Grafis, it was required to add the seam allowance individually after selecting the different individual pattern parts. But it was possible to give input the seam allowance after selecting all the parts at a time within the same window.

At the time of preparing mirror of the pattern parts by using Grafis, it was required to make mirror for individual patterns by selecting the different pattern parts individually. While using Gerber, it was possible to develop mirror of the pattern parts at a time by

selecting all the parts at the same time in a same window.

Different shapes of hem of pattern parts have been drawn through adjusting the interactive mode of the basic block in the Grafis system. Afterward it was clicked on the “test run” and all changes were transferred into other parts of pattern automatically. But in Geber system, the hems of pattern parts were drawn manually. At first, it was required to draw the hem shape manually and then traced it.

In order to modify the shape of sleeve curve, different shapes of sleeve curve were made by adjusting the interactive mode of the sleeve block in the Grafis system. Then it was clicked on “test run” and all changes were transferred into other parts of pattern automatically. By using Gerber system, different shape of sleeve curves were modified manually and finally traced it.

During dart modification, different shapes of darts were modified by adjusting the interactive mode of dart in the bodies block while using the Grafis system. Then it was click on “test run” to be active and all changes were transferred into other parts of pattern automatically. But**,** different shapes of dart of pattern parts were developed manually in the Gerber system.

In case of ladies item, sometimes darts are required for close fitting. The dart addition and relocation in pattern is always a difficult task within Gerber system. Because, whenever darts are added in the pattern parts, some changes are occurred within the patterns, thus need to adjust the pattern manually. There is no interactive dart adjusting tool in Gerber system. But, Grafis system has interactive dart adjusting tool.

After analyzing all the steps of pattern modification, it was experienced that this function is a unique property and easy to work within Grafis system. There is a special option such as ‘test run all'. After modifying the different shapes of different interactive blocks of a style, just clicked 'test run all' and all the patterns will be changed within a moment. On the other hand, in Gerber system, pattern modification is a difficult task. Because there is no interactive basic blocks but it exists in Grafis system. Although there are some auto shapes in Gerber system version 8.5, it's very poor in function and not possible to modify it later on when it will require**.**

For addition of side vent of pattern it was found that the Gerber system was difficult to work but Grafis system was very easy to work.

In the table 2, a comparison has been presented in between Gerber and Grafis system considering all sub operations of pattern modification.

3.3 Pattern grading

It was found two options of pattern grading while using the Grafis system. One is interactive grading and another is manual grading. During the interactive grading, it was possible to perform the grading of pattern parts in interactive mode not only for bodies blocks but also all others blocks. At first, sizes were taken from the size table and then went to the interactive mode to assign the sizes through the 'set break sizes’. After that, the values of grading amount were given input for each measurement place. Finally, it was clicked on 'test run all ' which enabled all the grading and transmitted to different pattern parts. For manual grading, all pattern parts were extracted into grade rule pattern to add the grade points and finally the values of grading amount were given input for each part separately.

Table 2: Comparison between Gerber and Grafis for pattern modification factors

Element	**Operations**	**CAD Systems**		**Leading System**
		Gerber	**Grafis**	
Pattern Modification	Shoulder forward	Complicated (Requires more time)	Easy (Requires less time)	**Grafis**
	Addition of seam allowance	Easy to work (Possible to hide during drawing)	Complicated to work (Not possible to hide during drawing)	**Gerber**
	Developing mirror of pattern	Easy to work (Possible to hide during drawing)	Complicated to work (Not possible to hide during drawing)	**Gerber**
	Developing of hem shape	Complicated to give the required shape (Require more time)	Easy to give the required shape (Requires less time)	**Grafis**
	Dart modification	Complicated to work	Easy to work	**Grafis**
	Modification of sleeve curve	Complicated to work	Easy to work	**Grafis**
	Addition of side vent	Complicated to work	Very easy to work	**Grafis**

During grading with Gerber system, it was only found the manual grading option. At first, the rule table was prepared in the Explorer and then assigned this rule

table in the different parts of the pattern. Finally, the grading values were given input for each grading point using 'edit delta' for each individual part of the pattern.

It was also noticed that during the styling process, Grafis internally creates a record of the modification steps, basically continuing the drafting instructions of the basic blocks. The record can then be re-called to create other sizes automatically thus, eliminating incremental grading. The Construction parameters can be applied during pattern development. This enables the user to comfortably modify already finished patterns by changing the construction parameter simply. The Gerber system has only the point grade rule system, which is old manual system. There is no option to save the all grade rule points all together even the record can‘t then be re-called to create other patterns automatically thus, eliminating incremental grading and the construction parameters can be applied during pattern development. The comparison between Gerber and Grafis system for the operations of pattern grading is presents in the table 3.

Table 3: Comparison between Gerber and Grafis for the operations of pattern grading

Element	Operations	CAD Systems		Leading System
		Gerber	Grafis	
Pattern Grading	Manual	Have Manual incremental system with point grade rule system,	Also have manual incremental grading but little bit difficult.	**Gerber**
	Auto	There is no auto grading rule.	There is auto grading in the Interactive mode, copy or recall possible	**Grafis**

3.4 Marker development

During marker development of our selected product by using Grafis system, it was found that along with normal marker making tools, there is an option for matching of pattern for side matching marker. The side matching was indicated through a green line. But this system has some limitations such as: it was not possible to open the marker from other formats directly except Grafis marker. On the other hand, in Gerber system, although there was no option for matching the pattern without manual system, it could open marker from some other formats directly such as: Lectra, Investronica and Assyst marker.

By using Grafis, markers can be created from different styles. Apart from the common functions such as butting pieces together, rotate, flip and buffer a large number of options and aids for specialist applications are available. These include matching points for laying checks and stripes, use of marker templates, automatic generation of fusing blocks, consideration of material flaws and shrinkage and many more. Special lay planning options for folded lays or tubular material and step-lays can be selected. In case of matching garments, sometimes it's needed to match the front part and back part of matching garment horizontally and vertically within the marker. The Gerber system have no option for matching of front and back part of a garment and need to do it manually within the marker. It's not only time consuming but also difficult while using the Gerber system. A brief and specific comparison is presented in the table 4.

Table 4: Comparison between Gerber and Grafis for marker development operation

Element	Operations	CAD Systems		Leading System
		Gerber	Grafis	
Marker Develop-ment	Marker making	Pattern matching is manual system	Pattern matching is auto system	**Grafis**

3.5 Data transferring facility

After marker making, next task was to transfer the data to subsequent process. It was only possible to import the 'standard dxf' and ‘Grafis’ data of pattern and export into different data formats by using the Grafis system. But during using Gerber system, there was lots of flexibility for the pattern and marker data in respect of exporting and importing. By using Gerber system, it was possible to import the data of pattern parts directly from other formats such as Lectra, Investronica, Assyst, Standard dxf, etc. and possible to export different data format like as AAMA(dxf), ASTM, Standard dxf ,IGES and so on.

Normally, all Grafis users who deal with production abroad or provide pattern services for companies will have to deal with export and import. According to basic rule, during data exchange between CAD systems a loss of information occurs as the patterns are reduced to an agreed data format. During export, the interactively adjustable patterns in Grafis are converted to a contour with grade rules including additional information on grain line, notches, text and symbols. The exported patterns contain no information regarding x values, body measurements and piece interdependency. Patterns from foreign systems can be imported into Grafis only as grade rule patterns. Grade rule patterns consist of a pattern perimeter with grade points. Each grade point is

assigned a grade rule table with size dependant point movement in x and y direction.

On the other hand, it's possible to import a model or pattern pieces from different data format in the Gerber system as well as it's possible to export a model or pattern pieces from the Gerber system. It's also possible to open the patterns or a model from other systems (Lectra design, Assyst design, Investronica design, IGES) directly. The comparison is presented in the table5.

Table 5: Comparison between Gerber and Grafis for data transferring operations

Element	Operations	CAD Systems		Leading System
		Gerber	Grafis	
Data Transferring System	Data import/ export	Easy from other systems	Not easy from other systems	**Gerber**

3.6 Advanced features

The development of clothing 3D simulation technology made a tremendous impact on the apparel field including fashion design, garments manufacture and marketing [7-9].The researches on the application of 3D clothing simulation in the garments industry have given more and more attention [9] .The Gerber system has the 3D simulation technology (Vsticher) auto nesting and so on [5] but the Grafis system has no 3D simulation technology. Only it has auto nesting advanced features [6].

Table 6: Comparison between Gerber and Grafis for advanced feature factor

Element	Operations	CAD Systems		Leading System
		Gerber	Grafis	
Advanced Feature	Auto motion	Have Full automation	No, but can be used	**Gerber**
	3D simulation	Possible	Not possible	**Gerber**

3.7 Purchasing cost

During investigating the price of both selected CAD systems, it was found that the Price of Gerber system is extensively high compare to Grafis system. The price of one set Gerber system is near about 8000 USD in Bangladeshi market, where as the price of one set Grafis system is near about 4000 USD.

Table 7: Comparison between Gerber and Grafis for price factor

Element	Factor	CAD Systems		Leading System
		Gerber	Grafis	
Price	Value of unit system	$ 8000	$ 4000	**Grafis**

3.8 Evaluating the performance of integrated system

Upon investigating the working capabilities, flexibilities and scopes of Gerber and Grafis CAD systems for our selected product, it was observed that the Grafis system has shown great advantages for most of the elements and the Gerber system has shown advantage for some elements. Afterward an integrated system has been developed taking the advanced elements from both CAD systems and applied all three systems (Gerber, Grafis and Integrated) to develop our selected product. After application of all systems, a comparison among all three systems has been done in respect of different operations used for the product development. The comparative analysis is presented in the figure1.

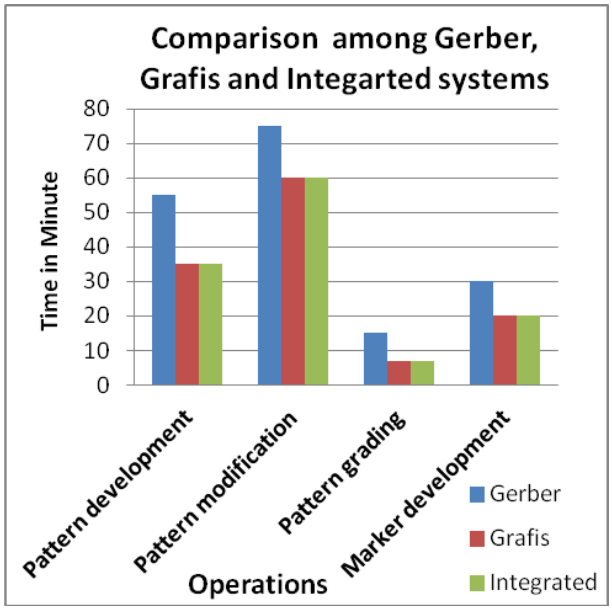

Figure1: Evaluation of the integrated system comparing with Gerber and Grafis system

Actually, it was possible to analyze four major operations (i.e pattern development, pattern modification, pattern grading and marker development) quantitatively during our product development. The results presented in the Graph (figure 1) evident that for all four major operations, the integrated system have showed significant advantages like as Grafis, as because

those elements were taken from Grafis system for integrated system.
After the quantitative analysis, a qualitative analysis has been done for "Data transferring facility" and "Advanced features" exist in the Gerber and Grafis systems (presented in the table:5 and 6). In respect of both cases, the Gerber system has shown more advantage than Grafis system. That's why to use the advantage of those elements within the integrated system; it was taken from Gerber system.
Further, another comparative analysis has also been done in respect of price factor, which is very much important for the end users. For this analysis, the price of five units of Gerber systems, five units of Grafis systems and five units of "Integarted systems" (One unit Gerber and four unit Grafis; which is a good combination to get all working facilities) has been calculated. As shown in the figure2, the price of "Integrated system" is little higher (approx. 16%) than Grafis system but 40% lower than the Gerber system, which very much significant. But working flexibility and scopes are same and or better (in some cases as discussed in the previous section) than individual Grafis or Gerber system.

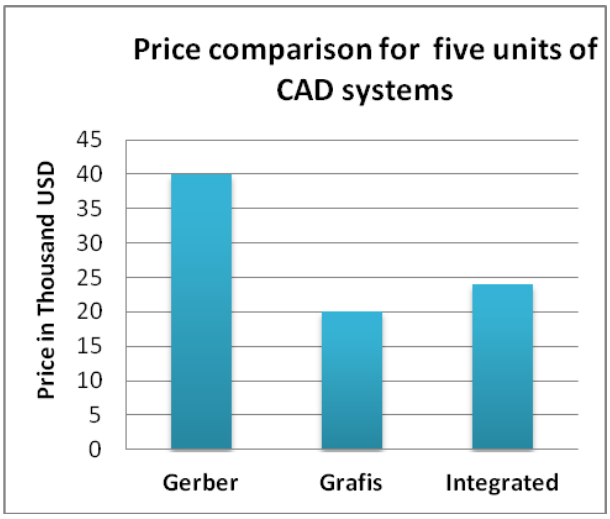

Figure 2: Comparison among Gerber, Grafis and Integrated systems in respect of price

4. Conclusions

The results from the practical application revealed that the Grafis system has shown more effective performance than Gerber in respect of Pattern development, Pattern modification, Pattern grading, Marker development and Purchasing cost. On the other hand, the Gerber showed better performance for Data transferring facility and advanced features. Moreover, the results from integrated approach have expressed the significant advantages for all the selected elements. This article has documented the advantages of integrated application of two CAD systems in garments manufacturing unit. During this time many garments manufacturing units are trying to increase their working flexibility and production rate through introducing more work stations with existing Gerber CAD system. The results of our study suggested that the integration of Grafis system with Gerber system would be one of the effective solutions for the expansions of their CAD facilities.

Acknowledgement:

This research has been carried out within the "Sinha Knitting Ltd", Dhaka, BANGLADESH, is a reputed export oriented knit garments manufacturer. Authors would like to provide sincere thanks to the management of above mentioned company for their all out support.

REFERENCES

[1] H. Lim, C. L. Istook, Automatic Pattern Generation Process for Made-to Measure, *Journal of Textile and Apparel, Technology and Management*, Vol. 7, Issue-4, pp 1-11, (2012).
[2] A. Beazley, T. Bond, Computer –aided pattern design and product development, *Blackwell Publishing Ltd.*, Oxford, UK, (2003).
[3] L.M. Baral, Feasibility study of CAD and CAM technology in garments industries of Bangladesh, *Advanced Materials Research*, Vols. 264-265, pp 1563-1567, Trans Tech Publications, Switzerland, (2011).
[4] C. L. Istook, Enabling mass customization: Computer-driven alteration methods, *International Journal of clothing science and technology*, Vol. 14, Issue-1, pp 61-76, (2002).
[5] Gerber CAD/CAM, Clothing designing, founder: Joseph-Gerber, Responsible for the content of this site: July (2014), Available at www.gerbertechnology.com
[6] Grafis CAD/CAM, Clothing designing, partner authorized to represent: Dr. Kerstin Friedrich, Responsible for the content of this site: June (2014), Available at www.grafis.de
[7] C. L. Istook, H. Su-Jeong, 3D Body Scanning Systems with Application to the Apparel Industry, *Journal of Fashion Marketing and Management*, Henry Stewart Publications,1361-2026,II, pp 120-132, (2001).
[8] A. Vilumsone, I. Dabolina, Computer aided garment designing, Bulletin of Polytechnic Institute of Iasi, Technical University " Gheorghe Asachi" of Iasi (2010).
[9] R. A. Khokon, CAD formation in real-time simulation of clothing with VIDYA-didactical projection of study processes, Master Thesis, The Niederrhein University of Applied Sciences, (2014).

ICMIEE-PI-140146

Similarity Analysis of Unsteady MHD Boundary Layer Flow of Heat and Mass Transfer about an Inclined Stretching Porous Sheet

Mohammad Ali [1,*], *Md.Abdul Alim* [2], *Mohammad Shah Alam*[3]
[1,3] Department of Mathematics, Chittagong University of Engineering & Technology, Chittagong-4349, BANGLADESH
[2] Department of Mathematics, Bangladesh University of Engineering and Technology, Dhaka-1000, BANGLADESH

ABSTRACT
The aim of the study is to investigate the similarity solution of unsteady MHD boundary layer flow of an incompressible, electrically conducting and viscous fluid about an inclined stretching sheet with suction by Quasi-linearization technique. So the present work is focused of the impact of the flow parameters on the velocity, temperature and concentration are computed, discussed and have been graphically represented in figures and also the shearing stress and rate of heat transfer shown in table 1 for various values of different parameters. In this regard the governing momentum boundary layer, thermal boundary layer and concentration boundary layer equations with the boundary conditions are transformed into a system of first order ordinary differential equations which are then solved numerically by using Runge-Kutta fourth-fifth order method along with shooting iteration technique. The results presented graphically illustrate that velocity field decrease due to increase of Magnetic parameter, porosity parameter, suction parameter and angle of inclination of the sheet and reverse trend arises for the increasing values of stretching parameter, unsteadiness parameter, Grashof number and modified Grashof number. The temperature field decreases for Magnetic parameter, porosity parameter, suction parameter and Prandtl number but the temperature field increases for the increasing values of stretching parameter, unsteadiness parameter, Grashof number and modified Grashof number. Again, concentration profile decreases for increasing the values of Magnetic parameter, porosity parameter, suction parameter and Schmidt number but concentration increases for increasing the values of stretching parameter, unsteadiness parameter, Grashof number and modified Grashof number. The present results in this paper are in good agreement with the work of the previous author.

Keywords: MHD; stretching sheet: angle of inclination; viscosity; porosity.

1. Introduction

The important applications of heat and mass transfer over a stretching sheet in spinning of fibers, extrusion of plastic sheets, polymer, cooling of elastic sheets etc. As a result the quality of final product depends on the rate of heat transfer so that the cooling procedure has to be maintained effectively. On the other hand, the MHD boundary layer flow of heat and mass transfer has significant applications in industrial manufacturing processes such as Magneto-hydrodynamics power generator, glass fiber production, plasma studies, cooling of Nuclear reactors, petroleum industries, and paper production etc. In this regard many investigators have studied the boundary layer flow of electrically conducting fluid due to stretching sheet in presence of magnetic field. For this reason, Elbashbeshy and Bazid [1] discussed the similarity solution for unsteady momentum and heat transfer flow whose motion is caused solely by the linear stretching of a horizontal stretching surface, Alharbi et.al [2] studied heat and mass transfer in MHD visco-elastic fluid flow through a porous medium over a stretching sheet with chemical reaction, Seddeek and Abdel Meguid [3] analyzed the effects of radiation and thermal diffusivity on heat transfer over a stretching surface with variable heat flux , Ali et al. [4] studied the Radiation and thermal diffusion effects on a steady MHD free convection heat and mass transfer flow past an inclined stretching sheet with Hall current and heat generation, Ibrahim and Shanker [5] investigated the unsteady MHD boundary layer flow and heat transfer due to stretching sheet in the presence of heat source or sink by Quasi-linearization technique. Ishak et al. [6] investigated the solution to unsteady mixed convection boundary layer flow and heat transfer due to a stretching vertical surface. Further, Ishak [7] studied unsteady laminar MHD flow and heat transfer due to continuously stretching plate immersed in an electrically conducting fluid. Ebashbeshy and Aldawody [8] analyzed heat transfer over an unsteady stretching surface with variable heat flux in presence of heat source or sink, Fadzilah et al. [9] studied the steady MHD boundary layer flow and heat transfer of a viscous and electrically conducting fluid over a stretching sheet with an induced magnetic field. Also, Bachok et al. [10] analyzed the similarity solution of the unsteady laminar boundary of an incompressible micro-polar fluid and heat transfer due to a stretching sheet and Mohebujjaman et al. [11] studied MHD heat transfer mixed convection flow along a vertical stretching sheet with heat generation using shooting technique. All of the above researchers in their studies were not consider the inclination of angle of the sheet and porosity. So the present work is focused on unsteady MHD boundary

* Corresponding author. Tel.: +88-01713109929
E-mail address: ali.mehidi93@gmail.com

layer flow of an incompressible, electrically conducting and viscous fluid about an inclined stretching sheet with suction by Quasi-linearization technique.

2. Governing Equations of the Present Problem and Similarity Analysis

Let us Consider a two dimensional unsteady laminar MHD viscous incompressible electrically conducting fluid along an inclined stretching sheet with an acute angle (α) , *X*- axis is taken along the leading edge of the inclined stretching sheet and *Y* is normal to it. Also, a magnetic field of strength B_0 is introduced to the normal to the direction of the flow. Again, suppose that the uniform plate temperature T_w is grater than that of fluid temperature (T_∞), where T_∞ is the ambient temperature of the fluid. Let *u* and *v* be the velocity components along the *X* and *Y* axis respectively in the boundary layer region. Under the above assumptions and usual boundary layer approximation, the dimensional governing equations of continuity, momentum, concentration and energy under the influence of externally imposed magnetic field are:

Equation of continuity:

$$\frac{\partial u}{\partial x}+\frac{\partial v}{\partial y}=0 \tag{1}$$

Momentum equation:

$$\frac{\partial u}{\partial t}+u\frac{\partial u}{\partial x}+v\frac{\partial u}{\partial y}=-\frac{1}{\rho}\frac{\partial p}{\partial x}+\nu\frac{\partial^2 u}{\partial y^2}+ g\beta(T-T_\infty)\cos\alpha+g\beta^*(C-C_\infty)\cos\alpha -\frac{\sigma B_0^2 u}{\rho}-\frac{\nu}{k^*}u \tag{2}$$

Energy Equation:

$$\frac{\partial T}{\partial t}+u\frac{\partial T}{\partial x}+v\frac{\partial T}{\partial y}=\frac{k}{\rho c_p}\frac{\partial^2 T}{\partial y^2} \tag{3}$$

Concentration Equation:

$$\frac{\partial C}{\partial t}+u\frac{\partial C}{\partial x}+v\frac{\partial C}{\partial y}=D_m\frac{\partial^2 C}{\partial y^2} \tag{4}$$

Using free stream velocity $u=U(x,t)=\frac{bx}{\sqrt{1-\gamma t}}$,

we get

$$\frac{\partial U}{\partial t}+U\frac{\partial U}{\partial x}=-\frac{1}{\rho}\frac{\partial p}{\partial x}$$

Hence equation (2) becomes

$$\frac{\partial u}{\partial t}-\frac{\partial U}{\partial t}+u\frac{\partial u}{\partial x}+v\frac{\partial u}{\partial y}=U\frac{\partial U}{\partial x}+\nu\frac{\partial^2 u}{\partial y^2}+ g\beta(T-T_\infty)\cos\alpha+g\beta^*(C-C_\infty)\cos\alpha-\frac{\sigma B_0^2 u}{\rho}-\frac{\nu}{k^*}u \tag{5}$$

The above equations are subject to the following boundary conditions:

$$\begin{aligned} &u=u_w,\ v=v_0(t),\ T=T_w, C=C_w \quad at\ \ y=0 \\ &u=U, T=T_\infty, C=C_\infty \quad as\ \ y\to\infty \end{aligned} \tag{6}$$

The velocity of the sheet $u_w(x,t)$, the surface temperature of the sheet $T_w(x,t)$, concentration $C_w(x,t)$, and the transverse magnetic field strength $B(t)$ are respectively defined as follows:

$$u_w=\frac{ax}{\sqrt{1-\gamma t}}, T_w-T_\infty=\frac{bx}{\sqrt{1-\gamma t}}, C_w-C_\infty=\frac{cx}{\sqrt{1-\gamma t}},$$

$$B(t)=\frac{B_0}{\sqrt{1-\gamma t}}$$

where, a is the stretching rate and b, c are positive constant with dimension (time)$^{-1}$. We introduce the steam function $\psi(x,y)$ as defined by $u=\frac{\partial\psi}{\partial y}$ and $v=-\frac{\partial\psi}{\partial x}$.

To convert the governing equations into a set of similarity equations, we introduce the following similarity transformation:

$$\psi=x\sqrt{\frac{a\nu}{1-\gamma t}}f(\eta), \eta=y\sqrt{\frac{a}{\nu(1-\gamma t)}},$$

$$\theta(\eta)=\frac{T-T_\infty}{T_w-T_\infty}, \varphi(\eta)=\frac{C-C_\infty}{C_w-C_\infty}$$

From the above transformations, the non-dimensional, nonlinear and coupled ordinary differential equations are obtained as follows:

$$f'''+ff''-f'^2-A\left(f'+\frac{1}{2}f''\right)-(M+N)f' +Gr\theta\cos\alpha+Gm\varphi\cos\alpha+\frac{1}{2}A\lambda+\lambda^2=0 \tag{7}$$

$$\theta''+\Pr f\theta'-\frac{1}{2}\Pr A\eta\theta'=0 \tag{8}$$

$$\varphi'' + Scf\varphi' - \frac{1}{2}ASc\eta\varphi' = 0 \qquad (9)$$

The transform boundary conditions:

$$\begin{aligned} &f = -f_w,\ f' = 1, \theta = \varphi = 1 \ at\ \eta = 0, \\ &f' = \lambda, \theta = \varphi = 0 \ \ as\ \eta \to \infty \end{aligned} \qquad (10)$$

Where f', θ and φ are the dimensionless velocity, temperature and concentration respectively, η is the similarity variable, the prime denotes differentiation with respect to η. Also

$$M = \frac{\sigma B_0^2(1-\gamma t)}{\rho a}, N = \frac{v(1-\gamma t)}{k^* a}, A = \frac{\gamma}{a}, \lambda = \frac{b\sqrt{(1-\gamma t)}}{a},$$

$$Gr = \frac{g\beta(T_w - T_\infty)(1-\gamma t)^2}{a^2 x}, Gm = \frac{g\beta^*(C_w - C_\infty)(1-\gamma t)^2}{a^2 x},$$

$$\Pr = \frac{\mu c_p}{k}, and\ \ Sc = \frac{v}{D_m}$$

are the Magnetic parameter, porosity parameter, unsteadiness parameter, stretching ratio, Grashof number, modified Grashof number, Prandtl number, and Schmidt number, respectively. The important physical quantities of this problem are skin friction coefficient C_f and the local Nusselt number Nu which are proportional to rate of velocity and rate of temperature respectively.

3. Methodology

The governing thermal boundary layer Eq. (3), concentration boundary layer Eq. (4) and momentum boundary layer Eq. (5), with the boundary conditions (6) are transformed into a system of first order ordinary differential equations which are then solved numerically by using Runge-Kutta fourth-fifth order method along with shooting iteration technique. From Eq. (7) – Eq.(9) it is observed that *f* is in third order and θ and φ are in second order. In order to solve this system of equations using Runge-Kutta method, the solution needs seven initial conditions but we have two initial conditions in f and one initial condition in each of θ and φ. The most important step of this scheme is to choose the appropriate finite value of η_∞. Therefore, to determine the value of η_∞, we have to start with some initial guess value and solve the boundary value problem consisting of Eq. (7)– Eq.(9). The solution process is repeated with another larger value of η_∞ until two successive values of $f''(0), \theta'(0)$ and $\varphi'(0)$ differ only after desired significant digit. The last value of η_∞ is taken as the finite value for determining the velocity, temperature and concentration, respectively. After getting all the initial conditions we solve this system of simultaneous equations using fourth order Runge-Kutta integration scheme. The effects of the flow parameters on the velocity, temperature and species concentration, are computed, discussed and have been graphically represented in figures and also the shearing stress and rate of heat transfer are shown in table1 for various value of different parameters. Now defining new variables by the equations

$$y_1 = f, y_2 = f', y_3 = f'', y_4 = \theta, y_5 = \theta', y_6 = \varphi, y_7 = \varphi'$$

The higher order differential Eq. (7), Eq. (8), Eq.(9) and boundary conditions (10) may be transformed to seven equivalent first order differential equations and boundary conditions are as follows:

$$dy_1 = y_2, dy_2 = y_3, dy_3 = -y_1 y_3 + y_1^2 + (M+N)y_2 + A\left(y_2 + \frac{1}{2}y_3\right) - \frac{A\lambda}{2} - \lambda^2 - Gr\cos\alpha\, y_4 - Gm\cos\alpha\, y_6,$$

$$dy_4 = y_5, dy_5 = -\Pr y_1 y_5 + \frac{1}{2}\Pr A\eta\, y_5, dy_6 = y_7,$$

$$dy_7 = -Sc\, y_1 y_7 + \frac{1}{2}ScA\eta\, y_7$$

And the boundary conditions are

$$\begin{aligned} &y_1 = -f_w, y_2 = 1, y_4 = 1, y_6 = 1 \ \ at\ \eta = 0 \\ &y_2 = \lambda, y_4 = 0, y_6 = 0 \ \ as \ \ \eta \to \infty \end{aligned}$$

4. Results and discussion

Numerical calculation for distribution of the velocity, temperature and concentration profiles across the boundary layer for different values of the parameters are carried out. For the purpose of our simulation we have chosen f_w = 1.0, λ= 2.0, M = 0.2, N = 0.2, A = 1.0, Gr = 0.5, Gm=0.5, Sc= 0.22, Pr = 1.0 and α = 35^o while the parameters are varied over range as shown in the figures. Fig.1 clearly demonstrates that the primary velocity starts from maximum value at the surface and then decreasing until it reaches to the minimum value at the end of the boundary layer for all the values M. It is interesting to note that the effect of magnetic field is more prominent at the point of peak value, because the presence of *M* in an electrically conducting fluid introduce a force like Lorentz force which acts against the flow if the magnetic field is applied in the normal direction as in the present problem. As a result velocity profile is decreased. Similar effect is also observed in Fig.5 and Fig.8 with increasing values of α and f_w. Fig.3, Fig.4, Fig.6 and Fig.7 show the velocity profile for various values of *λ, A, Gr* and *Gm*, it is observed that an increasing in *λ, A, Gr* and *Gm* lead to an increasing effect on velocity profile. From Fig. 2 it is observed that the velocity is decreased up to a certain interval of η and

then increased for increasing values of N. Fig.9 – Fig.16 show the temperature profile obtained by the numerical simulations for various values of entering parameters. Fig.13 clearly demonstrates that the thermal boundary layer thickness decreases as the Pr increases implying higher heat transfer. It is due to fact that smaller values Pr means increasing thermal conductivity and therefore it is able to diffuse away from the plate more quickly than higher values of *Pr*, hence the rate of heat transfer is reduced as a result the heat of the fluid in the boundary layer increases. Similar result has been found for the effect of *M*, *N* and f_w which are shown in Fig.9, Fig.10 and Fig.16 respectively and reverse trend arises for the increasing values of *λ*, *A*, *Gr* and Gm which are depicted in Fig.11, Fig.12, Fig.14 and Fig.15. From Fig. 9 it is observed that the temperature profile is decreased for increasing values of M which implies that the applied magnetic field normal to the flow of the fluid tends to reduce heat from the fluid and thus increases the rate of heat transfer as a result temperature is decreased. The effect of Gr on temperature profile is shown in Fig. 14. From this figure it is observed that, the temperature profile increases for increasing values of Gr; because the increase of Grashof number results in the increase of temperature gradients, which leads to the enhancement of the velocity due to the enhanced convection and thus temperature profiles are increased. Fig.17- Fig.24 shows the concentration profiles obtained by the numerical simulation for various values of entering non-dimensional parameters. From Fig.17, Fig.18, Fig.23 and Fig.24 it is observed that the concentration profile decreases for the effect of *M*, *N*, *Sc*, and f_w but reverse effect arises for the increasing values of *λ, A, Gr* and *Gm* which are shown in Fig.19, Fig.20, Fig.21 and Fig.22 respectively. Further the numerical solutions for the skin friction [$f''(0)$] and local Nusselt number [$-\theta'(0)$] have been compared with those of Pop et al. [12], Mahapatra and Gupta [13] and Sharma and Singh [14] when *M = 0, Gr = 0, Gm =0, N = 0, A = 0, α = 0* and f_w =1.0 and consider the Prandtl number *Pr*= 0.01. These results are given in Table.1 and it is observed that the agreement between the present results and those of Pop et al. [12], Mahapatra and Gupta [13] and Sharma and Singh [14] are familiar.

4. Conclusions

Following are the conclusions made from above analysis:

- The magnitude of velocity decreases with increasing magnetic parameter causing of Lorentz force reverse trend arise for stretching parameter and unsteadiness parameter.
- Increase in stretching parameter and unsteadiness parameter, the temperature is increased but reverse effect for Prandtl number.
- The noticeable increasing effects of stretching parameter, unsteadiness parameter, Grashof number and modified Grashof number but reverse trend arises for the increasing values of Schmidt number, magnetic parameter, porosity parameter and suction parameter on concentration profile.
- To compare the skin friction and rate of heat transfer with previous results and get almost similar results.

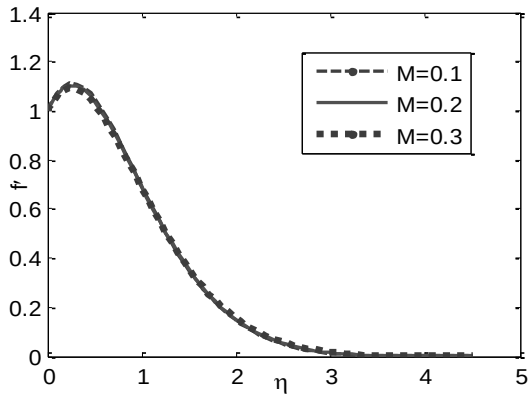

Fig.1 Velocity profile for various values of M

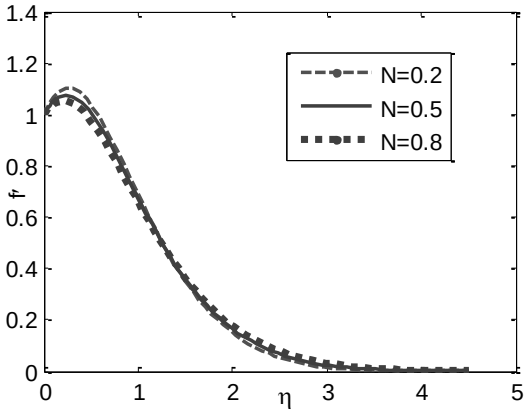

Fig.2 Velocity profile for various values of N

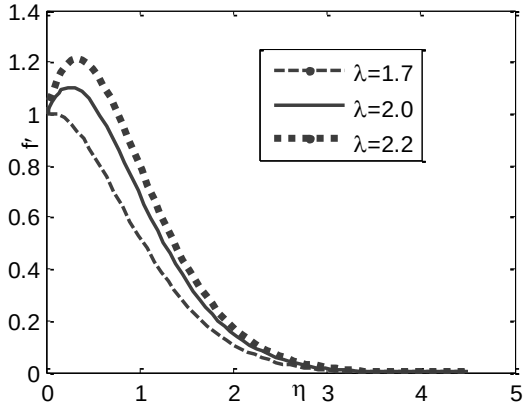

Fig.3 Velocity profile for various values of λ

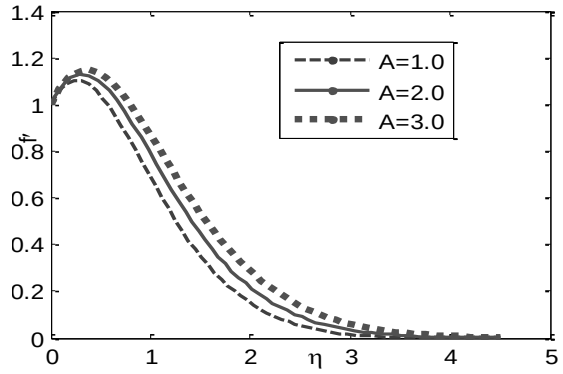

Fig.4 Velocity profile for various values of A

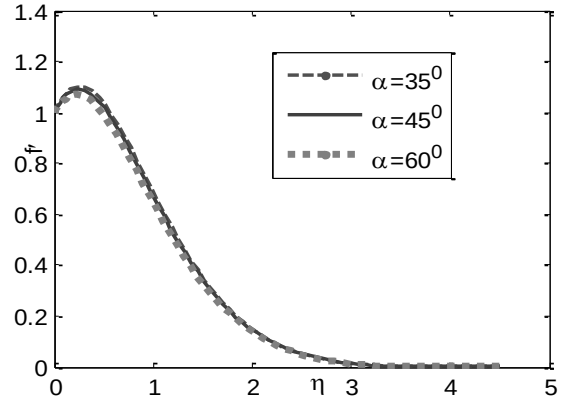

Fig.5 Velocity profile for various values of α

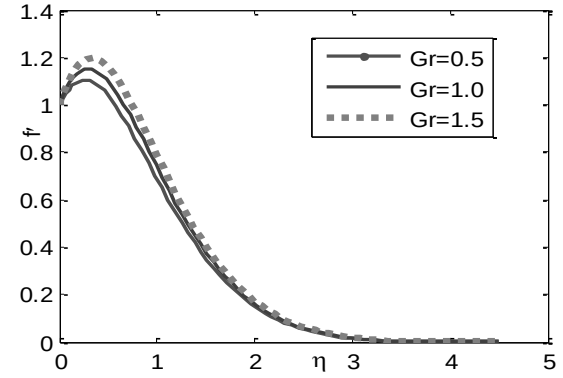

Fig.6 Velocity profile for various values of Gr

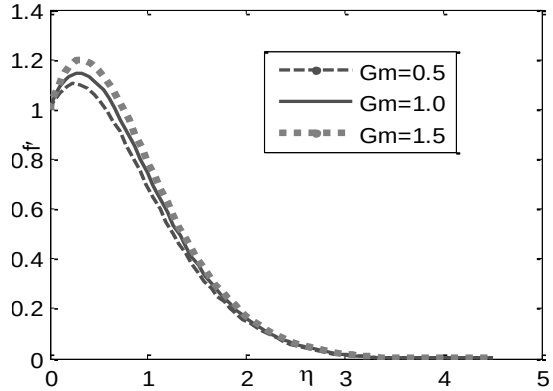

Fig.7 Velocity profile for various values of Gm

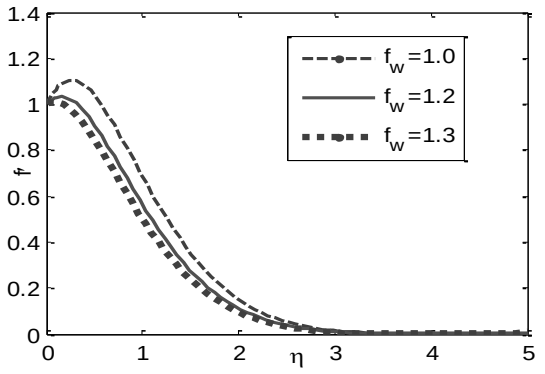

Fig.8 Velocity profile for various values of f_w

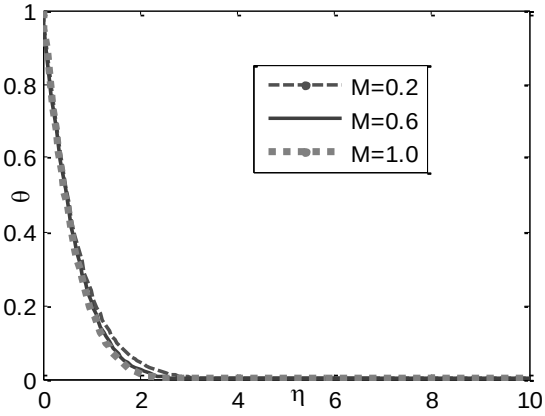

Fig.9 Temperature profile for various values of M

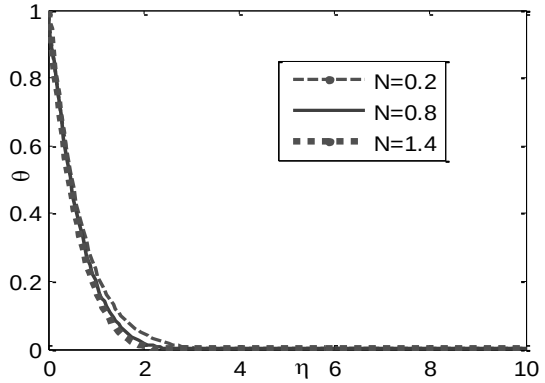

Fig.10 Temperature profile for various values of N

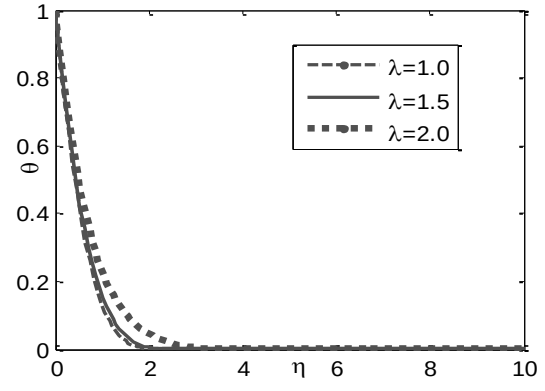

Fig.11 Temperature profile for various values of λ

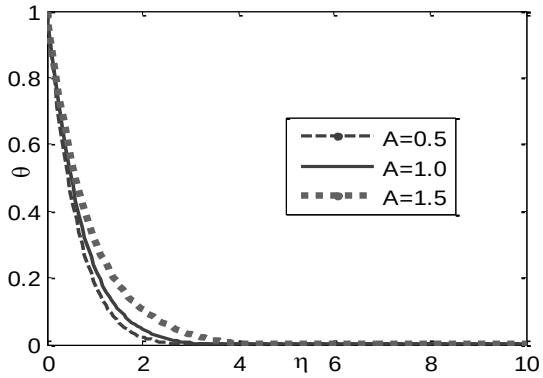

Fig.12 Temperature profile for various values of A

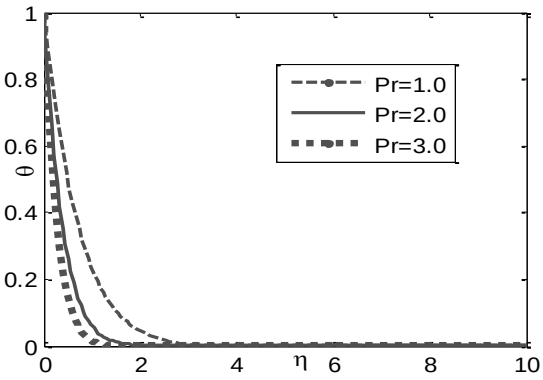

Fig.13 Temperature profile for various values of Pr

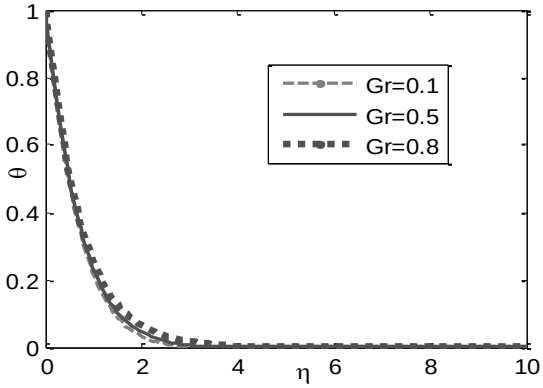

Fig.14 Temperature profile for various values of Gr

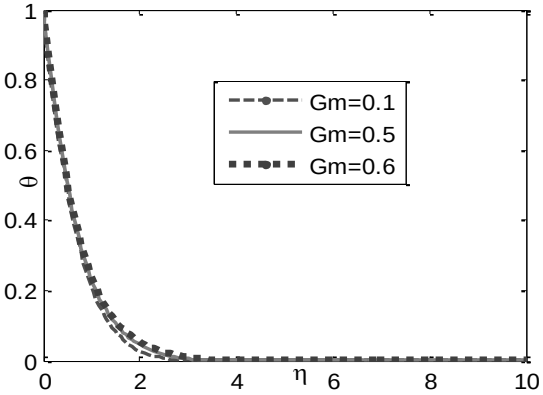

Fig.15 Temperature profile for various values of Gm

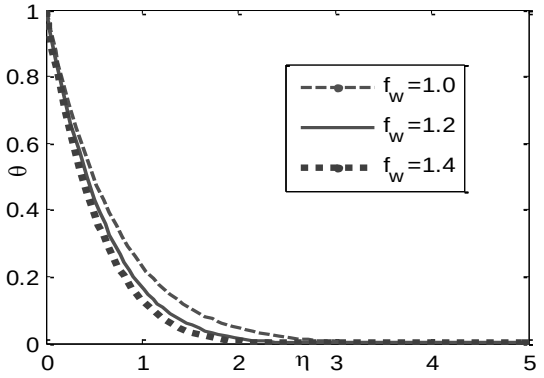

Fig.16 Temperature profile for various values of f_w

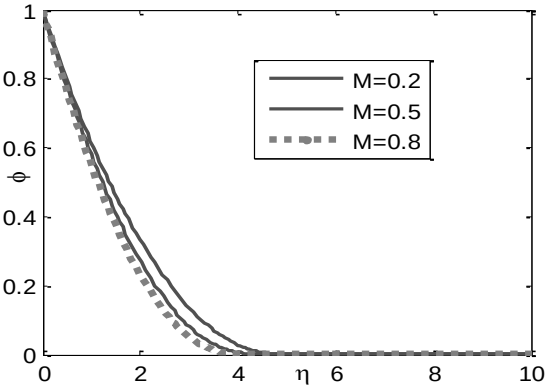

Fig.17 Concentration profile for various values of M

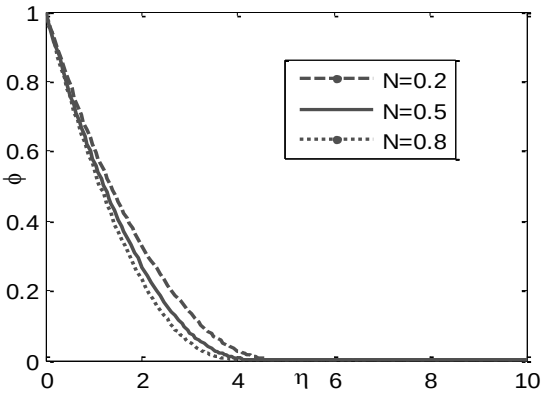

Fig.18 Concentration profile for various values of N

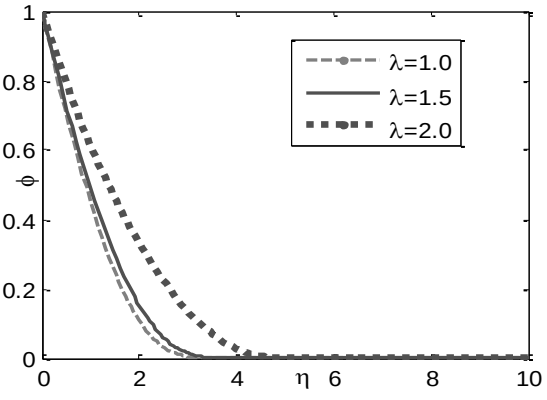

Fig.19 Concentration profile for various values of λ

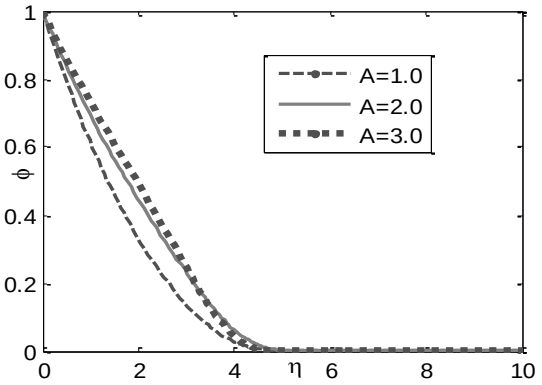

Fig.20 Concentration profile for various values of A

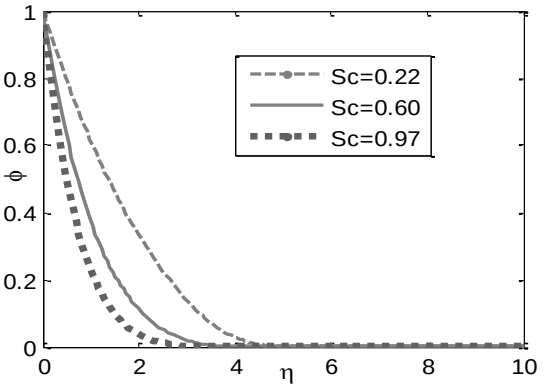

Fig.23 Concentration profile for various values of Sc

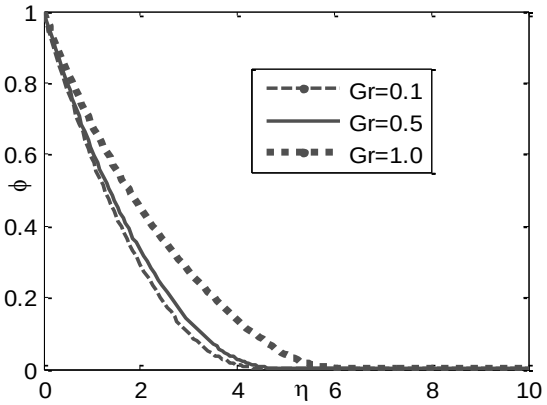

Fig.21 Concentration profile for various values of Gr

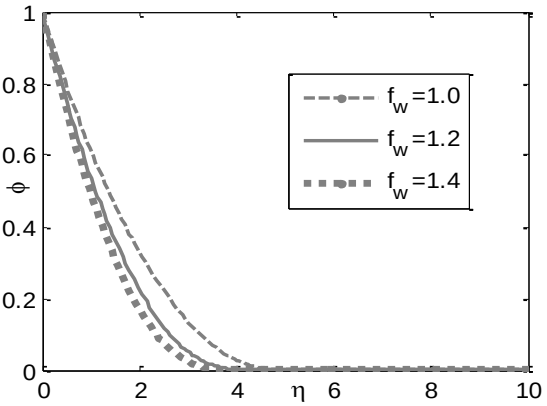

Fig.24 Concentration profile for various values of f_w

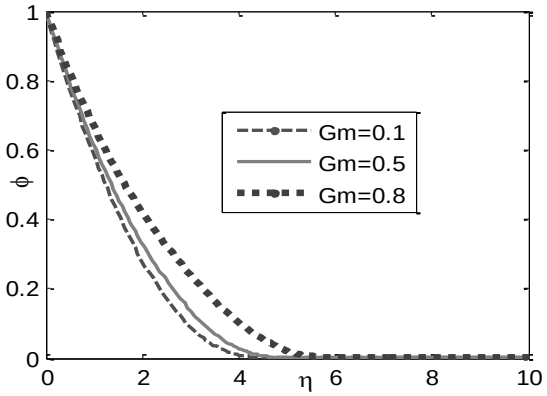

Fig.22 Concentration profile for various values of Gm

Table 1 Comparison of the skin friction [$f''(0)$] and local Nusselt number [$-\theta'(0)$]

λ	Pop et al.[12]		Mahapatra and Gupta[13]		Sharma and Singh [14]		Present results	
	$f''(0)$	$-\theta(0)$	$f''(0)$	$-\theta(0)$	$f''(0)$	$-\theta(0)$	$f''(0)$	$-\theta'(0)$
0.1	-0.9694	0.081	-0.9694	0.081	-0.969386	0.081245	-0.96782	0.099205
0.2	-0.9181	0.135	-0.9181	0.136	-0.9181069	0.135571	-0.911135	0.13539
0.5	-0.5573	0.241	-0.6673	0.241	-0.667263	0.241025	-0.7195	0.23926
2.0	2.0174	-	2.0175	-	2.01749079	-	1.9881	
3.0	4.7290	-	4.7293	-	4.72922695	-	4.72259	

NOMENCLATURE

c_p : specific heat at constant pressure, $Jkg^{-1}K^{-1}$
κ : thermal conductivity, $w\ m^{-1}K^{-1}$
α : angle of inclination, degree
g : acceleration due to gravity, ms^{-2}
γ : constant
σ : electrical conductivity, sm^{-1}
D_m : coefficient of mass duffisivity, m^2s^{-1}
μ : coefficient of viscosity, $kg\ m^{-1}s^{-1}$
ν :kinematics viscosity, m^2s^{-1}
ρ :fluid density, $kg\ m^{-3}$
B_0 :magnetic field intensity, Am^{-1}
β :thermal expansion coefficient, k^{-1}
β^* :concentration expansion coefficient, $\mu\ mm^{-1}k^{-1}$
u :velocity component along X axis, ms^{-1}
v :velocity component along Y axis, ms^{-1}
U :free stream velocity, constant
C :concentration, $kg\ m^{-3}$
C_w :stretching sheet concentration, $kg\ m^{-3}$
C_∞ :free stream concentration
T :fluid temperature, k^{-1}
T_w :stretching sheet temperature, k^{-1}
T_∞ :free stream temperature

REFERENCES

[1] E.M.A. Elbashbeshy and M.A.A. Bazid, Heat transfer over an unsteady stretching surface, *Heat Mass Transfer,* Vol.41, pp 1-4 (2004).

[2] Saleh M. Alharbi1, M. A. A. Bazid and Mahmoud S. El Gendy, Heat and mass transfer in MHD visco-elastic fluid flow through a porous medium over a stretching sheet with chemical reaction, *Applied Mathematics*,Vol.1, pp 446-455(2010).

[3] M. A. Seddeek and M. S. Abdel Meguid, Effects of Radiation and Thermal Diffusivity on Heat Transfer over a Stretching Surface with Variable Heat Flux, *Physics Letters A*, Vol. 348, pp 172-179 (2006)

[4] M. Ali, M. S. Alam, M. M. Alam and M. A. Alim, Radiation and thermal diffusion effects on a steady MHD free convection heat and mass transfer flow past an inclined stretching sheet with Hall current and heat generation, *IOSR Journal of Mathematics*, Vol. 9, pp 33-45 (2014).

[5] W. Ibrahim and B. Shanker, Unsteady MHD boundary layer flow and heat transfer due to stretching sheet in the presence of heat source or sink by Quasi-linearization technique, *International Journal of Applied Mathematics and Mechanics*, Vol. 8, pp 18-30(2012).

[6] Ishak A, Nazar R and Pop I, Boundary layer flow and heat transfer over an unsteady stretching vertical surface, *Mechanica*, Vol.44, pp 369-375 (2009).

[7] Ishak A, Unsteady MHD flow and heat transfer over a stretching plate, *Journal of Applied Science*, Vol.10, pp 2127-2131(2010).

[8] Ebashbeshy and Aldawody , Heat transfer over an unsteady stretching surface with variable heat flux in presence of heat source or sink, *Computers and Mathematics with Applications,* Vol. 60, pp 2806-2811 (2010).

[9] Fadzilah M, Nazar R, Norihan M and Pop I, MHD boundary layer flow and heat transfer of a viscous and electrically conducting fluid over a stretching sheet with an induced magnetic field, *Journal of Heat Mass Transfer*, Vol.47, pp 155-162 (2011).

[10] Bachok N, Ishak A and Nazar R., Flow and heat transfer over an unsteady stretching sheet in a micro polar fluid, *International Journal of Applied Mathematics and Mechanics*, Vol.8, pp 18-30(2011).

[11] Mohebujjaman M, Khalequ S and Samad M, MHD heat transfer mixed convection flow along a vertical stretching sheet in presence of magnetic field with heat generation , *International Journal of Basic and Applied Science*, Vol.10,(2010).

[12] S.R. Pop, T. Grosan and I. Pop, Radiation effect on the flow near the stagnation point of a stretching sheet, *Technische Mechani*k, Vol.25, pp 100-106 (2004).

[13] T.R. Mahapatra, and A.S. Gupta, Heat transfer in stagnation-point flow towards a stretching sheet, *Heat and Mass Transfer*, Vol.38, pp 517-521(2002).

[14] P.R. Sharma and G. Singh, Effects of Variable Thermal Conductivity and Heat Source / Sink on MHD Flow Near a Stagnation Point on a Linearly Stretching Sheet, *Journal of Applied Fluid Mechanics,* Vol.2, pp 13-21(2009).

ICMIEE-PI-140153

Electro-Mechanical Modeling of Separately Excited DC Motor & Performance Improvement using Different Industrial Controllers with Active Circuit Realization

A.F.M. Sajidul Qadir [1*]
[1] Department of Electrical, Electronic & Communication Engineering, Military Institute of Science & Technology, Mirpur Cantonment, Dhaka-1216, BANGLADESH

ABSTRACT
In this paper, Mathematical Modelling of a reference Separately excited DC motor has been done & Transfer Function has been derived with simulated result. Later Parameter Identification has been carried out to find the suitable design criteria for testing different controllers (P, PI, PD, PID controllers) with the machine. As it turned out to be a stable system (as per Routh–Hurwitz Stability Criterion), different controllers has been used to evaluate the Step response of Open loop & Closed loop system with simulated result. Controller tuning has been done to find the best result for controlling speed of the machine. Settling time, % Overshoot, Steady-State error & Rise time has been calculated for all the controllers. Later active RC realization of the best fitted controller has been done using Ideal PID Control Algorithm.

Keywords: Mathematical Modeling; DC Machine; Industrial Controller; Parameter Estimation; Transfer Function; Active Circuit Realization

1. Introduction

Separately excited DC motors have been widely used prime movers in many industrial applications such as electric vehicles, steel rolling mills, electric cranes, and robotic manipulators due to precise, wide, simple, and continuous control characteristics. The widely used traditional way of controlling low power DC motor is rheostatic armature control. Due to non-linearity properties, implementation of traditional control system is tedious and inefficient. The controllability, cheapness, higher efficiency and higher current carrying capabilities of static power converters brought a major change in the performance of electrical drives. The desired torque-speed characteristics can be achieved by the use of conventional proportional-integral-derivative (PID) controllers. The purpose behind this work is to deeply investigate the performance of DC machine and hence tuning the speed using the suitable controller & deriving physical realization of the system.

2. Modeling Approach of SEDM

The DC motor is basically a torque transducer. The torque developed in the motor shaft is directly proportional to the field flux & armature current. For modeling any physical active element, Transfer function of it needed to be derived which represents the mathematical form of the physical element. When an idealized physical system's Mathematical model is tested for various input conditions and tuned accordingly with controllers, the result represents the dynamic behaviour of the system. Since SEDM is extensively used in control system, for analytical purpose, it is necessary to establish mathematical models for control application of it. After that suitable design criteria will be established in consistent with the particular machine parameter. Assuming magnetic linearity, [1] the basic motor equations are:

$$T = K_f i_f i_a = K_m i_a \quad (1)$$

$$e_a = K_f i_f \omega_m = K_m \omega_m \quad (2)$$

Where $K_m = K_f i_f$ is a constant, which is also ratio $\frac{e_a}{e_m}$. The Laplace transform of equation Eq.(1) and Eq.(2) are:

$$T(s) = K_m i_a(s) \quad (3)$$

$$E_a = K_m \omega_m(s) \quad (4)$$

In the physical system, a switch is positioned after $\mathbf{R_a}$ and the switch be closed at **t=0** as because for Transfer Function, all initial conditions must be zero. After the switch is closed:

$$VV = e_a + R_a i_a R_a i_a + L_{aq} \frac{di_a}{dt} \quad (5)$$

From Eq.(2) and Eq.(5):

$$V = K_m \omega_m K_m + R_a i_a R_a i_a + L_{aq} \frac{di_a}{dt} \quad (6)$$

As the necessary differential equation is obtained which is required to derive Transfer Function of the reference system, Laplace transform of the equations can now be obtained. It is independent of input excitation and shows the relationship between input and output of the system. Laplace transform of Eq.(6) for initial zero condition is:

$$V(s) = K_m \omega_m(s) + R_a I_a(s) + L_{aq}(s) I_a(s) \quad (8)$$

$$V(s) = K_m \omega_m(s) + I_a(s)\, R_a\, (1 + s\tau_a) \quad (9)$$

* Corresponding Author. Tel.: +88-01922268656
E-mail Address: sajid.kaist@gmail.com

Where $\tau_a = \frac{L_{aq}}{R_a}$ is the electrical time constant of the armature. The dynamic equation for the mechanical system is:

$$T = i_a K_m = J\frac{d\omega_m}{dt} + B\omega_m + T_L \quad (10)$$

The term $\mathbf{B\omega_m}$ represents the rotational loss torque of the system. The Laplace transform of Equation of Voltage is:

$$T(s)=K_m i_a(s)=J(s)\omega_m(s)+B\omega_m(s)+T_L(s) \quad (11)$$

From Eq.(3) and Eq.(11) :

$$\omega_m(s) = T(s)-\frac{T_L(S)}{B\{1+S(\frac{J}{B})\}} = \frac{K_m I_a(S) T_L(S)}{B\{1+S(\frac{J}{B})\}} \quad (12)$$

Where $\tau_m = \frac{J}{B}$ is the mechanical time constant of the system. From Eq.(4) and Eq. (9):

$$I_a(s) = V - \frac{E_a(S)}{R_a(1+S\tau_a)} = V(s) - \frac{K_m\omega_m(S)}{R_a(1+S\tau_a)} \quad (13)$$

Taking Laplace transform, the transfer function from the input voltage **V(s)** to the angular velocity **ω(s)** directly follows:

$$\frac{\omega(S)}{V(S)} = \frac{K}{(R+LS)(Js+B)+K^2}$$

This is the desired transfer function of the SEDM which represents the ratio of system's input condition to the output. A block diagram representation of the Equation is as follows:

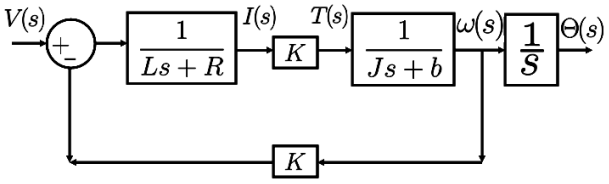

Fig.1 Block diagram representation of Transfer Function

2.1 Parameter Identification

Before any consideration of the above transfer function, the value of the parameters (**J, B, K, R, L**) must be known which is very important for the proper application of the DC Motor. [2] There are many methods of parameter identification. Some widely practiced methods are:

1. Gradient Algorithm
2. Stochastic State Estimation (Using Kalman Filter)
3. Least Square Algorithm

In these methods, Kalman filter can be used as an observer which helps to reduce the % of error. Using the 3rd method, parameters can be estimated even from open loop transfer function. Considering the table of specification of the reference Separately Excited DC motor provided by the manufacturer, the following values have been taken for the design purpose using the method described above. These values will be used in designing the desired system with recommended speed control. [3]

Table 1 Physical Parameters of SEDM

Moment of inertia of the rotor (J_m)	0.007 kg.m^2
Damping ratio of the mechanical system (b_m)	0.02 Nms
Electromotive force constant ($K=K_e=K_t$)	0. 1 Nm/Amp
Electric resistance (R)	1 Ω
Electric inductance (L)	0.1 H

Since the most basic requirement of a motor is that it should rotate at the desired speed, the steady-state error of the motor speed better be less than 1%. The other performance requirement is that the motor must accelerate to its steady-state speed as soon as it turns on. In this case, considering the full load speed 1500r/min, desired settling time is of 1 second. Since a speed faster than the reference may damage the equipment, an overshoot of less than 2% is desired. If the reference input (**r)** is simulate by a unit step input, then with a **1 rad/sec** step input the motor speed output should have:

- Settling time less than 0.2 seconds
- Overshoot less than 2%
- Steady-state error less than 1%
- Rise Time less than 0.2 second

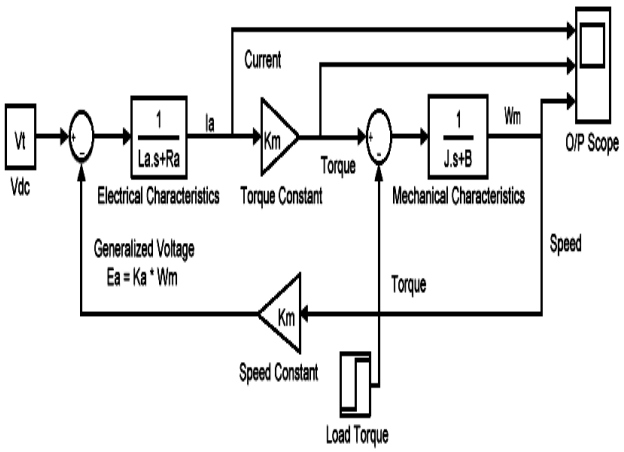

Fig.2 Simulink representation of the SEDM TF

With all the required specifications of the DC motor, a model of the system has been developed using SIMULINK. The system has been modeled using the characteristics transfer function of the electrical and mechanical parameters of the motor. The Electro-Mechanical model is obtained only after deriving the differential equations and Transfer function of all the

components of the system. Figure 2 shows the DC motor input armature voltage ($\mathbf{V_t}$) summed with the internal EMF. The result is then fed into the electrical characteristics transfer function block to produce the armature current ($\mathbf{I_a}$). It is then pass through a torque constant to produce torque. This is then summed with a torque load, giving an output torque which is then fed into the mechanical characteristics transfer function block. The output is the rotor speed ($\mathbf{W_m}$), which is fed back into the speed constant providing the constant EMF.

3. Controller Selection & Performance Improvement

To test the reference model, two performance measures have been chosen to use. These measures are widely used in analyzing the performance of the controller and also next generation Fuzzy-PID. They are:

1. *Transient Response:* One of the most important characteristics of control system is their transient response. The transient response is the response of a system as a function of time. It can be described in terms of two factors:

A. The swiftness of response, as represented by the rise-time (T_r).

B. The closeness of response to the desired response, as represented by the overshoot (O_s) and settling-time (T_s).

2. *Robustness:* A robust controller is capable of dealing with significant parameter variation provided that it's steady state error [$e(\infty)$] will be negligible. Examining the machines performance with different parameter values showing negligible steady state error usually assesses controller robustness.

Before testing any controller for the reference system, open-loop and close-loop response of the transfer function has to be measured for finding out the level of the parameters which has to be improved. So open-loop and close-loop response of the reference system has been measured followed simulation of by Proportional (P), Proportional Integral (PI) and Proportional Integral derivative (PID) controllers.

3.1 Step Response for Open Loop Control

As derived earlier, the transfer function of the SEDM for open loop control system is:

$$\frac{\omega}{V} = \frac{K}{(Js+b)(Ls+R)+K^2}$$

Using the electrical & mechanical parameters that have been defined in Table 1, the modified transfer function is:

$$\frac{\omega}{V} = \frac{0.1}{(0.007s+0.02)(0.1s+1)+0.01}$$

$$\text{Or } \frac{\omega}{V} = \frac{0.1}{0.0007S^2+0.009S+0.03}$$

$$\text{Or } \frac{\omega}{V} = \frac{1}{0.007S^2+0.09S+0.3} \qquad (14)$$

After running the necessary code (M-file) in Matlab, the step response has been generated as Fig.(3). The DC gain of the plant transfer function is 1/0.3, so 3.333 is the final value of the output to a unit step input. This corresponds to the steady-state error 0.2308, quite a high value. Furthermore, the rise time is about 0.513 second, and the settling time is 0.866 seconds. So, a controller has to be selected & tuned properly that will reduce the rise time, reduce the settling time, and eliminates the steady-state error.

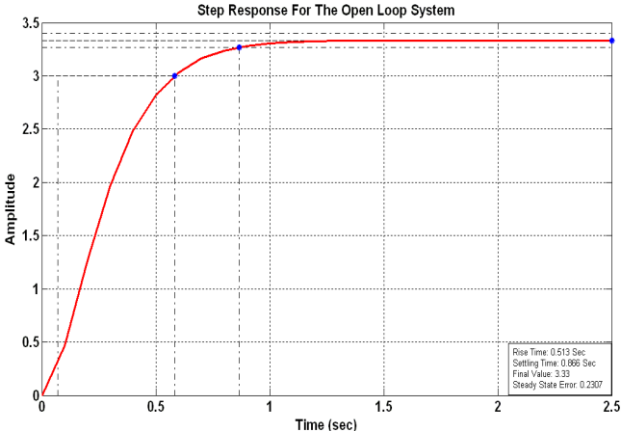

Fig.3 Open-loop step response of the transfer function

3.1.1 Checking System Stability

Stability of a system indicates it's usability. As the characteristic equation of open loop TF of the SEDM is algebraic in nature, Routh-Hurwitz stability criteria can be used to measure system's stability. The open loop TF is as derived earlier in Eq.(14):

$$\frac{\omega}{V} = \frac{1}{0.007S^2+0.09S+0.3}$$

Using Routh-Hurwitz theory, if the system prevails to be stable, than different controllers can be used to modify the transfer function to satisfy the design criteria.

Table 2 Routh-Hurwitz Table

S^2	0.007	0.03	0
S^1	0.09	0	0
S^0	0.0027	0	0

Here it can be seen that the system is stable, because there is no sign change in first column of the Routh table and all terms are positive. As the system turns out stable, different types of controller can be used with the machine to check performance.

3.2 Close-Loop Response

Close loop control improves machine performance by increasing the speed of response and improving on speed regulation. The step response plotted in Figure 1 shows a sluggish response of speed and current with time. The Closed Loop Speed Control presents an

enhanced control method. To validate it, different controllers will be tested in close loop control system to improve the overall speed regulation by decreasing the rise time, settling time and overshot. Based on the DC motor speed response measurement under a constant voltage input, important motor parameters such as the electrical time constant, the mechanical time constant, and the friction can be estimated.

3.3 Effects of Different Control Gain

There are 3 different conventional control gain namely K_p, K_i, K_d. They have varied effect on the system. They can be used alone or together. Using together is advisable because demerits of one type will be compensated by other one. So to eliminate huge oscillation, sluggish rise time and much delayed steady state final value, the combination of these controllers can be used. The feedback device that has been used is a Tachometer. Tachometer is a kind of sensor which is electromechanical devices that converts mechanical energy into electrical energy. [4]

3.3.1 Proportional Controller

K_p is termed as the proportional gain. After many trial & error, a suitable value has been taken for proportional gain. It is known that proportional controller decreases Rise Time, increases overshoot and decreases Steady-State error. It also has small effect on Settling Time. Considering all these effect, value of K_p has been taken.

$$K_p = 1$$

The close loop transfer function of the above system with a proportional controller is:

$$\frac{\omega}{V} = \frac{1 \times K_p}{0.007S^2 + 0.09S + (0.3 + K_p)}$$

$$\text{Or } \frac{\omega}{V} = \frac{1}{0.007S^2 + 0.09S + 1.3} \qquad (15)$$

After running the necessary code in Matlab (M-file), the response has been generated as follows:

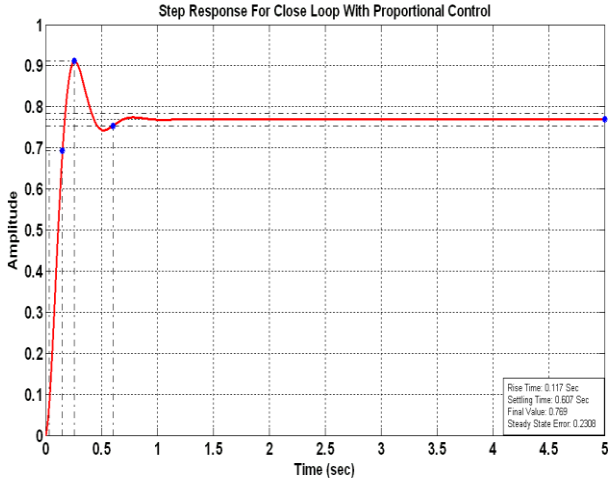

Fig.4 Close loop step response with Proportional Controller

So using Proportional controller, rise time is 0.117 seconds, settling time 0.607 seconds, Steady state error 0.2308 with a minor overshoot. The above plot shows that the proportional controller reduced rise time, increased the overshoot, and decreased the settling time by small amount. But the steady state error remained unchanged. Derivative controller decreases overshoot and settling time. So a combination of Proportional & Derivative controller has been used together to offset the effects.

3.3.2 Proportional Derivative (PD) Controller

K_d is termed as the derivative gain. The gain of proportional controller will remain same. The new derivative gain K_d has been taken as 5 after trial and error. All the values have been taken on expert guess.

$$K_p = 1, \qquad K_d = 5$$

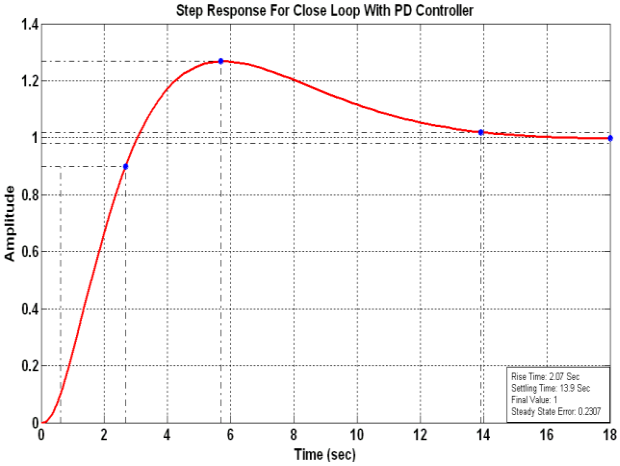

Fig.5 Close loop step response with PD Controller

The close loop transfer function of the above system with a PD controller is:

$$\frac{\omega}{V} = \frac{K_d S + K_p}{0.007S^2 + (0.09 + K_d)S + (0.3 + K_p)}$$

$$\text{Or } \frac{\omega}{V} = \frac{5S + 1}{0.007S^2 + 5.09S + 1.3} \qquad (16)$$

The derivative term reduces overshoot and settling time and has little effect on rise time and steady state error. After running the necessary code in Matlab (M-file), the response has been generated as above. So using PD controller, rise time is 2.07 seconds, settling time 13.9 seconds, Steady state error 0.2307 with a minor overshoot. The above plot shows that the PD controller increased rise time, increased the overshoot, and increased the settling time by huge amount. But the steady state error remained unchanged. So it is observed that PD controller has worst effect on the system. Now PI controller will be examined because they both decreases the rise time and eliminate the steady state error.

3.3.3 Proportional Integral (PI) Controller

It introduces a pole and a zero to the overall system. It is better than the previous Controllers. The gain of proportional controller will remain same. The new integral gain K_i has been taken as 8 after trial and error. All the values have been taken on expert guess.

$$K_p = 1, \qquad K_i = 8$$

The close loop transfer function of the above system with a PD controller is:

$$\frac{\omega}{V} = \frac{K_p S + K_i}{0.007S^3 + 0.09S^2 + (0.3 + K_p)S + K_i}$$

$$\text{Or } \frac{\omega}{V} = \frac{S+8}{0.007S^3 + 0.09S^2 + 1.3S + 8} \qquad (17)$$

The proportional and integral both term reduces the rise time and eliminates the steady state error, but it increases overshoot. After running the necessary code in Matlab, the response has been generated.

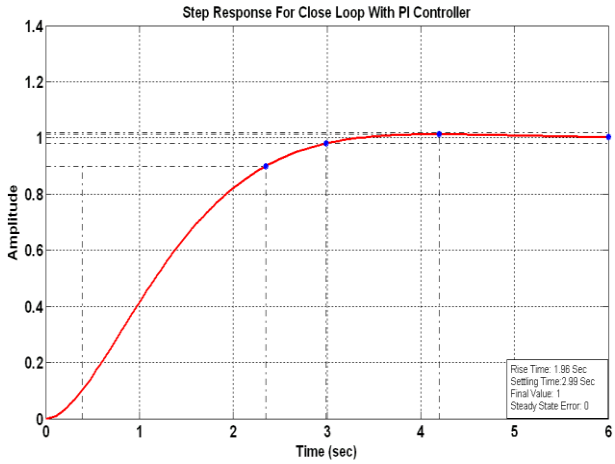

Fig.6 Close loop step response with PI Controller

It is observed from the graph that rise time is 1.96 seconds, settling time is 2.99 seconds. Steady state error is 0(zero). PI controller has much better effect on the system as it has decreased the settling time & rise time. More importantly, it eliminates the steady state error to zero. Also the system has negligible overshoot. Yet the system with PI is still far off from the design requirement.

3.3.4 Proportional Integral Derivative (PID) Controller

Two zeroes and a pole at origin is introduced by this controller. Proper selection of controller gains (K_p, K_i & K_d) improves stability and response of the overall system. The gain of proportional & integral controller will remain same. The new derivative gain K_d has been taken the same as that of PD control mechanism. All the values have been taken on expert guess.

$$K_p = 1, \qquad K_d = 5, \qquad K_i = 8$$

The close loop transfer function of the above system with a PD controller is:

$$\frac{\omega}{V} = \frac{K_d S^2 + K_p S + K_i}{0.007S^3 + (0.09 + K_d)S^2 + (0.3 + K_p)S + K_i}$$

$$\text{Or } \frac{\omega}{V} = \frac{5S^2 + S + 8}{0.007S^3 + 5.09S^2 + 1.3S + 8} \qquad (18)$$

PID controller brings the best of the entire available controller. The proportional and integral controller decreases the rise time & eliminate the steady state error while the derivative controller decreases the overshoot and settling time which is increased by P & I gain. After running the necessary code in Matlab, the response has been generated as follows:

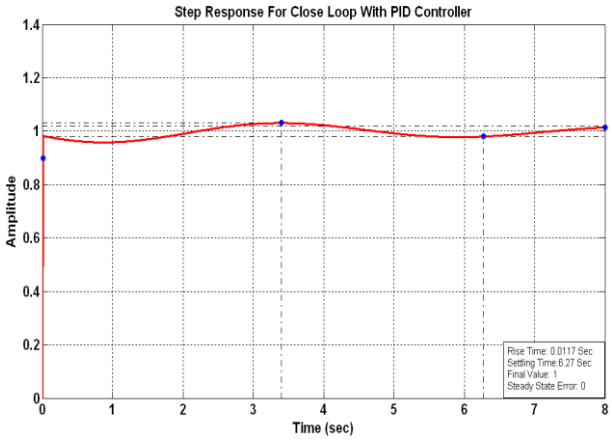

Fig.7 Close loop step response with PID Controller

From the graph, it is observed that rise time is 0.0117 seconds, settling time is 6.27 seconds, steady state error is 0 (zero). There are some very small scale oscillation or ripple in the system which increased the settling time of the system. So proper tuning of the gain is necessary.

3.4 Tuning the PID Controller

There exist many methods to tune PID controllers. Some common methods are listed used in the industry are: [5]

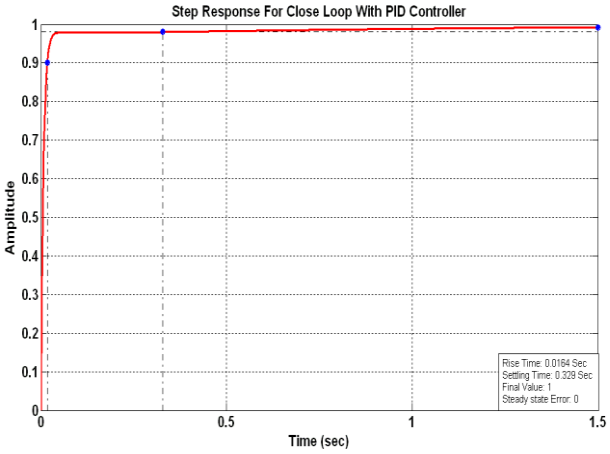

Fig.8 Close loop step response with Tuned PID

1. Ziegler–Nichols method
2. Skogestad's method
3. Good Gain method
4. Cohen-Coon method

As it is possible to take the proposed system of the paper offline, that's why 3rd method has been followed. Among these methods, 3rd method need no prior knowledge of the system & is easier of the methods mentioned.

As seen from the Fig.8, settling time decreased a lot if the gain values are taken as below:

$$K_p = 10, \qquad K_d = 1, \qquad K_i = 8$$

K_p & K_d is increased to decrease the rise time and overshoot. The Matlab code shows the graph as Figure 6. From the figure it is observed that rise time is 0.0164 seconds, settling time is 0.329 seconds, steady state error is 0(zero). Furthermore there is no overshoot. So these gain combination can meet the design requirement almost satisfactorily. The figure gives almost perfect system condition with very fast rise time, very fast settling time, zero steady state error with zero overshoot. So this particular combination of gain values gives near perfect system response with all the responses very fast and no overshoot, no steady state error. From above experimental data & figures, it can be concluded that perfectly tuned PID controller best suites the proposed design criteria to control the speed of SEDM (Separately excited DC Motor) & hence improve the performance of the machine.

3.5 Calculation of Steady State Error, Rise Time & Settling Time

For a unity feedback system without any controller attached to it, the steady state error response is:

$$e_{step}(\infty) = \frac{1}{1+lim_{s\to 0}\, G(s)} \qquad (19)$$

From Fig.3, T_r =0.513 sec, T_s = 0.866 sec. So for the reference SEDM, the steady state error is:

$$e_{step}(\infty) = \frac{1}{1+3.333} = 0.2308$$

For a unity feedback system with different controllers attached to it as of the figure below, the steady state error response is:

$$e(\infty) = lim_{s\to 0}\{1 - T(s)\} \qquad (20)$$

For Proportional Controller from Eq.(15):

$$T(s) = \frac{1}{0.007S^2+0.09S+1.3}$$

$$e(\infty) = lim_{s\to 0}\{1 - T(s)\} = 1 - 0.76923 = 0.2308$$

From Fig.4 of Step response of Proportional controller, T_r = 0.117 sec, T_s = 0.607 sec.

For PD Controller from Eq.(16):

$$T(s) = \frac{5S+1}{0.007S^2+5.09S+1.3}$$

$$e(\infty) = lim_{s\to 0}\{1 - T(s)\} = 1 - 0.76923 = 0.2308$$

From Fig.5 of Step response of PD controller, T_r = 2.07 sec, T_s = 13.9 sec.

For PI Controller from Eq.(16):

$$T(s) = \frac{S+8}{0.007S^3+0.09S^2+1.3S+8}$$

$$e(\infty) = lim_{s\to 0}\{1 - T(s)\} = 1 - 1 = 0$$

From Fig.6 of Step response of PI controller, T_r = 2.07 sec, T_s = 13.9 sec.

For PID Controller from Eq.(17):

$$T(s) = \frac{5S^2+S+8}{0.007S^3+5.09S^2+1.3S+8}$$

$$e(\infty) = lim_{s\to 0}\{1 - T(s)\} = 1 - 1 = 0$$

From Fig.7 of Step response of PID controller, T_r = 0.0117 sec, T_s = 6.27 sec.

4. Active Circuit Realization

PID (proportional Integral Derivative) control is one of the earlier control strategies. Its early implementation was in pneumatic devices, followed by vacuum and solid state analog electronics, before arriving at today's digital implementation of microprocessors. Since many process plants controlled by PID controllers have similar dynamics it has been found possible to set satisfactory controller parameters from less plant information than a complete mathematical model. These techniques came about because of the desire to adjust controller parameters in situ with a minimum of effort, and also because of the possible difficulty and poor cost benefit of obtaining mathematical models. The goal is to design a PID controller with the tuned gains found earlier with active circuits. This can also be termed as 'Physical Realization' of the controller.

4.1 Different Methods of Physical Realization

There are many methods of physically realizing a controller or compensator. Two general way of implementing controllers are:

1. Analog Implementation
2. Digital Implementation

Analog implementation is preferred over digital implementation when the system considered is not necessarily to be very fast in response such as responsive of μsec limit. Also digital implementation needs complex circuitry which is costly. That's why analog implementation has been preferred in this work. Analog implementation can be done in 3 ways: [6]

1. Parallel PID Algorithm
2. Series PID Algorithm
3. Ideal PID Algorithm

In Ideal PID Algorithm, a simple inverting amplifier is used to implement PID controller. Its response and tenability is slower than the other two algorithms but because of cost effectiveness, 3rd method has been chosen for the work. The classical implementation of PID controller or the active circuit realization of the controllers contains several active elements to realize the transfer function. For instance, parallel structures using Operational Amplifiers (Op-Amp) requires 5 amplifiers: Differentiator, P, I, D Op-amp and adder. At least 3 operational amplifiers are needed to implement a PID controller:

1. Integral - Need one Op-amp to perform integration of input signal.
2. Derivative - Need one Op-amp to perform derivative of input signal.
3. Proportional - Need one Op-amp to provide proportional gain.

Utilizing Operational amplifier, all the conventional industrial controller as well as compensators can be realized.

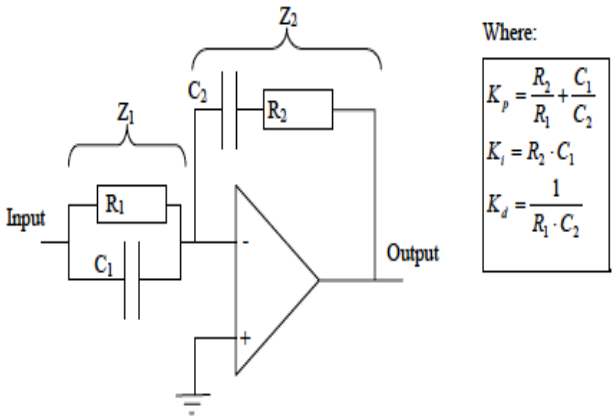

Fig.9 Ideal PID Implementation

The transfer function of the inverting amplifier is:

$$T = -\frac{Z_2}{Z_1} = \frac{V_0(s)}{V_i(s)} \qquad (21)$$

By judicious choice of $\mathbf{Z_1(s)}$ and $\mathbf{Z_2(s)}$, the circuit of Fig.9 can be used as a building block to implement PID controller. Using Eq.(21) and the Fig.9, it can be shown that:

$$\frac{V_{out}}{V_{in}} = -\left[\left(\frac{R_2}{R_1} + \frac{C_2}{C_1}\right) + S.C_1.R_2 + \frac{1}{R_1 C_2}.\frac{1}{S}\right] \qquad (22)$$

Above Eq.(22) corresponds to a PID controller. The transfer function of the PID controller is found as:

$$G(s) = K_p + K_d s = \frac{K_d S^2 + K_p s + K_i}{s} \qquad (23)$$

By putting the desired gains, a function of S will be formed. From Fig.8, if gain of PID controllers if taken as follows:

$$K_p = 10, \qquad K_d = 1, \qquad K_i = 8$$

Than the transfer function of the PID controllers will be as follows:

$$G(s) = \frac{K_d s^2 + K_p s + K_i}{s} = s + 10 + \frac{8}{s} \qquad (24)$$

Comparing the PID controller of Fig.9 with Eq.(24), the following three relationships were obtained:

Proportional Gain, $K_p = \frac{R_2}{R_1} + \frac{C_1}{C_2} = 10$

Derivative Gain, $K_d = R_2 C_1 = 1$

Integral Gain, $K_i = \frac{1}{R_1 C_2} = 8$

Since there are 4 unknowns (R_1, R_2, C_1, C_2) and 3 equations, practical value of any one parameter is chosen arbitrarily. If $C_2 = 0.3$ µF than remaining values are found as below:

$R_1 = 416.67\ K\Omega$

$R_2 = 3.34\ M\Omega$

$\frac{C_1}{C_2} = 10 - 7.999 \rightarrow C_1 = 0.6\ \mu F$

Using these values, the complete circuit is simulated in PSPICE. [7] Using PSPICE, PID implementation has been done by operational amplifier which is the basis of Ideal PID Algorithm. Fig. 10 is PSPICE schematics of active RC realization of PID controller of the reference system.

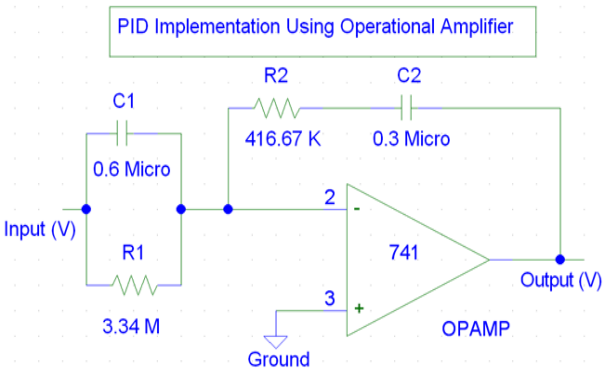

Fig.10 PSPICE Schematics of PID controller using Ideal PID Algorithm

5. Conclusion

In this paper, a novel approach has been adopted to model a Separately Excited DC Motor with mathematical differential equation to test it with different industrial controller and later to derive active RC realization. Transfer function has been derived from the basic machine equations. Suitable electrical and

mechanical parameters have been calculated to perfectly represent the DC Motor that has been used throughout the work. Finally specific design criteria have been set up to the best interest of the machine application. A Simulink representation has been done and added to check and validate the initial parameters which have been taken in modeling the machine's mathematical equivalence. Later, the open loop step response has been calculated to find the best suitable conventional controller for use with the machine and the system has been proved to be stable through Routh-Hurwitz method. After that, different controllers have been used with the system and it is observed that properly tuned PID controller is the best controller to get sharp and quick response from the system. $\mathbf{T_r}$, $\mathbf{T_s}$, Steady State Error and % overshoot for different configuration have been measured. Finally, the tuned PID controller has been designed using 'Ideal PID Algorithm' which uses operational amplifier as a building to physically realize the system. The Schematics have been drawn based on the values of the active circuits (Resistance, Capacitance) calculated by the Ideal PID Algorithm method. With the value of the feedback voltage known, a transient analysis can be done. This PID controller is fully compatible with the reference machine that has been used in the work.

REFERENCES

[1] Wei Wu, DC Motor Parameter Identification Using Speed Step Responses, *Modeling and Simulation in Engineering*, Vol. 2012, (2004).

[2] George Moleykutty, Speed control of separately excited DC motor, *American Journal of Applied Sciences*, Vol. 5, Issue 3, (2008).

[3] M. Salah, M. Abdelati, Parameters Identification of a Permanent Magnet DC Motor**,** *Modelling, Identification, and Control*, (2010).

[4] B.A.A. Omar, A.Y.M. Haikal, F.F.G. Areed, Design adaptive Neuro-fuzzy speed controller for an Electro-mechanical system, *Ain Shams Engineering Journal*, Vol.2, Issue 2, (2011)

[5] Dingyu Xue, Yangquan Chen, Derek P. Atherton, Linear Feedback Control, *Society for Industrial and Applied Mathematics*, Chapter 6, (2007).

[6] Norman S. Nise, Control Systems Engineering, *Wiley Publishers*, 4th Edition, Chapter 9, (2004).

[7] A.F.M. Sajidul Qadir, Electro-Mechanical Modeling of SEDM (Separately Excited DC Motor) & Performance Improvement Using Different Industrial Controllers, *Google Books*, 1st Edition, (2013).

ICMIEE-PI-140154

Design and Construction of a Model of a Magnetic Train

Md. Ariful Islam [1*], *Md. Shafiqur Rahman* [2], *Prof. Dr. Md. Syed Ali Molla* [3]

[1] Department of Mechanical Engineering, Khulna University of Engineering & Technology, Khulna-9203, BANGLADESH

[2] Department of Mechanical Engineering, Khulna University of Engineering & Technology, Khulna-9203, BANGLADESH

[3] Department of Mechanical Engineering, Khulna University of Engineering & Technology, Khulna-9203, BANGLADESH

ABSTRACT

The magical magnetic levitation has fascinated philosophers and scientists in the past. The recent advances, especially in magnetic materials and power electronics, have focused this attention on the application of electromagnetic suspension and levitation techniques to advanced ground transportation. There are different technology available for suspension and propulsion, but the entire field is given an encompassing title of 'maglev'. Only high speed ground vehicle has caught the imagination of the media. But there is also a wide range of industrial applications i.e. material handling, product transportation to which magnetic suspension techniques could be profitable. This project deals with the design and construction of a model of a simple maglev system with the existing technology available in this country. The suspension of the maglev system has been done by arrays of permanent magnets. The repulsive force between two permanent magnets has been used for floating the train body in the air. The propulsion has been done by Linear Induction Motor (LIM). The linear induction motor has been made by making electromagnet and placing them in a straight line and connecting them in a three phase sequence. The design of linear induction motor has been done considering the weight and velocity of the train and the design algorithm is completely user-interactive. During the design, end effects and edge effects are neglected. During the test, the train was run successfully with some vibration which can be reduced by using magnetic feedback control.

Keywords: Maglev, Suspension, Propulsion, LIM

1. Introduction

A magnetic train runs on the principle of Maglev. In Maglev system, a vehicle is suspended form guide ways and propelled through a definite course [1]. The mechanical methods commonly used in transportation like the use of wheels, bearings, axles etc. are obsolete in a Maglev system. In this project, the levitation has been achieved by permanent magnets and propulsion has been done by Linear Induction Motor (LIM).

2. Theory:

2.1 Permanent Magnet

When two similar poles of two permanent magnets are kept close to one another, a repulsive force is created which tends the magnets to swift away from one another. The hysteresis loop of the permanent magnetic materials describe their magnetic properties i.e. flux density B and field strength H [2].

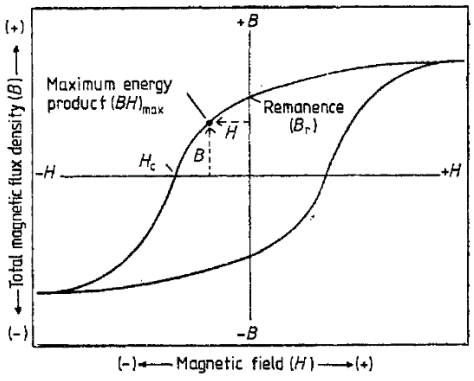

Figure 1: B-H loop of a permanent magnet illustrating the point where the product B-H is maximum.

The force of attraction or repulsion between two magnets is given by the expression $F= B^2/2\mu_0$ per unit area. When the permanent magnets repulse with one another the flux

* Corresponding author. Mob: +8801738294944

E-mail address: aiaariful@gmail.com

density (B) is no longer constant rather is varies at different sections. Due to this reason, according to Earnshaw's corollary, it is impossible for a body to be held in stable equilibrium against displacements in all directions if the system is constituted of permanent magnets only [3].

2.2 Linear Induction Motor:

A Linear Induction Motor (LIM) is an AC asynchronous motor that is designed to produce motion through a straight line. The basic principle of LIM operation is similar to that of a conventional rotating squirrel-cage induction motor.

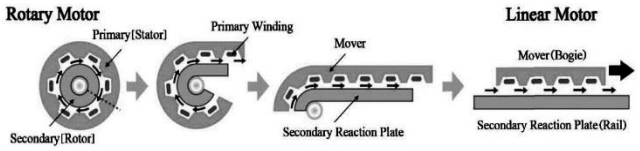

Fig 2: Concept of a linear induction motor from a rotary motor [4]

The Single sided LIM synchronous velocity Vs is the same as that of the rotary induction motor, given by

$$V = \frac{2\omega R}{p} = 2f\tau \qquad (1)$$

The Single sided LIM synchronous velocity Vs is the same as that of the rotary induction motor, given by

$$V = \frac{2\omega R}{p} = 2f\tau \qquad (2)$$

The parameter τ is the distance between two neighboring poles on the circumference of the stator, called pole pitch, defined as [5]

$$\tau = \frac{2\pi R}{p} \qquad (3)$$

The stator circumference of the rotary induction motor, 2πR, is equal to the length of the LIM stator core, L_s. Therefore, the pole pitch of a LIM is

$$\tau = \frac{2\pi R}{p} = \frac{Ls}{p} \qquad (4)$$

The current sheet strength, i.e., the amount of current per unit stator length (Ls) in a current sheet of a Single sided LIM can be calculated as in Nasar and Boldea [6] as follows:

$$J_m = \frac{2\sqrt{2}mk_w N_c I_1}{L_s} \qquad (5)$$

Winding factor,

$$k_w = k_p k_d \qquad (6)$$

k_p is the pitch factor which can be found by

$$k_p = \sin\left(\frac{\theta_p}{2}\right) \qquad (7)$$

K_d is the breadth or distribution factor given by

$$k_d = \frac{\sin\left(\frac{q_1\alpha}{2}\right)}{q_1 \sin\left(\frac{\alpha}{2}\right)} \qquad (8)$$

The power input to the stator windings is given by

$$P_i = mV_1 I_1 \cos\varphi \qquad (9)$$

Synchronous speed, V_s=2*pole pitch*frequency of current

For a slip of s, the speed of the secondary in a linear motor is given by

$$v_r = (1\text{-}s)v_s \qquad (10)$$

3. Design

3.1 Design Considerations

A low performance LIM was targeted as the cost was a major concern.

Size of each permanent magnet (24.4×19.25×20) mm.

Length of the train body = 16 cm.

Final width of the train 21.20 cm.

From experiment it has been seen that

Each permanent magnet can lift 112.5 gm.

Total weight of the train = Weight of the train body + Weight of the permanent magnets fitted with the body= 176+14*8 = 288 gm.

* Corresponding author. Mob: +8801738294944

E-mail address: aiaariful@gmail.com

3.2 Design of the Track

Length of the track is 100 cm.

Width of the track is 14.075 cm.

Height of the guide track is 7.2 cm from the base.

U shape guide ways was used.

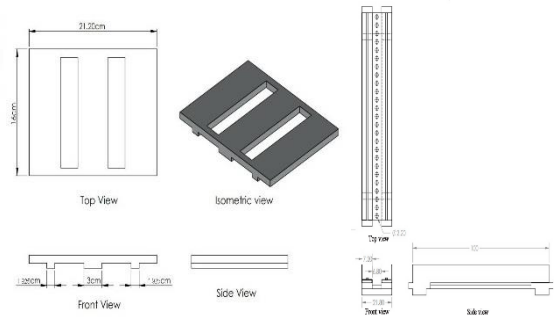

(a) (b)

Fig 3: Design of the (a) train body and (b) suspension track

3.3 Design of the Linear Induction Motor (LIM)

3.3.1 Targeted power for LIM

Synchronous speed of the linear induction motor

,v_s = 2*pole pitch*supply frequency in Hz.

So that the velocity of the primary designed linear induction motor was

$$v_s = 2*12*50 = 1200 \text{ cm/sec} = 12 \text{ m/sec}$$

Considering 15 % slip the velocity of the secondary in a linear induction motor

$$v_r = (1-.15)*12 \approx 10 \text{ m/sec}$$

Drag force acting on the train body

$$F_D = 0.5*1.204*10^2*1.8*21.20\times10^{-4} = 0.22 \text{ N}$$

Power required to overcome the aerodynamic drag is

$$P_d = 0.229*10 = 2.2 \text{ W}$$

Force required to accelerate the train in 10s from 0 m/s to 10 m/s is

$$F_a=0.288*1 = 0.288 \text{ N}$$

Power required to accelerate the train from 0 m/s to 10 m/s is

$$P_a = 0.288*10 = 2.88 \text{ W}$$

Frictional force in the guide plate

$$F_f = \mu_k N = 1.4*2.83 = 3.962 \text{ N}$$

Frictional power

$$P_f = 3.962*10 = 39.62 \text{ W}$$

So total power required to run the train = (2.2+2.88+39.62) = 44.7 W

3.3.2 General Specifications

Number of phases, m = 3

Line to line voltage,V_{line} = 220 V

Electrical frequency, f = 50 Hz

Number of poles, p = 8

Number of slot per pole per phase, q_1 = 1

Target electromagnetic thrust, F_s = 10 N

3.3.3 Determination of Pole Pitch and Slot Pitch

Optimum space required for each pole is 4 cm (Considering optimum bolt size with washer and winding space).

So, pole pitch, τ = 12 cm = 0.12 m

Slot pitch,

$$\lambda = (\tau/mq_1) = \frac{0.12}{3*1} = 0.04 \text{ m} = 4 \text{ cm}$$

3.3.4 Determination of Current

$$V_1 = V_{line}/\sqrt{3} = 220/\sqrt{3} = 127 \text{ V}$$

$$I_1 = \frac{Fs\ Vr}{mV1\ \eta\cos\varphi} = \frac{10*10}{3*127*.5} = 0.5 \text{ A}$$

3.3.5 Determination of Optimum Wire Size and Optimum no. of Turns

Total area of copper wire,

$$A_{wt} = 2\pi r_w L + 2\pi r_w^2$$

As r<<< l, so $2\pi r^2$ is negligible. So,

$$A_{wt} = 2\pi r_w L = \pi D_w L = \pi D_w * \pi D_c N_c = \pi^2 D_w D_c N_c.$$

Bolt size 1.2 cm

* Corresponding author. Mob: +8801738294944

E-mail address: aiaariful@gmail.com

Assume after winding, each pole size will be 2.2 cm

So,

$$D_c = \frac{1.2+2.2}{2} = 1.7 \text{ cm} = 0.017 \text{ m}$$

Again,

$$A_{wt} = (I_1/J_1) = \pi^2 D_c D_w N_c = 0.1 D_w N_c.$$

Again

$$J = \frac{2\sqrt{2}mKwNcI1}{Ls}$$

$$k_w = k_p k_d = 1*1 = 1 \text{ where}$$

$$k_p = \sin(\theta_p/2) = \sin 90^o = 1$$

$$k_d = \sin(q_1\alpha/2) / (q_1 \sin(\alpha/2) = \sin(1*\alpha/2) / 1*\sin(\alpha/2) = 1$$

$$J_1 = \frac{2\sqrt{2}*1*3*.5*Nc}{100} = 0.043N_c$$

So

$$D_w N_c = I_1 /(0.1*J_1) = 0.5/ (0.0043N_c)$$

$$\text{Or, } D_w N_c^2 = 116.2$$

For wire no. #25 D_w = 0.45mm = 0.00045m

So,

$$N_c = \sqrt{(116.2/.00045)} = 508.2 \approx 510.$$

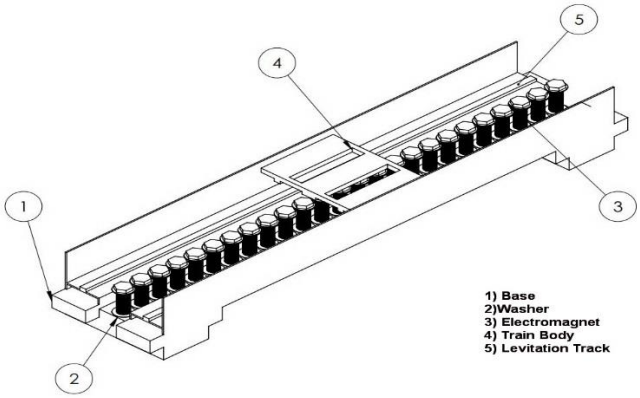

Fig 4: Design of the maglev system

4. Construction

Thai aluminum bar (21.2×1.5) cm was used for the structure as it has low weight and rigid enough comparing to the other available material. Permanent magnets were attached to the track in a single array using super glue. Sequence was maintained for winding i.e. 1-4-7-10 no. 2-5-8-11 no. bolt for making three phase winding. Copper wire was winded tightly so that the wire didn't lose and make good magnetic flux.

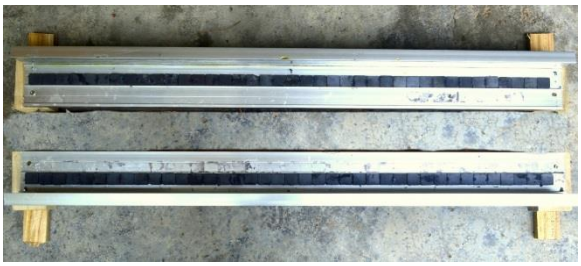

(a)

(b)

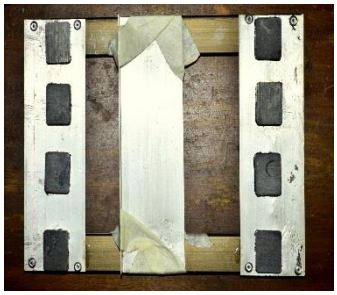

(c)

(d)

Fig 5: Constructed view of (a) Maglev track, (b) LIM (c) Train body (d) Final assembly

* Corresponding author. Mob: +8801738294944

E-mail address: aiaariful@gmail.com

5. Experiments and Performance Test

Maximum weight that can be carried by the train was 513 gm.

Maximum velocity achieved: 0.75m/s

Levitation achieved 1 cm

So physical air gap, g_m = 1 cm

Magnetic air gap, g_o = 1+.1 = 1.1 cm

Carter's coefficient, $k_c = \frac{\lambda}{\lambda - \gamma go} = \frac{4}{4 - 1.97 * 1.1} = 2.18$

Here,

$$\gamma = \frac{4}{\pi}\left[\frac{1.2}{2*1.1} arctan\left(\frac{1.2}{2*1.1}\right) - ln\sqrt{(1 + \left(\frac{1.2}{2*1.1}\right)\left(\frac{1.2}{2*1.1}\right)}\right]$$

= 1.97

So effective air gap g_e = 1.97*1.1 = 2.16 cm

6. Discussion and Conclusion

The maglev train ran successfully although having some difficulties. As the train body touched the guide plate, a frictional resistance force was produced. It created obstacle and lowered the speed of the train. Also sometimes the train body just vibrated instead of going forward. The main reason was that the force and velocity produced by the LIM could not match with the high frequency of the current.

NOMENCLATURE

A_s: Area of slot, m^2
A_w: Area of copper wire for one turn per slot, m

A_{wt}: Total area of copper wire, m^2

D_w: Diameter of copper wire, m

f: Electrical frequency, Hz

F_s: Electromagnetic thrust generated by rotor, N

g_e: Equivalent air gap, m

g_{ei}: Equivalent air gap considering edge effects , m

g_m: Mechanical air gap, m

g_0: Magnetic air gap, m
G: Goodness factor
I_1: RMS input phase current, A

V_1: RMS Input Phase, V

V_r: Rotor Velocity, m/s

V_s: Synchronous Velocity , m/s

φ : Angle between voltage and current ,

η: Efficiency
λ: Slot Pitch, m
μ_0: Permeability of free space, H/m

ρ_w: Volume resistivity of Copper, Ω-m

τ: Pole pitch, m

* Corresponding author. Mob: +8801738294944

E-mail address: aiaariful@gmail.com

REFFERENCES

[1] http://en.wikipedia.org/wiki/Maglev

[2]K.X. Quian, P. Zeng, W.M. Ru, H.Y. Yuan (2005) New Concepts and new design of permanent maglev rotary artificial heart blood pumps, Medical Engineering & Physics 28(2006) 383-388

[3] B V Jayawant. In Atsugi Unisia Corporation, Brighton BNl 9QT, UK. School of Engineering and Applied Sciences, University of Sussex. Electromagnetic Suspension and Levitation

[4] Poloujadoff, M., Linear induction machines, Part II – Applications, IEEE Spectrum, March 1971, pp. 77-86.

[5] http://cem.colorado.edu/archives/fl1997/thor.html

[6]S.A.Nasar and I.Boldea, Linear motion Electric Machines, John Wiley and Sons., New York 1976

ICMIEE-PI-140160

Analysis of Mechanical Properties of mild steel Applying Various Heat treatment

Mst.Nazma Sultana[1], Md.Ferdaus Hasan[2], Mehedi Islam[3]

[1, 2, 3] Department of Industrial Engineering and Management, Khulna University of Engineering & Technology, Khulna-9203,

BANGLADESH

ABSTRACT

In this study mild steel is selected as specimen for testing various mechanical properties. The effects of heat treatment (annealing, hardening, and tempering) on the mechanical properties of selected specimen are analyzed. Annealing, hardening and tempering are the most important heat treatment processes often used to change mechanical properties of engineering materials .The purpose of heat treating is to analyze the mechanical properties of iron, usually ductility, hardness, Yield strength, tensile strength and impact resistance. The heat treatment develops hardness, softness, and improves the mechanical properties such as tensile strength, yield strength, ductility, corrosion resistance and creep rupture. These processes also help to improve machining effect, and make them versatile. Samples of malleable iron are examined after heating at 900^0C and quenched in oil. The mechanical behavior of the samples is investigated using universal tensile testing machine for tensile test, compression test and Rockwell hardness tester for hardness testing. Samples revealed that with increasing temper temperatures: (a) hardness first increases to a maximum and then gradually decreases; (b) yield strength first decreases, then increases, and then increases again; (c) ultimate strength first increases to a maximum and then steadily decreases; and (d) ductility (% elongation) gradually decreases till 600ºC, and then increases rather sharply. The mechanical properties can easily be modified by heat treating to suit a particular design purpose. In the present study, selected samples are heat-treated at different temperature above the austenitic region and quenched followed by tempering in order to investigate the effect of different tempering temperature on the mechanical properties of iron. The changes in mechanical behavior as compared with unquenched samples are explained in terms of changes in tensile strength. Tensile test specimens are produced from malleable iron which is subjected to various forms of heat treatment processes like annealing, hardening and tempering. Results showed that the mechanical properties of malleable iron can be changed and improved by various heat treatments for a particular application. Results showed that the mechanical properties can be changed and improved by various heat treatments for a particular application. It was also found that the annealed samples with mainly ferrite structure gave the lowest tensile strength and hardness value and highest ductility value while hardened sample which comprise marten site gave the highest tensile strength and hardness value and lowest ductility value.

Keywords: Heat treatment process, mild steel, Mechanical properties, Universal Testing Machine, Rockwell hardness tester.

1. Introduction

The subject of mechanical testing of materials is an important aspect of engineering practice. Today, more concern is being given to the interpretation of test results in terms of service performance, as well as giving reliable indications of the ability of the material to perform certain types of duty. Mechanical tests are also employed in investigational work in order to obtain data for use in design to ascertain whether the material meets the specifications for its intended use.Heat treatment is defined as an operation or combination of operations involving heating and cooling of a metal or alloy for this case involving the mild steel in the solid state in such ways as to produce certain microstructure and desired mechanical properties (hardness, toughness, yield strength, ultimate tensile strength, Young's modulus, percentage elongation and percentage reduction). Annealing, normalizing, hardening and tempering are the most important heat treatments often used to modify the microstructure and mechanical properties of engineering materials particularly steels. Annealing is defined as a heat treatment that consists of heating to and holding at a suitable temperature followed by cooling at an appropriate rate, most frequently applied in order to soften iron or steel materials and refines its grains due to ferrite-pearlite microstructure; it is used where elongations and appreciable level of tensile strength are required in engineering materials In normalizing, the material is heated to the austenitic temperature range and this is followed by air cooling. This treatment is usually carried out to obtain a mainly pearlite matrix, which results into strength and hardness higher than in as received condition. It is also used to remove undesirable free carbide present in the as-received sample [1].

Steel is an alloy of iron with definite percentage of carbon ranges from 0.15-1.5% [2], plain carbon steels are those containing 0.1-0.25% [3]. Steel is mainly an alloy of iron and carbon, where other elements are present in quantities too small to affect the properties. The other alloying elements allowed in plain-carbon steel are manganese and silicon. Steel with low carbon content has the same properties as iron, soft but easily formed. As carbon content rises, the metal becomes harder and stronger but less ductile and more difficult to weld. There are two main reasons for the popular use of

* Corresponding author. Tel.: +88-01941055289
E-mail address: nazma.kuet@yahoo.com

steel: (1) It is abundant in the earth's crust in form of Fe_2O_3 and little energy is required to convert it to Fe. (2) It can be made to exhibit great variety of microstructures and thus a wide range of mechanical properties. Although the number of steel specifications runs into thousands, plain carbon steel accounts for more than 90% of the total steel output. The reason for its importance is that it is a tough, ductile and cheap material with reasonable casting, working and machining properties, which is also amenable to simple heat treatments to produce a wide range of properties [1].The purpose of heat treating carbon steel is to change the mechanical properties of steel, usually ductility, hardness, Yield strength, tensile strength and impact resistance. The standard strengths of steels used in the structural design are prescribed from their yield strength. Most engineering calculations for structure are based on yield strength. The heat treatment develops hardness, softness, and improves the mechanical properties (such as tensile strength, yield strength, ductility, corrosion resistance and creep rupture. These processes also help to improve machining effect, and make them versatile. They are found in applications such as train railroads, beams for building support structures, reinforcing rods in concrete, ship construction, tubes for boilers in power generating plants, oil and gas pipelines, car radiators, cutting tools etc [3].The mild steel or called low carbon steel as the main component to through the process of the heat treatment where it containing several characteristic. The general range of mild steel is 0.05% to 0.35%. Mild steel is a very versatile and useful material. It can be machined and worked into complex shapes has low cost and good mechanical properties. It is forms the vast bulk of the steels employed for general structural fabrication, sheet metal and so on. Bolts and studs are supposed to be made from mild steel (up to 0.25% carbon) with characteristic toughness and ductility.

2. Materials and Methods

Sample of ASTM A-36 mild steel was purchased from a local market located in Khulna, Bangladesh. All specimens of mild steel of dimensions 8×8×8 mm was cut using power hacksaw. The chemical composition of the mild steel sample was determined as given in Tables 1. Standard tensile and impact specimens were made from ASTM A-36 mild steel sample using lathe machine. Samples were subjected to different heat treatment: annealing, normalizing, hardening, and tempering in accordance to ASM International Standards [4].Heat treated specimens were tested for mechanical properties. The heat treatment conditions are listed in Table 2. Four specimens were prepared for each heat treatment type.

Table 1: Chemical composition of mild steel

Iron family	C%	Si %	Mn %	S %	P%	Fe %	Cu%
Mild steel	0.29	0.28	0.10	0.10	0.04	98.14	0.2

3. Results and Discussions

2.1 Determination of mechanical properties

Mechanical properties (hardness, tensile strength, toughness, yield strength, elongation and percentage of elongation) of the treated and untreated samples are determined using standard methods. For hardness testing, oxide layers formed during heat treatment were removed by stage-wise grinding and then polished. Average Rockwell Hardness Number (B) readings were determined by taking two hardness readings at different positions on the samples, using a Standard Rockwell hardness tester and tensile test using universal testing machine. Impact energy was recorded using the Izod impact tester. For tensile properties, tensile specimens were loaded into a 2000-kg Mosanto Tensiometer hooked up to a data logger. Load-elongation data were recorded and converted into stress-strain graphs. Yield strength, ultimate (tensile) strength, Young's modulus and ductility (% elongation and reduction) are determined based on these graphs, in accordance with ASTM standard test procedures (ASTM A-36) [5,6,7].

Condition	Annealed	Normalized	Hardened	Tempered
Temperature, ℃	910	910	910	450
Holding time, min	70	70	30	70
Cooling medium	Furnace	Air	Water	Air

2.2 Effect of Heat Treatment on Mechanical Properties

The effect of heat treatment (annealing, normalising, hardening, and tempering) on the mechanical properties (ultimate tensile strength, hardness, toughness, percentage elongation, and percentage reduction) of the treated and untreated samples is shown in Table 3. The untreated samples value of mechanical behavior was noted as follows: tensile strength 402.45 MPa, yield strength 220.03MPa, hardness 69.80 HRC, toughness J, percentage of elongation 23.16%, percentage of reduction 56.24% , young modulus 207.88Gpa, yield strength 217.31 N/mm^2 .

Table 3: Mechanical Properties of heat treated and untreated ASTM A -36 steel

Mechanical properties						
Heat Treatment	Tensile Strength (Mpa)	Hardness (HRC)	Percentage Elongation (%)	Percentage Reduction (%)	Yield Strength (MPa)	Young Modulus (GPa)
Untreated	402.45	69.80	23.16/15	56.24	220.03	207.88
Annealed	389.34	62.15	25.22	64.12	212.54	302.32
Normalised	452.13	120.36	22.70	63.23	242.26	288.12
Hardened	734.32	293.4	6.90	37.39	278.11	632.47
Tempered	421.76	100.01	23.20	69.01	232.78	293.63

Comparing the mechanical properties of annealed sample with the untreated sample, annealed sample showed that lower tensile strength (389.34MPa), yield strength 212.54 MPa and hardness (62.15HRC) and increase in reduction in area (25.22%), elongation (64.12%), modulus of elasticity (302.32GPa). The decrease in tensile strength and hardness can be associated with the formation of soft ferrite matrix in

the microstructure of the annealed sample by cooling. The mechanical properties of the normalized specimen are found to be 452.13 MPa, 242.26MPa, 120.36HRC, 63.23 % and 22.70 % for tensile strength, yield strength, hardness, percentage reduction and percentage elongation, respectively. The increase in tensile strength and hardness as compared to annealed and untreated sample was due to proper austenising temperature at 910^{o}C and higher cooling rate, which resulted in decrease in elongation, which was lower than those obtained for untreated and annealed samples due to pearlitic matrix structure obtained during normalization of ASTM A-36steel.

The mechanical properties of the hardened sample revealed that it had the highest value of tensile strength 734.32 MPa, yield strength 278.11 MPa and highest hardness (293.4 HRC) were obtained. The specimen was austenised at 910^{o}C for 30 minutes and then water quenched. This treatment increased the tensile strength and hardness but there was massive reduction in elongation and reduction in area 6.90%, and 37.39%, respectively.

The mechanical properties of tempered sample showed that the tensile strength, yield strength, hardness, percentage reduction and percentage elongation were 421.76 MPa, 232.78 MPa, 100.01 HRC, 69.01 % and 23.20%, respectively. Comparing the mechanical properties of tempered sample with hardened sample, it was found that there was decrease in tensile strength and hardness at tempering temperature 450^{0}C while the percentage elongation and percentage reduction increased which can be associated to the graphitization of the precipitated carbides that resulted in the formation of ferrite at tempering temperature of 450^{o}C. This showed that tempering temperature improved the degree of tempering of the martensite, softening the matrix and decreased its resistance of plastic deformation. However, the test results showed that annealing treatment gave an elongation superior to any other heat treatment studied. The variability in ultimate tensile strength, percentage elongation, percentage reduction hardness and toughness of treated and untreated ASTM A-36steel are shown in Figures 1 to 5, respectively.

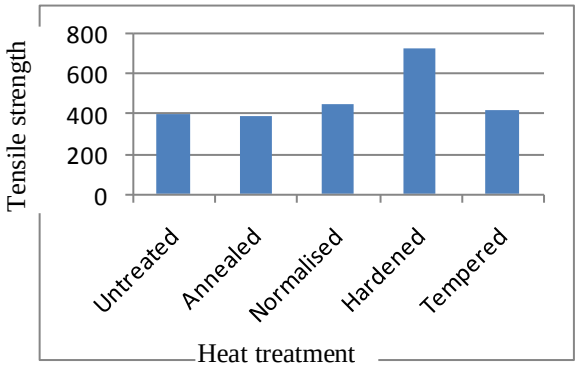

Fig. 1: Tensile Strength of treated and untreated samples of ASTM A-36steel

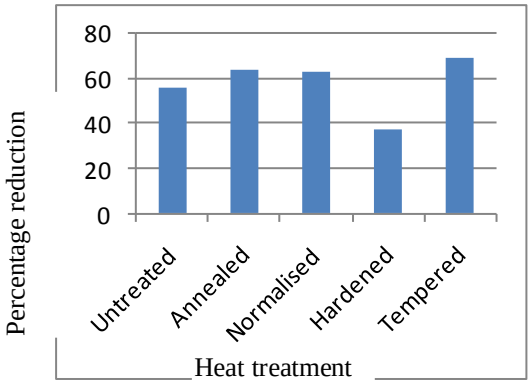

Fig. 2: Percentage reduction of treated and untreated samples of ASTM A-36steel

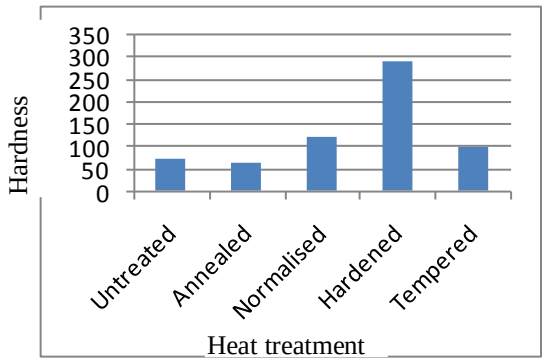

Fig. 3 Hardness of treated and untreated samples of ASTM A-36 steel

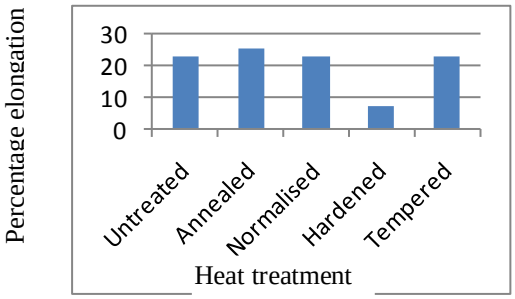

Fig. 4: Percentage elongation of treated and untreated samples of ASTM A-36steel

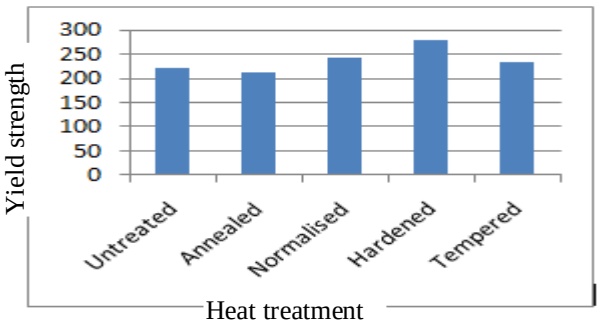

Fig. 5: Yield Strength of treated and untreated samples of ASTM A-36 steel

The value of tensile strength were observed to be in the order; hardened > normalized >tempered >untreated<annealed, possibly as a result of the

refinement of the primary phase after the subsequent cooling processes. The value of hardness was observed to be higher for the hardened steel specimen. The hardness of the steel increases with cooling rate and also with increasing pearlite percentage The reason being that martensite is one of the strengthening phases in steel. The increase in the hardness was due to the delay in the formation of peatrlite and martensite at a higher cooling rate. The yield strength value for the hardened specimen was also observed to be greater than that of normalized and annealed specimens, while the normalized specimen also has a greater value than that of tempered and annealed specimen. It was also observed from the graphs that for all the heat treated specimens, except for the hardened specimen, there were tremendous increase in the toughness of the material which indicates that hardened material, though have a very high tensile stress, but at the expense of its toughness, hence where toughness is a major concern. However if strength is also desired along with hardness, this should not be done. It is seen that annealing causes a tremendous increase in % elongation (ductility). It can be clearly seen comparing all the heat treatment processes, optimum Combination of Ultimate Tensile Strength, Yield Strength, % Elongation as well as hardness can be obtained through austempering only.

4. Conclusions

From the results obtained, it can be said that mechanical properties depends largely upon the various form of heat treatment operations and cooling rate. Hence depending upon the properties and the applications that may be required for any design purpose, a suitable form of heat treatment should be adopted. For high ductile and minimum toughness, annealed mild steel will give satisfactory results. According to the results of investigation on the effect of heat treatment on mechanical properties and microstructure of ASTM-A36 mild steel, the following conclusions were made: Tensile strength, yield strength and hardness of low carbon ASTM A-36 steel increased with plastic deformation while ductility and impact strength decreased due to strain hardening effect. Normalization treatment had also resulted in higher tensile strength and hardness than annealed samples. This treatment is recommended as final treatment after manufacturing. The tempered samples gave an increase in tensile strength and hardness than untreated sample as a result of formation of tempered martensite and resultant ferrite structure that were obtained. Hardened sample had the highest tensile strength and hardness with lowest ductility and impact strength when compared to other heat treated samples. Hardening is strongly recommended when the strength and hardness are the prime desired properties in design. The mechanical properties of ASTM A-36steel can be altered through various heat treatments. The results obtained confirmed that improvement in mechanical properties that can be obtained by subjecting ASTM A-36 steel to different heat treatments investigated in this study.

REFERENCES

[1] Dell, K.A., Metallurgy Theory and Practical Textbook. *American Technical Society*, Chicago, pp 351-353, (1989).

[2] John, V.B, Introduction to Engineering Materials, 2nd Edition, *Macmillan Publishing Company Ltd.*, pp 321-324, (1980).

[3] Alawode, A.J.,Effects of Cold Work and Stress Relief Annealing Cycle on the Mechanical Properties and Residual Stresses of Cold-Drawn Mild Steel Rod, M. Eng Thesis, *Mechanical Engineering Department*, University of Ilorin, Nigeria,(2002).

[4] ASTM E18. Standard Test Method for Rockwell Hardness of Metallic Materials, *American Society of Testing and Materials*, (2008).

[5] ASTM E23. Standard Test Method for Izod Bar Impact Testing of Metallic Materials, *American Society of Testing and Materials*, (2008).

[6] ASTM E8. Standard Test Method for Tension Testing of Metallic Materials, *American Society of Testing and Materials*, (2008).

[7] Jokhio, M.H.,Effect of Retained Austenite on Abrasive Wear Resistance of Carburised SAE 8822H Steel, Thesis in Manufacturing Engineering, Mehran *University of Engineering and Technology, Jamshoro*, (1991).

ICMIEE-PI-140163

Minimization of Makespan in Flow Shop Scheduling Using Heuristics

Md. Sanowar Hossain, Md. Asadujjaman, Md. Ashraful Alam Nayon, Priyanka Bhattacharya*

Department of Industrial & Production Engineering, Rajshahi University of Engineering & Technology, Rajshahi-6204, BANGLADESH

ABSTRACT

Production scheduling is one of the most significant issue in production and operations in any manufacturing system that has significant impact on cost reduction and increased productivity. Improper scheduling causes idle time for machines and hampers productivity that may cause an increased price of the product. So the main objective of this study is to minimize the makespan or total completion time. To do this study we have collected our data from Hatil complex limited, Mirpur, Dhaka, Bangladesh. This study presents Palmer's heuristic, CDS heuristic, NEH algorithm for solving the flow shop scheduling problem to minimize the makespan. NEH yields more elaborate results as compared to Palmer and CDS heuristic. Grant chart is used to verify the effectiveness of heuristics. By applying these three techniques we have gotten an optimal result for each case. The use of these techniques makes it possible to generate a schedule that minimizes the makespan.

Keywords: Flow Shop Scheduling, Makespan, CDS, NEH, Palmer's Heuristics.

1. Introduction

A wide range of knowledge of the general flow-shop scheduling problem is provided by the scheduling literature to get permutation schedules with minimization of make span. One of the earliest algorithm known as Johnson's algorithm [1] has been the basis of many flow shops scheduling heuristics. After that the researchers developed different heuristics for make span minimization in the flow shop scheduling for 'm' machine and 'n' job problems. Palmer [2] first proposed a heuristic for the flow shop scheduling problem with the objective of minimization of make span. Palmer's heuristic generates a slope index for jobs and sequences them in a descending order of the index. Campbell et al. [3] proposed Campbell, Dudek, and Smith (CDS) heuristic which is a generalization of Johnson's two machine algorithm and it generates a set of m-1 artificial two-machine problems from an original m-machine problem, then each of the generated problems are solved using Johnson's algorithm. Nawaz et al. [4] proposed Nawaz, Enscore, and Ham (NEH) heuristic algorithm which is probably the most well-known constructive heuristic used in the general flow-shop scheduling problem is based on the assumption that a job with high total processing time on all the machines should be given higher priority than job with low total processing time. Adding a new job at each step and finding the best partial solution it builds the final sequence in a constructive way. A review of flow shop scheduling with make span criterion had been given by Hijazi and Shaghafian [5]. Ibrahim [6] proposed a new heuristic to minimize the mean flow time for static permutation flow shop scheduling problem and showed that for the average flow time measure, the improved Chan and Bedworth's heuristic was the best among the four heuristics. Jin et al. [7] consider a hybrid flow shop with identical parallel machines. They proposed two approaches to generate the initial job sequence and used a simulated annealing algorithm to improve it. An improved heuristic for permutation flow shop scheduling was proposed by Chakraborty and Laha [8]. Ruiz and Stutzle [9] presented a new iterated greedy algorithm that had applied two phases iteratively, named destruction, where some jobs were eliminated from the incumbent solution, and construction, where the eliminated jobs are reinserted into the sequence using the well-known NEH construction heuristic. A model for scheduling a single semi continuous batching machine was developed by Tang and Zhao [10]. Their objectives were to schedule jobs on the machine so that the make span and the total completion time were minimized. Sahu [11] compared Gupta's, RA, CDS & Palmer's Heuristics in Flow Shop Scheduling on 8 jobs & 3 machines, 10 jobs & 8 machines and 10 jobs & 10 machines. He concluded that RA heuristic performs well for the problems considered when compared to other heuristics. Chia and Lee [12] developed the total completion time problem in a permutation flow shop with a learning effect. The concept of learning process played a key role in production environments. In addition, the performances of several well-known heuristics are evaluated when the learning effect is present. Vallada and Ruiz [13] worked on a cooperative meta-heuristic method for the permutation flow shop scheduling problem considering two objectives separately: total tardiness and make span. Damodaran and Velez Gallego [14] propose a constructive heuristic. Modrákand & Pandian [15] presented Flow Shop Scheduling Algorithm to Minimize Completion Time for n-jobs m-machines Problem. Chaudhry & Mahmood [16] considered minimization of makespan (total completion time) for *n* number of jobs to be processed on *m* machines using a general purpose spread sheet based genetic algorithm (GA). They showed that their proposed approach was able to find optimal solution for all the problems with different objective functions.

* Corresponding author. Tel.: +88-01913599639
E-mail address: jonikhan007@yahoo.com

Semančo and Modrák [17] showed a comparison of constructive heuristics with the objective of minimizing makespan in the Flow-Shop Scheduling Problem by using NEH; Palmer's Slope Index; CDS; Gupta's algorithm. Sagar et al. [18] presented an efficient heuristic method to minimize total flow time in no-wait flow shop scheduling. Malik &. Dhingra [19] presented comparative analysis of heuristics for make span minimizing in flow shop scheduling by using 5 heuristics for 10 jobs & 5 machines. Agarwa & Garg [20] worked with 5 heuristics named Gupta, RA, CDS, Palmer, NEH heuristic and applied these algorithm to solve 10machine, 10 job problem.

2. Methodology

With a view to minimize the make span the proposed heuristics/algorithm for 4-jobs and 10-machines problem from the real life has been used. Data is shown in table 8 that is collected from Hatil complex limited, Mirpur, Dhaka, Bangladesh which a leading furniture manufacturing company. Then, Palmer's heuristic, CDS heuristic and NEH algorithm are used and compared to get the optimal result.

3. Palmer's Heuristic

In flow shop scheduling, Palmer proposed a heuristic to minimize the make-span measure. He mainly proposed a slope index S_j, for each job. The formula for the slope index S_j is shown below.

$$S_j = (m-1)\,t_{j.m} + (m-3)\,t_{j.m-1} + (m-5)\,t_{j.m-2} + \ldots - (m-3)\,t_{j.2} - (m-1)\,t_{j.1}$$

Where j is the job and m is the total number of machines.

Procedure:

Step 1. Compute slope for each job.
Step 2. Arrange the jobs as per the decreasing order of slope.

Solution:

According to the procedure, firstly we have calculated the slope index for each job and have gotten $S_1 = 272$, $S_2 = -87$, $S_3 = 12$, $S_4 = 556$ arranging it as per decreasing order we have gotten $S_4 > S_1 > S_3 > S_2$. So the final sequence is J4-J1-J3-J2. For the original flow shop 4-jobs and 10-machines problem as given in Table 1, using this heuristic the J4-J1-J3-J2 sequence has been calculated and the make-span calculation is displayed in Table 2. Corresponding Gantt chart is shown in Fig.1.

Table 2 Solution of Palmer's heuristic with J4-J1-J3-J2

Job	M1	M2	M3	M4	M5	M6	M7	M8	M9	M10
J4	33	53	74	74	74	100	126	233	260	290
J1	66	103	128	128	151	193	231	343	343	373
J3	105	136	136	173	193	230	275	343	389	426
J2	145	176	212	238	268	300	335	343	433	470

Gantt Chart:

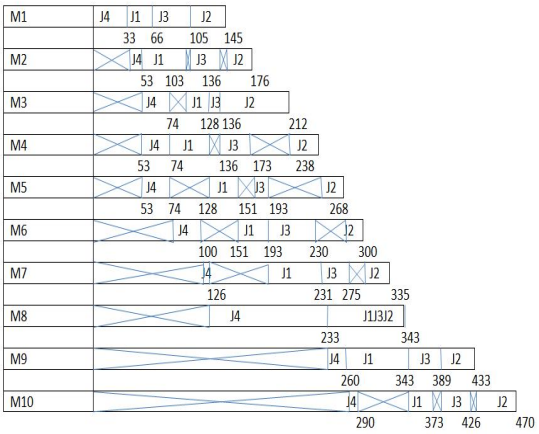

Fig.1 Gantt chart for the sequence J4-J1-J3-J2

In Fig.1 blank rectangle indicates that the machine is on working mode and the crossed rectangle indicates that the machine is on idle mode.

4. CDS Heuristic

CDS heuristics is basically an extension of the Johnson's algorithm. The main objectives of the heuristic are the minimization of make-span for n jobs and m machines in a deterministic flow shop scheduling problem. The CDS heuristic forms in a simple manner a set of an m-1 artificial 2-machine sub problem for the original m-machine problem by adding the processing times in such a manner that combines M1, M2,...,Mm-1 to pseudo machine 1 and M2, M3,... Mm to pseudo machine 2. Finally, by using the Johnson's 2-machines algorithm each of the 2-machine sub-problems is then solved. The best of the sequence is selected as the solution to the original m-machine problem. For the given flow shop problem as stated in table 1 of size10×4 using this heuristic the following sequences and make span has been established.

Procedure

Step 1:

Table 3 Taking M1 & M10

Job	M1	M10
J1	33	30
J2	40	37
J3	39	37
J4	33	30

Table 4 Optimal sequence when taking M1 & M10:

Sequence	Make span
J1-J3-J2-J4	492
J4-J3-J2-J1	487
J1-J2-J3-J4	499
J4-J2-J3-J1	485

Step 2:

Table 5 Taking M1+M2+M3+M4+M5 & M6+M7+M8+M9+M10

Job	M1+M2+M3+M4+M5	M6+M7+M8+M9+ M10
J1	118	220
J2	163	148
J3	127	164
J4	74	216

Table 6 Optimal sequence taking M1+M2+M3+M4+M5 & M6+M7+M8+M9+M10:

Sequence	Make span
J4- J1- J3- J2	470

Step 3:

Table 7 Taking M1+M2+M3+M4+M5+M6+M7+M8+M9 & M2+M3+M4+M5+M6+M7+M8+M9+M10

Job	M1+M2+M3+M4+M5 +M6+M7+M8+M9	M2+M3+M4+M5+M 6+M7+M8+M9+M10
J1	308	305
J2	274	271
J3	254	252
J4	260	257

So, optimal sequence: **J1-J2-J4-J3** and make span: 525

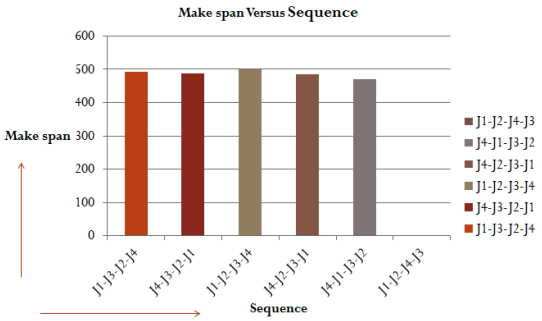

Fig.2 Makespan versus sequence curve for CDS heuristic

5. NEH Algorithm

Step 1: Find the total work content for each job using expression

$$T_j = \sum_{i=1}^{m} P_{ij}$$

Step 2: Arrange the jobs in a work content list according to decreasing values of Tj

Step 3: Select first two jobs from the list and from two partial sequences by inter changing the place of two jobs. Compute $C_{max}$the value of partial sequences. Oyt Of the two sequences, discard the sequence having larger value ofC_{max}, Call the lower value of C_{max}as incumbent sequence.

Step 4: Pick the next job and put in incumbent sequence. Calculate value of $C_{max}$of all sequences.

Step 5: If there is no job left in work content list to be added to Incumbent sequence, Stop go to step 4.

Table 8 Calculation of total completion time**:**

Job	M1	M2	M3	M4	M5	M6	M7	M8	M9	M10	Total
J1	33	37	25		23	42	38	110		30	338
J2	40	31	36	26	30	32	35		44	37	311
J3	39	31		37	20	37	44		46	37	291
J4	33	20	21			26	26	107	27	30	290

Decreasing order in term of total completion time is

Sequence	Make span
J4-J1-J3-J2	470
J1-J4-J3-J2	569
J1-J3-J4-J2	523
J1-J3-J2-J4	492
J4-J1-J2-J3	470
J1-J4-J2-J3	569
J1-J2-J4-J3	525
J1-J2-J3-J4	499

J1>J2>J3>J4

Step 1: Taking J1 & J2, we have,
Sequences: J1-J2 &J2-J1 and makespan 389 and 415 respectively

Step 2: Choosing J1-J2 & take J3
Sequences:
J3-J1-J2 & J1-J3-J2 & J1-J2-J3 and make span 437, 435 and 435 respectively

Step 3: Taking J1-J3-J2 & take J4
Taking J1-J2-J3 & take J4
Sequences:
J4-J1-J3-J2 & J1-J4-J3-J2 & J1-J3-J4-J2 & J1-J3-J2-J4
J4-J1-J2-J3 & J1-J4-J2-J3 & J1-J2-J4-J3 & J1-J2-J3-J4

Table 9 Sequence for NEH algorithm

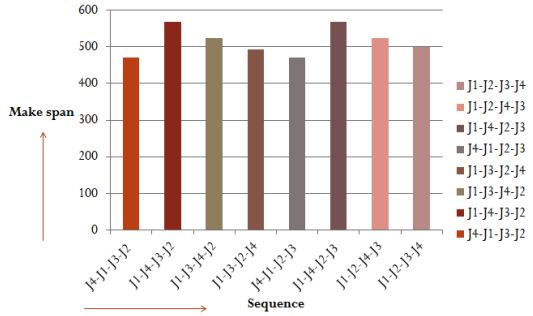

Fig.3 Makespan versus sequence curve for NEH algorithm

6. Result Analysis

Table 10 Comparison among Pamer, CDS and NEH

No. of observation	Technique	Optimal sequence	Make span
01	Palmer's Heuristic	J4-J1-J3-J2	470
02	CDS Heuristic	J4-J1-J3-J2	470
03	NEH Algorithm	J4-J1-J2-J3 J4-J1-J3-J2	470

We have applied three techniques to determine the optimal make span and dramatically we have got the same result for three cases. By applying Palmer's Heuristic and CDS Heuristic we have got only one sequence and by applying NEH Algorithm we have got two sequences and by applying any of the sequence between them we can get our optimum make span. From the above analysis we can say that make span 470 is the most optimum and no other optimum make span less than 470 is possible for the above problem.

7. Conclusion

This study tries to solve the problem of a flow shop scheduling with the objective of minimizing the makespan. The problem of 4 jobs and 10 machines have been considered for comparative analysis among Palmer's heuristic, CDS heuristic and NEH heuristic and we have got the same result by applying all of the three heuristics. From the analysis, it has proved that the make span 470 is the most optimum make span for the given problem and no other optimum make span is possible less than 470. This work can be useful to researchers for selecting the effective and efficient heuristics for solving the flow shop scheduling problems. The work can also be extended by increasing the size of the problems and removing any or all of the assumptions considered.

REFERENCES

[1] S. M. Johnson. Optimal two and three stage production schedules with setup times included, *Naval Research Logist Quarterly*, Vol. 1, pp. 61-68, (1954).

[2] D. Palmer, Sequencing jobs through a multi-stage process in the minimum total time – a quick method of obtaining a near optimum, *Operation Research*, Vol. 16, pp. 101-107, (1965).

[3] H. G. Campbell, R. A. Dudek and M. L. Smith, A heuristic algorithm for the n-job, m-machine sequencing problem, *Management Science*, Vol. 16, pp. 630 – 637, (1970).

[4] M. Nawaz,Jr. E. Enscore and I. Ham, A Heuristic Algorithm for the m-Machine, n-job flow-shop sequencing problem, *OMEGA - Elsevier*, Vol. 11, pp. 91 – 95, (1983).

[5] S. R. Hejazi, S. Saghafian, Flow shop-scheduling problems with make span criterion: a review, *International Journal of Production Research*, Vol. 43(14), pp. 2895-2929, (2005).

[6] M. A. Ibrahim, New Heuristics to Minimize the Mean Flow Time for Static Permutation Flow shop Problems, *Eng. Sci.* (1), Vol. 18, pp. 83-99, (2005).

[7] Z. Jin, Z. Yang and T. Ito, Metaheuristic algorithms for the multistage hybrid flow shop scheduling problem, *International Journal of Production Economics*, Vol. 100, pp. 322–334, (2006).

[8] U. K. Chakraborty, D. Laha, An improved heuristic for permutation flowshop scheduling. *International Journal of Information and Communication Technology*, Vol. 1, pp. 89–97, (2007).

[9] R. Ruiz, T. Stutzle, A simple and effective iterated greedy algorithm for the permutation flow shop scheduling problem, *European Journal of Operational Research*, Vol. 177, pp. 2033 – 2049, (2007).

[10] Tang, Zhao, Scheduling a single semi-continuous batching machine, *Omega*, Vol. 36, pp. 992-1004, (2008).

[11] A. K. Sahu, Efficient heuristics for scheduling tasks on a flow shop environment to optimize make span *National Institute of Technology, Rourkela INDIA*, (2009).

[12] Chia, Lee, Minimizing the total completion Time in permutation flow shop, *Computers and operations research*, Vol.6, pp. 2111-2121, (2009).

[13] R. Ruiz, E. Vallada. C. F. Martinez, In Computational Intelligence in Flow Shop and Job Shop Scheduling, *Springer Berlin / Heidelberg*, Vol. 230, (2009).

[14] P. Damodaran, M. C. V. Gallego, Heuristics for makespan minimization on parallel batch processing machines with unequal job ready times. *International Journal of Advanced Manufacturing Technology*, Vol. 49, pp. 1119-1128, (2010). V. Modrák, R. S. Pandian, Flow shop scheduling algorithm to minimize completion time for *n*-jobs *m*-machines problem, *Technical Gazette*, Vol. 17, pp. 273-2783, (2010).

[15] A. Chaudhry, S. Mahmood, No-wait Flowshop Scheduling Using Genetic Algorithm, *Proceedings of the World Congress on Engineering* ISSN: 2078-0966 (Online), Vol. 3, (2012).

[16] P. Semančo, V. Modrák, A Comparison of Constructive Heuristics with the Objective of Minimizing Makespan in the Flow-Shop Scheduling Problem,*Acta Polytechnica Hungarica*, Vol. 9, pp. 177-190, (2012).
[17] S. U. Sapkal, D. Laha, A heuristic for no-wait flow shop scheduling, *International Journal of advanced manufacturing Technology*, DOI 10.1007/s00170-013-4924-y (In Press). (2013).
[18] A. Malik, A. K. Dhingra, Comparative analysis of heuristics for make span minimizing in flow shop scheduling. *International Journal of Innovations in Engineering and Technology*. Vol. 2, pp. 263-269, (2013).
[19] A. K. Agarwal, R. Garg, Flowshop Scheduling Problem for 10-Jobs, 10-Machines By Heuristics Models UsingMake span Criterion, *International Journal of Innovations in Engineering and Technology*, Vol. 2, pp. 28- 37, (2013).

ICMIEE-PI-140166

Real-Time Monitoring and Controlling of Remote Electrical Device Using Microcontroller and Android Smart Phone via Internet

Md. Hanif Ali Sohag[1], *Md. Asif Ahamed* [2]
[1,2]Department of Electrical & Electronic Engineering,
Khulna University of Engineering & Technology, Khulna-9203, BANGLADESH

ABSTRACT
Smart phone can provide a vital role for controlling remote electrical devices easily. This paper represents a system to control household appliances (e.g. lights, fans, pumps, AC, etc.) by using Android smartphone via internet from any place in the world. This system includes an Android application, a microcontroller (ATmega8) with a Bluetooth module (HC-05) and a cloud-based application to provide an easier access to the remote electrical devices to the user. The cloud-based application also includes a logging facility to allow only authorized users to control the electrical appliances. We have tested the system in an Android smartphone running on Android 4.2.

Keywords: Android, Cloud computing, ATmega8, Real-time.

1. Introduction

With the advancement of technology and the continuous improvement of people's living standard, people are in pursuit of automated, intelligent, and convenient home control systems. Home automation is one of the most exciting developments in technology for the home that has come along in recent years. It is mainly the automation of the home, housework, or household activity. It may also include centralized control of lighting, heating, ventilation, and air conditioning of appliances, and other systems to provide improved convenience, comfort, energy efficiency, and security. It can be helpful to the people to access home appliances while away from their home and can incredibly improve the lives of the disabled. The home automation systems can be separated into two categories: locally controlled systems and remotely controlled systems. Locally controlled systems allow users to control their system from within their home via a stationary or wireless interface. Remotely controlled systems allow the users to control of their system from their mobile device, personal computer, or PDA via internet. Because of the popular usage of computers and high share rate of smart phones in the market [3], computers and Android smartphones are mostly chosen to design the home automation systems. However, there are some problems in the computer [1] monitoring system, such as inconvenience to carry, high cost, limited monitoring range and so on. Therefore, it is a good choice to design a system based on mobile phone. With the rapid development of 3G wireless technology and a variety of smart phones, smart home is no longer confined within the house. With smartphones based on Android platform [2] and mobile internet, people can monitor and control the home environment wherever they are.

Electrical safety and warnings were always a matter of great concern during the utilization of home appliances. Some people are not aware that without carrying out a safety inspection based on the visible indication could initiate fault and produce an electrical hazard. Any unusual electrical condition can occur due to certain fault conditions, for example- overloaded circuit of the appliance, damaged insulation, and misused of extension cords. Therefore, it is necessary to monitor the condition of appliances whether being at home or away. The internet based home automation system with real time monitoring facility can be much helpful to solve such problems.

In this study, we have developed a smart home monitoring system for monitoring and controlling electrical appliances in a residential environment. With this system, it is possible to check the real time status and control the electrical appliances via laptop, PDA (Personal digital assistant), mobile phone, or web interface. The system intelligently controls power consumption of all appliances connected to the smart home network, also contributing to energy savings in the household.

2. Working principle

This system includes two Android smart phone, a microcontroller (ATmega8), a Bluetooth module (HC-05), five relays, a Cloud-based application, and an Android application. This Android application has two options, Device side, and User side. User can control the remote electrical appliances by using the Android application or by using the web interface of the smart home automation system at anytime from anywhere of the world via internet. For this privilege, an active data connection is required in user's phone. User can also use this facility through laptop, tablet, or desktop computer.

The working steps of the system are given below.

1. When user touches on the icon of one or more electrical devices in the Android application to make it ON or OFF, the application sends a data to a particular server [7]. There is a web interface and a cloud based processing system in the server. For monitoring and

Md. Hanif Ali Sohag. Tel.: +88-01613103110
E-mail address: hanifalisohag@gmail.com

controlling the electrical appliances through laptop or desktop user needs to visit the system's website [8]. After successful login to the website, user can see the real time status of the electrical devices. Then the user can easily turned ON or OFF the electrical appliances according to his/her needs.

2. When the server receives data from the phone or command in the webpage, it sends a data to the Android phone, which is connected to the system at home via internet.
3. Receiving the data from the server Android smartphone transmits the data to the microcontroller via the Bluetooth module (HC-05).
4. Then the microcontroller will turn the electrical appliances ON or OFF according to the data.
5. The microcontroller receives the present status of the devices via ADC (Analog to digital converter) and sends it to the server via Bluetooth module, Android phone, and internet [9]. Application installed on the Android phone or tablet checks the status of the device in a time interval by connecting to the server.

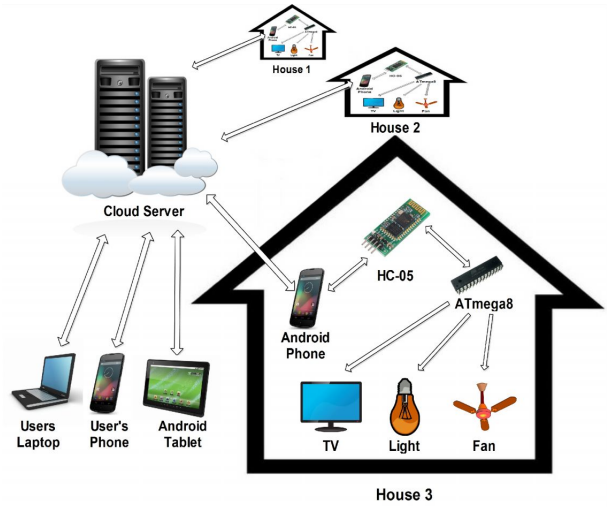

Fig.1 Operational diagram of the system.

3. Functional block diagram

Based on the working principle described in section 2, Fig. 2 shows the functional block diagram of the entire system.

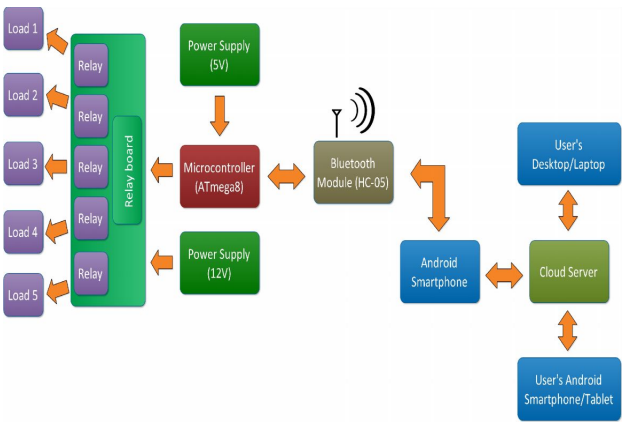

Fig.2 Functional block diagram of the system.

4. Hardware design and implementation

The main hardware components that make up the smart home automation system are Android smartphone and the microcontroller board. Other components are Bluetooth module and relays. These components are connected to the microcontroller board. We have implemented the code in C programing language by using WinAVR.

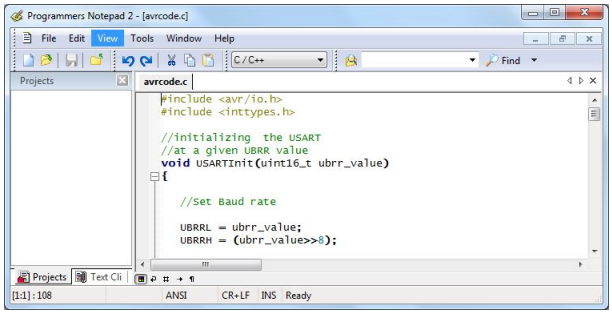

Fig.3 Coding of microcontroller program using WinAVR.

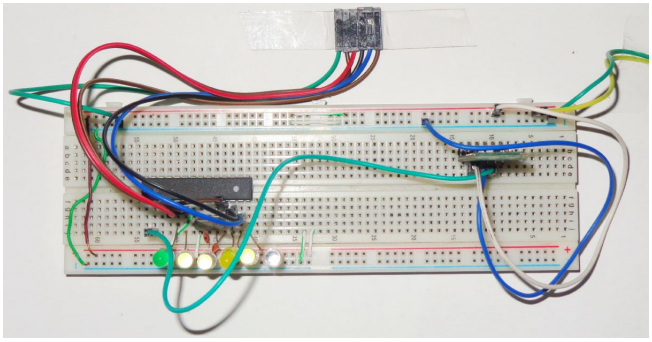

Fig.4 Experimental setup of the microcontroller board.

4.1 Microcontroller Board

An ATmega8 microcontroller does the operation of making the devices ON or OFF. A Bluetooth module (HC-05) is connected to the microcontroller, which communicates with the Android phone [4]. From the Android phone microcontroller gets the command for switching the device ON or OFF.

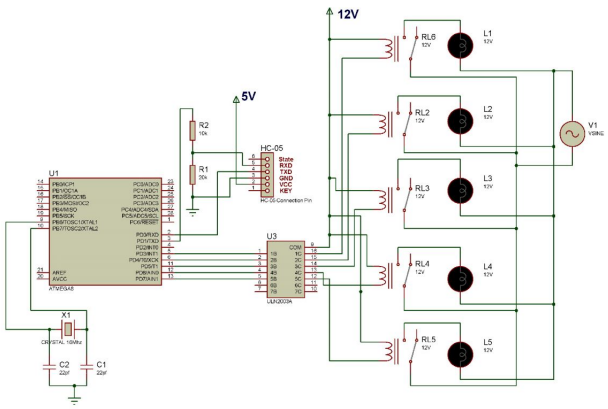

Fig.5 Circuit diagram of the microcontroller board.

4.2 Relay board

In relay board, there are five relays for five electrical appliances [10]. A 12V dc power supply is given to the relay board.

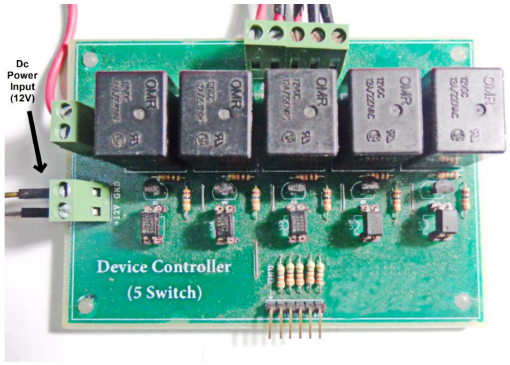

Fig.6 Relay board layout.

5. Software design and implementation

Android being truly open, developers can easily develop their required application on this platform. Developers are provided with four development components of Android: Activity, Service, Broadcast Receiver, and Content Provider [6]. Besides, Android uses XML document to design user interface, which helps the developers to design the application very easily. With the MVC (Model view controller) pattern, Android implements separation of the user interface design and writing code. The Android SDK provides a wide range of useful libraries, tools, and APIs, which is necessary to develop applications on the Android platform using the Java programming language. We use Android Software Development Kit (SDK) for developing the application of this home automation system. The application provides a friendly interface of the home automation system and users can easily check the real time status of the electrical appliances and control the appliances according to their needs.

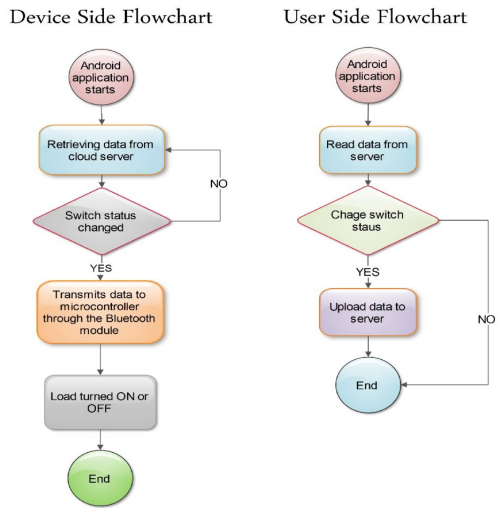

Fig.7 Flowchart of the device side and user side.

When user opens this application, a homepage will be presented to the user with the following options,

- Device side
- User's side

5.1 Android Application's Device Side

The Android provides full safety of the electrical appliances by providing logging facility for the users. Entering the exact username and password, the user has to start the device side part of the system. If logging info of the user exactly matches with the records of the web server, the user will be displayed the Bluetooth connectivity activity and has to choose the proper Bluetooth module (such as HC-05) and connect the Android phone with the Bluetooth module. Now an activity with the proper status of the electrical appliances will be displayed. To start receiving the data from the server, the user has to press the "START" button. The status of the different switches is mainly retrieved from the server. When the status received by the server is "ON", the application sends the data to the microcontroller through the Bluetooth module and the appliance with the proper switch number will be turned ON by the relay and if the status received is "OFF" and the appliance connected with the microcontroller is ON then it will be turned OFF.

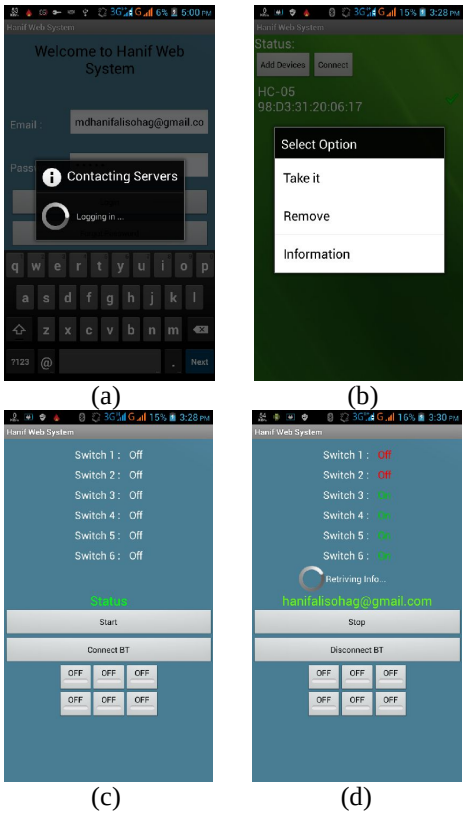

Fig.8 Screen shots of some processes, (a) Logging to the server, (b) Connecting to Bluetooth Module (HC-05), (c) Devices status, (d) Receiving information from the server.

The device side of the application also provides the control of the electrical switches through the Bluetooth if there is no net connection or the user is at the home.

5.2 Android Application's User's Side

In the user's side part of the Android application, logging and registration facility is provided for the user. The user must have to register for the first time to start the system. After successful registration, the user has to enter the correct username and password to log in to the cloud server through the Android application. If everything goes well a screen with the status of the electrical appliances will be displayed to the user. To check the real time status of the appliances connected with the system, the user has to press the "Check first" button. After checking the status, the users can now easily change the status of the appliances by checking the radio buttons "OFF" or "ON" and pressing the "Update" button.

Fig.9 Screen shots of some processes, (a) Registering to the server, (b) Logging to the server, (c) Devices status, (d) Devices status changed.

5.3 Web Part

The implementation of the smart home automation system involved several languages and software. The languages used to suit the development of the interface are HTML, PHP and MySQL. For designing the web interfaces and providing a user friendly interface to the user, the HTML language is used. For communicating with the web server from the Android smartphone, PHP is used. PHP is also used with MySQL database engine for data storing. The web server stores the user records and serves to the other components in the system. Cloud Platform based web server is used for supporting the bidirectional communication between local device and web server and also mobile device and web server.

6. System's Web Interface

The system can be monitored and controlled through the Web interface [5]. As a part of the system, we have designed a web based GUI for the smart home automation system and users can easily access the system through the laptops, PDAs or any multimedia mobile phone having internet facility.

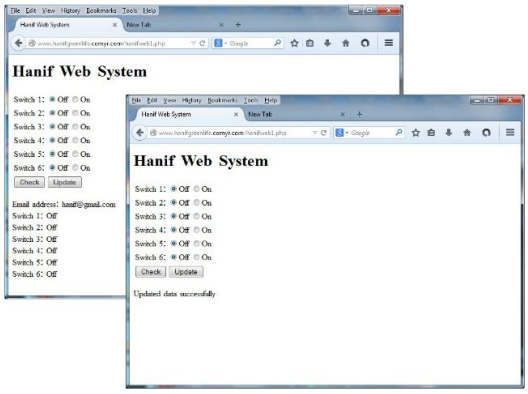

Fig.10 Screen shot of the web site of the system.

7. System Prototype

The system has three components. Those are a local device to transfer signals to home appliances, a web server to store customer records and an Android mobile running the Android application. When microcontroller receives a signal, it will turn the electrical appliances ON or OFF according to the user command.

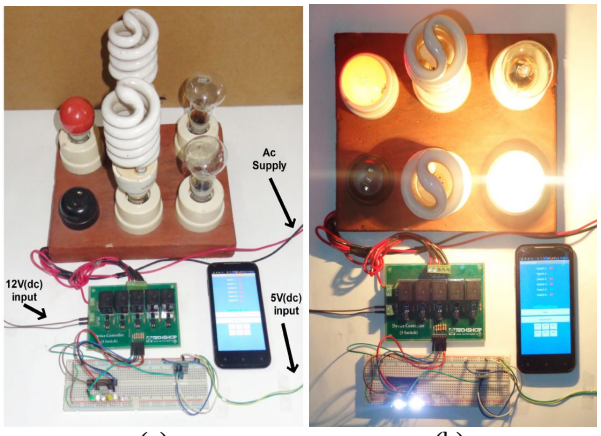

Fig.11 Developed prototype, (a) All bulbs are OFF, (b) Second and fifth bulbs are ON.

In Figure 11, five relays are used for five bulbs. Android phone communicates with the microcontroller via Bluetooth module. This android phone runs the device side of the application. In Figure 11(a), all bulbs are OFF by sending

commands from the user's phone, microcontroller turns the second and fifth bulb ON

7. Conclusion

The paper presents the design and implementation of a wireless home automation system and interfacing them to the web server based network using the Android smartphone. With the help of Android client, the web server, and the control protocols, a user can control the home appliances and monitor the status of each appliances at anytime from anywhere via internet by using a user-friendly interface. Compared with common used home automation systems based on Client/Server structure, this system does not need a dedicated IP address and server, so the home gateway maintenance issues is reduced. When the proposed design was applied to home appliances, it was found to function successfully. The obtained results confirm the feasibility of the proposed home automation system.

REFERENCES

[1] J. Lv, Z. Li, Q. Huang, M. Mao, Z, A new USB home appliances based on PC and infrared remote control protocol, International Conference On Computer and Communication Technologies in Agriculture Engineering (CCTAE), Chengdu, pp 572-575, June 2010.

[2] S. W. Chean, C. H. Yang, C. T. Liu, Design and Implementation of Live SD Acquisition Tool in Android Smart Phone, Fifth International Conference on Genetic and Evolutionary Computing (ICGEC), Xiamen, pp 157-162, 2011.

[3] H. Pieterse, M. S. Olivier, Android botnets on the rise: Trends and characteristics, Information Security for South Africa (ISSA), Johannesburg, Gauteng, pp 1-5, August 2012.

[4] S. Panth, M. Jivani, Home Automation System (HAS) using Android for Mobile Phone, International Journal of Electronics and Computer Science Engineering, ISSN 2277-1956, vol-3, no-1, 2014.

[5] P. M. Corcoran, J. Desbonnet, Browser-Style Interfaces to a Home Automation Networks, IEEE Trans. on Consumer Electronics, vol-43, no-4, Nov. 1997.

[6] O. Ling, Android core technology and explain examples, Beijing, Electronic Industry Press, 2013.

[7] A. Gurek, C. Gur, C. Gurakin, M. Akdeniz, S. K. Metin, I. Korkmaz, An Android Based Home Automation System, 10th International Conference on High Capacity Optical Networks and Enabling Technologies (HONET-CNS), Magosa, pp 121-125, December 2013.

[8] L. Ningqing, Y. Haiyang, G. Chunmeng, Design and Implementation of a Smart Home Control System, Third International Conference on Instrumentation, Measurement, Computer, Communication and Control (IMCCC), Shenyang, pp 1535-1538, September 2013.

[9] G.M.S. M. Rana, A. A. M. Khan, M. N.Hoque, A. F. Mitul, Design and implementation of a GSM based remote home security and appliance control system, International Conference on Advances in Electrical Engineering (ICAEE), Dhaka, pp 291-295, December 2013.

[10] R.K. Rajput, "Power System Engineering" in Firewall Media, pp 271-350, 2006

ICMIEE-PI-140169

Artificial Bee Colony, Firefly and Bat Algorithm in Unconstrained Optimization

*Md. Tajmiruzzaman, Md. Asadujjaman**
Department of Industrial & Production Engineering, Rajshahi University of Engineering & Technology, Rajshahi, BANGLADESH

ABSTRACT
Meta-heuristic algorithms have been proven to outperform deterministic algorithms in real world optimization problems. Artificial Bee Colony (ABC) Algorithm is a meta-heuristic optimization algorithm based on the intelligent behavior of honeybee swarm. Firefly algorithm is a recently developed algorithm inspired by the flashing behavior of fireflies. And a most recently developed algorithm is Bat algorithm which exploits the so-called echolocation of bats. In this paper, Artificial Bee Colony, Firefly and Bat algorithms are tested on some standard well-known bench-mark problems of unconstrained optimization to compare performance of these algorithms. The result indicates that, Artificial Bee Colony algorithm outperforms the other algorithms with Firefly algorithm performing better than Bat algorithm, although Bat algorithm scores best in convergence speed. This paper concludes that further in-depth researches for modification purposes and detailed parametric studies are needed for these algorithms to work best.

Keywords: Artificial Bee Colony Algorithm, Firefly Algorithm, Bat Algorithm, Unconstrained Optimization.

1. Introduction

Nature has always been an inspiration for researchers and scientists. Many nature-inspired algorithms have been developed to solve complex problems in optimization and in real world. In general, there are two main concepts developed in bio-inspired computation:

1) Evolutionary algorithms
2) Swarm based algorithms.

Evolutionary algorithms [1] are optimization techniques that base on Darwin's principle of survivor of the fittest. Such kinds of algorithms are Genetic algorithm, Evolution strategies, Genetic programming, Evolutionary programming, Differential evolution etc. Swarm intelligence is the collective behavior of decentralized, self-organized systems, either natural or artificial. Swarm intelligence was introduced by Beny, in 1989 [2]. The most well-known classes of swarm intelligence algorithms are as follows: Particle swarm optimization, Ant Colony Optimization, Artificial Bee Colony, Firefly algorithm, Cuckoo Search, Bat algorithm etc. In this paper, Artificial Bee Colony, Firefly and Bat Algorithms are checked for their performance in terms of convergence speed and precision in solving unconstrained optimization problem for single objective function.

The structure of the paper is as follows. In Section-2, Artificial Bee Colony, Firefly and Bat Algorithms are introduced. In section-3, benchmark test functions used in this paper are described briefly. Section-4 shows experimental settings of the algorithms and experimental analysis on the three algorithms. And finally, Section-5 concludes the work done.

2. Overview of the Algorithms

2.1 Artificial Bee Colony (ABC)

In 2005, D. Karaboga introduced a bee swarm algorithm called artificial bee colony algorithm for numerical optimization problems [4]; and B. Basturk and D. Karaboga compared the performance of ABC with that of some other well-known population based optimization algorithms [5]. The artificial bee colony contains three groups: scouts, onlooker bees and employed bees. The bee carrying out random search is known as scout. The bee which is going to the food source which is visited by it previously is employed bee. The bee waiting on the dance area is an onlooker bee. The bees search for the rich food sources around the hive. The employed bees store the food source information and share the information with onlooker bees. The number of food sources is equal to the number of employed bees and also equal to the number of onlooker bees. Employed bees whose solutions cannot be improved through a predetermined number of trials (that is "limit") become scouts and their solutions are abandoned [4]. in the optimization context, the number of food sources in ABC algorithm represents the number of solutions in the population. The ABC consists of four main phases:

Initialization Phase:
The food sources, whose population size is SN, are randomly generated by scout bees. Each food source, represented by x_m is an input vector to the optimization problem, x_m has D variables and D is the dimension of searching space of the objective function to be optimized. The initial food sources are randomly produced via the Eq.(1).

$$x_m = x_{min} + rand(0,1) \times (x_{max} - x_{min}) \quad (1)$$

Where x_{max} and x_{min} are the upper and lower bound of the solution space of objective function, rand (0, 1) is a random number within the range [0, 1].

* Corresponding author. Tel.: +88-01913599639
E-mail address: jonikhan007@yahoo.com

Employed Bee Phase:
Employed bee flies to a food source and finds a new food source within the neighborhood of the food source. The higher quantity food source is memorized by the employed bees. The food source information stored by employed bee will be shared with onlooker bees. A neighbor food source v_{mi} is determined and calculated by the following Eq.(2).

$$v_{mi} = x_{mi} + rand(-1,1) \times (x_{mi} - x_{ki}) \quad (2)$$

Where i is a randomly selected parameter index, x_k is a randomly selected food source, rand(-1,1) is a random number within the range [-1, 1]. The range of this parameter can make an appropriate adjustment on specific issues. The fitness of food sources is essential in order to find the global optimal. The fitness is calculated by the following Eq.(3), after that a greedy selection is applied between x_m and v_m.

$$fit_m(x_m) = \begin{pmatrix} \frac{1}{1+f_m(x_m)}, & f_m(x_m) > 0 \\ 1 + |f_m(x_m)|, & f_m(x_m) < 0 \end{pmatrix} \quad (3)$$

Where $f_m(x_m)$ is the objective function value of x_m.

Onlooker Bee Phase:
Onlooker bees calculates the profitability of food sources by observing the waggle dance in the dance area and then select a higher food source randomly. After that onlooker bees carry out randomly search in the neighborhood of food source. The quantity of a food source is evaluated by its profitability and the profitability of all food sources. Pm is determined by the Eq.(4).

$$p_m = \frac{fit_m(x_m)}{\sum_{m=1}^{SN} fit_m(x_m)} \quad (4)$$

Where $fit_m(x_m)$ is the fitness of x_m. Onlooker bees search the neighborhood of food source according to Eq.(5).

$$v_{mi} = x_{mi} + rand(-1,1) \times (x_{mi} - x_{ki}) \quad (5)$$

Scout Phase:
if the profitability of food source cannot be improved and the times of unchanged greater than the predetermined number of trials, which called "limit", the solutions will be abandoned by scout bees. Then, the new solutions are randomly searched by the scout bees. The new solution x_m will be discovered by the scout by using Eq.(6).

$$x_m = x_{min} + rand(0,1) \times (x_{max} - x_{min}) \quad (6)$$

Table 1 Pseudo code for ABC algorithm

1) **Begin**	9) **Generate** new solutions v_{mi} for the Onlooker bees using Eq.(5) and evaluate them
2) **Initialize** the solution population, i = 1, . . . , SN	10) **Keep** the best solution between current and candidate
3) **Evaluate** population	11) **Determine** if exist an abandoned food Source and replace it using a scout bee
4) cycle = 1	12) **Save** in memory the best solution so far
5) **Repeat**	13) cycle = cycle + 1
6) **Generate** new solutions v_{mi} for the employed bees using Eq.(2) and evaluate them.	14) Until cycle = M C N
7) **Keep** the best solution between current and candidate	
8) **Select** the visited solution for onlooker bees by their fitness	

2.2 Firefly Algorithm
The Firefly algorithm was introduced by Dr. Xin She yang [6,7] at Cambridge University in 2007 which was inspired by the mating or flashing behavior of fireflies. The FA is assumed as follows: 1) All fireflies are unisex, so that one firefly will be attracted to all other fireflies. 2) Attractiveness is proportional to their brightness, and for any two fireflies, the less brighter one will be attracted by the brighter one. However, the brightness can decrease as their distance increases. If there are no fireflies brighter than a given firefly, it will move randomly. 3) The brightness of a firefly is affected or determined by the landscape of the objective function. For a minimum optimization problem f(x), the light intensity I_i of a firefly i is determined by Eq.(7).

$$I_i = f(x_i) \quad (7)$$

Based on these three rules, the basic steps of the FA can be summarized as the pseudo code shown in Table 2. The initial positions of fireflies are generated at random ($x_i \in [x_{min}, x_{max}]^D$). The movement of a firefly i is attracted by another more attractive firefly j, which has better solution, is determined by Eq.(8).

Table 2 Pseudo code for Firefly algorithm

Objective function f(x), $x=(x_1,\ldots\ldots,x_D)^T$
Initialize positions of fireflies x_i (i=1,2,……,M)
Calculate Light intensities by $I_i=f(x_i)$
while (t< MaxGeneration t_{max}) **do**
  for i = 1 to M, all M fireflies **do**
    for j = 1 to M, all M fireflies **do**
      if $I_i > I_i$ **then**
        Move firefly i toward j by Eq.(8)
      end if
    end for j
  end for i
  Evaluate new solutions $f(x_i)$
  Rank the fireflies and find the current global best g_*
end while

$$x_i^{new} = x_i^{old} + \beta_{i,j}\left(x_j(t) - x_i^{old}\right) + \alpha(t)(rand(0,1) - 0.5)L \quad (8)$$

Where, the second term is due to the attraction. The attractive-ness β is determined by Eq.(9)

$$\beta_{i,j} = (\beta_o - \beta_{min})e^{-\gamma r_{i,j}^2} + \beta_{min} \quad (9)$$

Where, β_0 is the attractiveness at r = 0, β_{min} is the minimum value of β, and an absorption coefficient γ is crucially important in determining the speed of the convergence. Thus, the attractiveness will vary with the distance $r_{i,j}$ between firefly i and j.

$$r_{i,j} = \left\|x_i^{old} - x_j(t)\right\| = \sqrt{\sum_{d=1}^{D}(x_{i,d} - x_{j,d})^2} \quad (10)$$

The third term of Eq.(8) is randomization with α(t) being the randomization parameter;

$$\alpha(t) = \alpha(0)\left(1 - \left(\frac{10^{-4}}{0.9}\right)^{1/t_{max}}\right) \quad (11)$$

Where, Rand(0,1) is a random number generator uniformly distributed in [0, 1], and L is the average scale of the problem $|x_{max} - x_{min}|$. The brightest firefly k moves randomly according to Eq.(12)

$$x_k(t+1) = x_k(t) + \alpha(t)(rand(o,1) - 0.5)L \quad (12)$$

2.3 Bat Algorithm

Bat Algorithm, proposed by Yang, is inspired by echolocation characteristic of bats which they use to detect prey and to avoid obstacles [8]. These bats emit very loud sound and listen for the echo that bounces back from the surrounding objects [9]. Thus a bat can compute how far they are from an object. In order to transform these behaviors of bats to algorithm, Yang idealized some rules:

1) All bats use echolocation to sense distance, and they also know the difference between food/prey and background barriers in some magical way;
2) Bats fly randomly with velocity v_i at position x_i with a frequency f_{min} varying wavelength and loudness A_0 to search for prey. They can automatically adjust the wavelength (or frequency) of their emitted pulses and adjust the rate of pulse emission r ϵ [0,1], depending on the proximity of their target;
3) Although the loudness can vary in many ways, we assume that the loudness varies from a large (positive) A_0 to a minimum constant value A_{min};

Initialization of Bat Population:

Initial population is randomly generated from real-valued vectors with dimension d and number of bats n, by taking into account lower and upper boundaries.

$$x_{ij} = x_{minj} + rand(0,1)(x_{maxj} - x_{minj}) \quad (13)$$

where i=1,2,…n, j=1, 2,….d. x_{minj} and x_{maxj} are lower and upper boundaries for dimension j respectively.

Update Process of Frequency, Velocity and Solution:

The frequency factor controls step size of a solution in BA. This factor is assigned to random value for each bat (solution) between upper and lower boundaries [f_{min}, f_{max}]. Velocity of a solution is proportional to frequency and new solution depends on its new velocity.

$$f_i = f_{min} + (f_{max} - f_{min})\beta \quad (14)$$

$$v_i^t = v_i^{t-1} + (x_i^t - x^*)f_i \quad (15)$$

$$x_i^t = x_i^{t-1} + v_i^t \quad (16)$$

Where β ϵ [0, 1] indicates randomly generated number, x^* represents current global best solutions. For local search part of algorithm (exploitation) one solution is selected among the selected best solutions and random walk is applied .

$$x_{new} = x_{old} + \varepsilon\overline{A^t} \quad (17)$$

Where $\overline{A^t}$ is average loudness of all bats, Ɛ ϵ [0,1] is random number and represents direction and intensity of random-walk.

Update Process of Loudness and Pulse Emission Rate:

Loudness and pulse emission rate must be updated as iterations proceed. As a bat gets closer to its prey then loudness *A* usually decreases and pulse emission rate also increases. Loudness *A* and pulse emission rate *r* are updated by the following equations Eq.(18) and Eq.(19):

$$A_i^{t+1} = \alpha A_i^t \quad (18)$$

$$r_i^{t+1} = r_i^0[1 - e^{(-\gamma t)}] \quad (19)$$

Where α and γ are constants. r_i^0 and A_i are factors which consist of random values and A_i^0 can typically be [1, 2], while r_i^0 can typically be [0,1].

Table 3 Pseudo code for Bat algorithm

Objective function f(x), $x = (x_1,...,x_d)^T$
Initialize the bat population x_i (i = 1, 2,...,n) and v_i
Define pulse frequency f_i at x_i
Initialize pulse rates r_i and the loudness A_i

while (t <Max number of iterations)
Generate new solutions by adjusting frequency, and updating velocities and solutions by Eq.(14) to Eq.(16) .
if (rand > r_i)
Select a solution among the best solutions
Generate a local solution around the selected best solution
end if
Generate a new solution by flying randomly
if (rand < A_i & $f(x_i) < f(x_*)$)
Accept the new solutions
Increase r_i and reduce A_i
end if
Rank the bats and find the current best x_*
end while

3. Benchmark Test Functions

Seven well-known Benchmark functions are used in our experiment to test the performance of the three algorithms. These functions are useful to evaluate characteristics of any optimization algorithms [10]. Both the unimodal and multimodal functions are used. The separability and dimensionality of these functions are worth being studied carefully [3]. In Table 4, U= unimodal, S=separable, M=multimodal, N=non-separable

Table 4 Benchmark test functions

S. NO.	***Function***	***Formulation***	***Characteristics***	***Range***	***Global minimum point***
f_1	Sphere	$f(x) = \sum_{i=1}^{D} x_i^2$	U/S	[-5.12, 5.12]	x_i =0,.,0
f_2	Step	$f(x) = \sum_{i=1}^{D} (\lvert x_i + 0.5 \rvert)^2$	U/S	[-10, 10]	x_i =0,.,0
f_3	Rosenbrock	$f(x) = \sum_{i=1}^{D} [100(x_i^2 - x_{i+1})^2 + (1 - x_i)^2]$	M/N	[-5, 5]	x_i =1,.,1
f_4	Rastrigin	$f(x) = \sum_{i=1}^{D} [x_i^2 - 10\cos(2\pi x_i) + 10]$	M/N	[-15, 15]	x_i =0,.,0
f_5	Griewank	$f(x) = \frac{1}{4000}\sum_{i=1}^{D} x_i^2 - \prod_{i=1}^{D} cos\left(\frac{x_i}{\sqrt{i}}\right) + 1$	M/N	[-600, 600]	x_i =0,.,0
f_6	Schwefel	$f(x) = D * 418.9829 + \sum_{i=1}^{D} -x_i \sin\left(\sqrt{\lvert x_i \rvert}\right)$	M/N	[-500,500]	x_i =420,.,420
f_7	Ackley	$f(x) = 20 + e - 20e^{\left(-0.2\sqrt{\frac{1}{D}\sum_{i=1}^{D} x_i^2}\right)} - e^{\frac{1}{D}\sum_{i=1}^{D}\cos(2\pi x_i)}$	M/N	[-32, 32]	x_i =0,.,0

4. Experiments and Results

All the experiments are executed in a Fujitsu LH531 computer and the configuration of PC was Intel(R) Pentium(R) CPU B960 @ 2.20 GHz and 2 GB RAM. Each algorithm is tested with 30 independent runs for each test function and the population size (no. of bees, fireflies or bats) is fixed to 50 for each run. Three different sets of dimensions (variables) were taken into account viz: D=10, D=20, D=30 and maximum cycle numbers for each dimension were taken as 2000, 4000 and 6000 respectively. Parameter settings for three algorithms are given in Table 5. The experimental results for objective function values and processing times are shown in Table 6 and Table 7 respectively.

Table 5 Parameter settings

ABC	FA	BA
Limit: 100	α (randomness): 0.5	A_0 (loudness): 1.8
	γ(absorption): 1	α: 0.9
	β_0: 1	r_0 (pulse rate): 0.9
	β_{min}: 0.2	γ: 0.9
		Q_{min} (minimum frequency) : 0
		Q_{max} (maximum frequency): 2

Table 6 Objective function values for three algorithms

Functions	D	ABC			FA			BA		
		Best	Worst	Mean	Best	Worst	Mean	Best	Worst	Mean
f_1	10	2.5511e-17	1.0062e-016	7.6965e-017	9.0434e-008	2.5190e-007	1.7624e-007	8.2939e-007	1.2646	0.1244
	20	2.0769e-016	4.9192e-016	3.3509e-016	4.7583e-007	9.8592e-007	7.0852e-007	3.8730e-006	0.2416	0.0129
	30	4.1396e-016	9.4409e-016	6.6442e-016	1.1955e-006	2.3205e-006	1.6189e-006	1.2419e-005	2.2329e-005	1.6328e-005
f_2	10	3.7136e-017	1.7645e-016	8.5316e-017	3.1041e-007	1.1208e-006	6.9179e-007	1.0309	53.8202	17.7914
	20	2.5010e-016	4.6896e-016	3.3612e-016	1.5421e-006	4.1627e-006	2.9305e-006	2.4155	93.1103	36.3792
	30	4.1167e-016	7.7174e-016	6.2551e-016	5.2488e-006	9.5321e-006	6.8868e-006	1.1551	71.2719	23.4291
f_3	10	0.0017	0.2392	0.0290	4.2452	9.3845	6.3135	1.4919	246.829	43.1519
	20	0.0038	0.7961	0.0957	14.8867	18.4818	17.0887	9.0993	204.319	54.2309
	30	2.5162e-004	0.4781	0.1112	26.1359	27.9784	26.9346	17.0327	151.151	35.0552
f_4	10	0	0	0	0.9953	8.9548	5.2404	43.7783	336.286	152.193
	20	0	5.6843e-014	1.6106e-014	7.9605	47.7589	19.9003	205.954	637.753	374.197
	30	0	1.1937e-012	2.3874e-013	18.9078	30.8471	23.8821	424.844	919.313	630.294
f_5	10	0	0.0123	0.0025	1.9674e-004	0.1382	0.0210	29.5652	86.3512	62.4397
	20	0	4.3881e-011	1.9047e-012	7.2438e-004	0.0011	8.8518e-004	47.9587	297.395	160.523
	30	1.1102e-016	5.4412e-012	5.2344e-013	0.0012	0.0087	0.0030	146.711	417.807	282.642
f_6	10	-3.4e+3	-1.6e+3	-2.4e+3	769.857	1.7372e+003	1.2673e+003	-Inf	-Inf	-Inf
	20	-4.7e+3	-2.3e+3	-3.6e+3	2.2504e+003	3.4151e+003	2.7340e+003	-Inf	-Inf	-Inf
	30	-6.3e+3	-3.9e+3	-4.8e+3	3.8494e+003	6.1592e+003	5.1997e+003	-Inf	-Inf	-Inf
f_7	10	2.6645e-015	9.7700e-015	6.2172e-015	0.0022	0.0040	0.0032	11.7922	17.8919	15.6894
	20	2.0428e-014	3.1086e-014	2.6586e-014	0.0038	0.0055	0.0048	14.1646	18.2478	16.8652
	30	4.1744e-014	6.3061e-014	4.9679e-014	0.0054	0.0066	0.0060	15.7225	18.4957	17.2802

In Table 6, we can see ABC algorithm outperforms both Firefly and Bat algorithm with Firefly algorithm performing better than Bat algorithm in all the functions. For unimodal separable functions (sphere, step), ABC algorithm outperforms FA by a factor 10^{-10} and FA outperforms BA by 10^{-7}. All the algorithms showed some difficulties to reach global minima for schwefel function. Except this, other functions reach global minima or require only a few extra iterations to reach global minima. It can also be noticed that, as dimension increases, the difficulty with finding global minima also increases. In Table 7, we can see that BA converges much faster than FA (or even than ABC algorithm) and FA performs worst of the three algorithms.

Table 7 Processing time for three algorithms

Function	D	ABC			FA			BA		
		Best	**Worst**	**Mean**	**Best**	**Worst**	**Mean**	**Best**	**Worst**	**Mean**
	10	1.7811	1.9407	1.7933	18.142	18.442	18.261	1.6009	1.658	1.6135
f_1	20	3.6818	4.0251	3.7087	37.128	37.851	37.286	3.222	3.381	3.249
	30	5.7592	6.1313	5.7857	58.554	62.314	59.367	4.9783	5.1387	5.0023
	10	1.8109	2.0030	1.8220	17.674	18.353	17.934	1.6158	1.6645	1.63
f_2	20	3.7641	4.0917	3.7940	36.896	37.151	37.025	3.3071	3.5034	3.3350
	30	5.9447	6.3332	5.9920	58.622	59.387	58.872	5.0219	5.2680	5.0610
	10	2.1526	2.3195	2.1732	18.294	18.787	18.632	2.6183	2.6819	2.6286
f_3	20	4.7530	5.0703	4.7844	39.871	40.211	39.934	5.3558	5.4489	5.3852
	30	7.8199	8.1974	7.8453	60.486	60.834	60.635	8.3112	9.3287	8.4250
	10	2.2073	2.4376	2.2449	18.270	18.720	18.559	2.4014	2.4585	2.4167
f_4	20	5.2398	5.5808	5.2816	38.067	38.439	38.147	4.9231	4.9976	4.9444
	30	9.1117	9.6187	9.1856	59.336	60.222	59.623	7.5976	7.7640	7.6367
	10	4.6223	5.0921	4.6473	20.291	21.081	20.389	5.3466	5.5116	5.3897
f_5	20	10.978	11.365	11.046	42.540	45.628	43.292	10.963	11.142	11.020
	30	18.952	19.527	19.111	67.587	68.456	67.966	16.836	17.379	16.946
	10	7.3361	7.5628	7.4105	17.390	18.976	17.625	2.8161	3.1559	2.9904
f_6	20	16.313	18.324	16.969	36.411	36.921	36.571	7.5515	9.2466	8.3519
	30	26.438	27.345	26.775	57.383	58.159	57.659	15.299	16.866	16.062
	10	7.2599	7.5470	7.3308	18.130	18.249	18.173	3.0408	3.0941	3.0561
f_7	20	15.388	15.848	15.520	38.187	38.331	38.248	6.2228	6.3651	6.2526
	30	24.111	24.676	24.213	60.330	61.086	60.650	9.4868	9.6724	9.5449

5. Conclusion

This paper compared the performance of the three algorithms in terms of accuracy and convergence speed. We have used basic versions of these algorithms without finely tuning the parameters to compare the results. From simulation results, it is turned out that, ABC algorithm gives the best result and firefly algorithm has a faster convergence speed. Although these algorithms have some difficulties with higher multimodality, it can be concluded that, these difficulties can be overcome by some modification or improvement of the algorithms and some extensive parametric studies.

References

[1] A.E. Eiben, J.E. Smith, Introduction to Evolutionary Computing. *Springer-Verlag, Berlin*, (2003).

[2] G. Beni, J. Wang, Swarm Intelligence in Cellular Robotic Systems, *Proceed. NATO Advanced Workshop on Robots and Biological Systems, Tuscany, Italy*, June 26–30, (1989).

[3] G. Hadley, Nonlinear and Dynamics Programming, *Addison Wesley, Reading, MA* (1964).

[4] D. Karaboga, An idea based on honey bee swarm for numerical optimization, *Technical Report-TR06,Erciyes University, Engineering Faculty, Computer Engineering Department*, (2005).

[5] D. Karaboga, B. Basturk, A powerful and efficient algorithm for numerical function optimization: Artificial bee colony (ABC) algorithm, *Journal of Global Optimization*, 39-459-471,(2007).

[6] X. S. Yang, Firefly Algorithm, Stochastic Test Functions and Design Optimization, *Int. J. Bio-Inspired Computation*, Vol. 2, No. 2, pp.78–84 (2010).

[7] X. S. Yang, Nature-Inspired Metaheuristic Algorithms, *Luniver Press*,(2008).

[8] X. S. Yang, J. R. Gonzalez et al., A New Metaheuristic Bat-Inspired Algorithm, Nature Inspired Cooperative Strategies for Optimization (NISCO 2010), *Eds., Springer Press*, vol. 284, pp. 65-74, (2010).

[9] X. S. Yang and A. H. Gandomi, Bat Algorithm: A Novel Approach for Global Engineering Optimization, *Engineering Computations*, Vol. 29, Issue 5, pp.464 – 483,(2012).

[10] Marcin Molga, Czesław Smutnicki, Test functions for optimization needs, *3 kwietnia* (2005).

ICMIEE-PI-140177

Study of Lean facility Layout in Garment Manufacturing Process: Focusing Sewing Section of Men's Shirt

M. N. Shakib, M.M. Rahman, M. S. Parvez[*]*, A.S.M. Haque*
Department of Industrial & Production Engineering, Jessore University of Science & Technology, Jessore-7408, BANGLADESH

ABSTRACT
Facility layout is a settlement of machine, storage areas or work areas within the confines of a physical structure to increase the production rate. It is estimated that 20% to 40% production cost can be reduced by proper arrangement of machine, storage areas or work areas. By developing a good layout arrangement it can be possible to reduced bottlenecks in moving people or material, minimize material handling cost, reduced hazards to personnel, utilize labor efficiency, trim down idle time, make the most of available space effectively and efficiently and provide flexibility. Many researches have been done to get optimum arrangement of layout design. Here we specially perform Time Study, Learning curve, Waste identification of the line to get optimum target, and output, capacity of operator and to find the optimum arrangement of man, machine, and material of the production line.

Keywords: Facility layout, Learning curve, Time study.

1. Introduction

In current world the garments industries is led by fashion and gives emphasis on the use of modern technology. In modern civilized world the clothing industries has created a great application particularly in the emerging countries due to the increasing labor wage in developed countries, the apparel manufacturing has been transferring from the high pay developed countries to low pay developing countries. By purpose of low labor cost of Bangladesh before now gets a foremost position in this sector. This sector contributes about three-fourth of the national export earnings of Bangladesh. Garments sectors are one of the leading job sources to the employee of the country. The working environment of garments are not satisfactory, the industries are ran in such an environment that they are the victim of low labor utilization low labor productivity, high WIP, excessive manufacturing lead times, huge amount of waste and higher manufacturing cost. Garment Industries in developing countries are low intensive on labor productivity than other issues like sourcing of raw material and minimizing delivery cost because of the availability of cheap labor and its result is low labor productivity than developed countries. For example, efforts are very reasonable in Bangladesh but the productivity is poor among other developing countries [1]. Many Industries want higher productivity from labor without paying standard wage and incentives but they become fail to improve productivity because it is not a motivating factor to the workers. Even today the garments of developing countries are familiar to work with similar styles but numbers of styles are increasing rapidly with the revolution of fashion world. This becomes the new challenge for the garments industries. The garment industries are accustomed to work with same style and large volume product. But nowadays due to small order quantities and complex designs, the garment industry has to produce multiple styles even within a day; this needs higher flexibility in volume and style change over [2].In developing countries it is seen that they have rarely used modern technology and lean application because they maintain the traditional way to run the organization. Majority of them don't know the benefit of lean application and the also have no sufficient knowledge about lean tools and they also hesitate to employ industrial engineer as well as textile engineer with handsome amount of money and facilities. Such kind of traditional motive is one of the major obstacles for the garments industries in developing countries to strive with the rising challenges and also for attaining higher efficiency with work friendly environment.

2. Literature view

Lean Manufacturing is not exclusively new. This term derives from the Toyota Production System or Just, Henry Ford and other predecessors. Eli Whitney is most prominent as the originator of the cotton gin. Nevertheless, the gin was an insignificant achievement compared to his perfection of substitutable parts. Whitney established this about 1799 when he took a agreement from the U.S. Army for the manufacture of 10,000 muskets at the extraordinarily low price of $13.40 each. For the next 100 years manufacturers predominantly alarmed themselves with specific technologies. Throughout this time our scheme of engineering drawings settled, modern machine tools were completed and large scale processes such as the Bessemer process for making steel held the center of courtesy [3].Frederick W. Taylor [4] instigated to look at separate workers and work methods. The outcome was Time Study and standardized work. He called his concepts Scientific Management. Taylor was a provocative figure. The idea of applying science to management was comprehensive but Taylor simply

* Corresponding author. Tel.: +88-01827486660
E-mail address: sparvez.ipe@gmail.com

overlooked the behavioral sciences. In accumulation, he had a strange attitude towards factory workers [5]. Frank Gilbreth (Cheaper by the Dozen) added Motion Study and invented Process registering. Process charts fixated care on all work elements including those non-value added elements which generally occur between the "official" elements. Starting about 1910, Ford and his right-hand-man, Charles E. Sorensen, shaped the first inclusive Manufacturing Strategy. They took all the elements of a manufacturing system-- people, machines, tooling, and products-- and organized them in a nonstop system for manufacturing the Model T automobile. Ford was so unbelievably successful he rapidly became one of the world's richest men and placed the world on wheels. Ford is painstaking by many to be the first expert of Just in Time and Lean Manufacturing. Ford's success stimulated many others to copy his methods. But maximum of those who copied did not recognize the basics. Ford assembly lines were frequently engaged for products and processes that were inapt for them. At Toyota Motor Company, Shigeo Shingo and Taichii Ohno initiated to integrate Ford production and additional techniques into a method called Toyota Production System or Just in Time [6]. They documented the inventory. The Toyota people also familiar with the Ford system had contradictions and shortcomings, predominantly with respect to employees. With General Douglas MacArthur actively encouraging labor unions in the occupation years, Ford's punitive boldness and demeaning job structures were unworkable in post-war Japan. They were also impracticable in the American context, but that would not be apparent for some years. America's "Greatest Generation" carried over arrogances from the Great Depression that made the system work in spite of its defects. Toyota shortly exposed that factory workers had distant more to subsidize than just muscle power. This sighting perhaps created in the Quality Circle movement. Ishikawa, Deming, and Juran all completed main contributions to the quality movement. In this manner, small production runs started by Toyota became a advantage relatively than a burden, as it was able to reply much more rapidly to changes in demand by quickly substituting production from one model to another [8].Toyota didn't depend on the economies of measure production like American companies. It somewhat developed a culture, organization and operating system that uncompromisingly followed the elimination of waste, variability and inflexibility. To achieve this, it focused its operating system on responding to demand and nothing else. This in turn means it has to be flexible; when there are changes in demand, the operating system is a steady workforce that is required to be much more skilled and much more flexible than those inmost mass production systems. Over time, all these elements were associated into a new method to operations that shaped the foundation of lean or Toyota production System.

3. Methodology

To achieve optimum productivity by balancing the production line well here we performed Time study, Motion study, Root cause analysis Learning Curve as a part of our research work. By doing this we become able to know the actual capacity of the worker, the improvement of operators performance with time, the actual allowance time of the worker, the person who is actually responsible for the defects of the part, the reasons behind the dissimilarity of motion and so on. All of these helps to fix better scheduling, balancing line according to the operators capacity and operation sequence, reducing workers waiting time, speed up to the production line, to fix actual allowable allowance of time. By doing this, stitching operations will be standardized and production targets for each operation will be fixed. Furthermore, batch processing is transformed into single piece movement by the allegation of new layout. This will serve the purpose of WIP reduction. For the ease of operator movement between machines, sitting operations were converted into standing. The worker multi-skilling is achieved by the concept of assembly line balancing. As in cellular manufacturing the numbers of operators are less than the number of operations (machines), one operator has to perform at least three to four operations. This will help to increase operator skill. Finally, flexibility in production is achieved by reduced WIP and multi-skilled operators, who can work on multiple styles immediately.

3.1 Root Cause Analysis

The principle of root cause analysis is to sock at the root of a crisis by pronouncement and influential its root causes. Root cause analysis is "a group of problem solving methods intended at identifying the root causes of problems or measures or so on [7]. The carry out of root cause analysis is predicated on the certainty that problems are greatest solved by attempting to exact or reduce root causes, as opposed to simply addressing the directly observable symptoms."Our essential rule is the only way to explain a complicated problem is to determine its root causes. Various major problems are founded by analyzing root causes that are shown in Table 1.

Table 1: Major problem In Sewing Section

SL. Name	Problem Name
1	Skipped Stitch
2	Broken Stitch
3	Loose Tension
4	Uneven Stitch
5	Run Off Stitch
6	Slanted
7	High/Low
8	Puckering
9	Crooked
10	Overlap
11	Incomplete

12	Visible Joint
13	Wrong SPI
14	Spot
15	Oil Mark
16	Twisting
17	Label Mistake
18	Visible Top Stitch
19	Color Bone Make Uneven
20	Color Shading

By applying root cause Analysis method majority of this problem can be reduced in a significant amount which will give flexibility to balancing a line well as well as to ensure optimum productivity with defect free units and it will save huge amount of production time.

3.2 Learning Curve

A learning curve is a graphical representation of the increase of learning (vertical axis) with experience (horizontal axis). Learning curve is an industrial tool which has direct and indirect relationship with line balancing as well as facility layout [9]. Learning curves are mathematical models used to estimate efficiencies gained when an activity is repeated. The "learning effect" was first noted in the 1920s in linking with aircraft production. Learning curves draw from historic building practice to decide expected reductions in labor and materials costs. Expected reductions can be determined from the labor and materials content of the manufactured item, plus the number of repetitions of the initial production run. Cost estimate need to reflect the observed characteristic that costs will vary in proportion to the quantity produced. Now a days, learning curves are considered as an important tool or formula in garments industries for better scheduling, line balancing, capacity planning, etc. All of these ensure optimum productivity of the industries. The underlying view behind learning curves is that when people individually or collectively repeat an activity, there tends to be a gain in efficiency. Generally, this depicts the form of a decrease time required for doing the activity. Because cost is generally related to time or labor hours consumed, learning curves are very important in industrial cost analysis. A key idea underlying the theory is that every time the production quantity couples, we can expected a more or less fixed percentage decrease in the strength required to build a single unit (the Crawford theory), or in the average time required to build a group of units (the wright theory). These reductions occur not in big jumps, but more or less smoothly as production continue. Learning tends will be "lost" when there is a break in repetitions of the activity, or a change in the nature of the activity. The usual use of learning curves is to assessment the labor time and thereby cost of labor of a manufactured item that is made in significant quantities. Besides learning curve is used for designing of the manufacturing work force, and valuing costs of production when same tasks are repeated. Here we work with learning curves at some specific operation of a line in a garments industries and comparing these curves with ideal curve. Here we work with learning curves at some specific operation of a line in a garments industries and comparing these curves with ideal curve. The curve from the practical experience are shown in Fig.1

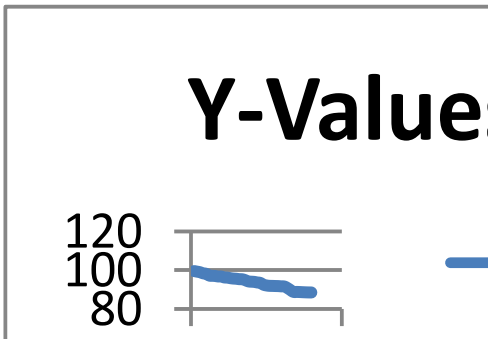

Fig.1 The curve obtained from the practical experience**.**

3.3 Waste Identification

We know that generally there are seven wastes are found in the working areas. In our research we found that all of these waste are not equally present and rise as a vital waste in one working areas. By this way we have identified some of the major waste which consists on our research areas, these are:

- Worker's waiting for raw material, information and machinery.
- Defective parts made by the operators.
- Unnecessary transportation.
- Over processing.

Excess idle time of the operators can also be considered as a waste. Here we perform experiment over two types of waste like waiting time and idle time. Major waste in the existing line are shown in Fig.2.

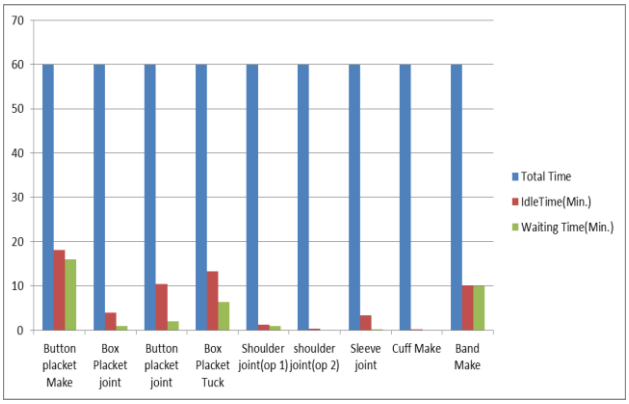

Fig.2 Major waste in the existing line (total time versus waiting & Idle time)

3.4 Time Study

The time study is conducted in a selected certain line whose product is Men's Formal Shirt because operations differ from style to style and it is difficult to correlate all these operations of individual styles. After that, at least two or three operators were selected for each operation so that the difference in timing can be cross checked from the experiential data of these two operators. To get better results, each operation time is taken for at least 5 cycles. Once time study is made by collecting raw data the performance rating is given to each operator and actual time is calculated for particular operation. Finally the Personal Fatigue and Delay (PFD) component is added on the calculated time and the operation time is identical. While conducting time study some parameters are kept fixed (for example machine speed, stitches per inch, type of machine used etc.) to get consistent results. The PFD factor is taken as 12%-15% of total time depending on the types of operation. This PFD is a little bit higher than normal industry standard; it is taken higher considering the standing operation and operator's movement inside the cell. Performance rating is also taken as the average of the performance of the 5 cycles.

3.5 SAM/SMV

Standard Allowed Minute (SAM) is used to measure task of a garment. SAM widely used by production people and industrial engineers in the garment manufacturing industry. SAM value plays a very important role for the estimation of cost of making a garment.

Standard Minute Value (SMV) = NT (1+ AF)

Normal Time (NT) = (Average Cycle Time) x (Rating Factor)

Process Target = 60/SMV

Operation Name	Machine Name	Cycle time	21.00	22.67	18.76	21.01	21.10	Allowance	Avg. cycle time	Avg. Rating
Collar Make	SNLS	Rating	1	0.97	1.05	1	1	13%	20.908	1.004

SMV = NT (1+AF)

= 20.908*1.004(1+13%)

=23.29/60 = 0.40

So, the process target = 60/0.40 = 150

3.6 Proposed Layout

From our experiment we become able to identify the problem or obstacle, the operator's capacity, the root cause of the defect and the major waste of the of the existing production line layout. By considering these problem we can proposed a significant layout for the production line with a view to solving the existing problem and for getting higher productivity as well as optimum productivity. Here we proposing cellular U-Shaped layout by considering the problem of the existing layout of the production line. In figure we have showed the proposed layout for the output section and the other two sections like make and output section will be arranged similarly according to the capacity of the operators, sequence of the operations and the types of machines. Proposed layout is shown in Fig.3.

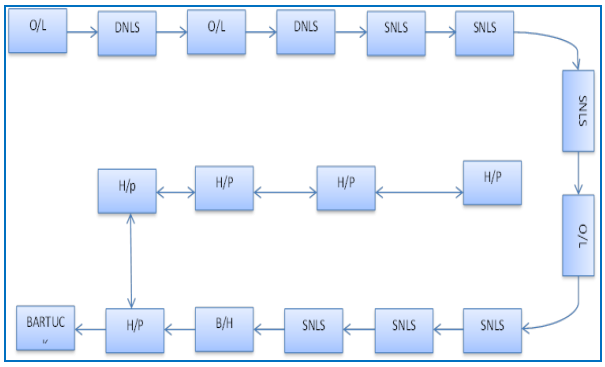

Fig.3 The proposed layout (output section)

Present capacity of the existing manufacturing systems which are summarized in table.2

Table 2

SL.	Operation	Manpower	M/C	SMV(Min)	Present Capacity
1	FRONT JOINT	1	O/L	.35	173
2	FRONT JOINT THREAD CUT	1	H/P	.18	325
3	SHOLDER TOP STITCH	1	DNLS	0.43	139
4	SLEEVE JOINT	1	O/L	o.3o	190
5	SLEEVE JOINT THREAD CUT	1	H/P	0.1	348
6	ARMHOLL	2	DNLS	0.45	270
7	ARMHOLL THREAD CUT	1	H/P	0.23	261
8	COLLER BODY MATCH	1	H/P	0.30	202
9	COLLER JOINT	1	SNLS	0.29	208
10	COLLAR HALA MARK	1	H/P	0.18	326
11	COLLAR TOP STITCH	1	SNLS	0.4	147
12	COLLAR TOP STITCH THREAD CUT	1	H/P	0.25	244
13	CIRE LABEL JOINT	1	SNLS	0.23	261
14	SIDE JOINT	2	O/L	0.71	170
15	SIDE JOINT THRED CUT	3	H/P	0.62	291

16	SAFETY STITCH	2	SNLS	0.51	234
17	CUFF+BODY MATCH	2	H/P	0.33	368
18	CUFF JOINT	2	SNLS	0.62	192
19	CUFF JOINT THREAD CUT	1	H/P	0.34	186
20	HEM	1	SNLS	0.67	89
21	HEM THREAD CUT	2	H/P	0.47	254
22	BUTTON HOLE	2	B/H	0.78	175

4. Result and Discussion

By considering the international demand and the rapid growth of garments in Asian country especially in Bangladesh, the lean facility layout can be a powerful tool of lean manufacturing. In the sewing floor of a RMG industry, to ensure a perfect environment must implement various layout tools to obtain the benefits of lean manufacturing as well as lean facility layout. Lean facility layout has a great influence in garments sectors. As the lean manufacturing reduces wastes that do not add any value to the product, it supports to reduce the manufacturing cost and increase productivity by increasing the labor utilization. Minimize manufacturing cost, increase productivity, maximize interest is the main motto of every manufacturing industries. If the labor utilization increases, a factory can save a handsome amount of cost annually; this will help the factory to exist in the competitive business world. In our research we are enabled to practically work in a garments where we observed the practical environment of a garments especially the practical environment of the sewing floor and we have conducted our research on sewing line by applying some useful lean techniques like Lean facility layout, Seven waste, Learning curve, Root cause analysis, SAM calculation. By these kinds of experiments we become able to know more about layout, the problems of a line, capacity of workers, learning rate of workers.

5. Conclusions and future works

The research is performed based on the practical experiment by using some lean techniques, find out the barriers of the existing line and try to solve these obstacles by applying right techniques right place. The authors feel that these objectives have been accomplished. The sewing floor of a ready-made garment industry is an ideal environment to introduced lean manufacturing tools as well as lean facility layout. From our research we become able to realize that the proper arrangement of layout has a great influence at the improvement of factory performance like better utilization of workers, higher productivity, smooth flow of task, reduce waste, balancing operators capacity and so on.

This research is limited to the only sewing section of the garments industry, but the lean facility layout can be studied and implemented in other areas of the shop floor of the garments like finishing, cutting, warehouse. In cutting section we can save a significant amount of fabrics by arranging the marker 'layout significantly. Allowance is taken as workers fatigue, motion variation, machinery problem and the factory maintain a standard without calculation but the allowance may vary with the types of fabrics. The line balancing is made as per manual calculation and assuming every operator knows at least three to four operations of individual cells, but operators may not essentially know this much operation confidently. This may cause imbalance of the line so while selecting operator for the particular cell it is necessary to check whether the operator is suitable for that work or not because the cell will perform best if all the group members have the same skill level. If it is not maintain then it will be very difficult to balance line. Performance rating of operators and helper has no mathematical equation; it is measured during time when cycle time is taken. This measurement may not be 100% correct because it is difficult to identify the performance of man. . In organization, manager need better knowledge about the capacity of the workers, problems in the line, future challenges. To gain these he should use the lean tools in the organization and also should try to improve the application of these tools. In this research the lean facility layout is experimented and tried to implement to improve productivity but this can be possible more significant by implementing group incentives and reward system. In this way we can use some motivation theory given by Gant and Gilbert, Taylor, Merrick, Henry Fayal and so on.

REFERENCES

[1]Shahidul, M. I. and Syed Shazali, S. T. Dynamics of manufacturing Productivity: Lesson Learnt from Labor Intensive Industries. Journal of Manufacturing Technology Management Vol. 22 No. 5, 2011, p. 664-678.

[2] Shahram, T. and Christian, M. The Impact of Lean Operations on the Chinese Manufacturing Performance. Journal of Manufacturing Technology Management Vol. 22 No. 2, 2011, p. 223-240.

[3] Crute, V., Ward, Y., Brown, S. & Graves, A. 2003, "Implementing Lean in aerospace - challenging the assumptions and understanding the challenges", Technovation,vol.23,no.12,pp.917-928.

[4] Taylor, F., The Principles of the Scientific Management, New York: Norton, 1967.

[5] Ana Valentinova Kovacheva (January 2010, Aarhus): Challenges in Lean implementation.

[6] Mid-America Manufacturing Technology Center, 'Lean Manufacturing Utilizes Multiple Tools to Help Companies Improve Performance Objectives, 'The Manufacturer's Edge. (winter 2000), p 1-2.

[7] Buffa, E.S., Sarin, R.K. (2002), *Modern Production operations and management*, 8th edition, Gopsons Paper Ltd., India, pp. 484, 672-674.
[8] Drew, J., Blair, M. and Stefan, R. (2004). Journey to Lean: Making Operational Change Stick. Gordonsville, VA, USA: Palgrave Macmillan. p. 5-25.
[9]USA,E.stumpP.E.,http://www.galorath.com/images/uploads/Learning Curves.

.

ICMIEE-PI-140179

Analysis of Renewable Sources as a Solution to Power Crisis in Bangladesh

*Molla Shoyeb Uddin Mithu[*1], Md Shafayate Hossain[2], Md Enamul Haque[3], Mohammad Didarul Alam[4], Hasan Shahriar Simanto[5], Sheikh Tanveer Hossaim[6]*

Department of Mechanical Engineering, Khulna University of Engineering & Technology, Khulna-9203, BANGLADESH

ABSTRACT
The incisive power crisis problem in Bangladesh can be solved through proper implementation of renewable energy technologies. Although Bangladesh is blessed with all types of renewable energy sources, still now renewable energy has not been given priority as a possible solution to power crisis. Existing sources like solar energy, wind energy, hydropower and potential sources like geothermal energy, wave energy, energy from the Bay-of Bengal have been discussed at a detailed manner here in this paper so that maximum possible energy can be extracted through these using the available subsisting technologies. Technology overview, cost analysis and implementation technique get circumstantial interpretation throughout the paper.
Keywords: Power crisis, renewable sources, implementation

1 INTRODUCTION

Renewable energy is generally defined as energy that comes from resources which are naturally replenished on a human timescale such as sunlight, wind, tides, waves and geothermal heat. Renewable energy replaces conventional fuels in four distinct areas: electricity generation, hotwater/spaceheating, motorcycle and rural energy services. About 16% of global final energy consumption presently comes from renewable sources with10 % of all energy from traditional biomass, mainly used for heating, and 3.4% from hydroelectricity. New renewables (small hydro, modern biomass, wind, solar, geothermal, and biofuels) account for another 3% and are growing rapidly. Although Bangladesh have all the above mentioned sources existing, its power generation from renewable sources stands below. The analysis of renewable sources can be an alternative solution to the acute problem of power crisis in Bangladesh.

2 PRESENT ENERGY SITUATION IN BANGLADESH

Bangladesh's energy infrastructure is quite small, insufficient and poorly managed. The per capita energy consumption in Bangladesh is one of the lowest (321 kwh) in the world. Noncommercial energy sources, such as wood fuel, animal waste, and crop residues, are estimated to account for over half of the country's energy consumption. Bangladesh has small reserves of oil and coal, but very large natural gas resources. Commercial energy consumption is mostly natural gas (around 66%), followed by oil, hydropower and coal.

Electricity is the major source of power for most of the country's economic activities. Bangladesh's installed electric generation capacity was 10289 MW in January, 2014; only three-fourth of which is considered to be 'available'. Only 62% of the population has access to electricity with a per capita availability of 321 kWh per annum which is interrupted by power cut.

3 RENEWABLE ENERGY POTENTIAL IN BANGLADESH

Bangladesh is expected to have enormous potentiality in renewable energy development. Country is blessed by considerable solar radiation. Bangladesh receives an average daily solar radiation of 4-6.5 kWh/m2. Solar photovoltaic (PV) are gaining acceptance for providing electricity to households and small businesses in rural areas. Development of off-grid solar home solutions has achieved international benchmark. According to a survey, there is an existing market size of 6 million households for Solar Home Systems (SHS) on a fee-for-service basis in the off-grid areas of Bangladesh.

Table-1: Renewable energy situation in Bangladesh

	Category	Achievement
1.	SHS	150 MW
2.	Solar Irrigation	1 MW
3.	Roof Top solar PV at Government, Power sector office buildings and at newly constructed buildings	14 MW
4.	Wind Energy	2 MW
5.	Biomass based	<1 MW

* Corresponding author. Tel.: +88-01739522330, +88-01979522330
E-mail address: shoyeb.msum.mithu479@gmail.com

	electricity	
6.	Biogas based electricity	5 MW
7.	Hydro power	230 MW
	Total	**403 MW**

Potential of Wind Energy is mainly in coastal areas and offshore islands. Bangladesh has strong potential for biomass gasification based electricity. More common biomass resources available in the country are rice husk, crop residue, wood, jute stick, animal waste, municipal waste, sugarcane bagasse etc. Exploration of these resources for electricity generation is still at preliminary stage. Potentials for utilizing biogas technologies derived mainly from animal, kitchen and municipal wastes may be one of the promising renewable energy resources for Bangladesh.

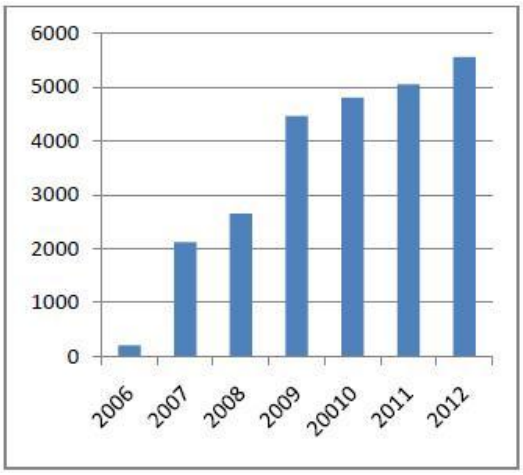

Fig-1:Biogas plants construction in Bangladesh

4 OVER VIEW ON DIFFERENT RENEWABLE ENERGY SOURSES IN BANGLADESH

4.1 BIOPOWER

Biopower, or biomass power, is the use of biomass to generate electricity. It is the third largest form of renewable electricity generation after hydropower and wind energy, and is a mature source of renewable power, with costs on par with conventional fossil energy plants. Electricity produced from biomass can be used as base-load or dispatchable power in the existing electric power sector and in industrial cogeneration.

4.1.1 Resources: Potential biopower resources – wood wastes, mill residues, forest residues, agricultural residues, cattle residues, and dedicated harbecious and woody energy crops are widely distributed through out the country.

4.1.2 Technology overview: Biopower technologies include those that directly combust biomass (direct-fired biomass and co-firing) in a furnace to produce steam that is used in a steam turbine generator (STG) and those that convert solid biomass to an intermediate gas or liquid that is then used in a prime mover to produce electricity.

Biopower system technologies include direct firing fired combustion, co-firing, gasification, pyrolysis, landfill gas generators, and anaerobic digestion generators. RE Futures investigated opportunities for additional technology improvements that can lead to reduced cost, focusing on increasing system efficiencies by combining direct combustion technologies with gasification technologies to produce a dynamic mixed fleet that gradually includes more gasification technologies.

The most important issue for large-scale deployment of biopower is feedstock competition with lignocellulosic biofuels and other uses for wood. In addition to the known air and water quality environmental issues associated with permitting and operation of biopower plants, the primary environmental issues that must be addressed for biopower are overall sustainability and land use change impacts resulting from growing dedicated biomass feedstocks to support large-scale deployment of biopower technologies. Proactive strategies to reduce capital and operating costs for early-generation systems, reduce uncertainty in feedstock cost and supply, standardize policies and incentives, and improve and standardize codes and standards are needed to maximize biopower's contribution to a high-renewable electricity future.

4.1.3 Technology cost and performance: Future capital cost, performance (generally represented as capacity factor or heat rate), and operating costs of electricity generating technologies are influenced by a number of uncertain and somewhat unpredictable factors. As such, to understand the impact of renewable energy technology cost and performance improvements on the modeled scenarios, two main projections of future renewable energy technology development can be evaluated: (1) renewable electricity-evolutionary technology improvement (RE-ETI) and (2) renewable electricity-incremental technology improvement (RE-ITI). In general, RE-ITI estimates reflect only partial achievement of the future technical advancements and cost reductions that may be possible, while the RE-ETI estimates reflect a more complete achievement of that cost-reduction potential considering only evolutionary improvements of currently fewer commercial technologies.

4.2 GEOTHERMAL ENERGY

Geothermal (meaning "earth heat") energy involves using the high temperatures produced beneath the earth to generate electricity from heated water, as well as for various direct uses (such as hot springs spas, lumber drying or aquaculture). The term geothermal is also

applied to the temperatures of the Earth near the surface which are used as a source of consistent temperatures for heating and cooling of buildings. Geothermal applications that involve water heated within the earth are also called hydrothermal processes.

Table-2: Geothermal gradients as noted in some deep wells of Bangladesh

Well Name	**Depth (Km)**	**Gradient (K/km)**
Hazipur	3,816	30,9
Bakhrabad	12,837	25.0
Titas	13,758	30,1
Habigonj	13,509	31,16
Rashidpur	13,851	26,8
Biyanibazar	14,107	28,7
Kailas Tila	14,139	27,8
Sylhet	12,377	31,1
Chhatak	12,33	33,8
Semutang	14,88	30,3

4.2.1 Resources: Naturally occurring large areas of hydrothermal resources are called geothermal reservoirs. Most geothermal reservoirs are deep underground with no visible clues showing above ground. But geothermal energy sometimes finds its way to the surface in the form of: volcanoes and fumaroles (holes where volcanic gases are released), hot springs, geysers. Most Geothermal Resources Are Near Plate Boundaries. The most active geothermal resources are usually found along major plate boundaries where earthquakes and volcanoes are concentrated. Most of the geothermal activity in the world occurs in an area called the Ring of Fire. This area encircles the Pacific Ocean.
When magma comes close to the surface, it heats ground water found trapped in porous rock or water running along fractured rock surfaces and faults. These features are called hydrothermal. They have two common ingredients: water (hydro) and heat (thermal). Geologists use various methods to look for geothermal reservoirs. Drilling a well and testing the temperature deep underground is the most reliable method for finding a geothermal reservoir.

4.2.2 Technology overview: Geothermal power plants use steam produced from reservoirs of hot water found a couple of miles or more below the Earth's surface. There are three types of geothermal power plants: *dry steam*, *flash steam*, and binary *cycle*.

Dry steam power plants draw from underground resources of steam. The steam is piped directly from underground wells to the power plant, where it is directed into a turbine/generator unit. There are only two known underground resources of steam in the United States: The Geysers in northern California and Yellowstone National Park in Wyoming, where there's a well-known geyser called Old Faithful. Since Yellowstone is protected from development, the only dry steam plants in the country are at The Geysers.

Flash steam power plants are the most common. They use geothermal reservoirs of water with temperatures greater than 360°F (182°C). This very hot water flows up through wells in the ground under its own pressure. As it flows upward, the pressure decreases and some of the hot water boils into steam. The steam is then separated from the water and used to power a turbine/generator. Any leftover water and condensed steam are injected back into the reservoir, making this a sustainable resource.

Binary cycle power plants operate on water at lower temperatures of about 225°-360°F (107°-182°C). These plants use the heat from the hot water to boil a *working fluid*, usually an organic compound with a low boiling point. The working fluid is vaporized in a *heat exchanger* and used to turn a turbine. The water is then injected back into the ground to be reheated. The water and the working fluid are kept separated during the whole process, so there are little or no air emissions.

Small-scale geothermal power plants (under 5 megawatts) have the potential for widespread application in rural areas, possibly even as distributed energy resources. Distributed energy resources refer to a variety of small, modular power-generating technologies that can be combined to improve the operation of the electricity delivery system.

4.2.3 Technology cost and performance: The capital costs for geothermal power plant projects are normally broken down by project phase: resource identification (permitting, leasing, surface and non-drilling exploration); drilling (exploration, confirmation, and production well drilling); and power plant construction. Hydrothermal costs vary widely. In general, the LCOE for hydrothermal projects typically range from $60/MWh to $90/MWh but can range from $40/MWh to $150/MWh depending on the resource characteristics and project development finance structure.

4.3 HYDROPOWER

Flowing water creates energy that can be captured and turned into electricity. This is called hydroelectric power or hydropower.

The most common type of hydroelectric power plant uses a dam on a river to store water in a reservoir. Water released from the reservoir flows through a turbine, spinning it, which in turn activates a generator to produce electricity. But hydroelectric power doesn't necessarily require a large dam. Some hydroelectric power plants just use a small canal to channel the river water through a turbine.

Another type of hydroelectric power plant - called a pumped storage plant - can even store power. The power is sent from a power grid into the electric generators. The generators then spin the turbines backward, which causes the turbines to pump water from a river or lower reservoir to an upper reservoir, where the power is stored. To use the power, the water is released from the upper reservoir back down into the river or lower reservoir. This spins the turbines forward, activating the generators to produce electricity.

A small or micro-hydroelectric power system can produce enough electricity for a home, farm, or ranch.

4.3.1 Implementation in Bangladesh: Micro Hydro Power Plants can be installed in the north-eastern hilly regions and in the existing irrigation canal system with sufficient head. Currently there is a Micro Hydro Power Plant with a 50 kW generator at Barkal area of Rangamati district implemented by the Bangladesh Power Development Board (BPDB). A larger hydroelectric plant was built in the Kaptai region using the Karnaphuli river during the 1960s, and was Bangladesh's only hydroelectric power plant for a long time. It is capable of producing a total of 230 MW of electricity.

4.4 OCEAN ENERGY: ENERGY FROM BAY OF BENGAL

The ocean can produce two types of energy: thermal energy from the sun's heat, and mechanical energy from the tides and waves. Oceans cover more than 70% of Earth's surface, making them the world's largest solar collectors. The sun's heat warms the surface water a lot more than the deep ocean water, and this temperature difference creates thermal energy. Just a small portion of the heat trapped in the ocean could power the world. Ocean thermal energy is used for many applications, including electricity generation. There are three types of electricity conversion systems: closed-cycle, open-cycle**,** and hybrid. Closed-cycle systems use the ocean's warm surface water to vaporize a working fluid, which has a low-boiling point, such as ammonia. The vapor expands and turns a turbine. The turbine then activates a generator to produce electricity. Open-cycle systems actually boil the seawater by operating at low pressures. This produces steam that passes through a turbine/generator. And hybrid systems combine both closed-cycle and open-cycle systems. Ocean mechanical energy is quite different from ocean thermal energy. Even though the sun affects all ocean activity, tides are driven primarily by the gravitational pull of the moon, and waves are driven primarily by the winds. As a result, tides and waves are intermittent sources of energy, while ocean thermal energy is fairly constant. Also, unlike thermal energy, the electricity conversion of both tidal and wave energy usually involves mechanical devices. A barrage (dam) is typically used to convert tidal energy into electricity by forcing the water through turbines, activating a generator. For wave energy conversion, there are three basic systems: channel systems that funnel the waves into reservoirs; float systems that drive hydraulic pumps; and oscillating water column systems that use the waves to compress air within a container. The mechanical power created from these systems either directly activates a generator or transfers to a working fluid, water, or air, which then drives a turbine/generator.

4.4.1 Resources: Bangladesh is blessed to be situated on the shore of Bay-of Bengal. So enormous amount of renewable energy can be extracted from the sea in following form:

(A) Natural Wave Energy: Ocean waves can be considered as a form of solar energy because they are formed by the far-field interaction of ocean surfaces and wind currents, which in turn, are the result of differential heating of Earth's surface. There is greater wave resource on the coast of Bay of Bengal.

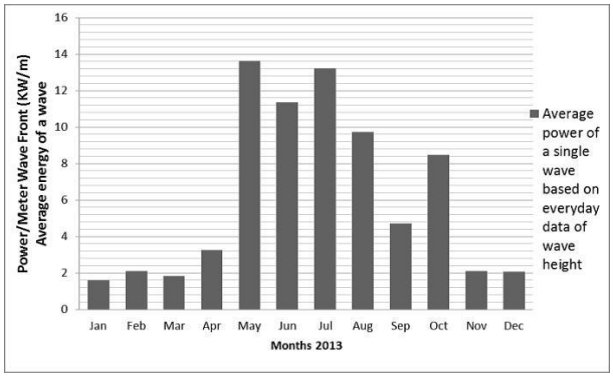

Fig-2: Average power of a wave based on everyday data of significant wave height in the year of 2013.

(B) Natural Tidal Energy: The current approach for computing the natural tidal energy resource at a site is to estimate the mean natural kinetic energy of the flow

through the channel at the site of interest without considering the interaction of the flow and the device. The natural tidal energy is then taken as some fraction of this mean energy accounting for any known access restrictions.

(C) Natural Ocean Current Energy: An ocean current is a continuous, directed movement of ocean water generated by the forces acting upon the mean flow, such as breaking waves, wind, Coriolis force, temperature and salinity differences, and tidal forces.

(D) Ocean Thermal Energy: Ocean thermal gradient energy is created by a temperature difference between surface water and deep water in the ocean. OTEC requires a temperature difference of approximately 20°C for practicable generation. Basically it may be a great source of energy because the required temperature difference can be easily maintained at the Bay of Bengal.

(E) Salinity Gradient Energy: At the mouth of rivers where freshwater mixes with saltwater in the ocean, energy is released from the mixing, resulting in a very small increase in the local temperature of the water. Actually research is undergoing on this but the salinity gradient conversion is discussed here for complete coverage of ocean energy technologies.

4.5 SOLAR ENERGY

Solar energy is radiant light and heat from the sun harnessed using a range of ever-evolving technologies such as solar heating, solar photovoltaics, solar thermal electricity, solar architecture and artificial photosynthesis.

4.5.1 Solar Energy in Bangladesh: Solar energy is the most easily available renewable source of energy in Bangladesh which can be implemented at comparatively low cost in a huge amount. The long term average sunshine data indicates that the period of bright sunshine hours in the coastal regions of Bangladesh varies from 3 to 11 hours daily.

The insolation in Bangladesh varies from 3.8 kwh/m2/day to 6.4 kwh/m2/day at an average of 5 kwh/m2/day. These indicate that there are good prospects for solar thermal and photovoltaic application in the country.

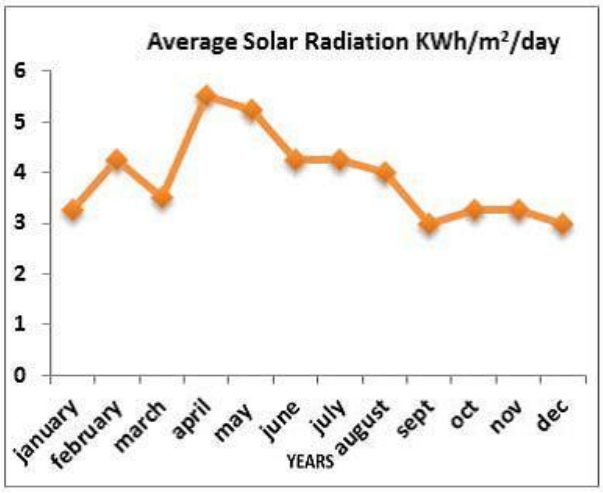

Fig-3: Monthly average solar radiation profile in Bangladesh

4.5.2 Technology Overview

(A) Solar photovoltaics: Photovoltaic technologies convert sunlight directly into electricity by enabling solar photons to "excite" electrons from their ground state, producing a freed (photo-excited) electron and a "hole" pair. The electron and hole are then separated by an electric field that is formed by the design of the PV cell and pulled toward positive and negative electrodes, generating DC electricity.

(B) Concentrating Solar Power: CSP technologies use mirrors or lenses to focus sunlight onto a receiver. The receiver contains a working fluid,78 which transfers the thermal energy to a heat engine that drives an electrical generator.

(C) Other Solar Technologies: Several additional solar technologies—including water heating, space heating, cooling, and lighting—do not generate electricity but do displace end-use electricity and fossil fuel consumption. Although these technologies are not explicitly modeled in RE Futures, they are likely to be an important complement to energy-efficiency investments for stabilizing or reducing end-use electricity demand as envisioned in several RE Futures modeling scenarios.

4.5.3 Technology cost: the cost of concentrating solar power generation depends greatly on the technology in question. The levelized cost of energy for concentrating solar plants range from USD 0.14 to USD 0.36/kWh for parabolic trough installations and USD 0.17/kWh to USD 0.29/kWh for solar tower installations.

4.6 WIND ENERGY

Wind power is the conversion of wind energy into a useful form of energy, such as using wind turbines to produce electrical power, windmills for mechanical power, wind pumps for water pumping or drainage, or sails to propel ships.

A blade acts much like an airplane wing. When the wind blows, a pocket of low-pressure air forms on the downwind side of the blade. The low-pressure air pocket then pulls the blade toward it, causing the rotor to turn. This is called lift. The force of the lift is actually much stronger than the wind's force against the front side of the blade, which is called drag. The combination of lift and drag causes the rotor to spin like a propeller, and the turning shaft spins a generator to make electricity.

Wind turbines can be used as stand-alone applications, or they can be connected to a utility power grid or even combined with a photovoltaic (solar cell) system. For utility-scale sources of wind energy, a large number of wind turbines are usually built close together to form awind plant. Several electricity providers today use wind plants to supply power to their customers.

Stand-alone wind turbines are typically used for water pumping or communications. However, homeowners, farmers, and ranchers in windy areas can also use wind turbines as a way to cut their electric bills.

Small wind systems also have potential as distributed energy resources. Distributed energy resources refer to a variety of small, modular power-generating technologies that can be combined to improve the operation of the electricity delivery system. Wind turbines, like windmills, are mounted on a tower to capture the most energy. At 100 feet (30 meters) or more aboveground, they can take advantage of the faster and less turbulent wind. Turbines catch the wind's energy with their propeller-like blades. Usually, two or three blades are mounted on a shaft to form a rotor.

4.6.1 Wind Energy in Bangladesh: The long term wind flow, especially in the islands and the southern coastal belt of Bangladesh indicate that the average wind speed remains between 3 to 4.5 m/s for the months of March to September and 1.7 to 2.3 for remaining period of the year. There is a good opportunity in island and coastal areas for the application of wind mills for pumping and electrification. But during the summer and monsoon seasons (March to October) there can be very low pressure areas and storm wind speeds 200 to 300 kmph can be expected. Wind turbines have to be strong enough to withstand these high wind speeds.

Table-3: Feasibility of wind condition at different places of Bangladesh

Site	Reference height(m)	Annual average speed(m/s)
Cox's Bazar	10	2.42
Sandip Island	5	2.16
Teknaf	5	2.16
Patenga Airport	5	2.45
Comolla Airport	6	2.21
Kheppura	10	2.36
Kutubdia Island	6	2.09
Bhola Island	7	2.44
Hatia Island	6	2.08

5 **DISCUSSION AND CONCLUSION**

Only 62% people of Bangladesh have access to electricity and it is interrupted by power cut. Moreover, the existing sources of power are non-renewable. So an initiative is taken to look back at our power sector and searching for alternative options. No doubt renewable energy is the most promising and most dependable one for this case of our country as it is blessed with adequate renewable energy sources. Biopower or biomass power has not yet been implemented most recently but it can be a great source of energy in upcoming future since power production cost is moderately lower. Geothermal energy is a great source of energy for developed countries. But for Bangladesh electricity from geothermal sources is pretty difficult and costlier. Since Bangladesh is bestowed with a good number of rivers and is located on the shore of Bay of Bengal, a lot of micro- power plants are possible which will be run by hydrow power and wave power. The vast field of renewable energy is still left for solar power. Solar energy is the most effective, most powerful and most promising source to cover extra amount of power. Implementation of wind turbine has to be given a wise rethink. Actually all the existing and auspicious sources of renewable energy in Bangladesh have been discussed through out the paper to show what types of sources we do have, what technology should be implemented and

what will be the costing nature for the implementation of renewable energy technology.

REFERENCES

[1] 'Renewables 2011' – Global States Report, 'REN21: Energy Policy Network for the 21st Century'

[2] SNV Domestic biogas news letter, issue 4, January 2011.

[3] EIA (U.S. Energy Information Administration). (2008). "Electricity Generating Capacity: Existing Electric Generating Units in the United States, 2008." Washington, DC: DOE. http://www.eia.gov/electricity/capacity/. Accessed 2011.

[4] Short, W.; Sullivan, P.; Mai, T.; Mowers, M.; Uriarte, C.; Blair, N.; Heimiller, D.; Martinez, A. (2011). Regional Energy Deployment System (ReEDS). NREL Report No. TP-6A20-46534. Golden, CO: National Renewable Energy Laboratory.

[5] Ashwood, A.; Bharathan, D. (2011). "Hybrid Cooling Systems for Low-Temperature Geothermal Power Production." NREL/TP-5500-48765. Golden, CO: National Renewable Energy Laboratory.

[6] DiPippo, R. (2008). "Environmental Impact of Geothermal Power Plants." Geothermal Power Plants: Principles, Applications, Case Studies and Environmental Impact, 2nd ed. Burlington, MA: Butterworth-Heinemann (Elsevier).

[7] Bain, R.L. (2007). World Biofuels Assessment – Worldwide Biomass Potential: Technology Characterizations. NREL/MP-510-42467. Golden, CO: National Renewable Energy Laboratory. http://www.nrel.gov/docs/fy08osti/42467.pdf.

Bergman, P. (2005). "Combined Torrefaction and

[8] Black & Veatch. (2012). Cost and Performance Data for Power Generation Technologies. Overland Park, KS: Black & Veatch Corporation.

[9] AP&T (Alaska Power and Telephone). (2010). "Solstice on the Yukon Ushers in the Dawn of In-Stream Hydrokinetic Energy for AP&T in Eagle Alaska." Press release. http://www.businesswire .com/news/home/20100622005679/en/Solstice-Yukon-Ushers-Dawn-In-Stream-Hydrokinetic-Energy. Accessed February 26, 2012.

[10] AEG (Aspen Environmental Group). (2011a). California Valley Solar Ranch Conditional Use Permit, and Twisselman Reclamation Plan and Conditional Use Permit: Final Environmental Impact Report (DRC2008-00097, DRC2009-00004). Prepared for County of San Luis Obispo Department of Planning and Building. http://www.sloplanning.org/EIRs/ CaliforniaValleySolarRanch. Accessed August 2011.

[11] DSIRE (Database of State Incentives for Renewables and Efficiency). (2011). http://www. dsireusa.org/. Accessed September 2011.

[12] Andersen, P.B.; Mac Gaunaa, C.B.; Buhl, T. (2006). "Load Alleviation on Wind Turbine Blades Using Variable Airfoil Geometry." Presented at EWEC 2006 European Wind Energy Conference and Exhibition, Athens, Greece, February 27–March 2.

[13] Asmus, P; Seitzler, M. (2010). Wind Energy Operations and Maintenance Report. London, England: Wind Energy Update.

[14] AWEA (American Wind Energy Association). (2008). Wind Energy Siting Handbook. http:// www.awea.org/sitinghandbook/. Accessed February 11, 2010.

ICMIEE-PI-140180

Mismatch between classroom furniture and anthropometric measurements of Bangladeshi primary school students

Bhadrabati Biswas, Farzana Bintay Zahid, Rahat Ara , M.S. Parvez[*]*, A.S.M. Hoque*
Department of Industrial and Production Engineering, Jessore University of Science and Technology, Jessore7408, BANGLADESH.

ABSTRACT
Furniture has a significant effect on human health. So, it is necessary to use anthropometric data to design the school furniture. Students spend about more than five hours per day at school with little or no breaks. Most classroom activities involve sitting for long period of time. Due to prolonged sitting on inappropriate classroom furniture, students feel back pain and other musculoskeletal disorders. Every effort should be made to ensure that students do not face this problem. In Bangladesh, an anthropometry survey indicated that the furniture used by students, were not manufactured according to ergonomics principle. So, the purpose of this study is to compare furniture dimensions within three different primary schools with the anthropometric measurements of the Bangladeshi students, in order to evaluate the potential mismatch between them. The study consists of 300 students where 150 girls and 150 boys of the 1-5th grade ranging from 5-10 years from different schools. Fifteen anthropometric measurements and five dimensions from the existing classroom furniture were measured and then compared together to identify any potential mismatch between them. This paper focuses on the variation of the existing classroom furniture and students' anthropometry and also focuses on the problem of using the traditional school furniture.

Keywords: Anthropometry, school, classroom furniture, mismatch, ergonomic-oriented furniture.

1. Introduction

Human health risk is varying from case by case basis. The factors that can influence human health are the work environment, external factors and personal dispositions. Students spend 80% of their school time at sitting position. Considering the amount of time spending at school and especially while sitting, it is fundamental that school furniture fit the student's requirements [1]. In Bangladesh, most classroom furniture is manufactured without proper ergonomic consideration; as a result school children are suffering in various problems. Thus, necessary anthropometric measures have to be considered to design classroom furniture. The benches used by the students are too high and too deep. This situation has negative effects on the sitting posture of the students especially when reading and writing. The design of the furniture for students has received little or no interest. So, the situation of school work becomes more serious. For students comfort it is necessary to take step to design school furniture immediately.

This paper is based on match between school furniture and children's anthropometric measurement. It is also showed the ergonomic problems of using benches at school and how the mismatch between school furniture and student anthropometric measurements.

2. Methodology

It may be unrealistic to attempt to develop a classroom furniture design that "fits all" since children continue to grow and often leave for the next grade at the end of the academic session. It is therefore, unwise to design specific or custom made furniture for a particular elementary school student. This research aims is to evaluate the mismatch between classroom furniture dimension with anthropometric measurement of primary school students to examine proper ergonomic-oriented classroom furniture dimension.

2.1 Sample

In this study a sample of 300 primary school students is randomly selected where 150 girls and 150 boys with no physical disabilities from three primary schools (police line school, Badsha Foysal School, Churamonkathi govt. primary school) located in the city of Jessore, Bangladesh. They are in 1-5 classes and ranged in age from 5-10 years. The schools are representative of the three types of elementary school administration.

2.2 Measurement and procedure

Various anthropometric measurements of normal healthy students (Fig.1) were taken in standard sitting and standing positions. Student's heights were measured by standing the students on barefoot in front of a wall with a scale. To measure the existing furniture dimensions standard measuring tape was used. A statistical-software named Microsoft Excel spreadsheet was used to calculate the mean value, maximum and minimum values, standard deviation value and also the percentile value. The measurements were taken according to the method described by researchers [2-4].

2.3 Anthropometric measurements

Anthropometric measurements are considered as the basis for the design of furniture ergonomically. Thus, designing the classroom furniture for this study the authors have considered the following anthropometric measurements [5].

* Corresponding author. Tel.: +88-01827486660
E-mail address: sparvez.ipe@gmail.com

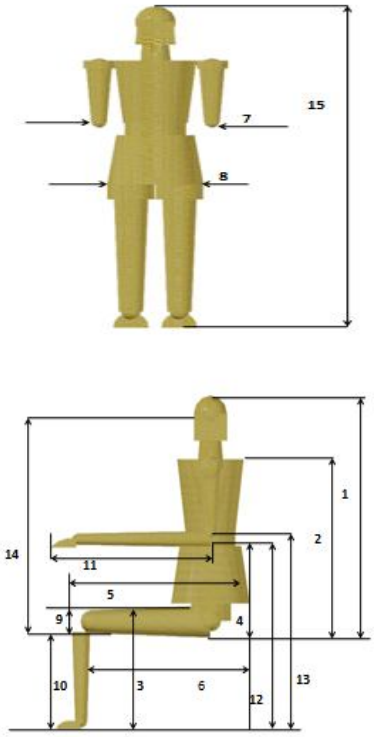

Fig.1 Anthropometric measurements

1. Sitting height 2.Shoulder height (sitting) 3.Knee height 4.sitting elbow height 5.buttock knee length 6.Buttock popliteal length 7.Elbow to elbow breadth 8.Hip breadth 9.Thigh clearance 10.Popliteal height 11.Forearm finger tip length 12. Sitting upper hip bone height 13.Sitting lowest rib bone height 14.Sitting eye height 15.stature

Sitting Height (SH): This is the vertical distance from the tip of the head to the surface of the sitting object (stool) [6].

Shoulder Height (ShH): This is the vertical distance from the top of the shoulder at the acromion process to the subject's sitting surface.

Knee height (KH):This is the vertical distance from the foot resting surface to the top of the knee cap[6].

Elbow Height (EH): This is the vertical distance from the bottom of the tip of the elbow (olecranon) to the subject's seated surface

Buttock knee Length (BKL): Distance was measured horizontally from the back of the uncompressed buttock to the front of the kneecap.

Buttock Popliteal Length (BPL): This is the distance from the posterior surface of the buttock to the posterior surface of the knee or popliteal surface [6].

Elbow to elbow breadth/elbow width (EW):

Horizontal distance across the lateral surfaces of the elbows (when the students write on the desk), spreading sideways was measured.

Hip Breadth (HB): The hip breath is the distance between the right side of the pelvic and the left side, measured when seated [6].

Thigh Clearance (TC): This is the vertical distance between a surface of the stool and the highest point on the top of the right thigh.

Popliteal Height (PH): This is the vertical distance from the popliteal space which is the posterior surface of the knee to the foot resting surface [6].

Forearm finger tip length (FFTL): Distance measured horizontally from the back of the elbow to the tip of the middle finger in a standard sitting position.

Sitting upper hip bone height (SUHBH): Distance measured vertically from a rest of foot to the upper hip bone.

Sitting lowest rib bone height (SLRBH): Distance measured vertically from a rest of foot to the lowest rib bone.

Eye Height (EH): Vertical distance from the sitting surface to the inner canthus (corner) of the eye.

Stature (St): Distance measured vertically from the footrest to the vertex.

2.4 Furniture measurements

Generally benches are used in Bangladesh primary schools. Those are made by local furniture companies and they lack of various standard dimensions, because the designers and manufacturers have not minimum knowledge about ergonomics. The dimensions of the classroom furniture (Fig.2) of the three different schools were measured. Thus, the following dimensions were measured for different school but same classroom furniture.

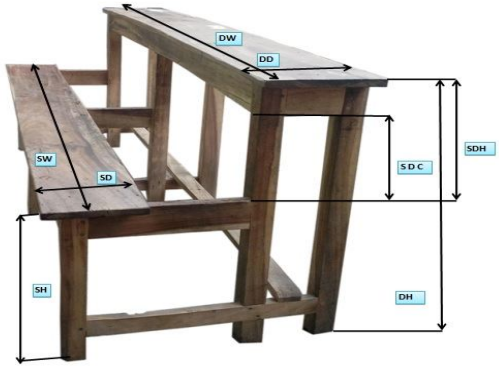

Fig.2 Representation of the classroom furniture measurements

SH=Seat Height, SW= Seat Width, SD= Seat Depth, SDH=Seat to Desk Height, SDC= Seat to Desk Clearance, DH= Desktop Height, DD=Desk Depth, DW=Desk Width

Seat height (SH): Seat height measured as the vertical distance from the floor to the middle point of the front edge of the seat.

Seat width (SW): Seat width measured as the horizontal distance between the lateral edges of the seat.

Seat depth (SD): Minimum distance measured horizontally from the front edge of the sitting surface to its back edge.

Seat to desk height (SDH): The vertical distance from the top of the front edge of the seat to the top of front edge of the desk .
Seat to desk clearance (SDC): The vertical distance from the top of the front edge of the seat to the lowest structure point below the desk .
Desk width (DW): Desk width measured as the horizontal distance between the lateral edges of the desk.
Desk depth (DD): Desk depth is the distance from the back to the front of the top surface of the desk.

2.5 Classroom furniture and body dimensions mismatch:
Anthropometric dimensions of each individual student were compared to the relative school furniture dimensions in order to identify a match or mismatch between students and the furniture they used. Mismatch is defined as discrepancy between the school furniture dimensions and the student's anthropometric measurement [7]. For designing and evaluation of school furniture and to define the range in which each furniture dimension is considered appropriate, applied anthropometric and ergonomic principles should be used. Different recommended relationships have been found in the literature to identify a match or mismatch. The most commonly used are describe below:

2.5.1. Popliteal Height (PH) against Seat Height (SH):

The Seat Height (SH) is required to be adjusted relative to the Popliteal Height (PH) and allowing the knee to be flexed so that the lower legs form a maximum of 30º angle relative to the vertical axis. Generally, PH should be higher than the SH [7]. The lower leg constitutes a 5–30^0 angle relative to the vertical and also the shin-thigh angle is between 95 and 120^0 [8]. Normally, PH does not have a value higher than 4 cm or 88% of the PH [7] to avoid compression in the buttock region [9]. So, a mismatch between PH and SH is defined when the seat height is either > 95% or < 88% of the popliteal height [7] and it is possible to establish a criterion for SH [8]. For this research work, 3 cm correction for shoe height is included to the popliteal height. Therefore, using this data a match criterion is established according to equation (1).

$$(PH+3)\cos 30^0 \leq SH \leq (PH+3)\cos 5^0 \qquad (1)$$

2.5.2. Buttock popliteal length (BPL) against seat depth (SD):
Seat Depth should be at least 5 cm less than the Buttock Popliteal Length [10]. However, the thigh would not be supported enough if the SD is substantially less than the BPL of the subjects. Various researchers [11-16] explain that the seat depth should be measured for the 5th percentile of the BPL distribution so that the backrest of the seat can support the lumbar spine without compression of the popliteal surface. Thus, a mismatch between SD and BPL is defined when SD is either < 80% or >95% of BPL [7]. Therefore, a match criterion is established according to equation (2).

$$.80BPL \leq SD \leq .95BPL \qquad (2)$$

2.5.3. Hip Breadth (HB) against Seat Width (SW):
The seat width must be large enough to accommodate the user with the largest hip breadth to attain stability and permit space for lateral movements [12-14]. Various researches [15-20] show that the HW should be thinner than the SW in order to have a proper fit in the seat and an optimal seat width is selected for the 95th percentile of HW distribution or the largest HW. The revised proposed equation displays that the SW should be at least 10% (to accommodate hip breadth) and at the most 30% (for space economy) larger than the hip breadth [8]. Thus, a match criterion is determined by equation (3).

$$1.10HB \leq SW \leq 1.30HB \qquad (3)$$

2.5.4. Sitting elbow height (SEH) against desk height (DH):
A number of studies [21-22] show that the elbow height is measured as the major factor for the desk height as the load on the spine reduces significantly when the arms are supported on the desk [20] and the desk height also be subject to on the shoulder flexion and shoulder abduction angles [7] and is strong-minded by the 5th percentile. So, the desk height should be 3-5 cm higher than the SEH [16]. Thus, a match criterion is established with a revised equation (4) that accepts the SEH as the lowest height of DH [20], and considering that the extreme height of DH should not be higher than 5 cm above the SEH.

$$SEH \leq DH \leq SEH+5 \qquad (4)$$

2.5.5. Thigh clearance (TC) against Seat to desk clearance (SDC):
The suitable seat to desk clearance needs to be greater than thigh clearance in order to make available leg movement [22]. The ideal seat to desk clearance should be 2 cm higher than knee height [7]. Therefore, a match criterion is recognized according to equation (5).

$$(TC+2) < SDC \qquad (5)$$

3. Results and Discussions
The aim of the current study was to evaluate the match between dimensions of the classroom furniture in school with student's anthropometric measurements. The result of this study showed considerable mismatch between students` body dimensions and classroom furniture.

The mismatch percentage between the classroom furniture dimensions which are: seat height, desk height, seat width, seat depth, seat to desk clearance and the anthropometric measurements of school students by gender and grade level are shown in Fig.3.The percentage of students which measurements match or mismatch the dimensions of the classroom furniture is presented by gender and grade level. From Fig.3, for class 1, seat height 64.44% (100% boy, 93.33% girl), seat depth 59.99% (56.66% boy, 63.33% girl), seat

width 94.99% (93.33% boy, 96.66% girl), desk height 94.99% (96.66% boy, 93.33% girl) and seat to desk clearance 3.33% (3.33% boy, 3.33% girl) were not appropriate for the students. For class 2, seat height 75% (80% boy, 70% girl), seat depth 84.99% (83.33% boy, 86.66% girl), seat width 78.33% (80% boy,76.66% girl), desk height 96.66% (96.66% boy,96.66% girl) were not appropriate for the students. For class 3, seat height 59.99% (63.33% boy, 56.66% girl), seat depth 94.99% (96.66% boy, 93.33% girl), seat width 86.66% (86.66% boy, 86.66% girl), desk height 74.66% (76% boy, 73.33% girl) and seat to desk clearance 3.33% (6.66% boy, 0% girl) were not appropriate for the students. For class 4, seat height 76.66% (76.66% boy, 76.66% girl), seat depth 91.66% (93.33% boy, 90% girl), seat width 94.99% (93.33% boy, 96.66% girl), desk height 91.66% (100% boy, 89.33% girl) and seat to desk clearance 36.66% (36,66% boy, 36.66% girl) were not appropriate for the students. For class 5, seat height 83.33% (86.66% boy, 80% girl), seat depth 96.66% (96.66% boy, 96.66% girl), seat width 100% (100% boy, 100% girl), desk height 100% (100% boys, 100% girls) and seat to desk clearance13.33% (3.33% boys, 23.33% girls) were not appropriate for the students.

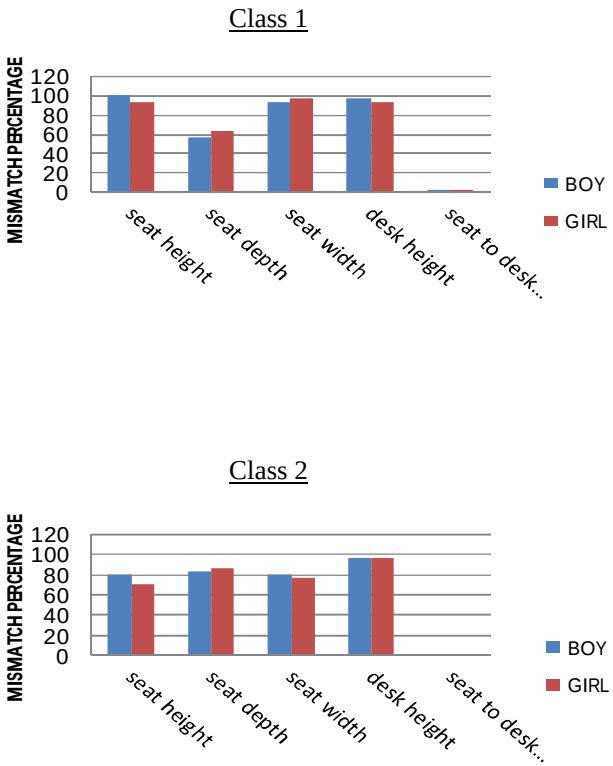

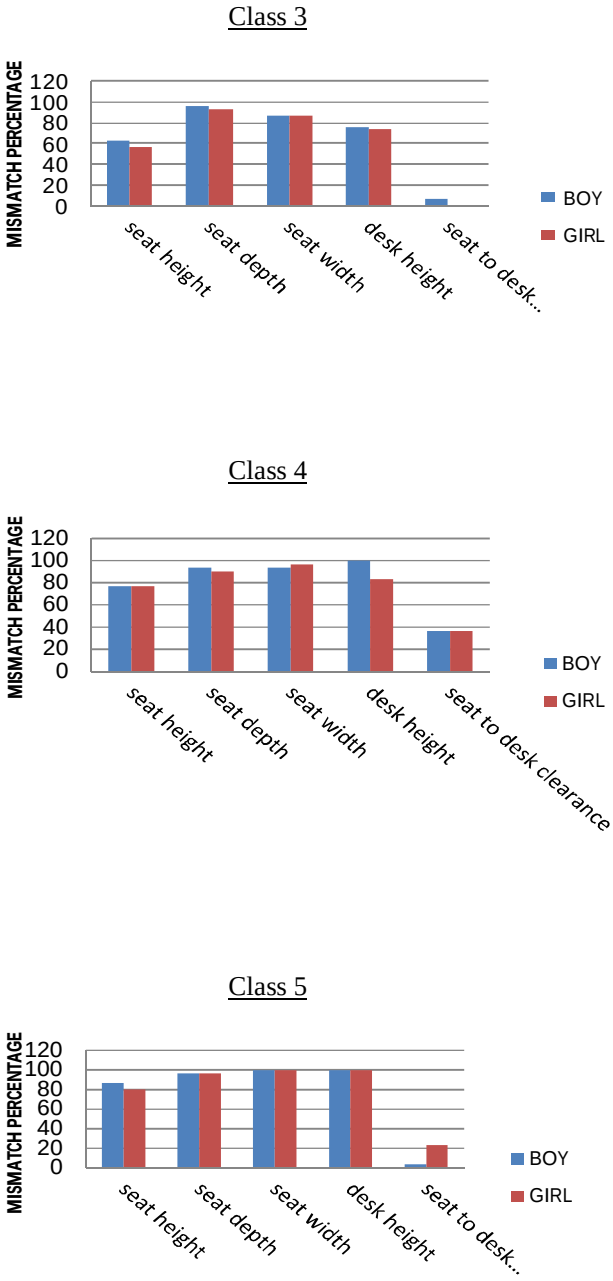

Fig.3 Mismatch percentages for different dimensions

For class 1, 100% boys and 93.33% girls used seat that were too high (high mismatch) and no low mismatch. For class 2 and 5 there were no low mismatch but had high mismatch. For class 3, there were 13.33% low mismatch and 50% high mismatch for boys and 3.33% low mismatch and 53.33% high mismatch for girls. And for class 4, 6.66% low mismatch for boys. The results indicated that the mismatch percentages decreased with grade level for both girls and boys. According to the current study based on average, the seat height only matched to 18.67% of boys and 24.67% of girls, which are obviously greatly below the lower limit of the

acceptance range. In other words, subjects are sitting on seats that are too high for them. According to filed observations most of subjects sitting with their legs not touching the floor. These positions can place high amounts of stresses on the popliteal arc that runs through the underside of the thigh and may cause serious discomfort and possibly risk injuries which are shown in Fig.4. This may lead to an increase in tissue pressure on the posterior aspect of the thighs. Since the mismatch forces students to slide forward on the seat of the classroom furniture, therefore seat height match appears to be necessary [12]. According to the current study, the seat width only matched to 25.33% of boys and 8.67% of girls, which are obviously greatly below the lower limit of the acceptance range. The high mismatch percentage for seat width dimension was as large for girls and boys for each class. An important element in the magnitude of the pressure under the buttocks is the form of the supporting surface. Some investigators have recommended that the seat width should be at least 45 cm, or 5 cm wider than the hip breadth [23, 24]. The breadth of sitting surface is determined according to the 95% percentile values of hip breadth. The seat should be wide enough to accommodate a user's hips and clothing, and comfortably allow use of the armrests. There is a need that a reasonable proportion of the population of potential users can easily get up and sit down and be satisfied with their seat design [25]. The anthropometric measure width of the hips should be lower than what should be allowed for width of the seat. There must be added, on each side, an extra width for movement of the arms if the seat is equipped with armrests.

(a) (b)

Fig. 4 Wrong furniture dimensions (a and b)
(a)Wrong seat height dimension causes student's feet unable to reach the ground.
(b)Wrong furniture dimensions force student to lift their arms and hunch their shoulders.

According to the current study, the seat depth only matched to 14.67% of boys and 14% of girls, which are obviously greatly below the lower limit of the acceptance range. The percentage of students 1-5th grade whose measurements had a bad fit with the seat depth of the classroom furniture shown in figure 3. Where benches were too deep (high mismatch) for 33.33% of boys and 6.66% of girls while they were too shallow (low mismatch) for class 1, 23.33% boys and 56.6% girls and for class 2, 3, 4 there was high mismatch and no low mismatch. But for class5, both girls and boys, there were 89.99% low mismatch and 6.66% high mismatch. As is apparent, the mismatch percentage increased with grade level for both girls and boys. On the other hand, too deep benches force students usually place their buttocks forward on the edge of the seat, especially while reading and writing.

4. Conclusion

The finding of the study is that there is a substantial inconsistency between the student's anthropometric measurements and school furniture dimensions. It is impractical and difficult to select the proper furniture for a large number of students, so, to design the furniture dimension's adjustable range design would be preferable. This paper intended to analyse the relation between body dimensions from a sample study of 300 Bangladeshi students from three schools with three different economical levels within the five classes. A considerable mismatch was identified between body dimensions (popliteal height, buttock popliteal length, hip breadth, sitting shoulder height, sitting elbow height and thigh clearance) of the school students and the classroom furniture dimensions (seat height, seat depth, seat width, backrest height, desk height and seat-to-desk clearance) available to them. The results indicated a considerable mismatch between body dimensions of the students and the existing classroom furniture. For both boys and girls seat heights and desktop heights of the classroom furniture were too high, which may result in pain on the posterior surface of the knee and shoulder region, discomfort respectively and tend to increase the risk for developing musculoskeletal problems amongst school students. The results of the study highlight the fact that classroom furniture is typically acquired and selected without any previous ergonomic concern, which will most likely result in its inadequacy.

REFERENCES

[1] H.I.Castellucci,P.M.Arezes,C.A.Viviani ,2009.Mis match between classroom furniture and anthropometric measures in Chilean schools. Applied Ergonomics 41 (2010) 563–568.

[2] Weiner, J.S., Lourie, J.A., 1969. Human Biology: a Guide to Field Methods. P.A. David, Philadelphia.

[3] Abeysekara, J.D.A., 1985. Design requirements and dimensions for a comfortable work seat for Sri Lankans. Journal of National Science Council of Sri Lanka 13 (1), 77–88.

[4] Pheasant, S., 2003. Bodyspace, second ed. Taylor & Francis, London.

[5] Dianat I, Karimi MA, Asl Hashemi A, Bahrampour S, 2013. Classroom furniture and anthropometric characteristics of Iranian high school students:

proposed dimensions based on anthropometric data. Appl Ergon. 2013 Jan;44(1):101-8.
[6] Clauser, C.E., Tebbetts, I.O., Bradtmiller, B., McConville, J.T., Gordon, C.C., 1988.Measurer's Handbook: US Army Anthropometric Survey (ANSUR) 1987e1988,Technical Report NATICK/TR-88/043.
[7] Parcells, C., Stommel, M., Hubbard, R.P., 1999. Mismatch of classroom furniture & student body dimensions: empirical findings & health implications. J. Adolesc. Health 24 (4), 265 273.
[8] Gouvali, M.K., Boudolos, K., 2006. Match between school furniture dimensions & children's anthropometry. Appl. Ergon. 37, 765-773.
[9] Garcı´a-Molina, C., Moraga, R., Tortosa, L., Verde, V., 1992. Gui´a de Recomendaciones para el Disen˜o de Mobiliario Ergono´ mico. Instituto Biomeca´ nico de Valencia, Valencia.
[10] Poulakakis, G., Marmaras, N., 1998. A model for the ergonomic design of office. In: Scott, P.A., Bridger, R.S., Charteris, J. (Eds.), Proceedings of the Ergonomics Conference in Cape Town: Global Ergonomics. Elsevier Ltd., pp. 500–504.
[11] Milanese, S., Grimmer, K., 2004. School furniture and the user population an anthropometric perspective. Ergonomics 47, 416–426.
[12] Helander, M., 1997. Anthropometry in workstation design. In: Helander, M. (Ed.), A Guide to the Ergonomics of Manufacturing. Taylor & Francis, London, pp. 17–28.
[13] Orborne, D.J., 1996. Ergonomics at Work: Human Factors in Design and Development, third ed. John Wiley & Sons, Chihester
[14] Sanders, M.S., McCormick, E.J., 1993. Applied anthropometry, work-space design and seating. In: Human Factors in Engineering and Design, seventh ed. McGraw-Hill, Singapore.
[15] Khalil, T.M., Abdel-Moty, E.M., Rosomoff, R.S., Rosomoff, H.L., 1993. Ergonomics in Back Pain: A Guide to Prevention and Rehabilitation. Van Nostrand Reinhold, New York.
[16] Pheasant, S., 1991. Ergonomics, Work and Health. Macmillan, Hong Kong.
[17] Evans, W.A., Courtney, A.J., Fok, K.F., 1988. The design of school furniture for Hong Kong school children: an anthropometric case study. Appl. Ergon. 19, 122–134.
[18] Gutie´rrez, M., Morgado, P., 2001. Gui´a de recomendaciones para el disen˜o del mobiliario escolar Chile. Ministerio de Educacio´n and UNESCO, Santiago de Chile.
[19] Mondelo, P., Gregori, E., Barrau, P., 2000. Ergonomı´a 1: Fundamentos, third ed. Alfaomega Grupo Editor – UPC, Me´xico
[20] Occhipinti, E., Colombini, D., Molteni, G., Grieco, A., 1993. Criteria for the ergonomic evaluation of work chairs. Le Medicina del Lavoro 84, 274–285.
[21] Dul, J., Weerdmeester, B., 1998. Ergonomics for Beginners. A Reference Guide. Taylor & Francis, London.
[22] Molenbroek, J.F.M., Kroon-Ramaekers, Y.M.T., and Snijders, C.J. 2003. Revision of the design of a standard for the dimensions of school furniture. Ergonomics 46, 681-694.
[23] Fernandez JE, Marley RJ. Applied occupational Ergonomics: A Text book. 2nd edition Cincinnati : International journal of Industrial Engineering press ;2007.
[24] ANSI/HFES 100-2007. Human factors Engineering of computer workstation;2007.
[25] BS EN ISO 9241-5. Ergonomic requirement for office work with visual display terminals (VDT_s)-part 5:workstation layout and postural requirements,1999.

ICMIEE-PI-140181

Vertical (VTOL) & short (STOL) takeoff and landing for modern jet powered aircraft: a Problem to carry heavy payload & its solution

Md Saifuddin Ahmed Atique [1], *Nafisa Nawal Probha*[2], *Asif Shahriar Nafi* [3]

[1] Department of Aeronautical Engineering,
Military Institute of Science & Technology (MIST), Mirpur Cantonment, Dhaka-1216, BANGLADESH
[2] Department of Aeronautical Engineering,
Military Institute of Science & Technology (MIST), Mirpur Cantonment, Dhaka-1216, BANGLADESH
[3] Department of Aeronautical Engineering,
Military Institute of Science & Technology (MIST), Mirpur Cantonment, Dhaka-1216, BANGLADESH

ABSTRACT
A vertical (VTOL) & short (STOL) takeoff and landing (V/STOL) aircraft is an airplane which is able to vertically takeoff or can takeoff with in a very short runway even in a paddy field. Vertical takeoff and landing (VTOL) aircraft is a subset of V/STOL aircraft that does not require any runways at all. A V/STOL aircraft needs to be able to hover. Vertical takeoff and landing (VTOL) or short (STOL) are desirable characteristics for any type of aircraft. Even VTOL aircrafts have too many advantages, but still there is only one drawback which has prevented them to be at the top of fighting aircraft i.e. the problem with payload. The VTOL aircraft can only carry very little payload, while taking off vertically due together power plant design which does not support heavy payloads. In this paper we will discuss how to increase their payload capability by using electromagnetic flux which will provide an extra bit of thrust during takeoff. Hence, increase the payload capability of aircraft.

Keywords: Keywords: Takeoff, landing, payload, aircraft

1. Introduction

Though vertical takeoff and landing (VTOL) or Short take off and landing (STOL) are most desirable characteristics for any type of aircraft but until the introduction of the gas turbine engine, the low disc loading rotor, as on the helicopter was only system capable of VTOL .For a pure jet engine, this V/STOL concept was developed by the principle that was proposed by M. Wibault. During 1960s, many countries around the world wanted to design an aircraft that will be able to take off and land easily from the aircraft career by reducing the cost of making large aircraft career and runways for therm. After that the Harrier, Mirage-IIIV, YAK-38, F-35, V-22 etc were developed and designed according to the desired mission and requirement of V/STOL aircrafts. Though there are different/STOL aircrafts now-a-days, but still now all of these V/STOL aircraft allow a very little amount of payload during takeoff. Here we will try to improve their payload capacity by using electro-magnetic flux. Though our research may not solve this problem fully but it will open a new horizon for new generation researchers.

2. Power plant-a historical view

Different types of power plants were used to make the operation of V/STOL aircraft smooth and successful as much as possible it was. But Rolls Pegasus –a turbofan engine was unique in this field. It was considered as a blessing for V/STOL aircraft during that time.

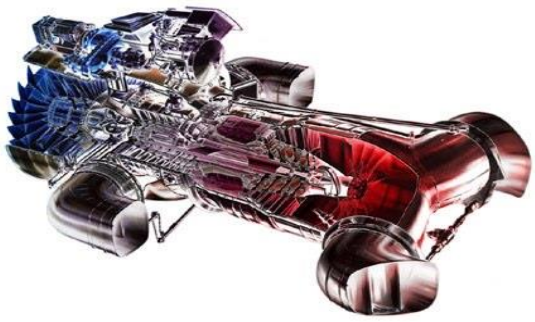

Fig.1 The Rolls-Royce Pegasus V/STOL Engine

This engine also provides the thrust vectoring system for the V/STOL aircraft of that period. This eradicated the necessity of traditional long runway and opened a new horizon for that aircraft which were responsible to take off and land from variety of ships at sea. This Rolls Royce Pegasus turbofan engine featured three low pressure and eight high pressure compressor stages which were driven by two low pressure and two high pressure turbine engine respectively. This Pegasus was first turbofan engine which had the initial compressor fan ahead of from bearing. But unfortunately at higher ambient temperature the maximum takeoff thrust provided by the Pegasus engine was limited. To overcome this problem and to increase the thrust during takeoff, water was sprayed into combustion chamber

* Corresponding author. Tel.: +88-01686334988
E-mail address: saifaerospace@gmail.com

and turbine to keep the blade temperature down let and to enable to engine to its optimum speed.

3. Power plant thrust equations

Let us consider a propulsive duct in which air of mass $\dot{m}_i$ enters the intake with velocity c_i and pressure. During the combustion process acceleration of air happens and it leaves through the nozzle with pressure p_j and velocity c_j.. The flow is assumed to be steady and reversible outside the duct .A_j and A_i are considered as the exhaust area and intake area respectively.

So, thrust due to the rate of change of momentum = $\dot{m}_j c_j - \dot{m}_i c_i$

And pressure Thrust = $(p_j - p_a)A_j - (p_i - p_a)A_i$

Net Thrust = $(\dot{m}_j c_j - \dot{m}_i c_i) + (p_j - p_a)A_j - (p_i - p_a)A_i$

We have by mass balance,

$\dot{m}_j = \dot{m}_i + \dot{m}_f$

Where $\dot{m}_j$, $\dot{m}_i$ and $\dot{m}_f$ are the mass flow rates of exhaust gases, air and fuel respectively.

Fuel air ratio = $f = \dot{m}_f / \dot{m}_i$

So, $\dot{m}_j = \dot{m}_i(1+f)$

So, Net Thrust = $\dot{m}_i\{(1+f)c_j - c_i\} + (p_j - p_a)A_j - (p_i - p_a)A_i$

For subsonic aircraft ($p_i \approx p_a$)& ($p_j \approx p_a$),

Neglecting small value of pressure thrust,

$T = \dot{m}_i\{(1+f)c_j - c_i\}$

4. Electromagnetic flux

A stationary charge produces an electric field in the surrounding space .When the charged particle is in motion it also creates a magnetic field around it .Electromagnetic Flux (EMF or EM Flux) is a spatial distribution of influence of charged particles around them while they are in motion .Because of mutual interaction of electric and magnetic fields created by the charged particles; an electromagnetic flux is generated.
From a classical perspective, the EMF can be regarded as a smooth, continuous field, propagated in a wavelike manner; whereas from the perspective of quantum field theory, the field is seen as quantized, being composed of individual particles.

4.1 Nature of electromagnetic field

Electromagnetic Field is produced due to combined interaction of electric field and magnetic field. Electric Flux is a property of electric field which can be defined as the number of electric lines of force that pass through a given area. The mathematical relation between electric flux and enclosed charge is known as Gauss's law for the electric field, one of the fundamental laws of electromagnetism which is,

$$\Phi_E = \oiint_s E.dA = \frac{q}{\varepsilon} \text{------ - - - - - - - - - } (i)$$

$$\Phi_B = \oiint_s B.dS = 0 \text{------ - - - - - - - - - } (ii)$$

When the electric charges are in motion, magnetic and electric fields are generated which produce forces on electric charges .These forces and their effects are described by Lorentz force law which is,

$$\vec{F} = q\vec{E} + q\vec{V} \times \vec{B}$$

Faraday's Induction Law states that induced electromotive force in any closed circuit is equal to the rate of change of the magnetic flux through the circuit. Mathematically,

$$\oint_s \vec{E}.dl = -d\Phi_B/dt \text{------ - - - - - - - - } (iii)$$

Faraday's Induction Law refers to changing magnetic field induces (negative) vortex of electric field.
Ampere's Law relates the net magnetic field along a closed loop to the electric current passing through the loop.
Mathematically,

$$\oint_s \vec{B}.dl = \mu_0 i + \frac{1}{c^2}\frac{d}{dt}(\Phi_E) \text{------ - - - - } (iv)$$

These Laws[(*i*) to (*iv*)] are the mathematical way of defining an electromagnetic field .These four laws are known as Maxwell's Equations which are the fundamental postulates of classical electromagnetic. All classical electromagnetic phenomena are explained by these equations. These equations are used to explain the behavior of an electromagnetic field.

4.2 Electro-magnetic field & its reciprocal behavior

A very practical feature of the electro-magnetic field is illustrated by maxwell's equation, Faraday's law and the ampere-maxwell law. At first, we will think about the faraday's law. According to this law, a changing magnetic field creates an electric field and it is the principle behind the electric generator. Ampere's law relates magnetic fields to electric current to produce them, It relates a magnetic field to its electric current source. It states that," a changing electric field creates a magnetic field.".Thus we can apply this law to generate a electric field and run an electric motor. Lovents force between two point charges is

$$\boldsymbol{F_{12} = (Q_1 Q_2 / 4\pi\epsilon_0\epsilon_r r^2)\hat{l}_r}$$

We can verified it with the help of coulombs law and Biot-savart law also-

$F_L = Q(v \times B)$

$dB/p = (\mu_0 I/4\pi r^2) dl \times l_r$

This is also known as the law of laplace.

5. Multi-frequency flux generator

Ultrasonic generators with multiple frequency technology are specially designed units that convert electrical energy into ultrasonic signals. Connected with immersible transducers, ultrasonic signals from the generator will be converted into corresponding mechanical vibrations able to "scrub off" surfaces immersed in liquid.

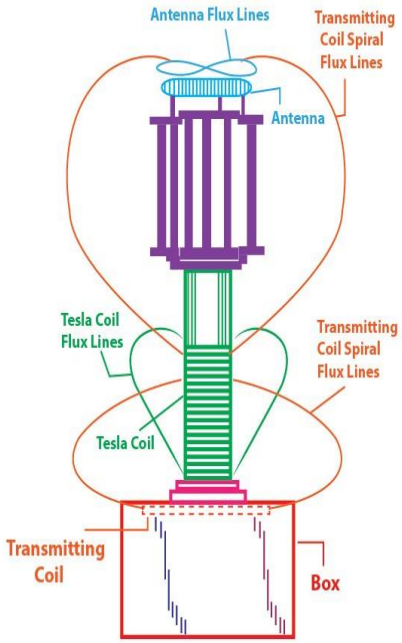

Fig.2 A typical flux generator

5.1 Features

1. Robust unit - Material in contact with cleaning solution is made of stainless steel
2. Thermostatic adjustable heating and timer function
3. Designed for use with water-based as well as solvent-based cleaning chemicals
4. Convenient drainage option
5. Mounted on stainless steel frame for secure fastening to the deck
6. Ideal partner for cleaning fuel and lube oil filters

5.2 Benefits

1. Allows usage of chemicals with less hazard
2. Flexible solution & low audible sound

6. Result and Calculation

By using different types of generator electromagnetic flux can be generated. We are interested here to use the generator shown in fig.2 for our calculation purpose. To increase the thrust produced by the aircraft, we can use this flux which is being generated by this flux generator.

Fig.3 A self conceptual designed V/STOL aircraft

Let us consider 127 KN is the maximum weight that can be carried by our considered aircraft (conceptual). Now by using electromagnetic flux we can provide an extra bit of thrust to the aircraft. We have done this by using the following calculations of table 1 and derived our result. Generally, here we have taken the radius of our coil of the flux is 0.02 m which we kept fixed. We changed the number of turns and varied the current with a view to increase the magnetic flux .By doing this experiment for several iteration and using 12000 turns of the coil we produced 23212.98 N of magnetic flux that is around 23.212 KN (shown in table-1). So, from here, we can summarized that around 23.212 KN force can be managed by using magnetic flux to assist the aircraft in vertical or short take off and certainly this 23.212 KN force is around 18% of this gross force required for this aircraft to perform this.

6.1 Calculation

(1) Number of turns (n) =100
Radius = 0.02 m
Magnetic flux $B=\frac{\mu oni}{2r}$ =0.0314
Force generated, F=2πIRBcosθ=0.039

(2) Number of turns(n)=1200
Radius (m) = 0.02
Magnetic flux $B=\frac{\mu oni}{2r}$ = 1.257
Force generated, F=2πIRBcosθ=6.314

(3) Number of turns(n)=1500
Radius (m) = 0.02
Magnetic flux $B=\frac{\mu oni}{2r}$ = 2.827
Force generated, F=2πIRBcosθ=21.3151

(4) Number of turns(n)=2000
Radius (m) = 0.02
Magnetic flux $B=\frac{\mu oni}{2r}$ = 6.283
Force generated, F=2πIRBcosθ=78.955

(5) Number of turns(n)= 2500
Radius (m) = 0.02
Magnetic flux B=$\frac{\mu oni}{2r}$ = 11.78
Force generated, F=2πIRBcosθ=222.05

(6) Number of turns(n)=5000
Radius (m) = 0.02
Magnetic flux B=$\frac{\mu oni}{2r}$ = 31.41
Force generated, F=2πIRBcosθ=789.42

(7) Number of turns(n)=10000
Radius (m) = 0.02
Magnetic flux B=$\frac{\mu oni}{2r}$ = 141.37
Force generated, F=2πIRBcosθ=7994.298

(8) Number of turns(n)=12000
Radius (m) = 0.02
Magnetic flux B=$\frac{\mu oni}{2r}$ = 263.89
Force generated, F=2πIRBcosθ=23212.98

Table 1 Calculation for force generated by flux

Serial no	Number of turns(n)	Radius (m)	Current (I)	Magnetic flux B=$\frac{\mu oni}{2r}$	Force generated, F=2πIRBcosθ
1	100	0.02	10	0.0314	0.039
2	1000	0.02	40	1.257	6.314
3	1500	0.02	60	2.827	21.3151
4	2000	0.02	100	6.283	78.955
5	2500	0.02	150	11.78	222.05
6	5000	0.02	200	31.41	789.42
7	10000	0.02	450	141.37	7994.298
8	12000	0.02	700	263.89	23212.98

Conclusion

From this study, we can see that V/STOL thrust can be increased around 18% by using electro-magnetic flux generator. We can easily increase this capability of generated thrust by increasing the number of turns of the coil and the current passing through it according to the mission requirement. Different types of fluxes i.e spiral ,horizontal can be used in this purpose. But there are some problems for the implementation of this as the flux generated by this can harm the aircraft instrument and structure ,so special care should be taken during the time of airframe manufacture. Therefore, no others only specially designed V/STOL aircraft can use this which are capable of withstanding the hazard produced by the flux.

REFERENCES

[1] Harshit Bhardwaj, Rajneesh Sharma,*Utilization of electromagnetic flux for increasing VTOL thrust*.

[2] Bishop,chris,ed, The eccyclopedia of modern Military weapons:*The comprehensive guide to Over 1000 weapons systems from 1945 to present Days. NY barnes & Noble 1999.*

[3] Donald,David. , *The complete Encyclopedia of world aircraft. NY:Barens and Noble,1997*.

[4] Gunston,Bill and Spick,Mike, *Mordern Air Combat combat: The Aircraft,Tactics and weapons employed in aerial combat today.*

[5] Muller,Claudio, *Aircraft of the world.NY:Muddle Ruddle Books,2004.*

[6] Munro,Bob and Chant,Christopher, *Jane's Combat aircraft.*

[7] Spick,Mike, *Brassey's Modern Fighters; The ultimate Guide to In-flight Tactics,Technology, weapons and equipment.*

[8] Wilson,Jim, *Combat : The Great American Warplane.*

[9] Winchester,Jim, *Military Aircraft of Cold War*

[10] Yefim Gordon, :Yokovler Yak-36,Yak-38 and Yak-41: The soviet '*Jump Jets',Midland Publishing 2008*.

ICMIEE-PI-140182

Application of Porter's Five Forces Model in Battery Manufacturing Industries of Bangladesh.

Md. Golam Kibria [1], Md. Al Amin[2], Usama Abdullah Rifat[3]
[1] Lecturer,
Department of Industrial Engineering and Management,
Khulna University of Engineering & Technology, Khulna-9203, BANGLADESH
[2,3] Graduate Student,
Department of Industrial Engineering and Management,
Khulna University of Engineering & Technology, Khulna-9203, BANGLADESH

ABSTRACT
This paper is concentrated on the analysis of Porter's Five Forces model in regard to battery industry of Bangladesh. The five forces are impact of supplier, power of customer, competition between existing manufacturers, threats of substitutes and entrance of new manufacturer. This paper has analyzed the five forces to find out how a battery industry can be put in an advantageous position in a highly competitive market. The strongest of the five forces has been shown as the power of customer and competitive rivalry. The elements controlling customers are customer volume, price sensitivity, option of substitute and product differentiation. Threat of substitutes include advent of new or improved technology, and improved performance. The weakest of the forces has been found as substitute product and bargaining power of supplier. It can be suggested that the companies should pay more attention in providing quality rather than thinking cost.

Keywords: Energy sector, Porter's Five Forces model, Operations strategy, Industrial Engineering.

1. Introduction (Top heading should be in bold)

Michael E. Porter first introduced and constructed the model of the five forces that shapes the company strategy in his book "Competitive Strategy: Techniques for Analyzing Industries and Competitors" in 1980. Porter's Five Forces model highlights the strength, potential profitability and balance of power between different organizations in a competitive market Although over time some limitations of this model has been found, still now this model works as the basis for determining the strategies to be adopted for surviving and expanding in this highly competitive and aggressive market .

The global battery industry witnessed good growth during the past decade and holds immense growth potential for the future. The global market size for batteries is expected to reach $86.6 billion by 2018. The industry is boosted by growing demand of battery in consumer electronic products and automotive vehicles. Growing demand of electric, hybrid electric, and plug-in hybrid electric vehicles are creating huge growth opportunities for the battery industry. Technological development, increasing disposable income of customers, development of new application for batteries, and decreasing prices of raw materials for manufacturing latest battery products further aided the battery Industry. [1]

The global market share of the lead-acid battery in 2010 was 36.2 billion U. S. dollars, a growth of 8.6% compared to 2009. The future of the industry, following the market growth of automobiles, motorcycles, and storage applications, is estimated to have a 2~5% annual market growth rate until 2015. Compared to the 2.8 billion U. S. dollars of nickel-based rechargeable batteries, and the near 10 billion U. S. dollars of lithium batteries sold, the lead-acid battery still has the highest market share of all electric storage device products today. [2]

Batteries are divided into two categories: primary and secondary. In 2009, primary batteries made up 23.6 percent of the global market. Frost & Sullivan (2009) predict a 7.4 percent decline of the primary battery in revenue distribution by 2015. Primary batteries are used in watches, electronic keys, remote controls, children's toys, light beacons and military devices. The real growth lies in secondary batteries. Frost & Sullivan say that rechargeable batteries account for 76.4 percent of the global market, a number that is expected to increase to 82.6 percent in 2015. [3]

Lead-acid accounts for half the demand of rechargeable batteries. This battery is mainly used for automotive and stand-by applications. Because of low cost and dependable service in adverse environmental conditions, lead-acid enjoys a steady increase. Multiple use of lead acid battery is growing fast in the country.

According to Bangladesh Accumulator & Battery Manufacturers Association (BABMA), annually about 2.8 million pieces of batteries are used by different sectors in the country with its 10 percent growth rate. Of these, 420,000 pieces are used by motor vehicles, 411,000 pieces by IPS and UPS users, 150,000 pieces by heavy equipment of the industries, 1,050,000 pieces by electric vehicles and electric-rickshaw, and 700,000 pieces by the solar system. [4]

Recent introduction of solar home system and electric vehicles has given a big boost to the use of lead acid batteries which prompted a number of local firms to come into the battery manufacturing business. At present, there are about 30 battery manufacturers, but six (6) are leading in the battery business as they hold 93 percent of the total market share while only 7 percent by the traders

Md. Golam Kibria. Tel.: +88-01939126205;
E-mail addresses: kibria.ipekuet@gmail.com
rifat2k10@gmail.com

who import batteries and sell those locally. Among the local manufacturers, Rahimafrooz has been leading the market with 35 percent market share, followed by Hamko with 18 percent market share. Volvo, Ramso, Rangs and some other companies are also active in the battery market. Rahimafrooz, meeting the compliances, has also been exporting batteries to more than 45 countries across the globe. [4]

2. Literature Review

Bacanu (2010), tried to find a reference framework for the competition that includes Porters competence strategy to achieve the goal of the competitive advantage through cost and differentiation strategy. The study showed that for some products a positive relation exists between the price level of current manufacturer and the new entrants. [5]

Bayraktar (2010), discussed the tools that link between the strategic option and the performance of the company. The survey includes (519) companies and the multi-regression analysis has been used. The study showed that there is a strong impact of the strategic option on improving the performance of the company. [6]

Hill (2010) aimed to improve a framework which identifies the circumstances under the dominance of the differentiation and the cost strategies. The study concludes that the differentiation strategy has an important role in pushing the cost down. [7]

Rada (2010), demonstrates the bargaining power of electro-mechanical suppliers of oil industry companies, especially when the suppliers can add value to their customers through selling the product using different methods to offer the product, namely the best offer, the modern offer, the prompt offer and the lowest price offer. [8]

Dr. Jaradat (2013), studied the application of Porter Model for five competitive forces on the food industrial companies in Jordan to select business strategies. [9]

Amrollahi (2013), conducted an analysis on Open Source Business with Porter's Five Forces. They studied many case studies and previous researches for this analysis and recognized that the issue of license and revenue model has to be precisely considered while a firm adopts the open source strategy. [10]

3. Overview of Current Manufacturers

Navana Limited, the flagship company of the Navana Group (previously Islam Group) was established in 1964. Aftab Automobiles Ltd. Introduced a Battery Manufacturing unit, concern of Navana Group in January 2002, and manufacturing different type of automotive batteries (from small car to big lorries) and marketing the same in the country. This company is manned by 82 staff (all inclusive) in manufacturing plant and by 20 staff (all inclusive) in sales and service center (both Dhaka and Chittagong).

Incorporated in 17th of July, 1996 with absolute determination to produce quality products and bring in cutting edge technology, White Products and Electronics Limited (WP&EL) was founded. Rangs Power Battery, manufactured in own factory under strict supervision of highly experienced engineers and strong QAD. It stores rated power and ensures uninterrupted service during its life span in Cars, Commercial vehicles, Rickshaws & Three Wheelers, IPS, Solar System and industrial use. Skilled Engineers & Technicians are engaged in after sale service centers evenly distributed all over the country. Achieved ISO 9001, ISO 14000 and OHSAS for its Quality Management, Environmental and Health Safety up to International Standard.

HAMKO Group started its journey in 1979 with the vision to excel in the accumulator industry. After 3 decades of business HAMKO is currently a leading producer of Lead Acid Batteries in Bangladesh. HAMKO is also a pioneer Battery Components and Chemical manufacturer serving and supporting other battery companies of the country. HAMKO Group is also contributing to proliferation of Renewable Power Generation as the supplier for Solar Batteries, Solar Panels and other related accessories to the rural electrification initiative by different NGOs and System integrators at home and abroad. HAMKO Group in its future ventures has a clear focus to advance in the Energy Technology sector, and contribute to mutual development of itself and all its partners and stakeholders.

Panna Group (PG) has sailed on its journey in the year of 1980. Panna Group adopted the strategy of developing a major Bangladesh based manufacturing business through acquisitions and other means from a raw materials trader. Panna Group introduced Panna Battery Ltd. a well-established organization and is recognized by Govt. of Bangladesh as a manufacturing and export outfit in 1978. It is also ISO 14001-2004, ISO 9001-2008, and BSTI certified company. They are holding the permanent membership of International Battery Council, USA. Their quality products are well established and popular in more than 17 countries of the world covering Asia, Africa, Latin America, Middle East, North America and Europe. Annual turnover is US$ 95 million. The group has bagged several awards including National Export Award and Engineering Export Award.

Rahimafrooz Batteries Ltd. (RBL) is the largest lead-acid battery manufacturer in Bangladesh. The company is one of the leading regional players, with market leadership at home and export endeavours to more than 44 countries around the world. It manufactures about 200 different varieties of batteries for automotive, motorcycle, IPS and other applications in its factory located at West Panisail, Zirani Bazaar, and Gazipur. The Company maintains high standards of operations, which are certified in both ISO 9001 as well as ISO 14001 standards. Furthermore, in order to ensure occupational health and safety of its employees, the company has also implemented the occupational health and safety management system, OSHAS 18001 standard.

4. The Study Population and Sample

The population of the study consisted of 30 battery industries located in different parts of Bangladesh. The

sample consisted of 5 industries from this population of 30.

5. Hypotheses and Research Model

H01 Influence of buyer power on cost strategy is average.
H02 Influence of buyer power on differentiation strategy is high.
H03 Influence of supplier power on cost strategy is very low.
H04 Influence of supplier power on differentiation strategy is very low.
H05 Influence of threat of new entrants on cost strategy average.
H06 Influence of threat of new entrants on differentiation strategy is high.
H07 Influence of threat of substitute product on cost strategy low.
H08 Influence of threat of substitute product on differentiation strategy is average.
H09 Influence of competitive rivalry on cost strategy is average.
H10 Influence of competitive rivalry on differentiation strategy is very high.

To find the effect of the five forces on cost strategy and differentiation strategy, t-distribution has been used with two-tail α. Effect of the five forces on the strategies has been quantified using Likert scale and then t-distribution has been used.

6. Analysis of the Five Forces

6.1 Bargaining Power of Buyer

The bargaining power of customers determines how much customers can impose pressure on margins and volumes. Customers bargaining power is likely to be high when they buy large volumes, there is a concentration of buyers, the supplying industry comprises a large number of small operators, the supplying industry operates with high fixed costs, the product is undifferentiated and can be replaced by substitutes, switching to an alternative product is relatively simple and is not related to high costs, customers have low margins and are price-sensitive, customers could produce the product themselves, the product is not strategically important to the customer, the customer knows about the production costs of the product, there is the possibility for the customer integrating backwards.

In this industry, buyers are fragmented, no buyer has any particular influence on price. But buyers influence product characteristics. There is no possibility of customers integrating backward. [11]

The results from t-distribution analysis is summarized in Table 1.

Table 1 Results of t-distribution analysis for bargaining power of buyer

Condition	*t*	Acceptable Range of	Result of Null Hypothesis
Influence of buyer power on cost strategy is average.	-0.5976	-2.132 to +2.132	Accept
Influence of buyer power on differentiation strategy is high.	0.5976	-2.132 to +2.132	Accept

6.2 Bargaining Power of Supplier

The term 'suppliers' comprises all sources for inputs that are needed in order to provide goods or services. Supplier bargaining power is likely to be high when, the market is dominated by a few large suppliers rather than a fragmented source of supply, there are no substitutes for the particular input, the suppliers customers are fragmented, so their bargaining power is low, the switching costs from one supplier to another are high, there is the possibility of the supplier integrating forwards in order to obtain higher prices and margins etc. This threat is especially high when the buying industry has a higher profitability than the supplying industry, the buying industry hinders the supplying industry in their development. In such situations, the buying industry often faces a high pressure on margins from their suppliers. The relationship to powerful suppliers can potentially reduce strategic options for the organization. [11]

Here suppliers have a very low level of influence over the industry. Most of the components are made locally and a good number of suppliers are available. Substitute of some resources are available through different suppliers. Same raw materials are obtained from different suppliers from different countries, so there is very low risk of the suppliers being united and trying to control the industry. Switching cost is not at all high as we see that there is different suppliers supplying at the same time. This industry is a well-established sector, so the supplier enjoy less power of bargaining. Some industries has internal suppliers, such as HAMKO battery has HAMKO plastic and KMI to supply them plastic cover and charging plates. We can conclude that suppliers are weak in this industry. The results from t-distribution analysis is summarized in Table 2.

Table 2 Results of t-distribution analysis for bargaining power of supplier

Condition	*t*	Acceptable Range of	Result of Null Hypothesis
Influence of supplier power on cost strategy is very low.	0.4564	-2.132 to +2.132	Accept
Influence of supplier power on differentiation	1.8257	-2.132 to +2.132	Accept

strategy is very low.			

6.3 Threat of New Entrants

The competition in an industry will be the higher, the easier it is for other companies to enter this industry. In such a situation, new entrants could change major determinants of the market environment (e.g. market shares, prices, customer loyalty) at any time. There is always a latent pressure for reaction and adjustment for existing players in this industry. The threat of new entries will depend on the extent to which there are barriers to entry. These are typically economies of scale (minimum size requirements for profitable operations), high initial investments and fixed costs, cost advantages of existing players due to experience curve effects of operation with fully depreciated assets, brand loyalty of customers, protected intellectual property like patents, licenses etc., scarcity of important resources, e.g. qualified expert staff, access to raw materials is controlled by existing players, distribution channels are controlled by existing players, existing players have close customer relations, e.g. from long-term service contracts, high switching costs for customers, legislation and government action. [11]

Demand for this product is very high, so possibility of new entrants is very high. Again technological requirement is not very high. But the entrance is bounded by very high initial cost, government policies and environmental laws. Economies of scale is very high in this sector for making profit. Again loyal customer base will not be created if product is not supplied in necessary amount, which is very important factor for running business. For lack of brand loyalty of customers, it will very hard to achieve economies of scale. So close customer relation is necessary to counter new competitor. The results from t-distribution analysis is summarized in Table 3.

Table 3 Results of t-distribution analysis for threat of new entrants

Condition	*t*	Acceptable Range of	Result of Null Hypothesis
Influence of threat of new entrants on cost strategy average.	-0.3835	-2.132 to +2.132	Accept
Influence of threat of new entrants on differentiation strategy is high.	0.5976	-2.132 to +2.132	Accept

6.4 Threat of Substitutes

A threat from substitutes exists if there are alternative products with lower prices of better performance parameters for the same purpose. They could potentially attract a significant proportion of market volume and hence reduce the potential sales volume for existing players. This category also relates to complementary products. Similarly to the threat of new entrants, the threat of substitutes is determined by factors like brand loyalty of customers, close customer relationships, switching costs for customers, the relative price for performance of substitutes, current trends etc. [11]

Performance constraints of this type of battery, such as poor cycle life, fading performance after repeated discharges, slow charging, and heavy weight may give rise to lithium batteries. The results from t-distribution analysis is summarized in Table 4.

Table 4 Results of t-distribution analysis for threat of substitute.

Condition	*t*	Acceptable Range of	Result of Null Hypothesis
Influence of threat of substitute product on cost strategy low.	-1.8257	-2.132 to +2.132	Accept
Influence of threat of substitute product on differentiation strategy is average	-0.4564	-2.132 to +2.132	Accept

6.5 Competitive Rivalry

Competition between existing players is likely to be high when there are many players of about the same size, players have similar strategies, there is not much differentiation between players and their products, and hence, there is much price competition, low market growth rates, Barriers for exit are high etc. [11]

Market situation for this industry is very good and growth rate is high, one has to ensure constant supply of product as per requirement and provide quality to sustain improvement. Products from different manufacturers don't differ much in specification and quality, so price competition is not very high. Making price a key to take advantage is not easy, again there is brand loyalty of customers. All the manufacturers generally employ the same strategy to achieve improvement. A small amount of manufacturers are in the market and most of them are producing below the demand rate. So competition is not very high in this sector. The results from t-distribution analysis is summarized in Table 5.

Table 5 Results of t-distribution analysis for competitive rivalry.

Condition	*t*	Acceptable Range of	Result of Null Hypothesis
Influence of competitive rivalry on cost	0.0	-2.132 to +2.132	Accept

strategy is average.			
Influence of competitive rivalry on differentiation strategy is very high	0.4564	-2.132 to +2.132	Accept

7. Conclusion

Generally three types of strategies are employed in an industry, namely cost strategy, differentiation strategy and focus strategy. Cost strategy and differentiation strategy has been analyzed in this paper in regard to the five forces. After performing survey required information has been obtained and t-distribution analysis has been performed. It has been found that not all the forces has the same impact on the strategies. It has been found that influence of buyer power on cost strategy is average, influence of buyer power on differentiation strategy is high. Influence of supplier power on cost strategy is very low, Influence of supplier power on differentiation strategy is very low. Influence of threat of new entrants on cost strategy average, Influence of threat of new entrants on differentiation strategy is high. Influence of threat of substitute product on cost strategy low, Influence of threat of substitute product on differentiation strategy is average. Influence of competitive rivalry on cost strategy is average, Influence of competitive rivalry on differentiation strategy is very high. Among the strategies, cost strategy is of more importance than differentiation strategy. In particular, the forces have an average impact on cost strategy, but bargaining power of supplier has relatively low impact than others. For differentiation strategy, the forces generally have a high influence, but influence of bargaining power of supplier is very low. So we can conclude that, bargaining of supplier is the least influential force. Whereas, competitive rivalry is the most influential force for both the strategies. It is a matter of great regret that such an important tool is not practiced yet by most of the firm. They are using their as usual operations strategy which do not give them competitive advantages. These firms should adopt operations strategies which help them reduce cost. They should thrive for continuously updating their process and technology. They should emphasize on researching for alternate technology which helps them to take strong leadership in battery industry.

REFERENCES

[1] Lucintel. (2013) *The Global Battery Industry 2013-2018: Trends, Profits and Forecast Analysis.* [Online] Available from: http://www.lucintel.com/reports/energy/the_global_battery_industry_2013-2018_trend_profit_and_forecast_analysis.aspx. [Accessed: 28th August 2014]

[2] Lu Xue-Long. (2011) *Global Lead-Acid Battery Market Development Status*. [Online] Available from: http://investtaiwan.nat.gov.tw/news/ind_news_eng_display.jsp?newsid=64. [Accessed: 28th August 2014]

[3] Battery University. (2011) *Global Battery Markets.* . [Online] Available from: http://www.batteryuniversity.com/learn/article/Global_ Battery_ Markets. [Accessed: 28th August 2014]

[4] The News Today. (2014) *Battery manufacturers defy recycling rule.* [Online] Available from: http://www.newstoday.com.bd/?option=details&news_id=2373925&date=2014-03-29. [Accessed: 28th August 2014]

[5] Bacanu, Differentiation vs. low cost strategies in Romania. Management & Marketing, vol. 5 (2), pp 135-142 (2010).

[6] Bayraktar and Tatogla, Assessing the link between strategy choice and operational performance of Turkish companies, 14th International Research, Expert conference "Trends in the development of machinery and associated technology", Mediterranean cruise, 11-18, September 2010.

[7] Hill, Differentiation vs. low cost or differentiation and low cost: A contingency frame work, An academy of management review, Vol 13(3), pp 401-412 (2010).

[8] Rada and Abrudan, The management of competitive of companies the supply electro mechanical equipment for oil industry, University of Oradea, Faculty of Electrical Engineering and Information Technology.

[9] Jaradat, Almomani and Salami, The impact of Porter model`s five competence powers on selecting business strategy "An Empirical Study on Jordanian Food Industrial Companies", Interdisciplinary Journal of Contemporary Research, Vol 5, pp 457-470 (2013).

[10] Amrollahi and Akhgar, Analyzing open source business with Porter's five, forces International Journal of Computer Theory and Engineering, Vol. 5, pp 162-165 (2013).

[11] Dagmar Recklies. (2001) *Porters Five Forces Model.* [Online] Available from: http://www.themanager.org/Models/p5f.htm. [Accessed: 10th June 2014]

ICMIEE-PI-140191

Optimization of Grinding Parameters for Minimum Surface Roughness using Taguchi Method

Subrata Talapatra[1,*], *Ishat Islam* [2]
[1]Department of Industrial Engineering and Management, University of Engineering & Technology, Khulna-9203, BANGLADESH
[2]Department of Industrial Engineering and Management, University of Engineering & Technology, Khulna-9203, BANGLADESH

ABSTRACT
The main aim of the machining is to obtain minimum surface roughness and smooth surface contains less wear and friction coefficients. Good surface quality has proper quality of functioning of the parts of product which is influenced by hardness, cutting speed, depth of cut, feed rate etc. In this experiment, FSG-1224 AD (1500 rpm) surface grinding machine is used for surface finishing, hardness is measured by Rockwell Hardness Tester (HRC) and TR-200 is used for measuring surface roughness. Mathematical model is developed to predict surface roughness using the experimental results with the help of Minitab 1513 software. Analysis of variance (ANOVA) was carried out to identify the significant factors affecting the response and the best possible factor level combination was determined through. Finally, a regression model for minimum surface roughness has been developed. The conducted optimal condition which is comparing with experimental results and predicted values.

Keywords: Surface Grinding Machine, Taguchi Method**,** Surface roughness, *S/N* ratio, Regression modeling.

1. Introduction

Production engineering is under constant pressure to satisfy industrial demands for improved productivity while simultaneously achieving high work piece quality. Furthermore, growing environmental awareness is an additional requirement that production engineers must increasingly address. There are still several gaps in the evaluation of process eco-efficiency and material effectiveness [1]. A typical surface is characterized by clean cutting paths and plowed material to the sideway of some grooves. However, many other marks can be found, such as cracks produced by the thermal impact, back-transferred material and craters produced by a grain fracture. Thus, need to machine to achieve smooth surfaces and high dimensional accuracy. Surface Grinding is an abrasive machining process widely used for the final shaping of components that require very smooth surfaces and a high dimensional accuracy. The performance attainable in this process as measured by levels of productivity, cost, and final part quality is determined by the selected combination of (i) the machine tool, (ii) work piece material (iii) grinding wheel (iv) setup parameters, (v) grinding parameters and (vi) grinding fluid [2]. In many cases, the selected parameters are too conservative and not adapted to maximize the utility of the machine tool and the grinding wheel. A similar practice is prevalent in the selection of grinding fluid application settings, where different oils are typically used to flood the grinding contact zone without considering more effective alternatives [3]. Although grinding has been used extensively in the production of precision components, these common practices confirm that it still remains one of the least understood and most inefficiently conducted machining process in the manufacturing industry.

2. Objectives

I. The main objective in this machining process is to minimize the surface roughness (Ra).
II. To determine the significant grinding parameters on the key process performance responses. (Feed force, Feed, Depth of cut, Temperature, System Roughness)
III. To optimize the grinding parameters.

3. Literature review

Nowadays, grinding is a major manufacturing process which accounts for about 20-25% of the total expenditure on machining operations in industrialized countries. In the grinding process, material is removed from the work piece by a rotating abrasive wheel. The grinding process can be classified into three parts; which are surface, cylinder and center less grinding. These processes are choose regarding with work piece shape. Surface grinding is the common operation for grinding flat surface and is likely to produce high tolerances, low surface roughness and planar surfaces. In surface grinding, shallow depth of cut is achieved with fast feed rates and the depth of cut can range from 0.01 to 0.05mm while feed rate is approximately 3m/s [4].The cutting speed, feed rate, and depth of cut have the greatest influence on the surface roughness. Increasing the feed rate significantly increases the surface roughness, as well as the depth of cut using the Taguchi method. Akkus et al. Found that the feed rate is the most significant factor that contributes to the surface roughness using ANOVA and regression. Chowdhury et al. Noticed that the rate of growth of flank wear increases irrespective of feed, with an increase in speed under both minimum quantity lubrication and dry conditions. According to

* Corresponding author. Tel.: +88-01727555334
E-mail address: sub_ksy @yahoo.com

Grzesik&Wanat the results show that by keeping equivalent feed rates (0.1 mm/rev for conventional, and 0.2 mm/rev for wiper inserts), the obtained surfaces have similar roughness parameters and comparable values of skewness and kurtosis. With wiper inserts and a high feed rate it is possible to obtain machined surfaces with <0.8 µm of Ra compared with conventional inserts that present high values of surface roughness. Kushnaw et al. Observed that the main factor affecting the inclination angle is the diameter of the periphery, and machined diameters depend on change in depth of cut and the cutting condition. Choudhury et al. discussed the development of surface roughness prediction models for turning EN 24T steel (290 BHN) using a response surface methodology. A factorial design technique was used to study the effects of the main cutting parameters such as cutting speed, feed, and depth of cut on surface roughness. The tests were carried out using uncoated carbide inserts without any cutting fluid [5].

4. Methodology

4.1 Taguchi Method

Taguchi method is the process of engineering optimization in a three steps approach namely system design, parameter design and tolerance design. In the system design, a basic functional prototype design will be produced by applying scientific and engineering knowledge. In parameter design, independent process parameter values will be optimized and where as in tolerance design, tolerances will be determined and analyzed for optimal values set by parameter design. Taguchi method is a powerful design of experiments (DOE) tool for optimization of engineering processes [6]. Steps of taguchi method is given in Fig.1.

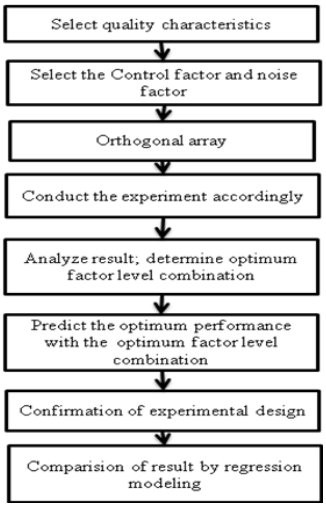

Fig.1 Steps of taguchi method

4.2 Experimental Procedure

In the present work, mild steel, cast iron and carbon steel have been selected for work materials. The work materials are 6 inch in length, 3 inch in width and 3/4 inch height. After filling, work pieces are grinded in surface grinding machine. (FSG-1224 AD, 1500 RPM), grinding spindle drive speed 50Hz/150, power rating 3.7 KW. Aluminum grinding wheel- WA36G5VBE is used as grinding wheel. Dioxol.M used as cutting fluid. The various process parameters of a surface grinding machine include depth of cut, material hardness, and work piece speed, grinding wheel grain size, and grinding wheel speed. The input processes parameters namely material hardness, work piece speed and depth of cut. The other parameters such as abrasive type and feed rate are kept constant. The number of experiments to be conducted can be reduced by using orthogonal array method of Taguchi optimization technique. Experimental Set-up for surface grinding is given in **Fig.2**.

Fig.2 Experimental Set-up for surface grinding

Selected process parameters are given in **Table 1**.

Table 1 Selected process parameters

Level	Hardness(HRC)	Work piece speed (ft/min)	Depth of cut(mm)
1	15	38	0.001
2	25	44	0.005
3	36	48	0.01

Surface roughness values are obtained from Surface Roughness Tester TR-200 Surface roughness tester for each experiment. The obtained values used for the Taguchi optimization process. L9 orthogonal array surface with roughness values is given in **Table 2**.

Table 2 L9 orthogonal array surface with roughness values

Exp.No.	Hardness	Work piece speed	Depth of cut	Ra
1	15	38	0.001	0.763
2	15	44	0.005	0.630
3	15	48	0.01	0.382
4	25	38	0.005	0.470
5	25	44	0.01	0.396
6	25	48	0.001	0.470
7	36	38	0.01	0.291
8	36	44	0.001	0.429
9	36	48	0.005	0.300

In the Taguchi method, the term 'signal' and 'noise' denote respectively 'desirable' and 'undesirable' value. Signal to Noise ratio is found out in each case using the criteria 'lower is better' as surface roughness is the factor of consideration. The objective of using the S/N ratio as a performance measurement is to develop products and processes that are insensitive to the noise factor.

Lower is better S/N = -10 log [1/n (Σyi2)] (n=1)

From this equation where n represents the number of experimental run. Signal to noise ratio for various experiments is given in **Table 3**.

Table 3 Signal to noise ratio for various experiments

Exp. No.	SNRA1
1	2.3495
2	4.0132
3	8.3587
4	6.5580
5	8.0461
6	6.5580
7	10.7221
8	7.3509
9	10.4576

Average S/N ratio for each parameter at each level is found out. Similarly the average surface roughness values for each parameter at each level are also found out. Average S/N ratios in each level, a main effect for S/N ratio, average surface roughness values in each level and effect of process parameter on roughness are given in **Table 4**, **Fig.3**, **Table 5** and **Fig. 4** respectively.
.

Table 4 Average S/N ratios in each level

Level	Hardness	Work piece speed	Depth of cut
1	4.907	6.543	5.413
2	7.048	6.470	7.010
3	9.510	8.452	9.042
Delta	4.603	1.982	3.629
Rank	1	3	2

From the table 5, hardness greatly influenced the surface roughness (Ra), followed by the depth of cut and work piece speed. Based on table 5,the optimum conditions for this study are 36(HRC),48(ft/min) and 0.01(mm) for hardness, work piece speed and depth of cut. So signal to noise ratio is high in level 3.The difference between the largest and minimum signal to ratio is calculated and the factors effect are ranked based on it.

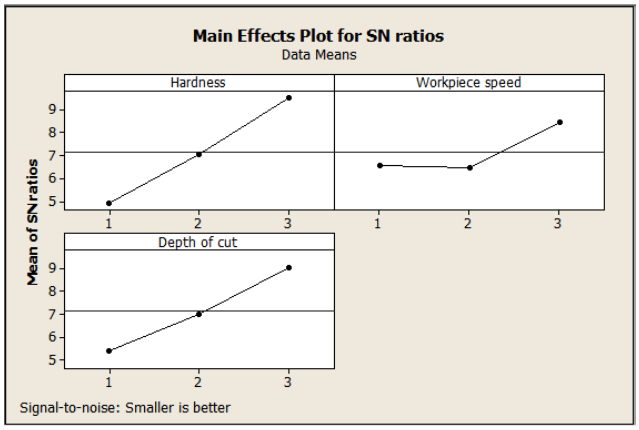

Fig.3 Main effects for S/N ratio

I. Level III for Hardness, H_3 = 9.510dB indicated as the optimum situation in terms of S/N values.
II. Level III for Cutting Speed, W_3 = 8.452dB indicated as the optimum situation in terms of S/N values.
III. Level III for depth of cut, D_3 = 9.042dB indicated as the optimum situation in terms of *S/N* values.

Table 5 Average surface roughness values in each level

Level	Hardness	Work piece speed	Depth of cut
1	0.5917	0.5080	0.5543
2	0.4457	0.4850	0.4667
3	0.3400	0.3843	0.3563
Delta	0.2517	0.1237	0.1980
Rank	1	3	2

From the table 6, at level 3(hardness, work piece speed and depth of cut), the surface roughness (Ra) is low. The difference between the largest and minimum signal to ratio is calculated and the factors effect are ranked based on it. As this table hardness greatly influenced the Ra, followed by the depth of cut and work piece speed. The optimum conditions for this study are 36(HRC), 48(ft/min) and 0.01(mm) for hardness, work piece speed and depth of cut.

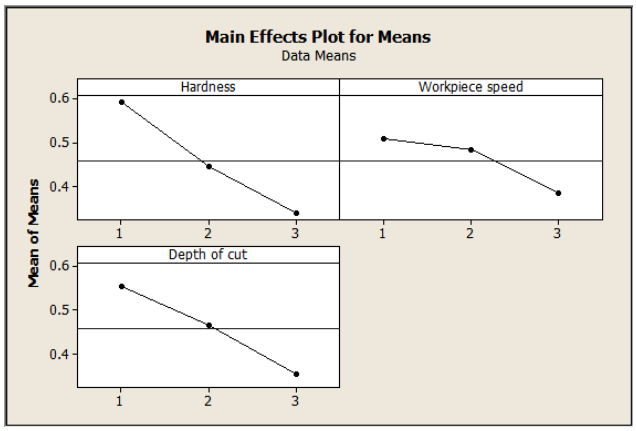

Fig. 4 Effect of process parameter on roughness

I. Level III for Hardness, H_3 = 0.3400Ra indicated as the optimum situation in terms of Surface Roughness values.

II. Level III for Cutting Speed, W_3 = 0.3843Ra indicated as the optimum situation in terms of Surface Roughness values.

III. Level III for depth of cut, D_3 = 0.3563Ra indicated as the optimum situation in terms of Surface Roughness values.

4.3 Interaction Plot

Whether interactions between factors exist or not can be shown by plotting a matrix of interaction plot. Parallel lines in an interaction plot indicate no interaction. However, the interaction plot doesn't tell if the interaction is statistically significant. Interaction plots are most often used to visualize interactions during DOE. Interaction Plots are used to compare the relative strength of the effects across factors [7]. Interaction plot for SNRA1of Ra is given in **Fig.5**.

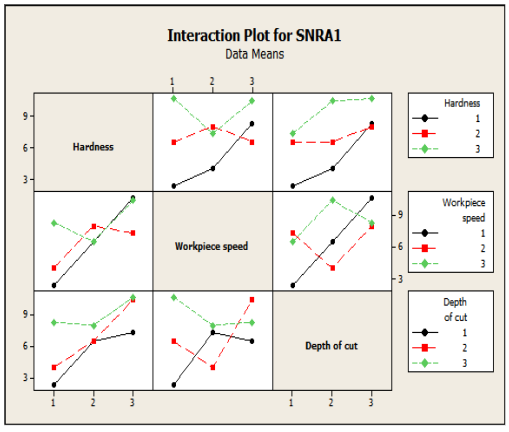

Fig.5 Interaction plot for SNRA1of Ra

From these figure (5 and 6), it can be seen that there are non-parallel line between hardness, workpiece speed and depth of cut. So, all factors depend on each others.

5. Calculations and result

5.1 ANOVA test

One way ANOVA test is used for obtaining the F value. Analysis of variance (ANOVA) of Ra is given in **Table 6**.

Table 6 Analysis of variance (ANOVA) of Ra

Source	DF	SS	MS	F	P
Regression	1	58.143	58.143	281.42	0.000
Residual error	2	1.446	0.207		
Total	8	59.589			

From this table F-value is 281.42 and P vale zero. that means there is a significant relationship between the response variable. To generalize the results, the Modeling of input parameters (Hardness, work piece speed, grains) and output parameter (Roughness) is done using Regression Modeling and Minitab1513 Software. Regression equation, different residual plots for testing the adequacy of the proposed model and Run test: Experiment No. *Ra* are given in **Table 7, Fig.6** and **Table 8** respectively.

Table 7 Regression equation

The regression equation is SNRA1=15.3-17.7 surface roughness				
Predictor	Coef.	SE Coef.	*T*	*P*
Constant	15.2680	0.5067	30.130	0.000
Ra	-17.671	1.053	-16.78	0.000

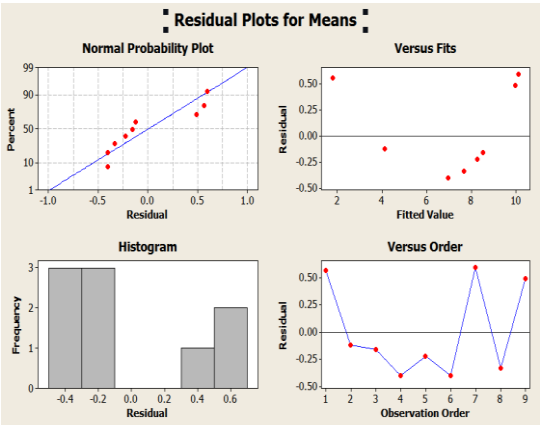

Fig.6 Different residual plots for testing the adequacy of the proposed model

I. Normal probability plot indicates the data are normally distributed and the variables are influencing the response. Outliers don't exist in the data

II. Residuals versus fitted values indicate the variance is constant and a non-linear relationship exists.

III. Histogram proves the data are not skewed and no outliers exist.

IV. Residuals versus order of the data indicate that there are systematic effects in the data due to time or data collection order.

Table 8 Run test: Experiment No. *Ra*

Runs test for experiment no. Runs above and below K=5
The observed no. of runs=2 The expected no. of runs=5.4444 4 observations above K,5 below *N is small, so the following approximation may be invalid. *P*-value=0.013
Runs test for surface roughness Runs above and below K=0.459
The observed no. of runs=6 The expected no. of runs=5.4444 4 observations above K,5 below *N is small, so the following approximation may be invalid. *P*-value=0.688

Confirmation experiments were conducted at the optimum set of the process parameters. The value of surface roughness at the optimum set of the process parameters was 0.340 µm and it fall near the predicted value of 0.300 µm. The difference between the value of the minimum and the actual surface roughness (*Ra*) is about 36%. Conformation of experiment is given in **Table 9**.

Table 9 Conformation of experiment

Surface roughness(Ra)	S/N ratio (dB)
0.300	10.4576

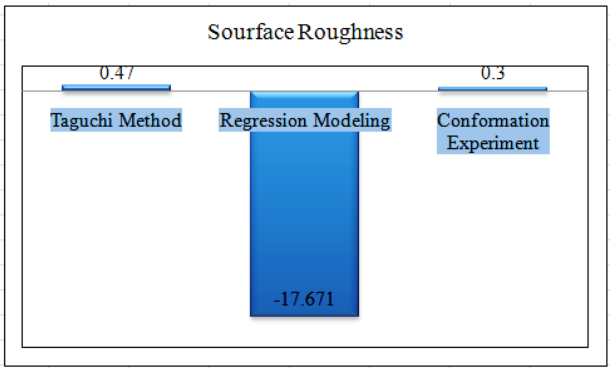

Fig.7 Comparisons of results

6. Conclusions

From main effects plotted, it is observed that there is decrease in surface roughness as material hardness increased from -15 to 36. The surface roughness decreases when work piece speed increases from 38 to 48 ft/min, similarly when depth of cut increases from 0.001 to 0.01mm surface roughness decreases. It can be observed that the difference between the value of the minimum and the actual surface roughness (*Ra*) is about 36%.

NOMENCLATURE

R_a : surface roughness
rpm : revolution per minute
HRC : Rockwell Hardness C scale
mm : millimeter
ft/min : feet per minute
ANOVA: Analysis of variance
µm : micrometer
DOE : Design of experiment
Kw : kilowatt
S/N : Signal to Noise Ratio
db : decibel
DF : Degree of freedom
SS : Sum of square
MS : Mean of square
F : statistical parameter
P : percentage

REFERENCES

[1]. California,Berkeley, Dornfeld, David, Combination of speed stroke grinding and high speed grinding with regard to sustainability, *Green Manufacturing and Sustainable Manufacturing Partnership*, (2011).

[2]. Sead Dzebo, Investigation of methods to improve process performance in centers less grinding of Inconel 718 And Ti-6al-4v Super alloys, *Georgia Institute of Technology*, (2009).

[3]. Angela Adamyan, David He, Ioan Marinescu, and Radu Coman, Multi-objective optimization of grinding processes with Two, Approaches:Optimal pareto set with Genetic Algorithm and Multi-attribute, Utility Theory.

[4]. M.A.Kamely,S.M.Kamil, and C.W.Chong,World, Mathematical modeling of surface roughness in surface grinding operation, *World Academy of Science, Engineering and Technology*,Vol:56, (2011).

[5]. S.Afr.J.Ind.Eng, Reducing surface roughness by optimizing the turning parameters, *South Africa jounal of Industrial Engineering*, Vol.24, No.2, (2013).

[6]. Deepak Pal, Ajay Bangar Rajnan Sharma, Ashis Yadav, Optimization of grinding parameters for minimum surface roughness by Taguchi Parametric Optimization Technique, *International Journal of Mechanical and Industrial Engineering (IJMIE)*,Vol.1, No.3, (2012).

[7]. Rt.Achyut.K., Panda,R.K.Singh, Optimization of Process Parameters by Taguchi Method: Catalytic degradation of polypropylene to liquid fuel,

International Journal of Multidisciplinary and Current Research, (2013).

ICMIEE-PI-140192

Gas Stove with Embedded Controlling System to Stop Misuse of Natural Gas in Bangladesh

Kazi Ehsanul Karim [1], *Jaber Al Hossain* [2,*], *Farhan Hossain* [3]
[1,2,3] Department of Mechanical Engineering, Khulna University of Engineering & Technology, Khulna-9203, BANGLADESH

ABSTRACT
Natural gas is the most essential resource in Bangladesh. Around 52% of energy supply of Bangladesh depends on natural gas. It is estimated that, approximately 20 TCF gas is reserved in Bangladesh. Though domestic users consume 12% of the gas supply, a big amount of this supplied gas is misused due to drying cloths, warming room and for other purposes during winter and rainy season. Through this research work, a microcontroller based embedded system (including arduino mega, ultrasonic sensor, servo motor) is designed to control this misuse and stop it. This embedded system will enable the gas flow through gate valve of gas stove whether there is any cooking pot on the gas stove. Thus the misuse of domestic gas will be stopped.

Keywords: Gas stove, Microcontroller based embedded system, Ultrasonic sensor, Valve and key system, servo motor.

1. Introduction

Proper use of natural gas is really essential for future energy production, domestic use and other purposes in Bangladesh. Recent statistics shows that, the growth rate of gas consumption is 10% [4] and the R/P ratio of Bangladesh is 17.8 years. Thus the reserved of natural gas will ends after 17.8 years. As the rate of natural gas consumption is 1000mmcfd, the domestic demand is 120mmcfd. Total customer of petrobangla is only 2369371 up to December, 2012 [1]. It becomes difficult for the government of Bangladesh to ensure natural gas supply to the remaining citizens. Moreover a big amount of this supplied gas for domestic purposes is misused. But this wasted gas can be used for further domestic gas connections. This paper presents a microcontroller based embedded system, which will enable the government to stop the misuse of natural gas effectively. Through the saved natural gas more new connections can be made. Thus other citizens can be benefitted.

2. Background

In order to stop the misuse of natural gas through natural gas stove, some research papers were published. In "Microcontroller based natural gas oven" [3], Authors only suggested a method using solenoid gas valve. But no practical construction was done. Thus there is no feasibility of this project. In the evaluation of pilot project, natural gas pre-paid meter was introduced for domestic users. Here a new billing methodology is proposed but no method for saving natural use was mentioned. In this research paper a method with practical construction for saving gas is shown.

3. Construction of mechanical Structure

In this project, a mechanical structure is constructed. In the constructed structure, a servo motor is connected with gas gate valve to operate the mechanical parts to start and stop the gas flow. Welded bars are joined with the gate valve and the rotating shaft of servo motor. So rotation of the output shaft of the servo motor controls the rotation of the gate valve. After every 90 degree rotation the gate valve opens and closes its paths respectively. The structure is shown in Fig.1. In Fig.2, it is shown that the gas gate valve is attached with the gas stove. In this position, the proposed embedded system will be placed.

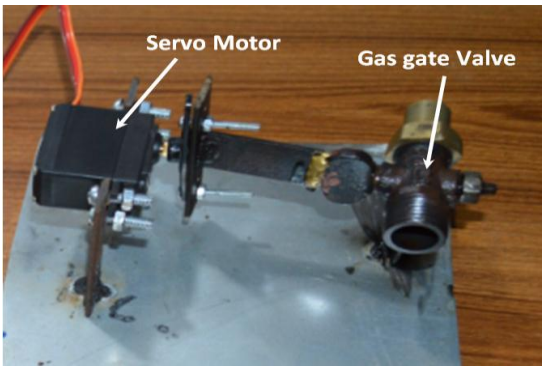

Fig.1 Constructed mechanical structure

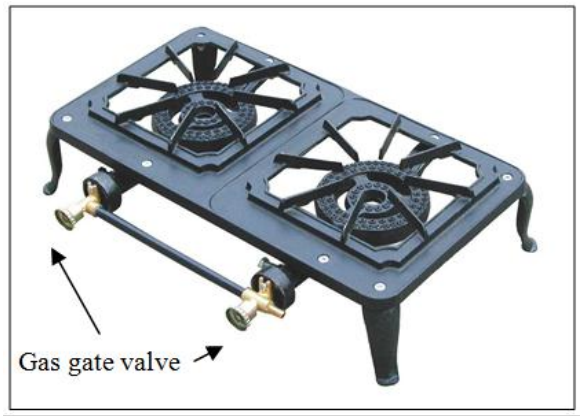

Fig.2 Natural Gas stove

4. Electrical components

In this research project, a microcontroller based embedded system is designed and interfaced with the mechanical structure. This embedded system consists of

* Corresponding author. Tel.: +88-01680387475
E-mail address: jaber.me.2010@gmail.com

an arduino Mega 2560, ultrasonic sensor – HC-SR04 and a servo motor.

4.1 Arduino Mega 2560

The operating voltage of arduino mega 2560 is 5V and the input recommended voltage is between 7V to 12V. It has 54 digital I/O pins among which 14 pins provide PWM output. It has 16 analog input pins. DC current per I/O pin is40 mA. Flash memory size is 256 KB of which 8 KB is used for boot loader. SRAM, EEPOROM and clock speed are 8 KB, 4 KB and 16 MHz respectively [7].

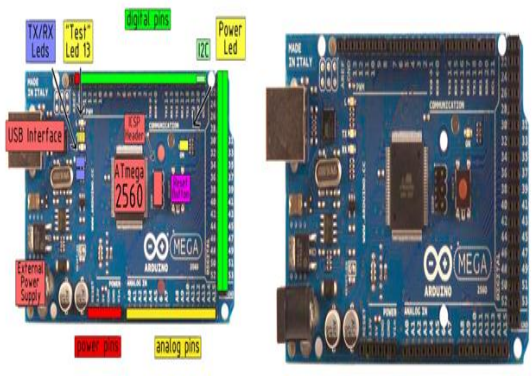

Fig.3 Arduino Mega 2560

4.2 Ultrasonic sensor – HC-SR04

It provides 2cm to 400cm non-contact measurement function. The ranging capacity can be extended to 3mm. It has ultrasonic transmitter, receiver and control circuit. Its working voltage, current, frequency and measuring angle are DC 5V, 15mA, 40Hz and 15 degree respectively. Trigger input signal is 10uS TTL signal and the echo output signal ranges in proportion.

Fig.4 Ultrasonic sensor – HC-SR04

4.3 Servo motor

The model of servo motor is Tower Pro MG 995. It is a metal geared motor. Its operating voltage lies between 4.8V to 7.2V and temperature range is 0 ^{o}C to 55 ^{o}C. The stall torque of this motor is 8.5Kg/cm at 4.8V and 10Kg/cm at 6V. Operating speed is 0.20 sec/60 degree at 0.16 sec/60 degree. It weighs 55g.

Fig.5 Tower Pro MG 995

5. Circuit arrangement

In the circuit arrangement, Echo pin is attached to arduino pin 7 and the Trig pin is attached to arduino pin 8. Onboard led is attached to led pin 13. VCC supply is 5V to the arduino. Maximum range of ultrasonic sensor is 25cm and the minimum range is 10 cm. Ultrasonic signal is sent after every 50ms duty cycle. The full circuit diagram is shown in Fig. 6

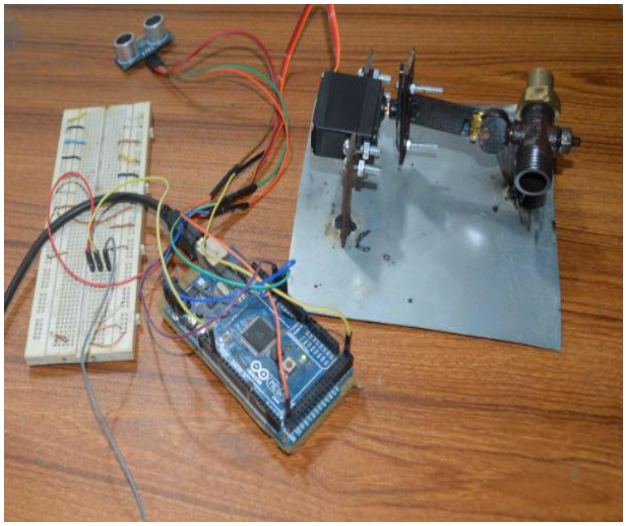

Fig.6 Interface of constructed mechanical structure and circuit arrangement

6. Control Mechanism

The embedded system enables the gas flow through gate valve whether there is any obstacle between the defined working ranges (10cm-25cm) of ultrasonic sensor. The range can be changed through arduino program according to the stove model. In this stage, the motor gives anti-clockwise rotation at 90 degree angle. This is shown in Fig.7 by using hand as an obstacle. Thus the gas flow was enabled through gate valve.

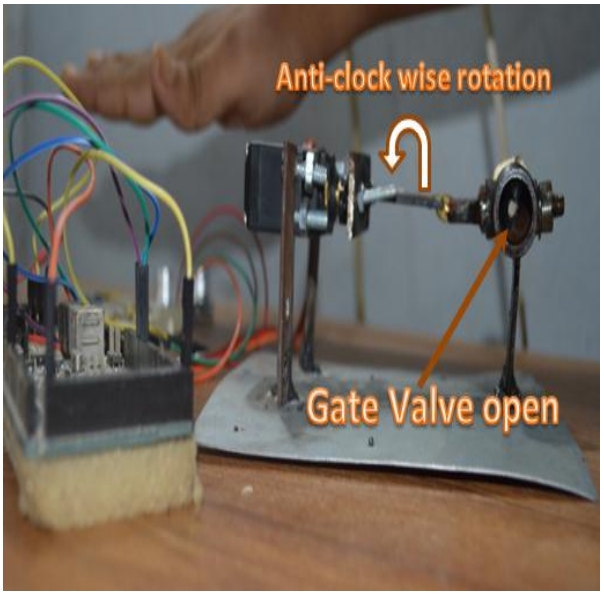

Fig.7 Gas flow enabled

If the obstacle is taken away from the working range, ultrasonic senor possess signal through microcontroller of arduino board. When this signal is forwarded to the servo motor, it gives clockwise rotation at 90 degree angle. Then the gas flow is disabled through gate valve. This phenomenon is shown in Fig.8.

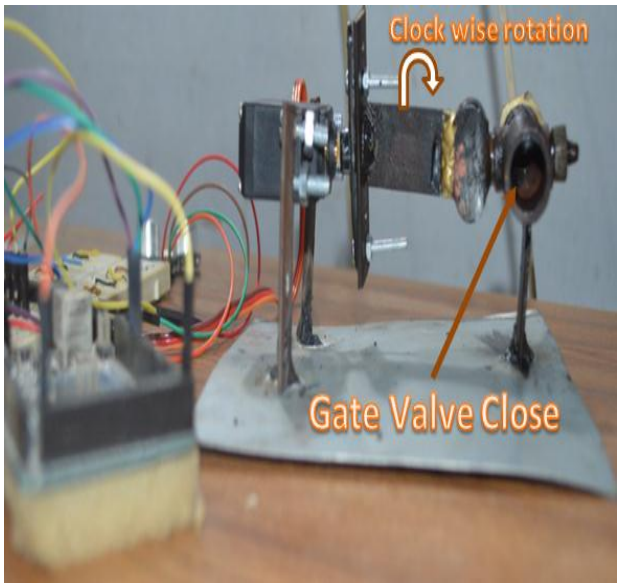

Fig.8 Gas flow disabled

When the gas flow is enabled, gas stove can be used for cooking purpose. Thus the embedded system make the gas stove to perform whether there is any cooking pot on it. In order to visualize the control mechanism, block diagram is shown in Fig.9. The flow chart is also given in Fig.10 which shows the whole working mechanism.

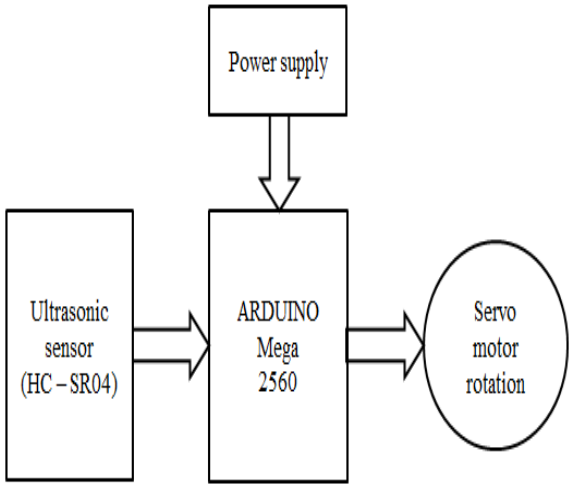

Fig.9 Block diagram of the flow system

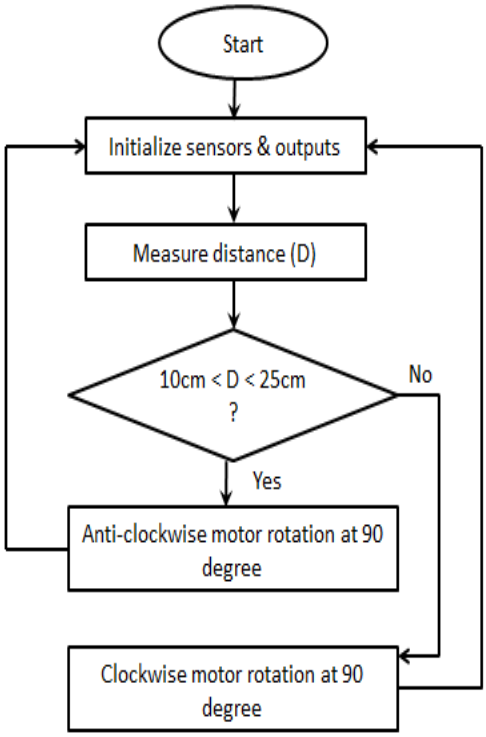

Fig.10 Flow chart of control mechanism

7. Cost analysis

It is shown in the annual report of Petrobangla [1] that the domestic consumption of natural gas from fiscal year 2011 to fiscal year 2012 was 89.29 BCF or 89290000000 CF. The number of domestic consumers of natural gas up to 2012 was 2369371 [1]. So consumption of one user is 37685.12 CF. Thus the daily consumption of one user is 103.25 CF. Past surveys showed that the individual consumer uses 8 hours a day to complete cooking purpose [5]. Though a big amount of natural gas is wasted for long time by most of the domestic users, it is assumed that 2 hours of the cooking

period is wasted by drying clothes, warming room for independent calculation. So the amount of wasted gas per day is 17.21 CF by an individual user. So the wasted amount of natural gas of one year by the total domestic user is 14883559 MMCF. According to the tariff structure of gas, the cost of bearing one household stove is BDT 146.25/MMCF. So the total cost of wasted gas is BDT 217.67 cores. For installation of the proposed system the government will need BDT 189.55 cores. Thus in first year of installation the profit of government will be BDT 28.12 cores. Moreover, this calculation shows that the yearly wastage of 6 users is 37689.9 CF which is more than the yearly consumption of one user. So using this embedded system, the government can connect natural gas to 394895 new consumers without new production. The amount saved gas by this embedded system will be 30, 612 MCF. The vast production cost of this embedded system with PCB system will be 189.55 cores BDT to connect this embedded system to the gas stove of 2369371 users. The profit of Government will be 213.24 cores BDT from 384895 new connections. So the profit will be 23.69 cores BDT. Thus 394895 new gas connections can be made which is 16.67% of existing connections.

8. Result and Discussion

This Microcontroller based embedded system can stop the misuse of Natural gas. The domestic users will be able to use the natural gas only for cooking purposes through this system. But there will be no further scope to use our natural gas for drying clothes or warming room. Thus more gas connections can be made by using the present production. Government could not provide new gas connections for several months due to gas crisis. But this embedded system will enable them to make new connections without new production. The independent calculation of this research work shows that 3, 94, 895 new connections can be made using the designed microcontroller based. So the implementation of this project is essential not only for the common people but also for the government. Thus the right of every citizen on natural gas will be fulfilled.

9. Conclusion

Proper use of natural gas is really essential for the welfare of common people. Thus the implementation of this research project will ensure the right of common people on natural gas of our country. In different research projects, many methods were shown for controlling the misuse of natural gas. But the proposed embedded system will efficiently stop the misuse with economic benefits. So the implementation of this project is really essential for our country.

Further work of this research project can be the development of power supply from rechargeable battery.

NOMENCLATURE

TCF : Trillion Cubic Feet
Mmcfd: Million Cubic Feet a day
MCF : Thousand Cubic Feet
Nm^3 : Standard Cubic Feet
R/P : Réserves-to-production ratio
BCF : Billion Cubic Feet
CF : Cubic Feet
PCB : Printed Circuit Board
MMCF: Million Cubic Feet

REFERENCES

[1] Hossain, Annual report 2012, Bangladesh oil, gas and mineral corporation (Petrobangla), Ministry of power, energy and mineral resources, Government of People's Republic Bangladesh, 2012.

[2] Gomes, "Natural gas in Pakistan and Bangladesh: current issues and trends", The Oxford for energy studies, NG 77, June 2013.

[3] Rahman, A. H. Ronee, "Microcontroller Based Smart Gas Oven", *International Journal of Advancements in Research & Technology,* Volume 1, Issue3, August-2012.

[4] M. S. Islam, "Research Report on Energy Sector of Bangladesh", *IDLC Finance Limited, March-2011*.

[5] M. Rahman and G. Sarwar, "Natural Gas Pre-paid metering for Domestic Customers: Evaluation of the Pilot Project by Titas Gas Transmission and Distribution Company Limited", *International Conference on Mechanical Engineering*, December, 2011.

[6] M. J. Hossain, M. A. Banu, R. Sobhan, "Bangladesh Gas Sector Development: Status, Policy Option and Challenges", CPD Dialogue, Report no. 24, May 2000.

[7] Margolis, "Arduino Cookbook," O'Reilly Media, 2nd Edition, 2011.

[8] Ali, Asad, M. S. Islam, "Contactless Smart Card Based Prepaid Gas Metering System", *International Conference on Industrial Engineering and Operations Management Bali, Indonesia*, January 7 – 9, 2014.

ICMIEE-PI-140194

Characterization of Coastal Water Deposits and its Subsequent Effect on Piping Materials

A.H.M Fazle Elahi[1], Zia Uddin Md. Chowdhury[2],Mohammed Enamul Hoque[3]*

[1]Department of Mechanical Engineering,
Khulna University of Engineering & Technology, Khulna-9203, BANGLADESH
[2]Department of Leather Engineering,
Khulna University of Engineering & Technology, Khulna-9203, BANGLADESH
[3]Department of Chemistry
Khulna University of Engineering & Technology, Khulna-9203, BANGLADESH

ABSTRACT
The coastal water has common feature of high salinity and hardness. Besides these there are deposited materials in water. Bangladesh has a total area of 147,570 km2 where coastal region covers almost 29,000 km2 or about 20% of the country. About 53% of the coastal areas are affected by salinity. CaCO3, Cl- and pH has the greater effect on material. The chemical characteristics of the water flowing through a pipe will influence whether the water is stable and will also affect the extent of any corrosive reaction. Sample water collected from coastal region was undergone some test to evaluate some characteristics such as Alkalinity, Hardness, COD, BOD, EC, TDS, Sulfate, Ammonia etc. Primary factors include alkalinity, hardness, and pH, but oxidizing agents, carbon dioxide, and dissolved solids can also influence corrosion. These deposits plays vital role for corrosion and for destroying electric conductivity of the metal. Here pH of the coastal area water is found to be 6.94~7.85, which illustrates the hardness of water. Brienell Hardness Number (BHN), Rockwell Hardness, Impact load capacity & Shear test have been done on GI & copper pipes that carry coastal area water. An image of affected material has been captured on Scanning electron Microscope (SEM) to investigate the condition of scale forming and corrosion. Scaling tends to be the result of water with a high hardness. Hard water typically contains a lot of calcium compounds which can precipitate out as calcium carbonate. Some processes to solve these problems has been proposed.

Keywords: Piping Material (GI), Water Characterization, Brinell Hardness Number (BHN), Scale forming, Impact of Water

1. Introduction: Bangladesh, lies in the northeastern part of South Asia, has a total area of 147,570 km2 where coastal area covers about 32% of the country [1]. Due to influence of tide and presence of salinity in coastal rivers, the livelihoods of over 50 million inhabitants of coast area depend on groundwater for meeting domestic, municipal, industrial and other needs. Numerous water quality problems exist in ground water and surface water systems in Bangladesh, especially in its southwestern coastal belt, where salinity is a very alarming issue at present [2]. Khulna city is located on the banks of the Rupsha and Bhairab Rivers in the southwest region of Bangladesh. However, the southwest coastal belt of the country is facing enormous challenges in meeting the rising freshwater demand due to limited water supply from the available ground water and surface water sources as they are affected by the salinity and other water quality problems [2],[3]. The salinity was started to increase in Khulna after the commencement of Farrakka Barrage operation of India in 1975, which significantly reduced the Ganges flow, located at upstream of the Gorai River, a major source of freshwater to the rivers surrounding Khulna [4]. As salinity in the groundwater is a key factor, a clear idea of the extent of fresh –saline groundwater in various depths is required for optimal development and use of this precious potable water resource. The southwestern coastal region is characterized by the Ganges tidal flood plains with low relief, criss-crossed by rivers, tidal marshes and swamps. Although groundwater is abundant in the region, saline water intrudes into the aquifer system due to reduction of upstream freshwater flow, shrimp farming and over abstraction of groundwater makes the situation worse. As a consequence the coastal area may suffer from acute storage of potable water. It has also negative impacts on human activities, livelihood, agricultural production, aquatic ecosystem, infrastructure etc.

The availability of water determines the location and activities of humans in an area and our growing population is placing great demands upon natural fresh water resources. Technological growth has also put the ecosystem we depend on under stress and the availability of water is at a very high risk [5-6]. It is important to analyze water to determine its suitability for drinking, domestic use industrial use, agricultural use etc. It is also important in water quality studies to know the amount of organic matter present in the system and the quantity of oxygen required for stabilization of the water. The impact of organic pollutants on water quality in this work is expressed in terms of the Biochemical Oxygen Demand, BOD and Chemical Oxygen Demand, COD which all depend on the Dissolved Oxygen, DO. Total organic Carbon, TOC and Total Dissolved Solids; TDS on the other hand are

* Corresponding author. Tel.: +88-01920804972
E-mail addresses: zia1.chowdhury@yahoo.co.uk

used to define the organic content of the water and the total ions in solution respectively. It is estimated that over 80% of the wastewater generated across the world are not presently collected or treated [7]. Ground water pollution by various organic and inorganic substrates may alter the quality of that water, which may cause adverse health effects on humans. Several works on water quality have focused on the physicochemical characteristics of waters [8], [9]. The aim of this study therefore, physic-chemical analysis of the water and the mechanical test of GI pipe, water flowing through a pipe will influence the mechanical properties and extent of any corrosive action due to salinity. High alkalinities values in water are associated with high dissolved solids which can create scale build up on water pipeline systems, especially hot water pipeline systems. Scale build up in the pipeline system can increase power consumption and also increase the costs to heat the water.

2.0 Materials and Methodology

2.1 Materials:

Generally Galvanized Iron is used as piping material. Galvanizing is a process of coating iron or steel with zinc in order to provide greater protection against corrosion for the iron or steel base. Chemical Composition of Soft Iron:-C = 0.03%Si = 0.05%Mn = 0.20%P = 0.01%S = 0.02%. Galvanized iron and steel's resistance to corrosion depends largely on the type and thickness of the protective zinc coating and the type of corrosive environment. The zinc coating on galvanized iron and steel may be corroded by: Acids, strong alkalis, and is particularly vulnerable to corrosion by sulfur acids produced by hydrogen sulfide and sulfur dioxide pollution in urban atmospheres. [10]

The zinc provides a barrier against corrosion so that the pipe may be exposed to the outdoor environmental elements. The protective barrier proves equally effective against damage from indoor humidity. The reason for this is the the zinc is oxidizes easier than the iron so even if the layer of zinc is broken the zinc will oxidize before the iron. [11]

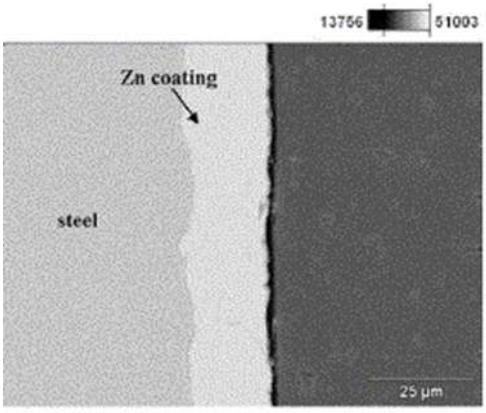

Fig.1: SEM image of cross section of galvanized Iron

The coating that develops during the galvanizing process is metallurgically bonded to the steel – virtually becoming a part of the steel itself. During the reaction in the kettle, the zinc interacts with the iron in the steel to form a series of zinc-iron alloy layers. The photomicrograph below is a cross section of the galvanized steel coating, showing a typical microstructure comprised of three alloy layers and a layer of pure metallic zinc.

Fig.2: The sample GI pipe used for carrying sample water

2.2 Methodology:

It is needless to emphasize the importance of water in our life. We need water for different purposes; we need water for drinking, for industries, for irrigation, for swimming, for fishing etc. Thus water for different purposes has its own requirements for the composition and purity and each body of water has to be analyzed on a regular basis to confirm to suitability. The types of analysis could vary from simple field testing for a single analysis to laboratory based multi component instrumental analysis. The representative sample of water that is taken should be the one that truly reflects the composition of the water sample to be analyzed. Due to varying period of time that may lapse between sample collection and analysis, storage conditions must be such as to avoid undesirable loses, contamination or other changes that could affect the results of the analysis. [12]

Khulna University of Engineering & Technology (KUET) is situated in southwestern part of Bangladesh, and the area of study is in the southwest coastal belt of the country, is facing enormous challenges in meeting the rising freshwater demand due to limited water supply from the available ground water and surface water sources as they are affected by the salinity and other water quality problems.

Water samples were collected in pre-cleaned plastic bottles from KUET in the form of ground water and surface water. The samples were analyzed for pH, DO, BOD, COD, TOC, TDS and alkalinities using standard analytical techniques. [13] Results obtained were expressed in bar diagram.

The pipe that carry the sample water has undergone some tests. Mainly the surface morphology of the GI material has been tested through Scanning Electron Microscope (SEM) images. Materials made with unique

sizes and structures of grain are viewed by microscope. Generally, there are two types of electron microscopes, transmission electron microscope (TEM) and scanning electron microscope (SEM). TEM shoots electrons through the sample and measures how the electron beam changes as it is scattered in the sample; SEM images the sample surface by scanning it with electron beams in a raster scan pattern. SEM is used to investigate the crystal growth or structure evolution processes in our work. It is a very powerful tool to study the crystal growth morphology and assist the micro and nanofabrication.

Besides the Brinell Hardness Number (BHN or HB) of the internal surface of the pipe has been determined by a Tensometer using conventional method. The value of BHN was compared with the conventional value to evaluate the changes of the pipe surface due to the impact of water.

Fig.3: Tensometer used for BHN test

3.0 Impact of Water:

Many water quality factors affect corrosion of pipes used in water distribution, including the chemistry and characteristics of the water (e.g., pH, alkalinity, biology), salts and chemicals that are dissolved in the water, and the physical properties of the water (e.g., temperature, gases, solid particles). The tendency of water to be corrosive is controlled principally by monitoring or adjusting the pH, buffer intensity, alkalinity, and concentrations of calcium, magnesium, phosphates, and silicates in the water. The following Table 1 illustrates the significance of major constituents of water and their subsequent significance.

Table 1: Major constituents of water and their effect

Constituent or physical property	Significance
Calcium (Ca) & Magnesium (Mg)	Cause hardness and most of the scale- forming properties of water;
Iron(Fe)	On exposure to air, iron in ground water oxidizes to reddish brown sediment. More than about 0.3 mg/L stains laundry and utensils reddish brown. Iron and manganese together should not exceed 0.3 mg/L.
Carbonate (CO_3^{2-})	Bicarbonateandcarbonateproducealkalinity.
Sulfate(SO_4^{2-})	Sulfate in water containing calcium forms hard scale in pipe. In high concentrations, sulfate in combination with other ions gives a bitter taste to water. Concentrations above 250 mg/L may have a laxative effect.
Nitrate(NO_3^-)	Concentrations much greater than the local average may suggest pollution. Nitrate encourages growth of algae and other organisms which produce undesirable tastes and odors.
Totaldissolved solids(TDS)	Total dissolved solids concentrations are useful for comparison to established water-quality standards. Water with more than 1000 mg/L of dissolved solids may contain minerals which impart a distinctive taste.
pH (Hydrogen-ion activity)	The pH is a measure of acidity. A pH of 7.0 indicates neutrality of a solution. Values higher than 7.0 denote increasing alkalinity; values lower than 7.0 indicate increasing acidity. Corrosiveness of water generally increases with decreasing pH, but excessively alkaline waters may also attack metals.
Hardnessas $CaCO_3$	Hard water consumes soap before a lather will form, deposits soap on bath tubs, and forms scale in boilers, water heaters, and pipes. Waters of hardness 0 to 60 mg/L are termed soft; 61 to 120 mg/L moderately hard; 121 to 180 mg/L hard; and more than 180 mg/L very hard.

4.0 Result Analysis:

4.1 Water Deposits

In present investigation the pH values of the ground water and surface water sample are found in 7.6 and 6.9, respectively. Acid-base reactions are very essential in ground water, because of their effect on pH and their ion chemistry in water influences materials. BOD of ground water and surface water sample were zero. In general, the BOD of groundwater must be zero because organic matters are mostly filtered through subsurface strata and thus leaving no space for the development of microorganisms which are responsible for water borne diseases. But some time there is BOD in water which is due to industrial effluent might have contributed some organic pollutants sometime percolate through the sub soil and reaches the ground water table forming contaminated pool, which is potential threat of water contamination in future. In present investigation COD of ground water and surface water sample were found 9

and 5mg/L. The COD is used to measure pollution load in terms of quantity of oxygen required for oxidation of organic matter to produce carbon dioxide and water. Water with high COD indicates that there is presence of organic waste and oxygen is required for the oxidation of these wastes so all oxygen is used for the oxidation of organic waste and that are why there is inadequate oxygen available in water sample.

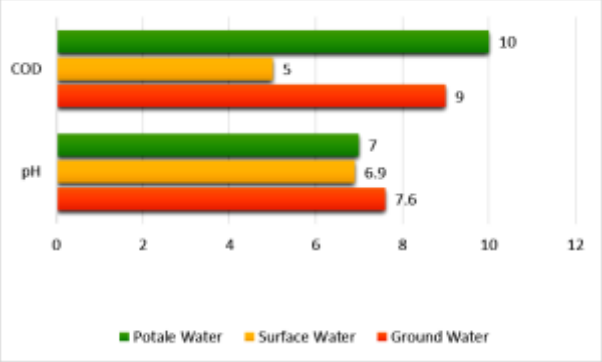

Fig.4: Comparison of COD and pH of three sample water

Alkalinity of ground water and surface water sample in present study came 412 and 399 mg/L. This indicates that water from sampling location is hard, this high alkalinity values indicates the presence carbonate and bicarbonate ions. Effect of alkalinity is that much low and much high values of alkalinity can cause nuisance problems. Alkalinity values less than 75 mg/L can change pH levels in water system and make the water corrosive. Corrosive water can then lead to potentially harmful metals dissolving from the plumbing into the drinking water which may cause several health effects by increasing metal concentration in water. High alkalinities values, over 500 mg/L are in water are associated with high dissolved solids which can create scale build up on water pipeline systems, especially hot water pipeline systems. Scale build up in the pipeline system can increase power consumption and also increase the costs to heat the water. The total hardness of ground water and surface water were found 750 and 446 mg/L. In present investigation TDS of the ground water and surface water sample were found 350 and 602 mg/L.

The salinity behavior of any water samples is generally characterized by its total dissolved solids content17. In the present study the range of total solids of ground water and surface water sample were found 390 and 650 mg/L. The term solid refers to the matter that are either filterable or in filterable and remain as residue upon filter paper by drying at a defined temperature after drying. Different forms of solids (TDS, TSS and TS) are defined on the basis of method applied for their determination. High concentration of total solids during summer was probably due to low level of water, the direct relationship between rainfall and total solids was attributed to an increased load of soluble salts as results of surface runoff. In water total solids, total dissolved solids and total suspended solids are composed mainly of carbonates, bicarbonates, chlorides, sulphates, nitrates, Ca, Mg, Na, K, Mn and other organic matter silts which are present either in dissolve or in suspended form.

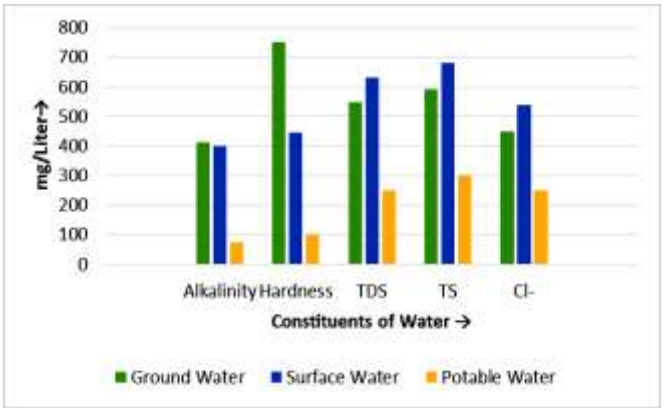

Fig.5: Graphical comparison of values of major constituents of three sample water

4.2 Material Properties

The Brinell Hardness has been measured using the following equitation. The values of load and Impression diameters are measured by Tensometer. Hardness is a vital mechanical property of material. Brinell hardness measurement principle is the test force F(N) with a certain size, the diameter D (mm) of hardened steel balls or carbide ball pressed into the surface of the metal under test, to maintain a predetermined time after the drop test force, the the indentation average diameter d (mm) measured with a reading microscope, and then the equation Brinell hardness HB value, or the value d from the prepared Brinell hardness table to detect HB Brinell hardness measurement method is suitable for cast iron, non-alloy, annealing and quenching and tempering steel, the determination should not be too hard, too small, too thin and the surface does not allow the larger indentation specimen or work piece. [14]

BHN: $$\frac{P}{\frac{\pi D}{2}\{D-\sqrt{(D^2-d^2)}\}}$$

Where
BHN = Brinell hardness number
P = load on the indenting tool (kg)
D = diameter of steel ball (mm)
d = measure diameter at the rim of the impression (mm)
It is desirable that the test load are limited to an impression diameter in the range of 2.5 to 4.75 mm.
Here, for interior surface of pipe
P= 9 KN= 917.745 Kg
D= 5 mm
D= 2.6 mm,

BHN (Internal surface)= 161 and
BHN (External surface) = 198

So BHN or HB of the affected (Used 14 Months) GI pipe is 161.
A GI pipe before using has a BHN of 260-350.
If used in normal conditions where potable water is transferring, after 14 months BHN is around 220~240.
There is a drastic change in BHN if used to transfer saline water.

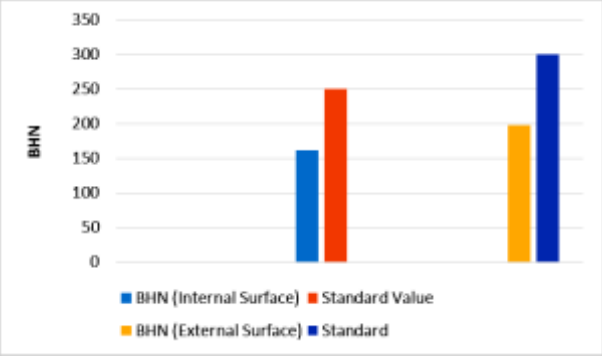

Fig.6: Comparison of Brinell Hardness for External and internal surface of GI pipe

Surface Morphology:
Electrochemical or Mechano-chemical behavior of a surface, such as corrosion or corrosive wear, is extremely complicated and involves various chemical, physical and mechanical factors. Fig. 2 shows the micrograph appearance of the GI pipe interior surface.

7(a)

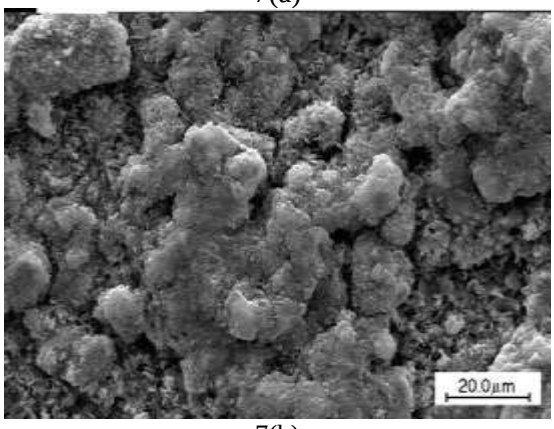

7(b)

Fig.7: Corroded pipe surface (a) 1000X and (b) 50000X (SEM)

Fig. 7 shows the appearance of the metal through electron microscope. Fig 7(a) is the view of 1000X by microscope and 7(b) is the view of 50,000X by SEM. Amounts of Pitting holes are observed on the surface of the metal in the SEM image. It shows that the susceptibility of the metal to breakage for corrosion was more in the internal surface of pipe. The pitting corrosion readily occurred on the surface of the pipe in the presence of Sulfate Reducing Bacteria (SRB).The surface of the pipe was still contained the polishing grooves in the internal surface. However, the grooves were not apparent in the 1000X view because Light cannot be used to see the Nano world, as its resolution is limited by its own wavelength, so optical microscopes are useless for nanotechnology. The large scale is formed in the internal surface of pipe which indicates that the severe corrosion has occurred.

5.0 Discussion & Conclusion

The characterization of sample water collected from ground and surface were illustrated in bar diagram figure 4 and figure 5. In figure 4 the values of organic compound for sample waters has been compared. The Chemical Oxygen Demand (COD) for surface and ground water are 5 and 9 respectively. The requisite amount for potable water suggested by World Health Organization (WHO) is 10. The hydrogen ion activity (pH) was around the standard value for both cases. Figure 5 focuses on the characteristics which are critical for corrosion and scale formation in the pipe. Alkalinity of surface and ground water are much more than the amount of potable water which indicates the presence of Bicarbonate (HCO3) and Carbonate (CO3). These compounds are reasonably responsible for scale forming. The hardness is also much higher in case of ground and surface water. Hardness can also be expressed as the equivalent amount of CaCo3. If the amount exceeds 180 mg/L for any water it is said as very hard. So the sample water is undoubtedly very hard as its hardness is more than 400 for both case. The amount of Total Dissolved Solid (TDS) and Total solid constituents are very high compared to the WHO standard. For these unexpected higher values of chemical compounds the properties of piping material has changed a lot. The pipe sample used for testing had carried sample water for not more than 14 months. The Brinell Hardness test shows there is a drastic change in the BHN or HB value for both the internal and external surface of the pipe. The microscopic image shows the corroded and scale formed internal surface of the pipe.

Reference:

[1] SOUZA, Maria ElizianePires; ARIZA, Edith; BALLESTER, MargaritROCHA, Luís Augusto; FREIRE, Célia M.A, “Comparative behaviour in terms of wear and corrosion resistance of galvanized and zinc-iron coated steels”, ISSN 1517-7076, RevistaMatéria, v. 12, n. 4, pp. 618 – 623, 2007

[2] D. Jedrzejczyk, "Effect Of High Temperature Oxidation On Structure And Corrosion Resistance Of The Zinc Coating Deposited On Cast Iron", A R C H I V E S O F M E T A L L U R G Y A N D M A T E R I A L S, Volume 57 2012 Issue 1, DOI: 10.2478/v10172-012-0003-x

[3] Juan G. Castaño, "Characterization of deposits formed in a water distribution system", Corrosion and Protection Research Group, University of Antioquia, 2012

[4] Zhe Zhang, Janet E. Stout, Victor L. Yu, RadisavVidic, "Effect of pipe corrosion scales on chlorine dioxideconsumption in drinking water distribution systems", WATER RESEARCH 42 (2008) 129– 136, Elsevier

[5] ShuPeng, Jintang Lu, ChunshanChe, Gang Kong, QiaoyuXu, "Morphology and antimony segregation of spangles on batch hot-dip galvanized coatings", Applied Surface Science 256 (2010) 5015–5020, Elsevier

[6] ZHANG, Z., LENG, W.H., SHAO, H.B., ZHANG, J.Q., WANG, J.M., CAO, C.N., "Study on thebehavior of Zn–Fe alloy electroplating", Journal of Electroanalytical Chemistry, v. 516, pp. 127 130,2001.

[7] ISAACS, H.S., ALDYKIEWICZ JR, A.J., THIERRY, D. SIMPSON, T.C., "Measurements of corrosion at defects in painted zinc and zinc alloy coated steels using current density mapping", Corrosion, v.52, n. 3, pp. 163-168, Mar. 1996.

[8] 17. Nithulal K. P, Karthikeyan K, Praveesh V, Devi V, Suriyanarayanan S and Vijay Kumar V. Drinking Water Quality Assessment of Ground Waters of BhachauKachchh, Gujarat, India with special reference to major Anions and Cations. Int. Res. J. Environment Sci. Vol. 3(5), 67-72 (2014)

[9] MahaMehanna and Bruce E. Logan* Tomonori Saito,JinglingYan,MichaelHickner, XiaoxinCao,Xia Huang,"Using microbial desalination cells to reduce water salinity prior to reverse osmosis",Energy & Environmental Science, Received 2nd February 2010, Accepted 16th June 2010,DOI: 10.1039/c002307h

[10] Gorham, Eville, "Chemical Composition of some waters from lowland lakes in Shopeshire,England", Freshwater Biological Association, Ambleside,England,September 24, 1996.

[11] RANJEETA CHOUDHARY, PUSHPA RAWTANI[1] and MONIKA VISHWAKARMA[2], "Comparative study of Drinking Water Quality Parameters of three Manmade Reservoirs i.e. Kolar, Kaliasote and Kerwa Dam", Current World Environment,Vol. 6(1), 145-149 (2011)

[12] Fei Liu, Junshu Wu, Kunfeng Chen and DongfengXue,"Morphology Study by Using Scanning Electron Microscopy", Microscopy: Science, Technology, Applications and Education,Méndez-Vilas and J. Díaz (Eds.),FORMATEX 2010

[13] World Health Organization, "Total dissolved solids in Drinking-water", Guidelines for drinking-water quality, 2nd ed. Vol. 2. Health criteria andother supporting information, WHO/SDE/WSH/03.04/16, Geneva, 1996

[14] Jin Xu*, Cheng Sun, Maocheng Yan, Fuhui Wang," Effects of Sulfate Reducing Bacteria on Corrosion of Carbon Steel Q235 in Soil-Extract Solution", International Journal of Electrochemical Science, 7 (2012) 11281 – 11296.

ICMIEE-PI-140195

Flexible job shop scheduling for parallel machine with genetic algorithm

Subrata Talapatra [1,], Md. Riyad hossain [2] , Md. Kamruzzaman Rasel [3] , Utpal Kumar Dey [4]*
[1, 2, 3] Department of Industrial Engineering and Management, Khulna University of Engineering & Technology, Khulna-9203, BANGLADESH
[4] Department of computer science and Engineering, Khulna University of Engineering & Technology, Khulna-9203, BANGLADESH

ABSTRACT
Optimized scheduling of Flexible Job-shop for Parallel Machine is the toughest combinatorial problems as they occupy very large search space. Solving this kind of combinatorial optimization problems with classical methods are time consuming or almost impossible. Genetic Algorithms (GAs) is a powerful tool to solve this kind of problem. This research develops a scheduling algorithm for solving these problems to minimize total tardiness and make span time. The algorithm consists of two major modules: machine selection module (MSM) that helps to select one of the parallel machines and operation scheduling module (OSM) to arrange the sequence of operation. Global selection (GS) technique is used to generate high quality initial population. To represent a solution of the FJSP, an improved chromosome representation is used while adopting uniform crossover and mutation operator. The result showed that proposed algorithm is much more effective and efficient to solve flexible job-shop scheduling problem for parallel machine.

Keywords: Flexible job-shop scheduling, Genetic Algorithm, Parallel machine, global search method.

1. Introduction

In 1985, first Davis applied Genetic Algorithms (GAs) to scheduling problems. While applying GAs to Scheduling problems the main problem is to find a suitable chromosome representation and genetic operators in order to create feasible schedules (Bilgesu Ak, & Erdem Koc, 2012). The classical method of solving job-shop scheduling problem (JSP) is time consuming and sometimes impossible. The JSP consists of a set of n jobs processed by a set of m machines with the objective to minimize certain criteria. At time zero each machine is fully available, processing only one operation at a time. Each job contains a pre-specified processing order and specific time on the machines that are fixed and known in advance. In modern manufacturing plant, a machine may have the flexible capability to be set up to process more than one type of operations. This leads to a modified version of JSP called flexible JSP (FJSP). There are two types of FJSP (Brucker & Schlie, 1990). For type I FJSP, jobs have alternative operation sequences and alternative identical or non-identical machines for each operation. The problem is to select operation sequences for jobs and determine job processing orders on machines. For type II FJSP, jobs can have only fixed operation sequences but alternative identical or non-identical machines for each operation. The problem is to arrange jobs to machines according to their operation sequences (James C. Chen, Cheng-Chun Wu, Chia-Wen Chen, & Kou-Huang Chen, 2012).

In this paper, we propose an effective GA to solve the FJSP. Global Selection (GS) and Local Selection (LS) are designed to generate high-quality initial population in the initialization stage which could accelerate convergent speed. In order to assist the initialization method and assure the algorithm perform well, we design an improved chromosome representation method ‘‘Machine Selection and Operation Sequence”. In this method, we try to find an efficient coding scheme of the individuals which respects all constraints of the FJSP. At the same time, different strategies for crossover and mutation operator are employed. Computational results show that the proposed algorithm could get good solutions.

The paper is organized as follows. Section 2 gives the formulation of FJSP and shows an illustrative instance. An overview of proposed genetic algorithm including machine Selection and Operation Sequence, encoding and decoding scheme, Global Selection technique is provided in Section 3. Section 4 presents the Numerical illustration and computational result of proposed genetic algorithm when it is applied to solve some realistic problem. Some final concluding remarks and future study directions are given in Section 5.

2 Problem definitions:

The FJSP consists in performing a set of n jobs {J_1, J_2, J_3…., j_i, ….. J_n} on a set of m machines {M_1, M_2, M_3…., M_k, ….. M_m}. A job J_i is formed by a sequence of operations {O_{i1}, O_{i2}, O_{i3}…., O_{ij}} to be performed one after the other according to the given sequence. Each operation requires one machine selected out of a set of available machines. All jobs and machines are available at time 0, and a machine can only execute one operation at a given time. Preemption is not allowed, i.e., each operation must be completed without interruption once it starts. Machine Setup time and movement time between operations are negligible. The processing time of operation O_{ij} on machine M_m is $P_{ijk} > 0$. Flexibility of FJSP can be categorized into partial flexibility and total flexibility. A system will be called partial if every

* Corresponding author. Tel.: +88-01814500041
E-mail address: riyad_iem09@yahoo.com

machine cannot perform every other operation because of some constraint or extremely high cost. Data associated with a partial flexible system are given in Table 1, in which rows stand for operations time and columns is for machines. In this Table, symbol 0 means that a machine cannot execute the corresponding operation. Problem can be formulated by using following nodes and symbols:

Z is the set of all machines
n is the number of the total jobs
m is the number of the total machines
i is the index of the i^{th} job
j is the index of the j^{th} operation of job J_i
k, x is the index of alternative machine set
O_{ij} is the j^{th} operation of job J_i
P_{ijk} is the processing time of operation O_{ij} on machine k
S_{ijk} is the start time of operation O_{ij} on machine k
E_{ijk} is the end time of operation O_{ij} on machine k

Assumptions made in FJSP as follows:

- All machines are available at time t = 0;
- All jobs are released at time t = 0;
- For each job, the sequence of operations is predetermined and cannot be modified;
- Each machine can only execute one operation at a time;
- Each operation Oij must be processed without interruption on one of a set of available machines;
- Recirculation occurs when a job could visit a machine more than once;
- The objective of the FJSP is to minimize the total completion time;

A basic representation of flexible job shop scheduling is as follows in **Table 1**.

Job	*O/P*	*M_1*	*M_2*	*M_3*	*M_4*	*M_5*
J_1	O_{11}	21	16	15	13	0
	O_{12}	0	18	12	14	0
J_2	O_{21}	23	10	17	0	15
	O_{22}	24	13	5	0	20
	O_{23}	0	17	14	15	28
J_3	O_{31}	18	13	5	19	13
	O_{32}	21	0	13	11	17
J_4	O_{41}	10	8	13	17	0
	O_{42}	9	14	15	0	10
	O_{43}	17	20	25	0	14

There are 5 jobs and 7 machines, where rows correspond to operations and columns correspond to machines. Each cell denotes the processing time of that operation on the corresponding machine. In the table, the ‘‘0” means that the machine cannot execute the corresponding operation, i.e., it does not belong to the alternative machine set of the operation. So this instance is a Partial FJSP.

3. Algorithm for Flexible job scheduling

The proposed algorithm is developed according to the concept of the genetic algorithm. The detailed procedure of the proposed algorithm is as follows:

3.1. Determining operation sequence

The sequence of operation should be arranged on that way so that every other operation of an individual job must be accomplished before processed to next immediate operation. For example, to perform the job j_2 of table 1 the sequence of operations O_{21} 0_{22} O_{23} should be maintained i.e. $O_{21} > O_{22} > O_{23}$.

3.2. Global selection

We define that a stage is the process of selecting a suitable machine for an operation. Thus this method records the sum of the processing time of each machine in the whole processing stage. Then the machine which has the minimum processing time in every stage is selected. In particular, the first job and next job are randomly selected. Detailed steps are as follows:

1. Create a new array to record all machines’ processing time, initialize each element to 0;
2. Select a job randomly and insure one job to be selected only once, then select the first operation of the job;
3. Add the processing time of each machine in the available machines and the corresponding machine’s time in the time array together;
4. Compare the added time to find the shortest time, and then select the index k of the machine which has the shortest time. If there is the same time among different machines, a machine is selected randomly among them;
5. Set the allele which corresponds to the current operation in the MS part to k;
6. Add the current selected machine’s processing time and its corresponding allele in the time array together in order to update the time array;
7. Select the next operation of the current job, and execute Step 3 to Step 6 until all operations of the current job are selected, then go to Step 8;
8. Go to step 2 until all jobs are all selected once.

The implementation of GS is given in Fig. 1.We assume that the sequence of job is $J_1 > j_2 > j_3 > j_4$ from table 1, as mentioned earlier processing time ‘0’ means the machine is unable to perform the operation. So, we easily see that the processing time on M_4 is the shortest in the alternative machine set of operation O_{11}. Hence, machine M_4 is selected to process the operation O_{11} of job J_1, and set corresponding allele in MS to the index of M_4 .Then the processing time is added to the corresponding position in time array. The selection process continued till finding a new chromosome as described above 8 steps.

Time array	0	0	0	0	0
Operation			O_{11}		
Available machines	M_1	M_2	M_3	M_4	
Processing time	21	16	15	13	
Added time	21	16	15	13	
Shortest time				13	
Selected machine				M_4	
Update time array	0	0	0	13	0
Machine Selection	4				

(a) O_{11}

Time array	0	0	0	13	0
Operation			O_{12}		
Available machines		M_2	M_3	M_4	
Processing time		18	12	14	
Added time		18	12	27	
Shortest time			12		
Selected machine			M_3		
Update time array	0	0	12	13	0
Machine Selection	4	3			

(b) O_{12}

Time array	0	0	12	13	0
Operation			O_{21}		
Available machines	M_1	M_2	M_4		M_5
Processing time	23	10	17		15
Added time	23	10	29		15
Shortest time		10			
Selected machine		M_2			
Update time array	0	`12	13		0
Machine Selection	4	3	2		

(c) O_{21}

Fig.1 The global selection technique for operation (a) O_{11} (b) O_{12} (c) O_{21}

Finally, the selected machines of operations O_{11} O_{12} O_{21} may be M_4-M_3-M_2 and chromosome is 4-3-2.

3.3. Generate the Initial Population

As shown in Fig 1, the structure of the chromosome used in this paper consists of two components. The first component of the chromosome represents the list of machines while the second component contains the sequence of operations to be processed used in executing the operations in the first component.

For example, consider the 4-job, 5-machine problem given in Table 1. Initial chromosomes are randomly created as shown in Fig 1. Each chromosome contains 10 genes. The numbers 1 and 2 which appear in the first component of the chromosome stand for jobs J_1 and J_2 respectively. According to the chromosome in Fig 2, the second component is [1 1 2 2 2 ...]. The first gene in the second component 1 means that the 1st operation of the 1st job is to be processed by the machine M_4. Here, Ch. = chromosome

Ch.	Machine selection										Operation sequence									
	4	3	2	3	2	5	1	3	5	5	1	1	2	2	2	3	3	4	4	4

Fig.2 Schematic representation of the chromosome structure

3.4. Crossover operation

The goal of the crossover is to obtain better chromosomes to improve the result by exchanging information contained in the current good ones. In our work we carried out uniform crossover operator to generate new chromosomes.

3.4.1. Machine Selection part

The crossover operation of MS is performed on two Machine Selection parts and generates two new Machine Selection parts each of which corresponds to a new allocation of operations to machines. Each machine of the new Machine Selection parts must be effective, i.e., the machine must be included in the alternative machine set of the corresponding operation. We adopt uniform crossover (Gao, Sun & Gen, 2008). MS crossover operator only changes some alleles, while their location in each individual i.e., their preceding constraints are not changed. Therefore, the individuals after crossover are also feasible. The procedure could be illustrated in Fig. 3.

3.4.2. Operation Sequence part

The crossover operation of OS is different from that of MS. During the past decades, several crossover operators have been proposed for permutation representation. Here we apply a Precedence preserving order-based crossover (POX) for the Operation Sequence. Detailed implementing steps of POX are as follows:

1. Generate two sub-job set Js1/Js2 from all jobs and select two parent individuals as p1 and p2;

2. Copy any allele in p1/ p2 that belong to Js1/Js2 into two child individuals c1/c2, and retain in the same position in c1/c2;
3. Delete the alleles that are already in the sub-job Js1/Js2 from p2/ p1;
4. Orderly fill the empty position in c1/c2 with the alleles of p2/p1 that belongs to in their previous sequence. In Table 1, there are only four jobs. So it is difficult to present the process of POX clearly.

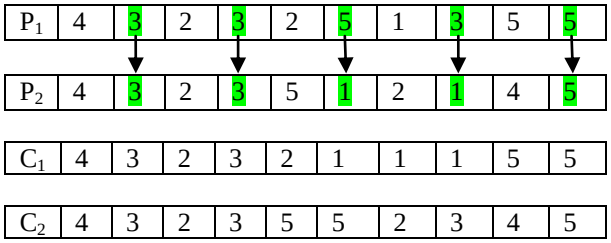

Fig.3 MS uniform crossover operator.

3.5. Mutation operator

Mutation introduces some extra variability into the population to enhance the diversity of population. Usually, mutation is applied with small probability. Large probability may destroy the good chromosome.

3.5.1. Machine Selection part

The machine selection mutation operation is performed by following steps:

1. MS mutation operator only changes the assignment property of the chromosomes. We select the shortest processing time from alternative machine set to balance the workload of the machines. Taking the chromosome from Fig. 3 for example, MS mutation is described as follows: Select one individual from the population;
2. Read the chromosomes of the individual from left to right and generate a probability value randomly; if all the chromosomes have been read, then end the procedure;
3. If the probability value is less than or equal to the mutation probability then go to Step 4; otherwise, go to Step 2;
4. Select the shortest processing time from the alternative machine set and assign it to the mutation position;

An illustrative instance is shown in Fig. 4. Suppose the mutative operation is O_{42}, before the mutation, O_{42} is processed on M5, which is the fourth machine in the alternative machine set, so the allele is 4. In the mutation, the rule that selecting the machine of the shortest processing time is obeyed, so M_1 is selected, and the allele in the chromosome changes into 1.

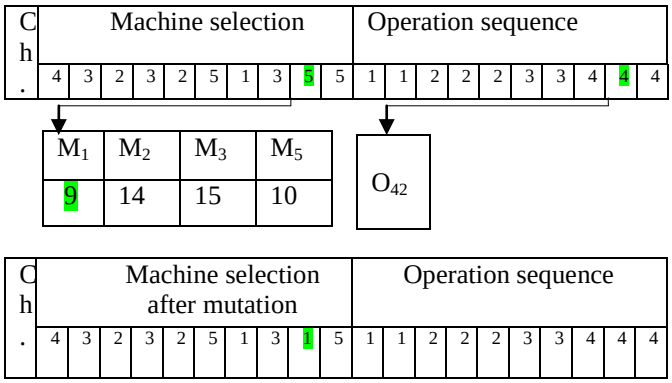

Fig.4 MS after mutation operation.

3.6. Overview of the proposed algorithm

The framework of the proposed genetic algorithm is illustrated in Fig. 5. Each individual in the initial population of MS part is generated by GS. This procedure makes it possible to assign each operation to the suitable machine considering the processing time.

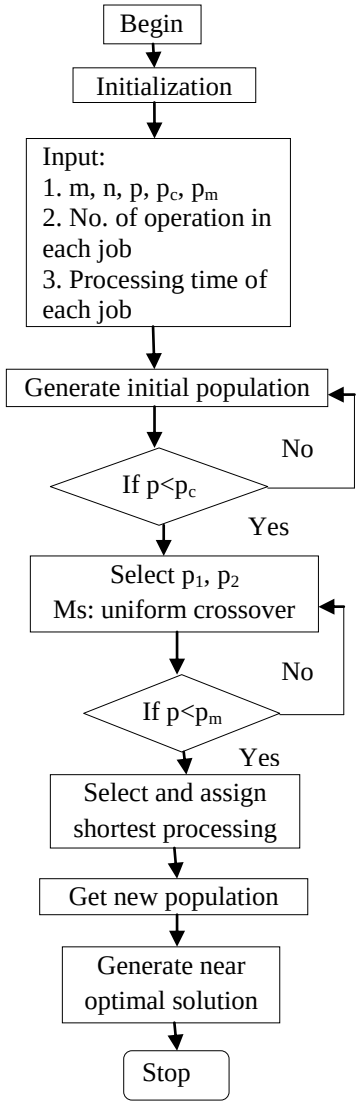

Fig.5 Overview of the proposed algorithm.

4. Numerical illustration and computational result

The genetic algorithm was coded in ANSI C++ programming language using only simple array data structure and implemented on a PC (Intel(R) Pentium(R), CPU B960 Intel processor of 2.20 GHz).

Firstly, we tested the performance of the algorithm using GS method. In Fig. 6 we draw the generation vs time completion curve that shows the decreased average time required to complete each and every operation. The optimal solution for a 4×5 problem can be achieved at 17th generation. In order to obtain meaningful results, we ran our algorithm for several times on different instance. The parameters used in this GA are chosen experimentally in order to get a satisfactory solution in an acceptable time span.

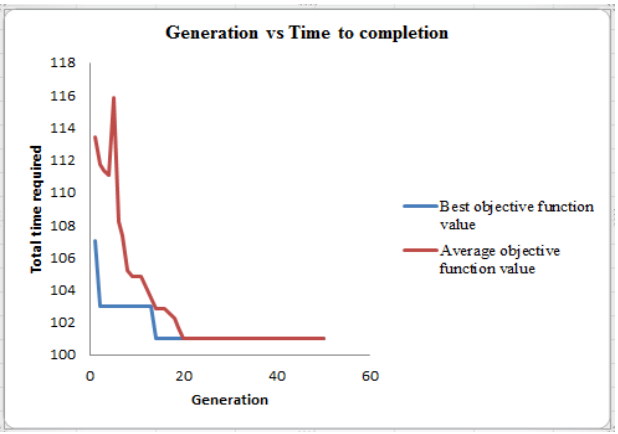

Fig.6 Decreasing of the total time required

Table2 Summary of data set and computational Performance

No.	n × m	Crossover probability (P_c)	Mutation probability (P_m)	Generation size	Iteration required. to get opt. result
1.	3 × 7	.25	.35	20	9th
2.	4 × 6	.25	.25	22	12th
3.	5 × 7	.20	.20	30	17th
4.	4 × 5	.25	.25	50	19th

5. Conclusion and future study

In this paper, a genetic algorithm for solving the flexible job-shop scheduling problem (FJSP) is proposed. A new chromosome representation scheme is proposed and an effective decoding method interpreting each chromosome into a feasible active schedule is designed. In order to enhance the quality of initial solution, a new initial assignment method i.e., global search technique is used to generate high-quality initial population integrating different strategies to improve the convergence speed and the quality of final solutions. Then different strategies for crossover, selection and mutation operator are adopted. This makes it possible to solve the problem of trade-off resources allocation.

Some realistic problems are solved by using our new algorithm. The computational results show that the proposed genetic algorithm leads to an effective scheduling considering time and quality compared with other genetic algorithms. The proposed algorithm can enhance the convergence speed and the quality of the solution. This algorithm can be used in solving large size flexible job shop scheduling problem.

In the future, it will be interesting to investigate the following issues: a better search technique can be developed along with global search technique in order to generate better results. Adjust an appropriate relation between crossover and mutation probability to enhance the chance of better solution.

REFERENCES

[1] Yazdani, M., Amiri, M., & Zandieh, M. (2010). Flexible job-shop scheduling with parallel variable neighborhood search algorithm. Expert Systems with Applications, 37(1), 678–687.

[2] Barnes, J. W., & Chambers, J. B. (1996). Flexible job shop scheduling by tabu search. Graduate program in operations research and industrial engineering, The University of Texas at Austin 1996; Technical report series: ORP96-09.

[3] Brandimarte, P. (1993). Routing and scheduling in a flexible job shop by taboo search. Annals of Operations Research, 41, 157–183.

[4] Gao, J., Sun, L. Y., & Gen, M. (2008). A hybrid genetic and variable neighborhood descent algorithm for flexible job shop scheduling problems. Computer and Operations Research, 35(9), 2892–2907.

[5] Guohui Zhang , Liang Gao, Yang Shi (2011). An effective genetic algorithm for the flexible job-shop scheduling problem. Expert Systems with Applications 38 (2011) 3563–3573.

[6] Garey, M. R., Johnson, D. S., & Sethi, R. (1976). The complexity of flow shop and jobshop scheduling. Mathematics of Operations Research, 1, 117–129.

[7] Ho, N. B., Tay, J. C., Edmund, M., & Lai, K. (2007). An effective architecture for learning and evolving flexible job shop schedules. European Journal of Operational Research, 179, 316–333.

[8] Jia, H. Z., Nee, A. Y. C., Fuh, J. Y. H., & Zhang, Y. F. (2003). A modified genetic algorithm for distributed scheduling problems. International Journal of Intelligent Manufacturing, 14, 351–362.

[9] Kacem, I. (2003). Genetic algorithm for the flexible job-shop scheduling problem. IEEE International conference on Systems, Man and Cybernetics, 4, 3464–3469.

[10] Lee, K. M., Yamakawa, T., & Lee, K. M. (1998). A genetic algorithm for general machine scheduling problems. International

Journal of Knowledge-Based Electronic, 2, 60–66.
[11] Pezzella, F., Morganti, G., & Ciaschetti, G. (2007). A genetic algorithm for the flexible job-shop scheduling problem. Computers and Operations Research, 35(10), 3202–3212.
[12] Tay, J. C., & Wibowo, D. (2004). An effective chromosome representation for evolving flexible job shop schedules, GECCO 2004. Lecture notes in computer science (Vol. 3103, pp. 210–221). Berlin: Springer.
[13] Watanabe, M., Ida, K., & Gen, M. (2005). A genetic algorithm with modified crossover operator and search area adaptation for the job-shop scheduling problem. Computers and Industrial Engineering, 48, 743–752
[14] Balin, S. (2011). Non-identical parallel machine scheduling using genetic algorithm. Expert Systems with Applications, 38(6), 6814–6821.
[15] Chan, F. T. S., Choy, K. L., & Bibhushan. (2011). A genetic algorithm-based scheduler for multiproduct parallel machine sheet metal job shop. Expert Systems with Applications, 38(7), 8703–8715
[16] M. Zhang, C. Luo, Parallel-machine scheduling with deteriorating jobs, rejection and a fixed non-availability interval, Appl. Math. Comput. 224 (2013) 405–411.
[17] P. Liu, N. Yi, X. Zhou, H. Gong, Scheduling two agents with sum-of-processing-times-based deterioration on a single machine, Appl. Math. Comput. 219 (2013) 8848–8855.
[18] C.-C. Wu, S.-R. Cheng, W.-H. Wu, Y. Yin, W.-H. Wu, The single-machine total tardiness problem with unequal release times and a linear deterioration, Appl. Math. Comput. 219 (2013) 10401–10415.
[19] D. Wang, Y.-B. Wu, J.-B. Wang, P. Ji, Single-machine scheduling with decreasing time-dependent processing times to minimize total absolute differences in waiting times, J. Chin. Inst. Ind. Eng. 29 (2012) 444–453.
[20] J.-B. Wang, X. Huang, Y.-B. Wu, P. Ji, Group scheduling with independent setup times, ready times, and deteriorating job processing times, Int. J. Adv. Manuf. Technol. 60 (2012) 643–649.
[21] W.-C. Lee, Z.-S. Lu, Group scheduling with deteriorating jobs to minimize the total weighted number of late jobs, Appl. Math. Comput. 218 (2012) 8750–8757.
[22] C.-L. Zhao, H.-Y. Tang, A note on two-machine no-wait flow shop scheduling with deteriorating jobs and machine availability constraints, Optim. Lett. 5 (2011) 183–190.
[23] X.-Y. Wang, M.-Z. Wang, J.-B. Wang, Flow shop scheduling to minimize makespan with decreasing time-dependent job processing times, Comput. Ind. Eng. 60 (2011) 840–844.
[24] S.-H. Yang, J.-B. Wang, Minimizing total weighted completion time in a two-machine flow shop scheduling under simple linear deterioration, Appl. Math. Comput. 217 (2011) 4819–4826.
[25] L.-H. Sun, L.-Y. Sun, M.-Z. Wang, J.-B. Wang, Flow shop makespan minimization scheduling with deteriorating jobs under dominating machines, Int. J. Prod. Econ. 138 (2012) 195–200.

ICMIEE-PI-140199

Design, Development & Comparison of Temperature Regulation Units for Neonatal Incubator by Analogous Methods

Zinat Ara Nisha[*,1], A.H.M Fazle Elahi*[2]

[1] Department of Applied Physics Electronics & Communication Engineering,
University of Dhaka, Dhaka-1000, BANGLADESH

[2] Department of Mechanical Engineering,
Khulna University of engineering & Technology (KUET), Khulna-9203, Bangladesh

ABSTRACT
According to the World Health Organization (WHO), an estimated 15 million infants worldwide are born preterm every year; 4 million infants die within a month of birth. 25% of these deaths are caused due to complications of prematurity, most often due to improper heat regulation, water loss and neonatal jaundice and due to other complications that could be avoided by use of simple interventions, such as keeping the infant warm for the first several weeks of life. An infant incubator provides stable levels of temperature, relative humidity and oxygen concentration. Temperature control system is the most important part of a baby incubator which has to be maintained around 37^{o}C. This paper focuses on the comparison of temperature control between advanced temperature control system and microcontroller based control system. The advanced temperature control system has been designed and developed incorporating a combination of Pulse Width Modulation (PWM) and simple ON-OFF control system, where thermistors have been used as temperature sensors. The range of variation of temperature against the set temperature (37^{o}C) has been found to be 2^{o}C. The system components of the microcontroller based control system includes DHT11 temperature sensor, relay, LCD display, fans, bulbs, heater and Arduino Uno microcontroller. For implementation, a software program has been developed in language C. It can control the temperature at the set level 37^{o}C very precisely with negligible temperature swing. At the same time it is cost effective, free of health hazard. It can be used commercially in the hospitals, at home and can be further modified in the laboratory.

Keywords: Temperature controlling method, Pulsed Width Modulation (PWM), Automatic controller, Intelligent infant incubator, Premature baby

1. Introduction

The premature infant care is one of the most sensitive and delicate areas in biomedical field. Until recently, there was just little attention for the care of newly born babies in developing countries. New-born babies with growth problems usually have a net body area greater than normal babies from same age. This in turn makes their heat loss greater than normal babies. Moreover, their net mass is less than the normal babies and makes them unable to keep their body temperature to the required level. With regard to sick babies, they usually can't control their body temperature without an external aid. The current recommended method of providing infant temperature regulation in resource constrained settings is Kangaroo Mother Care (KMC), the practice of placing new-borns directly onto the mother's chest [1]. But at the same time, KMC also has important limitations. As a consequence, preterm or premature infants in developing countries need a warm, clean environment to grow stronger. Incubators can provide millions of at risk infants with shorter hospitals stays and can enable infants who might otherwise have faced a lifetime of severe disability to experience active lives. The incubator is an isolated area environment with no dust, bacteria, and has the ability to control temperature, humidity, and oxygen to remain them in acceptable levels. [2]

2. Background

The first incubator was developed in 1857 named warmwännaen. In 1833, Pierre-Victor-Adolph published an account of another incubator, developed by Etienne Stephane Tarnier for use of enormous Paris Maternite named couveuse. In 1891 reports came of a new incubator design in France, designed by Alexander Lion of Nice. In early 21st century the incubator has become highly technological and improved.[3] Today developments are still constantly underway to try and create an ever more womb-like environment; controlling oxygen levels and other vital systems, with an array of sensors, monitors and alarms [4]. Hence till the world is here, infant incubator technology will be developing to next stage. There are different types of incubator such as Open box type incubator, Close type incubator, manually controlled incubator, Servo controlled incubator and Transport incubator [5]. Temperature regulation is of primary importance in an incubator. This is an analogy between two temperature controlling methods with the suggestion of the best one.

3. Controlling Methods

Temperature control system is an important integral part of a baby incubator. Selection of an appropriate temperature sensor is important for effective control of temperature in the incubator. There are a number of

* Corresponding author. Tel.: +88-01710-424749
E-mail address: zinat.ara.nisha@gmail.com

temperature controlling methods available for infant incubator. Here two methods are designed and developed where one is an advanced control system consists of a PWM circuit & ON-OFF circuit, the other one is based on microcontroller. This paper illustrates the best & accurate method of temperature controller for an infant incubator.

3.1 Advanced temperature control system

The advanced temperature control system is the combination of simple on-off control and PWM control systems. Comparing the sensitivity and response time of available temperature sensors like thermistor, thermocouple, RTD in the range of temperature 25-40^{o}C along with accuracy, repeatability, term stability, linearity, self-heating thermistor has been used for the advanced temperature control system. [6] The block diagram of the ON-OFF control circuit is shown below.

Fig. 1 ON-OFF control block diagram

To improve the temperature sensitivity of the system, the thermistor was placed in one arm (R4) of a Wheatstone bridge, as shown in Fig.2, rather than in a voltage divider circuit. Firstly a balance is obtained through adjustments of the resistors in the other arms (R1/R3 = R2/R4).

The unbalanced output voltage of the bridge as shown was used to give a measure of the temperature change. It is well known that this sensitivity is the greatest when R4 is almost equal to R2 [7].

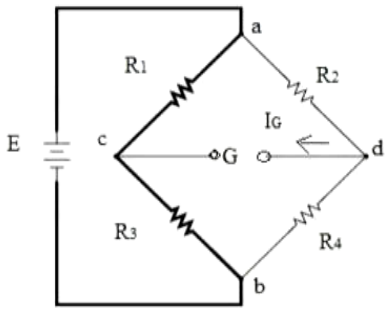

Fig. 2 Wheatstone bridge circuit

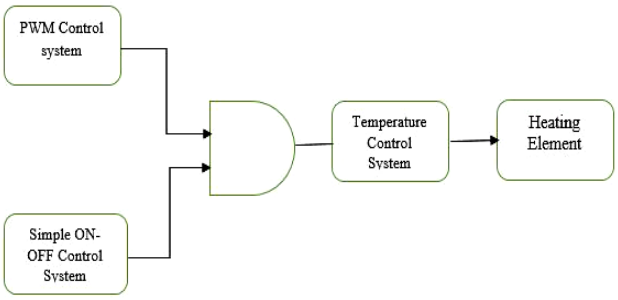

Fig. 3 Block diagram of the combined enhanced temperature control system

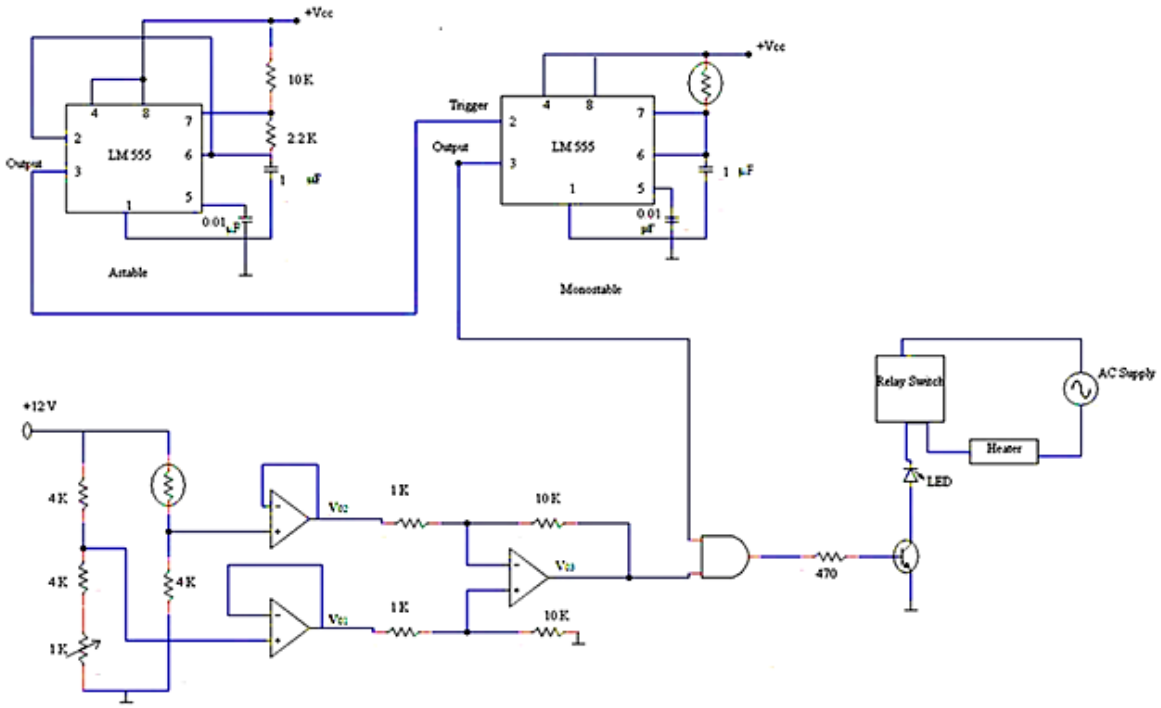

Fig. 4 Circuit diagram of a combined advance temperature control system

3.2 Temperature Control System with Microcontroller

The temperature in the neonatal chamber need to be sensed and read before controlling it. A sensor is placed in the compartment where the baby is kept and the sensed temperature is given to the Arduino Uno Microcontroller. Output devices for keeping temperature within the desired range are connected to the digital output pins of the microcontroller. The temperature is sensed using a DHT11 sensor.

Fig. 5 DHT11 sensor

This is a multifunctional sensor that gives temperature and relative humidity information at the same time. It can meet measurement needs of general purposes. It provides reliable readings when environment humidity condition is in between 20% RH and 90% RH, and temperature condition is in between 0°C and 50°C, covering needs in most home and daily applications that don't contain extreme conditions. [8]

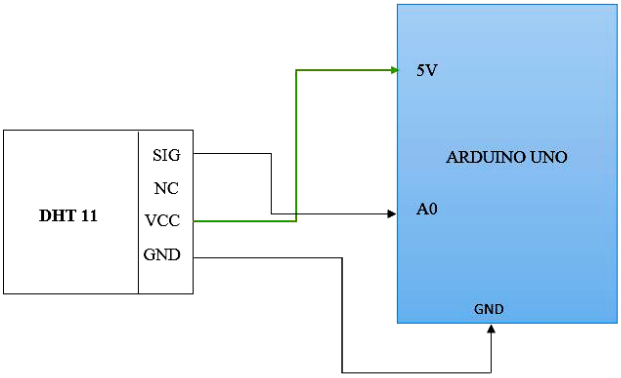

Fig. 6 Circuit for temperature sensing

The temperature sensed by DHT11 is given to Arduino Uno which is connected to a laptop/Computer. Signal pin of the sensor is connected to the analogue input pin A0 of the microcontroller. A program is written and uploaded to the Arduino which makes the temperature to be controlled within the desired range.

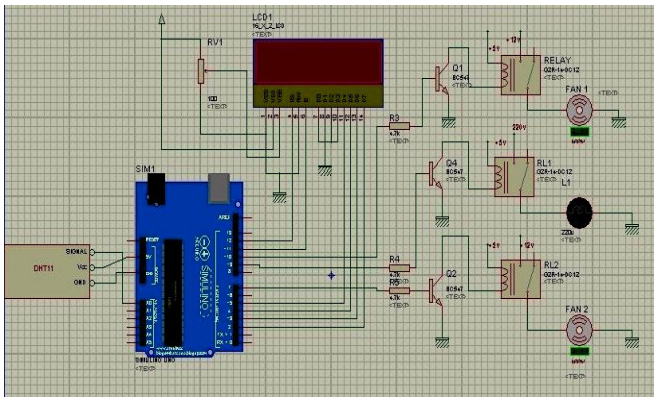

Fig. 7 Microcontroller circuit for temperature sensing

For controlling temperature there are two units; (a) Heating unit (b) Cooling unit. The heating unit consists of a 12 V dc fan and a 220V bulb. These are connected through relays with the digital output pin of Arduino board. The program is written to control the bulb and fans. The cooling unit consists of an Aluminum vessel containing ice and a 12V dc fan. This fan is connected with the digital output pin of the Arduino board through the relay. Whenever the temperature in the chamber goes beyond 37°C the bulb automatically switches off and the fan in the cooling unit turns ON. The program to run the control unit has been uploaded to the system through USB cable from computer. Fig 8 illustrates the logical expression for the program. It gives signal to the output when temperature is not set to 37°C. When it goes below this prescribed temperature the program switch ON the heating device and when it gets high the program start the cooling unit of the neonatal incubator.

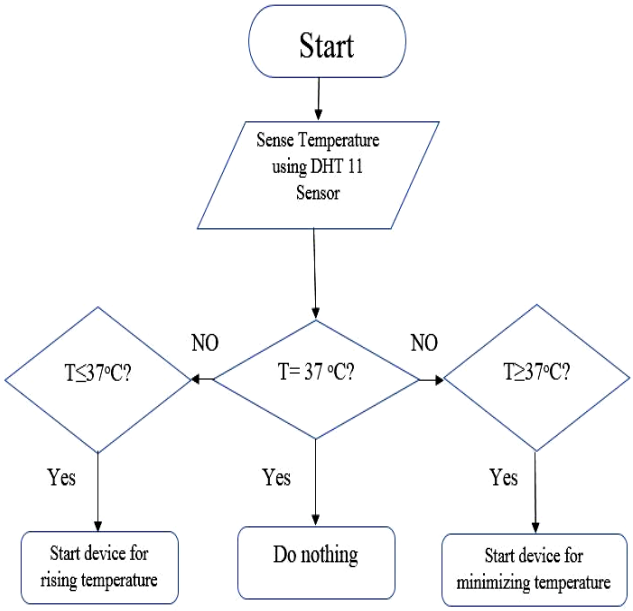

Fig. 8 Flowchart for system software development

4. Result Analysis

Two methods described above functioned to keep the temperature of an infant incubator within the desired range. Readings from two systems have been taken after implementing the systems with total incubator unit with same ambient condition at the same day**.**

4.1 Advanced temperature control system

The performance of the advanced temperature control system is shown in Fig 8. Once the temperature reaches the set value it remains almost constant, varying within a maximum and minimum of 37.9ºC and 36.0ºC, giving the range of variation of temperature of ≈2ºC.

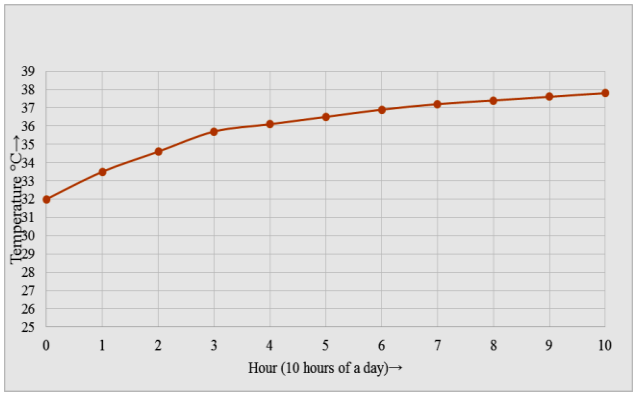

Fig. 9 Variation of temperature with respect to time for advanced temperature control system

4.2 Arduino controlled unit

Temperature of the incubator needs to be maintained at level of 37ºC. When temperature falls below 37ºC, digital output pins become high which are connected to the heating element according to the coding written in Arduino Uno. As a result, the heating unit is turned ON. When temperature goes above 37ºC, a relay is turned ON with which a cooling unit is connected. When the temperature is 37ºC both the heating and cooling units are OFF.

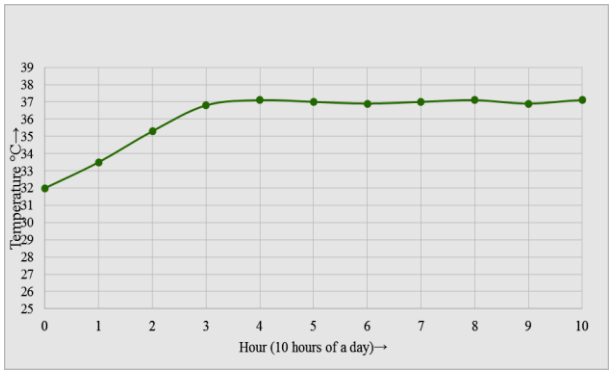

Fig. 10 Maintained temperature in the incubator using Arduino Uno microcontroller

5. Discussion & Result Interpretation

To achieve thermo-neutrality in neonatal body temperature controlling is most significant part. To keep the temperature of the compartment of an incubator in the desired level (37ºC) an advanced regulation system has been developed based on the combination of a PWM circuit and ON-OFF circuit. This unit keeps the temperature of the baby containing vessel within 36ºC to 37.9ºC. This result shows that the temperature is not constant at the desired value. The temperature swing of 2ºC is not acceptable in that case. To improve the system a new unit is designed using a microcontroller. Where temperature is read by a DHT 11 sensor and its signal is processed by an Arduino Uno board. The program helps Arduino to send signal to both heating and cooling devices for keeping the temperature at the constant level. This unit provides the baby compartment a temperature of 37ºC throughout the time. It can be easily stated that using microcontroller instead of a PWM circuit is more effective and efficient in case of controlling temperature for an infant incubator. However, both systems can be regulated for various temperature by only changing the program incorporated within the circuit.

6. Conclusion

Every year, about 1 million infants in the developing world die due to prematurity complications. Premature infants are born before the developing organs are mature enough to allow normal postnatal survival. An incubator is the only solution to avoid diseases of baby. The vital part of an incubator is to have a constant temperature and humidity desired for the neonatal during the time being. The microcontroller based system provides the constant temperature. But humidity control has not been included in this unit. It is achievable through this system by only enlarging the program of the Arduino to control the humidity. The DHT 11 is capable of sensing both temperature and humidity. For future development humidity controlling unit can be included in the existing system with a LCD display. There should be available oxygen supply in the incubator in case of emergency. An active noise control system for infant incubators can be introduced.

References

[1] Tisa T.A, Nisha Z.A, Kiber A; “Design Of An Enhanced Temperature Control System For Neonatal Incubator”, Bangladesh Journal of Medical Physics, Vol. 5, No. 1, Bangladesh 2012

[2] Michael. H. LeBlanc, Thermoregulation: Incubators, radiant warmers, artificial skins, and body hoods. Clin Perinatol, 1991. p. 403-422.

[3] Guler* and M. Burunkaya, “Humidity control of an incubator using the microcontroller-based active humidifier system employing an ultrasonic nebulizer” , J of Medical

Engineering & Technology, Vol. 26, No.2, 2002, p.82– 88
[4] Edward F. Bell and Margit-Andrea Glatzl-Hawlik, Environmental Temperature Control, in Polin RA, Fox WW, eds. Fetal and Neonatal Physiology. 1998, PA:WB Saunders: Philadelphia. p. 716-727.21.
[5] Michael H. LeBlanc, Relative efficacy of an incubator and an open radiant warmer in producing thermo neutrality for the small premature infant. Pediatrics,1982. 69: p. 439-445.
[6] P J J Sauer, H.J.D., and H K A Visser, New standards for neutral thermal environment of healthy very low birth-weight infants in week one of life. Arch Dis Child, 1984. 59: p. 18-22.
[7] Mack, James E.; Shoemaker, Thomas (2006). "Chapter 15 - Distribution Transformers". The Lineman's and Cableman's Handbook (11th ed.). New York: McGraw-Hill. pp. 15–1 to 15–22. ISBN 0-07-146789-0
[8] World Health Organization, Maternal or newborn health/ Safe motherhood unit, Division of reproductive health (Technical Support) “Thermal Protection of newborn

ICMIEE-PI-140200

Role of Advanced Composites Materials in Aerospace Applications - A Review of Current Status and Future Prospects

Md. Anisul Islam [1,*], *Nikhil Ranjan Dhar* [2]
[1] Department of Aeronautical Engineering, Military Institute of Science and Technology, Dhaka-1216, BANGLADESH
[2] Department of Industrial and Production Engineering, Bangladesh University of Engineering and Technology, Dhaka-1000, BANGLADESH

ABSTRACT
Aerospace components are characterized by having high strength to weight ratios in order to obtain lightweight structures and combine damage tolerance characteristics with high resistance under both static and dynamic loads. However, design engineers have to rely on trusted and tested materials. It is composites, which brought revolution in structural materials and has given various opportunities to design engineers to use new and better materials, which results increased efficiency, better utilization of available resources. Fiber-reinforced polymer composite materials are fast gaining ground as preferred materials for construction of aircraft and spacecraft. This paper gives a review several applications of composites materials in the aerospace sector, where they have been seen a significant growth in usages. Farther, the scope of developments of new composites is outlined and some directions for future work are given.

Keywords: Lightweight structures; damage tolerance; reinforced.

1. Introduction

Composites are multicomponent materials designed to achieve a combination of mechanical properties superior to the individual constituents. The unrelenting passion of the aerospace industry is to enhance the performance of commercial and military aircraft is constantly driving the development of improved high performance structural materials. The increased performance demanded of present day aerospace systems requires in turn an improvement in the materials of construction.

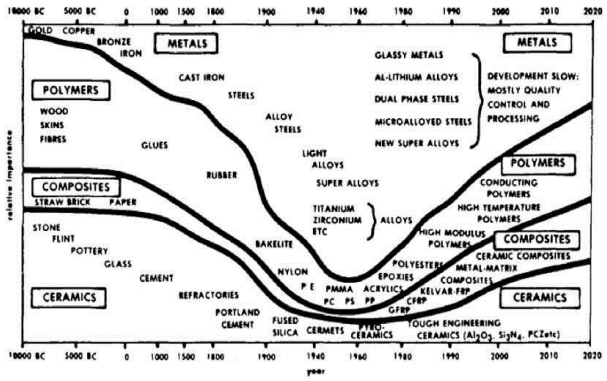

Fig.1 The evolution of materials for mechanical and civil engineering. [1]

Composite materials are particularly attractive to aviation and aerospace applications because of their exceptional strength and stiffness-to-density ratios and superior physical properties. The aircraft/aerospace market represents only 0.8% which is surprising in light its importance in the origins of composites. Of course, the aerospace products are fewer in number but are much higher in value. Most of the markets continue to grow Fig.1. Composites have found their place in the world and seem to be gaining market share, especially in products where performance is critical. Advantage of composite materials is that, they can be formed into more complex shapes than their metallic counterparts.

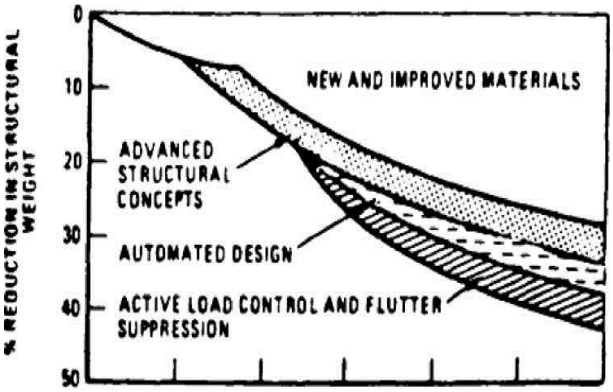

Fig.2 Trends in structural weight reduction for fighter aircraft, showing the significance of new and improved materials. [2]

This not only reduces the number of parts making up a given component, but also reduces the need for fasteners and joints, the advantages of which are twofold: fasteners and joints may be the weak points of a component — a rivet needs a hole which is a stress concentration and therefore a potential crack-initiation site, and fewer fasteners and joints can mean a shorter assembly times.

This applies both to airframes and engines. For example fighter aircraft must operate over broader combat envelopes with supersonic speed, high load factors and maximum Mach numbers. The major part that new and improved materials play in structural weight reduction is shown in Fig.2. It can be seen

* Corresponding author. Tel.: +88-01717518131
E-mail address: anisulislam49@gmail.com

clearly that the materials factor this factor greatly exceeds the contribution made by other advanced technologies such as structural concepts, automated design & active load control and flutter suppression.

2. Types of Composite Materials

A composite material typically consists of relatively strong, stiff fibers in a tough resin matrix. Wood and bone are natural composite materials: wood consists of cellulose fibers in a lignin matrix and bone consists of hydroxyapatite particles in a collagen matrix.

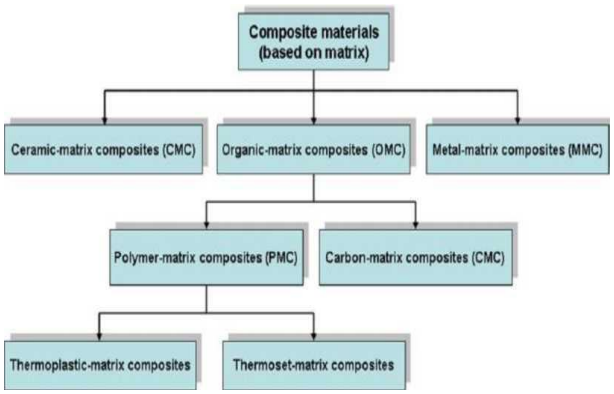

(a)

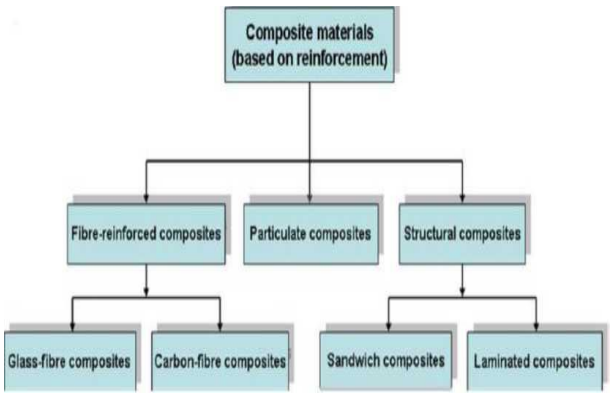

(b)

Fig.3 Classification of composite material (a) based on material matrix (b) based on reinforcement material. [3]

FRP composites are high strength Better known man-made composite materials, used in the aerospace and other industries are CFRP and GFRP which consist of carbon and glass fibers, both of which are stiff and strong (for their density), but brittle, in a polymer matrix, which is tough but neither particularly stiff nor strong. Very simplistically, by combining materials with complementary properties in this way, a composite material with most or all of the benefits (high strength, stiffness, toughness and low density) is obtained with few or none of the weaknesses of the individual component materials are CFRP and GFRP are fibrous composite materials; another category of composite materials is particulate composites. Advanced composites are generally classified based on their matrix and reinforcement shown in Fig.3.

3. Properties of composites materials

Composites are incredibly lightweight, especially in comparison to materials like concrete, metal, and wood. Often a composite structure will weigh 1/4 that of a steel structure with the same strength. This equates to serious fuel savings. Composite materials are extremely strong, especially per unit of weight. An example of this are the high tenacity structural fibers used in composites such as aramid and S-Glass, which are widely used in body armor. Composites are highly resistant to chemicals and will never rust or corrode. This is why the marine industry was one of the first to adopt the use of composites. Fiber reinforced composites have excellent elastic properties. When one bends metal, it will yield or dent. However, when composites are bent, they want to naturally snap back into place. Certain composites, such as composite made with fiberglass, are non-conductive. This is important because often a structure is needed that is strong, yet will not conduct electricity. For example, Aluminum ladders can be an electrocution hazard, while ladders made with fiberglass are not a risk if the ladder was to cross a power line.

3.1 Properties of Carbon-Carbon Composites

Table 1 High performance C-C composite plane shear and compression properties in room temperature. [4]

Construction	Fiber volume fraction			Shear strength (Mpa)	Shear elastic modulus (Gpa)	Compressive strength (Mpa)	Compressive elastic modulus (Gpa)
Direction	X	y	z	x-y	x-y	X	X
Unidirectional (1D)	.65	0	0	7-14	4-7	620	250
Fiber laminate (2D)	.31	.30	0	7-14	4-7	150	100
Woven Orthogonal (3D)	.13	.13	.21	21-27	1.4-2.1	Z 140	Z 90

Examination of the data shows that C-C composites can have highly attractive mechanical and thermal properties. Strength utilization of the fibers is 25 to 50%, depending on the fiber architecture and processing specifics shown in Table 1. In general, the shear strengths and shear moduli of C-C composites are low

compared with other materials. The same limitations exist for tensile properties in one- and two dimensional composites in directions normal to the fiber directions. These low properties are the result of processing that creates less than optimum bonding between the matrix and fibers to avoid brittleness and low fracture strengths along the fiber directions.

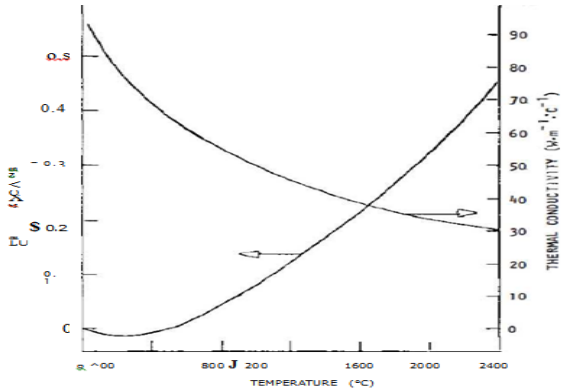

Fig.4 Representative high performance C-C composite thermal properties in principal fiber directions. [4]

Thermal expansion of C-C composite with variation of temperature and conductivity is shown in Fig.4. A principal reason for the structural attractiveness of C-C composites is that, although brittle, they can exhibit relatively high values of fracture toughness [5]. Shear displacement of the matrix relative to the fibers and eventual fracture of the fibers at points away from the primary zone of matrix failure create the fibrous pullout fracture surfaces indicative of toughness [6]. In general, carbon materials are unique in their retention of mechanical properties at high temperatures.

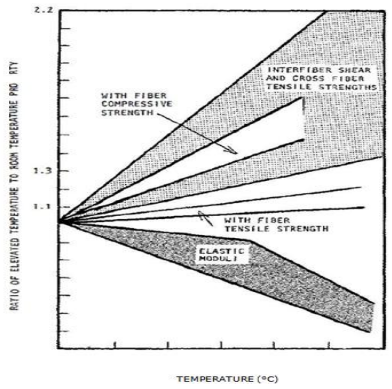

Fig.5 C-C composition high-temperature mechanical property trends. [4]

Fig.5 summarizes the effects of temperature on the mechanical properties of high-performance C-C composites. Moduli decrease or increase with temperature depending on the influence of matrix cracking relative to the basic thermal reductions in modulus of the constituents. This appears to depend on fiber architecture and specifics of the C-C processing. The creep or high-temperature time-dependent deformation of C-C composites has received only limited study [7-9]. Tests on small, single yarn unidirectional composite specimens at 2310°C and 770 MPa showed an initial transient creep in the direction of the fibers of about 2% over the first 2 hrs. and then a steady-state rate of about 0.37°K/h [7, 8].

3.2 Properties of Metal-Matrix Composites

The aerospace industry relies upon MMC billet produced by a powder metallurgy process. The primary process, performed by DWA Aluminum Composites, mixes matrix and reinforcing powder in a high-shear mixer, then outgases and consolidates the powder into billet. Unlike their organic counterparts, the metal alloy matrix in MMCs provides an important contribution to the strength of the composite. This results not only from the higher strength of metal alloys relative to organic resins typically used as matrices, but also from the fact that most MMCs currently have discontinuous reinforcements and a much higher matrix volume fraction. Metal-matrix composites are currently in service using matrices based on alloys of aluminum, titanium, iron, cobalt, copper, silver, and beryllium. Copper, silver, and beryllium MMCs are mostly used for thermal management and electrical contacts and titanium MMCs are used primarily for automotive, aerospace, and recreational products. By far the most widely produced MMCs are based on aluminum alloy matrices, and these are in current use for aerospace thermal management and electronic packaging, and recreational applications.

3.3 Properties of Fiber Reinforced Composites

FRC is high-performance fiber composite achieved and made possible by cross linking cellulosic fiber molecules with resins in the FRC material matrix through a proprietary molecular re-engineering process, yielding a product of exceptional structural properties. Through this feat of molecular re-engineering selected physical and structural properties of wood are successfully cloned and vested in the FRC product, in addition to other critical attributes to yield performance properties superior to contemporary wood. This material, unlike other composites, can be recycled up to 20 times, allowing scrap FRC to be reused again and again.

3.4 Ceramic Matrix Composites (CMC's)

While consisting of purely ceramic constituents, CMCs utilize a ceramic matrix with reinforcing ceramic fibers and are accepted as a composite system. This creates a material with the excellent thermal properties and with improved mechanical properties, overcoming the limitations of monolithic ceramic (i.e. toughness) and displaying other benefits. The possible applications of CMCs in aviation are generally in the hot section of the aero engines and include turbine disks, combustor linear, turbine aero foils, transition duct convergent flags and acoustic liners. The use of CMCs would allow

an increase in turbine inlet temperature from the current 1200°C to 1500°C, which would lead to a 6-8 per cent increase in fuel efficiency.

4. Literature Review

The maturation of computational structures technology and the development of advanced composite materials witnessed during the past 30 years have improved structural performance, reduced operational risk, and shortened development time and reduction in gross weight in typical air vehicles are shown in Fig.6.

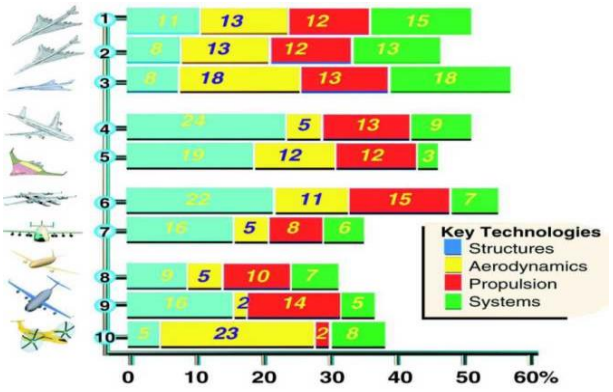

Fig.6 Projected vehicle total gross weight reduction in percent. [10]

The development of each of the component technologies is a multidisciplinary activity, which involves tasks in other disciplines.

Table 2 Features of aircraft structure [14]

Requirement	Effect
High reliability	♦ Strict quality control ♦ Extensive testing for reliable data ♦ Certification: Proof of design
Passenger safety	♦ Use of fire retardant materials ♦ Extensive testing: Crashworthiness
Durability-Fatigue and corrosion	♦ Extensive fatigue analysis/testing ♦ Al-alloys do not have a fatigue limit ♦ Corrosion prevention schemes ♦ Issues of damage and safe-life, life extension ♦ Thin materials with high integrity
Aerodynamic performance	♦ Highly complex loading ♦ Thin flexible wings and control surfaces ♦ Deformed shape-Aero elasticity ♦ Dynamics ♦ Complex contoured shapes ♦ Manufacturability: N/C matching; molding
Multi-role or function ability	♦ Efficient design ♦ Use: composites with functional

Affordable composite structures can be achieved by proper material selection, changing load paths, using robust low-cost manufacturing and joining/assembly techniques, and developing approaches for subsystem integration [11-13]. This will require composites to be considered as early as possible in the design process so that load paths are defined that offer manufacturability and do not penalize the composite structure's efficiency. Because the properties of composite materials are directionally dependent, they enable a structure's strength and stiffness to be tailored in directions that allow the most efficient management of airframe loads. They will be essential for creating durable and damage tolerant designs that can meet the long life requirements. [10] Important requirements of an aerospace structures and their effect on the design of the structure are presented in Table 2.

Two key developments in scientific-technological world have had a tremendous influence on the generation and satisfaction of the raised by the aerospace community: one, the advances in the computational power and the other, the composites technology using fiber reinforced polymeric materials.

Table 3 Typical composite materials systems in aerospace [14]

Fiber	Density (g/cc)	Modulus (GPa)	Strength (GPa)	Application areas
Glass				
E- glass	2.55	65-75	2.2-2.6	Small passenger a/c parts, aircraft interiors, secondary parts; Radomes; rocket motor casings.
S-glass	2.47	85-95	4.4-4.8	Highly loaded parts in small passenger a/c.
High modulus	1.48	160-170	2.3-2.4	Highly loaded parts
Carbon Standard modulus (high strength)	1.77-1.80	220-240	3.0-3.5	Widely used for almost all types of parts in a/c, satellites, antenna dishes, missiles, etc.
Ultra-high strength	1.80-1.82	290-310	7.0-7.5	Primary structural parts in high performance fighters, spacecraft.

In case of Aircrafts and other air breathing vehicles the use of advanced composites in the construction of aircraft and helicopters, weight savings of 20-30% are

achieved as compared to conventional materials [14]. Fairings, landing gears, engine cowls, rudder, fin boxes, doors, floor boards and many other interior gadgets are made of advanced composites in combination with metallic and nonmetallic honey comb cores and metals. In case of Space vehicles, two factors, high specific modulus and strength, and dimensional stability during large changes in temperature in space make composites the material of choice in space applications are listed in Table 3. Examples include the graphite/epoxy-honeycomb payload bay doors in the space shuttle like Antenna ribs and struts in satellite systems use graphite/epoxy for their high specific stiffness and its ability to meet the dimensional stability requirements due to large temperature excursions in space.

Table 4 Aircraft composite materials usage surveyed.

• Fighter Aircraft(US)	F-16,F-14,F-18,YF-23,F-22,JSF,UCAV
• Fighter Aircraft(Europe)	Gripen JAS-39, Mirage 2000, Rafael, Eurofighter Typhoon, Lavi.
• Fighter Aircraft(Russia) • Bomber(US)	MiG-29, Su series B-2
• Transport(US-Commercial)	B-777, B-767, MD-11
• Transport(Airbus, European)	A-320, A-340, A-380, Tu-204, ATR42, Falcon 900,A300-600 ST
• General Aviation	Piaggio, Starship, Premier 1
• Rotary Aircraft	V-22, Eurocopter Tiger, Comanche RAH-66

Operating efficiency and economy with passenger comfort are paramount in commercial transport aircraft. Table 4 shows that, the composites materials has already used in civil and commercial aircrafts.

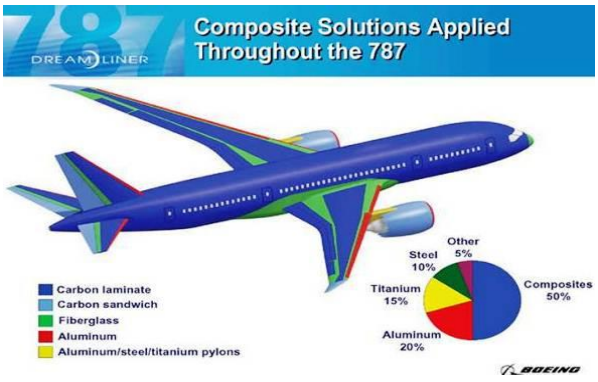

Fig.7 "Dreamliner" Boeing 787 composite solutions

Fig.7 shows that, "Dreamliner" Boeing 787 has already constructed of around 50% composites. Composites are especially adept at achieving overall weight reduction but also facilitate the construction of novel aerodynamic aircraft shapes such as the blended wing-body thus providing additional routes to improved fuel efficiency.

5. Manufacturing and testing

It is not my intention to deal at any great length with manufacturing technology since it falls outside the general scope of this paper. However, it is important to note that fabrication considerations strongly affect the designer in several ways. However, the production, manufacture and final disposal of high performance composites and similar materials for use in aircraft requires considerably more energy than metal components such as aluminum alloys. For example, aluminum can be recycled at about one 20th the energy that it takes to refine it from ores. The technique most commonly used today for fabricating high-performance composite structures is "filament winding." This is the technique currently used for fabricating rocket motor cases and other pressure vessels reinforced with glass fibers. It is significant that important weight reductions have been achieved with composites despite a conservative design approach. The difference results from reductions for factors like material property, variability, fatigue, stress concentrations at holes, cutouts and joints and allowance for minor damage and manufacturing defects. The use of more aggressive design allowable will depend on resolution of the technical uncertainties mentioned above.

6. Conclusion

Manufacturing and production engineers are searching for ways of reducing the costs and times to produce composite components. Prepreg materials are generally more expensive. For these reasons, Engineers are directing increasing interest at the use of "non-crimp" fabric (NCF). NCF is dry carbon fiber material, which is cheaper than prepreg. In terms of the manufacturing process there is an ongoing research effort throughout the industry to eliminate autoclaves. Vacuum bagging allows a pressure of up to one atmosphere to be applied to the laminate, although this falls short of what can be achieved in an autoclave. For this reason the geometries of component that can utilize this production approach may be restricted. Hopefully the money that is being invested in research in this area will enable such technology to be used in an increasing range of aerospace components.

7. Recommendation

The environmental case for developing understanding and increasing exploitation of composites is compelling. The reduction of airframe weight through the extensive use of carbon composites is just one of a range of technologies that must be deployed to meet such a challenging target to reduce the emission of CO2 from an aircraft by 50% by 2020. To meet the challenge that the widespread use of composite materials should throws up in aerospace community. It is safe to predict that, barring some unexpected catastrophic problem, composites usage will continue to increase at an accelerating rate. There are several reasons for believing

that, increasingly composites will become economically competitive with metals. These include, acquisition costs will drop because of lower material costs as volumes increase; and lower fabrication costs as this technology advances, aided by development of new, process-oriented resins. Rising fuel prices will provide an increasing premium for weight reduction. More requirements will be placed on toughened composites as new applications emerge such as cryogenic fuel tanks, large aerospace structures, space orbiting components, and lunar habitats. An approach to composite toughening should be developed Computational Chemistry technology to the point where an understanding exists between fracture energy and molecular polymer chemistry. This would be the ultimate screening tool; the polymer structure of a toughened resin can be predicted without the need to synthesize that polymer.

REFERENCES

[1] M. F. Ashby, "*Philosophy of Transportation*", Royal Society of London, pp. 322, 393, (1987)
[2] T.R. Rooney, "*Evaluation of Aircraft/Aerospace Structures and Materials*", AIAA, Dayton, OH, pp. 8.1-8.6, (1985)
[3] Vermeeren, "*An historic overview of the development of fiber metal laminates*", CAJR Applied Composite Materials, Vol. 10(4-5), pp. 189-205, (2003)
[4] J.E. Sheehan, K.W.Buesking and B.J. Sullivan, "*Carbon-Carbon Composites*", Annual Review of Material Science, Vol. 24, pp. 19-44, (1994)
[5] J. Cook, JE. Gordon, Proc. Royal Society of London, pp. 508-520, (1964)
[6] E. Fitzer, KH. Geigl, W. Huttner, Carbon 18, pp. 265-270, (1980)
[7] G. Sines, Z. Yang, BD. Vickers, "*Creep of carbon yarn and carbon-carbon composites at high temperatures and stresses*", UCLA-ENG-88-8, Los Angeles, UCLA Sch. Eng. App. Sci., (1988)
[8] G. Sines, Z. Yang, BD. Vickers, J. Am. Ceram. Soc. 72, pp. 54-59, (1989)
[9] LA. Feldman, A TR-88 (3728-02) -2. Los Angeles: Aerospace Corp.
[10] A.K. Noor, "*Structures technology for future aerospace systems*", Computers and Structures, Vol. 74, pp. 507-519, (2000)
[11] V.V. Kafarov, I.N. Dorokhov, A. Ramirez and N.I. Kafarova, "*Computer-aided design of multifunctional composite materials*", Computers and Chemical Engineering, Vol. 20(A), pp. 5431-5434, (1996)
[12] L. Sadler, A.V. Sarma, "*Fabricating affordable composites*", Proc. AIAA/ASME/ASCE/AHS/ASC 38th Structures, Structural Dynamics and Materials Conference, Part II, Kissimmee, FL. pp. 1002-1008, (1997)
[13] G.C. Krumweide, "*Affordable polymer composites for spacecraft applications*", Society for the Advancement of Materials and Process Engineering, Science of Advanced Materials and Process Engineering, Vol. 41, pp. 1122-1133, (1996)
[14] C.M. Satter, R.E. Freeland, "*Inflatable structures technology applications and requirements: For space deployable systems*", AIAA Space Programs and Technologies Conference, (1995)

ICMIEE-PI-140201

Material Transferring Robot in a Production System

Md. Mizanur Rahman [1*], *Md.Golam kibria* [2], *Mahadi Hasan Tushar*[3]
[1, 2, 3] Department of Industrial Engineering and Management, Khulna University of Engineering & Technology, Khulna-9203, BANGLADESH

ABSTRACT
There are many research work already performed for constructing the robot. Hence Robot is the important equipment in the industrial world. We are tried to create new required features of Robot. Maximum research of industrial robots are performed on Robotics arm, obstacles detection, Edge avoiding, line flower Robots. Here we implemented a Robot which gives some innovative or modifying features such as 1) It will transfer load automatically one location to another when maximum load throughput on it (for e.g. 3 kg weight). 2) It records how much units already transferred with respect to time. 3) If it faces obstacles in front of robot then robot starts counting time with beeping sound and it also increases the beeping sound to infinity with respect to time increasing. 4) It will give alarm when anyhow temperature of the industry gets in higher level or in firing situation. The structure of the Robot will be as an "Automatic guided vehicle" (AGV) which is may be used in the developed country in the world. The driving path of our robot is used line flowing to keep proper balance of the robot. The robot has a good aesthetic view and perfect assembly is performed. Mainly the robot works for a particular position in a production system to transfer required material.

Keywords: Keywords: Robot, material, obstacles, records unit, AGV.

1. Introduction

A robot [1] is a reprogrammable, multi-functional manipulator designed to move material, parts, tools, or specialized devices through variable programmed motions for the performance of a variety of tasks." (Robotics Institute of Amerca). Robots are primarily concerned with generating specific motion of the robot joints, simultaneously allowing tooling or sensors to perform certain functions, either when the arm is moving or at specific operational configurations. The material transferring robot may perform the operations themselves carry parts to other devices which perform the operations. In 2003 **"**OTC DAIHEN" introduced the ATMEGA AX series, a line of arc welding and handling robots. The AX series robots integrate seamlessly with the OTC D series welding power supplies for advanced control capabilities. In our material transferring robot we used ATMEGA8 microcontroller. In this microcontroller we loaded our desired AVR programming by using programmer software "PROVISP". Here we tried to implement material transferring robot in a production system like as in jute mill. In jute mill to make final yarn various operations and machines are included. Machines are breaker card, finisher card, 1st drawing, 2nd drawing, and 3rd drawing, spinning, twisting (Final yarn). The processing jute fiber in 1st drawing to 2nd drawing, 2nd drawing to 3rd drawing and spinning to twisting, twisting to storage buffer, final processing to storage five movements is required. The machine requires continuous processing and some labor need only to move the processing fiber. The application of material transferring robot is within these steps of making yarn.

2. Literature Review

The earliest known industrial robot, conforming to the ISO definition was completed by "Bill" Griffith P. Taylor in 1937 and published in Meccano Magazine, March 1938.[3][4] The crane-like device was built almost entirely using Meccano parts, and powered by a single electric motor. Five axes of movement were possible, including grab and grab rotation. The automation was achieved using punched paper tape to energize solenoids, which would facilitate the movement of the crane's control levers. The robot could stack wooden blocks in pre-programmed patterns. The idea [5] of using robotics for humanitarian demining has been proposed by numerous authors. For example, the quadric-pedal legged TITAN-IX (Hirose and Kunieda, 1991; Hirose and Kato, 1998; Hirose et al., 2005) and SIL04 (de Santos et al., 2003; Garcia et al., 2003) have been proposed to be able to walk through minefields with the TITAN-IX possessing the ability to reconfigure its legs for manipulation and its gait in case a leg is damaged, while SIL04 automatically adapts its gait to the terrain and uses a wide stance for traction. The Gryphon robot (Debenest et al., 2003; Freese et al., 2006; Tojo et al., 2004) successfully adds remote operation on top of a rugged, commercially available all-terrain vehicle base. In addition to robots, semiautonomous variants of wheeled and tracked mine clearing vehicles have been used with varying levels of success as they are

* Corresponding author. Tel.: +88-01722915126
E-mail address: sinha0911043@gmail.com

designed for and best suited to military requirement. The previous research work of industrial robot is not enough because we need more automation process in our industry. There is small number of industries that uses industrial automation but not 100% automation. We need more automation in our industry. When we want to automate our industry industrial, robot is the vital the things. Material transferring robot can automate only the carrying option of any industry.

3. Methodology

Table 1 Major Requirement.

Names	Ratings
Gear Motor	12V 200RPM
Wheel(front 1 & back 2)	19mm*38mm dia. 3P
Microcontroller	Atmega8
Motor driver	L-298
IR LED	5 Pairs
Vero Board	
programmer	ATmega8 program.
Transformer	12V 3A
Plastic Wood	4"*2"
Art Paper	For making path
Comparator	LM358P
capacitor	200uf,50v
Voltage stabilizer	7812,7805
FEVICOL Gum	
Drill machine	5mm dia,7 mm dia. bit
Wire	M to M, M to F
Thick tin base	5inch* 3inch
Welding heater	60 Watt

3. Production process

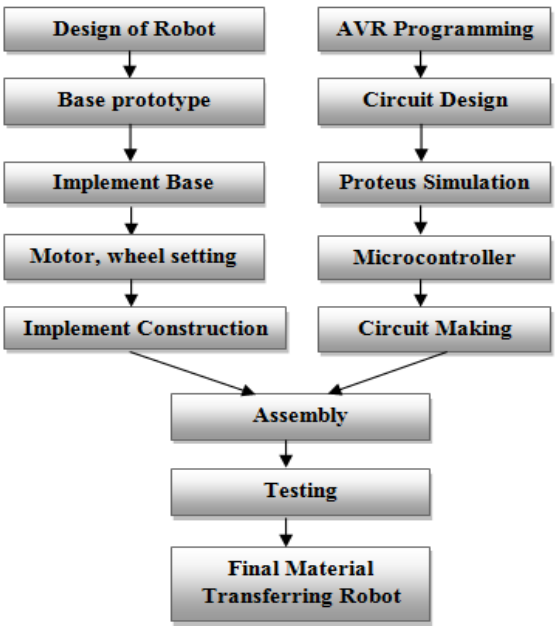

Fig.1 Production process of making material transferring Robot.

3.1.1 Design of Robot

Solid-work is design software. After planning of the thesis work is started. At first Here the possible design criteria is evaluated whose can affect in the final material transferring robot.

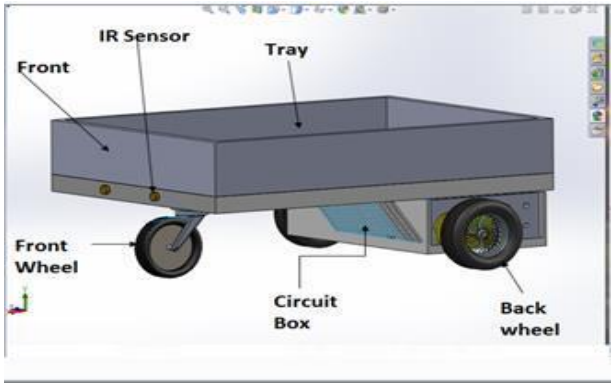

Fig.2 Initial solid-works design of material transferring robot

3.1.2 Hard Prototype for Base

After completing the solid works design of the robot, a prototype is designed for the base of robot. Here a thick cartoon paper is used as a prototype of base. The base length is 5" and the wide is 3". Also two holes are exists for adjusting the two gear motor.

Fig.3 Prototype of base

3.1.3 Implement Base and set with gear motor

Then the base from hard still is implemented and attached with the gear motor. Here a drilling machine is used with different drill bit's diameter. When the drilling operation is completed two screws are used to set the gear motor with base. It gives a strong relationship between the gear motor and the base.

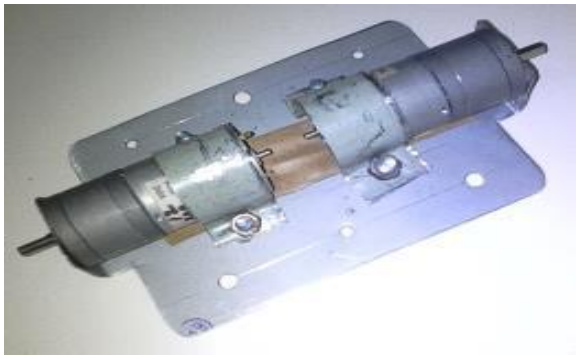

Fig.4 implementing the base with gear motor.

3.1.4 Wheel Set with Motor Gear

When the motor gears are set with the two wheels, there is a problem arises. First time it could not be the wheel with the gear motor because the gear motor diameter is less than the wheel diameter. Then it attached a cloth of piece with the wheel and possible to attached with it.

3.1.5 Implement Construction

This is the main point where many problems are arising again and again. When it was going to making the final construction of the robot various problems are faced. For giving the space to keep of circuit it is necessary to build up the screw holding system. Many scopes has been tried to develop the screw holding system in this stage and to make screw thread. That's why the waste pen is cut into small pieces and by the screw some internal threads made into it. Then it is attached the pen in the plastic wood surface of robot. Then the buildup surface with the help of FEVICOL gum is constructed. Here safety issue is considered with respect to safety criteria. When the construction of robot is made here is another problem arises. It could not move in straight axis and could not to keep balance within the straight axis. To solve this problem line flower robot part is used i.e. an external circuit is used with the constructed frame.

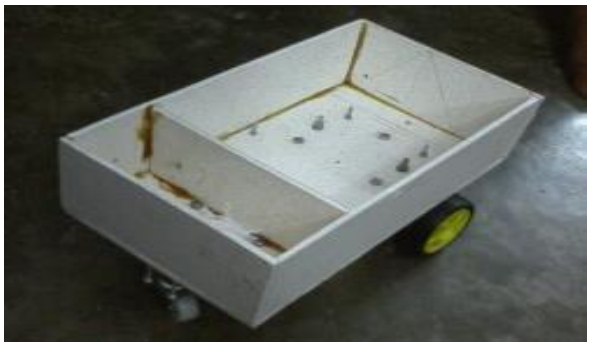

Fig.5 Constructed robot frame without circuit

3.1.6 AVR programming

AVR studio is programming software. Basically AVR is like a C or C^{++} programming. When the required programming is made then the program is combined with the Proteus software.

3.1.7 Circuit Design

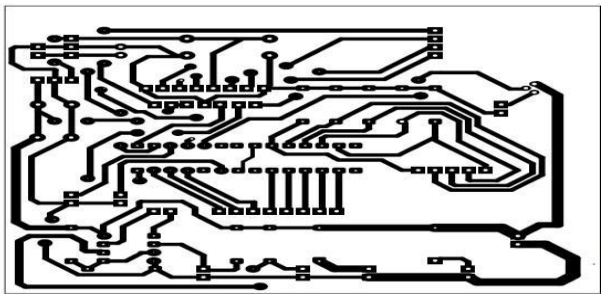

Fig.6 Mirror view of PCB design

Proteus software was used to design the circuit. First In ISIS design is performed and then in ARES PCB design is implemented. After print out the mirror of PCB design then heated the printed layout in PCB board. When the carbon attached with the PCB board it kept in $Fecl_3$. Then it is drilled by 1/32 inch drill bit. Initial and final view of PCB board design is given above.

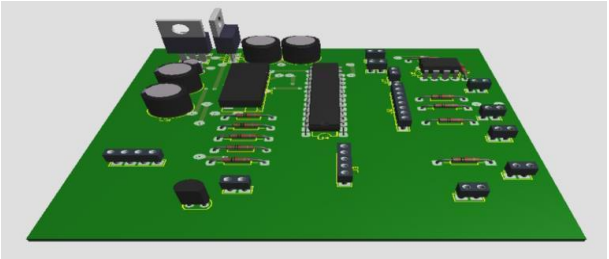

Fig.7 Desired view of PCB circuit design

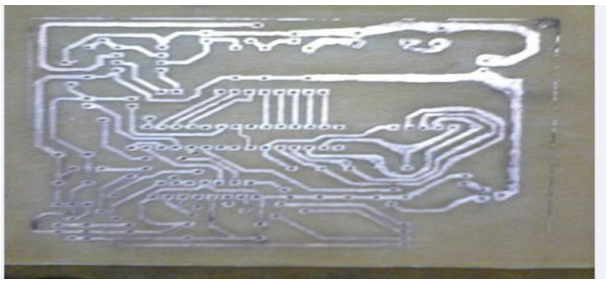

Fig.8 Implemented design in PCB board

3.1.8 Proteus Simulation

Proteus is a design and simulation software. In this thesis Proteus 7.7 is used for designing the circuit and simulation. Proteus show whether the circuit will work or not. Though the simulation is working, it is difficult to implement in the final product. When the design is completed, it leads for loading the program from programmer.

3.1.9 Microcontroller

ATmega8 microcontroller was used as a control unit. ATmega8 microcontroller consists of 512 bits of ROM, 12k bytes of flash memory. All of the work of robot controls the microcontroller. Specially, motor driver L298 takes logic input from the microcontroller according to microcontroller decision; it rotates clockwise or anticlockwise or rotates only one wheel to bulk. When sensors give input to microcontroller, microcontroller takes the decision what to do.

3.1.10 Circuit & Power Supply Making

Power supply making is important activity when a man works with a circuit. To get 12v supply a transformer to 12V converter 220V is purchased but it was giving 33v output. Then it is attached a 2200µf 50Volt capacitor, a safety resistor 10watt 1Ω and four diodes. Then it is tried to test whether the wheel is rotating or not. But the two wheels are rotating onetime clockwise and sometimes later anticlockwise. To solve this problem some capacitor attached with it. After attaching some

capacitor wheels are rotating only in clockwise direction. To make the circuit a Vero-board is used and also the essential requirement is used. The full circuit is made manually. The line flower circuit is attached under the base part. We made the final circuit in Vero-board because of design error in our PCB circuit. Line flower characteristics a circuit is shown below.

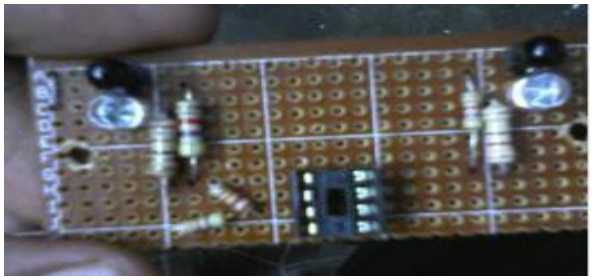

Fig. 9 Line flower sensor circuit

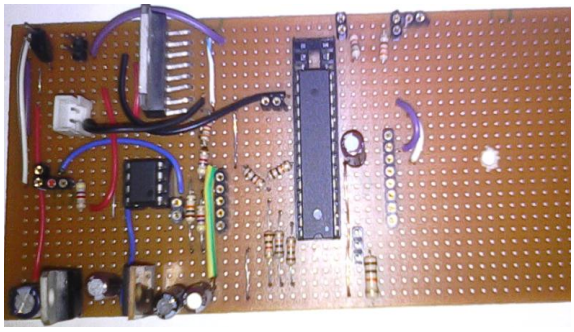

Fig. 10 Final Circuit

3.1.10.1 How Sensor Circuit Works?

A sensor circuit diagram is given below. Here a voltage stabilizer 7805, a comparator 358 and some resistor are used. This is a circuit diagram for sensing something nearby. When a something will pass through the space between infrared ray receiver and infrared ray transmitter an electric pulse is generated. Combination of transmitter and receiver is a complete circuit. When passing something space between the transmitter and receiver the resistance increases in circuit and output LED emits light. According to the microcontroller program it takes input as an electric pulse. In this thesis two types of sensor circuits are used one is for line flower and another is to detect obstacles in front of robot. Two types of sensor circuits are combined with the microcontroller unit. When the front circuit is sensing something, the microprocessor takes decision and stops the rotation of motor.

3.1.10.2 How first input takes the robot?

The robot for transferring is designed for 3kg weight. To take the first input three push buttons are used here. When 3kg weight throughput on it, the push buttons are completed the circuit and robot starts to move forward**.**

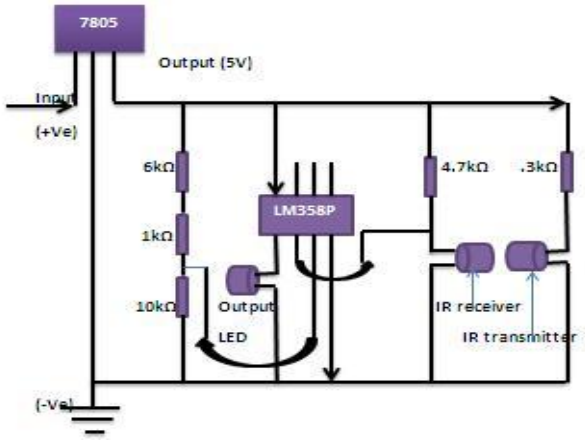

Fig.11 Common sensor circuit diagram

3.1.10.3 How the robot flow a straight line for moving itself?

Here some art papers, some black papers, FEVICOL gum and a tape for making the path of the robot are used. First five art papers ones end to another start point is joined by using FEVICOL gum. Then the black paper for design the straight line path is cut. The black paper's middle point of each of the paper; are also jointed and it creates a straight line which is shown in the final material transferring robot. After this the tape all-around of the art paper to give strength of the art paper is jointed. In the line flowing circuit two IR pair sensor are used. Here the coding is different to control the path of robot. When sensor senses that the black part is available, microcontroller takes decision to go the direction of black part of the path.

3.10 Assembly, examine & final selection

When all of the parts and subassembly is made, it is assembled all of those part and subparts. After assemble the parts it is need to checkup to ensure that the material transferring robot is worked. When the robot met the requirement of material transfer the material transfer robot is ready to serve.

Fig.12 Final view of material transferring robot

5. Result

The first the objectives (Transfer material, obstacles detect &record transfer unit) are fulfilled by our material transferring robot. But the fourth objective

(robot will give alarm in risky situation when temperature will rise up higher degree) is not fulfill by our robot. Hence the fourth objective is not so relevant with another three objectives, we just avoid it. Our robot has ability to give 93% efficiency of work. But our robot requires relatively higher initial cost.

6. Further research required

In our robot has some limitation because it can perform two automation works only. One is to transfer material or product from one place to another automatically and another is, can detect obstacles. According obstacles it can take decision whether it goes or not. Our robot is not fully automated because it cannot take material on into it automatically. To complete the total activity of material transfer automatically further research is required. In further research work may be different design of the robot which will have carrying capability and gripping capability together to perform full automation process. In addition it may be have additional arm for gripping the material or product with our robot. Again obstacles avoidance may be a further research option for who want to work with industrial robot.

7. References

[1] ISO Standard 8373:1994, Manipulating Industrial Robots – Vocabulary

[2] Turek, Fred D.. "Machine Vision Fundamentals, How to Make Robots See". *NASA Tech Briefs* 35 (6): 60–62. Retrieved 2011-11-29 (June 2011)

[3] "An Automatic Block-Setting Crane". *Meccano Magazine* (Liverpool UK: Meccano) 23 (3): 172. March 1938.

[4] Taylor, Griffith P. Robin Johnson, edition. *The Robot Gargantua*. Sheffield: Constructor Quarterly. pp. 6–13(1995)

[5] Ioan Doroftei, Yvan Baudoin, A concept of walking robot for humanitarian demining", Industrial Robot: An International Journal, Vol. 39 Iss: 5 pp. 441 - 449(2012),"

[6] KUKA-Roboter.de: 1973 The First KUKA Robot English, 28th of March 2010

[7] "History of Industrial Robots". Retrieved 2012-10 27. ISO 9283 preview

[8] Asif, U. and Iqbal, J."Motion planning using an Impact-based hybrid control for trajectory generation in adaptive walking", International Journal of Advanced Robotic Systems, Vol. 8 No. 4, pp. 212-24(2011)

[9] Baudoin, Y. and Colon, E. "Humanitarian demining and robotics: a difficult challenge", Proceedings of the Second International Conference on CLAWAR'99, Portsmouth, UK, pp. 911-21 (1999)

[10] John J. Craig, Introduction to Robotics, Mechanics and Control, Addison Wesley, 1989.

[11] Richard P. Paul, Robot Manipulators: Mathematics, Programming, and Control, MIT Press, 1981.

[12] Charles J. Spiteri, Robotics Technology, Saunders College Publishing, 1990.

ICMIEE-PI-140203

Feasibility Study on Power Generation in Bangladesh using Rice Husk as an Alternative Source of Fuel

Md. Amanullah Kabir[1] , Md.Saiful Alam Shabbir[2], A.H.M Fazle Elahi[3]*

[1, 2, 3] Department of Mechanical Engineering
Khulna University of Engineering & Technology, Khulna-9203, Bangladesh

ABSTRACT
Bangladesh is currently facing power crisis which has become worse in recent years. The cost of power generation that is increased drastically with an unprecedented surge in international fuel price. The rising cost of fuel is the main reason to seek the alternative source of fuel. Rice husk, which is a by-product of Rice processing is identified as an important and potential alternative fuel source for generating power. Bangladesh is an agricultural country which is dominated by Paddy cultivation. Bangladesh has reportedly over fifty thousand Rice mills–small, medium, large. They process Paddy collected from rural areas. The Rice mills use the thermal energy of steam which is generated in boilers by firing the Rice husk. It is globally well-known and convenient source of dry biomass energy of reasonable heat value. In Bangladesh context out of 38 million tons of total biomass produce from agro-residues, rice husk contributes about 28% by mass. Rice husk is considered to be an environment friendly fuel because it can minimize CO_2, SO_2 and NO_x emissions when compared with conventional fuel. In this research four major rice processing districts were selected to estimate potential husk available for electricity generation. The selected Rice mill Clusters are located at Bogra, Dinajpur, Rajshahi and Rangpur. More than hundred numbers of rice mills were surveyed in this research to know about annual Paddy processing capacity and surplus amount of husk from the four selected rice processing zones. Based on the collected data, potential power capacities were estimated in four selected districts considering the steam turbine technology. A systematic approach can give birth to a new industrial sector of Rice husk based power generation in Bangladesh.

Keywords: Rice mill, Rice husk, Alternative energy source, Power generation, Environmental impact.

1. Introduction

Bangladesh is an Agricultural country. In Bangladesh Rice is a staple food and accounts for about 93% of the total food produced in country. Bangladesh produces on average 33890 thousand MT (2011-2012) Paddy per year, giving approximately 6778 thousand MT Rice husk [1]. Generally Rice husk constitutes about one fifth or 23% (by weight) of the dried paddy Rice. Bangladesh has 53423 Rice Mills (Large, Medium, and Small). Approximately 95% Rice husk is produced by milling process of Rice Mills. Rice husk can be converted into different types of fuel through a variety thermo-chemical conversion process. So Rice husk can be used as a potential source of heat energy and one of the largest source of biomass because it contributes 26% of the total about 42390 thousand MT biomass produced in Bangladesh. At present in Bangladesh about 70-75% of Husk is consumed for steam production in mills. The average Calorific value of Rice husk in natural and dry state is 14700kJ/kg. The Moisture Content present in Rice husk, is ranged between 8.68-10.44%, ash content is ranged between 23.39-24.10% and the bulk density is ranged between 86-114 kg/m^3.The Paddy of 1 ton consumes approximately 30-60 KWh to give 600-700 kg of Rice and the Rice husk as a residue of 220 kg which is equivalent to power generation of 90-125 KWh. Bangladesh has a big crisis in energy sector in power generation because of simultaneous increase in cost of fuel and its consumption. At present installed capacity in power generation is 8716 MW, installed capacity is 8100 MW, demand forecast is 7518 MW, maximum peak generation is 6060 MW and maximum load shedding is 1058 MW. According to report of BPDP(2010-2011), power consumption pattern of the country - Domestic (44.49%), Agriculture (2.69%), Industrial (39.34%), Commercial (10.99%), others (2.49%) of total 6380 MKWh (cumulative) and sector wise number of consumer in rural electricity is 9085810 MKWh (Cumulative) and for power generation Import of coal and coke from other countries is 7.39 MT and fuel consumption by power plant is 151048 million Cft (natural gas), 182 million Litre (Furnace oil), 60 million Litre (HSD,SKD, SKO & LDO) [1]. So for the purpose of recover fuel consumption as well as fuel cost as possible by few percentage Rice husks can be used as a potential energy source.

Fig.1 Rice husk in a Rice mill

* Corresponding author. Tel.: +88-01750607736;
E-mail addresses: mdsaifulalam70@gmail.com

Already Electricity generation from Rice husk through various technologies is now being used in several developing countries like India, SriLanka, China, and Indonesia etc. In this research, our studied areas were mainly focused on the four districts which are Bogra, Dinajpur, Rajshahi and Rangpur located at the north zone in Bangladesh. The main purpose of this research is to give feasible idea about installation of Rice husk based Steam Turbine power plant in Bangladesh.

2. Methodology

Rice is mainly processed in two sections. One is in Household and other is in Rice mill. Around 5% of total paddy is used as seed for using next growing season and about 70% is processed in local mill and the rest of 25% paddy is processed in rural household level. In this research, Paddy which is processed in Rice mills, was considered the main potential source of Husk supply for electricity generation because household level cannot be considered due to its wide spread localized. Four districts - Bogra, Dinajpur, Rajshahi and Rangpur were selected for collecting data.

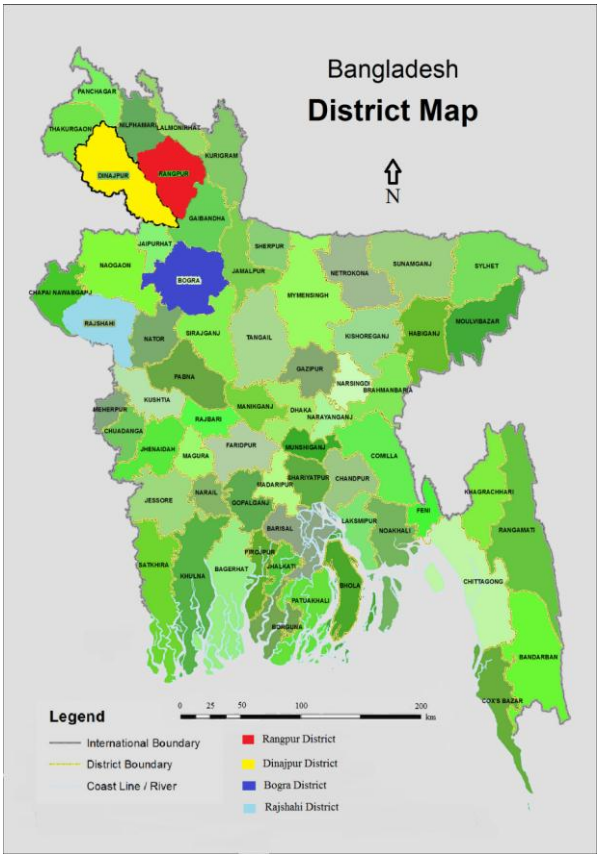

Fig.2 District Map of Bangladesh.

A survey Questionnaire was used to collect the information on annual quantity of Paddy, processed through interviews, observations for the studied Mills and internet sources etc. Over one hundred number of Rice mills were surveyed in this study. Data's of annual Paddy production trend of those districts were collected from BBS. Various thermo-chemical conversions of Rice husk were studied and total feasible electricity generation from Rice husk mixing with Coal was calculated by using steam turbine Technology. The Rice husk is produced as by-product which can be used as an important source of husk based electricity generated steam turbine plant.

3. Analysis of Rice Husk

Different types of analysis of Rice husk were taken based on various elemental analysis, collected data and finally electricity generation capacity of four districts were calculated which are varied with different color on the map. (I.e. Bogra, Dinajpur, Rajshahi, Rangpur) are given below:

3.1 Proximate Analysis of Rice Husk

Results from proximate analysis are shown in Table 1. Moisture content is one of the important criteria of a fuel for the selection of energy conversion process technology. Thermal conversion requires biomass fuels with lower amount of moisture content. Moisture content less than 10% is suitable for thermal conversion process. As Rice Husk has higher percentage of fixed carbon, volatile content and lower percentage of moisture content, it is suitable for thermal conversion process.

Table 1: Proximate analysis result of Rice husk

Volatile, %	Fixed Carbon,%	Ash,%	Moisture,%
58.90	19.70	13.20	8.20

3.2 Ultimate Analysis of Rice Husk

The percentage of organic elemental contents (i.e. Carbon, Oxygen, Hydrogen, Sulphur etc.) are listed in Table 2.

Table 2 Organic element contents of Rice husk

Carbon,%	Oxygen,%	Ash, %	Moisture, %	Hydrogen ,%	Nitrogen, %	Chlorine, %	Sulphur, %
39.1	34.70	13.2	8.2	4.59	0.18	0.09	0.04

3.3 District wise Number of Rice Mill

Total Rice Mills in four studied districts are given below [1]:

Table 3 Number of Rice Mills

Bogra	Dinajpur	Rajshahi	Rangpur
3781	1806	1052	1325

3.4 Elemental Analysis

Different elements of Rice Husk are given below [2]:

Table 4 Elemental Analysis

Element	Mg	Si	P	Ca	Cr	Mn	Fe	Cu	Zn	As	Hg	K	Pb
Rice Husk, mg/Kg	0.55	6.66	43.13	570	997.33	302.04	2127	210.76	38.23	0.76	0.98	2395	32.89

3.5 Electricity Generation Capacities

Estimated electricity generation capacities based on Rice husk as fuel by using Steam Turbine Technology in studied areas are given below:

Table 5 Electricity Generation Capacities

Rice Processing District	Available rice Husk in Thousand M.tons	Electricity Generation by using Steam Turbine Power Plant, kW
Bogra	59.49	5270.88
Dinajpur	89.92	7863.93
Rajshahi	149.25	12718.13
Rangpur	165.41	14095.18
Total =	464.07	39948.12

Husk supplies from Rice mill is not uniform quantity throughout the year. The Husk supply is surplus so that the husk is leftover after consumption and sometimes the husk supply is deficit than needed. By storing husk by uniform amount it can be used to steam boiler in deficit months. Electricity generation from Rice husk depends on availability of husk and its thermal conversion technology. In this research steam turbine technology was used. For steam turbine power plant consumption of Rice husk is 1.3 Kg per KWh as reported by Singh [3].Total potential power capacity in studied districts is estimated as 39948.12KW.

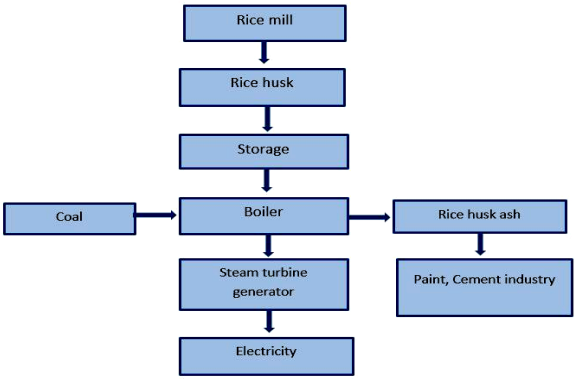

Fig. 3: Block Diagram of power generation from Rice husk.

4. Result Analysis

Over last 8 years there has been an increasing trend of Paddy production as well as Rice husk production. So, power generation from Rice husk by using Steam Turbine Technology is steadily increasing day by day. These analysis are shown in figures given below. Figure-4, Figure-5, Figure-6 represent the trend of Paddy production, Rice husk, estimated energy production respectively from 2004 to 2012. So, it can be assumed that power generation from Rice husk will increase in upcoming future years and Rice husk will add a remarkable amount of electricity in national grid of Bangladesh.

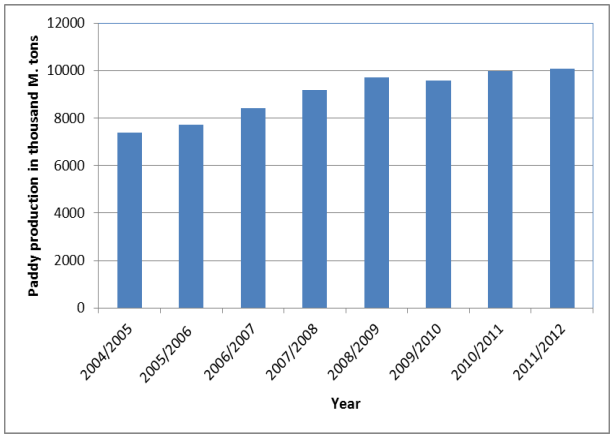

Fig. 4 Available Paddy production during 2004 to 2012

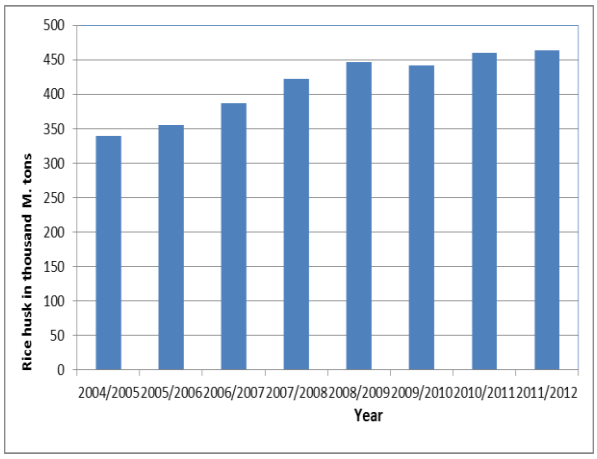

Fig. 5 Available Rice husk during 2004 to 2012

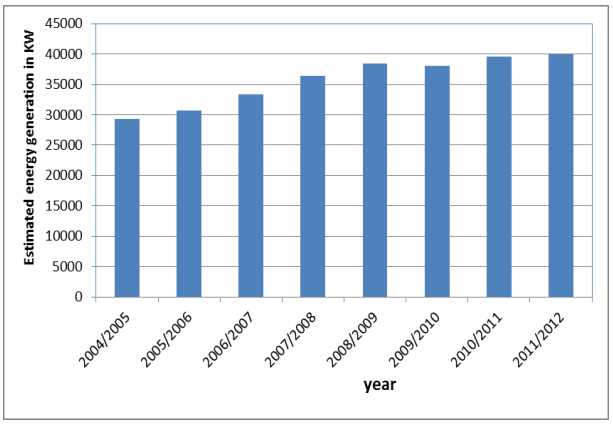

Fig. 6 Estimated energy generation by using Rice husk during 2004 to 2012

5. Environmental Impact

Fossil fuels can cause serious environmental impacts such as global warming, greenhouse effect by CO_2 and acidification by SO_x and NO_x [4].Combustion of fossil fuel can cause NO_x emissions when the combustion temperatures are higher than 1000^0C [5]. In addition to the environmental problems, impact of fossil fuels in an important economic issue for Bangladesh. So, it is necessary to focus on identifying suitable renewable sources for instance biomass. Biomass fuel can be used for reducing greenhouse effect because trees absorb CO_2 as they grow and these carbons are released from biomass combustion process. Since biomass contains a little amount of sulphur compared to coal, it is also expected that there will be lower SO_x emissions [6].Rice Husk burnt in boilers and produces Rice Husk ash as a residue which is a waste by product of Rice Husk has its different types of application depends upon the physical and chemical properties of it. Rice husk ash has been used widely in various industries such as processing of steel, cement and refractory industries etc. [6].If Rice husk ash is managed properly then it will be known as a beneficial environmental friendly biomass fuel.

6. Discussion

Rice Husk is a Carbon-neutral and renewable source of energy which reduces the emission of greenhouse gases to improve local environmental conditions. The use of Rice Husk fired in boilers for the generation of electricity, has already been applied in many developing countries throughout the world. Power generation from Rice Husk is modern use of this waste material. This research results in concluding that around 39.5MW generation capacity Steam Turbine plant can be installed in the selected districts to produce electricity from Rice Husk. From this research it is found that the installed capacity is increasing from the year 2004 to 2012. So, it can be said that the installed capacity will increase in upcoming years by increasing Paddy as well as Rice Husk production and remarkable amount of electricity will be added in national grid of Bangladesh. One major constraint raised a question about availability of Rice husk throughout the year. In Bangladesh Rice Husk is mainly used for preparing briquette fuel as an alternative to wood fuel. The major portion of Rice Husk is being consumed for briquette preparation and moreover, Rice husk is only available during crop season. If total produced Rice husk are collected and stored sincerely then the amount of electricity generated from Rice husk will be sufficient to meet the electricity demand for Rice processing purposes, irrigation process and minimization of load-shedding in studied districts. Similarly, more power generation can be possible if this process is applied throughout the country. It is financially possible to establish the Steam Turbine plant near the area where a large amount of Rice mill resides. Load-shedding is likely to have major influence over the profit of the Rice mills. So, owners of various Rice mills will be happier to have a continuous supply of electricity. More electricity generation will be helpful to stabilize irrigation process in Bangladesh. A small generation of 300KW electricity can run thirty two-cusec pumps; each with 10KW/hour electricity consumption can draw 7000Cft water from underground [7]. For the sustainable utilization of this biomass energy in Bangladesh, the governmental authority like Ministry of Power and Energy needs to inspire confidence and provide incentives for local business to invest in technologies for utilization of Rice husk potential.

7. Conclusion

Bangladesh research and technical institutions should be encouraged and supported to research further into these areas and support for local innovations. These initiatives can make Rice husk as a potential environmental friendly, secure energy source to minimize the fuel consumption especially coal and add remarkable electricity to national grid of Bangladesh. Lacking experience in this sector can be overcome by gaining confidence and learning from the experience of other countries like India, Thailand, and China etc. where already this sector is better established.

NOMENCLATURE

BBS	: Bangladesh Bureau of Statistics
BPDP	: Bangladesh Power Development Board
MT	: Metric Tons
Cft	: Cubic foot
MW	: Mega Watt
KW	: Kilo Watt
KWh	: Kilo Watt hour

REFERENCES

[1] Bureau of statistics, Ministry of planning, Bangladesh, "BBS Statistical yearbook of Bangladesh", 2012(32th Edition).

[2] Savitri Garivait, "Physical and chemical properties of Thai Biomass Fuels from Agricultural Residues", 2nd joint International conference on Sustainable Energy and Environmental, Bangkok, Thailand, 1-23 November 2006.

[3] Singh, R.I "Combustion of Bio-mass in an Atmospheric Fbc: An Experience & study", International Conference on Advances in Energy Research Indian Institute of Bombay, India, December 12-15, 2007.

[4] Streets,D.G. and waldhoff S.T, "Greenhouse – gas emission from biofuel combustion in Asia", Energy 24:841-855.1999.

[5] Rafaschiere, A., Rapaccini,M.and Manfrida,G., "Life cycle Assesment of electricity production from poplar energy crops compared with conventional fossil fuels", .Energy Conversion & Management 40:1477-1493, 1999.

[6] Kaltschmitt, M., Reinhardt,G.A and Stelzer,T., "Life cycle Analysis of biofuels under different environmental aspects", Biomass and Bioenergy.12(2):121-134, 1977.

[7] Arif Md. Walliullah Bhuiyan, "An improved method to generate Electricity and precipitated silica from Rice Husk perspective in Bangladesh", International Journal of Environmental Science and Development, vol. 2, No. 4, August 2011.

ICMIEE-PI-140214

Fatigue Estimation through Face Monitoring and Eye Blinking

Asma-Ul-Husna, Amit Roy, Gautam Paul, Milon Kanti Raha*

Department of Mechanical Engineering, Rajshahi University of Engineering & Technology, Rajshahi-6204, BANGLADESH

ABSTRACT

Face detection is the general case of face localization. It is a human-computer interface technology that determines the location of faces in arbitrary images. It detects face from input image from camera. From the face template eye pair is detected, where this system automatically locates the user's eye. Blinks are related to several environment states and the present report describes a simple, reliable way to measure blinks from the video stream of an eye obtained during eye tracking, where the source of the eye video is a video camera attached to a head-mounted eye tracker. Computer vision techniques are employed to determine the moments that a blink starts and ends for the purpose of calculating blinking rate. The video is first processed to show blocks of eyelid and pupil movements and is then analyzed for blink starts and ends. The moment of a blink start is reported when the eyelid starts to move quickly exceeding a predetermined threshold. The end of a blink arises when the pupil size increases by less than a separate threshold. Several different blink patterns from different stage are measured. Drowse condition is determined by the analysis of blinking rate from different situation. The system has ability to count blinking rate accurately around 94%. In this study observed that if the blinking rate is approximately 3 blink/minute then it can be considered as drowse condition.

Keywords: Fatigue, face monitoring, eye blinking rate, drowse condition.

1. Introduction

Face detection is a very important part of the developed eye-blink detection. An eye blink is defined as when the upper and lower lids are touching each other and the eye is temporarily hidden. A typical blink has amplitude of 400 μV and lasts for about 200 - 400 ms. A common definition of blink duration is the time difference between the beginning and the end of the blink, where the beginning and end points are measured at the point where half the amplitude is reached. The blinking activity is also affected by fatigue, disease and drowsiness etc. That is why blinking also has been used as one common parameter for measuring fatigue and drowsiness. The method of blinking detection can be broadly classified into following:

I. Image Analysis: Capture eye image by using camera. Several image processing steps are needed to observe the blinking.

II. Biological Approach: By using EOG [4] (Attach the surface electrode onto surrounding eye. Blinking is detected by measuring eye muscle potential in vertical and horizontal direction) or EEG [5] (Attach the surface electrode into skull surface in order to measure brain activity).

The method (II) is relative expensive and not convenience compared than method (I) since method (I) burden the user as several electrodes have to be attached onto user's skin. In this paper blinking rate detection is based on image analysis approach. Among the blinking application, the utmost important of blinking detection method is accurate against eye shape changes, varies of blinking speed and varies of users.

Firstly face is detected from captured image of camera. This process is done by the get_connected_component. Classifier 'haarcascade_frontalface_alt' is used to find out the face detection. Eye pair in a form of rectangle box is detected. Classifier 'haarcascade_mcs_eyepair_big' is used to detect eye pair. From the eye pair one eye is split. This method has 94% accuracy on eye state detection. By using simple model of head and eye, it determines the head-independent motions of the pupil and eyelids. Eye is tracked in real time. Opened eye template is used to find and track the eye position. Blinking is estimated by comparing the similarity between opened eye template and current image. When user closes the eye during blinking process, the similarity will decrease. Otherwise, the similarity will maximum when user fully open the eye. It detects blinking by tracking upper eyelid and measuring distance between its apex and center of iris. A counter is used to count accurate blink per minute. Blinking rate at different condition is measured. By this process it is easily represented the drowsy condition of eyes.

2. Methodology

The system initialize by capturing image from the web camera. User face is detected automatically from the image. This process is a real time process. There is no time dely. After detect face eye pair is detected. From the eye pair rectangle split one for single eye. Then detect pupil from the detected eye. Openness and closeness condition depends on threshold value. Blinking is estimated by comparing the similarity between opened eye template and current image. After this a general counter is used to find out blinking rate.

* Corresponding author. Tel.: +88-01719445005
E-mail address: evu_me04@yahoo.com

3. Eye blinking rate estimation

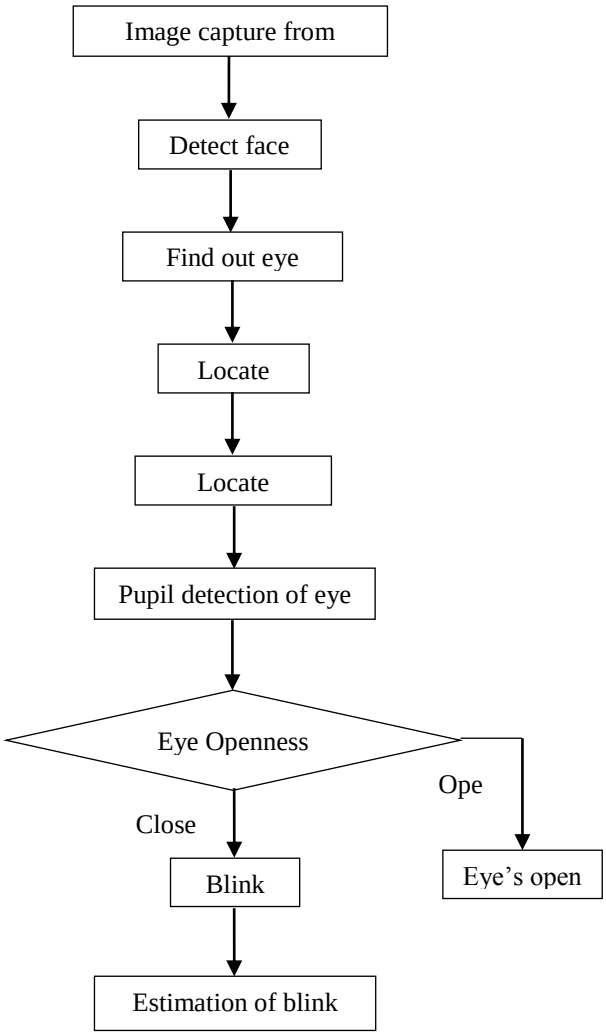

Fig. 1: Flow diagram of eye blinking rate estimation

The aim of the system is to create an eye blinking rate estimation system simple strategy, a regular web camera and the computer vision library OpenCV. OpenCV is incorporated with Microsoft Visual Studio. This system is done with some sample coding feature that helps to find out specific location of face. This system also helps to find out the eye blinking. By the system finally estimate the drowsiness condition and the eye blinking rate range.

3.1 Image Capture from Webcam

Build in camera of laptop (hp pavilion g4 22190TU) is used to capture image. 1.3MP camera has resolution 640x480.

3.2 Face Detection

The face detection is the first step in the implementation of the system. The first necessity is to load the classifiers. . The classier haarcascade frontalface alt.xml. is used for detect face. Face detection is done by get connected component. Cascade is loaded to execute the cvHaar Objects detection method. The image is grey scaled to make the Haar detection more robust. Since a grey image is more useful for the rest of the program as well, the grey image becomes the basis for the entire process. It firstly searches windows to image. Before that image need some minimal pre-processing. It analyzes the motion of face. Reset search windows for the accurate matching of the template. Then finally detect face.

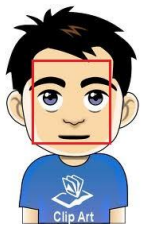

Fig. 2: Face detection

3.3 Eye Detection

Classifier 'haarcascade_mcs_eyepair_big' is used to detect eye pair. From the eye pair one eye is split. By using simple model of head and eye, it determines eyes in face.

The eye detection is done in a similar method to that of face detection in that it uses the same method but a different classifier. The classifiers used for the left and right eye detection are haarcascade_lefteye_splits.xml and haarcascade_righteye_splits.xml respectively. The eye detection is done separately for each eye Haar classifier.

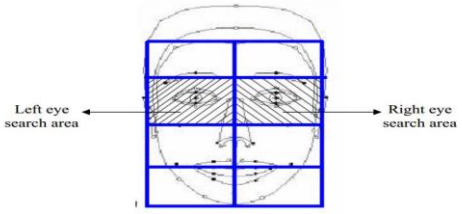

Fig. 3: Eyes detection from face

3.4 Blink Detection

Centroid is located from detected eye. Centroid is determined by simple geometric method. Width and height divided by two and common point of these is the Centroid of rectangle box. Where x and y represents two axis.

(*eye).x+ (*eye).width/2,……...….(i)

(*eye).y + (*eye).height...……..……...…(ii)

The pupil detection is very complex process. It is very tough to find out exact circle of the eye. To find out pupil some pre-processing is done by equalizing the histogram image. And finally find out the dark area of the eye. Then this combination is done with the help of threshold value.

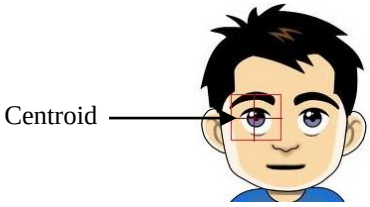

Fig. 4: Centroid detection

The moment of a blink start is reported when the eyelid starts to move quickly exceeding a predetermined threshold. The end of a blink arises when the pupil size increases by less than a separate threshold. If the pupil is found in the eye then the eye is open and if the component is not found then the eye is closed. And this close stage is defined as blinking stage.

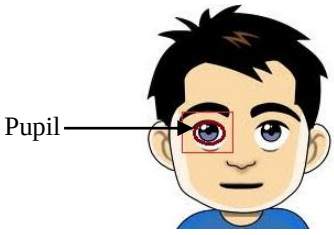

Fig. 5: Pupil detection

The moment of a blink start is reported when the eyelid starts to move quickly exceeding a predetermined threshold. The end of a blink arises when the pupil size increases by less than a separate threshold. If the pupil is found in the eye then the eye is open and if the component is not found then the eye is closed. And this close stage is defined as blinking stage.

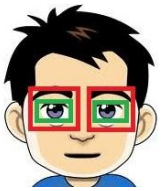

Fig. 6: Blink detection

3.5 Blink Estimation

A counter is used to count the blinking rate. This blinking rate is calculate by following formula

time_t end = time(NULL);

time_t diff = end - start;

double res=counter/(double)(diff/(double)60)

Firstly time is zero. Time is calculated by different between initial and ending time of blink.

If x number of blink found in y second then blinking rate is expressed as

Blinking rate= $\frac{x}{y} \times 60$ blink/min……..…(iii)

4. Experimental Result

Manuscripts should consist of the title, author(s), author's affiliation and address, abstract, keywords, and main text. Title, author(s), author's affiliation and address, abstract and keywords should be written according to the format given above.

Table 1 Blinking rate during conversation.

No. of persons	Blinking rate (blink/min)			Average blinking rate (blink/min)
Person 1 (age 23)	15.87	15.37	16.23	16.4
Person 2 (age 24)	14.54	18.3	16.11	
Person 3 (age 22)	17.43	14.6	19.2	

Table 2 Blinking rate during reading.

No. of persons	Blinking rate (blink/min)			Average blinking rate (blink/min)
Person 1 (age 23)	7.45	7.65	8.12	7.54
Person 2 (age 24)	6.52	6.92	7.6	
Person 3 (age 22)	8.31	7.47	7.84	

Table 3 Blinking rate during test (at noon 1.45-3 pm).

No. of persons	Blinking rate (blink/min)			Average blinking rate (blink/min)
Person 1 (age 23)	5.20	5.54	4.15	4.98
Person 2 (age 24)	5.11	4.98	5.15	
Person 3 (age 22)	4.76	4.85	5.04	

Table 4 Blinking rate during drowsiness (at midnight).

No. of persons	Blinking rate (blink/min)			Average blinking rate (blink/min)
Person 1 (age 23)	4.15	3.98	1.67	3.33
Person 2 (age 24)	3.22	2.64	2.18	
Person 3 (age 22)	2.95	2.73	2.25	
Night guard-1 (age 35)	4.1	3.92	4.6	
Night guard-1 (age 35)	3.8	2.7	3.7	

The present study measured the normal blinking rate at different conditions. Firstly blinking rate is measured at normal conversation time. From table 1 it shown that the average blinking rate is approximately 17 during conversation. Table 2 and 3 shown that the blinking rate during reading and rest period approximately 8 and 5 respectively. Table 4 shows that during drowsiness condition blinking rate is 3 approximately. From the above discussion it can be mention that when the blinking rate range approximately 3 then it's easily recognize the person is in drowse.

4.1 System accuracy and success rate

Table 5 System accuracy calculation

No. of Obs.	Actual Blink Rate (Blink/min)			Blink Rate Count by System Blink/min	Accuracy (Actual B/m– Practical B/m)/actual B/m×100%
1	17.7	15.87	90.5	1	17.7
2	16	15.37	95.2	2	16
3	7.94	7.45	94	3	7.94
4	7.13	6.92	97	4	7.13
5	5.2	5.11	98	5	5.2
6	4.6	4.15	90.4	6	4.6
7	4.27	3.98	93	7	4.27

The actual blinking rate is not exactly the same as the blink count by the system. Some environmental condition influence the system.. The system accuracy was calculated as 94%.

Blinking rate estimation is very complex process. Environment condition is the major factor to find out the blinking rate. Blinking rate also varies on different condition such as reading paper, conversation, rest period, soporific condition or drowsiness condition. The system can work perfectly with sufficient light condition, but worse condition need more time to find out face and eye blink. And also that time blinking rate is very low. In movement condition (body, head rotation) it's very hard to find exact blink rate. Though the system has some shortcoming it is done accurately as much as possible. This real time eye blinking estimation efficiency is higher than other non-real time process. Experimental results have shown that the proposed system is very sensitive to face background and head orientations. It can work only with frontal view.

5. Conclusion

OpenCV was incorporated in Microsoft Visual Studio effectively. Face and eye has been detected successfully by this real time process. Real time process help to find out the exact blinking rate that dignify the process work advancement. On the basis of eye blinking rate drowsy condition is mentioned.

This paper can be developed further by incorporating head movement cancellation, implementing a gaze tracker using a web-camera, implementing the system on a GPU, fatigue estimation though skin monitoring, implementing the system on automobile to improve its safety with attached alarming system, implementing the system on designed for use by people with severe paralyzed or afflicted with diseases such as ALS(Lou Gehrig's disease), high resolution camera can be used for better performance.

REFERENCES

[1] Park I.,Ahn J. and Byun H., "Efficient Measurement of Eye Blinking under Various Illumination Conditions for Drowsiness Detection Systems". Proceedings of IEEE the 18th International Conference on Pattern Recognition, 2006.

[2] Grauman K., Betke M., Gips J. and Bradski G. R., "Communication via Eye Blinks – Detection and Duration Analysis in Real Time". Proceedings of the IEEE Computer Society Conference on Computer Vision and Pattern Recognition, 2001.

[3] Hao Z. and Lei Q., "Vision-Based Interface: Using Face and Eye Blinking Tracking with Camera". iita, vol. 1, pp.306-310, 2008 Second International Symposium on Intelligent Information Technology Application, 2008.

[4] Krupinski R. and Mazurek P. "Estimation of Eye Blin king Using Biopotentials Measurements for Computer Animation Applications". Lecture Notes in Computer Science, Vol 5337/2009, pp 302-310, 2009.

[5] Rani B. A. and Mansor M. S. . "Detection of eye blinks from EEG signals for home lighting system activation". Proceeding of ISMA '09 6th International Symposium, pp 1-4, 2009.

[6] Arai K. and Mardiyanto R. "Eyes Based Electric Wheel Chair Control System",(IJACSA) International Journal of Advanced Computer Science and Applications, Vol. 2, No. 12, 2011 Japan.

[7] Wu J. and Trivedi M. M. ," Simultaneous Eye Tracking and Blink Detection with Interactive Particle Filters" Computer Vision and Robotics Research Laboratory,University of California, San Diego, Hindawi Publishing CorporationEURASIP Journal on Advances in Signal ProcessingVolume 2008, Article ID 823695, 17 pages doi:10.1155/2008/823695.

[8] Sigari M. S., Fathy M. and Soryani M. "A Driver Face Monitoring System for Fatigue and Distraction Detection" ,Iran University of Science and Technology,Tehran 16846, Iran, International Journal of Vehicular Technology, Tehran,Iran.Volume 2013, Article ID 263983,11pages.

[9] Svensson U. "Blink behaviour based drowsiness detection" Linköping University, Dept. Biomedical Engineering ,Linköping 2004.

[10] Arai K. and Mardiyanto R. "Real Time Blinking Detection Based on Gabor Filter" Department of Information Science, Saga University, Saga, Japan.

[11] Wild J.D. "Gaze Tracking Using A Regular Web Camera" Rhodes University, Grahamstown, South Africa,November 2012.

[12] Nski R. K. and Mazurek P. "Real–Time Low–Latency Estimation of the Blinking and EOG Signals" Department of Signal Processing and Multimedia Engineering,West Pomeranian University of Technology, Szczecin,Poland.

[13] Bradski G. and Kaebler A. "Computer Vision with the OpenCV Library" a book on OpenCV, page no 1-15.

[14] Official website of OpenCV "OpenCV http://opencv.org/".

ICMIEE-PI-140217

Velocity and temperature distributions of transitional and turbulent boundary layer flows along a vertical flat plate

Mohammad Zoynal Abedin[*]*, Mohammed Moinul Islam, Mashud Rana*
Department of Mechanical Engineering, Dhaka University of Engineering & Technology, Gazipur-1700, BANGLADESH

ABSTRACT

Time-developing transitional and turbulent boundary layer flows both in air and water along a heated vertical flat plate has been investigated by direct numerical simulation (DNS). The results reveal that the predicted heat transfer rates in the natural-convection boundary layer correspond quantitatively well with the existing observations. For the transitional natural-convection boundary layer, the velocity is initially zero and then increases to the peak and finally decreases to zero level. However, in the transitional mixed-convection boundary layer with aiding flow, the velocity profiles show a decreasing trend to a constant positive value in the outer boundary layer region. Also, the magnitude of the velocity profile increases with an increase in Grashof number due to the increasing trend in the boundary layer thickness. For the turbulent natural-convection boundary layer, the peaks of the velocity profiles both in air and water shift near to the wall as the value of Grashof number increases due to the fully developed turbulent condition. Unlike to the velocity profiles in air, the peaks for water shift slightly towards the outer boundary layer due to the higher Prandtl number. On the other hand, the temperature profiles in the boundary layers are initially at the peak values and finally decrease to zero. However, the temperature both in air and water falls more rapidly in the turbulent region compared to that in the transition region due to the thermal stability in the flow.

Keywords: Transition, Turbulent boundary layer, Natural convection, Mixed convection, DNS.

1. Introduction

The analysis of the boundary layer flows is important not only to clarify the fundamental characteristics of the boundary layer but also to evaluate the basic structures of the buoyancy-driven flows practically encountered in many applications.

The fundamental characteristics of the turbulent natural-convection boundary layer along a heated vertical flat plate were extensively investigated by many researchers [1-7]. There are several numerical approaches performed for the turbulent natural-convection boundary layer to evaluate the characteristics of the boundary layer flows [8-10]. The fundamental characteristics of turbulent mixed-convection boundary layer were investigated along various passages [12, 13] and the effects of freestream velocity on the turbulent mixed-convection boundary layer along a vertical heated plate were extensively investigated by Hattroi et al. [13, 14]. On the other hand, few expensive experiments were conducted for the turbulent mixed-convection boundary layer with opposing flow (freestream in the direction to the gravitational force) [15]. Due to the difficulty in obtaining the fluctuating characteristics of the boundary layer flows from the experiments, the numerical simulation techniques have been extensively used to evaluate the characteristics of the complex flow phenomenon.

Recently, some extensive numerical investigations have been carried out to clarify the characteristics in the natural- and mixed-convection boundary layer flows by time-developing DNS [16-21]. However, the effects of both freestream velocity and Prandtl number on the characteristics of the boundary layer flows in the natural- and mixed-convection have not yet been focused sufficiently and are eagerly awaited.

Therefore, in the present analysis, the DNS has been employed to investigate the nature of the velocity and temperature distributions of the boundary layer flows under the influence of the freestream velocity and Prandtl number.

2. Numerical procedure

The analysis of the transitional and turbulent boundary layer flows both in air and water along a heated vertical flat plate has been carried out by time-developing DNS. The flow is induced by heating an infinitely long vertical flat plate at a uniform temperature from a given time onward (τ = 0). The calculation domain and coordinate systems are shown in Fig. 1.

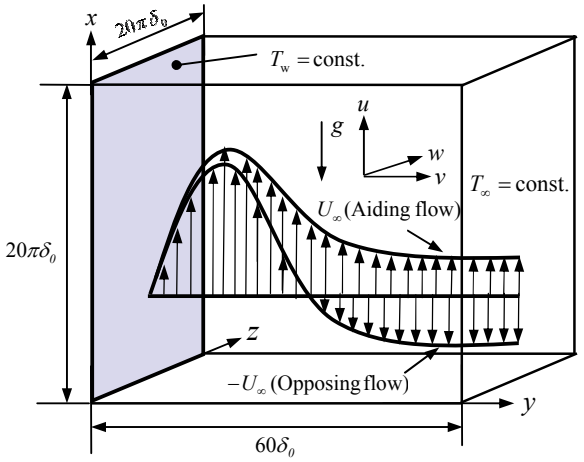

Fig.1 Calculation domain and coordinates.

* Corresponding author. Tel.: +88-02-9204710
E-mail address: abedin.mzoynal@duet.ac.bd

The coordinates in the vertical, wall-normal and spanwise directions are x, y and z, respectively, and the instantaneous velocities u, v and w are specified in the relevant directions. The instantaneous temperature is t and the wall and ambient temperatures, T_w and T_∞, respectively, are assumed to be constant.

The governing equations expressing the conservation of mass, momentum and energy with the Boussinesq approximation in the tensor notation can be written as follows:

$$\frac{\partial u_i^*}{\partial x_i^*} = 0 \tag{1}$$

$$\frac{\partial u_i^*}{\partial \tau^*} + u_j^* \frac{\partial u_i^*}{\partial x_j^*} = -\frac{\partial p^*}{\partial x_i^*} + \frac{\partial^2 u_i^*}{\partial x_j^{*2}} + Gr_{\delta_0}\theta \tag{2}$$

$$\frac{\partial \theta}{\partial \tau^*} + u_j^* \frac{\partial \theta}{\partial x_j^*} = \frac{1}{Pr}\frac{\partial^2 \theta}{\partial x_j^{*2}} \tag{3}$$

Here, $Gr_{\delta_0} = g\beta\Delta T_w \delta_0^3/\nu^2$ is the Grashof number based on the integral thickness of the velocity boundary layer δ_0 and the superscript '*' denotes variables that have been made dimensionless with δ_0 and ν.

The periodic boundary conditions have been applied for the x^* and z^* directions and the boundary conditions in the y^* direction are used in the wall normal direction.The above momentum and energy equations have been discretized by the second-order accurate central difference scheme on staggered grids and the detailed numerical simulation techniques for the present study are extensively reported in the literature of Abedin et al. [16-21].

The integral thickness of the velocity boundary layer δ, which is adopted as a characteristic length scale for the analysis, can be defined as:

$$\delta = \int_0^\infty \left|U - U_\infty\right| / \left(U_{max} - U_{min}\right)\, dy \tag{4}$$

Here, U is the mean velocity found by averaging the velocity in the (x - z) plane and U_{max} and U_{min} are the maximum and minimum mean velocities in the boundary layer, respectively. For pure natural convection, $U_{min} = U_\infty = 0$ and for mixed convection, $U_{min} = 0$ (aiding flow) and $U_{min} = -U_\infty$ (opposing flow).

3. Results and discussions

Time-developing DNS was advanced by adding various initial disturbances in the laminar boundary layer, which were created by reducing velocity fluctuations observed in the turbulent boundary layer to tiny fluctuations less than 5% for the intensities. Such disturbances added in the laminar boundary layer once decayed and then became activated showing the commencement of transition. However, these initial disturbances have an effect on the calculated results in the turbulent region [16, 17]. Therefore, we show the following turbulence statistics as ensemble averaged values of several iterations with different initial disturbances.

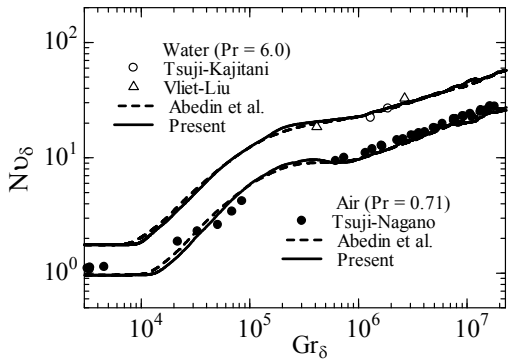

Fig.2 Code validation - Heat transfer rates in natural-convection boundary layer on length scale δ for air (Pr = 0.71) and water (Pr = 6.0).

3.1 Code validation

The predicted heat transfer rates in the natural-convection boundary layers both in air and water are validated with the analysis of previous investigations. Figure 2 depicts the Nusselt number Nu_δ against the Grashof number Gr_δ based on the integral thickness of velocity boundary layer. The predicted heat transfer rates obtained with the disturbance of less than 5% agree completely well with those obtained by the results in the numerical simulations done with the disturbance of less than 1% of Abedin et al. [16] for both air and water. Moreover, the present results of heat transfer rates correspond well with the results obtained by the experimental investigation of Tsuji-Nagano [5] for air and of both Vliet-Liu [1] and Tsuji-Kajitani [7] for water. Therefore, it can be concluded that the present analysis would provide credible findings in the characteristics of boundary layer flows along a heated vertical flat plate.

3.2. Transitional boundary layer flows

3.2.1. Velocity distribution

The predicted mean velocity profiles from laminar to turbulence in the natural-convection boundary layer ($Gr_{\delta_0} = 3000, Re_{\delta_0} = 0$) both in air (Pr = 0.71) and water (Pr = 6.0) are shown against y/δ_0 in Figs. 3 (a) and (b), respectively. The dimensionless velocity profile u/U_0 is used in the ordinate and the dimensionless distance y/δ_0 is used in the abscissa.

As can be seen in Fig. 3 (a), the velocity profiles from laminar to turbulence (Gr_δ = 7.37×103 ~ 6.91×106) in air are initially zero, then increase to their respective peak values and finally decrease to zero in the outer boundary layer region. It is also observed that the magnitude of the velocity profile increases to their peaks and shows wider span in the distributions with an increase in the Grashof number Gr_δ. This is due to the

increasing trend in the velocity within the increasing boundary layer thickness. On the other hand, the velocity profiles in water show similar behaviors with lower peaks and less wider span in the distribution (as seen in Fig. 3 (b)).

The predicted mean velocity profiles from laminar to turbulence ($Gr_\delta = 6.23\times10^3 \sim 2.31\times10^6$) in the mixed-convection boundary layer for aiding flow ($Gr_{\delta_0} = 3000, Re_{\delta_0} = 300$) both in air and water are presented in Figs. 4 (a) and (b), respectively. The profiles are seen to be initially at zero, then increase to their respective peak values and finally decrease to a constant positive value due to the aiding flow opposite to the gravity.

3.2.2. Temperature distribution

The predicted mean temperature profiles from laminar to turbulence in the natural-convection ($Gr_{\delta_0} = 3000, Re_{\delta_0} = 0$) and mixed-convection ($Gr_{\delta_0} = 3000, Re_{\delta_0} = 300$) boundary layer both in air (Pr = 0.71) and water (Pr = 6.0) are shown against y/δ_0 in Figs. 5 (a) and (b), respectively. The dimensionless temperature profile θ is used in the ordinate and the dimensionless distance y/δ_0 is used in the abscissa.

As can be seen from Fig. 5 (a) and (b), the temperature profiles both in air and water are initially at

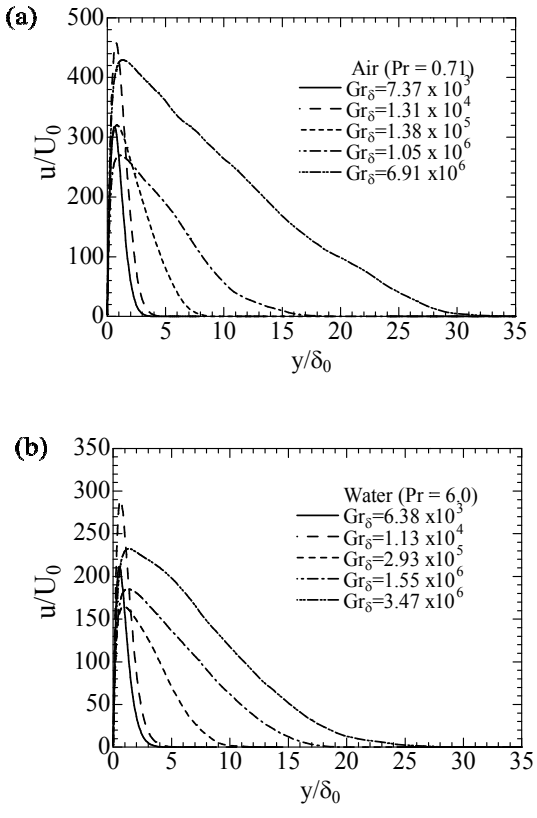

Fig.3 Mean velocity profiles from laminar to turbulence in natural-convection boundary layer ($Gr_{\delta_0} = 3000, Re_{\delta_0} = 0$) for (a) air (Pr = 0.71) and (b) water (Pr = 6.0).

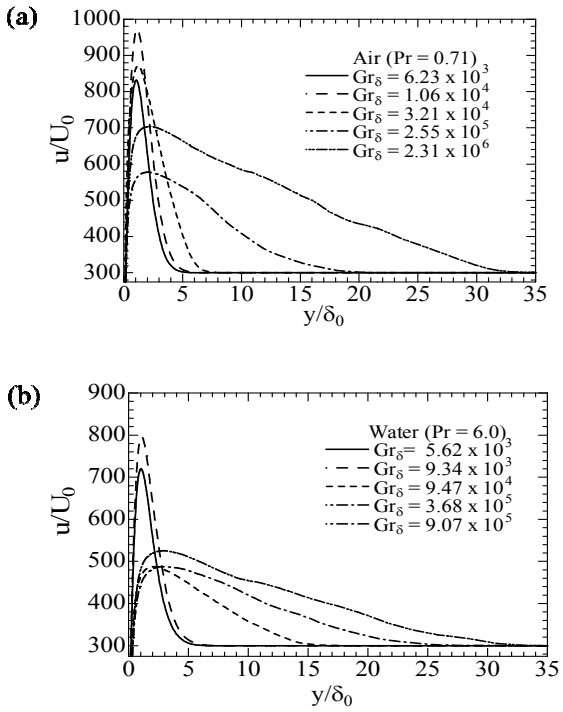

Fig.4 Mean velocity profiles from laminar to turbulence in mixed-convection boundary layers with aiding flow ($Gr_{\delta_0} = 3000, Re_{\delta_0} = 300$) for (a) air (Pr = 0.71) and (b) water (Pr = 6.0).

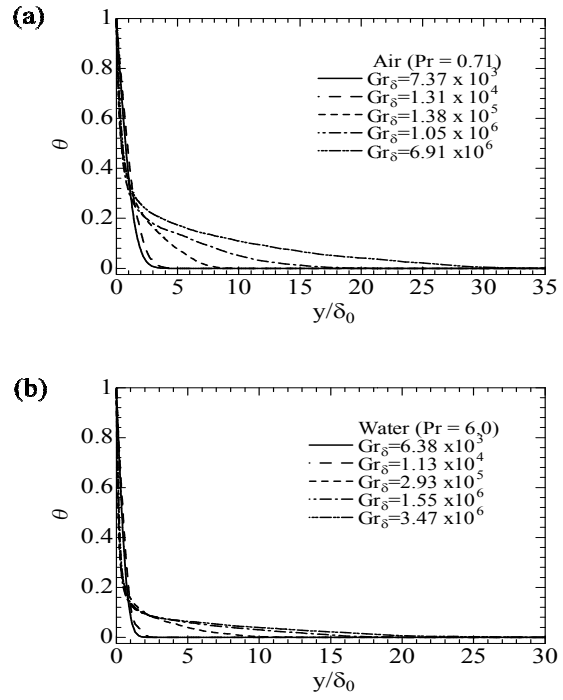

Fig.5 Mean temperature profiles from laminar to turbulence in natural-convection boundary layer ($Gr_{\delta_0} = 3000, Re_{\delta_0} = 0$) for (a) air (Pr = 0.71) and (b) water (Pr = 6.0).

their peaks and then decrease to zero. However, at outer boundary layer the profile falls moderately to zero for air and sharply to zero for water. The temperature of the water within the boundary layer becomes ambient at a shorter distance perpendicular to the heated wall compared to that in air due to the effects of high Prandtl number of water. Similar behaviors are observed in the temperature profiles in the mixed-convection boundary layer both for air and water as shown in Figs. 6 (a) and (b).

3.3. Turbulent boundary layer flows

3.3.1. Velocity distribution

The predicted mean velocity profiles from transition to turbulence in natural-convection boundary layer for air (Pr = 0.71) and water (Pr = 6.0) are shown against y/δ in Figs. 7 (a) and (b), respectively. In the figures, the dimensionless velocity profile U/U_{max} is used in the ordinate while the dimensionless distance y/δ is used in the abscissa. The term U is the mean velocity in x-direction; U_{max} is the maximum mean velocity measured in y-z plane and δ is the integral thickness of the velocity boundary layer.

As can be seen in Fig. 7(a), the velocity profiles from transition to turbulence ($Gr_\delta = 1.31\times10^4 \sim 6.91\times10^6$) in natural-convection boundary layer for air are all initially zero, then increases to their respective peak values and finally decreases to zero again. In addition, as the value of Gr_δ increases in the turbulent region the peak of the profile shifts near to the wall due to fully developed turbulence in the flow.

On the other hand, the velocity profiles from transition to turbulence ($Gr_\delta = 1.13\times10^4 \sim 3.47\times10^6$) for water are all initially zero, then increases to their respective peak values and finally decreases to zero again as seen in Fig. 7 (b). In addition, as the value of Gr_δ increases in the turbulent region the peak of the profile shifts near to the wall due to fully developed turbulence in the flow. However, unlike to the velocity profiles in air, the peaks shift slightly farther towards the outer boundary layer region due to the effect of higher Prandtl number of water.

3.3.2. Temperature distribution

The predicted mean temperature profiles from transition to turbulence in natural-convection boundary layer for air (Pr = 0.71) and water (Pr = 6.0) are shown against y/δ in Figs. 8 (a) and (b), respectively. In the figures, the dimensionless temperature profile $T/\Delta T_w$ is used in the ordinate while the dimensionless distance y/δ is used in the abscissa. The term T is the mean temperature in x-direction and ΔT_w is the difference between the wall temperature and ambient temperature.

As can be seen in Fig. 8 (a), the temperature profile from transition to turbulence ($Gr_\delta = 1.31\times10^4 \sim 6.91\times10^6$) in natural-convection boundary layer for air are initially at the peak with $T/\Delta T_w = 1.0$ and then decreases to zero. On the other hand, as can be seen in Fig. 8 (b), the temperature profile from transition to turbulence

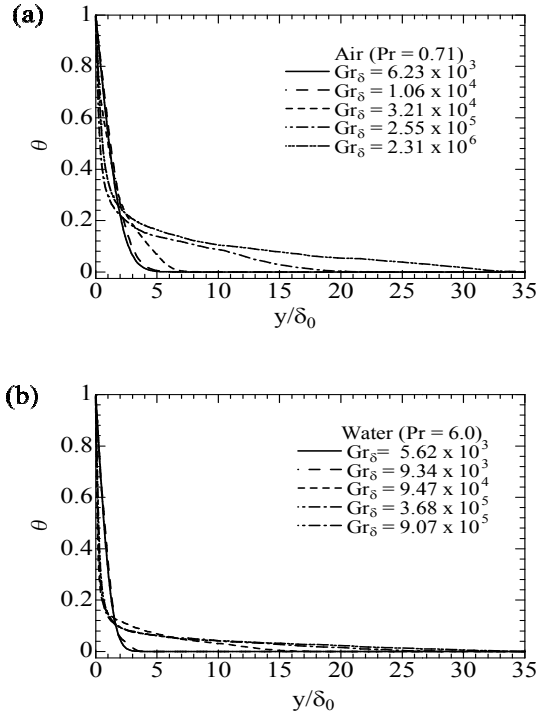

Fig.6 Mean temperature profiles from laminar to turbulence in mixed- convection boundary layer with aiding flow ($Gr_{\delta_0} = 3000, Re_{\delta_0} = 300$) for (a) air (Pr = 0.71) and (b) water (Pr = 6.0).

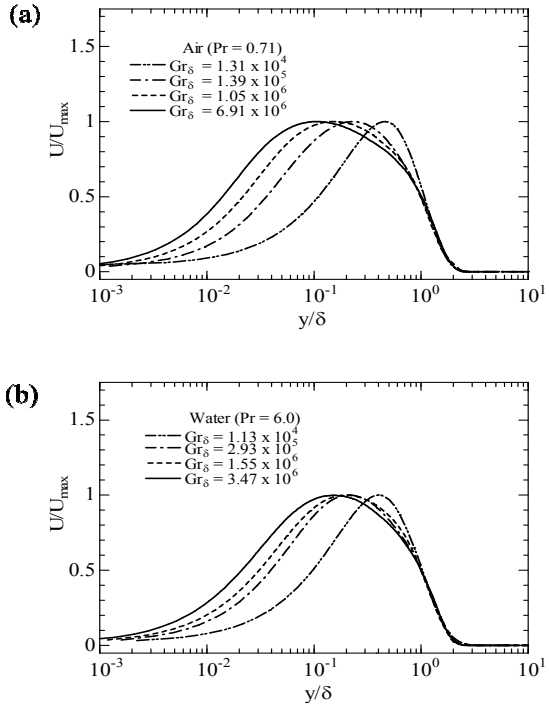

Fig.7 Mean velocity profiles from laminar to turbulence in natural-convection boundary layer for (a) air (Pr = 0.71) and (b) water (Pr = 6.0).

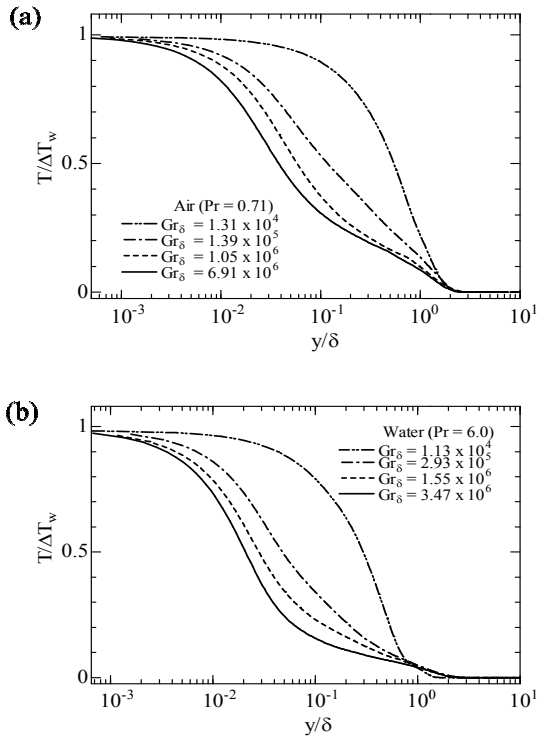

Fig.8 Mean temperature profiles from laminar to turbulence in natural-convection boundary layer for (a) air (Pr = 0.71) and (b) water (Pr = 6.0).

($Gr_\delta = 1.13 \times 10^4 \sim 3.47 \times 10^6$) in natural-convection boundary layer for water are also initially at their peaks and decreases sharply to zero. It is revealed from that the temperature profile falls more rapidly in the turbulent region of the flow compared to that in the transition region. This is due to the thermal instability in the transition region of the flow which leads to an unsteady nature of the temperature profile.

4. Conclusions

A numerical investigation is carried out in the transitional and turbulent boundary layer flows both in air and water along a heated vertical flat plate by time-developing DNS. The predicted results of heat transfer rates in the natural-convection boundary layer have been well compared and validated with the existing observations.

The following conclusions may be drawn from the present analysis:

- For the transitional natural-convection boundary layer both in air and water, the velocity profiles are initially zero and then increases to their respective peak values and finally decreases to zero level. The velocity increases with an increase in Grashof number due to the increasing trend in the boundary layer thickness. However, the temperature profiles both in air and water are initially at the peak and then decreases to zero analogous to the flows in the laminar flows.
- The velocity and temperature profiles in the transitional mixed-convection boundary layer with aiding flow in air show the similar behavior compared to the profiles observed in the natural-convection boundary layer.
- For the turbulent natural-convection boundary layer both in air and water, the velocity profiles show the identical nature compared to those in the laminar natural-convection boundary layer. However, the peak values of the profiles shift near to the wall as the value of Grashof number increases due to fully developed turbulent condition. Unlike to the velocity profiles in air, the peaks for water shift slightly towards the outer boundary layer due to the higher Prandtl number of water. On the other hand, it can be revealed that the temperature falls more rapidly in the turbulent region compared to that in the transition region due to the thermal stability.

Acknowledgements

The authors would like to acknowledge Professor Toshihiru Tsuji, Nagoya Institute of Technology, Japan, for his invaluable suggestions and great assistances in the time of simulation and experimentation.

NOMENCLATURE

c_p	specific heat at constant pressure, kJ/(kg K)
Gr_x	Grashof number based on x from leading edge of plate in space-developing flow, $g\beta\Delta T_w x^3/\nu^2$
Gr_δ	Grashof number based on integral thickness δ, $g\beta\Delta T_w \delta^3/\nu^2$
k	thermal conductivity, W/(m K)
Nu_δ	Nusselt number based on δ, hδ /k
Pr	Prandtl number, $\mu c_p/k$
Re_δ	Reynolds number based on integral thickness δ, $U_\infty \delta/\nu$
T	mean temperature, K
t	instantaneous temperature, K
U	mean streamwise velocity, m/s
u	instantaneous streamwise velocity, m/s
U_0	characteristics velocity, ν/δ_0, m/s
v	instantaneous transverse velocity, m/s
w	instantaneous spanwise velocity, m/s
x	distance from leading edge of flat plate, m
x_i	coordinate in tensor notation, m
y	distance from wall, m
z	spanwise distance, m

Greek symbols

α	thermal diffusivity, m^2/s
β	coefficient of volume expansion, 1/K
θ	dimensionless temperature, $(t - T_\infty)/\Delta T_w$
ΔT_w	temperature difference between wall and ambient, $T_w - T_\infty$, K
δ	integral thickness of the velocity boundary layer, m

μ viscosity, Pa.s
ν kinematic viscosity, m^2/s
ρ density, kg/m^3
τ time, s

Superscripts
$*$ normalized variables with δ_0 and ν for time-developing profiles

Subscripts
∞ ambient condition
0 initial condition
w wall condition

References

[1] G. C. Vliet, C. K. Liu, An experimental study of turbulent natural convection boundary layers, Trans. *ASME J. Heat Transfer*, Vol. C-91, pp. 517-531, (1969).

[2] K. Kitamura, T. Inagaki, Turbulent heat and momentum transfer of combined forced and natural convection along a vertical flat plate - aiding flow, *Int. J. Heat Mass Transfer*, Vol. 30, No.1, pp. 23-41, (1987).

[3] T. Tsuji, Y. Nagano, Characteristics of a turbulent natural convection boundary layer along a vertical flat plate, *Int. J. Heat Mass Transfer*, Vol. 31, No. 8, pp. 1723-1734, (1988).

[4] T. Tsuji, Y. Nagano, Turbulence measurements in a natural convection boundary layer along a vertical flat plate, *Int. J. Heat Mass Transfer*, Vol. 31 No. 10, pp. 2101-2111, (1988).

[5] T. Tsuji, Y. Nagano, Velocity and temperature measurements in a natural convection boundary layer along a vertical flat plate, *Exp. Therm. Fluid Sci.*, Vol. 2, pp. 208 -215, (1989).

[6] T. Tsuji, Y. Nagano, M. Tagawa, Experiment on spatial and temporal turbulent structures of a natural convection boundary layer, *Trans. ASME J. Heat Transfer*, Vol. 138, pp. 19-26, (1992).

[7] T. Tsuji, T. Kajitani, Turbulence characteristics and heat transfer enhancement of a natural convection boundary layer in water along a vertical flat plate, *Proc. 13th Int. Heat Transfer Conf.*, Sydney, TRB-08 of CD-ROM, (2006).

[8] W. M. To, J. A. C. Humphrey, Numerical simulation of buoyant, turbulent flow - 1. Free convection along a heated, vertical flat plate, *Int. J. Heat Mass Transfer*, Vol. 29, No. 4, pp. 573-592, (1986).

[9] R. A. W. M. Henkes, C. J. Hoogendoorn, Comparison of turbulence models for the natural convection boundary layer along a heated vertical plate, *Int. J. Heat Mass Transfer*, Vol. 32, No. 1, pp. 157-169, (1989).

[10] T. W. J. Peeters, R. A. W. M. Henkes, The Reynolds-stress model of turbulence applied to the natural convection boundary layer along a heated vertical plate, *Int. J. Heat Mass Transfer*, Vol. 35, No. 2, pp. 403-420, (1992).

[11] J. Wang, J. Li, J. D. Jackson, A study of the influence of buoyancy on turbulent flow in a vertical plane passage, *Int. J. Heat Fluid Flow*, Vol. 25, No. 3, pp. 420-430, (2004).

[12] N. Kasagi, M. Nishimura, Direct numerical simulation of combined forced and natural turbulent convection in a vertical plane channel, *Int. J. Heat Fluid Flow*, Vol. 18, No. 1, pp. 88-99, (1997).

[13] Y. Hattori, T. Tsuji, Y. Nagano, N. Tanaka, Characteristics of turbulent combined-convection boundary layer along a vertical heated plate, *Int. J. Heat Fluid Flow*, Vol. 21, No. 5, pp. 520-525, (2000).

[14] Y. Hattori, T. Tsuji, Y. Nagano, N. Tanaka, Effects of freestream on turbulent combined-convection boundary layer along a vertical heated plate, *Int. J. Heat Fluid Flow*, Vol. 22, No. 3, pp. 315-322, (2001).

[15] T. Inagaki, K. Kitamura, Turbulent heat transfer of combined forced and natural convection along a vertical flat plate (Effect of Prandtl number), *Trans. JSME*, Vol. B 54, No. 505, pp. 2515-2522, (1988). (In Japanese)

[16] M. Z. Abedin, T. Tsuji, Y. Hattori, Direct numerical simulation for a time-developing natural-convection boundary layer along a vertical flat plate, *Int. J. Heat Mass Transfer*, Vol. 52, No. (19-20), pp. 4525-4534, (2009).

[17] M. Z. Abedin, T. Tsuji, Y. Hattori, Direct numerical simulation for a time-developing combined-convection boundary layer along a vertical flat plate, *Int. J. Heat Mass Transfer*, Vol. 53, No. (9-10), pp. 2113-2122, (2010).

[18] M. Z. Abedin, T. Tsuji, Effect of freestream on thermally-driven boundary layers along a heated vertical flat plate, *Proc. 14th Int. Heat Transfer Conf.*, Washington D.C., USA, TRK-20 of CD-ROM, pp. 1-8, (2010).

[19] M. Z. Abedin, T. Tsuji, Transition behavior and turbulence characteristics in combined-convection boundary layers along a heated vertical flat plate, *Proc. 13 Asian Congress Fluid Mechanics*, Dhaka, Bangladesh, pp. 759-762, (2010).

[20] M. Z. Abedin, T. Tsuji, J. Lee, Effects of freestream on transition behaviors and turbulence characteristics of thermally-driven boundary layers along a heated vertical flat plate, *Int. J. Heat Fluid Flow*, 36, pp. 92-100, (2012).

[21] M. Z. Abedin, T. Tsuji, J. Lee, Turbulence characteristics and vortical structures in combined-convection boundary layers along a heated vertical flat plate, *Int. J. Heat Mass Transfer*, Vol.55, No. (15-16), pp. 3995-4002, (2012).

ICMIEE-PI-140219

Improvement of energy efficiency in a cement industry

Satwat Ahmed , S. M. Abid Hasan , Md. Kutub Uddin
Department of Mechanical Engineering, Khulna University of Engineering & Technology, Khulna-9203, BANGLADESH

ABSTRACT
The cement sector consumes noticeable energy of total industrial energy use. Therefore, a state of art review on the energy use and savings is necessary to identify energy wastage so that necessary measures could be implemented to reduce energy consumption in this sub-sector. In this paper, energy use at different sections of cement industries, specific energy consumption, types of energy use and various energy saving measures were reviewed and presented. Various energy savings measures were critically analyzed considering amount of energy that can be saved along with the implementation cost. This study compiled a comprehensive literature on the cement industries in terms of Thesis, peer reviewed journals papers, conference proceedings, books, reports, websites. This study identified that the cement industries are moving towards the use of alternative fuels to reduce environmental pollution along with the conventional fuels. It also observed that cement industries are moving from wet process to dry process as it consumes less energy compared to wet process.

Keywords: Energy Management, Cost Saving, Cement Manufacturing

1. Introduction

Managing and reducing energy consumption not only saves money but also helps in mitigating climate change and enhancing corporate reputation. The primary objective of energy management is to maintain optimum energy procurement and utilization, throughout the organization which may help in minimizing energy costs and mitigating environmental effects. In fact, energy management is widely acknowledged as the best solution for direct and immediate reduction of energy consumption.
Energy should be regarded as a business cost, like raw material or labor. Reduction and control of energy usage is vital for an organization as it:

Reduces costs: Reducing cost is the most compelling reason for saving energy. Most organizations can save up to 20% on their fuel cost by managing their energy use;

Reduces carbon emissions: Reducing energy consumption also reduces carbon emissions and adverse environmental effects. Reducing your organizations carbon footprint helps build a 'green' image thereby generating good business opportunities; and

Reduce risk: Reducing energy use helps reduce risk of energy price fluctuations and supply shortages.

Good energy management practices are compliant with these requirements and help fulfil regulatory obligations. Businesses worldwide are showing interest in appointment of a formal/informal energy manager to coordinate energy management activities. The main task of an energy manager is to set up a system to collect, analyze and report on energy consumption and costs.

In addition to financial benefits, energy management has other significant advantages for an organizations such as:

- Organizations achieve stronger market position by demonstrating 'green' credentials. Energy management improves competitive advantage as most consumers prefer to source from socially responsible businesses;
- Organizations adopting energy management systems can influence supply chains by preferring suppliers who adopt environment management practices; and
- Energy management creates a better workplace environment for employees by improving working conditions.[1]

This study also contains:

- Study of the Cement Industry Statistics
- Energy efficiency opportunities and barriers
- To minimize the energy costs without effecting production and quality
- To reduce the environmental effects
- Developing energy efficiency eradicating the limitations or implementing new processes

* Corresponding author. Tel.: +88-01923303316
E-mail address: s.a.sowad@gmail.com

2. Energy Management

"Energy Management System" is a term that has a number of meanings , but we are mainly concerned with the one that relates to savings energy in business, public sector/government organization, industries and homes. Energy management is the use of technology to improve the energy performance of an organization. To be fully effective it needs to be an integral part of an organization's wider management processes. Improving energy efficiency and using renewable energy resources is both important for improving profitability and reducing pollution. Improved energy efficiency will reduce the rate of depletion of fossil fuels and minimize the emission of greenhouse gases and other polluting gases. All organizatons need good management for long term success and efficient program.

Fig.1 Work Plan for Energy Management

Rising energy prices, climate change legislation and need to be enviornmently responsible all require effective energy management. Saving energy makes business sense and having a structured co-ordination and integrated approch to managing energy will maximize these benefits. Without this, cost-effective opportunities can be easily overlooked.

Energy management is the key to saving energy in the organization. Much of the importance energy saving stems from the global need to save energy. This global need affects energy prices, emission targets and legislation. All of which lead to several compelling reasons why you should save energy at your organization specifically.[2]

3. Auditing

An energy audit is a preliminary activity towards instituting energy efficiency programs in an establishment. It consists of activities that seek to identify conservation opportunities preliminary to the development of an energy savings program.[3]

The term energy management means many things to many people. One definition of energy management is:

"The judicious and effective use of energy to maximize profits (minimize costs) and enhance competitive positions"

(Cape Hart, Turner and Kennedy, Guide to Energy Management Fairmont press inc. 1997)

Another comprehensive definition is

"The strategy of adjusting and optimizing energy, using systems and procedures so as to reduce energy requirements per unit of output while holding constant or reducing total costs of producing the output from these systems" [4]

4. Methdology

The main issues of the proposed methodology are: historical data analysis, energy consumption characterization, energy consumption forecasting, energy consumption control, energy budgeting and energy machines management optimization. The methodology supports an industrial plant to:

- Identify areas of energy wastage - for example by determining the proportion of energy that does not directly contribute to production and that is often a source of energy savings;
- Understand energy consumption of the processes - by establishing a relationship between energy use and production;
- Highlight changes to energy consumption patterns - these are either a result of a specific action to improve efficiency or due to an unknown factor which may have a detrimental effect upon efficiency and may lead to process failure or poor quality product;
- Reach an optimal condition in terms of supplying, generation, distribution and utilization of energy in a plant by means of a continuous improvement approach based on energy action cost- benefit evaluation.[5]

The single operation described in the methodology steps has its own effectiveness in a context showing an awareness lack about energy management concept. Nevertheless, our intent is to point out the importance of introducing each step in a non-ending loop, granting continuous energy management improvements and a constant reduction of energy consumptions and costs.

Accordingly, in the following sections each step characterizing the proposed methodology will be described in detail. The different phases are:

- Energy cost & consumption data collection;
- Energy cost & consumption data analysis;
- Energy forecasting at plant level;
- Sub-metering energy use;
- Tariff analysis and contract renewal;
- Energy budgeting and control;
- Energy monitoring and control;
- Power plant management optimization;

5. Cement Manufacturing Process

Cement is a gray, finely ground combination of minerals which, when mixed with water, sand, gravel, and other materials forms concrete. Cement provides the chemical bond that holds the other materials together. Concrete, when newly mixed, is plastic and malleable, which allows it to be cast into shapes to build homes, sidewalks, superhighways, dams, skyscrapers and many other objects. Concrete is inert, nontoxic, naturally waterproof, and fire resistant. It is the world's most commonly used construction material.

The raw materials used to produce cement are primarily limestone, clay, shale, and silica sand. These materials are quarried, crushed, and, for economy, are usually transported to a nearby cement plant. The cement plant proportions the raw materials to the correct chemical composition and grinds the material to a fine consistency. Small quantities of iron ore, alumina, and other minerals may be added to adjust the raw material mixture.

Cement manufacturing requires exacting measurements and careful controls to produce a product that meets precise chemical and physical specifications. The first step in the cement manufacturing process is the quarrying of a combination of raw materials that when sized, blended, and processed yield the exact chemical composition required. These raw materials then undergo a series of high temperature chemical reactions and physical changes after which they are ground into a very fine, carefully sized powder. The steps of cement manufacturing are-

- Extraction of raw materials used in cement production;
- Preparation of raw materials (including grinding and mixing);
- Warehousing of meal;
- Baking of raw material meal (production of clinker);
- Maturing of clinker;
- Milling of clinker into cement;
- Warehousing of cement
- Packing and dispatch.[6][7][8]

6. Barrier to Energy Efficiency

A number of barriers to increased energy efficiency were identified in discussions with cement customers and utility representatives who are in close contact with their cement customers.

Following are some key barriers identified in the interview process.

***Limited capital*:** many of the energy efficiency equipment improvements in the cement industry involve large capital investments, and most customers cited limited capital availability as a key factor limiting increases in energy efficiency. One customer cited a $4 million capital budget, and another cited a $1 million capital budget. Two other customers did not indicate that they had any set budget to work with and had to justify all new capital expenditures on a case by case basis. Many targeted project cost many millions of dollars, so even the customers with assigned capital budgets are severely constrained.

***Production concerns*:** for all customers, keeping equipment operation and avoiding production disruptions was of the highest priority. Additionally, cement plants do not like to shut down except for once a year, largely because shut down stresses the ceramic insulation in the kiln.

Heat-up and cool down has to be done very carefully or the ceramic insulation will deteriorate.

***Limited staff time*:** staffing limitations were another key barrier to increased energy efficiency.

While all customers want to stay as efficient as possible, staff's number one priority is "keeping things running."

***Information*:** while all customers feel they have access to the information they need to make energy efficiency improvements, several customers indicated that they did not have time to focus on this information. Also, it appears that customer knowledge is mostly directed towards the "big ticket" equipment that are the primary energy users, and their understanding of the energy saving aspects of smaller items such are preventative O&M appears to be lower.

***Reliability concerns*:** since maintaining production is such a high priority, cement customers are very concerned about the reliability of all new equipment, including high efficiency equipment.

While the customers don't perceive differences in reliability between energy efficient and standard equipment, any installations of new equipment at the plant will generate some reliability concerns.

***Hassle*:** since staff time is limited, smaller energy efficiency projects are not pursued because they "are not worth the trouble."

***Facility uncertainty*:** one customer indicated that they were currently investigating the feasibility of a complete plant overhaul. Uncertainty over the overhaul project has halted any possible efficiency projects.

***Cost effectiveness*:** most customers have severe cost effectiveness criteria. Two customers (with less efficient plants) have payback cutoffs of 1.0 to 1.5 years. Only one customer indicated that they would consider projects with paybacks of up to three years.

***Exit fees*:** Customers have not proceeded to install cogeneration equipment that would utilize waste heat because they would be subject to departure charges. Without the departure charges, on-site generation with waste heat would be very close to being economic.

8. Case Study

8.1. Compressor

Compressed air is one of the most important and exclusive components in a plant where energy is used. Approximately 5% of the total energy of a cement industry is used to run compressor. So by taking some necessary steps to control air compressors consumption of energy, there could be significant savings for business.

Description about Existing system

In Seven Rings Cement industry there are three compressors. From those compressors one compressor is from the beginning of the industry. So the old one cannot give its maximum efficiency. The compressor needs to keep off at least 15 minutes over a day due to overheating. So it can be said that the compressor consume more electricity but give low efficiency and needs higher maintenance.

Losses calculation of the existing system

Capacity of the unit =180 ton/hour

Loss of cement production by the old compressor in 15 minutes=180/3*4ton/day

=15 ton/day

Cost of cement per 50 kg=450tk

So cost of the losses cement=15*1000*450/50

=135000tk/day.

Monthly losses=135000*25

=3375000tk.

Approximate maintenance cost=25000tk/month

Total loss per month=3375000+25000

=3400000tk

Cost of a compressor is 3000000tk

So, we can replace the compressor with the new one and sell the old compressor.

8.2 Motor

Increasing motor efficiency and taking measures to reduce the amount of energy it requires to run a motor can directly impact the bottom line of business. By replacing inefficient motors with premium efficient motors equates to significant cost savings over the life of the motor , not to mention the additional benefits of reduced down-time and increased productivity and reliability.

Electric motors are efficient at converting electric energy into mechanical energy. If the efficiency of an electric motor is 80%, it means that 80% of electrical energy delivered to the motor is directly converted to mechanical energy. The portion used by the motor is the difference between the electrical energy input and mechanical energy output.

Various Electric Motor Parameter

Efficiency=746*HP output/ watts input

%slip= (Synchronous speed – running speed)*100 / Synchronous speed

RPM= 120* frequency / no. of poles in winding

Power factor, P_f= Active power / Apparent power

Equations

For loads not sensitive to motor speed

Same horsepower and difference efficiency:

kW saved= HP *0.746*(100/Estd – 100/ Eee)

Annual saving, S= HP *L*C*N*(100/Estd- 100/ Eee)

For loads sensitive to motor speeds

Above equation should be multiply by speed ratio correction factor (SRCF).

$SRCF=(RPM_{EE} / RPM_{STD})^3$

Where,

S= Savings, L= % Load

HP=Horsepower, N=Operating hours

C= Energy cost (tk/kWh)

E_{EE}=% Efficiency of Energy Efficient Motor

E_{STD}=% Efficiency of Standard Motor

Available data

HP= 4760 HP for main motor

L= 90%

C= 7.5 tk/kWh, N=7200 hours

E_{STD}=91%, E_{EE}=94.1%

RPM_{STD}= Speed of the Standard Motor=786

RPM_{EE}=Speed of the energy efficient motor=810

Annual Cost Saving:

For loads not sensitive to motor speed:

S=4760*0.746*0.9*5.6*7200*(100/91 – 100/94.1) tk

=4664870 tk

For loads sensitive to motor speed:

S=4760*0.746*0.9*5.6*7200*(100/91 – 100/94.1) * $(810/786)^3$

=5105370 tk

Therefore it shows that the use of energy efficient motor for an existing system is not very effective because implementation cost is so high but for a new plant it may be little profitable.

There are 240 different types of motor in the factory.

Among them we work on-

Motor Name	Power (kW)	Speed (RPM)	Number
a)Mill main motor	3550	786	1
b)Roller press	900	987	2
c)Main fan motor (ID)	710	980	1
d)Separator motor	250	1485	1
e)Inlet bucket elevator motor	160	1470	1
f)Outlet bucket elevator motor	110	1470	1
g)Bag filter ID fan motor	75	1450	1
h)Air Slide	7.5	1450	8

Table 7.1- Different Types of Motors We Observed

8.3 Lighting

Enhancing lighting efficiency is one of the easiest ways to lower the energy bills. When planning o replacing lighting, consider the types of lights, the location, the lighting conditions, the appropriate lamp technology, the correct control systems by using PLC and other components of a commercial lighting system.

Name of lights	number	Power (Watt)	Working Hours
Tube light Set	214	40	24
Mercury light	20	1000	12
Street light	90	600	13
Energy Saving Bulb	100	63	24
Energy Saving Bulb	60	30	24
Energy Saving Bulb	40	35	24

Table 7.2- Different Types of Lights We Observed

Calculations

Total power used for lighting=

(214*40*24+20*1000*12+600*90*13+100*63*24+

60*30*24+40*35*24)

=387.572 kWh/ Day

Cost for lighting/year =387.572*365*7.

=1060980 tk

From the above data taken from the Seven Rings Cement Industry it can be said that they use very effective lighting system. So it is very much difficult to save energy from there. As in there total lighting system controlled manually sometimes it is not possible to switch off of street lights in time. By automatic control of lights in which switching of lights would be controlled by daylight intensity using Programmable Logic Control (PLC) this problem can be solved. This process also can save money. If every day one hour can be saved it will help to save money.

Calculations:

Cost for street lighting/ year=

(600*13*90*365*7.5+1000*12*20*365*7.5) /1000

=2578725 tk/ year

After using PLC systems

Cost for street lighting/ year =

(600*12*90*365*7.5+1000*11*20*365*7.5) /1000

=237150 tk / year

Therefore it shows that the use of PLC system is not very much effective but it is little profitable.

8.4. Dust Collection:

Dust collectors are used in many processes to either recover valuable granular solid or powder from process streams, or to remove granular solid pollutants from exhaust gases prior to venting to the atmosphere. Dust collection is an online process for collecting any process-generated dust from the source point on a continuous basis. Dust collectors may be of single unit construction, or a collection of devices used to separate particulate matter from the process air. They are often used as an air pollution control device to maintain or improve air quality.

Mist collectors remove particulate matter in the form of fine liquid droplets from the air. They are often used for the collection of metal working fluids, and coolant or oil mists. Mist collectors are often used to improve or maintain the quality of air in the workplace environment.

Fume and smoke collectors are used to remove sub-micrometer-size particulates from the air. They effectively reduce or eliminate particulate matter and gas streams from many industrial processes such as welding, rubber and plastic processing, high speed machining with coolants, tempering, and quenching.[6]

Five main types of industrial dust collectors are:

- Inertial separators
- Fabric filters
- Wet scrubbers
- Electrostatic precipitators
- Unit collectors

9. Conclusion

Energy efficiency in the cement industry and cost effective energy that can be achieved in the near future are analyzed in this report. The report focuses on the analysis of energy used in different sections, specific energy efficiency technologies and measures to reduce energy use without hampering product quality and quantity and the energy efficiency for cement production.

There is a lot of opportunities to reduce the energy consumption in both industrial and residential sector in Bangladesh. As there is a lack of energy in both electricity and fuel in Bangladesh therefore by proper management of energy the energy efficiency can be increased to 20% to 30%.

The whole auditing process was carried out by walk through audit and a very little engineering audit. In this thesis the field study is largely based on interviews with employees at the industry. When gathering information from personnel it is always a risk that it is affected by the interviews own opinion, standpoint and interests. A detailed auditing can be applied to avoid this mentioned risk and hence for the better solution.

There was a lack of provision of data as the data was considered highly confidential. And the auditing process was carried out within a short time. Therefore detailed and long term audit was not possible to carried out which would be more effective.

REFERENCES

[1] http://www.ecomena.org/tag/importance-of-energy-management/

[2] John Wiley and Sons, Wayne C. Turner, "Energy management handbook"

[3] http://www.powermin.nic.in.html

[4] Cape Hart, Turner and Kennedy, "Guide to Energy Management"

[5] Capobianchi Simona, Andreassi Luca, Introna Vito, Martini Fabrizio and Ubertini Stefano, "Methodology Development for a Comprehensive and Cost-Effective Energy Management in Industrial Plants"

[6] http://www.cis.org.rs/en/cms/about-cement/modern-production-of-potland-cement

[7] http://www.lafarge.com/SWF/animation-ciment-script-VA.html

[8] William T. Choate, "Energy and Emission Reduction Opportunities for the Cement Industry"

[9] https://www.wikipedia.org/

[10] N.A. Madlool, R. Saidur, M.S. Hossain, N.A. Rahim, "A critical review on energy use and savings in the cement industries"

ICMIEE-PI-140222

Automated Restaurant Food Service Management system using a Line Follower Robot

Asma-Ul-Husna[*]*, Dr. Md. Rokonuzzaman, Md. Shahinur Rahman, Mahjabeen Hossain Mim*
Department of Mechanical Engineering, Rajshahi University of Engineering & Technology, Rajshahi-6204, Bangladesh

ABSTRACT
This paper describes the concept of an application of a line follower robot as food service system (a line follower based food service system in a restaurant). Autonomous systems are gradually increasing day by day in our modern life. A Line follower robot is a good example of an autonomous system. A line follower robot moves by tracking a line of white color line on a black surface or vice versa. The tracking is done by using an array of IR sensor. Using this principle, a line follower robot can be applied as an autonomous food service system in a restaurant.

Keywords: Automated restaurant, food service management, line following robot, IR sensors

1. Introduction

A line follower robot is an autonomous robot that can move by tracking a line of white color on a black surface or vice versa. The idea of the project is to applying this principle of line following, the robot can be used as a food service system in a restaurant. The robot delivers food from the kitchen to the destination table number. The destination table no is input by key pressing. After receiving the food the robot automatically return to the kitchen for the next service. An entrepreneur can apply this concept in a small restaurant business to serve the customer as a smart way.

2. Problem detection

Since the concept of the project is to apply the system for food service and maintaining the service in a proper way in a small restaurant business, focusing on an entrepreneur who can't bear the cost of service man. Though Honda company has been established a humanoid servicing robot. It is now under research. But a humanoid robot is very costly to apply.

3. Related work

Some related application of line following robot are [1] 'Line following robot for library inventory management system' published in Emerging Trends in Robotics and Communication Technologies (INTERACT) 2010 International Conference, [2] 'Development and Applications of Line following Robot Based Health Care management system' published in International Journal of Advanced Research in Computer Engineering and Technology (IJARCET) Volume 2, Issue 8, August 2013

4. Design concept of the robot

The robot is based on line follower. An Array of infra-red sensors is used for tracking the line. The sensor array is placed at front of the body. An Arduino Mega2560 is used as control part of the robot. It processes the data from sensors and sends to the motors that move the body. A 12v Rechargeable battery is used for the power source of the robot. A proposed 3D view of the robot is shown in Fig.1

Fig.1 A 3D Model of the Robot

A movable tray is used to move forward when the robot reaches at the destination table no and move backward when the food is received. Fig.2 shows the actual robot body.

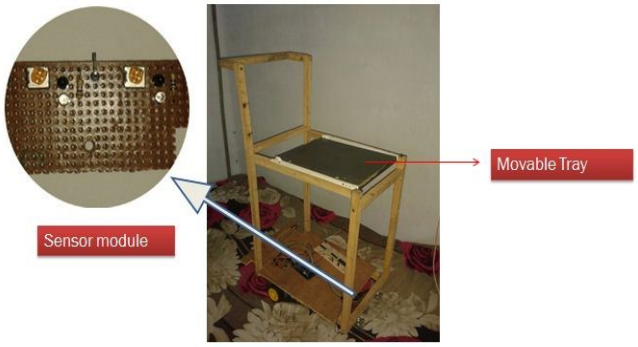

Fig.2 Actual Robot Body

4.1 Mechanical Construction

The whole body of the robot is placed on a chassis. The chassis contains the sensor module at the front, two wheel casters act like steering, and two DC gear motors with

* Corresponding author. Tel.: +88-01719445005
E-mail address: evu_me04@yahoo.com

wheel at back to move the body. The chassis metal is stainless steel. Since stainless steel has Modulus of elasticity about 200 GN/m^2, the chassis is able to carry weight of the whole body without any deformation. The Fig.3 shows the mechanical construction of chassis. The body material is used as wood for light weight and consideration of low cost. Any other light weight material such as aluminum can be used but then cost will be high.

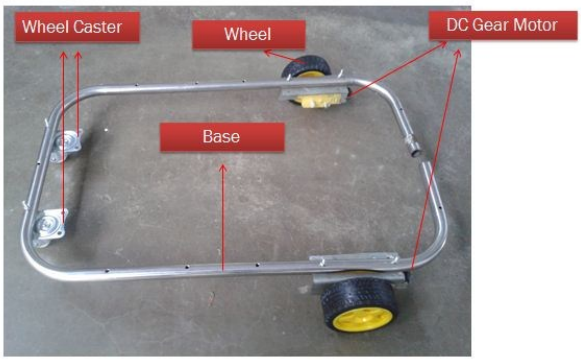

Fig.3 Chassis Construction

5. Design concept of the restaurant Layout or Track of the line.

The track for the robot is designed such a way that the robot can serve the food within a short time. In the line there is some indicating line which indicates where to stop the robot according to the corresponding table no. The tables are arranged with number beside the line. The Fig.4 shows the track line for the robot and table arrangement.

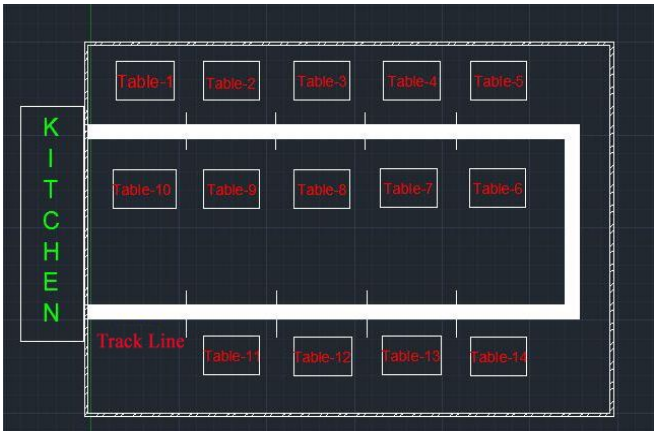

Fig.4Track for the robot

6. Control part of the robot

An Arduino mega2560 prototype board is used to control the robot. This is a micro-controller board based on ATmega2560 with 256KB Flash memory (of which 8KB is used by boot-loader), 8KB of SRAM, 54 digital I/O pins (of which 14 provide PWM output), 16 ADC, clock speed of 16 MHz and so many features from the data-sheet. The board operating on 5v DC, but recommended voltage is 7v to 20v. The controller board processes the data from the sensor array, and sends the control to the two DC motors. Fig.5 shows the control board

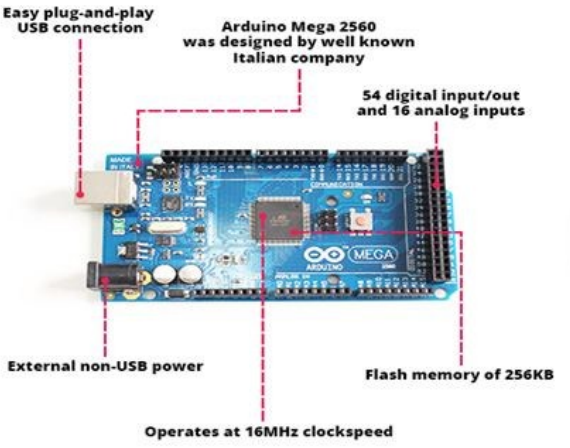

Fig.5 Arduino Mega2560 board

6.1 The Sensor module

The sensor module is used to trace the line. The sensor module is based on Infra-red light. The module contains 5 pairs of infra-red light emitter and receiver. The Fig.6 shows the sensor module.

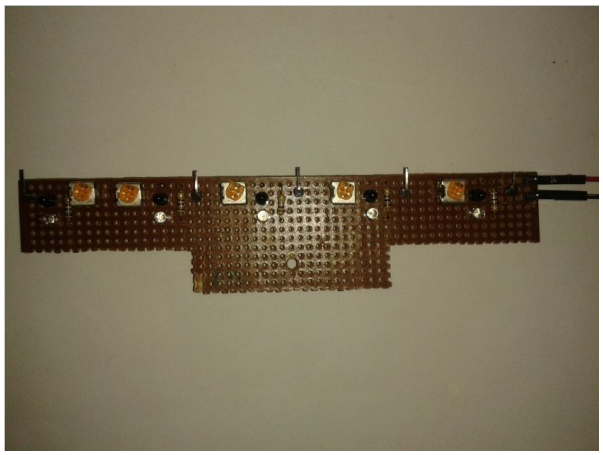

Fig.6 IR sensor module

The working principle of the sensor is shown in the Fig.7

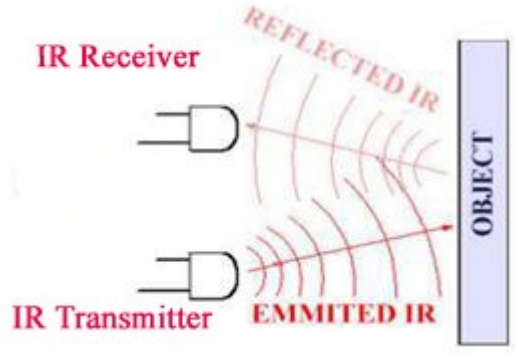

Fig.7 working method of sensor

The output voltage ranges of the sensors are 0v to 5v. This data is sent to the controller board to process.

6.2 Motor driver

Since the DC motor consume more current, a driver circuit is needed to provide the amount of current. The driver is L293D integrated circuit. It accepts the standard TTL logic levels and drives inductive loads (such as relays, DC motor, solenoid etc.) The device is a switching power transistor. It draws 600mA output current per channel, and operating through 5v to 36v. a several pin configuration of the driver is shown in Fig.8

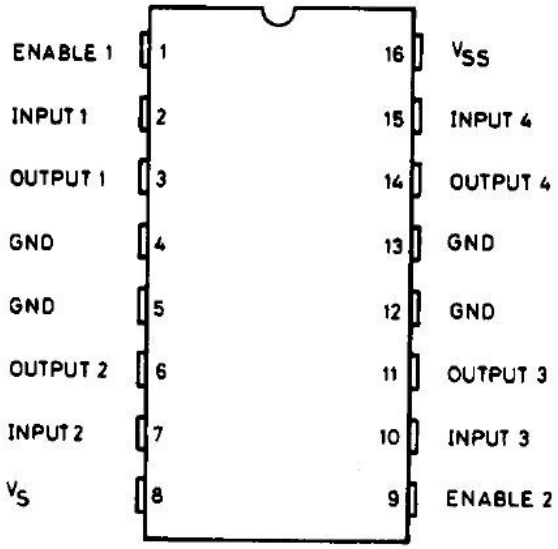

Fig.8 L293D motor driver.

7. Control Diagram of the robot

The overall control of the robot is shown in the Fig.9 in a block diagram.

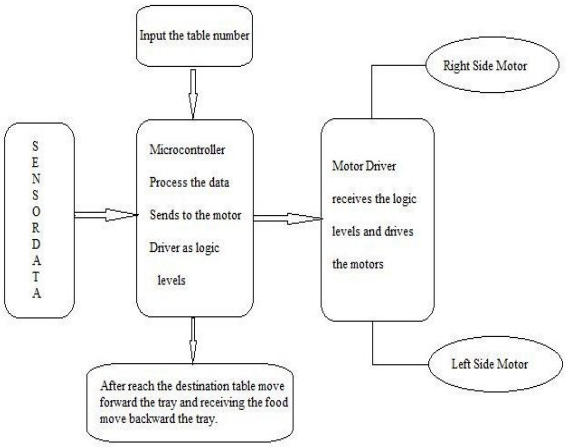

Fig.9 Control block diagram of the robot.

The robot takes the input table no. the sensors sense the track and send data as voltage input to the micro-controller. The micro-controller processes the data as digital logic and sends the data to the motor driver to drive the motors. After reaching the destination table the robot stops. The tray on the robot moves forward by using a servo motor. It moves backward when the food is received.

8. Differential Drive of motor

The differential drives mechanism help the robot to run at different speed of wheel while turning. Different input to the pin of motor driver creates differential drive. The table below shows the different voltage level at the pin of motor driver to create differential drive mechanism.

Table 1 differential drive mechanism

EN	IN1	IN2	Turn
HIGH	LOW	HIGH	CW
HIGH	HIGH	LOW	CCW
HIGH	LOW	LOW	STOP
HIGH	HIGH	HIGH	STOP
LOW	IGNOR	IGNOR	STOP

9. Performance

The performance of the robot depends on tracking of the line. The robot is able to trace the line very smoothly and moves fast. Since the objective of the service robot is to serve very short time, from this point of view the robot fulfills this requirement.

10. Discussion

Power supply is main fact to the performance of the robot. Less power drives the robot slow. The inductive loads (such as motor) consume more power. So use of rechargeable battery is very effective so that the battery can be charged fully before every run of the robot.

11. Future work

Since the robot can only reach the food and return for the next service but there is no scope of cleaning the table. So in future development of the robot it is focused on how to clean the table using an autonomous system.

11. Conclusion

The service robot is used in many fields such that from the industrial level to domestic service. There are many foods serving robot but their initial cost and maintenance cost are high. The overall cost of this project is considerable. Automation makes the life easier and reducing the time. This autonomous robot is also reducing the time and makes proper utilization of technology.

NOMENCLUTURE

MCU	: Micro-controller Unit
DC	: Direct Current
ADC	: Analog to Digital Converter
CW	: clock wise
CCW	: counter clock wise
EN	: Enable Pin of Motor Driver
GND	: Ground
I/O	: Input or Output
IN1	: Input pin 1 of motor Driver
IN2	: Input pin 2 of motor Driver
KB	: Kilo Byte
MHz	: Mega Hertz

PWM : Pulse Width Modulation
SRAM : Static Random Access Memory
TTL : Transistor-Transistor Logic
V_s : Supply voltage, V
V_{ss} : Logic supply voltage, V

REFENCES

[1] Autonomous Mobile Robot*, Sensing, Control, Decision Making and Application. Edited by Shuzhi Sam Ge, Frank L. Lewise*

[2] Designing Autonomous Mobile Robot, *by John Holland*

[3] Make An Arduino Controlled Robot, by*Michael Margolis*

[4] Arduino Robotics, *by John-Devid Warren, Josh Adams, HaraldMolle.*

[5] Fundamental of Robotic Mechanical System, *Theory, Methods and Algorithm*, *by Jorge Angeles*

[6] Introduction to AI Robotics, *by Robin R. Murphy*

[7] Robot Mechanism and Mechanical Devices Illustrated, *by Paul E. Sandin*

[8] Line Following for library inventory management inventory management system, *journal of Emerging Trends in Robotics and Communication Technologies (INTERACT), 2010 International on 3-5, Dec 2010, INSPECT Accession Number 11822531.Conference on 3-5, Dec 2010, INSPECT Accession Number 11822531.*

[9] Development and Applications of Line following Robot Based Health Care management system' *published in International Journal of Advanced Research in Computer Engineering and Technology (IJARCET) Volume 2, Issue 8, August 2013*

[10] PUSH-PULL 4 CHANNEL DRIVER WITH DIOD (l293D, L293D Datasheet), SGS-THOMSON MICROELECTRONICS

ICMIEE-PI-140224

Transportation Cost Optimization Using Linear Programming

Muztoba Ahmad Khan [1,*]
[1] Department of IPE, Bangladesh University of Engineering and Technology, Dhaka-1000, BANGLADESH

ABSTRACT
Optimization means using resources and existing technology at the best possible way. Better planning and its execution results in optimization of many problems. Quantitative models and mathematical tools such as linear programming allows for better result. We can use modern computing equipment for this purpose. Nowadays various problems of operational planning for transportation problems are solved by mathematical methods. Linear programming method is used to model most of these transportation problems. In this paper a real world application of a transportation problem that involves transporting mosquito coil from company's warehouse to distributor's warehouse is modeled using linear programming in order to find the optimal transportation cost. Excel Solver has been used to model and solve this problem.

Keywords: Optimization, Linear Programming, Transportation Cost, Supply Chain.

1. Introduction

To be successful in today's highly competitive marketplaces, companies must strive for greatest efficiency in all of their activities and completely utilize any possible opportunity to gain a competitive advantage over other firms. Among many possible activities, cost reduction in logistics is regarded as one of the core areas presenting enormous opportunities.

According to Jonsson there are two kinds of logistic costs: direct and indirect cost. Direct costs include physical handling, transportation, and storage of goods in the flow of materials together with the administration costs, whereas capacity and shortage costs are indirect costs. Jonsson also claims that direct logistics costs roughly vary between 10% and 30% of the turnover depending on the type of industry [1].

In such situation, it can be said that implementing optimization techniques to transportation of goods in order to schedule when and how much to send from each origin to its respective destination over a certain time period is a possible way to make improvements over the total cost of logistics.

In this paper a real world application of a transportation problem that involves transporting mosquito coil from company's warehouse to distributor's warehouse is modeled using linear programming in order to find the optimal transportation cost. Excel Solver has been used to model and solve this problem.

2. Linear Programming

Linear programming or linear optimization is a mathematical method for determining a way to achieve the best outcome (such as maximum profit or lowest cost) in a given mathematical model for some list of requirements represented as linear relationships. Linear programming is a specific case of mathematical programming (mathematical optimization) [2].

More formally, linear programming is a technique for the optimization of a linear objective function, subject to linear equality and linear inequality constraints.

Linear programs are problems that can be expressed in canonical form:

$$\begin{array}{ll} maximize & c^T x \\ subject\ to & Ax \leq b \\ and & x \geq 0 \end{array}$$

Where x represents the vector of variables (to be determined), c and b are vectors of (known) coefficients, A is a (known) matrix of coefficients, and $(.)^T$ is the matrix transpose. The expression to be maximized or minimized is called the objective function ($c^T x$ in this case). The inequalities $Ax \leq b$ are the constraints which specify a convex polytope over which the objective function is to be optimized. In this context, two vectors are comparable when they have the same dimensions. If every entry in the first is less-than or equal-to the corresponding entry in the second then we can say the first vector is less-than or equal-to the second vector [3].

Linear programming can be applied to various fields of study. It is used in business and economics, but can also be utilized for some engineering problems. Industries that use linear programming models include transportation, energy, telecommunications, and manufacturing. It has proved useful in modeling diverse types of problems in planning, routing, scheduling, assignment, and design [4].

3. Company Overview

J & J Essential Products (Pvt.) Ltd. is primarily a cosmetics and toiletries products manufacturing industry. However, they also produce some highly demanding products, i.e. electric bulb, mosquito coil etc. The cosmetics and toiletries products are branded as 'Jasmine' in the Bangladesh market place.

* Corresponding author. Tel.: +88-01919010349
E-mail address: muztobaahmad@yahoo.com

2.1 About the Factory

The factory [5] is located at BSCIC industrial area, Golora, Manikganj, Bangladesh. It has one 5 storied building (main factory building) of 35000 sq. ft., each floor area covering 7000 sq. ft.

2.2 Marketing & Distribution of mosquito coil:

The Company has set up regional offices in Dhaka, Chittagong and Bogra along with warehouse facilities. There are seven distributor's warehouses where the goods are delivered from company's warehouses. The company sends goods through four of its own vehicles and use public transport services. The company's sales and distribution costs account for 19% of total cost.

4. Problem Statement

Since the optimization model that will be developed is expected to be applicable to different instances, this section starts with depicting the scope of the problem which is followed by an extended description of the problem through a case provided by the company.

The problem is to determine the optimal quantity of mosquito coil that should be delivered from company's each warehouse to different distributor's warehouse in order to obtain the minimum transportation cost.

The company delivers mosquito coils from its three warehouses in Dhaka, Chittagong and Bogra to seven distributor's warehouses in Barisal, Chittagong, Dhaka, Rajshahi, Rangpur, Sylhet and Khulna without considering the optimal quantity. So if the company applies linear programming to find the optimal quantity of mosquito coil to be delivered, it will be able to minimize the transportation cost significantly, which will result in increased profitability.

In order to determine the optimal quantity of mosquito coil that should be delivered from company's each warehouse to different distributor's warehouse for obtaining the minimum transportation cost, the following information were collected from the Supply Chain Director of the company:

Shipping cost: Average shipping costs of per carton mosquito coil from company's warehouse to different distributor's warehouse are given in the table below:

Table 1 Average shipping costs of per carton coil.

Distributor's warehouse / Company's warehouse	Dhaka	Chittagong	Bogra
Dhaka	15	160	100
Chittagong	160	12	260
Rangpur	154	315	56
Barisal	245	410	190
Rajshahi	130	290	58
Sylhet	125	427	204
Khulna	215	375	160

*All units are in Bangladesh Taka (BDT)

Storage capacity: Storage capacity of company's different warehouses:

Table 2 Average shipping costs of per carton coil.

Dhaka	3980
Chittagong	1785
Bogra	4856

*All units are in cartons

Demands: Average demand of different distributor's warehouses:

Table 3 Average shipping costs of per carton coil.

Dhaka	1168
Chittagong	1560
Rangpur	1439
Barisal	986
Rajshahi	1658
Sylhet	2035
Khulna	1159

*All units are in cartons

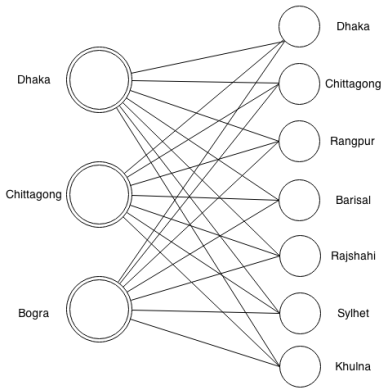

Fig.1 Illustration of the transportation network.

5. Mathematical Model Formulation

For the given problem, we formulate a mathematical description called a mathematical model to represent the situation. The model consists of following components:

Decision variables: These variables represent unknown quantities (number of items to produce, amounts of money to invest in and so on).

Objective function: The objective of the problem is expressed as a mathematical expression in decision variables. The objective may be maximizing the profit, minimizing the cost, distance, time, etc.

Constraints: The limitations or requirements of the problem are expressed as inequalities or equations in decision variables [6].

Followings are the decision variables, objective function and constraints specific to the problem of this paper:

Decision variables:

Three warehouses will be symbolized as:
Dhaka = A_1
Chittagong = A_2
Bogra = A_3

Seven distributor's warehouses will be symbolized as:
Dhaka = B_1
Chittagong = B_2
Rangpur = B_3
Barisal = B_4
Rajshahi = B_5
Sylhet = B_6
Khulna = B_7

Let the storage capacity of mosquito coils at A_i be a_i; where i=1, 2 and 3.

Let the requirements of mosquito coils at B_j be b_j; where j=1, 2, 3, 4, 5, 6 and 7.

Let C_{ij} be the cost of shipping one carton mosquito coil from A_i to B_j.

Let X_{ij} be the number of cartons of coil shipped from A_i to B_j.

Now let's assign the respective variables in Table 1:

Table 4 Average shipping costs with assigned variables.

Distributor's warehouse / Company's warehouse	Dhaka A_1	Chittagong A_2	Bogra A_3	Stock
Dhaka (B1)	$C_{2,1}$=15	$C_{2,1}$=160	$C_{3,1}$=100	b_1=1168
Chittagong (B2)	$C_{1,2}$=160	$C_{2,2}$=12	$C_{3,2}$=260	b_2=1560
Rangpur (B3)	$C_{1,3}$=154	$C_{2,3}$=315	$C_{3,3}$=56	b_3=1439
Barisal (B4)	$C_{1,4}$=245	$C_{2,4}$=410	$C_{3,4}$=190	b_4=986
Rajshahi (B5)	$C_{1,5}$=130	$C_{2,5}$=290	$C_{3,5}$=58	b_5=1658
Sylhet (B6)	$C_{1,6}$=125	$C_{2,6}$=427	$C_{3,6}$=204	b_6=2035
Khulna (B7)	$C_{1,7}$=215	$C_{2,7}$=375	$C_{3,7}$=160	b_7=1159
Requirement	a_1=3980	a_2=1785	a_3=4856	

Objective function:

The objective function contains costs associated with each of the variables. It is a minimization problem.

$$Minimize\ f\ = \sum_{i=1}^{3}\sum_{j=1}^{7} C\ (i,j)\ X(i,j)$$

Constraints:

The constraints are the conditions that force supply and demand needs to be satisfied. In the transportation problem, there is one constraint for each node.

The quantity of mosquito coils sent from A_i is $\sum_{j=1}^{7} X(i,j)$ and since the quantity of mosquito coils available at A_i is a_i, we must have $\sum_{j=1}^{7} X(i,j) \leq a(i), where\ i = 1, 2\ and\ 3$.

Now, the quantity of mosquito coils sent to B_j is $\sum_{i=1}^{3} X(i,j)$ and since the quantity of mosquito coils required at B_j is b_j, we must have $\sum_{i=1}^{3} X(i,j) \geq b(j), where\ j = 1, 2, 4, 5, 6\ and\ 7$.

It is assumed that we cannot send a negative quantity from A_i to B_j, so $X_{ij} \geq 0$ for all values of i and j.

6. Modeling the Problem using Excel Solver

This section will demonstrate, how to use Excel Solver to find the optimum transportation cost.

The first step is to organize the spreadsheet to represent the model. Once the model is implemented in a spreadsheet, next step is to use the Solver to find the solution. In the Solver, we need to identify the locations (cells) of objective function, decision variables, nature of the objective function (maximize/minimize) and constraints.

Step by step solution of the problem using Excel Solver is given below:

Step 1:
At first we will construct a table in excel that will contain the cost parameters between each destination.

Shipping Costs

	Dhaka	Chittagong	Rangpur	Barisal	Rajshahi	Sylhet	Khulna
Dhaka	15	160	154	245	130	125	215
Chittagong	160	12	315	410	290	427	375
Bogra	100	260	56	190	58	204	160

Step 2:
Now we will construct another table that will contain shipment, stock and requirements.

Shipments

	Dhaka	Chittagong	Rangpur	Barisal	Rajshahi	Sylhet	Khulna	Total Out	≤	Stock
Dhaka	0	0	0	0	0	0	0	0	≤	3980
Chittagong	0	0	0	0	0	0	0	0	≤	1785
Bogra	0	0	0	0	0	0	0	0	≤	4856
Total In	0	0	0	0	0	0	0			
	=	=	=	=	=	=	=			
Requirement	1168	1560	1439	986	1658	2035	1159			

Here "Total In" is the quantity of coils shipped to that particular distributor's warehouse from company's three warehouses.

i.e. for Dhaka it is "=SUM(I7:I9)"

And "Total Out" is the quantity of coils shipped from that particular warehouse to distributor's seven warehouses.

i.e. for Dhaka it is "=SUM(I7:O7)"

Step 3:
Now we will create a cell that will automatically calculate total cost based on the inputs in shipment table.

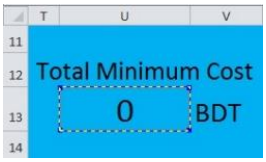

To calculate total cost we need the function SUMPRODUCT. This function will automatically sum all the product of unit and cost per unit.

i.e. Total Cost =SUMPRODUCT(J18:P20,I7:O9)

Step 4:
In this step we will setup Excel Solver according to this problem. First we will open Solver from Data tab and locate the Total Minimum Cost cell in to 'Set Objective' in solver (i.e. $U$13). As we want to minimize the function we will choose 'Min'. Also we will choose our solving method as 'Simplex LP'.

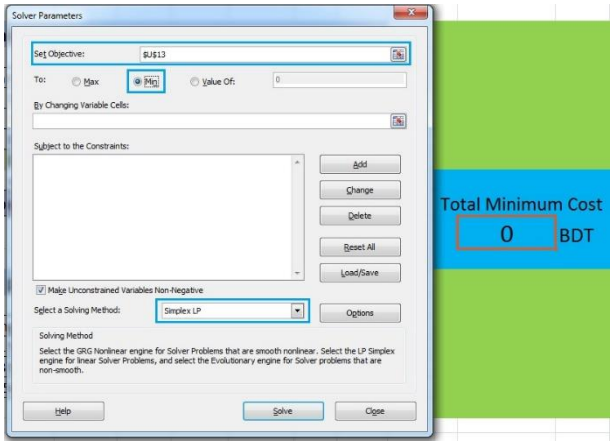

Step 5:
In this step we will locate the changing variables (i.e. the optimal quantities) in to 'By Changing Variable Cells:' option of Solver.

Here changing cells will be $I$7:$O$9

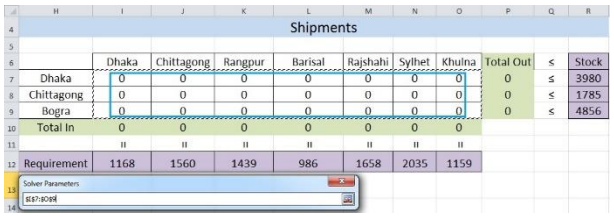

Step 6:
Now we will add constrains of this problem in Solver. As previously discussed, there are three constrains in this problem:

(1) Total Out is less than or equal to Stock
(2) Total In is equal to Requirement
(3) Shipment quantities are non-negative

To add constrains we will click add button on Solver and locate each constrains.

(1) Total Out is less than or equal to Stock ($P$7:$P$9 ≤ $R$7:$R$9)

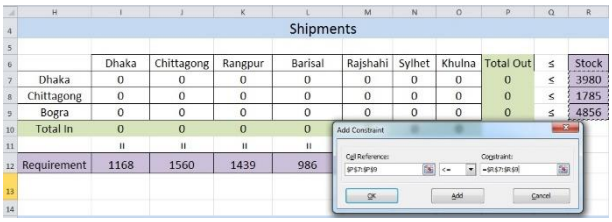

(2) Total In is equal to Requirement ($I$10:$O$10 = $I$12:$O$12)

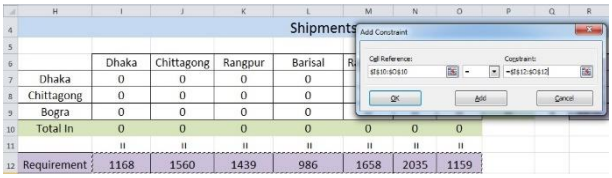

(3) Shipment quantities are non-negative (we will just select 'Make Unconstrained Variables Nonnegative')

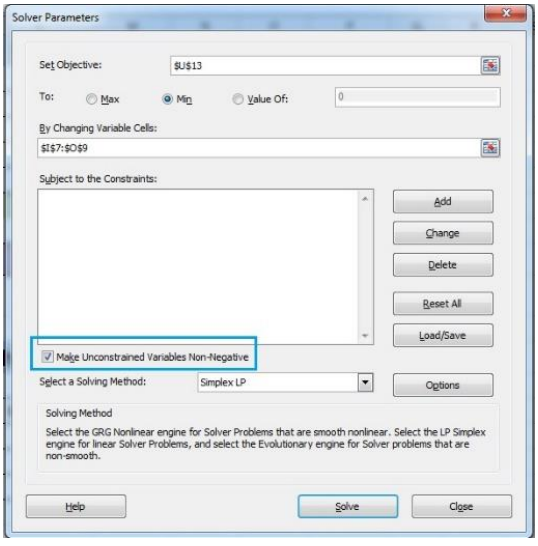

Step 7:

Now we are done with the setup, all that is left is to click on ‘Solve’ button. This way we will find the following solution from Solver:

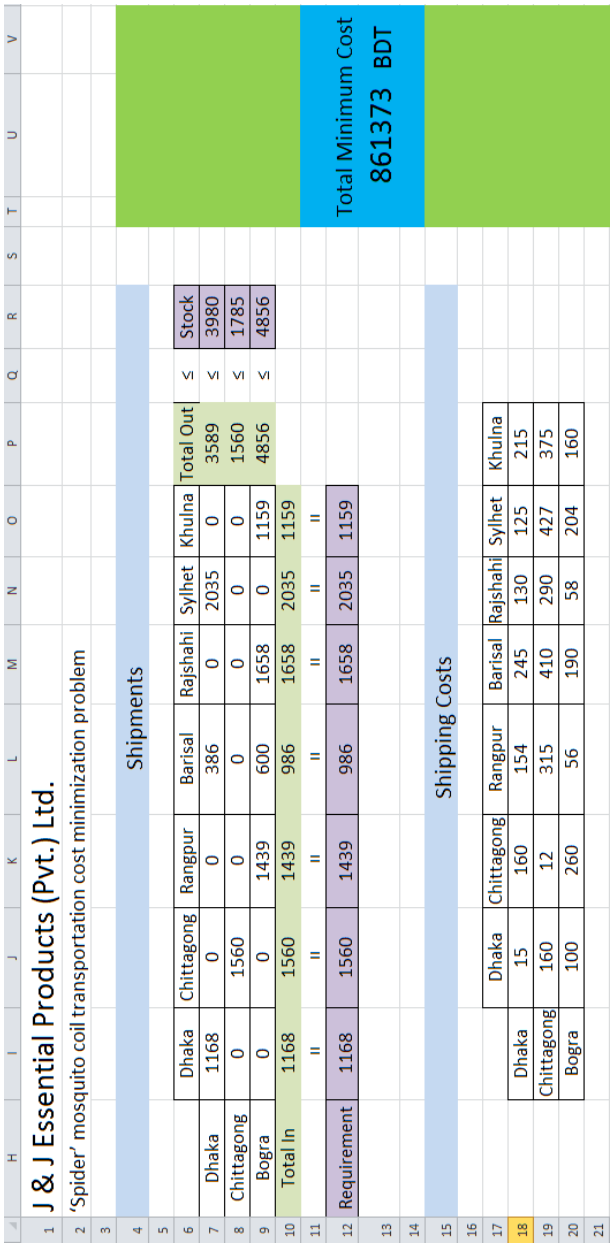

7. Limitations

In this problem we considered that supply will always exceed the demand. But in reality shortage of supply can exist.

Another importation limitation is that the company allocated 150 taka per carton for transportation cost when setting the trade price of their coil. So if the company makes a shipment that costs more than 150 taka per carton, it may incur loss.

7. Conclusion

Though this model has some limitations, still if the company applies the solution reached through this study, it will be able to minimize the transportation cost, which will result in increased profitability. In future a more optimized model of this problem can be developed by getting rid of the limitations mentioned above.

But again, certainly there will be some real life constrains, which we won’t be able to solve with any model. In those cases we will have to depend on our intuition and experience.

REFERENCES

[1] P. Jonsson, Logistics and supply chain management. *McGraw-Hill*, (2008).

[2] Wikipedia.org, (August, 2014). Linear programming, *Available from: http://en.wikipedia.org/wiki/Linear_programming*, [Accessed 15 August 2014].

[3] S. A. Phatangare, R. A. Deshmukh, P. K. Deshmukh, Public Cryptography Linear and Non Linear Programming Solver in Cloud Computing, *International Journal of Application or Innovation in Engineering & Management (IJAIEM)*, Vol. 2, pp 141-145, (2013).

[4] I. S. Fagoyinbo, R. Y. Akinbo, I. A. Ajibode, Y. O. A. Olaniran, Maximization of profit in manufacturing industries using linear programming techniques: Geepee Nigeria Limited, *Mediterranean Journal of Social Sciences,* Vol. 2, pp 97-105 (2011).

[5] J & J Essential Products (Pvt.) Ltd, Company Overview 2013, (2013).

[6] L. Chandrakantha, Using Excel Solver in Optimization problems, *Mathematics and Computer Science Department*, New York (2008).

ICMIEE-P1-140228

Seamless Jute Bag: a novelty in eco-friendly Packaging

Toufique Ahmed [1,*], *Shahidul Kader* [2]
[1] Department of Fabric Manufacturing Engineering, National Institute of Textile Engineering & Research, Dhaka-1350, BANGLADESH
[2] Department of Apparel Manufacturing Engineering, National Institute of Textile Engineering and Research, Dhaka-1350, BANGLADESH

ABSTRACT
In Bangladesh the annual demand of carrier bag is more than 14.1 million pcs and in the global market it is 500 billion pcs. Lion share of this huge market is occupied by petroleum derived non-biodegradable bag because of its cheap rate. But this market can be predominately occupied by producing seam or stitch less jute bag. The processing cost of this seamless bag will be very low as bag will be produced as like as fabric and no process is to be needed expect cutting. Beside, Jute is 100% biodegradable and able to consume up to 15 tons CO_2 and release 11 ton oxygen during its growing season which indicates its very environment friendly nature. According to our assumption the price of each seamless jute bag (having 63% cover factor) will $0.0683 and each weaving machine having 72 inch width will be able to produce 228 bags per hour.

Keywords: seamless bag, fully fashion bag, carrier bag, green packaging.

1. Introduction

With the growth of population and export items the demand of secondary packaging is increasing day by day. At present poly bag, paper bag are used in the purpose of secondary packaging. Non-woven synthetic bags are also used in large shopping malls. The reasons of the popularity of these bags are because of their low price. But these bags are non- biodegradable and create hazard to the environment. So the world is demanding a substitution of these bags. In this scenario, seamless jute bag would be a good alternative. Seamless means without sewing. The bags will be self stitched/selvedged when it is delivered from the loom. This characteristic will reduce the price of jute seamless bag.

Walter H Deubner invented the first packaging bag and by 1915, he was selling over a million shopping bags a year. The lightweight shopping bag that we see today dates back to the 1960s. From the mid-1980s, the use of plastic bags became common. Plastic bags soon replaced paper bags. [1]. Secondary packaging or carrier bags are classified into following types by Dr.Chris Edwards. [2]**:**

HDPE bags with prodegradant additive: this type of lightweight, plastic, carrier bag is made from HDPE with a prodegradant additive that accelerates the degradation process. These polymers undergo accelerated oxidative degradation initiated by natural daylight, heat and/or mechanical stress and embrittle in the environment and erode under the influence of weathering.

Low-density polyethylene(LDPE) bags: these are thick-gauged or heavy duty plastic bags, commonly known as "bags-for-life". The initial bag must be purchased from the retailer but can be replaced free of charge when returned.

Non-woven polypropylene (PP) bags: This type of bag is made from spun bonded non-woven polypropylene. The non-woven PP bag is stronger and more durable than a bag for life and is intended to be reused many times.

Cotton bags: This type of bag is woven from cotton, often calico. An unbleached cotton with less processing and is designed to be reused many times.

Paper bags: The paper bag was in effect the first "disposable" carrier bag, but was superseded in 1970s by plastic carrier bags which were seen as the perfect alternative as they did not tear when wet.

Biopolymer bags: Biopolymer carrier bags are a relatively recent development. The biopolymers are usually composed of either polylactic acid (PLA), made from polymerization of lactic acids derived from plant-based starch, or starch polyester blends. These biodegradable polymers decompose to carbon dioxide, methane, water, inorganic compounds or biomass. [3].

Woven Polypropylene (PP) bags: this type of bag is produced from woven PP fibres. Similarly to the nonwoven PP and LDPE bag, it is strong and durable and intended to be reused many times. To provide stability to the base of the bag, the bag comes with a semi-rigid insert.

Jute bag: jute bags are made from jute fibres spun into coarse strong strands making a strong and durable carrier bag. The jute bag is intended to be reused many times.

But it is found that High Density Poly Ethylene (HDPE) plastic bag would have a baseline global warming potential of 1.57 kg CO_2 equivalent, falling to 1.4 kg CO_2 if re-used once, the same as a paper bag used four times (1.38 kg CO_2). [4]. Plastic bags are created through the polymerization of ethylene, a gaseous hydrocarbon found in petroleum. While there are different types of polyethylene, all used as different kinds of plastic, the most commonly used for plastic retail bags is high density polyethylene, or HDPE. This

* Corresponding author. Tel.: +88-01710785325
E-mail address: atoufique@gmail.com

is manufactured from ethylene, a byproduct of gas or oil refining. [5].

Besides, on land conventional plastic carrier bags can last as litter for two years or longer before disintegrating, depending on product composition and environmental conditions. Additives in plastic carrier bags can contaminate soil and waterways and if ingested by animals can enter the food chain. Plastic carrier bags may accidentally be ingested by birds, fish, whales and other animals because they confuse them with prey species. Al least 267 species worldwide are affected by ingestion of plastic debris. Entanglement of wildlife (including seals, whales and marine turtles) in plastic carrier bags is also occuring. [5] Entanglement prevents feeding, swimming and reproducing and can cause drowning. The 2011 ICC report indictes that over the past 25 years 404 animals around the world were found entangled in plastic bags [6]. On the other hand paper bag has a limited opportunity to recycle .The disposal of ash from paper production also has an impact on eutrophication and fresh water aquatic eco toxicity. For producing paper bag trees are cut which indicates non eco-friedly nature. So in this scniero Jute bag would be very suitable alternative to the plastic bags. Because One hectare of jute plants can consume up to 15 tons of carbon dioxide and release 11 tons of oxygen during the jute growing season (about 100 days). [7]. Moreover jute is a natural, 100 percent bio-degradable and recyclable, ecological fibre plant.

2. Market analysis

For the last five years (from 2005 to 2009), export of raw jute in the world market has increased by 39.5 per cent, and export of jute products has increased by 57.6 per cent. In 2009, Bangladesh was the largest raw jute exporter with a share of about 85.7 per cent of the total global export. On the other hand, China occupied the topmost position among the exporters of jute goods accounting for 58.1 per cent of the total global export. India accounted for 8.5 per cent and Bangladesh for 6 per cent of export of jute products in the world market. Between 2005 and 2009, China's export of jute goods increased by 181.1 per cent, whilst that of Bangladesh declined by 11.1 per cent, although the benchmark figures for the two countries were significantly different.[9]

Table 1: world top jute and jute goods exporters

Jute goods				
Exporters	2005		2009	
World	2979.9	-	4695.5	-
Bangladesh	318.9	10.7	283.7	6.0
India	398.2	13.4	398.3	8.5
China	970.9	32.6	2729.6	58.1
Raw Jute				
World	139.5	-	194.5	-
Bangladesh	121.9	87.4	166.7	85.5
India	2.9	2.1	7.1	3.6
Tanzania	0.3	0.2	8.6	4.4

(Source: Trade Map Bangladesh) *(Million USD)*

In 2009, Bangladesh exported 322.6 thousand tones of raw jute worth USD 166.7 million. Her export was concentrated in two major markets, both of which were in Asia, Pakistan (32.2 per cent) and China (28.6 per cent). These two together accounted for more than 60 per cent of the raw jute exported by Bangladesh in 2009. **For jute yarn**, Bangladesh's major markets were Turkey, Belgium and India. In 2009, export of yarn has decreased for Belgium by 18 per cent; and for Turkey by 1 per cent and 4 per cent for two HS categories. In contrast, in India the growth was significant (79 per cent**). Export of jute woven fabric** registered very high growth in the markets of India, New Zealand and Korea, with 24 per cent, 120 per cent and 23 per cent respectively in 2009 compared to 2008. Indonesia was the largest market for ropes; however, export was 58 per cent lower compared to 2008. [9].

From this market analysis it is seen that Bangladesh has a very big international market and in exporting raw jute Bangladesh is unrivalled. But she lags behind in exporting jute goods. Capturing world packaging market may give good opportunity of exporting maximum jute goods.

2. 1 Market size

The world packaging market is very big and expanding day by day. The ongoing increasing in grocery items and affordability of inhabitants of developing countries make the packaging market as one of the biggest markets in the global village. Each and every item needs several packaging materials. Normally plastic bag is used for carrying different items. But due to their terrible effect on environment government of different countries are compelled to ban its use. For example: Bangladesh banned polyethylene bag in 2002, china banned the free distribution of plastic bag in 2008, inspiring by china Hong kong also banned the free distribution on plastic bags. Kenya has imposed extra tax on plastic bag and plans to ban ultra-thin plastic bag. Rwanda has banned plastic bags less than 0.1 mm thick, in 2003 South Africa banned the use of plastic bags, Uganda banned plastic bag in 2007 and many other countries impose various forms of bans on plastic bags. [10]. The apathy of using plastic bag will create a big opportunity of seamless jute bags. This bag will not be so cheap like plastic bag but will be cheaper than other alternatives. Jute goods manufacturers in Bangladesh export around 100,000 shopping bags a month on average to different countries. This number will be increased thousands times in near future if we make the shopping bag cheap and attractive.

2.2 Local Market

In Bangladesh, there is significant number of shopping mall, Agro shop, different consumer product retailer shop and chain store. They need of secondary packaging material (various shopping bags, promotional bags, sacks etc) to market their product in local market. These types of shops can be the target customer of seamless jute bag. Bangladesh government has taken

some initiatives for mandatory use of jute in packaging industry. An act name "Mandatory Jute Packaging Act-2010" has been issued. The law went an implementation from January 15 of 2013. [11] The act created a demand of 840 million jute bag for agriculture and non agriculture products. The use of jute in secondary packaging like shopping bags will certainly creates a new arena of jute. If the act is implemented successfully demand of jute bag will be 2,000,000 per day. [12]. Survey report showed that near about 10 million polyethylene bags were used everyday. It was estimated that about 14.1 billion bags were used annually at household levels in Bangladesh. [13]. So if the jute bags are supplied at cheap rate its domestic market demand would be about 10 million pcs per day.

2.3 International Market

The Global consumer packaging market value is $395bn and this value will reach $456bn in 2015.Global packaging market to reach $975 billion by 2018. Global packaging sales are projected to rise by 3% in real terms to $797 billion in 2013 and grow at an annual rate of 4% to 2018, according to a new market report by Smithers Pira. [14]. The global demand for shopping bags is estimated to be 500 billion pieces, worth around $500 billion a year, according to international Jute Study Group (IJSG). [15]. Demand for natural, biodegradable bags will gradually increase as more and more chain shops around the world phase out the use of polythene bags and use bio-friendly natural fiber bags instead. The US, Europe and China would be the biggest markets for shopping bags, once the ban on the use of plastic bags would fully come into force in a few years. [16]. It has been estimated that annual world demand for shopping bags is 500 billion pieces. World famous chain store Wal-Mart, Leading food retailers Tesco, the Co-operative Group, Sainsbury's, Morrison's and the John Lewis-Waitrose partnership are expanding grocery convenience formats. In the UK alone, the grocery market was worth £150.8 billon in 2010, an increase of 3.1 percent from 2009. [17]. In November 2013, the EC proposed an amendment to Directive 94/62/EC that would require MS (member states) to "take measures to achieve a reduction in the consumption of lightweight plastic carrier bags" (with a thickness of less than 50 microns, or 0.05 mm) [18]. So EU can be a large market for Bangladesh. The UAE announced to ban all plastic carrier bags by 2013. Following the decision a market of 9.0 billion pieces of jute shopping bags has been created there. [19]An estimated 99 billion plastic carrier bags were placed on the EU market in 2010 – almost 200 bags for each EU citizen [18]. So it can be told that if we deliver jute bag at bulk production and cheap rate, jute packaging would be a very potential source of foreign currency.

3. Materials and Methods

3.1 Loom

For producing seamless jute bag ordinary dobby or electronic dobby looms may be used. In Bangladesh most jute mills use power loom. For producing decorative weave dobby looms are used while for producing plain or twill tapet looms are used. Automatic looms are very common in cotton weaving but in jute weaving this type of modern looms is yet to be popular. Automatic loom consists of electronic dobby system which is more user friendly and capable of giving high range of figuring capacity. The feasibility of using automatic loom is experimented by Bangladesh Jute Research Institute (BJRI). They are using flexible double rapier loom (PICANOL GTX*Plus*) for producing jute and jute-cotton composite fabric. Picanol GTX*plus* is a versatile machine enabling the weaver to produce a very wide range of fabrics. The GTX*plus* enables operators to obtain good weaving results, even without optimal weaving expertise. The GTX*plus* rapier loom has been specially designed to achieve the best price/performance ratio. The specifications of Picanol GTX*Plus* are as follow:

Name: Picanol GTX*plus.*
Type: Flexible double rapier loom.
Reeded width: 72"
Heald frame capacity: 20
Shedding: Electronic dobby shedding (staubli)
Weft color capacity: 4
Power consumption: 7.5 kw
Machine RPM: 180-190 (theoretically 400)
Weave: any design.
Pattern input system: Digital console board.

3.2 Raw Materials

100% jute yarn in both warp and weft. Various count of yarn can be used for this bag. Although we suggest to use 8 lbs/spyndle yarn. Cotton, jute or Jute and cotton on warp and weft way also be used for producing seamless bag. For making the price cheap we suggest to use jute in both directions. 8 lbs/spyndle jute yarn can be used for manufacturing seamless bag. According to Bangladesh Jute Mills Corporation (BJMC) the price of CB 8 lbs/spyndle is $0.9 USD/kg or 70 Tk/kg.

3.3 Fabric construction

For producing seamless jute bag the following specification can be used
Here,
Ends/inch (EPI) = 16
Picks/ inch (PPI) or shots = 10
Warp count = 8 lbs/spindle
Weft count = 8 lbs/spindle
Fabric width = 70 inch
Total warp: 70x16= 1120

3.4 seamless bag design

The weaving plan along with drawing and lifting plan is given below:

Drawing process: Here we have to use minimum 6 heald frames. Straight draft is used here. The first 4 warp is drawn through initial 6 heald frames consequently. Then the next 2 warp of the repeat is drawn through 1 and 2 heald frame subsequently. (as shown in weaving plan in fig:1). As the total warp of

the full width fabric is 70 inch (1120 ends). Each bag contains 2" plain (28 warp), 15" double layer (210 warp) and again 2" plain (28 warp), so we have to draw 1st 28 warp through 1st 2 heald frames, then 210 warp through next 4 heald frame and again 28 warp through 1st 2 heald frame. In this way total 1000 yarn will be drawn.

Denting: As we are using 8 lbs/spydle jute yarn so 2 in a dent will be used. The reed count will be 14. In this case the reed with will be 68 inch.

Weaving: The pattern input system of PICANOL GTX*Plus* is very much user friendly and fully computerized. The bag will be produced by simply inputting the lifting plan (as shown in fig:1) will produce the bags.

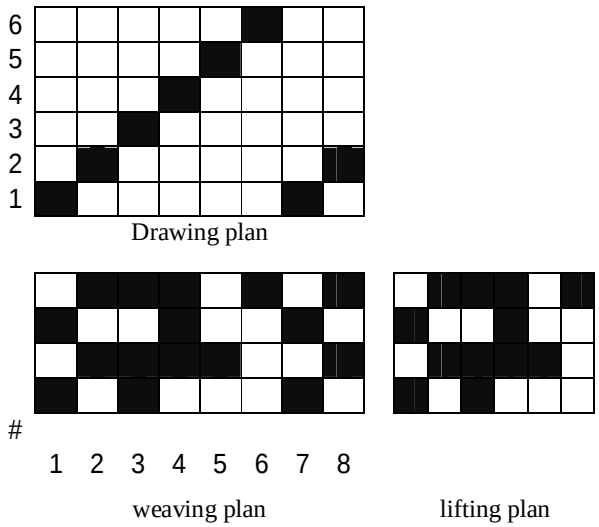

Fig.1 weaving, drawing and lifting plan

3.5 Bag specifications

Length: 19 inch,
Width: 17 inch
Stitched width: 1 inch at both side and bottom
Useable area: 18 inch x15 inch
Useable bag length: 18",
Useable bag width: 15 inch
Total warp / bag= 16x17 = 272,
Bag width: 17 inch
Total weft/ bag = 10x19= 190
Total bag along loom width = 4

Handle making can be possible either automatically or cutting. For automatic handle more 4 heald frame will be needed. For minimizing heald frame number we suggest to use manual cutting.

The 1 inch selvedge will provide sufficient strength from being torn. A simple model of seamless bags is illustrated in the following figure (fig:2). Here the dotted line indicates cutting direction.

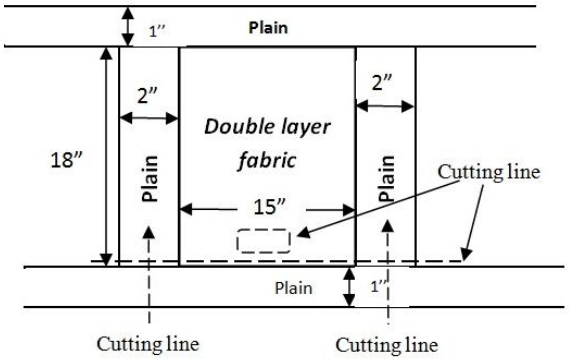

Fig.2 schematic diagram of seamless bag

4. Discussion of Results:

4.1 Production flow chart of ordinary jute bag: the process of conventional jute bag is illustrated below:

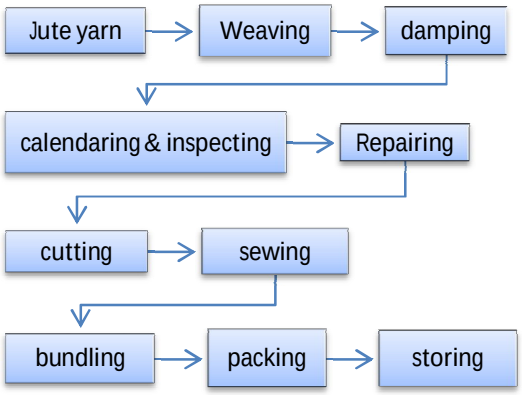

Fig.3 production process of ordinary jute bag [20]

Damping: water is added on the cloth for calendaring and to maintain desired moisture level in the final product.

Calendaring & inspecting : the cloth is pressed and heat is applied for the removal of crease and making the surface smooth and lustrous.

Cutting: the calendared roller is cut into pieces of required sizes to manufactured jute bag.

Sewing : sewing is done to produce bag of definite shape and size by sewing open ends of cut fabric

4.2 Production process of seamless jute bag

The process flow chart of seamless jute bag is as follow:

Warp way cutting: the warp way cutting may be performed either through mechanical cutting or manual cutting. Here 5 cutters are needed to make 4 bags simultaneously.

Weft way cutting: along the weft the fabric should be cut manually. Because this action should be performed after fabric withdrawal.
Handle making: to make a handle for carrying a dice can be used. So that it can be make at minimum effort.
Turing over: to stop the fraying of jute fabric. The bag should be turned over because jute yarn are coarser and very liable to fraying.

The flow process of seamless bag is illustrated below:

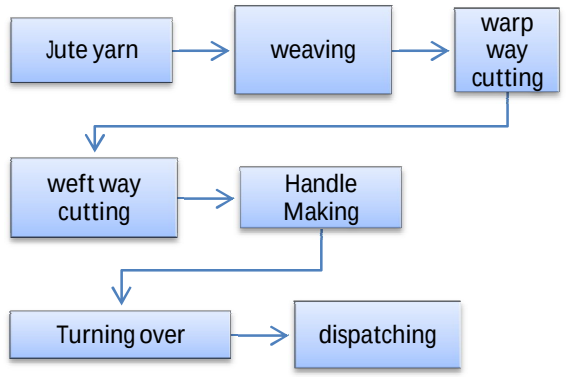

Fig.4 production process of seamless bag

4.3 Comparison:
If the two processes are compared then we see, in seamless bag there are no other processes except cutting whereas in conventional process sewing is needed to make bag along with cutting. So the cost of sewing, sewing yarn, time etc is saved. In the following graph (fig.5) a price comparison is illustrated (the price of seamless jute bag based on assumption) .

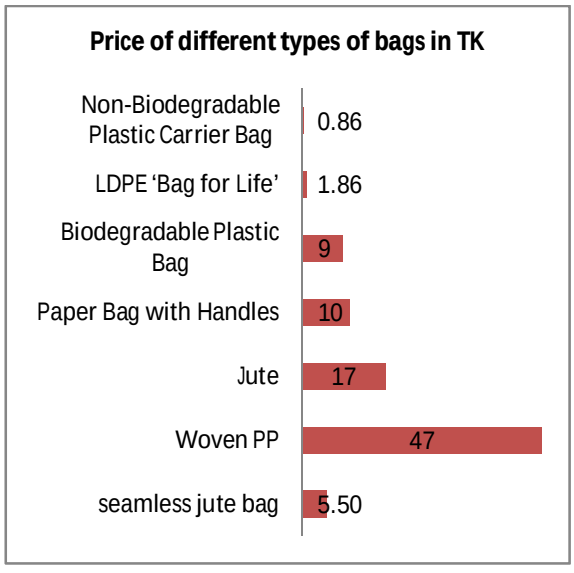

Fig.5 comparative prices of different bags. [21]

4.4 calcualtions

4.4.1 Production calculation

Production calculation formula = $\frac{PPM}{PPI}$ inch/min

= $\frac{PPM \times 60 \times 0.95}{PPI}$ inch/hr [say, machine efficiency is 95%]

= $\frac{190 \times 60 \times 0.95}{10}$ inch/hr

= 1083 inch/hr

= 1083/19 [length of bag = 19 inch]

= 57 × 4 [as 4 bags will be produce across loom width]

= 228 bags/hr

4.4.2 Time consumption

Time required to produce 4 bags simultaneously = $\frac{PPI \times bag\ length"}{PPM}$ min

= (10×19)/190 min

= 1 min

4.4.3 Yarn consumption calculation

Warp yarn consumption=

$\frac{EPI \times width \times \text{lenth} \times count \times crimp\% \times waste\%}{36 \times 14400 \times 2.2046}$ kg

= $\frac{16 \times 17 \times 19 \times 8 \times 1.05 \times 1.06}{36 \times 14400 \times 2.2046}$

= 0.040264 kg

Weft yarn consumption=

$\frac{PPI \times length \times \text{width} \times crimp\% \times waste\%}{36 \times 14400 \times 2.2046}$ kg

= $\frac{10 \times 19 \times 17 \times 8 \times 1.04 \times 1.06}{36 \times 14400 \times 2.2046}$

= 0.0248 kg

Total yarn consumption of a bag = 0.0402+0.0248 = 0.0585 kg

4.4.4 Cost calculation

Raw material cost of a bag = 0.0585 × 0.9 = $ 0.0526
USD = 4.07 BDT
In ordinary jute bag manufacturing, production processing cost is 40-60% of raw materials cost. But as seamless bag has high production and lowest process cost so we may take the weaving charge 30% of raw materials,. So selling price of each bag will be = $0.0526+ $0.0526×0.30= $0.0683 = BDT 5.29 ≈ 5.5 Tk. whereas in present market the price range of a jute bag is 17 Tk- 40 Tk in local market and in foreign market it is about $1.5-$1.7.

4.4.5 Cover factor calculation:

Warp cover, k1= $EPI \times \sqrt{warp count\ in\ lb/spyndle}$

= $16 \times \sqrt{8}$

= 45.25

Weft cover K2 = $PPI \times \sqrt{weft\ cont\ in\ lbs/spyndle}$

= $10 \times \sqrt{8}$

= 28.28

Fabric cover factor = $K_1 + K_2 - \frac{K_1 \times K_2}{120}$

= $45.25 + 28.28 - \frac{45.25 \times 28.28}{120}$

= 73.53 – 10.664

= 63%

Open area = 100-63 = 37%

5. Conclusion:

The present age is the area of consciousness. Each and everybody of this world need to be conscious about the world environment. Especially for Bangladesh because the country has already witnessed two devastating floods of 1998 and 2000 due to polythene bag. Bangladesh is world no. 1 in jute manufacturing; we have a big market in local and international stage. A vast consumer inside the country and different restriction on petroleum derived products throughout the world will make a very big and potential market of seamless bag. So if we utilize this jute in our packaging industry the nation must be benefitted. The proper implementation of seamless jute bag would add a new dimension to this effort.

REFERENCES

[1] **Modern Art Packaging.** History of Shopping Bag. [Online] http://www.shoppingbags.com/history-of-shopping-bags.html.

[2] **Dr. Chris Edwards, Jonna Meyhoff Fry.** *Life Cycle Assessment of Supermarket.* Bristol, United Kingdom : Environment Agency, 2011.

[3] **Nolan-ITU.** *The impacts of degradable plastic bags in Australi, Final Report to Department of the Environment and Heritage.* ExcelPlad Australia : Centre for Design at RMIT, September 2003.

[4] **Hickman, Martin.** *Plastic fantastic!carrier bags 'not eco-villains after all'.* s.l. : Unpublished Environment Agency, 20 February 2011.

[5] **J. Herbert.** (2010, March) http://www.suite101.com/content/the-life-cycle-of-a-plastic-baga214691#.

[6] **Deraik, Jose G.B.** Marine Pollution Bulletin. *The pollution of the marine environment by plastic debris, Marine Pollution Bulletin.* 2002.

[7] **ICC.** tracking trash,25 years of action for the ocean. [Online] 2011. http://act.oveanconservancy.org/pdf/Marine_Debris_2011_Report_OC.pdf.

[8] **IJSG.** Working for the Sustainable Environment. *Internation Juter study Group.* [Online] 8 14, 2014. http://jute.org/sustainable_env.html. *cycle-of-a-plastic-baga214691#.* [Online] March 13, 2010. [Cited: December 30, 2010.]

[9] **CPD.** *GLOBAL MARKET OPPORTUNITIES IN EXPORT OF JUTE.* Dhaka : Centre for Policy Dialogue (CPD), 2011.

[10] **BIO Intelligence Service.** *Assesment of impacts of options to reduce the single-use plastic carrier bags.* s.l. : European Comission-DG Environment, 2011.

[11] **Bangladesh Gazette.** Mandatory Jute Packaging Act2010. *Ministry of Textiles and Jute.* [Online] June 03, 2013.http://www.motj.gov.bd/wp-content/uploads/2014/06/gazatte.pdf.

[12] **Banglinews24.com.** Jute packaging act enacted 4 years back exists only on paper. . [Online] August 2, 2014. [Cited: August 14, 2014.] http://www.bengalinews24.com/english/business-economy-finance-banking-insurance-housing-finance-comerce-export-import-corporate-trade-chamber/2014/08/02/7714.

[13] **Bangladesh Centre of Advance Studies.** *Banning Polyethylene Shopping Bags: .* Dhaka : Bangladesh Centre of Advance Studies.

[14] **PIRA, Smithers.** Global packaging market to reach $975 billion by 2018. *Smithers Pira.* [Online] December 19, 2013. [Cited: August 14, 2014.] https://www.smitherspira.com/market-reports/packaging/news/global-packaging-industry-market-growth-2018.aspx.

[15] **IJSG.** world news. *Internation Juter study Group.* [Online] 8 14, 2014. http://jute.org/sustainable_env.html.

[16] **The daily star.** Bangladesh may lose market in diversified jute products. *The Daily Star.* [Online] November 26, 2013. [Cited: 14 10, 2014.] http://archive.thedailystar.net/beta2/news/bangladesh-may-lose-market-in-diversified-jute-products/.

[17] **Smith, Steve.** Emerging Space. *Online grocery shopping.* [Online] April 14, 2011. [Cited: August 10, 2014.] http://emergingspaces.co.uk/online-grocery-shopping/.

[18] **European parllamentary Research service.** Reducing the use of lightweight plastic carrier bags. *Europarl.* [Online] October 04, 2014. [Cited: August 12, 2014.]

[19] **The Financial Express.** BD fails to capture jute shopping bag market in UAE for scarcity of fabric. *The Financial Expess.* May 05, 2013.

[20] **IJSG.** *Jute Basics.* Dhaka : International Jute Study Group, 2010, 1st edition, pp78.

[21] **Dr. Chris Sherrington, Dr Dominic Hogg, Peter Jones, Brad Doswell, Chris Cullen, George Cole.** *Assistance to the Commission to Complement an Assessment of the Socio- economic Costs and Benefits of Options to Reduce the Use of Single-use Plastic Carrier Bags in the EU.* United Knigdom : European Commission DG Environment under Framework Contract No ENV.C.2/FRA/2011/0020, 2011.

ICMIEE-PI-140238

Heat transfer augmentation of cylinder block by using permeable fin over solid fin by using CFD Analysis

Jaber Al Hossain [1,*], *Kazi Ehsanul Karim* [2], *A. H. M. Fazle Elahi* [3]
[1, 2, 3] Department of Mechanical Engineering,
Khulna University of Engineering & Technology, Khulna-9203, BANGLADESH

ABSTRACT
Engines of two wheeler four stroke vehicle cannot be cooled by water cooling system due to lack of space. In this case efficient air cooling system should be applied for high performance of engine. Permeable fins can be used in engine cylinder to enhance the heat transfer rate. This paper is concerned about an experiment in which a solid annular fin was mounted on a cylinder. The cylinder was filled with water. At a constant temperature (100°C) of water the base & tip temperature of fin was measured and the temperature difference was calculated at different time. A graph of time vs. temperature difference was plotted. In simulation analysis temperature difference of same dimensions solid fin was found & a temp difference vs. time graph was plotted for these results. Both results obtained by experimental & simulation slightly deviated which showed the validity of the simulation work. Now in case of solid fin cylinder temperature difference between base & tip temperature was determined by simulation analysis. Same work was done for permeable fin cylinder. Temperature difference vs. time graph was plotted for both solid & permeable fin cylinder. From this paper it is found that permeable fin is about 10-15% efficient over solid fin. This paper also states that about 3-5% cost will be reduced by using permeable fin instead of solid fin.

Keywords: Permeable fin, heat transfer rate, CFD analysis, cooling system.

1. Introduction

During combustion of the air fuel mixture in the engine cylinder, temperature reaches as high as 6000°F (3316°C) [1]. A part of this heat is absorbed by cylinder wall, head and piston. They, in turn, must be cooled so that their temperature are not excessive. Cylinder wall temp must not increase beyond about 400 or 500°F. That's why engine cooling is necessary. In general, two types of cooling system are used, air cooling and liquid cooling. Air cooling system is mostly used in light vehicle like motor cycle due to lack of space. Air cooled engines have metal fins on the head and cylinder to help radiate the heat from the engine. Fin is an extended surface which is mounted on cylinder block to increase the rate of heat transfer to or from the environment by convection. The heat transfer enhancement can be achieved through some techniques: (1) extending the surface area to volume ratio, (2) enhancing the thermal conductivity of fin by different high conductive material and (3) enhancing the convective heat transfer coefficient between the surface of the fin and the surrounding fluid.

Bassam A/K Abu-Hijleh [2] numerically analyzed heat transfer of solid and permeable fins. They showed that permeable fins offered much higher nusselt number than the solid fins under same operating conditions. They assumed that the fins are made of highly conductive material. Ashok Tukaram Pise [3] investigated the heat transfer of permeable and solid fins by experimental analysis. They modified solid rectangular fins to permeable fins by drilling three holes in line at one half lengths of the fins of two wheeler cylinder block. They tested cylinder blocks having solid and permeable fin for different input. They showed that the heat transfer rate is more in permeable fins as compared to the solid fins. J. Ajay Paul [4] showed in their paper that the difference of heat transfer between 4mm thickness fins and 6mm thickness fins are negligible at zero velocity. They showed that the heat transfer from 6mm thickness fins is higher at high velocities. Mishra A.K. [5] investigated numerical analysis of heat transfer from air cooled engine cylinder fins. They showed that by using copper as fin material greatest effective cooling can be found.

This paper represents a numerical analysis of solid and permeable annular fins. The analysis was done by "Autodesk Simulation CFD 2014". Design and modelling was done by "SolidWorks 2013". The purpose of this analysis is to performance test of permeable fins over solid fins. The parameter of this analysis are heat transfer rate, temperature difference.

2. Experimental setup

2.1 Experimental Setup for Validation Process

The experimental setup consisted a cylinder, a solid annular fin, a 500W heater, a temperature meter and thermocouples. Here inside the cylinder water was used. The cylinder was made of aluminium. The height, outer radius and inner radius of cylinder were 254mm, 38mm, and 35mm respectively. The fin was made of aluminium. The thickness, outer radius and inner radius of fin were 1mm, 139.7mm and 38mm respectively. The fin was mounted on the cylinder by gas welding. The thermocouple wires were attached at tip and base of the fin to measure the fin temperature. Then the thermocouple wires were connected to the temperature meter. The cylinder was filled with water. A 500W heater was inserted into the cylinder to heat the water. A thermometer was inserted inside the cylinder to take the water temperature. Then the heater and temperature

* Corresponding author. Tel.: +88-01680387475
E-mail address: jaber.me2010@gmail.com

meter were connected to power. The fin temp was taken when the temperature inside the cylinder reached at 100°C temperature. After every 10 seconds the fin base and tip temperature were recorded. The experiment were continued for 300 seconds (5 minutes). The experimental setup is shown below in Fig 1.

Fig.1 Photographic view of experimental setup.

For validation of simulation analysis same dimension of cylinder and fin were used and simulation was run at same operating conditions.

2.2 Proposed numerical model

The material used for cylinder was cast iron. The height, outer and inner radius of the cylinder were 254mm, 38mm and 32mm respectively. The material used for solid and permeable fin was aluminium. The radius and thickness of the solid fin was 139.7mm and 6mm respectively. The thickness of permeable fin was 6mm. The dimensions of permeable fin are shown in Fig.2.

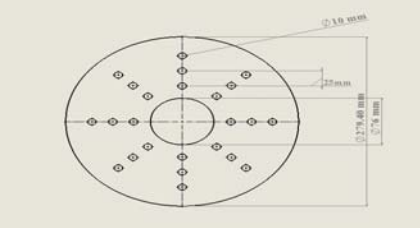

Fig.2 Dimensions of permeable fin.

An external volume was created for these models which was filled with air. The dimensions of external volume are given in Table 1

Table 1 Dimensions of external volume.

Direction/Angle	Value
X-length	0.7395m
Y-length	0.8414m
Z-length	2.2141m
X-offset	0.097m
Y-offset	0.1216m
Z-offset	0.2038m
Pitch angle	0
Yaw angle	0
Roll angle	0

The entire geometry was divided into four regions, (a) water, (b) cylinder, (c) solid or permeable fin and (d) surrounding air. The assemble geometry with external volume is given in Fig.3.

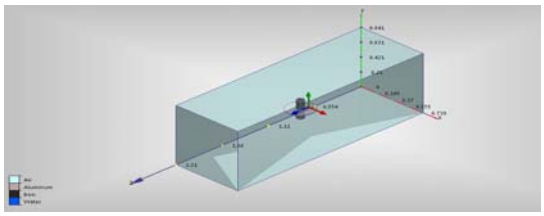

Fig.3 Assemble geometry with external volume.

3. Assumptions

The following assumptions are made for numerical simulation of fin:

a) Steady state heat transfer through the fin.
b) Constant temperature of water inside the cylinder.
c) Incompressible fluid.
d) The radiation heat transfer is neglected.
e) The properties of solid and fluid are constant.
f) The temperature does not vary along the fin thickness.
g) The ambient temperature is considered as 33°C uniformly.

4. Governing equations

The three dimensional heat flow was passed through cylinder and fin. It was simulated by solving the necessary governing equation viz. conservation of mass, momentum equation and energy equation using Autodesk® Simulation CFD 2014 code which is worked by finite element method.

5. Boundary conditions

The ambient temp and pressure were assumed as 33°C and 101325 Pa respectively. Density, specific heat, thermal conductivity and material properties were considered as constant. The temperature of water domain was fixed at 100°C. The inlet velocity of air was 0 km/h. The base and tip temperature of fin were taken after every 10 seconds. The analysis was done for 5 minutes.

6. Meshing and solving the model

For meshing and solving the model Autodesk® Simulation CFD 2014 was used. The meshing parameters used for the final simulation are given in Table 2

Table 2 Parameters for meshing the model.

Meshing Parameter	Setting/Value
Model mesh setting	Automatic
Surface refinement	Enabled
Volume growth rate	1.35
Surface growth rate	1.2
Enhancement growth rate	1.1

Gap refinement	Enabled
Fluid gap element	1
Thin solid elements	0.2
Mesh enhancement	Enabled
Number of layers	3
Layer factor	0.45

The solver settings are given in Table 3

Table 3 Solver settings

Parameter	Setting/Value	
Solution mode	Transient	
Time step size	10	
Inner iteration	5	
Time step to run	30	
Solution control	Intelligent solution control enabled	
Under relaxation factor	Velocity	0.5
	Pressure	0.5
	Temperature	1
	Turbulence	0.5
	Density	0.5
	Eddy viscosity	0.10
Flow	On	
Compressibility	Incompressible	
Heat transfer	On	
Gravity method	Earth	
Gravity direction	0,-1,0	

7. Validation

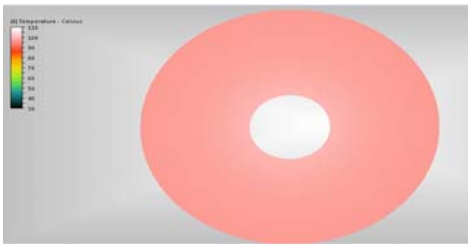

Fig.4 Temperature contour of solid fin at 300 seconds.

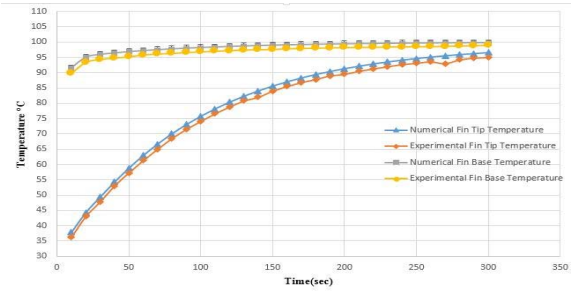

Fig.5 Comparison between experimental and CFD value.

Fig.5 shows the numerical and experimental value of solid fin temperature at tip and base. The deviation of numerical value from experimental value is maximum 5%.

8. Results and Discussions

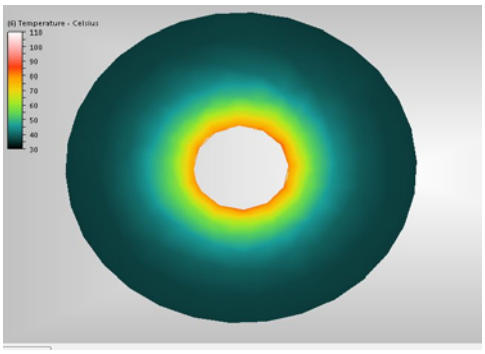

Fig.6 Temperature contour of solid fin at 10 seconds.

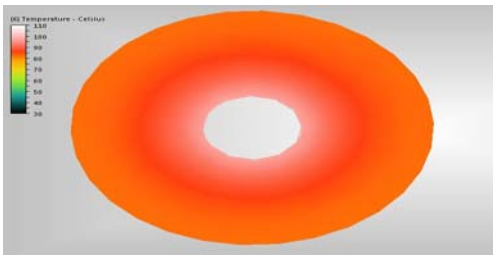

Fig.7 Temperature contour of solid fin at 150 seconds.

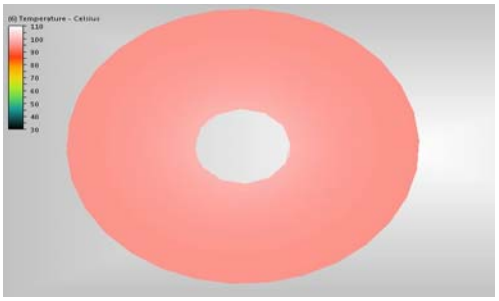

Fig.8 Temperature contour of solid fin at 300 seconds.

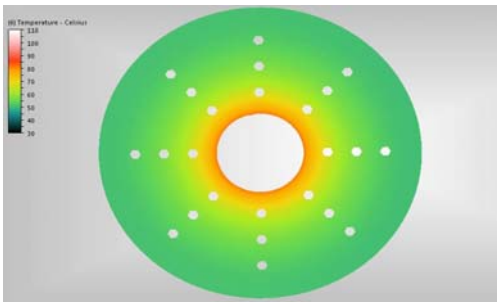

Fig.9 Temperature contour of permeable fin at 10 seconds.

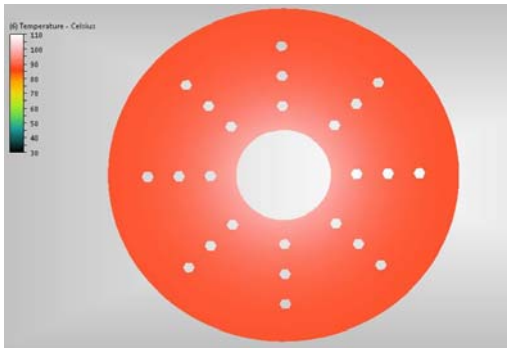

Fig.10 Temperature contour of permeable fin at 150 seconds.

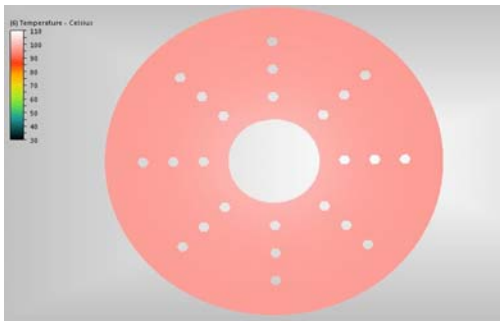

Fig.11 Temperature contour of permeable fin at 300 seconds.

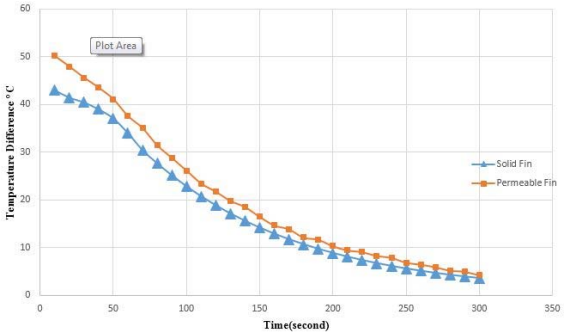

Fig.12 Temperature difference vs. Time for solid and permeable fin.

The temperature contours of solid fin and permeable fin at different time are shown in figures 6, 7, 8, 9, 10, 11.
From figures 6, 7, 8 it can be noted that the temperature of solid fin is increasing with respect to time. From figures 9, 10, 11 it can be appeared that the temperature of permeable fin is increasing faster than solid fin temperature with respect to time.
In Fig.12 a graph of temperature difference (°C) vs. time (sec) is plotted. This graph shows the change of temperature difference between fin tip and fin base with respect to time for solid and permeable fin. It is evident from this graph that in case of permeable fin the temperature difference is higher than solid fin. So it can be easily said from above discussion that the heat transfer rate of permeable fin is higher than solid fin.

8. Conclusion

Thus heat transfer rate of permeable fin is higher than solid fin, it can increase the efficiency of cooling system about 10-15%. There is a reduction of material. By this proposed method about 3-5% material can be eliminated. So there will be a reduction of cost.
One can extend this experiment by changing the geometry of permeable fin, by using different air velocity or by using different high conductive fin material.

REFERENCES

[1] Crouse, William H., Automotive Mechanics, *Tata McGraw-Hill Education*, New Delhi, 10th edition, 2007.

[2] Bassam A/K Abu Hijleh, Enhanced forced convection heat transfer from a cylinder using permeable fins, *Journal of Heat Transfer,* Vol.125, pp 804-811 (2003).

[3] Ashok Tukaram Pise, Investigation of enhancement of natural convection heat transfer from engine cylinder with permeable fins, *International Journal of Mechanical Engineering and Technology*, Vol.1, No. 1, pp 238-247 (2010).

[4] J. Ajay Paul, Experimental and parametric study of extended fins in the optimization of internal combustion engine cooling using CFD, *International Journal of Applied Research in Mechanical Engineering (IJARME),* ISSN: 2231-5950, Vol-2, Issue-1, 2012.

[5] Mishra A.K., Heat transfer augmentation of air cooled internal combustion engine using fins through numerical techniques, *Research Journal of Engineering Sciences*, ISSN 2278-9472, Vol.1(2), 32-40, August (2012).

ICMIEE-PI-140293

Generation of Various Micropattern Using Microlens Projection Photolithography

Md. Nazmul Hasan[1,], Md. Momtazur Rahman[2], and Md. Jahid Hasan[3]*
[1] Department of Mechanical Engineering, National Cheng Kung University, No. 1 university road, 701 Tainan, Taiwan
[2] Department of energy Science & Technology, University of Ulm, Helmholtzstraße 18, 89081 Ulm, Germany
[3] Department of Mechanical Engineering, Khulna University of Engineering & Technology, Khulna-9203, Bangladesh.

ABSTRACT
This paper discuss about review of various process for microlens array fabrication and their application in microlens projection photolithography. Microlens array fabricated by excimer laser machining used in photolithography to produce arrays of microstructures in photoresist. In this technique, the uniform UV illumination is used for exposure and by using a single mask with a single microlens array this system can produce arrays of micropattern in photoresist with a single exposure, which is very useful for mass production. Generated micropatterns can have 3D and uniform image by using a gray-scale mask. Multiple exposure with multiple mask can generate modified and combined pattern on the resist. This technique can generate microstructure with submicron resolution.

Keywords: Microlens array, photolithography, microstructure, excimer laser.

1. Introduction

Now a days, microlens arrays have become important optical elements that play a crucial role in advanced micro-optical devices and systems which is being used in optical data storage, digital display, optical communication and so on. Different technologies have been developed for the fabrication of microlens arrays. Some conventional methods used are listed as photoresist thermal reflow [1], photo thermal method [2], photo-polymer etching [3], micro-jet method [4], and micro-molding or hot embossing method [5]. Although the above-mentioned methods are widely used, the common problem for these methods is that the microlens surface profile is not controlled accurately and unexpected surface roughness is obtained. To fabricate a microlens array with better surface profile and roughness, excimer laser micromachining integrated with a planetary contour scanning method is developed [6]. But the filling factor of arrayed microlenses is limited and it cannot be used in mass production so the efficiency of this method is low. Later, the above method was upgraded into excimer laser dragging method for fabricating varieties of microstructures with arrays based on mask projection and mask/sample movement methods [7], [8]. Common excimer laser KrF (248nm) with wavelength in UV region is used for those machining. The process for material removal by excimer laser is through thermal ablation and/or photo ablation of the materials, i.e. the covalence bonding of the material is broken and vaporized by each laser pulse. The covalence bonding energy of polymer material is relatively low and it has good optical properties so it is suitable for excimer laser micromachining, and hence the photo-ablation mechanism can dominate the material removal [9], [10]. In this method less thermal effect is involved when the laser source can directly break the covalence bonding between polymer molecules, so smooth machined surface can be easily obtained [11].

A simple photolithographic method has been discussed in this paper that uses arrays of microlenses to generate arrays of micropatterns with submicron resolution. Conventional lithographic techniques form a single image for each exposure and require precision optical systems, expensive apparatus, chrome masks & steppers. Microlens array photolithography (MAP) can generate: (1) array of images by a single exposure because each lens forms an image of photomask. (2) simple repetitive features with minimal equipment & inexpensive masks. (3) Image can connect & overlap to generate varieties of pattern. (4) Patterns can have symmetries and periodicities. (5) Pattern size is as small as 500nm. This technique includes collimated flood illumination and masked illumination method which can produce arrays of repetitive micropatterns with shape same as mask pattern. The array of microlenses produce image of bright pattern of the mask and projects an array of size-reduced micropatterns onto the resist layer [12].

2. Experimental setup

Those experiments have been divided into two sections and some subsection:

2.1 Fabrication of plano-convex microlenses array:

In the following subsection some methods have been discussed to fabricate plano convex aspheric microlens array.

(1) Excimer laser planetary contour scanning method:
Excimer laser micromachining with planetary contour scanning method can accurately achieve pre-designed axially symmetrical 3D microstructures. This method based on the concept of machining probability and integration of both rotation and revolution of samples, and hence the machined surface profiles can be very accurate and smooth. The machining system includes a KrF(248nm) excimer laser, optical components for shaping laser beam, a 4-axis servo-controlled stage

* Md. Nazmul Hasan. Tel.: +886-0979211612
E-mail address: nazmul.eng@gmail.com

movement, and a personal computer for system control [6]. The machining pattern depends on the window opening profile in the photo-mask shown in fig.1. Since each single laser pulse removes a certain amount of sample material from object, the machining depth depends on the laser fluence and sample material properties. To fabricate 3D microlens, sample is moved by 4-axis stage system and synchronized with laser pulse firing sequences so that laser energy distributes uniformly on object surface. The machining profile of microlens can be directly observed by zoo lens microscope. Fig.1 shows a photo-mask with a typical window-opening pattern for fabrication of single microlens and fig.2 shows the procedure for fabricating arrays of microlens.

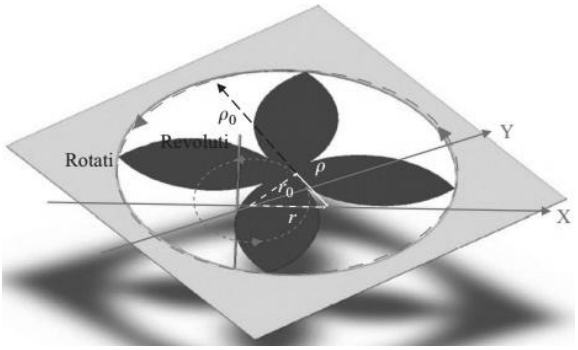

Fig. 1 Excimer laser machining of microlens using planetary contour scanning method [6].

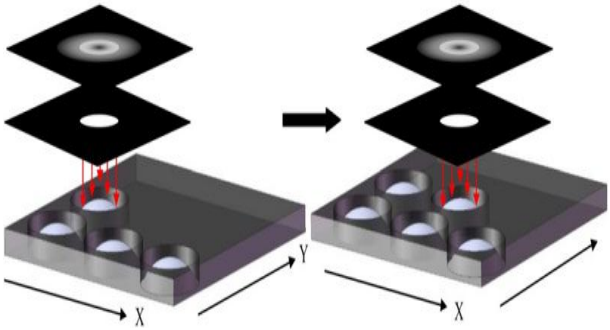

Fig. 2 The steps for fabricating an array of micro-lenses.

(2) Excimer laser dragging method: This method represents an improved excimer laser micromachining method over planetary contour scanning method for fabricating arrayed microstructures with a predesigned surface profile. This method is developed from a conventional biaxial laser dragging method. The excimer laser with stage system used in this method is same as previous method. A contour mask, called binary photo mask with a polynomial designed pattern through which laser light is passed and the pattern is made on the object surface along with a programmed scanning path. So the overall or overlapped laser energy projected on the sample surface has a predesigned spatial distribution. If the scanning paths are just straight lines and one direction only then one can get 2D microstructure. Since contour mask contains periodic patterns so scanning from another direction perpendicular to the first line is superimposed each other to create arrayed 3D microstructures in a very straightforward way known as the excimer laser dragging method [13]. Fig. 3 shows a rectangular array of plano-convex 3D microlens obtained by a contour mask with biaxial (x-y) laser line scanning/dragging method. An array of 10×10 microlenses with aperture sizes of 100μm with pitch 100 μm and a designed aspheric profile are obtained experimentally. The machined surface profiles are closely matched to desired ones with a deviation below 1μm and the average surface roughness around 5nm. The optical performance of the machined microlens array for minimizing the focal spot sizes are measured which approach to optical diffraction limit [11].

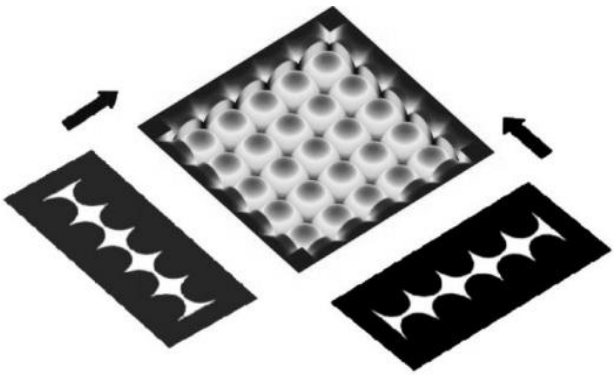

Fig. 3 Excimer laser machining with a contour mask and biaxial laser dragging method for fabricating arrayed microlens [11].

2.2 Microlens Projection Photolithography:
In the following subsections, some experimental setup and methods about microlens projection photolithography have been discussed.

(1) Microlens lithography using collimated illumination: This method depends on the shapes and profiles of the microlens arrays to control the irradiance distribution of the optical micropatterns [12]. It has very simple optical setup which includes a microlens array attach with photoresist by PDMS. The thickness of PDMS maintains the focal length of microlens so that each microlens can make pattern in the image plane. Fig. 4 shows the optical setup for the microlens lithography using collimated illumination. The micropatterns produced by this technique depend on three factors: (i) lenses size, shape and profile, (ii) image distance and (iii) lens refractive index. The patterns produced by this method are uniform over the whole illuminated area. Arrays of uniform micropatterns are generated over areas of 10 cm^2 by a single exposure using microlens array with sizes more than 1μm.

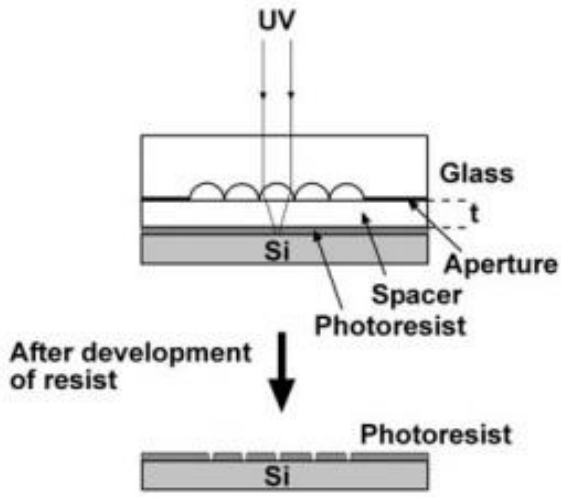

Fig. 4 Arrays of small holes in photoresist are fabricated by collimated flood illumination [12].

(2) Microlens lithography using patterned illumination: This method has simple equipment for optical setup which includes a UV illumination source, a photomask, a microlens array, PDMS for positions microlens array at focal length distance and a photoresist. An overhead transparency projector or a UV lamp is used as a light source for the illumination system or exposure. The mask which is patterned on photoresist is first designed with CAD software and then printed onto a transparency paper using a desktop printer. An optical diffuser such as ground glass is placed in front of the projector to homogenize the illumination. The diffuser scatters the illumination from the light source and produces a uniform illumination. This illumination passes through the clear areas of the transparency mask. The microlenses receive the patterned illumination and project an array of micropatterns on the photoresist surface. Fig. 5 illustrates the optical system for microlens projection photolithography.

The transparency mask was placed on top of the Fresnel lens of the projector which acts as a condenser lens that converge the illumination onto the image plane and generates a bright illuminated area on this plane. The image plane is about 40–60 cm from the Fresnel lens, depending on projector design. The lens array and the photoresist are positioned with PDMS spacer to patterned illumination into image plane. For a resist layer with a thickness of~400nm, the exposure took between 10 s to 5 min. The membrane is removed from the resist after exposure, and the resist is developed in a sodium hydroxide solution. The surface topology of the photoresist is examined with a scanning electron microscope [12].

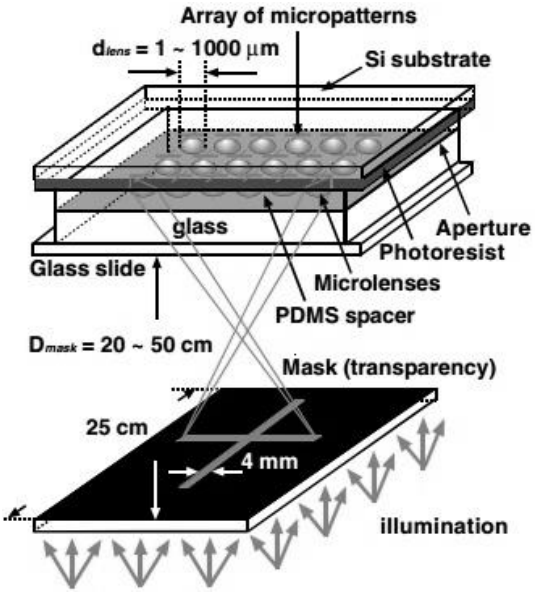

Fig. 5 Optical system for microlens projection lithography with masked illumination [12].

3. Result and discussion

3.1 Micropatterns produced by collimated flood illumination:

Microlens arrays under flood illumination can generate arrays of uniform micropatterns over the entire illuminated area more than $10cm^2$ [14]. The micropatterns shown in fig. 6 are produced by 1.5μm lens array.

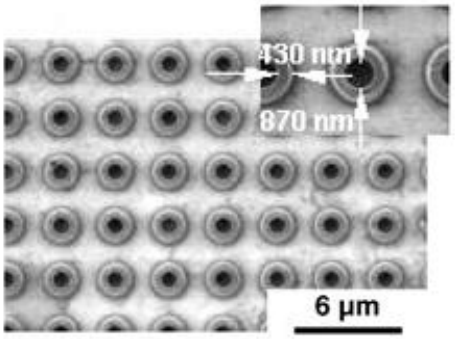

Fig. 6 An array of circular rings produced by 1.5μm microlens array [12].

3.2 Micropattern using arrays of plano-convex microlenses:

Fig. 7(a) and 7(b) illustrate two micropatterns generated by 10μm lens array. Micron and submicron scale patterns can be achieved by arrays of plano-convex microlenses. Demagnification i.e. the size reduction of the mask on photoresist is more than 1000 [12].

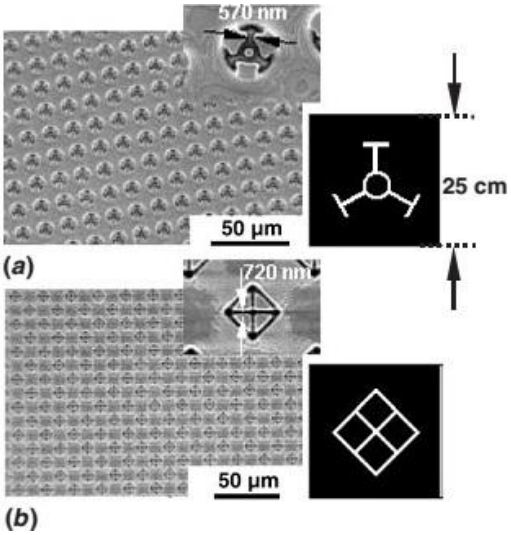

Fig. 7(a) and 7(b) SEM images of those patterns produced by array of 10µm plano-convex microlenses [12].

This technique can also generate arrays of complicated patterns with larger sizes of microlenses. Figures-8(a) and 8(b) show the patterns generated by square arrays of 40µm and 100µm lenses respectively. Fig.8(a) shows high quality micropattern of the logo 'VERITAS' by array of 40µm lenses. The circuit type pattern shown in fig. 8(b) is produced by array of 100µm square lenses. So this method can be applicable in the field of microelectro mechanical systems (MEMS).

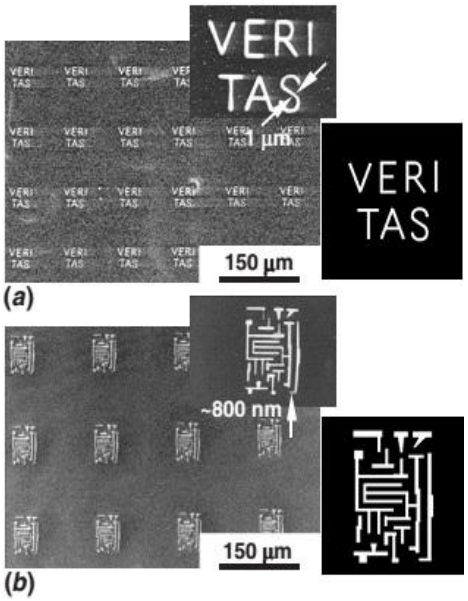

Fig. 8 SEM images of complicated patterns produced by different microlens arrays. (a) By array of 40µm lenses. (b) by arrays of 100µm lenses [12].

By this technique, generated micropattern can be overlapped and rotated with horizontal axis. When the size of cross mask (l) shown in fig.9 is larger than a critical length lc (l>lc=10cm), the reduced micropattern overlapped with each other to form a connected and continuous pattern [15]. Micropattern can be rotated with high-symmetry directions at 27° and 45° and highest periodicity at 27°. Figure 9(a) and 9(b) illustrate separated image and connected image respectively.

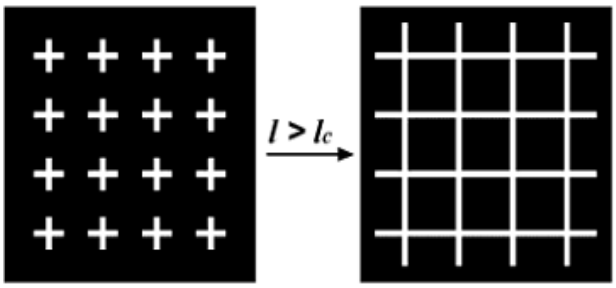

Fig. 9(a) and 9(b) separated and connected pattern produced by array of 100µm plano-convex microlenses [15].

3.3 Micropattern correction with gray-scale masks:

Gray scale mask has two advantages over binary mask: (i) reduce distortion of 2D micropatterns caused by diffraction and proximity effects [16]. (ii) Generate 3D microstructures. The patterns with gray-scale opacity on the binary masks can be printed easily. Figure-10(a) and 10(b) illustrate a comparison of two cross-shaped micropatterns arrays that is generated using a binary mask and gray-scale mask. The image of the cross-shaped micropatterns is not uniform across linewidth which is broaden at centre and tapered at the corner as shown in fig. 10(a). Gray-scale pattern produces an array of crosses with more uniform linewidth is shown in fig.10(b).

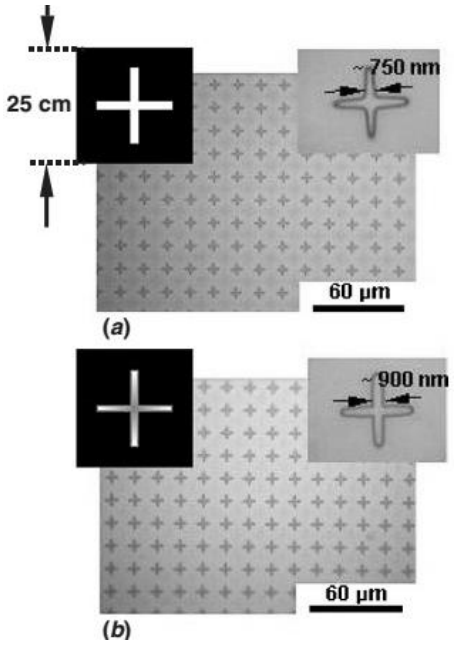

Fig. 10 SEM images of cross-shaped patterns produced by array of 10µm lenses: (a) using a binary mask (b) using a gray-scale mask [12].

3.4 Micropattern using multiple exposures with multiple mask:

Multiple exposures with multiple masks are used to modify microstructures as like as post processing. In this process different mask is used for each exposure without changing the position of lens array and photoresist. The profile of developed resist shows a modified, combined pattern of all the masks. Fig. 11(a) shows an array of hexagonal microstructures produced by gray-scale mask with single exposure. Then another exposure with binary mask that has a binary pattern of a tripole shown in fig. 11(b) generates an array of connected microstructures using two masks with double exposures. But it has a limitation that fine modification of a microstructure can be done only at specific locations.

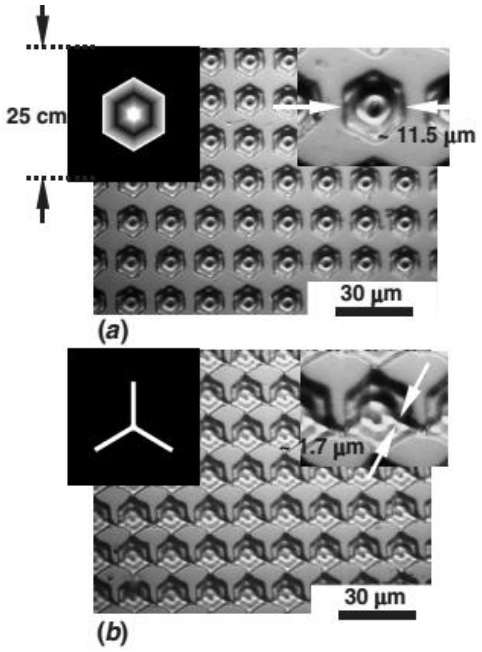

Fig. 11 SEM image of micropatterns using two exposures with two masks. (a) array of hexagonal microstructures using a gray-scale mask. (b) array of connected microstructures generated after second exposure through a binary mask as shown at the corner onto hexagonal microstructures [12].

4. Conclusion

This work demonstrates that a single microlens array can produce varieties of structures by a single mask. Microlens array can be fabricated by planetary contour scanning method. Since it has limitation to fabricate large microlens array so excimer laser dragging method is also presented which can create 100x100 lens array [11]. Various types of microlens projection photolithography technique is also presented which has very simple optical setup, low-cost and microstructure having dimensions from 300nm to more than 10µm. Micropattern fabrication with two types of illumination named as collimated flood illumination and patterned illumination is presented. In result and discussion section SEM image of various fabricated micropatterns such as simple, complicated and connected pattern are illustrated by various figures. Resulted micropattern can be modified by gray scale mask and multiple exposures with multiple masks. This technique will be useful in applications of repetitive microstructures: e.g., frequency-selective surfaces, flat-panel displays, information storage devices, sensor arrays and array based bio-systems.

REFERENCES

[1] Z. D. Popovic, R. A. Sprague, and G. A.Connell, Technique for monolithic fabrication of microlens arrays, *Applied Optics*, 27(7), pp 1281–1284, (1988).

[2] N. F. Borrelli, D. L. Morse, R. H. Bellman, and W. L. Morgan, Photolytic technique for producing microlenses in photosensitive glass, *Applied Optics*, 24(16), pp 2520–2525, (1985).

[3] M. B. Stern and T. R. Jay, Dry etching for coherent refractive microlens array, *International Society of Optics and Photonics*, 33(11), pp 3547–3551, (1994).

[4] D. L. MacFarlane, V.Narayan, J. A. Tatum, W. R. Cox, T.Chen, and D. J. Hayes, Microjet fabrication of microlens array, *IEEE Photonics Technology Letter*, 6(9), pp 1112–1114, (1994).

[5] S. Ziółkowski, I.Frese, H.Kasprzak, and S.Kufner, Contactless embossing of microlenses--a parameter study, *Optical Engineering*, 42(5), pp 1451–1455, (2003).

[6] C. C. Chiu and Y. C. Lee, Fabricating of aspheric micro-lens array by excimer laser micromachining, *Optical and Lasers in Engineering*, 4(9), pp 1232–1237, (2011).

[7] G. P. Behrmann and M. T. Duignan, Excimer laser micromachining for rapid fabrication of diffractive optical elements, *Applied Optics*, 36(20), pp 4666–4674, (1997).

[8] M. C. Gower, Industrial applications of laser micromachining, Optics Express, 7(2), pp 56–67, (2000).

[9] P. E. Dyer and J.Sidhu, Excimer laser ablation and thermal coupling efficiency to polymer films, *Journal of Applied Physics*, 57(4), pp 1420–1422, (1985).

[10] J. H. Brannon, Excimer-laser ablation and etching, *IEEE Circuits and Devices Magazine*, 6(5), pp 18–24, (1990).

[11] Chi-Cheng Chiu and Yung-Chun Lee, Excimer laser micromachining of aspheric microlens arrays based on optimal contour mask design and laser dragging method, *Optics express*, 20(6), pp 5922-5935, (2012).

[12] Wu, Ming-Hsien, and George M. Whitesides. Fabrication of two-dimensional arrays of microlenses and their applications in

photolithography, *Journal of micromechanics and microengineering*, 12(6), pp 747, (2002).
[13] H.Hocheng and K. Y. Wang, Analysis and fabrication of minifeature lamp lens by excimer laser micromachining, *Applid Optics*, 46(29), pp 7184–7189, (2007).
[14] Fujita, Katsumasa, Real-time confocal two-photon fluorescence microscope using a rotating microlens array, *Optical Engineering for Sensing and Nanotechnology (ICOSN'99)*, pp 390-393, (1999).
[15] Wu, Hongkai, Teri W. Odom, and George M. Whitesides. Connectivity of features in microlens array reduction photolithography: generation of various patterns with a single photomask, *Journal of the American Chemical Society*, 124(25), pp 7288-7289, (2002).
[16] Robertson, P. D., F. W. Wise, A. N. Nasr, A. R. Neureuther, and C. H. Ting, Proximity effects and influences of nonuniform illumination in projection lithography, *In Microlithography Conferences*, pp 37-43, (1982).

ICMIEE-PI-140240

Finite Element Analysis of Convective Heat and Mass Transfer Flow through a Channel with Heat Sources and Chemical Reaction Effect

Salma Parvin, Rehena Nasrin and M.A. Alim*
Department of Mathematics, Bangladesh University of Engineering and Technology, Dhaka-1000, Bangladesh

ABSTRACT
Present study performs the heat and mass transfer analysis for laminar double-diffusive mixed convection flow in a parallel plate reactor with four heated cylinders. An external fluid flow enters from the left inlet and exits from the right. After entering the reactor, the fluid passes four heated cylinder. Two-dimensional continuity, momentum, energy and concentration equations govern the developed mathematical model. The governing non-dimensional equations are solved by using Galerkin finite element method with triangular grid discretization system. Numerical simulations are carried out for different combinations of the heat source parameter and results are presented in terms of streamlines, temperature and concentration distributions. The results indicate that the average Nusselt and Sherwood numbers at the heat and contaminant sources strongly depend on the heat source.

Keywords: Double diffusive mixed convection, parallel plate reactor, finite element method.

1. Introduction

Combined heat and mass transfer problems with chemical reaction are of importance in many processes and have, therefore, received a considerable amount attention in recent years. In processes such as drying, evaporation at the surface of a water body, energy transfer in a wet cooling tower and the flow in a desert cooler, in chemical reaction engineering heat and mass transfer occur simultaneously.

Brown and Lai [1] numerically examined combined heat and mass transfer from a horizontal channel with an open cavity heated from below. Since heat and contaminant sources usually co-exist indoors, the present work is to numerically study the double-diffusive mixed convection in a vented cavity due to the discrete heat and contaminant sources. Parvin et al. [2] analyzed numerically the effect of double-diffusive natural convection of a water–Al_2O_3 nanofluid in a partially heated enclosure with Soret and Dufour coefficients. Azad et al. [3] investigated double diffusive mixed convection in an open channel with a circular heater on the bottom wall. They found that, average Nusselt number at the heat source decreases and overall mass transfer rate in terms of average Sherwood number increases with the rising of Lewis number. Muthucumaraswamy and Ganesan [4] studied effect of the chemical reaction and injection on flow characteristics in an unsteady upward motion of an isothermal plate. Das et at. [5] studied the effect of the first order homogeneous chemical reaction on the process of an unsteady flow past an infinite vertical plate with a constant heat and mass transfer. Chamkha [6] studied the MHD flow of a numerical of uniformly stretched vertical permeable surface in the presence of heat generation/absorption and a chemical reaction. He assumed that the plate is embedded in a uniform porous medium and moves with a constant velocity in the flow direction in the presence of a transverse magnetic field. Ibrahim et al. [7] have studied the effect of chemical reaction and radiation absorption on the unsteady MHD free convection flow past a semi infinite vertical permeable moving plate with heat source and suction. Kesavaiah et al [8] have studied the effect of the chemical reaction and radiation absorption on an unsteady MHD convective heat and mass transfer flow past a semi-infinite vertical permeable moving plate embedded in a porous medium with heat source and suction. Heat and mass transport in tubular packed reactors at reacting and non-reacting conditions was analyzed by Koning [9] where the most common models of wall-cooled tubular packed bed reactors were presented. The two dimensional axial plug flow model was used for a water gas shift reactor to compare heat conduction or mass diffusion with convective effect. Kugai [10] studied Heat and Mass Transfer in Fixed-bed Tubular Reactor. The two dimensional axial plug flow model was used for a water gas shift reactor to compare heat conduction or mass diffusion with convective effect in his study.

The objective of the present work is to investigate the effect of heat generation on the characteristics of the flow and heat/contaminant transport mechanism inside a chemical reactor channel in terms of streamlines, isotherms and iso-concentration lines.

2. Analysis

2.1. Physical Model

The domain under analysis is, as sketched in Figure 1(a)-(b), a two-dimensional cross section of a reactor channel of length L and height H with four heated tubes each of radius r, suffering the influence of a gravitational field. The centers of the heaters are located at (L/5, H/2), (2L/5, H/2), (3L/5, H/2) and (4L/5, H/2). The heaters are maintained at constant and uniform temperature T_h and concentration c_h. The air flow is entering from the left with velocity U_i, temperature T_i

* Corresponding author. Tel.: +88-01712085970
E-mail address: E-mail: salpar@math.buet.ac.bd

and concentration c_i, then passes the tubes and then the polluted hot air exhausted from the outlet opening at the right.

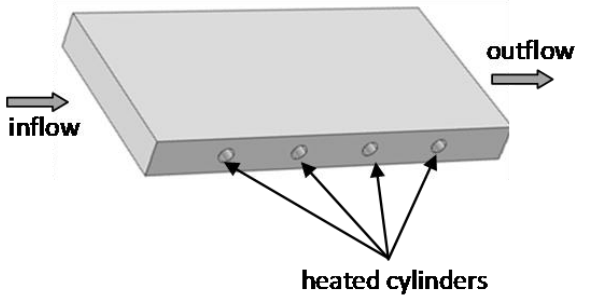

Fig-1(a). 3-D geometry of the considered reactor

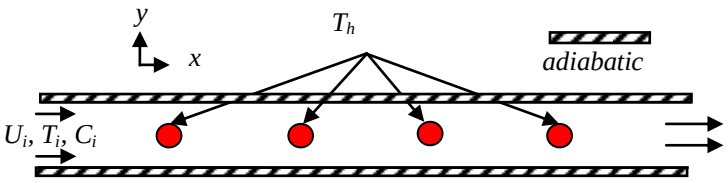

Fig-1(b). Schematic diagram of the problem

2.2. Mathematical Model

The governing mass, momentum, energy and species conservation equations have been presented by Deng et al. [11] for double-diffusive mixed convective flows driven by the combined effect of the internal buoyancy induced from temperature and concentration differences and the external mechanical driven forced flow from the inlet port. With use of the Boussinesq approximation, the dimensionless governing equations under steady-state condition are given by:

$$\frac{\partial U}{\partial X}+\frac{\partial V}{\partial Y}=0$$

$$U\frac{\partial U}{\partial X}+V\frac{\partial U}{\partial Y}=-\frac{\partial P}{\partial X}+\frac{1}{Re}\left(\frac{\partial^2 U}{\partial X^2}+\frac{\partial^2 U}{\partial Y^2}\right)$$

$$U\frac{\partial V}{\partial X}+V\frac{\partial V}{\partial Y}=-\frac{\partial P}{\partial Y}+\frac{1}{Re}\left(\frac{\partial^2 V}{\partial X^2}+\frac{\partial^2 V}{\partial Y^2}\right)+Ri\left(\theta+NC\right)$$

$$U\frac{\partial \theta}{\partial X}+V\frac{\partial \theta}{\partial Y}=\frac{1}{RePr}\left(\frac{\partial^2 \theta}{\partial X^2}+\frac{\partial^2 \theta}{\partial Y^2}\right)-H\theta$$

$$U\frac{\partial C}{\partial X}+V\frac{\partial C}{\partial Y}=\frac{1}{RePrLe}\left(\frac{\partial^2 C}{\partial X^2}+\frac{\partial^2 C}{\partial Y^2}\right)-KC$$

The above equations are non-dimensionalized by using the following dimensionless variables

$$X=\frac{x}{L},\ Y=\frac{y}{L},\ U=\frac{u}{Ui},\ V=\frac{v}{Ui},\ P=\frac{p}{\rho U_i^{\,2}},$$

$$\theta=\frac{T-T_i}{T_h-T_i},\ C=\frac{c-C_i}{\Delta c}$$

and the dimensionless parameters are Reynolds number (*Re*), Grashof number (*Gr*), Richardson number (*Ri*), Prandtl number (*Pr*), Lewis number (*Le*), the buoyancy ratio (*N*) and Chemical reaction parameter (*K*) and they are defined as follows:

$$Re=\frac{U_i L}{\nu},\ Gr=\frac{g\beta_T\left(T_h-T_i\right)L^3}{\nu^2},\ Ri=\frac{Gr}{Re^2},$$

$$Pr=\frac{\nu}{\alpha},\ Le=\frac{\alpha}{D},\ N=\frac{\beta_c\Delta c}{\beta_T\left(T_h-T_i\right)},\ K=\frac{kL^2}{D},$$

$$H=\frac{QL^2}{\alpha}$$

where ν, α, D, k and Q are kinematic viscosity, thermal diffusivity, solutal diffusivity, reaction coefficient and strength of heat generating source respectively. The buoyancy ratio measures the relative importance of solute and thermal diffusion in creating the density difference to drive the flow. It is clear that *N* is zero for pure thermally driven flows and infinity for pure solute driven flows.

The boundary conditions are

at the inlet: $U=1,\ V=\theta=C=0$

at the circular tube walls: $\theta=1,\frac{\partial C}{\partial n}=0$

at other surfaces: $\frac{\partial \theta}{\partial n}=0,\frac{\partial C}{\partial n}=0$

at all solid boundaries: $U=V=0$

The average Nusselt and Sherwood number may be expressed as

$$Nu=-\frac{1}{S}\int_0^S\sqrt{\left(\frac{\partial\theta}{\partial X}\right)^2+\left(\frac{\partial\theta}{\partial Y}\right)^2}\,dS \quad \text{and}$$

$$Sh=-\frac{1}{S}\int_0^S\sqrt{\left(\frac{\partial C}{\partial X}\right)^2+\left(\frac{\partial C}{\partial Y}\right)^2}\,dS$$

where *S* is the non-dimensional length of the heated/contaminant surface.

3. Computational methodology

Galerkin weighted residual method of finite element formulation is used to solve the governing equations for the present work. The application of this technique is well documented by Zienkiewicz and Taylor [12]. The nonlinear parametric solution technique is chosen to solve the governing equations. This approach will result in substantially fast convergence assurance. In addition,

the absolute convergence criteria are set to be 10^{-4} for velocities, energy and concentration.

4. Results and Discussion

The present investigation was carried out for heat generation parameter H (= 0, 1, 5 and 10) with Ri = 1, Re = 100, Pr = 0.7, Le = 1, N = 1, K = 1. Now in the following section, a detailed description of mixed convection with heat and mass transfer in a parallel plate reactor is given in terms of streamline, thermal and concentration contours for different H. In addition, the results for both average Nusselt and average Sherwood numbers at various H will be presented.

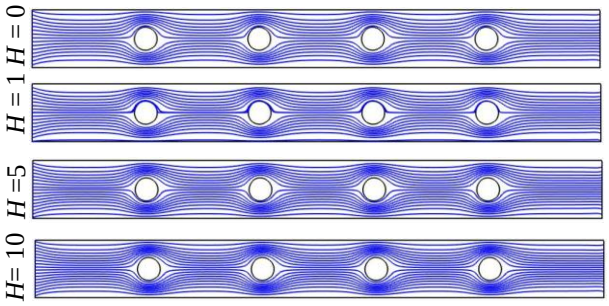

Fig-2. Effect of H on streamlines

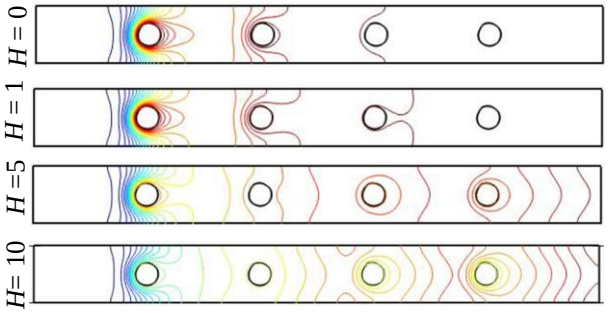

Fig-3. Effect of H on isotherms

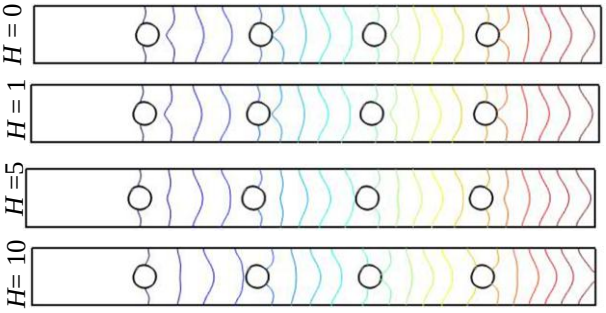

Fig-4. Effect of H on iso-concentrations

Figure 2-4 exhibits the effect of H on the streamlines, isotherms and iso-concentrations. In fact, the analysis is performed at pure mixed convection regime by fixing Ri = 1. The values of heat generation parameter are 0, 1, 5 and 10 are chosen to examine the evolution of streamline, isotherm and concentration patterns.

From Figures 2, it is observed that there is a common trend of the development of streamlines with increasing heat generation parameter. The streamlines are almost parallel to the channel wall and condensed in region between the circular heater and the channel wall. The streamlines become more condensed along the middle of the channel due to increasing heat generation effect. This indicates higher velocity.

As in Figure 3, isothermal lines have significant change due to the variation of H. variation. At H = 0, isothermal lines appear at the inlet portion of the channel. But for higher values of H, these lines spread all over the channel. It is seen from the figure that, at the highest value of H, the lower temperature lines remain at the left potion where as the higher temperature lines at the right exit port. Temperature gradient at the heat source becomes lower for increasing heat generation in the fluid. This happens because higher temperature of the fluid produces lower temperature difference between the heat source and the fluid. It is also clear that the higher temperature gradient exists at the first heater from the inlet and sequentially it reduces for the second, third and fourth.

Iso-concentration lines have also considerable change due to generating heat as shown in Figure 4. Iso-concentration lines spreads all over the channel. As heat generation increases these lines depart to the exit port which indicates higher mass transportation. This phenomenon is logical because heat generation causes higher velocity which leads to more concxentration transfer.

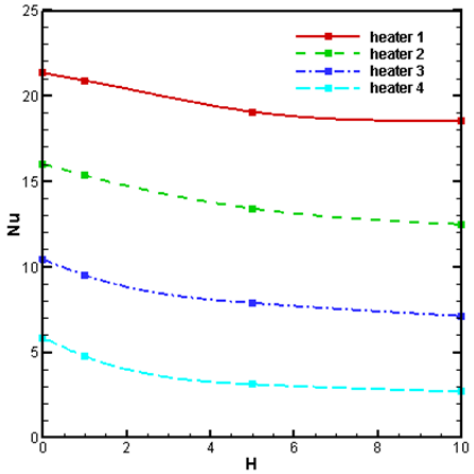

Fig-5. Effect of H on heat transfer

Figure 5 depicts the average heat transfer Nu at the four consecutive heaters for different H. Highest heat transfer rate is observed for the first heater and sequentially these values reduce for second, third and

fourth heater. This phenomenon is very logical because the flow intensity becomes lower for the last heater due to the obstacles. Increasing *H* decreases the value of *Nu* due to lowering the temperature difference

The average mass transfer *Sh* at the inlet port for different heat generation parameter is shown in Figure 6. Enhanced mass transfer rate are observed for increasing the heat generation.

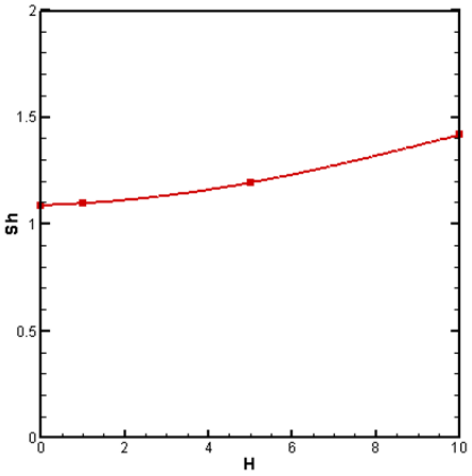

Fig-6. Effect of *H* on mass transfer

5.Conclusion

Laminar double-diffusive mixed convection flow in a parallel plate reactor with four heated cylinders for various heat generations has been studied. The following major conclusions are drawn:

- Increasing *H* has significant effects on flow, temperature and concentrations.
- Lower temperature and higher concentration gradient observe for higher *H*.
- Heat transfer reduces where as mass transfer enhance for rising values of *H*.
- The heater placed near the inlet and outlet gives respectively the highest and lowest heat transfer rate.

In general the effect of heat generation plays an important role in both heat and mass transfer for such type of reactor.

NOMENCLATURE

α : thermal diffusivity
β :expansion coefficient
ν : kinematic viscosity
ρ : density
θ : nondimensional temperature
C : nondimensional concentration
C : concentration
D : mass diffusivity
g : gravitational acceleration
Gr : Grashof number
H : height of the reactor
K : Chemical reaction parameter
L : length of the reactor
Le : Lewis number
N : buoyancy ratio
Nu : average Nusselt number
P : nondimesional pressure
Pr : Prandtl number
Re : Reynolds number
Ri :Richardson number
Sh : average Sherwood number
T : temperature
U,V : nondimensional velocity components
u,v : velocity components
X,Y : nondimensional coordinate
X,y : Cartesian coordinate

REFERENCES

[1] N. Brown and F .Lai, Correlations for combined heat and mass transfer from an open cavity in a horizontal channel, *International Communications in Heat and Mass Transfer*, Vol. 32(8), pp. 1000–1008, (2005).

[2] Salma Parvin, Rehena Nasrin, M.A. Alim, and N.F. Hossain, Double-diffusive natural convection in a partially heated enclosure using a nanofluid, *Heat Transfer—Asian Research*, 41 (6), pp 484-497, (2012).

[3] A.K. Azad, M.J.H. Munshi, M.M. Rahman, Double Diffusive Mixed Convection in a Channel with a Circular Heater , *Procedia Engineering* ,Vol. 56, pp. 157–162, (2013).

[4] R. Muthucumaraswamy, P. Ganesan, Effect of the chemical reaction and injection on flow characteristics in an unsteady upward motion of an isothermal plate, *J. Appl. Mech. Tech. Phys.*, **Vol. 42**, pp. 665-671, (2001).

[5] U.N. Das, R. Deka, V.M. Soundalgekar, Effects of mass transfer on flow past an impulsively started infinite vertical plate with constant heat flux and chemical reaction, *Forschung in Ingenieurwesen*, Vol. **60**, pp. 284-287, (1994).

[6] A.J Chamka, MHD flow of a numerical of uniformly stretched vertical permeable surface in the presence of heat generation/absorption and a chemical reaction. *Int. Comm. Heat and Mass Transf*., Vol. **30**, pp. 413-22, (2003).

[7] F.S. Ibrahim, A.M. Elaiw, A.A. Bakr, Effect of chemical reaction and radiation absorption on the unsteady MHD free convection flow past a semi infinite vertical permeable moving plate with heat source and suction, *Comm. in Nonlinear Sci. and Num. Simul*., Vol.**13**, pp. 1056-1066,(2008).

[8] DC.H. Kesavaiah, P.V. Satyanarayana and S. Venkataramana, Effects of the chemical

reaction and radiation absorption on an unsteady MHD convective heat and mass transfer flow past a semi-infinite vertical permeable moving plate embedded in a porous medium with heat source and suction. *Int.J. of Appl. Math. and Mech.*, Vol. **7**(1), pp. 52-69 (2011).

[9] B. Koning, Heat and mass transport in tubular packed bed reactors at reacting and non-reacting conditions, *Ph.D. Thesis*, University of Twente, Netherland, (2002).

[10] J. Kugai, Heat and mass transfer in fixed-bed tubular reactor, May 1st , (2008).

[11] Q. Deng, J. Zhou, C. Mei and Y. Shen, Fluid, heat and contaminant transport structures of laminar double diffusive mixed convection in a two-dimensional ventilated enclosure, *International Journal of Heat and Mass Transfer*, Vol. 47(24), pp. 5257–5269, (2004).

[12] O. Zienkiewicz and R. Taylor, *The finite element method*, Butterworth-Heinemann, 5th edition, 2000.

ICMIEE-PI-140241

Energy Saving, Low Cost Brick from Rice Husking & Saw Dust Ash

Sabbir Ahmed [1,*], *Fazle Rabbi* [1]
[1] Department of Mechanical Engineering, Rajshahi University of Engineering & Technology, Rajshahi-6204, BANGLADESH

ABSTRACT
The main objective of this thesis is to develop eco-friendly and low cost brick from rice husking and saw dust ash. This brick is eco-friendly because less amount of soil is needed than conventional brick, as well as waste material such as rice husk ash and saw dust ash are also used.
In this method 25% rice husking ash, 10% saw dust ash, 60% soil and 5% binding material such as silica (2%) Portland cement (1%) and lime (2%) were used to prepare the bricks. The bricks were made by mixing all elements properly with water. The mixture was molded. Then molds were dried in the high temperature. In Bangladesh every year almost 12 billion of bricks were made. By applying this process huge amount of soil can be saved .This process reduces not
only soil erosion but also waste disposal volume to make a better world.

Keywords: Light weight brick, Compressive strength, Environmental friendly, Thermal conductivity, Rural-development.

1. Introduction

Energy is one of the main prerequisites to ensure socio-economic development. The availability of energy sources and its proper utilization of energy are the prime concerns for achieving growth and progress in developing countries. Paddy is one of the most important agricultural crops in the world. More than 80 countries in the world produce paddy in large extent. Bangladesh is one of the largest producers of rice in the world. It produces about 28 million tones per year.
During milling of paddy about 78 % of weight is received as rice, broken rice and bran .Rest 22 % of the weight of paddy is received as husk. This husk is used as fuel in the rice mills to generate steam for the parboiling process. This husk contains about 75 % organic volatile matter and the balance 25 % of the weight of this husk is converted into ash during the firing process, is known as rice husk ash (RHA).
So for every 1000 kg's of paddy milled, about 220 kg's (22 %) of husk is produced and when this husk is burnt in the boilers, about 55 kg's (25%) of RHA is generated. Saw dust is also very common element which is usually found in saw mill. 23% of the weight of this saw dust is converted into ash during firing process. Energy saving and eco-friendly bricks from rice husking ash and saw dust ash can be probable solution to reduce these waste. Different ratio of rice husking ash, saw dust ash, lime, soil , sand, cement are used to prepare this eco-friendly brick. But the brick made from 25% rice husking ash, 10% saw dust ash, 60% soil and 5% binding material such as silica (2%) Portland cement (1%) and lime (2%) gives the maximum result.
These two types of ash can easily mix up with air which is very much harmful for environment. These can cause various kinds of diseases. Many researches are going on to reduce this ash content from environment. From the socio economic aspect this bricks are low cost than conventional type of bricks. So, it can be good replacement for tin-shed house.

2. Procedure

The rice husking ash and saw dust ash were perfectly sieved in-order to eliminate coarse particle.
Lime was grinded and sent to the mixture .Sand was sieved before sending to the mixture. Appropriate amount of water was fed to the mixture for prefect mixing. After mixing all materials in proper ratio, materials were unloaded .Brick Block was filled with mixing materials. Then it was kept in room temperature for several days. After removing the blocks desired brick was obtained. Five batches of experiments were carried out with different composition of Rice husk Ash, saw dust ash, lime, Sand, Binder.

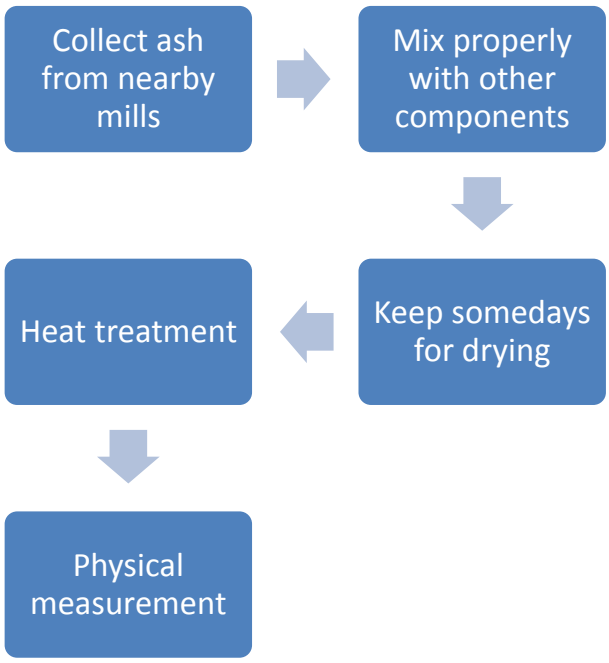

Fig.1 Experimental process

* Corresponding author. Tel.: +88-01755107987
E-mail address: sabbir112048@gmail.com

Calcium Carbonate

Mixture of rice husk &saw dust

Mixture of cement & sand

Ash of rice husk & saw dust

Fig.2 Different Components

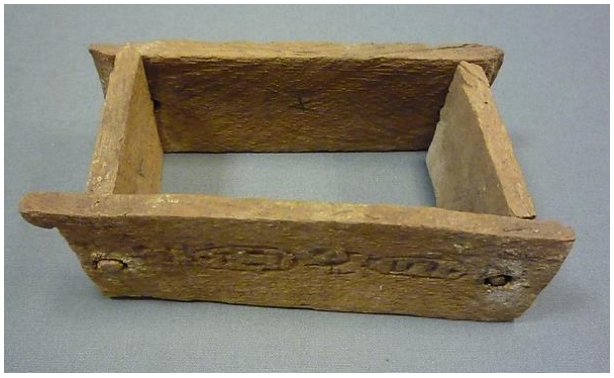

Fig.3 Hand made brick mold

Fig.4 Eco-friendly brick

3. Chemical formula

When Portland cement was mixed up with rice husking ash and saw dust ash it reacts, and improve early age strength of brick and also form calcium silicate hydrate gel around the cement[4].Calcium silicate hydrate formation in also very important to develop the micro structure of the brick.

The pore refinement or densification reduces the permeability of brick and improves the resistance against chloride diffusion into brick. The following reactions take place during the mixing:

Portland cement + H_2O =CSH +$Ca(OH)_2$… … (1)

Portland cement + H_2O + RHA + SDA = CSH + Unreacted silica … … (2)

There are two types of calcium silicate hydrate (CSH) gel which formed during reaction between RHA ,SWA and Portland cement:

$Ca(OH)_2 + SiO_2 = CaO.SiO_2.(H_2O) + CaO.SiO_2.2(H_2O)$

4. Compressive strength

Compressive strength of bricks at different percentage of rice husk ash & saw dust ash is shown in Fig 05 It is evident from Table 1 that the compressive strength of brick so formed increases with increase in rice husk ash content but decreases with the increase in rice husk ash content beyond 6%. Lime reacts with fine pozzolanic component to form calcium-silicate gel with soil particles. The silicate gel proceeds immediately to coat and bind soil particles. In time this gel gradually crystallized into well defined calcium silicate hydrates Such astobermorite and hillebrandite[2]

Table 1 Percentage of different batch material

Component	1st batch	2nd batch	3rd batch	4th batch	5th batch
RHA (%)	30	20	10	5	25
SDA (%)	20	15	20	5	10
Soil(%)	40	50	60	75	60
Lime(%)	5	8	3	10	2
Silica (%)	3	5	4	3	2
Cement (%)	2	2	3	2	1
Compressive strength (N/mm^2)	1.9	2.0	2.2	1.7	2.5

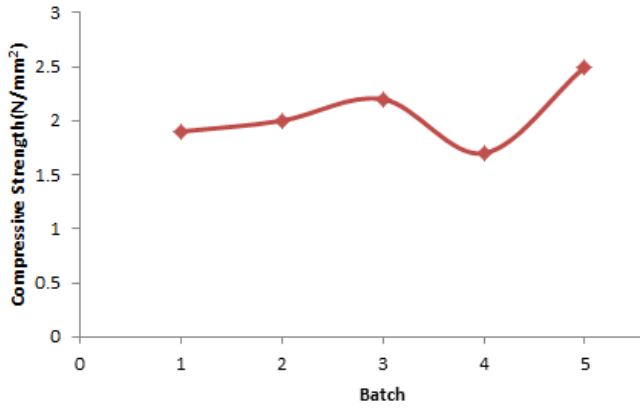

Fig.5 Batch vs Compressive Strength Curve

5. Water absorption capacity

Water absorption capacity is one of the basic requirements of brick. It directly affects the durability of bricks. The more infiltration of water in the brick, the less durable is the brick[1,5]. So, the internal structure of the brick must be intensive enough to prevent the intrusion of water. The water absorption capacity of eco friendly bricks decreases initially with the increasing of ash content up to a certain range. Then it increases with the increasing of ash content. Water absorption capacity of different batches is shown in Table 2 & Fig 6

Table 2 Water absorption capacity for different batches

Batch name	Water absorption capacity (%)
1st batch	27.25
2nd batch	20.75
3rd batch	19.50
4th batch	12.35
5th batch	20.00

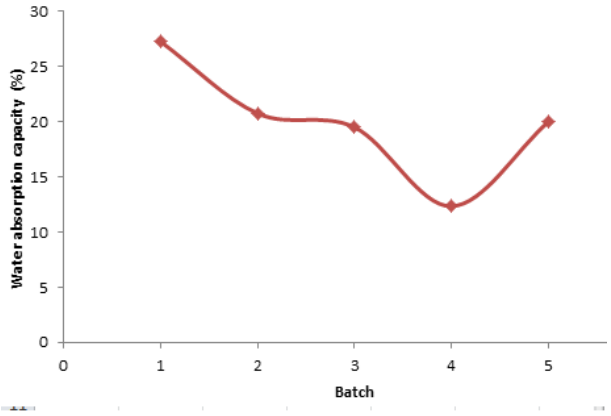

Fig. 6 Batch vs Water Absorption Capacity Curve

6. Density of bricks

Density of bricks is another important factor. The brick which density is low, cannot sustain sufficient load. It is observed, the density of brick decreases with the increases of ash contents[1]. Density of different batches is shown in Table 3 & Fig 7

Table 3 Density for different batches

Batch name	Density (t/m^3)
1st batch	1.05
2nd batch	1.25
3rd batch	1.30
4th batch	1.45
5th batch	1.27

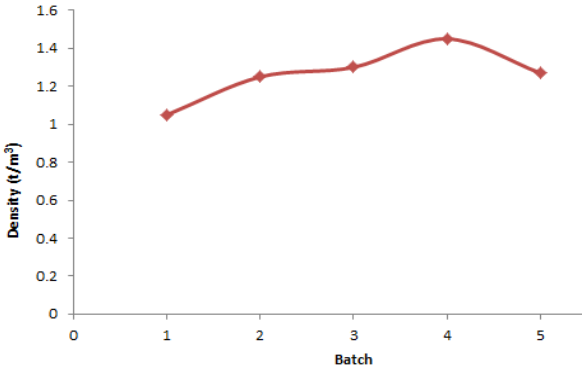

Fig. 7 Batch vs Density Curve

7. Thermal conductivity

Thermal conductivity is a property of material which described the heat conduction ability. We know by lowering the density of concrete, a lower thermal conductivity can be achieved[3]. From the result it is observed the conductivity can be decreased with the increasing ash contents. . Thermal conductivity of different batches is shown in Table 4 & Fig 8

Table 4 Thermal conductivity for different batches

Batch name	Thermal conductivity(W/mK)
1st batch	0.19
2nd batch	0.25
3rd batch	0.27
4th batch	0.35
5th batch	0.23

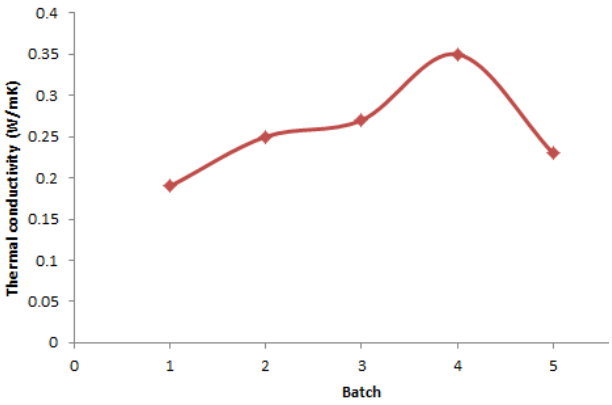

Fig. 8 Batch vs Thermal Conductivity Curve

8. Result analysis and discussions

From the experiment it is observed the compressive strength, thermal conductivity, density vary widely due to the variation of the percentage of ash content. These also depend on binding materials. Rice husk ash reacts with binder and forms calcium silicate hydrate (CSH) gel around the cement particles which is highly dense and less Porous, increase the strength of brick. From the graph we can see that, the compressive strength of batch 5 bricks is almost $2.5*10^{-3}$ KN/mm^2. But the compressive strength of conventional bricks which are usually used to make multi- stroyed building is almost $3.45*10^{-3}$ KN/mm^2[5]. Again due to the increases of the ash contents, the quality of the bricks is decreasing.

9. Conclusion

It is observed that this eco friendly brick is not efficient to be used in multi stroyed building. It can be used to make one stroyed building. The quality of the eco friendly bricks can be improved by varying the percentage of the components. This brick is also light in weight. It can be good replacement of tin shed house. Again these eco-friendly bricks have made these wastes a significant contributor to a holistic approach by the concrete brick industry to the global issue of environmental sustainability.

Acknowledgement

The supports from the Department of Mechanical Engineering&Department of Chemistry of Rajshahi University of Engineering &Technology are gratefully acknowledged.

NOMENCLATURE

RHA: rice husking ash
SDA: saw dust ash

REFERENCES

[1] Dr S. M. Ali Jawaid , Rice Husk Ash - Lime Blended Building Bricks, *International Journal of Earth Sciences and EngineeringISSN 0974-5904*, Vol. 03, No. 02, April 2010, pp. 302-309

[2] N.Vamsi Mohanl Prof. P.V.V.Satyanarayanal Dr. K. Srinivasa Rao, *Performance Of Rice Husk Ash Bricks .Engineering Research and Applications, (IJERA) ISSN: 2248-9622.*

[3] Ling, I. H. and Teo, D.C.L, EPS RHA Concrete Bricks – A New Building Material, *.Jordan Journal of Civil Engineering*, Volume 7, No. 4

[4] Md. Latiful Khabir, Md.Masrul Huda, Dr.Ruhul Amin and Sarker Kamruzzaman, Energy Saving Brick from Rice Husk Ash, *International Conference on Mechanical, Industrial and Materials Engineering 2013 (ICMIME2013)*Paper ID: ET-07

[5] John W. McBurney and Allan R. Eberle, Strength, water absorption, and resistance to freezing and thawing of sand-lime brick, *Part of Journal of Research of the National Bureau of Standards*, Volume 20,January 1938 research paper rp1065.

ICMIEE-PI-140244

Green Lean Approach to Minimize the Environmental Wastes of Cement Industry

Ashma Ahmed[1,*] *,Md. Abdul Quddus*[2]
Department of Industrial Engineering & Management, Khulna University of Engineering & Technology, Khulna-9203, BANGLADESH

ABSTRACT
The objective of this paper is to identify, assess and minimize the environmental wastes produced from processing side of a cement industry using value stream mapping (VSM).The usage of energy, workspace and material and air emission are considered as environmental factors derived from a hierarchy that is developed by EPA. The values of these environmental factors are incorporated in lean metrics and also in VSM which is called Environmental value stream mapping (EVSM). The paper addresses the various environmental wastes or non-value added activities in the processing side of the cement industry, using VSM approach to make the existing process greener. Finally, Future state of the map is drawn with Kaizen opportunities which minimize the environmental wastes.

Keywords: lean, VSM, environmental waste, cement industry, green manufacturing

1. Introduction

In today's competitive world, companies focus on eliminating wastes to increase their profit, growth and ensure customer satisfaction. Lean is a powerful and well-known tool for waste minimization. Products with superior environmental performance attract new customers. That's why organizations must comply with the federal rules and regulations towards environmentally friendly manufacturing. Lean manufacturing provides opportunities for improving the environmental performance along a production line.

Cement industry is one of the fastest growing sectors of Bangladesh. Due to huge local demand cement sector is developing rapidly. Cement industry produces lots of environmental waste. Therefore, it is categorized as red according to Environmental act, 1997. Environmental performance improvement is thus crucial for gaining competitive advantages.

2. Literature review

There are different techniques to measure environmental performance as there is no standard technique available: Green Productivity Index (GPI), Air Pollution Index (API), Ozone depletion Index, Global warming Index [8-10]. Most methods for assessing environmental impacts mentioned are not suitable for a company to implement [2] and lack in integration and assimilation of the traditional waste management approaches with that of the lean manufacturing approach to waste [14]. This is particularly apparent with respect to environmental mapping, as there has been relatively little exploration of Environmental Value Stream Mapping (EVSM).

EPA developed Lean and environment toolkit that draws heavily from the experience of the EPA's partners and organizations who have pioneered integrated approaches to lean and environmental decision making while at the same time delivering world class performance, exerting market leadership, and achieving bottom line results [15].

In this paper, the environmental wastes are identified, assessed and minimized applying a lean tool named Value Stream Mapping (VSM) as it is the simplest, easiest and more convenient and effective to implement in a company.

3. Concept of Lean Manufacturing, VSM and Environmental wastes

Lean manufacturing is a business model and collection of tactical methods that emphasize eliminating non-value added activities (waste) while delivering quality products on time at least cost with greater efficiency. Lean is practiced to eliminate waste, inconsistency and reduce the workload [11].There are seven types of waste in lean production and they are: a) defects, b) overproduction, c) unnecessary inventory, d) inappropriate processing, e) unnecessary motions, f) transport and g)waiting [3]. Five basic principles of lean manufacturing are: defining value, identifying value stream, work flow, pull the work and pursue to perfection [4].

VSM is the simple process of directly observing the flows of information and materials as they now occur, summarizing them visually and then envisioning a future state with much better performance [4]. A VSM gives a pictorial representation of activities, cycle time, lead time, information flow and material flow. Initial step for creating a VSM is to prepare current state map. The immediate step is to analyze the VSM and identify the areas of improvement. The final step is to draw future state map with the improvement ideas along the value stream map [13].

Environmental waste is any unnecessary use of resources or a substance released into the air, water, or land that could harm human health or the environment [5].

4. Objectives of the study

a) Getting an insight on the cement production process for the current state map.
b) To identify environmental factors of the manufacturing system from the hierarchy.

* Corresponding author. Tel.: +88-01731893146
E-mail address:sorna69cutee@gmail.com

c) Measuring environmental factors and incorporating them in a VSM.
d) Analyzing data to identify improvement areas.
e) Drawing future state map with the recommendations.

5. Methodology

The data presented in this paper were obtained from Bashundhara Cement Mills Ltd., Mongla. Data about the process at large were collected over one month from critical observations and conducting interviews. After that, environmental wastes were identified from hierarchy of environmental factors. Current state VSM was drawn based on the data collected. The environmental metrics were incorporated in the VSM which is called environmental value stream mapping (EVSM).Eventually future state map was drawn according to recommendations.

5.1 Hierarchy of environmental factors

The hierarchy of environmental factors in a manufacturing system shown in table1 was developed from a list obtained from EPA. These environmental factors help to document cost-benefits, resource quantities and environmental opportunities which form the basis of improving the environmental performance of an organization. Among the measures, only energy use, material use, workspace use and air emission are considered for incorporating environmental factors in a VSM in this paper.

Environmental measures			
Input measures	Non-product measures	Downstream product measures	Other measures
Energy use Land use Materials use Water use Hazardous materials use	Air emissions Water pollution Solid waste	Product impacts	Money saved Qualitative measures

Table **1** Hierarchy of environmental factors

5.2 Environmental VSM

There are different ways followed by EPA to address environmental values in a VSM:

a) Environmental data in a VSM
b) Comparison of resources needed with usage data.

The study is based on some assumptions:

a) Only Portland Composite Cement (PCC) is produced in the cement industry
b) The collected information and the results are reliable and accurate and were taken from the production activities
c) The top level of the organization was committed to identify the waste of its activities and develop the improvements.
d) The suggestions and improvement are reachable for the industry.
e) Only the material and process flow is analyzed,, information flow is not shown in the map to avoid complications.

6. Current state map

6.1Cement production process

In this case study, cement production means the finish grinding process. Clinker, Gypsum and blast furnace slag are assumed to be used as raw material. No clinker burning and processing is done here. All the raw materials are imported and unloaded at jetty area. Then they are stored in their respective silos and sheds. Production of cement involves following steps:

6.1.1 Grinding

At first processed clinker which is used as the main raw material is ground. Raw clinker is fed from silo through conveyor belt to the VRM feed building. Feed is given in two ways:

a) Main feed system
b) Reject feed system

Then clinker is transported to the Vertical Roller Mill (VRM) mill through enclosed belt conveyor. From the VRM mill, ground clinker is collected by dust collector and then sent to clinker silo for storage. Gypsum and slag is ground in the same way from gypsum shed and slag shed. Then they are also stored in different silos

6.1.2 Mixing

Normally mixing is done in two steps:

a) Ordinary Portland Cement (OPC) mixing: Only clinker and gypsum is mixed in mixing house at 95:5 proportions. OPC is then sent to OPC silos for storage.
b) Portland Composite Cement (PCC) mixing: OPC, slag and other materials (limestone, fly ash, moisture) in very small proportion is mixed to produce Portland Composite Cement (PCC).

Mixing is done in either ball mill or by a screw conveyor.

6.1.3 Packing

After mixing, PCC is stored in silos. Then it is sent to pack house for bagging. The bags are transported for final storage and shipping.

6.2 Process attributes

6.2.1 Blaine number

It is the measure of fineness of the cement particles, expressed in units of cm^2/g [1]. Normally, it ranges from (3000-5000) cm^2/g for Portland cement.

6.2.2 Re-circulation or rework rate

It is the percentage of raw feed mill that is fed back to be ground for obtaining desired fineness of the cement particles. Current state map is shown in fig.1.

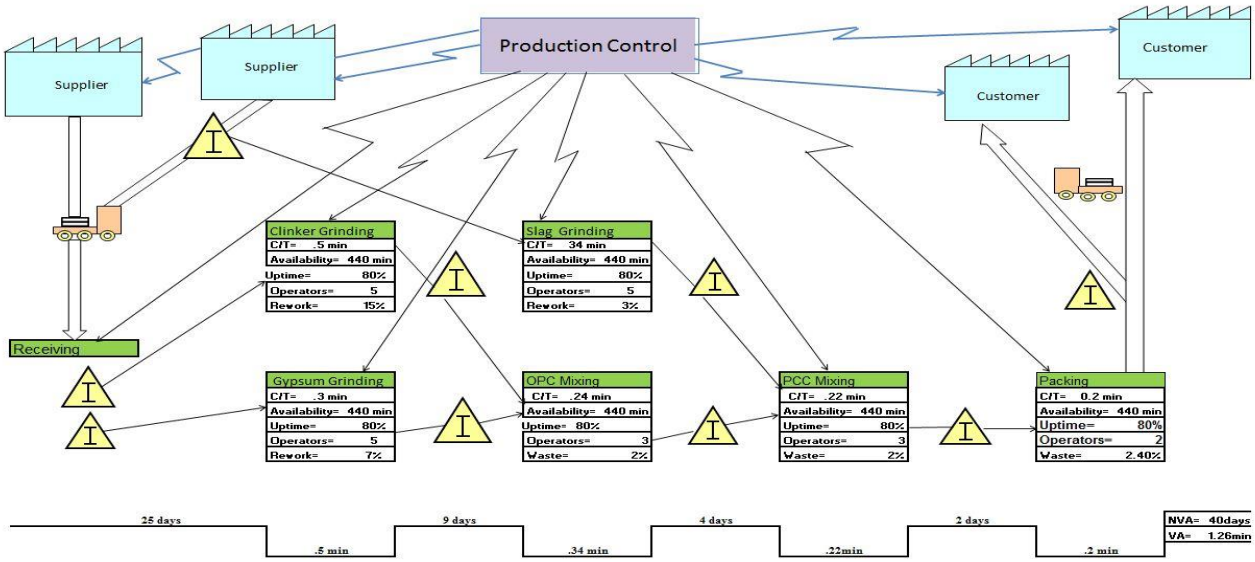

Fig.1 Current state map of the cement industry

6.3 Incorporating Environmental values in VSM

As discussed, the above input measures like energy used, workspace used and materials used and non-product measure like air (dust) emission from the hierarchy shown in figure are utilized for incorporating the environmental factors in a VSM.

6.3.1 Energy use

Assessment of energy use with a VSM helps to identify areas of improvement in environmental performance, safety and productivity and decreasing operating cost of an organization. Measuring energy consumption for each process will identify where excess energy is utilized. Measure energy can be used as a basis for minimizing energy consumption and maximizing energy efficiency for reducing costs and improving environmental quality.

6.3.2 Workspace used

Assessment of workspace use using a VSM gives an opportunity to improve space utilization and reduce energy use in those areas which indirectly reduces environmental impacts. The workspace used for inventory storage is shown below the inventory symbol. The workspace used for a machine is known as value-added workspace and the workspace used for storage of raw materials, inventory, tools and other substances are known as non-value added workspace.

6.3.3 Material use

Assessment of material use with a VSM gives an idea of how much material is used for each process. Material usage can also be minimized by comparing usage data with materials required data. Measurement of material usage gives an idea of how much material is wasted for each and every process.

6.3.4 Air emission

Only SPM emission from each process is considered here. Suspended particulate matter (SPM) refers to particles in the air of all sizes. SPM is a complex mixture of organic substances, present in the atmosphere both as solid particles and liquid droplets. Health impacts of PM vary depending on the size and the concentration of particles.

The incorporation of environmental values in a VSM is shown in fig.2 and summarized in the table 2.

Table 2 Incorporating environmental values in a VSM

Serial no	Process	Energy used in kWh/t		Workspace used in square feet		Material used in ton/day		SPM emission in µg/m3
		VA	NVA	VA	NVA	used	needed	
1	Receiving		0.2		40000			
2	Clinker grinding	50	0.2	24800	23000	7801.92	7224	153.24
3	Gypsum grinding	43	0.2	24800	5000	520	516	114.33
4	BFS grinding	40	0.2	24800	20000	2657.4	2580	94.73
5	OPC mixing	20	0.2	11450	25000			156.13
6	PCC mixing	20	0.2	11450	37000			148.21
7	Packing	15	0.2	10000	40000			288.8

* Corresponding author. Tel.: +88-01731893146
E-mail address:sorna69cutee@gmail.com

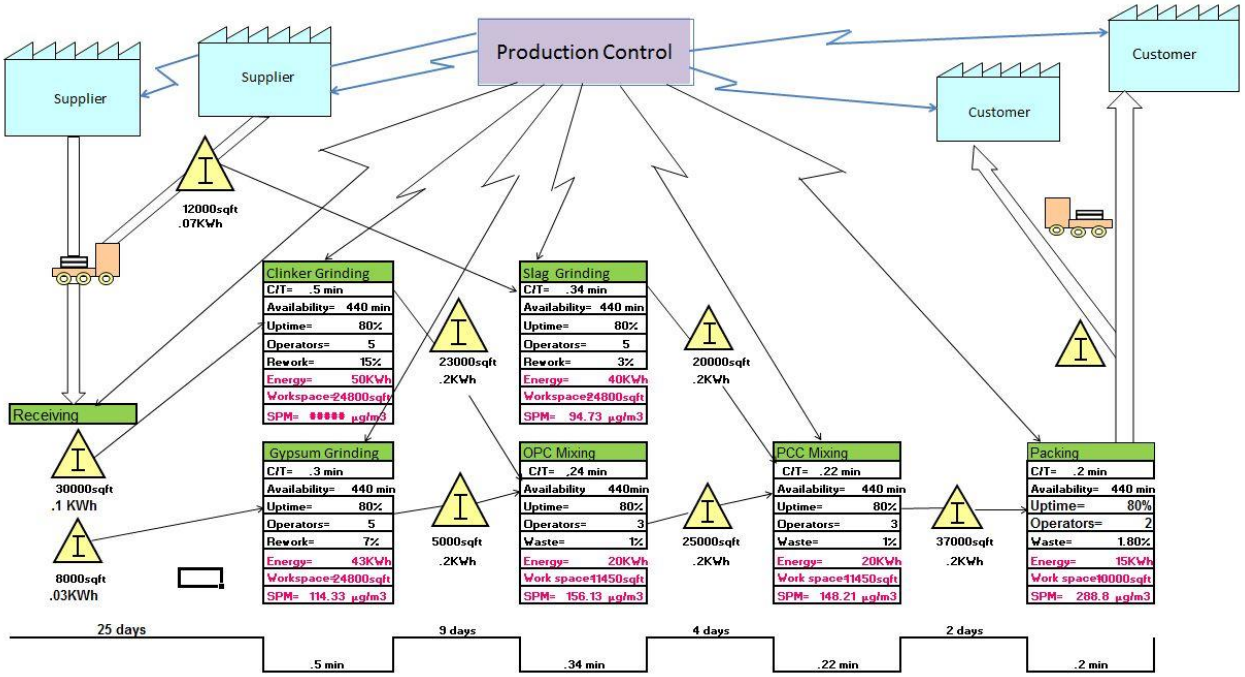

Fig.2: Incorporating environmental values in VSM

7. Future state mapping

Some proposed steps for future state mapping is suggested below. The first step is to reduce variability in blaine number of cement particles and recirculation rate. The higher the blaine number, the better the quality of cement, but it costs high in terms of time and energy as particles are re-circulated to obtain desired number. So, reducing and maintaining a standard range of blaine number results in less time and energy required with standard quality. Second step is to develop pull production system instead of push system with implementing JIT and Kanban production system. The Kanban system is used to inform each company, the production necessity, changing the too each forecast made with enormous forecasts antecedence for each agent. By implementing pull system, Kanban and JIT, overproduction and excess inventory can be reduced.

Suspended Particulate Matter (SPM) is a special concern of cement industry as it is harmful for human beings. Strategies stated below should be incorporated in the production system to control and minimize hazards.

Use of alternative source of energy and clinker substitutes can improve product quality economically and environmentally.

The proposed future state map and data are shown in fig.3 and table 2.

Table 2 Future state data (proposed)

Serial no	Process	Energy used in KWh/t		Workspace used in square feet		Material used in ton/day		SPM emission in µg/m3
		VA	NVA	VA	NVA	used	needed	
1	Receiving		0.2		30000			
2	Clinker grinding	45	0.2	24800	20000	6500	6300	145
3	Gypsum grinding	38	0.2	24800	5000	454	450	114.13
4	BFS grinding	35	0.2	24800	15000	2378	2250	94.73
5	OPC mixing	20	0.2	11450	20000			150
6	PCC mixing	20	0.2	11450	30000			140
7	Packing	15	0.2	10000	30000			180

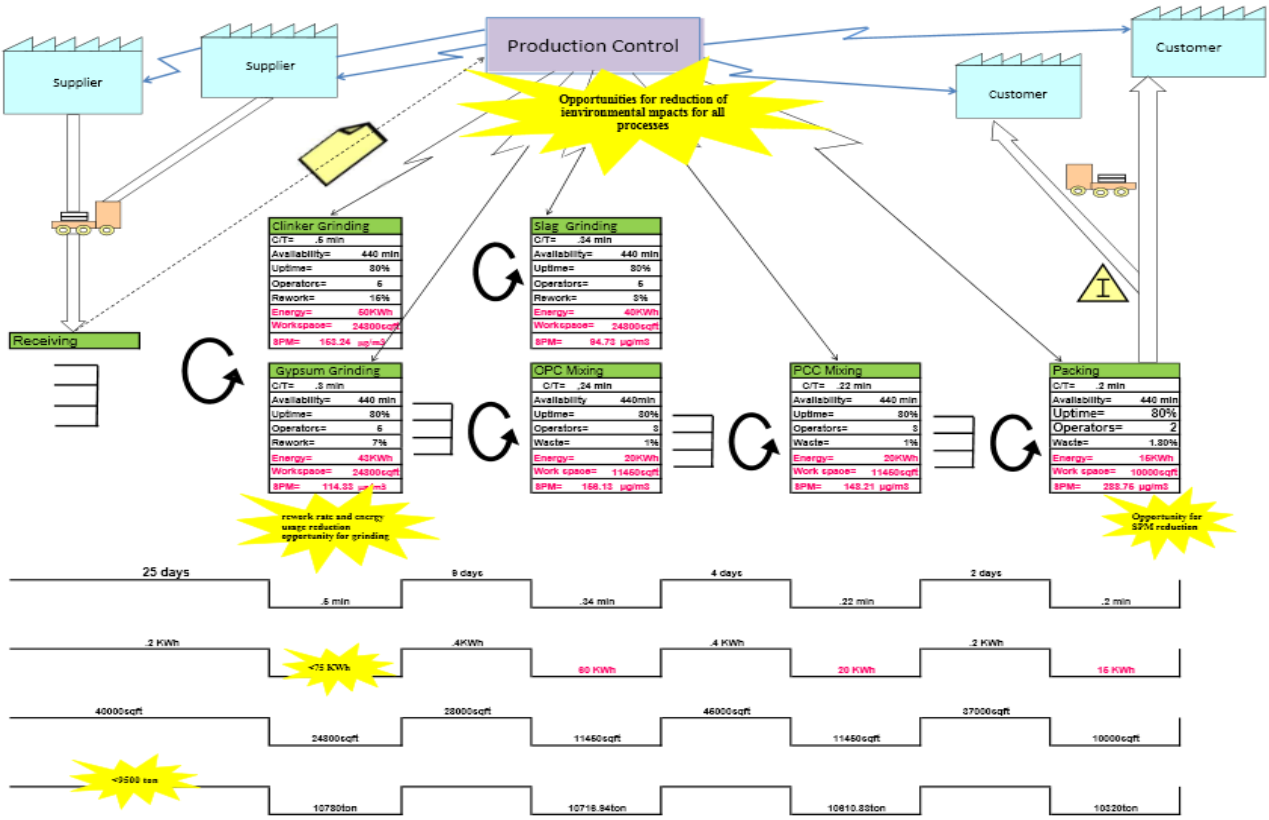

Fig.3 Future state of VSM (proposed)

The energy use can be reduced to 1% non-value added workspace use can be reduced to 20% by implementing JIT, Kanban and pull system. Material usage can be reduced to 1646 ton per day. Waste of materials due to scrap, rework or recirculation, spillage, emissions and other wastes can be reduced from 8% to 3.55%. Also air emission can be reduced specially in packing by adopting proposed measures.

8. Action plans

Following suggestions or recommendations can be applied to improve the current state of the cement industry:

a) Reduction of the variability in blaine number of cement particles.

b) Reduction of recirculation or rework rate of about 50% to reduce energy consumption.

c) Inventory reduction by implementing JIT (Just In Time) methodology.

d) Adoption of pulled production through supermarket.

e) Fostering communication and co-ordination between upstream and downstream of the production process to increase flexibility.

f) Incorporating sufficient safety measures to control and reduce SPM. Environment Management plan for minimizing dust is shown in table 3.

g) Change in facility layout to minimize workspace usage.

h) Adoption of 6S (5S+safety) to create and maintain a clean, orderly, and safe work environment.

i) Use of alternate sources of energy like biofuels, biomass; clinker substitutes such as pozzolans, fly ash [7].

Table 3 Environmental Management Plan for minimizing dust

Srl. no.	Activity/process	location	hazards	Strategies to minimize hazards
1	Transportation	Jetty area, sheds	Dust pollution, landscape and forest degradation	Sprinkle of water, minimum travel of transport, smaller speed limit of vehicles, use of pallets.
2	Grinding	Grinding mill	Dust pollution	Enclosed material handling system, ESP, bag dust collectors, masks for workers.
3	Cement production	Mixing plant	Dust pollution	Enclosed material handling system, ESP, bag dust collectors, mask for workers
4	packing	Packing plant	Dust pollution	Mask for workers

9. Limitations

The study has some limitations:

a) Monetary value of the waste reduction is not calculated.
b) Only SPM is considered as the air emission;PM10, PM2.5 and other particulate matters are not considered.
c) SPM data is collected for processing steps only; air emission due to transportation, vehicles, free flow are not considered.
d) Workspace is not measured in terms of volume other environmental factors from the hierarchy is not assessed.
e) Kaizen events are not considered.

10. Conclusion

It is rightly argued that whenever there is a product for a customer, there is a value stream. The challenge lies in seeing and working on it. VSM can be done in the same way for practically any business activity and expanded upstream or downstream. Cement Industry has a huge potential due to fast rising commercial and residential in Bangladesh. Use of inappropriate methods of processing, scarcity of raw materials and excess inventory is causing production losses and wastes as well as adverse effects in the environment. Minimizing production wastes as well as environmental wastes result in green organization and more customer satisfaction.

With the above action plans being in practice, the cement industry might look into the future with a positive outlook to be greener and of course lean. The future scope of work lies in exploiting other powerful tools of value stream to attack wastes and take appropriate actions to minimize those wastes. The concepts can be replicated for other cement industries to capture various scenarios and attack wastes in processing and distribution chains. Similarly, studies can be used to compare value streams in the context to the country specific situation.

NOMENCLATURE.

VSM : Value Stream Map
EVSM : Environmental Value Stream Map
SPM : Suspended Particulate Matter, µg/m3
kWh : Kilowatt hour
BFS : Blast Furnace Slag
OPC : Ordinary Portland Cement
PCC : Portland Composite Cement
EPA : Environmental Protection Agency
VA : Value added
N-VA : Non-Value Added

REFERENCES

[1] Alain Blasco, Particle size analysis reduces cement manufacturing cost, Engineerlive Magazine, (2013).
[2] Gavindarajulu, A.P., Using a value stream map to assess environmental impacts, Wichita State University, (2009).
[3] Ohno, T., The Toyota production system: beyond large scale production, *productivity press*, Portland, Oregon,(1998)
[4] Womack, K., D. Jones, Lean Thinking, Simon and Schuster, New york,(1996)
[5] U.S. Environmental Protection Agency (EPA), Lean and environment toolkit, Washington, D.C., USA, (2011).
[6] Tourki, T. Implementation of lean within the cement industry, De Montfort University, (2010).
[7] ClimateTechWiki, Clinker substitute, (2011).
[8] Gandhi, N. M., Selladurai, V. and Santhi, P. Green productivity indexing: A practical step towards integrating environmental protection into corporate performance, *International Journal of Productivity and Performance Management*, Vol. 55 Iss: 7, pp.594 – 606, (2006).
[9] Basu, D., Srivastava, R.K.and Vaishya, R.C., An assessment of air pollution impact for an Indian highway project: A GIS based approach, *Management of Environmental Quality: An International Journal*, Vol. 19 Iss: 5, pp.510 – 519, (2008).
[10] Bare, C.J., Norris, G.A., Pennington, D.W. and Mckone, T., The Tool for the Reduction and Assessment of Chemical and Other Environmental Impacts Issue, *Journal of Industrial Ecology*, Volume 6, Iss: 3-4, pp.49–78,(2008).
[11] Wu, Y.C., Lean Manufacturing: a perspective of lean suppliers, *International Journal of Operations and Production Management*, Vol. 23 Iss: 11, pp.1349 – 1376, (2003).
[12] U.S. Department of Energy, 2003. Energy and Emission Reduction Opportunities for the Cement Industry, Washington, D.C., USA.
[13] Braglia, M., Carmignani, G. & Zammori, F., A new value stream mapping approach for complex production systems, *International Journal of Production Research*, Vol. 44, Iss: 18-19,(2006).
[14] Roosen, T.J., Reducing Lean and Environmental Wastes: The Integration of Value Stream Mapping with Environmental Wastes to Improve Production, Performance, Efficiency and Process Flow, University of Canterbury, (2013).
[15] U.S. Environmental Protection Agency (EPA), Best practices and case studies, (2011).

* Corresponding author. Tel.: +88-01731893146
E-mail address:sorna69cutee@gmail.com

ICMIEE-PI-140250

A Review of Properties of Advanced Aerospace Materials

Md. Anisul Islam [1,*], *Istaqur Rahman* [2]
[1] Department of Aeronautical Engineering, Military Institute of Science and Technology, Dhaka-1216, BANGLADESH
[2] Department of Aeronautical Engineering, Military Institute of Science and Technology, Dhaka-1216, BANGLADESH

ABSTRACT
The use of advanced materials has always been a key element in the success of aerospace industry. Aerospace components should have damage tolerance characteristics with high resistance under both static and dynamic loads. To meet the specific requirements, new materials have been necessary to improve and advance aviation. This improvement will come from advances in synthesis/processing of materials. These advanced alloys are more demanding in terms of machinability as their structure and material properties are focused on improved resistance to dwell crack growth, environmental damage and creep strain, as well as higher levels of microstructure stability and high temperature yield stress. Modern machine tools with advanced machining processes are key enablers to achieve overall quality and productivity goals to meet future market requirements. In this paper, properties of advanced materials in general are discussed; specifically advanced materials in aerospace applications.

Keywords: conventional; combine damage tolerance; synthesis.

1. Introduction

Structural materials surround us and serve as the fabric of modern technology. These materials bear stresses and loads in housing, civil works, transportation vehicles and machines. Researchers are continuously working to develop new materials for aerospace applications. Even at the first powered flight, innovation in aerospace materials was present, with the Wright brothers using a 8% copper (by weight) aluminum alloy crank case. The increasing use of lower density materials, such as composites and titanium alloys, has led to an overall reduction in aircraft weight, which in turn gives a reduced fuel burn, increased range and cargo capacity. In recent years, when we think about improvements in materials , the goal is to move to an enhanced trend band as shown in Fig.1.

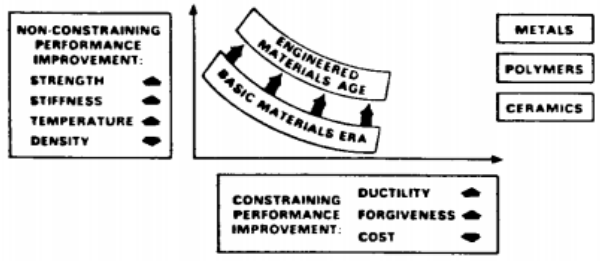

Fig.1 Trend bands exhibited by basic materials and enhanced trend band characteristic of engineered materials. [1]

where it is implied that parameters such as strength, ductility and temperature capability and "forgiveness" (ductility, fracture toughness, fatigue crack growth rate, etc.) should be maximized, while other characteristics such as density and cost should be reduced as far as possible Fig. 2.

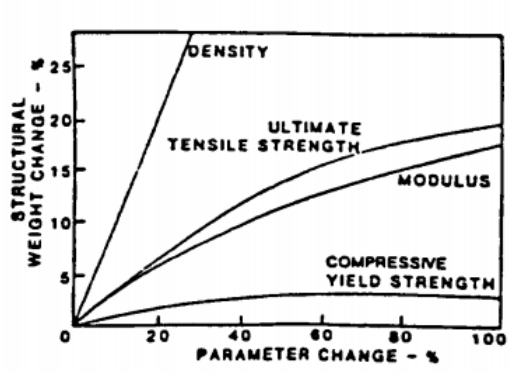

Fig.2 Effect of property improvement on structural weight. [1]

2. Properties of Aluminum Alloy

Aluminum has been the dominant material in the aircraft industry due to its attractive combination of light weight strength, ductility, corrosion resistance, ease of assembly and low cost. The aluminum industry has continued to develop a number of advanced materials of its own rapidly solidified alloys, metal matrix composites and aluminum-lithium alloys. Aluminum lithium alloys show promising property levels, particularly strength and elastic modulus. Aluminum alloys capable of operating at temperatures in the range of 200-300°C can also be produced by rapid solidification. For example, AA2219 alloy exhibits a 170 MPa tensile strength at 260°C. Newly developed RSP alloys, however, offer strengths of about 350 MPa at this temperature, and may remain usable up to 340°C. Most attention has focused on AI-Fe-X compositions such as Coca's CU78 AI-Fe-Ce, Pratt& Whitney's AI-Fe-Mo, and Allied Corp's AI-Fe-Zr-V. The weight savings attainable with these materials are anticipated to be 15% for airframe structures and up to 35% for engine components. Another potential use of RSP is to produce

* Corresponding author. Tel.: +88-01717518131
E-mail address: anisulislam49@gmail.com

light weight, high modulus aluminum alloys containing more than 3 wt. % lithium, as these alloys are difficult to cast by conventional ingot metallurgy methods. RSP AI-3% Li-2%Mg-0.2% Zr and A1-3% Li-2% Cu-0.2%Zr compositions. [2]

3. Properties of Aluminum based Composites

Metal matrix composites (MMC's), in which high strength/elastic modulus materials such as SiC, AI203, B4C, B, etc. are incorporated into aluminum alloys, offer unique combinations of strength, stiffness, wear resistance, and elevated temperature stability. The specific stiffness of aluminum aerospace alloys can be increased approximately 50% by adding 20 wt. % of SiC whiskers. MMC's containing particulate SiC are isotropic and can be tailored to match the expansion contraction Table 1 characteristics of other materials such as beryllium or stainless steel [2] AI-Li alloys containing SiC reinforcement are particularly attractive since they are much stiffer and lighter than conventional aluminum aircraft alloys.

Table 1 Tensile Properties of Aluminum MMC Extrusions. [2]

Material	Thermal Expansion Coefficient ($X10^{-6}/°C$)	Micro-yield Strength (MPa)	Elastic Modulus (GPa)	Density (g/cm^3)
Al 2124-T6 + 30 vol % SiC_p	12.4	117	117	2.91
Al 6061-T6 + 35 vol % SiC_p	12.1	124	131	2.88
Al-2124-T6	23.4	117	72	2.78
Be I-220	11.5	35	303	1.85
Electroless Ni Coating	12.1	-	200	7.75

4. Cryogenic Properties

Al-Li alloys most effectively utilized in certain space applications involving cryogenic environments. Preliminary results show that the yield strength, ultimate tensile strength, fracture toughness and elongation of all improve as the test temperature is reduced. Consequently, the strength toughness combination improves dramatically as temperature decreases, making the material for superior to any aluminum alloy currently used in cryogenic situations. Initial weld ability studies also suggest that with appropriate processing, acceptable post-weld properties can be achieved. AI-H alloys can therefore be seriously considered for applications such as the fuel tanks in the space shuttle, or for the proposed hypersonic and trans-atmospheric vehicles. [3]

5. Properties of Aerospace Super Alloys

Aerospace super alloys, such as nickel base and titanium alloys, Fig. 3 as well as other advanced engineering materials like structural ceramics and tantalum are usually employed in the manufacture of components for aerospace services because of their unique combination of properties like high strength at elevated temperatures, resistance to chemical degradation and wear resistance. The widespread use of jet engine has increased demand for materials that have excellent high temperature mechanical and chemical properties relative to steels and stainless steel alloys originally employed in jet engine applications. Engine efficiency increases and fuel consumption decreases with each increase in temperature. Heat resistant alloys with high melting temperatures are major materials used in the manufacture of aero-engine components. Demand for hotter, more powerful and more efficient engines led to the development of 'super- stainless' alloys, or super alloys. Ability to retain high mechanical and chemical properties at elevated temperatures makes super alloys, ideal materials for use in both rotating and stationary components in the hot end of jet engines. Components produced with super alloys are smaller and lighter than if they were made of conventional steel. About 50% wt. of aero-engine alloys are nickel base alloys [4] they exhibit higher strength to weight ratio, relative to steel that is denser. They are used in these aggressive environments because of their ability to maintain high resistance to corrosion, mechanical and thermal fatigue, mechanical and thermal shock, creep and erosion at elevated temperatures.

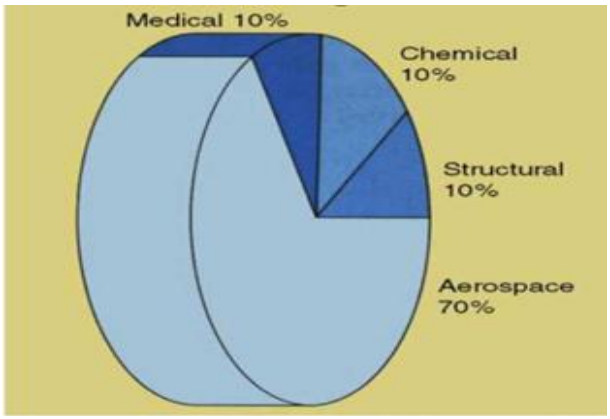

Fig. 3 Super alloy consumption. [4]

Titanium alloys were developed in order to satisfy the need for a class of strong and lightweight materials for aircraft engine and airframe manufacture, because of their outstanding strength to density ratios. They possess exceptional resistance to corrosion, which provide savings on protective coating like paints that will otherwise be used in the case of steel. Titanium alloys can also be used as airframe structure where the operating temperature exceeds 1308°C, the conventional maximum operating temperature or aluminum alloys. In aero-engines, titanium alloys are widely used in both low and high pressure compressors and for components subjected to high centrifugal loads such as disks and blades that have reduced flow diameters as well as for components which operate under severe fatigue conditions.

6. Mechanical Properties of Advanced Aerospace Materials

6.1 Fatigue Strength

High-cycle fatigue testing, to determine the fatigue strength, is always an important part of test programmers on aircraft structural materials. The practical significance of such tests is, however, restricted to notched fatigue, as cracks start at stress concentrations, especially fastener holes. Most of the notched fatigue tests comparing modem AI-Li and conventional alloys show that the AI-Li alloys have similar or better high-cycle fatigue strengths. From this figure the majority of results it may be concluded that the high-cycle notched fatigue strength of AI-Li alloys does not limit their application as replacements for conventional alloys.

6.2 Fracture Toughness and Crack Resistance

Fracture toughness and crack resistance data can be useful in two general ways. First, they may be used to screen and choose between candidate materials for classes of applications. Second, they may be used as design parameters to determine the residual strengths of actual structures, including the important damage tolerance problem of failsafe crack arrest in aircraft stiffened panel structures. Investigation of the fracture toughness's and crack resistances of modem AI-Li alloys has been done mainly for plate and sheet, and to determine whether these properties are at least equivalent to those of conventional alloys. However, as will be discussed below, some attention has been paid to the residual strength of aircraft stiffened panel structures.

6.2.1 Plate Materials

The longitudinal (L-T crack plane) fracture toughness's of modern AI-Li plate alloys generally compare well with those of conventional alloys .However, a contributing factor to the good performance of several AI-Li alloys is through-thickness delamination during fracture toughness testing. This susceptibility to delamination correlates with inters granular fracture and relatively low short transverse fracture toughness, 56'79 which though it may not be specified for a particular application, or class of applications, is traditionally associated with 'inferior metal quality'. Several suggestions have been made to explain low- and variable short transverse fracture toughness's of AI-Li alloys. These suggestions include the presence of brittle grain boundary phases, segregation of the impurity elements sodium and potassium to grain boundaries, segregation of lithium to grain boundaries, and strain localization at grain boundaries. 56'79 Recent work on 8090- T8771 plate indicates that lithium segregation to grain boundaries is mainly responsible for brittle inter granular fracture and low short transverse fracture toughness.

6.2.2 Sheet Materials

Unlike plate materials, the combinations of plane stress fracture toughness, crack resistance and yield strength of modem AI-Li sheet alloys are often inferior to those of equivalent conventional alloys. Fig. 4 & Fig. 5 provide representative 'state-of-the-art' examples, which show the following trends: 1. Damage-tolerant AI-Li alloys, which must be recrystallized, possess high fracture toughness and Ka-curve characteristics comparable with those of the industry-standard damage-tolerant 2024-T3 sheet alloy, but at slightly lower yield strengths. In the medium- and high-strength regimes theA1-Li alloys possess combinations of fracture toughness, KR-curve characteristics and yield strength significantly inferior to those of conventional alloys. In addition, two important phenomena specific to AI-Li alloys have been found. These are fatigue crack plane deviation in 8090-T81 sheet and a change in fracture characteristics depending on whether monotonic crack growth is stable or unstable.

6.3 Effect of Constituents and Dispersions' Morphologies on Fracture Toughness

Fig. 4 shows, Fracture toughness KQ of high purity (H) was higher than that of low purity (L) by about 20%. In order to identify the microstructural parameters, fracture toughness KIC of high purity (H) and low purity (L).

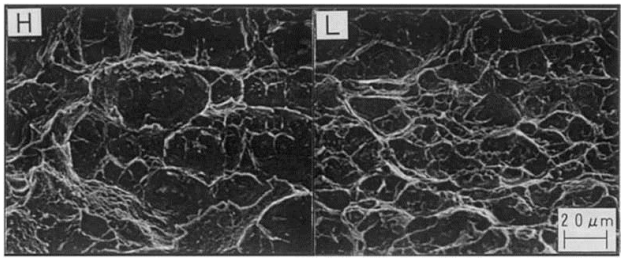

Fig. 4 Fractographs of specimens after fracture toughness test for 2024 aluminum alloys with high purity (H). [5]

After the microstructural and fractographical considerations as mentioned later. There is a linear relationship between the fracture toughness and the square root of the constituent spacing of the materials.

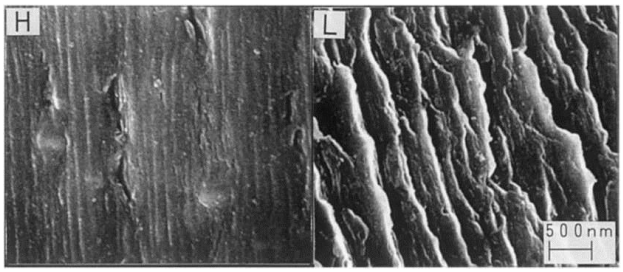

Fig. 5 Fractographs of specimens after fatigue crack propagation test for 2024 aluminum alloys with wide (H) and narrow (L) spacing of dispersoids. [5]

6.5 Other Properties and Considerations

Lightweight construction, consistent with meeting design intent, has become a universal requirement. For all transportation systems but the complexity of current

design and manufacturing methods now requires structural materials to satisfy a much wider variety of properties. This has led to many improvements in materials performance during the past few decades, which are mostly associated with an increase in our understanding of the relationships among composition, processing, microstructure and properties. Fig. 6 presents typical use of Al-Li alloy in various components of Airbus A340 aircraft.

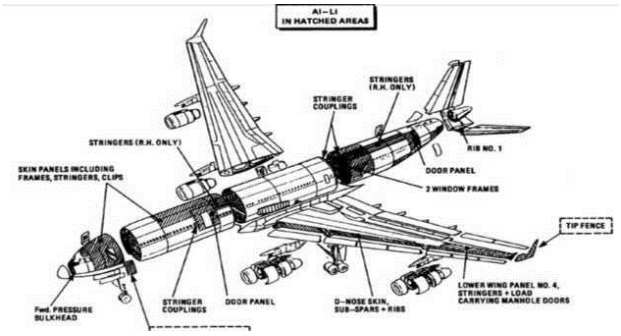

Fig. 6 AI-Li alloy components involved in full-scale fatigue testing of the Airbus A340.

7. Conclusion

Researchers of Advanced Materials and Processing have been actively developing a wide variety of novel, lightweight, high performance, high temperature advanced materials since the 1970s. Most of the 150 patents issued are related to polyimide materials and processes for making them. Some of these materials embody breakthroughs in performance and properties, while the others exhibit unique, one-of-a-kind properties that no other materials can duplicate. Most of these materials can be used as a composite matrix resin, a high temperature adhesive, an advanced coating, a thin film, and a molding article. The rest are better suited for specialized applications, such as atomic oxygen resistant films, thermal/cryogenic insulation foams, cryogenic fuel tanks, and colorless polyimide films. Because of their unique properties, these advanced materials and specialized technologies offer significant advantages for space exploration and other non-aerospace applications.

REFERENCES

[1] F. H. Froes, “Advanced metals for aerospace and automotive use”, Materials Science and Engineering, A 184 (1994) 119-133

[2] Manabu Nakai, Takehiko Eto, 2000,” New aspects of development of high strength aluminum alloys for aerospace applications”,Materials Science and Engineering A285, pp.62-68

[3] R. Arunachalam & M.A. Mannan 2000,” Machinability Of Nickel Based High Temperature Alloys”,Machining Science and Technology, 4:1, 127-168.

[4] Farhad Nabhani, 2001,” Machining of Aerospace Titanium Alloys”, Robotics and Computer Integrated Manufacturing, vol. 17, pp. 99-106.

[5] Heinz A., A. Haszler, C. Keidel, S. Moldenhauer, R. Benedictus and W.S. Miller, 2000,”Recent development in aluminum alloys for aerospace Applications”, Materials Science & Engineering, vol.280 (1), pp.102-107

ICMIEE-PI-140251

Interface Stress Analysis of Two Bonded Isotropic Materials by Finite Difference Method

A. I. Khan , Yeasin Bhuiyan, Abdus Salam Akanda*
Department of Mechanical Engineering, BUET, Dhaka-1000, BANGLADESH

ABSTRACT
Bi-layer composites, such as metal-metal, steel-polymer, concrete-steel etc., having different mechanical properties layer by layer are widely used for modern structures. This paper deals with the stress analysis of two bonded isotropic materials called bi-layer composite materials. Materials under consideration are assumed to be perfectly bonded together. A numerical model (Finite Difference Method) for rectangular geometry based on displacement potential function has been developed to investigate the problem. In each layer of the composite the mechanical properties are isotropic. Finite difference scheme has been developed for the management of boundary conditions so that all possible mixed boundary conditions can be applied in any boundary points as well as at the interface of isotropic layers. Special numerical formulations yield to new formula structures are employed at the interface as well as adjacent boundary points of the interface. An effective programming code has been developed in FORTRAN language to solve the problem of bi-layer composites. In order to compare the results by the present finite difference method, another numerical technique namely finite element method is used. Validation of the results is performed by using commercially available FEM package software. It is observed that the results agree well within the acceptable limit, which also confirms to the reliability of the finite difference method. At the interface, there is a single value for each displacement component but two different values for each stress component of the bi-layer composite having different mechanical properties in each layer. Like as usual critical zone of a bi-layer composite under mechanical loading, the interfacial zone is also a zone of critical stresses. Changing in Poisson's ratio in any layer has significant effects on the results of all layers of the bi-layer composite. Due to the mathematical expressions of stresses and displacements for two dimensional elastic problems, the study of the effects of Poisson's ratio is intricate rather the study of the effects of Modulus of elasticity is straightforward. In general, the material having higher modulus of elasticity experiences higher stresses.

Keywords: Bi-layer composites, displacement potential function, finite difference method.

1. Introduction

Now-a-days composite is a very common word because of its multipurpose application in many industries such as aerospace, automotive, marine, construction etc. The word "composite" means 'consisting of two or more distinct parts'. Composites are formed by combining materials together to form an overall structure that is better than the individual components. The constituent materials have significantly different physical or chemical properties, that when combined, produce a material with characteristics different from the individual components. The individual components remain separate and distinct within the finished structure. In bi-layer composite, there are two materials bonded together having different mechanical properties.

The concept of stress analysis of the bi-layer composite is relatively new. But increasing demand of the bi-layer composite made it very lucrative field for research. Zabulionis [1] performed stress and strain analysis of a bi-layer composite beam under hygrothermal loads considering slip at the interface of the layers. It was solved analytically assuming that load-slip relationships for the interlayer connections are linear and layers' stress and elastic displacement relation is linear. Long et al. [2] predicted the nominal stress-strain curves of a multi-layered composite material by FE Analysis. Sevecek et al. [3] analytically performed stress-strain analysis of the laminates with orthotropic (isotropic) layers using Classical Laminate Theory and compared it with finite element analysis considering the thermal loading. Some other researchers have used finite element technique for stress analysis of some layered materials [4-6]. Problems with various mechanical loadings were not present in these studies.

Later, the displacement potential function approach of the finite difference method had been extended for investigating bond-line stresses of tire tread section by Sankar et al. [7] and determination of the stresses for composite lamina considering directional mechanical properties was performed by Alam et al. [8]. But it was confined into single layer only. Therefore, stress analysis in layer to layer materials as well as at the interfaces is yet to be solved by this approach.

From the above survey it is evident that, the present study of finding state of stress and displacement in bi-layer composite for various mechanical loadings is not only an interesting practical subject, but also of great importance because of its presence in many structural components. Application of finite difference technique based on displacement potential function for the solution of interfacial stress as well as in the body will be a new attempt to extend the capability of displacement potential formulation.

* Corresponding author. Tel.: +88-01672122179
E-mail address: a.islam117@gmail.com

2. Governing Equations

Stress analysis in an elastic body is usually a three dimensional problem. But in most cases, the stress analysis of three-dimensional bodies can easily be treated as two-dimensional problem, because most of the practical problems are often found to conform to the states of plane stress or plane strain. In case of the absence of body forces, the equations governing the three stress components σ_x, σ_y and σ_{xy} under the states of plane stress or plane strain are:

$$\frac{\partial \sigma_x}{\partial x} + \frac{\partial \sigma_{xy}}{\partial y} = 0 \quad (1)$$

$$\frac{\partial \sigma_y}{\partial y} + \frac{\partial \sigma_{xy}}{\partial x} = 0 \quad (2)$$

$$\left(\frac{\partial^2}{\partial x^2} + \frac{\partial^2}{\partial y^2}\right)(\sigma_x + \sigma_y) = 0 \quad (3)$$

In absence of body forces, the equilibrium equations for two dimensional elastic problems in terms of displacements components are as follows

$$\frac{\partial^2 u}{\partial x^2} + \left(\frac{1-\mu}{2}\right)\frac{\partial^2 u}{\partial y^2} + \left(\frac{1+\mu}{2}\right)\frac{\partial^2 v}{\partial x.\partial y} = 0 \quad (4)$$

$$\frac{\partial^2 v}{\partial y^2} + \left(\frac{1-\mu}{2}\right)\frac{\partial^2 v}{\partial x^2} + \left(\frac{1+\mu}{2}\right)\frac{\partial^2 u}{\partial x.\partial y} = 0 \quad (5)$$

These two homogeneous elliptic partial differential equations Eq.(4) and Eq. (5) with the appropriate boundary conditions should be sufficient for the evaluation of the two functions u and v, and the knowledge of these functions over the region concerned will uniquely determine the stress components. Although the above two differential equations are sufficient to solve mixed boundary value elastic problems but in reality it is difficult to solve for two functions simultaneously. So, to overcome this difficulty, investigations are necessary to convert equations (Eq. 4 and 5) into a single equation of a single function.

A new potential function approach involves investigation of the existence of a function defined in terms of the displacement components. In this approach attempt had been made to reduce the problem to the determination of a single variable. Thus the problem is reduced to the determination of a single function $\psi(x,y)$ instead of two functions u and v, simultaneously, satisfying the equilibrium Eq.(4) and (5) [9-10] by defining a potential function $\psi(x,y)$ in terms of displacement components as follows as in the case of Airy's stress function $\varphi(x,y)$ [7],

$$u = \frac{\partial^2 \psi}{\partial x.\partial y} \quad (6)$$

$$v = -\left[\left(\frac{1-\mu}{1+\mu}\right)\frac{\partial^2 \psi}{\partial y^2} + \left(\frac{2}{1+\mu}\right)\frac{\partial^2 \psi}{\partial x^2}\right] \quad (7)$$

With this definition of $\psi(x,y)$, the Eq.(4) is automatically satisfied. Therefore, ψ has only to satisfy the Eq. (5). Thus, the condition that ψ has to satisfy is

$$\frac{\partial^4 \psi}{\partial x^4} + 2\frac{\partial^4 \psi}{\partial x^2.\partial y^2} + \frac{\partial^4 \psi}{\partial y^4} = 0 \quad (8)$$

Therefore, the problem is now formulated in such a fashion that a single function ψ has to be evaluated from bi-harmonic Eq.(8), satisfying the boundary conditions specified at the boundary.

2.1 General Boundary Conditions

In order to solve a problem in terms of potential function ψ of the bi-harmonic equation (Eq. 8), the boundary conditions should be expressed in terms of ψ. The boundary conditions of a problem are known restraints and loadings, that is, known values of components of stresses and displacements at the boundary. The boundary conditions at any point on an arbitrary shaped boundary are known in terms of the normal and tangential components of displacement, u_n and u_t and of stress components σ_n and σ_t. These four components are expressed in terms of u, v, σ_x, σ_y, σ_{xy}, the components of displacement and stress with respect to the reference axes x and y of the body as follows:

$$u_n = u.l + v.m \quad (9)$$

$$u_t = v.l - u.m \quad (10)$$

$$\sigma_n = \sigma_x.l^2 + \sigma_y.m^2 + 2\sigma_{xy}.l.m \quad (11)$$

$$\sigma_t = \sigma_{xy}.(l^2 - m^2) + (\sigma_y - \sigma_x).l\,m \quad (12)$$

Now these above boundary conditions can be expressed in terms of ψ by substituting the following expressions of the components of displacement and stress into Eq.(9) to (12).

$$u = \frac{\partial^2 \psi}{\partial x.\partial y} \quad (13)$$

$$v = -\left[\left(\frac{1-\mu}{1+\mu}\right)\frac{\partial^2 \psi}{\partial y^2} + \left(\frac{2}{1+\mu}\right)\frac{\partial^2 \psi}{\partial x^2}\right] \quad (14)$$

$$\sigma_x = \frac{E}{(1+\mu)^2}\left[\frac{\partial^3 \psi}{\partial x^2 \partial y} - \mu\frac{\partial^3 \psi}{\partial y^3}\right] \quad (15)$$

$$\sigma_y = -\frac{E}{(1+\mu)^2}\left[\frac{\partial^3 \psi}{\partial y^3} + (2+\mu)\frac{\partial^3 \psi}{\partial x^2 \partial y}\right] \quad (16)$$

$$\sigma_{xy} = \frac{E}{(1+\mu)^2}\left[\mu\frac{\partial^3 \psi}{\partial x^2 \partial y} - \frac{\partial^3 \psi}{\partial x^3}\right] \quad (17)$$

From the above expressions it is found that, as far as boundary conditions are concerned, either known restraints or known stresses or combinations of stresses and displacements, all can be converted to finite difference expressions in terms of ψ at the boundary.

2.2 Model Problem and its Boundary Conditions

A model problem is chosen for this study is shown in fig 1(a). It is a bi-layer composite under uniform axial loading. Length =1.5*width i.e. b=1.5*a. The interface lies at a distance of a/2 from the top or bottom edge of the bi-layer composite. The purpose of the paper is to investigate the interface stress and strain i.e. displacements. The modulus of elasticity and Poission's

ratio of the upper material of the bi-layer composite is E_1 and μ, and for lower material is E_2 and μ_2 respectively. The necessary boundary conditions are shown in fig 1(b). The left edge is rigidly fixed that makes $u_n, u_t=0.0$ for $0 \le x \le a$ and $y=0$. The upper and bottom edge is free and obviously $\sigma_n, \sigma_t=0$ for $0 \le y \le b$ and $x=0$ or a. The boundary conditions at the right edge is given in terms of normal and tangential components of stress $\sigma_n=P=2x\ 10^{-4}$ and $\sigma_t=0.0$ for $0 \le x \le a$ and $y=b$. The stress components are normalized by young modulus, E which is the average of E_1 and E_2.

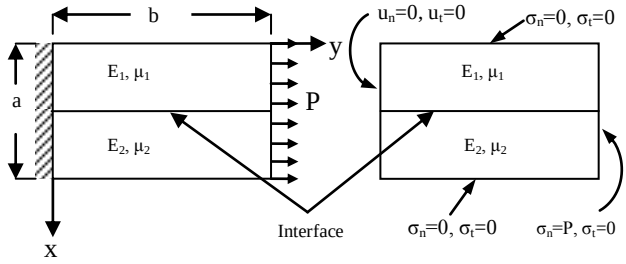

a) b)

Fig.1 a) Axially loaded member and b) Necessary boundary conditions.

3. Solution of the Problem

For the solution of the problem, a two dimensional mesh is generated based on rectangular coordinate system. The function ψ from the governing Eq.(8) is evaluated at various mesh points inside the body using central difference formula. The function ψ from the boundary conditions is evaluated in the same manner by forward and backward difference formula at the boundary points depending on the physical boundary. A FORTRAN code has been developed to investigate various aspect of the problem. The full procedure of the management of boundary conditions has already been discussed in the papers [11-13]. But at the interface of the bi-layer composite the above procedure [11-13] of the management of boundary conditions does not give satisfactory results. In this paper, a new procedure of the management of boundary conditions at the interface has been developed. Among boundary conditions those depend on material properties have to be managed under this new procedure. The displacement component, u has not to be modified by new procedure because it does not depend on material properties Eq.(13). The displacement component, v is dependent on the material properties and continuous over the bi-layer composite. At the interface, two materials are perfectly bonded together, hence the displacement component, v of the common node point is the average of the two displacement components v_1 and v_2 considering through the each side of the material. So, at the left side of the interface it could be written as-

$$v_1)_{i,j} + v_2)_{i,j} = 2v \qquad (18)$$

Stencil of this Eq.(18) is shown in fig. 2.

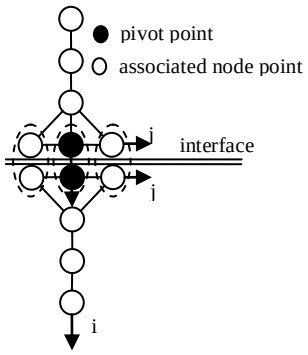

Fig. 2 Stencil of v at the left point of the interface line.

At the interface two points from upper and lower material are actually bonded together in a bi-layer composite. The normal stress acting at the interface boundary point is shown in Fig. 3(a) and shear stress acting at the interface is shown in fig. 3(b).

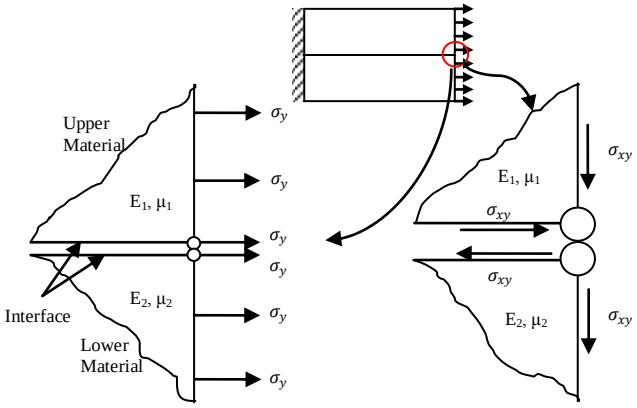

a) Normal stress b) Shear stress

Fig.3 a) Normal stress and b) Shear stress at the interface of bi-layer composite.

The average of normal stresses of upper material and that of lower material should be equal to the applied normal stress at that point. Thus it could be written as-

$$\sigma_{y1})_{i,j} + \sigma_{y2})_{i,j} = 2\sigma_y \qquad (19)$$

By similar fashion, the average shear stress at interface can be written as-

$$\sigma_{xy1})_{i,j} - \sigma_{xy2})_{i,j} = 2\sigma_{xy} \qquad (20)$$

The stencils of the above two Eq.(19) and (20) are shown in Fig. 4. If one needs to apply boundary conditions σ_y and σ_{xy} at the left boundary interface one can easily formulate finite difference equation by taking mirror reflection about a vertical plane through the member. This is also valid for any other boundary conditions. Besides the above modification of stencils of boundary conditions some other modifications near the interface region is necessary for better results. Due to this, several formula structures are derived for

solving the problem of the bi-layer composite. Although the formulae are correct in mathematical point of view but the coefficient matrices of the system of equations become ill-conditioned and provide ill results, thus become unsuccessful formulae. The stencils of boundary conditions which provide the most accurate solution of the problem from the view point of our experience and coincidences with FEM results are shown in fig.5 which signifies that more inclusions of nodal points of interface region provides better results. Here this modification is necessary only for right boundary because of presence boundary conditions σ_y=P and σ_{xy}=0. But, if left boundary is also subjected by same type boundary conditions then it is also necessary to apply this modification at the left boundary. There is no need of modification for boundary conditions u=0 and v=0 because the existing formulae of these boundary conditions includes nodal points of both materials.

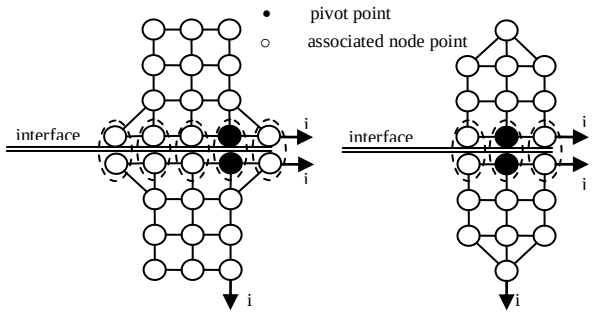

a) b)

Fig.4 Stencil of a) Normal stress and b) Shear stress at right edge of the member.

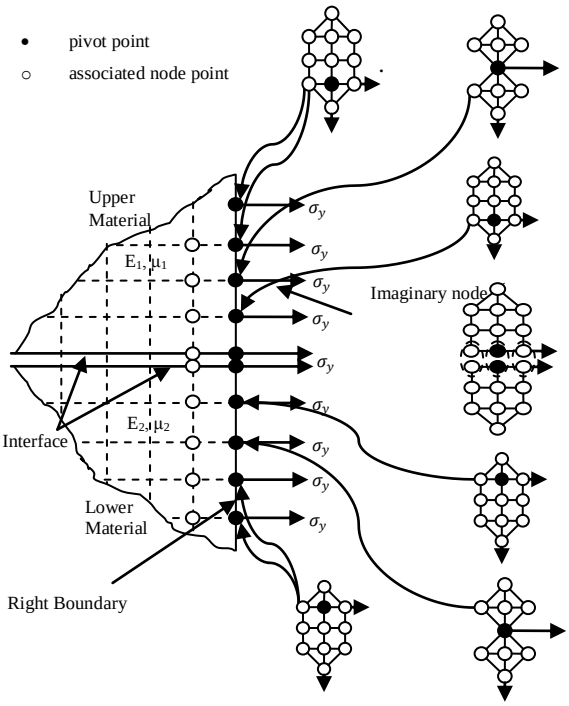

Fig.5 Suitable grid structures of tangential stresses at the adjacent points of the interface.

4. Results and Discussions

Since no analytical solution as well as FDM solution of the problem has not been found, the solution of the problem is represented as a comparison with FEM solution which is obtained by commercial software Ansys v14.0. In this paper only variation in poissons ratio of two materials is taken in account and it is taken as 0.32 and 0.28 for the upper and lower material respectively. The modulus of elasticity is taken as same in both material. Following the procedure stated in previous section and taking the mesh size 0.02 unit, results are obtained by both FEM and FDM methods.

In both FEM and FDM analysis, u and v are continuous over the bilayer composite and there is a single value for each parameter at the interface point. But in case of stresses, there are two values of each stress component one is for upper material and one is for lower material. Although there is a single nodal point at the interface actually it is a perfectly bonded two nodal points i.e. two nodal points from upper and lower material merge together and form a single interface point. By both the method, two values of each stress component are obtained and there is a discontinuity in the distribution of stress at the interface line of the bilayer composite material.

Fig.6 shows the comparison of displacement (v/b) distribution at various sections of the bilayer composite obtained by FDM and FEM analysis. At y/b=0.0, two results are exactly identical as the two lines merge together. At other sections of the material there are very small differences in two results. Near. In FEM results, the variation of the displacement component (v/b) is more likely identical at the upper and lower materials of the bilayer composite although there are different poissons' ratios in upper and lower materials. But in FDM results, there is non-identical displacement component (v/b) at the upper and lower materials. The displacement component (v/b) by FDM is smaller at the upper material (μ_1=0.32) than FEM result and at the lower material (μ_2=0.28), FDM result for displacement component (v/b) is larger than the FEM result. But the variation of the two results is not in significant amount. As there are different poissons' ratios in two materials of the bilayer composite, the FDM results are more logical in that sense.

The distribution of σ_{xy} as shown in fig.7 matches up with each other by FDM and FEM method in different sections of the bilayer except at the top and bottom boundary points of section at y/b=0.0. Actually, the upper corner point could be considered at the both top and left boundary. Similarly, the lower corner point could be considered at the both bottom and left boundary. If top boundary condition is applied at the upper corner point, there is mismatch in results of boundary point by FDM and FEM. In FDM, there is provision to apply either of the two boundary conditions

at the corner points. If left boundary conditions are applied at the upper and lower corner points, the FDM result becomes consistent with the FEM result as shown in fig.8.

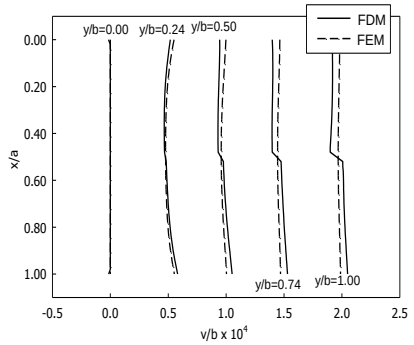

Fig.6 Comparison of displacement (v/b) distribution at various sections of the bilayer composite.

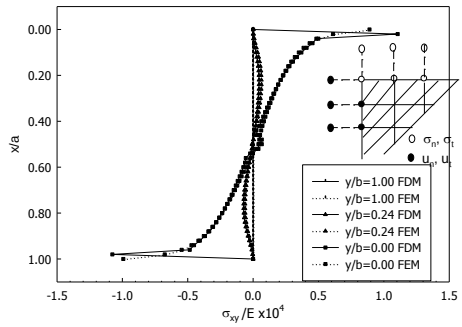

Fig.7 Comparison of shear stress distribution at different sections of the bilayer composite.

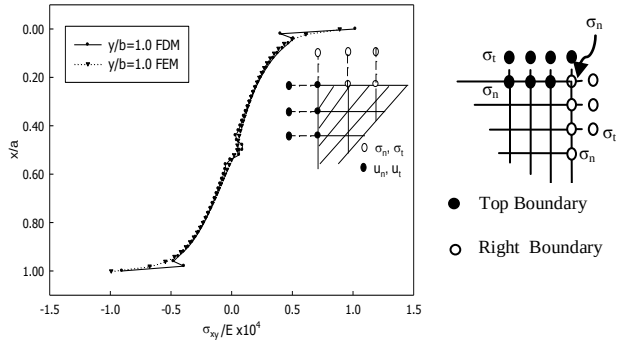

Fig.8 Comparison of normalized shear stress (σ_{xy}/E) distribution at y/b=0.0 of the bilayer composite.

The distribution of σ_y at various sections of the bilayer composite by FDM method is shown in fig.9. It indicates that for this particular problem stress at section y/b=0.0 is very significant as compared to the other sections of the material which is shown in fig.10 and most of the case it is simply equal to applied stress. From fig.9, it is seen that the FEM result shows smaller value of stress σ_y at the boundary corner points (most critical point in engineering point of view as it correspond the highest stress) than FDM result. This is obvious because in FEM method stress is calculated at every element and then extrapolated to find stress at the boundary. The distribution of stress σ_x at section y/b=0.0 as shown in fig.11 and indicates that, there is a bumping of the stress distribution curve at the interface of the bilayer composite. It is noted that, in FDM there is a provision of adjusting the corner point boundary conditions that is corner points could be considered at the either of the two boundaries i.e. at this point, either u=0,v=0 and σ_{xy}=0 or u=0,v=0 and σ_x=0 can be applied as boundary conditions. But the application of left boundary condition i.e. u=0,v=0 and σ_{xy}=0 at the corner point best accords the two solutions by FDM and FEM method. This so because if it is applied that u=0,v=0 and σ_x=0 at the left boundary corner then the FDM should gives σ_x=0 at this point and from the practical knowledge we know that at fixed support there always developed bi-directional resistive force and hence stress.

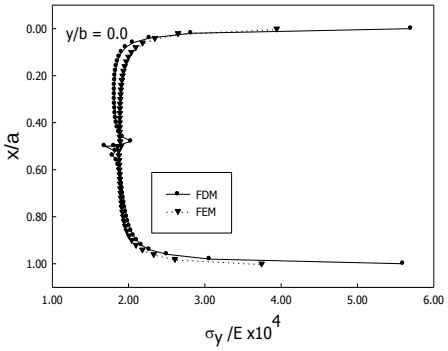

Fig.9 Comparison of normal stress (σ_y/E) distribution at y/b =0.0 by FDM and FEM.

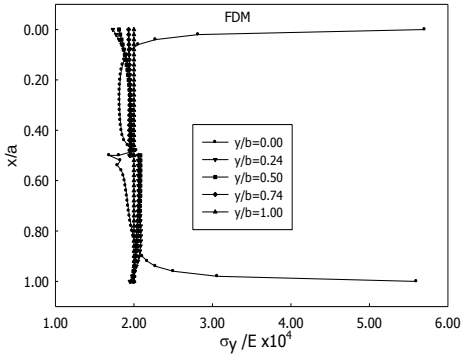

Fig.10 Normalized normal stress (σ_y/E) distribution at different sections of the material by FDM.

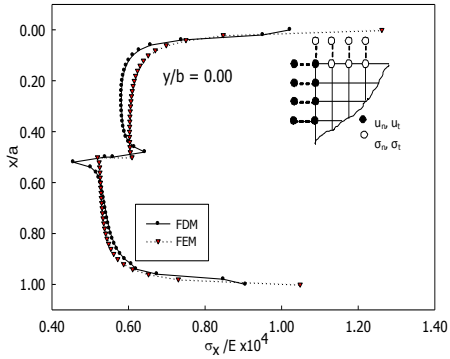

Fig.11 Comparison of normal stress (σ_x/E) distribution at y/b =0.00 considering the corner point at left boundary in FDM analysis.

5. Conclusions

The available FDM method for the numerical solutions of mixed boundary-value elastic problem based on the ψ-formulation can be applied to analysis of stresses and displacements of bi-layer composite by changing of formulation of finite difference equations of boundary conditions at the interface of bonding of two isotropic materials. The numerical formulations with greater inclusion points at the interface provide better solution of the bi-layer composite as they ensure proper compatibility between two materials.

NOMENCLATURE

E : Modulus of Elasticity, GPa
μ : Poisson ratio
ψ : Displacement potential function
σ_x : Normal stress component along x-direction
σ_y : Normal stress component along y-direction
σ_{xy} : Shear stress component in the xy plane
σ_n : Stress component normal to boundary
σ_t : Stress component tangential to boundary
u : Displacement component along x-direction
v : Displacement component along y-direction
l, m : Direction cosine of the normal at any physical boundary point
u_n : Displacement component normal to boundary
u_t : Displacement component tangential to boundary

REFERENCES

[1] Zabulionis D., "Stress and strain analysis of a bilayer composite beam with interlayer slip under hygrothermal loads", Scientific Journal "MECHANIKA", Nr.6(56), ISSN 1392 – 1207, pp 5-12, (2005).

[2] Long L., Iwasaki S., Yin F. and Nagai K. "Prediction of Nominal Stress-Strain Curves of a Multi-Layered Composite Material by FE Analysis", Materials Transactions, Vol. 51, No. 12, pp. 2188-2195, (2010).

[3] Sevecek O., Pletz M., Bermejo R., Supancic P. "Analytical Stress-Strain analysis of the laminates with orthotropic (isotropic) layers using Classical Laminate Theory", Materials Center Leoben Forschung GmbH, Presentation, (2011).

[4] Carreira R. P., Caron J. F., Diaz A. "Model of multilayered materials for interface stresses estimation and validation by finite element calculations", Materials Transactions, Vol. 51, No. 12, pp. 2188-2195, (2010).

[5] Wang Z., Wang W., Wang H. and Hu Y., "Stress Analysis on Layered Materials in Point Elastohydrodynamic-Lubricated Contacts", Tribology Letters (Springer), Vol. 35, Issue 3, pp. 229-244, (2009).

[6] Algbory A. M. R. M. "Stress analysis of the multi-layered thick cylinders", Al-Qadisiya Journal For Engineering Sciences, Vol. 4, No. 2, pp. 51-67, (2011).

[7] Nath, S.K.D., Akanda, M.A.S., Ahmed, S.R. and Uddin, M.W., "Numerical investigation of bond-line stresses of tire tread section", International Journal of Applied Mechanics and Engineering, Vol. 13, No. 1, pp. 43-61, (2008).

[8] Alam, M. T., Akanda, M.A.S and Mandal, A.C., "Stress analysis of composite lamina having a square hole by finite difference technique", Proceedings of International Conference on Mechanical & Manufacturing Engineering, pp. 1-6, Johor Bahru, Malaysia, May 21-23, (2008).

[9] Uddin, M. W., "Finite difference solution of two-dimensional elastic problems with mixed boundary conditions", M. Sc. Thesis, Carleton University, Canada, (1966).

[10] Idris A.B.M, "A new approach to solution of mixed boundary value elastic problem", M. Sc. Thesis, BUET, Bangladesh, (1993).

[11] Akanda, M. A. S., "Stress analysis of gear teeth", M. Sc. Thesis, BUET, Bangladesh, (1997).

[12] Akanda, M. A. S., Ahmed, S.R., Khan, M. R., and Uddin, M. W., "A finite-difference scheme for mixed boundary-value problems of arbitrary-shaped elastic bodies", Adv. in Engng Soft, Vol. 31, No. 3, pp. 173-184, (2000).

[13] Akanda, M. A. S., Ahmed, S.R. and Uddin, M. W., "Stress analysis of gear teeth using displacement potential function and finite-differences", Int. J. Numer. Meth. in Engng., Vol-53, No. 7, pp 1629-1649, (2002).

ICMIEE-PI-140253

Application of Branch and Bound algorithm for solving flow shop scheduling problem comparing it with tabu search algorithm.

[*] *Mr. Subrata Talapatra[1], Md. Shamsur Rahman[2], Chandnee Das[3], Utpal Kumar Dey[4]*
[1, 2, 3] Department of Industrial Engineering and Management (IEM)
[4]Department of Computer Science and Engineering
Khulna University of Engineering & Technology (KUET)
Khulna-9203, Bangladesh.

ABSTRACT
The leading position in contributing to the economics of many countries is hold occupied by the garments factory and it has great opportunity to enhance its area .In Bangladesh, the garment factory is the top of the organization, which takes the vital role in the economic sector. As the number of jobs and machines increase, the flow shop scheduling problems in the industry approaches to difficulty. Consider a regular flow shop cell with several bottleneck stages. If such were the case, the industry owners would provide more resources to these bottleneck stages. In this case it is so much important to eliminate the bottleneck in production section and improve the total productivity of the industry. This paper deals with the Branch and Bound technique for solving M machines and N jobs in flow-shop scheduling problem. Here the optimal sequence of jobs is obtained through minimizing the total elapsed time by a lower Bounding (LB) method based on the Branch and Bound algorithm. The working of the algorithm has been illustrated by numerical example and also a C++ code was used to generate an algorithm for finding the optimal solution. The input parameters are process time and operation sequence for each job in the machines provided. This research ensures the makespan optimal values of the schedules comparing with the Tabu search method.

Keywords: Flow-Shop, Branch and Bound, Scheduling, Makespan, C++ code, Tabu search algorithm.

1. Introduction

Consider n different jobs that need to be processed on m machines in the same order. Each job has one operation on each machine and the operation of job i on machine j has processing time Pij. This problem is called a flow shop problem [1,5].In a flow shop problem all jobs have the same ordering sequence on all machines. An optimal permutation schedule does not produce an appreciably worse performance than the optimal general flow shop schedule [4]. Also schedules are attractive from a practical point of view since they are easier to implement. The flow shop problem is NP-hard for m >=3 [3,7]. Optimal solutions can only be obtained via enumeration techniques such as Branch and Bound[6] . However, these methods may take a prohibitive amount of computation even for medium-size problems and become intractable for large problems. This leads to the development of many heuristic procedures. Heuristics for solving the flow shop scheduling problem can be divided into two categories: sequence generating heuristics and improvement heuristics. The former methods generate a schedule from scratch. Most of these methods are either extensions or based on the ideas behind Johnsons' s well known algorithm for solving two- and three-machine problems[2,4,8,9]. Starting with a solution produced by some sequence generating heuristic, improvement heuristics provide a scheme for obtaining a new sequence with improved performance measure. Methods of this type include neighborhood search techniques[5] such as simulated annealing and tabu search. Tabu search is a local search based optimization method which has been successfully used to solve many difficult combinatorial optimization problems, particularly in the scheduling area. It also exhibited considerable robustness.

2. Literature review

Many applied and experimental situations, which generally arise in manufacturing concern to get an optimal schedule of jobs in set of machines, diverted the attention of researchers and engineers. In flow-shop scheduling, the objective is to obtain a sequence of jobs which when processed in a fixed order of machines, will optimize some well defined criteria. Various researchers have done a lot of work in this direction. Johnson , first of all gave a method to minimise the makespan for n-job, two-machine scheduling problems. The work was further extended by Ignall and Scharge, Cambell[2], Maggu and Dass, Heydar,Yoshida and Hitomi, Lomnicki Palmer Bestwick and Hastings,Nawaz et al.Sarin and Lefoka , Koulamas,Dannenbring , etc. by considering various parameters.Yoshida and Hitomi considered two stage flow shop problem to minimize the makespan whenever set uptimes are separated from processing time. The basic concept of equivalent job for a job block has been introduced by Maggu and Dass. Singh T.P. and Gupta Deepak studied the optimal two stage production schedule in which processing time and set uptime both were associated with probabilities including job block criteria. Heydari dealt with a flow shop scheduling problem where n jobs are processed in two disjoint job blocks in a string consists of one job block in which order

* Corresponding author. Tel.: +88-01727555334
E-mail address: sub_ksy@yahoo.com

of jobs is fixed and other job block in which order of jobs is arbitrary. Lomnicki introduced the concept of flow shop scheduling with the help of Branch and Bound method. Further the work was developed by Ignall and Scharge , Chandrasekharan, Brown and Lomnicki , with the Branch and Bound technique to the machine scheduling problem by introducing different parameters. In practical situations processing times are not always deterministic so we have associated probabilities with their processing times of all the jobs on all the three machines. This hence the problem discussed here is wider and has significant use of theoretical results in process industries**.**

3. Assumptions

a) No passing is allowed.
b) Each operation once started must performed till completion.
c) A job is entity, i.e. no job may be processed by more than one machine at a time.

Notations:
We are given n jobs to be processed on three stage flow shop scheduling problem and we have used the following notations:
Ai: Processing time for job i on machine A
Bi: Processing time for job i on machine B
Ci: Processing time for job i on machine C
Pi: Expected processing time for job i on machine A
pi2: Expected processing time for job i on machine B
pi3: Expected processing time for job i on machine C
Cij: Completion time for job i on machines A, B and C.
S0: Optimal sequence
Jr: Partial schedule of r scheduled jobs.
Jr′: The set of remaining (n-r) free jobs

4. Mathematical Development

Consider n jobs say i=1, 2, 3 … n are processed on three machines A, B & C in the order ABC. A job i (i=1,2,3…n) has processing time Ai , Bi & Ci on each machine respectively, assuming their respective probabilities pi , qi & ri such that $0 \leq pi \leq 1, \Sigma pi = 1$, $0 \leq qi \leq 1$, $\Sigma qi = 1$, $0 \leq ri \leq 1$, $\Sigma ri = 1$. The mathematical model of the problem in matrix form can be stated as:

Step 1: Calculate expected processing time Pi1, Pi2 &Pi3 on machines A, B & C respectively
Step 2: To calculate
(i) LB1 =Max Pi1+Min (Pi2+pi3)
(ii) LB2=MinPi1+Max Pi2+Min Pi3
(iii) LB3=Min (Pi1+Pi2) +MaxPi3
Step 3: To calculate LB
Step 4: Continuing this way, until we reach at the end of the tree. Finally we get the optimal schedule of the jobs.

Consider 3 machines and 4 jobs are used in flow shop scheduling. Applying Branch and Bound method for reducing flow shop scheduling problem. The processing time of these 3 machines is Pi1, Pi2, and Pi3.Calculate the completed time by this method using this Branch and Bound steps. Calculation is done in below:

4.1. Algorithm development for branch &bound method

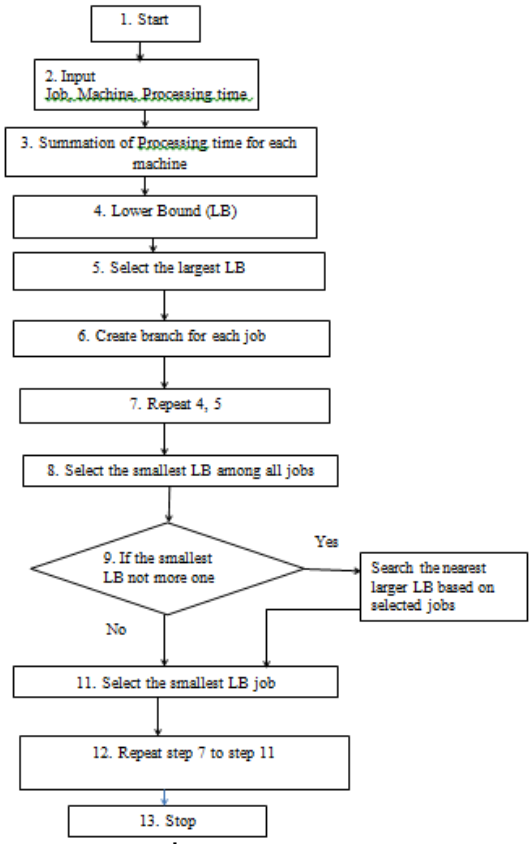

Fig1: Flow diagram of Branch-and-Bound algorithm

5. Data Analysis & Calculation

Job\Machine	M1	M2	M3
Processing time	Pi1	Pi2	Pi3
J1	77	11	82
J2	34	92	8
J3	88	36	30
J4	1	98	9
total	200	237	129

So the makespan is more than or equal to 237.

LB1:200+66=266
=max Pi1+min (Pi2+pi3)
LB2:MinPi1+max Pi2+Min Pi3
=1+237+8=246
LB3: Min (Pi1+Pi2) +MaxPi3=88+129=217

5.2. Branch & Bound's search tree diagram

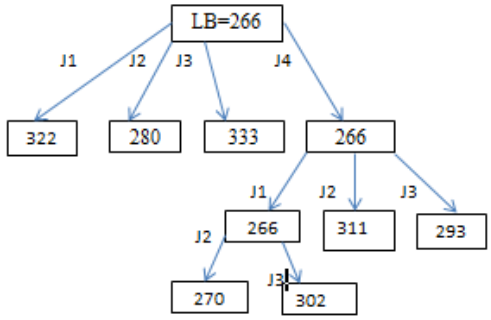

Fig2: Branches for the optimal sequence

Table 1 Verification between old sequence and new sequence job

Job\Machine	M1	M2	M3
J1	77	88	170
J2	111	203	211
J3	199	239	269
J4	200	337	346

Here, without using Branch and Bound method, total completion time is 346 minute for initial sequence of job.

Job\Machine	M1	M2	M3
J4	1	99	108
J1	192	110	192
J2	112	204	212
J3	270	240	270

After calculating by Branch and Bound method, we get the job sequence is J4-J1-J2-J3.The total completion time of this sequence is 270 minute. So, makespan is reduced.

Now this Branch and Bound result compare with tabu search algorithm results.

6. Tabu Search algorithm

A tabu search approach for solving the permutation flow shop scheduling problem. The proposed implementation of the tabu search approach suggests simple techniques for generating neighborhoods of a given sequence and a combined scheme for intensification and diversification that has not been considered before. These new features result in an implementation that improves upon previous tabu search implementations that use mechanisms of comparable simplicity. Tabu search is a local search based optimization method which has been successfully used to solve many difficult combinatorial optimization problems, particularly in the scheduling area. It also exhibited considerable robustness.

In its simplest form, tabu search requires the following ingredients:

a) initial sequence;
b) mechanism for generating some neighborhood of the current sequence;
c) tabu list;
d) Stopping criteria.

6.1. Flow diagram of proposed tabu search algorithm:

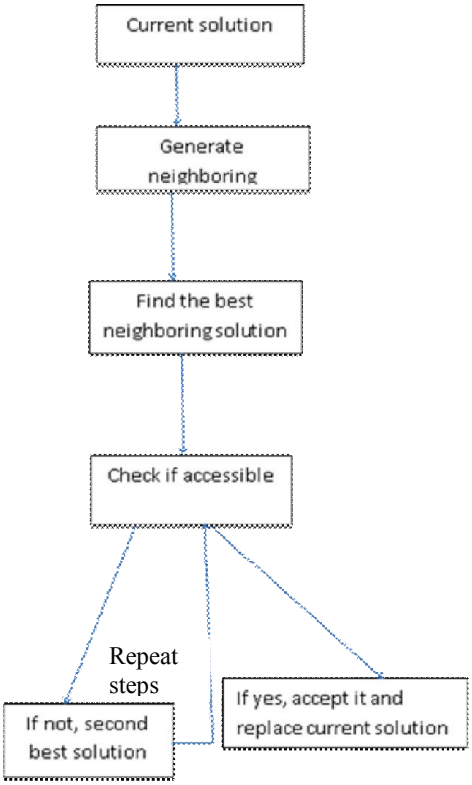

6.2. Step development of this Tabu search algorithm

a) Initial solution:

To get an initial starting solution here Branch and Bound method is applied.

b) Neighborhood structure:

Given a sequence s, we define N(s) as being the set of all sequences which can be obtained from s using one of the following schemes:

(1) Swapping: given a sequence s, let i and j be two positions in the sequence s. A neighbor of s is obtained by interchanging the jobs in positions i and j. The positions i and j can be specified in one of two ways:

a) Positions i and j are selected randomly; or
b) They are enumerated in some systematic way. Such as interchanging adjacent pair wisely.

(2) Insertion:

given a sequence s, let i and j be two positions in the sequences. A neighbor of s is obtained by inserting the job in position i in position j. The positions i and j can be specified in one of two ways:

a) Positions i and j are selected randomly; or

b) they are enumerated in some systematic way such as inserting every job in every position.

c) Selecting the best neighbor in the candidate list

The objective function is the makespan. Thus, we define ‘ best’ simply by reference to the objective function and the current tabu conditions, the best neighbor in the candidate list is the sequence that yields the smallest makespan. Possible ways to select the best neighbor include:

i. Choose the first sequence that improves makespan.
ii. Consider a subset of neighbors and’ search for the best sequence.
iii. Search the whole neighborhood and choose the best sequence.

In our algorithm, we adopted the first alternative, that is, we examine the neighborhood and take the first sequence which improves the current solution. If there is no move that improves the solution then we examine the whole neighborhood.

d) Tabu list:

The size of the tabu list is a very important parameter of a tabu search algorithm. The tabu list can be either fixed or variable.

e) Aspiration criteria

In order to override the tabu list when, there is a good tabu move, we introduced the aspiration criterion concept. We used the simplest form of aspiration criterion which is stated as follows: a tabu move is accepted if it produces a solution better than the best obtained so far.

f) Intensification and diversification scheme

As previously noted, an intensification scheme often takes the form of reinforcing attributes of good solutions while a diversification scheme typically consists of driving the search into regions not yet explored.

The random restarting approach, as its name suggests, consists of restarting the algorithm by a sequence that is randomly generated. The second scheme uses a frequency matrix which is constructed as follows. The frequency matrix is an n x n matrix whose columns are the n positions in a sequence and its rows are the n jobs. Each entry fij is incremented by 1 whenever job i visits position j. Using this frequency matrix, the sequence used to restart the algorithm is generated using the following procedure:

Step1. Let k = 1

Step2. Find the entry fij of the frequency matrix having the maximum value. The algorithm is stopped when there is no improvement between two consecutive calls of the diversification scheme. Other criteria could be used such as stopping after some maximum number of iterations or stopping after some maximum number of calls of the diversification scheme. This completes the description of our implementation of the tabu search algorithm. In the next section, we report and analyze our computational experiments.

Step3. Assign job i to position j

Step4. Delete row i and column j

Step5. Set k = k + 1

Step6. If k> n stop, otherwise go to Step 1.

g) Stopping criteria

The algorithm is stopped when there is no improvement between two consecutive calls of the diversification scheme. Other criteria could be used such as stopping after some maximum number of iterations or stopping after some maximum number of calls of the diversification scheme. This completes the description of our implementation of the tabu search algorithm. In the next section, we report and analyze our computational experiments.

After using Branch & Bound method and Tabu search method with c++ codding software, we get the following completion time:

Input: In this notepad the inputs are taken sequentially. Such firstly enter the number of machines then number of jobs and finally the job processing time. When all the data are taken then runs the c++ program and get the output.

Here,
No of machine is 3
No of job is 4
The Processing time of 3 machine is 77,11, 82 minutes.

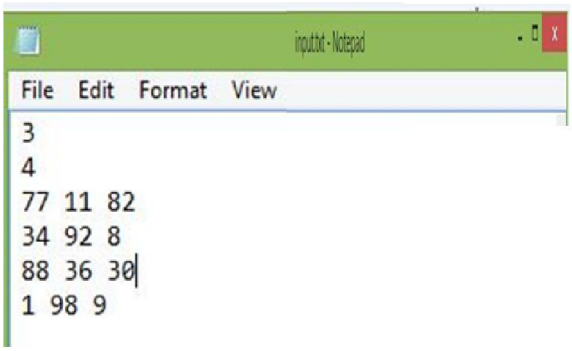

Output for Branch &Bound

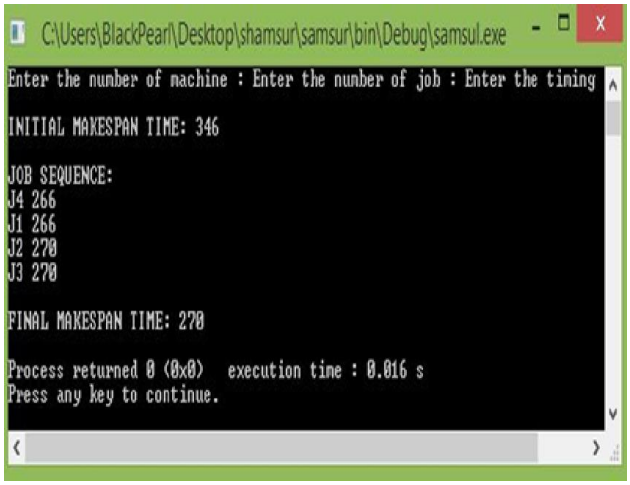

Output for Tabu search

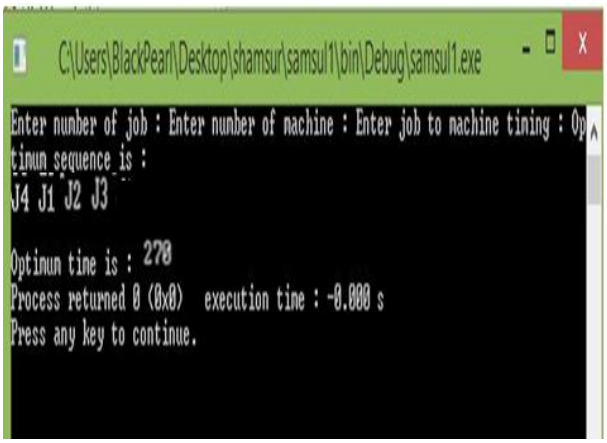

7. Gantt chart

Devised by Henry Gantt in 1910s, Gantt chart is the representation type of bar chart used to represent a feasible schedule of a scheduling problem. Gantt chart also provides the details about the precedence of operations under taken by the Jobs in various machines. The main advantage of the Gantt Charts is that visualizing the job schedule makes it very easy for the Project Manager to communicate the job schedule to various stakeholders as well as to the project team. Gantt chart is an apt medium for portraying a resultant schedule in a small problem, but a problem with large number of activities that is very difficult to represent the schedule. Gantt does not represent the relative size of work items or the total size of the project. Therefore, it becomes too tough in some cases to compare two projects with the same number of time of completion.

7.1. Reasons for using Gantt chart

Because of the many advantages offered by Gantt charts, thousands of companies use Gantt charts to become more productive, enhance their communications, forecast over the long term and track results. While some a naysayers believe they limit the size of the project that can be tracked, those using Gantt charts note an array of key benefits, including the five listed here. While there are a number of reasons to use Gantt charts below are five key reasons they are often advantageous :

a) **Avoid Completion Confusion**: Gantt charts were created to keep users on track, providing a visual timeline for starting and finishing specific tasks. By providing a visual overview of milestones and other key dates, these charts are thought to offer a more understandable and memorable method of maintaining timescale-based tasks and deliverables whether tracked on a daily, weekly, monthly or yearly basis. Below diagram shows the power of visualization found in Gantt charts. In a glance you can see that the interviews are done, there 50% more to do in training etc.

b) **Keep everyone on the Same Page**: Where there is a visual framework for the work to be done, there are fewer chances for misunderstanding, especially when it comes to highly complex tasks. Using Gantt charts allow all types of stakeholders to have the same information, set mutually understood expectations, and conduct their efforts according to the desired protocol.

c) **Understand Task Relationships**: These charts can make clear how various tasks are interrelated and perhaps rely on the completion of another to meet specific objectives. These task relationships revolve around understanding the timing of each task, which then impacts other tasks listed. This can better assure the optimum work flow, maximized productivity and overall project success. A Gantt charts makes it very easy to visualize related tasks.

d) **Effectively Allocate Resources**: By being able to look ahead on the Gantt chart, users can clearly discern where resources need to be anticipated, allocated or shared to maximize the use of those resources. The more closely the chart is followed, the better chance there is of keeping project costs within budget while also better assuring on-time completion.

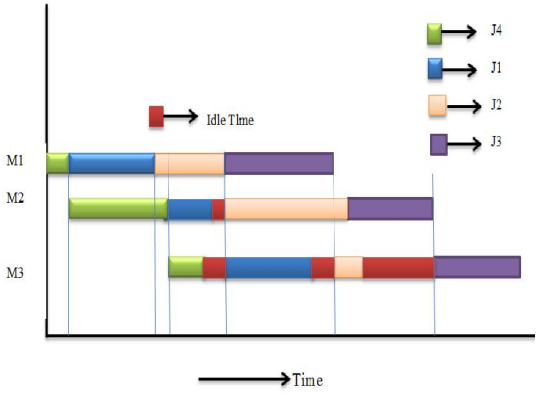

Fig 3 Gantt chart

In fig 3 the flow of jobs after scheduling through Branch and Bound method are shown graphically. It is seen that

as jobs are sequenced so the idle time is minimum. Here the red color indicates idle of the machine and other colors indicate machining or working time. Though this gantt chart shows working procedure so much easily, it has also some problems. These are this method is not designed to be the cure-all for an organization's project management ills. The main disadvantage is that Gantt Charts are not well suited for conveying complex dependencies or projects having significant potential variability in completion dates. There are some situations where other tools may indeed be more effective – particularly in scenarios when a particular milestone or critical task is missing because the project manager didn't include. Other limitations include the inability to include certain constraints like time, scope, and costs. Overall, however, Gantt chart advantages have been realized by all types of organizations for applicable applications.

8. Result and discussion

In this paper, applying this Branch and Bound algorithm and tabu search algorithm we can minimize the makespan(total completion time of the last job) of the tasks. We also can reduce waiting time between two jobs which can help for increasing the productivity of the flow shop. To complete above this tasks, first we apply Branch and Bound algorithm then we compare this algorithm with Tabu search algorithm. In Tabu search algorithm we generate the tabu list solution until we can get optimal solutions. We will mainly follow the Branch & Bound method, because it is the most effective for scheduling the total processes in any apparel industry. If we notice to the output Branch & Bound and Tabu search methods, then it is clearly understood that the Branch & Bound method is the best than others. Actually here we use Tabu search method as a parameter which ensures the Branch & Bound method's effectiveness. Here the optimum processing time using Tabu search method and the Branch & Bound is 270 unit times. Finally, the best optimal solution is obtained from Branch & Bound algorithm for n number of jobs and m number of machines through comparing with Tabu search method.

9. Conclusion and Recommendation

In flow shop scheduling, jobs are processed on machines in a set order .Flow shop scheduling problems area class of scheduling problems with a work shop or group shop in or with other resources 1,2…m in compliance with given processing orders. Especially, the maintaining of a continuous flow of processing tasks is desired with a minimum of idle time and minimum of waiting time. Reducing this waiting time we apply Branch and Bound algorithm and Tabu search algorithm in flow shop scheduling problem. The proposed implementation of the tabu search approach uses simple but effective techniques for generating neighborhoods and candidate lists, and a new combined intensifications and diversifications scheme that has not been considered before. These new feature results in an implementation of the tabu search approach. Better results are obtained.

Reducing flow shop scheduling problem some recommendations are provided:

1. Prevent recycling the tabu list in tabu search algorithm &generate the solution until we get our expected solution.
2. Further research should try to remove the total idle time from the overall process.
3. The research also improves the overall productivity of an apparel industry.

References

[1] K.R Baker,Introduction to sequencing and scheduling,viley,,,New York,1974

[2] H.G Campbell,R.A.Dudek,M.L.Smith,A heuristic algorithm for the n-job, m-machine sequencing problem,Management science16/B(1970) 630-637.

[3] E.G,Coffiman,Computer and job Scheduling Theory,Wiley,New York,1976.

[4] D.G.Dannenbring ,An Evaluation of flow shop sequencing heuristics,Management science 23(1977) 1174-1182

[5] S.French, Sequencing And Scheduling:An Introduction to the Mathematics of the job shop,Ellis Horwood,Chichester,UK 1982.

[6] E.Ignall,L.E.Scharge,Application of Branch and Bound technique to some Flow –shop problem,Operations research13(1965) 400-412

[7] A.H.G Rinnoy Kan,Machine Scheduling Problems:Classification,Complexityandcomputations,Martinus Nijhoff,The Hague,1976

[8] J.N.D Gupta,A functional heuristic algorithm for the flow shop scheduling problem,Operational Research Quarterly 22 (1971) 39-47

[9] T.S Hundal,J.Rajgopal,An extension of palmers heuristic for the flow-shop scheduling problem,International journal of production Research26(1988) 1119-1124

ICMIEE-PI-140254

Design, Construction and Performance Test of Generator and Condenser for a Small Capacity Vapor Absorption Cooling System

Faisal Ahmed, DipayanMondal, Mohammad Ariful Islam
Department of Mechanical Engineering, Khulna University of Engineering & Technology, Khulna-9203, BANGLADESH

ABSTRACT
The most commonly used refrigerant-absorbent pair is water/Li-Br where water acts as the refrigerant and the Li-Br acts as the absorbent. Generator and condenser of a small capacity Li-Br/water vapor absorption system was designed and constructed to compare actual performance with designed conditions, of 2 kW capacity and 50% Li-Br solution at constant pressure 9.66kpa. Properties of water/Li-Br solution are evaluated from standard curve fitting system. Construction material for condenser and generator coil are copper tube and rectangular stainless steel chamber for corrosion resistance and the system is kept under 9.66kpa pressure with absolutely leak proof and well insulated. The system was run for about 100 minutes. The performance is tested for variable mass flow rate and constant mass flow rate of water at the generator and condenser. The obtained minimum temperature is 25^{o}C which avoid crystallization temperature of Li-Br solution.

Key Words: Vapor absorption, Generator, Condenser, water/Li-Br refrigerant, intermittent cooling.

1. Introduction

An absorption refrigeration system uses heat source to provide the energy needed to drive the cooling system. Absorption refrigeration system is a popular alternative to regular compressor refrigeration system .Generator and condenser are two major part of an absorption system. Generator is used to supply heat to the refrigerant water and the absorber. This generator is varying for the cooling effect of the absorption system. Heat is supplied to the refrigerant water and absorbent lithium bromide solution in the generator from the hot water. The water becomes vaporized and moves to the condenser, where it gets cooled. As water refrigerant moves its pressure is reduced along with the temperature. This water refrigerant then enters the evaporator where it produces the cooling effect [1].A condenser is a device or unit used to condense a substance from its gaseous to its liquid state, typically cooling it. The latent heat is given up by the substance, and will transfer to the condenser coolant. The condenser water is used to cool the water refrigerant in the condenser and the water-Li Br solution in the absorber.

2. Working Procedure of a Single Effect Li-Br/Water Cooling System

A single-effect, Li-Br /water cycle is illustrated in Fig (1). With reference to the numbering system shown in figure, at point (1) the solution is rich in refrigerant and a pump forces the liquid through a heat exchanger to the generator (3). The temperature of the solution in the heat exchanger is increased. In the generator thermal energy is added and refrigerant boils off the solution. The refrigerant vapor (7) flows to the condenser, where heat is rejected as the refrigerant condenses. The condensed liquid (8) flows through a flow restrictor to the evaporator (9). In the evaporator, the heat from the load evaporates the refrigerant, which flows back to the absorber (10). A small portion of the refrigerant leaves the evaporator as liquid spillover (11) which is pumped back to the evaporator inlet again. At the generator exit (4), the steam consists of absorbent-refrigerant solution, which is cooled in the heat exchanger. From points (6) to (1), the solution absorbs refrigerant vapor from the evaporator and rejects heat through a heat exchanger. At point (1) the solution is reach in refrigerant and a pump (2) forces the liquid through a heat exchanger to the generator (3). The temperature of the solution in the heat exchanger is increased [4].

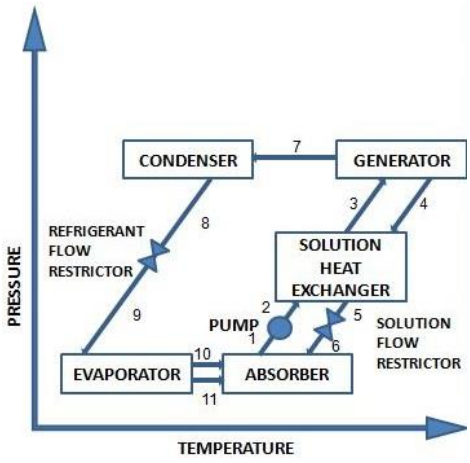

Fig.1 P-T diagram of LiBr-water absorption cooling cycle.

3. Design of a single effect Li-Br/Water absorption cycle system

To perform designing of equipment size and performance evaluation of a single-effect Li-Br/water absorption cooler basic assumptions are made.
The basic assumptions are:

- The steady state refrigerant is pure water.

Corresponding author. Tel.: +88-01922988336
E-mail address: faisalkuet08@gmail.com

- There are no pressure changes except through the flow restrictors and the pump.
- At points 1, 4, 8 and 11, there is only saturated liquid.
- At point 10 there is only saturated vapor.
- The pump is isentropic.
- There are no jacket heat losses.
- The capacity of the system is 2kW.

Table 1 Design parameters for the single effect Li-Br/water absorption cooler

Parameter	Symbol	Value
Capacity	Q_e	2 kW
Generator solution exit temperature	T_4	80 ^{0}C
Weak solution mass fraction	X_1	50% Li-Br
Strong solution mass fraction	X_4	55% Li-Br
Solution heat exchanger exit temperature	T_3	65 ^{0}C
Generator vapor exit temperature	T_7	80 ^{0}C

Table 2 Data for single effect Li-Br/water cooling system

Point	h (kJ/kg)	m (kg/s)	P (kPa)	T (^{0}c)	X (% LiBr)
1	92.4	0.0129	1.227	34.9	55
2	92.4	0.0129	9.66	34.9	55
3	145.4	0.0129	9.66	65	55
4	212.2	0.0118	9.66	90	60
5	154.3	0.0118	9.66	59.93	60
6	154.3	0.0118	1.227	44.5	60
7	2628	0.00017	9.66	85	0
8	185.3	0.00017	9.66	44.3	0
9	185.3	0.00017	1.227	10	0
10	2519.2	0.0009	1.227	10	0
11	40.35	0.0002	1.227	10	0

Table 3 Energy flows in generator and condenser of the system

Description	Symbol	KW
Capacity	Q_e	2
Heat input to the generator	Q_g	3.45
Condenser heat rejected	Q_c	2.62

4. System heat exchangers sizing Equations

In the heat transfer analysis, it is convenient to establish a mean temperature difference (ΔT_m) between the hot and cold fluids such that the total heat transfer rate Q between the fluids can be determined from the following expression:

$$Q = AU\Delta T_m \quad (1)$$

Where, A (m^2) is the total heat transfer area and U (W/m^2-°C) is the average overall heat transfer coefficient, based on that area.

$$\Delta T_m = F\Delta T_{ln} = F\left(\frac{\Delta T_0 - \Delta T_L}{\ln(\Delta T_0/\Delta T_L)}\right) \quad (2)$$

F= Correction factor.

The overall heat transfer -coefficient (U) based on the outside surface of the tube is defined as [6]

$$U = \frac{1}{(D_0/D_i)(1/h_i)+(D_0/D_i)F_i+(1/2k)D_0\ln(D_0/D_i)+F_0+1/h_0} \quad (3)$$

For the design of the heat exchangers, the cooling water inlet and outlet temperatures are assumed. The cooling water inlet temperature depends exclusively on the available source of water, which may be a cooling tower or a well. The Petukhov-Popov equation [5] or turbulent flow inside a smooth tube gives:

$$Nu = \frac{\left(\frac{f}{8}\right)Re\ Pr}{K_1+K_2\left(\frac{f}{8}\right)^{.5}\left(Pr^{\frac{2}{3}}-1\right)} \quad (4)$$

Friction Factor,

$f = [1.82 \log (Re) - 1.64]^{-2}$

Constant k_1=1.34; k_2= 11.7+ $\frac{1.8}{Pr^{2/3}}$

Nusselt's analysis of heat transfer for condensation on the outside surface of a horizontal tube, gives the average heat transfer coefficient as [6]

$$h_m = 0.725\left[\frac{g\rho_1(\rho_1-\rho_v)h_{fg}k_1^3}{\mu_1(T_v-T_w)D_0}\right]^{0.25} \quad (5)$$

The logarithmic mean temperature difference is [6]

$$\Delta T_{ln} = \frac{(T_{sat}-T_i)-(T_{sat}-T_0)}{\ln[(T_{sat}-T_i)/(T_{sat}-T_0)]} \quad (6)$$

For the average Nusselt number Churchill and Chu proposed [6] a correlation in free convection boiling regime on horizontal tube. The correlation is:

$$Nu_m^{\frac{1}{2}} = 0.60 + \frac{0.387\,Ra_D^{1/6}}{\left[1+\frac{0.59}{Pr^{\frac{9}{16}}}\right]^{8/27}} \quad (7)$$

here range $[10^{-4} < Ra_D < 10^{12}]$

Nu_m and Ra_D are based on pipe diameter. Namely

$$N_m = \frac{h_s D}{k}\ and$$

$$R_D = Gr_D\,\mathrm{Pr} = \frac{g\beta\,(T_w - T_\infty){D_0}^3}{\vartheta^2}\,Pr$$

Table 4 Design Parameters for generator & condenser

Tube dimension	Outer diameter D_o= 12.7 mm Inside diameter D_i=10.7 mm	
Chamber Pressure (Vacuum)	9.66kpa	
Condenser	Cooling water inlet temperature	Inlet=25°C
		Outlet=28°C
	Condensed water temperature	From 80°C to 44.3°C
	Mass flow rate of cooling water*(m)*	0.21 kg/s
	Condensed water mass flow rate	0.00107 kg/s
	Load	2.62kW
Generator	Generator solution	Entering: 50% LiBr at 65°C
		Leaving: 60% LiBr at 80°C
	Generator water vapor mass flow rate (*m*)	0.16507 kg/s
	Load	3.45 kW

5. Condenser Design

The overall heat transfer coefficient is given by Eq. (3) For this equation, the value of the fouling factors (Fi,F_O) at the inside and outside surfaces of the tube can be taken as 0.00009m2°C/W [6] and k for copper = 383.2 (W/m-°C). The heat transfer coefficients, hi ,ho, for the inside and outside flow need to be calculated.

The Petukhov-Popov equation Eq.4 applies for Reynolds numbers 10^4<Re< $5x10^6$and Prandtl numbers, 0.5<*Pr<2000*. The Petukhov-Popov equation agrees with the experimental results for the specified range within ± 5%.The water properties at the mean temperature of (25+28)/2=26.5°C

ρ = 997kg/m^3	ν = $0.8365\times10^{-6}$$m^2$/s
k = 0.610 W/m-°C	Pr= 5.85
C_p = 4180 J/kg-°C	μ= 0.86×10^{-3} kg/m.s

Q_c equals to 2.62 kW, therefore

$$m = \frac{Q}{C_p \Delta T} = \frac{2620}{4180 \times 3} = 0.21\ kg/s$$

$$Re = \frac{4m}{\pi D \mu} = \frac{4 \times 0.21}{\pi \times 0.0107 \times 0.86 \times 10^{-3}} = 29159$$

Substituting the above values into Eq. 4 and replacing $Nu_D = h_i D_i / K$, gives h_i = 11162.53 W/m^2°C.

The physical properties in Eq. (5) should be evaluated at the mean wall surface and vapor saturation temperature. The average temperature of the condensate film is (45.01+26.5)/2=35.75°C and its physical properties are,

ρ_l = 997kg/m3	k_l= 0.613 W/m-°C
ρ_v= 0.04125 kg/m^3	μ_l= 801.4×10^{-6}kg/m-s
T_w = 26.5°C	T_v= 45.01°C
D_o = 0.0127 m	

$$h_{fg} = -0.013T^2 - 2.2T + 2500.43 = 2416.5 \times \frac{10^3 j}{kg}$$

h_m= 9958.03 W/m^2-°C

By substituting the above values in Eq. (3) a resulting overall heat transfer coefficient of U=1657.932W/m^2-°C is determined.

Finally, LMTD from Eq. (6) $\Delta T_{ln} = 18.47$

The tube length L is determined by writing an overall energy balance, [6]

$$Q_{tube} = (\pi D_0 L) U_0 \Delta T_{ln} = m C_p (T_0 - T_i)$$

Which gives, *L=2.14 m*

6. Generator Design

The generator provides sensible heat and latent heat of vaporization. The heat of vaporization consists of the heat of vaporization of pure water and the latent heat of mixing of the liquid solution [15]. Typically, the heat of mixing is about 11% of the heat of vaporization for water/ lithium bromide. For designing of the generator following designing parameters are used as shown in Table 4.The heat transfer coefficients, h_i,$h_s$for the inside and outside flow need to be calculated.

Assume,	Here,
Hot water inlet T_1= 90°C	Solution TempT_3=T_{sol}= 65°C
Water outlet at T_2= 85°C	Refrigerant TempT_4=80°C

The Eq^n.(4) for turbulent flow inside a smooth tube Reynolds numbers 10^4<Re< $5x10^6$and Prandtl numbers, 0.5<*Pr<2000*. The Petukhov-Popov equation agrees with the experimental results for the specified range within ± 5%. Physical properties of water evaluated at (90+85)/2 = 87.5 °C

Dynamic Viscosity $\mu = 3.16 \times 10^{-4}$ kg/ms
Thermal Conductivity k = 0.67467 w/mk
Prandlt no.Pr = 1.9083

Mass flow rate (m) = $\frac{Q}{C_p \Delta T}$ = 0.16507 Kg/sec

Reynolds Number, Re = $\frac{4m}{\pi D_i \mu}$ = 62160.15

So,f= 0.01992;k_1= 1.0677;k_2= 13.151;
Nu= 207.84hence, hi=13105.28 w/m^2°C

Water-LiBr Solution Properties:
Percentage of water-LiBr solution X = 50%
Pressure P=9.66kpa andSolution Temp T_3= 65°C

Density:
Here $X_0 = X/100 = 0.5$
T_{sol} = 65℃ (0℃ $< T <$ 200℃)
ρ_x= 1145.36 + 470.84 X_o + 1374.79 X_o^2 – (0.33 + 0.57 X_o) (273 +T)=1515.165 Kg/m^3

Absolute Viscosity:
Range 45 %<X< 65%
Solution TemperatureT_{sol} =(65+273) K =338K

$$A_1 = -404.12 + 16.39X - 0.145X^2 = -37.097$$
$$A_2 = 28606.4 - 934.56X + 8.52X^2 = 3196.85$$
$$A_3 = 70.38 - 2.35X + 0.028X^2 = 4.85$$
$$B = A_1 + \frac{A_2}{T} + A_3 \ln(T) = 0.4868$$
so,$\mu = \frac{e^B}{1000} = 1.627 \times 10^{-3} Kg/msec$

Specific Heat :
$c_p = 0.097X^2 - 37.51X + 3825.4$=$2193.8 J/kgK$

Thermal Conductivity:
Solution Temperature T_{sol}=(65+273) K =338K
For T≥ 313 K;$k_1 = 0.308\frac{X}{100} + 0.62 = 0.47$
$$k_2 = -0.31\frac{X}{100} + 0.65 = 0.49$$
$$D_{12} = \frac{k_2 - k_1}{20}(T - 273) = 0.0277$$
so, $k = k_1 + D_{12}$=0.5034 w/mk

For the average Nusselt number Churchill and Chu proposed [6] a correlation in free convection boiling regime on horizontal tube. So for Eq. (7)
Prandlt no $Pr = \frac{\mu c_p}{k}$ =7.009
Kinematic Viscosity$\vartheta = \frac{\mu}{\rho} = 1.07 \times 10^{-6} m^2/sec$
Mean wall surface Temperature $T_w = \frac{90+85}{2} = 87.5$℃
T_∞= 65℃and Film Temp$T_f = \frac{T_w + T_\infty}{2} = 76.25$℃

$$\therefore, \beta = \frac{1}{T_f} = 0.0134\ ℃$$

Hence Rayleigh number $Ra_D = 36452647$
Average Nusselt number $Nu_m = (7.2828)^2$

So, heat transfer co-effiient on out side of tube $h_s = 2102.40\ w/m^2$℃and overall heat transfer coefficient of$U_o = 1038.80\ w/m^2$℃is determined.

LMTD is $\Delta T_{ln} = 14.427$

The tube length L is determined by writing an overall energy balance, [6]

$$Q_{tube} = (\pi D_0 L) U_0 \Delta T_{ln} = m C_p (T_0 - T_i)$$

Which gives, *L=5.77 m*

Table 5 Obtained heat exchanger size of generator **& condenser**

Parameter	Generator	Condenser
Tube length	5.77 m	2.14 m
Tube material	Copper	Copper

7. Construction of the Generator and Condenser

Heat exchangers are constructed according to the design. A stainless steel sheet made structure is providing enclose for condenser and generator assembly. Copper tubes are used for construct the generator and condenser coil.

7.1 Generator

To reduce the complexity of the system a vacuum box (made of galvanized iron plates) is used as an alternative of generator which has capacity of storing Li-Br/Water solution under desired vacuum pressure and temperature. Li-Br/Water solution should be feed manually into this to run the whole system. The generator coil is made of copper tube of 5.77 m. Length and width of the generator coil are30.48×10.16 cm. Tube spacing is 2.54 cm. Tube spacing are obtained by using several number of copper U bend. Copper tube and U bend are connected by gas welding.

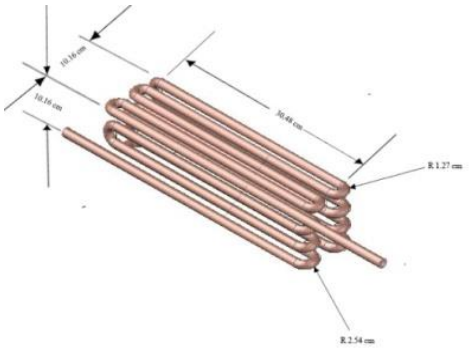

Fig.2 Photographic view of the Generator Coil

7.2 Condenser:

For the purpose of running a vapor absorption system a condenser is a must. Condenser condenses vapor obtained from. Condenser is made of copper tube of 2.14 m length. Tube spacing is 2.54 cm. Tube spacing are obtained by using several number of copper U bend. Copper tube and U bend are connected by gas welding.

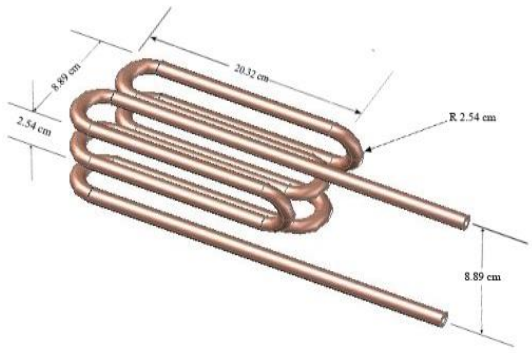

Fig.3 Photographic view of the condenser coil

7.3 Chamber construction

The chamber is made of stainless steel sheet of 2mm thickness. At first the rectangular structure of the box is made of 0.5 inch stainless steel square bar. Than the sheet are welded around the box. Water should be fed manually along the tube to run the whole system. A thermocouple arrangement and vacuum pressure gauge is installed for taking any adjustments and measurements. Fig shows various component of the system.

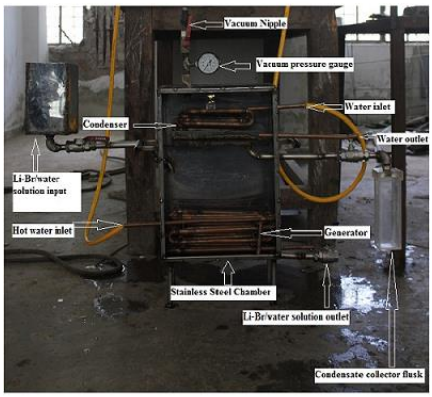

Fig.4 Various Component and water circulation system assembled inside the Chamber.

8. Result and Discussion

Variation of rate of condensation with hot water mass flow rate is shown if Fig. 6. The amount of condensate is dependent on the change of mass flow rate of the generator. As the amount of mass flow rate increases, the amount of condensate also increases. The increase in the mass flow rate in the generator increases the amount of heat rejection. As a result, amount of accumulated condensate increases. The increasing mass flow rate of hot water in generator causes the water present in the Li-Br solution to vaporize in large amount which then condenses in the condenser due to absorption of heat by the condenser.

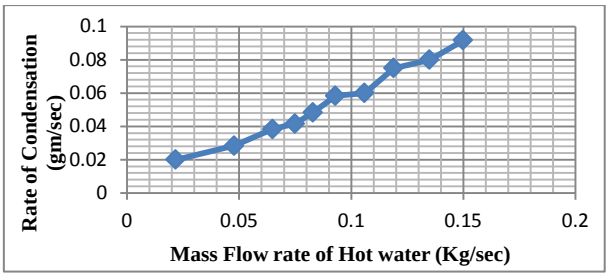

Fig.5 Variation of rate of condensation with hot water mass flow rate

The vaporized water from the Li-Br solution has much higher temperature than the condenser fluid. The inlet temperature of the condenser is at the atmospheric temperature. The vaporized water condenses in the condenser by rejecting heat. The heat is rejected to the condenser fluid. The increased flow in the condenser increases the amount of condensing rate. As a result the amount of condensate increases.

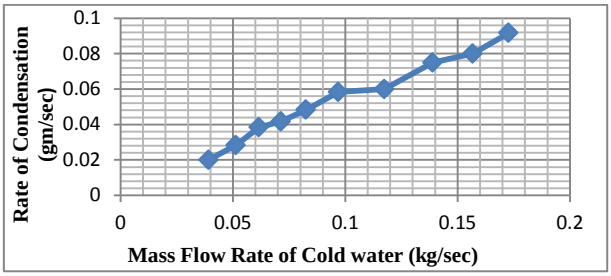

Fig.6 Variation of rate of condensation with cold water mass flow rate

The increase in the mass flow rate increases the amount of heat rejection by generator. As a result more water content from the Li-Br solution gets vaporized. This causes the increase in density of Li-Br solution. Because of being a salt particle, Li-Br present in the solution doesn't get vaporized. It remains constant while the whole solution is reducing. As a result the weight percentage of the Li-Br present in the solution increases with the increase of mass flow rate inside the generator.

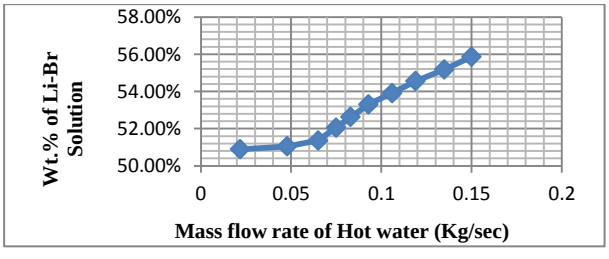

Fig.7 Wt. % of Li-Br Solution against mass flow rate of hot water

The amount of heat rejection is dependent on the inlet temperature. The high inlet temperature causes more heat rejection by generator. The more heat rejection causes more water present in the Li-Br solution to

vaporize. This increases the density of Li-Br solution. As a result the weight percentage of the Li-Br solution increases with the inlet temperature.

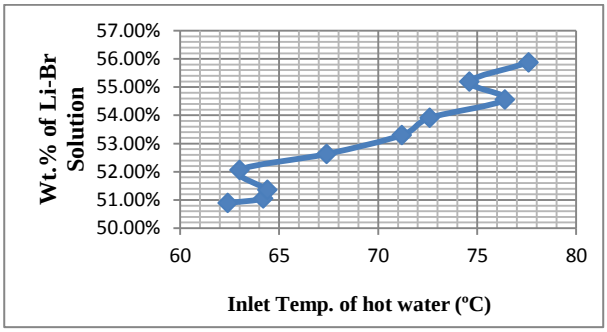

Fig.8 Wt. % of Li-Br Solution against Inlet Temperature of Hot water

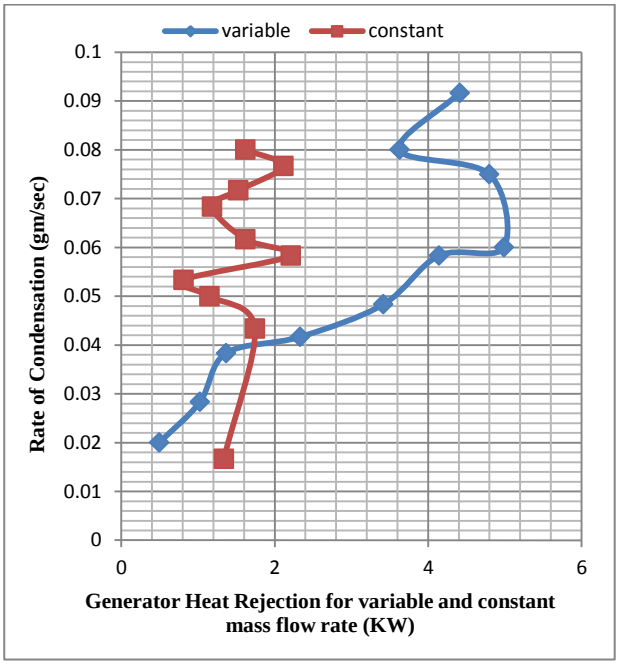

Fig.9 Comparison of the amount of condensate against generator heat rejection between variable and constant condition.

From the above graphical representation it can be seen that the amount of accumulation of condensate corresponding to the amount of heat rejection of generator for variable mass flow rate is very much same as for constant mass flow rate. Although it is seen that amount of heat rejection for variable mass flow rate is much higher than the constant mass flow rate. For the same amount of accumulated condensate, variable mass flow rate requires huge amount heat rejection of generator than the constant mass flow rate. The trend line for the variable condition shows the trend line to be less steep. But for constant condition the trend line is much steep. This graphical representation is actually a comparison between variable condition and constant condition.

9. Conclusion

A generator and condenser assembly for a small capacity vapor absorption refrigeration system has been designed in this project. Then heat exchangers used for each component are designed. Heat exchanger tube material and dimensions are determined. The unit designed is constructed and each heat exchanger is adjusted to the required output. In this way the designed parameters are ensured. Some performance test is made to evaluate performance of the system. It is so important to maintain each component at required pressure. Experimental result shows that the constructed generator and condenser can able to perform the required purse satisfactorily.

10. Nomenclature

c_p : specific heat at constant pressure, $kJ \cdot kg^{-1} \cdot K^{-1}$
Q_c : condenser Load KW
h : specific enthalpy, $kJ \cdot kg^{-1}$
p : saturation pressure, kPa
ρ : density $kg \cdot m^{-3}$

11. References

[1]. Perry, R. H. Perry's Chemical Engineer's Handbook, 6th ed.; McGraw-Hill: New York, 1992; Chapter 12.

[2]. Marcriss RA, Gutraj JM, Zawacki TS. Absorption fluid data survey: final report on worldwide data, RLN/sub/8447989/3, Inst. Gas Tech., 1988.

[3]. Kang YT, Christensen RN. Transient analysis and design model of LiBr-H2O absorber with rotating drums. ASHRAE Trans 1995;101:1163–74.

[4]. Priedeman DK, Christensen RN. GAX absorption cycle design process. ASHRAE Trans 1999;105(1):769–79.

[5]. ASHRAE, Handbook of Fundamentals, Atlanta, 1997.

[6]. Ozisik, M. 1985. Heat Transfer-A Basic Approach. McGraw-Hill Book Company. ISBN 0- 07-066460-9.

[7]. Herold, K.E. and Klein, S.A. 1996. Absorption Chillers and Heat Pumps. CRC Press, Inc. USA, ISBN 0-8493-9427-9.

ICMIEE-PI-140260

Numerical investigation of mixed convection flow of Cu-water nanofluid in a wavy wall channel

*Nayeem Uddin Ahmed[1], Meem Tasfia Zaman[2] and Md. Mamun Molla[3]**
[1,2]Department of Electrical and Computer Engineering, North South University, Dhaka- 1229, BANGLADESH
[3*]Department of Mathematics and Physics, North South University, Dhaka- 1229, BANGLADESH

ABSTRACT
In this research, the improved thermal features of nanofluids are studied by investigating the laminar fluid flow over a two dimensional sinusoidal wall channel whose top and bottom wavy sections are heated. The nanofluid used is composed of copper (Cu) nanoparticles suspended in water (H_2O) which acts as the basefluid. The flow is characterized by a range of Reynold numbers (*Re*) with varying volume fractions for a particular Grashof Number (*Gr*). In addition, the effect of mixed convection, which takes both natural and forced convection of the fluid into account, is examined by altering the Richardson number ($Ri = Gr/Re^2$). The governing equations which include the continuity, Navier-Stokes and energy equations are in Cartesian coordinates which are non-dimensionalised and then transformed into curvilinear coordinates. The transformed equations are then discretized using finite volume method, applying the appropriate boundary conditions. The consequent numerical results are represented in the form of local Nusselt number graphs, isotherms, streamlines, temperature and velocity profiles.

Keywords: Nanofluid, Finite Volume Method, volume fraction, mixed convection, Richardson number

1. Introduction

Thermal management of electronic devices is of paramount importance in the world today due to the widespread use and availability of such systems. Heat generated by electrical or electronic circuits must be rapidly dispelled in order to improve their efficiency and prevent their premature failure. Thus, various techniques of heat dissipation are used today, which involves the use of heat sinks, cooling fans, heat pipes as well as electrostatic and convective cooling fluids. Each of these methods mentioned above has their associated pros and cons, thus allowing constant research to be dedicated to locating superior alternatives.

One of the techniques used only recently to enhance heating or cooling in different mechanical and electronic systems involves the use of Nanofluids. Nanofluids are dilute liquid suspensions of nanoparticles with at least one of their principal dimensions smaller than 100nm. Such particles include copper, copper (II) oxide, tin (IV) oxide, aluminium oxide, silicon carbide etc. The solvents for these suspensions, also known as base fluid, include water, oil, ethanol or ethylene glycol. From the literature available, nanofluids have been found to possess improved thermo-physical properties such as thermal conductivity, thermal diffusivity, viscosity and convective heat transfer coefficients compared to those of the base fluids.

Experiments involving nanofluid flows through a straight, circular pipe in a laminar flow regime and constant heat flux boundary condition were carried out by Ebrahimnia-Bajestan *et al*. [1] to investigate the corresponding heat transfer performance and pressure drop. The effects of particle concentrations, diameter, Brownian motions, Reynolds number, type of the nanoparticles and base fluid on the heat transfer coefficient were determined. The results indicated that the particle volume concentration, Brownian motion and aspect ratio of nanoparticles similar to flow Reynolds number increased the heat transfer coefficient, while the nanoparticle diameter had an opposite effect.

A simpler version of the study mentioned above was represented in a numerical analysis done by Abouali and Falahatpisheh [2]. They investigated the internal free convection of Al_2O_3 water nanofluid in a vertical annulus with different physical and geometrical parameters to explore the heat transfer behavior. Thermal conductivity models of Wasp and Kenny [3], Jang and Choi [4] were used in numerical model and results were compared with experimental data of Putra *et al*. [5]. Pak and Chos model was used for viscosity [6]. Different aspect ratio from 1 to 5, Grashof numbers in the range between 10^3 to 10^5, as well as varying particle volume fraction of 0% to 6% were studied. The study revealed that the thermal conductivity model of Wasp and Kenny [3] greatly overestimates the Nusselt number of experimental data of Putra *et al*. [5] for 3-D cylinder, whereas the Jang and Choi model agrees [4].

The most comprehensive explanation of forced convection in a wavy channel was given by Wang and Chen [7]. Their study involved analysis of the effects of Reynolds and Prandtl number on the skin friction and Nusselt number in a wavy geometry. This was done by implementing a simple coordinate transformation on the non-dimensional governing equations and then finding the solutions using spline alternating direction implicit method. The results exhibited that the curves for the local skin-friction coefficient and the local Nusselt number have the same recurrence rate as the sinusoidal surface at smaller wavy amplitudes and lower Reynolds numbers. However, as these two quantities increased, a consequent rise in the local Nusselt number was also observed in the converging section of the wavy-wall indicating that a corrugated wall can be an effective medium of heat transfer.

*Corresponding author. Tel.: +88-02-55668200(Ext.1519); fax: +88-02-55668202
E-mail addresses: mmamun@northsouth.edu, mmamun@gmail.com

The first experimental study on corrugated surfaces was conducted by Rush *et al*. [8] where the local heat transfer and flow behavior for laminar and transitional flows was examined. The geometry was constructed for a channel with a 10:1 aspect ratio with the walls being 12 to 14 wavelengths long. A total of 12 test sections was created varying either the wave amplitude, phase angle or vertical wall spacing in each case. It was concluded that instabilities observed in the flow cause a heat transfer enhancement in the wavy channels. It was also established that a larger relative amplitude of the wavy section delayed the onset of instability in the channel. However the consequence of this factor reduced significantly for higher Reynold numbers.

Employment of sinusoidal walls in the nanofluid cavity was quickly becoming prominent due to increased surface area and better heat transferring capabilities. As a result of this, Heidary and Kermani [9] investigated the use of copper-water nanofluid in a wavy channel. The analysis involved changing the nanofluid volume fraction and wave amplitude and studying their effects on the average and local Nusselt number as well as the skin friction coefficient for a range of Reynolds numbers from 50 to 1500. It was observed that the addition of nano-particles to the purefluid along with the presence of wavy walls significantly improved the heat exchange between the wall and the fluid due to its improved thermal conductivity and increased temperature gradient with higher Reynolds numbers. In addition, the heat exchange was enhanced with increasing wave amplitudes too due to increased disturbance with the main flow at higher wave amplitudes. The skin friction coefficient was maximized at points along the duct having minimal cross sections and it was independent of the nanoparticle volume fraction.

Laminar mixed convection in a horizontal curved tube using water/Al_2O_3 nanofluid was numerically investigated by Alikhani et al. [10]. A two-phase approach subjected to mixed convection condition was used to investigate the nanofluid flow. Three dimensional elliptical approach was used to solve the governing equations and study the simultaneous effect of the buoyancy and centrifugal forces. The results showed that the increase in particle concentration significantly augments the average convective heat transfer. In addition, it was also observed that the nanoparticle concentration increases the strength of the secondary flow.

More work on mixed convection was done by Kherbeet et al. [11] who presented a mathematical evaluation of laminar mixed convection flow over a 2D horizontal microscale backward-facing step (MBFS) placed in a duct. The governing equations along with the boundary conditions were solved using the finite volume method (FVM). The upstream wall and the step wall were considered adiabatic, while the downstream wall was heated by uniform heat flux. Different types of nanoparticles such as Al_2O_3, CuO, SiO_2 and ZnO, with volume fractions in the range of 1–4% and nanoparticle diameter between \$25\$ nm to \$70\$ nm were used. The Reynolds number was in the range of 0.05 to 0.5. The results revealed that the Nusselt number increased with increase in volume fraction and Reynolds number as well as the decrease in nanoparticle diameter. The nanofluid consisting of SiO_2 nanoparticles was observed to have the highest Nusselt number.

Studies regarding turbulent flows were extended to wavy boundaries by Assato and Lemos [12] who investigated non-linear turbulence models used in complex flows. The main highlights of this investigation included the proposal of two models- i) a new implicit numerical treatment for non-linear diffusive terms and ii) analysis of linear and non-linear eddy-viscosity models in predicting turbulent flows. For comparing these two models, symmetric converging-diverging channel and concave-convex wall channel, were used. A boundary fitted non-orthogonal coordinate system was utilized for creating the grids. The discretization of governing equations was completed through control-volume method and the SIMPLE method was applied for handling pressure-velocity coupling. The results of this investigation showed that, the implicit technique was the only way to get converged result for high Re-model. This technique also helped to enhance the computational robustness of the relaxation process.

To the best of our knowledge, there is no paper in the literature that has interpreted mixed convection flow of nanofluid in a sinusoidal walled channel. The discussed geometry has its top and bottom wavy surface being heated. The fluid flow is characterized by varying Reynolds Numbers between 10 and 40 and the volume fraction from 0% to 20% respectively, for a Grashof number of 10^3. In addition the role played by mixed convection is studied by altering the Richardson number from 0 to 2. The effect of these parameters on the rate of convective heat transfer is presented in local Nusselt number graphs. Furthermore, variations in the fluid flow pattern and temperature inside the channel is presented in streamlines, isotherms, velocity and temperature profiles.

2. Mathematical model

The continuity, momentum and energy equations are respectively derived from the Navier-Stokes equation and can be expressed as follows-

$$\frac{\partial \mathrm{u}}{\partial \mathrm{x}} + \frac{\partial v}{\partial y} = 0 \tag{1}$$

$$\frac{\partial u}{\partial \mathrm{t}} + u\frac{\partial u}{\partial x} + v\frac{\partial u}{\partial y} = -\frac{1}{\rho}\frac{\partial P}{\partial x} + \frac{\mu}{\rho}\left[\frac{\partial^2 u}{\partial x^2} + \frac{\partial^2 u}{\partial y^2}\right] \tag{2}$$

$$\frac{\partial v}{\partial \mathrm{t}} + v\frac{\partial v}{\partial y} + u\frac{\partial v}{\partial x} = -\frac{1}{\rho}\frac{\partial P}{\partial y} + \frac{\mu}{\rho}\left[\frac{\partial^2 v}{\partial y^2} + \frac{\partial^2 v}{\partial x^2}\right] + g\beta\left(T - T_\infty\right) \tag{3}$$

$$\frac{\partial T}{\partial \mathrm{t}} + u\frac{\partial T}{\partial x} + v\frac{\partial T}{\partial y} = \kappa\left[\frac{\partial^2 T}{\partial x^2} + \frac{\partial^2 T}{\partial y^2}\right] \tag{4}$$

The following substitutions are then applied to the governing equations to convert them to non-dimensional form:

$$X=\frac{x}{\mathrm{L}},\ Y=\frac{y}{\mathrm{L}},\ U=\frac{u}{u_r},\ V=\frac{v}{v_r},\ \Theta=\frac{T-T_c}{\mathrm{T_h}-\mathrm{T_c}},\ P=\frac{p}{\rho u_r^2}$$

$$\mathrm{Pr}_f=\frac{v_f}{\alpha_f},\ Ra=\frac{g\beta(T_h-T_c)L^3\,\mathrm{Pr}_f}{{v_f}^2},\ Gr=\frac{Ra}{\mathrm{Pr}_f},\ \mathrm{Re}=\frac{u_r L}{v_f} \quad (5)$$

$$Gr=\frac{g\beta(T_h-T_c)L^3}{{v_f}^2},\ v_{nf}=\frac{\mu_{nf}}{\rho_{nf}},\ \alpha_{nf}=\frac{K_{nf}}{\rho(C_p)_{nf}}$$

The non dimensionalied continuity, u-momentum, v-momentum and internal energy equations are given as follows-

$$\frac{\partial \mathrm{U}}{\partial \mathrm{X}}+\frac{\partial V}{\partial Y}=0 \quad (6)$$

$$\frac{\partial U}{\partial \tau}+U\frac{\partial U}{\partial X}+V\frac{\partial U}{\partial Y}=-\frac{1}{(1-\phi)+\phi\frac{\rho_s}{\rho_f}}\frac{\partial P}{\partial X}+\frac{1}{\mathrm{Re}(1-\phi)^{2.5}\left[(1-\phi)+\phi\frac{\rho_s}{\rho_f}\right]}\left[\frac{\partial^2 U}{\partial X^2}+\frac{\partial^2 U}{\partial Y^2}\right] \quad (7)$$

$$\frac{\partial V}{\partial \tau}+U\frac{\partial V}{\partial X}+V\frac{\partial V}{\partial Y}=-\frac{1}{(1-\phi)+\phi\frac{\rho_s}{\rho_f}}\frac{\partial P}{\partial Y}+\frac{1}{\mathrm{Re}(1-\phi)^{2.5}\left[(1-\phi)+\phi\frac{\rho_s}{\rho_f}\right]}\left[\frac{\partial^2 V}{\partial X^2}+\frac{\partial^2 V}{\partial Y^2}\right]+Gr\frac{\Theta}{\mathrm{Re}^2}\left[\frac{1}{1+\frac{(1-\phi)\rho_f}{\varphi\rho_s}\frac{\beta_s}{\beta_f}}+\frac{1}{1+\frac{\phi\rho_s}{(1-\phi)\rho_f}}\right] \quad (8)$$

$$\frac{\partial \Theta}{\partial \tau}+U\frac{\partial \Theta}{\partial X}+V\frac{\partial \Theta}{\partial Y}=\frac{1}{\mathrm{Re}}\frac{1}{\mathrm{Pr}}\frac{\frac{K_{nf}}{K_f}}{\left[(1-\phi)+\phi\frac{(\rho C_p)_s}{(\rho C_p)_f}\right]}\left[\frac{\partial^2\Theta}{\partial X^2}+\frac{\partial^2\Theta}{\partial Y^2}\right] \quad (9)$$

Next to tackle the complexity of the wavy geometry the non-dimensional equations are transformed to curvilinear coordinates which utilizes the introduction of the Jacobian.

Transformed U momentum equation

$$\frac{\partial U}{\partial \tau}+\frac{1}{|J|}(UA_{11}+VA_{21})\frac{\partial U}{\partial \zeta_1}+\frac{1}{|J|}(UA_{12}+VA_{22})\frac{\partial U}{\partial \zeta_2}=-\frac{1}{\left[(1-\phi)+\frac{\phi\rho_s}{\rho_f}\right]|J|}\left[A_{11}\left(\frac{\partial P}{\partial \zeta_1}\right)+A_{12}\left(\frac{\partial P}{\partial \zeta_2}\right)\right]+\frac{1}{\mathrm{Re}(1-\phi)^{2.5}\left[(1-\phi)+\phi\frac{\rho_s}{\rho_f}\right]|J^2|}\left[\begin{array}{l}(A_{11}^2+A_{21}^2)\frac{\partial^2 U}{\partial \zeta_1^2}+2(A_{11}A_{12}+A_{21}A_{22})\frac{\partial^2 U}{\partial \zeta_1\partial \zeta_2}\\+(A_{12}^2+A_{22}^2)\frac{\partial^2 U}{\partial \zeta_2^2}\end{array}\right] \quad (10)$$

Transformed V-momentum equation

$$\frac{\partial V}{\partial \tau}+\frac{1}{|J|}(UA_{11}+VA_{21})\frac{\partial V}{\partial \zeta_1}+\frac{1}{|J|}(UA_{12}+VA_{22})\frac{\partial V}{\partial \zeta_2}=-\frac{1}{\left[(1-\phi)+\frac{\phi\rho_s}{\rho_f}\right]|J|}\left[A_{11}\left(\frac{\partial P}{\partial \zeta_1}\right)+A_{12}\left(\frac{\partial P}{\partial \zeta_2}\right)\right]+\frac{1}{\mathrm{Re}(1-\phi)^{2.5}\left[(1-\phi)+\phi\frac{\rho_s}{\rho_f}\right]|J^2|}\left[(A_{11}^2+A_{21}^2)\frac{\partial^2 V}{\partial \zeta_1^2}+2(A_{11}A_{12}+A_{21}A_{22})\frac{\partial^2 V}{\partial \zeta_1\partial \zeta_2}+(A_{12}^2+A_{22}^2)\frac{\partial^2 V}{\partial \zeta_2^2}\right]+Gr\frac{\Theta}{\mathrm{Re}^2}\left[\frac{1}{1+\frac{(1-\phi)\rho_f}{\phi\rho_s}\frac{\beta_s}{\beta_f}}+\frac{1}{1+\frac{\phi\rho_s}{(1-\phi)\rho_f}}\right] \quad (11)$$

Transformed Internal energy equation

$$\frac{\partial \Theta}{\partial \tau}+\frac{1}{|J|}(UA_{11}+VA_{21})\frac{\partial \Theta}{\partial \zeta_1}+\frac{1}{|J|}(UA_{12}+VA_{22})\frac{\partial \Theta}{\partial \zeta_1}=\frac{1}{\mathrm{Re}}\frac{1}{\mathrm{Pr}}\frac{\frac{K_{nf}}{K_f}}{\left[(1-\phi)+\phi\frac{(\rho C_p)_s}{(\rho C_p)_f}\right]|J|^2}\left\{\begin{array}{l}(A_{11}^2+A_{21}^2)\frac{\partial^2\Theta}{\partial \zeta_1^2}+(A_{12}^2+A_{22}^2)\frac{\partial^2\Theta}{\partial \zeta_2^2}\\+2(A_{11}A_{12}+A_{21}A_{22})\frac{\partial^2\Theta}{\partial \zeta_1\partial \zeta_2}\end{array}\right\} \quad (12)$$

3. Computational geometry and Boundary conditions

The following figure shows the shape of the implemented wavy channel and the summarized boundary conditions. Fluid enters through the left and exits through the right end of the channel.

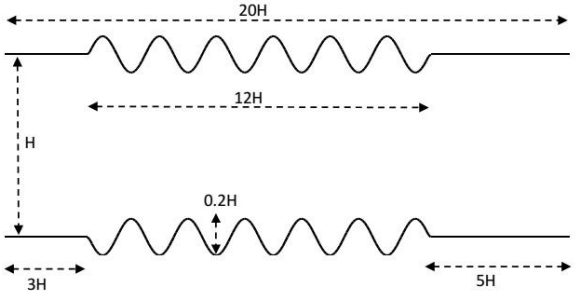

Fig.1 Body fitted mesh of computational geometry

Inflow-

$$T = T_c, U = U_{in}, U = 6\left(\frac{1}{4} - y^2\right), V = 0, x = 0, -\frac{H}{2} \le y \le \frac{H}{2}, H = 1$$

Wall- (13)

$$T = T_w = T_h, U = V = 0, \quad y = y(1 + \alpha \sin x) \qquad (14)$$

Exit plane-

$$\frac{\partial T}{\partial x} = 0, \frac{\partial u}{\partial x} = 0 \quad at \quad x = L, \quad -\frac{H}{2} \le y \le \frac{H}{2}, H = 1 \qquad (15)$$

4. Results and discussion

4.1 Code validation

In order to assess the accuracy of our numerical code, the algorithm was tested at Reynolds number 250 and volume fraction 0% for a wavy channel. As can be seen from the local Nusselt number graph the results of the current experiment are in excellent agreement with that of Heidary and Kermani [2].

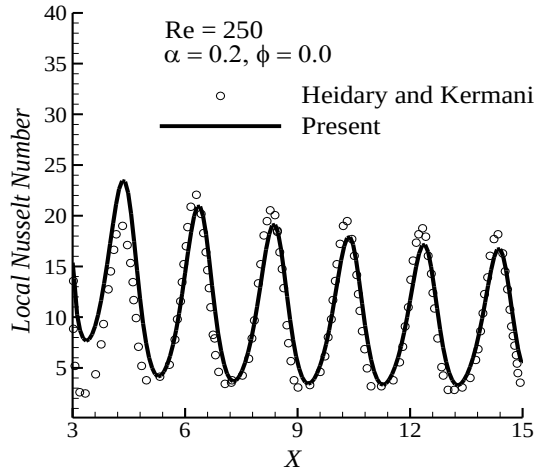

Fig.2 Comparison of Local Nusselt number of the current study with that of Heidary and Kermani [2]

4.2 Grid independence test

To perform this test, graphs of the local Nusselt number were observed at Reynolds number 500, Grashof number 10^4 and volume fraction, 20% for three different grid arrangements; 71 X 251, 100 X 300 and 120 X 300. The overlapping curves for all three grid sizes validate the grid independence test.

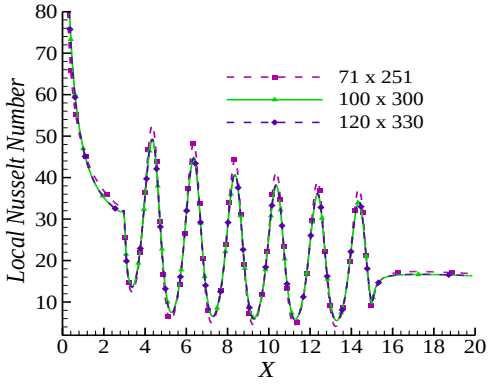

Fig.3 Local Nusselt number for three different grid sizes at Re = 500, Gr = 10^4 and Φ = 20%

4.3 Results

Presence of Ri usually indicates the onset of mixed convection which takes both natural and forced convection into account. A value of Ri = 0, indicates the presence of forced convection only whereas large values of Ri (beyond 100) mean that the effects of natural convection are dominant. Intermediate values of Ri between 0.1 to 10 signifies that the roles played by both natural and forced convection are important and is thus ideal to display the consequences of mixed convection.

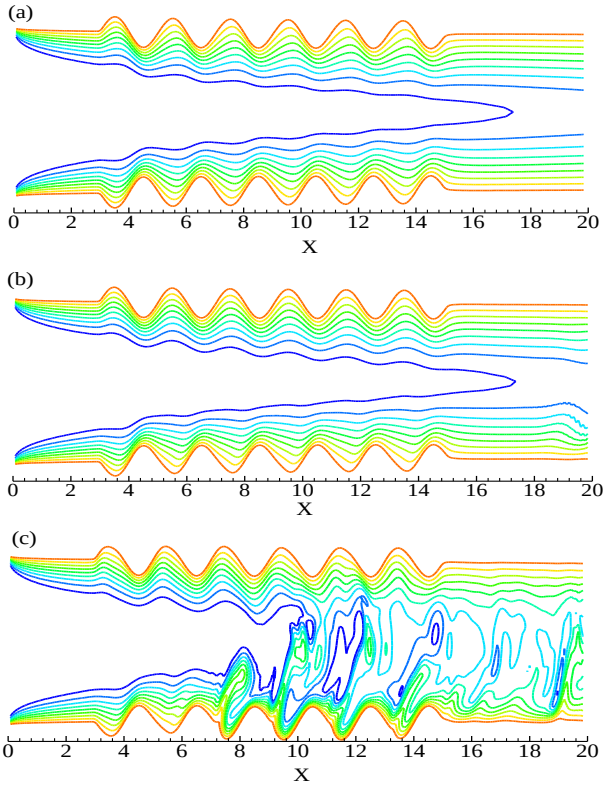

Fig.4 Isotherms for nanofluid (Φ = 20%) at (a) Ri = 0, (b) Ri = 1 and (c) Ri = 2 at Re = 100

Fig. 4(a) shows the isotherm contours in the channel for forced convection, Ri = 0. As can be seen from the figure, the isotherms are concentrated near the channel walls, setting up a high temperature gradient leading to enhanced heat transfer. The fluid flow is laminar in this case as depicted by the well oriented isotherms. However, this behavior change as the Richardson number is increased gradually. For Ri = 1, the thickness of the thermal boundary increases slightly and the isotherms at the channel outlet start showing signs of distortion due to the inception of mixed convection. For higher values of Ri, the nature of the fluid flow transitions from laminar to turbulent due to the increase in the buoyancy term. In these cases, conduction

minimizes and convection largely dominates the primary method of heat transfer.

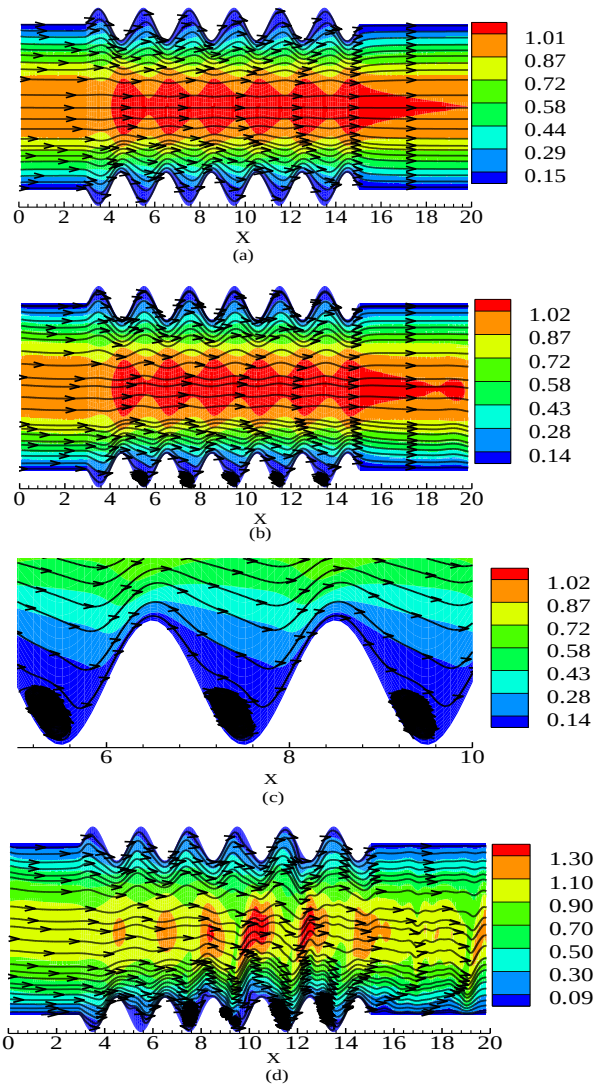

Fig.5 Streamlines for nanofluid (Φ = 20%) at (a) Ri = 0, (b) Ri = 1 with (c) its magnified view and (d) Ri = 2 at Re = 100

Concurrent to the results shown by the isotherms previously, the uniform streamlines present in Fig. 5(a) signify laminar fluid motion when Ri = 0. These features are largely maintained when the Richardson number is increased to 1 in (b). In both these cases the fluid passing through the center of the channel constantly exhibits the highest velocity as expected when the fluid motion is undisturbed. However a significant amount of turbulence can be observed near the upper and lower peripheries of the channel when the Richardson number is increased to 2. The streamlines lose their uniform distribution and large vortices are developed at the furrow of the wavy channel which become more prominent for higher Richardson numbers. The resulting vortices lead to a backflow of the fluid in the associated regions which partially obstruct the fluid flow traversing from the channel inlet to outlet in the wavy sections. However a higher Richardson number leads to lower levels of viscosity which in general increases the fluid velocity in the midsection of the channel.

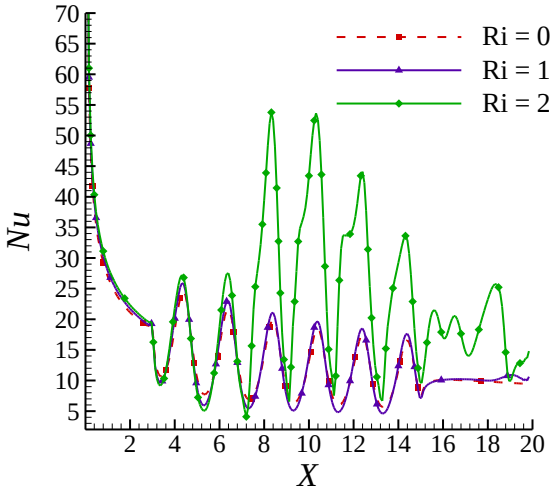

Fig.6 Local Nusselt number at different Richardson numbers and Reynolds number = 100

For Ri = 0 (forced convection) and Ri = 1 (onset of mixed convection) the frequency of the graph in fig.6 matches that of the wavy surface. As expected, the minimum and maximum values occur in the largest and smallest cross sections of the channel respectively. The peak values for Ri = 1 are slightly greater than those for Ri = 0 since the former takes the effects of both natural and forced convection into account. The graph for Ri = 2 initially overlaps the graphs of Ri = 0 and 1 for the first two cycles of the wavy section. However the formation of eddies near the furrows of the wavy channel from the third cycle onward shown by Fig.5 (d) creates circulations in the given areas which rapidly increases the rate of heat transfer. As a result, there is a large overshoot in the local Nusselt number slightly upstream from the troughs of the wavy channel after the third cycle. The size of the vortices in the subsequent furrows decreases, leading to smaller peaks in the local Nusselt number.

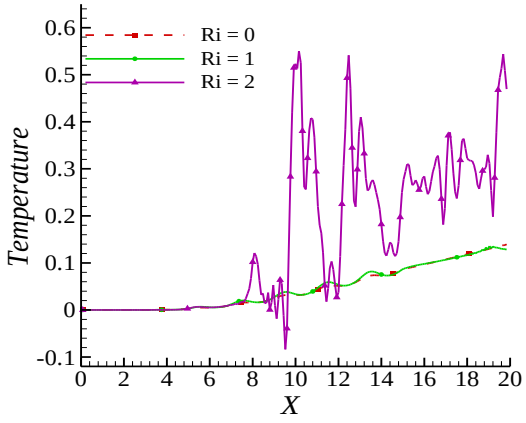

Fig.7 Temperature distribution at various Richardson number and Re = 100

For the temperature distribution shown in Fig.7, the graphs for Ri = 0 and 1 are again overlapping for the most part due to laminar fluid flow. Here, the graph of Ri = 1 shows a slightly higher temperature than for Ri = 0. Turbulent flow for the cases of Ri = 2 lead to the large fluctuations in temperature at the mid plane of the channel as shown in the figure. The eddies created at the furrows of the wavy sections store high temperatures as shown and this creates a higher temperature gradient leading to enhanced heat transfer.

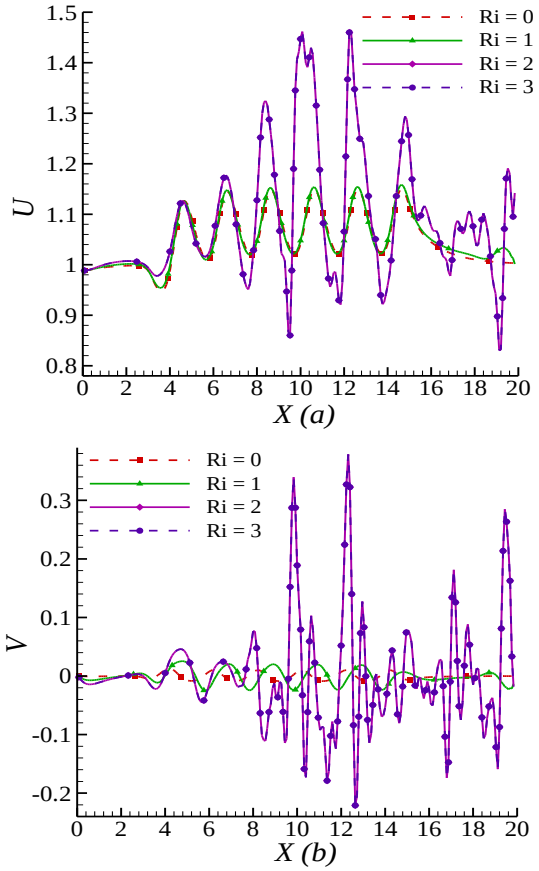

Fig.8 (a) U velocity and (b) V velocity at different Richardson numbers and Re = 100

Fig.8 (a) above shows the U velocity of the nanofluid along the length of the channel for different Richardson numbers at a Reynolds number of 100. The positive values for all the graphs signify that the net movement of the fluid is from the channel inlet to the outlet. The graphs of Ri = 0 and 1 coincide and show minimum and maximum values at the widest and narrowest sections of the channel respectively. The graph of Ri = 2 show higher magnitudes than those for Ri = 0 and 1 since increase in the Richardson number reduces the viscous nature of the fluid.

In fig.8 (b) the fluctuation in the V velocity values from positive to negative for Ri = 0 indicate that the vertical movement of the fluid is bidirectional at the mid plane of the channel. The graph for Ri = 1 shows a similar shape with higher minimum and maximum values. Turbulence in the case of Ri = 2 lead to the larger overlapping fluctuations attaining greater peak values. In this case the larger V velocity magnitudes are a result of the high temperature stored by the vortices which create strong convection currents inside the channel.

5. Conclusion

The highlights of this research are summarized below-

- Onset of mixed convection was investigated by altering the Richardson number from 0 to 2.
- For higher Richardson numbers the temperature gradient with the channel surface was greater leading to higher rates of heat transfer.
- Streamline profiles indicated that the flow pattern of the nanofluid is laminar for forced convection, but transitions to turbulent flow for higher Richardson numbers.
- The temperature of a nanofluid increased with the increase in Richardson number due to inception of more turbulence.
- In addition, the local Nusselt number graphs showed that the average rate of heat transfer is almost doubled when the Richardson number is increased from 0 to 2.
- The net horizontal flow of the nanofluid is from the channel inlet towards the channel outlet as indicated by the positive U velocity values.
- Fluctuations in both U and V velocities is more pronounced for higher Richardson numbers.

NOMENCLATURE

$\overline{Nu}$	: average Nusselt number, no unit
F	: body force, N
H	: channel width, m
Ra	: Rayleigh number, no unit
Re	: Reynolds number, no unit
Ri	: Richardson number, no unit
Gr	: Grashof number, no unit
Pr	: Prandtl number, no unit
A	: cofactor, no unit
CV	: control volume
x, y	: dimensional cartesian coordinates, m
P	: dimensional pressure, pa
u, v	: dimensional velocity components, $m \cdot s^{-1}$
X, Y	: dimensionless cartesian coordinates
P	: dimensionless pressure
U, V	: dimensionless velocity components
K_f	: fluid thermal conductivity, $W \cdot m^{-1} \cdot K^{-1}$
E	: internal energy, J
J	: Jacobian, no unit
K_{nf}	: nanofluid thermal conductivity, $W \cdot m^{-1} \cdot K^{-1}$
L	: reference length, m
K_s	: solid thermal conductivity, $W \cdot m^{-1} \cdot K^{-1}$
C_p	: specific heat at constant pressure, $kJ \cdot kg^{-1} {}^{o}C^{-1}$
S(x)	: surface geometry function, m
T	: temperature, K
t	: time, s

Subscripts

c	: cold, no unit

i , j : coordinate numbers in Jacobian transformation - i, j = 1,2

x, y, z : direction along axis, no unit

H : hot, no unit

N_f : nanofluid, no unit

Greek

ρ : density, $kg \cdot m^{-3}$

ζ_1, ζ_2 : dimensionless coordinates for Jacobian transformation

τ : dimensionless time, no unit

μ : dynamic viscosity, $kg \cdot m^{-1} \cdot s^{-1}$

β_f : fluid thermal expansion coefficient, K^{-1}

β_{nf} : nanofluid thermal expansion coefficient, K^{-1}

υ : kinematic viscosity, $m^2 \cdot s^{-1}$

Θ : non dimensional temperature, no unit

ϕ : solid volume fraction, no unit

ψ : streamline function, $m^2 \cdot s^{-1}$

β : thermal expansion coefficient, K^{-1}

REFERENCES

[1] C. Wang, C. Chen, Forced Convection in a wavy wall channel, International Journal of Heat and Mass Transfer 45 (12) (2002) 2587-2595.

[2] O. Abouali, A. Falahatpisheh, Numerical investigation of natural convection of Al_2O_3 nanofluid in vertical annuli, Heat and Mass transfer 46 (1) (2009) 15–23.

[3] E. Wasp, J. Kenny, Solid-liquid flow slurry pipeline transportation, Heat and Mass transfer.

[4] S. Jang, S. Choi, Role of Brownian motion in the enhanced thermal conductivity of nanofluids, Applied Physics Letters 84 (21) (2004) 4316.

[5] N. Putra, W. Roetzel, S. Das, Natural convection of nano-fluids, Heat and Mass Transfer 39 (8–9) (2003) 775–784.

[6] B. Pak, Y. Cho, Hydro dynamic and heat transfer study of dispersed fluids with submicron metallic oxide particles, experimental Heat Transfer 11 (2) (1998) 151–170.

[7] C. Wang, C. Chen, Forced convection in a wavy-wall channel, International Journal of Heat and Mass Transfer 45 (12) (2002) 2587–2595.

[8] T. Rush, T. Newell, A. Jacobi, An experimental study of flow and heat transfer in sinusoidal wavy passages, International Journal of Heat and Mass Transfer 42 (9) (1999) 1541–1553.

[9] H. Heidary, M. Kermani, Effect of nano-particles on forced convection in sinusoidalwall channel, International Communications in Heat and Mass Transfer 37 (10) (2010) 1520–1527.

[10] S. Alikhani, A. Behzadmehr, M. Saffar-Avval, numerical study of nanofluid mixed convection in a horizontal curved tube using two-phase approach, Heat and Mass Transfer 47 (1) (2011) 107–118.

[11] A. S. Kherbeet, H. A. Mohammed, B. Salman, The effect of nanofluids flow on mixed convection heat transfer over microscale backward-facing step, International Journal of Heat and Mass Transfer 55 (21) (2012) 5870–5881.

[12] M. Assato, M. Lemos, Turbulent flow in wavy channels simulated with nonlinear models and a new implicit formulation, Numerical Heat Transfer, Part A: Applications 56 (4) (2009) 301–324.

ICMIEE-PI-140262

A mismatch between seat measurements and body dimensions of truck drivers in Bangladesh

Tamanna Mahamud, Shams-E Ara Noor, Pobitra Kumar Halder, Sarojit Kumar Biswas*
Department of Industrial and Production Engineering, Jessore University of Science and Technology, Jessore-7408, BANGLADESH

ABSTRACT
In Bangladesh, truck drivers face many problems such as back pain, neck pain, headache and musculoskeletal diseases because of improper seat design. Therefore, it is essential to use ergonomic consideration and appropriate sitting posture for drivers' seat design for comfort. The study outlines the mismatch between seat dimensions and anthropometric characteristics of thirty Bangladeshi truck drivers, aged ranging from 30 to 50 years. Here, five trucks of same model of Tata had been considered for four seat dimensions and relative four anthropometric measurements of drivers. The potential mismatch between seat dimensions and anthropometric measurements in this study indicated that the seat dimensions were not ergonomically fit for the drivers. The paper also proposed the seat dimensions that increase the match percentages with body dimensions and will improve drivers' sitting posture.

Keywords: Sitting posture; Mismatch; Anthropometric dimensions; Seat measurements; Truck driver.

1. Introduction

The scientific study of people and their work is known as ergonomics [1]. For determining the furniture is safe to use, the designer of furniture needs to apply the anthropometry of the specific user [2]. Trucks are one of the most common transportation which has been widely used in Bangladesh. Truck driving is one of the hardest professions. Seat is the place where truck drivers have to spend most of their time. The seat plays a vital role in fulfilling drivers comfort expectation and removing fatigue [3]. Here, most of the truck seats are made without ergonomic consideration because the seat manufacturers are illiterate and have no knowledge about anthropometry. Uncomfortable and awkward sitting postures are responsible for musculoskeletal injuries, back pains or lumber pains, neck pains, foot cramp and this also puts pressure on the muscles, the ligaments and on lumbosacral joint and so on. Therefore, useful ergonomic measures need to be considered for avoiding these remarkable problems. The main goal of this study is to determine the possible mismatch between seat dimension and anthropometric characteristics and to recommend proposed dimensions for relieving health problems, ensuring comfort and reducing fatigue of truck drivers.

2. Major problems of truck drivers

In our country, truck driver faces many long term physical effects due to driven in sitting on poor driving seat. These physical problems include foot cramp, neck pain, numbness, eye strain or headache, obesity, muscle weakness, hypertension, musculoskeletal disorder. All these problems area are compared with the normal people who are not driving the truck. Thirty normal people were considered for this sample of data. The comparison shows that the percentage of this problem is higher than that of normal people. It is estimated that, almost 93.33% of driver suffer from back pain and 86.67% suffer from neck pain whereas the values for normal people is 40% and 33.33% respectively. Thus, anthropometry study should be considered for relieving the problem and leading better life for truck driver.

3. Methodology/procedure

2.1 Sample, measuring technique and procedure

In this study a sample of 30 drivers from Central Storage Depot (CSD) in the Khalishpur, Khulna with ages ranged from 30 to 50 years was arbitrarily selected for the purpose of various anthropometric measurements of drivers. For data collection, five trucks of TATA were considered. In the study various anthropometric measurements of drivers when they were sitting in an erect position on an adjustable seat with horizontal surface whose lower and upper legs were pointed at right angles and standing in a standard position, having shoeless and wearing light normal vest with no pockets and seat dimension of these trucks were taken by anthropometer, a measuring tape and a height measuring scale. The mean value, maximum and minimum values, standard deviation (SD) value, and also the percentile value were calculated by statistical software called Microsoft Excel.

2.2 Anthropometric measurements

The anthropometric measurements are the basis of this research. Four anthropometric measurements are considered as shown in Figure 1.

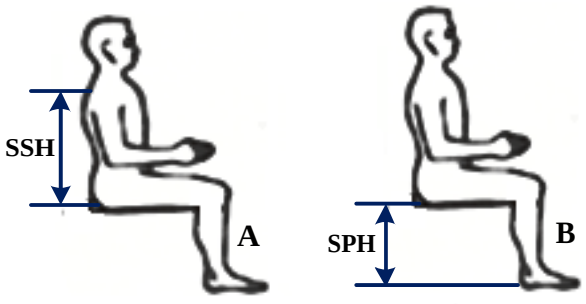

* Corresponding author. Tel.: +88-01913597592
E-mail address: pobitra.halder@gmail.com

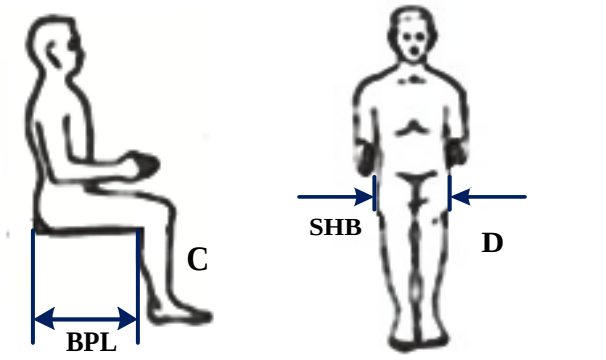

Fig.1 Anthropometric measurements of driver: A) Sitting shoulder height (SSH), B) Sitting popliteal height (SPH), C) Buttock popliteal length (BPL), D) Hip breadth (HB) [4]

Shoulder elbow length: In a standard sitting position, distance measured from the acromion to underside of the elbow.

Sitting popliteal height: The distance measured vertically from the underside of the foot to the underside of the thigh at the knees.

Buttock-popliteal length: Taken with a 90º angle knee flexion as the horizontal distance from the posterior surface of the buttock to the posterior surface of the knee where the posterior surface of the lower legs fit the underside of the thigh during the attendant sits completely erect with thighs fully supported and sitting surface spreading far into the hollow of the knee, supporting freely the feet flat on the floor.

Hip breadth sitting: The maximum horizontal distance measured across the hips in the sitting position.

2.3 Seat measurements

In this study, four existing seat dimensions relative to anthropometric measurements are considered as described in Figure 2.

Seat height: The vertical distance that measured from the floor to the middle point of the front edge of the seat.

Seat depth: The horizontal distance measured from the back edge of the sitting surface of the seat to the front edge.

Seat width: Distance measured horizontally between the lateral edges of the seat.

Backrest height: Distance measured vertically from the upper edge of the backrest to the sitting surface.

2.4 Seat and body dimension mismatch

This can be possible by using most recommended relationships. The most common relationships are described below.

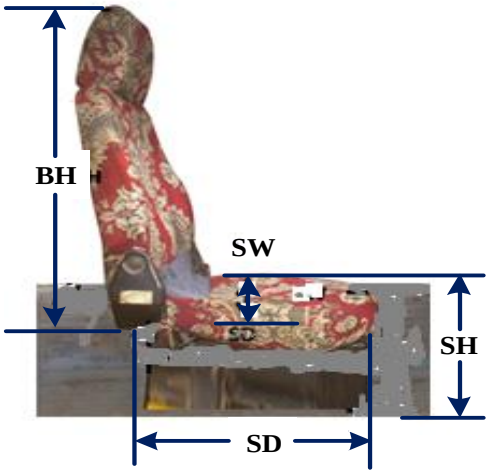

Fig.2 Existing seat dimensions of TATA: Seat height (SH), Seat width (SW), Seat depth (SD), Backrest height (BH)

Popliteal height and seat height mismatch: According to the literature popliteal height should be higher than seat height to allow the lower legs forming a 5º-30º angle relative to the vertical and the shin-thigh angle is between 95º and 120º [5]. A mismatch of the popliteal height against the seat height is defined when seat height is either > 95% or < 88% of the popliteal height [6] and it is possible to form a criterion for SH [5]. Thus, a match criterion is defined by the use of equation 1.

$$(PH+3)\ \mathrm{Cos}\ 30^{o} \leq SH \leq (PH+3)\ \mathrm{Cos}5^{o} \quad (1)$$

Buttock popliteal length and seat depth mismatch: A mismatch of the BPL against the seat depth is defined when seat depth is either < 80% or >95% of BPL [6]. A well-fitting seat needs to be a depth of between 80% and 95% of the users BPL [2]. Thus a match criterion is formed, according to equation 2.

$$0.80\ BPL \leq SD \leq 0.95\ BPL \quad (2)$$

Hip breadth and seat width mismatch: The modified proposed equation by Gouvali and Boudolos [5] recommended that seat width should be a minimum of 10% (to accommodate hip breadth) and a maximum of 30% (for space economy) larger than the hip breadth. Therefore, a match criterion is established by the application of equation 3.

$$1.10\ HB \leq SW \leq 1.30\ HB \quad (3)$$

Sitting shoulder height and backrest height mismatch: According to the recommendation of Gouvali and Boudolos [5] and Agha [7], the backrest should be kept lower than or almost on the upper edge of the scapula and an optimum height of the backrest should be at 60%-80% of shoulder height. Thus, a match criterion is demonstrated according to equation 4.

$$0.60\ SSH \leq BH \leq 0.80\ SSH \quad (4)$$

3. Result and discussion

The descriptive statistics of the anthropometric dimensions of drivers and the existing seat dimensions of driving seat are presented in Table 1 and Table 2.

Table 1 Relevant anthropometric data of truck drivers

Anthropometric measurement (cm)			Percentile value		
	Mean	SD	5th	50th	95th
SSH	61.5	2.41	57.7	62	64.15
SPH	43.3	1.21	41.85	43	45
BPL	44.17	2.12	41.7	44	47.3
SHB	40.71	2.54	36.35	41	44.3

Table 1 shows that, the mean SPH of the truck drivers is 43.3 cm (SD 1.21). Similarly, the mean SSH, BPL and SHB are 61.5 cm, 44.17 cm and 40.17 cm with SD of 2.41, 2.12 and 2.54 respectively.

Table 2 Dimensions of existing truck driver seats of TATA

Seat dimension (cm)			Percentile value		
	Mean	SD	5th	50th	95th
SH	47.28	0.19	47.04	47.3	47.48
SW	46.22	0.19	46.02	46.2	46.46
SD	38.24	0.21	38.02	38.2	38.48
BH	48.32	0.24	48.04	48.3	48.58

Table 2 shows that, the mean of SH, SW, SD and BH are 47.28 cm, 46.22 cm, 38.24 cm and 48.22 cm with a standard deviation of 0.19, 0.19, 0.21 and 0.24.

The percentages of drivers whose anthropometric measurements are matched or did not match (high mismatch or low mismatch) the mean values of existing seat dimensions of the 5 trucks of TATA are presented in Table 3.

Table 3 Match/mismatch percentages for drivers of TATA

Seat dimensions	Match (%)	Mismatch (%)		
		Low	High	Total
SH	26.67	0	73.33	73.33
SW	73.33	26.67	0	26.67
SD	93.33	6.67	0	6.67
BH	73.33	0	26.67	26.67

The mismatch percentage of SH is 73.33%, SW is 26.67%, SD is 6.67% and BH is 26.67% for drivers. This result denoted that the dimension of SH is too high (high mismatch) for drivers (70.33%) and is almost appropriate for 26.67% drivers. The dimension of SW is almost appropriate for the majority of the drivers (73.33%) and is too low (low mismatch) only for 26.67% drivers. The dimension of SD is too shallow (low mismatch) for 6.67% and almost acceptable for 93.33% drivers. In the case of BH about 26.67% drivers are not suited because of too large (high mismatch) BH dimension whereas 73.33% drivers are suited to the BH dimension.

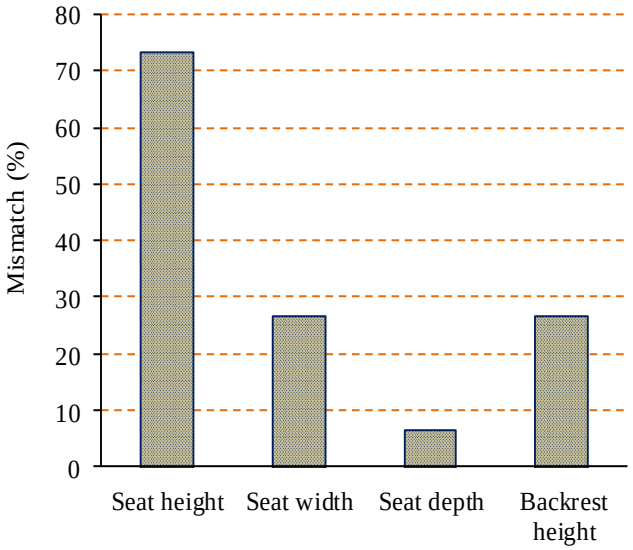

Fig.3 Mismatch percentages for drivers

Figure 3 represents the mismatch percentages for drivers. Almost 73.33% of drivers' SPH do not match to the measurement of SH. Because of this high mismatch, drivers are not able to support their feet on the floor. This causes to serious discomfort or possible injury, increased in tissue pressure on the posterior surface of the knee [8, 9] and also causes low back pain if the posture is prolonged.

4. Proposed seat dimension

To improve the existing four seat dimensions of the three types of truck with considering drivers anthropometry, the dimensions of single seat are proposed for drivers. Table 4 shows the four proposed dimensions of seat based on the anthropometric data which are appropriate for three types of truck.

Table 4 Proposed seat dimensions (cm) and match/ mismatch percentages for drivers

Seat dimensions	Dimension (cm)	Match (%)	Mismatch (%)		
			Low	High	Total
SH	43	100	0	0	0
SW	49.8	80	0	20	20
SD	38.5	100	0	0	0
BH	44	100	0	0	0

In the table 4, it can be seen that as compared to the existing four seat dimensions, the new proposed dimensions better match the driver's anthropometry, with the percentages ranging from 80% to 100%. The newly proposed four dimensions for improving the match percentage of the sampled drivers are shown in Figure 4.

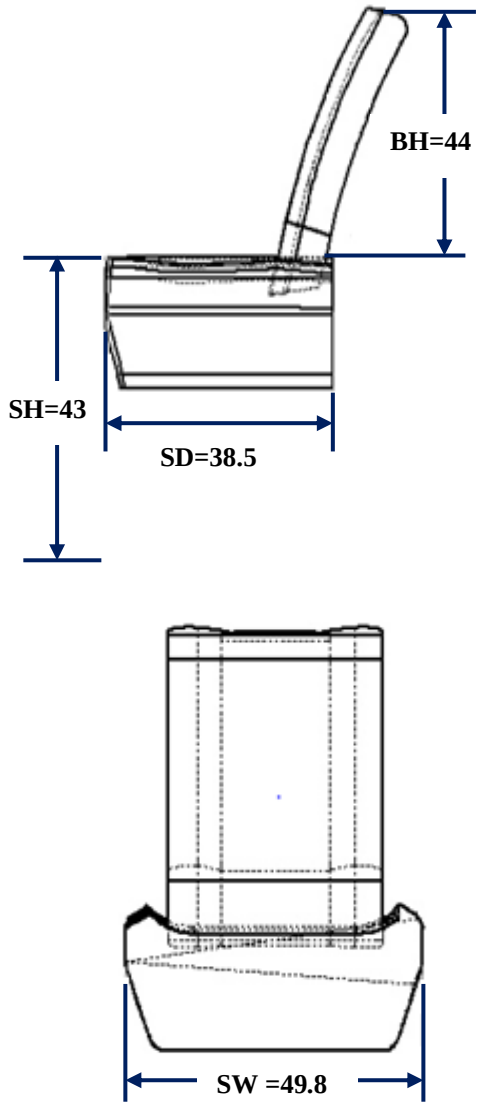

Fig.4 Proposed seat dimensions for truck drivers (cm)

5. Conclusion

The main focus of the study is on seat for Bangladeshi truck drivers. There is a considerable mismatch between body dimensions of drivers and their seat dimensions. This condition predisposes to increase pain and discomfort and tend to increase musculoskeletal and other health related problem amongst truck drivers. The findings of the study clearly indicate that the design and allocation of truck seat for drivers should be made for avoiding unnecessary demands upon them. So, the proposed dimensions for the truck seats were given based on anthropometric data obtained for reducing the mismatch related problems and ensuring comfort of drivers.

REFERENCES

[1] The nation. Ergonomics solution to occupational health problems. www.nation.lk/edition/health/item/12091-ergonomics-solution-to-occupational-health-problems.htm.

[2] A. Nazif, N. Kamar, S. Ezrin Hani, C. K. Lee, I. Ahmad Rasdan, A Study on the Suitability of Science Laboratory Furniture in Malaysian Secondary School, *Asia Pacific Symposium on Advancements in Ergonomics and Safety (ERGOSYM2011)*, Perlis, Malaysia, (5-6 December 2011).

[3] T. C. Fai, F. Delbressine, M. Rauterberg, Vehicle seat design: state of the art and recent development, *World Engineering Congress*, pp. 51-61, Penang Malaysia, (2007).

[4] A. S. Onawumi, E. B. Lucas, Ergonomic Investigation of Occupational Drivers and Seat Design of Taxicabs in Nigeria, *ARPN Journal of Science and Technology*, vol. 2, no. 3, pp. 214-220, (2011).

[5] M. K. Gouvali, K. Boudolos, Match between school furniture dimensions and children's anthropometry, *Applied Ergonomics*, vol. 37, pp. 765-773, (2006).

[6] C. Parcells, M. Stommel, R. P. Hubbard, Mismatch of classroom furniture and student body dimensions: empirical findings and health implications, *Journal of Adolescent Health*, vol. 24, no. 4, pp. 265-273, (1999).

[7] D. Chaffin, G. Anderson, Bernard J. Martin, Occupational biomechanics, New York: John Wiley and Sons, 2nd ed. (1991).

[8] S. Milanese, K. Grimmer, School furniture and the user population: an anthropometric perspective, *Ergonomics*, vol. 47, pp. 416–426, (2004).

[9] S. R. Agha, School furniture match to students' anthropometry in the Gaza Strip, *Ergonomics*, vol. 53, 344–354, (2010).

ICMIEE-PI-140264

Effect of different casting variables on casting quality

Tasmia Zaman [1,*], *A. Hafiz Zaman* [2]
[1] Department of Glass and Ceramic Engineering, Rajshahi University of Engineering & Technology, Rajshahi-6204, BANGLADESH
[2] Department of Mechanical Engineering, Rajshahi University of Engineering & Technology, Rajshahi-6204, BANGLADESH

ABSTRACT
Quality of castings is partly affected by the type and extent of residual stresses, which may lead to undesirable distortions and dimensional changes in critical parts and components. So it is essential to study the effects of casting variables on residual stress. In this research, the effects of variables like chemical composition and pouring temperature on tensile property, elongation, residual stress/strain as well as microstructure have been studied. For this purpose commercially pure Al and Al-Si-Cu-Mg alloy was taken. Pouring temperature was varied from 700 to 900^{o}C. Effect of mold hardness on residual stress was studied by varying mold hardness. Visual inspection was done to observe the presence of oxide films at surface. Microstructure of the cast samples using scanning electron microscope (SEM) was done to visualize the presence of oxide films inside the casting. UTS, percent elongation and residual stress were measured for each sample. The results showed that all of the mentioned casting parameters had clear effects on tensile property as well as residual stresses. The residual stresses and UTS decreased with decreasing pouring temperature and mold hardness. It was also found that microstructure and mechanical properties are influenced significantly by the mentioned parameter.

Keywords: Residual stress, SEM, green sand mold, oxide film, pouring temperature.

1. Introduction

Historically, the development of casting practices for Aluminum and its alloys is a relatively recent accomplishment. Aluminum alloys were not available in any substantial quantity for casting purposes until long after the discovery in 1886 of the electrolytic process of reduction of Al_2O_3 by Charles Martin Hall in the United States and Paul Heroult in France. Although Hall's invention provided Al at a greatly reduced cost, the full value of Al as a casting material was not established until alloys suitable for foundry processes were developed. Since about 1915, a combination of circumstances-gradually decreasing cost, the expansion of air transportation, development of specific casting alloys, improved properties, and the impetus provided by two world wars has resulted in an ever-increasing use of Al castings [1].

Cast Aluminum-Silicon alloys are being increasingly used in automotive and aerospace industries for critical structure applications because of their excellent castability, low density, acceptable mechanical properties and low cost. Mechanical properties of this family of cast alloys are strongly affected by the shape, size and distribution of the silicon eutectic and different intermetallics in the microstructure. Chemical composition of the alloy, solidification conditions and modification are the most important casting parameters which are able to change the mentioned features of the silicon eutectics and intermetallics [2].

Sand casting is an important process for casting molten Aluminum alloys. It can be used to prepare castings of any shape and size. Molten metal is poured into a mold cavity formed out of sand (natural or synthetic). The sand cavity is formed by using a wooden pattern. The pattern resembles the real casting part. The upper part of sand mold box is called cope and lower part is called drag. The pattern is made slightly oversize to allow for the metal contraction as it cools down. The liquid flows into the gap between the two parts, called the mold cavity. Sand castings have a rough surface and are machined later. The metal from the sprue and risers is cut from the rough casting. The riser is a reservoir of liquid metal to supply a contracting, cooling casting with make-up metal. It is used to prevent internal or external voids due to shrinkage. Residual stresses in a cast component are those stresses which may remain in the casting after it has been removed from the mold [3].

The main causes of residual stresses in cast components might be: the pouring temperature differences within the castings, hindrance of contraction by the mold, and transformations in the solid metal during cooling [4,5]. According to the following Eq.(1), Eq.(2), and Eq.(3) there is a clear relationship between the residual stresses of the major parts of a component and their difference in cooling rate:

$$E = \sigma / \varepsilon \quad (1)$$

$$\varepsilon = \Delta L / L = \alpha \Delta T \quad (2)$$

$$\sigma = \alpha E \Delta T \quad (3)$$

Shape change can decrease the residual stresses produced during cooling. Hence, change of shape during solidification has a significant effect on residual stress. So Eq.(3) will develop into the following formula Eq.(4):

$$\sigma = \alpha . E . \Delta T (1 - \varepsilon^{1}) \quad (4)$$

* Tasmia Zaman. Tel.: +88-01911546371
E-mail address: zaman.tasmia@yahoo.com

On the other hand, according to Chevorinov's rule, the solidification time of molten metal is related by the following Eq.(5):

$$t = C\,(V/A)^2 = C\,M^2 \quad (5)$$

Among the general methods for residual stress measurement, X-ray diffraction, hole drilling and sectioning are the most common methods applied to Aluminum alloys. Although the first two methods are non-destructive, the problem is that they are sensitive to microstructure (and texture) and geometry, respectively. The sectioning as a destructive method seems to be an acceptable method for measuring the macro stress within the Aluminum cast components [6,7].

2. Experimental setup

Experimental setup was done according to the following procedure:

2.1 Mold preparation

Initially six molds, three greensand molds and three metal molds were prepared. Round tensile test bars of 25 mm in diameter and L_1 150 mm in length were required for the experiment. Shape of required dimensions was made in each mold.

2.2 Melting and pouring

Around 8.0 Kg of pure Al and Al-Si-Cu-Mg alloy were melt separately at 900^{o}C. The molten metal and alloy were poured in different molds at different pouring temperatures (700, 800 and 900^{o}C). Castings were named as G_1, G_2, G_3 for green sand mold and M_1, M_2, M_3 for metal mold.

2.3 Tensile test

Tensile samples of specific dimensions (D_o=10 mm and L_o=50 mm) were prepared from the test bars. Then tensile tests were conducted using universal testing machine (UTM). Finally, ultimate tensile strength (UTS) and percent elongation were calculated.

2.4 Residual stress measurement

To measure the residual stress castings were made in bar shapes. Two lines were drawn on the center bar of the casting and their spacing was measured. It was noted as L_1. Then the middle of the bar was cut and again the distance between the lines were measured. It was named as L_2. After that strain was calculated. Eq.(6) shows the formula for residual stress calculation.

$$\sigma = \varepsilon E \quad (6)$$

2.5 Visual inspection

Broken samples were collected after performing the tensile test and visual inspection was done. The surface of broken samples was observed carefully.

2.6 SEM analysis

Fracture surface of the broken samples were observed under the scanning electron microscope (SEM).

3. Results and Discussions

3.1 Mechanical property test

The cast samples (both metal and alloy) were taken for tensile property test. It was found that, pouring temperature as well as the mold material had important effect on tensile property. The tensile strength or UTS decreased gradually with increasing pouring temperature. The effect of pouring temperature for pure Aluminum metal was vital. In case of Aluminum alloy, the effect was minor. Aluminum and its alloys oxidize readily in both the solid and molten states to provide a continuous self-limiting film. The rate of oxidation increases with temperature and is substantially greater in molten than in solid Aluminum. The high pouring temperature might have caused the oxide film formation in both cases. Moreover, turbulence during faster pouring might fold the oxide film. Presence of any oxide film during cooling will remain as inclusion or porosity in the cast. Thus the quality of cast will decrease. At temperatures higher than the melting point range results comparatively large crystals, low strength. Due to high pouring temperatures, gases are entrapped in the castings, leading to defects known as blowholes. It might have also decreased the tensile property of the cast samples.

Table 1 Mechanical property of pure Al cast.

Metal	Mold	T	UTS	% elongation
Al	Sand	900	45	0.85
		800	83	0.95
		700	86	1.3
	Metal	900	33	0.4
		800	45	0.65
		700	50	0.87

Table 1 shows the data for pure Aluminum sample cast. It shows the UTS have increased with decrease in temperature.

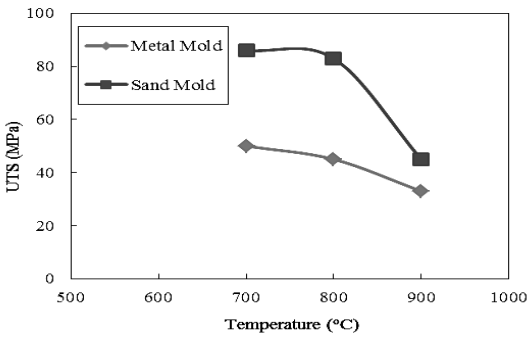

Fig.1 Effect of pouring temperature on UTS for Al metal.

Fig.1 shows the schematic representation of effect of pouring temperature on UTS. In case of mold material sand mold casts gave better result than metal mold. It was true for both metal and alloy samples. Metal mold had chilling effect which caused faster cooling. Higher cooling rate resulted poor structure with entrapped gases.

Table 2 Mechanical property of Al-alloy cast.

Alloy	Mold	Temperature	UTS	% elongation
Al alloy	Sand	900	102.5	0.13
		800	140	0.18
		700	165.5	3.9
	Metal	900	43.78	0.4
		800	79.37	0.6
		700	128.99	2.55

Table 2 shows the temperature effect on tensile property in case of alloy samples. It has been observed that pinholes in aluminum castings are caused by the absorbed hydrogen. This can be minimized by pouring the alloy at temperatures just necessary for casting. Therefore, once this optimum pouring temperature is identified, it should be properly applied.

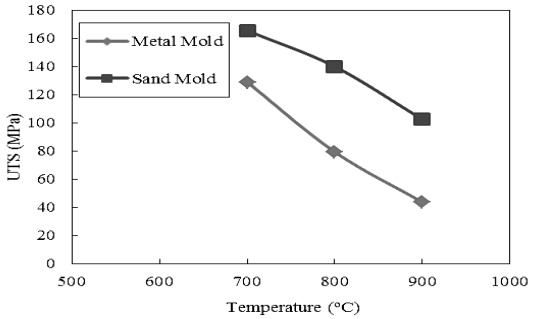

Fig.2 Effect of pouring temperature on UTS for Al alloy.

Fig.2 shows the effect of pouring temperature on tensile property of Al ally samples. Alloy samples gave better result compared to pure Al samples. This can be explained by the fact that, pure Al forms oxide film while alloy of Al with Cu and other alloying elements forms oxide precipitates or particles which have less adverse effect than continuous oxide film. Thus composition of alloy also changes the quality of cast.

3.2 Percent elongation measurement

The percent elongation was seen to increase with decreasing pouring temperature for both metal and alloy samples. Sand and metal mold gave same effect but percent elongation for sand mold samples was much higher than the metal mold. Fig.3 and Fig.4 shows the variation of percent elongation with pouring temperature and mold material.

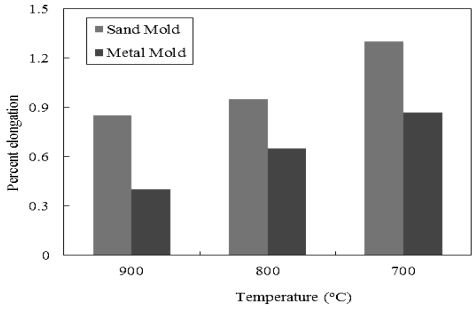

Fig.3 Effect of pouring temperature on percent elongation for Al metal.

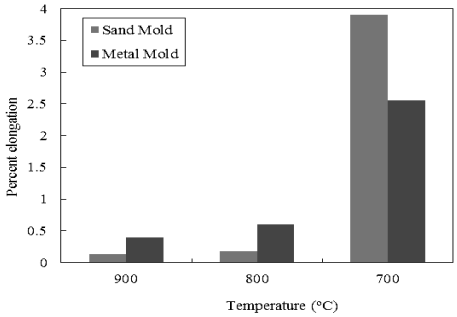

Fig.4 Effect of pouring temperature on percent elongation for Al alloy.

3.3 Residual stress test

Residual stress was measured for each pouring temperatures. It was found that as pouring temperature increased the residual stress also increased. Metal mold samples gave poor result than sand mold. The faster cooling rate in metal mold samples caused residual stress which resulted poor property. Table 3 shows that measured residual stress for all samples. The Al samples gave higher result than Al alloy samples in terms of residual stress.

Table 3 Effect of residual stress on cast Al & Al-alloy.

Mold	Temperature	Residual Stress	
		Al	Al-Alloy
Sand	900	231.93	200
	800	161.65	125
	700	116.67	110
Metal	900	240.11	230.9
	800	210.54	170
	700	160	123

Fig.5 and Fig.6 shows the graphical representation of residual stress Vs. pouring temperature.

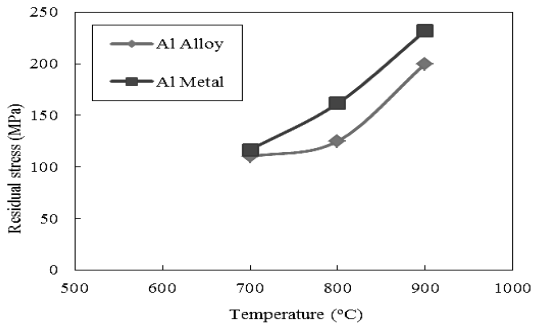

Fig.5 Effect of pouring temperature on residual stress for sand mold samples.

Metal mold samples had higher residual stress. It resulted poor castings due to the chilling effect. The formation of dendrite might cause adverse effect.

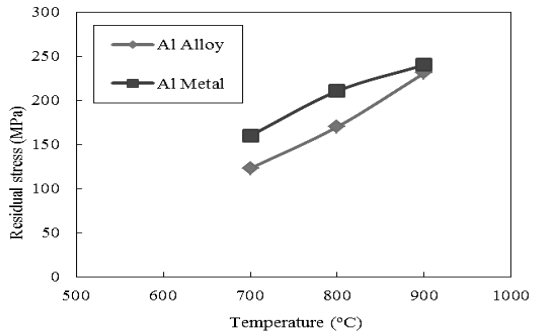

Fig.6 Effect of pouring temperature on residual stress for metal mold samples.

3.4 Quality assessment

The melting point of pure Al is around 660^{o}C. Higher the pouring temperature higher the undercooling. This resulted poor structure.

3.5 Visual inspection

The fracture surface of the tested samples was observed carefully. The higher pouring temperature samples gave very rough surface with open voids. On the other hand, the low pouring temperature caused samples with comparatively ductile surface.

3.6 SEM analysis

The micrograph of the samples can be seen in Fig.7 and Fig.8. The micrographs showed the clear effect of pouring temperature.

The melt poured at 900^{o}C temperature gave poor microstructure than the others. Cast samples of Al metal had large amount of voids in the SEM graph. The voids might have caused adverse effect on mechanical property.

High pouring temperature with fast cooling encloses gas bubbles inside the cast. These entrapped gases are very dangerous for cast product. They create pores or voids. The quality of cast thus becomes poor. High temperature makes more reactive melt which easily react with atmosphere and form oxides. Presence of oxide particles act as inclusion.

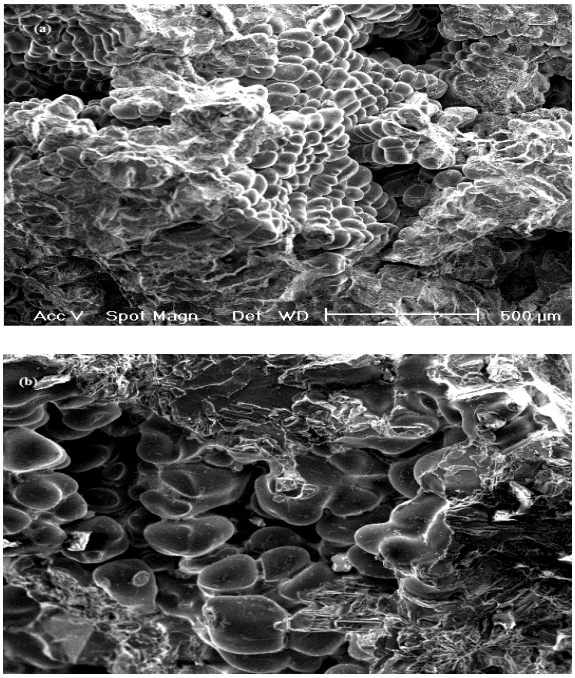

Fig.6 SEM micrographs of (a) pure Al sample & (b) Al alloy sample (pouring temperature 700^{o}C).

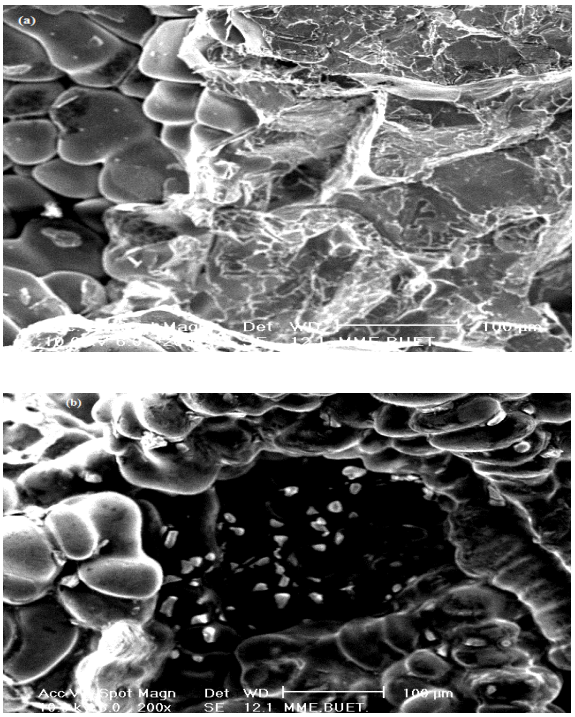

Fig.7 SEM micrographs of (a) Al alloy sample & (b) pure Al sample (pouring temperature 900^{o}C).

4. Conclusions

In terms of better cast quality and good mechanical property, 700^{o}C was the optimum pouring temperature. 700±50^{o}C is the region where good quality casts are produced with good mechanical properties. So pouring temperature is an important parameter in case of Al castings.

Thermal residual stresses are primarily due to differential expansion when a metal is heated or cooled. As soon as the pouring temperature increases, the amount of residual stress also increases.

NOMENCLATURE

ε^{1} : Ductility at failure
t : Time, sec
C : Constant
V : Local volume, m^3
M : Casting modulus
A : Surface area, m^2
α : Thermal expansion coefficient
σ : Residual stress, MPa
ΔT : Degree of undercooling, ^{o}C
T : Temperature, ^{o}C

REFERENCES

[1] J. L.Warrendale, Pouring Rate of Some Ferrous and Non-Ferrous Metals, *American Society of Metallurgical Engineers*, pp 37-45, (1981).

[2] P.L. Jain, Principle of Foundry Technology, *MIR Publications Moscow*, pp 22-64, (1986).

[3] P.L. Grill, Principle of Metal Casting, *McGraw-Hill Book Company New York*, pp 160-166, (1982).

[4] N.C. Lancer, Guidelines for Establishment of Foundry, *MIR Publishers Moscow*, pp 72-75 (1981).

[5] ASME, Pouring Temperature Ranges for Metals and Alloys, *Publication of American Society of Mechanical Engineering*, Vol. III, (1996).

[6] O. P. Adeleke, Effect of Pouring Temperature on Solubility of Gases, B. Eng Project Submitted to Mechanical Engineering Department, F.U.T. Minna, pp 17-18, (1992).

[7] M. F. Spotts, Design of Machine Elements*, Hall of India Private Limited, New Delhi*, pp 705-709, (1988).

ICMIEE-PI-140266

Development of programmable logic controller based self-controlled egg incubator

A. Hafiz Zaman [*1], Md. Emdadul Hoque [1], Md. Jakir Hossen[1] , Sourav Sarker [1]*

[1] Department of Mechanical Engineering, Rajshahi University of Engineering & Technology, Rajshahi-6204, BANGLADESH

ABSTRACT

An incubator is a device that performs or facilitates various forms of incubation. In this paper, we introduced a Programmable Logic Controller (PLC) based system which can control its temperature and humidity automatically and application of this system into an egg incubation system. A self-controlled egg incubator (SCEI) has been developed here. The system consists of three major processes. Such as mechanical, electrical and control process. Temperature range for proper incubation is 35-40°C, Humidity range- 55-65% and the required turning angle - 28.80°. If the temperature inside the incubator chamber is lower than 35°c then the temperature sensor gives a signal to the PLC, PLC will make an electric heater turn on and keep it on till the temperature reaches 39°c. In the case of humidity, if it is higher or lower than our desired range, then PLC makes the blower running which suck the air from inside the incubator chamber and makes it pass through the humidifying & dehumidifying chamber. So the humidity reaches to the desired level.

Keywords: Egg Incubator, Programmable Logic Controller (PLC), Temperature & Humidity Sensors.

1. Introduction

An incubator can be defined as a device that performs or facilitates various forms of incubation. It may also refer to a device for maintaining the eggs of birds or reptiles to allow them to hatch. Egg incubator is a widely used machine in the poultry sectors. Poultry is an emerging and important sector that has been contributing progressively to our economy for the past decade. Poultry is one of the fastest growing and most promising industries with the brightest of futures for our country. Poultry sector are playing a very vital role in the reduction of poverty, malnutrition and unemployment problems of our country. In the natural or conventional incubation system, the mortality rate of chicks is high. From a survey, it is noticed about five out of twenty eggs or more are damaged in a natural incubation system [1]. The only reason is the improper control of temperature. The purpose of this project is to the design and development of an egg incubator system named as Self Control Egg Incubator (SCEI) that is able to incubate various types of eggs, properly so that the mortality rate is reduced. Temperature range for proper incubation is 35-40°C [3], Humidity range- 55-65% [2] and the required turning angle - 28.80°.

2. Experimental setup

The incubation system consists of PLC, wooden chamber humidifying & dehumidifying chamber, temperature sensor (LM-35), humidity sensor (HSM-20G), air blower, air circulating pipes, silica gel, wet sponge etc. which are described in the followings:

2.1 PLC

PLC can be termed as the brain of an automated system. The PLC used in this experiment is given below.

BRAND	SIEMENSE
MODEL	**LOGO 6ED1052-1MD00-0BA6**

2.2 Wooden chamber

Due to availability and low cost the wood made objects are always preferable. As the wood is a good insulator too and the project theme associate with the control of temperature its importance is increased to some extent.

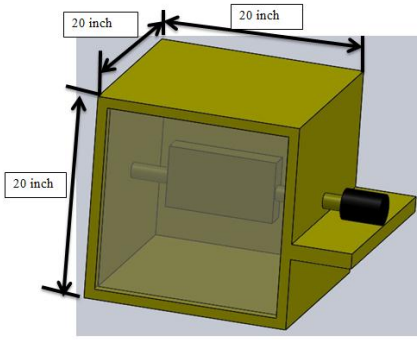

Design with dimension

Front View

Back View

Fig.1 Incubation chamber

* Corresponding author. Tel.: +88-01671193009
E-mail address: a.hafizmecha09@gmail.com

2.3 Humidifying & dehumidifying chamber

This is a cylindrical shaped chamber and acts as a heart in this control system. The chamber is internally divided into two equal portions and both the portions has inlet and outlet ports The cylinder is required to hold the drawers that contain silica gel and sponge which wet with water.

Fig.2 Humidifying and dehumidifying chamber construction

Height of the cylinder	30 inch
Diameter of the cylinder	12 inch
Construction material	Galvanized sheet

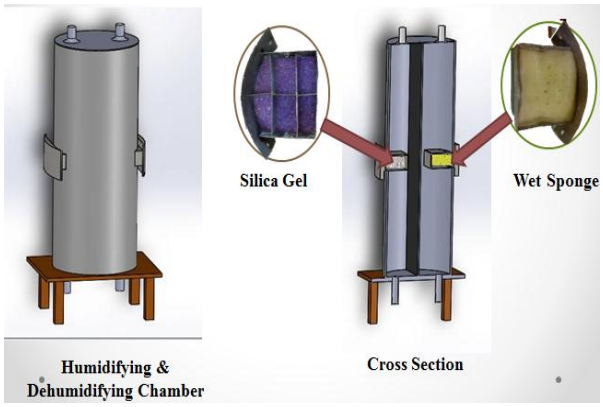

Fig.3 Humidifying and dehumidifying chamber

When the dry air is made passed through the portion with wet sponge, the air extracts moisture from it and the conditioned air (moist air) is circulated in the incubation chamber again. When moist air is made passed through the portion with silica gel, then the silica gel extracts moisture from the passing air and the conditioned dry air will be again circulated in the chamber.

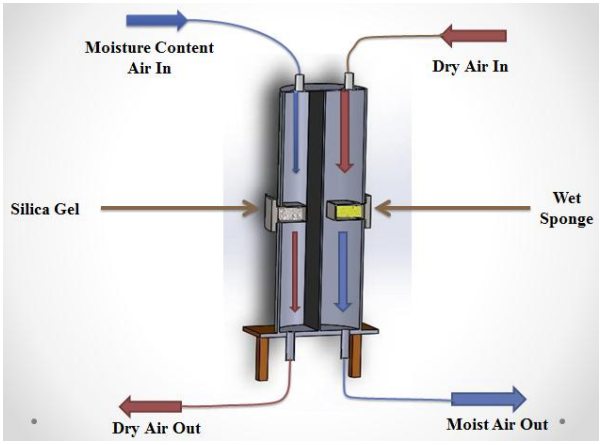

Fig.4 Cross section of humidifying and dehumidifying chamber

2.4 HSM-20G humidity sensor

Humidity sensor is used to sense the value of humidity in the square room whose humidity is to be controlled. It use voltage 7V DC, Storage temperature Tsg-40 to 85$_0$ C. Storage humidity range Rhstg 0 to 100% RH. Operating temperature range Ta -30 to 80^{o}C.

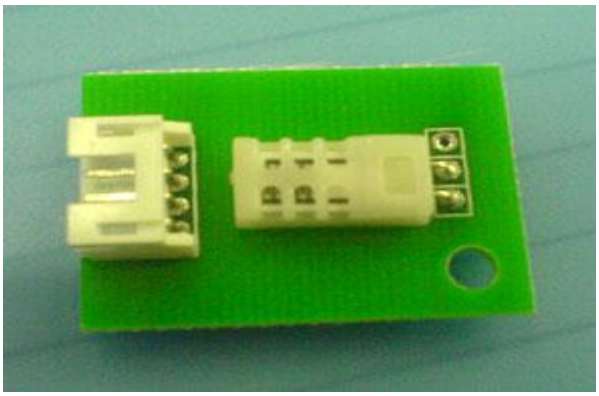

Fig.5 HSM-20G humidity sensor

2.5 Air Blowers

Two blowers are required to force the process air and reactivation air through the cylindrical shaped chamber.

Fig.6 Air blower

2.6 Construction

The main structure of the incubation system is as followings:

Fig.7 Self-controlled egg incubator

2.7 Working principle

For proper incubation, the temperature inside the incubator chamber is needed to be maintained between 35^0c to 40^0c. If the temperature inside the incubation chamber falls below 35^0c then the temperature sensor (LM-35) will send a signal to the PLC and the PLC will turn on the electric heater placed inside the incubation chamber. When the temperature inside the chamber reaches to 40^0c then PLC will turn off the electric heater. Thus the temperature is maintained between the desired ranges**.** In this experiment, a 40watt incandescent bulb has been used as an electric heater. A 24volt DC fan has been attached to the back side of the chamber for providing proper ventilation and equal distribution of the heat.

Again in case of humidity, desired range for proper incubation is 55% to 65%. So the humidity inside the incubation chamber is needed to be maintained between these limits. For controlling the humidity inside the chamber, two electric air blowers, humidifying & dehumidifying chamber and air circulating pipe has been used here. A humidity sensor (HSM-20G) has been used to measure the humidity condition inside the incubation chamber. If the humidity inside the chamber is lower than 55% then the PLC will turn on the blower1 (Fig.8). Blower 1 will suck the air from inside the incubation chamber and will make it pass through the portion 1 of the humidifying and dehumidifying chamber where wet sponge has been placed. The dry air passing through the portion-1(Fig. 8) will extract moist from the wet sponge and comparatively moist air will be again circulated to the incubation chamber. Once the humidity inside the incubation chamber reaches to 60%, the PLC will turn off the blower-1.

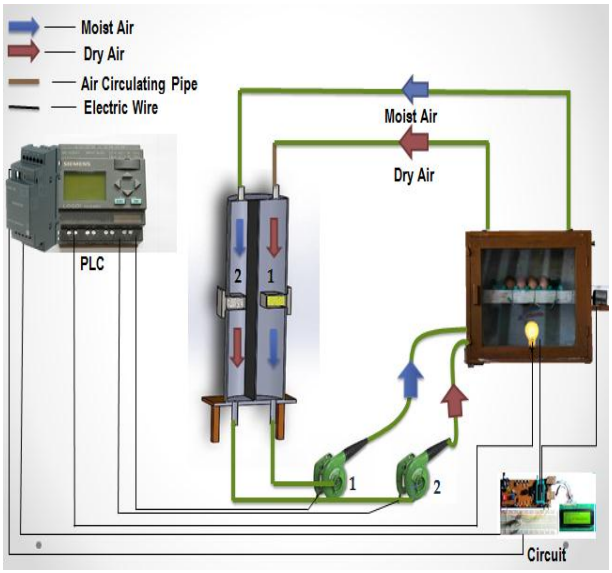

Fig.8 Flow diagram

Again in the case of excess humidity, that is when the humidity inside the chamber is above 65% then the PLC will turn on the blower-2, this blower will suck the moist air from inside the chamber, and then make this moist air pass through the portion two where silica gel has been placed. Silica gel is a desiccant material which will extract moist from the air. Then the dry air is again supplied to the incubation chamber. Thus the humidity inside the incubation chamber is maintained between desired ranges.

3. Experimental Results

Fig.9 shows a time vs. temperature curve. It indicates when the heater will turn on and when it will be off. The data was taken between 2 pm to 5 pm on 5th September, 2013.The heater was switched on when the temperature falls to 30°c and switched off when temperature reached to 40°c. Then when the temperature again fell down, the PLC switched on the electric heater again. This procedure was continued for a long time, but data recorded between 2 pm to 5 pm is presented in following figure.

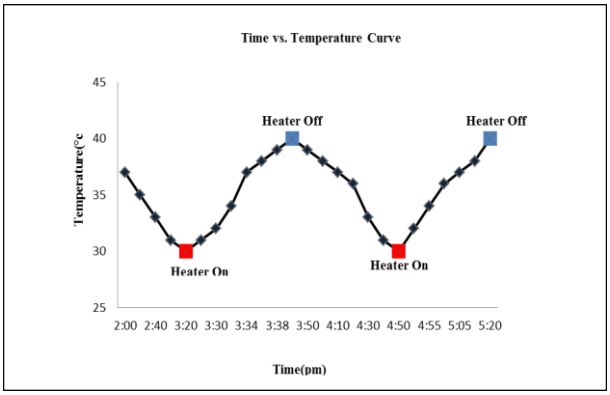

Fig.10 Time vs. temperature curve

Fig.11 shows a time vs. relative humidity curve that represents the dehumidification operations of the system. Data were taken between 2:00 pm to 4:30 pm on 5th September, 2013. Initially the relative humidity inside the chamber was around 72%, so the blower-2 was turned on as soon as the power is supplied to the system and the system starts working. When the relative humidity inside the incubator reached 55%, the blower-2 was turned off.

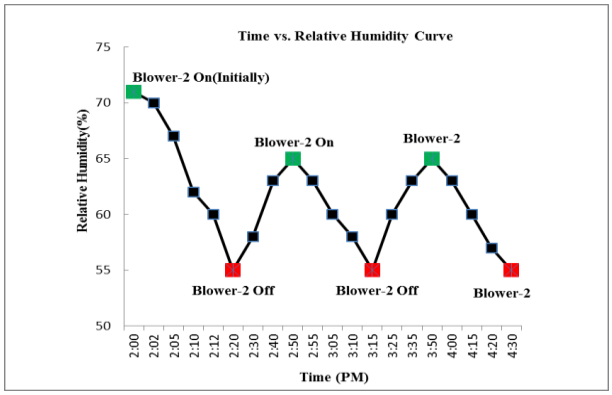

Fig.11 Time vs. relative humidity curve (dehumidification)

Fig.12 shows a time vs. relative humidity curve for humidification operation. Actually the humidification operation is required in the winter season in Bangladesh as the relative humidity falls below the desired range in winter. The data were taken between 2:00pm to 4:00 pm on 11th December, 2013. Initially the relative humidity inside the chamber was lower than the desired range, so the blower-1 was switched on as soon as the system started running, and the blower-1 is switched off when the relative humidity reached to 65%.

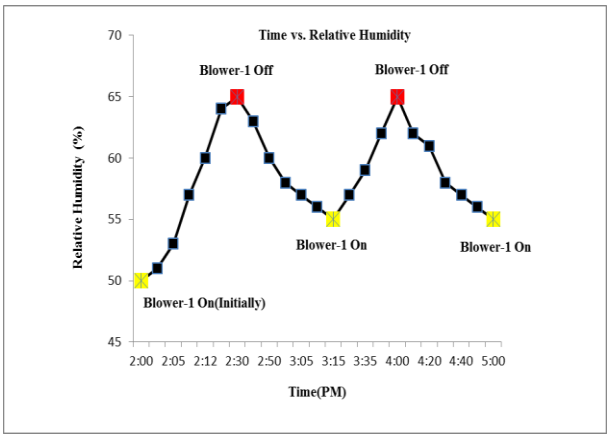

Fig.12 Time vs. relative humidity curve (humidification)

Temperature and humidity has a proportional relationship. Temperature of a system increases with increase in relative humidity. This relation might was also considered during designing the system. Fig.13 shows a relationship between temperature and humidity.

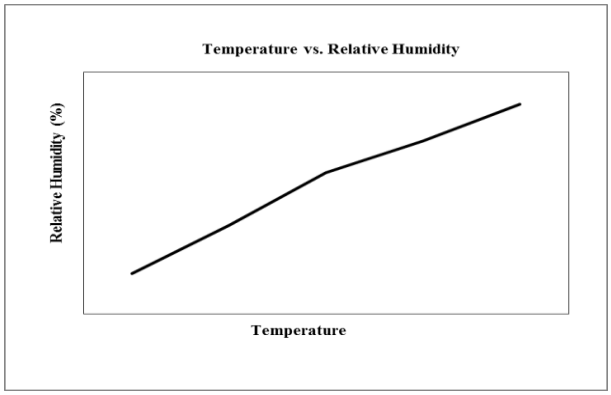

Fig.13 Temperature vs. relative humidity curve

The switching operation of the electric heater has been shown in fig. 14. The electric heater was made switched on and off by using PLC. Since the PLC got the temperature reading from inside of the incubation chamber by using temperature sensor (LM-35).

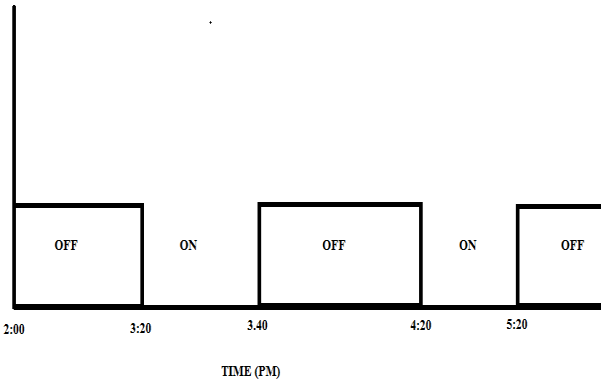

Fig.14 Switching sequence of electric heater

The switching sequence of blower-2 for the dehumidification operation has been shown in the fig.15.

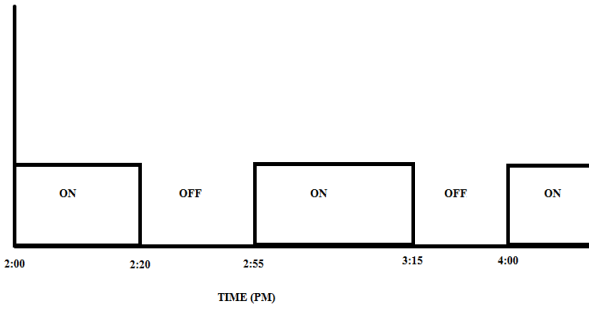

Fig.15 Switching sequence for blower-2

Fig. 16 shows the switching sequences of the blower-1 for the humidification operation which is required mainly in winter season in Bangladesh.

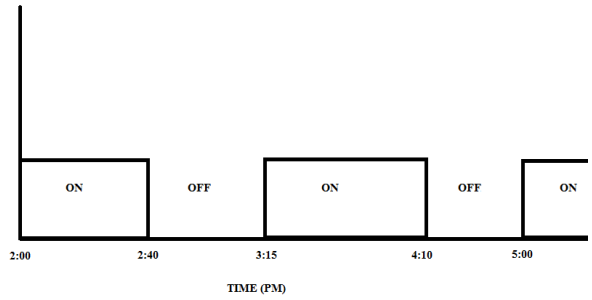

Fig.16 Switching sequence of blower-1

4. Scopes & limitations

Though this Self-controlled egg incubator has great scopes in poultry sectors, but it has some limitations too.

4.1 Scopes

This project consists of multi-purpose capability due to use of PLC as automatic control device. However this technology can be applied not only in egg incubation system but also in air conditioning system, cold storage and many other industrial purposes.

4.2 Limitations

This project may results a little higher initial cost. Moreover this incubator requires a little bit higher space for set up. This incubator is not suitable for portable use.

.

5. Conclusion

As poultry sector is one of the most important sectors for the social and economic development of a country like Bangladesh, so there is no need to tell the importance of an egg incubator. In this paper, a PLC based self-controlled egg incubator has been developed and result of performance test of the system has been also given. Since PLC is an expensive device, this egg incubator is more suitable for the large farms, no much for the small poultry farms. Though development can be made on this project by doing more research.

REFERENCES

[1] M. B. M. Adid, Development Of smart Egg Incubator System (SEIS) for various types eggs, University of Malaysia, vol. 1, pp 1-50, Pahang. (2008)

[2] T. P. Mote, S. D. Lokhande., Temperature control System Using ANFIS, Vol. 2, Isue-1,Page-156,March (2012).

[3] S.C Ekwuozor, P.S Aguh , Design of a automatic electrically powered egg incubator system, Vol. 3, pp 1-20, April (2004).

ICMIEE-PI-140272

Design of an Accessible Door System in High Floor Buses for Wheel Chair Users

Md. Hafizur Rahman [1,*], *S.M. Mahbobur Rahman*[1], *Asif Tanvir Bhuiya*[1], *Shadman Sakib*[2]
[1] Department of Mechanical Engineering, Khulna University of Engineering & Technology, Khulna-9203, BANGLADESH
[2] Department of Naval Architecture & Marine Engineering, Bangladesh University of Engineering & Technology, Dhaka-1000, BANGLADESH

ABSTRACT
A large portion of the physically disabled community of the world is currently using wheel chairs which is not universally accessible. In many countries, public transport system depends on high floor bus and a wheel chair user fails to access to that comfortably. This research aims to demolish that problem of inaccessibility through a modification of the high floor bus door. The basic methodology here, consists of movable door-step system (one vertically and other horizontally) which allows the lifting of a wheel chair into the bus. Two linear actuators and two rack and pinion mechanisms are involved in this system. In this research, through simulation analysis the feasibility of the lifting step is tested. Eventually, the cost is discussed for performing this type of modification in a public bus in Bangladesh. So, this work will help people to find an effective mean to make public buses accessible for disabled persons.

KEYWORDS: Universally accessible, linear actuator, rack and pinion mechanism, Simulation analysis

1.0 Introduction

Almost 7 percent of the world population belongs to physically disabled society. Most of them use wheel chairs for overcoming accessibility boundary. Yet, wheel chairs are not universally accessible and in countries like Bangladesh all public buses are high floor and a disabled person faces major difficulty if he wants to travel by bus like a privileged person. In countries like USA by dint of ADA act (Americans with Disabilities Act of 1990) the public transportation system are habituated with modified bus with low floor and modified door. Moreover for the safety conditions inside the bus WTORS (wheelchair tie down and occupant restraint system) is adapted for rendering comfort for a physically disabled personnel. [1] But, in countries like Bangladesh there is no low floor bus system. Yet, a lot of people here are dependent on wheelchair and currently unable to move long distance because of the lack of facility of access and safety in the public bus. This research work aims to make a mean for allowing the wheel chair users to enter comfortably into the public bus. In the first phase of this paper, the model of such a door system is provided. And then, in the second phase, a modification in the interior of the bus is rendered following WTORS system. [1] Finally the simulation of wheel chair lifting plate is analyzed and cost for such a modification to currently available bus system is discussed. The control loop of the program algorithm and the electric circuit diagram needed for these modifications are also provided with this research paper. For simulation analysis the CAD platform of solid works is used which is very popular in recent years and Vivek kaundal also used this platform for design and simulation in his research work in 2012. [2]

2.0 Background research

It is an old demand of people to provide facility to the one who is not physically privileged. Research has been accomplished in 20th century and in the United States, all new mass transit vehicles placed into service after July 1, 1993 became accessible to persons in wheelchairs [3] and until the 2000s, this requirement was most commonly met by the inclusion of a wheelchair lift. Low-floor transit vehicles (buses, streetcars, light rail cars) – fitted with ramps or bridge plates rather than lifts – later began to become more common than lifts for heavy-duty transit vehicles, while lifts continued to be used in para-transit vehicles. [4] Currently in few low floor buses there is a cross arm mechanism present which is used for lifting the wheel chair up to bus interior. But none of these systems can

Fig.1 A wheelchair lift in the front door of a low floor city bus in San Francisco

* Corresponding author. Tel.: +88-01685125882, +88-01736941309
E-mail addresses: mhrsazal@gmail.com

be implemented for high floor buses as there is about 15 inch distance between the ground and lower base of a traditional bus door. So a reasonable lifting mechanism is needed to be taken place which is the main motto of our research work. By field inspection in CRP (Centre for rehabilitations of the Paralyzed), Savar, Bangladesh the real scenario regarding this matter was readily understood. CRP made a mean for shifting disabled patients with wheel chairs into one of their buses using a 50 inch inclined surface. But that requires a long free distance in road which is most of the time unavailable in jam pact cities like Dhaka. So, a better solution is now needed to take into account.

3. Design of the model

In Bangladesh, BRTC (Bangladesh Road Transport Corporation) buses are most available. So, the system is designed based on the structure of a BRTC bus. In general, BRTC buses have 2 doors, one in front side closer to driver and the other at the middle. Here the

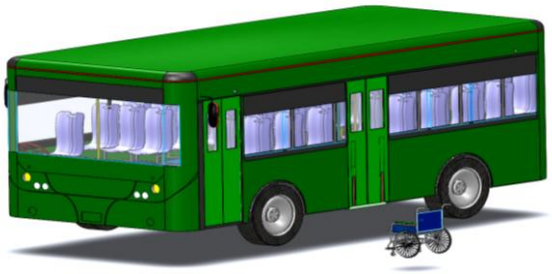

Fig.2.1 Bus comes at stoppage

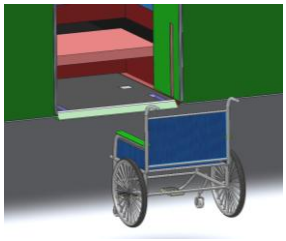

Fig.2.2 Door opens

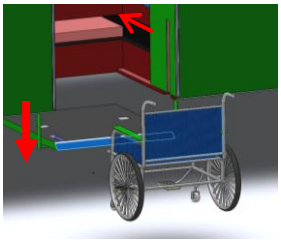

Fig.2.3 Step comes down

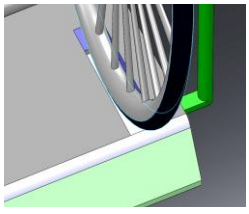

Fig.2.4 Chair gets in

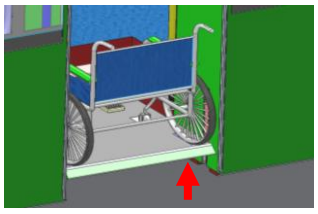

Fig.2.5 Step moves up

design is done for the middle door. The mechanical model of the door system was prepared and simulated using solid works CAD platform. We are going to describe the system in two phases.

3.1 First phase

The Door system and the methodology of lifting:

As we stated earlier, our lifting system consists of 2 movable steps (fig.2) instead of two fixed conventional steps of public bus. Among the steps one is vertically movable (first step plate fig.3) and the other is horizontally movable (second step plate fig. 4). The first step plate of the bus door can move vertically from the ground to the height of the base of the bus using two linear actuators. When the doors are open, (Fig.2) this vertically movable step can be moved using the actuator by pressing a switch. For free movement of the actuator the door is modified by cutting a portion (fig.5). This open portion is protected with a small plate that has rollers in two sides. So, when actuator moves up, this portion also moves up, when actuator moves down, this plate also moves down vertically dew to gravitational force inside the hollow portion of the door. And the plate attached to the actuator is made inclined at an angle of 45 degree at the forward edge for the ease of wheel chair driving into it. The 2nd step can come out and go hidden under the base of the bus using a rack and pinion mechanism. So, when a wheel chair user comes in front of the bus, the linear actuator will be turned on by the help of a switch and the vertical plate attached to it will go down. In the meantime the 2nd step will go hidden under the bus basement using the motor controlled rack and pinion mechanism.

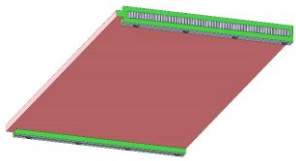

Fig.3 Horizontally movable plate with roller and rack slots

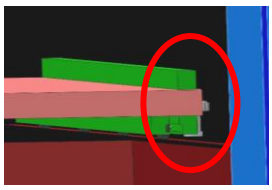

Fig.4 Horizontally movable plate installed in the bus connected to pinion gear

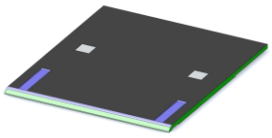

Fig.5 Vertically movable plate with 4 slots for the placement of 4 wheels

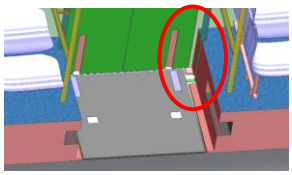

Fig.6 Vertically movable plate installed in the bus door connected to linear actuators.

Initially after the plate comes down, a wheel chair user can go up to the plate and fix the wheels at the modified cut surface (fig.3) so that the wheels don't roll during lifting. Secondly, when the wheel-chair load is charged on the plate, load sensor will guide the actuator for the lifting of the 1st step plate. When this plate comes at the interior base height of the bus, the actuator will be stopped and the user will comfortably go inside and take his position to a separated modified interior portion (fig.7) and fix his chair with the support of belts. Finally, after the wheel chair user has gone inside, the load sensor will guide the system and the doorsteps will get

rearranged for the normal condition, for the general passengers.

3.2 Second phase
Interior portion modification:
The bus has a separate portion close to the door at the middle of the bus where there is an empty space for the placement of the wheel chair (fig.7). A wheel chair user will set his chair there and tie it with safety belts. The belt mentioned here is designed following WTOR System (fig.8); highly popular in the USA. This system prevents the wheel chair from rolling inside a vehicle during jerk or sudden break.

4. Terminologies used in description

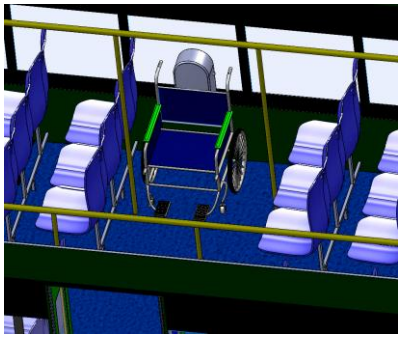

Fig.7 Modified interior portion of the bus for a wheel chair supported with the WTROS system

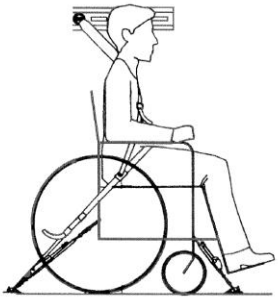

Fig.8 A typical wheelchair tie down and occupant restraint system (WTORS).

4.1 Universally accessible
This term refers the ability to access anywhere as per demand. The wheel chairs used now-a-days in Indian sub-continent are not of that type. Most of the times it is manually operated and travelling a long distance becomes impossible using such a wheel chair. That's why we are proposing the design to be implemented in the bus to help the disabled persons to make a way out to travel a long distance.

4.2 Movable step system
Movable step system (fig.2) means the two plates of our door system are movable linearly. The vertically movable plate is attached to the actuators which can move vertically at a range of 35 inches (15 inches lower and 20 inches upper than the normal lower step of the bus. The other plate has two threaded surfaces which will be used as rack and a motor controlled pinion gear is installed beside it to guide it to ensure linear movement horizontally.

4.3 Rack and pinion mechanism
A rack and pinion is a type of linear actuator that comprises a pair of gears which convert rotational motion into linear motion. A circular gear called "the pinion" engages teeth on a linear "gear" bar called "the rack"; rotational motion applied to the pinion causes the rack to move, thereby translating the rotational motion of the pinion into the linear motion of the rack

4.4 Linear Actuator
An actuator is something that converts energy into motion. It also can be used to apply a force. An actuator typically is a mechanical device that takes energy usually that is created by air, electricity or liquid and converts it into some kind of motion. That motion can be in virtually any form, such as blocking, clamping or ejecting. Actuators typically are used in manufacturing

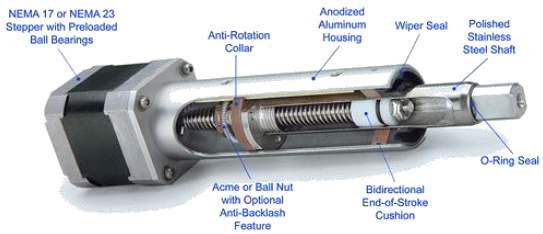

Fig.9 Linear Actuator

or industrial applications and might be used in devices such as motors, pumps, switches and valves. In our study, we used linear hydraulic actuator that is able to generate great power.

4.5 Load Sensor
A Load Sensor is defined as a transducer that converts an electrical output signal. Load Sensors are also commonly known as Load Transducers or Load Cells.

Fig.10 Load Sensor

4.6 Arduino board
For controlling the system, an Arduino MEGA board is used. Arduino is a single-board microcontroller, intended to make the application of interactive objects or environments more accessible. The hardware consists of an open-source hardware board designed around an Atmega 2650 microcontroller. Current models feature a USB interface, 6 analog input pins, as well as 14 digital I/O pins which allow the user to attach various extension boards.

4.7 Wheelchair Tie Down and Occupant Restraint System (WTORS):

The Society of Automotive Engineers (SAE) Recommended Practices J2249, provides best practice guidelines for the design, testing and performance requirements for WTORS. SAE J2249 states that a person seated in a wheelchair, should utilize both a wheelchair tie down device (e.g. docking, four-point strap), designed to secure the wheelchair in a forward facing position; in conjunction with an occupant restraint that consists of both a pelvic and upper torso belt, anchored directly to the vehicle or to the components of the wheelchair tie down device. [4]

5. Electrical Circuit:

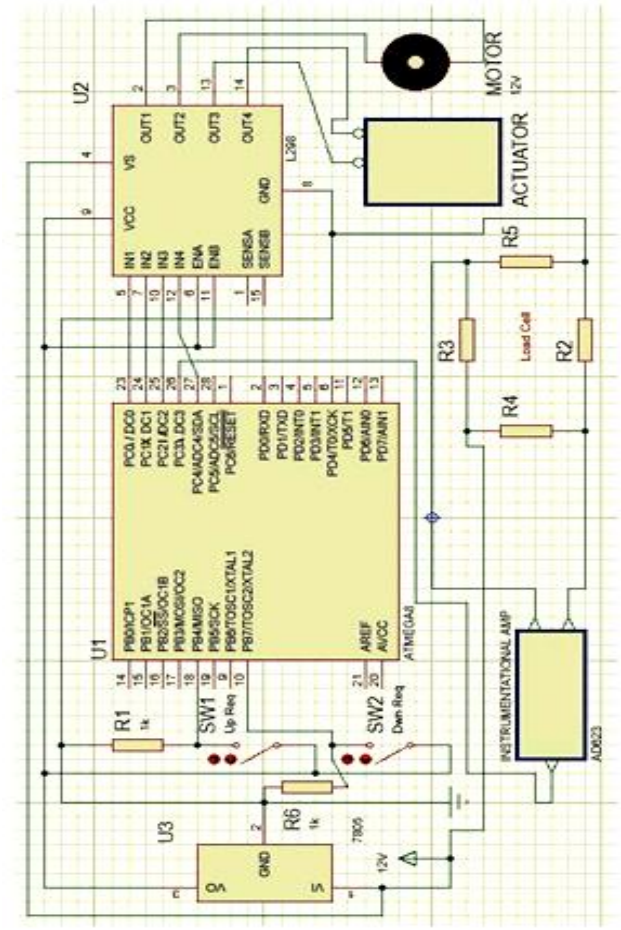

Fig.11: control circuit

In actual design 2 actuators and 2 motors are used. As they are identical only one connection is shown in figure.11 In real circuit another actuator and another motor should be added parallel to other actuator and other motor.

6. Program Algorithm (Control loop)

In order to perform the automation commands successively, a coded instruction should be provided via program algorithm which will act as the control loop. Here, the attached algorithm satisfied this purpose.

If (Up_Req PIN = HIGH)
- Rotate motor clockwise to limit (Sliding stair inward)
- Pull down the vertical stair to limit
- If (Load cell value > Threshold)
  - Wait (5 sec.)
  - Pull up the vertical stair to limit
  - Wait (while (Load cell value > Threshold))
  - Wait (5 sec.)
  - Lower the vertical stair to the original position
  - Rotate motor clockwise to limit (Sliding stair outward)

If (Down_Req PIN = HIGH)
- Rotate motor clockwise to limit (Sliding stair inward)
- Pull up the vertical stair to limit
- If (Load cell value > Threshold)
  - Wait (5 sec.)
  - Pull down the vertical stair to limit
  - Wait (while (Load cell value > Threshold))
  - Wait (5 sec.)
  - Pull up the vertical stair to the original position
  - Rotate motor clockwise to limit (Sliding stair outward)

7. Simulation Analysis:

Material used is Aluminum that is usually preferred for door step construction of a bus Dew to reliability and strength. We used here Aluminum 6063 T-6 alloy. The simulation was done in Solid works 2010 CAD platform. Firstly, the plate was divided into meshes and then Von Mises stress, Equivalent Strain, Expected displacement and factor of safety of the wheel chair lifting plate were studies.

Table.1: Plate information

Sr.	Part	material	Mass(kg)
1.	Vertical plate	Al 6063 T-5	64.69 kg

Table.2: Properties of Aluminium 6063 T-6 alloy:

Sr.	Properties	magnitude	unit
1.	Elastic Modulus	6.9 x 10^10	N/m^2
2.	Poisson's Ratio	0.33	N/A
3.	Shear Modulus	2.58 x 10^10	N/m^2
4.	Density	2700	kg/m^3
6.	Tensile Strength	185000000	N/m^2
7.	Yield Strength	145000000	/K

7.1 Simulated Outputs:

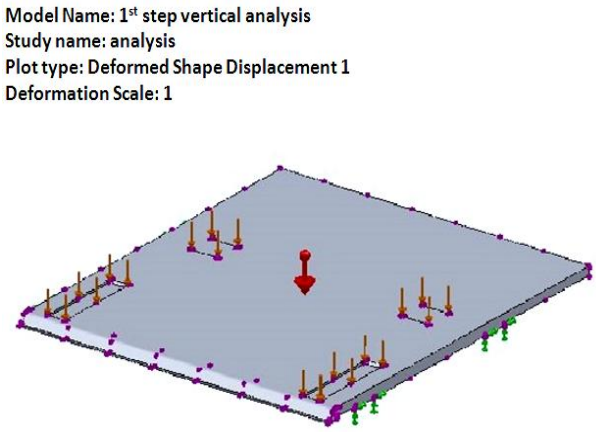

Fig.12 Mesh Diagram of vertically movable plate dew to wheel chair load

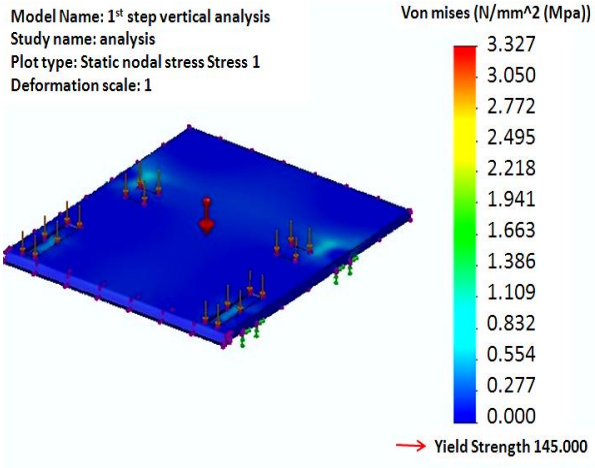

Fig.13 Von Mises Stress Analysis

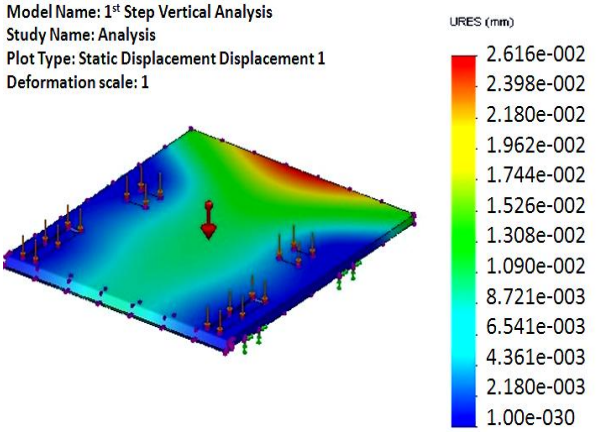

Fig. 14 Resultant Displacement (mm)

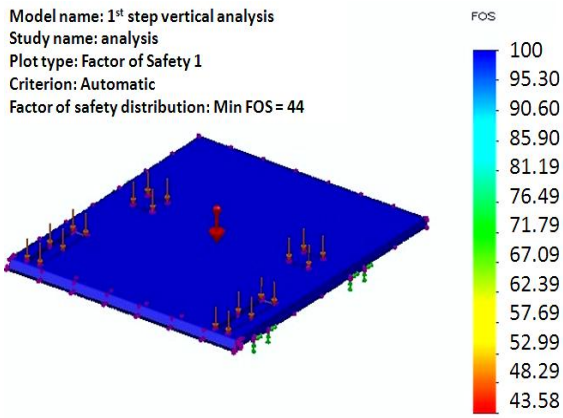

Fig.15 Factor of Safety at different positions of the plate

Table.3 Mesh Information

Mesh Type:	Solid Mesh
Mesher Used:	Standard mesh
Automatic Transition:	Off
Jacobean Check:	4 Points
Element Size:	0.82304 in
Tolerance:	0.041152 in
Quality:	High
Number of elements:	124745
Number of nodes:	204335
Time to complete mesh(hh;mm;ss):	00:00:24
Computer name:	mhrsazal

8. Terminologies used in simulation

8.1 Meshing

The partial differential equations that govern fluid flow and heat transfer are not usually amenable to analytical solutions, except for very simple cases. Therefore, in order to analyze fluid flows, flow domains are split into smaller subdomains (made up of geometric primitives like hexahedra and tetrahedral in 3D and quadrilaterals and triangles in 2D). The governing equations are then discretized and solved inside each of these subdomains. Typically, one of three methods is used to solve the approximate version of the system of equations: finite volumes, finite elements, or finite differences. Care must be taken to ensure proper continuity of solution across the common interfaces between two subdomains, so that the approximate solutions inside various portions can be put together to give a complete picture of fluid flow in the entire domain. The subdomains are often called elements or cells, and the collection of all elements or cells is called a mesh or grid. The origin of the term mesh (or grid) goes back to early days of CFD when most analyses were 2D in nature. For 2D analyses, a domain split into elements resembles a wire mesh, hence the name [2].

8.2 Von Mises Stress

The von Mises yield criterion suggests that the yielding of materials begins when the second deviatory stress invariant J2 reaches a critical value. For this reason, it is sometimes called the J2-*plasticity* or J2 flow theory. It is part of a plasticity theory that applies best to ductile materials, such as metals. Prior to yield, material response is assumed to be elastic.

8.3 Factor of Safety (FOS)

For structural applications FOS is the ratio of the allowable working unit stress, allowable stress or working stress. The term was originated for determining allowable stress. The ultimate strength of a given material divided by an arbitrary factor of safety, dependent on material and the use to which it is to be put, these gives the allowable stress.[5]

$$\mathrm{FS} = \frac{S_{\mathrm{al}}}{\sigma_{\mathrm{ap}}}$$

Where,

S_{al} = Allowable strength

σ_{ap} = Applied stress (Allowable stress)

FS = Factor of Safety

9. Cost analysis

Sr. no	Name of parts	Price /piece (BDT)	Number needed	Price (BDT)
1	Linear actuator	5000	2	10000
2	DC motor	300	2	600
3	WTROS system	4000	1	4000
4	Miscellaneous	2000	-	2000
				Total: 16600

10. Results and discussion

Through mesh analysis the stability of the model is readily understood as the maximum displacement for the material plate dew to the loading of a wheel chair with its user is less than a millimeter and the maximum stress is developed at four positions where wheels are touching the vertically movable plate and the stress is not acting at any alarming magnitude. The minimum factor of safety in mesh analysis comes as 43 which is more than enough for the stability condition.

The cost that is obtained is very reasonable and if government takes this project into concern for the sake of the physically disabled community of Bangladesh the cost can be further reduced.

Here, in this research work, we integrated the mechanical design, electrical circuit and program algorithm of the system which allows us to lift a wheel chair user comfortably into the high floor bus. Here there are still scopes of developing this system, the lifting system and materials can be modified by further research in this field.

Through mesh analysis the stability of the model is readily understood as the maximum displacement for the material plate dew to the loading of a wheel chair with its user is less than a millimeter and the maximum stress is developed at four positions where wheels are touching the vertically movable plate and the stress is not acting at any alarming magnitude. The minimum factor of safety in mesh analysis comes as 43 which is more than enough for the stability condition.

The cost that is obtained is very reasonable and if government takes this project into concern for the sake of the physically disabled community of Bangladesh the cost can be further reduced.

Here, in this research work, we integrated the mechanical design, electrical circuit and program algorithm of the system which allows us to lift a wheel chair user comfortably into the high floor bus. Here there are still scopes of developing this system, the lifting system and materials can be modified by further research in this field.

11. Conclusion

Accessibility is the first need of a person to communicate and to keep pace with the world. But here in Bangladesh dew to having no mechanism to transport a wheel-chair user in public bus, the accessibility to everywhere for a physically challenged person remains uncertain. This research has showed the current situation of bus system in countries like Bangladesh and stated a cheap way to come out from this situation by modifying the door system. It also created scopes of further research for developing this system for the noble sake of the wheel chair users.

REFERENCES

[1] Greg Shaw, Wheelchair rider risk in motor vehicles: A technical note, Journal of Rehabilitation Research and Development Vol.37 No.1, Pages 89—100, January/February 2000.

[2] Vivek Kaundal, Rajesh Singh, Low Cost Robotic Wheel Chair for Disabled People in Developing Countries, Conference on Advances in Communication and Control Systems 2013.

[3] Getting on board, Trolleybus Magazine No. 190, pp. 86–87, National Trolleybus Association (UK). ISSN 0266-7452, July–August 1993.

[4] K. Ashley Rotko, MS, Patricia Karg, MS, Thomas Songer, PhD, Shirley Fitzgerald, PhD, Examination of Wheelchair Tie down and Occupant Restraint Systems (WTORS): Use and Effect on Motor Vehicle Related Injuries, 2006

[5] David G. Ullman, "The Mechanical Design Process", McGraw-Hill publishers, 2009

ICMIEE-PI-140275

Design a Solar and Pedaling powered Rickshaw

Sheikh Mohammad Waliullah, Md. Saddam Hossain, Md. Nazmul Hasan, Md. Tanvir Ibny Gias*
Department of Mechanical Engineering, Khulna University of Engineering & Technology, Khulna-9203, BANGLADESH

ABSTRACT
The Indian subcontinent is a place where three wheeler rickshaws are driven by human power for transportation system. As a result, large portion of energy are wasted by human being through pedaling. Since pedaling is one kind of kinetic energy, so it can be converted into electric energy by using dynamo which produce 6 W electricity. As sun & pedal are the source of energy, so these energy can be stored into the battery which is used to supply power to the motor to drive the rickshaw automatically. The implementation of this system would be beneficial and efficient, because these are not only depending on the availability of sun.

Keywords: Solar panel, Dynamo, Battery, DC Motor.

1. Introduction

The "Rickshaw" is a common vehicle in Indian subcontinent. Due to its popularity, it has become a symbol of Bangladesh and especially for its design and arts. These vehicles are small and narrow allowing easy maneuverability in congested Asian metropolises. Bangladesh is home of more than a millions of rickshaws [1, 2]. Most of the Rickshaw of Bangladesh is human-powered vehicle for hire, usually with two seats for carrying passengers in addition to a driver seat. This non-motorized form of public transport is basically a three wheeler vehicle capable of carrying two passengers excluding the driver, or a pay-load of 150-200 kg [3].

Rickshaw is an eco-friendly vehicle considering environmental pollution. Most of the transport vehicles in Bangladesh are petrol and diesel-powered and these are responsible for air and noise pollution. There are presently nearly half a millions of petrol-powered motorbikes and thousands of petrol or diesel-powered three wheelers [4].

Recently electric rickshaws are being introduced which do not contains any pedal arrangement. So its driving speed is totally dependent on the charge of battery which diminishes gradually on use [5]. But in these electric rickshaws require high motor and battery capacities having charging and economical problem. Electric hybrid rickshaw combines the advantages of the pedal and electric auto rickshaws in single arrangements which are tried out without changing the main structure of existing rickshaw. The hybrid system improves battery operation time [6].

Electric rickshaws first introduced on a commercial basis in 2004 from china and marketed it in 2008. The government of Bangladesh banned import and assembly of electric vehicles because of power crisis. Each EMR (Electric Motorized Rickshaw) consumes at best five watts of electricity during off-peak hours to recharge the batteries and 50,000 Rickshaws consume at best 25 MW [7].

For the power crisis of Bangladesh, it will be convenient to use alternative power source in electric rickshaws. Alternative energy solutions convened a great deal of consideration in the last decade due to the need of sustainable and environmental friendly energy sources. The aim of this paper is to propose a new type of Hybrid "Green" Rickshaw that operates in an environment friendly way. A solar system and a dynamo system have introduced in this rickshaw considering economical aspect.

2. Obstacles to the development of rickshaw

Electric rickshaw becomes popular vehicle. So many research works have been analyzed and many recommendations were proposed for improvement of rickshaw. But no notable change has been implemented in this vehicle in our country [2, 5, and 7]. There are many causes behind this situation which is related to some prevailing socio-economic barriers. There are no significant changes in the existing rickshaw-design. It has been carried out up to road level in the last few decades due to

- Rickshaw owners are not interested to purchase improved rickshaws as well as to modify their own rickshaws for financial problem.
- No organizers are coming forward to motivate the buyers for new ones.
- Mass production is not available in market.
- Lack of government legislation to maintain a standard specification.
- High price of electricity and electrical equipments.

3. Proposed Methodology

In this system sun is the main source of energy which provides power through solar panel to store this power in the battery for riding the rickshaw. A dynamo is used in the rickshaw's front wheel which can provide power. This power will be stored in an additional battery of 6v. This 6v battery will supply power to the rickshaws horn for giving signal to other people. It also supplies power to the rickshaw's light at night for safe movement. This

* Corresponding author. Tel.: +88-01913508189
E-mail address: shnrubel@gmail.com

system needs two kinds of equipment where one is mechanical and other is electrical equipment.

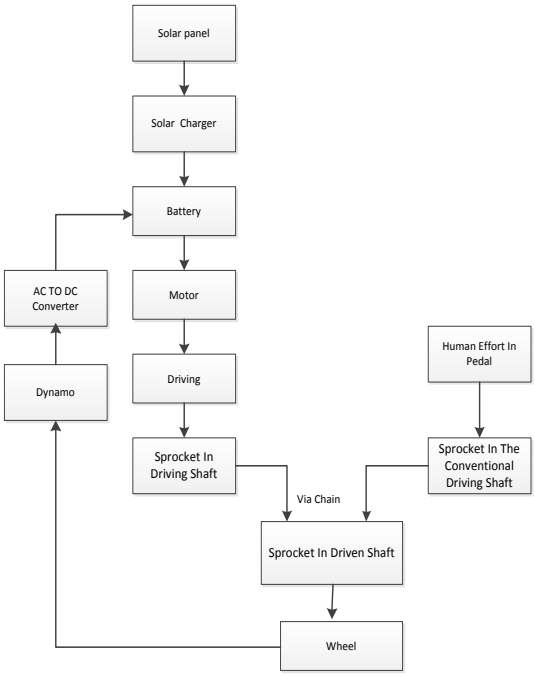

Fig.1 Block diagram of power transmission

3.1 Mechanical equipments

The mechanical equipments used in rickshaw are

1. Mechanical shaft.
2. Chain sprocket.
3. Mild steel pipe.
4. Mild steel bar.

In this system the frame of rickshaw will carry all the loads. An electric dc motor is used in this mechanism. Two additional mild steel bars are used to support the motor. The mild steel bar provides a better support for the motor and an additional chain sprocket is assembling with the motor in this mechanism. It transmits power from the motor to the shaft. A solar panel is assemble in the upper portion of rickshaw with the help of two mild steel pipe which mounted vertically and joined with the lower portion of the frame of rickshaw. The mild steel pipe has no connection with the hood of rickshaw. The hood can easily move.

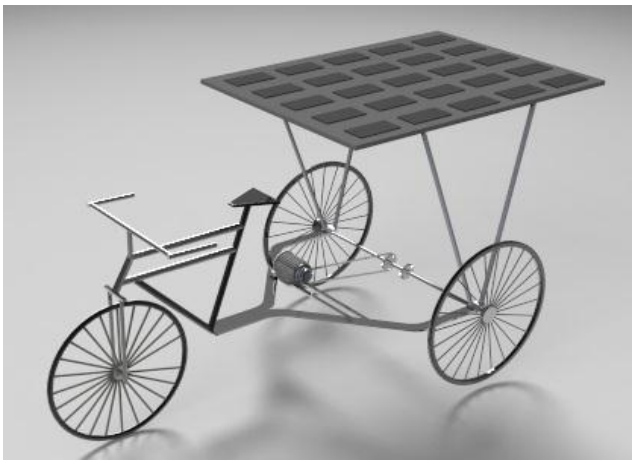

Fig.2 SolidWorks design for the fabrication of Mechanical equipments.

3.2 Electrical equipments

The main electrical equipments those are used in this system are discussed below-

- Solar Panel: A solar panel is a set of solar photovoltaic (PV) modules electrically connected and mounted on a supporting structure. A PV module is a packaged, connected assembly of solar cells. Solar panels can be used as a component of a larger photovoltaic system to generate and supply electricity in commercial and residential applications. A panel is designed to absorb the sun's rays as a source of energy for generating electricity or heating. In this system 4 pieces 40W solar panel is used which can easily recharge the battery.
- Motor: The DC motor helps to convert electrical energy into mechanical energy. It is used in majority of household applications and electronic devices and it is also widely used in electric rickshaw. In this system 48V 500W brushless DC motor is used.

Fig.3 48V 500W Dc motor

- Battery: A dry cell battery is an electrochemical device that produces voltage

and delivers electrical current. The battery is the primary "source" of electrical energy used in vehicles today. In this system 1 piece of 6V 14Ah battery and 4 piece of 12V 30Ah Super Start Dry Charged NS40ZL JIS standard batteries are used.

Fig.4 Battery

- Dynamo: It is a device which changes energy of movement into electrical energy. It turns mechanical energy from the rickshaw's movement into electricity that can be used to power the rickshaw's battery. In this system one piece of 12V 6W dynamo is used to store power in a 6V 14Ah battery.

Fig.5 12V 6W dynamo [8]

3.2.1 Electric circuit diagram

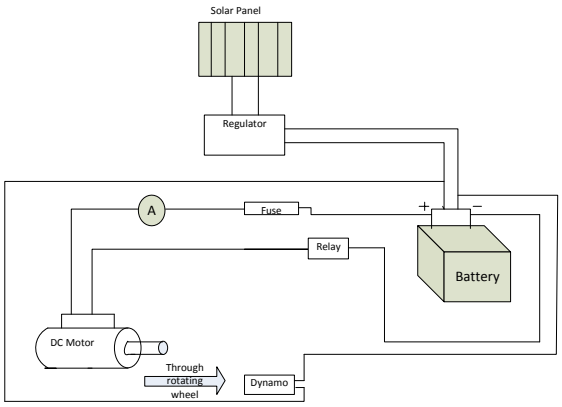

Fig.6 Electrical circuit diagram

3.3 Designing set-up

In this system 4 piece of 12V 30Ah Super Start Dry Charged NS40ZL JIS standard battery is used which is located inside the seat box. The battery is located inside the seat box for protecting it from the rain, as the rain water can damage the battery. After giving full charge to the battery it can easily support 4-5 hours with the load of 3 people including the rickshaw puller. The total system controlled by a switch which is located in the rickshaw's handle. The switch starts the motor for automatic riding. The horn is located in front of the rickshaw and the horn switch is located near the handle. The light is located in the lower portion of the rickshaw's frame. The additional battery of 6V will supply power to both the light and the horn. The motor is located in the lower portion of rickshaw's frame with the help of mild steel bar. The mild steel bar gives a strong support as the motor's weight is very heavy.

Fig.7 Experimental view

3.4 Observation of solar panel

In this system the solar panel was connected in direct sunlight with main electrical circuit and measured the voltage by digital multi-meter. The meter was used to measure the open circuit voltage and the short circuit current. No power was generated when the open circuit voltage and short circuit current was measured.

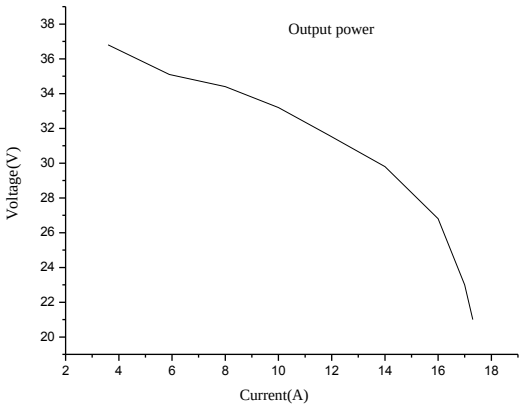

Fig.8 Plot of Voltage versus Current of solar panel

The Fig 8 shows an intuitive view of data. The output of this solar panel shows a characteristic behavior of solar panel. The maximum power is generated at the operating point which forms the 'knee' in the curve. The maximum power is produce approximately 428.8 watts.

To measure the load of the solar panels, the power resistor was connected and measured over time to identify the complete output characteristics.

Table 1: Measured output values with the power resistance.

Time	Ampere (A)	Voltage(V)	Power(W)
11.30am	8	34.4	275.2
12.00pm	10	33.2	332
12.30pm	12	31.6	379.2
1.00pm	14	29.8	417.2
1.30pm	16	26.8	428.8
2.30pm	17	23.1	392.7

4. Advantages and Drawbacks

4.1 Advantages

- To save the electric utility.
- There is no environmental pollution.
- Convenient use of renewable energy.
- Lighting and traffic signal indicators in a rickshaw provides with the dynamo battery.

4.2 Drawbacks

- In this system space is limited for solar panel setting. As solar panel covers comparatively large area on top of the rickshaw's body so it creates a problem.
- The performance of solar cell in not satisfactory in comparison with its price.
- The dynamo provides small amount of energy to the battery.
- Needs more time for charging of a battery due to the change of intensity of suns ray.

5. Discussion

In this system renewable energy is used to reduce the waste of national power. The main purpose of this system is to use solar power through solar panel and to recharge the battery as solar power is available and cost-free. Dynamo is used in rickshaw's wheel to store some energy in an additional battery. The additional battery supplies power to the light and the horn. For this eco-friendly system around 6-7 hours are required to recharge the 48V 30Ah battery by solar power which can be used 4-5 hours. This eco-friendly solar and pedaling powered rickshaw will be more efficient after the improvement of solar cell, charging system and dynamo mechanism.

6. Future improvement

The model will be more efficient in future if dynamo system will be upgraded to produce power with the help of alternator and other electronic equipment's. Besides, efficiency may be increased by using upgraded solar cells.

REFERENCES

[1] Ali, M. and Islam, R. (2005) Livelihood Status of the Rickshaw Pullers of Bangladesh, the Good Earth, Dhaka.

[2] Gallagher, R. (1992) the Rickshaws of Bangladesh Dhaka University Press: Dhaka.

[3] S. Gadepalli, "Rickshaws in the new millennium", The Daily Star, 30 June 2006, from http://www.thedailystar.net/2006/06/30/d606300901105.htm

[4] World Bank (2007), Project Performance Assessment Report, Dhaka Urban Transport Project, World Bank, Washington DC.

[5] Hossain, A.B. Effect of Non-motorized Transport on the Performance of Road Traffic in Metropolitan Dhaka. M.Sc. Dissertation, CE, BUET. (1996).

[6] S.C. Saha, A. Goswami and Md. Ehsan, Design and development of an electric hybrid rickshaw, International Conference on Mechanical Engineering 2011 (ICME2011) 18-20 December 2011, Dhaka, Bangladesh.

[7] Rajvanshi, A.K. Human Power, winter 1999–2000, 49, pp. 15–1

[8] http://www.examiner.com/review/tech-review-spinpower-i4-iphone-4s-bicycle-dynamo-charger.

ICMIEE-PI-140277

Ergonomic design of garments furniture for Bangladeshi workers based on anthropometric measurement

M. I. Ali, M. S. Rahman, M.S. Parvez, A.S.M. Hoque
Department of Industrial and Production Engineering, Jessore University of Science and Technology, BANGLADESH.

ABSTRACT
Garments industry is one of the biggest sectors in Bangladesh for earning foreign currency. Generally in garments industry, workers work more than eight hours by shifting mostly by sitting or standing in one position. However, an anthropometry survey showed that the furniture used by garments worker in Bangladesh were not manufactured ergonomically. As a result, workers suffer various musculoskeletal disorders. The study evaluated the potential mismatch between garments furniture dimensions and anthropometric characteristics of garments workers. Seventeen anthropometric measurements and five furniture dimensions from existing garments furniture were measured and then compared together to find out any potential mismatch. The results indicate that a considerable mismatch between body dimensions and existing furniture, with seat height (79%), seat depth(94%), seat width(36%), and table height(79%) being the furniture dimensions with a higher level of mismatch. The main purpose of this paper is an ergonomics approach to design garments furniture to achieve appropriate balance between workers and their workplace.

Keywords: Anthropometric measurement; Garments Furniture; Mismatch.

1. Introduction

In garments industries workers have to work for more than eight hours repeatedly either by sitting or by standing in one position. So, definitely stress developed in their musculo-skeletal system. Garments industries in Bangladesh have in general very poorly designed workspace, sewing table, sitting chair, Inspection table, Ironing table, limits of work space etc. without considering any ergonomic issue. As a result, the workers feel, back pain, neck pain, fatigue, blood circulation problem, discomfort are related to the anthropometric factors of ergonomics. Ergonomics deals with making the workstation as efficient, safe and comfortable as possible. This can increase worker productivity, provide worker safety and physical and mental comfort and job satisfaction .The aim of ergonomic is the evaluation and design of facilities, environment, jobs, training method, and equipment to equal the capabilities of the users and workers, and thereby to condense the probable for fatigue, error, and unsafe acts[1]. Anthropometry is one of the basic parts of ergonomics that refers to the measurement and collection of the physical dimension of the human body. It is used to improve the human fit in the workplace or to determine problems existing between facilities or equipment and the employees using them [2]. Anthropometric data are used in ergonomics to specify the physical dimensions of workspaces, equipment, furniture and clothing to "in shape the task to the man" [3] and to ensure that the physical mistakes between the dimensions of equipment and products and matching user dimension are avoided. Generally anthropometric measurements are expressed as percentiles. A percentile is defined as a measure used in statics representing the value below which a given percentage of observations in a group of observations fall. For example, the 95^{th} percentile is the value below which 95 percent of the observation may be found.

2. Methodology

For the purpose of this study 400 (200 male and 200female) garments worker were taken from Babylon Dresses ltd. Mirpur, Dhaka, Bangladesh, in order to, collect various anthropometry measurements. Dimensions of existing furniture also taken by a standard measuring tape in order to, mismatch with anthropometric measurements. Dimension were taken in standard sitting and standing positions, wearing light cloths and barefooted. Worker body dimension measured when the worker seated erect on a flat horizontal surface, their lower and upper legs were at right angles (knees bent at 90^0) and feet (without shoes) placed on the flat floor. Comparisons have been made between worker anthropometry measurement and existing furniture dimension. Data have been analyzed by determining mean value, standard deviation value, percentile value using Microsoft office excel worksheet. During this study, 5^{th} percentile, and 95^{th} percentile was calculated as a limit range. Then the anthropometric measurements and furniture dimension were combined to calculate whether there is match or mismatch between them by using quantitative equation.

2.1 Anthropometric dimensions of the worker:

The anthropometric measures (Fig.1) were collected in the seated and standing positions in a bare foot. The following anthropometric measurements were taken for each worker:

Sitting height: This is the vertical distance from horizontal sitting surface to the highest point of the head.

* Corresponding author. Tel.: +88-01610291124
E-mail address: imraan.just@gmail.com

Sitting eye height: This is the vertical distance from a horizontal sitting surface to the eye.

Sitting shoulder height: The vertical distance from a horizontal sitting surface to the top of the shoulder at the acromion.

Sitting elbow height: The vertical distance from a horizontal sitting surface to the tip of the elbow with flexed at 90^0.

Hip breadth: The maximum horizontal distance between the hips in the sitting position.

Elbow to elbow breadth: The horizontal distance across the lateral surfaces of the elbows spreading sideways was measured.

Thigh clearance: The vertical distance from a horizontal sitting surface to the highest point on the thigh.

Knee height: The vertical distance from the foot resting surface to the top of knee cap just in back and above the patella with knee flexed at 90^0.

Buttock knee length: The horizontal distance from the posterior surface of the buttock to the front of the knee cap.

Buttock Popliteal length: The horizontal distance from the posterior surface of the buttock to the popliteal surface.

Popliteal height: The vertical distance from the foot resting surface to the popliteal space.

Functional forward reach: The horizontal distance from the scapula to forward fingertip, when arm at 90^0 angle position.

Stature: The vertical distance from the floor to the top of the head, while the participant stood erect, looking straight ahead.

Standing eye height: This is the vertical distance from floor surface to the eye.

Standing shoulder height: The vertical distance from floor surface to the top of the shoulder at the acromion.

Standing elbow height: The vertical distance from floor surface to the tip of the elbow with flexed at 90^0[4].

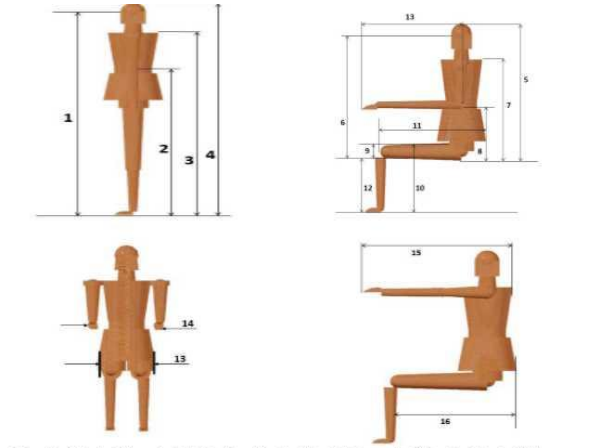

1. Eye Height, 2. Elbow height, 3. Shoulder height, 4.Stature, 5. Sitting height, 6. Sitting eye height, 7. Sitting shoulder height, 8. Sitting elbow height, 9. Thigh Clearance, 10. Knee height 11. Buttock knee length, 12. Buttock popliteal height, 13. Hip breadth, 14. Elbow to elbow breadth,15. Functional forward reach, 16. Buttock popliteal length.

Fig.1 Anthropometric measurements

2.2 Garments Furniture Measures:

The following dimensions (Fig.2) of the garments furniture which were measured:

Chair Seat height (SH): The vertical distance from the floor to the highest point on the front of the seat.

Chair Seat depth (SD): The horizontal distance from the back of the sitting surface of the seat to its front.

Chair Seat width (SW): The horizontal distance from the outer left side of the sitting surface of the seat to outer right side.

Chair Backrest height (B): The vertical distance from the top side of the seat surface to the highest point of the backrest.

Table height (T): The vertical distance from the floor to the top of the front edge of the table.

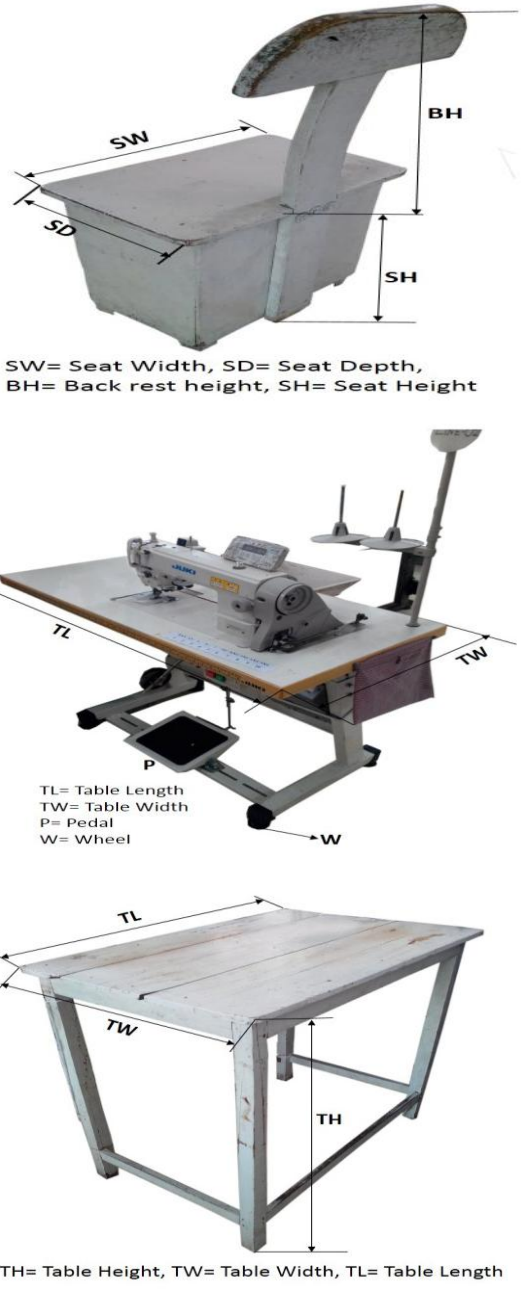

Fig.2 Garments furniture measurements.

2.3 Mismatch between garments furniture and body dimensions:

The anthropometric measurements of each individual worker were compared with relative furniture dimension in order to identify match or mismatch. In the literature different suggested relationships have been found to identify match or mismatch. Following equations are commonly used:

2.3.1 Popliteal Height (PH) against Seat Height (SH):

In literature, the seat height (SH) needs to be adapted comparatively to popliteal height, allowing knees to be flexed so that the lower legs form a maximum of 30^0 angle relative to vertical axis [5]. As shown the equation (1) below declares that the seat height(SH) should be lower than popliteal height(PH) so that the lower leg forms a 5-30^0 angle relative to the vertical and the shin-thigh angle is between 95^0 and 120^0 [5]. For this study, 3 cm correction for pedal height is including to the popliteal height. Therefore the match criteria were defined according to the eqn.1.

$$(PH+3)\cos 30^{o} \leq SH \leq (PH+3)\cos 5^{o} \quad \ldots\ldots (1)$$

2.3.2Buttock popliteal length (BPL) against seat depth (SD):

In the literature [6] the seat depth should be designed for the 5thpercentile buttock popliteal length distribution so that the backrest of the seat can support the lumbar spine without compression of the popliteal surface. Therefore a mismatch between buttock popliteal length and seat depth is either<80%or >95% of buttock popliteal length [7]. Thus the match criterion was determined by Eq^{n}.2

$$0.80BPL \leq SD \leq 0.95BPL \quad \ldots\ldots (2)$$

2.3.3 Sitting shoulder height (SSH) against backrest height (BH):

In order to facilitate of the trunk and arms, the backrest height needs to be adapted below the scapula [9]. Other researches [5] recommended to keep the backrest lower than or at most on the upper edge of the scapula (which is 60% to 80% of shoulder height). Therefore, a match criterion is established by equation (3).

$$0.60SSH \leq BH \leq 0.80SSH \quad \ldots\ldots (3)$$

2.3.4 Hip Breadth (HB) against Seat Width (SW):

In literature,[8] seat width should be designed for the 95% of hip breadth distribution and also recommended the seat width should be at least 10%(to accommodate hip breadth) and at the most 30% larger than the hip breadth (for economy space[5]. Therefore, a match criterion is established by equation (4).

$$1.10HB \leq SW \leq 1.30HB \quad \ldots\ldots (4)$$

2.3.5 Sitting elbow height (SEH) against table height (TH):

In the literature[7] suggested that the table height should be adopted to elbow-floor height, so that it would be minimum when shoulders are not flexed and maximum when shoulders are at 25^0 flexion and 20^0 abduction (elbow rest height x 0.8517 + shoulder height x 0.1483). The equation is modified [5] based on the fact that elbow-floor height is the sum of elbow rest height and seat height. Thus, a match criterion is determined by equation (5).

$$EH + (PH+3)\cos 30^{\circ} \leq TH <= (PH+3)\cos 5^{\circ} + 0.8517\ EH + 0.1483\ SH \quad \ldots\ldots (5)$$

3. Results

3.1 Anthropometric measures of the garments workers related design:

The results of 200 female worker's anthropometry data are summarized in Table 1 and Table 2 also summarized the results of 200 male worker's anthropometry data. For the purpose of analysis and design, the data are offered mean, 5th, and 95th percentile value.

Table 1 Anthropometric results for female workers

Dimension	5th %tile	Mean	95th %tile
Sitting			
Sitting height	71.95	77.26	84
Eye height	61.95	66.79	72
Shoulder height	49	53.99	59
Elbow height	16	19.79	24
Hip breadth	30	32.4	38
Elbow to elbow breadth	35	40.92	46
Thigh clearance	12	13.66	16
Knee height	47	49.03	51
Popliteal height	39	41.42	49
Buttock knee length	48	50.88	55
popliteal length	38	40.64	45
Forward reach	64	68.67	75
Standing			
Stature	150	154.46	161
Eye height	137.95	143.76	151
Shoulder height	125	129.79	138
Elbow height	91	95.39	101
Forward reach	64	68.67	75

Table 2 Anthropometric results for male workers

Dimension	5th %tile	95th %tile	Mean
Stature	155.95	173	107.99
Eye height	145.85	161	159.97
Shoulder height	130.95	146	146.89
Elbow height	96	109.05	120.85
Forward reach	72	83	89.91

3.2 Dimensions of existing garment furniture:

The critical dimensions of current garment furniture's are summarized in Table 3 that represents the existing furniture dimensions.

Table 3 Existing garment furniture dimensions

Furniture dimensions		Dimension(cm)
Sewing chair	Seat height	45
	Seat width	36
	Seat depth	43
	Back rest height	38
Sewing table	Table height	72
Inspection, cutting, and Ironing table	Table height	91

3.3 Comparison between garment worker's anthropometric measurement and garment furniture:
Match or mismatch was determinate based on above mentioned equation in the method section. Table 4 summarized the number and percentage of workers whose measurements match or did not match with the existing furniture.

Table 4 Number and percentage of female workers who match or mismatch with existing garment furniture.

Comparison between anthropometry and furniture dimensions	Match (%)	Low Mis match (%)	High Mis match(%)	Total Mis match (%)
SH and PH	**21**	**0**	**79**	**79**
SD and BPL	**6**	**0**	**94**	**94**
SW and HB	**64**	**36**	**0**	**36**
BH and SH	**100**	**0**	**0**	**0**
TH and EH	**21**	**0**	**79**	**79**

From Table 4 results show that the existing sewing table height and seat height of chair was appropriate for 21% of the workers, and only 6% of workers match with seat depth. Of these, 79% of workers used seats and tables were too high (high mismatch) than popliteal height and elbow height. The mismatch percentage for seat width is 36 % (low mismatch) which is smaller than hip breadth of workers. The results also show that 94% of workers used seats were too depth (high mismatch) than buttock popliteal length.

4. Discussion

The study estimated the possible mismatch between garment furniture and anthropometric characteristics of 400(200male and 200 female) Bangladeshi garment workers. Results, (from Table 4) show that there is a considerable mismatch between body dimensions of the garments workers and the existing garment furniture available to them. Table 4 indicates that, mismatch (high mismatch) percentages for the seat height is 76%that means workers are sitting on chairs are too high. The results indicate that, seat depth mismatch percentages are too high 94% (high mismatch) consequently, majority of the workers usually place their buttock forward on the edge of the seat during sewing operations. Thus, the back of workers does not touch the back rest shown in Fig. 4

Fig. 4 working positions at existing sewing workstation

Seat width mismatch percentages are 36% (low mismatch) for workers that mean chairs are narrow designed. Due to, worker who have large hip breadth cannot get enough space to sit. The mismatch percentages for the sewing table height are too high 79% (high mismatch) thus; the height of the table exceeds their elbow rest height, so the workers are forced to lift their arms during sewing operations (shown in Fig 4), which may cause more muscular load, discomfort and pain in the shoulder area [7] or have to bend their trunk forward, a posture which increase the spinal load.

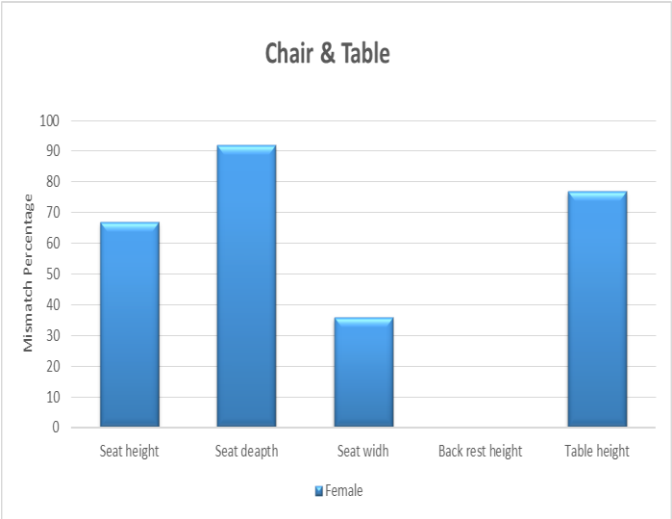

Fig. 5 Mismatch percentages for different dimensions (existing)

The mismatch (percentages) between the anthropometric characteristics of garments workers and the existing garments furniture are shown in Fig. 5

5. Conclusion

The study indicates that, there are considerable mismatches between the garments furniture and anthropometric characteristic of workers. The seat height, seat depth, and sewing table height are being the dimensions with a higher level of mismatch. Based on estimation by applying mismatch equations(equation 1-equation 5) and reported to the workers that the existing furniture are not safe and comfort to use and they can cause health problems for the worker. The seats heights, table height, are too high for majority workers. On the other, hand seat depths are too length and the seat widths are too narrow for female workers. This occurred due to design the furniture without maintaining ergonomic issues. As a result the workers feel discomfort.

REFERENCES

[1] Chengular, S.N., Rodgers, S.H., & Bernard, T.E.(2004). *Kodak's ergonomic design for people at work.* Hoboken, NJ: John Wiley & Sons, Inc.

[2] Friend, M.A. , & Kohn, J.P. (2007). *Fundamentals of occupational safety and healthfourth edition.* Lanham, MD: Government Institutes.

[3] Grandjean, E. and Vigliani, E.(Eds),1980, *Ergonomics Aspects of Visual Display Terminals, London*: Taylor & Francis.school children: an anthropometric case study. Appl. Ergon. 19, 122–134.

[4] Helander, M., 1997. Anthropometry in workstation design. In: Helander, M. (Ed.),A Guide to the Ergonomics of Manufacturing. Taylor & Francis, London, pp. 17e28.

[5] Molenbroek, J.F.M., Kroon-Ramaekers, Y.M.T., and Snijders, C.J. 2003. Revision of the design of a standard for the dimensions of school furniture. Ergonomics 46, 681-694.

[6] Gouvali, M.K., Boudolos, K., (2006) Match between school furniture dimensions & children's anthropometry. *App. Ergo.* 37, 765-773.

[7] Milanese, S., Grimmer, K., 2004. School furniture and the user population: an anthropometric perspective. Ergonomics 47, 416–426.

[8] Parcells, C., Stommel, M., Hubbard, R.P., 1999. Mismatch of classroom furniture & student body dimensions: empirical findings & health implications. J. Adolesc. Health 24 (4), 265–273.

[9] Evans, W.A., Courtney, A.J., Fok, K.F., 1988. The design of school furniture for Hong Kong .

ICMIEE-PI-140282

Autonomous Robot Path Planning Using Particle Swarm Optimization in Dynamic Environment with Mobile Obstacles & Multiple Target

Md. Rakibul Islam[1], Md. Tajmiruzzaman[2], Md. Mahfuzul Haque Muftee[3], Md. Sanowar Hossain[4]*
[1*, 2, 4] Department of Industrial & Production Engineering,
Rajshahi University of Engineering & Technology, Rajshahi- 6240, BANGLADESH
[3] Department of Computer Science & Engineering,
Rajshahi University of Engineering & Technology, Rajshahi- 6240, BANGLADESH

ABSTRACT
Now a day, there are even demands for application of robots in homes and hospitals. The goal of this research is to plan a trajectory and minimizing the path lengths with collisions avoidance for a mobile robot in dynamic environment. In this paper, an intelligent approach for navigation of a mobile robot in dynamic environment with multiple targets is proposed. Particle Swarm Optimization (PSO) method is used for finding proper solutions of optimization problems. PSO has been demonstrated to be a useful technique in robot path planning in dynamic environment with mobile obstacles and multiple goals, as a feasible approach for self organized control of robot to avoid obstacle throughout the trajectory. The authors here has been used a grid based search approach for robot. The positions of the obstacles will be changed randomly. Finally, simulation results confirm the effectiveness of our algorithm**.**

Key words: Robot Path Planning, Particle Swarm Optimization, Trajectory Planning, Moving Obstacles

1. Introduction

Autonomous mobile robots used in the environment where many human beings are working, cooperating with robots. In these environments, the collision-free path planning is one of the major problems to realize autonomous mobile robots. Since there are many stationary or moving obstacles in these environments, autonomous mobile robots should plan their own path that can avoid not only stationary obstacles but also moving ones such as human workers and other robots. The main problem in robot path planning is to find a motion trajectory from a starting position to a goal position regarding to some optimization criteria. Path Planning is one of the most vital issues in the navigation of mobile robot, which means to find out an optimized collision free path from the start state to the goal state according to some performance merits. It can be classified into two categories global path planning with all the information of the robot's known environment and local path planning in a partly or totally unknown environment [1]. In global navigation methods cost of environmental change, especially in dynamic environment is very high, because supply a new map is difficult. Therefore, research on the local navigation is necessary. These methods could be able to detect the unknown environment, and it does not need to environment model. In this paper, a new method of local navigation based on particle swarm optimization technique is proposed.

There have been many algorithms for global path planning, such as artificial potential field, visibility graph, and cell decomposition etc. PSO is a heuristic search technique that is inspired by the behavior of bird flocks. Although PSO is relatively new, the relative simplicity, the fast convergence and the population-based feature [2] have made it a considerable viable alternative for solving the robot path planning problem. PSO has been used for hazardous target search applications, such as landmine detection, fire fighting, and military surveillance, and are an effective technique for collective robotic search problems.

Swarm intelligence is an emerging research area with similar population and evolution characteristics to those of genetic algorithms. Swarm intelligence is used to solve optimization and cooperative problems among intelligent agents, mainly in computer's networks, mobile robotics [3] and cooperative and/or decentralized control [4]. Swarm intelligence is inspired in nature, in the fact that contribution among living animals of a group contribute with their own experiences to the group, making it stronger in face of others. In This method, an optimization problem based on position of obstacles, and goal is designed and then PSO is used to solve the optimization problem. Every step of the algorithm, the global best position of particle is selected and the robot moves on the points in order to reach the goal. Whenever sensors detect changes in their environment or whenever the robot reaches to a local goal the local, processor of robot updates its data.

2. A Review of Previous Research

To solve the navigation problem for the robot, researchers have proposed various methods. In conventional navigation methods such as cell decomposition (Latombe, 1990) [5] and road map (Wang. 2000) [6], due to the high volume of calculations, we are not able to solve problems in complex environments. Artificial potential field method (Shi, 2009) [7], because of simplification frequently is used for local navigation. But due to stop at local minima, this method will fail. In recent years a series of intelligent ideas, such as genetic algorithms and particle swarm optimization because of the robust and ability to the Simultaneous calculations to solve the navigation

* Corresponding author. Tel.: +88-01774686877
E-mail addresses: rbn_khan@yahoo.com

problems are used. Ghorbani and colleagues (Ghorbani, 2009) [8], use the genetic algorithm for solving the problem of mobile robot navigation. Sugiwara and colleagues, (*Sugawara*, 2004) [9], used ants colony algorithm to solve the problem of navigation in a dynamic virtual environment. Qu and colleagues, (Qu, 2009) [10] used neural networks for navigation and obstacles avoid in dynamic environments. PSO, by Kennedy in 1995, based on observation of the collective behavior of certain species of animals such as birds and fish have been proposed (Eberhart, 1995& Kennedy, 1995) [11]. Due to simplicity, this method is used in robot navigation. Doctor and colleagues (*Doctor*, 2004) [12], using the PSO method for navigation an unmanned vehicle that can converge well. Chen and colleagues, (Chen, 2006) [13], suggests a soft and efficient navigation method for mobile robot using the Stochastic PSO. Qin and colleagues (Qin, 2004) [14] used the Chaotic PSO with Mutation operator for navigation and moving the robot meets the immediate needs. Hao and colleagues, (Hao, 2007) [15] proposed a method of obstacles avoiding using the PSO and polar coordinate system in a dynamic environment.

3. Particle Swarm Optimization

The proposal of such algorithm appeared from some scientists that developed computational simulations of the movement of organisms such as flocks of birds and fish schooling. Such simulations were heavily based in manipulating the distances between individuals, that is, the synchrony of the behavior of the swarm was thought as an effort to keep an optimal distance between them.

In theory, at least, individuals of a swarm may benefit from the prior discoveries and experiences of all member of the swarm when foraging. The fundamentals of developing particle swarm optimization (PSO) are a hypothesis in which the exchange of information among beings of a same species offers some sort of evolutionary advantage.

Similarly to genetic algorithms (GAs), PSO is an optimization tool based in a population, where each member is called a particle, that is, each particle is a potential solution to the analyzed problem. However, unlike GAs, PSO does not have operators, like crossover and mutation. PSO does not implement the survival of the fittest individuals; instead, it implements the simulation of social behavior.

The PSO algorithm works as follows, initially, a random position population exists, each of these particles has a speed and the particles start to "fly around" the search space. Each particle has a memory, allowing it to remember the best position it has visited in history (*pbest*), and also the fitness in that position.

The best position ever achieved by the whole swarm is denominated the global best (*gbest*). The basic concept of PSO algorithm is to accelerate the particles towards *pbest* and *gbest*, considering a random weight at each time step. Mathematically, the particles move following the equations:

$$V_{id}^{t+1} = W \times V_{idt} + c_1 \times rand_1 \times (P_{id} - X_{id}^{t}) + c_2 \times rand_2 \times (Pgd_{id} - X_{id}^{t}) \quad (1)$$

$$X_{id}^{t+1} = X_{id}^{t} + V_{id}^{t+1}\Delta t \quad (2)$$

Where $\Delta t = 1$, t represents the actual iteration and $t + 1$ represents the next iteration V_{id} and X_{id} represent the particle speed and position respectively, $rand_1$ and $rand_2$ are two random numbers with uniform distribution in [0,1], used to maintain populations' diversity.

Eq. (1) is used to update each particle's speed, and Eq. (2) represents the position update, according to its previous position and its speed, considering $\Delta t = 1$.

Positive constants c_1 and c_2 are denominated cognitive and social components, respectively. These are the acceleration constants, responsible for varying the particle speed towards *pbest* and *gbest*. Constants c_1 and c_2 are not critical factors for determining the algorithm convergence; however, a correct tuning may cause the algorithm convergence to occur faster.

The use of W, called inertia weight was proposed by Shi and Eberhart (1998) [16]. This parameter is responsible for dynamically adjust the speed of the particles, so, it's responsible for balancing between local and global search, consequently, needing less iterations for the algorithm to converge. A small value of inertia weight implies in a local search, by the other side, a high value leads to a global search.

Applying a high inertia weight at the start of the algorithm and making it decay to a low value through the PSO algorithm execution, makes the algorithm globally search in the start of the search, and search locally at the end of the execution. Eq. (3) shows how the inertia weight is updated, considering $iter_{max}$ the maximum number of iterations of the algorithm and $iter$ the actual iteration.

$$W = W_{max} - \frac{W_{max} - W_{min}}{iter_{max}} \times iter \quad (3)$$

The first step of the PSO algorithm is to start each particle with random numbers, considering that the random number must belong to the search space. Next a loop starts being executed, and it remains until the stopping criteria is met, the stopping criteria may be the convergence of the algorithm, a maximum number of iterations, or anything else. Inside the loop the value of the fitness and the *pbest* of each particle are determined. Once all particles have been analyzed, it's calculated the *gbest*, and with this value, the velocity and position of all particles is achieved.

4. Trajectory Planning

The position of the robot is represented by Cartesian coordinates such as x- and y-coordinate positions and its velocity is modified by PSO.

As the particles initiated moves through the search space for finding the next optimum position for the robot to move, the positions lying inside any obstacle should be discarded and the path, generated after choosing the next position, should not collide with any obstacle.

4.1 Objective function

The path-planning, in this study, is nothing but a constrained optimization where the obstacles represent constraints and the length of path has to be optimized (minimized) i.e. the Euclidean distance from current position to the goal is the objective function.
The positions which give the minimum value of the objective function i.e. the positions nearest to the goal point must be selected for the next move of the robot in every iteration of the algorithm.
In this study, we have used a simple objective function

$$F = \sqrt{(x_i - x_g)^2 + (y_i - y_g)^2}; i = 1, 2, 3, \ldots\ldots, N \quad (4)$$

Where, N is number of particles. (x_i, y_i) is current position of i-th particle and (x_g, y_g) is co-ordinate of goal point.

4.2 Proposed Approach

The overall steps of the algorithm are as follows:

Step 1: A preset number of particles are generated around the robot's initial position and within its sensing range.

Step 2: Each particle takes a new velocity and position based on the constantly updated PSO equations.

Step 3: All the particles are checked if the lines connecting the new positions of the particles to the robot's current position intersect any obstacle; if any particle intersects, then the particle is relocated to another new position.

Step 4: A candidate for the robot's next position is determined by the position of the best particle (i.e., the one nearest to the goal). Set it as the robot's next position and go to Step 2.

Step 5: Execute Steps 2–4 until the goal is within the robot's sensing range and can be accessed via a straight line.

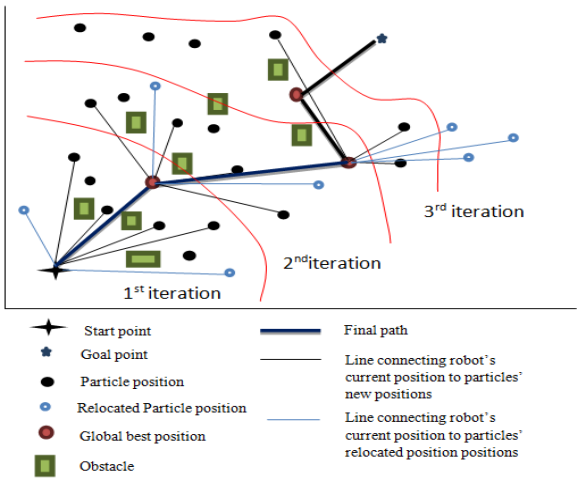

Fig.1 Obstacles avoidance and path generation

We have used relocation method instead of penalty method for obstacle avoidance, because in penalty method, some particles will be lost but in relocation method, particles' positions are relocated, so no particles are lost.
The algorithm part for relocation of particles' positions is:

```
for i =1 to M, M is no. of obstacles do
    for j=1 to N, N is no. of particles do
        Find I, I is matrix of intersection points of
        obstacle and line connecting the new position
         of the particle to the robot's current position.
          while ( I ~= empty) do
             Find new position of the particle
              for k=1 to M do
                 Find I
                 if(I==empty )
                   Break
                 end if
              end for k
          end while
    end for j
end for i
```

5. Simulation

5.1 Settings and environment

All the experiments are executed in a Fujitsu LH531 computer and the configuration of PC was Intel(R) Pentium(R) CPU B960 @ 2.20 GHz and 2 GB RAM. The environment used for the trajectory planning is a 20x20 meters field. And as we have mentioned earlier, we have used a grid based environment, where robots can choose only integer-valued co-ordinates for the candidate points of trajectory. As for creating a dynamic environment, once we have assigned some positions to the obstacles initially before starting iterations, the obstacles move randomly in a range of (-1,1) for both x and y co-ordinates in each iteration. The PSO parameters are: maximum number of iterations 100, maximum inertia weight 0.9 and minimum inertia weight 0.4 and $c1 = c2 = 2$.

5.2 Simulation result

The MATLAB simulation results of our research work for autonomous robot path planning in dynamic and static environment is summarized in table 1 for different combinations.

Obstacle No.	Static Obstacles	Dynamic Obstacles	Swarm No.	Target No.	Path Length	Time (S)
4	4	0	30	1	26.24	2.57
8	8	0	35	1	28.64	4.71
12	12	0	40	1	27.69	4.82
12	8	4	50	1	30.56	6.45
12	0	12	50	1	32.35	6.70
12	0	12	50	2	43.26	6.9

Table 1 Simulation results for the proposed algorithm

These results for different combinations are also shown in different figures below. The figure 1 through figure 3 has

been shown for static environment. The figure 4a and 4b is for partly dynamic and partly static environment and the figure 5a through figure 5d is used to show the fully dynamic environment. These upper-mentioned cases are for single goal. Finally, the figure 6 is used to show for the case of multiple goals as two goals.

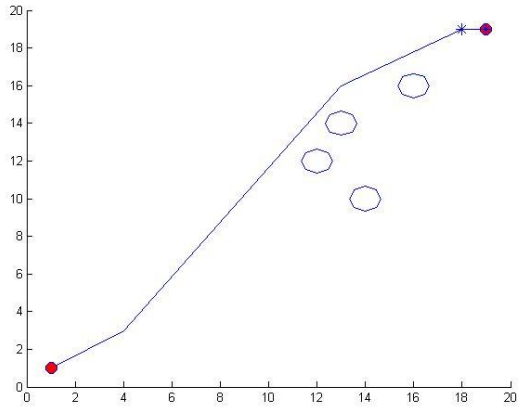

Fig.2 Path generated for the working environment using PSO (Static obstacles = 4; Dynamic obstacles = 0; Swarm size = 30; Goal = 1)

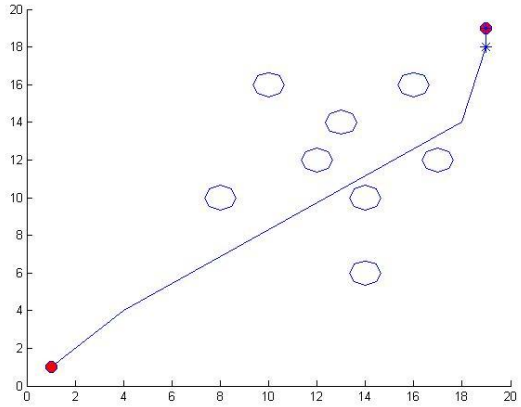

Fig.3 Path generated for the working environment using PSO (Static obstacles = 8; Dynamic obstacles = 0; Swarm size = 35; Goal = 1)

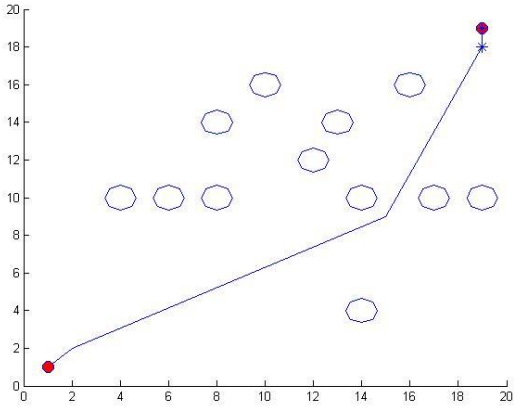

Fig.4 Path generated for the working environment using PSO (Static obstacles = 12; Dynamic obstacles = 0; Swarm size = 40; Goal = 1)

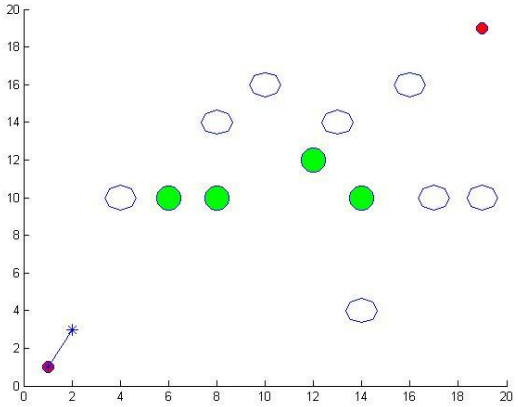

Fig.5a (Starting**)** Path generated for the working environment using PSO (Static obstacles = 8; Dynamic obstacles = 4; Swarm size = 50; Goal = 1)

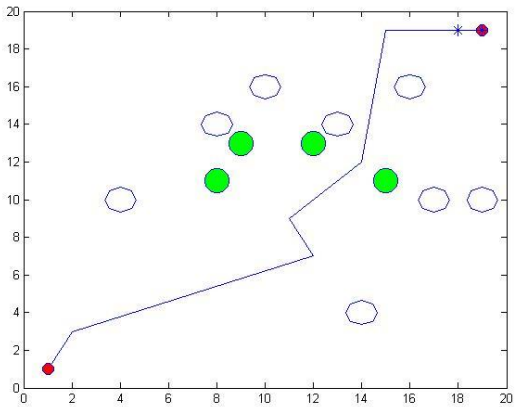

Fig.5b (End**)** Path generated for the working environment using PSO (Static obstacles = 8; Dynamic obstacles = 4; Swarm size = 50; Goal = 1)

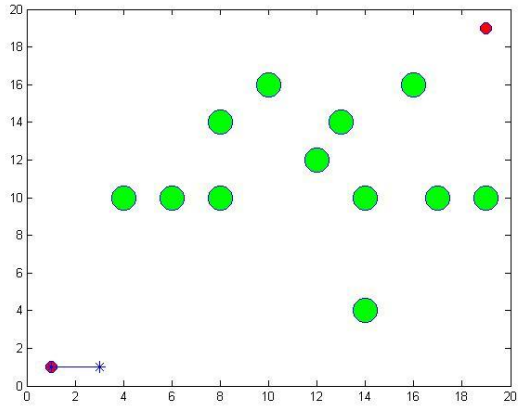

Fig.6a (Starting**)** Path generated for the working environment using PSO (Static obstacles = 12; Dynamic obstacles = 0; Swarm size = 50; Goal = 1)

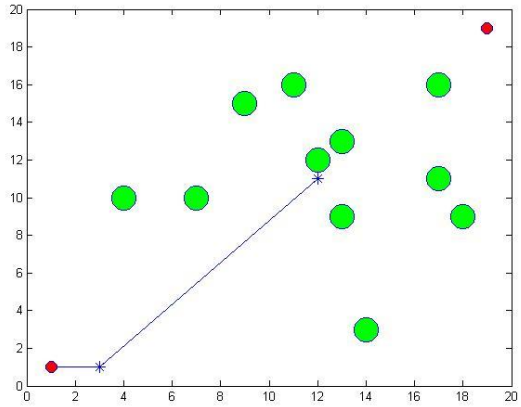

Fig.6b (Middle**)** Path generated for the working environment using PSO (Static obstacles = 12; Dynamic obstacles = 0; Swarm size = 50; Goal = 1)

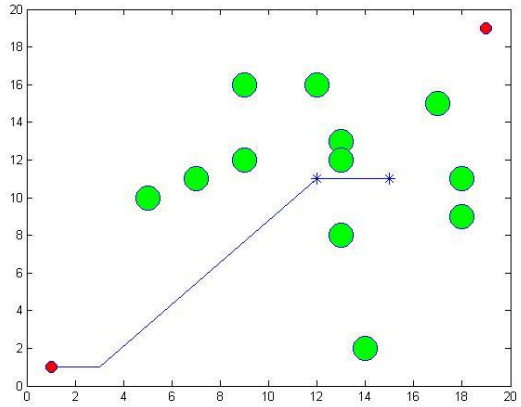

Fig.6c (Middle**)** Path generated for the working environment using PSO (Static obstacles = 12; Dynamic obstacles = 0; Swarm size = 50; Goal = 1)

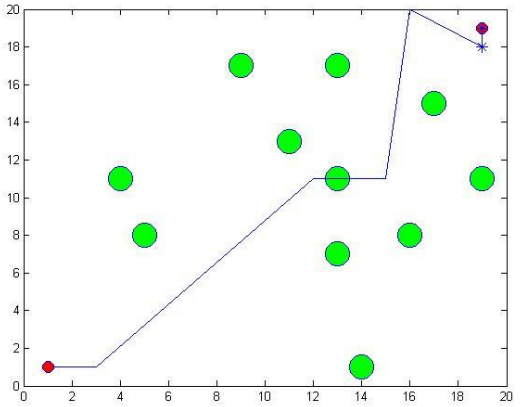

Fig.6d (End**)** Path generated for the working environment using PSO (Static obstacles = 12; Dynamic obstacles = 0; Swarm size = 50; Goal = 1)

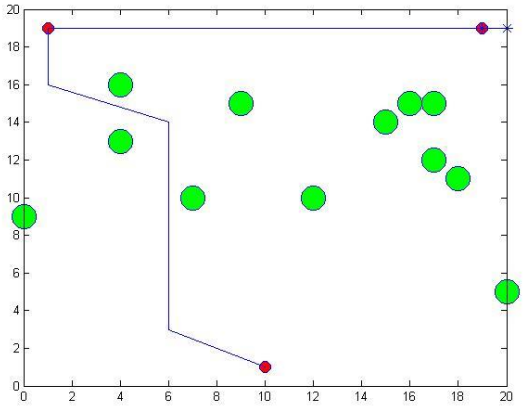

Fig.7 Path generated for the working environment using PSO (Static obstacles = 12; Dynamic obstacles = 0; Swarm size = 50; Goal = 2)

6. Conclusion & Future Works

A sensor-based path planner is presented in this paper. The proposed method is able to deal simultaneously with both global and local planning requirements. The advantages of the approach can be summarized by the fact that the trajectories obtained are smooth and safe, and at the same time, free of local traps due to the integration of the real-time sensor information in the recalculation of the path.

The method is easy to implement, the algorithm is very fast and can work online. It works in cluttered and changing environments with moving obstacles. As demonstrated along this work, the method can perform in all types of environments without restrictions in the form of the obstacles.

Obstacles in the environment by the robot sensors, in a limited radius around it are detected. The robot will come. It cannot be said with certainty that the path travelled by the robot to the global is optimum because the environ-

ment is dynamic and unknown. The proposed method is flexible, that way you can change any parameters, or control the degree of importance of avoiding or moving toward the goal. As future work we have the intention to apply other types of nature inspired algorithms to the path planning problem. We can also improve the performance by the hybridization of various nature inspired algorithms.

7. References

[1] L. Li, T. Ye, M. Tan, and X. Chen, Present state and future development of mobile robot technology research, *Robot*, vol. 24(5), pp.475-480, (2002).

[2] M. Reyes-Sierra, and C.A. Coello, Multi-objective particle swarm optimizers: a survey of the state-of-the-art, *Int. J. Comput. Intell.* Res. 2 (3), 287–308, (2006).

[3] Y. Liu, and K.M. Passino, Stable social foraging swarms in a noisy environment, *IEEE Transactions on Automatic Control*, vol. 49, no. 1, pp. 30-44, (2004).

[4] J.S. Baras, X. Tan, and P. Hovareshti, Decentralized control of autonomous vehicles, *Proceedings of the 42nd IEEE Conference on Decision and Control, Maui, Hawaii, USA*, pp. 1532-1537, (2003).

[5] J. C. Latombe, Robot motion planning, *Springer Verlag*, (1990).

[6] Y. Wang, Two novel approaches for unmanned underwater vehicle path planning: constrained optimization and semi-infinite constrained optimization, Robotica, vol. 18, pp. 123-14, (2000).

[7] P. Shi and Y. Zhao, An efficient path planning algorithm for mobile robot using improved potential field, *IEEE International Conference on Robotics and Biomimetics*, pp. 1704-1708, (2009).

[8] A. Ghorbani, Using Genetic Algorithm for a Mobile Robot Path Planning, *International Conference on Future Computer and Communication*, pp. 164-166, (2009).

[9] K. Sugawara, Foraging behavior of interacting robots with virtual pheromone, *Proceedings of the International Conference on Intelligent Robots and Systems*, pp. 3074-3079 vol. 3, (2004).

[10] H. Qu, Real-time robot path planning based on a modified pulse-coupled neural network model, *Neural Networks, IEEE Transactions on*, vol. 20, pp. 1724-1739, (2009).

[11] R. Eberhart and J. Kennedy, A new optimizer using particle swarm theory, *in Proceedings of the Sixth International Symposium on Micro Machine and Human Science*, pp. 39-43, (1995).

[12] S. Doctor and G. Venayagamoorthy, Unmanned vehicle navigation using swarm intelligence, *in Proceedings of International Conference on Intelligent Sensing and Information Processing*, pp. 249-253, (2004).

[13] X. Chen and Y. Li, Smooth path planning of a mobile robot using stochastic particle swarm optimization, *in Proceedings of the IEEE International Conference on Mechatronics and Automation*, pp. 1722-1727, (2006).

[14] Q.Y. Qin, Path planning for mobile robot using the particle swarm optimization with mutation operator, *in Proceedings of International Conference on Machine Learning and Cybernetics, pp.* 2473-2478 vol. 4, (2004).

[15] Y. Hao, Real-Time Obstacle Avoidance Method based on Polar Coordination Particle Swarm Optimization in Dynamic Environment, *in IEEE Conference on Industrial Electronics and Applications*, pp. 1612-1617, (2007).

[16] Y. Shi, and R. C. Eberhart, Parameter selection in particle swarm optimizer, *Proceedings Seventh Annual Conference on Evolutionary Programming, V.W. Porto, N. Saravan, D. Waagen, and A.E. Eiben (eds.). Berlin: Springer-Verlag*, pp. 591-601, (1998).

ICMIEE-PI-140283

Numerical investigation of natural convection heat transfer of nanofluids inside a wavy cavity

Md. Maruf Billah[1] *, Neethila Nabanita Poddar*[1] *and Md. Mamun Molla*[3]*
[1,2]Dept. of Electrical and Computer Engineering, North South University, Dhaka-1229, BANGLADESH
[3*]Dept. Mathematics and Physics, North South University, Dhaka-1229, BANGLADESH

ABSTRACT
In this research, heat transfer efficiency of nanofluids, through natural convection, inside a sealed wavy cavity has been examined numerically. Copper has been used as nanoparticles for primary investigation, with water as the base fluid. The governing Navier-Stokes and energy equations have been transformed into Cartesian curvilinear coordinates and then solved numerically using the finite volume method imposing several boundary conditions. Numerical code written in FORTRAN programming language is used to simulate the dimensionless, discretized governing equations. The study has been conducted for a range of Rayleigh numbers ($10^3 < Ra < 10^6$) and different volume fractions ($0 < \phi < 0.2$). The code is validated with previous published results and found to be in good agreement. The obtained results are illustrated in terms of the isotherms, streamlines, velocity and temperature profiles as well as the rate of heat transfer. It is observed that volume fraction of nanoparticles and the Rayleigh number affect the flow and heat transfer characteristics of nanofluids within the cavity.

Keywords: Nanofluids, Natural convection, curvilinear coordinates, Finite volume method, Wavy cavity.

1. Introduction

Heat transfer characteristics have been a major concern in the scientific world and have been the focus of many scientific researches because many devices and equipments starting from major industrial machines to the computers at home require cooling. For most of those equipments, like a flat-plate solar collector or a solar thermal collector, the performance improves with the increase in heat transfer efficiency. The conventional heat transfer materials like water, air, ethylene glycol, engine oil and so on were used as coolants but they have their limitations. The lower heat transfer performances of these conventional fluids obstruct the performance enhancement and compactness of heat exchangers. So the concept of nanofluid emerged which was first coined by Choi [1], a pioneer in this field.

Nanofluids are dispersion of nanometer sized particles (nanoparticles) in the conventional base fluids mentioned above. Nanoparticles can be metallic and non-metallic and may contain aluminum, copper, titanium etc. These suspensions of nanoparticles in base fluids have been reported to have increased the heat transfer characteristics of the fluids and thus enhance the efficiency of the system. This increase in heat transfer is mainly due to high thermal conductivity of the nanoparticles. Xuan and Li [2] conducted theoretical study to find that the heat transfer increases with the introduction of nanoparticles. Minsta et al. [3] and Pang et al. [4] also showed the enhancement of thermal conductivity of nanofluids in their research. Many studies and research works have been done on nanofluids to understand their characteristics properly. There were numerical and experimental works on nanofluids with various geometries such as, square cavity (Esmaeil [5]), triangular cavity (Yu et al. [6]), pipe (Abouali et al. [7]), inclined angle (Oztop [8]) and so on, and with various governing parameters (Rayleigh number, volume fraction, Grashof number, etc).

The literature reviewed reveals that many efforts were given to understand the characteristic of the nanofluids. Many studies were done with square cavity. Khanafer et al. [9] was one of the first to use nanofluids inside the cavity and his work was extended by Violi et al. [10] for square cavity. As the literature review suggests, there were also some works on square cavity with wavy wall, like Abu Nada et al. [11], Farhadi et al. [12], Mansour et al. [13] and Sonam singh et al. [14]. These papers studied the different parameters of nanofluids in different geometries of wavy wall cavity to understand their effects. However, to the best knowledge so far, none of them did any study on natural convection flow with left wall heated wavy and right wall cold wavy and top and bottom adiabatic flat.
So the main aim of this study is to investigate the effects of vertical wavy walls, heated from the left, on the flow of the nanofluids and the effects on the heat transfer characteristics of the nanofluids. This study intends to draw a qualitative comparison, based on the simulation findings, between flat and wavy walls. A mathematical model has been developed, based on which the simulations are done and the results are discussed.

2. Mathematical modeling

A two-dimensional (2D) rectangular cavity of height *H* and width *L is* considered for the present study. The top and bottom wall is entirely adiabatic. No-slip and no penetration assumptions were imposed on the walls. The entire left sidewall is hot and the right sidewall is cool (see Fig. 1.). Considering this cavity contains nanofluid, which is Newtonian, incompressible laminar, to

*Corresponding author. Tel.: +88-02-8852000(Ext.1519); fax: +88-02-8823030
E-mail addresses: mmamun@northsouth.edu, mmamun@gmail.com

investigate the flow and thermal behavior when left wavy wall is heated under several conditions.

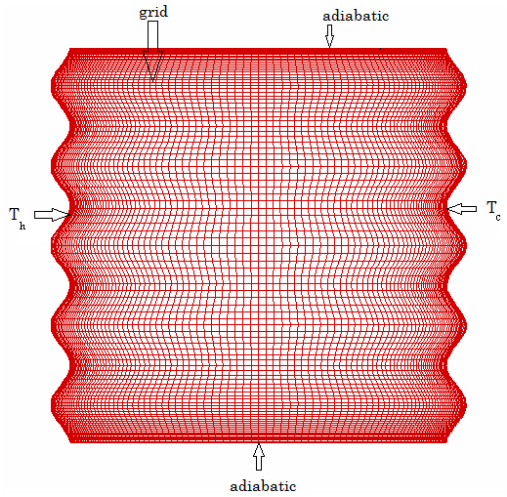

Fig. 1: Schematic for the physical model

The governing Navier-Stokes and energy equations for the present study taking into the account the Boussinesq approximation can be written as:

$$\frac{\partial \mathrm{u}}{\partial \mathrm{x}}+\frac{\partial v}{\partial y}=0 \tag{1}$$

$$\frac{\partial u}{\partial \mathrm{t}}+u\frac{\partial u}{\partial x}+v\frac{\partial u}{\partial y}=-\frac{1}{\rho}\frac{\partial P}{\partial x}+\frac{\mu}{\rho}\left[\frac{\partial^2 u}{\partial x^2}+\frac{\partial^2 u}{\partial y^2}\right] \tag{2}$$

$$\frac{\partial v}{\partial \mathrm{t}}+v\frac{\partial v}{\partial y}+u\frac{\partial v}{\partial x}=-\frac{1}{\rho}\frac{\partial P}{\partial y}+\frac{\mu}{\rho}\left[\frac{\partial^2 v}{\partial y^2}+\frac{\partial^2 v}{\partial x^2}\right]+g\beta(T-T_\infty) \tag{3}$$

$$\frac{\partial T}{\partial \mathrm{t}}+u\frac{\partial T}{\partial x}+v\frac{\partial T}{\partial y}=\kappa\left[\frac{\partial^2 T}{\partial x^2}+\frac{\partial^2 T}{\partial y^2}\right] \tag{4}$$

The boundary conditions for the present investigation are presented as:

Left wall: at $x = 0$, $0 \le y \le 1$: $T = 1$, $u = v = 0$

Right wall: at $x = 1$, $0 \le y \le 1$: $T = 0$, $u = v = 0$

Top wall: at $y = 1$, $0 \le x \le 1$: $\frac{\partial T}{\partial y}=0$, $u = v = 0$

Bottom wall: at $y = 0$, $0 \le x \le 1$: $\frac{\partial T}{\partial y}=0$, $u = v = 0$

It is important that the terms in our equation are in a form that is independent of the dimensions of the geometry and hence is feasible for comparison. So the governing equations are non-dimensionalized using the following dimensionless parameters.

$$X=\frac{x}{\mathrm{L}},\ Y=\frac{y}{\mathrm{L}},\ U=\frac{uL}{\alpha_{\mathrm{f}}},V=\frac{vL}{\alpha_{\mathrm{f}}},\Theta=\frac{T-T_{\mathrm{c}}}{\mathrm{T_h}-\mathrm{T_c}},\ P=\frac{pL^2}{\rho_f\alpha^2{}_{\mathrm{f}}}$$

$$\mathrm{Pr}_f=\frac{\nu_f}{\alpha_{\mathrm{f}}},\ Ra=\frac{g\beta(T_h-T_c)L^3\,\mathrm{Pr}_f}{\nu_f{}^2},\ \tau=\frac{\alpha_{\mathrm{f}}t}{L^2},\ \nu_{nf}=\frac{\mu_{nf}}{\rho_{nf}},\ \alpha_{nf}=\frac{K_{nf}}{(\rho c_p)_{nf}} \tag{5}$$

Here, the effective viscosity for a suspension containing small spherical solid nanoparticles is given as μ_{nf} and the effective density of a fluid containing solid nanoparticles is given by ρ_{nf} .

The dimensionless governing equations is of the following form,

$$\frac{\partial \mathrm{U}}{\partial \mathrm{X}}+\frac{\partial V}{\partial Y}=0 \tag{6}$$

$$\frac{\partial U}{\partial \tau}+U\frac{\partial U}{\partial X}+V\frac{\partial U}{\partial Y}=-\frac{1}{(1-\phi)+\phi\frac{\rho_s}{\rho_f}}\frac{\partial P}{\partial X}+\mathrm{Pr}\frac{1}{(1-\phi)^{2.5}\left[(1-\phi)+\phi\frac{\rho_s}{\rho_f}\right]}\left[\frac{\partial^2 U}{\partial X^2}+\frac{\partial^2 U}{\partial Y^2}\right] \tag{7}$$

$$\frac{\partial V}{\partial \tau}+U\frac{\partial V}{\partial X}+V\frac{\partial V}{\partial Y}=-\frac{1}{(1-\phi)+\phi\frac{\rho_s}{\rho_f}}\frac{\partial P}{\partial Y}+\frac{\mathrm{Pr}}{(1-\phi)^{2.5}\left[(1-\phi)+\phi\frac{\rho_s}{\rho_f}\right]}\left[\frac{\partial^2 V}{\partial X^2}+\frac{\partial^2 V}{\partial Y^2}\right]+Ra\,\mathrm{Pr}\,\Theta\left[\frac{1}{1+\frac{(1-\phi)\rho_f}{\phi\rho_s}}\frac{\beta_s}{\beta_f}+\frac{1}{1+\frac{\phi\rho_s}{(1-\phi)\rho_f}}\right] \tag{8}$$

$$\frac{\partial \Theta}{\partial \tau}+U\frac{\partial \Theta}{\partial X}+V\frac{\partial \Theta}{\partial Y}=\frac{\frac{K_{nf}}{K_f}}{\left[(1-\phi)+\phi\frac{(\rho C_p)_s}{(\rho C_p)_f}\right]}\left[\frac{\partial^2 \Theta}{\partial X^2}+\frac{\partial^2 \Theta}{\partial Y^2}\right] \tag{9}$$

3. Numerical method and validation

The governing equations (6)-(9) were transformed to curvilinear coordinates $x=x_1=(\zeta_1,\zeta_2)$ and $y=x_2=(\zeta_1,\zeta_2)$ so that complex geometry can be handled. The determinant of the Jacobian matrix, J, is defined as :

$$|J|=\begin{vmatrix}\frac{\partial x_1}{\partial \zeta_1} & \frac{\partial x_1}{\partial \zeta_2}\\ \frac{\partial x_2}{\partial \zeta_1} & \frac{\partial x_2}{\partial \zeta_2}\end{vmatrix}\quad \text{Therefore,}\quad |J|=\frac{\partial x_1}{\partial \zeta_1}\frac{\partial x_2}{\partial \zeta_2}-\frac{\partial x_1}{\partial \zeta_2}\frac{\partial x_2}{\partial \zeta_1} \tag{10}$$

$$|J|=\frac{\partial x_i}{\partial \zeta_j}A_{ij},\ \text{where}\quad A=\begin{vmatrix}\frac{\partial x_2}{\partial \zeta_2} & -\frac{\partial x_2}{\partial \zeta_1}\\ -\frac{\partial x_1}{\partial \zeta_1} & \frac{\partial x_1}{\partial \zeta_2}\end{vmatrix}$$

The final transformed equation into curvilinear coordinate are:
Continuity Equation:

$$\frac{A_{11}}{|J|}\frac{\partial U}{\partial \zeta_1}+\frac{A_{12}}{|J|}\frac{\partial U}{\partial \zeta_2}+\frac{A_{21}}{|J|}\frac{\partial V}{\partial \zeta_1}+\frac{A_{22}}{|J|}\frac{\partial V}{\partial \zeta_2}=0 \qquad (11)$$

Momentum equation:
U-momentum

$$\frac{\partial U}{\partial \tau}+\frac{1}{|J|}\left(UA_{11}+VA_{21}\right)\frac{\partial U}{\partial \zeta_1}+\frac{1}{|J|}\left(UA_{12}+VA_{22}\right)\frac{\partial U}{\partial \zeta_2}=-\frac{1}{\left[(1-\phi)+\frac{\phi\rho_s}{\rho_f}\right]}\left[\frac{A_{11}}{|J|}\left(\frac{\partial P}{\partial \zeta_1}\right)+\frac{A_{12}}{|J|}\left(\frac{\partial P}{\partial \zeta_2}\right)\right]+\Pr\frac{1}{(1-\phi)^{2.5}\left[(1-\phi)+\phi\frac{\rho_s}{\rho_f}\right]|J^2|}\left[\begin{array}{l}\left(A_{11}^2+A_{21}^2\right)\frac{\partial^2 U}{\partial \zeta_1^2}+2(A_{11}A_{12}+A_{21}A_{22})\frac{\partial^2 U}{\partial \zeta_1 \partial \zeta_2}\\+\left(A_{12}^2+A_{22}^2\right)\frac{\partial^2 U}{\partial \zeta_2^2}\end{array}\right] \qquad (12)$$

$$\frac{\partial V}{\partial \tau}+\frac{1}{|J|}\left(UA_{11}+VA_{21}\right)\frac{\partial V}{\partial \zeta_1}+\frac{1}{|J|}\left(UA_{12}+VA_{22}\right)\frac{\partial V}{\partial \zeta_2}=-\frac{1}{\left[(1-\phi)+\frac{\phi\rho_s}{\rho_f}\right]}\left[\frac{A_{11}}{|J|}\left(\frac{\partial P}{\partial \zeta_1}\right)+\frac{A_{12}}{|J|}\left(\frac{\partial P}{\partial \zeta_2}\right)\right]+\Pr\frac{1}{(1-\phi)^{2.5}\left[(1-\phi)+\phi\frac{\rho_s}{\rho_f}\right]|J^2|}\left[\left(A_{11}^2+A_{21}^2\right)\frac{\partial^2 V}{\partial \zeta_1^2}+2(A_{11}A_{12}+A_{21}A_{22})\frac{\partial^2 V}{\partial \zeta_1 \partial \zeta_2}+\left(A_{12}^2+A_{22}^2\right)\frac{\partial^2 V}{\partial \zeta_2^2}\right]+Ra\,\Pr\Theta\left[\frac{1}{1+\frac{(1-\phi)\rho_f}{\phi\rho_s}}\frac{\beta_s}{\beta_f}+\frac{1}{1+\frac{\phi\rho_s}{(1-\phi)\rho_f}}\right] \qquad (13)$$

Internal energy equation:

$$\frac{\partial \Theta}{\partial \tau}+\frac{1}{|J|}\frac{\partial \Theta}{\partial \zeta_1}\left(UA_{11}+VA_{21}\right)+\frac{1}{|J|}\frac{\partial \Theta}{\partial \zeta_1}\left(UA_{12}+VA_{22}\right)=\frac{\frac{K_{nf}}{K_f}}{\left[(1-\phi)+\phi\frac{(\rho C_p)_s}{(\rho C_p)_f}\right]|J|^2}\left\{\begin{array}{l}\left[\frac{\partial^2 \Theta}{\partial \zeta_1^2}\right]\left(A_{11}^2+A_{21}^2\right)+\left[\frac{\partial^2 \Theta}{\partial \zeta_2^2}\right]\left(A_{12}^2+A_{22}^2\right)\\+2\frac{\partial^2 \Theta}{\partial \zeta_1 \partial \zeta_2}(A_{11}A_{12}+A_{21}A_{22})\end{array}\right\} \qquad (1ss4)$$

The transformed equations (11-14) were discretized using finite volume method. The discretized governing equations were used for simulation in code written in FORTRAN programming language.

The present code was tested for grid independence using three different grid arrangements: 81×81, 101×101 and 121×121. Temperature profiles are plotted at mid section of cavity for Ra=10^5, ϕ =10% and Pr =6.2, as illustrated by Figure 2. It is observed that the shape of the curve changes consistently for all three grid sizes, which shows that grid independence, has been established.

Moreover the numerical codes were validated with the benchmark results of de Vahl Davis [15], as shown by table 1 and were found to be in good agreement.

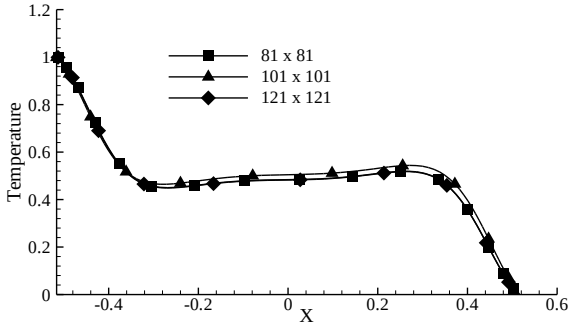

Fig.2 Temperature profiles at mid section of cavity for different grid combinations

Table1 Validation of present study with benchmark results of Davis [15] in terms of the average Nusselt number Nu_{avg} for the pure fluid

Ra	10^4	10^5	10^6
Present	2.45	4.49	8.78
Davis [15]	2.24	4.52	8.80

4. Results and Discussion

In this section**,** numerical results for the streamlines and isotherms contours as well as temperature, velocity and local Nusselt number profiles have been presented graphically that demonstrate the effects of the controlling parameters namely solid volume fraction ($0 \le \phi \le 0.2$) and the Rayleigh number ($10^4 \le Ra \le 10^6$).

4.1 Isotherms and streamlines

Fig. 3 illustrates comparison of the isotherms (on the left) and streamlines (on the right) between nanofluid (ϕ = 0.2) and pure fluid (ϕ = 0) for Rayleigh numbers 10^4 to 10^6. As seen in the diagrams (Fig. 3), for low Rayleigh numbers (*Ra* =10^4), the isotherms are distributed approximately parallel to the vertical wavy walls. As Rayleigh number increases, the isotherms become horizontal at the central region of the cavity and vertical at the thin boundary layers. This behavior occurs because at a low *Ra* value, the heat transfer is only due to conduction between the hot and the cold walls. However, with increase in *Ra*, the heat transfer is done by convection rather than conduction due to increased buoyancy. It is also observed that the left and right wavy walls affect the shape of the isotherms and streamlines.

As illustrated in the Fig. 3, at Ra=10^4, an oval shaped cell is formed in the clockwise direction with ψ_{min} = -0.0154747 for pure fluid and ψ_{min} = -0.00860596 for nanofluid (ϕ = 0.2). As Rayleigh number increases, the length of central vortex increases and the streamlines elongate parallel to the horizontal walls for both pure and nanofluids. At *Ra* =10^6, ψ_{min} = -1.88113 for pure fluid and ψ_{min} = -1.05468 for nanofluid. This shows that absolute value of stream function increases

with Rayleigh number but decreases with particle volume fraction. Moreover, it is observed that at *Ra* $=10^6$, the central vortex of the pure fluid occupies a larger area than that of nanofluid. The central streamline contour of nanofluid becomes divided into two distinct vortices, whereas the central vortex for pure fluid does not break up. Similar results were obtained by Khanafer et al. [9] for the flat square cavity, which attributed this behavior to the dispersion effect. It is clearly observed that as Rayleigh number increases, boundary layers become thinner and denser causing steeper velocity and temperature gradients near the boundary. With higher Rayleigh number, the streamline gradient increases, representing an increase in velocity and an enhancement of the absolute circulation strength of the fluid flow.

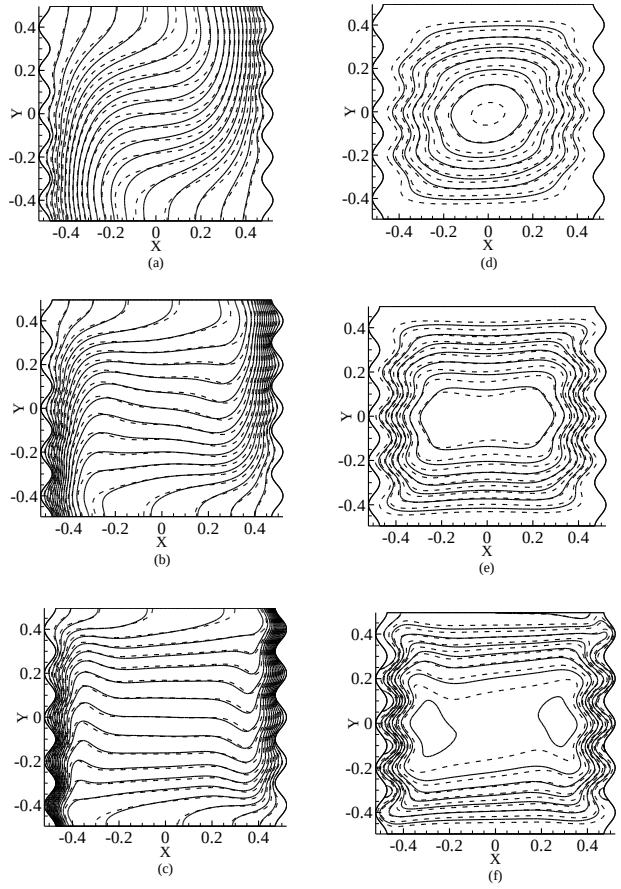

Fig.3 Comparison between nanofluid (-) (ϕ = 0.2) and pure fluid (- - -) (ϕ = 0) for isotherms at Rayleigh Numbers (a) 10^4 (b) 10^5 (c) 10^6 and for streamlines at Rayleigh numbers (d) 10^4 (e) 10^5 (f) 10^6

4.2 Vertical and horizontal velocity profiles

To demonstrate the effects of Rayleigh number and volume fraction on fluid flow, velocity profiles are plotted at mid planes of the wavy enclosure. The Figs.4 (a)-(b) show that the velocity profiles undergo a parabolic variation near the adiabatic and isothermal walls respectively. In addition, the velocities at the center of the enclosure and at the walls are almost zero compared to those at the boundaries near the walls, where fluid flow occurs at higher velocities.

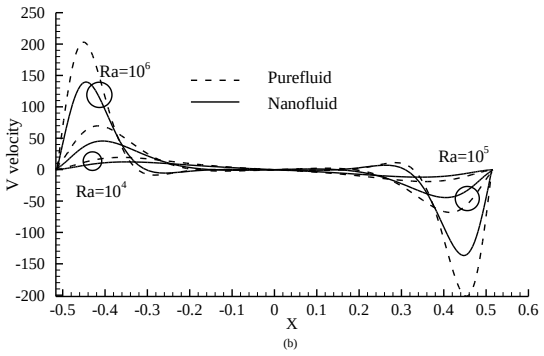

Fig.4 Comparison of vertical velocity profiles for nanofluid (-) and pure fluid (- - -) at mid section of cavity for different Rayleigh numbers.

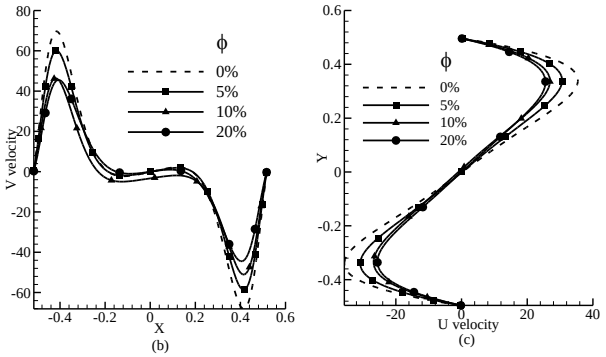

Fig.5 Comparison of vertical and horizontal velocity profiles for nanofluid (-) and pure fluid (- - -) at mid section of cavity for different volume fraction and at Ra= 10^5.

This is due to the fact that no-slip and no penetration assumptions are imposed on the walls. From Fig. 5, it is observed that for ϕ= 0, the maximum stream function value is obtained as ψ_{max} = 5.09334 at *Ra* $=10^4$. When solid volume fraction is increased to ϕ = 0.05, the maximum value of stream function decreases to ψ_{max} = 4.48676. Similar trend is also found for *Ra* $=10^5$ and *Ra* $=10^6$. This shows that the absolute magnitudes of both vertical and horizontal velocities decrease with increasing volume fraction. This is because increase in volume fraction causes decrease in intensity of buoyancy and thereby reduces fluid flow intensity. Similar results were found in many previous studies (Mansour et al. [13]) with various geometries and conditions.

4.3 Nusselt number

From Table 2, it is evident that the average Nusselt number Nu_{avg} increases with increase in Rayleigh number and volume fraction. This observation is in agreement with other research works (Khanafer et al. [9], Abu-Nada et al. [10], and Violi et al. [11]). As

volume fraction of nanoparticles increases, the divergence in average Nusselt number becomes greater especially for higher Rayleigh numbers due to predominant effects of convective heat transfer. Use of nanoparticles in fluid increases the Nu number by about 34% for $Ra = 10^5$ and 35% for $Ra = 10^6$ at $\phi = 0.2$ compared to pure fluid. The results indicate that with increase in particle concentration, thermal conductivity in fluid improves, thereby causing an enhancement in mean *Nu* number (heat transfer performance).

Table 2 Variation of Average Nusselt number for different values of volume fraction and Rayleigh numbers.

Nu_{avg}	$Ra = 10^4$	$Ra = 10^5$	$Ra = 10^6$
ϕ = 0%	1.7731	3.7182	7.3324
ϕ = 5%	2.0498	4.2925	8.4736
ϕ = 10%	2.2885	5.3791	9.5124
ϕ = 20%	2.6769	5.6643	11.327

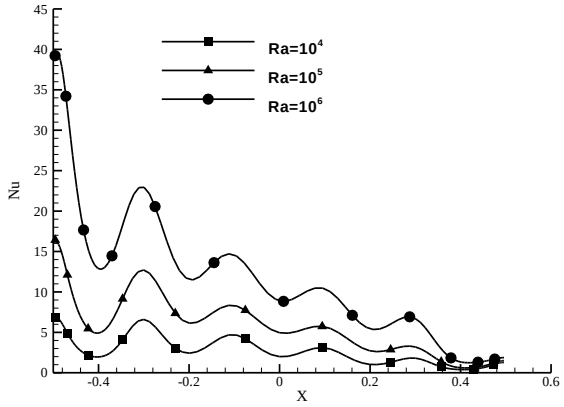

Fig.6 Variation of local Nusselt number with Rayleigh number at $\phi = 0.2$.

From Fig. 6, it is observed that the lowest heat transfer occurs at $Ra = 10^4$ and the highest heat transfer is observed at $Ra = 10^6$. By definition, *Nu* number is the ratio of convective to conductive heat transfer. As described earlier, for low Rayleigh numbers, heat transfer within the cavity is dominated by conduction because viscous force is greater than buoyancy force.

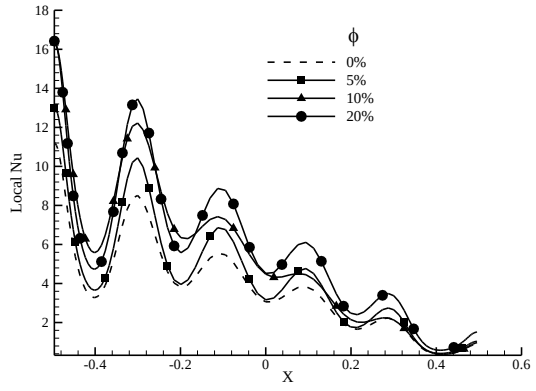

Fig. 7 Variation of local Nusselt number with volume fraction at $Ra=10^5$.

Hence the value of *Nu* is lower and variation is less for $Ra = 10^4$. As *Ra* increases, a stronger buoyancy effect is induced and greater thermal energy transfer occurs, causing an increase in Nu. Moreover, Fig. 7 illustrates that the use of nanoparticles gives rise to higher *Nu* compared to pure fluid for the same *Ra*, indicating improvement of heat transfer with increase in volume fraction.

4.4 Comparison between different nanoparticles

Fig. 8 demonstrates variation of local Nusselt number for three different nanoparticles- Cu, Al_2O_3 and TiO_3. It is clearly observed that the highest heat transfer occurs for Cu and the lowest for TiO_3. This is because TiO_3 has the lowest thermal conductivity (Ks) compared to Cu and Al_2O_3. Hence the results reinforce that in comparison to the other two nanoparticles, Cu is more feasible due to higher enhancements of heat transfer.

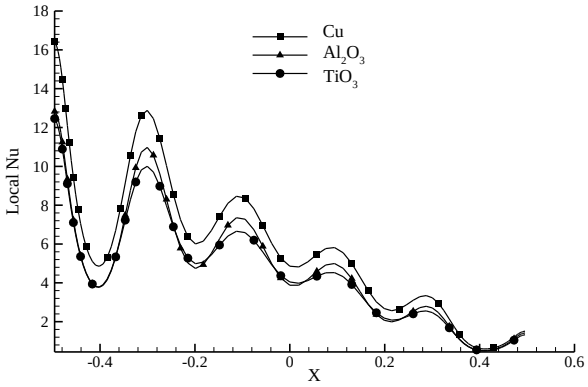

Fig.8 Variation of local Nusselt number for different nanoparticles at $Ra = 10^5$ and $\phi = 0.2$.

4.5 Comparison between flat and wavy surface heating

Fig. 9 shows that the shape of local *Nu* profile is strongly dependant on the geometry of the enclosure.

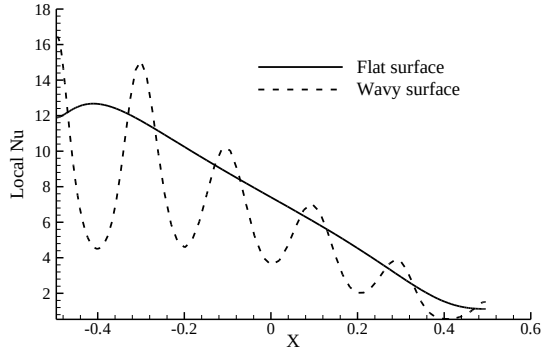

Fig. 9 Variation of local Nusselt number for wavy and flat surface heating

Table 3 Percentage difference of average Nu_{avg} for flat and wavy surface heating

	Wavy	Flat	% difference
Nu_{avg}	5.6643	7.2743	22.132

In case of the wavy surface, the local Nusselt number value changes continuously depending on the shape of the heated surface. Table 3 reveals one important finding that the average Nusselt number decreases and is almost 22% less for a wavy wall compared to a flat surface. This is because, a cavity with wavy walls have a larger surface area than that for flat walls. However, at the boundary, the local Nusselt number for wavy-wall shows almost 37% increase than the flat wall, indicating a much higher heat transfer with increased convection due to increased buoyancy force. The wavy wall of the geometry used is a sine function with amplitude of 0.05. Although the local Nusselt number for wavy wall decreases rapidly than that of flat wall, it has certain peak regions where heat transfer is more than the non-wavy surfaces. These are the regions where the local Nusselt numbers are higher for wavy surfaces.

4.6 Comparison between aspect ratio A =1 and A = 0.5

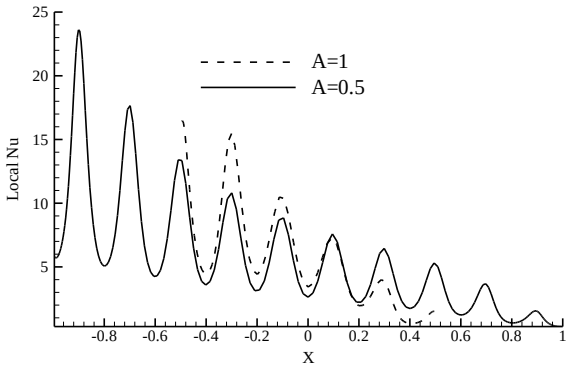

Fig. 10 Variation of local Nusselt number with aspect ratio at $Ra = 10^5$ and ϕ =0.2.

The variation of the local Nusselt number for the two different aspect ratios is compared in Fig.10. The solid lines represents aspect ratio A =0.5 and the dotted line represents aspect ratio A =1. The overall pattern of the two graphs is similar, and in both the graphs local Nusselt number variation is sinusoidal. This variation is due to the wavy surface pattern of the left heated wall. However, it is evident from the graph that the highest heat transfer, at a particular instance, takes place with the aspect ratio A = 0.5 near the boundary. The maximum value of local Nusselt number for A = 0.5 is 24. Whereas, the maximum value for A =1 is 17, which is about 29% lower than that for aspect ratio A = 0.5.

5. Conclusion

The results found show that the nanofluids exhibit much better heat transfer efficiency, in terms of average Nusselt number, than the purefluids in case of the wavy cavity. Similar heat transfer efficiency increment, for nanofluids, is also found in the literature for flat surface cavity. In this research work, it has been found that the streamline contours, temperature profiles, average Nusselt number and local Nusselt number are affected by the wavy surface of the cavity. In particular, the local Nusselt number varies much with the wavy surface. It is observed that the flow rate for both pure fluid and nanofluid increases with the increase in Rayleigh number, but the flow rate of pure fluid is higher than the nanofluid at all Rayleigh numbers. Also the absolute magnitude of both vertical and horizontal velocities decreases with the increase of volume fraction, from φ = 0 to ϕ = 0.2. The heat transfer efficiency, depicted by Nusselt number, seems to increase with the increase in Rayleigh number, $Ra = 10^4$ to $Ra = 10^6$, for each volume fraction. Moreover, the Nusselt number increases with the increase in volume fraction. It was found that, the use of nanoparticles of volume fraction ϕ = 0.2, increases the Nusselt number by 34% for $Ra = 10^5$ and 35% for $Ra = 10^6$, compared to that of pure fluids. This shows an increase in heat transfer efficiency for nanoparticles. However, if these results of wavy surface are compared with that of flat surface, then a decrease in average Nusselt number, by 22%, for the wavy surface is observed. Although the local Nusselt number shows certain places with higher heat transfer efficiency, as high as 37% than the flat surface, the overall heat transfer is assumed to have decreased for the wavy surface.

Moreover, while focusing on different nanoparticles and the aspect ratios, it was found that Copper has the highest Nusselt number which is 5.66 among the three nanoparticles used, which in turn shows that Copper has the highest heat transfer rate. Change in aspect ratio also changes the heat transfer rate. If a nanofluid, having a nanoparticle of volume fraction ϕ = 0.2, is considered, then the value of average Nusselt number for A = 0.5 will be 29% more than that of A =1. This shows a much higher heat transfer occurs for a lower aspect ratio.

NOMENCLATURE

A : cofactor
C_p : specific heat (J kg^{-1} K^{-1})
g : gravitational accleration (m s^{-2})
J : Jacobian
K_f : fluid thermal conductivity (W $m^{-1}K^{-1}$)
K_{nf} : nanofluid thermal conductivity (W $m^{-1}K^{-1}$)
L : reference lenght (m)
Nu : Nusselt number
Nu_{avg} : average Nusselt number
Pr : Prandlt number
P : dimensionless pressure
p : dimensional pressure (N m^{-2})
Ra : Rayleigh number
T : dimensional temperature (K)

u,v : dimensional velocity components (m .S^{-1})
U,V : dimensionless velocity components
x,y : Cartesian coordinates (m)
X,Y : dimensionless coordinates
Greek symboles
Θ : non dimensional temperature (K)
ϕ : solid volume fraction
ψ : streamline function, (Ψ/α_f)
β : thermal expansion coefficient, (k^{-1})
β_{nf} : nanofluid thermal expansion coefficient, (k^{-1})
τ : non dimensional time ($T\text{-}T_c/\Delta T$)
α : thermal diffusivity, ($m^2\ s^{-1}$)
v : kinematic viscosity, ($m^2\ s^{-1}$)
μ : dynamic viscosity, (kg $m^{-1}\ s^{-1}$)
$\zeta_1\ \zeta_2$: dimensionless coordinates in Jacobian transformation

REFERENCE

[1] S. U. Choi, J. Eastman, Enhancing thermal conductivity of fluids with nanoparticles. *International Mechanical Engineering Congress and Exhibition*, San Francisco, USA, November 12-15 (1995).

[2] Y. Xuan, Heat Transfer Enhancement Of Nanofluids. *International Journal of Heat and Fluid Flow*, *21*(1), 58-64. (2000).

[3] H. Mintsa, G. Roy, C. Nguyen, D. Doucet, New temperature dependent thermal conductivity data for water-based nanofluids, *Int. J. Thermal Sciences*, 48 (2009) 363-371.

[4] C. Pang, J. Jung, J. W. Lee, Y. T. Kang, Thermal conductivity measurement of methanol-based nanofluids with Al_2O_3 and SiO_2 nanoparticles. *International Journal of Heat and Mass Transfer*, *55*, 5597-5602. (2012).

[5] K. Esmaeil, Numerical feasibility study of utilizing nanofluids in laminar natural convection inside enclosures. *Heat and Mass Transfer*, *49*, 41-54. (2012).

[6] Z. Yu, X. Xu, Y. Hu, L. Fan, K. Cen, Numerical study of transient buoyancy-driven convective heat transfer of water-based nanofluids in a bottom-heated isosceles triangular enclosure. *International Journal of Heat and Mass Transfer*, *54*(1-3), 526-532. (2011).

[7] O. Abouali, A. Falahatpisheh, Numerical investigation of natural convection of Al2O3 nanofluid in vertical annuli. *Heat Mass Transfer*, *43*, 15-24 (2009).

[8] Abu-Nada, E., & Oztop, H. F. (2009). Effects of Inclination Angle on Natural Convection in Enclosures Filled with Cu–water Nanofluid. *International Journal of Heat and Fluid Flow*, *30*(4), 669-678.

[9] K. Khanafer, K. Vafai, M. Lightstone, Buoyancy-driven heat transfer enhancement in a two-dimensional enclosure utilizing nanofluids, *International Journal of Heat and Mass Transfer* 46 (19) ,3639-3653. (2003).

[10] K. C. Lin, A. Violi, Natural convection heat transfer of nanofluids in a vertical cavity: Effects of non-uniform particle diameter and temperature on thermal conductivity, *International Journal of Heat and Fluid Flow* 31 (2), 236-245. (2010).

[11] E. Abu-Nada, H. F. Oztop, Numerical analysis of al2o3/water nanofluids natural convection in a wavy walled cavity, *Numerical Heat Transfer*, Part A: Applications 59 (5) 403-419 (2011).

[12] M. Jafari, M. Farhadi, K. Sedighi, E. Fattahi, Effect of wavy wall on convection heat transfer of water-al2o3 nanofluid in a lid-driven cavity using lattice boltzmann method, *International Journal of Engineering-Transactions* A: Basics 25 (2) (2012) 165.

[13] M. Mansour, M. Bakier, Free convection heat transfer in complex-wavy-wall enclosed cavity filled with nanofluid, *International Communications in Heat and Mass Transfer* 44 (2013) 108-115.

[14] S. Singh, R. Bhargava, Numerical study of natural convection within a wavy enclosure using mesh free approach: Effect of corner heating, *The Scientific World Journal* (2014).

[15] G. de Vahl Davis, Natural convection of air in a square cavity: a bench mark numerical solution, *International Journal for Numerical Methods in Fluids* 3 (3) 249-264. (1983).

[16] F.-H. Lai, Y.-T. Yang, Lattice boltzmann simulation of natural convection heat transfer of Al_2O_3 water nanofluids in a square enclosure, *International Journal of Thermal Sciences* 50 (10) 1930-1941. (2011)

ICMIEE-PI-140285

A brief study of the prospect of hybrid solar irrigation system in Bangladesh

Md Abul Hasnat [1,*], *Muhammad Naimul Hasan* [1], *Najmul Hoque* [1]
[1] Department of Mechanical Engineering, Rajshahi University of Engineering & Technology, Rajshahi-6204, BANGLADESH

ABSTRACT
Solar energy is an efficient alternative source of energy in Bangladesh for its geographical location. After its long term success the solar energy use in irrigation phenomenon to replace conventional energy. This paper presents the prospect of a hybrid solar irrigation system with both technical and financial point of view. In an existing solar irrigation system PV panel is applied to produce DC current and by the inverter it converts into AC current and finally operates 3 phase submersible AC pump. By applying the hybrid system, it is possible to increase the operating hour and cultivate more agricultural land without any extra installation cost. In this system the solar energy and grid electricity use alternately to operate same pump. After the financial analysis of solar and proposed hybrid solar irrigation system the payback period is decreased 5 to 7 years. Therefore the hybrid system release the excessive load on the grid connected irrigation system.

Keywords: Solar, Hybrid, Irrigation, Bangladesh, Grid electricity.

1. Introduction

Bangladesh is an agro based country in the South Asia. Most of the people of it's depends upon the agricultural work for their living. It holds lots of agricultural land and the amount of total cultivable land is 8.52 million hectares. About 37.266 % million metric ton crops and other vegetables are cultivated in various seasons in this land [1]. Though Bangladesh is a realm of the river, but it has huge water crisis for irrigation, especially in summer and winter season. Moreover the amount of lands beside the river and canal are not so much so as to cultivate this land by these water sources. Particularly in the semi-arid region (Barind tract) there is a sufficient lack of water for irrigating the lands. As a solution in Bangladesh most of the farmer uses underground sources of water for irrigating purposes. This is done by picking up the bore water through the pump. Here there are almost about 2 lakh such type of pump used for picking up water. These pumps are running by grid electricity and diesel oil. From the statistic it has seen that about 25% electricity of the entire output is employed for operating these pumps, which stands for that irrigation pumps consume 1300 MW electricity in a day. In the irrigation sector of Bangladesh nowadays there are approximately 84% irrigation are depend on diesel oil. Meanwhile about 1.34 million diesel operating pumps emit 0.9 million tons of exhaust per year [2]. So for the green milieu it is high time to decline the use of conventional fossil fuel and create the alternative sources of energy. Though Bangladesh is an agricultural country and huge amount of energy are consumed in this sector. So agriculture sector is a good concern to replace by renewable sources of energy.

It is also illicit phenomenon that applies just the conventional energy without creating any renewable sources. In the wisdom of renewable energy Bangladesh is abandoning to use solar energy rather than wind, hydro and tidal energy. Bangladesh situated between 20° 34´-26° 38´ north latitude and 88° 01´-92° 41´ east longitude [3]. So geographically the solar radiation effect in this region is satisfactory to utilize solar energy. The solar radiation is vary from 4 to 6.5 kWh/m^2 in various districts of Bangladesh [4]. This solar energy makes a strong renewable sources in Bangladesh. The Bangladesh government vision is to replace the 10% conventional energy by renewable energy within the year 2020 and the solar energy considers as great renewable sources of energy . For this purpose solar power pump is introduced in recent year by various government and private organization over the country. Infrastructure Development Company Ltd. (IDCOL) has a plan to set up approximately 18,750 solar power pump over the country between 2016 yr.

Only the primary obstruction of solar power pump of its higher installation cost and long term payback period. Generally in the existing solar irrigation system DC current is converted into AC current and directly run the AC pump without using any battery. Moreover at low sunshine and during night time it is not possible to run the system. So in this situation to sustain the project it needs to supply water all the day and night. Solar energy is far behind to use at night and also for higher maintenance cost of the battery system is totally shut down during the night. For this situation it is difficult to earn profit from the project. The idea of the hybrid system increases the working hour while solar energy has failed to run the pump. So if hybrid system is replaced by the solar irrigation system, then it is possible to earn profit from the project and cultivate more land in the region.

Now a day's hybrid irrigation system is used in various countries all over the world. It is usually used to overcome the limitations of continuous supply of energy and to supply energy in remote places. Hybrid power system is a combination of different sources of producing electricity that confirms the uninterrupted supply of electricity [5]. Generally wind solar hybrid energy system is used most of the country for irrigation sector. This hybrid system is an admirable sources of renewable energy which release the

* Corresponding author. Tel.: +88-01674888710
E-mail address: ah.roxy@gmail.com

gravity of conventional energy and retain the environment green. But this solar wind hybrid system is very much expensive to setup. It is not possible for developing countries like Bangladesh to install such type solar wind hybrid energy system. It is why not only for its exorbitant installation cost, but also not possesses a moderate wind speeds for its geographical location. But equally it has inherent of abandoning sunshine and then the solar irrigation pump has installed in recent years, it is possible to combine the photovoltaic system with grid electricity to run the pump as a means of the hybrid solar energy system. Through this hybrid solar irrigation system there is no any additional installation cost. This paper presents the prospect of a hybrid solar irrigation system in Bangladesh. For this, both technical and financial analysis of the solar irrigation system and grid connected pumping system is considered and finally combined the analysis for further results. Methodology and study area are described in the second and third section while the technical analysis is summarized in the fourth section. The fifth section is compiled with financial analysis. Finally at the last section is deliberated with the conclusion and prospect of the hybrid solar irrigation system.

2. Methodology

The methodology was occupied to find out the prospect of hybrid solar irrigation system in Bangladesh is concise here. At first the area was selected at where the solar irrigation system and grid connected irrigation system has already installed. Then by making a visit in these designated areas required technical information were gathered. The economic essential information was noted by making questionnaire to the agrarian and the employers. Afterward finding all the necessary evidence the final analysis was done showing the actual scene of the hybrid solar irrigation system. For technical analysis overall efficiency, discharge of water, operating hour and liter per watt peak were considered. And for financial analysis consider the simple payback period, NPV and IRR. Finally, compare the financial improvement of the hybrid solar irrigation system after solar irrigation system.

Photo.1 Solar irrigation system in Naogaon

3. Study area

The study area was selected based on the districts where the solar and grid electricity irrigation is running at least several years. By these, three districts were selected namely Rajshahi, Naogaon and Jessor. In Rajshahi there are about three solar irrigation projects and in Naogaon there is one solar irrigation project. In Mirjapur and Mandoel under Godagari and in Poba under the Rajshahi Solar irrigation project is built up by KOICA. Here 5hp AC submersible pump is running directly by 5.16 kW photovoltaic panels. In Shapahar, Naogaon Solar irrigation project is built up by Grameen Shakti namely Grameen Shakti Solar Pump Pilot Project shown in the Photo 1. Here 10hp submersible pump is operated by 11.2 kW photovoltaic panels. In Jessor ten solar irrigation project is newly set up by IDCOL. Here 10 HP submersible pump is also run by 11.84 kW photovoltaic panels. For the analysis consider the 10 HP solar pump system for its accessibility and large discharge capacity of water. Besides grid electricity connected pump is available in several districts of Bangladesh. For analyzing the grid connected pumping system Rajshahi and Naogaon district are randomly selected. The grid connected pumping system is shown in Photo 2.

Photo.2 Grid connected pumping system

4. Technical analysis

Hybrid solar irrigation system is an improvement of the existing solar irrigation system. In this system both the solar energy and grid connected electricity used simultaneously as alternative sources. For the analysis solar irrigation and grid connected pumping system is considered. Finally proposed the improved hybrid system which reduces the conventional energy from grid connected pumping system and also reduce the net cost of the solar irrigation system.

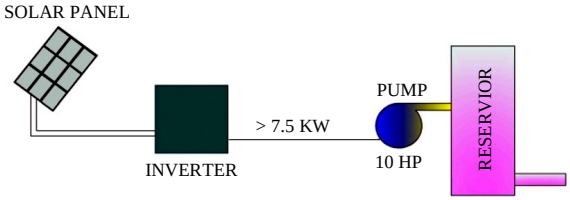

Fig.1 Solar irrigation project

4.1 Solar irrigation system

From the visited areas, it has seen that the existing solar irrigation system consists of mainly photovoltaic panels, inverter and AC pump. Photovoltaic panels generate DC current using solar radiation. This DC current is then

converted to AC current through the inverter [6]. Finally a submersible AC pump is running by using this AC current. The diagram of the solar irrigation system shown in Fig.1. As there is no use of any battery here for minimizing the maintenance cost so there is no chance for preservation of extra power. The entire panel power kept much higher than the pump power to run the pump uninterruptedly. In the considered system a 10hp submersible AC pump is running when the power produce from the panel is above 7.5 kW. The corresponding technical parameter of solar irrigation project is presented in the Table 1.

Table 1 Solar irrigation project specification

Parameter	Unit	Value
Maximum power	kW	11.2
Panel number	no.	64
Per panel capacity	W	175
PV array area	m^2	81.7
Pump head	ft	100

The overall efficiency of this system is calculated by the ratio of the power supply to the pump (kWh/day) to the average solar radiation (kWh/day) that incident on the photovoltaic panel.

$$\eta = \frac{P_1 \times t}{A \times I} \quad (1)$$

By using Eq.(1) the overall efficiency was found about 16.52% for 11.20kW power supply to the pump. It may change from system to system for different PV array area, solar radiation and per panel capacity. The average solar radiation of the visited area is assumed 5 kWh/m^2. Another technical parameter Liter per Wp was determined by the ratio of the water supply per year to the maximum Wp given by the equation.

$$L_p = \frac{Q \times t \times 365 \times 1000}{P_2 \times 60} \quad (2)$$

The Liter per Wp for this system was calculated by the Eq.(2) and it was found 9680 for a year when the discharge was 550 L/min and the average operating time was 8 to 10 hours per day. The Liter per Wp also varies from system to system depending upon the pump capacity and panel ability. In Table 2 the calculated value is shown.

Table 2 Solar irrigation project evaluation

Parameter	Unit	Value
Operating time	h/day	8-10
Flow rate	liter/min	550
Average water supply	liter/day	2,50,000
Litter watt peak	liter/Wp/y	9,680
Average solar radiation	kWh/m^2	5
Overall efficiency	%	16.52

In this analysis, it determines that the main problem of the solar irrigation project is less operating time due to dependence on sunshine. Also the solar irrigation project is switch off during the cloudy and gloomy environment. Hence decrease the supply of water and also lost the public draw.

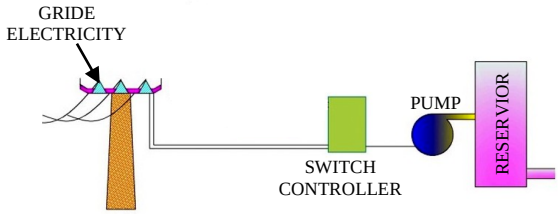

Fig.2 Grid connected irrigation system

4.2 Grid connected irrigation system

Grid connected irrigation system is a popular medium of irrigation. In this system grid electricity is used to run the AC pump directly. There are 2HP to 12HP pump are used according to various demand. The project design and equipment is very simple. The project consists of a submersible AC pump and switch controller. In the Fig.2 the grid connected irrigation project is shown. When the electricity is available that time the pump supply water. The respective information of the grid connected irrigation is given in Table 3.

Table 3 Grid connected irrigation project information

Parameter	Unit	Value
Pump capacity	HP	10
Head of pump	ft	60
Discharge	liter/min	900
Operating time	hour	20
Consume electricity	kWh/day	150

By the study it was found that the discharge of the pump varies from 600 to 700 liter/min and the pump is in operation about 16 to 20 hours according to demand. In this case a huge amount of electricity is consumed for irrigation. There are above 1300 MW electricity are used for cultivating land under grid connected pumping project. Thus it is desirable to put back the grid connected irrigation system with alternative sources totally or partly

4.3 Hybrid solar irrigation system

The hybrid solar irrigation is an improvement system rather than solar irrigation system. Though the solar irrigation system is a good practice of renewable energy, but the main problems are the longest payback period and less operating time comparable to grid connected irrigation system. On the other hand the grid connected irrigation system used up a large amount of conventional energy and pollute the surroundings by using fossil fuel. The hybrid solar irrigation system minimizes the two major problems of the previous system. The proposed hybrid solar irrigation system are shown in the Fig 3. In hybrid solar irrigation system the task consists of two units, solar is one unit which is renewable sources of energy and other is a grid connected unit which is conventional sources of

energy. The two units are united by the controller switch. In solar unit the DC current is converted into AC current by the inverter. On the other hand, in the grid connected unit the grid electricity directly supply AC current. And by the both unit finally run the AC pump to lift water and supply for irrigation. When the solar panel failed to produce 7.5 kW power the 10hp pump cannot be started with the solar unit that time the grid connected connection is available to run the same AC pump [7].

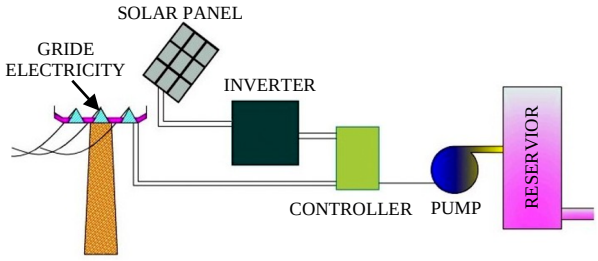

Fig.3 Hybrid solar irrigation system

In this system there no technical variation only the two units work separately according to the condition. The average sunshine in the Bangladesh is about 8 to 10 hours and this respective time solar energy is applied for irrigation [8]. But at the evening to next morning this energy cannot use without any battery storage. For saving the maintenance and replacement cost battery is eliminated in large production unit. So the system was shut down about 14 to 16 hours per day. To increase the operating time and production in hybrid system, it has the opportunity to run the pump at night while the solar energy is absent. Therefore at night hour 10 pm to 6 am it is perfect to feed the pump. This increase the 8 hour operating time and remaining time of the day it should keep idle for better life of the pump. The daily operating and idle time of the solar irrigation and hybrid solar irrigation system are presented in Fig 4. Its indicated that daily idle time is decreased in the hybrid solar irrigation system and increase the operating time. The hybrid system increases the operating time in existing solar irrigation system so this project will more viable and profitable. [9]

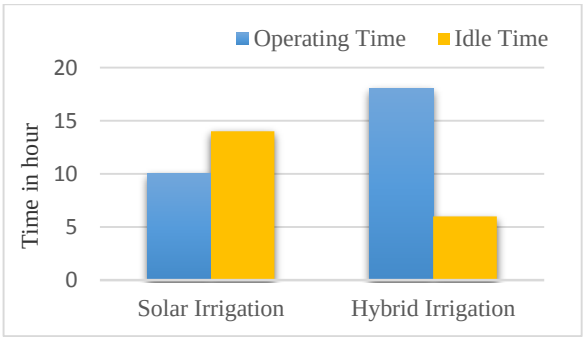

Fig 4 Daily Operating and Idle time of the systems

5. Financial Analysis

Generally a project is acceptable when the project is financially viable. Besides the technical improvement it is another concern about the investment and its quick return. In solar irrigation project the installation cost is much higher and it is tough to recover the total investment earlier in its project life time. By the field visit, it has seen that the installation cost is variable from 30 lakh to 50 lakh BDT for setup 10HP submersible AC pump. Now a day these types of projects are established by the government and non-government association. Infrastructure Development Company Limited (IDCOL) with the World Bank, KFW, KOICA, JICA, ADB and Bangladesh Climate Change Resilience Fund are financially supported to set up the project in rural areas of Bangladesh. In Grameen Shakti solar irrigation project the 70% of its total investment was donated from IDCOL and KFW and 30% of the total cost was invested by Grameen Shakti. Though the solar irrigation system is an alternative sources for irrigation but for its high investment cost it is not suitable for the full investment without any grant. Thus the hybrid solar irrigation system may be a good prospect to recover the investment within a shortest possible of time. [10]

In terms of financial analysis, both the solar irrigation project and grid connected pumping project was considered and finally estimate the analysis of grid connected hybrid solar irrigation system. For financial analysis Net present value (NPV), Internal rate of return (IRR) and simple payback period were calculated both for solar irrigation and hybrid solar irrigation system. The survey had indicated that the expected project life of the system is 20 years. The total expense calculated from the installation cost, maintenance cost, repair cost, replacement cost and operator salary. On the other hand the total income of the project comes from the charge of the water supply to the cultivable land. There are approximately 80 to 100 bigha lands are cultivated by the 10HP irrigation pump in a season. In case of solar irrigation system water supply charge for different crops are shown in the Table 4.

Table 4 Average charge to supply water per season

Type of cultivation	Charge BDT/Bigha
Paddy	1750
Wheat	560
Potato	560
Onion	210
Garlic	210

On the other hand in the grid connected pumping system water supply charge for paddy per season is about 3000 to 3500 BDT. And for per hour water supply the charge from the farmer is about 100 to 120 BDT in a different district. There is no running charge for solar irrigation, but when the irrigation is conducted by the grid electricity about 1000 BDT is charged for running costs. In a grid connected pumping system per unit electrical charge for irrigation are shown in Table 5 [10]. In finance observation the project is viable when higher NPV and the higher IRR rate and also desirable shorter payback period. NPV is calculated by bringing all the expenses and income from the investment year to the expected lifetime with various

lending and deposit interest. The various lending and deposit cost were collected from the Bangladesh Bank [11].

Table 5 Charged of electricity for irrigation

Distributor	BDT/Unit
DPDC / DESCO	2.51
BREB	3.39-3.96

In the Table 6 for the different discount rate the NPV is shown for both the solar irrigation project and hybrid solar irrigation project. From field visit feedback these financial analysis assuming both the project expected life time is 20 years. There were no replacement on solar panel and pump. But the inverter was replaced after 10 years. Also assuming in the hybrid solar irrigation system added the extra installation cost only for electricity supply line and switch controller. For hybrid solar irrigation system the net income is increased by increasing water supply more than 8 hours and expense is include the electricity charged for per unit use.

Table 6 NPV of the project

Discount Rate	Solar irrigation	Hybrid solar irrigation
2.5	128644.8527	2899070.514
7.17	-	588926.3382
8.4	-	173995.1968
8.61	-	108972.1892
10.29	-	-358623.4856

IRR is another financial parameter calculated from the graph including the NPV for the different discount rate for both the solar irrigation and hybrid solar irrigation project. The NPV vs. discount rate in Fig.1 denoted the discount rate where the NPV is zero that point is considered as the project IRR.

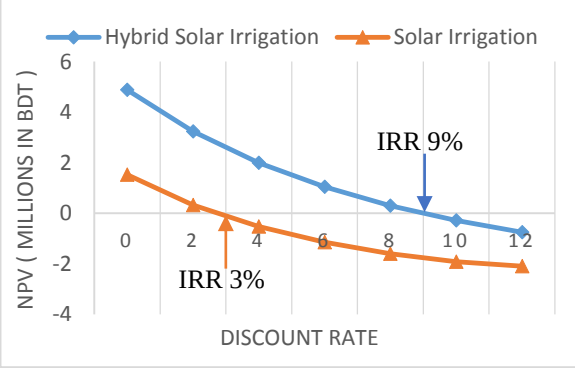

Fig.5 NPV vs. Discount Rate

Besides the NPV and IRR the simple payback period is the vital term of the project financial analysis and it should be minimum as possible. The IRR and simple payback period are presented in Table 7. In solar irrigation by the survey report, assumption and analysis the simple payback period is about 14.57 years and while improving the hybrid solar irrigation system the simple payback period is reduced at 9.11 years only. Therefore in the hybrid solar irrigation the simple payback period is decreased 5 to 7 years from the existing solar irrigation project.

Table 7 IRR and simple payback period

Parameter	Solar irrigation	Hybrid solar irrigation
IRR (%)	3	9
Simple Payback period (y)	14.57	9.11

By the financial analysis, it is found that the hybrid solar irrigation system is more feasible than the solar irrigation project.

6. Conclusion

As a developing country, Bangladesh has a massive dependency on agriculture. Therefore water is mandatory to cultivate the land basically in the agro seasons. The grid connected irrigation project depends only grid electricity which accelerate energy crisis more than a hybrid system. The ultimate conversation is concise in the following points:

a. Solar irrigation is considered as a new epoch for alternating the conventional energy sources in irrigation sector which reduces the excess load on the electricity.
b. The average efficiency is found to be 16.52% and the water supply per day is 2,50,000 liter in case of solar irrigation.
c. Solar irrigation project is not financially feasible due to high initial cost and less operating time. Such as 30 to 50 lakh BDT are required for installing a 10 hp solar pumping project.
d. In terms of solar irrigation the simple payback period is found 14.57 years and operating time is about 8 to 10 hours per day.
e. Besides in a hybrid solar irrigation system the simple payback period is found 9.11 years which reduce up to 5 years to return the investment and operating time increases about 8 to 12 hours per day.
f. After introducing hybrid solar irrigation the NPV and IRR are also increased and simple payback period is decreased than solar irrigation system.
g. Moreover this hybrid system reduces the CO_2, NO_X and SO_2 emission and declines the oil importation that requires (about 1,44,000 billion liters of oil every year) to operate more than two lakh diesel pumps.

A hybrid solar irrigation system may create the intensity to the private organizations for investment. Also the government should install some project to make this hybrid system more dynamic.

NOMENCLATURE

P_1 : Pump power, kW
P_2 : Panel power, kW
A : Surface area of panel, m^2
I : Solar radiation, kWh/m^2
t : Operating time, hr/day
Q : Flow rate, liter/min

η : Overall efficiency, %
W_p : Watt peak, W
L_p : Liter per watt peak, liter/Wp/y

REFERENCES

[1] S. I. Khan, S R Mizanur and Q Islam. Design and analysis of a low cost solar water pump for irrigation in Bangladesh, *Journal of Mechanical Engineering*, Volume ME 43, NO 2, (December 2013).

[2] C K Sharad, Y K Dhananjay, S K Lalit and S L Dheeraj. Experimental study on hybrid power system combining solar energy and animal energy for minor irrigation. *International Journal of Environmental Engineering and Management*. ISSN 2231-1319, Volume 4, pp 457-470, (2013).

[3] Hoque N and Kumar S. Performance of photovoltaic micro utility systems. *Energy for Sustainable Development*, Volume 17, pp 424-430, (October 2013).

[4] Islam MR, Islam MR, Beg MRA. Renewable energy resources and technologies practice in Bangladesh. *Renewable and Sustainable Energy Reviews*, Volume 12, pp 299-343, (February 2008).

[5] S Yndra, N Badari , T Srikanth and N Laxmi. Design and integration of wind solar hybrid energy system for drip irrigation pumping application. *International Journal of Modern Engineering Research*, Volume 2, pp 2947-2950, (August 2012).

[6] M. Mozammel Haque, Photovoltaic water pumping system for irrigation, *4th International conference on Mechanical Engineering*, pp 21-26. (December 2001).

[7] Islam Sadrul, M. A. H. Mondal and M. Ahiduzzaman, A study of grid connected solar pv irrigation system in semi-arid region of Bangladesh. *Int. J of Sustainable Water & Environment System,* Volume 1, pp 33-38 (2010).

[8] SH Khan, TU Rahman and S Hossain. A brief study of the prospect of solar energy in generation of electricity in Bangladesh. *Journal of Selected Areas in Renewable and Sustainable Energy (JRSE),* (June 2012).

[9] Kabir Lutful S.M. and Chowdhury Hasib. A low cost multiple motor switched powered irrigation system, *Journal of Electrical Engineering*, Volume EE 38, (December 2012).

[10] Harishankar S, S R Kumar, K P Sudharsan, Vignesh U and Viveknath T Solar powered smart irrigation system, *Advanced in Electronic and Electric Engineering*, ISSN 2231- 1297, Vol. 4, pp 341-346, (April 2014).

[11] Investment Rate, Bangladesh Bank. Website: *http://www.bangladesh-bank.org* [accessed on 19 May, 2014]

ICMIEE-PI-140286

Continuous desalination process of sea water using solar energy in Bangladesh

Md. Rashedur Rahman [1,*], *Md Abul Hasnat* [1], *Sardar Masud Rana* [1]
[1] Department of Mechanical Engineering, Rajshahi University of Engineering & Technology, Rajshahi-6204, BANGLADESH

ABSTRACT
Safe drinking water sources are limited and only 3% of total earth's water are drinkable. Approximately 97% of earth's water are salty and not allowed to use without desalination. For purifying the water a huge amount of conventional energy are depleted. In this paper presents the continuous desalination process of sea water using solar energy without any electricity or external power. The desalination process is designed through using flat plate and parabolic solar collector. The flat plate solar collector preheats the water and increase the temperature about 55℃ to 60℃. Then parabolic solar collector heating the water and allowed to vaporization above 85℃ temperature. In this process water supply in the heating pot continuously through the float valve system and at the time of heating the flat plat preheat the water. Finally collected the fresh water using condenser pipe. For large water output multi system of the panel can be applied.

Keywords: Solar, Water, Desalination, Bangladesh, Renewable energy.

1. Introduction

Water is the essential resource to sustain our existence. Mankind scarcely pass a single day without water. Though our earth is abundant of water resource we face scarcity of fresh water. The total volume of water on Earth is estimated at 1.4 billion km³, with 97.5% being salt water and 2.5% being fresh water. However, only about 0.014% of the total is directly available for human beings and other organisms as fresh water [1]. People living in coastal areas and any other region of different countries are facing salinity in water and excessive salinity cause stomach problem and discomfort of taste. According to WHO normal salinity limit in water up to 500 ppm but seawater's salinity is normally range from 35,000 to 45,000 ppm [2]. Producing fresh water from saline water by Electro dialysis, Mechanical vapor compression and Reverse Osmosis process need much electrical energy and abundant installation costs. Some processes need much conventional fuel energy. However for rural people and who are living in remote place can use solar powered water desalination unit to collect fresh water. Besides producing fresh water from saline water using solar energy is environment friendly and save conventional energy and cost.

Desalination using solar energy practiced from the former historic period of history. In 1774, a French chemist named Lavoisier used large glass lenses, which was mounted on structures to concentrate solar energy on distillation flasks [3]. Also in 1872, a Swedish engineer named Carlos Wilson build a large scale solar distillation plant to supply a mining community with drinking water in Chile [4]. From 1965 to 1970 to provide fresh water to small communities on Greek Islands solar distillation plants were built [5]. In 2009 Galveza developed a desalination process of sea water using solar powered membrane distillation unit [6]. Modern developments have discovered that solar powered desalination methods are superior to the alternatives including Reverse Osmosis, ED for fresh water delivery in remote areas [7].

Bangladesh located between 20° 34´-26° 38´ north latitude and 88° 01´-92° 41´ east longitude [8]. The solar radiation effect in Bangladesh is comparatively high for its position in the world map. The solar radiation effect in this region is satisfactory to utilize solar energy for both photovoltaic solar panel and solar collector. So solar energy in Bangladesh is strong alternative sources rather than hydro, wind and tidal energy [9]. The annual solar intensity in Bangladesh is about 1400 to 1700 w/m^2 which can easily use to concentrate in parabolic solar collector to evaporate saline water and finally condensing the steam fresh water is collected [10].

In this paper present the continuous desalination process where eliminate the electric power or external energy and apply only the solar energy as suitable renewable sources. Two types of solar collector are used for effective output of the system. By using only parabolic dish collector is not so efficient and time consuming for the continuous desalination process. Because feeding water needs much time to raise its vaporized temperature from ambient temperature in desalination pot. So flat plate solar collector is used as a preheater to heat up the saline water initially and then final heating is done by the parabolic solar collector. In this continuous desalination process at the time of heating other amount of water preheat in the system. This combined system accelerates the desalination process and decrease the time to raise the vaporized temperature and also increase the overall efficiency of the system. Finally distilled water is collected by condensing the vapor water and can use for a particular operation. Though distilled water is tasteless calcium and mineral can be added for drinking purpose. The experimental setup of the project is described in the second section of this paper and the third section is decorated with the working procedure of the system. The fourth section is compiled with the data collection and analysis and fifth section posses with calculations. Finally in the last section of the paper discuss the conclusion and outcomes of the experimental project.

* Corresponding author. Tel.: +88-01743989298
E-mail address: rashed.ruet09@gmail.com

2. Experimental setup

In this experiment eliminate all kinds of electric and external power. The experimental setup of continuous desalination system is made out only using solar energy. The total system constructs with three detached units. For continuous desalination the following three units work together.

1. Preheating Unit
2. Heating Unit
3. Condensing Unit

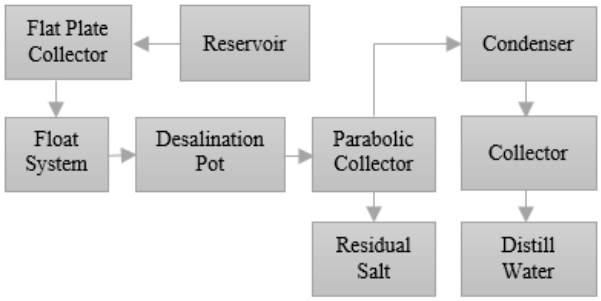

Fig.1 Flow diagram of desalination process

2.1 Preheating unit

In the experiment the main concern is that to supply salty or sea water in heating unit and finally heating the water until its vapor. It is more effective to preheat the water before final heating. When the heating unit works and started to vapor it's taken large time for vaporization. The heating operation was done in a closed system and that time no water is allowed to supply the heating unit. In this idle time the preheating unit is used to preheat the water. The preheating unit consist of a flat plate solar collector, inlet reservoir tank and pipeline with get valve. The inlet reservoir tank is used for input water through the system and flat plate solar collector is used for preheating water.

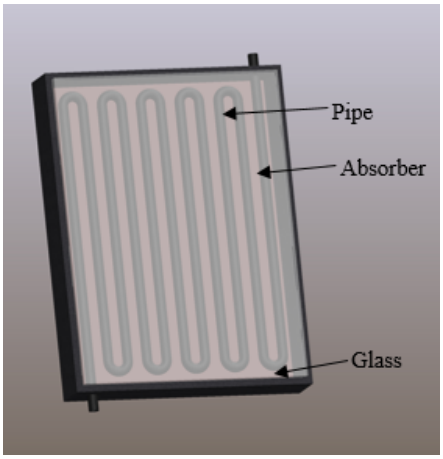

Fig.2 Flat plate solar collector

A flat plate solar collector consists of pipe line covered with dark colored absorber plate and transparent glass which placed in metallic box. The flat plate solar collector is shown in the Fig.2. The main function is that to capture solar radiation from sunlight and absorbed the heat in the absorber. The transparent glass is used as a trap to prevent the heat loss. [11]

2.2 Heating unit

Heating unit is the final operational unit. In this unit pre heated water is allowed for heating until its vaporization. The unit consists of parabolic solar collector, desalination pot and a floating system valve. The parabolic solar collector is made of iron rim decorated with a number of glass pieces focusing on a single point. The parabolic solar collector is shown in the Fig.3. It is used to concentrate the heat in the desalination pot and finally vaporized the preheated water in this desalination pot. The floating system worked as a lock system to prevent supply water from preheating unit at the time of heating. But when steam is produced in the desalination pot the volume of water is decreasing and for minimizing the water the float system allowed water in the pot. This float system supplies water continuously in the desalination pot and produce steam continuously.

Fig.3 Parabolic solar collector

2.3 Condensing unit

Condensing unit consists of a condenser and reservoir tank. The vaporized water turned to a liquid state by the condenser pipe. The condensing pipe is set aside to air cooling rather than power cooling to save electric power. Manual cooling like chiller and water used for rapid cooling of the condenser pipe. Thus the vaporized water from heating unit is directly converted into liquid. It is the final step to collect condensing water and reserved the condensed liquid water in the reservoir tank. Though distilled water is tasteless to drink some mineral rock is kept in the reservoir of mineralized water.

3. Working procedure

For continuous desalination process seawater passes through the inlet port of flat plat plate solar collector from the reservoir. Sea water then fills the pipeline of preheating unit. Preheating unit absorbs ample solar energy to heat up the sea water quickly. When the vaporization starts in distillation unit this time preheating unit increase temperature of sea water about 40-50 ℃. Sea water when

filled up the desalination pot at certain level floating system valve automatically closed. At this time no preheated sea water will enter into desalination pot until abundant sea water vaporized. In a parabolic dish solar collector sun rays incident upon the segments of the mirror. All incidents rays focused to the focal area that mean the lower surface of desalination pot. Incident solar intensity varies with 1100-1500 W/m^2 in experimented areas. This solar intensity is enough to vaporize the sea water. Sea water normally starts vaporization prominently after 15 minutes of the process starts. Approximately 30 minutes later its mass flow rate is about 0.1-0.2 Kg/hr. Mass flow rate varies with different times of the day. When ample water vaporized and passes through the outlet port to the condenser water level falls float system valve opened to fill up the level. The vaporization process maintains about 70-100℃ so salt cannot vaporized because boiling point of salt much higher than water. Some vapor condensed in the desalination pots upper inclined surface and droplet creates. Droplet goes to the outlet port along with the inclined surface due to gravity. Outlet port situated at the end of inclined surface. Due to the vapor pressure in the desalination pot generated vapor enter into the condenser pipe which is ice chilled. Upper portion of the condenser is ice chilled so that steam can quickly condensed. Another portion can condense in the condenser by natural air. Condenser pipe constructed such way that condensed pure water can flow down to the collector by gravity action. In collector distilled water is mineralized by calcium and magnesium rocks. The experimental setup of desalination process is shown in Fig.4.

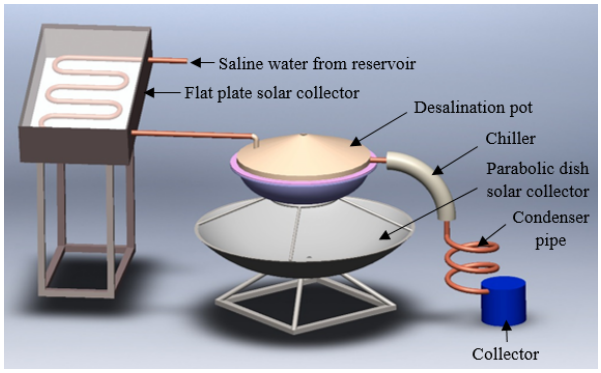

Fig.4 Experimental setup of desalination process

4. Data collection and analysis

This desalination process is done by the solar energy and ultimately solar energy depended on sunshine. So the data of the experiment are vary according to different day and time. It assumes that the vaporization is started partially above 85℃ temperature and by the experiment, it found that only 30 minutes need to raise the final temperature above the desired temperature in parabolic solar collector while preheating at 64℃ temperature. The flat plate solar collector preheats the water before supply in the desalination pot. For flat plate solar collector the different temperature at the same time interval is shown in Fig.5. It takes an average 30 minutes to increase the temperature from 32℃ to 64℃.

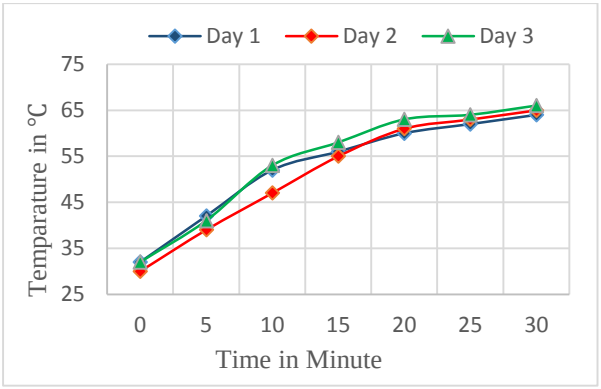

Fig.5 Temperature Vs. Time for flat plat collector

In the parabolic solar collector the preheated water, which temperature is above 60℃ allowed for final heating and it took 25 to 30 minutes to raise temperature above 85℃. The different temperature at different time of parabolic solar collector are shown in Fig.6.

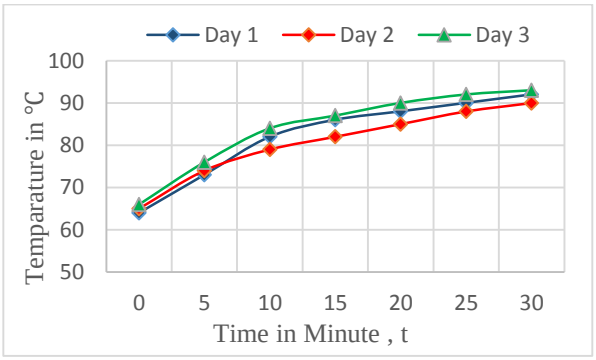

Fig.6 Temperature Vs. Time for parabolic collector

For the data analysis the fate plate solar collector initial temperature is assumed T_1 and the final temperature is assumed T_2. The final temperature of the flat plate is considered as the initial temperature of the parabolic solar collector and finally the ultimate temperature is assumed T_3. For the desalination process more rapid at the time of vaporization at parabolic collector the flat plate collector preheat the water for next vaporization process. The combined work of the two collectors at the same time interval are shown in the Fig.7.

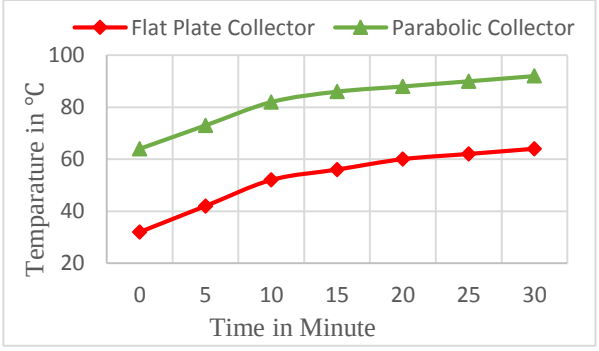

Fig.7 Temperature Vs. Time for combined system

5. Calculations

The efficiency of both flat plate solar collector and parabolic solar collector is calculated separately and finally find out the overall efficiency and mass flow rate. The surface area of the flat plate is 0.8387 m^2. There are 11 pieces of pipes which diameter is 0.5 inches and length 36 inch. The volume of pipe is equal to the water volume and it converts into the mass of water. It found 1.294 kg water allowed to preheat from 32℃ temperature to 64℃ temperature in the flat plate solar collector. The average solar intensity for both the collector is assumed 1400 W/m^2.

$$\eta_1 = \frac{m \times S \times (T_2 - T_1)}{A_1 \times I \times t} \quad (1)$$

By the equation 1 the efficiency of the flat plate solar collector is calculated and it was found 8.39%.

The surface area of the parabolic dish solar collector is calculated by equation 2 using the diameter 44 inch and height 7 inch.

$$A_2 = \left(\frac{\pi}{6}\right)\left(\frac{r}{h^2}\right)\left[(r^2 + 4h^2)^{\frac{3}{2}} - r^3\right] \quad (2)$$

The surface area of the parabolic solar collector is found 1.097 m^2. By this collector the temperature is increased from 64℃ to 92℃ and 35 g steam is produced within 30 minutes. In this distillation pot always 1 kg water allowed to heat. The efficiency of the parabolic solar collector is calculated by using equation 3 and it found 7.09%.

$$\eta_2 = \frac{mS(T_3 - T_2) + \Delta m \times Lv}{A_2 \times I \times t} \quad (3)$$

The continuous desalination process is done with combined system. In this system finally increase the temperature above 92 ℃ from 32 ℃ . The overall efficiency is equal to the summation of the both efficiency. Finally it found that the overall efficiency is 15.48% and mass flow rate of condense water 1.67 g/min.

6. Conclusion

The continuous desalination process of sea water was done by flat plate and the parabolic dish solar collector. The variation of the sunshine affects the producing rate of steam and slow down the output production. The following conclusions were drawn from the experiment:

a. Conventional desalination process as Electro dialysis, Mechanical vapor compression, and Reverse Osmosis can be replaced by this continuous desalination method for eliminating the electric energy.
b. Low installation cost and environment friendly.
c. Using solar energy as renewable sources it has zero running cost.
d. In flat plate collector water temperature raises up to 60℃ and in parabolic dish solar collector its temperature raises up to its vaporization temperature.
e. The individual efficiency of parabolic solar collector and flat plate solar collector are 7.09% & 8.39% respectively. But unification of these two system give overall efficiency is 15.48%.
f. The mass flow rate of condense water is found 1.67 g/min.
g. Higher efficiency and mass flow rate can be expected with larger unit and more series connection of the collectors.

NOMENCLATURE

A_1 : Flat plate surface area, m^2
A_2 : Parabolic dish surface area, m^2
r : Parabolic dish radius, m
h : Parabolic dish depth, m
η : Efficience, %
T_1 : Inlet temperature of water in flat plate, ℃
T_2 : Outlet temperature of water in flat plate, ℃
T_3 : Final temperature of water in parabolic dish, ℃
S : Specific heat of water, $J \cdot kg^{-1} \cdot °K^{-1}$
L_v : Latent heat of vaporization, $J \cdot kg^{-1}$
m : Mass of water in the desalination pot, kg
Δm : Mass of vapor produced, kg
I : Solar intensity, W/m^2
t : Total time required, sec

REFERENCES

[1] Saffa Riffat, Mahmoud Shatat and Guohui Gan; An innovative psychometric solar-powered water desalination system; *International Journal of Low-Carbon Technologies*, December 28, 2013.
[2] Mahmoud Shatat and Saffa B. Riffat; Water desalination technologies utilizing conventional and renewable energy sources; *International Journal of Low-Carbon Technologies*, December 28, 2013.
[3] Delyannis E. Historic background of desalination and renewable energies. Solar Energy 2003; 75(5):357–66.
[4] Intermediate Technology Development Group. Solar Distillation: Technical Brief. The Schumacher Centre for Technology & Development.Website:*http://www.itdg.org/docs/technical_information_service* (8 June 2014).
[5] Soteris A. Kalogirou; Seawater desalination using renewable energy sources; *Progress in Energy and Combustion Science*; V 31 , pp: 242–281 (2005).
[6] Galveza, J.B., L. Garcia-Rodriguezb and I. Martin-Mateosc, 2009. Seawater desalination by an innovative solar-powered membrane distillation system: The MEDESOL project. Desalination, 246:567-576. DOI: 10.1016/j.desal.2008.12.005
[7] Abdel-Rehim ZS, Lasheen A. Improving the performance of solar desalination systems. Renew Energy 2005;30:1955–71.
[8] Hoque N and Kumar S. Performance of photovoltaic micro utility systems. *Energy for Sustainable Development*, Volume 17, pp 424-430. (October 2013).
[9] Islam MR, Islam MR, Beg MRA. Renewable

energy resources and technologies practice in Bangladesh. *Renewable and Sustainable Energy Reviews*, Volume 12, Issue 2, pp 299-343, (February 2008).

[10] SH Khan, TU Rahman and S Hossain. A brief study of the prospect of solar energy in generation of electricity in Bangladesh. *Journal of Selected Areas in Renewable and Sustainable Energy (JRSE),* June 2012 edition.

[11] Fabio Struckmann; Analysis of a Flat-plate Solar Collector; Project Report 2008 MVK160 Heat and Mass Transport; May 08, 2008, Lund, Sweden.

ICMIEE-PI-140287

Polymer composites: a blessing to modern aerospace engineering

Md Saifuddin Ahmed Atique [1,*], *Nafisa Nawal Probha* [2], *Asif Shahriar Nafi* [2],

[1] Department of Aeronautical Engineering, Military Institute of Science and Technology, Mirpur Cantonment Dhaka-1216, BANGLADESH
[2]Department of Aeronautical Engineering, Military Institute of Science and Technology, Mirpur Cantonment Dhaka-1216, BANGLADESH
[3] Department of Aeronautical Engineering, Military Institute of Science and Technology, Mirpur Cantonment Dhaka-1216, BANGLADESH

ABSTRACT
Modern aerospace industry is highly progressive and polymer composite materials have a positive and significant impact on it. This paper demonstrates details about the components of advance polymer composites, its properties and its uses in aerospace industries. Polymer composites are highly efficient and environment friendly. Traditional materials are susceptible to fatigue and corrosion when composite materials provide resistance to both of this along with its significant amount of weight reduction. Due to high strength and stiffness of its fiber, polymer composite provides high "strength to weight" & "stiffness to weight" ratios. Apart from this, they possess good shear properties and low density .As a result, new generation aerospace engineers and aircraft designers are turning to polymer composite materials to make their flying vechicle and aircraft lighter, stronger and of course more fuel efficient. Our paper will briefly describe about the uses of fiber reinforced polymer composites in aerospace industry and how does it consider as a blessing in this field.

Key Words: Polymer composites, aerospace engineering, fiber, aircraft

1. Introduction

A Composite material is a material system composed of two or more macro constituents that differ in shape and chemical composition and which are insoluble in each other. A Composite material is a material system composed of two or more macro constituents that differ in shape and chemical composition and which are insoluble in each other.

The term composite is often used both in the modern context of Fiber Reinforced Plastics (FRP) and also in the wider context to cover honeycomb structures and bonded metal laminates for primary structural applications. The fibers or matrix (resin) alone cannot be used for any applications because of the limitations in other properties. The fibers provide the stiffness, and the matrix provides the glue to produce a stiff structure that is very light. Plastics and fibers generally are less dense than the metals, but the fibers have greater stiffness, providing for a larger stiffness-to-weight ratio. Fibers are thin and integrity is not maintained. Fibers are comparatively heavier. In matrix materials the modulus and strength values are less and hence matrix alone cannot be used for any structural applications. But when these two materials are combined we get a composite material which is light weight, stiff, strong and tough. Beyond doubt, the new material here we are developing is much more suitable for special purpose (light weight & strong) than compared to the previous one we got.

2. Why Aerospace?

'Safety' and 'security' are the most important words in the field of aerospace. Imagine a structural failure in a car and an airplane. If the skin of the car gets ripped off while driving no disaster is going to happen. But in the case of the aircraft, a great disaster will occur. Let's see the following pictures:

Fig.1 Fuselage damage to Aloha Airlines Flight 243, April 1988

Besides these, the performance of an airplane is highly influenced by its weight and overloading it will cause serious problem. By using composite materials, we can overcome this problem .Aircraft operate in very corrosive environment and inspection for corrosion

* Corresponding author. Tel.: +88-01686334988
E-mail address: : saifaerospace@gmail.com

damage are carried out often. Composites don't corrode. They also help to reduce the development of the crack.

3. Components of advanced polymer composite

Advanced polymer composites generally contain reinforcing fibers. They are in the form of continuous filamentary tows or fabrics and properly formulated polymeric matrices. Structural adhesives (mostly in the form of supported or unsupported film) and honeycomb cores are also used for making sandwich structures and metallic laminates.

3.1 Fibers

Fibers are widely used as reinforcements. Glass, aramid and carbon fibers are in extensive use amongst the fibers available. Boron or other exotic fibers are also used in modest quantities for applications requiring very high service temperatures like the ones which we need for the skinning of the aircrafts. The properties of glass, aramid and carbon fibers are given in the tables 1 to 5.

Table 1 typical properties of glass fibers

Fiber	'E' glass	'R' glass	'D' glass
Density(g/cc)	1.44	1.38	1.41
Tensile strength(MPa)	3600	3620	3447
Tensile Modulus(GPa)	83	127	175
Elongation of break(µm)	4	1.85	2.9
Filament diameter (µm)	-	-	-

Table 2 typical properties of aramid fibers

Fiber	Kevler 29	Kevler 49	Kevler 149
Density(g/cc)	1.44	1.38	1.41
Tensile strength(MPa)	3600	3620	3447
Tensile Modulus(GPa)	83	127	175
Elongation of break(µm)	4	1.85	2.9
Filament diameter (µm)	-	-	-

Table 3 properties of high tensile carbon fiber (2)

Fiber	T-300	T-400	T-800
Density(g/cc)	1.75	1.80	1.81
Tensile strength(MPa)	3528	4412	5588
Tensile Modulus(GPa)	230	250	294
Elongation of break(%)	1.5	1.8	1.9

Table 4 properties of high modulus carbon fibers

Fiber	M-30	M-40	M-50
Density(g/cc)	1.7	1.81	1.91
Tensile strength(MPa)	2920	2744	2450
Tensile modulus(GPa)	294	392	492
Elongation of break(%)	1.3	0.6	0.5
Filament diameter(µm)	6.3	6.5	6.3

Table 5 properties of high modulus high strain carbon fibers

Fiber	M 35J	M 40J	M 46J
Density(g/cc)	1.70	1.77	1.84
Tensile Strength(MPa)	5000	4410	4210
Tensile Modulus(GPa)	343	384	440
Elongation of break(%)	1.6	1.2	1.0
Filament Diameter(µm)	5.2	6.2	5.1

3.2 Matrix

Matrices are holders in which fibers are embedded. A matrix acts as binder which surrounds the fibers. For example; when we considering carbon fiber reinforced polymer, carbon fiber is the filler and polymer is the matrix. Matrix properties like Stress-Strain behavior & adhesion properties are important factors which mostly determine the ability of the matrix to distribute stresses. Polymer Matrix can be divided into two groups –

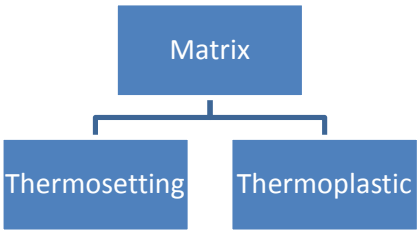

Both type of matrix are greatly used in industrial applications but thermoplastic system is preferred over thermosetting because of no involvement of chemical reaction as it results in release of gas or heat.

(1) Thermosetting

In a thermosetting resin, the raw uncured molecules are cross linked through a catalytic chemical reaction. Through this reaction they are converted into hard brittle solids, creating strong bonds between one another through the formation of three dimensional networks of polymer chains. Once a thermosetting composite is formed; it cannot be reformed or reversed. That is why recycling of thermosetting composite is difficult. Thermosetting resins have excellent properties like resistance to solvents, corrosives, heat and high temperature and also have good fatigue strength, elasticity and adhesion properties. Epoxy resin, unsaturated polyester resin and vinyl ester are the most used thermosetting polymer matrices. Epoxy resins are

better in case of stiffness properties as compared to polyester resins. The interface bond strength between epoxy resin and filler is also greater than the polyester thermosetting.

Table 6 Properties of epoxy and polyester

Property	Epoxy	polyester
Viscosity at 25ºC μ(Cp)	12000-13000	250-350
Density	1.16	1.09
Heat Distribution Temperature(HDT)	50	54
Flexural Strength(MPa)	60	45
Tensile Strength(MPa)	78	40
Maximum elongation	4	1

Vinyl ester resins offer good process ability for liquid processing techniques such as RTM.

(2) Thermoplastic

Thermoplastics are of very high molecular weight and their strength and stiffness are emerged from the properties of their monomer units. Amorphous and Crystalline polymer's properties have profound effect on the properties of thermoplastic composites. For Amorphous polymers chain slippage occurs and it leads to high strain to failure, toughness and damage tolerance. Crystalline polymers have increased strength and temperature resistance. Some examples of Amorphous and Crystalline matrices are as follows

Table 7 Examples of amporphus & crystalline matrices

Amorphus	Crystalline
ABS	Nylon 6/6(etc)
PC	PPA
PSU	Acetal(POM)
PEI	PE
PES	PPS
PS	PEK

Table 8 Comparison of mechanical properties

Properties	polycarbonate	polypropylene
Density mg/m^3	1.14-1.31	0.89-0.92
E modulus GPa	2.21-2.44	0.9-1.35
Ultimate strength MPa	65-72.4	17.2-37
Yield strength MPa	58.6-70	20.7-37.2
Tensile strength MPa	6-50	5-37
Max elongation(%)	10-125	10-600

4. Properties of Matrix

It is undoubtedly true that the high strength of composites is largely dependent on the fiber reinforcement but the importance of matrix material cannot be avoided as it supports the fibers and distribute the load evenly on the fibers.

The desired properties of matrix material for the formation of a good composite are as follows-

i. High toughness
ii. Room temperature cure preferable
iii. Low moisture absorption
iv. Low shrinkage
v. Low thermal expansion
vi. Higher elastic modulus(more than fiber)
vii. Excellent chemical resistance
viii. Easily process able
ix. Dimensional stability

4.1Thermal Properties

Polymer matrix determines the elevated temperature properties and the maximum use temperature of composite material. Glass Transition Temperature (Tg) is an important parameter for dimensional stability of a composite under influence of heat; it also has effect on most of the physical properties of matrix system. The polymer softens as Tg is approached. There are many different ways to measure Tg such as using DSC (Differential Scanning Calorimeter) apparatus, HDT technique.

4.2 Toughness

In aerospace applications high elasticity modulus, high strength and greater damage tolerance of composites are preferred. In polymer matrix composites, the transverse modulus is dictated by the matrix modulus while the longitudinal modulus is dictated by the fiber modulus. That's why transverse strength and shear strength is matrix dominated. However, for a brittle matrix toughness can be achieved by several processes. One of them is by using reactive dilute but in this process the high temperature withstanding capability is lost. Another way is inclusion of dispersed phase in the glassy matrix.

C1: 120C curing epoxy based system not formulated for toughness

C2: 175C curing system based on widely used MY 720 and DD

Here in the following figure we can see a comparison of Toughness of carbon fiber composites based on their toughness. As in aerospace or aeronautical engineering purpose the toughness of the material that we are going to use it should be high enough so special care should be taken while selecting the material. A composite material that may have posses other significant properties required for use in aerospace/aeronautical purpose but wit out being it blessed by the properties of enough toughness definitely it will not be considered as an idle material for this special track of engineering. So the toughness of the selected material should be high enough to satisfy the aeronautical/aerospace engineers.

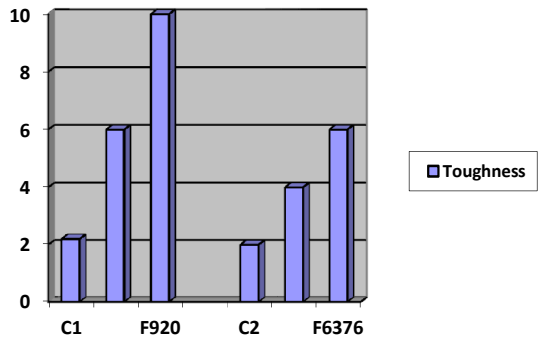

Fig.2 Comparison of toughness of carbon fibre Composites

Here,
C1: 120C curing epoxy based system not formulated for toughness
C2: 175C curing system based on widely used MY 720 and DD

4.3 Humidity and Chemical Resistance
The material selection for the generation of a composite for a particular application largely depends on the severity of the environment. For aggressive environment resins are preferred. Although epoxies have a greater solvency and thermal resistance than vinyl esters, they are difficult to process and more expensive. That's why vinyl ester is mostly used in industrial sectors.
All polymers generate heat and toxic smoke when exposed to fire. However when composites contain upto 70% fiber(by weight) which are non-combustible they are almost fire resistant.
Recent Development in Matrices-
Toughening of a resin usually degrades its yield strength, modulus and Tg. To overcome these problems and for the development of matrices of improved fracture toughness and impact performance and straight up cure cycle; R&D oriented manufacturers have developed a number of matrices which can meet the needs of new demanding aerospace sectors. Composite properties of these matrices are given below in the table.

Table 9 Composite properties of matrix

Matrix and fiber	0º Laminate Properties			
	Tensile strength	Tensile Modulus	ILSS,MPa	G_{IC}(Tough Ness)
F914+T300	1650	135	118	350
F6376+1M6	2696	172	131	
F924+T800	2610	169	130	666
VxM18+M 40JB	2370	221	84	

5. Sandwich Structures
In aerospace industry the effectiveness of composite materials in reducing component weight and increasing fuel economy has greatly been proved. The idea of sandwich structure has become increasingly popular because of the development of man-made cellular materials.
Sandwich structure consists of

i. A pair of thin stiff, strong skins(faces, facings or covers)
ii. A thick, lightweight core to separate skins & carry the loads from one skin to other
iii. An adhesive attachment which is capable of transmitting shear and axial loads to and from the core.Sandwich structures are very light and stiff which are the main demands of aerospace industry.

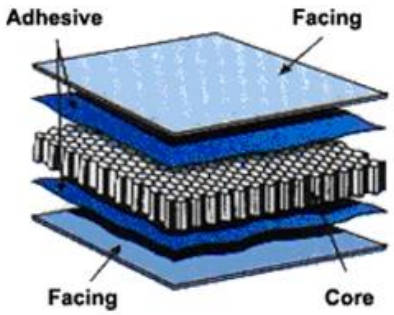

Fig.3 An Illustration of layer orientation of a sandwich structure

6. Advantages of carbon fiber composites
There are various advantages of using advanced composite material specially carbon fiber composite material in aerospace industries as well as others engineering. For example,
1. High resistance to fatigue and corrosion is provided by advanced carbon fiber composite.
2. Composite materials provide high "strength to weight" or "stiffness to weight" ratio. So, weight savings are significant ranging from 25-45% of the weight of the traditional metallic machine design.
3. Composite provides high resistance to impact damage and improve torsional stiffness.
4. Manufacturing and assembly are simplified because of part integration and thereby reducing cost in aerospace industries.
5. Improved friction and wear properties.
6. Composite makes it easy to tailor the basic material properties of a laminate which has allowed new approaches to the design of aero elastic flight structure.

7. Application of composites in aerospace

Composite materials are widely used in the aircraft manufacturing industries and it has allowed the aerospace engineers to overcome the obstacles that have been faced by them when they used the traditional materials individually. As the polymer composite provides the properties of light weight, high temperature resistance etc. so that during the last few decades its application in aerospace industry has rapidly increased to design high performance and economical aircraft. Boeing a leading aircraft manufacturing industry has used a significant amount of composite at their new passenger aircraft "Boeing 787/Dream liner". The following figure shows us the amount of composite with respect to other materials used in Boeing 787/Dream liner.

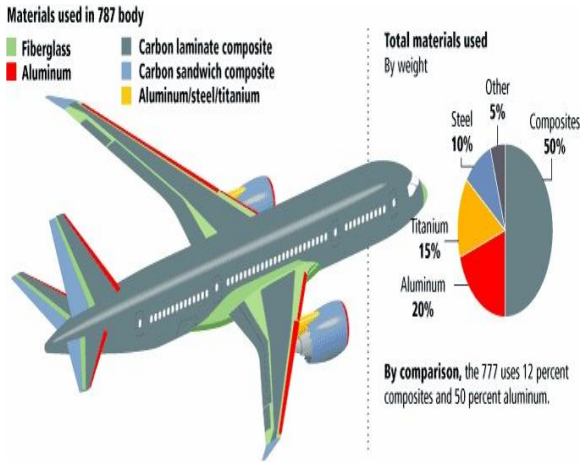

Fig.4 Percentages of composite material along with others in Boeing 787/Dream liner

The figure shows that now a day's around 50% material used in Boeing 787 is composite material with comparison to the Boeing 777 which used only 12% of composite and 70% aluminum. Apart from aircraft, now a day's for design and manufacturing rocket and missiles the new generation aerospace engineers are widely using composite of carbon, aramid and glass. Carbon –carbon composites are used for manufacturing the nose tips and heat shields of reentry vehicles.

8. Blessing to modern aerospace engineering

Polymer composite has proved as a blessing to modern aerospace/aviation industries. For a flying vehicle it is most important to be lighter than air and at the same time it should be strong enough to withstand the gust load and other aerodynamic loads which impose on it. But it was very difficult for the aerospace engineers to select such a material which will provide enough strength to weight ratio when they worked with the traditional individual material. But this problem was solved by the grace of polymer composite which is very much light (important for fuel efficiency) and provide enough strength against the gust and aerodynamic loads. Now with the help of a comparison between Boeing 777 (launched in 2000) and Boeing 787 (launched in 2007) we will prove our statement regarding the debt of polymer composite materials in aerospace industries.

Table 10 Comparison between Boeing 777 & 787

Boeing 777	Boeing 787/ Dream liner
Launched in 2000	Launched in 2007
12% Composites	50% Composites
50% Aluminum	20% Aluminum
8% Titanium	15% Titanium
20% Steel	10% Steel
10% Others	5% Others

Because of using 50% polymer composite material instead of using greater amount of aluminum, steel or others traditional materials makes Boeing 787 almost 20% more fuel efficient and 35,000 lbs lighter compared to its previous origin Boeing 777.That is how polymer composite contributes to modern aerospace industries.

Conclusion

It is always important to choose the right material for right job. For example, In order to designing a commercial gas cylinder metals can be a good selection because it provides sufficient strength, ductility and keeps the manufacturing cost moderate. Here, the weight is not a significant factor, so we can select a low alloy steel (ASTM A414-Grade G). On the other hand when we fall our focus on aerospace engineering here the weight reduction (light weight) is more significant than the cost. So, for manufacturing aerospace pressure vessel aerospace engineer choice is composite material which provides light weight along with strength and ductility.So, a wise aeronautical engineer/aerospace engineer will always choice a polymer composite (Kevlar 49 aramid fibers) for designing an aerospace pressure vessel. Since, aerospace/aeronautical is an advanced branch of engineering where the term "safety" & "reliability" is more important than cost and so, the use of fiber reinforced polymer composite is taking its strong position in this field very rapidly. When we make unique combination of safety, reliability, light weight, strength and efficiency then there is no alternative to this polymer reinforce composite because it is aerospace which requires a lot of care. Otherwise the consequences will be dangerous and drastic.

REFERENCES

[1] Vijai Kumar , *Advanced Composite Materials in Typical Aerospace Application.*

[2] Dr. P. Mitra , *Advanced polymer composites with special reference to carbon fiber reinforced polymer (CFRP).*

[3] R. Velmurugan, *Composite material for aerospace application*

[4] Tim Edward, *Composite material revolutionize aerospace engineering.*

[5] Krisham K Chawla, *Composite Material: Science and Engineering.*
[6] Roger Naslian, Brayan harris, *Ceramic matix Composies, component, preparation micro-Structure and properties.*
[7] Bryan Harris: *Engineering Composite Materials.*

ICMIEE-PI-140290

Observation of mechanical properties of fiber reinforced polymer matrix composite

Tasmia Zaman [1,*], *Abdullah Al Mahmood* [1], *A. Hafiz Zaman* [2]
[1] Department of Glass and Ceramic Engineering, Rajshahi University of Engineering & Technology, Rajshahi-6204, BANGLADESH
[2] Department of Mechanical Engineering, Rajshahi University of Engineering & Technology, Rajshahi-6204, BANGLADESH

ABSTRACT
Polymer Matrix Composite (PMC) is the material consisting of a polymer (resin) matrix combined with a fibrous reinforcing dispersed phase. PMCs are very popular due to their high tensile strength, stiffness and fracture toughness along with low cost and simple fabrication methods. The work was done to prepare a Polypropylene based PMC with different reinforcing dispersed phase and compare their mechanical properties. All the available dispersing media (polymer) was taken initially for hardness test. Polypropylene gave the highest hardness in shore scale. So it was taken as the final matrix media. Glass and Jute fiber was used as dispersed phase. Both hand lay-up and hot pressing techniques were used to fabricate the composite material. Finally, tensile test and flexural test was performed on the prepared composites. Glass fiber polymer composite gave better result than the others. On the other hand, hot pressing technique gave better texture of the finished product than the hand lay-up technique.

Keywords: PMC, flexural test, tensile strength, hand lay-up, hot pressing.

1. Introduction

Polymer matrix composites (PMCs) are comprised of a variety of short or continuous fibers bound together by an organic polymer matrix. Unlike a ceramic matrix composite (CMC), in which the reinforcement is used primarily to improve the fracture toughness, the reinforcement in a PMC provides high strength and stiffness. The PMC is designed so that the mechanical loads to which the structure is subjected in service are supported by the reinforcement. The function of the matrix is to bond the fibers together and to transfer loads between them [1].

Polymer matrix composites are often divided into two categories: reinforced plastics, and advanced composites. The distinction is based on the level of mechanical properties (usually strength and stiffness); however, there is no unambiguous line separating the two. Reinforced plastics, which are relatively inexpensive, typically consist of Polypropylene resins reinforced with low-stiffness glass fibers. Advanced composites, which have been in use for only about 15 years, primarily in the aerospace industry, have superior strength and stiffness, and are relatively expensive. Advanced composites are the focus of this assessment [2].

Chief among the advantages of PMCs is their light weight coupled with high stiffness and strength along the direction of the reinforcement. This combination is the basis of their usefulness in aircraft, automobiles, and other moving structures. Other desirable properties include superior corrosion and fatigue resistance compared to metals. Because the matrix decomposes at high temperatures, however, current PMCs are limited to service temperatures below about 600^{o}F (316^{o}C) [3].

Experience over the past 15 years with advanced composite structures in military aircraft indicates that reliable PMC structures can be fabricated. However, their high cost remains a major barrier to more widespread use in commercial applications [4].

Most advanced PMCs today are fabricated by a laborious process called lay-up. This typically involves placement of sequential layers of polymer-impregnated fiber tapes on a mold surface, followed by heating under pressure to cure the lay-up into an integrated structure. Although automation is beginning to speed up this process, production rates are still too slow to be suitable for high-volume, low-cost industrial applications such as automotive production lines [7].

New fabrication methods that are much faster and cheaper will be required before PMCs can successfully compete with metals in these applications. One of those methods includes hot pressing technique [6].

Aerospace applications of advanced composites account for about 50 percent of current sales. Sporting goods, such as golf clubs and tennis rackets, account for another 25 percent. The sporting goods market is considered mature, with projected annual growth rates of 3 percent. Automobiles and industrial equipment round out the current list of major users of PMCs, with a 25 percent share [5].

The next major challenge for PMCs will be use in large military and commercial transport aircraft. PMCs currently comprise about 3 percent of the structural weight of commercial aircraft such as the Boeing 757, but could eventually account for more than 65 percent. Because fuel savings are a major reason for the use of PMCs in commercial aircraft, fuel prices must rise to make them competitive [2,3].

The largest volume opportunity for PMCs is in the automobile. PMCs currently are in limited production in body panels, drive shafts, and leaf springs. Additional near-term markets for PMCs include medical implants, different reciprocating industrial machinery, storage and

* Tasmia Zaman. Tel.: +88-01911546371
E-mail address: zaman.tasmia@yahoo.com

transportation of corrosive chemicals, and military vehicles and weapons [6-8].
Beyond the turn of the century, PMCs could be used extensively in construction applications such as bridges, buildings, and manufactured housing. Because of their resistance to corrosion, they may also be attractive for marine structures. Realization of these opportunities will depend on development of cheaper materials and on designs that take advantage of compounding benefits of PMCs, such as reduced weight and increased durability. In space, a variety of composites could be used in the proposed aerospace plane, and PMCs are being considered for the tubular frame of the NASA space station [1-3].

2. Experimental setup

2.1 Hardness test
Hardness may be defined as the resistance to plastic deformation or penetration, usually by indentation. However, the term may also refer to stiffness or temper or to resistance to scratching, abrasion, or cutting. The greater the hardness of composite, the greater the resistance to deformation. There are basically two types of hardness tests, again which can be divided into different types. They are: Indentation hardness test which includes Rockwell hardness test, Brinell hardness, Vickers hardness test, Knoop hardness test, Shore test and Scratch hardness test. Among these, Vickers and Knoop are micro hardness tests while Rockwell, Brinell and Shore are macro hardness tests. On the other hand, Shore test can be measured in Shore A, Shore D, Shore O, Shore H and Shore OO scale. The hardness testing of plastics is most commonly measured by the Shore (Durometer) test. This method measures the resistance of the plastic towards indentation. Shore Hardness, using either the Shore A or Shore OO scale, is the preferred method for 'softer' plastics. Hardness measuring instrument called Shore A and Shore OO durometer was used for this experiment. The reading was dimensionless.

2.2 Hand lay-up technique
The most popular type of PMC fabrication is Hand lay-up process. The Hand lay-up is a manual, slow, labor consuming method. To perform the operation, at first a sheet of mild steel was placed on the ground to avoid dust. Then a releasing paper called “milot paper” was placed on it. A jute mat of 232mm x 237mm x 0.45mm dimension was taken as fiber and was placed on the “milot paper”. Around 150gm of Polypropylene was taken to prepare 3mm thick matrix. The Polypropylene was spread over the jute mat. Di ethyl methyl ketone per oxide was used as hardener. Hardener was about 1.5% of the total weight of matrix. After all these, the second “milot paper” was placed and a roller was used to roll the prepared composite. At last, heavy loads were placed on the composite and held there for three days to be hardened. After being hardened, the “milot papers” were removed. Same technique was applied for glass fibers.

2.3 Hot pressing technique
In this type of molding the curing of the reinforced plastic is accelerated by the use of heat (180^oC) and pressure (~15 MN/m^2). At first the molds (both male and female) were treated with “silicone mold release” spray. The mold dimension was 228mm x 230mm. After that, some PP (polypropylene) particles were spread over the female mold. Then, the jute mat was placed on it. Again, the other half PP particles were spread on it. Then, the male mold was given on the female mold. The mold was placed in the hot press machine (hydraulic). The temperature given was 180^oC. 100KN load was given for 50mins. During the process, the lower plate of the machine moves upward and the upper plate remained fixed. After the fixed period of time, all the parameters of the machine were made zero and the mold was water sprayed for cooling quickly. Then, the mold was out of the machine and the composite was taken out from the mold. Same technique was applied for glass fibers.

2.4 Tensile test
Tensile test was performed by preparing the samples of accurate dimensions. The composite samples were tested under universal testing machine. The percent elongation and ultimate tensile strength (UTS) were determined.

2.5 Flexural strength test
The flexural stress was calculated by the following Eq.(1), Eq.(2) and Eq.(3):

$$R=0.01L^2/6d \quad (1)$$

$$D=0.05L^2/6d \quad (2)$$

$$\sigma=3PL/2bd^2 \quad (3)$$

3. Results and Discussions

3.1 Hardness test
Different dispersing media was used for this experiment. Teflon, Polyvinyl chloride (PVC), Polypropylene (PP) and rubber was taken for the hardness test. Hardness was measured in Shore scale. Two scales were taken- Shore A and Shore OO. Polypropelyne gave consistent result in both scales. It also gave highest hardness. So polypropylene was chosen as the dispersing media.

Table 1 Hardness data of different polymers.

Shore Scale	Teflon	PVC	PP	Rubber
Shore A	98.9	75.06	98.93	45.8
Shore OO	93	94.5	96.67	84.3

Table 1 shows the data obtained during Shore hardness test. Both Teflon and Polypropylene gave good hardness.

But as the data for Teflon was fluctuating in different scales, so Polypropylene was taken finally.

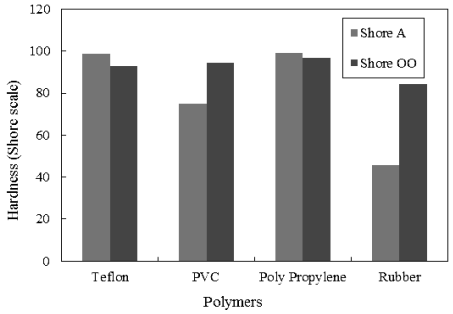

Fig.1 Hardness of polymer in shore scale.

Fig.1 shows the comparison of hardness measured in Shore scale for different polymers.

3.2 Visual inspection

Jute-Polypropylene composite, Glass-Polypropylene composite and only Polypropylene (only dispersing media with no dispersed phase) samples were made using both hand lay-up and hot pressing techniques. Prepared samples were taken initially for visual inspection. Hand lay-up method gave little smooth surface with some bubbles present in the samples. But the adhesion was good. Hot pressing technique gave samples with relatively smooth surface with no bubbles present. So it concluded that hot pressing gave better texture of composite samples than the hand lay-up technique.

3.3 Tensile test

Tensile test was performed using Universal Testing Machine (UTM). Both Ultimate Tensile Strength (UTS) and percent elongation was measured. Table 2 shows the data obtained for hot pressing technique samples during tensile test.

Table 2 Tensile strength data for different composites.

Parameters	Jute- PP	Only PP	Glass- PP
b	13.7	13.7	13.3
D	3.5	4.95	2.0
L	50	50	50
Maximum load	1.172	1.140	1.843
%Elongation	2.624	6.24	2.95
UTS	24.8	16.8	69.29
Fracture type	Brittle	Brittle	Brittle

Data shows that, Glass-PP composite gave the highest tensile strength. On the other hand, only PP samples gave higher percent elongation which was expected. But it can be also seen from the obtained data that, only PP gave lower tensile strength. In order to increase strength composite must be made. Jute-PP composite gave both lower strength and percent elongation compared to Glass-PP composite.

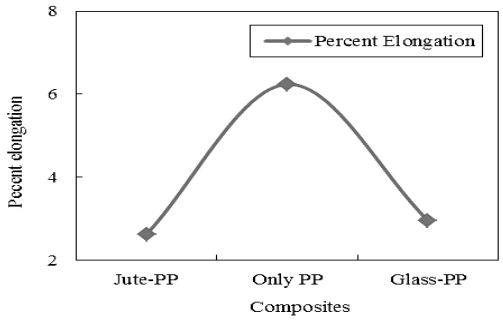

Fig.2 Percent elongation test for different materials.

Fig.2 shows the variation of percent elongation with different material and Fig.3 shows the graphical representation of tensile strength test data for different composites.

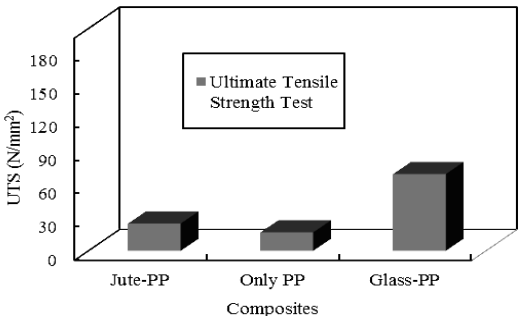

Fig.3 Ultimate tensile strength test for composites.

3.4 Flexural strength test

Flexural strength was measured for different composites. Again the Glass-PP composite gave better result than others.

Table 3 Flexural strength data for different composites.

Parameters	Jute- PP	Only PP	Glass- PP
b	12.5	12.6	12.6
d	2.8	4.65	2.0
L	44.8	74.4	3.2
Maximum load	0.0705	0.0072	0.206
R	1.2	1.98	0.853
D	5.97	9.92	4.26
σ	48.3	2.95	196.19

Table 3 shows the data obtained for flexural strength test. Glass-PP gave around five time higher flexural strength than Jute-PP composite. On the other hand, only PP gave very poor result compared to the other composites.

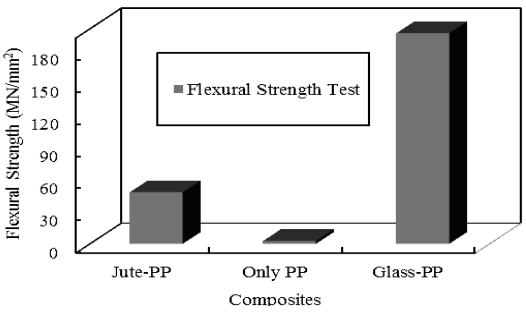

Fig.4 shows the graphical representation of flexural strength of different materials.

4. Conclusions

The work was done to study the variation of mechanical property with dispersed phase in composites. Polypropylene itself is a hard polymer compared to Teflon, PVC, rubber etc. So it contributed a vital role for the formation of high strength composites.

In case of dispersed phase which is also known as second phase size, amount and distribution is very important factor. According to the rule of mixture, both fiber and matrix has contribution to the composite strength. The tensile test showed that, maximum UTS was seen for glass fiber composite. Then came the jute-matrix composite and at last Polypropylene. Glass fiber has a higher strength than jute fiber.

Again, the percent elongation of only Polypropylene was higher than the others. It is because as only polymer is present it is very soft and ductile. So the percent elongation was high.

For flexural test, glass-matrix composite showed maximum flexural strength, which was around 196.19 MN/m^2. Only Polypropylene gave low flexural strength around 2.95 MN/m^2.

Brittle fracture was seen in case of both composites.

Presence of bubbles has adverse effect on mechanical properties. Hand lay-up technique made samples gave poor texture compared to hot press technique. Bubbles decreased the tensile strength and flexural strength of hand lay-up samples. So the hot pressed samples were finally taken for test.

NOMENCLATURE

b : Width of beam, mm
d : Depth of beam, mm.
L : Support span length, mm.
R : Rate of cross head motion, mm/mm
D : Maximum deflection
P : Maximum load, KN
σ : Stress in the outer fibers at mid-point, MN/mm^2

REFERENCES

[1] F.L. Matthews, R.D. Rawlings, *Composite Materials: Engineering and Science,* Boca Raton: CRC Press, ISBN 0-8493-0621-3, (1999).
[2] L. Hollaway, *Handbook of Polymer Composites for Engineers*, (1994).
[3] R. M. Jones, *Mechanics of Composite Materials* (2nd ed.), ISBN 9781560327127, (1999).
[4] A. K. Kaw, *Mechanics of Composite Materials,* (2nd ed.), CRC. ISBN 0-8493-1343-0, (2005).
[5] R. E. Smallman, R.J. Bishop, *Modern Physical Metallurgy and Materials Engineering*, (6th ed.) (1999).
[6] D. Fatih, H. Homayoun, D. Todor, B. Prasannakumar, Delamination of impacted composite structures by cohesive zone interface elements and tiebreak contact, *Central European Journal of Engineering,* Vol. 2, pp 612–626, (2012).
[7] E. Gunter, *Designing with Plastics*, (2006).
[8] D. V. Rosato, D. V. Rosato, J. Murphy, *Reinforced plastics handbook,* (2004).

ICMIEE-PI-140291

Utilization of Waste Plastic to Save the Environment

Nahid Newaj [1], Mahadi Hasan Masud [2]
[1] Department of Industrial & Production Engineering,
Rajshahi University of Engineering & Technology, Rajshahi-6205, BANGLADESH

[2] Department of Mechanical Engineering,
Rajshahi University of Engineering & Technology, Rajshahi-6205, BANGLADESH

ABSTRACT
Go green & go green is the prime demand of the environment. In this paper we will discuss the way to get green environment by utilizing the waste plastic. The use of plastic is essential today, so it is not the matter of concern today whether it can be used or not, the main matter of concern is the utilization of plastic wastes. For fulfilling this objective plastic waste should be converted into resources e.g. it can be used as fuel, landfill, in energy generation & for making road. Small business can be started to buy this plastic wastes to save the environment. Hence according to the environmental desire, by following the above discussed things with proper waste management we may hope about a clean and green environment. Plastics have now become indispensable materials in the modern world and application in the industrial field is continually increasing. The properties of the oil derived from waste plastics were analyzed and found that it has properties similar to that of diesel. Waste plastic oil (WPO) was tested as a fuel in a D.I. diesel engine and its performance characteristics were analyzed and compared with diesel fuel (DF) operation. It is observed that the engine could operate with 100% waste plastic oil and can be used as fuel in diesel engines.

Keywords: Plastic Waste, Waste Plastic Oil, Plastic Road.

1. INTRODUCTION

The term "global warming" refers to the increase in the average temperature of global surface air and oceans. Global Warming has adverse effect on environment and it is increasing day by day. So in order to reduce global warming it's necessary to think about something. Greener technology is the best way to solve this problem [1]. Green technology means to develop new methods to use natural environment and resources which reduces negative impact of human activities.

With the increase in generation, use of plastic is increasing and plastic waste becoming a major obstacle to greener technology. Waste plastic is often the most visible component in waste dump and landfill. Recent studies says to us that plastics remain 4500 years long on the earth and since plastic waste is growing rapidly hence the improper disposal of plastics causes problems as distant as breast cancer, reproductive problems in humans and animals, genital abnormalities and much more. Plastics wastes are found in different forms which almost 5% of the municipal solid wastes which is toxic in nature. It is a common sight in both urban and rural areas to find empty plastic bags and other type of plastic packing material littering the roads as well as drains. Due to its biodegradability it creates stagnation of water and associated hygiene problems [2]. So this paper will concern about, sources of plastic wastes, how plastic waste affects the environment and how we can utilize the plastic wastes.

The plastic consumption is shown in table 1

Table1. Plastics consumption, by major world areas, in kg and GNI dollars per capita:

Main world areas	Plastics consumption, 000s tons	Population millions	Kg/capita	GNI/capita
Europe W, C, E	40 000	450	90	18 000
Eurasia, Russia, others	4 000	285	14	1 600
North America	45 000	310	145	32 000
Latin America	11 000	500	22	3 500
Middle East, incl. TR	4 000	200	20	2 500
Africa, North & South	2 500	190	13	2 000
Other Africa	500	610	<1	300
China	19 000	1285	14	800
India	4 000	1025	4	450
Japan	11 000	125	90	35 000
Other Asia Pacific, rest	13 000	1120	11	600
Total world	154 000	6 100	25	5 200

Author. Tel.: +88-01768440929
E-mail address: newaj.nahid@gmail.com

2. NEED FOR THE STUDY

1) Disposal of waste plastic is a major problem.
2) It is non-biodegradable.
3) Burning of these waste plastic bags causes environmental pollution.
4) Dump yard and waste pits mainly consists of low-density polyethylene.
5) To find its utility of waste plastic in road construction.
6) To know about all the application of waste plastic

3. SOURCES OF PLASTIC WASTE [4]

There are many sources of plastic waste, municipalities are one of them. The term municipal solid waste (MSW) describes those waste materials that are collected by the municipality itself or by the authorized organization. The municipal solid wastes come from residential, commercial, institutional and industrial sources MSW consists of waste materials such as news paper, cans and bottles, food waste, food packaging, clothing, appliances, yard wastes, household hazardous waste, corrugated boxes, office papers and plastics film etc. MSW normally does not include processing residuals from the industry as this material has residual value and most of the industries will know the commercial method to dispose this material of some value. The respective part of each category in the MSW stream differs in various communities. Plastic wastes and plastic recycling can be classified as follows:

Waste Plastic: Consists of plastic resin or product that must be reprocessed or disposed of
Industrial Plastic: waste is generated by various industrial consumers.
Post consumer Plastic: waste is generated by the consumer.
Nuisance Plastic: Wastes are those that cannot be processed under the existing knowledge and technology.

Scrap Plastic: Waste is generated by fabricators or converters and can be re-processed. Waste plastics are recycled by four methods viz. primary recycling, secondary recycling, tertiary recycling and quaternary recycling is the processing of scrap plastics in to same or similar types of products of scrap plastics in to plastic goods with less demanding properties. In case the plastic wastes does not possess requisite quantity; tertiary processing of the waste done to recover chemicals. Unrecyclable waste is finally converted in to energy under controlled conditions.

Fig-1 shows the flow of plastic waste, most of the plastic wastes generated by the resin manufacturer, compounder, fabricator, converter, distributor and recyclers. The consumer generates only nuisance plastics generated by industrial sectors in landfills or in incinerator.

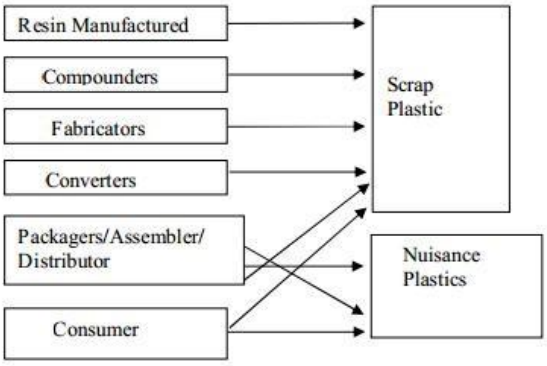

Fig. 1: Sources of plastic waste

4. INCORRECT PLACE FOR PLASTIC WASTE

Due to ignorance of the people, the plastic waste that can be a source of resources were thrown at wrong places which is responsible for pollution of environment and creates problem to the health of human beings living around those places [5]. It is also hazardous to the animals. Indiscriminate throwing of plastic cause accidental ingestion by the animals, that causes blockage of the digestive system, leads to bloat even death. The plastic waste causes landfill and incineration. Here are some self explanatory figures of waste and the plastics [6]

Fig. 2: Plastic waste at wrong places

Fig. 3: Plastic waste at wrong places

Fig. 4: Plastic eaten by animals

5. PLASTIC WASTES AS RESOURCES

a) The reprocesses will use the pallets for manufacturing.
b) Plastic wastes can be used for energy generation.
c) Plastic wastes can be used for landfill.
d) Waste Plastic Oil as A Diesel Fuel in The Diesel Engine
e) It can be used for making road [7]

Among all the resources we will discuss about some.

5.1. PLASTIC WASTE FOR LANDFILL

20-25% of landfill weight is plastics. Landfills are most common way to dispose of Municipal Solid Waste (MSW) in the US, with an overall increase in MSW consistent with increases in the population.

Plastics made up only 1% of MSW in 1960. This has increased to 12% (30 million tons) in 2008. 43% of this is containers and packaging, 22% is nondurable goods, and 35% is from durable goods. This means that 11.3 million tons of just containers and packaging end up in landfills each year.

Most people agree that recycling is a preferred method of dealing with plastics. However, only 24% of municipal waste is recycled and 9% is composted, for a total of only 33% of waste that is recovered.

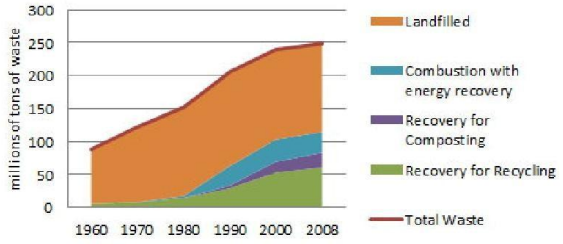

Fig. 5: Plastic waste in different stages

5.2. PLASTIC OIL IN DIESEL ENGINE

There are two series of waste plastic cracking. The first series of polymer cracking experiments was carried out in a glass reactor at atmospheric pressure and in a temperature range 350-420°C, the second one in autoclaves under hydrogen pressure (~3-5MPa) in temperature range 380-440°C. The application of catalyst results in lowering of polymers cracking temperature, density of obtained liquid and increased the gas fuel yield. The main problems with the use of neat plastics oil in diesel engines are high smoke levels and relatively low thermal efficiency due to high viscosity and carbon residue as compared to diesel[9]. But it is concluded that the engine performance is Good.

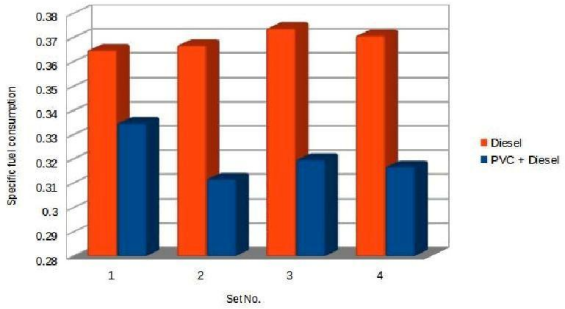

Fig. 6: Comparison of specific fuel consumption

In this above bar chart it is showned that the rate of fuel consumption of PVC+Disel fuel is less than the pure Disel. And further more in the bar chart which is shown in below showed that the thermal efficiency of PVC+Disel fuel is more than pure Disel. So it will be a great opportunity to make the plastic waste as a good fuel mixture known as plastic oil.

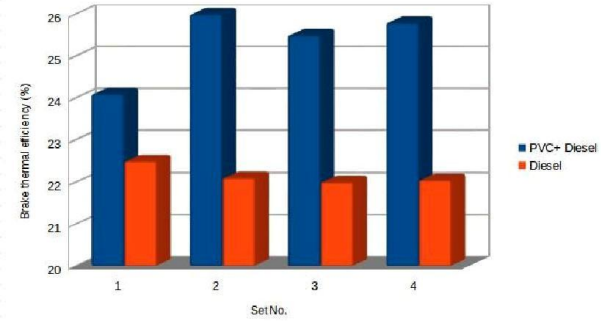

Fig. 7: Comparison of Brake thermal efficiency

In this regard Senthilkumar Tamilkolundu et al.[3] investigated Total Fuel Consumption (TFC), Brake Power (BP), Specific Fuel Consumption (SFC) and BT) for PVC/diesel oil Brake Thermal Efficiency.

5.3. PLASTIC WASTE FOR MAKING ROAD

UNEP has developed a programme on integrated solid waste management to support capacity building and technology transfer [7]. In order to contain this problem experiments have been carried out whether this waste plastic can be reused productively in the construction of roads [8]. The experimentation at several institutes indicated that the waste plastic, when added to hot aggregate will form a fine coat of plastic over the aggregate and such aggregate, when mixed with the binder is found to give higher strength, higher resistance to water and better performance over a period of time.

Fig. 8: Plastic waste road

Fig. 9: Plastic waste road in Bangalore

6. CONCLUSION

In the full paper we discuss about the sources and incorrect places of plastic wastes, also mentioned the application area of plastic waste. By the proper utilization of plastic waste in the mentioned area we can hope for a green environment. Now a day's plastic waste is a common phenomenon in our daily life. If we can properly utilize this waste & make them as a handy one then we can save our nature as well as we can be benefitted economically. In fine we can say that Bangladesh is one of the wasteful countries so the proper authority should have the necessary steps for waste minimization for this point of view this papers information will be beneficiary one.

7. REFERENCES

[1]. Dr. V. Vasudevan, TEC, Madurai, and CRRI, New Delhi

[2]. Appea A. K., Al-Qadi, I. L., Bhutta, S. A., and Coree, B. J., "Quantitative Assessment of Transmission Layer in Flexible Pavements," 77Th Transportation Research Board, Paper No. 980994, Washington, DC, 1998.

[3]. Senthilkumar Tamilkolundu et al. The Evaluation of blend of Waste Plastic Oil-Diesel fuel for use as alternate fuel for transportation. 2nd International Conference on Chemical, Ecology andEnvironmental Sciences (ICCEES'2012) Singapore April 28-29, 2012.

[4]. D. Ashutosh, Tewari A., M. K. Chaturvedi, "Plastic waste and its recycling", VSRD Technical and Non Technical Journal, Vol-I(1), 2000, 30-34

[5]. IRC, "Guidelines for the Design of flexible pavements," IRC: 37-1970, Indian Roads Congress.

[6]. Battiato, G., and Verga, C., "The AGIP Visco elastic Method For Asphalt Pavement Design," Proceedings of The Fifth International Conference On The Structural Design Of Asphalt Pavements, Netherlands, August 23-26 1982 pp.59-66.

[7]. Barksdale, R. D., Brown, S. F., and Francis, C., "Potential Benefits of Geosynthetics in Flexible Pavement Systems," National Cooperative Highway Research Program, Report No. 315, Transportation Research Board, Washington, D. C. 1989.

[8]. ISI, "Indian Standards Specifications for Roads Tar", IS: 215, Indian Standard Institution

[9]. M. Mani. Et al. characterization and effect of using waste plastic oil and diesel fuel blends in compression ignition engine. Energy36 (2011), 212-219

ICMIEE-PI-140296

An Adaptive Mesh Refinement Scheme for the Solution of Mixed-Boundary Value Problems

A. I. Khan[1,], Abdus Salam Akanda[1] and Asma Akhter[2]*
[1]Department of Mechanical Engineering, BUET, Dhaka-1000, BANGLADESH
[2]Department of Industrial Engineering and Management, KUET, Khulna-9203, Bangladesh

ABSTRACT
Some numerical simulations of multi-scale physical phenomena consume a significant amount of computational resources, since their domains are discretized on high resolution of meshes. An enormous wastage of these resources occurs in refinement of sections of the domain where computation of the solution does not require high resolutions. This problem is effectively addressed by adaptive mesh refinement (AMR), a technique of local refinement of a mesh only in sections where needed, thus allowing concentration of effort where it is required. Sections of the domain needing high resolution are generally determined by means of a criterion which may vary depending on the nature of the problem. Fairly straightforward criteria could include comparing the solution to a threshold or the gradient of a solution, that is, its local rate of change to a threshold. The objective of this paper is to develop an adaptive mesh refinement algorithm for finite difference scheme using potential function approach of fourth order bi-harmonic partial differential equation. In the AMR algorithm developed, a mesh of increasingly fine resolution permits high resolution computation in sub-domains of interest and low resolution in others. Then, the AMR scheme has been applied to solve a mixed boundary value elastic problem. In this work, the gradient of the solution has been considered as the criterion determining the regions of the domain needing refinement. Also the same problem is solved by classical Finite Difference Method (FDM) approach which uses uniform mesh over the whole numerical field. Finally, the solutions of both methods are presented as a comparative study to visualize the superiority of adaptive mesh refinement FDM technique over classical FDM technique. This analysis of superiority is done on basis comparison of solutions of both techniques with well known published results.

Keywords: Adaptive mesh refinement; Potential function approach, Classical finite difference method.

1. Introduction

Elasticity is now a classical subject and its problems are even more classical. But somehow these stress analysis problems are still suffering from a lot of shortcomings. Two factors may really be responsible for it. Both these factors involve management of the boundary of elastic problems: one is the boundary conditions and other is the boundary shape. There are various methods available for the solution of partial differential equations, which are needed for the stress analysis of structures. The FDM is one of the oldest numerical methods known for solving PDE's. The difference equations that are used to model governing equations in FDM are very simple to computer code and the global coefficient matrix that is produced by FDM possesses a banded structure, which is very effective for good solution. In spite of these characteristics, the necessity of the management of boundary shape has lead to the invention of the FEM and it's over whelming popularity, specifically because of the side by side development of high power computer machines. Of course, the adaptations of the FEM relieved us from our major inability of managing odd boundary shapes but we are constantly aware of its lack of sophistication and doubtful quality of the solutions so obtained. That is why FDM is chosen as solving method over FEM. There is present another factor of impediment to quality solutions of elastic problems is the treatment of the transition in boundary conditions. Several attempts were made to overcome both these two difficulties faced in the management of boundaries by FDM [1-2] and successfully overcome against these difficulties. But, using these [1-2] procedures, FDM simulations of some multi-scale physical phenomenon consumes a significant amount of computational efforts and resources because their domain are discretized on high resolution of meshes to achieve a good solution. To reduce the computational efforts and resources, several adaptive mesh refinement algorithms [3-14] have been developed over the last thirty years. But all such studies have limited application of solving the problems of either heat transfer or fluid mechanics. Moreover, the governing equation for the problems is either second order or lower. Mesh refinement is desirable to improve spatial solution. However, the uniform mesh refinement is not perfect for the applications of which the solution may need different resolutions for different regions. For example, for the mixed-boundary value problems, fine resolution is typically required for regions boundary. But for the evolving stress analysis of elastic fields with complicated structures, AMR techniques are more preferred to locally increase mesh densities in the

* Corresponding author. Tel.: +88-01672122179
E-mail address: a.islam117@gmail.com

regions of interest, thus saving the computer resources. The strategies of AMR can fall into two categories from the viewpoint of way of multi-resolution fulfilled. The first category includes these adaptive algorithms involved local mesh/stencil refinement. In these algorithms, either the existing mesh is split into several smaller cells or additional nodes are inserted locally, thus obtained the *h*-refinement. This group can be further categorized by the mesh type, i.e. hierarchical structured grid approach [3, 5-6] and unstructured mesh refinement approach [4]. The second category of adaptive algorithms involves global mesh redistribution. These methods move the mesh pint inside the domain in order to better capture the dynamic changes of solution and usually referred as moving mesh method or *r*-refinement [12-14] and at present, this category has application in FEM only. In this paper, AMR technique of fourth order bi-harmonic PDE is developed based on *h*-refinement by splitting the existing mesh into smaller cells. This approach is established on regular Cartesian meshes and at fine/coarse cell interfaces, special treatment is required for the communications between the meshes at different levels [15].

2. Governing Equations

Stress analysis in an elastic body is usually a three dimensional problem. But in most cases, the stress analysis of three-dimensional bodies can easily be treated as two-dimensional problem, because most of the practical problems are often found to conform to the states of plane stress or plane strain. In case of the absence of body forces, the equations governing the three stress components σ_x, σ_y and σ_{xy} under the states of plane stress or plane strain are:

$$\frac{\partial \sigma_x}{\partial x} + \frac{\partial \sigma_{xy}}{\partial y} = 0 \quad (1)$$

$$\frac{\partial \sigma_y}{\partial y} + \frac{\partial \sigma_{xy}}{\partial x} = 0 \quad (2)$$

$$\left(\frac{\partial^2}{\partial x^2} + \frac{\partial^2}{\partial y^2}\right)(\sigma_x + \sigma_y) = 0 \quad (3)$$

Substitution of the stress components in Eq.(1-3) by their relations with the displacement components u and v make Eq.(3) redundant and transform Eq.(1) and (2) to

$$\frac{\partial^2 u}{\partial x^2} + \left(\frac{1-\mu}{2}\right)\frac{\partial^2 u}{\partial y^2} + \left(\frac{1+\mu}{2}\right)\frac{\partial^2 v}{\partial x.\partial y} = 0 \quad (4)$$

$$\frac{\partial^2 v}{\partial y^2} + \left(\frac{1-\mu}{2}\right)\frac{\partial^2 v}{\partial x^2} + \left(\frac{1+\mu}{2}\right)\frac{\partial^2 u}{\partial x.\partial y} = 0 \quad (5)$$

The problem thus reduces to finding u and v in a two dimensional field satisfying the two elliptic partial differential Eq.(4) and (5). Further the problem is reduced to the determination of a single function ψ instead of two functions u and v, simultaneously, satisfying the equilibrium Eq.(4) and (5) [9-10]. In this formulation, as in the case of Airy's stress function φ [7], a potential function $\psi(x,y)$ is defined in terms of displacement components as

$$u = \frac{\partial^2 \psi}{\partial x.\partial y} \quad (6)$$

$$v = -\left[\left(\frac{1-\mu}{1+\mu}\right)\frac{\partial^2 \psi}{\partial y^2} + \left(\frac{2}{1+\mu}\right)\frac{\partial^2 \psi}{\partial x^2}\right] \quad (7)$$

When the displacement components in the Eq.(4) and (5) are substituted by Eq.(6) and (7), Eq.(4) is automatically satisfied and the condition that ψ has to satisfy becomes

$$\frac{\partial^4 \psi}{\partial x^4} + 2\frac{\partial^4 \psi}{\partial x^2.\partial y^2} + \frac{\partial^4 \psi}{\partial y^4} = 0 \quad (8)$$

Therefore, the problem is now formulated in such a fashion that a single function ψ has to be evaluated from bi-harmonic Eq.(8), satisfying the boundary conditions specified at the boundary.

2.1 General Boundary Condition

The boundary conditions at any point on an arbitrary shaped boundary are known in terms of the normal and tangential components of displacement, u_n and u_t and of stress σ_n and σ_t. These four components are expressed in terms of u, v, σ_x, σ_y, σ_{xy}, the components of displacement and stress with respect to the reference axes x and y of the body as follows:

$$u_n = u.l + v.m \quad (9)$$

$$u_t = v.l - u.m \quad (10)$$

$$\sigma_n = \sigma_x.l^2 + \sigma_y.m^2 + 2\sigma_{xy}.l.m \quad (11)$$

$$\sigma_t = \sigma_{xy}.(l^2 - m^2) + (\sigma_y - \sigma_x).l\,m \quad (12)$$

The boundary conditions at any point on the boundary are specified in terms of any two known values of u_n, u_t, σ_n and σ_t. In order to solve the mixed boundary-value problems of irregular-shaped bodies using present formulation, the boundary conditions are required to be expressed in terms of ψ. This can be done substituting the following expressions of the components of displacement and stress into Eq.(9) to (12).

$$u = \frac{\partial^2 \psi}{\partial x.\partial y} \quad (13)$$

$$v = -\left[\left(\frac{1-\mu}{1+\mu}\right)\frac{\partial^2 \psi}{\partial y^2} + \left(\frac{2}{1+\mu}\right)\frac{\partial^2 \psi}{\partial x^2}\right] \quad (14)$$

$$\sigma_x = \frac{E}{(1+\mu)^2}\left[\frac{\partial^3 \psi}{\partial x^2 \partial y} - \mu\frac{\partial^3 \psi}{\partial y^3}\right] \quad (15)$$

$$\sigma_y = -\frac{E}{(1+\mu)^2}\left[\frac{\partial^3 \psi}{\partial y^3} + (2+\mu)\frac{\partial^3 \psi}{\partial x^2 \partial y}\right] \quad (16)$$

$$\sigma_{xy} = \frac{E}{(1+\mu)^2}\left[\mu\frac{\partial^3\psi}{\partial x^2\partial y} - \frac{\partial^3\psi}{\partial x^3}\right] \quad (17)$$

It is evident from the expressions of boundary conditions Eq.(9) to (12) that no matter what combinations of two conditions are specified on the boundary, the whole range of conditions that ψ has to satisfy Eq.(8) within the body and any two of the Eq.(9) to (12) at points on the boundary can be expressed as finite difference equations in terms of ψ(x,y).

2.2 Model Problem and its Boundary Conditions

A model problem chosen for this study is shown in Fig. 1. It is simple plate with an embedded crack at center of the plate. The length a/b=1, while crack length is one fourth of 'a' or 'b'. The boundary conditions are expressed in terms of stresses and displacement in normal and tangential directions. The problem treated here is, therefore, obviously a two dimensional problem with mixed boundary conditions. Due to the material and loading symmetry only right half section is taken for analysis. The top and bottom edge is free and thus obvious σ_x, σ_{xy}=0. At the right edge there is present a normal tensile stress thus σ_y =P=2e^{-4} and σ_{xy}=0. And at the left edge, σ_{xy}=0 and v=0 except crack position where σ_y =0 and σ_{xy}=0. Here, the stress components are normalized by the young modulus, E (e.g. $\sigma_y=\sigma_o/E$). For this problem the Poisson's ratio is taken as μ=0.3.

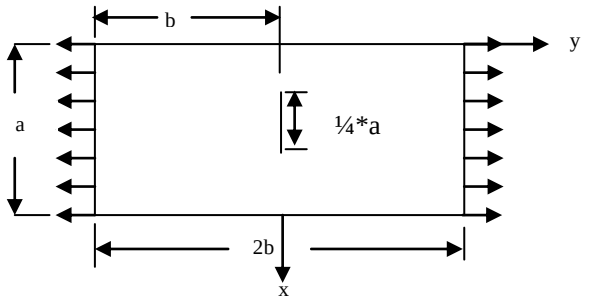

a) Physical problem.

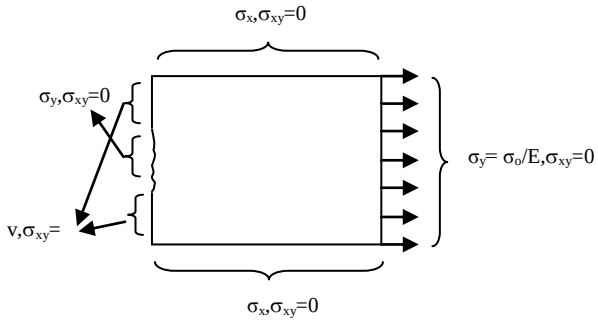

b) Right half section with boundary conditions.

Fig.1 Physical geometry of the elastic problem and its boundary conditions.

3. Solution of the Problem

For the solution of the problem, a two dimensional mesh is generated based on rectangular coordinate system. The function ψ from the governing Eq.(8) is evaluated at various mesh points inside the body using central difference formula. The function ψ from the boundary conditions is evaluated in the same manner by forward and backward difference formula at the boundary points depending on the physical boundary. A FORTRAN code has been developed to investigate various aspect of the problem. The full procedure of the management of boundary conditions has already been discussed in the papers [17-18]. But that procedure gives better result when the meshes are discretized base on uniform grid throughout the domain. Under AMR technique, for this particular problem the domain is discretized as follows [fig.2]. Uder classical FDM there is only one sizes mesh of length h_i and k_i in direction x- and y- respectively, whereas, the AMR technique has three different size of mesh. The high resolution of meshes under AMR technique is taken in the vicinity of the crack. Here, in this thesis the discretization is done by such a way that both methods have almost equal no. of nodal points. To satisfy governing equation and boundary condition over the whole field, some new stencils of governing equation and boundary conditions have been developed. The details of applications procedure of these stencils is given in [15].

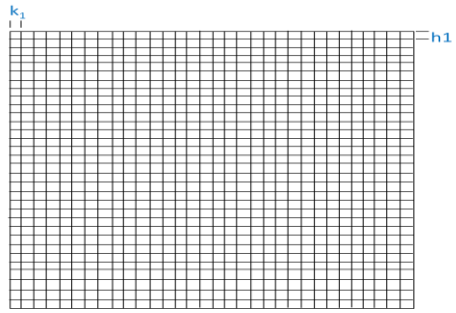

a) Discretization under Classical FDM.

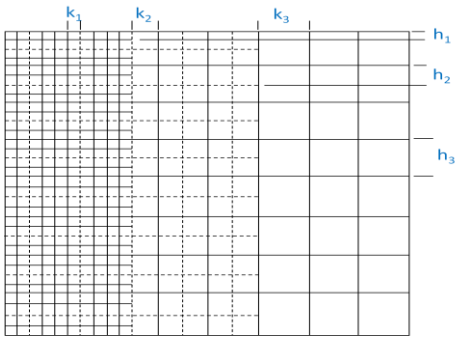

b) Discretization under AMR technique.

Fig.2 Discertization of the domain under classical FDM and AMR technique.

4. Results and Discussions

Following the procedure stated above and taking mesh size 0.0167 unit for classical FDM and for AMR that is taken as 0.0083 for smallest mesh, 0.0167 for medium mesh and 0.033 for largest mesh [fig.2], results are obtained by both classical FDM and AMR technique of half section of the problem. In fig.3 displacement in x-direction is shown for two section namely y/b=0.0 and 1.00, and it shows that displacement obtained by both methods is same. But at the tip of the crack, the AMR technique gives better results than classical FDM due to high resolution. In fig.3 displacement in y-direction is shown for two sections and shows that results are almost same, although, AMR shows a smaller value than classical FDM. But the deviation is not very much significant. From this study, it can be concluded that the AMR technique has no improvement of results over classical FDM in terms of displacement of the model.

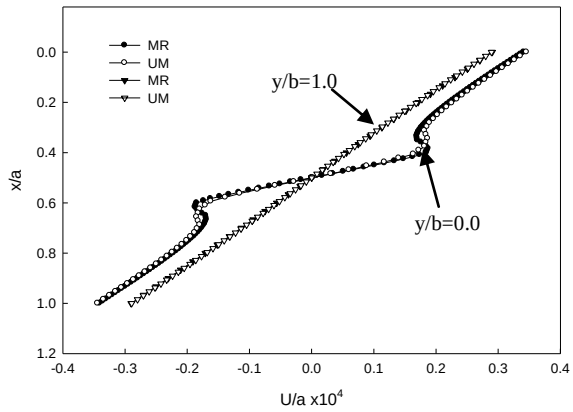

Fig.3 Comparison of the results for normalized displacement (U/a) obtained by mesh refinement (MR) technique and uniform mesh (UM) technique with almost equal no. of nodal points.

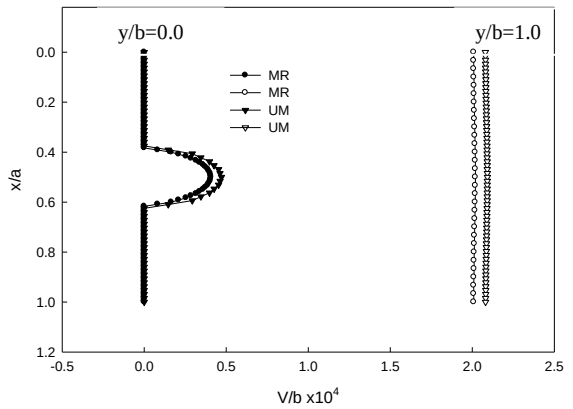

Fig.4 Comparison of the results for normalized displacement (V/b) obtained by MR technique and UM technique with almost same no. of nodal points.

The most significant component of stresses of this problem is stress in y-direction i.e. σy, which is shown in fig.5. From this graph it is seen that for almost equal no. of nodal points the AMR technique gives a higher value of σ_y than classical FDM. A validation of these results can be shown as follows. Analytical solution of this considered problem is given in literature [19]. Consider a mode I crack of length 2*a* in the infinite plate of Fig.6. By using complex stress functions, it has been shown that the stress field on a *dx dy* element in the vicinity of the crack tip is given by

$$\sigma_y = \sigma\sqrt{\frac{a}{2r}}\cos\frac{\theta}{2}\left(1+\sin\frac{\theta}{2}\sin\frac{3\theta}{2}\right) \qquad (18)$$

This equation tells that at the tip of the crack i.e. at r=0 and θ=0 the value of stress should be infinite. But for our case, it is seen that [fig.5] the stress is finite value and in classical method, it is only 2.25 times of applied stress ($\sigma_y/E= 2e^{-4}$) and in AMR technique, it is 3.5 times of the applied stress. An explanation of this phenomenon can be given as, in FDM method; it is never possible to take a node at the tip of the crack, because one always stays behind the tip of the crack by a distance of half mesh length. By taking r=0.5* mesh length and θ=0 from eq.18, it is found that the stress value should be 3.74 times of the applied stress and this is very close to the results of AMR technique. So it is verified that AMR technique is better than classical FDM for the solution of problems which required different level of resolution at different region of the problem. The comparison of results for σ_y at other section of the plate is shown in fig.7 and it is seen that, at other section results is almost same in both methods. The comparison of stress component in x-direction is shown in fig.8 and it is seen that in AMR technique results is higher than that of classical FDM.

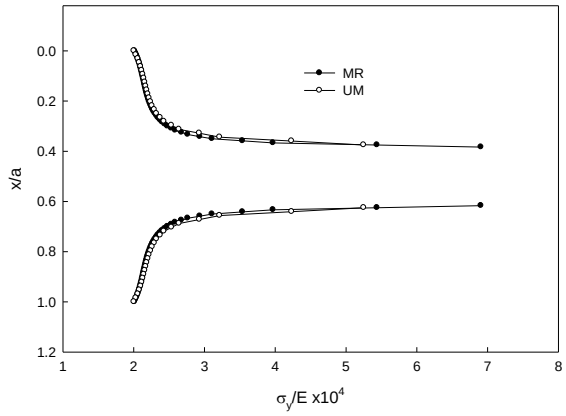

Fig.5 Comparison of the results for normalized normal stress (σ_y/E) obtained by MR technique and UM technique with almost equal no. of nodal points.

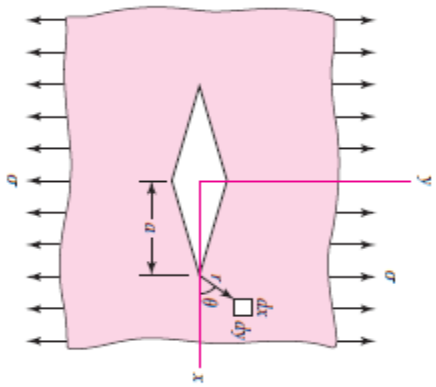

Fig.6 Plate with embedded crack under uniform tension.

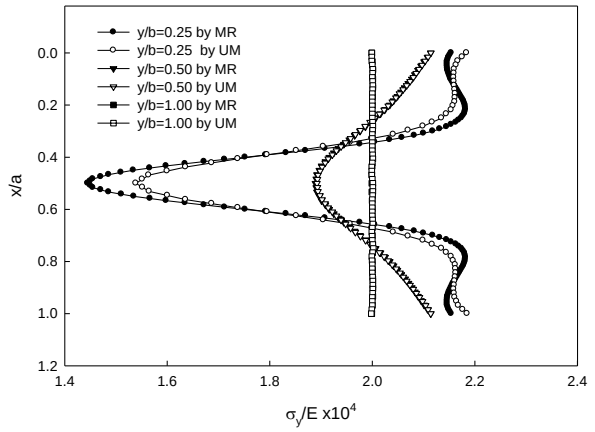

Fig.7 Comparison of the results for normalized normal stress (σ_y/E) obtained by MR technique and UM technique at different section of plate.

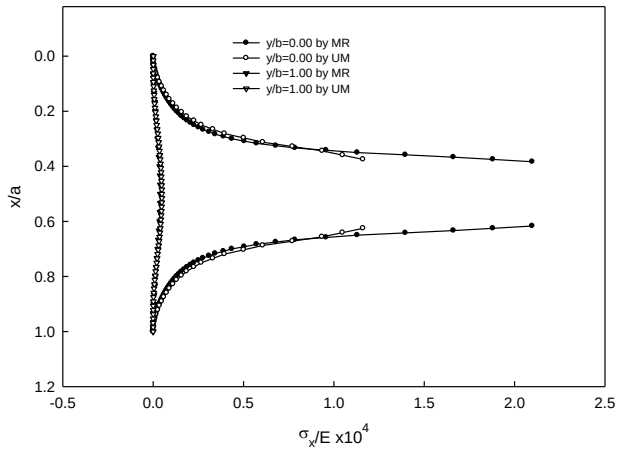

Fig.8 Comparison of the results for normalized normal stress (σ_x/E) obtained by MR technique and UM technique with almost equal no. of nodal points.

5. Conclusions

The adaptive mesh refinement technique, for the problem which need different resolution at different region of the domain, described here in this paper is already proven to be advantageous over conventional finer mesh generation technique of the finite difference method. Redistribution of nodes in AMR technique improves the accuracy of the solutions near stress concentration zone. The AMR technique requires a lesser amount of computational memory due to lesser number of unknown parameters. Thus the AMR technique could be a strongest weapon to solve problem which cannot be solved by uniform mesh generation technique due to memory shortage of computational resources.

NOMENCLATURE

E : Modulus of Elasticity, GPa
μ : Poisson ratio
ψ : Displacement potential function
σ_x : Normal stress component along x-direction
σ_y : Normal stress component along y-direction
σ_{xy} : Shear stress component in the xy plane
σ_n : Stress component normal to boundary
σ_t : Stress component tangential to boundary
u : Displacement component along x-direction
v : Displacement component along y-direction
l, m : Direction cosine of the normal at any physical boundary point
u_n : Displacement component normal to boundary
u_t : Displacement component tangential to boundary

REFERENCES

[1] Akanda, M. A. S., Ahmed, S.R., Khan, M. R., and Uddin, M. W., "A finite-difference scheme for mixed boundary-value problems of arbitrary shaped elastic bodies", Advances in Engineering Software, 31(2000), No. 3, 173-184.

[2] Akanda, M. A. S., Ahmed, S.R. and Uddin, M. W., "Stress analysis of gear teeth using displacement potential function and finite-differences", International Journal for Numerical Methods in Engineering, 53(2001), No. 7, 1629-1649.

[3] M.J. Berger, J. Oliger, Adaptive mesh refinement for hyperbolic partial differential equations, J. Comput. Phys. 53 (1984) 484–512.

[4] J.Z. Zhu, O.C. Zienkiewicz, Adaptive techniques in the finite element method, Commun. Appl. Numer. Meth. Vol. 4 pp. 197–204 (1988).

[5] Berger M. and Colella P., "Local adaptive mesh refinement for shock hydrodynamics". - J. Comput. Phys., vol. 82, pp. 64-84, (1989).

[6] J.O. Dow, I. Stevenson, Adaptive refinement procedure for the finite difference method, Numer. Meth. PDEs, vol. 8 pp 537-550 (1992).
[7] M.J. Berger, R. LeVeque, Adaptive mesh refinement for two-dimensional hyperbolic systems and the AMRCLAW software, SIAM J. Numer. Anal. 35 2298–2316 (1998).
[8] Johansen H. and Colella P., "A Cartesian grid embedded boundary method for poisson's equation on irregular grids". – J. Comput. Phys., vol. 147, pp. 60-85,(1998).
[9] Ceniceros H. D. and Roma A. M., "Study of long-time dynamics of a viscous vortex sheet with a fully adaptive non-stiff method". – J. Comput. Phys., vol. 16, No.12, pp. 4285-4318, 2004.
[10] McCorquodale P., Colella P., Grote D. and Vay J. L., "A node-centered local refinement algorithm for poisson's equation in complex geometries". – J. Comput. Phys., vol. 201, pp. 34-60, (2004).
[11] L.K. Bieniasz, Experiments with a local adaptive grid *h*-refinement for FDM solution of BVPs in singularity perturbed second-order ODEs, vol. 195 pp. 196-219(2008).
[12] T. Basebi, R.M. Thomas, A study of moving mesh methods applied to a thin flame propagating in a detonator delay element, Comput. Math. Appl. 45 131–163 (2003).
[13] E.D. Wilkes, S.D. Phillips, O.A. Basaran, Computational and experimental analysis of dynamics of drop formation, Phys. Fluids 11(12) (1999) 3577–3598.
[14] D.M Greaves, A.G.L. Borthwick, G.X. Wu, R.E. Taylor, A moving boundary finite element method for fully nonlinear wave simulations, J. Ship Res. 41 181–194(1997).
[15] A. I. Khan, a local mesh refinement scheme for finite difference solution of mixed boundary-value elastic problems, M. Sc. Thesis, Bangladesh University of Engineering and Technology, Bangladesh, (2014).
[16] Uddin, M. W., "Finite difference solution of two dimensional elastic problems with mixed boundary conditions", M. Sc. Thesis, Carleton University, Canada, (1966).
[17] Akanda, M. A. S., Ahmed, S.R., Khan, M. R., and Uddin, M. W., "A finite-difference scheme for mixed boundary-value problems of arbitrary-shaped elastic bodies", Adv. in Engg. Soft, Vol. 31, No. 3, pp. 173-184, (2000).
[18] Akanda, M. A. S., Ahmed, S.R. and Uddin, M. W., "Stress analysis of gear teeth using displacement potential function and finite-differences", Int. J. Numer. Math. in Engg., Vol-53, No. 7, pp 1629-1649, (2002).
[19] Richard G. Budynas, J. Keith Nisbett, Shigley's mechanical engineering design, ninth edition, McGraw-Hill Book Company Inc., New York, 2008 pp-242.

ICMIEE-PI-140299

Effects of Radiation on Unsteady MHD Boundary Layer Flow about an Inclined Porous Stretching Sheet with Variable Thermal Conductivity

Mohammad Shah Alam[1], *Mohammad Ali*[*2]
[1,2] Department of Mathematics, Chittagong University of Engineering & Technology, Chittagong-4349, BANGLADESH

ABSTRACT
The goal of this study is to investigate the effects of radiation on unsteady MHD boundary layer flow of an incompressible, electrically conducting and viscous fluid about an inclined stretching sheet with variable thermal conductivity embedded in porous medium. The flow is considered under the influence of a stretching velocity and a uniform magnetic field. The governing partial differential equations are transformed into ordinary differential equations by using similarity transformation and stretching variable. The governing momentum boundary layer, thermal boundary layer and concentration boundary layer equations with the boundary conditions are transformed into a system of first order ordinary differential equations which are then solved numerically by using Runge-Kutta fourth-fifth order method along with shooting technique. The effects of the flow parameters on the velocity, temperature and species concentration are computed, discussed and have been graphically represented in figures and also the shearing stress and rate of heat transfer are shown in table for various values of different parameters. The results presented graphically illustrate that velocity field decrease due to increasing of Magnetic parameter, porosity parameter and unsteadiness parameter and reverse trend arises for the increasing values of stretching parameter but there is no effect of Radiation and perturbation parameter on velocity profile. The temperature field decreases for Magnetic parameter, porosity parameter but the temperature field increases for the increasing values of stretching parameter, unsteadiness parameter, radiation and perturbation parameter. Again, concentration profile decreases for increasing the values of Magnetic parameter, unsteadiness parameter, porosity parameter, radiation and perturbation parameter but concentration increases for increasing the values of stretching parameter. By considering the hot plate the numerical results for the skin friction and the local Nusselt number are compared with the results reported by other author when the magnetic field and modified Grashof number are absent. The present results in this paper are in good agreement with the work of the previous author.

Keywords: MHD; unsteadiness; stretching sheet; radiation; porosity

1. Introduction

Heat transfer in boundary layer over a stretching sheet has important applications in extrusion of plastic sheets, polymer, spinning of fibers, cooling of elastic sheets etc. The quality of final product depends on the rate of heat transfer as a result the cooling procedure has to be controlled effectively. The MHD boundary layer flow of heat and mass transfer problems about an stretching sheet have become in view of its significant applications in industrial manufacturing processes such as plasma studies, petroleum industries, Magneto-hydrodynamics power generator, cooling of Nuclear reactors, boundary layer control in aerodynamics, glass fiber production and paper production. The MHD flow in electrically conducting fluid can control the rate of cooling and the desired quality of product can be achieved. In this regard many investigators have studied the boundary layer flow of electrically conducting fluid, heat and mass transfer due to stretching sheet in presence of magnetic field. Accordingly, Elbashbeshy and Bazid [1] presented an exact similarity solution for unsteady momentum and heat transfer flow whose motion is caused solely by the linear stretching of a horizontal stretching surface, Alharbi et.al [2] studied heat and mass transfer in MHD visco-elastic fluid flow through a porous medium over a stretching sheet with chemical reaction, Seddeek and Abdel Meguid [3] analyzed the effects of radiation and thermal diffusivity on heat transfer over a stretching surface with variable heat flux , Ali et al. [4] studied the radiation and thermal diffusion effects on a steady MHD free convection heat and mass transfer flow past an inclined stretching sheet with Hall current and heat generation, Ibrahim and Shanker [5] investigated the unsteady MHD boundary layer flow and heat transfer due to stretching sheet in the presence of heat source or sink by Quasi-linearization technique. Ishak et al. [6] investigated the solution to unsteady mixed convection boundary layer flow and heat transfer due to a stretching vertical surface. Further, Ishak [7] studied unsteady laminar MHD flow and heat transfer due to continuously stretching plate immersed in an electrically conducting fluid. Ebashbeshy and Aldawody [8] analyzed heat transfer over an unsteady stretching surface with variable heat flux in presence of heat source or sink, Fadzilah et al. [9] studied the steady MHD boundary layer flow and heat transfer of a viscous and electrically conducting fluid over a stretching sheet with an induced magnetic field. Also, Bachok et al. [10] analyzed the similarity solution of the unsteady laminar boundary of an incompressible micro-polar fluid and heat transfer due to a stretching sheet and Mohebujjaman et al. [11] studied MHD heat transfer mixed convection flow along a vertical stretching

* Corresponding author. Tel.: +88-01713109929
E-mail address: ali.mehidi93@gmail.com

sheet with heat generation using shooting technique. So the present work focused on unsteady MHD boundary layer flow of an incompressible, electrically conducting and viscous fluid about an inclined stretching sheet with variable thermal conductivity embedded in porous medium by Quasi-linearization technique.

2. Mathematical Formulation of the Problem and Similarity Analysis

Consider a two dimensional unsteady laminar MHD viscous incompressible electrically conducting fluid along an inclined stretching sheet with an acute angle (α) , *X*- direction is taken along the leading edge of the inclined stretching sheet and *Y* is normal to it and extends parallel to *X*-axis. A magnetic field of strength B_0 is introduced to the normal to the direction to the flow. The uniform plate temperature T_w ($>T_\infty$), where T_∞ is the temperature of the fluid far away from the plate. Let *u* and *v* be the velocity components along the *X* and *Y* axis respectively in the boundary layer region. Under the above assumptions and usual boundary layer approximation, the dimensional governing equations of continuity, momentum, concentration and energy under the influence of externally imposed magnetic field are:

Equation of continuity:

$$\frac{\partial u}{\partial x}+\frac{\partial v}{\partial y}=0 \tag{1}$$

Momentum equation:

$$\frac{\partial u}{\partial t}+u\frac{\partial u}{\partial x}+v\frac{\partial u}{\partial y}=-\frac{1}{\rho}\frac{\partial p}{\partial x}+\nu\frac{\partial^2 u}{\partial y^2}+ g\beta(T-T_\infty)\cos\alpha+g\beta^*(C-C_\infty)\cos\alpha - \frac{\sigma B_0^2 u}{\rho}-\frac{\nu}{K}u \tag{2}$$

Energy Equation:

$$\frac{\partial T}{\partial t}+u\frac{\partial T}{\partial x}+v\frac{\partial T}{\partial y}=\frac{\kappa}{\rho c_p}\frac{\partial^2 T}{\partial y^2}-\frac{\partial q_r}{\partial y} \tag{3}$$

Concentration Equation:

$$\frac{\partial C}{\partial t}+u\frac{\partial C}{\partial x}+v\frac{\partial C}{\partial y}=D_m\frac{\partial^2 C}{\partial y^2}+\frac{D_m K_T}{T_m}\frac{\partial^2 \mathrm{T}}{\partial \mathrm{y}^2} \tag{4}$$

Using free stream $u=U(x,t)=\dfrac{bx}{\sqrt{1-\gamma t}}$, we get

$$\frac{\partial U}{\partial t}+U\frac{\partial U}{\partial x}=-\frac{1}{\rho}\frac{\partial p}{\partial x}$$

Hence equation (2) becomes

$$\frac{\partial u}{\partial t}-\frac{\partial U}{\partial t}+u\frac{\partial u}{\partial x}+v\frac{\partial u}{\partial y}=U\frac{\partial U}{\partial x}+\nu\frac{\partial^2 u}{\partial y^2}+g\beta(T-T_\infty)\cos\alpha + g\beta^*(C-C_\infty)\cos\alpha-\frac{\sigma B_0^2(u-U)}{\rho}-\frac{\nu}{K}(u-U) \tag{5}$$

By using the Rosseland approximation, we have the radiative heat flux, $\mathrm{q_r}=-\dfrac{4\sigma^*}{3\mathrm{K_0}}\dfrac{\partial \mathrm{T}^4}{\partial \mathrm{y}}$ where σ^* is the Stefan-Boltzman constant, $\mathrm{K_0}$ is the Rosseland mean absorption coefficient. Assuming that, the difference in temperature within the flow are such that T^4 can be expressed as a linear combination of the temperatures. We expand T^4 in Taylors series about T_∞ as follows:

$T^4=T_\infty^4+4T_\infty^3(T-T_\infty)+6T_\infty^2(T-T_\infty)^2+\ldots\ldots$ and neglecting the higher order terms beyond the first degree in $(T-T_\infty)$; we have $T^4\approx -3T_\infty^4+4T_\infty^3T$.

Therefore $q_r=-\dfrac{16\sigma^*}{3K_0}T_\infty^3\dfrac{\partial T}{\partial y}$ .So the equation (3) becomes

$$\frac{\partial T}{\partial t}+u\frac{\partial T}{\partial x}+v\frac{\partial T}{\partial y}=\frac{\kappa}{\rho c_p}\frac{\partial^2 T}{\partial y^2}+\frac{16\sigma^*}{3K_0}T_\infty^3\frac{\partial^2 T}{\partial^2 y} \tag{6}$$

According to Arunachalam and Rajappa [15] and Chaim [16], the thermal conductivity is taken of the form $\kappa=\kappa^*(1+\varepsilon\theta)$, where u and v are the velocity components along x and y directions, *T*, T_w and T_∞ are the fluid temperature, the stretching sheet temperature and the free stream temperature respectively while C , C_w and C_∞ are the corresponding concentrations, κ is the variable thermal conductivity of the fluid, κ^* is the thermal conductivity of the fluid, *K* is the permeability of the porous medium, C_p specific heat with constant pressure, α is the angle of inclination , γ is the constant, μ is the coefficient of viscosity, ν is the kinematic viscosity , ε is the perturbation, σ is the electrical conductivity, ρ is the fluid density, β is the thermal expansion coefficient, β* is the concentration expansion coefficient, B_0 is the magnetic field intensity, *U* is the free steam velocity, *g* is the acceleration due to gravity, D_m is the coefficient of mass diffusivity, T_m is the mean fluid temperature, K_T is the thermal diffusion ratio respectively. The above equations are subject to the following boundary conditions:

$$u=u_w,\ v=0,\ T=T_w, C=C_w \quad at\ \ y=0$$
$$u=U, T=T_\infty, C=C_\infty \quad as\ \ y\to\infty \tag{7}$$

The velocity of the sheet $u_w(x,t)$, the surface temperature of the sheet $T_w(x,t)$, concentration $C_w(x,t)$, and the transverse magnetic field strength $B(t)$ are respectively defined as follows:

$$u_w = \frac{ax}{\sqrt{1-\gamma t}}, T_w - T_\infty = \frac{bx}{\sqrt{1-\gamma t}}, C_w - C_\infty = \frac{cx}{\sqrt{1-\gamma t}},$$

$$B(t) = \frac{B_0}{\sqrt{1-\gamma t}}$$

where, a is the stretching rate and b, c are positive constant with dimension (time)-1. We introduce the steam function $\psi(x,y)$ as defined by $u = \frac{\partial \psi}{\partial y}$ and $v = -\frac{\partial \psi}{\partial x}$.

To convert the governing equations into a set of similarity equations, we introduce the following similarity transformation:

$$\psi = x\sqrt{\frac{av}{1-\gamma t}}\, f(\eta), \eta = \sqrt{\frac{a}{v(1-\gamma t)}}\, y, \theta(\eta) = \frac{T - T_\infty}{T_w - T_\infty},$$

$$\varphi(\eta) = \frac{C - C_\infty}{C_w - C_\infty}$$

From the above transformations, the non-dimensional, nonlinear and coupled ordinary differential equations are obtained as follows:

$$f''' + ff'' - f'^2 - A\left(f' + \frac{1}{2}f''\right) - (M+N)f' + Gr\theta\cos\alpha + Gm\varphi\cos\alpha + \frac{1}{2}A\lambda + \lambda^2 = 0 \quad (8)$$

$$(1 + R\,\mathrm{Pr} + \varepsilon\theta)\theta'' + \mathrm{Pr}\, f\theta' - \frac{1}{2}\mathrm{Pr}\, A\eta\theta' = 0 \quad (9)$$

$$\varphi'' + Scf\varphi' - \frac{1}{2}ASc\eta\varphi' - S_0\theta'' = 0 \quad (10)$$

The transform boundary conditions:

$$f = 0\ f' = 1, \theta = \varphi = 1\ at\ \eta = 0,$$
$$f' = \lambda, \theta = \varphi = 0\ as\ \eta \to \infty \quad (11)$$

Where f', θ and φ are the dimensionless velocity, temperature and concentration respectively, η is the similarity variable, the prime denotes differentiation with respect to η. Also

$$M = \frac{\sigma B_0^2(1-\gamma t)}{\rho a}, N = \frac{v(1-\gamma t)}{Ka}, A = \frac{\gamma}{a},$$

$$\lambda = \frac{b\sqrt{(1-\gamma t)}}{a}, Gr = \frac{g\beta(T_w - T_\infty)(1-\gamma t)^2}{a^2 x},$$

$$Gm = \frac{g\beta^*(C_w - C_\infty)(1-\gamma t)^2}{a^2 x}, \mathrm{Pr} = \frac{\mu c_p}{\kappa^*},$$

$$Sc = \frac{v}{D_m}, R = \frac{16\sigma^* T_\infty^3}{3K_0}\ and\ S_0 = \frac{K_T(T_w - T_\infty)}{T_m(C_w - C_\infty)}$$

are the Magnetic parameter, porosity parameter, unsteadiness parameter, stretching ratio, Grashof number, modified Grashof number, Prandtl number, Schmidt number, Radiation parameter and Soret number respectively. The important physical quantities of this problem are skin friction coefficient C_f and the local Nusselt number Nu which are proportional to rate of velocity and rate of temperature respectively.

3. Methodology

The governing concentration boundary layer Eq. (4), momentum boundary layer Eq. (5) and thermal boundary layer Eq. (6) with the boundary conditions (7) are transformed into a system of first order ordinary differential equations which are then solved numerically by using Runge-Kutta fourth-fifth order method along with shooting iteration technique. First of all, the coupled ordinary differential Eq. (8) – Eq. (10) are third order in f and second order in θ and φ which have been reduced to a system of seven simultaneous ordinary differential equations for seven unknowns. For the purpose of numerically solve this system of equations using Runge-Kutta method, the solution requires seven initial conditions but two initial conditions in f, one initial condition in each of θ and φ are known. However, the values of f', θ and φ are known at $\eta \to \infty$. These end conditions are utilized to produce unknown initial conditions at $\eta \to 0$ by using shooting technique. The most important step of this scheme is to choose the appropriate finite value of η_∞. Thus to estimate the value of η_∞, we start with some initial guess value and solve the boundary value problem consisting of Eq. (8)– Eq.(10) to obtain $f''(0), \theta'(0)$ and $\varphi'(0)$. The solution process is repeated with another larger value of η_∞ until two successive values of $f''(0), \theta'(0)$ and $\varphi'(0)$ differ only after desired significant digit. The last value η_∞ is taken as the finite value of the limit for the particular set of physical parameters for determining velocity, temperature and concentration, respectively, are

$f(\eta), \theta(\eta)$ and $\varphi(\eta)$ in the boundary layer. After getting all the initial conditions we solve this system of simultaneous equations using fourth order Runge-Kutta integration scheme. The effects of the flow parameters on the velocity, temperature and species concentration, are computed, discussed and have been graphically represented in figures and also the shearing stress and rate of heat transfer shown in table for various value of different parameters. Now defining new variables by the equations

$$y_1 = f, y_2 = f', y_3 = f'', y_4 = \theta, y_5 = \theta', y_6 = \varphi,$$
$$y_7 = \varphi'$$

The higher order differential Eq. (8), Eq. (9), Eq.(10) and boundary conditions (11) may be transformed to seven equivalent first order differential equations and boundary conditions are as follows:

$$dy_1 = y_2, dy_2 = y_3, dy_3 = -y_1 y_3 + y_1^2 + (M+N)y_2 +$$
$$A\left(y_2 + \frac{1}{2}y_3\right) - \frac{A\lambda}{2} - \lambda^2 - Gr\cos\alpha\, y_4 - Gm\cos\alpha\, y_6,$$
$$dy_4 = y_5, dy_5 = \frac{-\Pr y_1 y_5}{1 + R\Pr + \varepsilon y_4} + \frac{\Pr A\eta\, y_5}{2(1 + R\Pr + \varepsilon y_4)},$$
$$dy_6 = y_7, dy_7 = -Sc\, y_1 y_7 + \frac{1}{2}ScA\eta\, y_7 + \frac{S_0 \Pr y_1 y_5}{1 + R\Pr + \varepsilon y_4}$$
$$- \frac{S_0 \Pr A\eta\, y_5}{2(1 + R\Pr + \varepsilon y_4)}$$

And the boundary conditions are

$$y_1 = 0, y_2 = 1, y_4 = 1, y_6 = 1 \quad at\ \eta = 0$$
$$y_2 = \lambda, y_4 = 0, y_6 = 0 \quad as \quad \eta \to \infty$$

4. Results and discussion

Numerical calculation for distribution of the velocity, temperature and concentration profiles across the boundary layer for different values of the parameters are carried out. For the purpose of our simulation we have chosen $\lambda = 0.1$, $M = 1.0$, $N = 0.6$, $A = 1.0$, $Gr = -0.2$, $Gm = -0.2$, $Sc = 0.22$, $Pr = 1.0$, $S0 = 0.2$, $\varepsilon = 1.0$, $R = 0.5$ and $\alpha = 60^o$ while the parameters are varied over range as shown in the figures. Fig.1 clearly demonstrates that the primary velocity starts from maximum value at the surface and then decreasing until it reaches to the minimum value at the end of the boundary layer for all the values *M*. It is interesting to note that the effect of magnetic field is more prominent at the point of peak value, because the presence of *M* in an electrically conducting fluid introduces a force like Lorentz force which acts against the flow if the magnetic field is applied in the normal direction as in the present problem. As a result velocity profile is decreased. Similar effect is also observed in Fig.2 and Fig.4 with increasing values of *N* and *A* and reverse trend arise for λ is shown in Fig.3 but there is no effect of *R* and ε which are shown in Fig.5 and Fig.6. Fig.7 – Fig.12 show the temperature profile obtained by the numerical simulations for various values of entering parameters. The temperature is decreased for the increasing effect of *M* and *N* but opposite effect arises for the values of λ, *R* and ε. From Fig.10 it is observed that the thermal boundary layer is increased up to certain values of η and then decreased for increasing values of A whereas the reverse trend is observed for the increasing values of *A*, *R* and ε in concentration profiles which are shown in Fig.16-Fig.18. Also, Fig.13 - Fig.18 show the concentration profiles obtained by the numerical simulation for various values of entering non-dimensional parameters. From Fig.13, and Fig.14, it is observed that the concentration profile decreases for the effect of *M* and *N* but reverse effect arises for the increasing values of λ [Fig.15]. Further the numerical solutions for the skin friction [$f''(0)$] and local Nusselt number [$-\theta'(0)$] have been compared with those of Pop et al. [12], Mahapatra and Gupta [13] and Sharma and Singh [14] when $M = 0$, $Gr = 0$, $Gm = 0$, $N = 0$, $A = 0$, $\alpha = 0$ and consider the Prandtl number $Pr = 0.05$, $R = 0.2$, $K = 2.0$, $\varepsilon = 1.0$. These results are given in Table1 and it is observed that the agreement between the present results and those of Pop et al. [12], Mahapatra and Gupta [13] and Sharma and Singh [14] are familiar.

4. Conclusions

Following are the conclusions made from above analysis:

- The magnitude of velocity decreases with increasing magnetic parameter causing of Lorentz force and similar effect is observed for porosity and unsteadiness parameter but reverse trend arise for stretching parameter.
- The temperature and concentration boundary layer are decreased for the effect of magnetic and porosity parameter and increased for stretching parameter.
- For the effect of Radiation and perturbation parameter, the temperature is increased but concentration decreased up to a certain value of η and then increased.
- For the effect of unsteadiness parameter, the temperature is increased up to a certain value of η and then decreased but opposite result is observed in concentration.

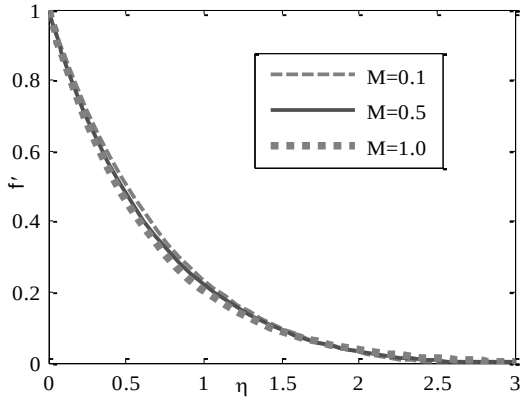

Fig.1 Velocity profile for various values of M

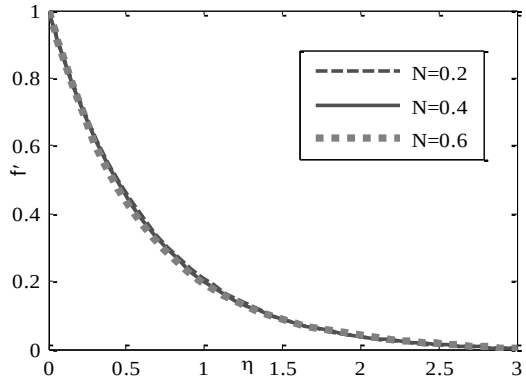

Fig.2 Velocity profile for various values of N

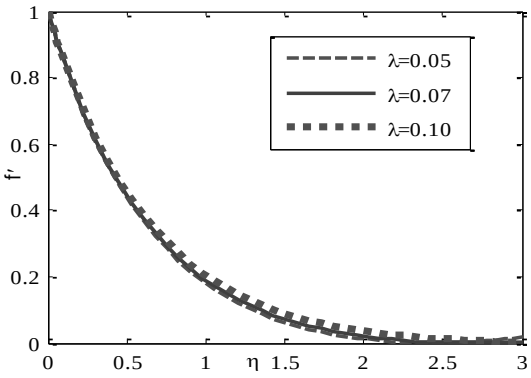

Fig.3 Velocity profile for various values of λ

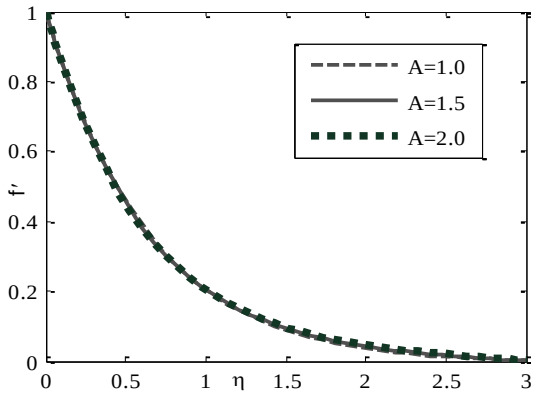

Fig.4 Velocity profile for various values of A

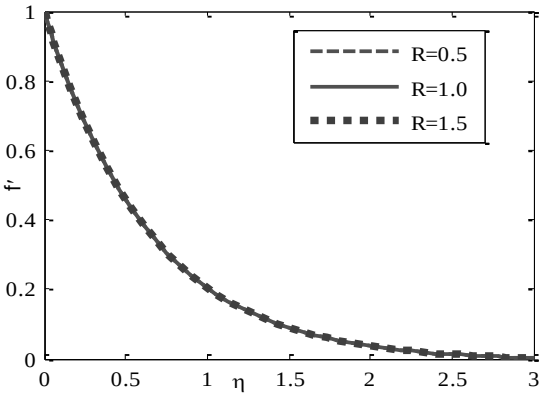

Fig.5 Velocity profile for various values of R

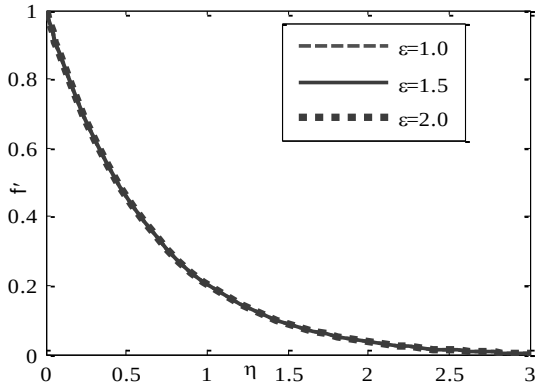

Fig.6 Velocity profile for various values of ε

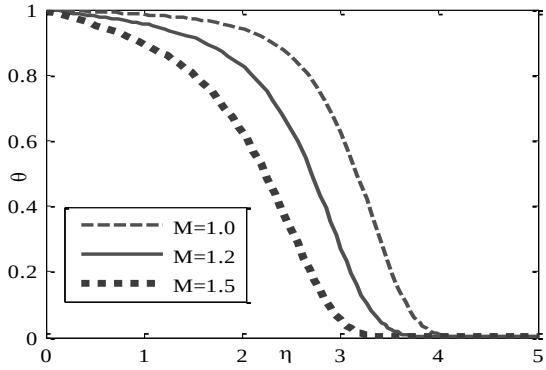

Fig.7 Temperature profile for various values of M

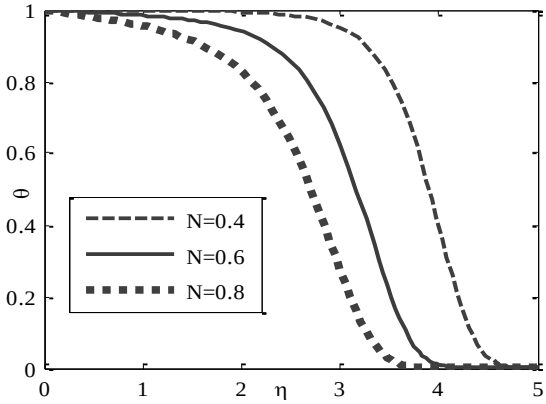

Fig.8 Temperature profile for various values of N

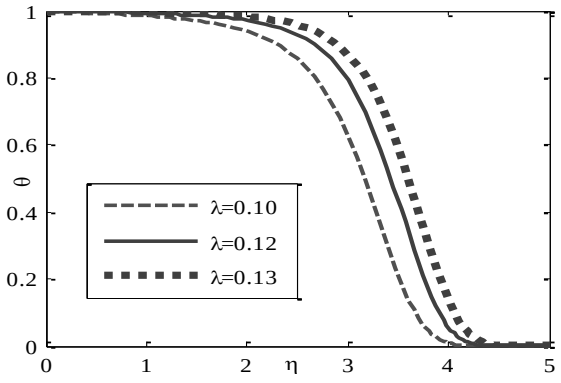

Fig.9 Temperature profile for various values of λ

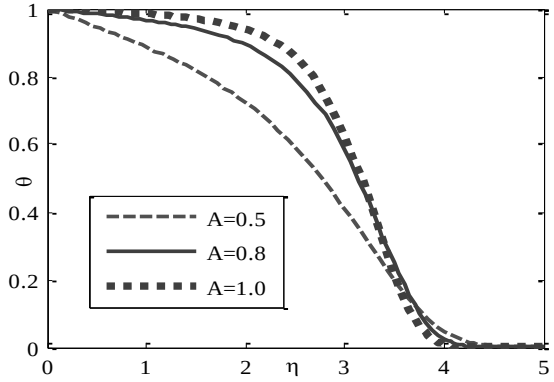

Fig.10 Temperature profile for various values of A

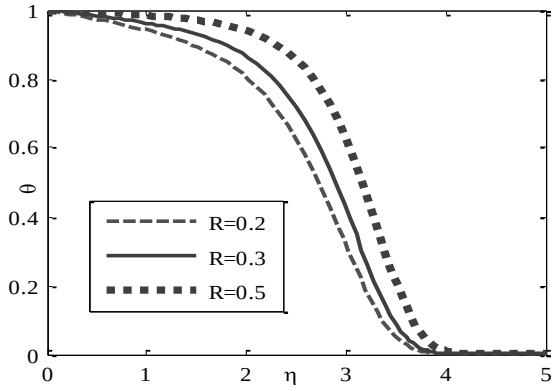

Fig.11 Temperature profile for various values of R

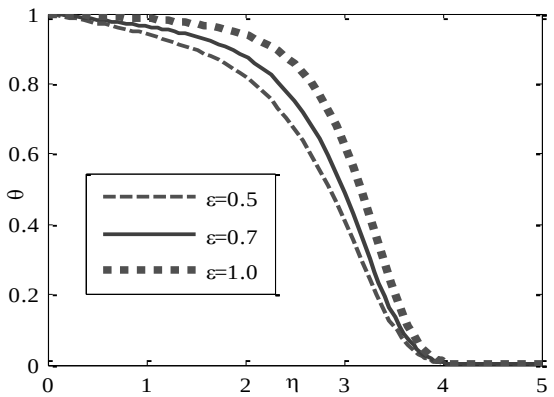

Fig.12 Temperature profile for various values of ε

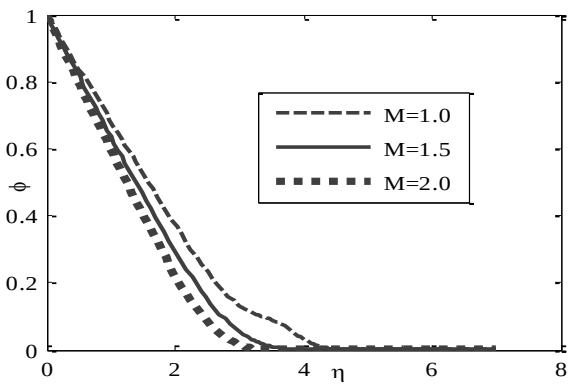

Fig.13 Concentration profile for various values of M

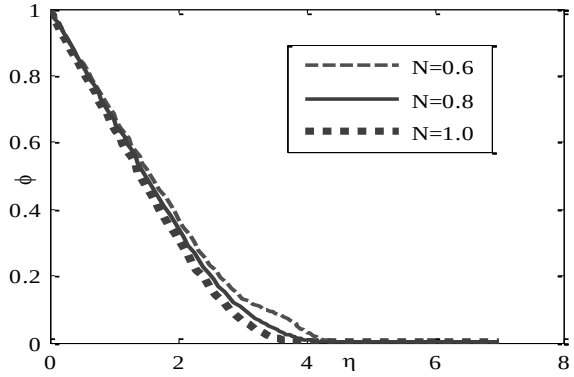

Fig.14 Concentration profile for various values of N

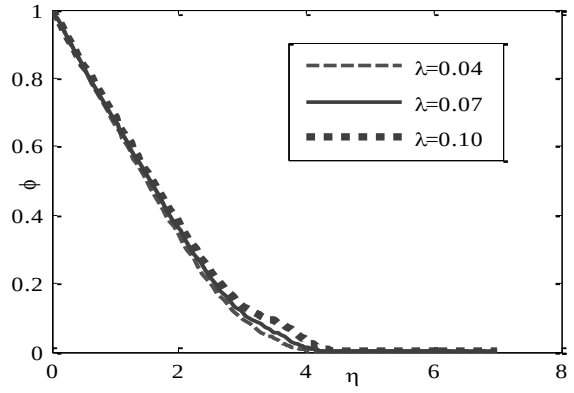

Fig.15 Concentration profile for various values of λ

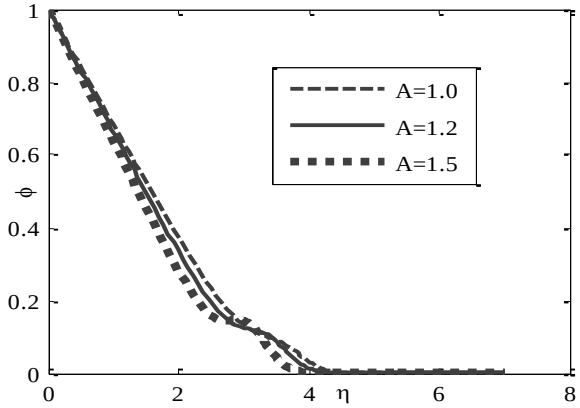

Fig.16 Concentration profile for various values of A

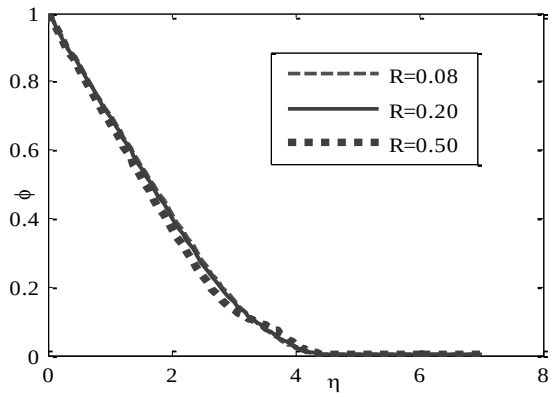

Fig.17 Concentration profile for various values of R

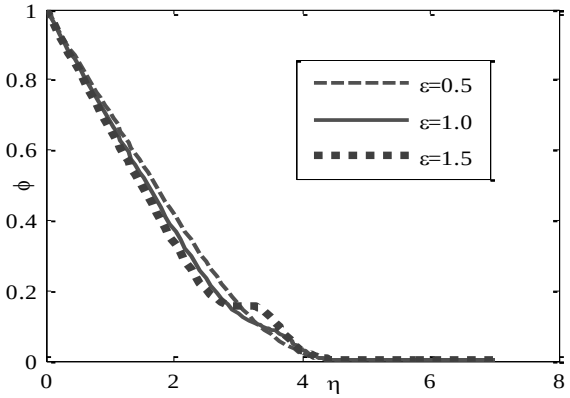

Fig.18 Concentration profile for various values of ε

Table 1 Comparison of the skin friction [$f''(0)$] and local Nusselt number [$-\theta(0)$]

λ	Pop et al.[12]		Mahapatra and Gupta[13]		Sharma and Singh [14]		Present results	
	$f''(0)$	$-\theta(0)$	$f''(0)$	$-\theta(0)$	$f''(0)$	$-\theta(0)$	$f''(0)$	$-\theta(0)$
0.1	-0.9694	0.081	-0.9694	0.081	-0.969386	0.081245	-0.97017	0.081005
0.2	-0.9181	-	-0.9181	-	-0.9181069	-	-0.91886	-
0.5	-0.6673	0.135	-0.6673	0.136	-0.667263	0.135571	-0.667909	0.135331
2.0	2.0174	0.241	2.0175	0.241	2.01749079	0.241025	2.00317	0.2410321

REFERENCES

[1] E.M.A. Elbashbeshy, M.A.A. Bazid, Heat transfer over an unsteady stretching surface, *Heat Mass Transfer*, Vol.41, pp 1-4 (2004).

[2] Saleh M. Alharbi1, Mohamed A. A. Bazid, Mahmoud S. El Gendy, heat and mass transfer in MHD visco-elastic fluid flow through a porous medium over a stretching sheet with chemical reaction, *Applied Mathematics*,Vol.1, pp 446-455(2010).

[3] M. A. Seddeek and M. S. Abdelmeguid, 'Effects of Radiation and Thermal Diffusivity on Heat Transfer over a Stretching Surface with Variable Heat Flux, *Physics Letters A*, Vol. 348, pp 172-179 (2006)

[4] M. Ali, M. S. Alam, M. M. Alam and M. A. Alim, Radiation and thermal diffusion effects on a steady MHD free convection heat and mass transfer flow past an inclined stretching sheet with Hall current and heat generation, *IOSR Journal of Mathematics*, Volume 9, pp 33-45 (2014).

[5] W. Ibrahim and B. Shanker, Unsteady MHD boundary layer flow and heat transfer due to stretching sheet in the presence of heat source or sink by Quasi-linearization technique, *International Journal of Applied Mathematics and Mechanics*, Vol. 8, pp 18-30(2012).

[6] Ishak A, Nazar R and Pop I, Boundary layer flow and heat transfer over an unsteady stretching vertical surface, *Mechanica*, Vol.44, pp 369-375 (2009).

[7] Ishak A, Unsteady MHD flow and heat transfer over a stretching plate, J*ournal of Applied Science*, Vol.10, pp 2127-2131(2010).

[8] Ebashbeshy and Aldawody , Heat transfer over an unsteady stretching surface with variable heat flux in presence of heat source or sink, *Computers and Mathematics with applications*, Vol. 60, pp 2806-2811 (2010).

[9] Fadzilah M, Nazar R, Norihan, M and Pop I, MHD boundary layer flow and heat transfer of a viscous and electrically conducting fluid over a stretching sheet with an induced magnetic field, *Journal of Heat Mass Transfer*, Vol.47, pp 155-162 (2011).

[10] Bachok N, Ishak A and Nazar R, Flow and heat transfer over an unsteady stretching sheet in a micropolar fluid, *mechanica*, *International Journal of Applied Mathematics and Mecanics.* Vol.8, pp 18-30(2011).

[11] Mohebujjaman M, Khalequ S and Samad M, MHD heat transfer mixed convection flow along a vertical stretching sheet in presence of magnetic field with heat generation , *International Journal of Basic and Applied Science*, Vol.10,(2010).

[12] S.R. Pop, T. Grosan and I. Pop, Radiation effect on the flow near the stagnation point of a stretching sheet, *Technische Mechani*k, Vol.25, pp 100-106 (2004).

[13] T.R. Mahapatra, and A.S. Gupta, Heat transfer in stagnation-point flow towards a stretching sheet, *Heat and Mass Transfer*, Vol.38, pp 517-521(2002).

[14] P.R. Sharma and G. Singh, Effects of Variable Thermal Conductivity and Heat Source / Sink on MHD Flow Near a Stagnation Point on a Linearly Stretching Sheet, *journal of Applied Fluid Mechanics,* Vol.2, pp 13-21(2009).
[15] M. Arunachalam and N.R. Rajappa, Forced convection in liquid metals with variable thermal conductivity and capacity, *Acta Mechanica*, Vol.31, pp 25-31 (1978).
[16] T.C. Chaim, Heat transfer in a fluid with variable thermal conductivity over stretching sheet, *Acta Mechanica,* Vol. 129, pp 63-72 (1998).

ICMIEE-PI-140-301

An investigation on the variation of woven fabric properties made from regular ring spun, compact & SIRO spun yarn.

Kazi Sowrov [1], *Prof. Mashud Ahmed* [2]

[1] Department of Fabric Manufacturing Engineering,
Bangladesh University of Textiles, Dhaka-1208 . BANGLADESH

[2] Department of Fabric Manufacturing Engineering,
Bangladesh University of Textiles, Dhaka-1208 . BANGLADESH.

ABSTRACT
Woven fabric properties are greatly dependent on yarn properties especially on yarn structures. Object of this paper is to show the variations of the woven fabric properties made from different structured yarns. Three different types of yarns – regular ring spun, compact & SIRO spun yarn were used to produce 1/1 plain woven fabric to study the recommended properties- tensile strength, tearing strength, abrasion resistance, pilling resistance and dye absorbency. The yarns were made from 100% cotton with combing process and the fabrics with construction of 24X24/90X60, 20". According to results, the structural differences of ring, compact and SIRO spun yarns have significant influence on the fabric properties. Fabrics woven from compact yarns were found to have better tensile strength, tearing strength and pilling resistances than fabrics woven from regular ring spun and SIRO spun yarn. Fabric made from compact yarn found to have poorer abrasion resistance compared to other fabrics. In case of dye absorbency fabrics made from SIRO spun yarn were found to have better results. The results were very significant and will surely help the woven fabric manufacturers to choose the exact type of yarn for their recommended fabric properties.
.

Keywords: Regular ring yarn, compact yarn, SIRO yarn, woven fabric, physical properties.

1. Introduction:

Properties of spun yarns are mainly affected by fiber properties and yarn structure. Yarn structure is principally influenced by the spinning system. In fact, each spinning system tends to produce a distinctive yarn structure. Recent refinements in spinning technologies have yielded significant improvement in yarn structure. Siro and compact spinning are the new spinning systems to have made a breakthrough until recently.

All these three types of yarns are produced by ring spinning system i.e yarn is produced by ring machine. The basic difference among their production proess are as below: the compact yarn is produced by the same technique as the conventional ring spun yarn but have an extra compacting zone that us which is equipped by the suction system. In this zone, maximum free & protruding fibers becomes parallel & condensed. Immediately after this condensing zone, this fibrous bundle is twisted in normal & conventional style. When two parallel fiber strand,seperated at a distance,are drafted simultaneously in the drafting zone and after they emerged from the front roller nip,they converge to form a yarn by twisting.And that yarn is called "SIRO" yarn.SIRO spun yarns are produced on a conventional ring frame.The process was invented around 1975-76 by the laboratories of the Commonwealth scientific International Research Organisation (CSIRO) Division of Textile industry in Australia.

Woven fabric has several important properties.Among them the following physical and mechanical properties were studied because yarn structure effects them mostly. The intended properties are as follows:

(a)Tensile strength: The tensile strength of a textile is the maximum amount of tensile stress that it can take before failure.(b) Tearing strength: It is the applied load which is used not to initiate a tear but to propagate an existing tear. (c) Abrasion resistance: Abrasion is just one aspect of wear & is the rubbing away of the component fibers & yarns of the fabric. (d) Pilling resistance: Pilling is the surface fault of woven fabrics which is recognized by the clear appearance of pills. (e) Dye absorbency: Dye absorbency of a fabric means the capacity of fabrics to accept dyes.

2. Literature Cited:

Sunay Omeroglu, and Sukriye Ulku works on Tensile Strength, Pilling and Abrasion Properties of Woven Fabrics Made from Conventional and Compact Ring-Spun Yarns and they found Fabrics woven from compact yarns were found to have higher tensile strength and pilling and abrasion resistances than fabrics woven from ring yarns[1]. Alsaid. A. Almetwally and Mona. M. Salem works on "Comparison Between Mechanical Properties of Fabrics Woven From Compact & Ring spun Yarns" and they found that there is no significant difference between both type of fabrics regarding tearing strength and abrasion resistance. But in relation to tensile strength, air permeability and stiffness, compact fabrics were superior to ring fabrics[2]. BI Song-mei works on The application, development and economical analysis of SIRO spun. The SIRO spun principle, technological requirements, processing equipment, product specialties and

* Corresponding author. Tel.: +88-01819014932,+88-0171823559
E-mail address: kazisowrov@gmail.com,ahmed.mashud@yahoo.com

processing program are described by him in his paper detail [3]**.** Zhang Changle wonks on SIRO spinning, the similarities and the differences of the structure and the performance among SIRO yarn, single yarn and plied yarn. By his experiment he found that The SIRO yarn has a few hairiness, good abrasion resistance, short production processing and can obtain a good economic benefit [4] Chen Yixing works on The Properties and Structure of SIRO spun Yarn. The effects were investigated of various parameters of a modified spinning frame for SIRO spun on the yarn properties with a 2~4-factors method. A comparison of the properties was made between two-fold yarn, SIRO spun yarn and single yarn, and it was proposed that some recommended parameters might contribute to the performance improvement of cotton SIRO spun yarn. The amount of strand-twist and the structure feature of SIRO spun yarn was described [5] Kirecci Ali , Kaynak Hatice Kubra , Ince Mehmet Erdem works on Comparative Study of the Quality Parameters of Knitted Fabrics Produced from SIRO spun, Single and Two-ply Yarns twist multiplier on the properties. They found that , the spirality values of plied yarn fabrics are slightly lower than those of SIRO spun yarn fabrics at finer yarn count values. These results indicate that SIRO spun yarn may be a good alternative for plied yarn due to its extremely low production cost and high quality values [6].

3. Experimental Setup:

Yarn Sample: 100% cotton combed yarn of count 24^{s}Ne. The yarn specification is as below:

Table 1: Yarn Specification

Specification	Ring	Compact	SIRO
Actual count	23.53	23.59	23.67
CV%	0.66	.69	0.77
IPI	28.00	40.1	47.9
CSP	2856	3228	3038
E%	8.93	8.67	8.77
TPI	17.54	17.54	17.54
Fiber MIC Value	4.57	4.57	4.57
Fiber Staple Length(mm)	28.26	28.26	28.26
Type	Comb	Comb	Comb

Fabrics Sample: All the fabrics were made with the following constructions- 90X60/24X24, 20",1/1 plain weave. The testing procedures and testing methods are as below:

Table 2: Fabric testing methods

Sl no	Name of the Test	Sample Size	Test Standard
1	Tensile Strength	$6inch \times 4inch$	ISO 13934-2-2014 Textiles
2	Tearing Strength	$7.5cm \times 10cm$	ASTM D1424-09(2013)
3	Abrasion Resistance	38mm(Diameter)	ISO 12947-1-1998 Textiles
4	Pilling Resistance	140mm(Diameter)	ISO 12945-2-2000 Textiles
5	Dye Absorbency	$4cm \times 1cm$	AATCC Test Method 79

4. Results & Analysis:

4.1 Results:

Table 3: Tensile Strength

No of observation	Warp Way			Weft Way		
	Ring	SIRO	Compact	Ring	SIRO	Compact
1	396	407	411	263	229	278.4
2	397	408	412	264	228	278
3	395	406	410	262	230	277.6
4	396	407	411	263	229	278.3
5	396	407	411	263	229	279.3

Graphical Representation:

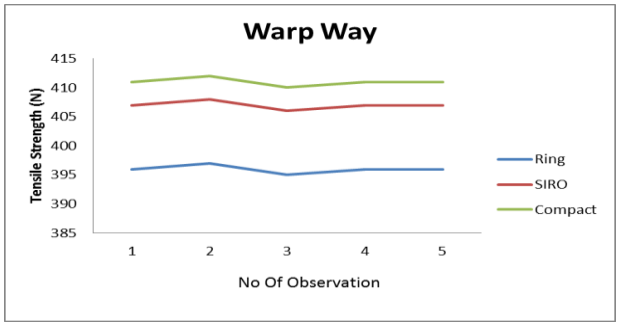

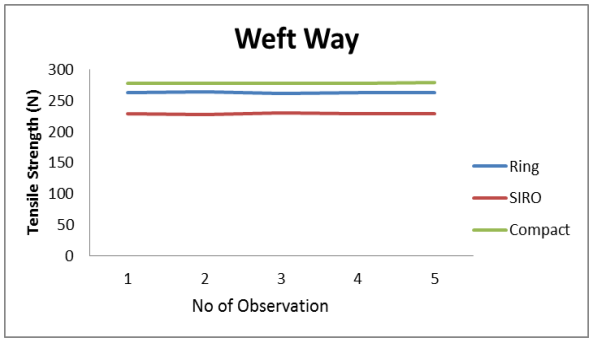

Table 4 : Tearing Strength:

No of Observation	Warp Way			Weft Way		
	Ring Spun	Compact	SIRO	Ring Spun	Compact	SIRO
1	16.07	16.0	15.01	12.51	13.19	13.41
2	16.3	17.0	15.07	13.03	12.19	12.41
3	15.9	15.0	15.05	11.99	14.19	14.41
4	16.01	16.0	14.9	12.51	13.25	13.31
5	16.05	16.0	15.01	12.51	13.13	13.51

Graphical Representation:

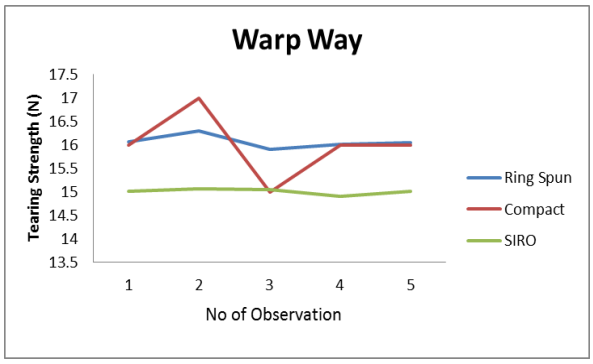

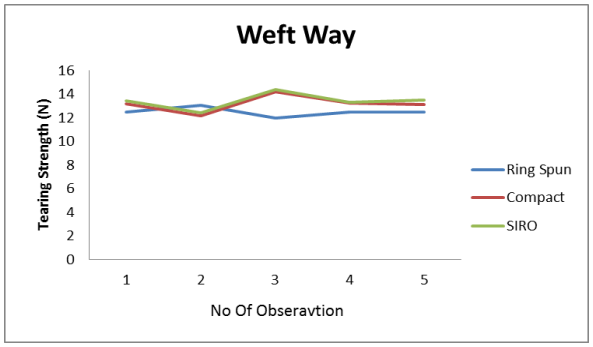

Table 5: Abrasion Resistance:

Yarn Type	Weave and construction	Revolution	Grade	Result
Ring spun	1/1 Plain 24×24/90×60	10000	3-4	No yarn were broken
Com Pact			3	Two or more yarn were broken
SIRO			3-4	No yarn were broken

Table 6: Pilling Resistance:

Yarn Type	Weave and construction	Revolution	Grade	Comment
Ring spun	1/1 Plain 24×24/90×60	2000	2-3	Moderate surface pilling
Com Pact			4	Slight surface fuzzing
SIRO			2-3	Moderate surface pilling

Table 7: Dye Absorbency

Yarn Type	Weave and Construction	Result (Dye absorbency)
Ring Spun	1/1 Plain 24×24/90×60	3.3
Compact		3.2
SIRO		3.4

Graphical representation:

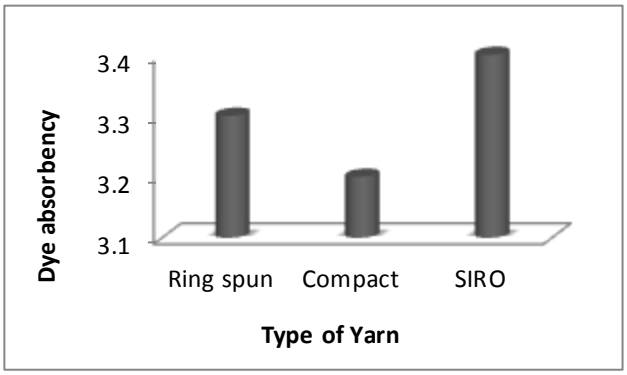

4.2 Analysis:

1.Tensile Strength:
Warp way (avg):
Compact(411N)>SIRO(407N)>Ring spun(407N)
Weft way (avg) :
Compact(278N)>Ring spun(263N)>SIRO(229N)
2.Tearing Strength :
Warp way (avg) :
Ring spun(16.07N)>Compact(16N)>SIRO(15.01N)
Weft way (avg) :
SIRO(13.41N)>Compact(13.19N)>Ring spun(12.51N)
3.Abrasion Resistance:
Ring spun and SIRO(3-4)>Compact(3)
4.Pilling Resistance:
Compact(4)>Ring spun and SIRO(2-3)
5.Dye Absorbency:
SIRO(3.4)>Ring spun(3.3)>Compact(3.2)

4.3 Discussion:

The tensile strength, pilling and tearing strength of the fabrics woven from compact, ring and SIRO yarns were investigated. Compact yarns have better fibre orientation than ring yarns and SIRO yarns, which results in better yarn properties and performance improvements in woven fabrics, especially those made from compact yarns.

In case of abrasion resistance no significant differences were obtained. slightly higher abrasion resistance in fabric made from ring spun and SIRO yarn. The reason for this may be the possibility that the breakage of any yarn on the fabric's surface is high after a certain level of abrasion.

In case of dye absorbency fabric made from SIRO yarn have better dye absorbency and then ring spun yarn due to their fluffy structure and comparatively low dye absorbency of fabric made from compact yarn due to their compact structure.

5. Conclusion:

By this work, it was tried to show that different yarn have a significant influence on most physical & mechanical properties of woven fabric. It is proved that fabric made from ring spun, compact and SIRO yarn differ significantly regarding fabric properties. Finally it can be concluded that fabrics made from compact yarn has better physical & mechanical properties.

REFERENCES

[1]. Sunay Omeroglu, Sukriye Ulku . An investigation about tensile strength, pilling and abrasion properties of woven fabrics made from conventional and compact ring-spun yarns, *FIBRES & TEXTILES in Eastern Europe* 2007

[2] . Alsaid. A. Almetwally and Mona. M. Salem, Comparison between mechanical properties of fabrics woven from compact and ring spun yarns, *AUTEX Research Journal*, Vol. 10, No1, March 2010

[3]. BI Song-mei, The application, development and economical analysis of SIRO spun yarn, *Journal of Anhui Institute of Mechanical and Electrical Engineering*; 2000-03

[4]. Zhang Changle The Spinning Principle and the Product Development of SIRO Spinning. *Journal of Textile Research 1986-09*.

[5] Chen Yixing The Properties and Structure of Siro Spun Yarn[J];*Journal of Textile Research*;1986-09.

[6] Kireçci A., Kaynak H. K., Ince M. E.; Comparative Study of the Quality Parameters of Knitted Fabrics Produced from Sirospun, Single and Two-ply Yarns. *FIBRES & TEXTILES in Eastern Europe* 2011, Vol. 19, No. 5 (88).

[7] Yang Rui-Hua, Xue Yuan, Wang Shan-Yuan; Comparison and Analysis of Rotor-Spun Composite Yarns and Sirofil Yarn. *FIBRES & TEXTILES in Eastern Europe* 2010, Vol. 18, No. 1 (78).

[8] Soltani P, Johari MS. Effect of Using the New Solo-siro Spun Process on Structural and Mechanical Properties of Yarns. *FIBRES & TEXTILES in Eastern Europe* 2013; 21, 3(99)

[9] Beceren Y., Candan C., Cimilli S., Ülger K.; Properties of Plain Knits from Siro-SpunViscose/Spandex Yarns. *FIBRES & TEXTILES in Eastern Europe* 2010, Vol. 18, No. 1 (78)

[10] *Principal of Textile Testing*. - J.E.BOOTH
[11] *Physical testing of textiles*. - B P Saville
[12] *Manual of Textile Technology*. - W. Klein

ICMIEE-PI-140304

Study on the Mechanical Properties of Glass Fiber Reinforced Polyester Composites

A.H.M Fazle Elahi [1], Md. Milon Hossain [2], Shahida Afrin[3], Mubarak A. Khan[4]*

[1] Department of Mechanical Engineering,
Khulna University of Engineering & Technology, Khulna-9203, BANGLADESH

[2] Department of Textile Engineering,
Khulna University of Engineering & Technology, Khulna-9203, BANGLADESH

[3]Abdur Rab Serniabat Textile Engineering College,
University of Dhaka, Dhaka-1000, BANGLADESH

[4]Institute of Radiation and Polymer Technology,
Bangladesh Atomic Energy Commission, Dhaka-1000, BANGLADESH

ABSTRACT
Glass fiber reinforced unsaturated polyester (GFRP) based polymer composite was prepared using hand layup process. Four layers of GF were impregnated by polyester resin and pressed under load of 5kg for a day. Then the fabricated composite were heat treated from 60 degree Celsius to 150 degree for 1 hour and finally taken for mechanical test. Tensile strength, tensile modulus, elongation at break, impact strength, shear strength and hardness of the fabricated composite were measured. The experiment showed wonderful improvement in the mechanical properties of the fabricated composite resulted from the heat treatment. The maximum tensile strength of 200.6 MPa is found for 900C heat treated sample. Inverse relationship between heat and mechanical properties of the composite was observed above 1000C. Finally, the excellent elevated heat resistant capacity of GFRP composite shows the suitability of its application to heat exposure areas such kitchen furniture materials, marine, electric board etc.

Keywords: Glass fiber, Polyester-resin, Composite material, Mechanical Properties test, Tensile test

1. Introduction

Composite materials are one of the most significant inventions of the material sciences. Composite materials are used in furniture, packaging, assembly boards, paneling, fencing, kitchen to civil constructions, automobile and marine industries, military purposes and even space or aircraft manufacturing. So, composites are a versatile and valuable family of materials that can be used in many fields with high quality and low cost applications. Currently, synthetic fiber-reinforced thermoplastic composites are widely used because of their excellent mechanical properties and durability [1]. Composite materials produce a combination property of two or more materials that cannot be achieved by either fiber or matrix when they are acting alone. Fiber-reinforced composites were successfully used for many decades for all engineering applications. Glass fiber-reinforced polymeric (GFRP) composites were most commonly used in the manufacture of composite materials due to their low cost, high tensile strength, high chemical resistance, and insulating properties. The matrix comprised organic, polyester, thermo stable, vinylester, phenolic and epoxy resins. Suitable compositions and orientation of fibers made desired properties and functional characteristics of GFRP composites was equal to steel, had higher stiffness than aluminum and the specific gravity was one-quarter of the steel. The various GF reinforcements like long longitudinal, woven mat, chopped fiber (distinct) and chopped mat in the composites have been produced to enhance the mechanical and tribological properties of the composites [2-3]. Glass fiber reinforced unsaturated polyester resin (UPR) composite materials have become the alternatives of conventional structural materials, such as wood and steel in some applications, because of its good mechanical properties. Mechanical properties of fiber-reinforced UPR composites depend on the properties of the constituent materials, the nature of the interfacial bonds, the mechanisms of load transfer at the inter-phase and the adhesion strength between the fiber and the matrix [4].

Glass fiber reinforced (GFRP) Composite is the largest segment in the composite industry, worth several billions. Glass fiber is made from extremely fine fibers of glass. It is a lightweight, extremely strong, and robust material. Although strength properties are somewhat lower than carbon fiber and it is less stiff, the material is typically far less brittle, and the raw materials are much less expensive. Its bulk strength and weight properties are also very favorable when compared to metals, and it can be easily formed using molding processes. The glass fibers are most extensively used as a raw material for composite materials. Glass fiber accounts for about 90% of the reinforcements used in composite consumption, globally. Most of the GFRP Composites are used in construction and transportation sectors. The demand for renewable energy in the form of wind turbines, demand for light-

* Corresponding author. Tel.: +88-01912-239243; fax: +88-041-774403
E-mail address: fazle.elahi.ashek@gmail.com

weight fuel efficient aircrafts & cars, and the demand for GFRP pipe, tank and other corrosion resistant equipment are major drivers increasing its demand in the coming years.

2. Background

Many researchers investigated the mechanical behavior of GFRP in different media. Environmental and moisture content impact of GFRP was investigated previously [5-6]. Thermal behavior of glass fibers were investigated by many researchers with the change of temperatures which is the basis of the experiment presented in this paper. Shokry studied the effect of five temperature levels (25, 50, 100,150 and 200°C) as well as three times of exposure (60, 120 and 180 minutes). The experiment showed that temperature has considerable effect on different properties of GRP. The results of the investigations show that the tensile strength, compressive strength and hardness for GPR composite decrease proportionally to temperature increase [7]. Properties of E-glass/epoxy composites at 650C for 1000 hours were studied by Abdel-Magid et al. The values of module of elasticity, stress-strain was examined and compared with the values obtained at room temperature. A decrease in module of elasticity and break of elongation was noticed from the experiment. The authors concluded that longer exposure of the samples to higher temperatures caused ductile breaks on E-glass/epoxy composites [8]. Behavior of E-glass fiber unsaturated polyester composites, subjected to moderate and high temperatures was investigated by Laoubi et al. [9]. The characterization of the resin and the composite, after heating, revealed that at moderate temperatures (lower than 100 °C) an improvement of the properties of materials is observed in the experiment. A thermogravimetric analysis (TGA) revealed that the thermal degradation of the composite occurs in two steps: the first between 130 and 200 °C and the second between 250 and 440 °C. When the temperature reaches the temperature of decomposition (Td), a fall of the mechanical properties was recorded for both resin and composite. Bisht and Chauhan investigated the effect of temperature on the tensile properties of E-glass/unsaturated polyester composite [10]. It was found from the experiment that temperature and tensile strength is inversely proportional.

The main objective of this experiment is to investigate the influence of various temperature levels of glass fiber reinforced unsaturated polyester composite. Four plies of glass fiber were reinforced to polyester resin and its response to different mechanical properties of the fabricated composite by temperature variations were determined and exhibited in this study.

3. Experimental

3.1 Materials

Unsaturated polyester and methyl ethyl ketone peroxide (MEKP) were supplied by Polyolefin Co. Limited; Singapore and E-glass fiber of GSM 300 was purchased from Saint-Gobain Vetrotex, India.

3.2 Method of Composite Fabrication

The composite specimens were prepared in open mold cold compression method. Unsaturated polyester resin and MEKP hardener were taken in a beaker. They were then mixed well and made ready for laminating reinforced mats. The composite samples were fabricated by hand lay -up technique. At first, a melot paper was placed on dried bottom part. Then some of the prepared resin mixture was spread evenly on the paper. After that, a piece of non-woven glass was placed on the resin mixture and a part of resin mixture was spread on the mat. Another piece of glass fabric was placed and similarly rest of the resin mixture spread on the mat and so on. A melot paper was placed on the mat following which top part of the open mold was kept on the paper. The prepared samples were allowed to cure under pressure at room temperature.

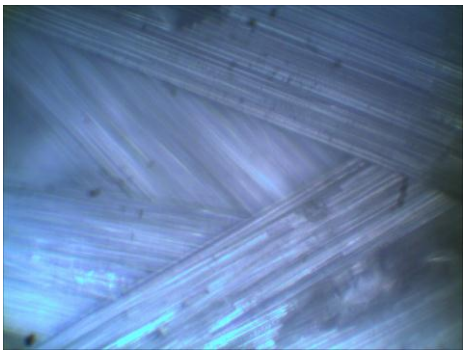

Fig. 1 Microscopic view of glass fiber (1000X)

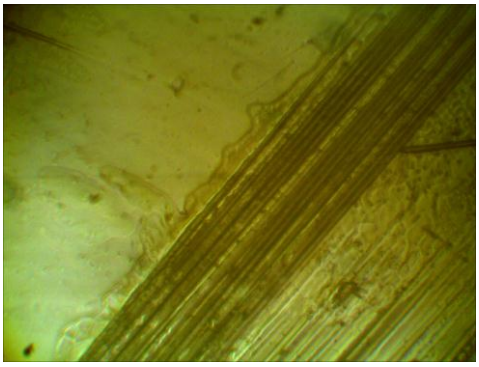

2 (a)

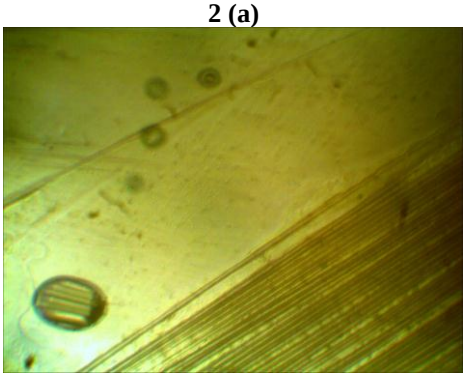

2(b)

Fig. 2 Microscopic view of fabricated composite (1000X)

The above figures are microscopic view at 1000X zoom. Fig. 1 provides information about fiber alignment and shows how the fiber is bonded within different layer. Fig. 2(a) shows the composite surface and the bonding with polyester resin. Fig. 2(b) shows there are some bubbles formed in between the layers during fabrication. The bubble formed part has been omitted from the mechanical test specimen to get precise results.

3.3 Mechanical Testing of Composite

Tensile, impact, shear and hardness (BHN) tests were conducted. For each test and type of composites, five specimens were tested and the average values were reported.

3.3.1 Tensile Test:

Tensile tests were conducted according to ASTM D 638-01 [11] using a Universal Testing Machine (Hounsfield series, model: INSTRON 1011, UK) with a cross-head speed of 10 mm/min. The dimensions of the test specimen were (ISO 14125): 60 mm × 15 mm × 2 mm3.

3.3.2 Impact Test:

Impact test for different fabricated composites were carried out according to ASTM D-256. The length and width of the samples used in impact test were 61.5 mm and 12.7 mm respectively. Impact strength was calculated using the following formula-

$$\text{Impact strength} = \frac{\text{Impact Energy}}{\text{Area}} = \frac{J}{A}$$

The unit of impact strength is Joule per square meter.

3.3.3 Shear Strength:

The shearing modulus of elasticity is called modulus of rigidity. Shear strength was measured using punch diameter 3.15 mm. The shear strength was calculated according to ASTM D5868 by using the following equation.

$$\text{Shear Strength, } S = \frac{P}{\pi D t}$$

Where, P = Applied load

D = Diameter of punch

t = Thickness of the composite

3.3.4 Determination of Hardness:

The test was carried out using 305.92 Kg(f) and the diameter of ball intender was 5 mm. The diameter of the impression produced is measure by means of a microscope containing an ocular, usually graduate in tenths of a millimeter, permitting estimates to the nearest 0.05mm. Hardness is obtained by dividing the applied load by the area of the surface of the indentation, which is assumed to be spherical. If P is the applied load (in kg), D is the diameter of the steel ball intender (in mm) and d is the diameter of eh indentation (in mm), then Brinell number (BHN) of the composite-

$$\text{BHN} = \frac{P}{\frac{\pi D}{2}(D - \sqrt{D^2 - d^2})}$$

BHN = Brinell hardness number

P = load on the indenting tool (kg)

D = diameter of steel ball (mm)

d = measure diameter at the rim of the impression (mm)

It is desirable that the test load are limited to an impression diameter in the range of 2.5 to 4.75 mm.

4. Results and Discussion

Non-woven glass mat was reinforced in thermoset polyester matrix by hand layup process with the fabric content 40%. The mechanical properties such as tensile strength, tensile modulus, elongation at break, were evaluated. Shear strength and hardness of the fabricated composite were also reported in this experiment. Five samples of which four designated as HT 60, HT 90, HT 120 and HT 150 were heat treated from 600C to 1500C for one hour and last one was untreated. The impact of heat on different samples was compared to the untreated sample.

4.1 Tensile Strength:

Fig. 3 demonstrates the tensile strength of GFRP before and after exposure to heat. Effects of heat on the composite were recorded and found that sample expose to temperature 900C shows highest tensile strength while sample exposed to heat 1500C shows lowest strength. Tensile strength increases gradually from untreated sample to temperature 900C and then start decreasing with the increase of temperature. This may be due to the internal phase change during heat treatment.

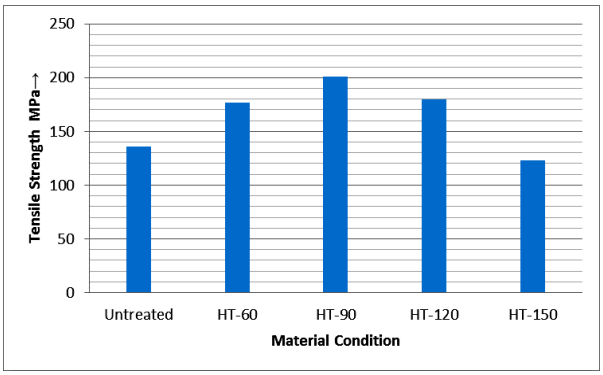

Fig. 3 Tensile strength of GFRP

4.2 Tensile Modulus:
Tensile modulus of GFRP is presented in the Fig. 4 Same pattern of the tensile strength test after the heat treatment is visible here. With the increase of temperature tensile modulus also increased and reaches to the maximum value at 900C compared to untreated sample. Further increase of temperature reduces the tensile modulus of the GFRP and lowest modulus is found at 1500C by value 1.072 GPa. Highest increase of the modulus was found 77.82% at 900C compared to untreated sample. Decreases in strength can be attributed to the hydrolysis of the, disruption of the matrix/fiber interface, and/or degradation of the fibers themselves.

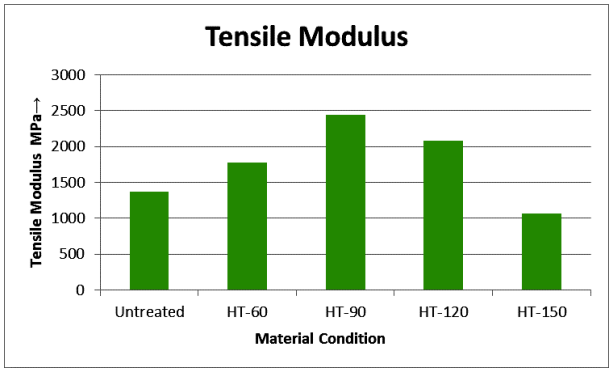

Fig. 4 Tensile modulus of GFRP

4.3 Impact Strength:
Fig. 5 depicts the impact properties of GFRP. Some fluctuation is observed in impact strength with different temperature ranges. Sample treated with 900C shows the highest impact strength of 155.178 KJ/m2 controversially sample treated with 1500C shows dramatic fall in impact strength by 43.83% compared to untreated sample. Almost zero change is found in the sample treated in initial temperature.

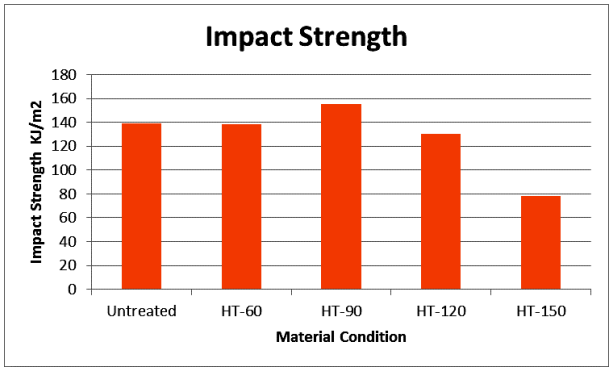

Fig. 5 Impact strength of GFRP

4.4 Elongation at Break:
Elongation at break percentage of GFRP is shown in Fig. 6. Highest elongation is observed in untreated sample by value 21.88%. After heat treatment slight decrease is found in elongation percentages. Negligible effect of temperature variation is found on elongation at break percentage.

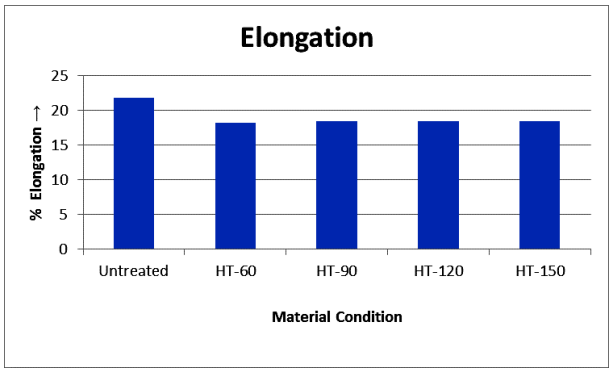

Fig. 6 Elongation at break % of GFRP

4.5 Shear Strength:
Shear strength of GFRP is presented in Fig. 7. An increasing trend in shear strength is observed of GFRP. Temperature is directly proportional to shear strength i.e. with the increase of heat shear strength also increases and reaches to its maximum value 112.742 MPa at 1500C. While all samples shows shear strength greater than 100 MPa untreated sample shows only 96.04 MPa.

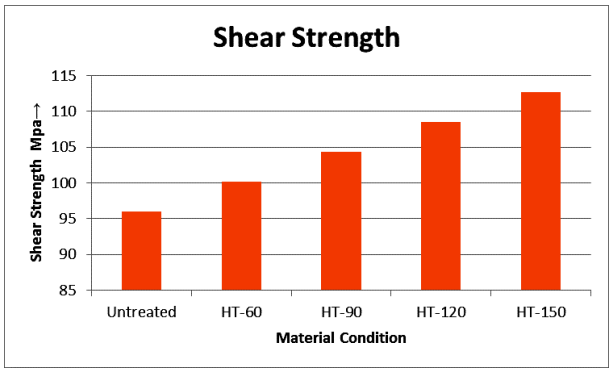

Fig. 7 Shear strength of GFRP

4.6 Hardness:
Fig. 8 depicts the hardness of GFRP. Likewise most of the other properties of GFRP, BHN value of fabricated composite is highest for sample treated at 900C.

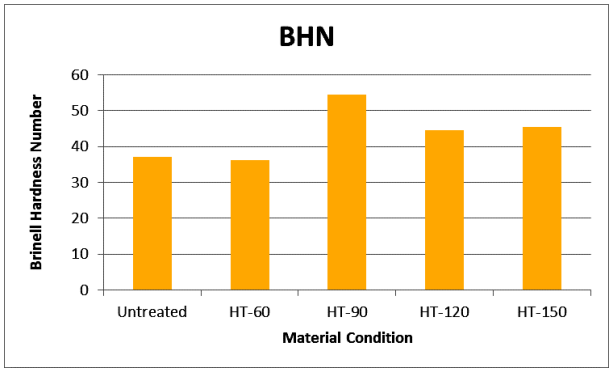

Fig. 8 Hardnes of GFRP

Apparently no change in hardness was visible for the initially heat treated sample. Further increase of temperature increase the hardness of the composite while more temperature reduces the hardness and negligible change is found in the final temperature.

5. Conclusion:

The effect of different temperature on GFRP was experimentally investigated. The GFRP were found to be temperature sensitive. Treatment of the composite below 1000C shows highest increase in their different mechanical properties whereas above the boiling temperature there is a huge loss of their mechanical properties. This vivid impact of temperature can be attributed to internal change of fiber matrix adhesion of the composite and evolution of the linkage of resin due to heat.

References:

[1] Haydar U. Zaman, Mubarak A. Khan and Ruhul A. Khan, "Physico-Mechanical and Degradation Properties of Banana Fiber/LDPE Composites: Effect of Acrylic Monomer and Starch", Composite Interfaces 18 (2011) 685–700.

[2] TP Sathishkumar, S Satheeshkumar and J Naveen, "Glass fiber-reinforced polymer composites – a review", Journal of Reinforced Plastics and Composites 2014, Vol. 33(13) 1258–1275.

[3] Mariana Etcheverry and Silvia E. Barbosa, "Glass Fiber Reinforced Polypropylene Mechanical Properties Enhancement by Adhesion Improvement", Materials 2012,5, 1084-1113

[4] LUO Weicai, WANG Xiao, HUANG Ronghua, FANG Pengfei, "Interface Enhancement of Glass Fiber/Unsaturated Polyester Resin Composites with Nano-Silica Treated Using Silane Coupling Agent", Wuhan University Journal of Natural Sciences2014, Vol.19 No.1, 34-40

[5] H. Abdullah, S. Al Araimi and R. A. Siddiqui, "THE EFFECTS OF WEATHERING ON MECHANICAL PROPERTIES OF GLASS FIBER REINFORCED PLASTICS (GRP) MATERIALS", IIUM Engineering Journal, Vol. 1, No. 2, 2000.

[6] P. Sampath Rao, M. Manzoor Hus ain, D. V. Rav i Shankar, "An Investigation on Strength Degradation of Gfrp Laminates Under Environmental Impact", International Journal of Composite Materials 2012, 2(4): 48-52.

[7] Khaled M. Shokry, "Effect of Temperature on Mechanical Properties of Glass Reinforced Plastic GRP", World Applied Sciences Journal 31 (7): 1341-1344, 2014

[8] Beckry Abdel-Magida, Saeed Ziaeea, Katrina Gassb, Marcus Schneiderc, "The combined effects of load, moisture and temperature on the properties of E-glass/epoxy composites", Composite Structures, Volume 71, Issues 3–4, December 2005, Pages 320–326.

[9] K. Laoubia, Z. Hamadia, A. Ahmed Benyahiab, A. Seriera, Z. Azari, "Thermal behavior of E-glass fiber-reinforced unsaturated polyester composites" Composites Part B: Engineering, Volume 56, January 2014, Pages 520–526

[10] Devnidhi Bisht, Hemant Chauhan, "Estimating Effects of Temperature on Tensile Strength of Eglass Composite with Unsaturated Orthophthalic Polyester", International Journal of Emerging Technology and Advanced Engineering, Volume 4, Special Issue 1, February 2014.

[11] A. A. Kafi, M. Z. Abedin, M. D. H. Beg, K. L. Pickering and M. A. Khan, "Study on the Mechanical Properties of Jute/Glass Fiber-Reinforced Unsaturated Polyester Hybrid Composite: Effect of Surface Modification by Ultraviolet Radiation," Journal of Reinforced Plastics and Composites, Vol. 25, No. 6, 2006, pp. 575-588.

ICMIEE-PI-140305

Experimental and Numerical Investigation of an Air to Water Heat Exchanger

Mohammad Didarul Alam [1,*], *Shaikh Tanveer Hossain*,[1] *Md. Hasan Shahriar Simanto* [1], *Molla Shoyeb Uddin Mithu*[1], *Mohammad Ariful Islam* [2].

[1] Undergraduate students of Department of Mechanical Engineering, Khulna University of Engineering & Technology, Khulna-9203, BANGLADESH
[2] Department of Mechanical Engineering, Khulna University of Engineering & Technology, Khulna-9203, BANGLADESH

ABSTRACT
Heat exchangers are devices that facilitate heat transfer between two or more fluids at different temperature. Many types of heat exchanger have been developed for using at varied levels of technological sophistication and air to water heat exchanger is one of them. This paper investigates the performance of an air to water heat exchanger using experimental and numerical techniques and determines its heat transfer characteristics, logarithmic mean temperature difference (LMTD), heat exchanger efficiency etc. Inside the exchanger hot air passes through a specially prepared copper tube which is accurately centered inside a brass tube to form the annulus along which the cooling water flows. Some readings of steady state condition have been taken for parallel and counter flow by changing air flow rate where other parameters were constant. For numerical simulation, the heat exchanger has been drawn by using a CAD software and it has been simulated by using Autodesk® Simulation CFD 2015. Graphical representations for both the cases (parallel and counter) has been analyzed here. The simulation results of the air to water heat exchanger behavior had well agreement with the available experimental data. Efficiency improvement might be seen as a profound concern in future analysis of this paper.

Keywords: CFD simulation, Tube to tube heat exchanger, Heat exchanger characteristics.

1. Introduction

Heat transfer science is concerned with the analysis of the rate of heat transfer taking place in a system. It has long been established by observation that when there is a temperature difference in a system, heat flows from the region of high temperature to that of low temperature. There are a lot of heat transfer applications available in our practical world. In practice the most common advantageous example is heat exchanger. Heat exchanger is a device that exchange heat between hot and cold fluid. Various heat exchanger applications are available such as boiler, condenser, water heater, automobile radiator or cooling coil, refrigeration, air conditioning etc. Different types of classification of heat exchangers available in engineering practice are widely discussed on Froas and Ozisik [1] Walker [2] and Kakac, Shah, and Bergles [3]. Heat exchangers can be classified based on the transfer process, compactness, construction type, flow arrangement and heat transfer mechanism [4], [7]. Heat exchanger performance is one of the most vital term in heat research field because of its vast range of applications. Numerous researches have been done already about the performance of heat exchanger.

In Vindhy Vasiny Prasud Dubey and Ray Rajat Verma [5] the performance of a shell and tube type heat exchanger under the effect of varied operation condition was analyzed and it was seen that the computational results were almost same compared with the experimental results.

Ozzbilin Guraras and Yusuf Ali Kara [6] made a computer based design model for a shell-tube heat exchanger. In that exchanger single phase fluid flows on both shell and tube side. According to the conclusion of that paper, circulating cold fluid in shell side and hot fluid in tube side is advantageous.

In this paper, a tube to tube heat exchanger is selected because tube to tube heat exchanger is one of the most advantageous for its simplicity and cheapness. The specified heat exchanger's performance is analyzed and compared here both experimentally and numerically.

2. Experimental analysis

The apparatus is a concentric pipe heat exchanger in which hot air flowing through the center tube is cooled by water flowing in the annulus (Fig.1). The direction of water was reversed to study both parallel and counter flow condition where air temperature, water flow rate were taken constant except the air velocity. The overall heat transfer coefficient can be determined for the heat exchanger either directly or by considering the heat transfer coefficient of the air to tube and tube to water separately. An electrically driven variable speed fan supplies filtered air and the air is heated by an electric heater under variable resistor control. The air leaving the heater passes through an isothermal approach length, in which the temperature and velocity are stabilized before entering the section. The inner test pipe is prepared by copper which is accurately centered inside a

* Corresponding author. Tel.: 01676284638
E-mail address: rahatalam48@gmail.com

brass tube to form the annulus along which the cooling water flows. Air leaving the test section passes through a 2nd isothermal length which ensures that exit condition doesn't affect the flow. Thermo-couple is provided to measure the air temperature and mercury thermo-meter is used to measure water temperature. Two manometers are used to measure the static pressure at inlet and the pressure drop along the tube. A calibrated measuring beaker and stop watch are used to measure the flow rate of water. A number of steady state reading has been taken for both parallel & counter flow.

2.1 Equations

LMTD (log mean temperature difference)= $\frac{\Delta t_{a-\Delta t_b}}{ln\frac{\Delta t_a}{\Delta t_b}}$

Heat loss by air $Q_h=m_aC_{Pa}\Delta t_a$
Heat gain by water $Q_c = m_w C_{pw}\Delta t_w$

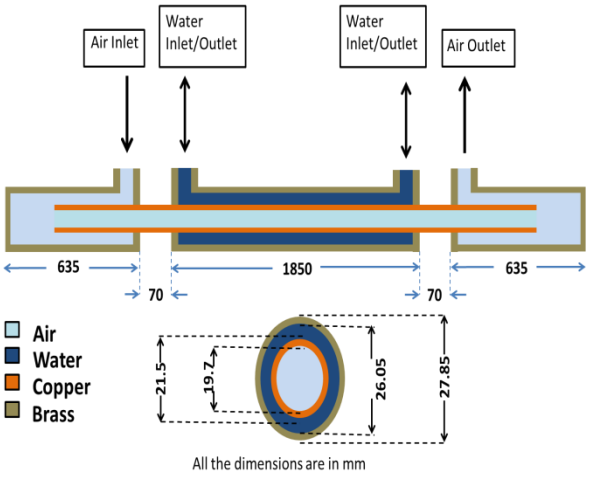

Fig.1 Experimental setup.

3. Numerical analysis

The commercial code Autodesk® Simulation CFD 2015 was adopted to simulate a three-dimensional steady-state turbulent flow and heat transfer in the computational model. It employs the FEM to reduce the governing partial differential equations (PDEs) of a CFD problem to a set of algebraic equations. Autodesk® Simulation CFD uses segregated algorithm along with iterative matrix solver for solving the equations iteratively until convergence is reached.

3.1 Governing Equations:

The governing equations for fluid flow and heat transfer are the Navier-Stokes or momentum equations and the First Law of Thermodynamics or energy equation.

3.2 Geometry & boundary condition:

The three dimensional geometry of the model was drawn in a CAD software and then exported to Autodesk® Simulation CFD. To reduce the computational domain without affecting the result, only the length of the pipe along which the heat transfers was considered in the CAD model. The inner pipe was assigned as copper and outer pipe was assigned as brass (Fig.2). Air and water volume was also assigned properly.

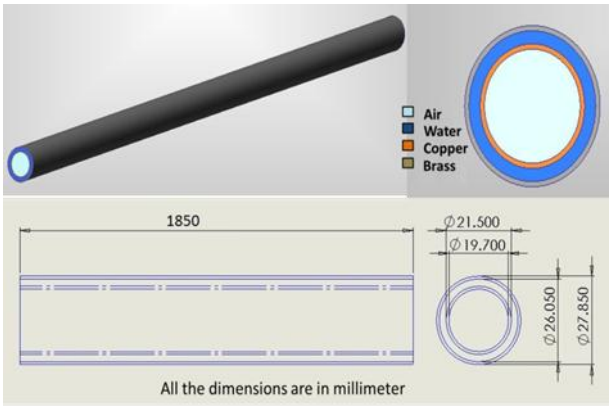

Fig.2 Numerical model

The hydraulics and thermal boundary conditions used in this simulation are given in the Table 1.

Table 1 Boundary conditions

ASSIGNED TO	TYPE
Air Inlet Surface	Velocity Normal (36 m/s) Temperature (85 Celsius)
Air Outlet Surface	Pressure (0 Pa Gage)
Water Inlet Surface	Volume Flow Rate (0.002182 m3/min) Temperature (30 Celsius)
Water Outlet Surface	Pressure (0 Pa Gage)

3.3 Grid generation

The solution accuracy greatly depends on the grid generation. Automatic mesh scheme (provided by Autodesk® Simulation CFD) followed by advanced mesh enhancement was used to generate fine mesh. Surface meshing and boundary layer meshing was also introduced. Mesh Enhancement adds element layers along all fluid-solid interfaces. This boundary layer mesh formation gives opportunity to have more precise result of temperature and velocity distribution (Fig.3). Following meshing criteria was given (Table. 2) :

Table 2 Mesh settings

Meshing parameter	**Setting/Value**
Surface refinement	1
Gap refinement	1
Resolution factor	1.0
Edge growth rate	1.1
Minimum points on edge	2
Points on longest edge	10
Surface limiting aspect ratio	20
Refinement length	0.0

Meshing parameter	Setting/Value
Fluid gap elements	1.0
Thin solid elements	0.2
Mesh enhancement	1
Enhancement blending	1
Number of layers	3
Layer factor	0.45
Layer gradation	1.05
Number of Nodes	1093567
Number of Elements	4528926

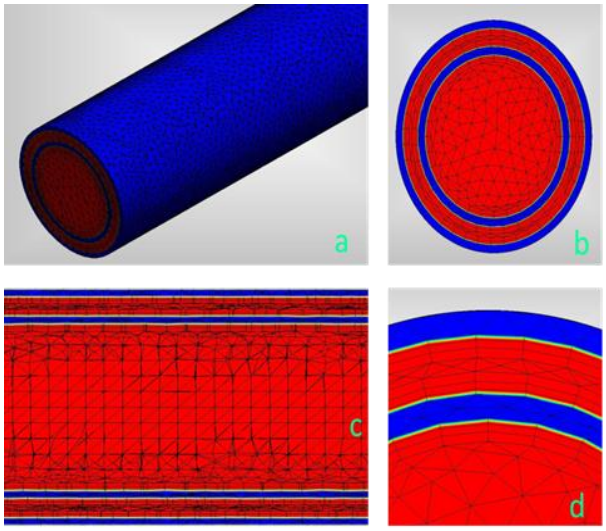

Fig.3 A sample of generated mesh (a) global view (b) radial cross-section view (c) transverse section view (d) boundary layer mesh formation

3. 4 Solving the Simulation

In the analysis a convergence criterion of 0.00001 was satisfied for all dependent variable .The number of iterations to run during the analysis was such that convergence plot was flattened and the convergence criterion was satisfied. *k-epsilon* turbulence model was used for running this simulation. It is typically more accurate but more computationally intensive and slightly less robust. *ADV 1 (Monotone streamline upwind scheme)* was used as advection scheme for its numerical stability. Following solver settings was used in the simulation process (Table. 3):

Table 3 Solver settings

Solution parameters	Settings/Values
Flow	On
Compressibility	Incompressible
Heat Transfer	On
Auto Forced Convection	On
Gravity Components	0, -1, 0
Radiation	Off
Turbulence	On
Solution mode	Steady State
Intelligent solution	Off

Solution parameters	Settings/Values
Advection scheme	ADV 1
Turbulence model	k-epsilon

4. Result and discussion

As mentioned earlier an experiment has been conducted with the full model and it is seen that for all the cases counter flow is more efficient than parallel flow. Inlet water volume flow rate, inlet water temperature and inlet air temperature were kept constant; only inlet air velocity was varied for each observation. Some typical data from experimental results showing efficiency and LMTD is given in Table 4.

Table 4 Experimental result

Flow type	Temperature of air (°C)		Temperature of water (°C)		Efficiency %	LMTD (°C)
	Inlet	Outlet	Inlet	Outlet		
Parallel	85.0	36.0	30.0	33.41	53	17.14
Counter	85.0	40.0	30.0	33.43	86	25.00

From numerical simulation, it is visualized that fully developed air flow inside the copper tube was generated gradually within 0.0263 mm (Fig 4) length from the inlet. The reynold number of the air flow was around 38000-38500 which indicates the air flow was fully turbulent.

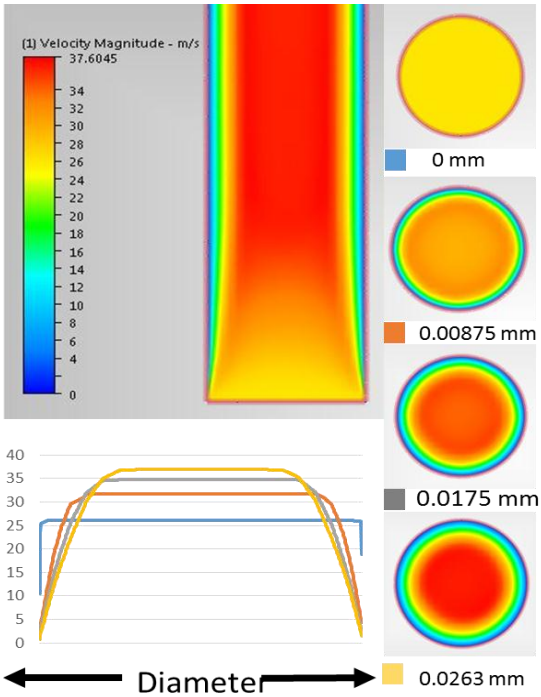

Fig.4 Formation of fully developed flow

Temperature colour contour of air at different sections of pipe is shown in the Fig. 5. Colour contour shows air touching the copper pipe has the lowest temperature, but

on the other hand the outlet air temperature is more likely uniform.

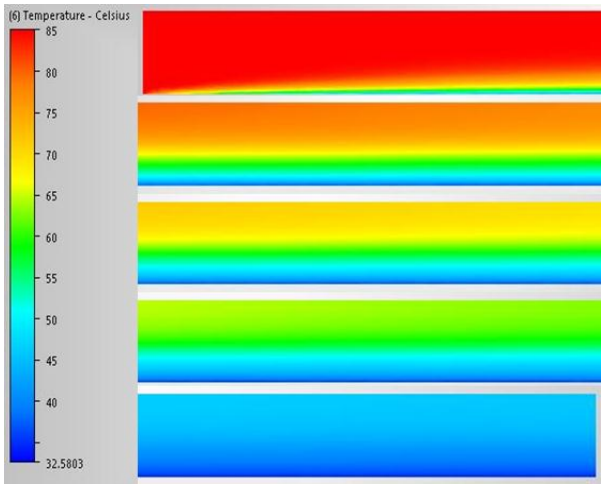

Fig.5 Temperature colour contour of air (1/2 of the cross section along the length)

Fig. 6 and Fig. 7 shows temperature colour contour (1/2 of the cross section along the length) of water at inlet, middle and outlet section for parallel and counter flow respectively. From Fig. 6 and Fig. 7 it can be inspected that for parallel flow the rate of heat gain is more than the counter flow at the inlet but the temperature is higher for the counter flow at the outlet.

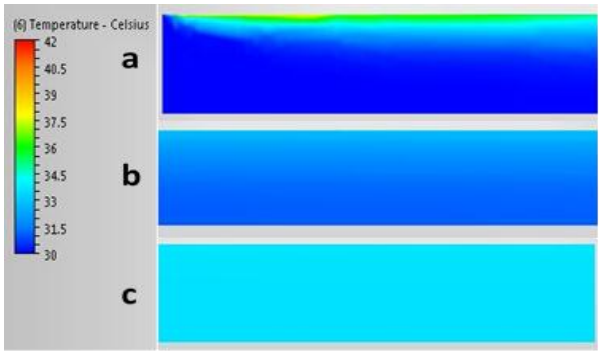

Fig.6 Temperature colour contour of water (parallel) (a) inlet (b) middle (c) outlet

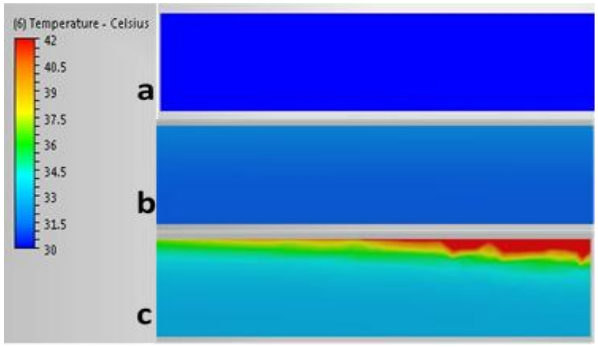

Fig.7 Temperature colour contour of water (counter) (a) inlet (b) middle (c) outlet

From CFD simulation results, temperature of air and water from inlet to outlet has been plotted against the pipe length for both cases (parallel & counter flow) in Fig. 8 and Fig. 9 respectively. Fig.8 shows that the temperature gradient (both air and water) is higher at inlet for parallel flow. In contrast, the temperature gradient (both air and water) is almost constant along the length for counter flow (Fig. 9).

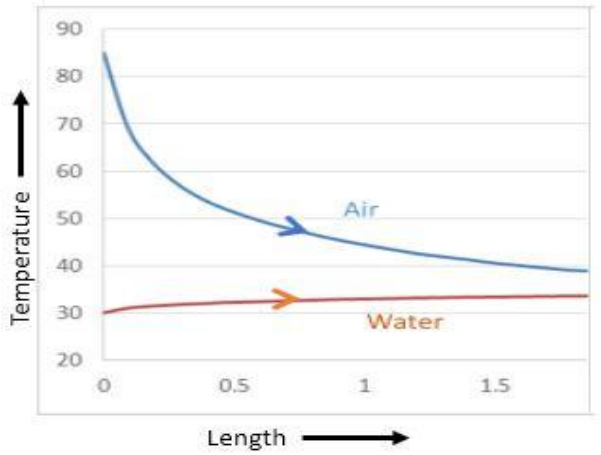

Fig.8 Temperature distribution for parallel flow

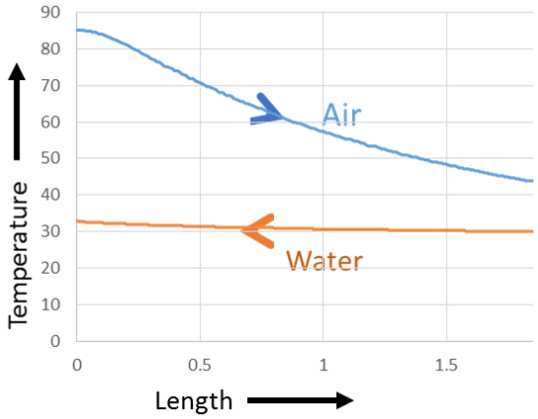

Fig.9 Temperature distribution for counter flow

Magnitude of air velocity as a fraction of free stream velocity and air temperature as a fraction of the input temperature has been plotted (Fig. 10) along the diameter of the pipe at different distances from the inlet for parallel flow.
Similarly, magnitude of water velocity as a fraction of free stream velocity and water temperature as a fraction of the output temperature has been plotted (Fig, 11) along the diameter of the pipe at different distances from the inlet.
Fig. 10 and Fig 11 both contains a velocity profile along with three temperature profiles at three different distances of the pipe. As fully developed flow was achieved within a short length of the flow for both water

and air so the velocity profile is almost the same for the rest of the length which is indicated by the figures too. For the temperature profiles the heat exchange is happening from start to end of the pipe so temperature profile will change with the length. Fig.10 shows temperature profile of air continuously decreases with the increasing of flow distance. The situation is just the opposite in Fig.11 which shows continuous increment of the temperature profile with the increment of length. This indicates air losses heat gradually with the advancement of length at the same time water gains.

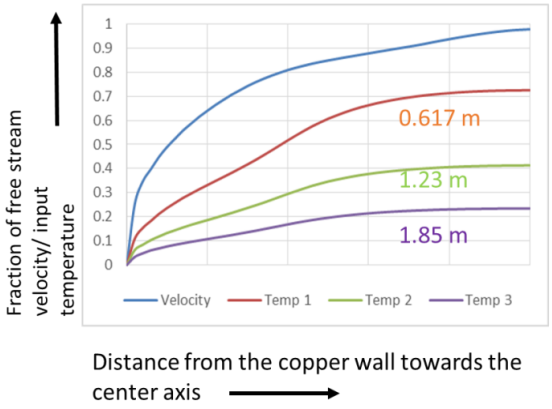

Fig10. Velocity boundary layer and temperature boundary layer (air)

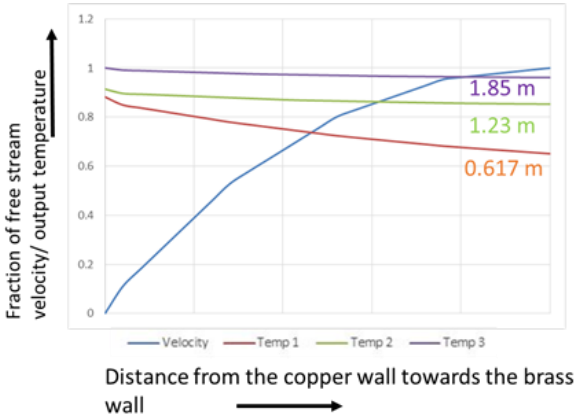

Fig.11 Velocity boundary layer and temperature boundary layer (water)

5. Conclusion

Numerical and experimental steady state heat transfer mechanism in tube to tube heat exchanger has been investigated. This investigation concludes several decisions:

1 The computational results are almost same as the experimental results.

2 In case of counter and parallel flow, counter flow is more efficient than parallel flow.

3 Increasing Reynolds number by rising hot air velocity increases the heat transfer rate.

4 Flow of hot air in tube and cold water in annulus side is much more efficient than flow of hot air through annulus and cold water in tube.

NOMENCLATURE

c_{pa} : specific heat at constant pressure, $kJ \cdot kg^{-1} \cdot K^{-1}$ for air.

c_{pw} : specific heat at constant pressure, $kJ \cdot kg^{-1} \cdot K^{-1}$ for water.

T : temperature ^{o}C

Δt_a : temperature difference between air and water at the inlet of exchanger.

Δt_b : temperature difference between air and water at the outlet of exchanger.

m_a : mass flow rate of air. $k_g.s^{-1}$

m_w : mass flow rate of water. $k_g.s^{-1}$

REFERENCES

[1] Fraas, A.P. and M. N. Ozisik, Heat Exchanger Design, Wiley, New York (1965).

[2] Walker, G. , Industrial Heat Exchangers, Hemisphere, Washington (1982).

[3] Kakac, S., R. K. Shah and A. E. Bergles (eds), Low Reynolds Number Flow Heat Exchangers, Hemisphere, Washington (1982).

[4] M. N. Ozisik, Heat Transfer - A Basic Approach, McGraw-Hill Book Company, International edition, (1985).

[5] Vindhy Vasiny Prasud Dubey and Ray Rajat, Performance Analysis of Shell and Tube Type Heat Exchanger Under The Effect of Varied Operating Condition, IOSR Journal of Mechanical and Civil Engineering (IOSR-JMCE) e-ISSN: 2278-1684,p- ISSN: 2320-334X, Volume 11, Issue 3 Ver. VI (May- Jun. 2014), PP 08-17 .

[6] Yusuf Ali Kara, Ozbilen Guraras, A computer program for designing of Shell and tube heat exchanger, Applied Thermal Engineering 24(2004) 1797–1805.

[7] J.P. Holman, Heat Transfer, McGraw-Hill Book Company, 10th Edition (2009).

[8] M. Hatami, D. D. Ganji, M. Gorji-Bandpy, CFD simulation and optimization of ICEs exhaust heat recovery using different coolants and fin dimensions in heat exchanger, Neural Computing and Applications, ISSN: 0941-0643.

[9] Autodesk® Simulation CFD 2015, Commercial CFD Software, © 2014 Autodesk Inc.

[10] Autodesk® Simulation CFD 2015, Online Help, Autodesk Inc.

ICMIEE-PI-140307

Development of an Automatic Board Cleaning system using Microcontroller

Imam-Ul-Ferdous *[1], *A.H.M Fazle Elahi* [2]

[1, 2] Department of Mechanical Engineering,
Khulna University of Engineering & Technology, Khulna-9203, BANGLADESH

ABSTRACT

Now-a-days white boards are widely used in almost every educational institute. About 70-80% educational institute around the world uses white board as the writing medium in their class room. They are large in size, for that reason it is very time consuming process to erase the writings from the board with duster. Using duster also reduce the visual quality of the board. If a class continue about one hour then about 8-10% time become waste because of cleaning the board using duster. Considering this "The board wiper", an automatic system can solve these problems. The board wiper will shorten the time and also the effort. It takes around 8 sec to clear the board without destroying the quality. The wiper has horizontal movements and it wipes the board twice at a short time. The wiper consists of electric motor, supports, a wiper bar and a microcontroller to give that an automation figure. It is possible to control the wiper by a remote control system and this allows the controller to wipe the board from a reasonable distance. And it has an advantage to remove the wiper if it's necessary to clean and the whole wiper system can be established at a very low cost. So, "The Automatic board wiper" is a spectacular replacement of "duster" and it can be suggested to use this to reduce the effort of the board user as well as to introduce the classroom with an automation system.

Keywords: Board wiper, Automation, control system, Automatic duster.

1. Introduction

When we said teaching and learning process we will focus on teacher and student, who are person that delivering and receiving information and knowledge. How do they deliver their knowledge to student? Nowadays, there are many methods which are used by teachers to deliver their knowledge such as computer, note given by teacher and at last but not the least whiteboard or blackboard as medium to deliver the information to student. The invention of blackboards was a revolutionary change in the history of mankind which led to the development of the society. One of the problems we are experiencing in our classroom is erasing the blackboard. Chalk dust scatter causing extreme nuisance especially for people who have asthma. Also, chalk dust causes skin irritation and serious health problems. [1] Blackboards require lot of time to get rubbed which increase the demand of whiteboards. The first whiteboards were very expensive and was made of enameled steel but seeing the growing demand in the market cheaper whiteboards made of steel with polyester or acrylic coating of white color on it were launched. Innovations in the field of whiteboards were done since a long time. Different types of whiteboards like laminated chipboard, high pressure laminated boards and porcelain boards were launched in the market for cheaper alternatives. [2] Modifications were also done in cleaning and rubbing methods of whiteboards. Remote control motorized cleaners were innovated to reduce the human efforts required for cleaning. This type of cleaner is operated by motors and is controlled by switch or remote.

2. Background

In the very past cave man used the wall of the cave as the writing medium. There they used the board to capture various memories or the story of their own culture and daily activities. As the time goes on and a civilized society was being formed the scenario begun to change. In the middle age people began to use a big slice of the wood piece as the board, and coal as the pen medium. [3] But it was not so comfortable and it became nasty. Then the black board had been introduced. It's nothing but a black canvas where a chalk is used as the pen medium. Chalk is a composite of calcium carbonate and it looks like a stick. It was comfortable but it creates dust during wiping the board using the duster. A duster is device which is used to wipe the writings from the board. Though the black board has not lost its popularity as in present time and it's being used widely across the world. But a white board is the modified version of the black board. Here a marker pen is used as pen medium and as duster a piece of cloth or a foam duster. As the white board has the advantage of not creating the dust as it only make the duster dirty and it is very much comfortable using marker pen as it comes in different colors. Across the world now white board is the best writing medium during teaching. Now almost everything is automated. And the automation system has the capacity to reduce the human effort and to make any arrangement easier. And those became possible for micro-controlling system. The Arduino microcontroller is an open-source hardware controller which is designed to ease any mechanism by using electronic commands.

* Corresponding author. Tel.: +88-01717581021
E-mail address: imam.ul.ferdous@gmail.com

3.0 System Components

The whole system is based upon two individual parts. One is the wiping system which ensure to erase writings and other is the controlling part which control the wiping system. The wiping system consists of the necessary arrangement which enable the wiper slide over the board and the controlling system consists of micro-controller which control the motor, rpm, and the time of rotation.
The controlling unit contain the following elements:

3.1 Arduino UNO:

The Arduino Uno is a microcontroller board based on the ATmega328 .It has 14 digital input/output pins (of which 6 can be used as PWM outputs), 6 analog inputs, a 16 MHz ceramic resonator, a USB connection, a power jack, an ICSP header, and a reset button. It contains everything needed to support the microcontroller. One of its most important features is its ease of programmability. [4]

Fig. 1: Arduino UNO Microcontroller

3.1 Motor Driver: (L293D IC)

The L293D is a monolithic integrated, high voltage, high current, 4-channel driver. Using the chip it is possible to use DC motors and power supplies of up to 36 Volts and maximum current of 600mA per channel.

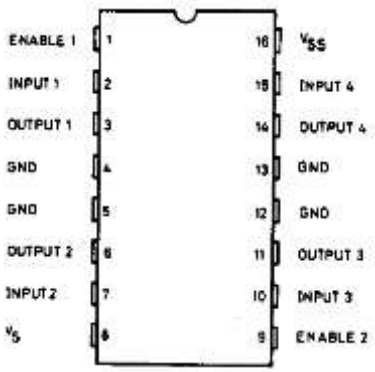

Fig. 2: Motor driver

The other components for control system are enumerated below.

3.2 10K Ohm resistor (Brown, Black, Orange, Gold)
3.3 50V 10uF Capacitor.
3.4 4 piece 6V DC motor.
3.5 A switch (push)
3.6 Breadboard.
3.7 Jumper.
3.8 9V DC power supply.

The elements that are used for building the wiping section consists of stainless steel, aluminum pipe, wood, pulleys ,foam, cord and cloth.

4.0 Methodology:

For rotating a motor both clockwise and anti-clockwise a motor driver is used along with the Arduino. The L293D chip is also what's known as a type of H-Bridge. The H-Bridge is typically an electrical circuit that enables a voltage to be applied across a load in either direction to an output. [5] This means it is possible to reverse the direction of current and thus reverse the direction of the motor. It works by having 4 elements in the circuit commonly known as corners: high side left, high side right, low side right, and low side left. By using combinations of these it is possible to start, stop and reverse the current. Here the care about in all of this is the 2 input pins per motor that do this logic and these, more importantly it can be controlled from the Arduino board. The voltage regulation allows for 2 power sources – 1 direct source, up to 36V for the motors and the other, 5V, to control the IC which can be supplied from the Arduino power supply. Capacitors is used in this circuit to smooth out the power load to the motors as much as possible to help avoid any spikes and stabilize the current.
It starts with the 16 pins on the L293D chip and has 2 sides, 1 for each motor. Pin 1 Starts and stops the motor whether it is on or off comes from the Arduino digital PWM pin 9. Pin 2 is the Logic pin for the motor goes to Arduino digital pin 4. Pin 3 is for one of the motor terminals can be either +/-. Pin 4 and 5 are grounded. Pin 6 is for other motor terminal. Pin 7 is the Logic pin for the motor (input is either high or low) goes to Arduino digital PWM pin 3. Pin 8 is for Power supply for the motor. Pin 9 Enables and disables the 2nd motor on or off (high or low). Pin 9 is the Logic pin for the 2nd motor (input is either high or low).pin 11 is for one of the 2nd motor terminals can be either +/-. Pin 12 and 13 are grounded. Pin 14 is for the 2nd motor's other terminal. Pin 15 logic pin for the 2nd motor (input is either high or low). Pin 16 Connected to +5V, in this case the power from motor supply. Next it switch on Arduino digital pin 2 and the GND pin from Arduino connected to the GND rail on the project board. The capacitor is used in between the power supply – making sure that the negative and positive terminals are correctly aligned. [6]

5.0 Design, Modeling & Construction

5.1 Design

Table 1: Functions of switch and Motor Rotation:

Switch	Motor 1	Motor 2	Motor 3	Motor4
1st push	Clockwise	Anticlock wise	Clockwise	Anticlock wise
2nd push	Anticlock wise	clockwise	Anticlock wise	clockwise
3rd push	Clockwise	Anticlock wise	Clockwise	Anticlock wise
4th push	Anticlock wise	clockwise	Anticlock wise	clockwise

A single motor driver can run highest two DC motor, so two motor driver is needed for running four DC motor. The motor arrangement follows the same but for four motors the +ve and –ve terminals are arranged for executing the targeted motion. Fig. 3 shows that the wiper can move up and down with the motor clockwise and anticlockwise rotation.

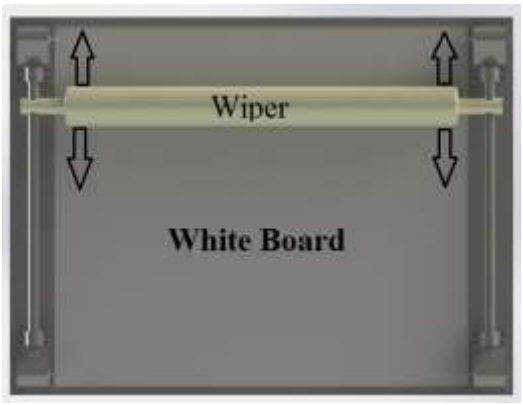

Fig. 3: Complete design of an Automatic board cleaner

5.1.1 Main Structure:

When a motor rotates it can create torque. This torque can be converted to linier motion. It is the basic principle of this machine. Here the wiper bar can slide over the board. Two stainless steel pipe is setup at the both side of the board. The wiper bar attached to the s-s pipe in a way that the bar can easily slide. Using cord and pulley arrangement the bar connected to the motors. When the motor rotates the pulleys attached to the motor also rotates. Then the pulley spin up the cords on it and the wiping bar moves vertically. There are four motors to drive the wiper bar. Two at the upper side and other two at the bottom side at four corners. Every complete move (from upper side to bottom side or lower side to upper side) of the wiper bar wipe the board completely. The control box controls all the motors in such manner that the motors spin in the same direction.

Fig. 4: Main structure design

5.1.2 Wiper Bar:

It is made of aluminum pipe and has two drill at both side that enables it to slide following the stainless steel pipe slider. Aluminum pipe is preferred due to its light weight and agility. Cloth and a piece of foam is used as wiping material. The cloth which used here is very soft and the foam makes sure that the cloth can easily sweep over the board.

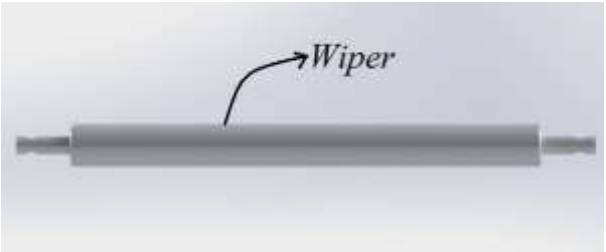

Fig. 5: Designed wiper roller

5.1.3 Control Box:

The control box consists of an Arduino and a circuit board with necessary elements. The control box is situated at the outer side of the main structure. It is connected through wire to the motors. An external power source is also connected to the control box to supply the power.

5.2 Modeling:

The circuit diagram is shown below at Fig. 6. Here Atmega-328 is used instead of Arduino UNO. Four motors are connected through two motor drivers. A switch is used as input. When switch becomes ON current flows to the motor driver through drivers. Here current is passed according to the program loaded in the microcontroller. Then motor starts respective of the microcontroller program.

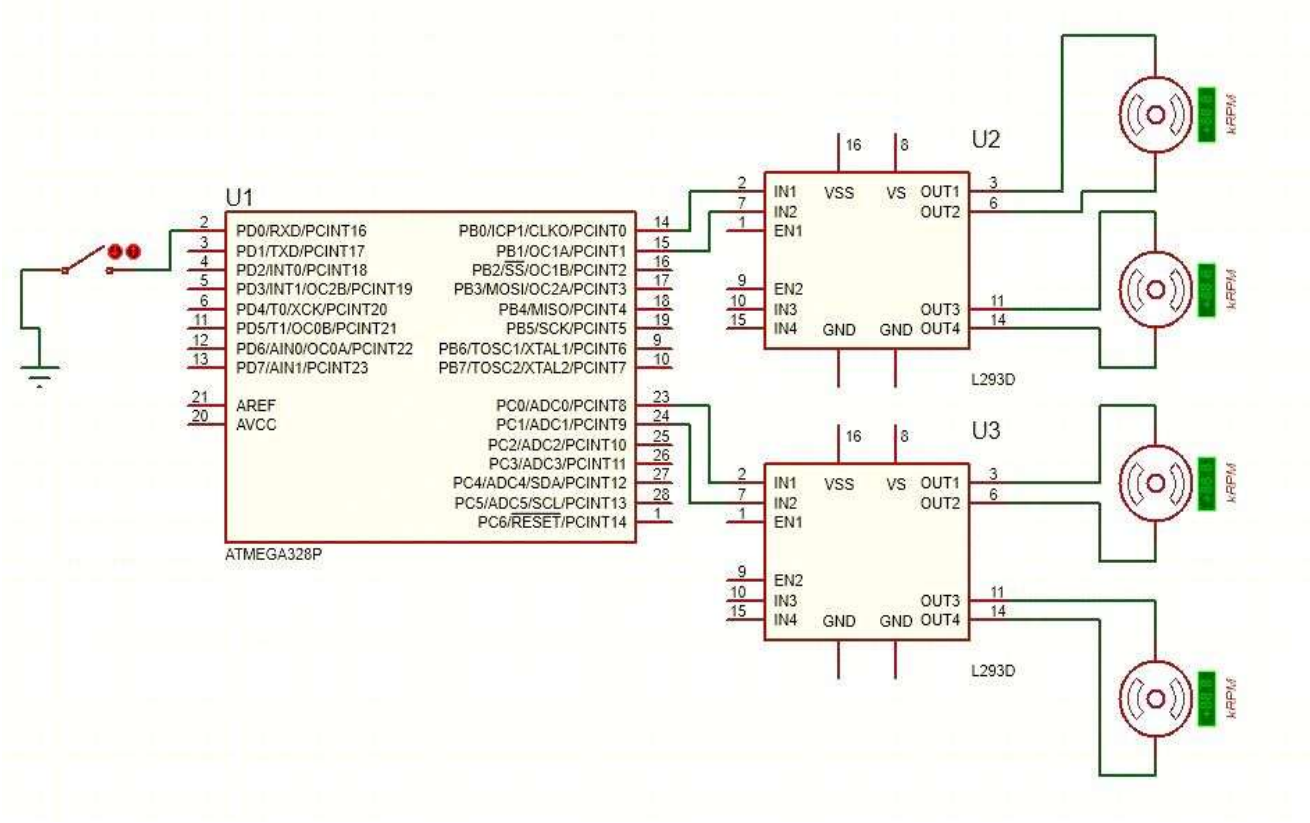

Fig. 6: Circuit diagram of the whole system for the board cleaner

Figure 6 illustrates the control system circuit diagram drawn by Proteus. The system is constructed according to this diagram. The corresponding pin numbers are exactly connected to the motors through motor drivers. The logical expression for the system is shown below as a flow diagram at Fig. 7.

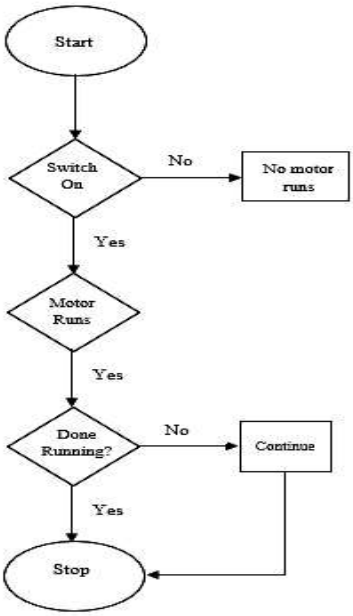

Fig. 7: Flow diagram of control system

5.3 Construction

After completing the virtual design main design has been executed. Material is same as it determined. The main structure dimension is also same. But some attachment is added for better performance. The main constructed model is shown in figure below.

Fig. 8: Constructed board cleaner

Fig. 8 represents the full constructed view of the Automatic Board Cleaner integrated within the white board. Here two stainless steel piers are supporting the wiper which is made of aluminum pipe surrounded with a foam and a cover. For wiping purpose the foam is attached with a cloth. The cloth has a zipper arrangement that helps the foam to attach with the aluminum bar as a round shape. It is possible to remove the bar and wash the cloth after a certain time.

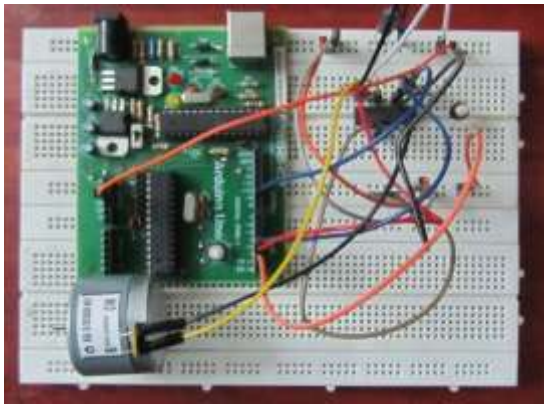

Fig. 9: Fabricated control circuit

Fig. 9 shows the connection of the designed circuit. For checking purpose only a motor is connected within the embedded system. Bread boards are used to connect all electronic components.

6.0 Time analysis

6.1 Using manual Duster:

For this project the prototype board was 4 feet wide and 2.5 feet longer. Using manual duster for complete cleaning the time requires averagely 25 sec.

6.2 Using Automatic Wiper:

Several data was taken to determine the time requires for completing the wiping process. Table-2 shows the time for five observations.

Table 2: Time requires for complete wiping.

Observation No.	Motor 1	Motor 2	Motor 3	Motor 4	Position Of wiper	Time (Sec)
01	Clockwise	Anticlockwise	Clock wise	Anticlockwise	Upward	8.3
02	Anticlockwise	clockwise	Anticlockwise	clock wise	Down ward	9
03	Clockwise	Anticlockwise	Clock wise	Anticlockwise	Upward	7.8
04	Anticlockwise	clockwise	Anticlockwise	clock wise	Down ward	8.9
05	Clockwise	Anticlockwise	Clock wise	Anticlockwise	Upward	6.2

7.0 Discussion and Conclusion

It is observed that the time requires for complete cleaning the board using this machine is average 8.04 sec. On the other hand while using the manual process the time is about 25 sec which is nearly about three times of the machine time. Though there have some lagging in to start the motor, but averagely it is optimum. The machine is reducing both time and human effort. It also maintaining the visual quality of the board. This construction consists of Arduino microcontroller. But it is possible to fabricate the circuit using Atmega-328p, Atmega-128p and other chip. For that reason it is very easy to crest the controlling circuit which enable us to create the machine easily. On the other hand to construct the main structure very simple tool work is need, and the materials use in this not very costly and available in market. So, it is not complicated to construct this machine and it will help to introduce an automation system. The system can be further developed by integrating a Bluetooth remote for controlling the switch. Infrared sensors can be used to convert this system to a smart white board.

References

[1] Praveen.G, "Microcontroller Based Automatic Electronic Duster", Proceedings Of International Academic Conference On Electrical, Electronics And Computer Engineering, 8th Sept. 2013, Chennai, India ISBN: 978-93-82702-28-3

[2] Bhushan Tukaram Chougule, Puneet Math, "Automated Motorized Sensing Whiteboard", International Journal Of Advanced Research In Engineering And Technology (IJARET), ISSN 0976 –6480(Print), ISSN 0976 – 6499(Online) Volume 5, Issue 3, March (2014), Pp. 155-163,

[3] Tsado Jacob, "A Remote Controlled Motorized White Board Cleaner", AU J.T. 15(4): 273-280 (Apr. 2012), Nigeria

[4] Puneet Mathur, Bhushan Tukaram Chougule, Ravina Nangare, "Automated Motorized Whiteboard", International Journal Of Engineering, Business And Enterprise Applications (IJEBEA), ISSN (Print): 2279-0020,ISSN (Online): 2279-0039, 6(1), September-November., 2013, Pp. 01-04

[5] Shmuylovich And Salcman, "Whiteboard Presentation Of Interactive And Expandable Modular Content,"U.S.Patent 057106 A2,Sept.07,2012

[6] Kuleshov, V.S. And Lakota, N.A. 1988. Remotely Controlled Robots and Manipulators. Mir Publications, Moscow, Russia

ICMIEE-PI-140308

Application of Particle Swarm Optimization in Aggregate Production Planning and Comparison with Genetic Algorithm

Md. Rakibul Islam[1], Md. Shahriar Aziz[2], Md. Mahfuzul Haque Muftee[3], Md. Sanowar Hossain[4]*
[1, 2, 4]Department of Industrial & Production Engineering,
Rajshahi University of Engineering & Technology, Rajshahi- 6240, BANGLADESH
[3]Department of Computer Science & Engineering,
Rajshahi University of Engineering & Technology, Rajshahi- 6240, BANGLADESH

ABSTRACT
This paper is aimed towards application of particle swarm optimization for constrained optimization as aggregate production planning and comparison of the result with genetic algorithm under uncertain demand in a predefined range. As in aggregate production planning 80% decision depends on cost only, we have eliminated other objective functions of APP in this case. We have used some data from CCKL, one the leading company in RMG sector in Bangladesh. There was a 24 variables problem with 24 constraints which was solved in MATLAB and the results between the aforementioned algorithms were compared. It is found that under these constraints PSO produces better result. In contrast with GA, PSO requires far less parameters to adjust and minimal time. Due to these reasons the authors suggest using PSO in such multi constraint problem.

Key words: Particle swarm optimization (PSO); Genetic Algorithm (GA); Aggregate Production Planning (APP)

1. Introduction

Aggregate production planning is concerned with the determination of production, inventory, and work force levels to meet fluctuating demand requirements over a planning horizon that ranges from six months to one year. Typically the planning horizon incorporates the next seasonal peak in demand. The planning horizon is often divided into periods. For example, a one year planning horizon may be composed of six one-month periods plus two or three month periods. Normally, the physical resources of the firm are assumed to be fixed during the planning horizon of interest and the planning effort is oriented toward the best utilization of those resources, given the external demand requirements. A firm must plan its manufacturing activities at a variety of levels and operate these as a system. Planners must make decisions on output rates, employment levels and changes, inventory levels and changes, back orders, and subcontracting. Aggregate planning determines not only the output levels planned but also the appropriate resource input mix to be used.

Aggregate planning might seek to influence demand as well as supply. If this is the case, variables such as price, advertising, and product mix might be used. If changes in demand are considered, then marketing, along with operations, will be intimately involved in aggregate planning. Aggregate planning is essentially a big-picture approach to planning.

There are many solving procedure for APP problem but in this paper we have used two new algorithms PSO and GA. PSO has been used by many applications of several problems. The algorithm of PSO emulates from behavior of animals societies that don't have any leader in their group or swarm, such as bird flocking and fish schooling. Typically, a flock of animals that have no leaders will find food by random, follow one of the members of the group that has the closest position with a food source (potential solution). The flocks achieve their best condition simultaneously through communication among members who already have a better situation. Animal which has a better condition will inform it to its flocks and the others will move simultaneously to that place. This would happen repeatedly until the best conditions or a food source discovered. The process of PSO algorithm in finding optimal values follows the work of this animal society. Particle swarm optimization consists of a swarm of particles, where particle represent a potential solution.

Most APP models can be formulated as linear programming problems but this is not the case for the proposed model. This warrants an opportunity of application for near-optimal heuristics to solve this multiple objectives optimization problem. In this study, PSO is a relatively new approach for solving optimization problem is employed to solve the proposed APP problem due to its simplicity, speed, and robustness. The PSO allows a group of particles to search for the solution. Knowledge gained by each agent is shared among one another in order to iteratively find an improved solution.

2. Literature Review

Aggregate production planning has lured a significant academic researchers & practitioners because of its immense importance. Shorten product life cycle in market & fickle customer perceptions push the researchers to choose this broad area to research.APP is the problem to determine the resource capacity needed to meet demand in the production line. Many researchers have studied to solve this type of management problems. Linear programming model with linear cost structure was proposed by Hanssman and Hess (1960) [1] to schedule production and employment. Multiple regressions were also used to determine proper coefficients of APP decision model (Bowman, 1963) [2] proposed a search-

* Corresponding author. Tel.: +88-01774686877
E-mail addresses: rbn_khan@yahoo.com

base simulation model. Some heuristic optimization techniques have been developed to solve APP problems. A search decision rule (SDR) was developed to generate an acceptable solution for APP (Taubert, 1968) [3]. Mellichamp and Love (1978) [4] presented the adaptable production switching heuristics (PSH) model whose results were quite consistent with the actual managerial practices.

The newer works included the use of spreadsheet software to solve APP problems in easier accessible way (Techawiboonwong and Yenradee, 2003) [5]. Das et al. (2000) [6] integrated APP, master production scheduling, and short-term production scheduling to a common data model.

Some meta-heuristic algorithms were also employed to solve APP problems. Stockton and Quinn (1995) [7] proposed a genetic algorithm based method for solving an APP problem. Wang and Fang (1997) [8] applied genetic algorithm (GA) based method with fuzzy logic to imitate the human decision procedure. Instead of locating exact optimal solution, this algorithm searched for a family of inexact solutions within acceptable level. Then, a final solution was selected by examining a convex combination of these solutions. Kumar and Haq (2005) [9] solved an APP problem by using ant colony algorithm (AGA), genetic algorithm (GA), and hybrid genetic-ant colony algorithm (HGA). From the outcomes obtained, GA and HGA showed comparably good performance. Constrained optimizations are often being solved by different direct & indirect approaches. Among indirect approaches genetic approach is mostly lucrative because of its consistent & optimized results (Ioannis, 2009) [10].Genetic algorithm is furnished with different genetic parameters like crossover, mutation, selection functions etc and different researchers used different combinations to solve constrained & unconstrained optimization problems (Bunnag & Sun, 2005) [11].

Particle Swarm Optimization (PSO) is another relatively new bio-inspired algorithm that may be used to find optimal or near-optimal solutions to numerical and quantitative problems. It was originally developed by a social psychologist, James Kennedy and Russel Eberhart (1995) [12]. The algorithm was modeled the flocking behavior seen in many species of birds. It embeds some mechanisms that are quite robust and can avoid local optima trap. Moreover, its evaluating function does not have to be twice differentiable. These make the PSO very attractive as one of the most efficient and effective optimization algorithm. Furthermore, the PSO is very easy to implement with few lines computer code. It has been applied to solve a wide variety of applications. El Mounayri et al. (2003) [13] used PSO to predict parameters of surface roughness in end milling. Prakasvudhisarn (2004) [14] used PSO to determine minimum tolerance zones of all basic form features for discrete parts inspection. The PSO was also extended to solve discrete problems. Kennedy and Eberhart (1997) [15] modified PSO to handle discrete binary variables. Experiments were conducted on standard test functions. The obtained outcomes showed that the PSO still performed well in terms of quality of solutions, robustness, and speed. Later, PSO was applied to other discrete problems including lot sizing problem (Tasgetiren and Liang, 2003) [16], flow-shop scheduling (Lian et al. 2006) [17].

Some researchers applied PSO to solve optimization problems with constraints. Hu et al. (2003) [18] modified the PSO to solve constrained nonlinear problems by preserving only feasible solutions. In this method, the PSO checks whether the current particle violates any constraints or not. If none of constraints is violated, mechanisms of PSO will continue normally. Otherwise, a wasted iteration occurs. This will loop until a feasible solution is found.

3. Algorithm

3.1 Particle Swarm Optimization

PSO is a new technique to deal with the problems whose solutions can be represented as a point in a *D*-dimensional solution space. PSO is initialized with a population of random particles $(X_1, X_2, \dots, X_D)$ which distribute uniformlyaround search space at first. Assuming that, the position and velocity of the i^{th} particle is represented by *D*-dimensional vectors $X_i = (x_{i1}, x_{i2} \dots., x_{iD})$ and $V_i = (v_{i1}, v_{i2}, \dots., v_{iD})$,respectively. The best previous position (*pbest*) of the i^{th} particle is defined as $P_i = (p_{i1}, p_{i2}, \dots, p_{iD})$, and the best position of the population (*gbest*) is denoted by $P_g = (p_{g1}, p_{g2}, \dots, p_{gD})$. The new velocity and position are updated according to following equations:

$$V_i^{k+1} = wV_i^k + c_1 r_1 (P_i - X_i^k) + c_2 r_2 (P_g - X_i^k) \quad (1)$$

$$X_i^{k+1} = X_i^k + V_i^{k+1} \quad (2)$$

Where $i = 1, 2, \dots, N$ and *N* is the size of the population; $k = 1, 2, \dots, K$ and K is the maximum number of iterations; w is the inertia weight; c_1 and c_2 are two positive constants,usually we choose $c_1 = c_2 = 2$; r_1 and r_2 are two randomfunctions in the range from 0 to 1. In PSO, the constraint conditions of velocity and position are:

$$-v_{max} \le v_{id} \le v_{max}, \; x_{min} \le x_{id} \le x_{max} \quad (3)$$

Where v_{max} is the maximum velocity, which allows actually serves as a constraint that controls the maximum global exploration ability PSO can have; x_{min} and x_{max} are the lower boundary and upper boundary of the solution space. The performance of each particle is measured according to a pre-defined fitness function which is problem dependent. Each particle observes the "fitness" of itself and its neighbors and emulates successful neighbors by moving towards them. This extremely simple approach has been surprisingly effective across a variety of problem domains.

In PSO, the inertia weight w plays a considered important role, because the balance between the global and local exploration abilities is mainly controlled by the inertia weight. Therefore, the parameter w will influence the

PSO'sconvergence behavior and choose a suitable *w* will help algorithm find the optimum solution accurately and rapidly. Large inertia weight at the beginning helps to find good seeds and the later small inertia weight facilitates fine search. So, a linearly decreasing inertia weight technique is developed, which linearly vary from 0.95 at the beginning of the search to 0.4 at the end. This technique has proven to be very efficient for balancing between the global and local exploration abilities. For this reason, this technique is used in our research and the inertia weight is determined by following equation:

$$w = w_{start} - \frac{w_{start} - w_{end}}{k} k \quad (4)$$

Where w_{start} and w_{end} denote the start and end value ofinertia weight, respectively.

The procedure of standard PSO can be summarized as follows (Algorithm 1):

Step 1: Initialize the size of the population *N*
Initialize the dimension of the solution space *D*
Initialize the maximum number of iterations *K*
Initialize the inertia weight w_{start} and w_{end}

Step 2: For each particle
Initialize the particle position X_i randomlyInitialize the particle velocity $V_i$randomlyInitialize the current position as P_i
Evaluate the fitness value
InitializeP_g according to the fitness value

Step 3: Calculate new inertia weight according to (4).

Step 4: Update velocity of each particle according to (1),
If$v_{id} > v_{max}$, then $v_{id} = v_{max}$
If$v_{id} < -v_{max}$, then $v_{id} = -v_{max}$

Step 5: Update position of each particle according to (2),
If $x_{id} > x_{max}$, then $x_{id} = x_{max}$
If $x_{id} < x_{min}$, then $x_{id} = x_{min}$

Step 6: Evaluate the fitness values of all particles. For each particle, compare its current fitness value with the fitness of its ***pbest***. If current value is better, then update ***pbest*** and its fitness value. Furthermore, determine the best particle of current population with the best fitness value. If the fitness value is better than the fitness of ***gbest***, then update ***gbest*** and its fitness value with the position and objective value of the current best particle.

Step 7: If the maximum number of iterations or any other predefined criterion is met, then stop; otherwise go back to Step 3.

3.2Genetic Algorithm

Genetic Algorithms were invented to mimic some of the processes observed in natural evolution. Many people, biologists included, are astonished that life at the level of complexity that we observe could have evolved in the relatively short time suggested by the fossil record. The idea with GA is to use this power of evolution to solve optimization problems. The father of the original Genetic Algorithm was John Holland who invented it in the early 1970's. The GA proposed by Holland (1975) to encode the features of a problem by chromosomes, where each gene represents a feature of the problem. Genetic Algorithms (GAs) are adaptive heuristic search algorithm based on the evolutionary ideas of natural selection and genetics. As such they represent an intelligent exploitation of a random search used to solve optimization problems. Although randomized, GAs are by no means random, instead they exploit historical information to direct the search into the region of better performance within the search space. The basic techniques of the GAs are designed to simulate processes in natural systems necessary for evolution; especially those follow the principles first laid down by Charles Darwin of "survival of the fittest". Since, in nature competition among individuals for scanty resources results in the fittest individuals dominating over the weaker ones.

In general, GA consists of the following steps:

Step 1: Initialize a population of chromosomes.

Step 2: Evaluate the fitness of each chromosome.

Step 3: Create new chromosomes by applying genetic operators such as reproduction, crossover and mutation to current chromosomes.

Step 4: Evaluate the fitness of the new population of chromosomes.

Step 5: If the termination condition is satisfied, stop and return the best chromosome; otherwise, go to Step 3.

The ability of the algorithm to explore and exploit simultaneously, a growing amount of theoretical justification, and successful application to real-world problems strengthens the conclusion that GAs are a powerful, robust optimization technique.

4. Problem Formulation

4.1 Problem Description & Notation

Authors have used a 2 product 2 period scenario for this case. We've employed the following notations for formulating the APP problem which predominantly akin in different literatures (Wang and Fang, 2001; R. C. Wang & T. F. Liang, 2004) [19, 20].

D_{nt} Forecast demand for nth product in period t (units)

a_{nt} Regular time production cost per unit for nth product in period t (TK. /unit)

Q_{nt} Regular time production for nth product in period t (units)

i_a Escalating factor for regular time production cost (%)

b_{nt} Overtime production cost per unit for nth product in period t (TK. /unit)

O_{nt} Overtime production for nth product in period t (units)

i_b Escalating factor for overtime production cost (%)

c_{nt} Subcontracting cost per unit for nth product in period t (TK. /unit)

S_{nt} Subcontracting volume for nth product in period t (units)

i_c Escalating factor for subcontract cost (%)
d_{nt} Inventory carrying cost per unit for n[th] product in period t (TK. /unit)
I_{nt} Inventory level in period for n[th] product (units)
i_d Escalating factor for inventory carrying cost (%)
e_{nt} Backorder cost per unit of n[th] product in period t (TK. /unit)
B_{nt} Backorder level for n[th] product in period t (units)
i_e Escalating factor for Backorder cost (%)
K_t Cost to hire one worker in period t (Tk. /man-hour)
H_t Worker hired in period t (man-hour)
m_t Cost to layoff one worker in period t (Tk. /man-hour)
F_t Workers laid off in period t (man-hour)
i_f Escalating factor for hire and layoff cost (%)
i_{nt} Hours of labor per unit of n[th] product in period (man-hour/unit)
r_{nt} Hours of machine usage per unit of n[th] product in period t (machine-hour/unit)
V_{nt} Warehouse spaces per unit of n[th] product in period (man-hour/unit)
W_{tmax} Maximum labor level available in period t (man-hour)
M_{tmax} Maximum capacity available in period t (machine-hour)
V_{tmax} Maximum warehouse space available in period t (ft^2)

4.2 Objective Function

Most practical decisions made to solve APP problems usually consider total costs. Total costs as objective function (Wang and Fang, 2001) [19]. The total costs are the sum of the production costs and the costs of changes in labor levels over the planning horizon T. Accordingly, the objective function of the proposed model is as follows:

$$\boldsymbol{MinZ} = \sum_{n=1}^{N}\sum_{n=1}^{T}[a_{nt}Q_{nt}(1+i_a)^t + b_{nt}O_{nt}(1+i_b)^t + c_{nt}S_{nt}(1+i_c)^t + d_{nt}I_{nt}(1+i_d)^t + e_{nt}B_{nt}(1+i_e)^t + \sum_{t=1}^{T}(K_tH_t + m_tF_t)(1+i_f)^t \quad (5)$$

4.3 Constraints

Constraints on carrying inventory:

$$I_{nt} - B_{nt} = I_{n(t-1)} - B_{n(t-1)} + Q_{nt} + O_{nt} + S_{nt} - D_{nt} \; for \forall n, \forall t \quad (6)$$

Constraints on Labor levels:

$$\sum_{n=1}^{N} i_{nt}(Q_{nt} + O_{nt}) \le W_{tmax} \; for \forall t \quad (7)$$

$$\sum_{n=1}^{N} i_{n(t-1)}(Q_{n(t-1)} + O_{n(t-1)}) + H_t - F_t - \sum_{n=1}^{N} i_{nt}(Q_{nt} + O_{nt}) = 0 \quad for \forall t \quad (8)$$

Constraints on Machine capacity & Warehouse space:

$$\sum_{n=1}^{N} r_{nt}(Q_{nt} + O_{nt}) \le M_{tmax} \; for \forall t \quad (9)$$

$$\sum_{n=1}^{N} V_{nt} I_{nt} \le V_{tmax} \; for \forall t \quad (10)$$

Others:

$$I_{nt} \ge I_{ntmin} \; for \forall n, \forall t \quad (11)$$

$$B_{nt} \le B_{ntmax} \; for \forall n, \forall t \quad (12)$$

$$S_{nt} \le S_{ntmax} \; for \forall n, \forall t \quad (13)$$

No negativity constraints on decision variables are:

$$Q_{nt}, O_{nt}, S_{nt}, I_{nt}, B_{nt}, H_t, F_t \ge 0 \; for \forall n, \forall t \quad (14)$$

5. Case Description

The Comfit Composite Knit Limited is the sister concern of Youth Group, which is one of the pioneer company of Ready Made Garments (RMG) sector in Bangladesh. This company readily produced knit ware items among them some are fancy & some are expensive. The jacket items as well as cardigan items are most expensive and most time & cost incurring manufacturing items. So it needs a lot of precise observations & perfect manufacturing practices to catch up the market& satisfy the buyers within specified lead time. Since they are the most expensive items, major concentration was on one particular style of hooded jacket (Product 1) & another special type of ladies cardigan (Product 2).

The APP decision problem for CCKL's Knit garments manufacturing plant presented here focuses on developing an interactive Genetic Algorithm approach for minimizing total costs. The planning horizon is 2 months long, including May and June. The model includes two types of knit ware items, namely the hooded jacket (Product 1) and special type of ladies cardigan (Product 2).According to the preliminary environmental information, Tables 1 & 2 summarizes the forecast demand, related operating cost, and capacity data used in the CCKL case. Other relevant data are as follows.

I. Initial inventory in period 1 is 500 units of product 1 and 200 units of product 2. End inventory in period 2 is 400 units of product 1and 300 units of product 2.
II. Initial labor level is 225 man-hours. The costs associated with hiring and layoffs are Tk. 22 and Tk. 8 per worker per hour, respectively.
III. Hours of labor per unit for any periods are fixed to 0.033 man-hours for product 1 and 0.05 man hours for product 2. Hours of machine usage per unit for each of the two planning periods are 0.1 machine-hours for product 1 and 0.08, machine-hours for product 2. Warehouse spaces required per unit are 1 square feet for product 1 and 1.5 square feet for product 2.
IV. The expected escalating factor in each of the costs categories are 1%.

Table 1 Forecasted demand, maximum labor, machine, warehouse capacity, back order level, subcontracted volume & minimum Inventory data

Item (Unit)	Period		Item	Period	
	1	2		1	2
D_{1t}	**1350-1450**	**2950-3050**	S_{1tmax} (pieces)	200	350
D_{2t}	**1550-1650**	**750-850**	S_{2tmax} (pieces)	100	100
W_{tmax} (man-hours)	225	225	I_{1tmax} (pieces)	300	500
M_{tmax} (machine-hours)	400	500	I_{2tmax} (pieces)	150	200
V_{tmax} (ft2)	1000	1000	B_{1tmax} (pieces)	200	600
			B_{2tmax} (pieces)	150	100

Table 2 Related operating cost data for the CCKL case

Product	a_{nt} (tk./unit)	b_{nt} (tk./unit)	c_{nt} (tk./unit)	d_{nt} (tk./unit)	e_{nt} (tk./unit)
1	22	40	27	3.5	42
2	20	40	30	4	47

6. Results & Findings

After running the problem in MATLAB 2014a by a pc with the configuration AMD A6 4400m dual core, 4 gb ram, radeon hd 7520g graphics card for both genetic algorithm and PSO significant difference were noticed. In this problem PSO excelled in all criterion. It had the better objective function value in shortest time. In this case we have used $c_1 = c_2 = 1.49$ and the inertia range 0.1 to 1.1. On comparison GA took ridiculously high time and inferior result. For a 3 variable 3 constraints problem GA took 10.536 seconds while for this particular problem it took as much as 177.684 second. So even with time consideration, PSO is more suitable than GA. The APP decision problem presented in the CCKL case was solved using the PSO and GA, as summarized in Table 3.Consequently, the optimal value when applying PSO to minimize the total costs was Tk. 230075.1925. In contrast with the GA approach, the results were Tk. Finally, the PSO approach is useful for solving APP decision problems and can generate better decisions than other models within very short time.

Table 3 Objective function value & required time

Algorithm	GA	PSO
Z	275931	230075.1925
Time	177.684s	2.107s

Table 4APP plan for the CCKL case

	GA		PSO	
Variables	Period 1	Period 2	Period 1	Period 2
Q_{1t}	405.999	1.98E-05	569.2108	999.7696
Q_{2t}	2.34E-05	212.6665109	629.2627	445.9673
O_{1t}	403.9996	3276.999959	568.8371	999.1826
O_{2t}	1824.667	212.6665381	628.7374	446.0327
S_{1t}	200.0002	2.28E-05	200	350
S_{2t}	1.55E-05	100.000023	99.99999	99.99999
I_{1t}	299.9997	499.9993055	428.0479	500
I_{2t}	466.6667	199.9991704	150	200
B_{1t}	2.00E+02	2.80E-05	1.00E-05	600
B_{2t}	4.84E-05	99.99998836	150	99.99999
H_t	120.2314	11.44432553	100.4556	5.01894
B_t	2.27E+00	8.03E-06	1.00E-05	5.090898

Table 5 Corresponding demand value within the range

Demand Value	Period 1	Period 2
D_{1t}	1410	2977
D_{2t}	1558	792

7. Conclusion & Future Works

The results show that PSO is much more feasible in this type of case. Besides, fewer parameters selection has made it much easier to work with PSO. For these reasons we can use PSO instead of GA in various engineering problem. In future we can work with total uncertain condition. Besides some modifications regarding velocity upgrade or velocity clamping can be made which will

result in even faster performance. And obviously there's an option that we can perform some comparative study of PSO with other algorithms and find suitable options for solving engineering optimization problems.

8. References

[1] F. Hanssman, and S. Hess, A linear programming approach to production and employment scheduling, *Management Technology*, 1(1): 46-50, (1960).

[2] E.H. Bowman, Consistency and optimality in managerial decision making, *Management Science*, 9(2):310-321, (1963).

[3] W. Taubert, A search decision rule for the aggregate scheduling problem, *Management Science*, 143(6):343-359, (1968).

[4] J.M. Mellichamp, and R.M. Love, Production switching heuristics for aggregate planning problem, *Management Science*, 24(12): 1242-1251, (1978).

[5] A. Techawiboonwong, and P. Yenradee, Aggregate production planning with workforce transferring plan for multiple product types, *Production Planning & Control*, 14(5): 447-458, (2003).

[6] B.P. Das, J.G. Rickard, N. Shan, and S. Macchietto, An investigation of integration of aggregate production planning, master production scheduling and short-term production scheduling of batch process operations through a common data model, *Computers and Chemical Engineering*, 24: 1625-1631,(2000).

[7] D.J. Stockton, and L. Quinn, Aggregate production planning using genetic algorithms, *Proc. Instn. Mech. Engrs., Part B, Journal of Engineering Manufacture*, 209(B3): 201-208, (1995).

[8] D. Wang, and S.C. Fang, A genetics-based approach for aggregated production planning in a fuzzy environment, *IEEE Transactions on System, Man, and Cybernetics-Part A: Systems and Humans*, 27(5): 636-645, (1997).

[9] G.M. Kumar and N.N. Haq, Hybrid genetic-ant colony algorithms for solving aggregate production plan, *Journal of Advanced Manufacturing Systems*, 4(1): 103-111, (2005).

[10] G.T. Ioannis, Solving constrained optimization problems using a novel genetic algorithm, *Applied Mathematics and Computation*, Vol. 208, pp. 273–283, (2009).

[11] D. Bunnag & M. Sun, Genetic algorithm for constrained global optimization in continuous variables, *Applied Mathematics and Computation*, Vol. 171, pp. 604–636, (2005).

[12] R. Eberhart, and J. Kennedy, A new optimizer using particle swarm theory, *Proceeding of the 6th International Symposium on Micro Machine and Human Science*, pp. 39-43, (1995).

[13] H. El-Mounayri, Z. Dugla, and H. Deng, Prediction of surface roughness in end milling using swarm intelligence, *Proceedings of IEEE Swarm Intelligence Symposium*, pp. 220-227, (2003).

[14] C. Prakasvudhisarn, A particle swarm search for determination of minimum zone, *proceeding of the Seventh International Conference on Industrial Managemen*t, pp. 109-115, (2004).

[15] J. Kennedy, and R.C. Eberhart, A discrete binary version of the particle swarm algorithm, *IEEE International Conference on Systems, Man, and Cybernetics*, 5: 4104-4108, (1997).

[16] M.F. Tasgetiren, and Y.C. Liang, A binary particle swarm optimization algorithm for lot sizing problem, *Journal of Economic and Social Research*, 5(2): 1-20, (2003).

[17] Z. Lian, X. Gu, and B. Jiao, A novel particle swarm optimization algorithm for permutation flow-shop scheduling to minimize makespan, *Chaos, Solitons, and Fractals, In press*, (2006).

[18] X. Hu, R.C. Eberhart, and Y. Shi, Engineering optimization with particle swarm, *Proceedings of the 2003 IEEE on Swarm Intelligence Symposium*, pp. 53-57, (2003).

[19] R.C. Wang, R.C & H. H. Fang, Aggregate production planning with multiple objectives in a fuzzy environment, *European Journal of Operational Research*, Vol. 133, pp. 521–536, (2001).

[20] R.C. Wang & T.F. Liang, Application of fuzzy multi-objective linear programming to aggregate production planning, *Computers and Industrial Engineering*, Vol. 46, No. 1, pp. 17–41, (2004).

ICMIEE-PI-140311

Optimization of Metal Removal Rate for AISI 1020 Mild Steel in Turning Operation by Lathe Machine

Md. Maksudul Islam , Lipon Kumar Sarkar, Dr.Md. Rafiquzzaman
Department of Industrial Engineering and Management, Khulna University of Engineering & Technology, Khulna-9203, BANGLADESH

ABSTRACT
This research work deals with an optimization of turning process by the effect of machining parameters applying ANOVA &Taguchi methods to improve the quality of manufactured goods and engineering development of designs for studying variation. Turning is a metal cutting process by which metals from the outer periphery of a cylindrical work piece is removed and the volume of metal removed per unit time is known as metal removal rate or MRR. Basically MRR is an important criterion in production engineering to increase the productivity and quality. MRR varies with the variation of cutting parameters of different metals. In this project work, AISI 1020 mild-steel is considered as work piece while spindle speed, feed rate and depth of cut are considered as cutting parameters. During turning process it is expected that the highest material removal rate is accomplished in order to achieve highest production at reduced time and cost and therefore it becomes very important issue to precisely study the effect of turning parameters. The results of analysis show that depth of cut and spindle speed have the most significant contribution on the material removal rate and feed rate has less significant contribution on the material removal rate.

Keywords: Analysis of Variance (ANOVA), Material Removal Rate (MRR), Taguchi Method, Depth of Cut.

1. Introduction

This paper represents the effect of various parameters on metal removal rate in turning operation. The paper also presents a mathematical formulation of metal removal rate in turning operation and to optimize this formula experimentally is the primary purpose of this project work.

In the turning operation, vibration is a frequent problem, which affects the result of the machining and in particular the surface finish. Tool life is also influenced by vibrations. Severe acoustic noise in the working environment frequently results as a dynamic motion between the cutting tool and the work piece. In all cutting operations like turning, boring and milling vibrations are induced due to deformation of the work piece. In the turning process, the importance of machining parameter choice is increased, as it controls the surface quality required. [1]

Dr Genichi Taguchi is a Japanese quality management consultant who has developed and promoted a philosophy and methodology for continuous quality improvement in products and processes. Within this philosophy, Taguchi shows how the statistical design of experiments (SDOE or DOE) can help industrial engineers design and manufacture products that are both of high quality and low cost. His approach is primarily focused on eliminating the causes of poor quality and on making product performance insensitive to variation. DOE (Design of Experiment) is a powerful statistical technique for determining the optimal factor settings of a process and thereby achieving improved process performance, reduced process variability and improved manufacturability of products and processes. Taguchi (1986) advocates the use of orthogonal array designs to assign the factors chosen for the experiment. The most commonly used orthogonal array designs are L8 (i.e. eight experimental trials), L16 and L18. The power of the Taguchi method is that it integrates statistical methods into the engineering process. Bendell *et al.* (1989) and Rowlands *et al.* (2000) report success of the Taguchi method in the automotive, plastics, semiconductors, and metal fabrication and foundry industries. [2]

The Taguchi method has been widely used in engineering analysis and is a powerful tool to design a high quality system. Moreover, the Taguchi method employs a special design of orthogonal array to investigate the effects of the entire machining parameters through the small number of experiments. By applying the Taguchi technique, the time required for experimental investigations can be significantly reduced, as it is effective in the investigation of the effects of multiple factors on performance as well as to study the influence of individual factors to determine which factor has more influence. [3]

The aim of this experimental investigation is to estimate the effects of cutting speed, feed rate, and depth of cut on Material Removal Rate in Turning of mild steel. Design of experiment techniques, i.e. Taguchi's technique have been used to accomplish the objective and to generate optimized value. Here L27 orthogonal array used for conducting the experiments and ANOVA

* Corresponding author. Tel.: +88-01790847464, +88-01673898882
E-mail addresses: rafiqbitr@yahoo.com, maksudkhandakar@gmail.com

technique was employed to analyze the percentage contribution and influence of Process Parameters.

2. Methodology

2.1 Specification of Work Material

For performing turning operations AISI 1020 (plain carbon steels is also named as) mild steel materials have been used. They were in the form of cylindrical bar of diameter 32mm and length 100mm. The material composition of AISI 1020 steel has given below [4].

Table 1 Chemical composition of AISI 1020 steel.

C	Si	Mn	Cr	Ni	P	S	Fe
0.20	0.22	0.66	0.055	0.18	0.015	0.028	Balanced

2.2 Process parameters

Table 2 Process parameter for investigation.

Level	Speed (s) (rpm) A	Feed rate(f) (mm/rev) B	Depth of cut(d) (mm) C
1	112	0.125	0.25
2	175	0.138	0.30
3	280	0.153	0.35

2.3 Taguchi Method

The Taguchi experimental design method is a well-known, unique and powerful technique for product or process quality improvement. It is widely used for analysis of experiment and product or process optimization. Taguchi has developed a methodology for the application of factorial design experiments that has taken the design of experiments from the exclusive world of the statistician and brought it more fully into the world of manufacturing [5]. Traditional experimental design methods are very complicated and difficult to use. Additionally, these methods require a large number of experiments when the number of process parameters increases. In order to minimize the number of experiments required, Taguchi experimental design method, a powerful tool for designing high-quality system. This method uses a special design of orthogonal arrays to study the entire parameter space with minimum number of experiments [6]. Taguchi strategy is the conceptual framework or structure for planning a product or process design experiment

2.4 Analysis of Variance (ANOVA)

Analysis of variance (ANOVA) is a statistical method for determining the existence of differences among several population means. While the aim of ANOVA is the detect differences among several populations means, the technique requires the analysis of different forms of variance associated with the random samples under study- hence the name analysis of variance. The original ideas analysis of variance was developed by the English Statistician Sir Ronald A. Fisher during the first part of this century. Much of the early work in this area dealt with agricultural experiments where crops were given different treatments, such as being grown using different kinds of fertilizers. The researchers wanted to determine whether all treatments under study were equally effective or whether some treatments were better than others [7].

ANOVA is used to determine the influence of any given process parameters from a series of experimental results by design of experiments and it can be used to interpret experimental data. Since there will be large number of process variables which control the process, some mathematical model are require to represent the process. However these models are to be developing using only the significant parameters which influences the process, rather than including all the parameters.

3. Experimentation and mathematical modeling

3.1 Choice of orthogonal array design

The choice of a suitable orthogonal array (OA) design is critical for the success of an experiment and depends on the total degrees of freedom required to study the main and interaction effects, the goal of the experiment, resources and budget available and time constraints. Orthogonal arrays allow one to compute the main and interaction effects via a minimum number of experimental trials (Ross, 1988). ‘‘Degrees of freedom’’ refers to the number of fair and independent comparisons that can be made from a set of observations. In the context of SDOE, the number of degrees of freedom is one less than the number of levels associated with the factor. In other words, the number of degrees of freedom associated with a factor at *p*-levels is (*p*-1). As the number of degrees of freedom associated with a factor at two levels is unity. The number of degrees of freedom associated with an interaction is the product of the number of degrees of freedom associated with each main effect involved in the interaction (Antony, 1998) [2].

3.2 Mathematical formulation and experimental data

The experiment is conducted for Dry turning operation (without cutting fluid) of using mild steel as work material and high speed steel as tool material on a conventional lathe machine. The tests are carried for a 100 mm length work material. The process parameters used as spindle speed (rpm), feed (mm/rev), depth of cut (mm). The response variable is material removal rate and the experimental results are recorded in Table 3. Material removal rate is calculated by following formula.

Let,

D_i = Initial diameter of the metal bar,

D_f = Final diameter of the metal bar,

L = Cutting length of workpiece,

t = time

Now,

Volume $= \pi/4L\ D^2_i - \pi/4L\ D^2_f$

$= \pi/4L\ (D^2_i - D^2_f)$
$= \pi/4L\ (D_i + D_f)\ (D_i - D_f)$
$= \pi\ L\ \{(D_i + D_f)/2\}\ \{(D_i - D_f)/2\}$
$= \pi\ L$ (Average diameter) (Depth of cut)

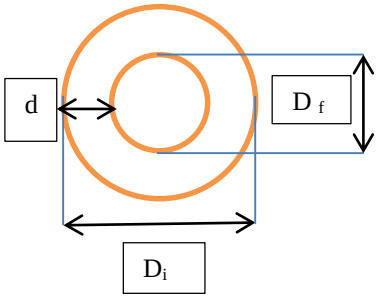

Fig.1 Schematic view of cutting section.

From Fig.1,

$D_i - D_f = 2d$ [Where, d = Depth of cut]

$\Rightarrow \quad d = (D_i - D_f)/2$

And,

$(D_i + D_f)/2$ = Average diameter of the cutting section = D_{avg}

So, Experimental formula for M.R.R

$$= \frac{\pi \times L \times d \times D_{avg}}{t} \quad mm^3/sec$$

Creating orthogonal arrays for the parameter design indicates the number of condition for each experiment. The selection of orthogonal arrays is based on the number of parameters and the level of variation for each parameter.

For the maximum material removal rate, the solution is "Larger is better" and S/N ratio is determined according to the following equation:

$$S/N = 10 \log_{10} \{n^{-1} \sum y^{-2}\}$$

Where,

S/N = Signal to Noise Ratio,
n = No. of Measurements,
y = Measured Value

Table 3 Experimental data and results for L27 Orthogonal array

Sl No	Spindle Speed (rpm) A	Feed Rate (mm/rev) B	Depth of Cut (D.O.C)(mm) C	Time, t (sec)	Average dia, (D_{avg} mm)	Material Removal Rate (M.R.R) (mm^3/sec) X
01	112	0.125	0.25	307	33.47	8.56
02	112	0.125	0.30	287	32.97	12.89
03	112	0.125	0.35	256	32.47	13.94
04	112	0.138	0.25	208	31.95	12.06
05	112	0.138	0.30	325	31.45	9.12
06	112	0.138	0.35	294	30.98	11.58
07	112	0.153	0.25	298	30.47	8.03
08	112	0.153	0.30	291	29.96	9.70
09	112	0.153	0.35	296	29.49	11.11
10	175	0.125	0.25	315	28.97	7.22
11	175	0.125	0.30	288	28.42	9.30
12	175	0.125	0.35	262	27.90	11.70
13	175	0.138	0.25	220	27.47	9.80
14	175	0.138	0.30	222	26.96	11.44
15	175	0.138	0.35	275	25.30	10.11
16	175	0.153	0.25	235	24.675	8.24
17	175	0.153	0.30	142	24.135	16.01
18	175	0.153	0.35	196	23.96	13.30
19	280	0.125	0.25	181	23.375	10.14
20	280	0.125	0.30	168	22.87	12.83
21	280	0.125	0.35	146	22.475	16.93
22	280	0.138	0.25	176	21.886	9.81
23	280	0.138	0.30	129	21.425	15.65
24	280	0.138	0.35	149	20.97	15.47
25	280	0.153	0.25	163	20.135	9.70
26	280	0.153	0.30	178	19.73	10.45
27	280	0.153	0.35	179	19.235	11.82

Table 4 ANOVA for the response Material Removal Rate (MRR)

Source	DOF	Sum of squares	Mean of squares	F ratio	% of contribution
Speed(s)	2	17.97	8.9835	32.667	21.42
Feed (f)	2	2.73	1.3634	4.958	3.25
DOC(d)	2	62.65	31.3281	113.920	74.68
Error	2	0.55	0.275		0.65
Total	8	83.90			100

From the above Table 4, it is observed that the depth of cut (74.68%), spindle speed (21.42%) have great influence on metal removal rate. The parameter feed rate (3.25%) has small influence. Since this is a parameter based optimization design, from the above values it is clear that depth of cut (74.68%) is the prime factor to be effectively selected to get the effective material removal rate.

Design of experiment for material removal rate L9 orthogonal array is prepared by carrying out a total number of 9 experiments along with 2 verification (X and Y data) experiments. For Y data, 9 set of new experiments is conducted in terms of data representation of Table 4. In L9 array 9 rows represent the 9 experiment to be conducted with 3 columns at 3 levels of the

corresponding factor. The matrix form of this array is shown in Table 5.

Classical experimental design methods are too complex and are not easy to use a large number of experiments have to be carried out when the number of process parameters increases. To solve this problem, the Taguchi method uses a special design of orthogonal arrays to study the entire parameter space with only a small number of experiments [8].

Table 5 Calculation of Signal to Noise ratio for MRR

Parameter				MRR		Signal to noise ratio
Exp No	A	B	C	X	Y	(SN ratio)
01	112	0.125	0.25	8.56	8.57	61.66
02	112	0.138	0.30	9.12	9.135	58.695
03	112	0.153	0.35	11.11	11.10	63.92
04	175	0.125	0.30	9.30	9.32	56.37
05	175	0.138	0.35	10.11	10.10	63.10
06	175	0.153	0.25	8.24	8.26	55.32
07	280	0.125	0.35	16.93	16.95	61.37
08	280	0.138	0.25	9.81	9.89	56.83
09	280	0.153	0.30	10.447	10.47	51.88

The experimental data for the material removal rate values and the calculated signal-to-noise ratio are shown in Table 5. The S/N ratio values of the material removal rate are calculated, using higher the better characteristics. Conceptual S/N ratio approach of Taguchi method provides a simple, systematic and efficient methodology for optimizing of process parameters and this approach can be adopted rather than using engineering judgment. This implies that engineering systems behave in such a way that the manipulated production factors that can be divided into three categories:

I. Control factors, which affect process variability as measured by the S/N ratio.
II. Signal factors, which do not influence the S/N ratio or process mean.
III. Factors, which do not affect the S/N ratio or process mean.

In practice, the target mean value may change during the process development applications in which the concept of S/N ratio is useful are the improvement of quality through variability reduction and the improvement of measurement. The S/N ratio characteristics can be divided into three categories when the characteristic is continuous: nominal is the best, smaller the better and larger is better characteristics. Based on Taguchi prediction that the bigger different in value of S/N ratio shows a more effect on material removal rate or more significant. Therefore, it can be concluded that, increase changes the depth of cut reduces the material removal rate significantly and it is shown in Table 6. Here delta is the difference between the maximum and minimum value of signal to noise ratio for each parameter. The highest delta value is ranked as first parameter which possesses the maximum influence in metal removal rate of AISI 1020 steel.

Table 6 Response table for Signal to Noise Ratio for MRR

Level	Spindle speed Factor A	Feed rate Factor B	DOC Factor C
1	61.425	59.87	57.94
2	58.263	59.50	55.65
3	56.760	57.04	62.86
Delta(max-min)	4.665	2.83	7.21
Rank	2	3	1

From Table 6 it is clear that the depth of cut is the most significant parameter for maximizing metal removal rate as its rank is first.

4. Results and Discussions

4.1 Equation for optimization of metal removal rate

From the linear regression analysis (running a program in IBM SPSS Statistics) the following equation has derived:

M.R.R =1.409+0.011(spindle speed) - 21.176(feed rate) +36.00(depth of cut)

4.2 Graphical representation

In the above experimental results, two techniques of data analysis have been used. Both techniques draw similar conclusions. The depth of cut has found to be the most significant effect to produce high value of average metal removal rate (MRR). The explanation for the influence of cutting speed on metal removal rate is still not available. This could be explained in terms of the velocity of chips that is faster at high cutting speed than at low cutting speed. This leads to a shorter time for the chips to be in contact with the newly formed surface of workpiece and the tendency for the chips to wrap back to the new face form is little as compared to low speed. The condition of seizure and sub layer plastic flow occurred at high speed and the term flow-zone is used to describe secondary deformation in this range [9]. The time taken for the chips at this flow-zone for high speed cutting is short as compared to lower speed, as the velocity of chip is faster [10]. The use of S/N ratio for selecting the best levels of combination for metal removal rate (MRR) value suggests the use of high value of depth of cut in order to obtain good removal rate. Therefore, it is preferable to set the depth of cut to a high value. Therefore, one can say that the set values for level '3' and '1' are both suitable to obtain good quantity of metal removal rate (MRR). From the result, the interaction of factor C and factor A is more important than the effect of the individual factors. In other words, in order to get the best result it requires experience to combine these two factors to achieve a suitable

combination of depth of cut and spindle speed. Form the minitab graph it is clear that spindle speed and depth of cut have the maximum influence for high metal removal rate.

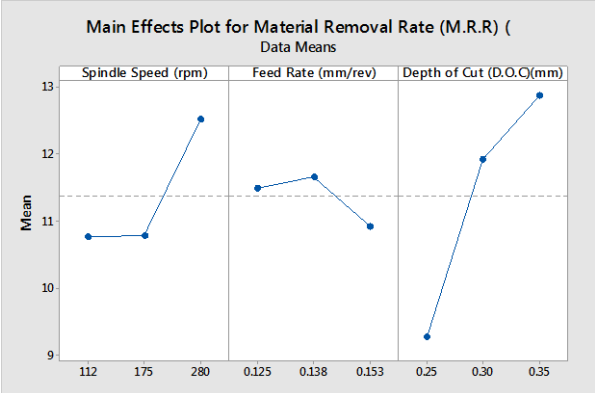

Fig.2 Main effects plot of mean value for MRR

5. Scope of Future Works

Some recommendations are given below:

I. The verification of the model for MRR may be developed by using other parameters.
II. Same analysis can be conducted for milling, facing, drilling, grinding and other metal removing processes.
III. Optimization of cutting parameters may be done by Fuzzy Logic and genetic algorithm.
IV. Same analysis may be done for other materials (like Copper, Brass and Aluminum etc.).
V. Consideration of tool wear, surface roughness, and power consumption may be done.
VI. Cutting fluids or lubricants are not used in this project work, cutting fluids can be used.

6. Conclusion

This paper illustrates the application of the parameter design (Taguchi method) in the optimization of metal removal rate of AISI 1020 steel in turning operation. ANOVA is required to know the contribution of each factors and their quantitative percentage during operation. To get the accurate percentage of contribution L27 orthogonal array is used in ANOVA analysis whereas for Taguchi's method L9 orthogonal array is used. Taguchi's method of parameter design can be performed with lesser number of experimentations and for this reason 9 consecutive experiments (L9 in Taguchi's method) have taken instead of 27 consecutive experiments (L27 in ANOVA). For both ANOVA and Taguchi's method, same result has been found that the depth of cut is the most significant parameter. The percentage of contribution of the depth of cut parameter is 74.68% in ANOVA analysis and the depth of cut is the first rank in Taguchi's method. Taguchi's method can be applied for analyzing any other kind of problems as described in this paper. It is found that the parameter design of the Taguchi method provides a simple, systematic, and efficient methodology for optimizing the process parameters and it is one of the most effective tools in the field of optimization problem solution.

NOMENCLATURE

s : Spindle speed, rpm.
f : Feed rate, mm/rev.
d : Depth of cut (DOC), mm.
D_i : Initial diameter of the metal bar, mm.
D_f : Final diameter of the metal bar, mm.
L : Cutting length of workpiece, mm.
t : time, sec.
D_{avg} : Average diameter of the cutting section, mm.
M.R.R. : Metal removal rate, mm^3 /sec.
A : Factor for spindle speed.
B : Factor for feed rate.
C : Factor for depth of cut.
S/N ratio : Signal to noise ratio.
X : Metal removal rate for first stage.
Y : Metal removal rate for second stage

REFERENCES

[1] G.M.Sayeed Ahmed, Hakeemuddin Ahmed , Syed Safiuddin Samad, "Experimental Investigation of Effect of Tool Length on Surface Roughness during Turning Operation and its Optimization" IOSR Journal of Mechanical and Civil Engineering (IOSR-JMCE) e-ISSN: 2278-1684,p-ISSN: 2320-334X, Volume 7, Issue 2 (May. - Jun. 2013), PP 73-80.

[2] Jiju Antony and Frenie Jiju Antony ,"Teaching the Taguchi method to industrial engineers" http://www.emerald-library.com/ft.

[3] Strojniški vestnik, **"**Application of Taguchi Method for Surface Roughness and Roundness Error in Drilling of AISI 316 Stainless Steel" - Journal of Mechanical Engineering 58(2012)3, 165-174.

[4] Sayed Shafayat Hossain, Md. Maksudul Islam & Md. Sajibul Alam Bhuyan, "A Case Study of Heat Treatment on AISI 1020 Steel"; Global Journal of Researches in Engineering: A, Mechanical and Mechanics Engineering, Volume 14, Issue 5, Version 1.0, Year 2014.

[5] S.R.DAS, R.P.NAYAK, D.DHUPAL; International Journal of Lean Thinking Volume3, Issue 2(December 2012).

[6] Mahendra korat, Neeraj Agarwal; "Optimization of different Machining parameters of En 24 Alloy steel in CNC Turning by use of Taguchi method", International journal of engineering research and application. ISSN: 2248-9622.

[7] M. Adinarayana, G. Prasanthi, G. Krishnaiah; "PARAMETRIC ANALYSIS AND MULTI OBJECTIVE OPTIMIZATION OF CUTTING PARAMETERS IN TURNING OPERATION OF AISI 4340 ALLOY STEEL WITH CVD CUTTING TOOL", IJRET: International Journal of Research in Engineering and Technology eISSN: 2319-1163 | pISSN: 2321-7308.

[8] T.G.Ansalam Raj and V.N .Narayanan Namboothiri; "An improved genetic algorithm for the prediction of surface finish in dry turning of SS 420 materials" manufacturing technology today 47, pp 313-324, 2010.

[9] E. M. Trent, Metal Cutting, 3rd ed., Butterworths, Heinemann, 1991

[10] Kareem Idan Fadheel and Dr. Mohammad Tariq;"OPTIMIZATION OF END MILLING PARAMETERS OF AISI 1055 BY TAGUCHI METHOD", International Journal of Advanced Research in Engineering and Technology (IJARET), ISSN 0976 –6480(Print), ISSN 0976 – 6499(Online) Volume 5, Issue 3, March (2014), pp. 09-20.

.

ICMIEE-PI-140327

Inevitable Environmental Degradation due to Textile Waste in Bangladesh: Is there Really a Solution?

*Jahid M M Islam[1], Md. Mahbubur R. Bhuiyan[2] and Mubarak A Khan[1]**

[1]Institute of Radiation and Polymer Technology, Bangladesh Atomic Energy Commission, Dhaka-1000, Bangladesh

[2]Echotex Limited, Kaliakoir, Gazipur, Bangladesh

ABSTRACT
Experiments revealed that proper ionizing radiation can completely detoxify the waste water and sludge to water soluble non-toxic form and the resulting residues can be used as liquid fertilizer as dyes are mostly stable nitrogenous compound and their degradation leads to produce water soluble nitrogenous salts which are readily available for uptaking by plants. Besides, sludge produced by the chemical or biological ETP contains minerals and biomasses that enrich soil fertility. Field trials showed excellent plant growth promotion without any adverse effect where raw sludge showed significant toxicity. Grown plants were subjected for toxicity, heavy metal content test etc. and were found safe for human consumption. Animals (rabbit) fed by this plants (grown in the treated sludge and effluent containing soil) showed no sign of complexity at any phase of life or during pregnancy. Besides, eco-brick and composite materials were also produced from sludge which can be employed as an alternative of conventional construction material. Possibility of reuse of the treated effluent in the dyeing plants is another great finding. All this experiments suggested that employment of ionizing radiation for textile effluent treatment is very potential to protect environment from this devastating pollution.

Keywords: Textile sludge, Gamma radiation, Detoxification, field trial.

*Corresponding author: Email-makhan.inst@gmail.com

INTRODUCTION

Environmental pollution has become a significant world concern. The main causes of this contamination are industries, which generate and deliver to the environment waste products often without any treatment. Most of these contaminants biodegrade very slowly, becoming dangerous for people, plants and animals. Damage to human health related to improper treatment of residues has led to strict environmental protection laws and consequently the need for research in the treatment of effluents [1-3] and sludge.

The variables involved in the environment's recuperation are numerous, mainly by the great variety of chemical compounds and raw materials used by industry. The most complicated industrial effluents are organic compounds, especially synthetic agents. Their degradation is difficult using conventional methods. The quality and quantity of industrial wastes change depending on the material used, and related processing technique. The aim of the conventional techniques employed is to reduce the volume and toxicity of the effluents but even with treatment, inevitably some waste still remains. Textile industries consume a large amount of water and use toxic products in its processes. Consequently, they produce and release large volumes of effluents, which after treatment, generate great amount of sludge. The final disposal of this sludge remains a challenge, as it contains a lot of toxic materials and depositing them in the usual ways will deteriorate the environment. Biological treatment such as activated sludge has been the choice of the majority of the facilities [4]. However, this process generates a great quantity of sludge [5] that is basically formed by the excess of biomass and substances that were not degraded during the biological treatment.

The aim of this research is to undertake a thorough study to discover if at the end of ionization processing of textile sludge; it can be used as a bio-fertilizer. Not only is this an attractive means of treating what is essentially a waste product, but recycling it to be used as fertilizer means we have achieved the state of zero waste production.

EXPERIMENTAL

Sample Collection

The combined textile sludge was collected from the Eco Tex textile industry, Kaliakoir, Gazipur. Then it was packed in small polybags (3 Kg/bag) and were sealed.

Gamma Irradiation of the Textile Sludge

The samples were irradiated by cobalt-60 gamma radiation source at different radiation doses (5KGy, 10KGy, 15KGy, 20KGy and 30KGy). The dose rate was 4.5 kGy/h.

Characterizations of Raw & Irradiated Sludge

Both raw and irradiated sludge were characterized by the means of pH, conductivity, TDS (total dissolved solids) and COD (Chemical oxygen demand) as well as solubility and biodegradability. All these parameters were measured with standard chemical methods.

* Corresponding author. Tel.: +88-01819252292
E-mail address: makhan.inst@gmail.com

Solubility Test of Raw and Irradiated Sludge
Sludge was dried in an oven for 12 hours at a temperature of 105^{o}C. After cooling grinded samples were kept in oven and dried at same temperature for several hours for the completion of drying. Then samples were sieved with a 0.5µm sieve. The resulting samples were weighted in a test tube and excess amount of distilled water was added. Samples were subjected to vortex and then kept for one hour. They were finally centrifuged to precipitate the insoluble portions and weighted after drying. Solubility was calculated in percentage.

Biodegradability Test
Garden soil was prepared my mixing with sludge samples at several ratios. The resulting samples were collected at different time interval, mixed with distilled water and kept for settle down. The grain patterns of the samples were compared and the biodegradability was estimated.

Seed Germination Test
Soil bed for germination was prepared using both treated and untreated sludge and then placed in Petri dishes. 30 *Basella alba* seeds were planted in each Petri dish, and left in an area were adequate amount of air and sunshine could be obtained. Seed germination was observed and counted after five days. The studies were triplicated for each samples and average value was taken.

Field trial
The experimental field was divided in three plots of equal areas, each of them were 9 sq. feet (3ft × 3 ft.). Then the irradiated (by 15kGy) sludge and raw sludge was mixed with the garden soil in 1:2 ratio. Plots having only garden soil served as control. The vegetables were sowed into the prepared plots after three days. No additional fertilizer was used.

Measurement of Plant Morphological Characteristics
Plant heights, width & number of leaves were observed for ten weeks consecutively. The plant heights were measured from soil surface to the top of the main plant stem. In order to measure the number of leaves, every visible leaves of each plants were counted, including the tips of new leaves just beginning to emerge.

Elemental Analysis
The samples were washed with the distilled water to remove the dust particles. After that the samples were dried at 100^{o}C for 6-8 hours. Dried samples were then ground into a fine powder using a mortar and stored in a polythene container until used for the elemental analysis by 3MV Tandem Accelerator. Before analysis sample pellets were prepared using pellet preparation equipment. For the preparation of pellet 1.5 mg sample were taken.

RESULTS AND DISCUSSIONS

Effect of Gamma Ray on Solubility of Sludge
Sludge of the textile mostly contains metal hydrated oxides and organic compounds. Most of these compounds breakdown in simpler molecules when irradiated. So, the solubility of sludge increases. It was found that almost 17.70% of sludge became soluble at 15 kGy dose of gamma radiation.

Table -1: Effect of gamma radiation on solubility of sludge

Samples	Raw sludge	5kGy	10kGy	15kGy	20kGy	30kGy
Percentages of solubility	6.30%	8.80%	6.50%	17.70%	8.30%	11.30%

Biodegradability Test
Biodegradability test of different dose of irradiated sludge and raw sludge is carried out four weeks consecutively by comparing the morphology of pure soil. After 4 weeks, it was observed that 15KGy irradiated sludge was miscible in pure soil completely whereas untreated sludge showed no notable miscibility. These results suggested that, the biodegradability of sludge can me reduced up to 4 weeks by gamma radiation treatment while untreated sludge takes around one year for biodegradation.

Chemical Oxygen Demand
The chemical oxygen demand analysis for sludge samples (1g/500mL) showed very interesting result. The highest COD at 20kGy with 26mg/L and lowest COD at raw sludge with 13mg/L were found. It can be assumed that there was an increase in COD with radiation occurred because the interactions (coagulation) between the minerals and organic matters decreased with radiation which led to increase available organic substances for titration. This phenomena was also justified by the increased biodegradability.

Germination Test
The rate of seed germination in the soil preparations is given in table 2. Soil prepared with 15kGy irradiated sludge showed same germination rate as plain soil (73%). The result for raw sludge showed poor germination rate within the same time period which indicated the toxic effect of untreated sludge.

Table-2: Rate of germination of irradiated sludge, raw sludge and pure soil

Sample ID	Seeds germinated from 30 seeds	Percentages (%)
Soil	22	73%
Raw sludge	12	40%
5KGy irradiated sludge	15	50%
10KGy irradiated	13	43%

sludge		
15KGy irradiated sludge	22	73%
20KGy irradiated sludge	21	70%
30KGy irradiated sludge	16	53%

Field trial observation

Irradiated sludge showed better crop growth compared to pure garden soil in all aspects. Although the weight and height of crops grown in raw sludge also showed better results, but was obvious toxicity in the plants since the leaves were showing brown spots and discoloring.

The mixture of 15KGy irradiated sludge & soil lead to plants with green colored leafs, maximum growth and maximum diameter. Other hand, the plants of pure soil showed low growth rate as no fertilizer was used. So treated sludge was uptaked by plants as fertilizer without any sign of toxicity.

Figure-1: Growth Amaranthus Viridis (Local Name: Danta Shak) Grown in Soil, Raw Sludge and Irradiated Sludge mixed soil preparations

Heavy Metal Detection Test

Plants grown in different soil preparation were subjected to heavy metal content test (table -3). Heavy metals were detected in the samples but they were within the acceptable limits. No significant metal content difference was found in the plants grown in plain soil and the plants grown in sludge preparations. As heavy metal containing dyes are banned for use in textile industry, these results were quite expected and justified.

Table-3: Comparison of heavy metal content of plants grown in different soil preparation

Conc (ppm)	Ti	V	Cr	Co	Ni	Cu	Zn
Raw Sludge	587.6	424.6	241.6	1413	0	0	80.42
Irradiated sludge	1652	840.8	1007	2042	181.9	48.46	120
Soil	8388	306.1	462.5	738.5	114.9	10.15	73.29

Conclusion

On the basis of above review it can be concluded that sludge can be treated by gamma radiation to be very important biological organic fertilizer/soil conditioner for sustainable agriculture. It improves organic matter status of the soil. It also adds macro and micronutrients to the soil. Improvement in organic matter content in soil helps in improving soil physical conditions, rejuvenating soil health and stimulating biological activity. Higher level of soil organic matter can sequester carbon and mitigate greenhouse gas emissions. Regarding the pathogen in textile sludge, their number can be significantly reduced by radiation treatment. It can also be assumed that gamma radiation is the most attractive and favorable method of this solid waste management. It is not only managing a waste product effectively, but also presenting a way to turn into a useful product.

References

[1]. Palaniappan, M, et al. "Clearing the Waters." *United Nations Environment Programme*. (2010). Web. 20 Jul. 2013. <http://www.unep.org/PDF/Clearing_the_Waters.pdf>.

[2]. "Industrial Waste." *Environmental Protection Agency*. Web. 20 Jul 2013. <http://www.epa.gov/epawaste/nonhaz/industrial/index.htm>.

[3]. Gomes, L, et al. "Ecotoxicity of Sludges Generated by Textile Industries: a Review." *JBSE : Journal of Biomechanical Science and Engineering*. 7, 89-96, 2012.

[4]. R. Anliker. "Ecotoxicology and environmental safety." 1, 59-74, 1979.

[5]. Kunz et al., International Encyclopedia Compilation. 14, 1122, 2002.

ICMIEE-PI-140331

Extraction of Bioactive Macromolecules from Locally Available Natural Resources and Application as Natural Tea Growth Promoter

*Jahid M M Islam[1], M Saifur Rahaman[1], M Mahbub Bhuiyan[2] and Mubarak A Khan[1]**

[1]Institute of Radiation and Polymer Technology, Bangladesh Atomic Energy Commission, Dhaka-1000, Bangladesh

[2]Echotex Limited, Kaliakoir, Gazipur, Bangladesh

ABSTRACT
This study was designed to evaluate the potential uses of natural biomaterials as tea growth promoter and anti-fungal agent. Bio-macromolecules were extracted from locally available natural resources i.e. prawn shell, sea weed etc. Extracted macromolecules were treated with Co-60 gamma radiation at different doses and were used to evaluate the growth promoting activity on tea plants. The aim of this study was to measure the effects of various concentrations and ratios of irradiated bio-macromolecule's solution in order to get the best response on tea plants in terms of various growth attributes. Samples were applied through foliar spraying at 7 days interval. The growth attributes like- total number of buds, fresh and dry weight of buds, average leaf area, and weight per bud and anti-fungal activities were determined after the foliar application for 15 weeks. The results showed increase in productivity (about 50%, based on fresh weight of tea leaves) and it reduced the total fungal count dramatically (more than 100 times in contrast with the control).

Keywords: Natural growth promoter, Gamma radiation, Tea plant, Bio-macromolecules.

*Corresponding author: Email-makhan.inst@gmail.com

INTRODUCTION

Today's over populated world demands more production of crops to fulfill its demand, within its limited hand. For instance, the use of chemical fertilizer for the production of more crops is popular in the recent times. However, the foods are produced using commercial chemical plant growth promoters, might have some harmful effects (Mollah et al., 2009). Chemical fertilizers which are used in agricultural land create environmental pollution (air and water) and facilitate the growth of weeds. For that, scientists are now interested to use natural polymer or bio-fertilizer as plant growth promoter instead of chemical fertilizer.

Biomaterials are new promising materials that possess important properties like biodegradability or lack of toxicity. The advantages of using these biomaterials are that, they are naturally available, cheap and have no destructive effect on overall environment including plants and animals which may be occurred in case of application of chemical fertilizers and pesticides.

Chitosan is a linear polysaccharide derived from chitin, a major component of the shell of crustaceans and the second most abundant biopolymer in nature next to cellulose and is commercially available [Kast et al., 2003]. It has the potential in agriculture with regard to controlling plant diseases and promoting the plant growth (Ghaouth et al., 1992, Ohta et al., 1999). These molecules were shown to display toxicity and inhibit fungal growth and development (Hadwiger, 1984).

On the other hand, alginates are widespread in nature; occurring in various organisms. Sargassum (brown algae) is the main source of sodium alginate (Na-alginate), which is abundantly found in the Coral Island, St. Martin's in Bangladesh (Aziz et al., 2001). Na-alginate, the natural growth promoter is friendly for environment. Alginate is the major structural polysaccharide extracted from brown seaweeds (Khan et al., 2010). Its empicical formula is Na-$C_6H_7O_6$. It is composed of three types of block polymers namely polyglucouronate (poly-G), polymannuronate (poly-M) and copolymer of poly-G and poly-M in random sequences (Hang et al., 1967).

Recently oligosaccharide derived from depolymerization of alginates and chitosan are promising candidate to the plant growth promotion applications. It was found that the influence of average molecular weight of chitosan on its fat-binding ability in vitro was very important and the reduction of molecular weight leads to a significant increase in the amount of fat bound by 1 g of chitosan (Czechowska-Biskup et al., 2005). Alginate of molecular weight less than 10 kD showed strong effect on the growth promotion of rice and peanut (Hien et al., 2010).

Several methods have been tried to produce low molecular weight chitosan, among them (oxidative degradation, acid hydrolysis, electrochemical process, ultrasonic treatment, thermal depolymerization,

* Corresponding author. Tel.: +88-01819252292
E-mail address: makhan.inst@gmail.com

enzymatic methods, micro fluidization combined with an ultrafiltration treatment, ultraviolet degradation, synergetic degradation with ultraviolet light and hydrogen peroxide and gamma radiation) gamma radiation degradation is relatively simple one step and an eco-friendly process and can be employed for the large scale production of . Radiation processing is the most promising method, since the process is simple, it is carried out at room temperature and no purification of the product is required after processing which allows extensive modification without waste and is a powerful tool that can be used to reduce molecular weight through chain scission mechanism without causing alteration to the main backbone structure of chitosan (Chmielewski and HajiSaeid, 2004).

This research work is concerning on the effect of radiation processed chitosan and Na-alginate on tea plants in the field trial basis to make a comparative study among treated and untreated plants.

MATERIALS AND METHODS

Preparation of 2% Chitosan (CH) Solution

Extraction of chitosan from shrimp shells and preparation of 2% solution in 2% acetic acid were done at the laboratory of Institute of Radiation and Polymer Technology of Bangladesh Atomic Energy Research Establishment according to standard procedure [Freier, 2008].

Preparation of 2% Na-Alginate (AL) Solution

Extraction of Na-Alginate from brown seaweed Sargassum [Khan et al., 2010] (Collected from Saint Martins Island) and preparation of 2% solution in water were done at the laboratory of Institute of Radiation and Polymer Technology of Bangladesh Atomic Energy Research Establishment according to standard procedure.

Radiation Degradation

Chitosan and Na-alginate solutions were irradiated by gamma radiation emitted from a Co-60 source at 40 kGy and 20 kGy doses respectively for degradation with a view to preparing oligosaccharides from them.

Selection of the experimental plots

The plant growth promotion activity was experimented in the field trial basis in Uttarbag-Indranagar teas state, Moulavibazar, Sylhet. Nine Plots having healthy tea trees from two divisions were selected. Among these nine plots 3 plots were for control, 3 plots were for Chitosan treatment and 3 plots were for Na-alginate treatment. The number of bushes per plot were counted for both divisions.

Evaluation of Growth Promoting Activity

The irradiated solutions of chitosan and Na-alginate were diluted to 500 ppm and 300 ppm respectively using pond water for testing the viability and reassuring it at the peasant level. The solutions were sprayed by using normal hand sprayer in the morning when photosynthesis of trees start. Foliar applications of biomaterials were done at every 7 days interval.

Evaluation of plant growth promotion activity

The leaves produced for each plant per plucking, their average numbers per plot and their average weight per plucking for each plot were calculated. Data collection started from the beginning of the first plucking. Measurements were recorded approximately at every 2 weeks interval and continued until 17th plucking. The results were finally tabulated and summed up using Microsoft Excel 2013 software. Then the results were graphically represented to evaluate the promotion activity.

RESULTS & DISCUSSION

The results for the field trial growth promotion experiments for division 1 and 2 are shown in the graphs 1 and 2 respectively. The graphs contain data for yields in Kg per plucking per plot.

Two varieties of tea trees were treated for this experiment. In division 1, tea seedlings of age 30 years and in division 2 tea variety TV23 of age 15 years were taken for this present work. From the graphs it is apparent that, for two varieties of tea trees, effectiveness of the two plant growth promoters (PGPs) is time dependent.

For both divisions, best results were found with alginate treatment. From figure 1, maximum yield with alginate treatment is found to be 21.67 % higher than that for control. However from figure 2, i.e. division 2 more prominent result with alginate treatment was found, and which was 71.47 % higher than that for control.

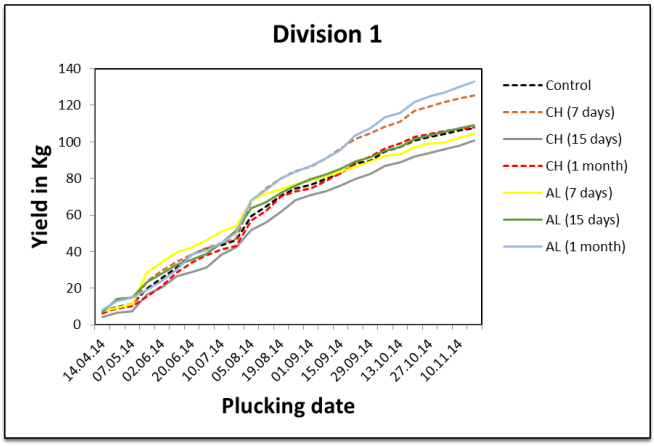

Figure 1. Yield of Tea leafs in Kg per plot of Division 1.

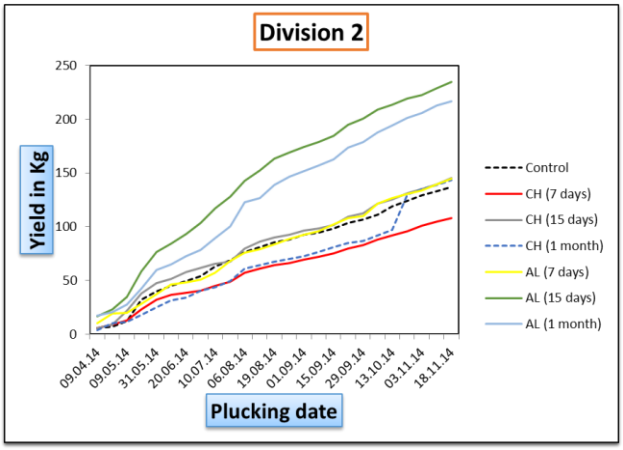

Figure 2. Yield of Tea leafs in Kg per plot of Division 2.

For chitosan treatment the results were not so much significant as that was for alginate. For division 1, yield of tea from seedlings of 30 yeas age, was found to be 14.757 % higher than that of control. On the other hand, for division 2 containing TV23 variety tea plants, the yield was only 5.632 % higher compared to the control.
From figure 1, it can be concluded that the optimized application intervals with alginate and chitosan treatment are 1 month and 7 days respectively. Whereas for division 2 15 days for alginate and 1 or half month for chitosan treatment are recommended.
There are some other conclusions that can be drawn from the figures, that, for TV23 tea plants both chitosan and alginates can be used as growth promoter; and for seedlings in division 1, alginate is the best solution.
Some negative trends in the tea yields for both division were also observed. For both chitosan and alginate treatment, from figures, low yields of tea are clear in contrast to the yield of the control, for some plots, may be due to the lack of due time spraying and red spider attack, as reported by the monitoring personnel in the tea state.

CONCLUSION

Field trial of tea growth promotion activities by the natural PGPs has been successful in spite of some inadvertent situations. Increase of budding, reduction of harvesting time were remarkable in this experiment. It can be summed up for the results found from this work as, these PGPs should be used for other promising fruits, that can bring more and more foreign revenues for 3rd world country like us. Moreover gamma radiation treatment, as a greener way to produce effective plant growth promoters should be taken under mass consideration by the research organizations as well the government to reduce the poisoning the environment by reducing the use of harmful chemicals.

REFERENCES

Chmielewski, A. G.; Haji-Saeid, M., Radiation technologies: past, present and future, Radiation Physics and Chemistry, Volume 71, Issue 1-2, p. 17-21.

Czechowska-Biskup, R., Rokita, B., Ulanski, P., Rosiak, J.M., Nucl. Instrum. Meth. B, 236 (1–4), 2005, 383–390.

Hien, N.Q., Naotsugu, N., Le, X.T., Fumio, Y., Vo, H.D., Hiroshi, M., Keizo, M., Tamikazu, K. (2000). Growth-promotion of plants with depolymerized alginates by irradiation. Journal of Radiation Physics and Chemistry, 59, 97–101.

Khan, R. A., Khan, M. A., Das, A. K., Debnath, K. K., Dey, K., Kha, A., Saha, S., Huq, T., Noor, N., Sarker, B. and Saha, M. (2010). Thermo-Mechanical and Interfacial Properties of Calcium Alginate Fiber-Reinforced Linear Low-Density Polyethylene Composite. Polymer Plastics Technological and Engineering, 49, 602–608.

Hang, A., Myklestad, S., Larsen, B., Smidsrod, O. (1967). Correlation between chemical structure and physical properties of alginates. Acta Chemical. Scandinavica, 21, 691-790.

Aziz, A., Nurul Islam, A.K.M., Pervin, R. (2001). Marine algae of St. Martin's Island, Bangladesh. Bangladesh Journal of Botany, 30 (2), 135–140.

Mollah, M. Z. I., Khan, M. A., Khan, R. A. (2009). Effect of gamma irradiated sodium alginate on red amaranth (Amaranthus Cruentus L.) as growth promoter. Journal of Radiation Physics and Chemistry, 78, 61-64.

K. Ohta, A. Zaniguhi, N. Konishi, T. Idosoki, "Chitosan treatment affects plants growth and flower quality in Eustoma grandiflorum", Horticulture Science, vol. 34, pp. 233-234, 1999

Kast C. E., Frick W., Losert U., and Bernkop-Schnürch A., "Functional properties of chitin and chitosan", International Journal of Pharmaceutics, pp.256, 183, 2003.

Ghaouth E. A., Arul J., Grenier J., and Asselin A., "Effects of Chitosan on Cucumber Plants: Supperession of Pythium aphanidennatum and induction of defence reactions",

Phytopathology, vol. 84, pp. 313-320, 1992.

Hadwiger L. A., "Chitosan: natural regulator in plantfungal pathogen interaction increases crop yields", Academic Press: San Diego, pp. 4, 1984.

Freier T., "Processing of Chitosan and Chitosan Derivatives", www.faqs.org/patents/app/20080254125, 2008

ICMIEE-PI-140333

Laminar Boundary Layer Flow Separation Control at the Leading Edge of an Airfoil

G.M Hasan Shahariar[1], Mohammad Rashedul Hasan[2], Dr. Mohammad Mashud[3]

[1,2,3] Department of Mechanical Engineering,
Khulna University of Engineering & Technology, Khulna-9203, BANGLADESH

ABSTRACT
In this paper, laminar boundary layer flow separation control at the leading edge of two dimensional NACA 2412 airfoil is investigated numerically through a commercial fluid dynamic code ANSYS FLUENT and to study the effects of laminar separation bubble on airfoil aerodynamic characteristics. Flow was fully turbulent with the Reynolds number of 6.85×10^5 and For these flows, the Reynolds Average Navier-Stokes equation with k-ω SST transition model are shown to accurately predict the characteristics of laminar separation bubble. In the present case, a flap with a length of 4% the camber at a distance of 12% the chord length from the leading edge is placed on the airfoil's upper surface at an angle of 5, 10, 15 degree. The numerical simulation reveals details of the actuation in modifying the leading edge flow giving insight in the induced effect by using flap. The effectiveness of the flap is observed in a wide range of angles of attack with lift co-efficient, drag co-efficient and surface pressure distribution of the airfoil.

Key Words
Laminar separation bubble, Flow separation control, CFD, Airfoil, Flap, RANS;

1. Introduction

The performance of almost all model aircraft is strongly influenced by laminar separation bubbles, which may occur at low Reynolds numbers. Such a separation bubble is caused by a strong adverse pressure gradient, which makes the laminar boundary layer to separate from the curved airfoil surface. The pressure rise is related to the velocity drop towards the trailing edge of the airfoil, which can be seen in the velocity distribution of the airfoil through Bernoulli's equation.

The boundary layer leaves the surface approximately in tangential direction, resulting in a wedge shaped separation area. The separated, but still laminar flow is highly sensitive to disturbances, which finally cause it to transition to the turbulent state. The transition region is located away from the airfoil at the outer boundary of the separated flow area. The thickness of the now turbulent boundary layer grows rapidly, forming a turbulent wedge, which may reach the airfoil surface again. The region where the turbulent flow touches the surface again is called reattachment point. The volume enclosed by the regions of separated laminar flow and turbulent flow is called a laminar separation bubble. Inside the bubble the flow may be circulating, the direction near the airfoil surface may even be the opposite of the direction of the outer flow. There is almost no energy exchange with the outer flow, which makes the laminar separation bubble quite stable.

The laminar separation bubble on the airfoil is classified into a short bubble and a long bubble. With increasing angle of attack, the chordwise length of the short bubble shortens and its position moves toward the leading edge. With further increase in the angle of attack, the short bubble fails to reattach on the airfoil surface, which is known as a short bubble burst and this bubble burst causes the airfoil stall. The long bubble, which is formed after the burst, increases its chord wise length as the angle of attack is increased beyond the stall angle. The stall characteristics of the airfoil are strongly dependent upon these two types of bubbles. The negative pressure peak near the leading edge is observed when the short bubble is formed. When the long bubble is formed after the bubble burst, this negative pressure peak is destroyed and a relatively flattened pressure distribution is formed. [1]

Recent improvements on airfoil performance were achieved by increasing the maximum lift and suppressing the stall. Many investigations on the airfoil flow control have been conducted. Some classical devices such as a leading-edge slat and a vortex generator [2] have been developed as passive control devices to control the airfoil lift. Recently, active control devices such as a jet blowing into the boundary layer [3] and oscillatory actuators and synthetic jet actuators [4] have been investigated. And many other investigations have been conducted. Another way to control the flow separation near the trailing edge is by the use of trailing-edge flap actuation [5].

However, both passive and active lift control devices were designed for the suppression of boundary-layer separation and they were not aimed for the control of the behavior of the bubble formed near the leading edge. In this paper, the control of the bubble formed on the NACA 2412 airfoil with the application of flap is pursued.

2. Numerical Method

In this study, laminar flow separation control at the leading edge over NACA 2412 airfoil is computationally investigated using computational fluid dynamics (CFD) code with commercial ANSYS Fluent 14.5 software based on finite volume technique. Here, the chord length

E-mail addresses: hasanshahariar.kuet@gmail.com, rashedulhasan.047@gmail.com , mdmashud@yahoo.com

of the airfoil is 1m. NACA 2412 airfoil has a maximum camber of 2% located 40% (0.4 chords) from the leading edge with a maximum thickness of 12% of the chord. Reynolds number for the simulations was $Re=6.85\times10^6$. The density of the air at the given temperature is $\rho=1.225kg/m^3$ and the viscosity is $\mu=1.7894\times10^{-5}kg/ms$. A flap with a length of 4% the camber at a distance of 12% the chord length from the leading edge is placed on the airfoil's upper surface at an angle of 5, 10, 15 degree respectively. The numerical simulation was done for NACA 2412 airfoil with and without flap at an angle of attack from 0 degree to 16 degree at a wind velocity of 10 m/s. The Reynolds average Navier-Stokes equations ware solved using the green gauss cell based gradient option and the IMPLICIT density based solver was selected with a second order implicit transient formulation for improved accuracy. The turbulent viscosity was computed through k-ω SST transition model. All solution variables were solved via second order upwind discretization scheme.

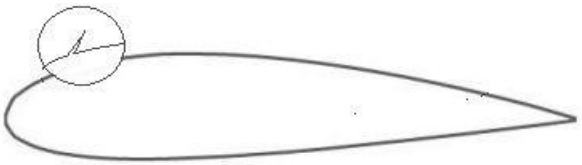

Fig.1 NACA 2412 airfoil with flap at the leading edge

2.1 Boundary Condition:
The computational domain extended 15C upstream of the leading edge of the airfoil, 15C downstream of the trailing edge, and 20C above the pressure surface. Velocity inlet boundary condition was applied upstream (Inflow) with speed of (U=10 m/sec) and outflow boundary condition was applied downstream. Free stream boundary conditions are used in the upstream, downstream and outer boundaries. No-slip boundary conditions are used at solid surfaces.

It involves inlet, outlet & wall boundary, the velocity components are calculated for each angle attack case as follows. The x component of velocity is calculated by $x=u\cos\alpha$ and the y component of velocity is calculated by $y=y\sin\alpha$, where α is the angle of attack in degrees. Ansys recommends turbulence intensities ranging from 1% to 5% as inlet boundary conditions. In this study it is assumed that inlet velocity is less turbulent that pressure outlet. Hence, for velocity inlet boundary condition turbulence intensity is considered 1% and for pressure outlet boundary 5%. In addition, Ansys also recommends turbulent viscosity ratio of 10 for better approximation of the problem [6].

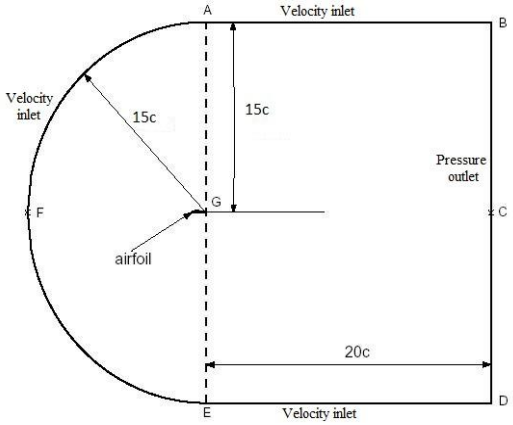

Fig.1 The dimensions and boundary conditions of the computational domain

2.2 Mesh Topology:
The grid used for the single airfoil is generated by the GAMBIT program, and is shown in Figure 2. The application of wall functions to modeling the near-wall region may significantly reduce both the processing and storage requirements of a numerical model, while producing an acceptable degree of accuracy. The non-dimensional wall parameter is defined as:

$$y^+ = \frac{\rho y_p}{\mu}\sqrt{\frac{\tau_\omega}{\rho_\omega}} \qquad (1)$$

Here, y_p is the distance from the first computational node to the wall and the subscript ω denotes wall properties [4]. Consequently, the grid size giving the grid independent results are selected and the total number of cells is adopted as 45,297 nodes. For solution convergence criteria was selected as 1^{0-5}.This indicates the value taken as the result were constant for consecutive 2000 iterations. Other criterions like continuity residuals were also monitored.

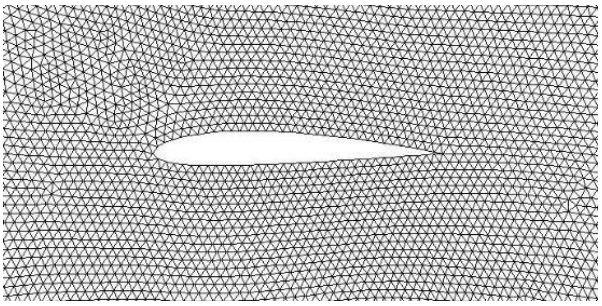

Fig.3 Mesh around NACA 2412

E-mail addresses: hasanshahariar.kuet@gmail.com, rashedulhasan.047@gmail.com , mdmashud@yahoo.com

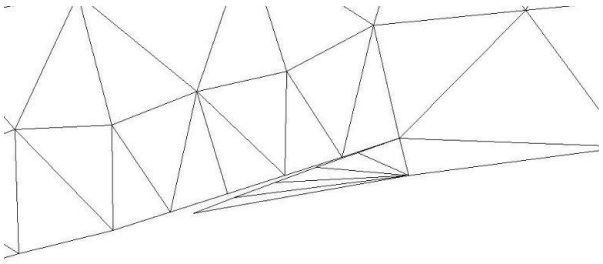

Fig.4 Mesh near the flap at 10 degree flap angle

2.3 Grid independence study:

The first step in performing a CFD simulation should be to investigate the effect of the mesh size on the solution results. Generally, a numerical solution becomes more accurate as more nodes are used, but using additional nodes also increases the required computer memory and computational time. The appropriate number of nodes can be determined by increasing the number of nodes until the mesh is sufficiently fine so that further refinement does not change the results. Figure 5 shows the effect of number of grid cells in coefficient of lift at stall angle of attack (16°). This computational model is very small compared to that of NASA's validation cases.

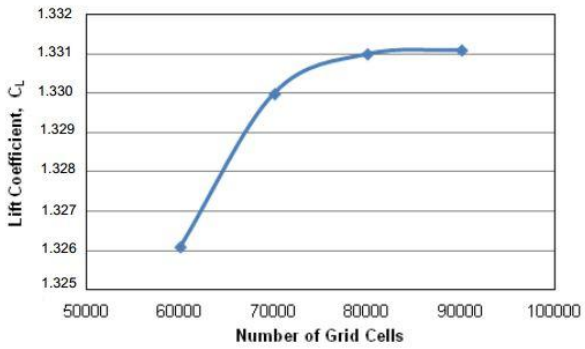

Fig.5 Variation of lift coefficient with number of grid cells [7]

3. Results & Discussions:

Figure 6 shows the lift coefficient (C_l) versus angle of attack (α) curve of NACA 2412 airfoil with a flap angle of 5, 10, 15 degree and compares them with the NACA 2412 airfoil without flap at a wind velocity of 10 m/s. The maximum lift coefficient defines the angle at which the airfoil will stall and the stall occurred at the angle of attack of 11° where $C_{l,max}$= 0.841. The graph depicted in figure 3 also shows the drag coefficient variations with the angle of attack. Here, the drag co-efficient increases as the increase of angle of attack of wind velocity.

From the both curve it is found that the airfoil performance is significantly improved due to the control of flow separation by using flap at the leading edge. It has also been found that the lift increases about 20.6% & 13.27% and drag reduces about 26.12% & 19.55% at the flap angle 5 & 10 degree respectively for 10 degree

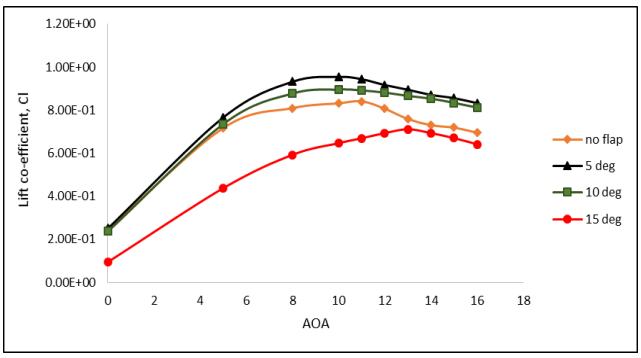

Fig.6 Lift co-efficient vs angle of attack at 10 m/s

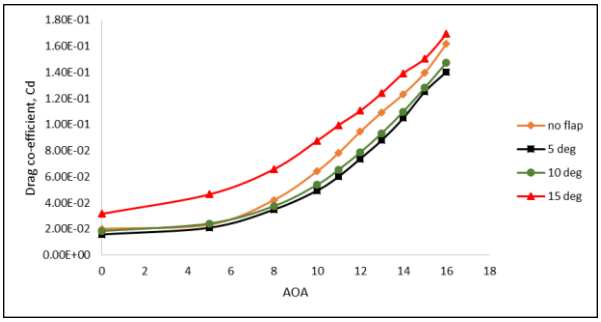

Fig.7 Drag co-efficient vs angle of attack at 10 m/s

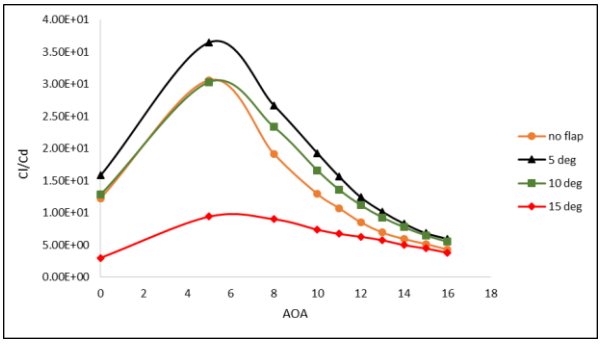

Fig.8 Lift-Drag ratio vs angle of attack at 10 m/s

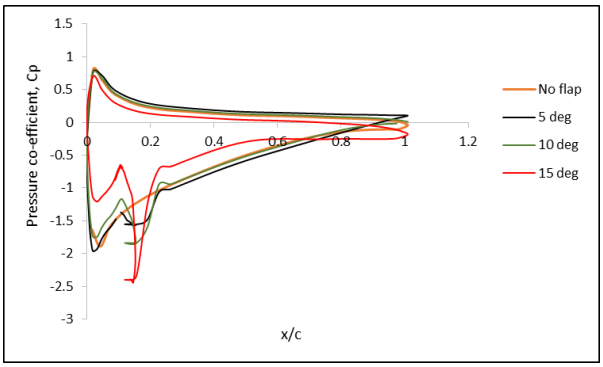

Fig.9 Surface pressure distribution over the airfoil at 8 degree angle of attack

angle of attack. Because of attaching flap at the leading edge, there formed bubbles which create so much negative pressure on the upper surface of the airfoil. Thus the reattachment of flow happened rapidly which

E-mail addresses: hasanshahariar.kuet@gmail.com, rashedulhasan.047@gmail.com , mdmashud@yahoo.com

reduces the flow separation region. As a result lift co-efficient increases and drag co-efficient decreases. But at 15 degree flap angle, lift reduces about 18.2% and drag increases about 30.75% at 10 degree angle of attack. From figure 8 it also seen that the lift to drag ratio is increases about 49.61% & 28.68% at flap angle of 5 & 10 degree respectively for 10 degree angle of attack but it decreases about 42.8% at 15 degree flap angle for the same angle of attack than the clean airfoil. Figure 9 shows the surface pressure distribution along the chord wise position of the airfoil with and without flap at 8 degree angle of attack.

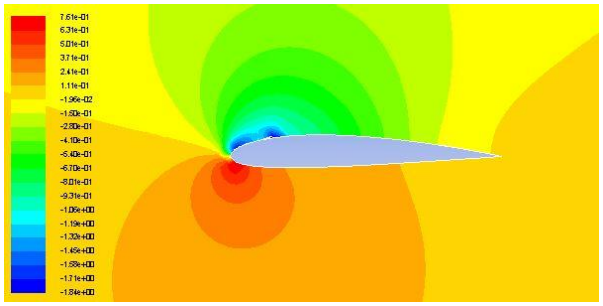

Fig.10 Pressure contours of NACA 2412 with 10 degree flap angle at 8 degree angle of attack

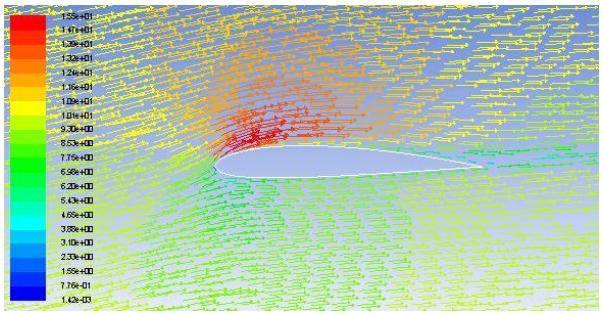

Fig.11 Velocity vector around NACA 2412 with 5 degree flap angle at 8 degree angle of attack

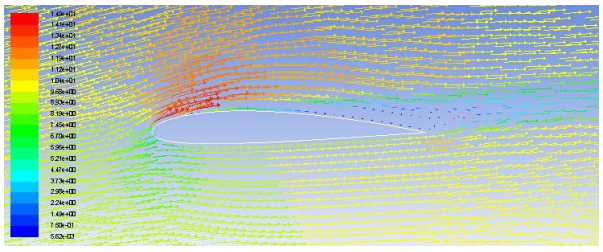

Fig.12 Velocity vector around NACA 2412 with 15 degree flap angle at 8 degree angle of attack

Figure 10 shows the contours of pressure at a flap angle of 10 degree for 8 degree angle of attack. It also seen from the figure 11 & 12 that, at 5 degree flap angle the flow separation region is quite smooth and short than 15 degree for 8 degree angle of attack. So, there have been found a better aerodynamics characteristics for NACA 2412 airfoil with 5 degree flap angle.

4. Conclusion:

For the purpose of burst suppression of the laminar separation bubble, flaps are tested on the NACA 2412 airfoil for different flap angles at a Reynolds number of 6.85×10^5.

- The results indicates that the burst of the bubble is suppressed and both the maximum lift coefficient and the stall angle are improved when the burst control plate (flap) is at an appropriate position (flap angle 5 degree).
- It has also been found that the lift increases about 20.6% & 13.27% and drag reduces about 26.12% & 19.55% at the flap angle 5 & 10 degree respectively for 10 degree angle of attack. Thus it can be strongly recommended to use bubble burst control mechanism to increase the aerodynamics performance of airfoil.

NOMENCLATURE

C_p : Pressure co-efficient over the airfoil surface
C_l : Lift co-efficient
C_d : Drag co-efficient
α : Angle of attack
μ : Dynamic viscosity
ρ : Air density
RANS: Reynolds Average Navier Stokes equation
C_l/C_d: Lift to Drag ratio
NACA: National Advisory Committee for Aeronautics

REFERENCES

[1] Kenichi Rinoie, Masafumi Okuno, and Yasuto Sunada, “Airfoil Stall Suppression by Use of a Bubble Burst Control Plate”, AIAA JOURNAL, Vol. 47, No. 2, February 2009

[2] Bragg, M. B., Gregorek, G. M., “Experimental Study of Airfoil Performance with Vortex Generators,” Journal of Aircraft, Vol. 24, No. 5, 1987

[3] Huang, L., Huang, P. G., LeBeau, R. P., and Hauser, T., “Numerical Study of Blowing and Suction Control Mechanism on NACA0012 Airfoil,” Journal of Aircraft, Vol. 41, No. 5, 2004

[4] Munday, D., Jacob, J. D., and Huang, G., “Active Flow Control of Separation on a Wing with Oscillatory Camber,” AIAA Paper 2002- 0413, 2002

[5] Melton, L. P., Yao, C. S., and Seifert, A., “Active Control of Separation from the Flap of a Supercritical Airfoil,” AIAA Journal, Vol. 44, No. 1, 2006

[6] Wilcox, David C, "Turbulence Modeling for CFD", Second edition, Anaheim, DCW Industries, 1998.

[7] Eleni, Douvi C., Tsavalos I. Athanasios, and Margaris P. Dionissios. "Evaluation of the turbulence models for the simulation of the flow over a National Advisory Committee for Aeronautics (NACA) 0012 airfoil." Journal of Mechanical Engineering Research 4.3 (2012): 100-111

E-mail addresses: hasanshahariar.kuet@gmail.com, rashedulhasan.047@gmail.com , mdmashud@yahoo.com

ICMIEE-PI-140335

Seismic Fragility Evaluation of a Moment Resisting Reinforced Concrete Frame

PKM Moniruzzaman [1*], *Fouzia H Oyshi* [2] , *Ahmed F Farah* [3], *Faysal M Omar* [4]
[1] Department of Wood Science, The University of British Columbia, Vancouver, CANADA
[2] Department of Civil Engineering, Bangladesh University of Engineering and Technology, Dhaka, BANGLADESH
[3] Department of Structural Engineering, Sakarya University, Sakarya, TURKEY
[4] Department of Civil Engineering, EELO University, Borama, SOMALILAND

ABSTRACT
This study examines the seismic behavior of a seven-storey moment resisting reinforced concrete frame under 9 different ground motion (GM) records through incremental dynamic analysis (IDA). The IDA results allowed a thorough understanding of changes in the structural response as the intensity of the GM increases. The selected earthquake hazard is based on maximum considered earthquake ground motions. The seismic performance is quantified through nonlinear collapse simulation on a set of archetype models developed in SeismoStruct. The drift behavior, record-to-record variability of the response and height-wise distribution of drift demand were reported. On the other hand, for collapse evaluation, ground motions are systematically scaled to increasing earthquake intensities until median collapse is established and analyzed the model as a form of IDA. Using collapse data obtained from IDA results, the collapse fragility curve defined through a cumulative distribution function, which related the ground motion intensity to the probability of collapse.

Keywords: Incremental dynamic analysis, seismic capacity, inter-storey drift, reinforced concrete structure.

1. Introduction

Reinforced concrete (RC) is concrete that contains embedded steel bars, plates, or fibers having higher tensile strength and/or ductility that strengthen the concrete's relatively low tensile strength and ductility [1-5]. Reinforced materials are embedded in the concrete in such a way that the two materials resist the applied forces together. In reinforced concrete, the tensile strength of steel and the compressive strength of concrete work together to allow the member to sustain tensile, shear and compressive stresses over considerable spans [4]. Such a material can be used for making any size and shape, for utilization in the construction. The worldwide use of reinforced concrete construction stems from the wide availability of reinforcing steel as well as the concrete ingredients [2]. With the rapid growth of urban population in both the developing and the industrialized countries, reinforced concrete has become a material of choice for residential construction [5].

In the consequence, RC frames consist of horizontal elements (beams) and vertical elements (columns) connected by rigid joints. These structures are cast monolithically- that is, beams and columns are cast in a single operation in order to act in unison. RC frames provide resistance to both gravity and lateral loads through bending in beams and columns. On the other hand, moment-resisting frames are rectilinear assemblages of beams and columns that resist forces by bending. In moment resisting frames, the joints, or connections, between columns and beams are designed to be rigid [2,,5]. The bending rigidity and strength of the frame members is the primary source of lateral stiffness and strength for the entire frame. Resistance to lateral forces is provided primarily by rigid frame action-that is, by the development of bending moment and shear force in the frame members and joints [1]. At a rigid joint, the ends of the columns and beams cannot rotate. This means that the angle between the ends of the columns and beams always remain the same. This causes the columns and beams to bend during earthquakes depending on the geometry of the connection [4]. Therefore, these structural members are designed to be strong in bending. Frequently, reinforced concrete construction is used in regions of high seismic risk. By virtue of moment resistance frames, rigid joints should be designed carefully to make sure they do not distort [2,4]. However, the 1994 Northridge earthquake revealed a common flaw in the construction, and building codes [2].

There is a lack of information about the dynamic performance of RC moment resistance frames. Thus, the progress and adoption of moment resistance frames, particularly in practice, has been hindered by the lack of performance-based criteria and design methodology for this type of structural system. To address this issue and examine the seismic response of this system under different earthquake records, incremental dynamic analyses (IDAs) were performed on seven-storey RC frame. The IDA results allowed a thorough understanding of changes in the structural response as the intensity of the Ground Motion (GM) increases. For collapse evaluation, ground motions are systematically scaled to increasing earthquake intensities until median collapse is established and analysed the model as a form of IDA. Using collapse data obtained from IDA results, the collapse fragility curve defined through a cumulative distribution function, which related the ground motion intensity to the probability of collapse.

2. Methodology

2.1 Description of the structure

In order to investigate the seismic performance of a RC moment resisting frame, a case study building was

* Corresponding author. Tel.: +1-778 866 2364
E-mail address: pkm.moni@alumni.ubc.ca

adopted which has 7-story, 166 m2 residential building located in Dhaka, Bangladesh (Figure 1). This structure is made of reinforced concrete frame building, is located on stiff soil and in an area in which near-fault ground motions are not prevalent (Zone 2 in [3]). In layout plan, the building has 19 m x 8.5 m and 4 bays x 2 bays (Figure 1). The long direction is oriented East-West. The building is approximately 21 m tall. The slabs are 115 mm deep. Columns in the south frame are 305 mm wide by 508 mm deep, i.e., oriented to bend in their weak direction when resisting lateral forces in the plane of the frame. Beams are generally 254 mm wide by 508 mm. The concrete has a nominal strength of 25 MPa and the reinforcement steel is scheduled as Grade 60 (400 MPa) (Table 1).

Fig.1 The studied structure: a) Full scale building, b) building layout, c) finite element model

2.2 Finite element modeling and model validation

The building was modeled in a simulation environment, SeismoStruct 5.2.2 [6] for analysis considering a 2D interior frame in the East-West direction. The concrete and steel materials were modeled using the built-in models in SeismoStruct. For instance, Menegotto-Pinto steel model and Mander et al. nonlinear concrete model were implemented [6]. On the other hand, RC rectangular sections were used to model the beam and column sections. The beams were divided longitudinally into 5 elements and each beam and column element was divided transversely into 300 by 300 fiber elements. The model was validated against the time period of the structure as calculated according to BNBC code. In the current study, the time period was 0.47 second which is about 2% lower than the code value.

Table 1 Material properties.

Materials	Properties	Values
Concrete	Compressive strength (MPa)	25
	Tensile strength (MPa)	2.5
	Ultimate strain (%)	0.35
Steel	Modulus of elasticity (MPa)	200000
	Yield strength (MPa)	400
	Strain hardening parameter (α)	0.5

3. Incremental dynamic analysis

This study examines the seismic behavior of seven-storey RC moment resisting frame under 9 different ground motion (GM) records through incremental dynamic analysis (IDA). The IDA results allowed a thorough understanding of changes in the structural response as the intensity of the GM increases. The drift behavior, record-to-record variability of the response and height-wise distribution of drift demand were reported.

3.1 Selected ground motion records

A set of 9 GM records were used to conduct nonlinear incremental dynamic time history analyses on the moment resisting reinforced concrete frame model. The GM records were selected in a bin of relatively large magnitudes of 5.5– 7.6. Soil type C was considered for all the records. The selected ground motions were scaled with the Dhaka response spectrum. The ground motions are matched with Dhaka spectrum using SeismoMatch software [6]. A typical time history records for the unscaled and scalded records are shown in Figure 2. The spectrums of the unscaled and scaled records are shown in Figure 3. These GMs are presumed to be representative of events that have the potential to cause severe GMs at the considered location [7,8].

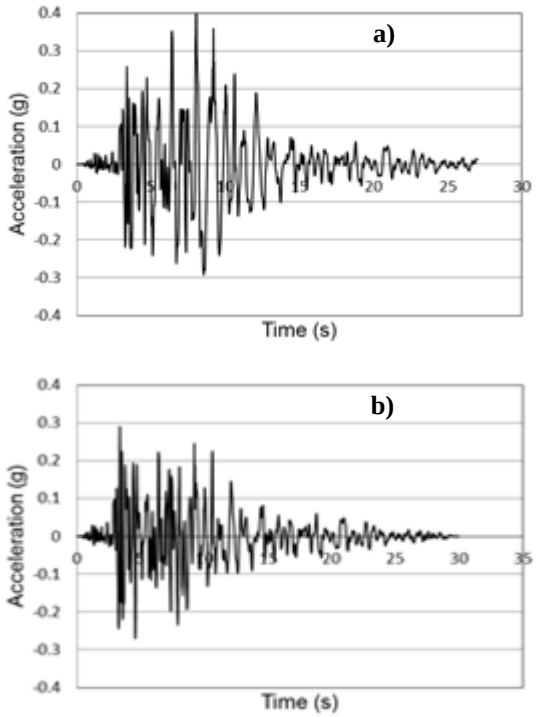

Fig.2 A typical earthquake record: a) unscaled, b) scaled

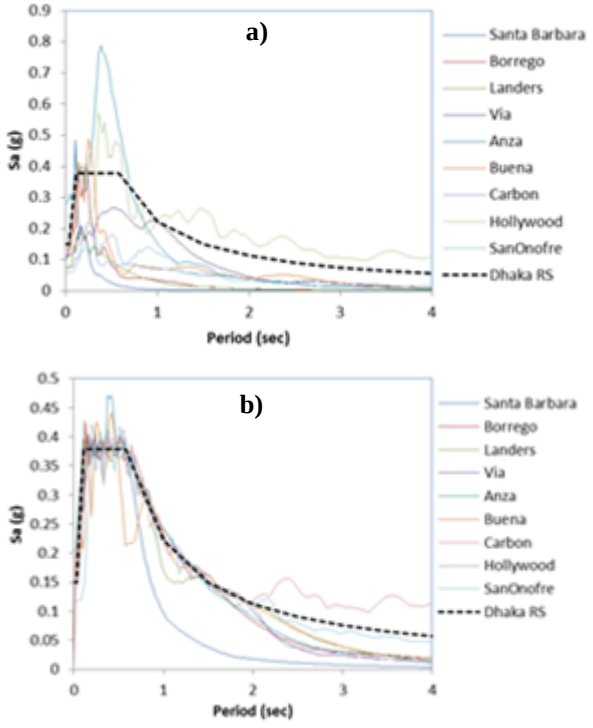

Fig.3 The ground motion records with Dhaka response spectrum: a) unscaled, b) scaled

4. Results and discussion

The IDA method was studied to examine the response of the RC moment resisting frame subjected to varied earthquake excitations. The IDA technique was developed in detail by [9]. IDA involves performing a series of nonlinear time history analyses on the modeled structure subjected to one or more GM records [8]. Each record is scaled to several intensity levels so as to cover the entire range of structural response, from elastic behavior through yielding to collapse (or until a defined 'failure' limit state occurs) [9]. In this study, the 5% damped spectral acceleration at the fundamental mode period of the structure, Sa(T1, 5%), was used as an intensity measure. In order to examine the structural response of the frame under earthquake excitations, the maximum inter-storey drift (MID) ratio were selected as damage measures. It should be noted that the inter-storey drift ratio was defined as the relative displacement of each storey divided by the storey height. Moreover, the analysis was continued until Sa =2.4g or until numerical non-convergence occurred which indicated the global dynamic instability.

4.1 Inter-storey drift ratio

The nonlinear time history analyses were conducted on the modeled frame, from which the IDA curves shown in Figure 4 are generated. The inter-storey drift ratio was computed as the difference in the displacements of two immediate floor levels divided by the height of that floor [7]. The IDA curves display the full range of behavior, showing quite large record-to-record variability. On the basis of the plot of Sa(T1, 5%) versus inter-storey drift ratio, the frame experienced a wider range of response measured as inter-storey drift. The IDA curves start as a straight line signaling the linear elastic range which stays straight up to 1.5% inter-storey drift ratio (Figure 4). Then the tangent slope changes as a result of nonlinearity. It is worth mentioning that the larger dispersion of the demand measure implies the necessity for considering a sufficient number of Ground motion records.

By increasing the intensity of earthquakes, the inter-storey drift ratio is also increasing from a linear to nonlinear range. The analysis was performed upto a Sa=2.4 g. However, all the GMs did not reach to Sa=4.5g, while some of the records reached to dynamic instability around Sa= 3g. From the IDA curves, it is observed that the inter-storey drift demand varied in a wide range. For instance, at Sa=2.0 the inter-storey drift ratio for the 9 GMs varied from 2.2%-8.0%.

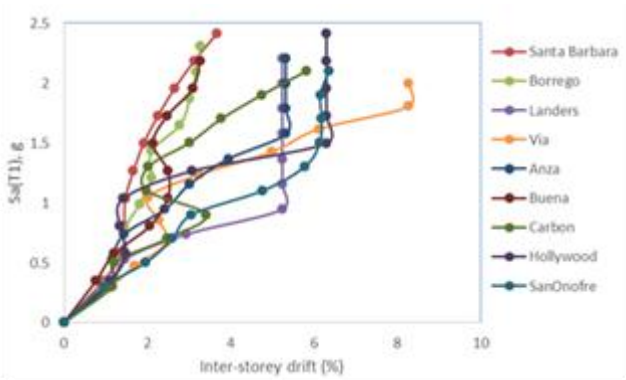

Fig.4 IDA curves for 9 ground motions

4.2 Nonlinear response along the height of the frame

In order to explore the effect of earthquake intensity on the distribution of inelasticity over the height of the building, the responses of each storey in terms of MID are provided through the use of IDA curves. Figure 5 illustrates a record-to-record specific picture of each storey subjected to earthquake records. At first storey the MID is varied linearly up to Sa= 1.5g. On the other hand, all the storey from 2nd to top floor the MID become inelastic after the design Sa (T1) = 0.7g.

In order to explore inelastic demand over the height of the building, the median values of MIDs were generated. Moreover, for each storey under the 9 GM records at three different intensity levels, i.e. Sa(T1) = 0.7g, 1.5g, and 2.1g were reported. Figure 6 show the inter-storey drift distribution along the height of the frame.

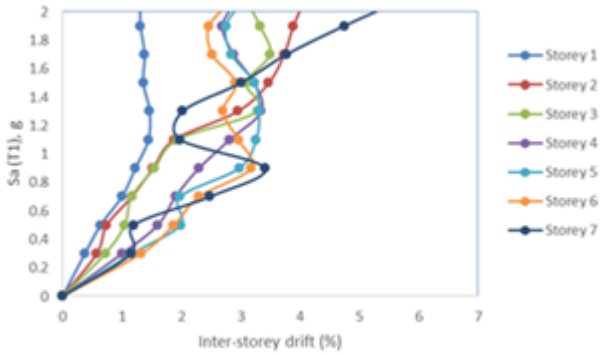

Fig.5 IDA curves for all stories

At Sa (T1)= 0.7g, the inter-storey drift at top floor varies up to 3.9% with a standard deviation of 17%. Similarly, at 1.5g and 2.1g level, the top floor inter-storey drift ratio goes up to 6% and 6.6%, respectively with a standard deviation of 23%, 42%, respectively (Figure 6). Therefore, it is observed that the variation of inter-storey drift ratio spread along the height of the frame. This is because as the intensity increases, the top storey reached to it nonlinear range.

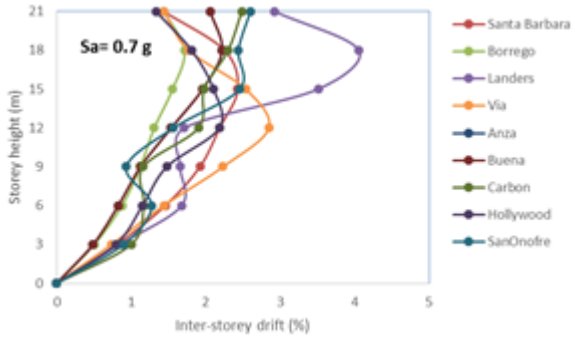

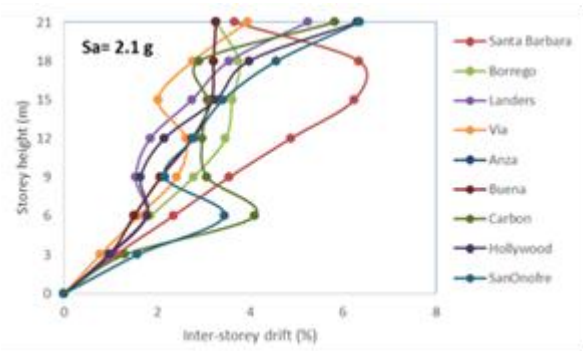

Fig.6 Inter-storey drift ratios for all stories at different Sa (T1) levels

The median inter-storey drift ratio is also plotted in Figure 7 along the height of the frame with a variation of Sa (T1). Comparing the NBCC [2] inter-storey drift limit of 2.5%, it can be concluded that the RC frame can be withstood up to Sa of 0.7g. Therefore, a strengthening scheme is necessary for the structure under severe GM excitations.

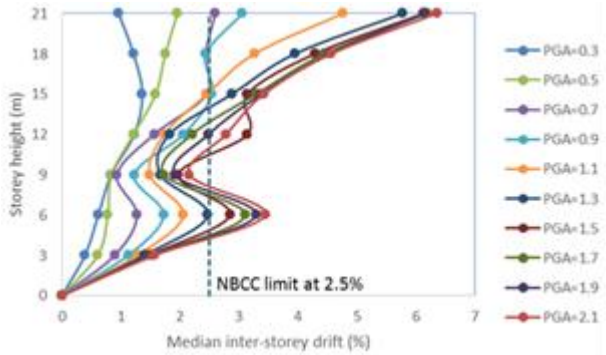

Fig.7 Median inter-storey drift ratios at different Sa(T1)

5. Seismic performance

The seismic performance of the RC moment resisting frame building was evaluated according to methodology describe in FEMA P695 [7]. The key notes to get the performance are stated below:

- Performance is quantified through nonlinear collapse simulation on a set of archetype model developed in SeismoStruct [6].
- The selected earthquake hazard is based on Maximum Considered Earthquake ground motions.
- Safety is expressed in terms of a collapse margin ratio (CMR).

5.1 Collapse margin ratio (CMR)

Safety of the studied building was expressed in terms of Collapse Margin Ratio (CMR). In order to quantify the safety, the collapse level ground motions are considered as the intensity that would result in median collapse of the seismic-force-resisting system, whereas, median collapse occurs when one-half of the structures exposed

to this intensity of ground motion would have some form of life-threatening collapse.

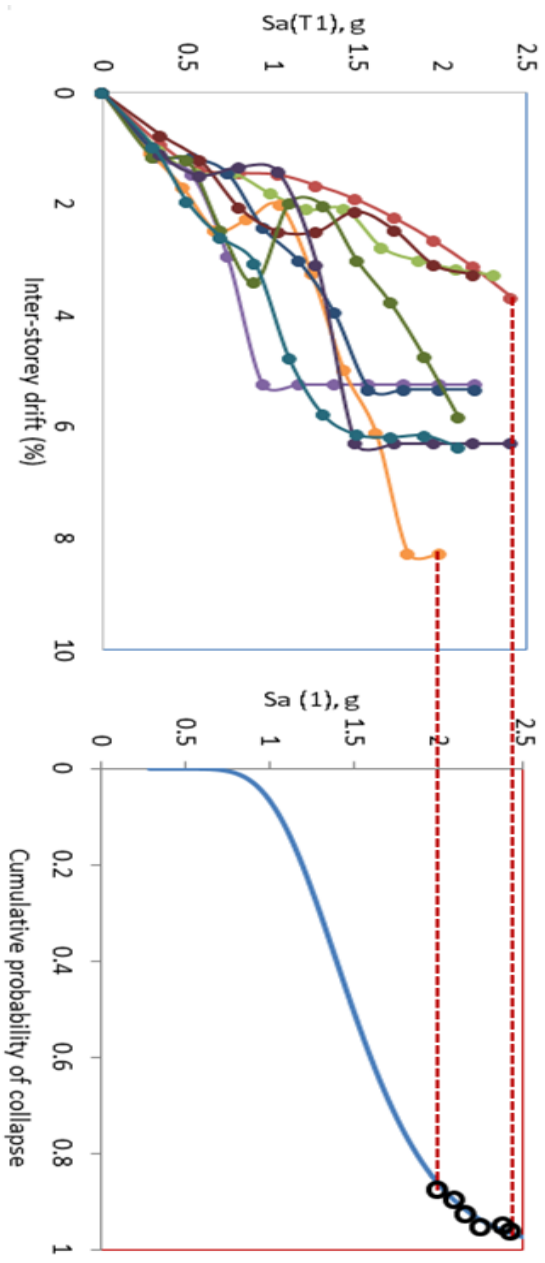

Fig.8 Incremental dynamic analysis response with the collapse fragility curve

The collapse margin ratio, CMR, is the ratio of the median 5%-damped spectral acceleration of the collapse level ground motions to the 5%-damped spectral acceleration of the MCE ground motions at the fundamental period of the seismic-force-resisting system.

For collapse evaluation, ground motions are systematically scaled to increasing earthquake intensities until median collapse is established and analyzed the model as a form of IDA. Using collapse data obtained from IDA results, the collapse fragility curve defined through a cumulative distribution function (CDF), which related the ground motion intensity to the probability of collapse. Figure 8 shows an example of a cumulative distribution plot obtained by fitting a 3 parameter lognormal distribution to the collapse data. Figure 9 shows the probability of collapse of the given structure under a given ground motion. Besides, the CMR value for the given RC moment resisting frame building is obtained as of 4.72. The value indicates the structure is safe under the design earthquake load.

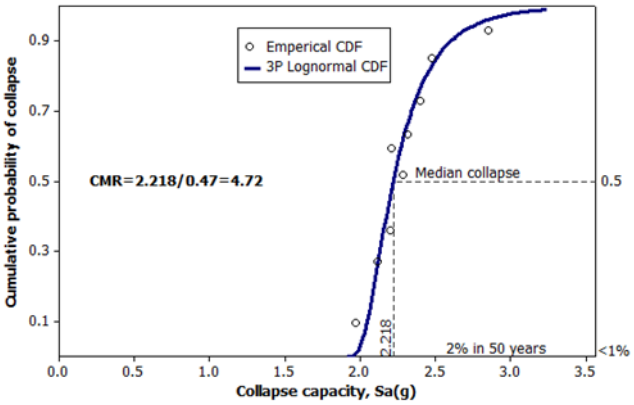

Fig.9 Collapse fragility curve

6. Conclusions

The present study provided a better understanding for the seismic performance of a RC moment resisting frame. A nonlinear incremental dynamic analysis procedure was developed in a finite element program, SeimoStruct. The results obtained discussed in the previous sections can be summarized as follows:

- From the IDA curves, it is observed that the inter-storey drift demand varied in a wide range. For instance, at Sa=2.0 the inter-storey drift ratio for the 9 GMs varied from 2.2%-8.0%.
- Comparing the NBCC inter-storey drift limit of 2.5%, it can be concluded that the RC frame can be withstood up to Sa of 0.7g.
- Structural safety is expressed in terms of a collapse margin ratio.
- The obtained CMR indicates the safe condition of the given structure.

REFERENCES

[1] CSA A23.3. Design of concrete structures. *Canadian Standards Association*. Rexdale, Ontario, Canada. (2004).

[2] NBCC. National Building Code of Canada. *National Research Council Canada*, Ottawa, Ontario, Canada. (2005).

[3] BNBC. *Bangladesh national Building Code*, Dhaka, Bangladesh. (1993).

[4] ACI 318. Building code requirements for structural concrete (ACI 318-02) and commentary (ACI 318R-02). *American Concrete Institute*. (2002).

[5] ACI 318. Building code requirements for structural concrete. American Concrete Institute, ACI Committee 318, Farmington Hills, Michigan. (2005).

[6] SeismoSoft, SeismoStruct. *A Computer Program for Static and Dynamic nonlinear analysis of framed structures*. Available from: http://www.seismosoft.com. (2008).

[7] FEMA P695. Quantification of Building Seismic Performance Factors. *Federal Emergency Management Agency*, Washington, D.C. (2009).

[8] ASCE. Seismic Evaluation and Retrofit of Existing Buildings, ASCE/SEI 41-13. *American Society of Civil Engineers*, Reston, Virginia. (2013).

[9] Vamvatsikos D, Cornell AC. Incremental dynamic analysis. *Earthquake Engineering & Structural* 31(3): 491–514. DOI: 10.1002/eqe.141. (2002).

ICMIEE-PI-140336

Seismic Fragility Evaluation of Reinforced Concrete Structures Considering Height Effects

PKM Moniruzzaman [1*], *Tanmoy Biswas* [2] , *Ahmed Shirwa* [3]
[1] Department of Wood Science, The University of British Columbia, Vancouver, CANADA
[2] Department of Civil Engineering, Bangladesh University of Engineering and Technology, Dhaka, BANGLADESH
[3] Department of Structural Engineering, Suleyman Demirel University, Isparta, TURKEY

ABSTRACT
This study examines the seismic behavior of a reinforced concrete structure having different heights under 9 different ground motion (GM) records through incremental dynamic analysis (IDA). The IDA results allowed a thorough understanding of changes in the structural response as the intensity of the GM increases. Three different heights of a structure, namely, 4, 7 and 10 storey were considered in this study. The selected earthquake hazard is based on maximum considered earthquake ground motions. The seismic performance is quantified through nonlinear collapse simulation on a set of archetype models developed in SeismoStruct. The drift behavior, record-to-record variability of the response and height-wise distribution of drift demand were reported. On the other hand, for collapse evaluation, ground motions are systematically scaled to increasing earthquake intensities until median collapse is established and analyzed the model as a form of IDA. Using collapse data obtained from IDA results, the collapse fragility curve defined through a cumulative distribution function, which related the ground motion intensity to the probability of collapse.

Keywords: Incremental dynamic analysis, seismic capacity, inter-storey drift, reinforced concrete structure.

1. Introduction

Reinforced concrete (RC) is concrete that contains embedded steel bars, plates, or fibers having higher tensile strength and/or ductility that strengthen the concrete's relatively low tensile strength and ductility [1-5]. Reinforced materials are embedded in the concrete in such a way that the two materials resist the applied forces together. In reinforced concrete, the tensile strength of steel and the compressive strength of concrete work together to allow the member to sustain tensile, shear and compressive stresses over considerable spans [4]. Such a material can be used for making any size and shape, for utilization in the construction. The worldwide use of reinforced concrete construction stems from the wide availability of reinforcing steel as well as the concrete ingredients [2]. With the rapid growth of urban population in both the developing and the industrialized countries, reinforced concrete has become a material of choice for residential construction [5].

In the consequence, RC frames consist of horizontal elements (beams) and vertical elements (columns) connected by rigid joints. These structures are cast monolithically- that is, beams and columns are cast in a single operation in order to act in unison [1]. RC frames provide resistance to both gravity and lateral loads through bending in beams and columns. Frequently, reinforced concrete construction is used in regions of high seismic risk to provide resistance against moment force [3]. By virtue of moment resistance frames, rigid joints should be designed carefully to make sure they do not distort [2,4]. However, the 1994 Northridge earthquake revealed a common flaw in the construction, and building codes [2]. There is a lack of information about the dynamic performance of RC structures. Thus, the progress and adoption of this type of structural system, particularly in practice, has been hindered by the lack of performance-based criteria and design methodology. Thus the aim of this paper is to address this issue and examine the seismic response of this system having different heights through incremental dynamic analyses (IDAs). The IDA results allowed a thorough understanding of changes in the structural response as the intensity of the Ground Motion (GM) increases. For collapse evaluation, ground motions are systematically scaled to increasing earthquake intensities until median collapse is established and analyzed the model as a form of IDA. Using collapse data obtained from IDA results, the collapse fragility curve defined through a cumulative distribution function, which related the ground motion intensity to the probability of collapse.

2. Methodology

2.1 Description of the structures

In order to investigate the seismic performance of RC structures, a case study building having different heights was adopted which has 166 m^2 area, located in Dhaka, Bangladesh. In the parametric study, three different height of a structure, namely, 4, 7 and 10 storey were considered to predict the seismic response depends on the height of the structures. These structures are made of reinforced concrete frames, are located on stiff soil and in an area in which near-fault ground motions are not prevalent (Zone 2 in [3]). In layout plan, the buildings have 19 m x 8.5 m and 4 bays x 2 bays (Figure 1). The long direction is oriented East-West. The buildings are approximately 12, 21, and 30 m tall in the name of 4^{th}, 7^{th} and 10^{th} storey, respectively. The slabs are 115 mm deep. Columns in the south frame are 305 mm wide by 508 mm deep, i.e., oriented to bend in their weak direction when resisting lateral forces in the plane of the frame. Beams are generally 254 mm wide by 508 mm.

* Corresponding author. Tel.: +1-778 866 2364
E-mail address: pkm.moni@alumni.ubc.ca

The concrete has a nominal strength of 25 MPa and the reinforcement steel is scheduled as Grade 60 (400 MPa).

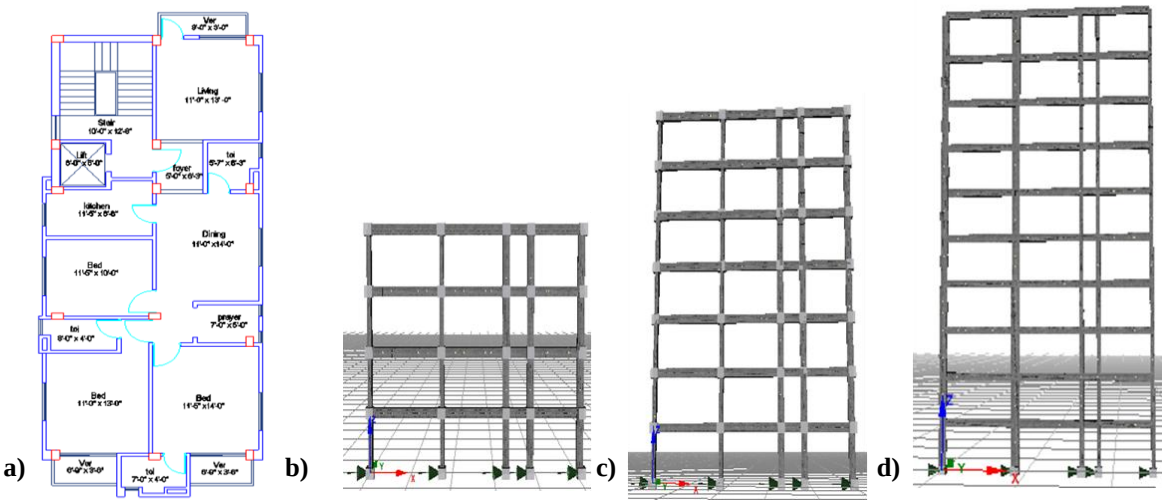

Fig.1 The studied structures: a) building layout, and b) 4th storey, c) 7th storey and d) 10th storey finite element models

2.2 Finite element modeling and model validation

The buildings were modeled in a simulation environment, SeismoStruct 5.2.2 [6] for analysis considering a 2D interior frame in the East-West direction. The modeled structures are shown in Figure 1. The concrete and steel materials were modeled using the built-in models in SeismoStruct. For instance, Menegotto-Pinto steel model and Mander et al. nonlinear concrete model were implemented [6]. The material properties are shown in Table 1. On the other hand, reinforced concrete rectangular sections were used to model the beam and column sections. The beams were divided longitudinally into 5 elements and each beam and column element was divided transversely into 300 by 300 fiber elements.

The models were validated against the time period of the structures as calculated according to BNBC code [3]. In the current study, the time period was 0.34, 0.47 and 0.73 second for the 4th, 7th, and 10th storey buildings, respectively, which are about 1-2% lower than the code calculated values.

Table 1 Material properties.

Materials	Properties	Values
Concrete	Compressive strength (MPa)	25
	Tensile strength (MPa)	2.5
	Ultimate strain (%)	0.35
Steel	Modulus of elasticity (MPa)	200000
	Yield strength (MPa)	400
	Strain hardening parameter (α)	0.5

3. Incremental dynamic analysis

This study examines the seismic behavior of RC structures under 9 different ground motion (GM) records through incremental dynamic analysis (IDA). The IDA results allowed a thorough understanding of changes in the structural response as the intensity of the GM increases. The drift behavior, record-to-record variability of the response and height-wise distribution of drift demand were reported.

3.1 Selected ground motion records

A set of 9 GM records were used to conduct nonlinear incremental dynamic time history analyses on the RC structure models. The GM records were selected in a bin of relatively large magnitudes of 5.5– 7.6. Soil type C was considered for all the records. The selected ground motions were scaled with the Dhaka response spectrum. The ground motions are matched with Dhaka spectrum using SeismoMatch software [6]. A typical time history records for the scalded records are shown in Figure 2. The spectrums of the unscaled and scaled records are shown in Figure 3. These GMs are presumed to be representative of events that have the potential to cause severe GMs at the considered location [7,8].

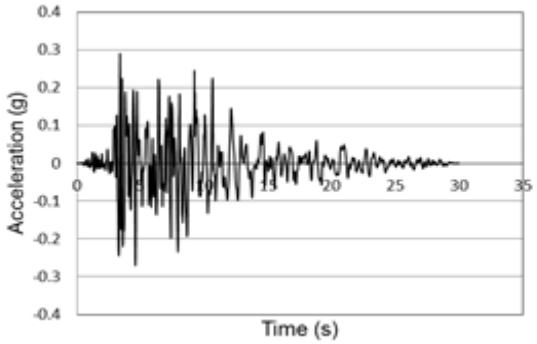

Fig.2 A typical scaled earthquake record

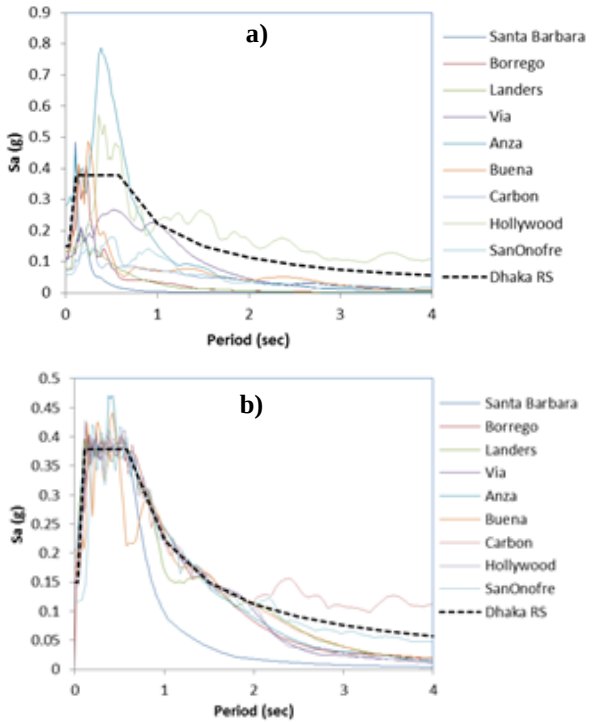

Fig.3 The ground motion records with Dhaka response spectrum: a) unscaled, b) scaled

4. Results and discussion

The IDA method was studied to examine the response of the RC structures having different height levels subjected to varied earthquake excitations. The IDA technique was developed in detail by [9]. IDA involves performing a series of nonlinear time history analyses on the modeled structures subjected to one or more GM records [8]. Each record is scaled to several intensity levels so as to cover the entire range of structural response, from elastic behavior through yielding to collapse (or until a defined 'failure' limit state occurs) [9]. In this study, the 5% damped spectral acceleration at the fundamental mode period of the structures, Sa(T1, 5%), was used as an intensity measure. In order to examine the structural response of the structures under earthquake excitations, the maximum inter-storey drift (MID) ratios were selected as damage measures. It should be noted that the inter-storey drift ratio was defined as the relative displacement of each storey divided by the storey height. Moreover, the analysis was continued until Sa =4.1g or until numerical non-convergence occurred which indicated the global dynamic instability.

4.1 Inter-storey drift ratio

The nonlinear time history analyses were conducted on the modeled structures, from which the IDA curves shown in Figure 4 are generated. The inter-storey drift ratio was computed as the difference in the displacements of two immediate floor levels divided by the height of that floor [7]. The IDA curves display the full range of behavior, showing quite large record-to-record variability. On the basis of the plot of Sa(T1, 5%) versus inter-storey drift ratio, the structures experienced a wider range of response measured as inter-storey drift. The IDA curves start as a straight line signaling the linear elastic range which stays straight up to 4, 1.5 and 2.3% inter-storey drift ratio for the 4th, 7th and 10th storey buildings, respectively (Figure 4). Then the tangent slope changes as a result of nonlinearity. It is worth mentioning that the larger dispersion of the demand measure implies the necessity for considering a sufficient number of Ground motion records.

By increasing the intensity of earthquakes, the inter-storey drift ratio is also increasing from a linear to nonlinear range. The analysis was performed up to a Sa=4.1 g. However, all the GMs did not reach to Sa=4.1g, while some of the records reached to dynamic instability around Sa= 3.5g. From the IDA curves, it is observed that the inter-storey drift demand varied in a wide range. For instance, at Sa=2.0 the inter-storey drift ratio for the 9 GMs varied from 2.2-3.7%, 2.2-8.0%, and 1.5-3.7% for the 4th, 7th and 10th storey buildings, respectively (Figure 4).

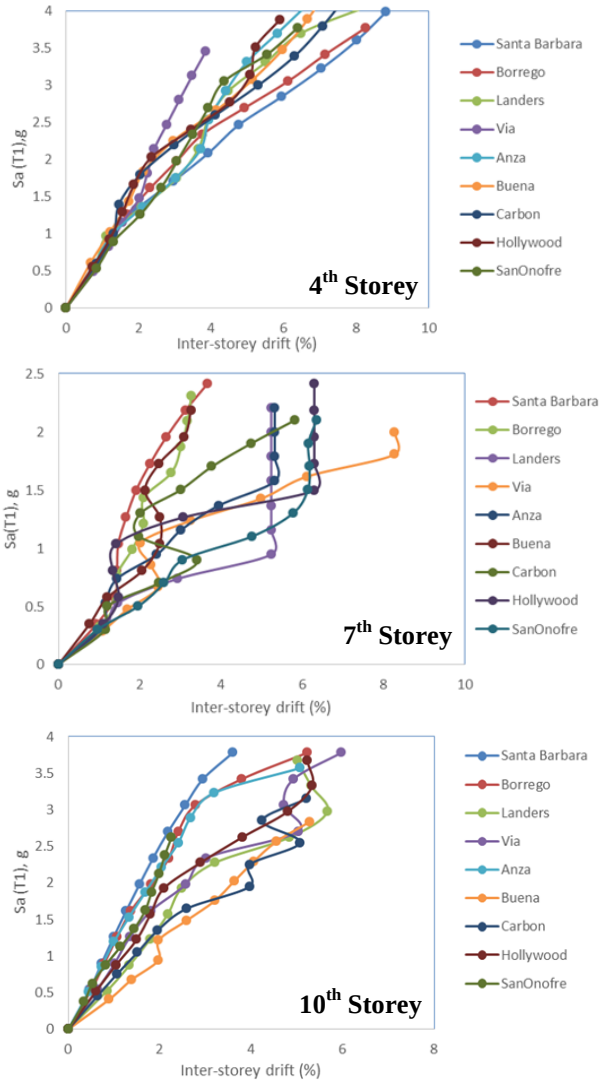

Fig.4 IDA curves for 9 ground motions

4.2 Nonlinear response along the height of the structures

In order to explore the effect of earthquake intensity on the distribution of inelasticity over the height of the buildings, the responses of each storey in terms of MID are provided through the use of IDA curves. Figure 5 illustrates a record-to-record specific picture of each storey subjected to earthquake records. For the 4th storey building, at first storey the MID is varied linearly up to Sa= 1.2g. Their 7th storey and 10th storey counterparts were 1.5 and 2.5 g, respectively.

In order to explore inelastic demand over the height of the buildings, the median values of MIDs were generated. Moreover, for each storey under the 9 GM records at three different intensity levels were noted. Table 2 shows the Sa(T1) response in the range of 0.7g to 4.0g. It indicates the inter-storey drift distribution along the height of the structures.

For the 7th storey building, at Sa (T1)= 0.7g, the inter-storey drift at top floor varies up to 3.9% with a standard deviation of 17%. Similarly, at 1.5g and 2.1g level, the top floor inter-storey drift ratio goes up to 6% and 6.6%, respectively with a standard deviation of 23%, 42%, respectively.

Their 10th storey counterpart was showed similar behavior, whereas, their 4th storey counterpart was showed a less variation in the inter-storey drift distribution at the design period with a range of 1.3% to 1.5%. However, it is observed that the variation of inter-storey drift ratio spread along the height of the structures. This is because as the intensity increases, the top storey reached to it nonlinear range.

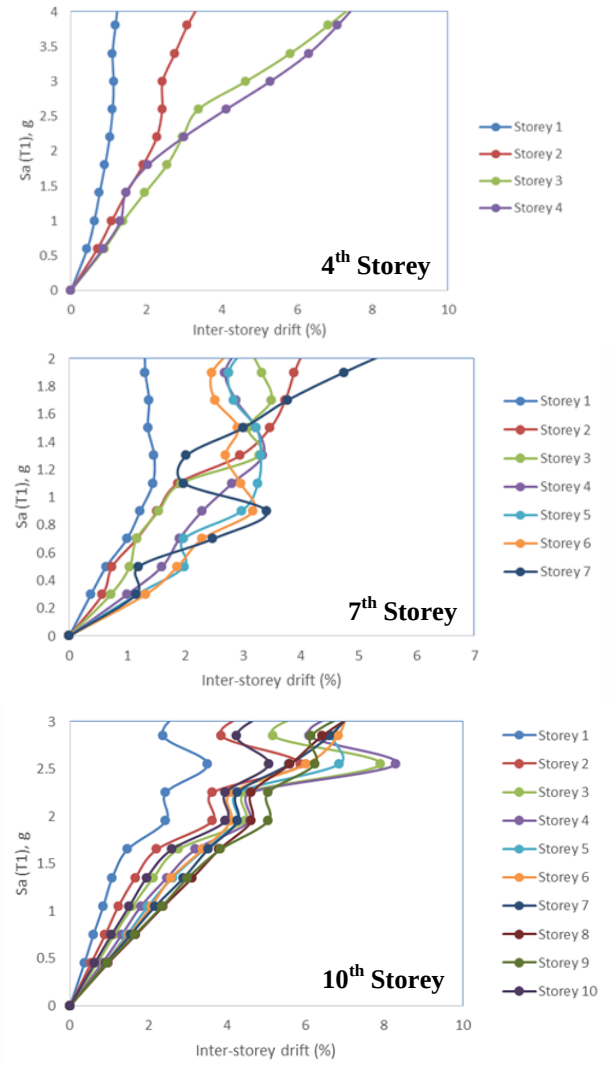

Fig.5 IDA curves for all stories

Table 2 Inter-storey drift ratios for all stories at different Sa (T1) levels.

4th Storey	7th Storey	10th Storey
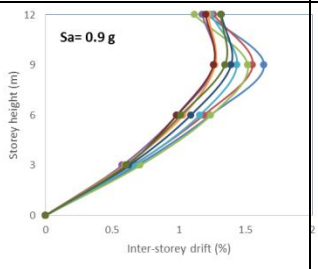	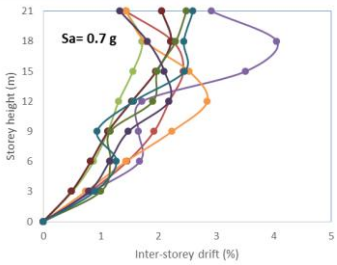	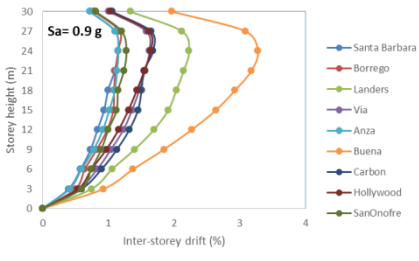
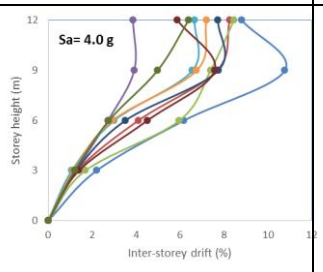	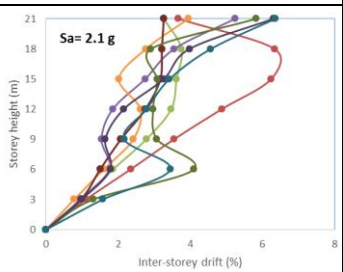	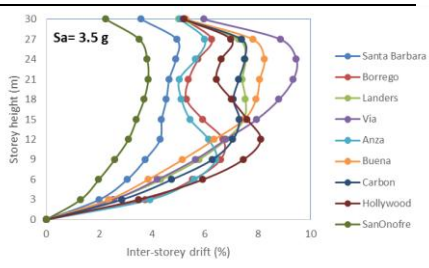

The median inter-storey drift ratio is also plotted in Figure 6 along the height of the structures with a variation of Sa (T1). Comparing the NBCC [2] inter-storey drift limit of 2.5%, it can be concluded that the RC structures can be withstood up to Sa of 1.5g, 0.7g and 0.9g for the 4th, 7th and 10th storey structures, respectively. Therefore, a strengthening scheme is necessary for the structures under severe GM excitations.

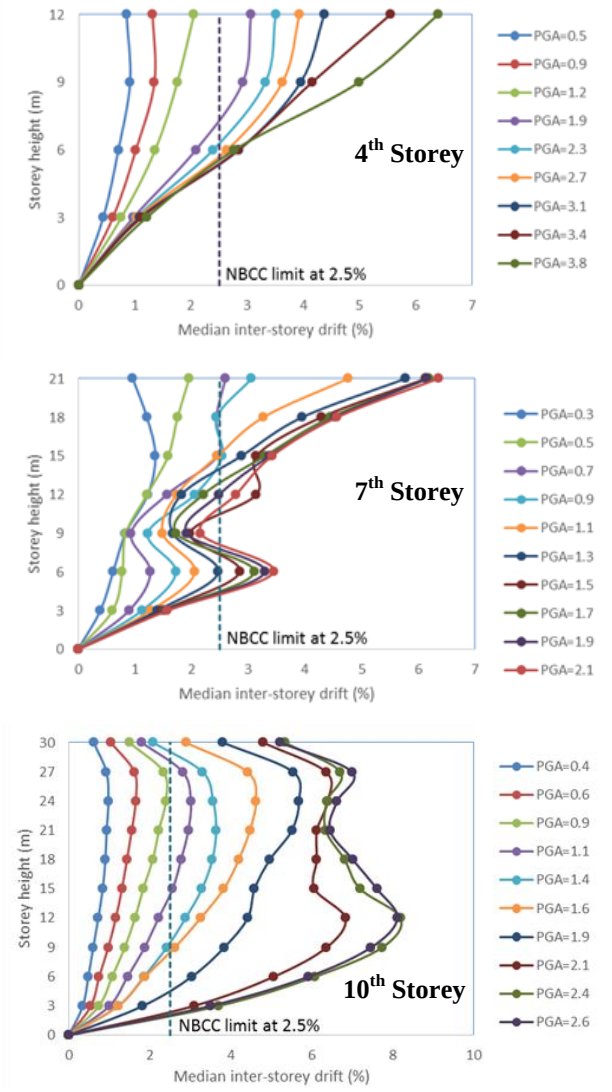

Fig.6 Median inter-storey drift ratios at different Sa(T1)

5. Seismic performance

The seismic performance of the RC structures was evaluated according to methodology describe in FEMA P695 [7]. The key notes to get the performance are stated below:

- Performance is quantified through nonlinear collapse simulation on a set of archetype models developed in SeismoStruct [6].
- The selected earthquake hazard is based on Maximum Considered Earthquake ground motions.
- Safety is expressed in terms of a collapse margin ratio (CMR).

5.1 Collapse margin ratio (CMR)

Safety of the studied buildings was expressed in terms of Collapse Margin Ratio (CMR). In order to quantify the safety, the collapse level ground motions are considered as the intensity that would result in median collapse of the seismic-force-resisting system, whereas, median collapse occurs when one-half of the structures exposed to this intensity of ground motion would have some form of life-threatening collapse.

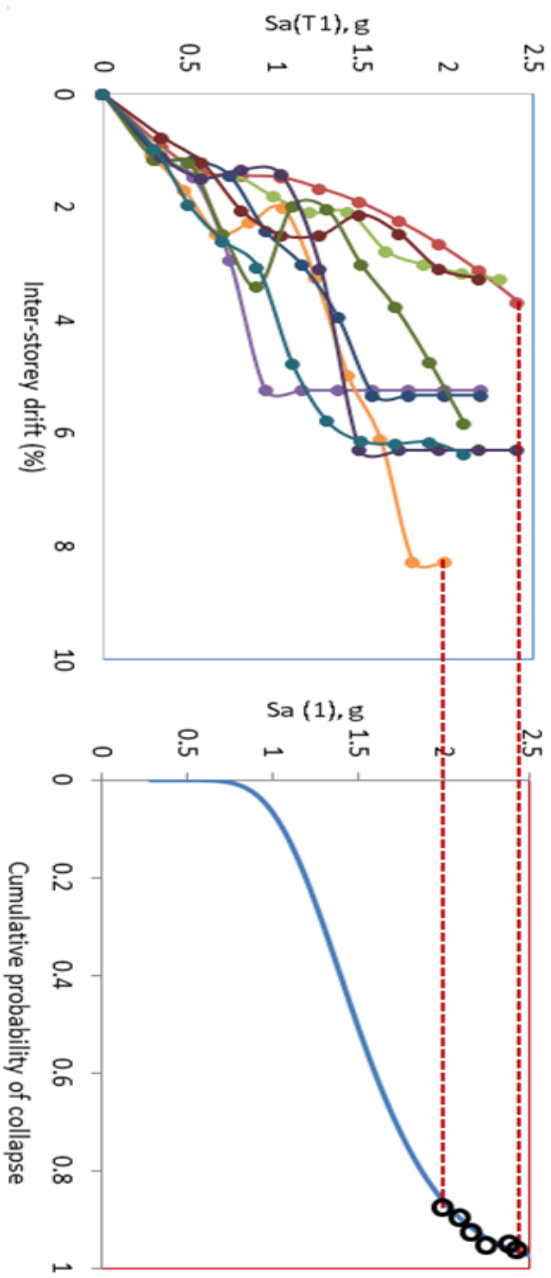

Fig.7 Incremental dynamic analysis response with the collapse fragility curve (7th storey building)

The collapse margin ratio, CMR, is the ratio of the median 5%-damped spectral acceleration of the collapse level ground motions to the 5%-damped spectral acceleration of the MCE ground motions at the fundamental period of the seismic-force-resisting system.

For collapse evaluation, ground motions are systematically scaled to increasing earthquake intensities until median collapse is established and analyzed the model as a form of IDA. Using collapse data obtained from IDA results, the collapse fragility curve defined through a cumulative distribution function (CDF), which related the ground motion intensity to the probability of collapse.

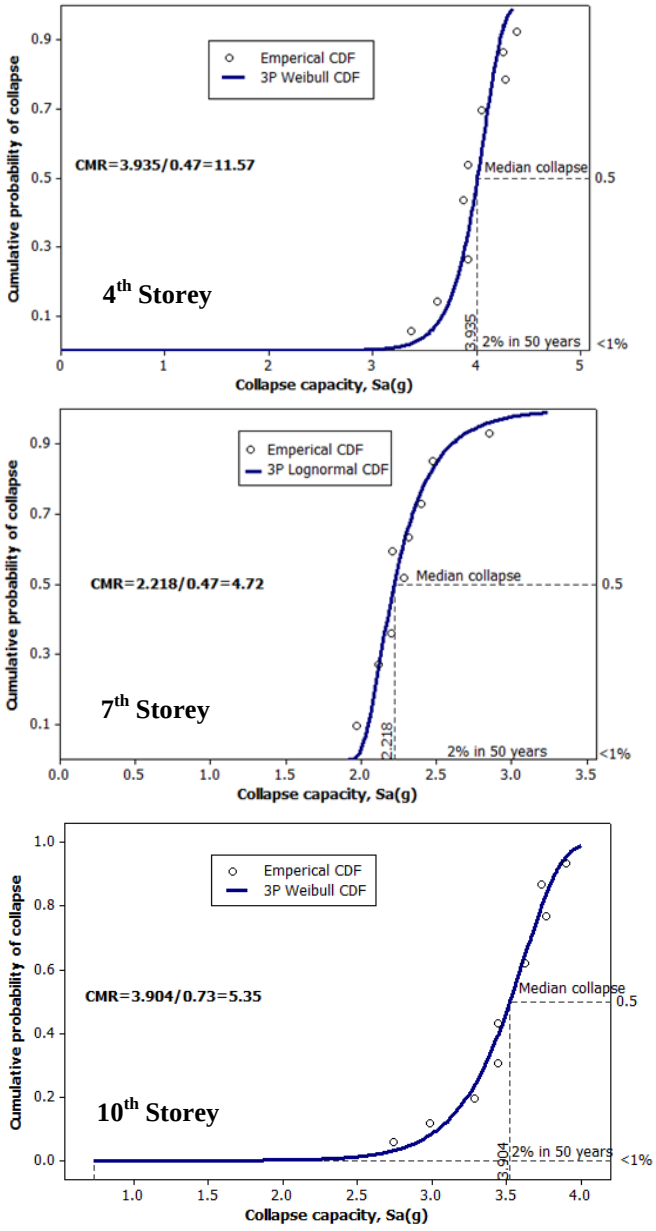

Fig.8 Collapse fragility curve for the studied structures

Figure 7 shows an example of a cumulative distribution plot obtained by fitting a three parameters lognormal distribution to the collapse data. Figure 8 shows the probability of collapse of the given structures under a given ground motion. Besides, the CMR for the given RC structures are obtained as of 11.57, 4.72, and 5.35 for the 4th, 7th, 10th storey building, respectively. The values indicate the structures are safe under the design earthquake loads. However, CMR of the 4th storey building indicates that it was very conservatively designed.

6. Conclusions

The present study provided a better understanding for the seismic performance of the RC structures having different heights. A nonlinear incremental dynamic analysis procedure was developed in a finite element program, SeimoStruct. The results obtained discussed in the previous sections can be summarized as follows:

- From the IDA curves, it is observed that the inter-storey drift demand varied in a wide range. For instance, at Sa=2.0 the inter-storey drift ratio for the 9 GMs varied from 2.2-3.7%, 2.2-8.0%, and 1.5-3.7% for the 4th, 7th and 10th storey buildings, respectively.
- The RC structures can be withstood up to Sa of 1.5g, 0.7g and 0.9g for the 4th, 7th and 10th storey structures, respectively, with compared to NBCC limit.
- Structural safety is expressed in terms of a collapse margin ratio and the obtained CMRs indicate the safe condition of the given structures.

REFERENCES

[1] CSA A23.3. Design of concrete structures. *Canadian Standards Association*. Rexdale, Ontario, Canada. (2004).

[2] NBCC. National Building Code of Canada. *National Research Council Canada*, Ottawa, Ontario, Canada. (2005).

[3] BNBC. *Bangladesh national Building Code*, Dhaka, Bangladesh. (1993).

[4] ACI 318. Building code requirements for structural concrete (ACI 318-02) and commentary (ACI 318R-02). *American Concrete Institute*. (2002).

[5] ACI 318. Building code requirements for structural concrete. *American Concrete Institute*, ACI Committee 318, Farmington Hills, Michigan. (2005).

[6] SeismoSoft, SeismoStruct. *A Computer Program for Static and Dynamic nonlinear analysis of framed structures*. Available from: http://www.seismosoft.com. (2008).

[7] FEMA P695. Quantification of Building Seismic Performance Factors. *Federal Emergency Management Agency*, Washington, D.C. (2009).

[8] ASCE. Seismic Evaluation and Retrofit of Existing Buildings, ASCE/SEI 41-13. *American Society of Civil Engineers*, Reston, Virginia. (2013).

[9] Vamvatsikos D, Cornell AC. Incremental dynamic analysis. Earthquake Engineering & Structural 31(3): 491–514. DOI: 10.1002/eqe.141. (2002).

ICMIEE-PI-140337

APPLICATION OF REENGINEERING PRINCIPLES IN A LOCAL INDUSTRY

[1] Sayem Ahmed, Minhajul Islam, Rafi Ahmed, Saifullah-Al-Munsur, And S. K. Biswas [2].
[1] Graduates of Industrial & Production Engineering, AUST, Bangladesh.
[2] Professor, Department of Mechanical and Production Engineering, AUST, Bangladesh.

ABSTRACT:
This paper proposes a redesigned plant layout for the plant as the overall performance of an industrial firm is significantly affected by the design of its manufacturing facility. Also attempt was given to determine the standard time of doing the jobs through the use of time study principles to increase the production efficiency and thus finding out the appropriate production time to meet the ultimate production goal of the industry, and attempts have also been made for analyzing and maintaining safety of workers in time of production and on other hazardous issues of the organization. Finally some safety standards for the plant have been recommended. The findings have been recommended for implementation and improvement. The case study was made in a local industry located at Tejgaon area of Dhaka. It is hoped that if the industry implements the findings, productivity will increase.

Keywords: Re-engineering, Time study, Plant Layout, Safety Engineering.

1. Introduction: [1] – [5]

There are many problems in industries in our country, which in the opinion of the authors, reduce overall performance of the industry. Often every industry overlooks many related problems, as a result the cost of the production increases. The main problem of many industries is production time loss the main cause of which might be for not following the use of the standard time for the purpose. In many cases the industries follow thumb rule in every process which violates Taylor's Scientific Management theory directly. So we think, the industry faces huge productivity & efficiency loss in the process. In this study and research work standard time for making different products by applying time study principles in a renowned local ice cream industry was found. Application of time study might help in reducing the actual time loss of the process. Further, we think, many of the industries don't usually follow the necessary safety precautions. As a result number of accidents has been increasing day by day. As the cost of the accident is quite large, this might affect the overall profit of the industry. In this study an appropriate plant layout for reducing process time as well as for avoiding accident has been found and recommended some safety instructions, which might reduce the accident and overall total production cost of the industry. So finally we can say that these findings might help the industry to increase profit and efficiency by following standard time and maintaining safety of the worker and machine. It might be further noted that many industries sometimes don't follow many standard theories related to Production Planning & Control. Moreover we have also observed that, location / layout /material handing etc. too initiated problems in many cases. The management people of the industry did not allow us to study the selected industrial organization in detail. Even we have been asked not to disclose the name and identity of the industry.

In the following analysis and discussions, the recommendations and comments for improvement have been mentioned separately (after discussions) in each section.

2. Present Layout and its improvement: [2], [4]

The overall performance of an industrial firm is significantly affected by the design of its manufacturing facility. As Local Ice Cream Company under study has an existing layout, we observed and studied the existing layout critically. The total area of the plant is too small and non-expandable, as for this the decision making of layout change will be too hard because it will cost high monetary value and hamper the production time. It was found that products of production floor 2 have to be moved through production floor 1 and ultimately to be placed into the cold storage, which is situated beside production floor 1. As a result during transportation in production floor 2 of products towards cold storage a haphazard situation is created which can be considered as waste as this requires extra movement of materials. A well-designed facility layout might help in efficient material handling requiring small transportation time, and paths It is hoped that this, in turn, leads to low work-in-process levels, effective production management, decreased cycle times and manufacturing inventory costs, improved on-time delivery performance, and consequently higher product quality. The efficiency of a layout is typically measured in terms of material transportation cost which is directly influenced by the distance a unit load travels.

*Corresponding author, Tel.: +88-01817-746070, +88-01813-261758
E-mail address: skbaust@yahoo.com, skbiswas.mpe@aust.edu, skbcuet@yahoo.com

2.1 Proposals for improvement:

(i) A conveyor system to move materials of production in floor 2 to be stored in central cold storage may be designed and installed. This might be more efficient if the position of cup filling machine is reversed in product flow direction from presently followed product flow direction and ultimately the packaging place for cup filling machines products, can then be placed in opposite direction by the side of hardening tunnel from the present place of packaging of ice creams. As a result hardening tunnel of production floor 2 will process both cup filling machines products and *Royal Sundae* products and thus these end products will be moved towards cold storage through vertical conveyor which will also convey *Rollo 23 and Mark Line* machines products. The vertical conveyor can easily be inserted to production floor 1 by breaking the wall between production floor 1 and 2. As a result extra material transportation will be reduced, as well as wastes will be reduced in number.

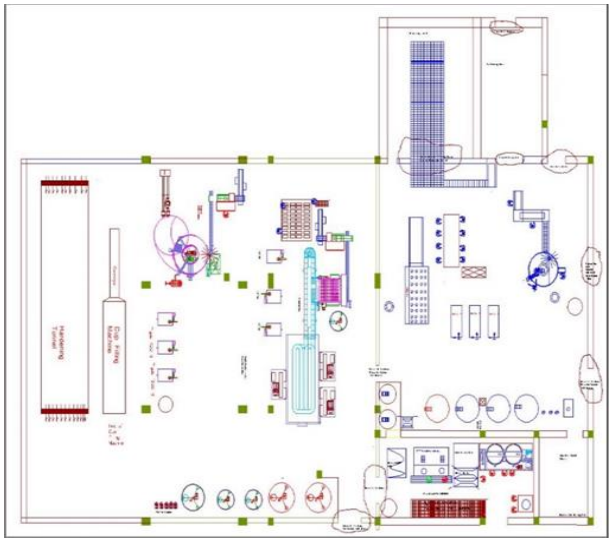

Fig.1: Existing Plant Layout

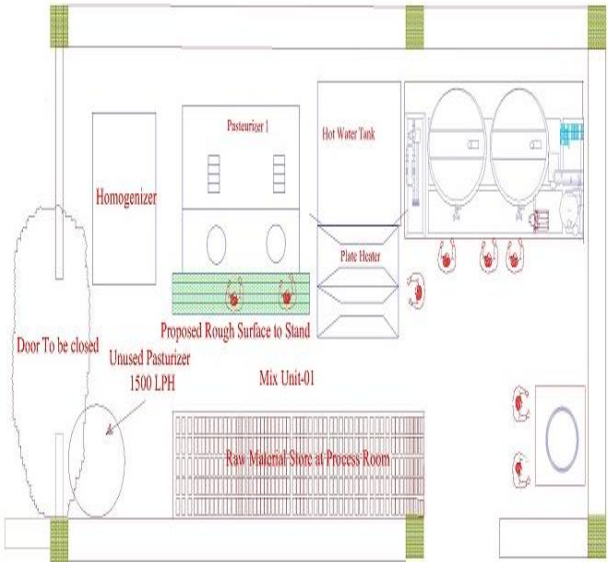

Fig.2: Proposed Mix Units working surface

(ii) The working surface bench used during pouring of raw material into the mix tank was seen as very slippery, which may cause severe accident to workers or damage to raw materials. To prevent this situation the bench where workers stand may be redesigned and rough surface may be introduced, please refer to figure-2.

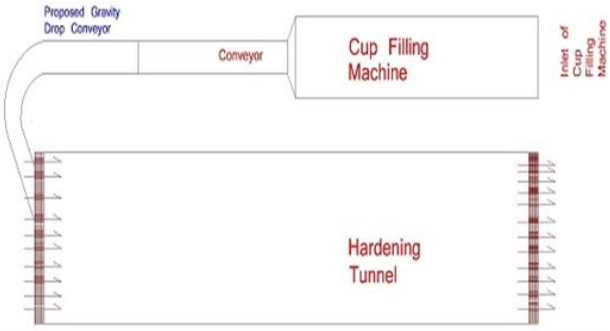

Fig.3: Proposed gravity drop conveyor (top view)

(iii) It was observed that Cup filling machine has a conveyance problem at present. When carnival ice cream gets out from the conveyor of the machine, a worker collects those ice creams in a tray and places this tray in the hardening tunnel. Problem is that during his or her movement towards hardening tunnel with the tray the cup filling machine continues to produce carnival ice cream during the same time as the process is a continuous one. So to prevent end product falling out from the conveyor usually an extra worker seats beside the inspection workers and this extra worker collects those stuck ice cream, during the tray carrier workers movement, with the help of a stick. But if we introduce a gravity drop conveyor from the conveyor of cup filling machine to the hardening tunnel as shown in **figure-3** the extra worker to collect stuck ice creams during tray carrier's movement can be eliminated.

3. Time study: [5]

The objective of doing Time study is to determine standard time of doing a job. In order to carry out time study, a number of interviews were taken of management officials e.g., of Managing director, Chief engineer, Deputy General Manager (DGM), Assistant engineer as well as of many workers of the industry of case study. Standard time is the amount of time a qualified worker should spend to complete a specified task, working at sustainable rate, using set methods, tools and equipment, raw material, workplace arrangement and with allowing adequate time for such items as unavoidable or machine delays, rest to overcome fatigue, and also for personal needs. It is generally done (i) to improve the accuracy of planning of set target (ii) to assign workers in an appropriate manner (iii) to set the direction of efforts aimed at improving skills of workers, etc.

3.1 Calculation of Actual Time for Mix Unit:

Table 1: Actual time required for 1st tank:

Process step	Required time (in minutes)
Start	-
Pouring hot water	4.29
Mixing ingredients	9.56
Mix ready and sending	17.18

Table 2: Actual time required for 2nd tank:

Process step	Required time (in minutes)
Start	-
Pouring hot water	4.42
Mixing ingredients	8.62
Mix ready and sending	18.78

Here, we found that total actual time for sending two mix batches was (17.18+18.78) min = 35.96 minutes.
But by company estimate standard time was found to be 30 minutes. So, time equivalent to 5.96 min per cycle can be saved.

Proposals for improvement:
To yield better production of flow in mix unit the following proposals may be helpful for the company.
As we know from the continuity equation, Q=AV (where, Q=flow rate, A=area, V=velocity). Thus we can make a trade-off between A and V. We can consider the following options:

a) Increasing the area of the delivery pipe
b) Increasing the delivery speed / velocity

- The first option of increasing area is quite expensive because of complex design and use of Stainless Steel (SS) pipe
- The second option of increasing the delivery speed can be done by using high capacity pump(s).

As the first option is costly and complex, so, the velocity of delivery can be increased by using high capacity pumps.

3.2 Allowance factor:

The standard allowance factor is very difficult to determine. So, each industry usually determines allowance factor after thorough study and investigation considering among other factors (i) Degree of skill-ness of worker (ii) Work details (iii) No of processes allotted to workers (iv) Miscellaneous other factors. In this study the allowance factor was calculated by 'Production Study' method. In this method, the worker is continuously monitored for a definite period of time and actual time for normal activity, unavoidable delay and avoidable delays are recorded without letting the worker know about the study. Thus the allowance factor was calculated as follows:

Activity	No. of hours observed	% of Normal Activity
Normal	5.4	100
Unavoidable delay	1.4	25.92
Avoidable delay	1.2	22.22
Total time reqd.	**8**	

Allowance factor = 1 + (unavoidable delays (hours) / normal activity (hours))

$= 1 + (1.4/5.4)$
$= 1.259$
$\cong 1.26$

3.3 Performance Rating (PR):

PR depicts the efficiency of workers. As most of the machines are automatic and semi-automatic, it was not possible to calculate the performance rating of workers. Here, we've used 85% efficiency of the workers to calculate the standard time of doing a work. This value was the estimate of the organization.
In the following calculations as machine processing time remained fixed for every cycle, hence it was excluded in measuring standard time. Here only the actual working times of workers have been considered.

3.4 Calculating Standard Time for various items:

(i) For Chocolate ½ liter box:

Table 3: Data for Chocolate ½ liter box

Activity	Observed time (sec)	Normal time (sec)	Standard time (sec)
Dosing	4	3.4 (4*0.85)	Standard Time (ST) ST = NT(Normal Time)*AF (Allowance Factor) = 16.455*1.26 = 20.73
Placing lid	3.167	2.69	
Collecting box	1.6	1.36	
Labeling	6.53	5.4	
Collecting in tray	2.5	2.125	
Tray to storage	1.75	1.48	
Total time in seconds		**16.455** without machine time	

But, the actual time as it was found by the company in the production floor was 22 sec; so, 1.27 sec per piece can be saved in making this type of ice-cream.

Proposals for improvement:
By given information it was known that the company did not do and apply any time study before. So, the standard time was unknown to the management. By applying thumb rule, the authority assumed that the processing time was 22 sec/piece. But by applying time study method, it has been found the standard time of doing was 20.73 sec/piece. Measurement of the standard time for only one dosing system was done in this study. As two dosing systems are running simultaneously, so output will be about 1120/2 = 560 pieces/hour for each of the dosing system.

If the workers perform their work with care without wasting time, they can produce at least 900 pieces / hour by following standard time, i.e., by saving 1.27 sec per piece of this type of ice cream.

i) For producing ½ liter chocolate box it was observed during study that 14 workers are necessary for the operation. But the company actually uses 16 workers for that operation. So, 2 workers can be reduced from that operation.

ii) For labeling operation and placing lid the management uses 4 and 3 persons respectively. But if the cover is redesigned to serve both as a cover and preservation system, it might save minimum 2 workers. In foreign countries this type of labels are widely used.

(ii) For Doi ice-cream:

For this too similar calculation was done as given below:

Table 4: Data for Doi ice-cream:

Activity	Observed time (sec)	Normal time (sec)	Standard time (sec)
Placing the cup	0.61	0.518 (0.61*0.85)	ST = NT*AF = 19.607*1.26 = 24.70
Cup filling	0.61	0.61 (done by m/c)	
Pouring solid milk	0.61	0.518	
Collecting lid	1.25	1.062	
Placing lid	2.44	2.074	
Collecting cup in tray	1.17	0.9945	
Storing in hardening tunnel	0.75	0.637	
Time elapsed in hardening tunnel	3300	3300 (done by m/c)	
Collecting cup from hardening tunnel	7	5.95	
Preparing packet	0.75	0.637	
Placing cup in the packet	0.94	0.79	
Serving spoon	1.5	1.275	
Taping	1.05	0.89	
Storage	5	4.25	
Total time in seconds		**19.607** (without machine time)	

But, as per present estimate of the company the actual time in the production floor was found to be 30 sec. Therefore, at present the process is taking about more time of 5.30 (i.e., 30.0-24.7) sec per piece in making ice-cream.

(iii) For Ice-cream type 2 in 1:

Table 5: Data for 2 in 1:

Activity	Observed time (sec)	Normal time (sec)	Standard time (sec)
Dosing and slicing	1	1 (done by m/c)	ST = NT*AF = 9.239*1.26 = 11.64
Hardening	1289	1289 (done by m/c)	
Hardening to clamping	20	20 (done by m/c)	
Releasing in conveyor	30	30 (done by m/c)	
Passing by conveyor	30	30 (done by m/c)	
Wrapping	9	7.65 (9*0.85)	
Collecting and placing in a paper box	1.13	0.96	
Packaging	0.68	0.578	
Storing in cold storage	0.06	0.051	
Total time in seconds		**9.239** without machine time	

But, the actual time as found by the company officials in the production floor to be 21 sec Therefore, at present the process is taking about more time of 9.36 sec per piece.

Proposals for improvements:

It was actually seen from the observations made by us that due to improper clamping and distorted holding plate the waste in ice–cream making machine (Mark Line) was about 66 ice-creams per 15 minutes. To reduce these wastes the following proposals can be followed:

i) The clamping unit and releasing unit of mark line seemed to be defective. If the system is redesigned including mechanism of clamping and the way of releasing of ice-cream to conveyor then the waste might be reduced.

ii) The ice-cream holding plate has been found to be distorted due to the repetitive force of the pneumatic hammer. Consequently the clamper sometimes fails to grip ice cream properly in its defined position due to the misaligned position of the plate. So, a rubber pad can be wrapped around the hammer that will dissipate the concentrated force of pneumatic hammer.

iii) If the height of the plastic in the exit section from the hardening tunnel is reduced then it is expected that

the plastic might not produce any scratch on the surface of the ice-cream.

In the conclusion it can be said that if the company improve as per proposals made then the waste of the ice-cream production may reduce. By analysis and observations it can be inferred that by following job rotation, actually 16 workers are sufficient instead of 20**.** And if the problem of clamping unit can be solved then the no of workers might further be reduced to (16-4) = 12 instead of 16. It was seen in the study that the yellow rectangle showed 4 workers engaged in existing clamping problem, if the problem can be solved then these 4 workers can be eliminated from the process.

4. Safety hazards and Recommendations: [3]

In the following the observations have been made from the study relating to safety and hazard. Thus along with the mentioned safety issues the proposals for improvement relating to machines used for making ice-cream, processes and related other issues have been made under each.

a) Mix unit:

Safety issues:

i. Slippery floor due to fat spilling
ii. Standing bench that is made of stainless steel which is used to pour ingredients into mixing tanks, is very slippery and dangerous
iii. Raising loads from the floor in upward direction for supplying ingredients in the mixing tank. This causes back pain of the worker
iv. Liquid glucose is handled with bare hand
v. Unorganized work materials

Recommended proposals for improvement:

i. Rough textured floor surface can be used. It can be considered that adhesive friction is a positive grip due to the penetration of one surface into the other. Textured surfaces and abrasive surfaces are considered as safest.
ii. Texturing of the standing bench surface or carpeting of non-slippery materials like rubber, gratings, diamond or checkered plate, knurled, dimpled corrugated expanding metal can be made.
iii. Semiautomatic lifting system can be used for loading (using hydraulic jack) as we know hydraulic jack is a device that uses force to lift heavy loads. After raising up to a certain height, the workers can use them easily.
iv. Special non-sticky gloves can be used.
v. "5-S", Japanese concept meaning: *Sort, Set in order, Shine, Standardize and Sustain,* method to organize things around the mix unit can be implemented.

b) Rollo 20: (Malai)

Safety issues:

i. Electric wires were found in exposed condition.

Recommended proposals to solve the issue:

i. Contact with electric current is a serious cause of workplace injuries. Electric wires should be insulated from the workers. Consistent monitoring can be done

c) Mark Line: (Rocks, 2 in 1)

Safety issues:

i. When ice-cream is released from clamp, a worker places it in the running conveyor. The worker works with one hand only which causes pain and hand become stiff in the long run.

Recommended proposals for solution:

i. According to principles of motion economy two (2) hands should remain in simultaneous motion as far as possible. Thus this principle is needed to be followed.
ii. The clamping and releasing system can be resigned to remove worker from that point

d) Rollo 23: (Chocobar)

Safety issues:

i. In time of maintenance work, the maintenance person sometimes stand and walk over the machine with unhygienic shoes

Recommended proposals for solution:

i. The person should wear hygienic foot protector / shoes during maintenance and general work period.

e) Royal Sundae/Mango Mellow Machine:

Safety issues:

i. The workers don't put on masks, hand gloves and caps always.

Recommended proposal for solution:

i. Awareness in workers can be created to correctly maintain the safety regulations

f) Light Problems:

Safety issues:

i. In 2nd floor, at nut cutting room, low level of light has been detected measuring only 9.2 lux. Insufficient light can cause serious eye problems and laceration

Recommended proposal for solution:

i. Sufficient light can be ensured to avoid the problems. For seeing requirement, concerned with moderately fine detail and intermittent work, the recommended light level is 322 lux

g) Sound Problems:

Safety issues: Relating to this issue the sound levels were measured as follows:

i. Repetitive force of the pneumatic hammer on the plate which carry ice cream at the Mark Line machine causes continuous sound of 95-98 dB
ii. Hardening section causes sound of around 90 dB
iii. At the Boiler room, there was sound of over 91 dB
iv. In Ammonia plant the range of sound intensity was 88 dB

It is known that, if the range of sound intensity crosses 80 dB it will create risk of hearing loss when worker works over 8 hours per day. It also causes slow deterioration of employees' health.

Recommended proposals for solution:

i. Rubber pad can be a useful solution for the first issue. A rubber pad can be wrapped around the hammer that will dissipate the concentrated force so the sound level may be reduced
ii. Comfortable ear plugs can be supplied to the workers and the workers can be motivated to use the ear plugs

h) Cold Storage problems:

Safety issues:

i. It was found that the temperature of the storage area was actually -28 ^{0}C. If a worker is new in the factory or he joins the work after a vacation at first he needs to adapt to that low temperature. Otherwise he might become sick. Fever or headache might affect him. Usually in the ice cream factory the workers don't get any chance to adapt to that level of low temperature.

Recommended proposals for solution:

i. Acclimatization (the body's gradual adjustment to a change in climate or working conditions and its rapid return to a "normal" state when removed from the stressful situation) process can be maintained and implemented.
ii. Generally, a two week program is required which will gradually get the worker and his body to become used to this cold environment. It is therefore suggested that on the first day the worker can be exposed to 50% of the work load and time which can eventually become the same as the total required. In each day thereafter, a 10% increase in exposure can be scheduled, building up to a 100% of the total exposure on the sixth day. If any worker remain absent from work for nine or more consecutive days for any reason, a four day acclimatization period, beginning with a 50% exposure the first day and with daily increments of 20%, is considered as necessary. His can be practiced for workers working in cold area only.

i) Ammonia Plant:

Safety issues: The following issues were identified:

i. Improper ventilation;
ii. Easily accessible discharge valve;
iii. Safety value can only handle maximum pressure of 17 bar;
iv. Mixture of air and gas occurs;
We know breathing of air containing 500-10000 ppm of ammonia, which can cause sudden death from spasm of inflammation of the larynx. Concentration exceeding 700 ppm of ammonia can cause permanent eye injury.

Recommended Proposals for improvement:

i. Proper ventilation system should be introduced
ii. Discharge valve should be placed in a safe position
iii. Condenser should always be kept clean due to avoid high pressure
iv. If air and gas is mixed together, then the gas can be cooled by air purging
v. There must be a sensor which can detect over 500 ppm of ammonia in the air and capable of sounding an alarm

j) Other Major accident areas:

It was found that in Cone biscuit machine area sometimes remain filled with smoke and heat.

Recommended solutions:

i. Smoke and heat detector can be used to buzz an alarm and a water sprayer can be installed which spill water in case of outbreak of fire.

Conclusion:

About the study relating to productivity increase, safety management, layout improvements, etc., in a word with a view to apply reengineering principles, an attempt has been made to minimize the production time loss, in the industry under case study, by applying Time and Motion Study principles in different processes, by improving the plant layout and also by proposing some safety rules that can be followed to reduce the accident. Thus it is hoped that productivity will certainly increase if all or at least some of the recommendations mentioned in this paper are implemented. This report discussed the existing and modified plant layout. There is no layout that ends to be the best. A given layout can be best in one set of conditions and yet poor in different set of conditions. We feel if this local ice cream company implements the suggestions it might get a better as well as economical solution for overall improvement.

Acknowledgement:

Our sincere thanks go the high officials of local ice cream company who allowed us to use various floor data although they did not allow us to disclose their identity**.**

REFERENCES

[1]Groover, Mikell P. (2007), "Work Systems and Methods, Measurement, and Management of Work", Pearson Education International.

[2]Joseph Prokopenko, "A Practical Handbook, Productivity Management".

[3]Rahman M. H., (2009), "Management of Occupational Safety Health & Environment", 1st Edition, Adorn Publication, 2009.

[4]Heizer & Render, "Operations Management", 8th Edition.

[5]Krazewski and Ritzaman, "Operations Management".

[6]Ralph M. Barnes, "Motion and Time Study: Design and Measurement of Work", 17th Edition.

[7]Mayer, "Production and Operations Management".

[8]Sayem, Minhaj, Rafi, Saifullah, "Application of Reengineering Principles in a local industry", B.Sc. Eng. thesis submitted to the Dept. of MPE, AUST, in 2014.

ICMIEE-PI-140338

QUALITY ASSURANCE PROGRAM & IMPLEMENTATION OF ISO, A CASE STUDY

[1]*Abrar Fahim Samad, Amit Banik, Md. Jakaria Rahman, Dipanjan Ghosh,*
Graduates of IPE, Ahsanullah University of Science & Technology (AUST),
[2] *S.K.Biswas*, Professor, MPE (Mechanical & Production Engineering) department, (AUST)

ABSTRACT
Quality assurance has become the major concern for any kind of organization in this competitive business world. Every organization wants to ensure best quality for their product their product or service i.e. in a word we can say all want to ensure 'Quality Assurance' by imposing different methods or processes. This paper discusses the importance and implementation process of **ISO** for product quality assurance in Bangladeshi industries. To cope up with the increasing competition of business around the world and to provide the people a better experience with good quality product and service the local industries needs to implement international standards to confirm the quality assurance up to the satisfaction of customers ultimately. The RANGS workshop limited (RWL), a leading automobile repair shop as well as automobile supplier in Bangladesh, gained ISO 9001:2008 certificates in year 2011.All related documents of RWL have been checked during implementation phase of ISO. This paper discusses all steps of implementation of ISO and also the most important steps in ISO implementation, the audit section of that organization.

Keywords: ISO, Quality Assurance Program

1. Introduction: [1], [2]

Before purchasing any product or receiving any service every customer wants to get the best with a reasonable price. Here the question comes, Quality Assurance. It has become the trump card for any organization in this competitive business world. To ensure quality some methods and procedures are followed depending on the organization types. Some standards and also technology work as a helping tool. ISO [3] and ERP [4] are the most common and effective tool to ensure quality and also for its continual improvement. Industries are growing rapidly in our country and the issue for ensuring quality has become more important to the industries / organizations. Implementation of ISO and ERP requires hard work, time and money but it has some unique benefits [5]. ISO provides senior management with an efficient management process and also sets out areas of responsibility across the organization, identifies and encourages more efficient and time saving processes, reduces product costs, provides continuous assessment and improvement. Some Improved quality and service and last of all independent audits demonstrate commitment to quality. Installing an ERP system has many advantages-both direct and indirect. The direct advantages include: Improved efficiency, Information integration for better decision-making, faster response time to customer queries etc. Modern ERP systems are built for the internet-enabled world with e-commerce capabilities and provision for integration and collaboration with supply chain partners, customer portals, and enhanced tracking of incoming material and outgoing product to extend the visibility and control. We believe that implementation of ISO and ERP for quality assurance can change the overall scenario in our local business. It will also help to break down the barrier of global business. In our study we could finish the ISO part in detail but we too studied the implementation of ERP briefly. In this paper we only focused our concentration in ISO implementation.

2. Objective of research and case study:

- To know the process of implementation of ISO in any industry in Bangladesh
- Study of the importance of quality assurance in industries
- Preparing ourselves to implement ISO in local industries
- Study of the implementation process of ISO in RWL as a case study

3. Background of the study:

Any Production entity / service organization / any type of Production plant can be represented like the following in a broad sense [6]. Usually input like human, material, technology, and societal variables etc. and also the conversion process play an important role in final product, profit, customer satisfaction, etc. The very survival of any production / service entity depends on customer satisfaction along with the efficiency in managing the affairs of the organization. And Customer satisfaction is ultimately related to the quality assurance program of the organization / industry.

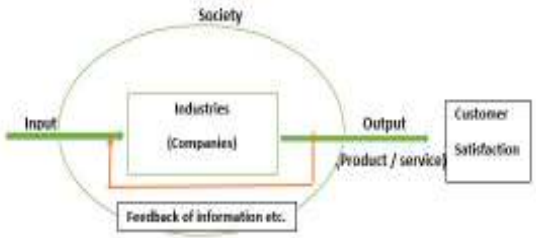

Fig. 3.1: Black Box Representation of Organization

* Corresponding author. Tel.: +8801838261758, +8801817746070
E-mail address: skbaust@yahoo.com, skbiswas.mpe@aust.edu, skbcuet@yahoo.com

In a word we can say that, to satisfy the customer with the best quality product or service has become the most important problem / objective for any organization to remain on the racing track with the increasing competition both locally and internationally i.e., throughout the whole world. We are living in the age of globalization, developed technologies and information, etc. In this age all customers are very much aware about what they want, while buying products or receiving service from any organization. So it has become a duty for the companies to ensure the quality and to improve them continually. Because quality has no finish lines just like 100 meter sprint. The companies are continuously trying to provide better quality or service and the customers too will come to get them. To ensure the quality, International Organization for Standardization (ISO) has developed standards called ISO 9000 that is for Quality Management of service & product quality in addition to various other local / regional agencies / organizations. In the following a brief discussion on ISO has been made.

4. ISO:

The word ISO [7], [8] came from a Greek word "Isos" which means "Equal". That means "Equal to Standard" [6]. Some popular ISO standards are mentioned below, but there are many others:

Table 4.1: ISO Standards

ISO 9000	Quality management
ISO 14000	Environmental management
ISO 26000	Social responsibility
ISO 50001	Energy management
ISO 31000	Risk management
ISO 22000	Food safety management

ISO 9000: The standard is a guide-line for world class business practice [9]. The unique part of the standard is that it allows each company to evaluate each element of the standard and decide how to meet the requirements of that element effectively. In very simplified terms, the standard tells an organization to check what it is doing to ensure quality and then does what it requires. Finally documentation or proof that it has been done as what it said. It can be applied to construction, engineering, manufacturing, health care etc. There are many standards in the ISO 9000 family [10], including:

ISO 9001:2008 - sets out the requirements of a quality management system

ISO 9000:2005 - covers the basic concepts and language

ISO 9004:2009 - focuses on how to make a quality management system more efficient and effective

ISO **9001:2008** sets out the criteria for a quality management system and is the only standard in the family that can be certified. It can be used by any organization, large or small, regardless of its field of activity. In fact ISO 9001:2008 is implemented by over one million companies and organizations in over 170 countries. [10]

4.1 Benefits of ISO 9001:

- Provides senior management with an efficient management process,
- Sets out areas of responsibility across the organization,
- Identifies and encourages more efficient and time saving processes,
- Highlights deficiencies,
- Reduces organizational costs,
- Provides continuous assessment and improvement, etc.

4.2 Application in Production Flow:

ISO 9000 series of standards has variety of application in a production process. The related flow chart is given below:

Fig. 4.1: Application of ISO 9000 series in production process

A basic of ISO 9000 is Quality Management. A principle is a fundamental truth or law and therefore quality management principles are the fundamental truths or laws that form the basis of quality management [11]. These principles have been identified to facilitate the achievement of quality objectives and form the foundation for effective quality management. Names of some of such principles are: customer focused organization; leadership; involvement of people; process approach; system approach to management; continual improvement; actual approach to decision making; mutually beneficial supplier relationships, etc.

4.3 Requirements ISO 9001:2008:

We studied various articles and books about quality management and ISO at the very beginning of our study. After reviewing the related literatures and also consulting the related official in RWL we found some core information about it. To implement ISO 9001:2008 in any type of organization we need to understand the requirements of it at first. Basically for implementing ISO 9001:2008 there are almost twenty requirements that an organization has to fulfill to get certification. But it is not fixed. It varies from organization to organization, from business to business. Those basic 20 clauses/requirements are: [each main clause has a few

sub clauses which are not mentioned here due to space limitation.]

1. Management responsibility
2. Quality System
3. Contract Review
4. Design Control
5. Document Control
6. Purchasing
7. Customer-supplied material
8. Product Identification & Traceability
9. Process Control
10. Inspection and Testing
11. Inspection, Measuring and Test Equipment
12. Inspection and Test Status
13. Control of Nonconforming Product
14. Corrective Action
15. Handling , Storage, Packaging and Delivery
16. Quality Records
17. Internal Quality Audits
18. Training
19. Servicing
20. Statistical Techniques

Along with those twenty requirements there are eight requirements that are usually considered as common for every organization. These especial eight requirements are:
1. Scope
2. Normative reference
3. Definitions
4. Quality, management systems
5. Management responsibility
6. Resource management
7. Product and / or service realization and
8. Measurement, analysis, and improvement

The details about these clauses may be found in literatures [12]

4.4 Implementation Process of ISO 9001:2008 at RWL:
ISO implementation consists of some organized procedure [13]. The certification procedure can be described briefly as similar procedures which are needed to be followed for getting any other ISO related certificates.

General ISO Certification Process:
i) Auditing by the 1st party:
It is the first step of the audit. Auditing means checking or conformance with defined standards. In it generally all the ISO implementation requirements are formally checked and audited. It was done by RWL itself.
ii) Auditing by the 2nd party:
Usually it is done by any local ISO related audit agency to see that the application submitting organization / company fulfills the requirements to get ISO certificate as per set standard. But most of the organizations along with RWL avoid this step because of cost and time.
iii) Auditing by the 3rd party:
It is done by the ISO affiliated body. ISO does not certify any organization by itself. Their affiliated body usually certifies the organization which applies for getting certificate. RWL got its certification from TÜV SÜD. There are many affiliated bodies like SGS, UKAS etc. While choosing the 3rd party proper research and study are needed because it involves huge amount of cost and time, i.e., we can say extreme care should be taken when choosing the certification body as certification from the wrong one might not be worth.

For the whole work the following procedures have been followed by RWL to get the desired ISO certificate. Thus this can be considered as work done before getting ISO certification. Generally all organizations interested to get quality certification like ISO certification should follow the procedures mentioned in this Section.

a. Formation of ISO team:
ISO team was formed generally by including the Head from each of the departments of the company. The formation can be shown in a block diagram:

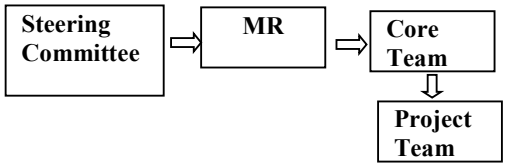

Fig 4.2: Formation of ISO Team

Basically steering team refers about cost and other involvements to the project sponsors, as ISO implementation involves cost and time. Mainly the CEO along with his high officials acts as the steering committee. Then the committee selects MR. after that core team is formed by selecting the head of every department such as supply chain, production, quality control, marketing etc. Core team members selects 2 to 3 person from his department. Those 2/3 persons from every departments actually works as the Project team and MR guides this team from the very beginning. One important task of this project team is to share information and updates with the rest of the employees in the organization so that everybody knows what's going on at that time.

b. Selection of Management Representative (MR) at RWL:
After forming ISO team then the top management of the RWL selected their Management Representative (MR) as **Engr. Md. Rajibul Amin** and made him totally responsible for the project of implementation of ISO 9001:2008. Basically MR will work as the project leader.

c. Assigning / hiring a consultant:
A consultant is a person who gives necessary guidance. Implementing ISO standard is very hard and complex work. So it is difficult for any organization to implement ISO standards without any previous experiences. So the company generally hires a consultant. Top management of the RWL then selected its consultant from CATS Academy India Pvt. Ltd. This has not been made compulsory yet. Polar Ice-Cream BD did not assign any consultant for their ISO 22000 certification for food safety. This is totally dependent on the organization.

d. Task given by the Consultant:
Consultant usually helps MR in implementation of ISO 9001:2008. In RWL too it was done like that and consultant helped MR by giving him necessary guidance. Actually the consultant gave / suggested necessary tasks / guidance to MR which was essential for the audit by the 3rd party. MR needs to finish the job along with his team members within the given period of time.

e. Feedback to the consultant:
MR finishes those tasks with the help of his team and gave feedback to the consultant. It is a dynamic process. And the whole team needs to be aware of that. In RWL too it was followed and done in time.

f. Reviewing the progress:
The consultant reviews the progress. Basically if every criterion is fulfilled then MR will go for the next step and if not he may take time for correction. After that the organization applies for certification to the ISO affiliated body. For RWL too it was followed accordingly.

g. Visit of Affiliated body:
Affiliated body then visits the company if requested and performs the audit. It is the last stage of certification. If everything is all right then the company gives certificate within 3 months. The same was done for RWL.

Predetermined charges are needed for the whole processes of the audit and certification.

RWL spent almost 2 years for the whole procedure as stated above and finally got ISO 9001:2008 certificate at **12th July, 2011**.

While doing the study / research work it became clear that ISO 9001:2008 standard can also be applied in the educational institutions too. For assuring the quality of education ISO 9001:2008 can be a very effective tool along with other national / international standards. In our country implementing ISO standards in educational sector it is very much uncommon but literatures say it has been implemented in other parts of the world in educational Institutions. It is a matter of hope that now the people are becoming very much aware about quality in every aspects and this awareness will make a better scope to seeing the implementation of ISO 9000 standards in other sectors including educational sector in near future.

5. Global adoption
The growth in ISO 9001 certification is shown in the Figure 5.1 as given below:
Source: ISO Survey 2011

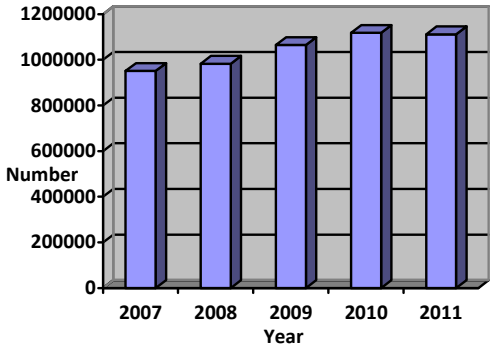

Fig 5.1: Growth in ISO 9001 certification

It is very much clear from the above chart that global adaptation of ISO 9001 standard is increasing day by day. In recent years there has been a rapid growth in China, which now accounts for approximately a quarter of the global certifications [14]. In our country this rate is also increasing but not in a dramatic way. To become a promising global competitor we need to focus on this area. But the matter of great hope is that while doing this study we came to know that not only the production companies of our country but also many service organizations at present are showing their interest to implement ISO 9001 standard as competition in our country and also outside the country is growing at a relatively faster rate day by day.

6. Discussion:
Quality assurance has become the major concern for any kind of organization in this competitive business world. Every organization wants to ensure their product or service quality i.e. in a word it can be said that every organization wants to ensure 'Quality Assurance' by imposing different methods or processes. ISO documents say that in an ISO 9001:2008 certified company the top management gets fully involved in a committed way to the customer satisfaction and quality improvement. Thus the standard revolves around "customer satisfaction". The result is: in most of the Bangladeshi industries it has now become a buzz word. Organization which is really serious about this aspect will go beyond the ISO standards and ensure total customer satisfaction and expectations of customers thus a certified organization will grow eventually. There will be more and more demand from customer's side. And the top management needs to take it as a challenge. The spirit of the standard will set directions for quality

improvement; to bring in team work; to change frames of minds; to bring in ownership and responsibility for the actions; to improve clarity and improve discipline, etc. The system will become a handy tool for effective control of operations; create confidence in the minds of the customers; and ensure continuous and consistent improvements in all fronts. ISO 9000 QMS is under criticism for long also. It requires huge paper work for documentation and record keeping. The cost associated with implementation and operations are also considered as an additional burden, which creates a question regarding ability of its adoption in small organizations. But the fact is that this ultimately pays off. Positive attitude towards quality improvement is the only solution to remove any hindrances. Nevertheless, ISO 9000 QMS is certainly not a cure for all, what many people or organizations think. It can serve as a complementary system to TQM.

7. Conclusions:

Now-a-days the market of any product has become globalized. For that reason, company has to compete with the companies not only of those which are inside the country but also of others around the world. To sustain in the market, acquiring customer satisfaction towards the product or service becomes an important criterion to be considered. Thus, ISO 9001:2008 certification is considered as an important tool of quality assurance. If the product is ISO certified, then customer can distinguish that from others and becomes interested to use. Although now a days, it is sometimes said that, this certificate can also be achieved by unfair means in many places including those in the 3rd world countries. There is a rumor prevailing in the market that, some of the affiliated bodies of ISO sometimes supply the ISO certificate in exchange of money without monitoring the standard of the organization. But it can be assumed that such rumor should not be taken into consideration at all. For getting the ISO certificate time, money and the strong willingness of top management is needed with all its merits and demerits, the ISO 9000 approach provides a systematic, documented and an all pervasive linkage through the value chain. It formally and publically commits the management for taking responsibility for this qualitative revitalization thorough a well-defined and interactive process. Quality today has become a business strategy and thus the ISO 9000 certification system acts as launching pad for Total Quality Management.

This study and research work is theory based. So no calculation has been referred. Implementation of ISO is a very hard work to do. But if the management and the employees believe that they can do then it is possible. Rangs Workshop Limited (RWL) took it as a challenge and they have done very hard work to fulfill the challenge. The authors observed, studied and verified all sequential processes towards achieving the ISO 9001:2008 by the RWL and also the review of all related documents was made. Due to limitation of space samples of the documents of RWL have not been shown.

RWL later implemented ERP in 2013, which is software based. We got a limited chance to use ERP software in a limited environment. But that was the most exciting experience to us. They are currently using IFS [15] version 8 and hoping to update it with the latest version of 8.5. RWL is the 1st company in Bangladesh who have got ISO certificate in automobile sector. The company is also running ERP successfully. These two things made RWL a unique organization and the management is getting tremendous benefits out of the implementation of both ISO and ERP.

8. Acknowledgement:

It was a good opportunity for the authors to get a chance to work at RWL because information obtained and procedures learnt, would not have been possible to know for the outsiders to the organization. Our heartfelt thanks go to the RWL management as a whole and our special thanks go to Engineer Mr. Rajibul Amin, MR for RWL for the implementation of ISO. We also are thankful to AUST authority for giving us permission to work at RWL.

9. Abbreviations:

ISO - International Organization for Standardization
ERP- Enterprise Resource Planning
TQM-Total Quality Management
QMS – Quality Management System
RWL –Rangs Workshop Limited
MR - Management Representative
TÜV SÜD - is an international service corporation focusing on consulting, testing, certification and training.
SGS - Société Générale de Surveillance, is a multinational company headquartered in Geneva, Switzerland which provides inspection, verification, testing and certification services.
CATS - CATS Academy India Pvt. Ltd has evolved as a business solutions provider, garnering the trust and goodwill of clients and associates alike.
IFS – IFS is a globally recognized leader in developing and delivering business software for enterprise resource planning (ERP)
CEO – Chief Executive Officer of any organization, who is mainly responsible for every decisions of that organization, sometimes may also be known as MD, GM, Chairman / Head of the Organization, etc.

10. References:

[1] Operations Management by Chase and Acqualino, Pearson publication.

[2] B.Sc. Eng. Thesis on Study and familiarization of implementation process of ISO and ERP for product quality assurance and efficient production in Bangladeshi industries.
(Case study: Rangs Workshop limited, Tejgaon)
By: Abrar Fahim Samad, Amit Banik, Dipanjan Ghosh, Md Jakaria Rahman
3, page 40-158

[3] Quality Assurance and TQM by K.C. Jain, chapter-3, page 40-158

[4] Enterprise Resource Planning by Alexis Leon 2nd edition

[5] http://www.iso.org/iso/home/standards/benefits of standards.htm

[6] Operations management: strategy and analysis by Lee J. Krajewski, Larry P. Ritzman

[7] http://www.iso.org/iso/home.html

[8] http://www.thefreedictionary.com/Isos

[9] Quality Control and Management by Ahsan Akhtar Hasin, chapter 24, page 321-325

[10]http://www.iso.org/iso/home/standards/management-standards/iso_9000.htm

[11]http://www.transitionsupport.com/8_QM_Principles.htm

[12] http://en.wikipedia.org/wiki/ISO_9000

[13] Reviewed document of Polar Ice-Cream BD and RWL for audit plan, production and quality assurance

[14] Total Quality Management by Dale H. Besterfield, 3rd edition, chapter 10, and page 254-256 and 3rd edition, chapter 3, and page 258-269

[15] http://www.ifsworld.com/en/about-ifs/

ICMIEE-PI-140339

PRODUCTIVITY ANALYSIS AND SUGGESTIONS FOR IMPROVEMENT A CASE STUDY IN A LOCAL COMPANY

[1]*Md. Abdul Mottalib, Rashedul Islam, JahidHasan*
[1]Graduates from IPE, AUST (Ahsanullah University of Science & Technology), Dhaka
[2]*S.K.Biswas*, Professor, MPE (Mechanical & Production Engineering), AUST, Dhaka,
[3]*A.K.M SolaymanHoque*, Chief Engr., BSEC, Dhaka.

ABSTRACT
Productivity is the efficiency with which a firm converts inputs into outputs. Productivity improvement is always a focus area in a manufacturing industry/company. One of the major causes of company's decline in profit margin is low productivity. This paper focuses on productivity improvement of a local Tube Light production company in Dhaka. It is found that the main problem of the company under investigation might be related to improper production process of tube light, design, layout and wastage of final product due to non-conformity (rejection) with designconformity (rejection) with design. We found the lack of good layout also created bottleneck in the flow of semi-finished and finished products in the shop floor. It has been seen that backdated machineries also created bottleneck. In this article it has also been discussed the application of the principles of lean manufacturing for reducing seven types of wastes such as over production, waiting, transportation, motion, inventory, over processing, defective units. It was concluded that for producing mount the two end wires should be placed accurately in correct position and the right flange tube with good properties and best raw materials can be imported for reducing wastes and also for decreasing bottlenecks upgraded machineries are necessary. Finally it is hoped that if the recommendations are accepted and implemented then positive results will surely be achieved along with huge increase of profit margin.

Key words: Productivity analysis and improvement, Tube light manufacturing, Leanmanufacturing.

1. Introduction: [5],[9],[10]

Productivity is the quotient obtains by dividing output by input of production. In this way it is possible to define the productivity of capital, investment or raw materials according to whether how the output is being considered in relation to capital, investment or raw materials etc. Thus, productivity is defined as the efficient use of resources-labor, capital, land, materials, energy, information-in the production of various goods and services. This is usually stated as:

$$\textbf{Productivity} = \frac{\textbf{Output}}{\textbf{Input}}$$

The European Productivity Agency (EPA) has defined productivity as follows:"Productivity is an attitude of mind. It is a mentality of progress of the constant improvement of that which exists. It is the certainty of being able to do better today than yesterday, and continuously. It is the constant adaptation of economic and social life to changing conditions, it is a continual effort to apply new techniques and methods, and it is the faith in human progress."Productivity can also be defined as the relationship between results and the time it takes to accomplish them Productivity compares at production and shop-floor, organizational, sectorial and national levels, etc., with resources consumed.

Bangladesh is a developing country and a lot of industry stands behind on its economic growth, but it is a matter of sorrow that because of different problems related to wastage; backdated machineries, improper management of inventory system; lacking of good supply chain management; management problems related to worker efficiency, worker motivation and distribution problem; lack of research & development, improper supervision on imported material; etc., the productivity remains comparatively low and these industries fail to get their desired or planned goal.

The authors did this study in a local tube light production company at Dhaka for finding out different problems related to productivity and with the aim of giving recommendation on productivity improvement. The authors found out that (i) wastage in backdated machineries is the main culprit for lower productivity and (ii) major wastage came from improper "mount making" (a part of tube light), (iii) the properties of flange tube from which mount was made were not good enough to withstand in high temperature, etc., therefore the wastage of final product was relatively big along with other problems as discussed later.
So, it is not possible to eliminate or solve all the problems but the authors tried their best to find out some possible problems of wastage of final product and they finally mentioned some suggestions to implement. We think, if these are implemented the company can achieve its desirable profit.

*Corresponding author, Tel.: +88-01817-746070, +88-01813-261758
E-mail address: skbaust@yahoo.com, skbiswas.mpe@aust.edu, skbcuet@yahoo.com

2. Objectives of the study

At the outset of the study, authors set objectives as (i) Analysis of decline in productivity and its improvement through waste elimination. (ii) Making recommendation for improvement of safety and planning for hazardous process (iii) and recommendation of possible changes in present layout system in the plant under case study.

3. Methodology of the study

- At first, the authors decided to explore the whole industry and learn about the whole production system of the industry also want to learn about the different machineries and their working systems.
- After knowing about the whole industry, the authors tried to find out the possible causes of bottlenecks related to production and about various leakages in the industry.
- After that the authors tried to work for achieving set objectives already mentioned earlier.
- The authors collected various data related to productivity improvement, and also talked to related workers and officers of that industry with different issues related to safety and hazardous environment.
- Finally the authors calculated the wastage at individual machine then by incorporating the whole process and found the total wastage.
- Then, recommendation relating to improvement of present system of manufacturing has been made.

4. Case study (Company A)

As requested by the authority of the company the authors decided not to disclose the name of the company and henceforth it will be called "Company A". The fluorescent lamp is an electric lamp consisting of a glass tube, coated on inside with a fluorescent substance that gives off light when acted upon by electricity. Fluorescent lamps and incandescent lamps are the two major sources of electric light today. Typical fluorescent lamps consist of a long glass tube that seals the inner components from atmosphere. These inner components include two electrodes that emit a flow of electrons; mercury vapor, which is the source of ultraviolet radiation; argon gas, which helps in starting the lamp, and of course fluorescent coating on the inner surface of the tube[1]. A step-by-step breakdown of the phases of the process, checking the inputs, checking the outputs, and operations that take place during each phase were checked and observed carefully. A process analysis was made later to improve the understanding of how the process operates, and to determine potential targets for process improvement through removing waste and increasing efficiency[2].

4.1 Manufacturing process

During study we checked the whole process of the manufacturing system of the industry "Company A" systematically and gradually. The whole working process of manufacturing of the fluorescent tube light is shown below in **Fig. 4.1**

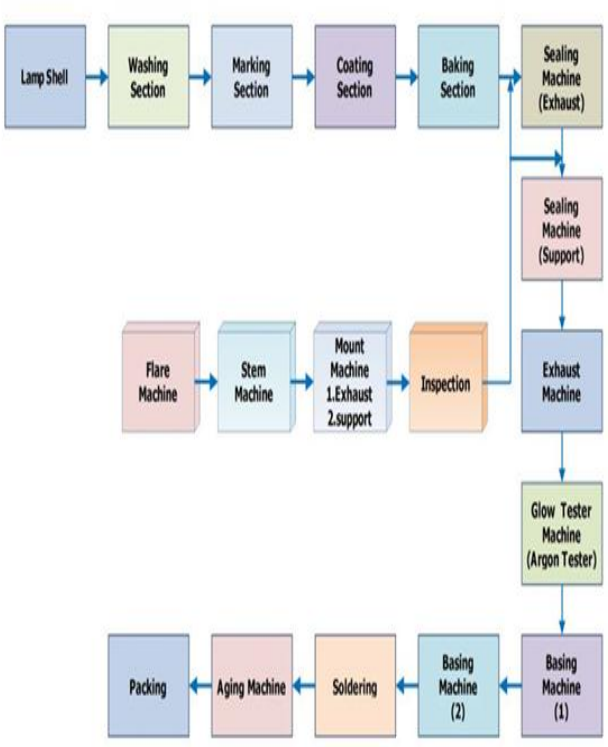

Fig.4.1 Production flow process of company

5. Productivity and wastage Analysis

5.1 Classification of Productivity[10][3]

Productivity can be classified as follows

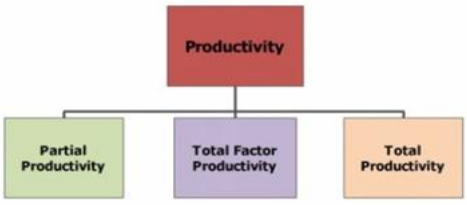

Fig.5.1 Classification of Productivity

A. Partial Productivity
It is the ratio of output to one class of input. For example, labor productivity (the ratio of output to labor input) is a partial productivity measure. Similarly, capital productivity (the ratio of output to capital input) and material productivity (the ratio of output to materials input) are examples of partial productivity

Partial productivity (labor) = Output/Labor input.

B. Total-factor Productivity
It is the ratio of net output to the sum of associated labor and capital (factor) inputs. By "net output, "we mean total output minus intermediate goods and services purchased. It can be noticed that the denominator of this ratio is made up of only the labor and capital input factor.

$$\textbf{Total factor Productivity} = \frac{\textbf{Output}}{\textbf{Labor+Capital}}$$

C. Total productivity
It is the ratio of total output to the sum of all input factors. Thus, a total productivity measure reflects the joint impact of all the inputs in producing the output.

$$\textbf{Total Productivity} = \frac{\textit{Output}}{\textbf{sum of input}}$$

All activities in manufacturing processes that do not add any value to the products are considered as wastes. It is necessary to find all sorts of wastes. All activities in manufacturing process that do not add any value to the products are considered as wastes. It is necessary to find all sources of wastes in manufacturing processes. The main concern of an industry is to reduce the percentage of waste from their production system with an aim to improve productivity. That's why, it is necessary to suggest the ways of wastage elimination.

The Japanese are true believers in eliminating waste. Waste in Japan, as defined by Toyota's Fujjo Cho is "anything other than the minimum amount of equipment, materials, parts and workers (working time) which are absolutely essential". In most organizations, few people in the organization have the ability to change a product or service to increase the value it offers to the customer, but everyone can reduce waste if he/she desires and truly examines.

5.2 Analysis and Finding Percentage of wastage for manufacturing of fluorescent tube light

In "company A" several semi-automated, manual processes are used to produce fluorescent lamps. It was found that in producing these lamps major wastage occurred in several sectors of production process. Machines of the industry were found to be backdated which lost its total depreciation value many years back. Wastes at different machining operation, as actually found, were listed in **Table 5.1**

5.3 Elements of Wastage Elimination
The following elements may be considered relating to waste elimination [3], [4]**:**

- Focus Factory Networks
- Group technology,
- Quality at the Source ,
- JIT production,
- Uniform plant loading,
- Kanban production control system,
- Minimize setup time.

In the case of "company A.", the major causes of wastage are found for improper quality of raw materials (especially for making "*Flange tube*"), non-uniform plant loading and more setup time. Overall production process wastage in this industry is occurred for these three basic elements [7], [8] and [9].

Table 5.1 Average wastage at different machining process

Number of Process	Name of Process	Standard Production per day	Experimental Production per day	Amount of wastage per machine per day	Percentage of Wastage (%)
1	Washing & drying	4800	4000	56	1.4
2	Marking	4240	4000	40	1
3	Coating	6400	6000	96	1.6
4	Backing machine	4240	3224	21	0.62
5	Neck cleaning machine	4240	2984	17	0.57
6	Sealing machine	4000	2928	176	6.01
7	Exhaust machine	4000	2904	256	8.81
8	Basing machine	4800	2448	104	4.25
9	Final inspection	-	-	-	4
	Total production process wastage				28.26(%)

Wastage statement for last 10 (ten) years
In case of "company A" overview of the percentage of wastage for last eleven fiscal years is listed into the **Table 5.2** these data are collected from sales and marketing department of the industry. These shows the industry's past and present situation in case of per year wastes. (Annual Reports of "company A")[7&8]

Table 5.2 wastes statement from 2003 to 2014

Serial no.	Fiscal Year	Percentage of wastage (%)
01	2003-2004	16.33
02	2004-2005	19.92
03	2005-2006	19.90
04	2006-2007	21.99
05	2007-2008	20.99
06	2008-2009	21.97
07	2009-2010	21.72
08	2010-2011	23-22
09	2011-2012	21.98
10	2012-2013	19.18
11	2013-2014	28.26

5.4 Overall Wastes Calculation
The overall wastage calculation of "company A" for the fiscal year 2013 is listed below in Table 5.3[7&8].
Table 5.3 Per year overall wastes in "company A" for the fiscal year '13-'14.

Input	551934 Pcs.
Total production	396000 Pcs.
wastes	155934 Pcs.
Percentage of Wastes	28.26 %

Total cost of wastes for per unit market price cost,
To produce one 4 feet40 inches watt tube light, the estimated cost of production is =94 Tk.
Therefore total cost for wastes during production
= (1, 559, 34×94) Tk.
=14,657,796 Tk. (1)

$$\text{Productivity} = \text{Output/Input}$$
(Before reducing wastes at desired level)

$$= \frac{396000}{551934} \times 100\%$$

$$= 71.74\ \%$$

Here it is clear that, the total cost of production for wastes is about 14,657,796 Tk. This is a big loss of the industry. This huge amount of production loss which actually occurred in the industry hindered to achieve its desired goals as targeted. Now it is essential for this industry to reduce the wastes. If the industry wants to improve its total productivity it is necessary that with respect to input the amount of wastes must be reduced. If the proper implementation of the proposal as discussed in recommendationis done by the industry, the wastage may be reduced from 28.26% to 19.26 % and thus the total production might be increased if wastages are reduced.

Table 5.4 Overview of industry production line for reducing to 19.26% wastes in fiscal year 2013-14[9]

Input	551934 Pcs.
Total production(Output)	4,45,632 Pcs.(increased from 396000 Pcs)
Output increased	49,632 Pcs.
Wastes	106302(Reduced from 1,55,934 Pcs)
Number of wastes reduction	49,632 Pcs

Using the above Table, we get,
Total cost of production for wastes
= (106302×94) Tk.
= 9,992,388 Tk. (2)

Productivity=Output/Input
(After reducing waste to suggested level)

$$= \frac{445632}{551934} \times 100\%$$

$$= 80.74\%$$

Here the difference between the Eq. (1) and Eq. (2) show the amount of reduction wastes after implementation. Thus the amount of wastes reduction becomes around 4.7 million Tk.

6. Layout Design

6.1 Existing layout

The existing layout of "Company A" has been found to be very poor. Machines were arranged as product layout orientation. There was no uniform production operation in different machines therefore bottleneck in flow was created in different areas especially in coating section. It was found that the production rate was 750 pcs./hour in total on an average. After coating operation the flow of production becomes too slow and in baking section the production rate becomes 320 pcs./hour and that was around half of the previous operation. Another important thing was the movement of mount and it was used to be done manually therefore that was time consuming also. The existing layout is shown in **Fig.6.1**. Flow description can be found in details in [9].

6.2 Proposed Layout

To overcome various production related problems a proposed layout was suggested[9]. The proposed layout is shown in **Fig.6.2**. In proposed layout the authors recommended two parallel lines of production after coating section and two different conveyors might be used in the proposed two different sections. That might increase the production rate of the company. Two conveyor belts were also suggested from mount making section to sealing section which might also enhance the production rate. A proper ventilation system might also be incorporated in whole industry and in coating section air cooling system may be instated. If possible present inventory of final products keeping area near the entrance might be rearranged.

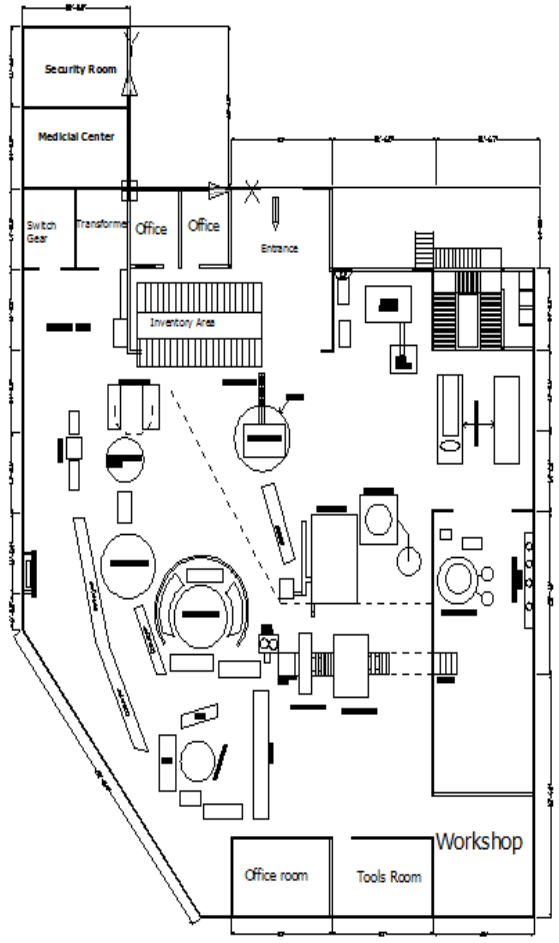

.

Fig.6.1 Existing Layout of "Company A"

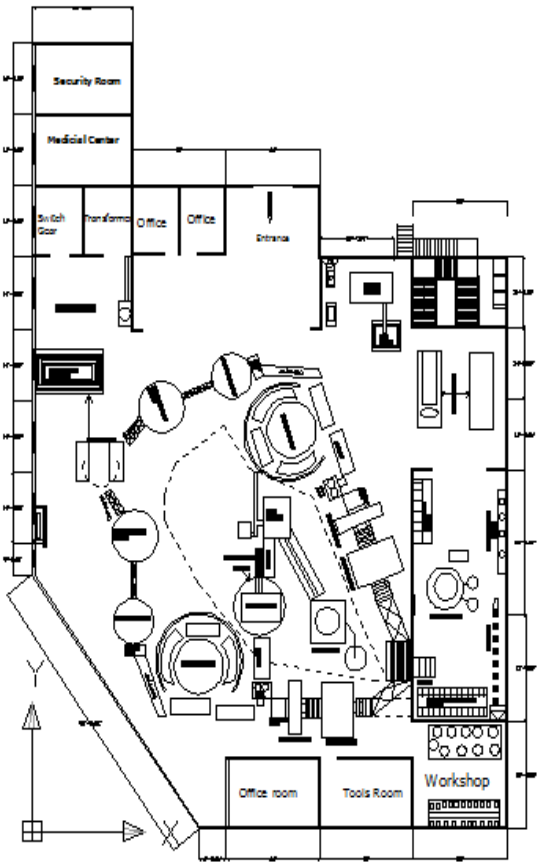

Fig.6.2 Proposed layout of "Company A"

6. Problem as Observed

The authors thought that following problems might be the cause of low productivity that generated from case study of "company A":

i. Poor exhaust system existed,
ii. Unfavorable working condition because of hot surroundings,
iii. Flow of combustible gas for manufacturing process was not continuous,
iv. The properties of flange tube was not good enough,
v. Some machines were found to be too old,
vi. Some portion in exhaust operation area was too hot to be operated manually,
vii. Workers were not conscious about hazardous situations and also about safety standards,
viii. Small broken glass were found in scattered condition here and there,
ix. Poor marketing policy,
x. Bottle neck in production flow process was found in different sections
xi. Improper implementation of 5'S and Kaizen,etc.

7. Recommendations

Here are our suggestions and recommendations for improving the situation:

i. As the inside surroundings are so hot so proper exhaust system should be installed,
ii. The imported properties of material of flange tube should be checked continuously for quality,
iii. Continuous flow of gas for production should be confirmed,
iv. Automated handling system should be increased for improving efficiency,
v. Old machineries are needed to be replaced,
vi. Proper marketing strategy should be implemented therefore advertisement in television / radio / billboard / other media, should be provided,
vii. Although mentioned in company's booklet, 5S' and kaizen, etc., were seen not to be implemented properly. So, That should be properly done for the sake of improving the productivity.
viii. Proper motivation should be done by providing incentives / reward system / other motivational mprinciples, etc.,
ix. To eliminate flowbottlenecks found in coating and baking section, the authors recommended a proposed layout (as shown in **Fig.6.2**) where two parallel lines of production after coating section have been proposed to be installed.

7. CONCLUSION

The authors are of the opinion that if the suggestions made in this paper are implemented, the overall productivity of the company might increase.

8. ACKNOWLEDGEMENT

The authors gratefully acknowledge the suggestions / opinions / advices ect., given by the Company A officials. The authors are also thankful to the authorities of Company A for allowing them to study the problems mentioned in this paper which was essential as a partial requirement of B. Sc. Eng. degree.

9. REFERENCES

[1] Turnkey.taiwantrade.com.tw/en/Contnt.aspx?ID=66
[2] Diagnosis of multi-operational machining processes through variation propagation analysis QiangHuang, Shiyu Zhou, Jianjun Shi (Department of Industrial and Operations Engineering, The University of Michigan, Michigan, USA)
[3] Heizer& Render, Operations management
[4] K.C. Jain and L.N. Aggarwall, Production Planning Control and Industrial Management
[5] Ahsan Akhtar Hasin, Quality Control and Management
[6]R.Panneerselvam, Production and Operations Management
[7] MIS Report of 2003, 04, 05....2013 of company A
[8] Annual Report of 2003, 04….2013 of company A
[9] A. Mottalib, F. Yasmin, R. Islam, J. Hasan,"Study and improvement of the condition of a local industry through the application of re-engineering & productivity improvement methods. (Case study:" Eastern Tubes Ltd, Tejgaon"), a thsis submitted to MPE Dept., AUST, 2014
[10]D. J. Sumanth, Total Productivity Management

ICMIEE-PI-140340

PROBLEMS OF TERTIARY ENGINEERING EDUCATION OF BANGLADESH AND SOME SUGGESTIONS FOR POSSIBLE IMPROVEMENTS

Dr. Shyamal Kanti Biswas [1],
[1]Professor, Mechanical & Production Engineering,
Ahsanullah University of Science & Technology, Dhaka, Bangladesh.

ABSTRACT
We think, tertiary Engineering Education in Bangladesh at present is having some problems. This can be known from the occasional various remarks of related educationists, related officials of the country or organizations through media or seminars or from various newspaper articles or news. To discuss this many seminars/conferences have been arranged by many organizations in recent days. The causes of the present scenario might be many and also opinions and suggestions for improvement might vary too. Remaining attached with engineering higher education of the country for more than 4 decades in local public institutions of higher studies, the author got a chance to have a close look on the problems. This paper tried to outlin the problems related to accreditation or decline in quality and also some suggestions for possible improvements of tertiary engineering education. In this paper the author wanted to put forward his personal views about the problem and also some personal suggestions for possible improvement.

Key words: Quality Assurance in Education, Washington Accord / ABET / ISO / International Mobility Forum, BAETE, etc., criteria for accreditation.

A. Introduction

In this paper some personal opinions are mentioned aiming at not to hurt anybody. We feel tertiary Engineering education in developing countries is needed to be given relatively more attention especially as, we believe, the growth and development of any country is dependent on qualified human resources in the Technological fields. We appreciate the initiative of the UGC & Govt. of Bangladesh in entering into a contract with World Bank for improving the present state of tertiary education in Bangladesh by establishing HEQEP (Higher Education Quality Enhancement Program) and under that program various activities have already been started. Besides, many seminars to discuss the issue are being arranged by many organizations including professional bodies.[10][11]

We all know that many years back Japan took a especial plan to improve the education system in Japan by establishing 8-9 imperial universities and other appropriate measures and neighboring Sri-Lanka also took a plan to improve the educational level in that country. Japan and Sri-Lanka started getting the benefits from the programs they initiated earlier. Also Indian leaders conceived during '40s - '50s that India's future development might be dependent on improvements in tertiary Engineering / Technical education, development of highly knowledgeable human resources, development of heavy industries, acquiring latest technology in all sectors etc. Thus India initiated, along with other measures, establishing IITs under direct control of central Government and giving full autonomy in their developments and within a link program with bench marked famous Technical Universities of USA / Europe / Asia. At present IITs are now ranked among best universities and their graduates are being attracted in global markets too. In the last few decades our national Governments formed multiple education commissions to solve problems in this sector. But sometimes before the full implementation of the recommendations of one commission another new such commission was formed. Such commissions sorted out many problems and also suggested solutions and many such suggestions have been implemented. It is desirable that a separate education commission aiming to sort out and solve problems only related to Engineering / Technical education and profession should be formed by the Government immediately, as we all know that any country needs qualified and technically skilled human resources to solve problems related to infra-structure development of the country and also we believe that future development of any country is quite dependent on advancement of Technology.

*Corresponding author, Tel.: +88-01817-746070, +88-01813-261758
E-mail address: skbaust@yahoo.com, skbiswas.mpe@aust.edu, skbcuet@yahoo.com

A) Quality Assurance in Higher Education[9]

Universities offering tertiary engineering degrees of which all are not internationally accredited yet. Supplying quality graduates to job market from any educational Institution is essential like that of industrial goods. For goods ISO standards / Regional standards / standards of respective countries etc. are usually followed. For Education various National standards / respective Professional Organizational standards / Regional standards etc. have been designed and can be followed. For Engineering or Technical education, ABET / ISO / Washington Accord / International Mobility Forum / National Professional society like Engineer's Institutions' standard/ National accreditation board like BAETE of Bangladesh standards / other regional standards, etc., can be followed. In many cases the procedure is either difficult or much attention is not always given for follow-up by appropriate authories, and also interest in implementation is not enough as there is no compulsion to follow. Internationally accredited programs are now frequently desired to remain in / enter into the competitive global market and for that getting accreditation is the cry of the day now.

Accreditation record in Bangladesh is not at all good. Among widely followed various types of world / regional rankings even our best universities like Dhaka University, BUET, etc., are not ranked high, rather conditions are worsening rapidly[3] .Therefore, it is high time to look back to our old heritage and march forward keeping in pace with world thinking in these days of high competition and globalization as it will not be wise to remain satisfied believing that we are good now or were good earlier. Otherwise our graduates will suffer in world market and at the same time we might fall back in our development efforts.

Black box representation of an University:

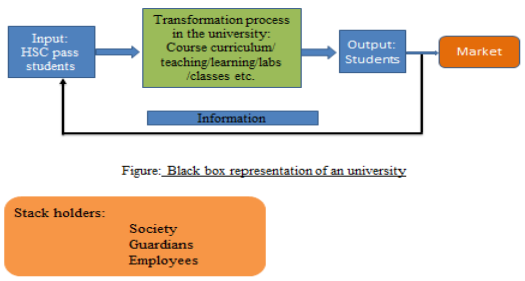

Figure: Black box representation of an university

Like Industrial goods some factors which can be controlled by respective educational institutions / universities like providing proper teaching-learning methodologies and facilities e.g., teaching by following standard updated latest curriculum / Syllabus, recruiting qualified and knowledgeable teachers / staffs, following standard class routine / program, providing proper classroom size and class room facilities, using proper audio-visual aids & maintaining other proper teaching-learning environment; following standard grading system and other types of merit evaluation systems for students'; maintaining proper teacher-student ratio; providing proper laboratory, library facilities and other related infrastructural facilities; providing proper guidance / consultation to students; maintaining off-time recreational / refreshment arrangements inside campus; etc., should be strictly monitored and maintained.

In addition other controllable factors like maintaining proper teachers' / staffs' evaluation process; motivational policies to attract highly qualified teachers / brilliant students to remain and to join in teaching profession; maintaining university-industry or organizational relationship; regularly getting feed-back from employers through Tracer Study program; developing other related programs to allow students to develop his / her own physical / mental capabilities, etc. must be maintained for the interest of the graduates / employers / owners of private companies / universities.

In my personal opinion accredited degrees must be made a requirement for job offer. We also know that it is the time for moving forward, market economy and globalization and also is the age of rapid technology change and environmental change. So, no compromise about the quality of education should be made for the development of the country and also for producing qualified human resource.

Many educationists tried to put forward their opinions about improvement / accreditation: Prof M H Khan[1] emphasized on the following for the improvement of quality in education:(i) teaching programs require external (peer review) and internal academic auditing (ii) Academic autonomy of teachers should be ensured within the guidelines of ethics, (iii) properly designed grading systems should strictly be implemented to indicate the merit of students, (iv) Curriculum and syllabus should be developed to meet the academic challenges (v) Accountability of the weaker students should be shared by them as well as by their guardians. Some other authors stressed on Out-come Based Education[5],[6]. Biswas et al.[4],[7]and[8] discussed the importance of quality control and importance of accreditation of education and in a key note paper Biswas[10] discussed the present scenario of tertiary education of Bangladesh. Both Prof M H Khan[1] & Prof. Iqbal Mahmud[2] stressed on peer review and academic auditing. Prof Iqbal Mahmud[2] discussed his ideas on accreditation and quality which has been summarized in Figure 1 in the following:

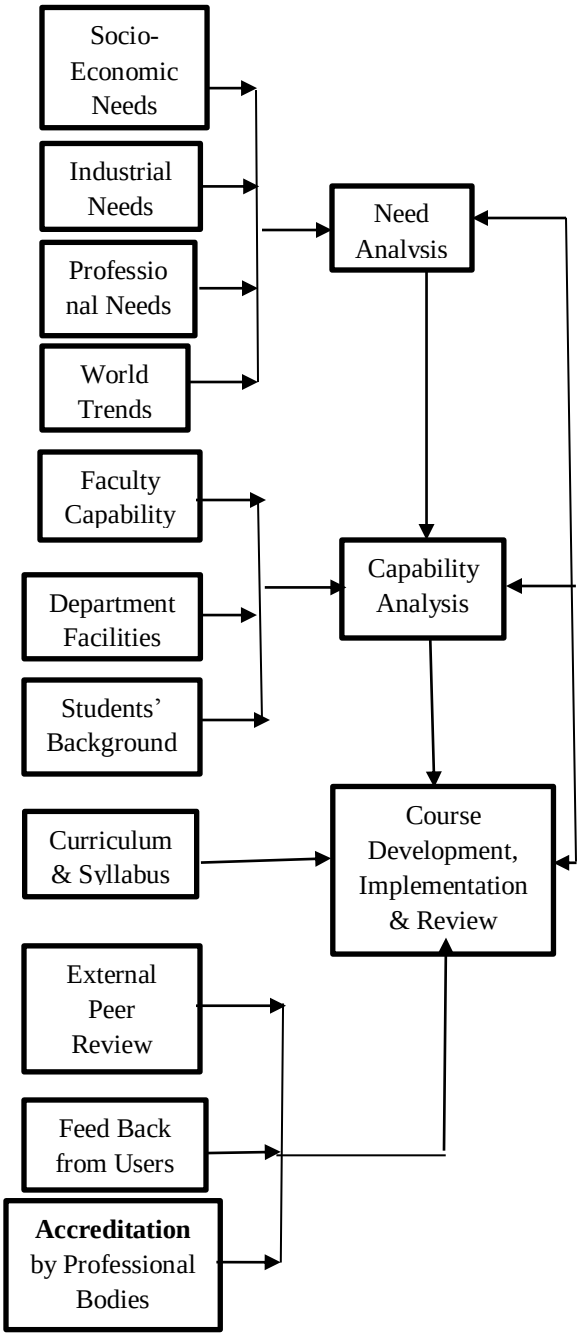

Figure: 1

B) State of tertiary education in some developing countries like India, Pakistan, Malaysia, Saudi Arabia, Bangladesh[9].

At Present some university programs in Saudi Arabia / Malaysia / India are internationally accredited. In Pakistan and in Bangladesh too accreditation of university programs are given emphasis now. We think, the scenario of tertiary Engineering education in Bangladesh can be improved by giving relatively more attention by the UGC (university Grants Commision, Bangladesh) like (i) Ensuring relatively more autonomy to the universities at least regarding quality of education, (ii) Regular monitoring to see whether the universities are following approved rules, (iii) A binding to follow uniform recruitment rules for teachers / staffs / officers of the universities, (iv) A binding to follow uniform and similar service rules and other benefits in all universities, (v) A binding to follow strictly the approved student intake rules, (v) Controlling almost all approved controllable and uncontrollable factors, For this *Strengthening the authorities of the UGC and allowing it to function as higher education commission is essential*. Also Decision giving time must be shourtened if possible.

C)Problems of tertiaryEducation in Bangladesh[11]

I think, the following are the major problems related to tertiary engineering education in Bangladesh:

(i) Absence of proper accreditation requirement or ignorance / avoidance of accreditation requirements:

Proper Quality assurance / accreditation program must be followed at least to satisfy the requirements of the present employers. Preferences in job placement, in promotion, and in salary determination, may be given to the graduates of highly accredited degree programs. *Programs of Universities failing to get accreditation repeatedly must not be allowed to continue.*

(ii) Absence of strict and uniform guidelines for recruitment / promotion in universities:

(a) ***Teachers' recruitment and promotion:***

Strict and uniform qualification test for the recruitment of all university teachers must be followed . The following points may be considered: (i) Under no circumstances, no teacher having same higher degree should be given theoretical class / practical classes of students' studying to get the same degree as that of teacher. Hence no teacher should be appointed as Lecturer in Engineering without having at least a M.S. or M. Phil or equivalent degree in relevant field. (ii) No teacher in Technical / Engineering universities should be promoted / appointed as Assistant Professor / Associate Professor / Professor without having a Ph.D. degree and other required academic qualifications and experiences, (iii) The entry requirement in teaching posts may be made as at least M.S / M.Phil. degree in the relevant field and if such qualified teachers are not available, conditional appointments of very brilliant persons having only B.Sc. Engineering degree or equivalent as Lecturers may be made in the next 5-10 years in local universities to teach only at practical/sessional / tutorial classes and if needed post

of Tutor / Junior Lecturer may be created for such teachers in the presently followed hierarchy of teaching posts. (iv) ***Research / publication requirement should be made mandatory for recruitment as Assistant Professor / Associate Professor / Professor and preference should only be given to candidates having strong research background and publication records*** (v) Industrial / Outside Organizational practical experience for a limited period may be made mandatory for recruitment as teacher at tertiary level of engineering / technical education, (vi) No graduates of one university should be recruited as teacher in that university at least in the first few years after graduation. Such practice is sometimes followed in some foreign universities. (vii) ***No promotion to higher teaching posts should be made without having a PhD degree but only considering present qualifications and experiences like long service record, having excellent contributions in administrative / departmental works, long teaching record, etc.,*** (viii) Any teacher of any university if he/she marries any colleague / student of that university, he/she should not be allowed to continue in teaching post in that university.

Besides the above points the following may also be followed (i) Non-academic jobs should not be given to academic staffs in general, (ii) Part time teachers should not be employed if possible, etc. (iii)Teachers preferring to enter into administrative post must be identified and be allowed to remain in administration as far as possible and teachers in academic line should not be taken to non-academic posts as far as possible. Except Head's and Dean's post all other higher administrative posts of any university may be filled up by qualified persons / Professors of other universities.

Examples of foreign universities may be followed for those points as discussed above for recruitment.

(b) ***Staff recruitment:***

Transparency in staff requirement must be established strictly. All universitiy staffs should be recruited strictly by following approved qualification test.

(iii) Absence of required basic knowedge in Science and English for Technical Education in new students' intake:

(a) Students' intake:

Fresh students must be admitted strictly by following approved admission criteria. All types of 'quota' if any should be abolished and if possible one central admission test should be held for all applicants on any particular date. Strict control during new intake is to be maintained with respect to basic knowledge in Science, Mathematics and English as any higher Technical education without a solid background on these subjects becomes a burden later. *It is now considered that level of English language in local higher secondary passed students is poor and thus is not sufficient for technical education.*

(b) Residential facilities:

If possible proper residential facilities, having strict rules to reside, should be developed, to free students from annoyance of searching accommodation and food. For this, rules followed in other foreign countries may be followed.

(c) Facilities for co-curricular& extra-curricular activities:

Facilities for all types of approved co-curricular or extra-curricular activities should be provided by the respective university to develop like a perfect human being.

(iv) Problems of privatization and lean control:

Although officially many private universities have been permitted to operate locally but there is a rumor that some are not strictly following the conditions set by the authorities. So, universities failing to follow approved set rules must be forced to discontinue operation. ***Universities should not be thought as profit making business enterprise at all. There should not be any system to purchase a degree or completing a set program with minimum effort.*** Besides, strict control to check the performance of the private and public universities by the UGC should be enforced at least for quality and also to monitor the implementation of other set conditions / rules.

(v) Politicization of education & outside interference in running day to day affairs and policy making:

Education should be made totally free from all political influence. University laws / regulations must be made so that there remain no scope for political appointment or to interfare in any type of decision making. Everybody should remember that ***if education is lost everything is lost forever.***

(vi) Absence of non-uniform rules & regulations in many universities:

Rules like those (i) for recruitments; (ii) service rules like leave rules, rules for higher studies etc.; (iii) for payments of all types of financial benefits, etc., should be made uniform in various universities failing in that might cause serious dissatisfaction in all employed teachers & other staffs of universities.

It should not be advisable to forget that people usually compares what he/she is getting with others.

(vii) Absence of strict demand of job providers:

Job Providers too should follow strict rules for all recruitments. Organizations / Industries should maintain close relationship with universities. Industry- university forum should be established in all universities at least for course-curriculum review, research funding / tracer study / Study tour and internship/job placement, etc. Each organization / industry should have one R & D department to solve its own problems as well as for future development of any new product. ***No recruitment should be made for non-accredited degrees and under influence. Minimum level of quality must be ensured in all jobs.*** All engineers serving in any practical job must have local professional society membership.

(viii) Professional accountability of teachers / staffs /officers of universities and Service length:.

Strict accountability procedure must be defined and must be communicated at the time of recruitment. ***No service be made permanent and all services should be made on contract basis for a limited period***. No extension / promotion should be given to teachers if he/she fails in defined accountability, having adverse evaluation report by authorities / students and failing to fulfill set publication and research criteria and having bad service records, etc. Evaluation by the Students' as well as by the authority should be made mandatory for promotion and continuation in teaching service. ***The doctrine "Publish or Perish" may be followed if required***. For staffs too similar criteria may be developed.

(ix) Absence of tracer study / job placement / Alumni Association and counseling programs:

Each university should have tracer study program to know how its graduates are performing. Also each university should have strong job-placement program and Alumni association. Alumni association can help universities in many social / institutional development activities and tracer study can help universities in updating curriculum and syllabus. ***Universities should review / update curriculum and syllabus on a regular basis*** to cope with the requirements of job-providers, change in Technology developments, etc.

(x) Strategic policy relating to education:

Long term strategic plan for the development of higher education especially the engineering education must be defined / launched for the development of the country. The author thinks that there must be clearly defined national policy about the relationship among the tertiary engineering education, industrial development, establishment of heavy industries and general development of the country.

xi) Other related matters relating to tertiary Education:

(a) Granting special pay scale and especial service length to attract brilliant persons to teaching profession.

Special Salary scale for teaching profession is needed to be provided to relieve teachers of economic hardship at all level should be made so that teachers can remain mentally free from economic problems, only then university teachers will be able to concentrate on quality and research.***Teachers' service length should be extended up to a approved limit*** to get the benefit of their experiences and knowledge in the field. Examples of other famous foreign universities may be followed in this respect. ***Posts of supernumery, Professor emitus or by other names may be created to attract really deserving Professors to remain in teaching***

(b) Diverting relatively more national budget to Education sector.

More emphasis on the development of education should be given through allotting more national budget on education sector.

(c) ***Establishing development / link program with bench-marked universities of developed countries to develop local universities.***

It was done for BUET, Agriculture University at Mymensingh, and for IITs of India at birth. For the sake of future development and also to get share / guidance of bench-marked universities link programs between local universities with famous foreign universities should be made for the greater interest of the educational quality and also for the development of tertiary Engineering education.

D)Suggestions for possible improvement in Tertiary engineering education in Bangladesh.

1. Strict accreditation requirement in all educational institutions of higher education must be made.
2. Syllabus / curriculum must be updated in every 2-3 years considering local industrial requirements / Technology change / Globalization effect, etc.
3. Strict approved academic guidelines for accountability in teaching job should be enforced giving emphasis on ethics.
4. Strict approved guidelines for recruitment of teachers / administrators / officers / staffs in all universities must be followed.
5. Uniform admission policy for new students must be enforced and if possible one central admission test for all universities may be taken.
6. Establishment of exchange / link programs with Bench marked universities may be established.
7. Strict Government policy so that education cannot be considered as business is to be made and universities selling certificates or not fulfilling quality requirements must be closed down.

8. Minimizing of outside interference in university affaires shuld be made effective and universities should be given full autonomy at least for academic development and quality masnagement.
9. No political appointment at any level should be made. Politics should be banned in universities.
10. Retirement age of teachers in general should be made higher and creation of special salary structure for teachers should be made and other motivational policy like creation of especial teaching posts like Supernumery Professor, Professor Emeritus etc. for really deserving professors may be implemented.
11. Initiation of government interference to remove the opinion differences among Engineers / technologists / diploma holders should be started soon. For this, practices in developed countries can be followed.
12. Continuing education / on-job training / apprenticeship, etc. programs for graduates and Study tour / Internship / industrial attachment,etc. programs for students may be implemented soon and may be encouraged. Job-fair / product exhibition / seminars / workshops should be held regularly to demonstrate creativity in students.
13. All universities should start offering post graduate degrees immediately to enhance research activities. Teachers must be provided with sufficient funds to do research. Industries should start R & D program soon and university-industry forum must be established soon to solve related problems. Tracer Study program, formation of Alumni Association / Job Placement cell, etc., may be created may be done /created soon.
14. Strict follow-up program for students' / teachers' performance evaluation be made effective.
15. Private university zones like export processing zones with many common facilities, without highlighting failures of private universities only, may be created by the Government. Regular and strict follow up program should be followed for all public & private universities by the appropriate authorities.

E) Conclusion

Some of the present problems in tertiary Engineering / Technical education have been discussed in author's own view. Also some suggestions have been given for possible improvements. In fact the total education should be made influence free from all sectors A separate education commission to improve tertiary engineering education should be formed soon by the Govt. consisting of thinkers in this line. Students should be brought under the control of teachers and strict quality control on all sectors of education and accountability at all sectors should be strictly established. Role of UGC should be made relatively more-broad based. UGC should act like ombudsman. Accreditation of University degrees should be made compulsory for any job or entry to higher education and also for continuation as university teacher. Peer review of univ programs may be implemented.

F) REFERENCES:

1. Prof Dr. M.H.Khan, Ex-VC BUET and AUST: "Quality Assurance in Engineering Education in Bangladesh" National Seminar on Quality Assurance in Engineering Education, IEB, Sept.'13.
2. Prof. Dr. Iqbal Mahmood, Ex VC BUET, "Quality Assurance in Engineering Education", a seminar paper.
3. Prof. Dr. Ataul Karim, Vice President for Research, Old Dominican University, Virginia, USA, a personal communication.
4. Dr. Harun Chy et. al. "Quality Assurance & Accreditation of Engineering Education in Bangladesh, 5th BSME international Conference at Dhaka and an Elsevier, '12 publication..
5. Prof. Dr. Anisul Hoque, East-West University, Dhaka, "Quality Assurance & Out-come based Engineering Education- Bangladesh perspective", National Seminar on Quality Assurance in Engineering Education, IEB, Sept.'13.
6. Prof. Dr. Rafiqul Islam, Naval Architecture & Marine Eng. Dept., BUET, "Self-Assessment exercise towards Outcome based Education", National Seminar on Quality Assurance in Engineering Education, IEB, Sept.'13.
7. Soma C hakraborty, S ,K Biswas, et.al:, 'Quality Assurance in Tertiary Engineering Education and Suggestion for Improvement', presented in ICMERE-2, CUET, June, '14.
8. Tonmoy Dhar, S. K. Biswas, et.al:, 'Implementation of ISO 9000 in Educational Institutions', presented in ICMERE-2, CUET, June, '14.
9. Wikipedia (separate for each Country), Education in Japan /Malaysia / Sri Lanka/ Pakistan / Saudi Arabia and India, Internet
10. S K. Biswas, Key note paper at in ICMERE-2, CUET, June, '14. on 'Problems of Higher Education of Bangladesh and some suggestions for improvement'.
11. National Seminar on 'Engineering Education in public and Private universities: Bangladesh Context', Organized by IEB, Aug. 30 , 2014.

ICMIEE-PI-140342

FUZZY MODEL FOR PRIORITIZING DISTRIBUTION CENTER WITH MULTIPLE CRITERIA, A CASE STUDY

[1] Sayem Ahmed, Minhajul Islam, Rafi Ahmed, Saifullah-Al-Munsur, S. K. Biswas [2], and Mahmudul Hasan [3].
[1] Graduates of Industrial & Production Engineering, Ahsanullah University of Science & Technology, Bangladesh.
[2] Professor, Mechanical & Production Engineering, AUST, [3] Lecturer, MPE, AUST.

ABSTRACT:
A company must deliver or distribute lots of diversified products to several distribution centers throughout the country from its storages or distribution department. 'Distribution center selection problem' is concerned with how to select the ultimate distribution centers from the potential set so that decision can be taken promptly based on optimized input criteria. However, it is not only a very complicated and demanding task for decision makers to select the most beneficial distribution center, but also it implicates uncertainty and produces erroneous results if single criterion is considered. As traditional methods are not very appropriate to analyze the priority with multiple criterions, the decision makers of the company require an efficient, reliable and promising tool to help them in selecting the best distribution center. This paper proposes a new method for prioritizing the distribution center by using MATLAB Fuzzy Logic Tool box to help the distribution department in selecting the most deserved distribution center. The main task in the proposed model involves determining the numerical score for distribution centers considering their respective performance in various qualitative and quantitative evaluation criteria and then selecting the most beneficial distribution center having highest score. Thus best distribution center for a local big Ice-cream company was found and it was finally known that the company used the same distribution center by thumb rule. Thus it can be said that the administration of the company got a technically sound basis for selection.

Keywords: Fuzzy Logic, Supply Chain Management, MATLAB, Distribution process of goods.

1. Introduction:

A distribution center is that through which a company or an organization delivers its products or services to the potential customers. As customers are the main focus point of an organization and their demands are served by the distribution centers, so the distribution centers deserve considerable attention of management. A dedicated distribution management system is often required for smooth flow of operations in distribution centers. A distribution center acts as a regional central point / place for the distribution of its products / services ultimately to the customers of a company / organization in a particular region. So, the performance of distribution centers directly or indirectly, affects the image of the organization. Distribution centers are set up strategically throughout the country. Some distribution centers may not be fruitful for the company. But it might be necessary to establish from the viewpoint of the competitive advantage. So it is essential to evaluate and prioritize the distribution centers based on their performance and beneficence. Apparently it seems to the management of distribution centers that it is an easy job but the situation becomes critical when several distribution centers submit their demands at a time and the organization do not have sufficient inventory of products to meet the demands of all the distribution centers. The management has to take decision like which demand of which distribution center will have to be satisfied first. And that makes complex the whole situation. So, a logical and mathematical model for this type of decision making can be very convenient and useful to the managers and through this decision makers can raise their confidence level in time of decision making.

Fuzzy Logic Toolbox in MATLAB is a tool for solving problems with multiple criteria. This paper presents a methodology which is based on fuzzy logic approach to provide a better way of decision making on prioritizing the distribution centers that will dictate which center should be delivered first. The most important factors like demand, sales, profit contribution, lead time and transportation cost are taken into account in modeling the problem. The result shows that the prioritization of distribution centers varies with the variations in the considered situation. The outcome of this model will represent a distinct numerical ranking value for each of the distribution centers. As multiple criteria decision making is quite complex, it is hoped that this modeling approach will surely be an outstanding helping hand for the decision makers.

2. Methodology of the study / research:

In order to carry out this study, steps that have been followed are mentioned below:

i. Identification of multiple criteria which influence the priority ranking of the distribution centers across the country.
ii. Defining the rules by some basic logic and conceptions for relating the inputs with the output.
iii. Selecting the membership function and range for each criteria and sub criteria (i.e. low, medium, high)

*Corresponding author, Tel.: +88-01817-746070, +88-01813-261758
E-mail address: skbaust@yahoo.com, skbiswas.mpe@aust.edu, skbcuet@yahoo.com

iv. Evaluating the surface for effective and valid development of the rules generated during the research.
v. Developing the data and finding the output decision for prioritizing the distribution center.

3. Basics of Fuzzy Modeling:

3.1 Fuzzy Set Theory:

Zadeh (1965) came out with the fuzzy set theory to deal with vagueness and uncertainty in decision making in order to enhance precision. Thus the vague data may be represented using fuzzy numbers, which can be further subjected to mathematical operation in fuzzy domain. Thus fuzzy members can be represented by its membership grade ranging between 0 and 1. A triangular fuzzy number (TFN) M is shown in figure:

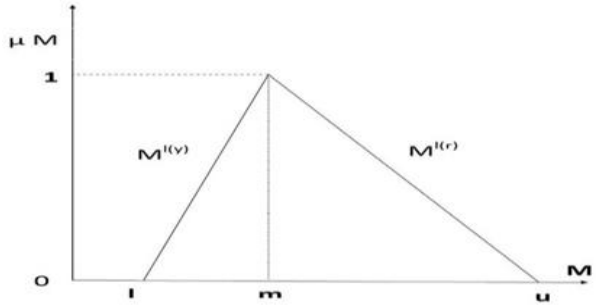

Fig.1: A Triangular Fuzzy Number

A TFN is denoted simply as (l/m, m/u) or (l, m, u), represented the smallest value, the most promising value and the largest possible value respectively. The TFN having liner representation on left and right side can be defined in terms of its membership function as

$$\mu(x/M) = \begin{cases} 0, & x<1, \\ (x-l)/(m-l), & l \le x \le m, \\ (u-x)/(u-m) & m \le x \le u, \\ 0, & x>u, \end{cases}$$

A fuzzy member with its corresponding left and right representation of each degree of membership is as below:

$\tilde{M}=(M^{l(y)}, M^{l(r)})= (l +(m-l)y, u+(m-u)y), y \in [0,1]$

Where l(y) and l (r), denotes the left side representation and the right side representation of fuzzy number respectively.

The fuzzy summation and fuzzy subtraction of any two TFN are also TFNs, but the multiplication of any two TFNs is only approximate TFNs. The data can be assessed using the linguistic scale along with corresponding triangular fuzzy scale.

If $M_1= (a_1, b_1, c_1)$ and $M_2= (a_2, b_2, c_2)$ are two TFNs, then their operational laws can be expressed as follows:

$M_1+M_2= a_1+ a_2, b_1+b_2, c_1+c_2$

$M_1-M_2= a_1-a_2, b_1-b_2, c_1-c_2$

$M_1*M_2=a_1a_2, b_1b_2, c_1c_2$

$\lambda *M_1 =\lambda a_1, \lambda b_1, \lambda c_1$ where $\lambda > 0, \lambda \in R$

$M_1^{-1} = (1/c_1, 1/b_1, 1/a_1)$

3.2 Fuzzy inference system (FIS):

Fuzzy inference system is also known as fuzzy rule based system, fuzzy models, fuzzy associative memories (FAM), or fuzzy controllers when used as controllers.

i. A rule base containing a number the membership function
ii. A database which defines the membership functions
iii. A decisions-making unit which performs the inference
iv. A fuzzification interface which transforms the crisp inputs
v. A defuzzification interface which transform the fuzzy

Usually, the rule base and the database are jointly referred to as the **knowledge base.**

The steps of fuzzy reasoning (inference operations upon fuzzy if-then rules) performed by fuzzy inference systems are

i. Compare the input variables with the membership functions on the premise part to obtain the membership values (or compatibility measures) of each linguistic label. (This step is often called fuzzification).
ii. Combine (through a specific T-norm operator, usually multiplication or min) the membership values on the premise part to get firing strength (weight) of each rule.
iii. Generate the qualified consequent (either fuzzy or crisp) of each rule depending on the firing strength.
iv. Aggregate the qualified consequence to produce a crisp output. (This step is called defuzzification.)

4. Prioritize Distribution Centers:

Distribution refers to the steps taken to move and store a product from the supplier stage to a customer stage in the supply chain. Distribution is a key driver of the overall profitability of a firm because it affects both the supply chain cost and the customer experience directly.

A distribution center is a principal part, the order processing element, of the entire order fulfillment process. Distribution centers are usually thought of as being demand driven. So when we prioritize ranking of the distribution centers we only consider demand. But the demand is the only one of many factors that affect the overall profitability of the firms for prioritizing the distribution centers. When assessing and selecting the distribution center according to priority the following factors other than quoted demand must be considered:

a. Demand
b. Sales
c. Profit-Margin
d. Lead-Time
e. Transportation-Cost

Distribution centers must be prioritized on each of these factors because they all affect the total profitability and effective functioning of the firms.

Local Ice-cream Industries Limited is a renowned ice-cream industry in Bangladesh. For its smooth flow of operation and distribution across the country, the company has set up 16 distribution centers at different locations of the country. The whole country is served through these distribution centers. The company's 16 distribution centers are –

1. Dhaka North
2. Dhaka South
3. Dhaka East
4. Dhaka West1
5. Dhaka West2
6. Dhaka Institute
7. Dhaka Trolley
8. Khulna
9. Barisal
10. Jessore
11. Rangpur
12. Bogra
13. Rajshahi
14. Comilla
15. Sylhet
16. Chittagong

Here in our thesis, we have developed a model by using Fuzzy logic multi-criteria decision making (MCDM) and using MATLAB. Different distribution centers have been ranked/prioritized based on those criterions. The combined effect of all these criterions on different distribution centers is shown and specific ranking point is attached to the centers.

5. Rule Formation:

In the proposed model, five input variables are used to prioritize distribution center of a company. The five variables are Demand, Sales volume, Lead time, Profit margin, Transportation cost. All of them have three divisions- High, Medium, Low. So there may be many combinations to formulate different rules using the input, the total number of rules in this model is 3X3X3X3X3 or 243. Rules are generated with five stated inputs using "and" command.

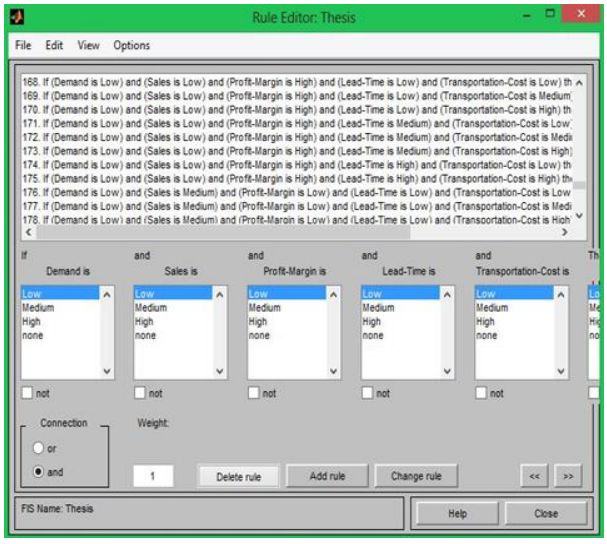

Fig.2: Rule editor

In rules generation, weighted method is used (between 0 – 1). Here one (1) is used for highest importance and lower than one (1) is used to identify relatively lower importance respectively. Like 0.7 is described lower weightage than 0.85.

For instance, comparing two DCs, criteria's for the first one are high demand, low sales, low profit-margin, low lead-time and high transportation-cost then priority-ranking is low (0.74) i.e. weightage value is 0.74. On the other hand, criteria's for the second one are high demand, high sales, high profit-margin, medium lead-time and low transportation-cost then priority-ranking is high(1) i.e. weightage value is 1.

6. Surface Viewer:

Surface actually represents the three dimensional relationship between various input and output. The variation in output against the input variables depends on the developed rules. The very random fluctuations in surface represent the weakness and at the same time indicate erroneous development of the rules generated. With a view to representing the sustainability and strength of the developed rule the surfaces should exhibit an approximate ascending and descending pattern. Throughout our work, we tried our best to ensure a reasonable approximate for ascending and descending pattern. Even though, the surface represented in our model exhibit some sort of ups and downs, but it can be considered as almost correct because all of the rules could not have been generated due to time constraint. If all of the possible rules could have been developed, it can be said for surity that the surface would have been more accurate. But, Generating such number of huge rules would be not only tedious but also time consuming and perhaps infeasible to some extent.

Surface analysis from some selected inputs which was obtained from MATLAB Fuzzy Toolbox is given below in figure 3 and 4.

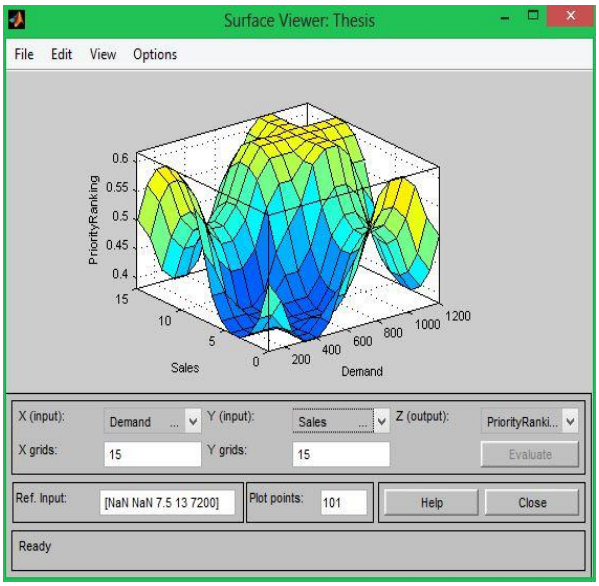

Fig.3: Surface for Demand vs Sales

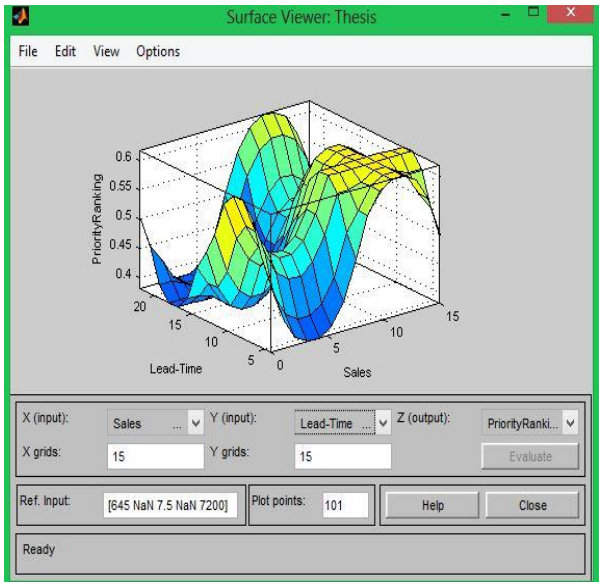

Fig.4: Surface for Sales vs Lead Time

7. Result and Analysis:

In this section, priority ranking of the distribution center has been determined. This priority ranking represents the distribution center based on the predetermined input criterions. To determine the ranking, Fuzzy toolbox of MATLAB software has been used. Finally, from this priority ranking the most beneficial distribution center for delivering the ordered amount has been selected.

From our observation, we have seen that **(table-1)** the most beneficial distribution center is "Dhaka East" whose priority ranking is 0.747.

The applied fuzzy logic on "Dhaka East" distribution center is shown below:

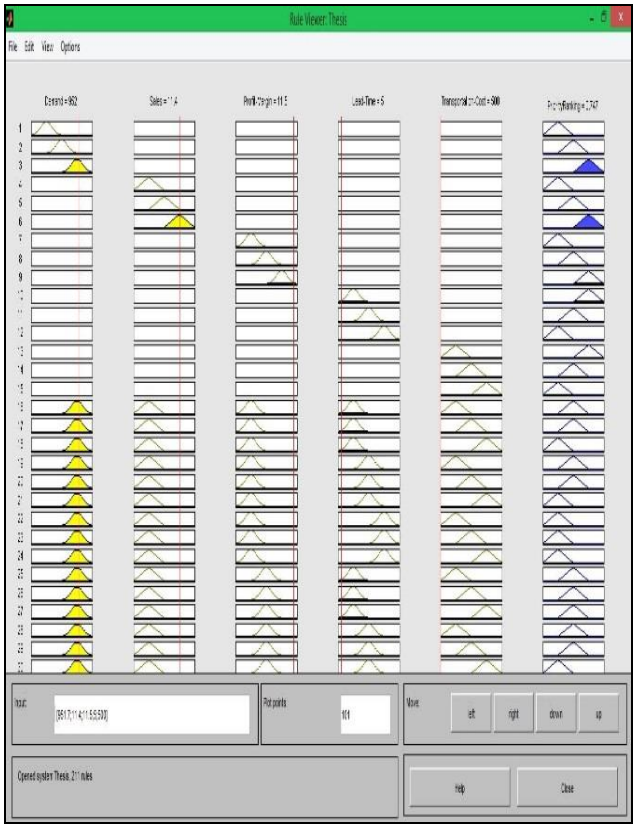

Fig.5: Highest ranked distribution center

Table 1: Priority Evaluation of Distribution Centers Based On MCDM

Center No.	Distribution Centre	Input Variables					Priority Ranking
		Demand (m^3)	Sales (%)	Profit (%)	Lead time (hrs.)	Transportation cost (Taka)	
1	Dhaka North	1127.026	13.5	7	6	5340	0.582
2	Dhaka South	1193.813	14.3	9.5	6	800	0.733
3	Dhaka East	951.711	11.4	11.5	5	500	**0.747**
4	Dhaka West1	989.2785	11.85	8	6	800	0.624
5	Dhaka West2	955.8852	11.45	7.5	6	500	0.619
6	Dhaka Institute	108.5284	1.3	5	6	500	0.42
7	Dhaka Trolley	91.83176	1.1	5.5	6	800	0.42
8	Khulna	258.7986	3.1	4	20	13620	0.25
9	Barisal	166.9668	2	4	16	13620	0.31
10	Jessore	166.9668	2	4	15	13620	0.368
11	Rangpur	166.9668	2	4	11	13670	0.46
12	Bogra	175.3152	2.1	5	9	9590	0.5
13	Rajshahi	166.9668	2	4	11	11630	0.444
14	Comilla	705.4349	8.45	6.2	8	5160	0.528
15	Sylhet	267.1469	3.2	6.8	11	9940	0.443
16	Chittagong	855.7051	10.25	8	18	10000	0.496

8. Conclusion:

Prioritization of the distribution center is undoubtedly crucial for any company when order is placed by several distribution centers at a time. The company might not have sufficient inventory of finished product to fulfill the order of all the ordering distribution centers. The company may fall in a dilemma to decide which distribution center's demand will be met and delivered first. Prioritizing the distribution center depends on multiple criterions, we think, massive uncertainty can be involved in this regard. At present, many companies use thumb rule and their past experiences to decide about such complex situation. But it costs a lot of time, mental pressure, decision might be wrong and there is no scientific and logical method to make decisions on it. This uncertain characteristic affiliated with the prioritization of the distribution centers leads to the utilization of fuzzy logic which facilitates the prioritization process by making it credible and accurate. During the generation of the model, at first some criteria have been determined based on which prioritized distribution center has been evaluated. Two hundred and forty three rules have been generated to provide relationship between five inputs and output that is for priority ranking. Finally, output has been calculated numerically and this output was generated according to the rules developed in fuzzy toolbox. The decision regarding prioritizing distribution centers is given by the Mamdani FIS. To generate the output data, all necessary data have been collected from Local Ice Cream Company. At the end of the work, this numerical output has been converted into the alphabetical output with the help of a code developed in MATLAB. In a nutshell, the result obtained represents the prioritized distribution center according to the criteria those have been adopted in the model. The accuracy of the output may be improved by considering many more criteria and those criteria may be varied from company to company. But, In general this is a generalized model and can be applied in different company with the proper determination of the input variables.

Acknowledgement:

Our sincere thanks go the high officials of local ice cream company who allowed us to use various floor data although they did not allow us to disclose their identity**.**

REFERENCES

[1] Aras, H., Erdogmus, S. and Koc, E. (2004), "Multi-criteria selection for a wind observation station location using analytic hierarchy process", Renewable Energy 29, pp. 1383-1392.

[2] Cheng, (1996), "Evaluating naval tactical missile systems by fuzzy AHP based on the grade value of membership function", European Journal of Operational Research. v96. 343-350.

[3] DCLG (Department for Communities and Local Government) (2009), "Multi-criteria analysis: a manua", West Yorkshire: Communities and Local Government Publication.

[4] Ertuğrul, I. and Karakasoglu, N. (2008), "Comparison of fuzzy AHP and fuzzy TOPSIS methods for facility location selection", International Journal of Advanced Manufacturing Technology39, pp. 783-795.

[5] Farahani, R.Z., Steadieseifi, M., and Asgari, N. (2010), "Multiple criteria facility location problems, A survey. Applied Mathematical Modelling 34", pp. 1689-1709.

[6] Fernandez, I and Ruiz, M.C. (2009), "Descriptive model and evaluation system to locate sustainable industrial areas", Journal of Cleaner Production 17, pp. 87-100.

[7] Jaideep Motwani, Mohamed Youssef, Yunus Kathawala, Elizabeth Futch, (1999) "Supplier selection in developing countries: a model development", Integrated Manufacturing Systems, Vol. 10 Iss: 3, pp.154 – 162.

[8] Jian Liu, Fong-Yuen Ding, Vinod Lall, (2000), "Using data envelopment analysis to compare suppliers for supplier selection and performance improvement", Supply Chain Management: An International Journal, Vol. 5 Iss: 3, pp.143 – 150.

[9] Md. Mahmudul Hasan, Md. Abu Sayeed Shohag, (2013), "A Fuzzy Model for supplier selection with multiple criteria".

[10] Saaty, T.L. (1994), "How to make a decision: the analytic hierarchy process", Interfaces 24(6), pp. 19-43.

[11] Tuzkaya, G., Önut, S., Tuzkaya, U.R. and Gülsün, B. (2008), "An analytic network process approach for locating undesirable facilities: an example from Istanbul, Turkey", Journal of Environmental Management 88, pp. 970-983.

[12] Tzeng, G.H., Teng, M.H., Chen, J.J. and Opricovic, S. (2002), "Multicriteria selection for a restaurant location in Taipei", International Journal of Hospitality Management 21, pp. 171-87.

[13] Wu, C.S., Lin, C.T. and Lee, C. (2010), "Optimal marketing strategy: A decision-making with ANP and TOPSIS", International Journal of Production Economics 127, pp. 190-196.

[14] Youssef, M. A., M. Zairi, and B. Mohanty. (1996), "Supplier Selection in an Advanced Manufacturing Technology Environment: An optimization Model." Benchmarking for Quality Management & Technology 3: 60-72.

[15] Zahedi, F. (1986), "The analytic hierarchy process: a survey of the method and its applications." Interface 16(4): 96-108.

[16] Yong, D. (2006), "Plant location selection based on fuzzy TOPSIS", International Journal of Advanced Manufacturing Technology 28, pp. 839-844.

[17] Saaty, T.L. (1980), "Fundamentals of Decision Making and Priority-Theory with the Analytic Hierarchy Process", Pittsburgh: RWS Publications.

ICMIEE-PI-140343

An Assessment of the Underground Roadway Water Quality for Irrigation Use around the Barapukuria Coal Mining Industry, Dinajpur, Bangladesh

**M. Farhad Howladar[1], Pulok Kanti Deb[1], ATM Shahidul Huqe Muzemder[1], and Mohammad Islam Miah[2]*

[1]Department of Petroleum & Mining Engineering, Shahjalal University of Science & Technology, Sylhet-3114.
[2]Department of Petroleum & Mining Engineering, Chittagong University of Engineering & Technology, Bangladesh.
E-mail : farhadpme@gmail.com islam.pge20@gmail.com

ABSTRACT

The study area Barapukuria Coal Mine is situated in the Parbatipur Upazilla, Dinajpur District, and north-west part of Bangladesh. The area is criss-crossed by a number of streams under three rivers namely the Khorkhori, the Jamuna (local name) and the Ghirnai. Most of the streams are locally originated which are filled by rain water. From long period, the local people used various sources of water for agricultural purposes before the development of Barapukuria Coal Mine, on the other hand presently using a large quantity of mine discharged water for agricultural purposes especially for irrigation. As it is well known that currently the influences of underground coal mining activities has become a leading issue in the changes of water resources and their uses around the mining area. While the mining area thoroughly bounded by the irrigated land where underground water is the main sources of irrigation use. In the case of Barapukuria Coal Mine, a huge volume of water is pumping regularly from the underground tunnel roadway to surface. Thus it is a matter of question regarding its quality for irrigation and other uses. From this view point, this study monitored and assessed the quality of inflow water in the roadway for different years for irrigation purpose. The investigation shows that the roadway water is suitable for irrigation purposes where the overall quality of water is dominantly controlled by the rock weathering and evaporation natural processes in the area. In fact, the suitability of roadway water for irrigation was evaluated based on SSP, Salinity Hazard, Sodium Percent, Sodium Adsorption Ratio, Residual Sodium Carbonate, US salinity diagram, Wilcox's diagram, Kelly's ratio, Permeability Index, Magnesium Hardness, Total Hardness and so on. On the whole, the concentration of such parameters, major cations, anions, trace elements (e.g. As, Cd, Zn, Cr, Cl, Al, Mn), and others elements (e.g. TSS, DO, DOB, Oil and Grease, C. Count, T. Coliform, F. Coliform etc.) did not exceed the permissible limit for irrigation purposes hence suitable for irrigation uses. Conversely, the slight Mg hazard with moderately hard to hard tendencies of water bodies suggests a restriction for frequent utilization of this water for irrigation. Thus this study strongly recommends for continuing the ongoing monitoring program with necessary precautionary measures for maintaining the quality of roadway water in the underground tunnel of the mine.

Key words: Barapukuria coal mine, Underground tunnel roadway, Inflow water quality, Irrigation use.

1. INTRODUCTION

The Barapukuria Coal Mine (BCM) is situated in the Parbotipur Upazila, Dinajpur District, which lies between the latitudes 23°31′45″ and 23°33′05″N, and the longitudes 88°57′48″ and 88°58′53″E [1] shown in Fig. 1. As for the exploration report, the hydrogeological condition around the mine is much complicated as a result the mine industry endured various problems to develop new roadway and safely take out coal from underground. During the development work of coal mine in 1996, a severe water inrush accident occurred consequently thoroughly inundated the underground roadway. In this case, this waterlogged condition has been resolved using forced pumping activities and this water drained into the nearby agricultural field. As we know, the drainage from mine is well recognized as a cause of landscape disturbance as being highly impactful to water resources and, as a cause of social and economic problems [2,3,4&5]. On the other hand, the discharged huge volume of water from the water bearing formation affects groundwater elevations equally which may be more distinct as underground mines are more deeper and of larger aerial extension than the open cut mines.

* Corresponding author. Tel.: +88-01731195918
E-mail address: farhadpme@gmail.com

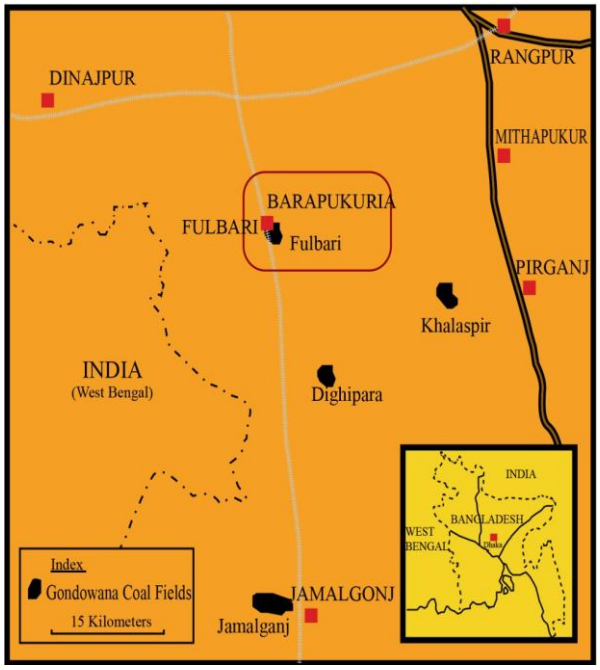

Fig. 1 The location map of the BCM field, Dinajpur, Bangladesh.

The lowering of groundwater level can occur over miles due to major mining operations [2&6]. However, mining affects water resources, both surface and groundwater, at various stages of the life cycle of the mine and even after its closure. The mining process itself, mineral processing operations, mine dewatering, seepage of contaminated lactates, flooding of mine workings, and discharge of untreated water are some important processes with related mine water problems [7&8]. Especially, the coal mine roadway water containing various hazardous materials may be dangerous to the surrounding environment. Contaminants released from the coal can pollute the water, soil and air, and can affect human health. For that reason, the areas where hazardous wastes are accumulated must be examined to avoid pollution. From long period, the local people used various sources of water for agricultural purposes before the development of BCM. But at present they are using huge amount of coal mine discharge water for their agricultural purposes especially for irrigation. Thus, from these points of view, it is very much essential to understand the total discharge rate of water from the aquifer to underground roadway, their quality, drainage system and utilization. In the study area, a group of researchers carrying out different research works from the early period of mine operation to present, but yet not a single research considered on the monitoring of the discharge rate of water, their quality and likewise their relation to lowering the water level around the mine. Under this situation, the prime objectives of the present studies are to ascertain the intensity of discharge water from the year 2001 to 2011, their quality for irrigation use around the area. Finally, discuss and compare the present results, and recommends the necessary steps for the present and future safety of underground tunnel, mining industry, surrounding environments and others.

2. MATERIALS AND METHODS

In order to understand and assess the inflow water quality in the roadway and the contemporary situation of water level around the BCM Industry, this study carried out intensive field inspections for collecting different relevant data such as the monitored groundwater samples from different location of the tunnel of the mining industry and their laboratory analysis. Moreover, field investigation was also carried out to observe the management system of mine drainage water and their utilization around the area. During field investigation, groundwater quality monitored data for a year as 2013 and water samples have been collected from Deep belt entry (Dupi Tila), Tract belt entry (Gondwana), Coal bearing water (Tract Gate), 430m Main Sump, Inrush Point, 1101, 1104, 1105, 1109, 1111, 1116, 1203, 1204 and 1210 faces, Outside boundary drain water, and Production level coal phase of the mine, and instantly measured some physical parameters such as Electrical Conductance (EC), Total Dissolved Solid (TDS), pH and Temperature. During field work, pH has been measured with a portable pH meter (HANNA pocket pH meter). The EC meter (HANNA HI 7039pS meter) was used to measure the EC, Temperature and TDS. The major cations like calcium (Ca), magnesium (Mg), sodium (Na), potassium (K), and anions like bicarbonate (HCO_3), carbonate (CO_3), chloride (Cl), nitrate (NO_3) and sulfate (SO_4) with some minor elements As, Cd, Zn, Cr, Cl, Al, Mn and other parameters, chemical analyses were carried out using appropriate certified and acceptable international procedures outlined in the standard methods for the Examination of Water and Wastewater [9]. The results were evaluated in accordance with the overall quality and irrigation standards given by the WHO & US salinity diagram and others for the classification of irrigation water [10].

The Permeability Index (PI) values have been calculated to know the suitability of water for irrigation use around the mining area while the soil permeability is affected by the long term use of irrigation water as it is

influenced by Na, Ca, Mg and HCO_3 content of the soil [7]. Based on the PI values, Doneen (1964); Raghunath (1987) and WHO (1989) provide a classification to assess the suitability of groundwater for irrigation 11,12&13]. The PI is defined as Equation 1:

$$PI = \frac{(Na + \sqrt{HCO_3}) \times 100}{(Ca + Mg + Na)} \quad \ldots\ldots\ldots\ldots\ldots\ldots (1)$$

where all concentrations are in meq/L.

3. DATA ANALYSIS AND RESULTS

3.1 Evaluation of Inflow Water for Its Possible Irrigation Utilizations

To understand the quality of water, a considerable number of water samples for a year of 2013 has been collected from various points of the underground tunnel such as Deep belt entry (Dupi Tila), Tract belt entry (Gondwana), Coal bearing water (Tract Gate), 430m Main Sump, Inrush Point, 1101, 1104, 1105, 1109, 1111, 1116, 1203, 1204, 1210 faces, Outside Boundary Drain Water and Production Level Coal Phase. These water samples have been analyzed in the laboratory, and results are plotted in the diagram (Table 1**)** for explaining the variations of water quality parameters of samples. From data analysis, some test parameters have been mentioned as Table 1 to Table 3 for underground roadway water. The outcome from data analysis gives significant values for determining water quality and compared these different quality parameters like physical and chemical parameters of tunnel roadway water with the standard acceptable limit recommended by WHO (2011) and EQS (1991), which confirms that the concentration of all parameters are within acceptable limit[14 & 15] and not much divergence occurred in the tunnel. Moreover the minor elements such as As, Cd, Zn, Cr, Cl, Al, Mn, and others, such as TSS, DO, DOB, Oil and Grease, C. Count, T. Coliform, F. Coliform etc. are also in the tolerable limits and can be used for different purposes with minor treatment. Meanwhile, the mining industry locates thoroughly in the plain land where the land use is dominated by agriculture workings and main crop is rice. The most of the lands within the mining area are cultivated in a natural way along with crops are harvested in two to three times in a year.

Table 1: Physicochemical characters of underground roadway water for the year 2013

Test Parameter & Units	**1101 Coal Phase**	**1206 Coal Belt Gate (3-L)**
pH	6.82	8.27
EC, µS/cm	156.80	151.60
Turbidity, NTU	90	153
Total Alkalinity, mg/L (as $CaCO_3$)	128	133
TH, mg/L (as $CaCO_3$)	45	70
CO_3, mg/L	7.20	11
HCO_3, mg/l	180.15	210.45
Fe (III), mg/L	0.60	0.40
Ca (II), mg/L	30	40
Mg (II), mg/L	15	30
Na (I), mg/L	7.7	5.40
K (I), mg/L	3.10	2.80
As (III), mg/L	0.012	0.011
TDS, mg/L	116	115
SO_4, mg/L	1.33	1.70
PO_4, mg/L	1.20	1
SiO_2, mg/L	35.50	36
NO_3, mg/L	0.18	0.12
Cl, mg/L	5.32	5.96
NH_3, mg/L	NF	0.44
Cd (II), mg/L	0.05	0.028
Zn (II), mg/L	0.21	0.24
Cr (III), mg/L	0.09	0.017

Table 2: Physicochemical characters of underground roadway water, 2013 year.

Test Parameter & Units	**1210 Coal Phase**	**1106 Coal Phase Belt Gate (3-R)**
pH	8.03	7.33
EC, µS/cm	91.20	174.30
Turbidity, NTU	28	34
Total Alkalinity, mg/L (as $CaCO_3$)	113	125
TH, mg/L (as $CaCO_3$)	80	71
CO_3, mg/L	9	6
HCO_3, mg/l	145.65	177.3
Fe (III), mg/L	0.45	0.34
Ca (II), mg/L	55	45

Mg (II), mg/L	25	26
Na (I), mg/L	6.20	7.20
K (I), mg/L	2.80	3.30
As (III), mg/L	0.012	0.013
TDS, mg/L	83	127
SO_4, mg/L	1.30	1.23
PO_4, mg/L	1.20	1.10
SiO_2, mg/L	35	35.4
NO_3, mg/L	0.13	0.17
Cl, mg/L	6.39	6.03
NH_3, mg/L	0.25	0.17
Cd (II), mg/L	0.030	0.026
Zn (II), mg/L	0.26	0.24
Cr (III), mg/L	0.012	0.015

Table 3: Physicochemical characters of underground roadway water of a year (2013)

Test Parameter & Units	**1203 Coal Phase (2-L)**	**1206 R/W Track Gate (2-R)**	**Mother Rock (R/W)**
pH	7.75	7.63	7.71
EC, µS/cm	352	323	403
Turbidity, NTU	90	198	27
Total Alkalinity, mg/L (as $CaCO_3$)	134	111	145
TH, mg/L (as $CaCO_3$)	55	46	59.50
CO_3, mg/L	6	21	26
HCO_3, mg/l	135.8	225.35	255.3
Fe (III), mg/L	0.52	0.47	0.39
Ca (II), mg/L	35	29	38.5
Mg (II), mg/L	20	17	21
Na (I), mg/L	4.10	3.50	5.50
K (I), mg/L	2.13	1.90	2.70
As (III), mg/L	0.014	0.012	0.015
TDS, mg/L	256	241	301
SO_4, mg/L	1.40	1.50	1.31
PO_4, mg/L	1.50	1.40	1.54
SiO_2, mg/L	42.50	53	45
NO_3, mg/L	0.15	0.19	0.18
Cl, mg/L	5.04	5.68	5.54
NH_3, mg/L	0.13	0.18	0.14
Cd (II), mg/L	0.024	0.035	0.032
Zn (II), mg/L	0.27	0.28	0.23
Cr (III), mg/L	0.017	0.016	0.014

Especially in the case of irrigation, the farmers are mostly dependent on the underground water, but currently they faced the problem to properly irrigate their land because of land subsidence, availability of underground water and so on. In this situation, the mine authority can supply this huge inflow water to a local farmer for irrigation and other uses. But before supplying this inflow water to the inhabitants, the authority might have to maintain the proper quality of water. Thus, considering this enormous quantity of inflow water in the underground tunnel and demand of water in the area, this research principally assesses the quality of water for irrigation. The quality of water for irrigation use normally evaluates by some essential issues such as EC, Sodium Absorption Ratio, Soluble Sodium Percentage, Sodium Percentage, Magnesium Hazard, Residual Sodium Carbonate, Permeability Index and United States Department of Agriculture classification. Along with the above indicators, some additional indices have been calculated to categorize the groundwater for irrigation like Kelly's Ratio and TH [16]. In general, when the concentrations of Ca and/or HCO_3 are a substantial form in the water, which are considered to be employed for irrigation consequently a variable fraction of this constituent will precipitate in the soil as $CaCO_3$ following this reaction as 2 [17].

$$Ca^{2+} + 2HCO_3^- = CaCO_3 + H_2O + CO_3 \text{ ---------- (2)}$$

As it is well known that salinization is the major cause of loss of production, which also severely limits the choice of crops, adversely affect crop germination and yields, and can cause soils to be difficult to work [18]. In fact, it is essential that all evaluations about irrigation water quality allied to the assessment of the soils to be irrigated [2&19]. In the present studies, the important hydro-chemical properties of underground tunnel water utilized to determine its suitability for irrigation and as a whole the inflow water in most cases was found to be suitable for irrigation shown in Table 4.

Table 4: Suitability of groundwater for irrigation based on different classification scheme

Classifi-cation Scheme	**Categories**	**Ranges**	**No. of samp-les**	**Percent of samp-les**
EC	Permissible	<1,500	7	100%
	Not permissible	1500-3000	0	Nil

	Hazardous	>3000	0	Nil
Salinity Hazard EC (µS) (Raghunath 1987)	Excellent	<250	4	57.14%
	Good	250-750	3	42.86%
	Medium	750-2250	0	Nil
	Bad	2250-4000	0	Nil
	Very Bad	>4000	0	Nil
Na% (Wilcox 1955)	Excellent	<20	7	100%
	Good	20-40	0	Nil
	Permissible	40-60	0	Nil
	Doubtful	60-80	0	Nil
	Unsuitable	>80	0	Nil
Na% (Eaton 1950)	Safe	<60	7	100%
	Unsafe	>60	0	Nil
SSP (Shah and Mistry 2013)	Good	<50	7	100%
	Bad	>50	0	Nil
SAR (Richards 1954)	Excellent	<10	7	100%
	Good	10–18	0	Nil
	Doubtful	18–26	0	Nil
	Unsuitable	>26	0	Nil
RSC (Richards 1954)	Good	<1.25	5	71.43%
	Medium	1.25-2.5	2	28.57%
	Bad	> 2.5	0	Nil
PI (Doneen 1964)	Class-I	>75	0	Nil
	Class-II	25-75	7	100%
	Class-III	<25	0	Nil
KR (Kelly 1940)	Good	<1.0	7	100%
	Unsuitable	>1.0	0	Nil
MH (Szabolcs and Darab 1964)	Suitable	<50	6	85.71%
	Harmful &Unsuitable	>50	1	14.29%
TH (Sawyer et al. 2003)	Soft	<75	0	Nil
	Moderately Hard	75-150	2	28.57%
	Hard	150-300	5	71.43%
	Very hard	>300	0	Nil

3.2 PI Status of Water for Irrigation Use

In this research, the calculated PI values have been plotted in Fig. 2. In the case of class I and II, waters are grouped as well for irrigation with 75% or more of maximum permeability, whereas class III is unsuitable with 25% of maximum permeability [20].

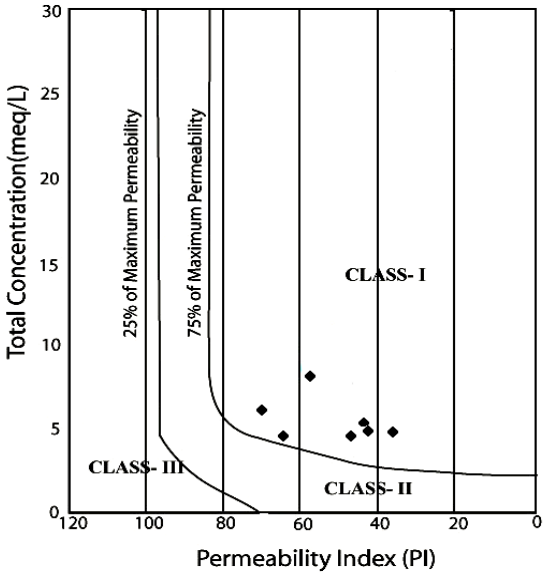

Fig. 2 Classification of irrigation water based on PI (After Ramesh and Elango 2011).

In the present research, the PI values vary from 35.81 to 69.25% (Table 4) which thoroughly belong to the class II reflects the inflow water is suitable for irrigation and quality is medium to excellent.

4. CONCLUSIONS

This study monitored and assessed the volume of inflow water in the roadways of underground tunnel with their quality for irrigation use around the BCM. In other cases of this water quality for irrigation, the results of chemical analyses for the major ions of water samples for different years collected from different points of the roadways of the mine are presented. The quality investigation is carried out with the evaluation of major, minor and other components such as pH, Ca, Mg, Na, K, HCO_3, CO_3, Cl, NO_3, SO_4, specific conductance, alkalinity and hardness, TDS and dissolved oxygen, and the minor elements such as As, Cd, Zn, Cr, Cl, Al, Mn and, others are TSS, DOB, Oil and Grease, C. Count, T. Coliform, F. Coliform etc., respectively, which indicates a sign of good quality of water as per WHO and EQS standards. On the basis of these results certain parameters such as TH, PI, SSP, SAR, Na%, potential salinity, RSC, KR, magnesium ratio, index of base exchange and GR were computed for irrigation purpose only, which implied that all the parameters are varied from good to excellent category hence suitable for irrigation. At the end, this study suggests that the present roadway water quality status must be maintained by taking a strict precautionary measure

with the ongoing monitoring of inflow water quantity and quality of the mine.

ACKNOWLEDGEMENTS

The financial assistance from Ministry of Science and Technology, Government of Bangladesh, Dhaka is highly acknowledged (Project grant No: 39.009.006.01.00.042.2012-2013/EAS-4/579) otherwise this research was entirely unattainable.

NOMENCLATURE

BCM : Barapukuria Coal Mine
EC : Electrical Conductance
PI : : Permeability Index, meq/L
TDS : Total Dissolved Solid
WHO : World Health Organization

REFERENCES

[1] CMC, Preliminary Geology and Exploration Report of Barapukuria Coal Mine, Bangladesh, (1994).

[2] Howladar MF, Deb PK, Muzemder ATMSH, Ahmed M., Evaluation of water resources around Barapukuria coal mine industrial area, Dinajpur, Bangladesh. Applied Water Sci. doi: 10.1007/s13201-014-0207-5, (2014).

[3] Bian Z, Lei S, Inyang H, Chang L, Zhang R, Zhou Q, He X, Integrated method of RS and GPR for monitoring the changes in the soil moisture and groundwater environment due to underground coal mining. J Environ Geol 57:131-142, (2009).

[4] Dinelli E, Lucchini F, Fabbri M, Cortecci Z, Metal distribution and environmental problems related to sulfide oxidation in the Libiola copper mine area (Ligurian Apennines, Italy). J Geochem Explor 74:141-152. doi: 10.1016/S0375-6742 (01) 00180-7, (2001).

[5] Davis CE, Duffy RJ, King Coal vs. reclamation federal regulation of mountaintop removal mining in Appalachia. Admin Soc 41:674-692, (2009).

[6] Steve BMS, James R, Kuipers PE, Technical report on underground hard-rock mining: Subsidence and hydrologic environmental impacts. Center for Science in Public Participation, Bozeman, MT, pp 72, (2002).

[7] Nagaraju A, Suresh S, Killham K, Edwards K. H, Hydrogeochemistry of waters of Mangampeta barite mining area, Cuddapah Basin, Andhra Pradesh, India, Turkish. J Eng Env Sci 30, (2006).

[8] Younger PL, Banwart SA, Hedin RS, Mine Water, Hydrology, Pollution, Remediation. Kluwer, pp 442, (2002).

[9] APHA, Standard Methods for the Examination of Water and Wastewater, 19th edn. Washington, (1995).

[10] WHO, Guidelines for Drinking Water Quality., Vol 1, 2nd edn. Geneva, pp 130, (1993).

[11] Doneen LD, Water Quality for Agriculture. Dept. of Irrigation, University of California, Davis pp 48, (1993).

[12] Raghunath HM, Groundwater. Wiley, Delhi, (1987).

[13] WHO, Health Guidelines for the Use of Wastewater in Agriculture and Aquaculture. In: Report of a WHO Scientific Group: Technical Report Series-778, Geneva, (1989).

[14] WHO, Guidelines for Drinking Water Quality. 4th edn. WHO, Geneva, (2011).

[15] EQS, Environmental Quality Standards, Guidelines for Bangladesh. Dept. of Environment, Bangladesh, (1991).

[16] Ya W, Jiao JJ, Origin of groundwater salinity and hydrogeochemical processes in the confined quaternary aquifer of the Pearl River Delta, China. J Hydrol 112-124, 438-439, (2012).

[17] Shah SM, Mistry NJ, Groundwater quality assessment for irrigation use in Vadodara district, Gujarat, India. World Academy of Science, Engineering and Technology. 79:1625-1630, (2013).

[18] Bhardwaj V, Singh DS, Surface and groundwater quality characterization of Deoria district, Ganga Plain, India. J Environ Earth Sci 63:383-395, (2011).

[19] Ayers RS, Wescot DW, Water Quality for Irrigation. FAO Irrigation and Drainage Paper No. 20, Rev 1, FAO, Rome, (1985).

[20] Ramesh K, Elango L, Groundwater quality and its suitability for domestic and agricultural use in Tondiar river basin, Tamil Nadu, India. J Environ Monit Assess Springer. doi: 10.1007/s10661-011-2231-3, (2011).

ICMIEE-PI-140345

A Case Study of Appropriate Supplier Selection of RFL industry by using Fuzzy Inference System (FIS)

Dr. Tarapada Bhowmick, Md Raiyan Tahsin Haque,Pritom Kumar Mondal

Department of Industrial Engineering and Management, Khulna University of Engineering & Technology, Khulna-9203, BANGLADESH

ABSTRACT

Best supplier selection has become the prerequisite of the business success of any organization. In this era of industrialization the supplier selection process is going in a traditional manner which is very impractical practice. All though there are some research works regarding this issue, but there are some limitations in decision making process. This paper is stood against these limitations and totally focused on appropriate supplier selection using Fuzzy Inference System (FIS). The successful conversion of the qualitative factors into quantitative value makes the system error free which is being performed by FIS, a calculative decision making tool. A successful algorithm is designed for calculating the acceptance probability of suppliers by which the decision making phase is become convenient. Using MATLAB a built in software and the necessary predetermined variables with relevant membership function, the entire process reflects the best system for supplier selection.

Keywords: Supplier selection, Fuzzy inference system (FIS), Rule viewer, Surface viewer.

1. Introduction

In today's extremely competitive environment, effective supply chain management (SCM) is a pivotal issue as all the companies are trying to attain the goals of low cost, high quality, flexibility and more customer satisfaction. The suppliers who offer products or services that match or exceed the need of business can be recognized as effective supplier. The supplier selection process deploys a tremendous amount of firm's financial resources. Optimization of the supplier selection process depends upon the effectiveness of following steps like identifying suppliers, soliciting information from suppliers, setting contract terms, negotiating with suppliers and evaluating suppliers. The supplier selection process has undergone significant changes like increased quality guidelines, improved computer communication and increased technical capabilities during the past twenty years. Recently a new dimension is being added in the supplier evaluation process which is providing product or service when it is required, by the concept of Just-In-Time (JIT) manufacturing strategies. The idea of forming an outsource system is meant to establish a dynamic organization through the synergetic combination of dissimilar companies with different core competencies to perform a given business project to achieve maximum degree of customer satisfaction.[2] The selection of suppliers includes both tangible and intangible factors and the decision becomes complicated by lots of criteria and sub-criteria. There are huge numbers of supplier evaluation attributes like price, quality, delivery time, service, performance history, reliability, capacity etc. and managers, however, often need to make tradeoffs on these attributes.[1] In today's global economy, enterprise are increasingly striving to develop long-term strategic partnership with a few competent and innovative suppliers and collaborates with them in non-core process outsourcing in order to improve organizational performance and generate long-term competitive advantage. Today the average U.S. manufacturer spends roughly half its revenue to purchase goods and service which makes a company's success dependent on their interactions with suppliers. [3] So supplier should be selected based on how their actions will impact all the performance and competitive elements of the supply chain. On the other hand, academics and practitioners alike have recently shown interest of working with the concept of the optimization of supplier selection and business evaluation process in doctoral research. [4]

Organizations are looking for those manufacturers who can produce the goods with good qualities, low price and can deliver the goods on shorter lead time. In most of the cases manufacturers are failed to deliver the goods on due time because of the unfaithful supplier. There are cases when suppliers are delivering raw materials on due time but their quality is questionable. So manufacturers should be very careful of selecting the suppliers. Tremendous numbers of research are going on regarding supplier selection. Previously developed supplier selection methods can be classified in four major types: rating/linear weighting, total cost approaches, mathematical programming and statistical approaches.[5] Linear weighting method is the most common method in practice, assigns different weights to a number of criteria and the supplier with the best weighted total score is selected.[6] Mathematical programming models can optimize the explicitly stated objective and proved more effective than the linear weighting method.[7] In recent research works, the combination of these two models is being used widely. There are some works where linear programming and analytical hierarchy process (AHP) are being integrated

* Corresponding author. Tel.: +88-01676260936
E-mail address: pritom.ipe08@gmail.com

to choose best supplier and to assign the optimum order quantity among selected suppliers.[8] Later AHP and preemptive goal programming based multi-criteria-decision-making (MCDM) methodology are being integrated and which are being proved to be very effective to satisfy capacity constraint.[9] The most recently developed method is Fuzzy goal programming approach which considers multiple objectives and deals with some of the parameters that are fuzzy in nature.[7]

During recent years, how to determine suitable suppliers in the supply chain has become a key strategic consideration. However, the nature of these decisions usually is complex and unstructured. In general many quantitative and qualitative factors such as quality, price, flexibility and delivery performance must be considered to determine suitable suppliers. In this method linguistic values are used to assess the ratings and weights for these factors. These linguistic ratings can be expressed in fuzzy numbers or fuzzy logic. Since human judgments including preferences are often vague and cannot estimate his preference with an exact numerical value. Fuzzy logic is a form of many-valued logic or probabilistic logic which deals with this decision vagueness. In contrast with traditional logic theory, where binary sets have two valued logic; true or false, fuzzy logic variables may have a truth value that ranges in degree between 0 to 1.Fuzzy logic has been extended to handle the concept of partial truth, where the truth value may range between completely true and completely false. Fuzzy theory can be collaborated with linear programming problems with a fuzzy objective and fuzzy constraints.[10] There are different ways to express fuzzy logics like trapezoidal or triangular fuzzy members or Gaussian membership functions. But most newly developed one is fuzzy inference system (FIS) which is a calculative decision making tool where both qualitative and quantitative factors are calculated in a probabilistic manner. FIS based works are not randomly used but there are some research works are available. Where there is a probabilistic result FIS are for accurate result. It is not easy to select an effective supplier because all the suppliers must be judged against some predetermined criteria. In these types of situations fuzzy inference system (FIS) is very effective because it considers the relationship between the criteria themselves; criteria and alternatives. In traditional approach all the supplier have been ranked in a fixed scale for all criteria and the supplier who achieves the highest score will be selected. But it has a serious limitation of not considering the weight of the selected criteria. To overcome this limitation Fuzzy Logic Toolbox built on MATLAB is used which provides tools to create and edit fuzzy inference systems within the framework of MATLAB. FIS utilizes the concept of fuzzy logic to transfer the expert's evaluation of these supplier selection criteria into a value which represents the acceptance probability. This developed approach considers a number of different unique criteria and the relationship between these criteria that may have significant effect on selection process and for which the chances of diverting the decision into the wrong direction which is considered as the most serious problem in the traditional approach has been eliminated.

2. Methodology

Supplier selection is the process by which the buyer identifies, evaluates and contracts with suppliers. The appropriate supplier selection is indeed a very tough job. In this paper supplier selection procedure is accomplished by completing the following steps.

2.1 Data collection

Data collection is the process of gathering information about alternative suppliers. Here both primary and secondary data are being collected. By direct interviewing, questioning some predetermined questionnaire and observing all alternative suppliers are the way followed for gathering primary data. By going through the previous history and published or unpublished reports of the suppliers, secondary data are being collected.

2.2 DoE for finding out important criteria

Design of Experiment (DoE) is a structured, organized method that is used to determine the relationship between different criteria affecting a process and the output of the process. DoE involves designing a set of ten to twenty experiments, in which all the relevant criteria are being varied systematically. The numbers of supplier evaluation criteria are being reduced by DoE according to the severity of their effect on selection process which is being done to make the process less time consuming and effective.

2.3 Measuring the acceptance probability using FIS

Fuzzy inference is the process of formulating the mapping from a given input to an output using fuzzy logic. The mapping then provides a basis from which decisions can be made. The following usual steps are being needed to accomplish for supplier selection using FIS.

- Input fuzzification: This step is to take the inputs and determine the degree to which they belong to each of the appropriate fuzzy sets by Gaussian Membership function.
- Antecedent matching: Here necessary rules have been made for supplier evaluation. Once the input has been fuzzified, the degree to which each part of the antecedent has been satisfied for each rule will be known.
- Rule fulfillment: A consequent of a rule is a fuzzy set represented by a membership function. In this step, the consequent is reshaped using a function associated with the antecedent.
- Consequent aggregation: Here all the rules have been combined in some manner in order to make a decision. Aggregation is the process by which the fuzzy sets that represents the output of each rule are combined into a single fuzzy set.
- Output defuzzification: Taking fuzzy set as input, defuzzification outputs a crisp value, which is

suitable for analysis and control. Actually acceptance probability of alternative suppliers is being calculated here.

1.4 Experimental Tools and Data

In this paper Fuzzy Logic Toolbox built on MATLAB is used which provides tools to create and edit fuzzy inference systems within the framework of MATLAB. The toolbox also provides Graphical User Interface (GUI) tools for building, editing and observing FIS in the fuzzy logic toolbox. There are five primary GUI tools: FIS Editor for displaying general information about FIS, Membership Function Editor for defining the degree of an element's membership in a fuzzy set which is being done by selecting qualitative range (worst, bad, good and best) for each supplier evaluation criteria, Rule Editor for constructing necessary supplier evaluation rules, Rule viewer for observing the changes in the result which have been occurred due to the small change in the input data and Surface viewer for showing relationship among two distinct criteria and the result, which represents the weight of those criteria.

3. Computational Study

Initially 25 different criteria have are been selected but all those criteria do not have the same effect on supplier evaluation method. By applying Design of Experiment (DoE) total number of criteria is being reduced to nine and these selected nine criteria affects the process most. This study is carried out for the supplier selection of 'Brass Metal' of RFL Industry and from previous data it is been found that there are 9 potential candidates for supplying this metal. Table1shows all the 9 selected criteria and the relative score of each candidate against these criteria which have been collected from previous data. Here 'S1' represents 'Supplier 1' and so on.

Table 1: Checklists for suppliers

Criteria	S1	S2	S3	S4	S5	S6	S7	S8	S9
Wastage	8	5	5.6	9	7.5	9	10	4	8
Ductility	10	9.5	8	7	7	7.8	9	8	8
Fluidity	7	7	9	8	6	7	6.5	9	10
Hardness	8.6	9	8	9	6	8.3	4	8	7.4
Responsiveness	7	6	7	8	7	8	7.8	9	5
Supplier Location	8	8	8	5	7	9	6	9.5	6
Technical Capabilities	7	8	7	8	9	6	7.9	7	8
Cost Effectiveness	5	7	9	6	6	8	9.2	6	7
Reputation	6	7	4	9	8	6	10	7.6	9

By using MATLAB software at first the input variables are inserted and the input variables are divided in to four ranges: Worst, Bad, Good and Best by Gaussian membership function. The input variables are the relative scores of the alternative suppliers against those selected criteria collected from previous data. Again by using the Gaussian membership the output variables which represent the process capability are being divided into seven ranges: Not Preferable (NP), Less than Equally Preferable (LEP), Equally Preferable (EP), Mutually Preferable (MP), Strongly Preferable (SP) and Very Strongly Preferable (VSP).

For calculating the acceptance probability of the alternative suppliers 65 different rules have been created and these rules are being created by establishing relations among all the selected criteria for each individual alternative supplier. The samples of rule building logics are as following:

- If (Wastage is Best) and (Ductility is Best) and (Fluidity is Best) and (Hardness is Best) and (Responsiveness is Best) and (Supplier Location is Best) and (Technical-Capabilities is Best) and (Cost_ Effectiveness is Best) and (Reputation is Best) and Then (Result is VSP)
- If (Wastage is Worst) and (Ductility is Worst) and (Fluidity is Worst) and (Hardness is Worst) and (Responsiveness is Worst) and (Supplier location is Good) and (Technical-Capabilities is Good) and (Cost_ Effectiveness is Good) and (Reputation is Good) and Then (Result is SP)

For example the relation among the scores of supplier 1 for all selected criteria will support any of the built 65 rules and thus transforming the output of that selected rule for supplier 1 into numerical value, acceptance probability will be calculated by Rule Viewer.

4. Result & Discussion

In this study nine suppliers are primarily selected to evaluate in FIS base analysis. These suppliers are evaluated on the basis of nine criteria and all these criteria do not affect the result evenly. To understand this effects surface viewer is a must. The Surface View is a three dimensional view which represents the relationship among two inputs and the results. The relation of Cost Effectiveness and Fluidity of Material with the Result is shown in Fig.1:

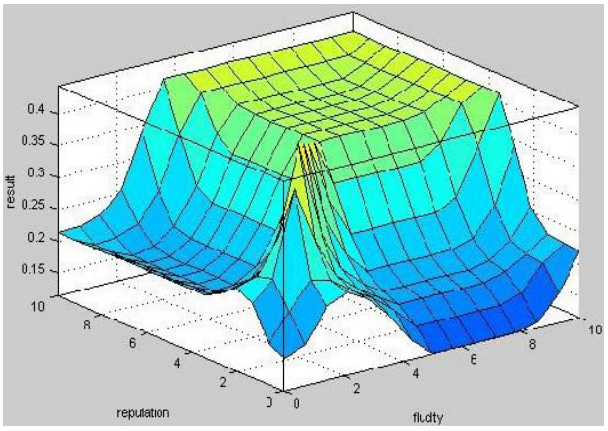

Fig.1: Surface Viewer (Cost Effectiveness and Fluidity with Result)

From the surface viewer it is seen that with the step wise increase of Cost effectiveness and Fluidity of Material, the result is also increased in ruled manner. It is also very helpful to understand the effect of a particular criteria on the result whether the effect is less or more than the other criteria.

In the Rule Viewer interface of MATLAB the score of each supplier against all the selected 9 criteria collected from previous data are put and thus the acceptance probability of all the alternative suppliers are calculated. For all the 9 suppliers the evaluation is performed by changing the value of input in the Rule Viewer interface to judge the efficiency of Rule viewer.Fig.2 is showing the Rule Viewer interface and acceptance probability which is 0.416 for supplier 1.

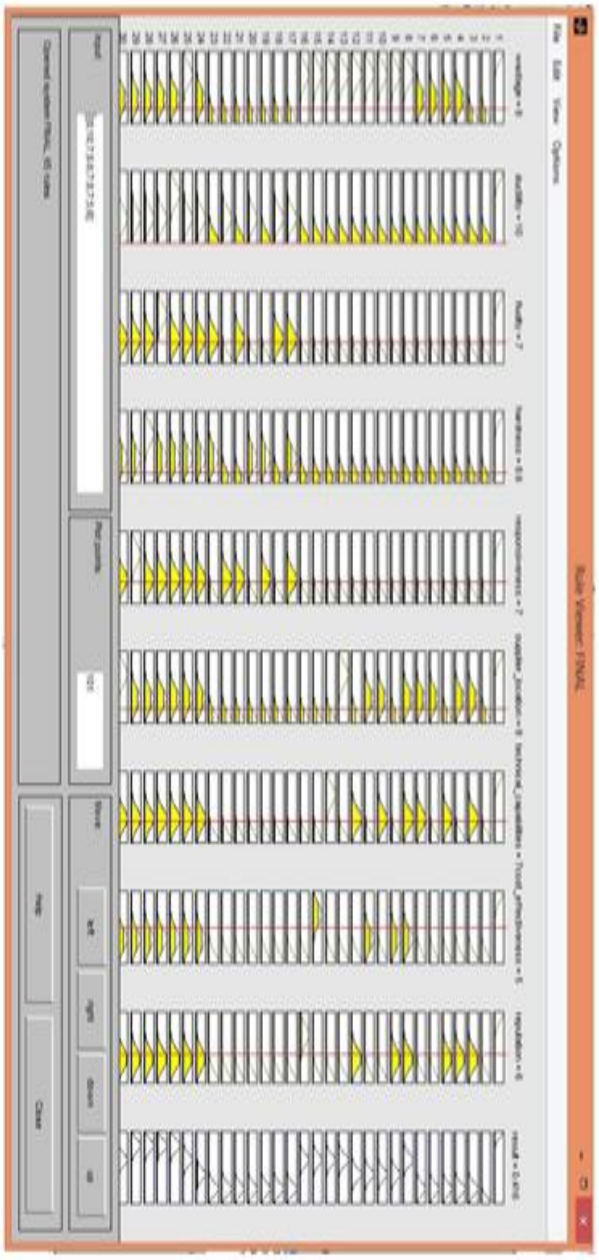

Fig.2: Rule Viewer for Supplier 1

In this study nine suppliers are selected to evaluate in FIS base analysis. Here suppliers are both judged with traditional approach and Fuzzy Inference System (FIS). The comparison between the results of these approaches is also shown. Table 2 shows the score calculated by traditional approach and acceptance probability calculated by FIS of each supplier.

Table 2: Score and Acceptance Probability of Suppliers

Supplier	Traditional Score	Acceptance Probability
S1	66.6	.416
S2	66.5	.419
S3	65.6	.430
S4	69	.492
S5	63.5	.438
S6	69.1	.488
S7	70.4	.438
S8	68.1	.487
S9	68.4	.438

In traditional system “Supplier 7” is selected for obtaining best score. In Fuzzy Inference System “Supplier 4” is selected for obtaining best acceptance probability which is .492 or 49.2%. From the research work it is become practical that there is a great variation between Traditional an FIS based work. Using FIS the calculative probability of acceptance is perfect on the basis of fuzzy logic, because these kind of qualitative factors are conveniently and correctly calculated only in Fuzzy Inference System. The rules are quite sensitive in the sense that a small amount of variance in the input will cause significantly different inference consequence, due to the crisp value. It indicates that FIS provides the facility of understanding the changes in the result by changing the value of all or some of the input variables. Traditional approach is quiet simple because here the final score of a particular supplier is the summation of the scores of that supplier against all the nine criteria. In this approach the weights of all the criteria are considered equal but it is not the true case. But FIS calculates and compares the weights of all the criteria and uses them in the calculation of acceptance probability. So the result becomes more accurate and more reliable.

5. Conclusion

Trough out this paper, an efficient approach for the evaluation technique of the best supplier selection based on readily available information and knowledge of experience is been accumulated. The developed approach considers a number of different unique factors that may have significant effect on selection process and utilizes the concept of fuzzy logic to transfer the experts’ evaluation of these factors into a value, representing the acceptance probability. The graphical

user interface (GUI) of MATLAB is used to determine the probability of acceptance for each supplier by using fuzzy logic. The works are been made more simple and attractive by the use of GUI tools. The FIS approach is been proved very efficient because it successfully considers the qualitative factors which is in linguistic form as well as quantitative factors.

REFERENCES

[1] G.W. Dickson, An approach of vendor selection system and decisions, Journal of purchasing, Vol. 2, No. 1, pp.5-17,(1996).

[2] K.L. Choy, W. B. Lee, A generic supplier management tool for outsourcing manufacturing, Supply Chain Management: An International Journal, Vol. 8, Issue 2, pp140 – 154, (2003).

[3] Beil Damian, Supplier selection, Stephen M. Ross School of Business, July 2009.

[4] Garfany Reza Mohammady, Supplier selection and Business process improvement, Doctoral Program in Business Creation, Strategy and Management, Department of Business Economics, Faculty of Economics and Business Studies, UniversitatAutonoma de Barcelona, 2004-2005.

[5] Z. Degraeve, E. Labro, F. Roodhooft, An evaluation of vendor selection models from a total cost of ownership perspective, European Journal of Operation Research, vol. 125, pp 34-58,(2000).

[6] F. Roodhoft, J. konigs, Vendor selection and evaluation: an activity based costing approach, European journal of Operation Research, vol. 96, no. 1, pp 97-102, (1997).

[7] M. Kumar, P. Vrat, R. Shankar, A fuzzy goal programming approach for vendor selection problem in a supply chain, Computers and Industrial Engineering, vol. 46, pp 69-85, (2004).

[8] S. H. Ghodsypour, C. O'Brain, A decision support system for supplier selection using an integrated analytic hierarchy process and linear programming, International Journal of Production Economics, Vol. 56-57, pp 199-212, (1998).

[9] G. Wang, S. H. Huang, J. P. Dismukes, Product driven supply chain selection using integrated multi-criteria decision making methodlogy, International Journal of Production Economics, vol. 91, pp 1-15, (2004).

[10] H. J. Zimmermann, Description and Optimization of Fuzzy Systems, International Journal of General Systems, Vol. 2, pp 209-215, (1976).

ICMIE-PI-140349

Modeling Progressive Damage and Failure for Polymer-Matrix Composites

*Alma Leanos, Md Shariful Islam and Pavana Prabhakar**
Department of Mechanical Engineering, The University of Texas at El Paso, TX-79902, USA

ABSTRACT
A model to predict the damage evolution and failure in unidirectional fiber-reinforced polymer-matrix composites (PMC) is developed using CCM-Schapery-Crack Band theory. Polymer matrix progressive damage is modeled using Schapery Theory (ST), which is later extended up to failure in order to account for more catastrophic failure mechanisms. The degrading elastic parameters of the fiber-reinforced PMC are obtained as a function of damage to finally determine the amount of damage associated with a PMC under uniaxial, biaxial, multiaxial and combined transverse/axial-shear loading.

Keywords: Polymer Matrix Composites, Damage Mechanics, Finite Element Method, Progressive Damage.

1. Introduction

In the last two decades, the advancement of composite materials has been generating technological and economic improvements. Advanced composite materials have been used in aircrafts, automobiles, industrial machinery, sporting goods and in many other applications. These applications require high-performance constituents, e.g. carbon fibers, glass fibers, polymers, ceramics, metals. Therefore, to assure the efficiency of these composite materials, a progressive damage and failure analysis has to be performed. According Pankow [1] the manufacturing of textile composite materials is becoming more economically feasible. The production of large scale composite structures has been continuously increasing in recent years. Therefore, as stated by Cox and Yang [2] analytical predictions of damage and failure are needed in the early stages of the design, reducing time and money spent on manufacturing the material to test the design.

According Pineda [3] the lay-up and directionality of the load applied to a fiber-reinforced PMC determine the global damage and failure mechanisms generated in the PMC. The extent of damage in PMCs is dependent on various material parameters, of which the fiber volume fraction, matrix and fiber properties along with the type of loading have shown to be critical. The influence of these parameters on the damage in fiber reinforced PMCs have been investigated by several researchers. Most of the non-linearity observed can be attributed to the damage evolution in the polymer matrix. Fiber breaking in PMCs is rather abrupt, whereas other damage mechanisms like microcracking, fiber-matrix debonding, transverse cracking, etc. are progressive in nature. For example, tensile loading in the transverse direction may cause microcracks or voids to grow resulting in transverse cracks[4], Schapery[5]. Interlaminar separation, also known as delamination, may occur when transverse cracks intersect an interface between two adjacent layers within a laminate[6], rendering the laminate weak in shear and transverse loading. Another types of loading is compression where the degradation of the polymer matrix has an influence on the failure of the laminate. Under compressive loading along the fiber direction, shear strains are generated in the matrix due to excessive rotation of fibers causing the matrix to damage, and vice-versa. The laminate fails in the form of kink band or micro-buckling [7-10]. Therefore, it is very critical to account for the damage occurring in the polymer matrix in order to determine the extent of damage accumulation in the fiber-reinforced PMC.

Therefore, the purpose of this paper is to model progressive damage and failure to determine the amount of damage associated with a unidirectional fiber-reinforced PMC under any load configuration. To predict the progressive damage of the PMC, this model is based on a thermodynamically-based work potential theory developed by Schapery[11]. Past publications have used crack density, geometry, strain energy release rate, and other crack models to predict damage evolution [12-14]. The progressive damage in PMC is accounted by matrix micro-damage, which yields to more severe failure mechanisms. Therefore, ST has been extended up to failure in order to account for the maximum strain and amount of damage at which the fiber-reinforced PMC completely fails.

2. Methodology

2.1 Progressive Damage

Failure initiation in the PMC is given by its critical strains, which are obtained by physical experiments of a small-scale PMC. Elastic properties of the fiber and matrix, as well as the fiber volume fraction and matrix Poisson's ratio are known variables of the model. The fibers are modeled as elastic transversely isotropic material, which properties are shown in Table. 1. Likewise, the polymer matrix is modeled as elastic-plastic isotropic material, therefore, the equivalent stress-strain response is nonlinear, as shown in Fig. 1. This non-linearity in the stress-strain response of the polymer matrix is the representation of micro-structural damages that manifest progressive damage in the composite, reducing its stiffness. In other words, progressive damage is represented as the region before the critical strain and it is accounted by matrix microdamage, i.e. microcracking,

* Corresponding author. Tel.: +1 (915) 747-5863
E-mail address: pprabhakar@utep.edu

void growth, fissuring, shear banding and fiber-matrix debonding.

Table 1 Fiber Properties.

E_{11} (GPa)	$E_{22}=E_{33}$ (GPa)	$\upsilon_{12} = \upsilon_{13} = \upsilon_{23}$	$G_{12}=G_{13}$ (GPa)	G_{23} (GPa)
276	8.76	0.35	12.0	3.244

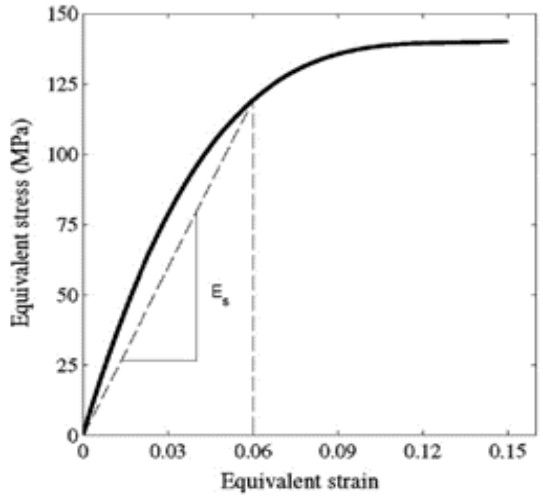

Fig.1. Equivalent stress-strain response of the polymer matrix.

According Pineda [3] the response of a composite in compression (axial or transverse) can be very different from that in tension. This means, it is easier for cracks to advance more in tension than in compression. Transverse cracks in compression progress under pure mode 2 and 3 or mixed mode conditions and there are other mechanisms associated to the failure of the PMC, which are fiber kinking and microbuckling. For this reason compressive loads are not taken into account in this model. As suggested by Sicking [15], it is assumed that the material is elastic and there is no plastic deformation upon unloading. However, plastic deformation can be incorporated to the model as stated by Schapery [11]. The concentric cylinder model (CCM) is used to determine the upscaled PMC mechanical properties, utilizing only the basic constituent (fiber and matrix) properties, as explained in the article by Prabhakar and Waas[16].

The CCM equations corresponding to the elastic regime are extended into the inelastic regime, to homogenize the lamina beyond the elastic regime, using a series of values of secant moduli of the pure matrix material as opposed to a single value of elastic modulus. That is, `$E_m$' of the matrix is not a single value, but a series of values `E_s', where `$E_s$' is the secant modulus of the pure matrix as shown in Fig. 1. By substituting a series of values of `Es' in expressions for E_{11}, E_{22}, G_{12}, G_{23} obtained from the CCM, we obtain the corresponding series of values for these constants as a function of stress (or strain), based on the assumption of stress based or strain based derivation of the CCM equations. Here, E_{11} (fiber dominated) is strain based, and E_{22}, G_{12} and G_{23} (matrix dominated) are stress based calculations. This implies that matrix dominated properties are expressed as a function of stress; while fiber dominated properties are expressed as a function of strain.

2.2 Schapery Theory

Schapery Theory (ST) accounts for the progressive damage in the matrix of the PMC. According to ST, the total work potential, W_T, is equal to the sum of the recoverable work potential (elastic region), W, and the dissipated (irrecoverable) energy, W_S [11].

$$W_T = W + W_S \tag{1}$$

Schapery (1989, 1990) shows that:

$$\frac{\partial W_T}{\partial S_m} = 0 \tag{2}$$

In general, S_m accounts for any damage that a composite may experience. Therefore, W_s will be only function of a single value of S (W_s=S). Thus, equation 1 yields:

$$W_T = W + S \tag{3}$$

Since every time a composite material is loaded it undergoes structural changes (damage), thus, the mechanical properties of the fiber-reinforced PMC are affected. Likewise, the recovered energy is obtained once the material is unloaded and it follows the elastic path. In other words, dissipated energy S is shown to be the area above the unloaded line, while the elastic strain energy density W is the area below this line (triangular shaded area), as shown in Fig. 2.

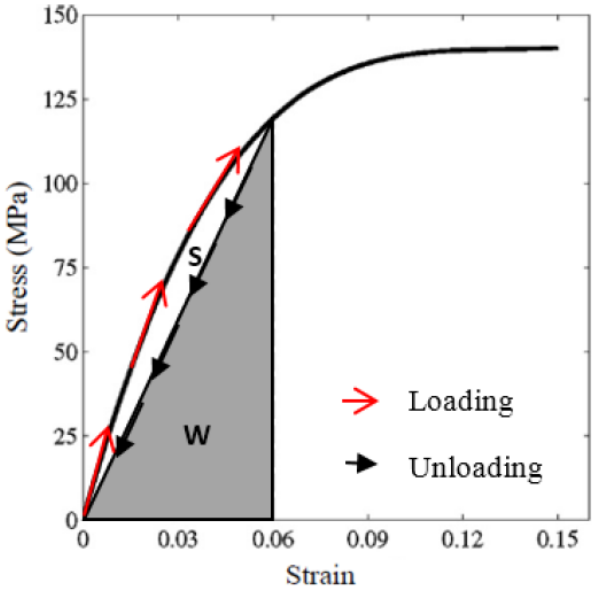

Fig.2. Stress-strain curve showing the elastic (*W*) and irrecoverable (*S*) portions divided by unloaded line.

Differentiating with respect to S, we have:

$$\frac{\partial W}{\partial S} = -1 \quad (4)$$

It is known that the amount of energy dissipated cannot be recovered, therefore:

$$S \geq 0 \quad (5)$$

Moreover, since the fiber-reinforced PMC is a unidirectional lamina, it is considered to be a transversely isotropic material and from the stress-stress relation $\{\sigma\} = [C]\{\varepsilon\}$ or simply $\sigma_i = C_{ij}\varepsilon_j$ for i, j =1,2,3…6, the elastic strain energy can be related to the elastic constantsC_{ij}.

$$W = \frac{1}{2}C_{11}\varepsilon_{11}^2 + C_{12}(\varepsilon_{11}\varepsilon_{22} + \varepsilon_{11}\varepsilon_{33}) + \frac{1}{2}C_{22}(\varepsilon_{22}^2 + \varepsilon_{33}^2) + C_{23}(\varepsilon_{22}\varepsilon_{33}) + \frac{1}{2}C_{44}\varepsilon_{23}^2 + C_{55}(\varepsilon_{12}^2 + \varepsilon_{13}^2) \quad (6)$$

Where:

$$C_{11} = \frac{E_{11}^2(\nu_{23}-1)}{\Delta} \quad (7)$$

$$C_{12} = \frac{-E_{11}E_{22}\nu_{12}}{\Delta} \quad (8)$$

$$C_{22} = \frac{E_{22}(E_{22}\nu_{12}^2 - E_{11})}{(1+\nu_{23})\Delta} \quad (9)$$

$$C_{33} = \frac{-E_{22}(E_{22}\nu_{12}^2 - E_{11}\nu_{23})}{(1+\nu_{23})\Delta} \quad (10)$$

$$C_{44} = 2G_{23} \quad (11)$$

$$C_{55} = 2G_{12} \quad (12)$$

$$C_{66} = C_{55} \quad (13)$$

$$\Delta = 2E_{22}\nu_{12}^2 + E_{11}(\nu_{23} - 1) \quad (14)$$

Substituting Equation 6 into Equation 4, the derivative of the elastic strain energy with respect to the damage has to be equal to -1. It should be noted that now the C_{ij} are functions of the damage parameter (S). Therefore, we have,

$$\frac{\partial W}{\partial S} = \frac{1}{2}\frac{\partial C_{11}}{\partial S}\varepsilon_{11}^2 + \frac{\partial C_{12}}{\partial S}(\varepsilon_{11}\varepsilon_{22} + \varepsilon_{11}\varepsilon_{33}) + \frac{1}{2}\frac{\partial C_{22}}{\partial S}(\varepsilon_{22}^2 + \varepsilon_{33}^2) + \frac{\partial C_{23}}{\partial S}(\varepsilon_{22}\varepsilon_{33}) + \frac{1}{2}\frac{\partial C_{44}}{\partial S}\varepsilon_{23}^2 + \frac{\partial C_{55}}{\partial S}(\varepsilon_{12}^2 + \varepsilon_{13}^2) = -1 \quad (15)$$

Where, the critical strains of the fiber-reinforced PMC are constant and the microdamage functions (degrading elastic constants as a function of damage) are second order differential equations, so they can be solved for the damage evolution *S*.

2.3 Extended Schapery Theory

More catastrophic failure mechanisms due structural changes occur once the critical strain of the PMC is reached and the PMC stiffness decreases drastically until the PMC completely fails, as shown in Fig. 3. The critical strain is characterized as the damage initiation point, where the tangent stiffness tensor is not positive anymore and there is some damage located into the smallest length scale of the finite element volume (single element) [17]. Since the shaded area of the stress-strain response of a PMC (Fig. 3) describes the energy per unit volume dissipated during the failure process, the total amount of energy dissipated in the element tend to zero as the element length scale also approaches zero, leading to pathological dependence of the solution on the mesh density.

Under transverse tension and shear loading some transverse cracks might appear on the matrix. These transverse cracks are more severe than matrix microdamage because they are growing abruptly rather than progressive. Therefore, transverse cracking and fiber breakage are common failure mechanisms in fiber-reinforced PMC. The Crack Band model is used to manifest these failure mechanisms. This model relates the fracture toughness of the material to a characteristic finite element length scale, both are assumed to be constant throughout the model to overcome pathological mesh dependency. This means that the total strain energy release rate upon complete failure (shaded area in Fig. 3) is always equal to the fracture toughness of the material by scaling the stiffness, which is assumed to decrease linearly after the critical strain, to a characteristic length.

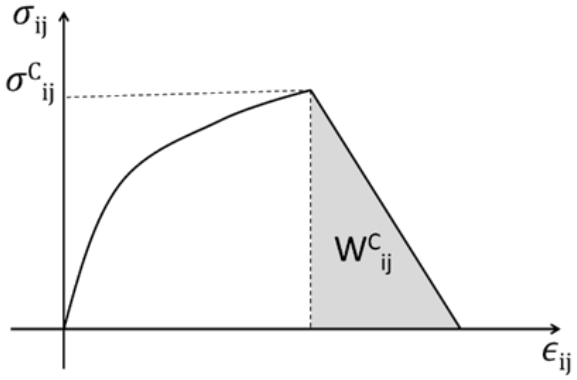

Fig.3 Schematic representation of stress-strain response of fiber-reinforced PMC up to complete failure.

3. Results and Discussions

The stress–strain response for the homogenized lamina of PMC are obtained by the CCM model and the nonlinearity of E_{22}, G_{12} and G_{23} is verified and it is attributed to progressive damage of the polymer matrix. It is important to state that the axial response of the PMC is linear since it depends mainly on the axial stiffness of the fibers, which is very high compared to the stiffness of the polymer matrix. Otherwise, the transverse and shear axial responses are dominated by the behavior of the matrix, this is the reason of the non-linear stress-strain response. Then, the ST has been extended up to the failure state, at which the maximum strain supported by the PMC is reached and it completely fails, as seen in Fig. 4 (a) and (b). Since the stiffness in the 1 direction is much higher compared to the other directions, Fig. 4 (b) reproduces a better view of the non-linear stress-strain responses.

The elastic constants C_{ij} are plotted against the amount of damage (S), as shown in Fig. 5. black curves, while the fitted curves (second order polynomials) are colored. It can be observed in Fig. 5. (a) that the elastic constant in the 1 direction has much higher values than the other constants. Then, to better visualize these other constants, the plot is zoomed and shown in Fig. 5 (b). Similarly, Table 2, shows the results obtained for different configurations of strain loading, i.e. uniaxial, biaxial, multiaxial and combined axial/transverse-shear loading.

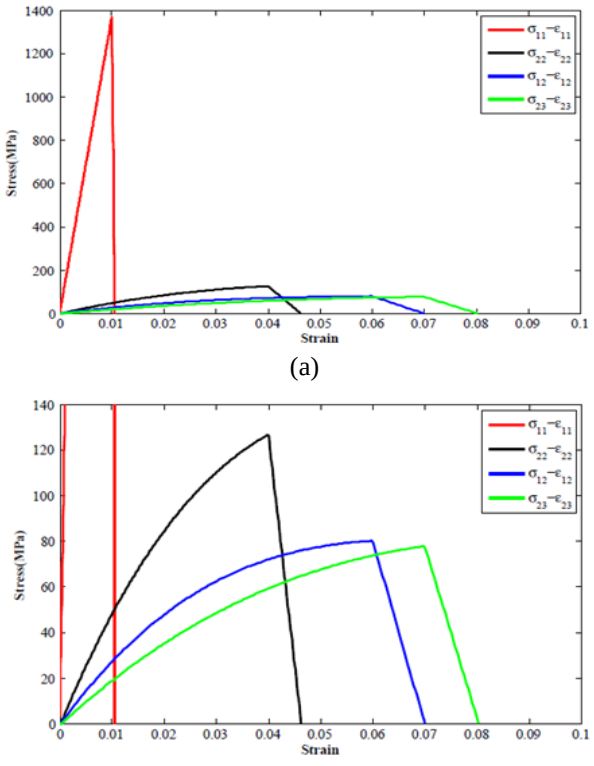

(a)

(b)

Fig.4 Stress-strain responses of a homogized lamina up to failure. (a) Complete representation of the responses (b) Zoomed plot to visualize nonlinearity.

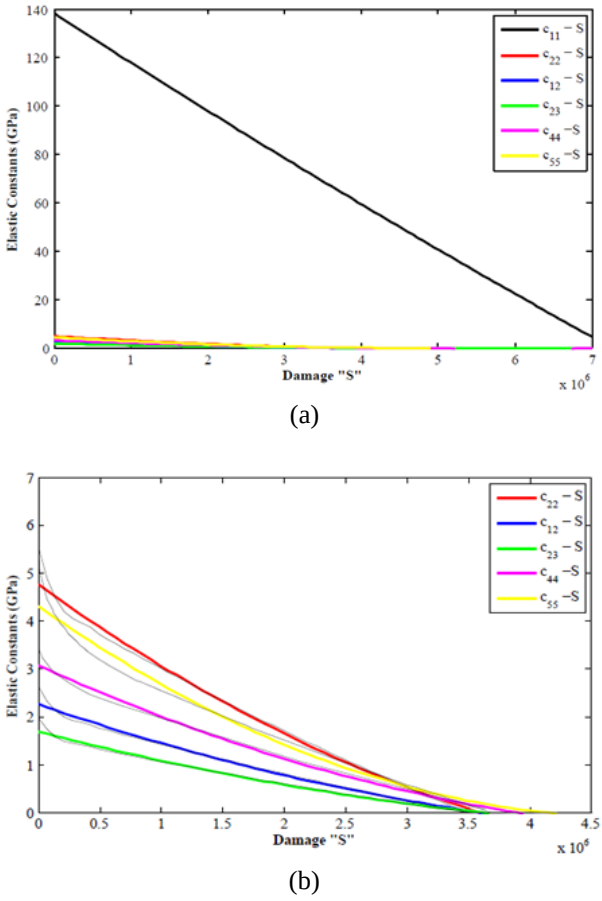

(a)

(b)

Fig.5 Elastic constants (*Cij*) vs amount of damage (*S*). (a) Complete representation (b) Zoomed plot to visualize a comparison of original plots and approximated curve.

Table 2 Results obtained for amount of damage (*S*) for different configurations of strain applied.

ε_{11}	ε_{22}	ε_{33}	ε_{12}	ε_{23}	Amount of Damage
0.005					0
	0.03				1.43E3
	0.04				1.95E5
	0.05				2.80E5
	0.06				3.3E5
	0.06	0.03			3.56E5
0.05	0.06	0.03			3.89E5
				0.05	3.4E5
			0.03		3.86E5
	0.03		0.03		3.92E5
	0.03		0.03	0.05	3.95E5
			0.05		4.17E5

4. Conclusions

A thermodynamically-based work potential theory developed by Schapery was presented to account for the effects of progressive matrix microdamage in fiber-

reinforced PMC. Shapery Theory was expended up to the failure state to capture more catastrophic failure mechanisms as transverse cracking and fiber breakage. This model was based in the CCM and Crack Band models, which were useful to determine the homogenized mechanical properties of the fiber-reinforced PMC and to relate the fracture toughness of the PMC with a finite element characteristic length scale, respectively. It is concluded that the amount of damage is bigger for multiaxial and combined axial/transverse-shear strain loading configuration. For uniaxial and biaxial strain, the amount of damage is small if this value is less than the critical strain of the PMC in the corresponding direction. However, damage increases drastically once the critical strain is reached. A finite element computational model can be developed to verify these results, which is currently being studied.

NOMENCLATURE

E_{ij} : Stiffness, GPa
ε_{ij} : Strain
υ_{ij} : Poisson's ratio
G_{ij} : Shear modulus, GPa
E_m : Elastic modulus of matrix, GPa
E_s : Secant modulus, GPa
W_T : Total work potential
W : Recoverable work potential
Ws : Dissipated energy
S : Damage parameter
Cij : Elastic constants

REFERENCES

1. Pankow, M.R., *The deformation response of three-dimensional woven composites subjected to high rates of loading.* 2010.
2. Cox, B. and Q. Yang, *In quest of virtual tests for structural composites.* Science, 2006. 314(5802): p. 1102-1107.
3. Pineda, E.J., et al. *A novel multiscale physics based progressive failure methodology for laminated composite structures*. in *Forty-nineth AIAA/ASME/ASCE/AHS/ASC structures, structural dynamics, and materials conference, Schaumburg, Illinois*. 2008.
4. McCartney, L., *Mechanics of matrix cracking in brittle-matrix fibre-reinforced composites.* Proceedings of the Royal Society of London. A. Mathematical and Physical Sciences, 1987. 409(1837): p. 329-350.
5. Schapery, R., *A theory of mechanical behavior of elastic media with growing damage and other changes in structure.* Journal of the Mechanics and Physics of Solids, 1990. 38(2): p. 215-253.
6. Talreja, R., *Multi-scale modeling in damage mechanics of composite materials.* Journal of materials science, 2006. 41(20): p. 6800-6812.
7. Fleck, N., *Compressive failure of fiber composites.* Advances in applied mechanics, 1997. 33: p. 43-117.
8. Fleck, N., L. Deng, and B. Budiansky, *Prediction of kink width in compressed fiber composites.* Journal of applied mechanics, 1995. 62(2): p. 329-337.
9. Schapery, R., *Prediction of compressive strength and kink bands in composites using a work potential.* International Journal of Solids and Structures, 1995. 32(6): p. 739-765.
10. Yerramalli, C.S. and A.M. Waas, *A failure criterion for fiber reinforced polymer composites under combined compression–torsion loading.* International Journal of Solids and Structures, 2003. 40(5): p. 1139-1164.
11. Schapery, R., *Mechanical characterization and analysis of inelastic composite laminates with growing damage.* Mechanics of composite materials and structures, 1989: p. 1-9.
12. Talreja, R., *Transverse cracking and stiffness reduction in composite laminates.* Journal of Composite Materials, 1985. 19(4): p. 355-375.
13. Dvorak, G.J., N. Laws, and M. Hejazi, *Analysis of progressive matrix cracking in composite laminates I. Thermoelastic properties of a ply with cracks.* Journal of Composite Materials, 1985. 19(3): p. 216-234.
14. Lee, J.-W., D. Allen, and C. Harris, *Internal state variable approach for predicting stiffness reductions in fibrous laminated composites with matrix cracks.* Journal of Composite Materials, 1989. 23(12): p. 1273-1291.
15. Sicking, D.L., *Mechanical characterization of nonlinear laminated composites with transverse crack growth*, 1992.
16. Prabhakar, P. and A.M. Waas, *Upscaling from a micro-mechanics model to capture laminate compressive strength due to kink banding instability.* Computational Materials Science, 2013. 67: p. 40-47.
17. Bazant, Z.P. and L. Cedolin, *Blunt crack band propagation in finite element analysis.* Journal of the Engineering Mechanics Division, 1979. 105(2): p. 297-315.

ICMIEE-PI-140353

CONCEPTUAL DESIGN OF A BUSINESS JET AIRCRAFT

Jannatun Nawar [1,], Nafisa Nawal Probha [2]*
Adnan Shariar [3], Abdul Wahid[4], Saifur Rahman Bakaul[5]
[1,2,3,4] Student, Department of Aeronautical Engineering, Military Institute of Science & Technology, Dhaka-1216,
[5] Associate Professor , Department of Aeronautical Engineering, Military Institute of Science & Technology, Dhaka-1216,

ABSTRACT
The modern jet transport is considered as one of the finest integration of technologies. Its economic success depends on performance, low maintenance costs and high passenger appeal and design plays a vital role in summing up all these factors. Conceptual design is the first step to design of an aircraft. In this paper a business jet aircraft is designed to carry 8 passengers and to cover a range of 2000 NM with maximum Mach No of 0.7 and with maximum ceiling of 29,000 ft. The conceptual design consisted of initial sizing, aerodynamics and performance analysis. Through trade studies and comparison with other business jet aircrafts a final model of the aircraft was built to achieve the requirements.

Key Words: Business jet, Conceptual design, Initial Sizing, Aerodynamics, Aircraft performance, Trade study.

1. Introduction

Airplane design is an art with scientifically approach. It requires both the intellectual engineering and sensible assumptions. Aircraft design is actually done to meet certain specifications and requirements established by potential users or pioneer innovative, new ideas and technology. Now-a-days business jet aircraft is one of the most popular forms of transport aircraft. A business jet is a jet aircraft designed to transport passenger and goods. It is also known as biz jet, executive jet or private jet. Biz jet is used by public bodies, government bodies and armed forces and used to parcel deliveries, transporting people and evacuation in case of casualties. This paper will illustrate about the conceptual design of a business jet.

Aircraft design has three distinct phases that are carried out in sequence. In chronological order, conceptual design, preliminary design and detail design. Conceptual design is the first step of designing aircraft. The main focus of this paper is to design a business jet transport aircraft conceptually. In conceptual design the configuration arrangement, size and weight and performance parameters will be calculated. The first thing required in a conceptual design is the design requirements which guide and evaluate the development of the overall aircraft configuration arrangement. In this paper we have tried to design gross weight, wing and tail geometry and some performance parameters with trade study.

Conceptual design is a series of activities which includes some basic question and answers. What requirements drive the design, what should it look like, what tradeoffs should be considered, what technologies should be used and do these requirements sale a viable and salable plane all these sums up conceptual design in a nutshell. This paper covers every aspects of conceptual design.

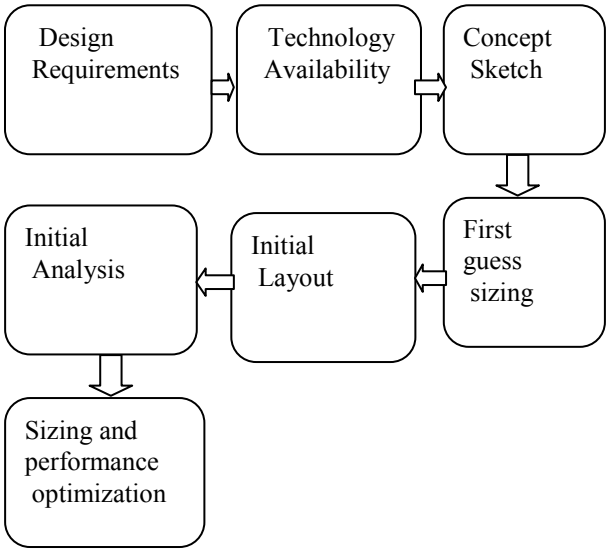

Fig 1: Block Diagram of Conceptual Design

2. Design Requirements

Mach no	0.7
Range	2000 NM
Maximum Ceiling	29,000 ft
Payload	8 pax
Endurance	30 min
Max g	+2.5, -1.2

3. Initial Layout Analysis

The actual design effort usually started with a conceptual sketch. This is the 'Back of a Napkin' drawing which gives a rough indication of what the design may look like. It first starts with a conceptual sketch.

Corresponding author: Squadron Leader Dr. Saifur Rahman Bakaul, Associate Professor, Military Institute of Science and Technology, Bangladesh. Tel.: +8801975104040, email: saif1833@yahoo.com, saif@ae.mist.ac.bd

3.1 Concept Sketch

A conceptual skecth is a rough skecth to show how the future design will look like. In this design a rough hand made skecth was first drawn as a initial sketch.

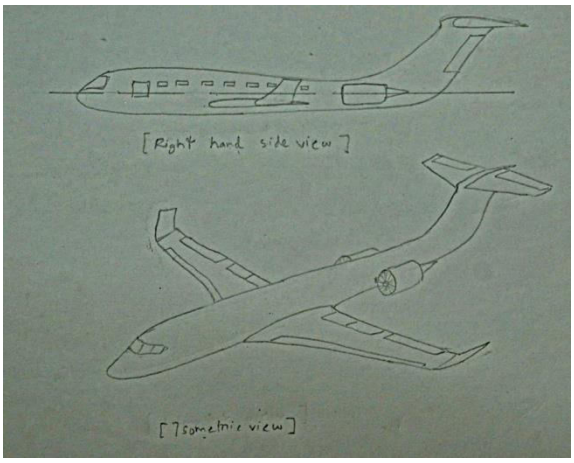

Fig.2: Initial Sketch

3.2 Initial Sizing

The conceptual design is used to estimate aerodynamics and weight fractions by comparison to previous design. In this paper first we estimated the required total weight and fuel weight to perform the design mission by 'Sizing' process.

3.3 Sizing from the Conceptual Sketch

Sizing is the most important calculation in aircraft design. It determines size of the aircraft, specially the take off-weight. Design take off gross weight can be calculated using the following equations,

$$Wo = \frac{Wcrew + Wpayload}{1 - \left(\frac{We}{Wo}\right) - \left(\frac{Wf}{Wo}\right)}$$

In this paper a jet for 8 passengers each of approximate 200 lbs, 2 crew members and 40 lbs of luggage for each passenger is considered. Fuel fraction is calculated based on the mission to be using approximations of the fuel consumption and aerodynamics.

3.4 Mission Profile

In this paper a simple cruise mission profile is considered as most transport and general aviation design use this profile. So there are five legs including takeoff, climb, cruise, loiter and landing. For warm up and take off, climb and landing we have taken weight fractions from the historical data.

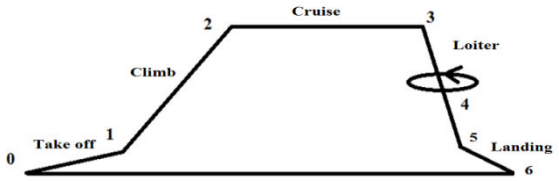

Fig 3: Mission Profile

Table.1: Historical mission segments weight fractions [1]

Mission Segment	Weight Fraction
Warm up and takeoff	0.970
Climb	0.985
Landing	0.995

For calculating weight fractions for cruise and endurance a Lift-to-Drag ratio which is a measure of the design's overall aerodynamic efficiency is needed .Using aspect ratio of 10.67 and from analyzing different business jet we have taken maximum Lift-to-Drag ratio as 23. Thus fuel fraction for cruise is 0.995 and for endurance is 0.991is found. An overall weight fraction of 0.8055is found and from this, takeoff gross weight is calculated 11035.624 lb. So it is a mid-sized business jet. Here the empty weight is 6439.16 lb and 2275.2146 lb of fuel is needed.

3.5 Engine Selection:

Design mach no is 0.7 and so analyzing both historical data and different jet aircraft High Bypass Turbofan engine. High BPR turbofan engine is used for high thrust and good fuel efficiency. Rolls-Royce/MAN Turbo RB193 .

4. Aerodynamics

Before designing layout, a number of parameters including aerofoil(s), the wing and tail geometries, wing loading as it affects the cruise speed, takeoff speed and landing distances, stall speed, handling qualities during all flight phases,

4.1 Aerofoil selection

(1)Camber aerofoil allows the airflow to remain attached have to be calculated. Thus it increases lift and reduces drag and also it produces lift at zero angle of attack. A five digit aerofoil analyzing different types of wing used so we used 65-2XX series is selected where last two digits define position of maximum camber. From calculation we have got the position of mean camber at .12 of mean chord i.e. 12%. Thus our aerofoil is NACA 65-212.

Fig 4: NACA 65-212 Aerofoil

4.2 Wing Geometries

(1)From different business jet and other transport aircraft historical trend the wing loading is 120 is found but considering different aerodynamic facts a wing loading of 80 is taken and so our wing area becomes 137.94 square feet. The relevant aspect ratio is 10.67 and so wing span is 38.35 ft.

(2)The maximum co-efficient of lift is 1.5. As wing sweep increases lateral stability, a leading edge sweep of 20 degree is taken. A twist angle of 3 degree to prevent tip stall is taken. Wing incidence angle is given 2 degree to minimize drag during cruise. As it is a subsonic aircraft so a positive dihedral of 5 is taken.

(3)Virtually all high-speed commercial transport aircraft are low wing so we have chosen a low wing aircraft as it gives us advantage for landing gear stowage.

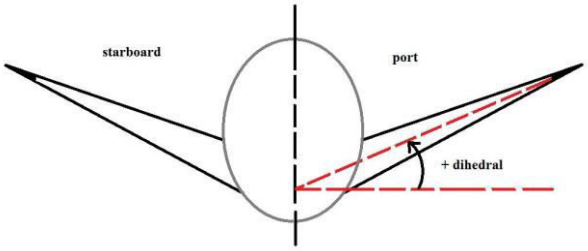

Fig 5: Low wing with dihedral

(4)We have chosen winglet as it increases lift-to-drag ratio by 20%. The following figure explains why winglet is chosen over the conventional wingtip.

4.3 Flap Selection

In this design double slotted fowler flap was used.

Fig 6: Fowler flap

From calculation, leading edge sweep angle is 20 degree. For flap maximum co-efficient of lift was calculated to be 2.82.

4.4 Stall Characteristics

For mach no 0.7, aerofoil thickness ratio of 14% is selected. So it is a moderately thick aerofoil where stall starts from leading edge.

4.5 Tail Geometries

(1)Tails are little wings and it provides for trim, stability and control. Here T-tail is considered as our tail arrangement not because of it is stylish but it allows the use of engines mounted in pods on the aft fuselage.

(2)Leading edge sweep of the horizontal tail is usually set 5 degree more than the wing sweep so it is 25 degree. For T-tail no aspect ratio and taper ratio needed for horizontal tail and for vertical tail taper ratio is 1 and aspect ratio is 0.8.

5. Landing Gear Arrangement

Today's most commonly used landing gear arrangement is 'tricycle gear'. So it is used with two main wheels aft of center of gravity, ahead of the main wheels.

As the aircraft is under 50,000 lb(11,036 lb) so two main wheels per strut will be used so we will get advantage in case of flat tire. The tires carries 90% the total weight of the aircraft so it is an important parameter. The diameter of the main wheels as 14.52 in and width is 9.12 in is calculated and the recommended tire pressure is 80 psi.

6. Fuselage Design

For a jet transport, fuselage length is 36.7 ft. Internal cabin system, aerodynamics related calculations etc are required to estimate Fuselage diameter. For rough estimation, taking circular fuselage, fineness ratio is 8 and diameter is 4.58 ft.

7. Vertical Stabilizer

From the historical data taper ratio for vertical stabilizer is 0.6-1.0[2] and the taper ratio considered is 1.0 in this design. T-tail reduces end plate effect by 5 percent. So tail volume coefficient is calculated 0.0855. From historical data, tail arm for aft mounted engine is about 45-50 %.[3] For a better design a tail arm should be as big as possible 50 % of fuselage length was taken and it was calculated to be 18.35 ft. Vertical stabilizer surface area was calculated to be 24.66 ft. square feet. Typical aspect ratio is 0.7-1.2. In this design a aspect ratio of 0.8; a higher aspect ratio was not chosen as increase in aspect ratio increases span which needs a stronger structure. Thus the weight will be increased so a lower aspect ratio was chosen.

8. Horizontal Stabilizer

Leading edge sweep for horizontal stabilizer is 5 degree greater than the sweep angle for wing. So it was taken as 25 degree. From statistical data tail volume coefficient for horizontal stabilizer is 1.00 but for clean air it was reduced 5% and taken as 0.95. Horizontal stabilizer surface area was calculates 27.25 square feet.

9 .Performance Analysis

Thrust-to-weight ratio directly associates the performance of the aircraft. It is not constant and it varies during flight as fuel burns. By analyzing historical data we estimated it for takeoff is 0.35 and

for cruise is .0434[4] and it was calculated using the following equation:

$$\frac{T}{W} = \frac{1}{(\frac{L}{D})_{cruise}}$$

From Oswald efficiency as .8[5] and using aspect ratio we calculated our co-efficient of drag is 0.1344. For a jet propelled aircraft to maximize range it has to fly at $C_l^{0.5}/C_d$ and the associated velocity can be calculated as 655 ft/sec and maximum range is 1975 NM which was calculated. Maximum climb angle calculated is 17 degree using the following equation:

$$sin\theta_{max} = \frac{T}{W} - \sqrt{4kC_{Do}}$$

And for maximizing this angle velocity needed is 310 ft/sec. The maximum rate of climb is,

$$V_{(\frac{R}{C})max} = \left(\frac{2}{\rho_\alpha}\sqrt{\frac{k}{3C_{Do}}}(\frac{W}{S})\right)^{.5} = 60\ ft/sec$$

Its associated velocity is 867 ft/sec. Maximum distance covered in a gliding path is 70 NM and associated velocity is 310 ft/sec. Maximum endurance is calculated to be 1.11 hrs and the velocity associated is 500 ft/sec. Maximum velocity is 1600 ft/sec which is much more than our required velocity. Stalling velocity is,

$$V_{stall} = \sqrt{\frac{2W}{\rho S C_L}} = 212 ft/sec$$

Takeoff distance was calculated to be 5100 ft and landing distance is 3445 ft.

10. Trade Study:

Trade study is an important part of conceptual design. It helps the designer to choose the best convenient design parameters. From the above trade study it can be seen that the best thrust to weight ratio will be 0.40 and wing loading will be 80.

Table.2: Trade study

Thrust to weight ratio	Wing Loading	Takeoff distance(ft)	Landing distance (ft)
0.30	80	6100	3444.4
0.35	80	5100	3444.4
0.40	80	5000	3444.4
0.35	85	5800	4255.9
0.35	75	5200	3825.8

11. V-n Diagram

V-n diagram is a very important diagram for both the designers and the pilots. It is actually a graph showing the limiting factors of design and flying. It shows stall region, corner velocity, maximum velocity, maximum and minimum load factor etc.

Table.3: Different factors of V-n diagram

Maximum g	+2.5, -1.95
Maximum velocity	725.9 ft/sec
V_{NE}	871 ft/sec
Maximum lift coefficient for positive load factor	2.82
Maximum lift coefficient for negative load factor	1.5
Ceiling	29,000 ft

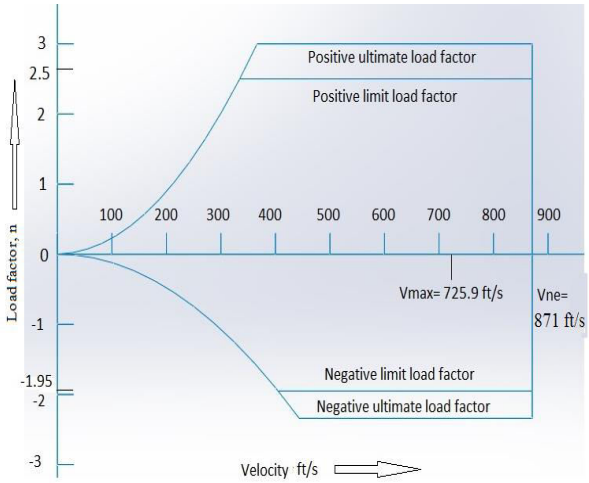

Fig 7: V-n diagram

12. Final Model

After all the calculations and the estimations done a final aircraft model was designd which is shown in the next page with the help of Solid Works software.

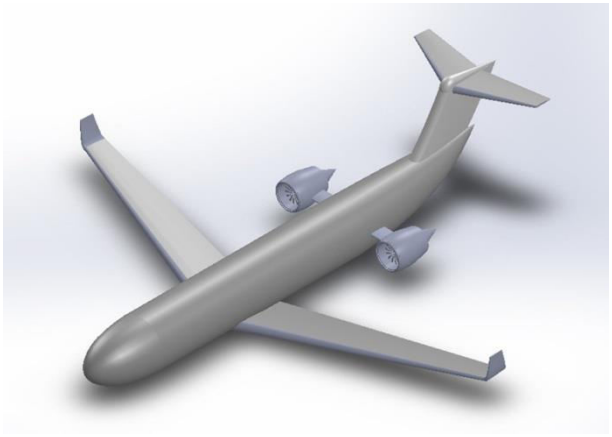

Fig 8: Isometric view

Fig 9: Front view

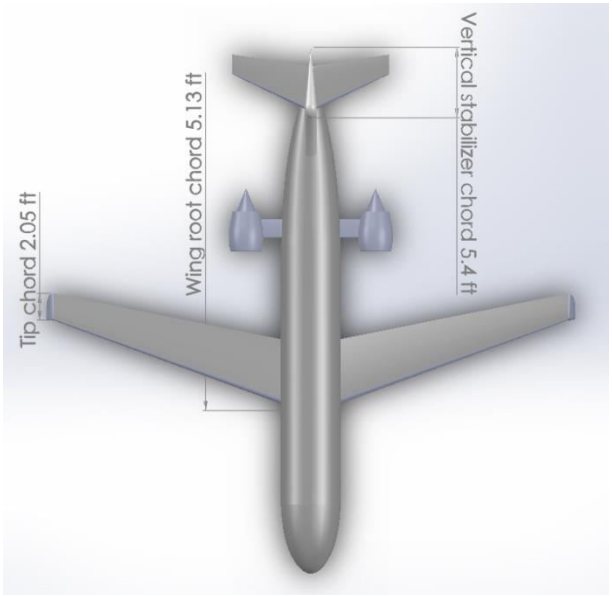

Fig 10: Top view

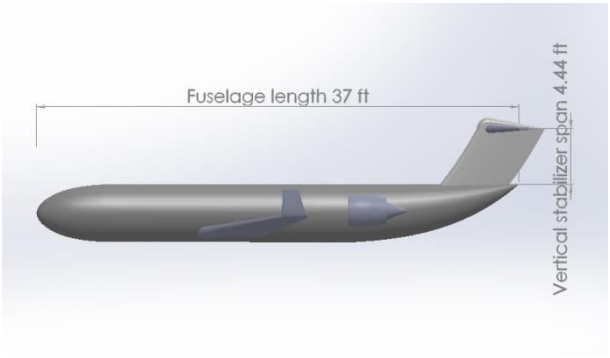

Fig 11: Right hand side view

13. Novel Ideas

During the design process some novel ideas were developed. These are explained in details below:

(1)T-tail was considered not because it is stylish but it allows the use of engines to be mounted on the aft fuselase in pods. Its not only stylish but it also reduces tail area due to endplate effect. Though it is heavier than the conventional wing it reduces buffet on the horizontal tail.

(2)Winglet was chosen as the wing tip as it offers lower drag. It is both cambered and twisted so the rotating vortex flow at the wing tipcreates a forward lift component which reduces total wing drag.

(4)As it is a small aircraft so aft-engine arrangement was used in this desing to maintain adequete wing nacelle and nacelle-ground clearances. As there is no wing-pylon interferance so less drag is created. Less assymetric yaw after engine failure with engine close to fuselage and lower fuselage height are also the advantages of using aft- engine arrangement.

14. Comparison with Similar Aircraft

Parameter	HONDA HA-420 JET AIRCRAFT	Designed Aircraft
Crew	2	2
Passenger	6	6
Fuselage Length	42.6ft	36.7ft
Wing span	39.9ft	38.35ft
Takeoff weight	9200lb	11035.624lb
Engine	GE Honda HF 120 turbofan engine	Rolls-Royce/MAN Turbo RB193 .
Maximum range	1180nmi	1975nmi
Maximum velocity	709.026ft/s	1581.469 ft/s

A comparison is done between the designed aircraft and HondaHA-420 Jet aircraft. Both the aircraft has almost same wing span and same passenger number. But with almost double range the weight increased only 2000 lb. It is a remarkable success in design.

Corresponding author: Squadron Leader Dr. Saifur Rahman Bakaul, Associate Professor, Military Institute of Science and Technology, Bangladesh. Tel.: +8801975104040, email: saif1833@yahoo.com, saif@ae.mist.ac.bd

15. Conclusion

In comparison with other business jet aircraft the total weight of the aircraft that was calculated is a compatible one. Maximum range calculated is almost close to the requirement assumed but the maximum velocity calculated exceeds the required velocity. Comparing with statistical data the takeoff distance and the landing distance calculated is a good one. The aerofoil chosen is a compatible one with the design requirement. Some during the design process some requirements were fulfilled but some were not. But still the calculation of total weight was remarkable one with a higher range thus this design is totally fuel efficient and economical.

NOMENCLATURE

W_o : Total gross Weight, lb
W_f : Fuel weight, lb
W_e : Empty weight, lb
T : Thrust, lb
L : Lift, lb
D : Drag, lb
Θ : Climb angle, degree
C_{D0} : Zero Lift Drag co-efficient
V : Velocity, m/s
R/C : Rate of climb, m/s
$\dot{\rho}$: Density, kg/m^3
W/S : Wing loading
C_L : Lift coefficient
n : Load factor
Vne : Velocity never exceed

References

[1] Daniel P. Raymer, Aircraft Design: A Conceptual Approach, Fourth Edition, AIAA, page 21
[2] Daniel P. Raymer, Aircraft Design: A Conceptual Approach, Fourth Edition, AIAA, page 84
[3] Daniel P. Raymer, Aircraft Design: A Conceptual Approach, Fourth Edition, AIAA, page 85
[4] Daniel P. Raymer, Aircraft Design: A Conceptual Approach, Fourth Edition, AIAA, page 99
[5] John D. Anderson Jr. Aircraft Performance and Design, Tata-McGraw-Hill edition

ICMIEE-PI-140354

Energy simulation to estimate building energy consumption using EnergyPlus

Md. Jahangir Alam[1,], Mohammad Ariful Islam[2], Biplob Kumar Biswas[1]*

[1]Department of Chemical Engineering, Jessore University of Science and Technology, Jessore- 7408, Bangladesh
[2]Department of Mechanical Engineering, Khulna University of Engineering & Technology, Khulna-9203, Bangladesh

ABSTRACT
To achieve sustainable and green design, performance simulations are often used to verify these criteria and modify the design. The conventional approach of manual trial-and-error is too time-consuming to be practical. The evaluation of building energy consumption usually requires building energy profiles on month and category basis. EnergyPlus-Windows-32-8.1.0.009, simulations were integrated to obtain this information but generating simulations requires a significant amount of experience, time, and effort to enter detailed building parameters. This paper presents a simple methodology to estimate source and site energy, where maximum energy requirement are 1485.14 MJ/m^2 and 447.6 MJ/m^2; respectively for D (mass type wall with attic) category within different categories (A-F) building. Moreover utility use per total floor area also calculated. Maximum U -factor with or without film are 0.512, 0.554 W/m^2.K; respectively for wall of building. For one year max tariff charge is 63.5$ on electrical source energy consumption for D category building. In addition to summer and winter clothes maximum and minimum uncomfortable time are 436.25 (for D-category and 390.75 (for E-category) hours as annual. The methodology has been applied to hypothetical buildings placed in Jessore, Bangladesh.

Keywords: Building Energy simulation, HVAC System, Human comfort, Energy Plus

1. Introduction

Concerning the rude use of energy and with climate change caused by gas emissions have impacts for civil construction. Population growth and economic progress have led to an increase in the demand for energy. The worldwide increase in demand for energy has put rising pressure on identifying and implementing ways to save energy. Energy efficiency is an important factor related to the energy issue; according to Omer [1] a building has three parameters directly related to energy consumption: thermal comfort (thermal conditioning), visual comfort (lighting) and air quality (ventilation). An annoying factor in the varied environment is the fact that the degree of industrialization in the building and construction industry is rather low. Each building is essentially a prototype. This is coupled with traditionally high costs and a complex planning process, this is usually hierarchical according to the different trades acting as a barrier for innovation. In order to make innovation possible, improved components and operational concepts are necessary to achieve an optimal design of buildings. Energy saving concepts includes passive and active measures. In the passive approach, investigation of innovative building envelope characteristics, increasing the use of natural ventilation, and the application of building thermal mass as energy storage are providing promising opportunities for energy efficiency. The active measures involve optimization of HVAC system operation taking into account the combination and performance of technologies.

Daylight is an important strategy in obtaining a more efficient architecture which is integrated with the climate in which it is inserted, and therefore it is necessary to study the ambient light. In order to carry out a more advanced study there is a need for data related to the daylight of the location in which the building will be constructed. However, the analysis of the ambient daylight must also take into account the heat exchange which occurs through the windows. Studies such as those by Ochoa and Capeluto [2], Li and Wong [3], and Ghisi and Tinker [4] use the joint simulation of the daylight and heat gain of a building in order to verify the performance of the design decisions taken, to study the daylight in dense areas and to analyze the ideal window size in climatised buildings. Energy consumption analysis of buildings is a difficult task because it requires considering detailed interactions among the building, HVAC system, and surroundings (weather) as well as obtaining mathematical/physical models that are effective in characterizing each of those items. The dynamic behavior of the weather conditions and building operation, and the presence of multiple variables, requires the use of computer aid in the design and operation of high energy performance buildings. Drawbacks in using computer simulations include the considerable amount of detailed input data and time from even experienced users [5-6]. Furthermore, simulation tools may not be cost-effective at the first stage of analysis, which makes others tools, such as screening tools, a better option. Several methodologies to estimate energy consumption have been developed. Some of them are based on statistics and other on simulations [5,7–13]. On-line building energy predictions based on neural networks and genetic algorithms [14–16] can also be used in some applications. In general, it is accepted that weather data

* Corresponding author. Tel.: +88-01911613187
E-mail address: jahangirche@gmail.com

can play an important role on forecasting energy consumption in buildings [7]. Papa et al. [17] proposed a normalized energy use index (NEUI) based on a temperature function. In their work, they discussed the influence of weather variables such as solar radiation and air velocity, and conclude that temperature is the most important factor on energy consumption. Their reasoning is that, since the equipment daily energy consumption is always the same, and because there is not significant variation of daily routine, changes in HVAC energy consumption is predominantly a function of temperature. To obtain the temperature function to compute the NEUI, they used EnergyPlus as a simulation tool. Since even more detailed building simulations will not reproduce exactly the energy consumption profile, there is an accepted degree of uncertainty in the estimated energy demands as consequence of the accuracy of the tool and inputs that the user needs to be aware of in order to make the final conclusions [6,18,19].

In the residential sector 47% of the total energy consumption in the Bangladesh, that justifies a variety of initiatives for building energy consumption reduction. As examples, the Building Technologies Program of the DOE Energy Efficiency and Renewable Energy Office is working to achieve the goal of net-zero energy buildings, and the Bangladeshi Green Building Council promotes the design, construction, and operation of high performance green buildings through the Leadership in Energy and Environmental Design program. Jessore is a district in the southwestern tip of Bangladesh. Energy consumption in the Jessore building sector is momentous. For reducing that, the entire external building envelope must be designed in accordance with the Bangladeshi building code.

Source energy is the most equitable unit of evaluation. Source energy represents the total amount of raw fuel that is required to operate the building. It incorporates all transmission, delivery, and production losses. On other hand site energy, which is the amount of heat and electricity consumed by a building as reflected in your utility bills. U value is a measure of heat loss in a building element such as a wall, floor or roof. It can also be referred to as an ‘overall heat transfer co-efficient’ and measures how well parts of a building transfer heat. This means that the higher the U value the worse the thermal performance of the building envelope.

Bangladesh has a subtropical monsoon climate characterized by wide seasonal variations in rainfall, high temperatures and humidity. There are three distinct seasons in Bangladesh: a hot, humid summer from March to June; a cool, rainy monsoon season from June to October; and a cool, dry winter from October to March. In general, maximum summer temperatures range between 30°C and 40°C. April is the warmest month in most parts of the country. January is the coldest month, when the average temperature for most of the country is about 10°C. Lightweight cotton clothing is advised throughout the year, with an umbrella or raincoat for the monsoon season. Be prepared for high temperatures and humidity, no matter where you go. A sweater and warmer clothing is advised for cooler evenings. Warmer clothing is advised for the northern mountainous areas of Bangladesh, which can have quite cold winters.

2. Simulation Technique

The global increase in demand for energy has generated pressure on saving energy. Consequently, Energy efficient buildings are an important factor related to the energy issue. Various building energy simulation softwares are used now-a-days to simulate building energy consumption and to design energy efficient building such as EnergyPro, EnergyPlus, EAB, REScheck etc. Among them EnergyPlus is developed by US department of Energy and it is getting popular to simulate and design of energy efficient building.

The methodology proposed in this paper is based on energy calculation obtained using data from EnergyPlus. It is a widespread and accepted tool in the building energy analysis community around the world [21]. This program combines the best capabilities and features from BLAST and DOE-2 along with new capabilities. EnergyPlus models heating, cooling, lighting, ventilating, and other energy flows as well as water in buildings. The Building Energy Software Tools Directory [22], which is a directory providing information on 375 building software tools for evaluating energy efficiency, renewable energy, and sustainability in buildings, introduces EnergyPlus as a tool for application on energy simulation, load calculation, building performance, simulation, energy performance, heat balance, and mass balance. EnergyPlus is free of use and can be downloaded from the official website [20]. Support from the U.S. government, worldwide use, capabilities, and resources, are the main reasons EnergyPlus has been chosen as the simulation tool to generate the data used in this study to estimate energy consumption. EnergyPlus has been used in other studies as source of energy consumption. Stadler et al. [21] used EnergyPlus as source of site end-energy loads for the analysis of distributed generation (DG) technology. Similarly, Fumo et al. [23] used it for the analysis of combined cooling, heating, and power (CCHP) systems. As an example of how EnergyPlus has been used to estimate building energy performance as reference for other cases, Griffith and Crawley [24] used EnergyPlus to propose a methodology for evaluating energy performance for the U.S. commercial buildings sector to estimate the technical potential on zero-energy buildings. They used data from the 1999 Commercial Buildings Energy Consumption Survey (CBECS) to create a baseline building energy model as it were being built in 2005.

It is obvious that an energy simulation needs to be performed to solve the design optimization problem.

EnergyPlus was used to simulate the space conditioning load of the building. EnergyPlus is an energy analysis and thermal load simulation program [25]. It has been widely used, like its predecessor programs, BLAST and DOE-2, by architects, engineers, and researchers. In the top view of building shown in Fig. 1, the exterior wall system is composed of four exterior walls, namely 4WE, 1SE, 3NE and 2EE.

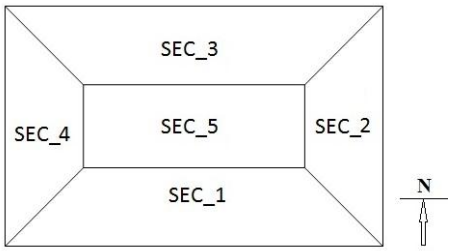

Fig. 1: Top view of building.

where the first number represents the section number, the second letter represents the orientation, and the third letter "E" represents "Exterior". Therefore, "3NE" denotes the north-facing exterior wall of section 3. The main components of the enclosure system in **Table 1** and all sections physical parameters are summarized in Table 2.

Table 1 Physical parameters of the building-I

Categories	Enclosure	
	Wall Type	Roof Type
A	Steel Framed	Insulation entirely above deck
B	Steel Framed	Attic and other
C	Mass	Insulation entirely above deck
D	Mass	Attic and other
E	Wood Framed	Insulation entirely above deck
F	Wood Framed	Attic and other

Table 2 Physical parameters of the building -II

Enclosure Section	**Area [m^2]**	**Volume [m^3]**
N_1_FLR_1_SEC_1	91.06	346.02
ZN_1_FLR_1_SEC_2	35.09	133.33
ZN_1_FLR_1_SEC_3	91.06	346.02
ZN_1_FLR_1_SEC_4	35.09	133.33
ZN_1_FLR_1_SEC_5	47.71	181.32
Total	300	1140
Conditioned Total	300	1140

For internal heat gains, all section was set to have 5 people per 100 m^2 and they were assumed to be in the building from 08:00 to 17:00 on regular work days and Friday is weekend day. Lighting level was set to be 10.76 W/m2 for all five sections. The air flow rate is 0.22 m^3/s (max.) on exterior part of the building. Since the study was concerned with the categories (A-F) of buildings conditioning load and energy consumption.

To analyze the categories of building, an obvious approach is designing different type materials in wall and roof, simulating each case to obtain the energy consumption and comparing the results. Many building performance simulation programs including EnergyPlus cannot be directly integrated. Therefore, one needs to develop customized codes to link the performance simulation program to the optimization algorithm. The most convenient way to run EnergyPlus is using the EPLaunch program that comes with the EnergyPlus downloadable package. EP-Launch has an interface through which the user can open IDF-Editor to edit the input file, specify the location of the EPW weather data file, and run a single simulation. Although being easy to use, the approach of running EnergyPlus in EP-Launch cannot be integrated into modeFRONTIER. Another way to run EnergyPlus is using RunEPlus batch file. The command is simply one line in DOS mode, i.e., "RunEPlus <input file name> <weather data file name>.

After properly editing the RunEPlus.bat file and writing the DOS command lines, a work flow to perform insulation optimization was established. The work flow consisted of four steps. Step 1 contained all the input variables, i.e., the insulation of six walls. DOE (Design of Experiment) initializing the input variables and the optimization algorithm were defined in step 2. Step 3 was the linkage that enables the integration of EnergyPlus. A DOS batch file was written and several support files such as Energyþ.ini, Energyþ.idd, DElight2.dll, and ExpandObjects.exe were transferred to the working directory. Optimization objectives were defined in step 4. Other nodes were mainly to perform calculations and other tasks needed. This four-step work flow can be used as a general format for many optimization problems encountered in architectural design. The range and step of the input variables were defined in step 1. In this study, the input variables were transferred to the "InputFile" node. In this node, one can open the input file, 1.idf, of EnergyPlus and specify the location of each variable. The work flow ends with two optimization objectives, namely minimizing source & site energy consumption and minimizing summer or winter clothes uncomfortable time with lowest energy cost.

3. Result and discussion

Fig. 2 shows total source energy with the categories (A-F) of building. By simulation, it has been obtained that total energy required is 410-450 GJ as source energy and the conversion factor for site to source energy is

3.31with respect to electricity used. From the Fig. 2, highest value of source energy per total building area required for D category building is 1485.14 MJ. On the other hand the lowest values is 1368.92 MJ for A-category building and the sequence is D>E>F>C>B>A.

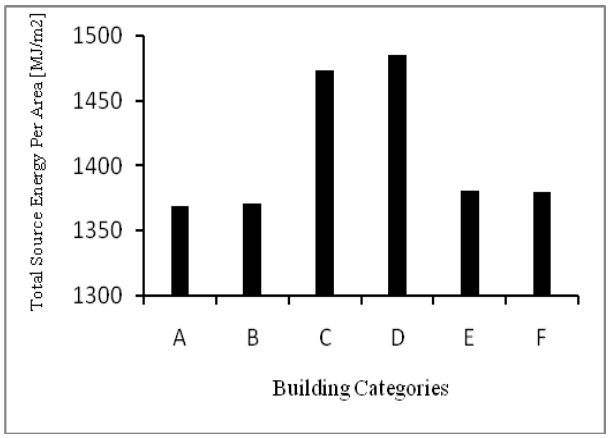

Fig. 2: Source energy per total area with the categories (A-F) of building

Utility use per total floor area as electricity intensity has been measured by the quantity of energy required per unit output or activity and total energy coming from utility as electricity with different categories (A-F) is about 120-140 GJ, as well as using less energy of a building reduces the intensity with building category that shows in Fig. 3. The electrical intensity needed for A-category building per total area as lighting and other are 110.91 and 128.72 MJ/m^2; respectively but the minimum electricity intensity required for steel framed wall, A-building is 412.52 MJ/m^2 and the progression is D>E>F>C>B>A. And 447.6 MJ/m^2 is maximum value of total electrical intensity used in building D.

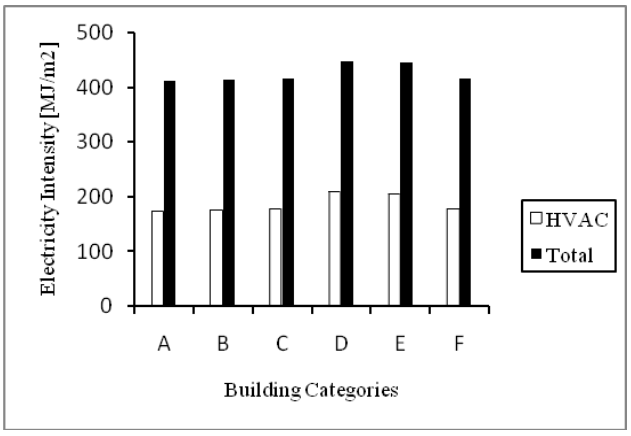

Fig. 3: Utility use per total area of building as electricity intensity with different category of building.

Fig. 4 shows thermal performance of building A with respect to U value. From the figure we can say that, with or without film the thermal performance of wall is almost 1.6 times greater than ceiling of buildings. For building A with no film, the U factor of wall and ceiling are 0.385 & 0.288 W/m^2.K; respectively that are almost 6 and 4 % higher than of building A with film. For other type of buildings, the U-factor shows similar value.

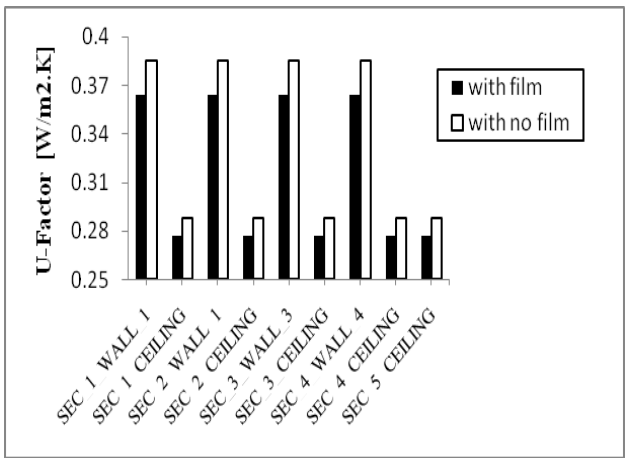

Fig. 4: U-factor in different section of building A.

The annual energy charge on electricity for all categories buildings is about 2600 to 2900 ($) in jessore, Bangladesh. From Fig. 5 the annual tariff charge (63.5 $) on electricity is maximum for the building D at the month of August because of high source energy used. The lowest tariff is 58.95 $ of building A & B at that month. During month December to January annual tariff charge is minimum value comparing other months.

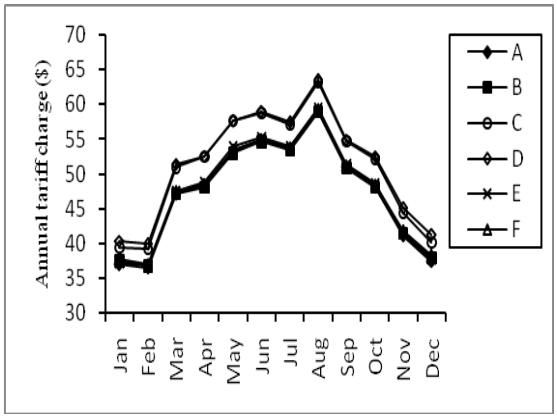

Fig. 5: The annual tariff charge on electricity in different categories (A-F) building

Fig. 6 shows that January to March clothes uncomfortable time increase almost linearly. From March to June maximum uncomfortable time is observed for all categories buildings for the reason of hot humid summer. Following June to December clothes uncomfortable time decrease randomly. From the Fig. 6, evaluate a value that is near to the ground at the month of December for all categories buildings. Since categories A-F buildings, the clothes uncomfortable time is highest as a value of 396.5 hours at June in Building A and the lowest value is 413 hours

at that month in building C. building arrangement with considering summer or winter clothes uncomfortable time is D>B>F>C>A>E. As of above discussion, C & A category building required moderate energy but feasible with respect to comfortable time than other category buildings.

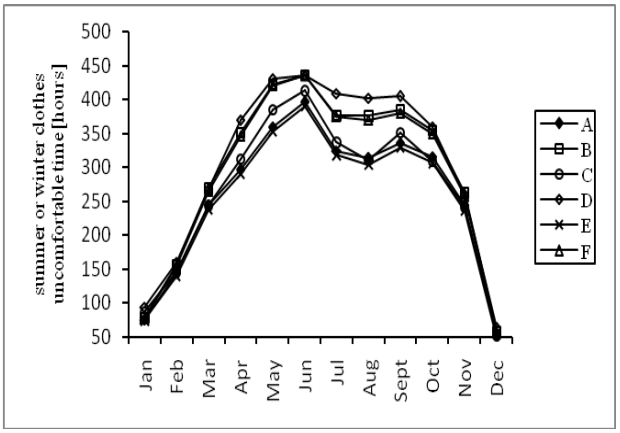

Fig. 6: summer or winter clothes uncomfortable time throughout the year in different categories (A-F) building

4. Conclusion

This paper has shown that it can be used to integrate EnergyPlus-Windows-32-8.1.0.009, to conduct optimization. Some basic computer knowledge is required to establish the work flow. To achieve sustainability, many design objectives considered are related to physical performances of the building and thus, they need to be simulated using computer programs. Using an office building in Jessore, Bangladesh as an example, we have demonstrated how to integrate EnergyPlus into the optimization software tool to search for the best result to minimize the source and site energy as well as winter or summer clothes uncomfortable time at lowest energy cost with different categories (A-F) building. The sequence for source & site energy is D>E>F>C>B>A. On behalf of utility per total floor area, the progression of electrical intensity is D> C>E>F> B>A. Building with or without film, the thermal performance of wall is greater (almost 1.6 times) than ceiling of buildings. Also, maximum tariff charge is 63.5 $ on electricity for D category building annually. Preferable building order with respect to summer or winter clothes uncomfortable time is D> B > F>C>A >E. From above result we can say that, category of C & A building required moderate energy but feasible with considering comfortable time than other category buildings. EnergyPlus is successfully integrated into the optimization software tool through writing a DOS batch file. In the future, there is a need to study how to integrate other building performance simulation programs. By doing so, the technique can be used to solve more residential building design optimization problems.

REFERENCES

[1] A. M. Omer, Renewable building energy systems and passive human comfort solutions, *Renewable & Sustainable Energy Reviews*, Vol. 12, pp 1562–87, (2008).

[2] C. E. Ochoa, I. G. Capeluto, Strategic decision-making for intelligent buildings: comparative impact of passive design strategies and active features in a hot climate, *Building and Environment*, Vol. 43, pp 1829–39, (2008).

[3] D. H. V. Li, S. L. Wong, Daylighting and energy implications due to shading effects from nearby buildings, *Applied Energy*, Vol. 84, pp 722–29, (2007).

[4] E. Ghisi, J. A. Tinker, An ideal window area concept for energy efficient integration of daylight and artificial light in buildings, *Building and Environment*, Vol. 40, pp 51–60, (2005).

[5] Y. Zhu, Applying computer-based simulation to energy auditing: a case study, *Energy and Buildings*, Vol. 38, pp 421–428, (2006).

[6] T. Catalina, J. Virgone, E. Blanco, Development and validation of regression models to predict monthly heating demand for residential buildings, *Energy and Buildings*, Vol. 40, pp 1825–1832, (2008).

[7] A. Hernandez, F. A. Sanzovo, Use of simulation tools for managing buildings energy demand, *Building Simulation 2007*, pp 1883-1889, (2007).

[8] F. W. H. Yik, J. Burnett, I. Prescott, Predicting air-conditioning energy consumption of a group of buildings using different heat rejection methods, *Energy and Buildings*, Vol. 33, pp 151–166, (2001).

[9] [9] S. Chirarattananon, J. Taveekun, An OTTV-based energy estimation model for commercial buildings in Thailand, *Energy and Buildin*gs, Vol. 36, pp 680–689 (2004).

[10] Y. Pan, Z. Huang, G. Wu, C. Chen, The application of building energy simulation and Proceedings: Building Simulation 2007 – 1889 – calibration in two high rise commercial buildings in Shangai, *Building Simulation Conference*, Australia, November, (2006).

[11] F. Gugliermetti, G. Passerini, F. Bisegna, Climate models for the assessment of office buildings energy performance, *Building and Environment*, Vol. 39, pp 39–50, (2004).

[12] F. S. Pedrini, R. Westphal, Lamberts, A methodology for building energy modeling and calibration in warm climates, *Building and Environment*, Vol. 37, pp 903–912, (2002).

[13] F. S. Westphal, R. Lamberts, Building simulation calibration using sensitivity analysis, *Ninth International IBPSA Conference*, August, (2005).

[14] R. Yokoyama, T. Wakui, R. Satake, Prediction of energy demands using neural network with

model identification by global optimization, *Energy Conversion and Management*, Vol. 50, pp 319–327, (2009).
[15] J. Yang, H. Rivard, R. Zmeureanu, On-line building energy prediction using adaptive artificial neural networks, *Energy and Buildings*, Vol. 37, pp 1250–1259, (2005).
[16] O. E. Canyurta, H. K. Ozturka, A. Hepbaslib, Z. Utlu, Estimating the Turkish residential–commercial energy output based on genetic algorithm (GA) approaches, *Energy Policy*, Vol. 33, pp 1011–1019, (2005).
[17] R. P. Papa, P. R. S. Jota, L. S. Assis, Energy index evaluation of buildings in function of the external temperature, *Building Simulation 2007*, pp 1890-1894, (2007).
[18] S. Gamou, R. Yokoyama, K. Ito, Optimal unit sizing of cogeneration systems in consideration of uncertain energy demands as continuous random variables, *Energy Conversion and Management*, Vol. 43, pp 1349–1361, (2002).
[19] M. Deru, B. Griffith, P. Torcellini, Establishing Benchmarks for DOE Commercial Building R&D and Program Evaluation, National Renewable Energy Laboratory, *National Renewable Energy Laboratory, Pacific Grove, California*, pp 1-12, (2006).
[20] U.S. Department of Energy, Energy Efficiency and Renewable Energy Office, Building Technology Program, EnergyPlus. http://apps1.eere.energy.gov/buildings/energyplus/.
[21] M. Stadler, R. Firestone, D. Curtil, C. Marnay, On-site generation simulation with EnergyPlus for commercial buildings, *Lawrence Berkeley National Laboratory*, (2006).
[22] U.S. Department of Energy, Energy Efficiency and Renewable Energy Office, Building Technology Program, Building energy software tools directory. Available from: http://apps1.eere.energy.gov/ buildings/tools directory/.
[23] N. Fumo, P. Mago, L. Chamra, Energy and economic evaluation of cooling, heating, and power systems based on primary energy, *Applied Thermal Engineering*, Vol. 29, pp 2665–2671, (2009).
[24] B. Griffith, D. Crawley, Methodology for analyzing the technical potential for energy performance in the U.S. commercial buildings sector with detailed energy modeling, *National Renewable Energy Laboratory, Pacific Grove, California*, pp 1-7, (2006).
[25] US Department of Energy. Getting started with EnergyPlus; 2009. http://apps1.eere.energy.gov/buildings/energyplus/.

ICMIEE-PI-140355

Effect of Compaction during Manufacturing of Textile Composites.

Md Shariful Islam and Pavana Prabhakar[*]
Department of Mechanical Engineering, The University of Texas at El Paso, TX-79902, USA

ABSTRACT
The influence of fiber tows on the deformation and damage evolution in fiber reinforced composites is investigated by considering a micromechanical model of fibers within matrix that is undergoing compaction and subsequently subjected to mechanical loads. The stresses developed due to compaction of the matrix during the VARTM manufacturing process is modeled using the finite element (FE) framework. Nonlinear material behavior due to post-damage response that can lead to cracking in the matrix is incorporated through a crack band model that preserves mesh objectivity in the FE calculations. The mechanical response of the composite along with damaging capability due to compaction and subsequent mechanical loading is investigated in detail in this paper. The influence of the curing process is not considered in this paper. But, the final quality of the composite, subjected to varying compaction, is investigated using a mesoscale model.

Keywords: Textile Composite, Damage, VARTM, Finite Element Method, Compaction.

1. Introduction

Textile composites are finding extensive use in the aerospace and automobile industry due to their high stiffness to volume ratio, easy formability and drapability[1]. For a rapid development of these materials in terms of high strength and durability, there is a need for a thorough understanding of the material state, and the influence of processing on the material response in subsequent service applications. Therefore, along with design aspects, like geometrical design and weaving, manufacturing induced defects have to be accounted for. These defects act as global failure initiation points within the composite. Therefore, in order to minimize any premature failure in the final composite manufactured, it is crucial to investigate process induced defect in these composites.

The most commonly used manufacturing technique for textile composites is the Vacuum Assisted Resin Transfer Molding (VARTM). In this technique, layers of dry fabric of the textile are place on top of each other, and subjected to vacuum. Further, liquid resin is transferred through the dry fabric through injection tubes, and is subjected to pressure and temperature as a curing process to manufacture the composite. The effects of compaction before or during the resin infusion are that the yarn has a very complicated shape and the fiber volume fractions vary locally[2, 3]. Nesting occurs between the yarns [2-4]. Further, compaction creates complicated contact zones between the yarns [1-3] [5]. Grail et al.[6] developed a new finite element mesh generation method for textile preform and compacted reinforcement.

The inputs to the manufacturing process influence the outcome of the composite in different ways. The pressure applied to the dry fabric, the rate of resin injection, the temperature during curing, are a few processes that may alter the quality of the final laminate. Therefore, it will be useful to the industry, if there are computational tools which are able to predict the final outcome of the VARTM process.

In this paper, the influence of the compaction on woven glass fabric during the VARTM process is investigated. In this context, the tensile response of the woven composite subjected to varying compaction is computationally studied. As a first approach, compaction on fabric layer during manufacturing and tension on the final composite was considered in this paper. Stresses developed during the curing process of resin are not considered in this paper which is under consideration as a next step.

2. Mesoscale Model

Four layers of glass fabric (as reinforcement) and Epon 638 with Epikure 9553 hardener (as matrix) was used in the paper. Fig. 1 shows the RVE with woven fiber tows and matrix. Fig. 2(a) shows a single layer of glass fabric with an exaggerated view. Geometry of the RVE was modeled with TexGen software, which is specially designed to model textile composites. The geometry of the model was then exported to ABAQUS commercially available software) to perform the finite element analysis.

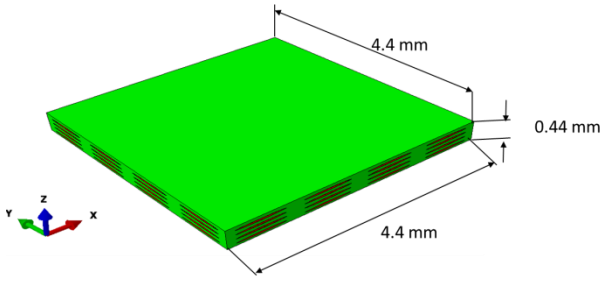

Fig.1 RVE of woven composite

The computational modeling approach is divided into two parts: 1) Compaction of the fiber tows with uncured

* Corresponding author. Tel.: +1 (915) 747-5863
E-mail address: pprabhakar@utep.edu

resin, and 2) Tensile response of the post-cured composite with damaging capability included in the matrix.

2.1 Computational Modeling of Compaction

In the compaction step, the RVE shown in Fig. 1 is used. The properties of the glass fiber used in this model are E_f= 85 GPa and $\upsilon_f = 0.22$. For the compaction model, it is assumed that the liquid resin fills the entire space between the dry fabrics. Therefore, prior to solidification of the resin, it was considered that 5 % of the resin has already cured. The matrix properties at this stage are E_m=0.081 GPa and $\upsilon_m = 0.48$ [6]. The homogenized tow properties were calculated using these properties of fiber and matrix using the concentric cylinder model[7]. Table 1 shows the homogenized properties of tows in the uncured state.

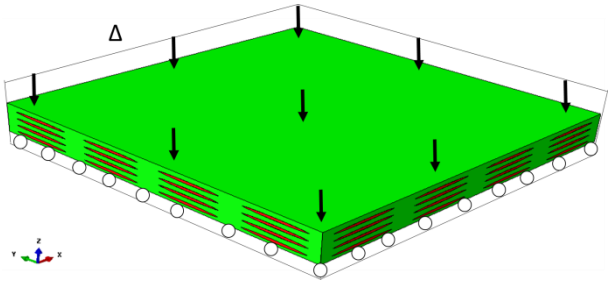

Fig.2 Boundary Conditions for Compaction Modeling

The boundary conditions used in the compaction modeling are shown in Fig. 2. Displacement of the bottom surface was restricted in the z-direction, and a displacement condition simulating a compaction was applied on the top surface. All other faces were maintained to be flat, i.e. the faces all allowed to breathe while remaining flat. Five different compactions, i.e. 5%, 7.5%, 10%, 30% and 50% of the thickness of composite were considered to study the effect of compaction of the final composite.

Table 1 Homogenized Tow Properties with 5% cured Matrix.

E_{11} (GPa)	$E_{22}=E_{33}$ (GPa)	$\upsilon_{12} = \upsilon_{13}$	υ_{23}	$G_{12}=G_{13}$ (GPa)	G_{23} (GPa)
51.03	0.254	0.307	0.24	0.111	0.105

2.2 Tensile Modeling of the Compacted Composite

The models corresponding to the different compaction values are subjected to tensile loading post-cure. As mentioned above, the curing process is not modeled in this paper. Therefore, the cured matrix properties were considered for the tensile loading step. That is, the cured matrix properties are E_m=4.95 GPa and $\upsilon_m = 0.375$ [6]. Table 2 shows the corresponding homogenized tow properties. Boundary condition for this case is shown in Fig. 3. Flat boundary conditions mentioned used for the compaction step was used for free surfaces in this current step as well.

Table 2 Homogenized Tow Properties of Final Composite

E_{11} (GPa)	$E_{22}=E_{33}$ (GPa)	$\upsilon_{12} = \upsilon_{13}$	υ_{23}	$G_{12}=G_{13}$ (GPa)	G_{23} (GPa)
53.01	13.67	0.375	0.25	6.044	5.468

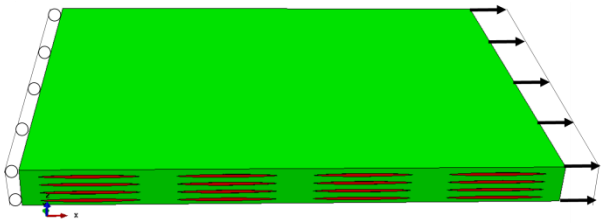

Fig.3 Boundary Conditions for Tension Modeling.

2.3 Damage Capability in Matrix: Crack Band Model

Including damage capability in materials adds a region with negative tangent stiffness to the constitutive law. Classical finite element method (FEM) converges to a single solution with mesh refinement, as long as the tangent stiffness of the constitutive law is greater than or equal to zero. But, a negative tangent in the constitutive law makes the model pathologically mesh dependent. That is, the results change as the element size is reduced. Therefore, the energy dissipated during the failure process has to be scaled with the element size to make the problem mesh objective. Crack band model (CBM) introduced by Bazant and Oh [8] is an efficient method to account for the element size during material damage.

The damaging regime is modeled by adding a traction-strain law beyond a critical strength value in the constitutive law. The traction-strain law is determined by converting a traction-separation law utilizing the characteristic element length "L_c" as shown in Fig. 4. The two inputs to the traction-separation law are the cohesive/critical strength (σ_c) and fracture toughness (G_c) of the material.

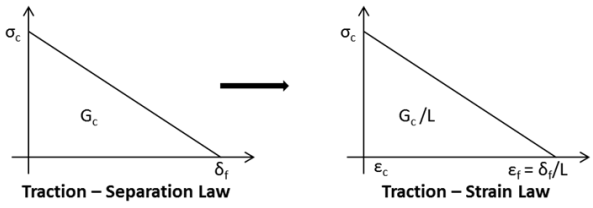

Fig.4 Converting traction-separation law to traction-strain law.

In CBM, a typical stress-strain material law is generated by adding a linearly decreasing damage path, with the characteristic length included, to follow the initial linearly increasing regime as shown in [8]**Error!**

Reference source not found.. The initial linear stiffness of the material is "*E*, which is a function of the degree of cure. As the strain within an element in the FEM model exceeds the critical strain corresponding to the critical stress, the stiffness of the element is reduced accordingly by entering the damage path in [8]**Error! Reference source not found.**. The degraded stiffness value is determine as $E=\sigma_i/\varepsilon_i$, corresponding to the strain in the element.

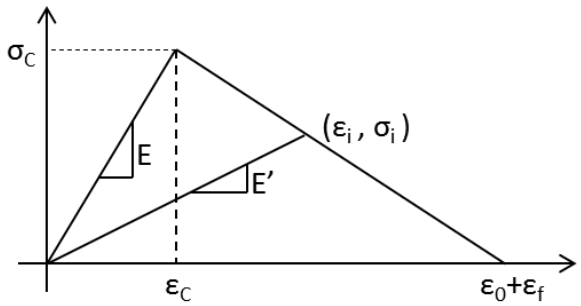

Fig.5 CBM: modified stress-strain material law incorporating failure.

3. Results and Discussions

For the compaction modeling, 5 different displacements for compaction were used, i.e., 5%, 7.5%, 10%, 30% and 50% of the thickness of the composite (in the z-direction). Table 3 shows the original and deformed dimensions because of compaction. Here, the original length of the RVE is L = 4.4mm, and the thickness t = 0.44mm, the corresponding dimensions after different compaction are given in the table.

Table 3 Original and Deformed Dimensions after Compaction.

Model	L (mm)	t (mm)
Original	4.4	0.44
5 % Compaction	4.40564	0.418
7.5 % Compaction	4.40846	0.407
10 % Compaction	4.41128	0.396
30 % Compaction	4.43383	0.308
50 % Compaction	4.45638	0.22

Fig. 6 shows the load-displacement diagrams for tensile response for different compaction and varying critical stress values (σ_c) for the matrix. The initial stiffness for 5%, 7.5% and 10% compaction is almost same for all values of, but this stiffness reduced because of more compaction (30% or 50% compaction). So, the amount of compaction plays an important role on the initial stiffness of the final composite. Fig. 6 also shows that the global tensile failure load decreases with increase in compaction.

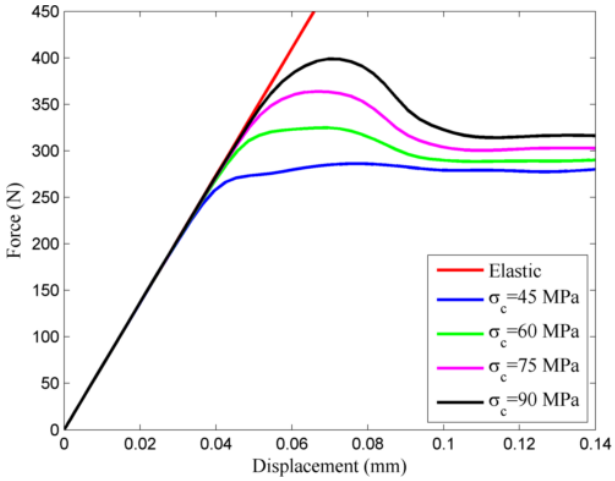

(a)

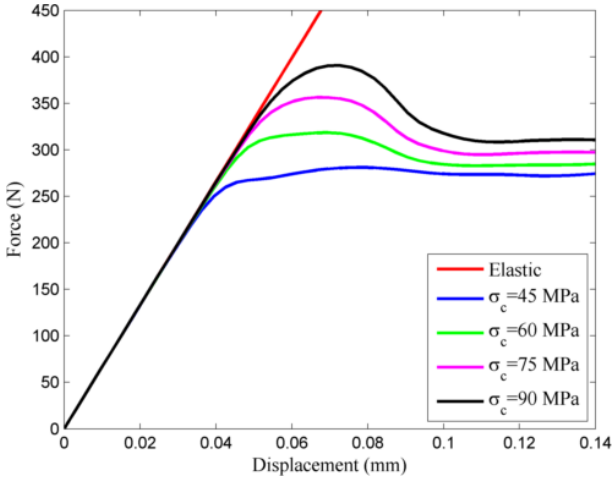

(b)

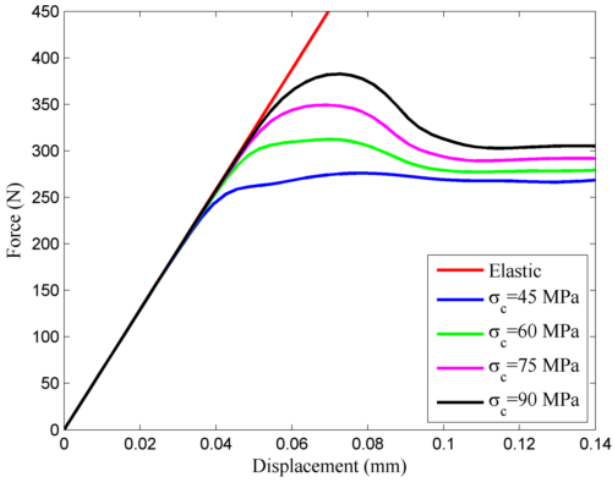

(c)

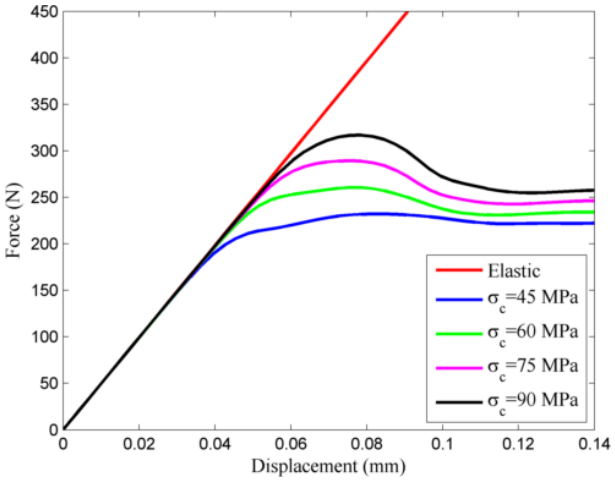

(d)

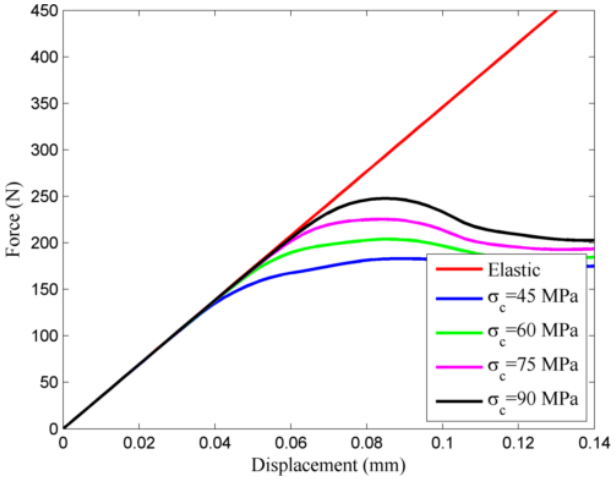

(e)

Fig.6 Load Displacement Response corresponding to Varying σ_c at Different Compactions of (a) 5%, (b) 7.5%, (c) 10%, (d) 30%, and (e) 50%.

The tensile load corresponding to first damage initiation in the composite is plotted in Fig. 7(a) for varying compaction and σ_c values. It is observed that the loads reduce with increasing compaction and reducing σ_c. similar behavior is observed for tensile loads at first failure points for different compaction and varying σ_c in Fig. 7(b). Fig. 7(a) and Fig. 7(b) indicate that when the compaction is increased from 5% to 50%, the loads for damage initiation reduces by 50%, and for the first failure point reduces by approximately 43%. For illustration, the damaged and the failed regions in the composite for 5% compaction and σ_c = 45MPa, are shown in red in Fig. 8(a) and Fig. 8(b). This indicates that the composite with greater compaction during manufacturing will fail prematurely when subjected to service loads.

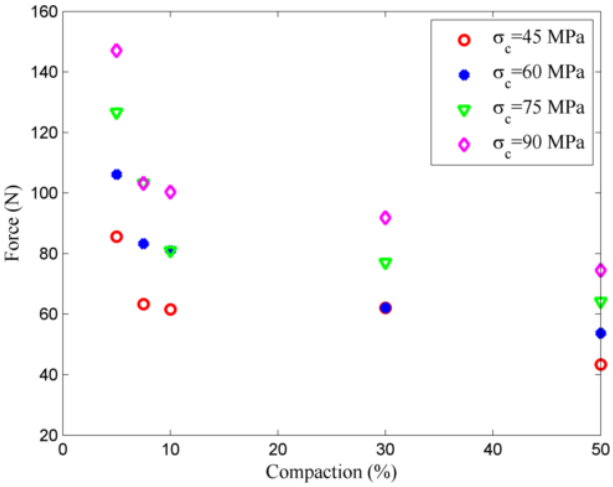

(a)

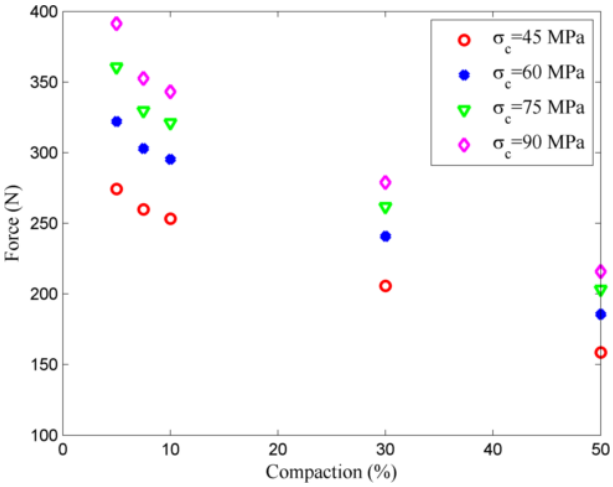

(b)

Fig.7 Loads at (a) First Damage and (b) Failure Points.

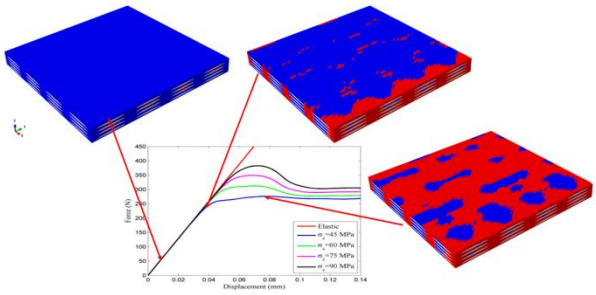

(a)

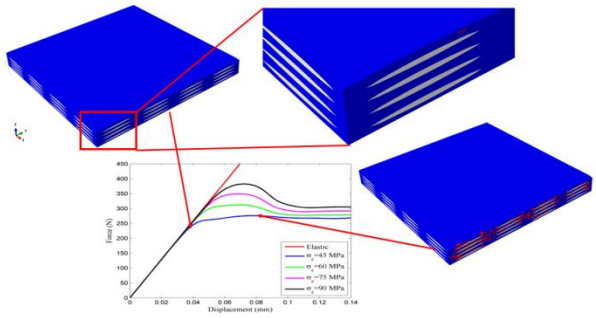

(b)

Fig.8 Example of Damaged and Failed Regions;
Compaction = 5% and σ_c = 45MPa

4. Conclusions

The effect of compaction during manufacturing of woven fabric composite by VARTM process is investigated in this paper. The damaging capability of matrix included in the finite element model by means of crack band model which preserves the energy dissipated during the failure process with varying element size and hence reduces the mesh sensitivity of the finite element analysis. The stresses developed during the curing process is not considered in the present paper, but it will be considered in the future work.

NOMENCLATURE

E_f : Stiffness of fiber, GPa
E_m : Stiffness of matrix, GPa
υ_f : Poison's ratio of fiber
υ_m : Poison's ratio of matrix
G_c : Fracture toughness of matrix
σ_c : Critical stress of matrix, MPa
L : Length of RVE, mm

REFERENCES

1. Mouritz, A., et al., *Review of applications for advanced three-dimensional fibre textile composites.* Composites Part A: Applied Science and Manufacturing, 1999. **30**(12): p. 1445-1461.
2. Olave, M., et al., *Internal geometry variability of two woven composites and related variability of the stiffness.* Polymer Composites, 2012. **33**(8): p. 1335-1350.
3. Karahan, M., et al., *Internal geometry evaluation of non-crimp 3D orthogonal woven carbon fabric composite.* Composites Part A: Applied Science and Manufacturing, 2010. **41**(9): p. 1301-1311.
4. Chen, B., E.J. Lang, and T.-W. Chou, *Experimental and theoretical studies of fabric compaction behavior in resin transfer molding.* Materials Science and Engineering: A, 2001. **317**(1): p. 188-196.
5. Lomov, S.V., et al., *Nesting in textile laminates: geometrical modelling of the laminate.* Composites Science and Technology, 2003. **63**(7): p. 993-1007.
6. Heinrich, C., et al., *Generation of heat and stress during the cure of polymers used in fiber composites.* International Journal of Engineering Science, 2012. **53**: p. 85-111.
7. Hyer, M. and A. Waas, *Micromechanics of linear elastic continuous fiber composites.* Comprehensive composite materials, 2000. **1**: p. 345-375.
8. Bažant, Z.P. and B.H. Oh, *Crack band theory for fracture of concrete.* Matériaux et construction, 1983. **16**(3): p. 155-177.

ICMIEE-PI-140101

An Android Controlled Mobile Robot for Stereo Vision and Live Streaming with Robotic Arm

Md. Muhaimin Rahman, Ashik-E-Rasul, Nowab Md. Aminul Haq, Md. Mehedi Hassan
Department of Mechanical Engineering, Bangladesh University of Engineering & Technology, Dhaka-1000, BANGLADESH

ABSTRACT
Mobile robotics and Android Operating System are two of the most advancing technologies at present. On the other hand, stereo vision technology is becoming more and more popular among the present youth. This project combines all of these advancing and developing technologies for humane purpose. The robot uses two smart phones with android operating system to send videos to the control server continuously and that will generate a stereoscopic image, a 3D live video from those images. In addition to that, a robotic arm is placed in front of that robot to pick any desired object . The whole process is be controlled by another smart phone with android operating system. The robot also can be controlled by the server computer only. Its usage are many. First of all, it can be sent to any place which is humanly impossible and do any task needed. For being small in size, it can be sent to any dangerous places like caves or underground operations also can be done by this robot. We hope this project can reduce the cost, human error, promote human trust and enable a robotic application which never has been possible before .

Keywords: Stereo Vision, Image Processing, Android OS, Mobile Robot.

1. Introduction

This paper focuses on a multipurpose mobile robot for stereo vision, live streaming controlled manually by an Android OS operated cell phone. It has a robotic arm to pick and place objects. The robot will have another two cell phones with Android OS used as their robotic eyes. An android application will transmit images captured by the cell phones continuously over wireless network to the server computer. The server computer will process the images using to generate stereo images out of them. Using those images, it will map any unknown area.

This paper is segmented into three parts. First portion details the architectural and mechanical construction. In the second portion, electrical design of the system is discussed. The final portion covers the software development and the algorithm of the robot.

2. Mechanical Construction

The mechanical body the robot consists of three main parts. Chassis with four wheel drive, pan and tilt mechanism and a robotic arm.

2.1 Chassis with four wheel drive:
The chassis of the robot body is made by bending aluminum sheets and acrylic sheet. Four wheels are connected to four high torque gear motors to facilitate a four wheel drive.

2.2 Pan and Tilt mechanism:
The android phones can be panned 180 degrees at different speed with a 180 degree high torque servo motor. However they can also be tilted with another 180 degree servo motor.

2.3 Robotic arm:
The robotic arm is at the front side of the robot. It has two degrees of freedom. The gripping mechanism used here is "Four Bar Linkage End Effector."[1]. In this mechanism, the gripper is operated with a gear drive connected to a servo motor. The up-down motion of the arm can be controlled by another servo. Gears involved in the gripping mechanism were made from acrylic sheet with precise laser cutting.

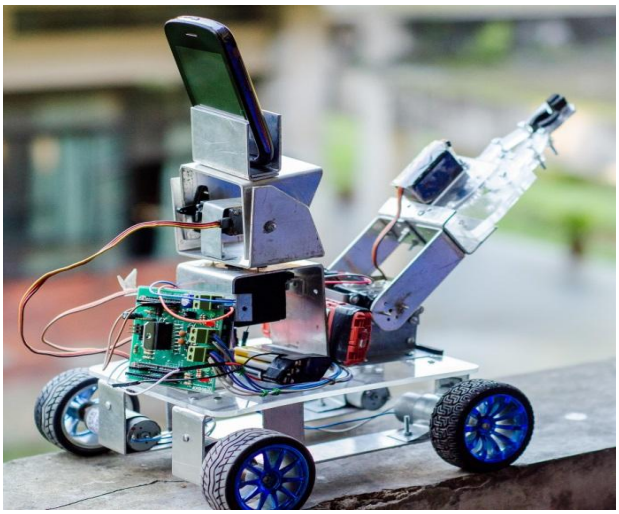

Fig. 1 Prototype

2.4 Steering:
For steering, "Skid Steering Method" [2] is used in this robot. This method engages one side of the tracks or wheels and turning is done by generating differential velocity at opposite side of a vehicle as the wheels or tracks in the vehicle are non-steerable.

Generally, differential drive concept is used in making robots which are two wheel drive robots. But that method has some disadvantages. In differential drive method, the robot does not drive as expected. It neither drives along a straight line nor turn exactly at expected

* Corresponding author. Tel.: +88-01557335807
E-mail address: sezan92@gmail.com

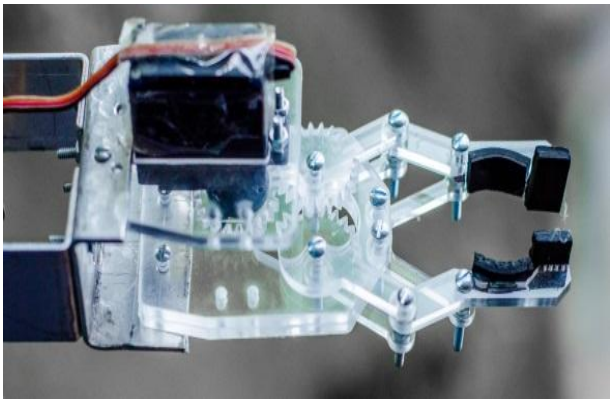

Fig. 2 Gripping Mechanism of the Claw

angles, especially when we use DC motors. So to over-come these problems, we used the skid-steering method.

3. Electrical Design

For locomotion, four wheels with four gear motors are used. For camera movement two servo motors are used and for the arm another two servo motors are used. These motors are controlled remotely from an android operated cell phone. A Bluetooth module 'HC-05'[3] is used to connect the system to the cell phone wirelessly. Whole Electrical System is described below,

3.1 Arduino

Arduino is a single-board microcontroller, intended to make the application of interactive objects of environments more accessible. The Hardware consists of an open source hardware board designed around an 8-bit Atmel AVR microcontroller. Here we've used Arduino Uno R3.[4] It has six analog output pins or "Pulse Width Modulation" or "PWM" pins. These pins

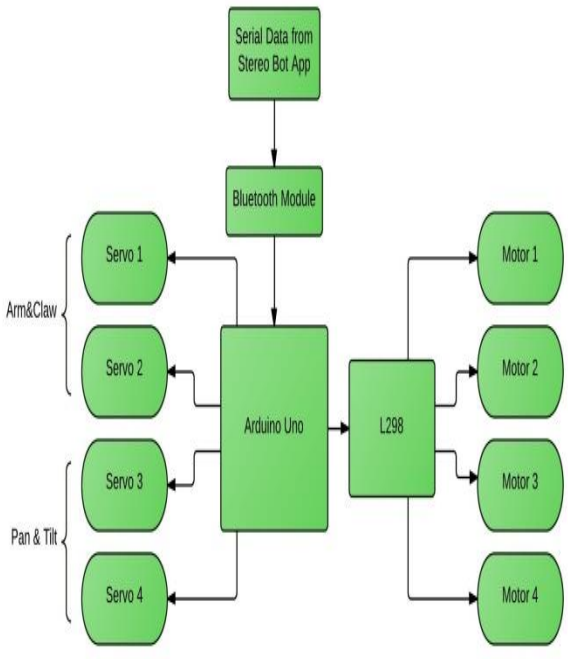

Fig. 3 System Block Diagram

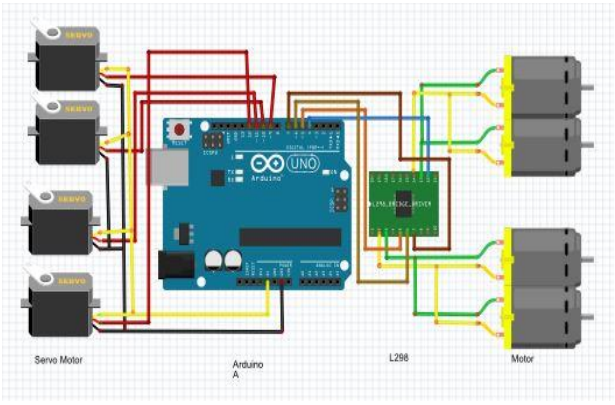

Fig. 4 Circuit Diagram using fritzing®

are enough for controlling the gear motors and servo motors.

3.2 Gear Motor Control

For locomotion, four high torque and high speed gear motors are used. Arduino boards cannot provide sufficient current and voltage for controlling these motors. So, a motor shield with dual bridge motor controller named L298 [5] is used. Four diodes are added to the motor shield to protect the circuit damage from back electromotive force generated from the motors. Two PWM pins D5 and D6 are connected to the input pins of the motor controller. The other pins are D4 and D7 respectively. PWM pins are used to control the speed of motors.

3.3 Servo Motor Control

A servo motor is a rotary actuator that allows for precise control of angular position, velocity and acceleration. In this particular robot, four high torque, coreless, metal gear dual bearing "Tower Pro MG995" - Standard Servo Motors are used. Two of them are used to control the arm. Remaining two of them are used to

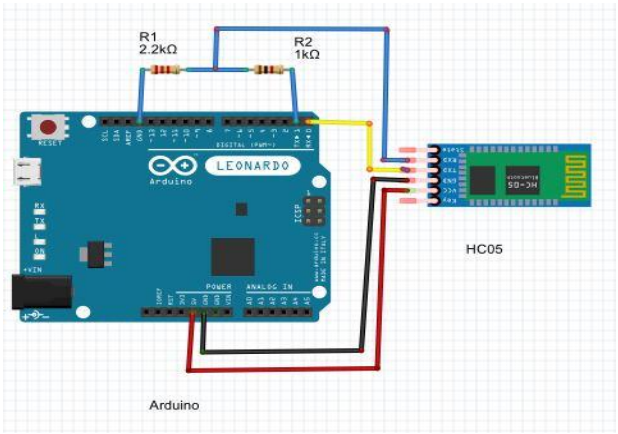

Fig.5 Arduino connection with HC05 using fritzing®

control the Camera pair. One servo motor rotates the cameras and the other one tilts the camera pair. Servo motors work on the pulses from microcontroller.

Changing the duty cycles of the pulses will change the angle of the servo motors. For zero degree position duty cycle must be 388 micro seconds, for ninety degree position duty cycle must be 1240 micro-seconds [6].

3.3 Bluetooth Communication

An Android Application will control the robot using Bluetooth connection. So, a Bluetooth module named HC-05 is used. This module works on 3.3 voltage level, while about all other electronic components work on 5 volt level. That means, to work with this module, we must make the signals voltage about 3.3 volt. To do that, a circuit connection like Fig.5 was made.

3.4 Software Development

3.4.1 Generating Stereoscopic Images

Stereo Vision: "Stereo vision is the extraction of 3D information from Digital Images." [7] At least two images of the same object is needed from two cameras. Here we used two cell phones as robotic eyes. The Distance between the two lenses is known as Baseline. The system will generate stereo images from those two images. There are some important steps to generate this image.

a) Stereo Image Rectification

First step for stereoscopic vision is to rectify stereo images. Image rectification is a transformation process used to project two-or-more images onto a common image plane. It corrects image distortion by transforming the image into a standard coordinate system.[8] We took help of MATLAB® documentation[9] regarding this very important process . The necessary steps are given below

Step 1: Reading the stereo image pair (Fig. 6)

Fig.6 Captured Images

Step 2: Generating points of correspondence. Points of interest are collected between two images and potential matches are found out using Speeded-Up Robust Features (SURF) algorithm. They will find blob-like features in both images [10].

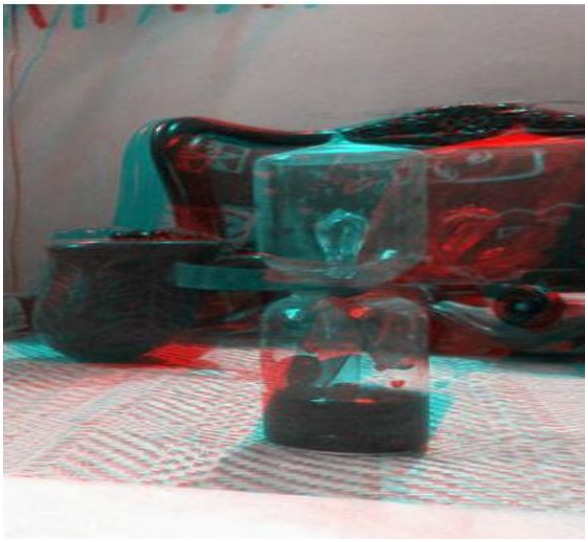

Fig. 7 Rectified Stereo Image

Step 3: Finding Putative Point Correspondences using Sum of Absolute Differences SAD. This algorithm takes absolute difference between each pixel in the original block and corresponding pixel in the block being used for comparison. These differences are summed to create a simple metric of block similarity. [11]

Step 4: Epipolar Constraints must be satisfied by the matched points. So, in this step , fundamental matrix was computed to check the inliers meet the epipolar constraint or not. [12] Then, outliers were removed using epipolar constraint.

Step 5: In this last step, the rectification transformation was computed. As a result, corresponding points appeared on the same rows. Finally, images were rectified using projective transformations and the overlapping area was cropped. (Fig.7)

b) Depth mapping

In 3D computer vision system, "Depth mapping" is referred to the process of measuring relative distances of surfaces of scene objects from a view point. At least two images are needed for depth mapping. Processing more images will result in more accurate depth map.[16]. It is worthy of mentioning that, we took a great help from MATLAB® documentation[9] in this regard. There are four steps for this particular process,

1) Basic Block Matching:
2) Sub-pixel Estimation
3) Dynamic Programming
4) Combined Pyramiding and Dynamic Programming.

The Block Matching block estimates motion between two images or two video frames using blocks of pixels. [13]. For every pixel in the right image, the 11-by-11-pixel block is extracted around it and searched along the same row in the left image for the block that best matches it.

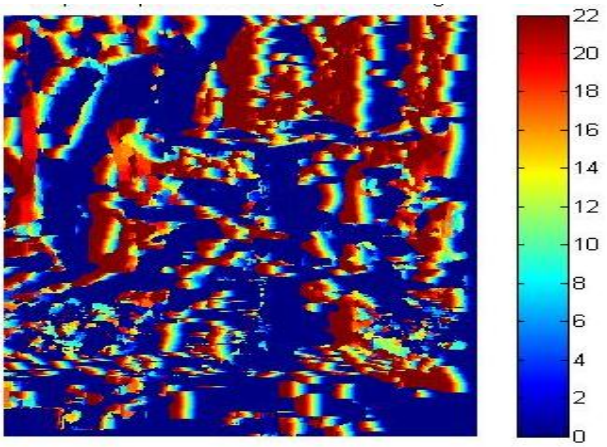

Fig. 8 Depth Map by Basic Block Matching

The pixel's location in the first image is searched in a range of pixels around, and the sum of absolute differences (SAD) is used to compare the image regions (Fig.7). "Templatematcher" system object was used to perform block matching. But in this step a noisy disparity image is created, which can be improved by introducing smoothness constraint. To remove these problems, "Subpixel Estimation" is used. At the end of this process, block matching was rerun .The result is given in the. The pseudo code is given below.

1) Set minimum and maximum row bounds for image block
2) Compute disparity bounds
3) Construct template and region of interest
4) Is there proper Template matcher object?
5) Run the" Templatematcher" object
6) Do "Subpixel Refinement"
7) Run Block Matching
8) Show the final figure

The final result with above process is shown in Fig.8. To improve the noise in the resulted figure, image pyramiding method and dynamic programming were used. [14][15] This improved the accuracy of the stereo image. The final result is shown in Fig. 9.

c)Backprojection:
Back Projection is the process of showing the position of every pixel in the three-dimensional image in a three-graph [9]. That is, it positions the objects in the plot and using that plot we can determine the exact position of every object. It's pseudo code is as following,

1) Declare Camera Intrinsic Matrix
2) Create a sub-sampled grid for back projection
3) Median Filter to smooth out noise
4) Derive conversion from disparity to depth with tie points
   4.1) Set Disparity values in pixels
   4.2) Set World "z" values in meters based on seen measurements.

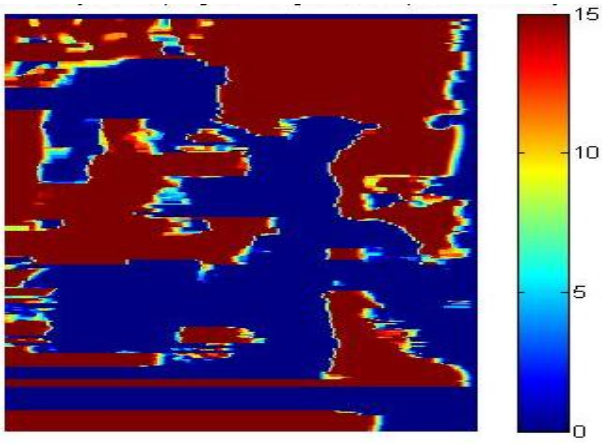

Fig.9 Depth Map for dynamic programming and sub-pixel accuracy.

5) Convert disparity to distances from camera using least square method
6) Set threshold
7) Remove near points
8) Show the 3-D plot.

To show this plot, intrinsic parameters of the cameras must be determined. Here, camera calibration toolbox[16] from California Institute of Technology was used to determine the intrinsic parameters . The parameters are shown in the following Table.

Table.1 Intrinsic Parameters of the Cameras

Parameters	x	Y
Focal Length	7305.527	-6009.122
Principal Point	239.5	319.5
Skew Factor	0	0

To measure the distances from the camera, an equation [17][18] is used in this process.

$$z_{world} = f + \frac{1+b}{d}$$

Here,

$$z_{world} = Distance\ from\ the\ Camera$$
$$f = focal\ length\ of\ the\ Camera$$
$$b = stereo\ baseline\ of\ the\ cameras$$
$$d = disparity$$

We know the focal length of the cameras. But we need to determine the baseline. That is done in MATLAB® . We gave input for known disparities the known distances of points from cameras. Doing simple regression analysis, the baseline can be measured. The final plot is shown in Fig. 10

3.4.2 Android Application for robot control:

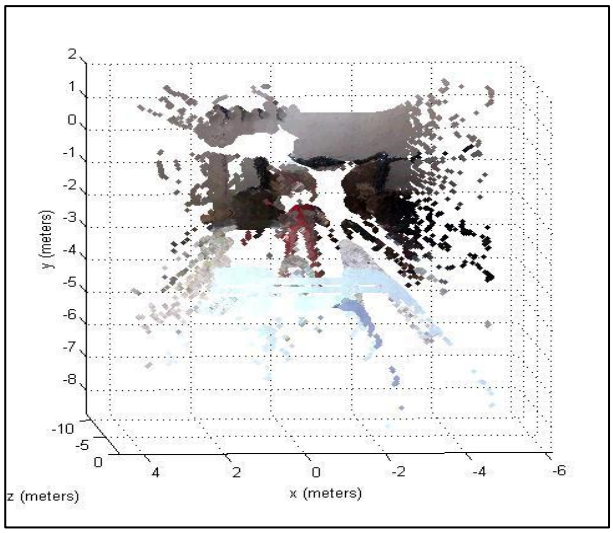

Fig. 10 Three dimensional plot after back projection

An android application named "Stereo Bot App" was developed to control the movement of the robot. Stereo bot connects HC-05 Bluetooth Module with the smart phone. While the connection is established serial data can be sent either from phone to Arduino or from Arduino to phone. The app works in two different control modes: Button control and accelerometer control. As described earlier, serial data can be sent to Arduino from two different user interfaces. The user Interface is given in the Fig.12. When an on screen button is touched a predetermined character assigned to that button is sent over Bluetooth network. For example, if forward button is pressed, 'w' character is sent. Other buttons work in a similar way.

Another control mode of Stereo Bot App is controlling using Accelerometer. Android's accelerometer can detect rotation of the phone around x, y and z axes and express the rotations in numerical values. These values

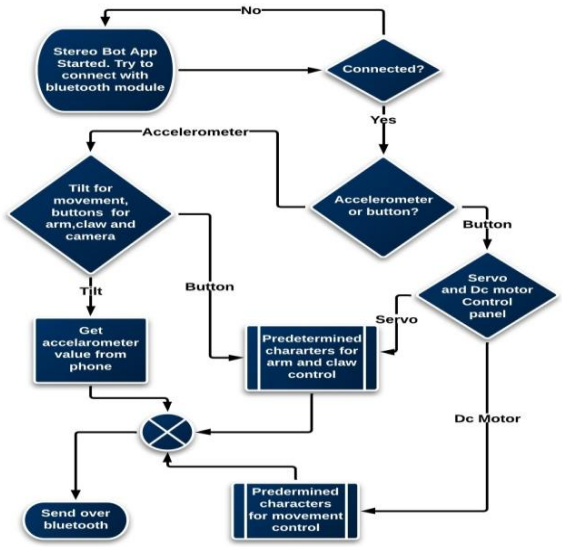

Fig. 11 Android Application Algorithm

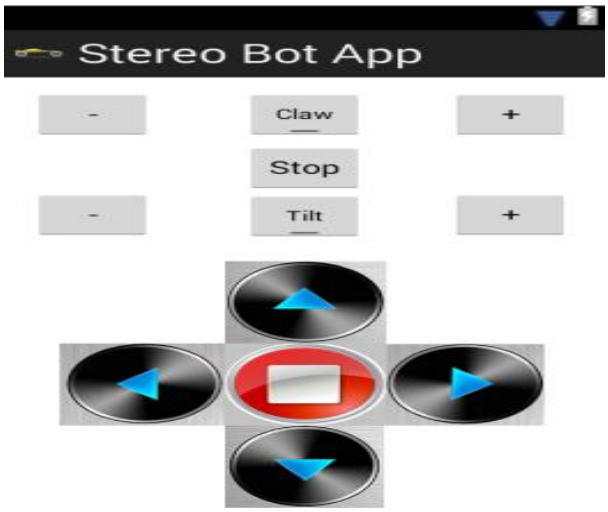

Fig. 12 Android Application interface

are measured at an interval of 250 milliseconds. Working principle of accelerometer control is described in the table. The corresponding robot movements are illustrated in Table 2..

Table.2 Accelerometer Value and Robot Movement.

Axes value	Robot Movement	Assigned Character
y<-4	Forward	W
y>4	Backward	S
x<-4	Left	A
x>4	Right	D
-2<x<2	Stop	X
-2<y<2	Stop	X

A plot is generated based on accelerometer data provided by "SensoDuino®". (Fig.13) However, for

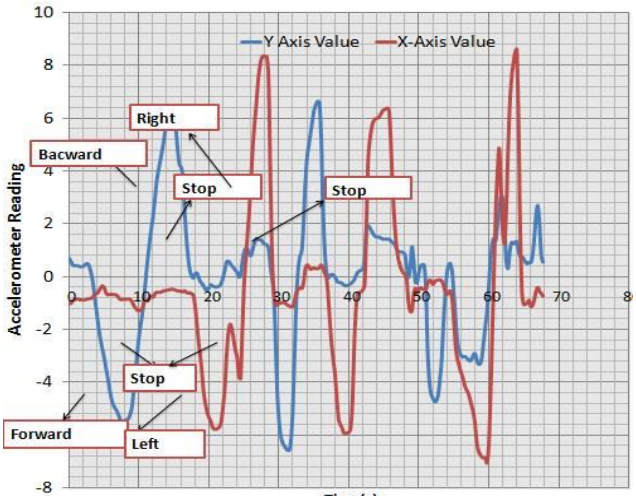

Fig. 13 Accelerometer reading vs time curve

arm-claw and pan-tilt control some on screen buttons are to be used.

REFERENCES

[1] Michael L. Turner, David A. Perkins, Andrew P. Murray,Pierre M. Larochelle "SYSTEMATIC PROCESS FOR CONSTRUCTING SPHERICAL FOUR-BAR MECHANISMS", ASME International Mechanical Engineering Congress and Exposition , Orlando, Florida USA. (2005)

[2] K. Kozlowsk, K. Pazderski, I. Rudas, J. Tar, "Modeling and Control of 4-Wheel Skid-Steering Mobile Robot: From Theory to Practice," in *International Journal of Applied Math and Computer Science*, Vol 14, n. 4, pp 477-496, (2004)

[3] HC-05 Bluetooth Module Datasheet. Available from http://www.scribd.com/doc/128811636/Datasheet-Bluetooth-Module-Hc05 . Accessed 17 November, 2014.

[4] Massimo Banzi, *Getting Started with Arduino*, O'Reilly Media Inc. (2009)

[5] L298 Datasheet. Available from https://www.sparkfun.com/datasheets/Robotics/L298_H_Bridge.pdf . Accessed 17 November , 2014

[6] Riazollah Firoozian, Electrical DC Servo Motors, *Servo Motors and Industrial Control Theory* , Springer Science & Business Media, Dec 4, 2008

[7] Richard Szelisk, *Computer Vision: Algorithms and Applications*, Springer Science & Business Media, Sep 30, 2010 .

[8] A. Fusiello, E. Trucco, and A. Verri. A compact algorithm for rectification of stereo pairs. *Machine Vision and Applications*, 12(1):16-22, 2000.

[9] MATLAB and Computer Vision Toolbox Release 2012b, The MathWorks, Inc., Natick, Massachusetts, United States.

[10] Herbert Bay, Andreas Ess, Tinne Tuytelaars, Luc Van Gool, "SURF: Speeded Up Robust Features", Computer Vision and Image Understanding (CVIU), Vol. 110, No. 3, pp. 346—359. (2008)

[11] E. G. Richardson, Iain. *H.264 and MPEG-4 Video Compression: Video Coding for Next-generation Multimedia*. Chichester: John Wiley & Sons Ltd. (2003)

[12] R A Hamzah, M. S. Hamid, H. N. Rosly, N. M. Z. Hashim and Z. A. F. M. Napiah ,"An Aligned Epipolar Line for Stereo Images with Multiple Sizes ROI in Depth Maps for Computer Vision Application .", International Journal of Information and Education Technology, Vol. 1, No. 1, April 2011.

[13] Aroh Barjatya, Block matching algorithms for motion estimation, 'Tech. Rep., Utah State University. (2004)

[14] Oliver Schreer, Peter Kauff, Thomas Sikora, Rendering with Geometry Compensation, *3D Videocommunication: Algorithms, concepts and real-time systems in human centred communication*, pp 167, John Wiley & Sons, (Nov 1, 2005).

[15] Burt, P. J. "Fast filter transform for image processing". *Computer Graphics and Image Processing* , (May 1981).

[16] Bouguet, JY. "Camera Calibration Toolbox for Matlab." Computational Vision at the California Institute of Technology. http://www.vision.caltech.edu/bouguetj/calib_doc/

[17] M. Okutomi , T. Kanade, A Multiple-Baseline Stereo, IEEE Transactions on Pattern Analysis and Machine Intelligence, v.15 n.4, p.353-363, (April 1993)

[18] Md. Shafayat Hossain, Ahmedullah Aziz, and Mohammad Wahidur Rahman "RAFI - A STEREO VISION BASED AUTONOMOUS MOBILE AREA MAPPING ROBOT WITH 16 DOF", International Journal of Artificial Intelligence & Applications (IJAIA), Vol.4, No.1, January 2013.

[19] Stephan Gobel, Ruben Jubeh, Simon-Lennert Raesch and Albert Zundorf: "Using the Android Platform to control Robots". Software Engineering Research Group, Kassel University.

ICMIEE-PI-140358

Analysis of Bio-heat Transfer Problem Using Finite Element Approach

A M M Mukaddes, Md. Atiqur Rahman and Abdullah Al Razi
Department of Industrial and Production Engineering, SUST, Sylhet-3114
Bangladesh
Email: mukaddes1975@gmail.com

ABSTRACT

Bio-heat transfer is the study of external or internal heat transfer in the biological body. In different therapeutic treatments especially in cancer treatment, heat is used to cure infected cells. The required temperature that will kill the infected cell should be known before starting the thermal treatment on human tissue. The useful ways to measure the temperature distribution on human tissue are finite difference method as well as analytical method in some cases. There are few reports of finite element solution of bio-heat equation in the literature. Though finite element approach is one of the efficient techniques to find the temperature distribution in physical body, there have been very few reports of using this method for this particular issue. In this paper a finite element model has been developed to analyze the bio-heat transfer equation which is also well known as Pennes equation. Crank-Nicolson method has been used for the time discretization of the unsteady part of the problem. The developed system can be used to predict the temperature in human tissue under certain external heating conditions.

Keywords: Finite element, bio-heat, Pennes equation, unsteady problem

1. Introduction

Heat transfer is an important component of biological activities. For example, skin plays a variety of important roles including sensory, thermoregulations and body defense etc. Amongst these, the most important one is thermoregulation: skin functions thermally as a heat generator, absorber, transmitter, radiator, conductor and vaporizer, thus acting as an important barrier for the human body to various outside conditions. Except some environmental conditions skin/tissue has also to face some experimental conditions during some therapeutic treatments. Cancer treatment, treatment of burn injuries and diagnosis of other thermal diseases requires the information of temperature distribution in living tissue. Therefore studying of the bio-heat transfer has become popular in the bio-mechanical engineering research area.

In some therapeutic treatment, heat is used to kill or remove the infected cell. For example, the primary objective of the hyperthermia is to raise the temperature of the infected cell to a therapeutic value, typical 42-46^0 C, and then deactivate it thermally.

Over the years, several mathematical models have been developed to describe the heat transfer within living biological tissues. These models have been widely used in the analysis of hyperthermia in cancer treatment, laser surgery, thermal comfort treatments, and many other applications. Many experimental and theoretical studies have confirmed the important role played by thermal processes during hyperthermia [1]. The most widely used bio-heat model was introduced by Pennes in 1948 [2]. It is based on the classical Fourier law, and has been greatly simplified after introducing the concept of blood perfusion to study the bio-heat transfer and assessment of skin burns. Reports on analytical solution and numerical solutions of the bio-heat transfer problem are found in the literature. They can be distinguished by the boundary conditions used on the skin surface, blood perfusion, heat flux on the skin surface and solution techniques. In some analytical cases sinusoidal heat flux [3] and sometimes cooling of the skin [4] are considered as boundary conditions. Researches related to the bio-thermo-mechanical are reviewed in [5]. The result of boundary element method and finite element method for the numerical solution of the steady-state bio-heat transfer model of the human eye are compared in [6, 7]. The finite element method is used for the thermal-magneto static analysis in biological tissues in [8].

ADVENTURE_Thermal is a parallel FEM open source module to solve the large scale 3D heat

E-mail address: mukaddes1975@gmail.com

conduction problems. The module considers the general heat conduction equation for the solid body. It supports different types of boundary conditions. Both steady and unsteady problem can be solved using this module. The hierarchical domain decomposition method is used to solve the problems in parallel computer. Development of ADVENTURE_Thermal is a continuing process. But this module cannot be used to find temperature distribution in biological bodies. The inclusion of bio-heat transfer functions in this module is necessary.

In this paper a finite element model [9, 11] has been developed for the numerical solution of the 1D unsteady Pennes equations with different spatial heating. The Crank-Nicolson method is used for the time discretization. This method is compared with other time discretization schemes. A C code has been developed which can be used to measure the temperature distribution in the human tissue. Later the function for the 3D bio-heat equation solution will be included in the ADVENTURE_Thermal.

The bio-heat transfer equation is introduced in the section 2 while section 3 describes the finite element discretization method. The time discretization scheme is explained in section 4. Before the conclusion some numerical results are shown in section 5.

2. Bio-heat transfer

For the study of bio-heat transfer in human tissue the most useful one is Pennes equation which is:

$$\rho c\frac{dT}{dt} = k\frac{d^2T}{dx^2} + w_b\rho_b c_b\,(T_a - T) + Q_m + Q_r(x,t) \qquad (1)$$

where ρ, c, k are respectively the density, the specific heat, and the thermal conductivity of the tissue; ρ_b, c_b denote density and specific heat of blood; w_b the blood perfusion; T_a the known arterial temperature, and $T(x,t)$ is unknown tissue temperature; Q_m is the metabolic heat generation, and $Q_r(x,t)$ the heat source due to spatial heating with respect to time t. Specific heat and density of both blood and tissue are changeable with respect to conditions. Natural and force heat convection coefficient between skin and surroundings can also be changed with change of temperature, air flow, postures etc.

For a one dimensional problem of length L Let, $T(x,0) = T_0(x)$ is initial temperature, T_c is the body core temperature and often regarded as a constant, h_0 is the apparent heat convection coefficient between the skin surface and the surrounding air, T_f is the surrounding air temperature. Thus the boundary conditions for this particular 1-D problem can be written as:

$$T = T_0(x) = T_c\,, \qquad at\ \ x = L$$

$$-k\frac{dT_0(x)}{dx} = h_0\big[T_f - T(x)\big],\ \ at\ \ x = 0 \qquad (2)$$

Here, the skin surface is defined at $x = 0$ and the body core at $x = L$.

The analytical solution of the differential equation (1) with boundary conditions of equation (2) was developed by Zong-Shan Dang and Jing Lui [10]. The bio-heat equations (1) and (2) have also been solved using the finite difference method and boundary element method. In this paper the finite element approach is developed to solve the bio-heat equation (1) and (2).

3. Finite element discretization

The first step of the finite element discretization is to develop a weak form that is a weighted-integral statement and is equivalent to both the governing differential equation as well as certain type of boundary conditions. The simplest form of the equation (1) is

$$\rho c\frac{dT}{dt} = k\frac{d^2T}{dx^2} - CT + q \qquad (3)$$

where, $C_b = w_b\rho_b c_b$

and $q = C_b T_a + Q_m + Q_r(x,t)$.

The weak form [9] of the differential equation (3) was derived as

$$\int_{x_a}^{x_b}\left[W\rho c\frac{dT}{dt} + k\frac{dW}{dx}\frac{dT}{dx} + CWT - Wq\right]dx + (WQ)_{x_a} + (WQ)_{x_b} = 0\ . \qquad (4)$$

where W is the weight function and Q is the secondary variable.

In this paper, a linear element is considered whose temperature function is given as:

$$T_h^e(x) = \sum_{j=1}^{2}\varphi_j^e(x)T_j^e \qquad (5)$$

Using the linear approximation of equation (5) finally a linear equation was derived [9]. That is:

$$[C]\{\dot{T}\} + [K]\{T\} = \{q\} + \{Q\} \qquad (6)$$

where C is the capacitance matrix, K is heat conductive matrix and T is unknown temperature and others are known vectors. This set of linear equation was solved using the well-known time discretization method.

Corresponding author: mukaddes1975@gmail.com

4. Time Discretization Scheme

A simple time integration scheme for equation (6) was derived by assuming that C and K are constant. In such case matrix differential equation can be discretized on time [11] as:

$$C\frac{T^{n+1}-T^n}{\Delta t}+\alpha KT^{n+1}+(1-\alpha)KT^n=q+Q \quad (7)$$

where T^{n+1} and T^n are the vectors of unknown nodal values at times $n\Delta t$ and (n+1) Δt respectively. α is a weighting factor which must be chosen in the interval between 0 and 1. In equation (7) the standard approximation for time derivative

$$\dot{T}=\frac{T^{n+1}-T^n}{\Delta t}$$

was used. When the value of α is considered 0.5, the process is called the popular Crank-Nicolson method.

The discretized equation (7) can be written as:

$$(\tfrac{1}{\Delta t}C+\alpha K)T^{n+1}=\left[\tfrac{1}{\Delta t}C-(1-\alpha)K\right]T^n+Q+q \quad (8)$$

and can also be written in the general form:

$$HT^{n+1}=F^n \quad (9)$$

where $H=(\frac{1}{\Delta t}C+\alpha K)$ and

$$F^n=\left[\tfrac{1}{\Delta t}C-(1-\alpha)K\right]T^n+q+Q$$

The equation (8) or (9) was solved using an iterative procedure. The initial temperature is known and then temperature of the next step can be calculated from the solution of equation (8) via the Gauss elimination technique.

5. Analysis and Numerical Results

A FEM code has been developed using the C language to solve the numerical solution of the finite element model described in the previous section. Both steady and unsteady state results are presented here.

Problem statement:

In this paper, a tissue of length 3 cm from the skin surface is considered for the calculation. The convection boundary conditions and temperature boundary conditions are considered on the skin surface and body core respectively. The tissue properties and parameters of the boundary conditions (Table 1) are applied as given in [10]. Both steady and unsteady problems are analyzed. Analytical results and numerical results for different time step are reported.

Steady state results

Steady problem is analyzed first. For FEM analysis 21 meshing nodes and 20 linear elements are considered. The temperature profile for 21 nodes is shown in Figure 1. The steady state results are compared with the analytical solution developed by Zong-Shan Dang and Jing Lui [10]. The comparative results are shown in Table 2 for the mesh of 21 nodes. According to the Table 2, the FEM results match with the analytical results.

Table 1 Thermo mechanical properties of tissue

Symbols	Values
k	0.5 W/m ^{0}C
h_0	10 W/m^2 °C
h_f	100 W/m^2 °C
T_f	25 °C
T_a	37 °C
T_c	37 °C
Q_m	33800 W/m^3.
C	4000 J/kg.°C
c_b	4200 J/kg.°C
P	1000 kg/m^3
ρ_b	1000 kg/m^3
W_b	0.0005 ml/s/ml

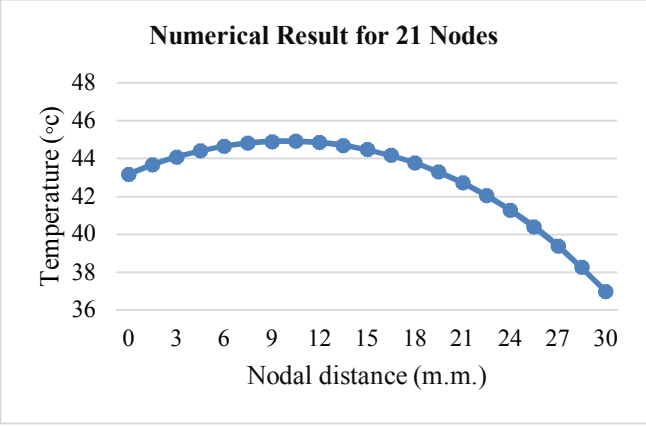

Figure- 1 Steady state results (21 nodes)

Corresponding author: mukaddes1975@gmail.com

Table-2 FEM and analytical solution

Dist. (m.m.)	Temp.(◦C) (Ana.)	Temp. (◦C) (FEM)
0	43.1913	43.1965
1.5	43.6912	43.6964
3	44.1021	44.1074
4.5	44.428	44.4332
6	44.672	44.6771
7.5	44.8363	44.8413
9	44.9224	44.9274
10.5	44.9313	44.9362
12	44.863	44.8677
13.5	44.7168	44.7213
15	44.4909	44.4957
16.5	44.1846	44.1887
18	43.7935	43.7974
19.5	43.3145	43.3181
21	42.743	42.7462
22.5	42.0736	42.0764
24	41.2999	41.3024
25.5	40.4147	40.4166
27	39.4095	39.4108
28.5	38.2749	38.2755
30	37	37

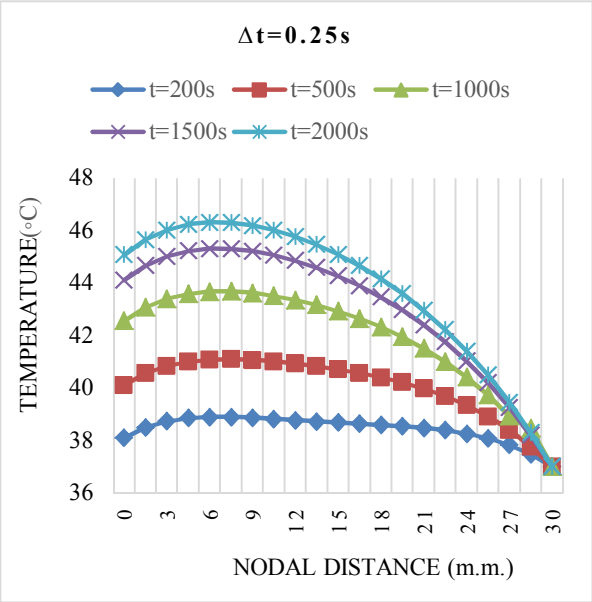

Figure-2 Temperature at different time ($\Delta t = 0.25s$)

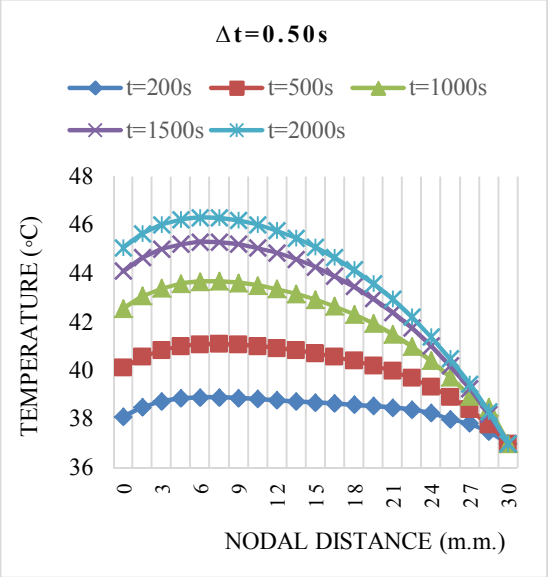

Figure-3 Temperature at different time ($\Delta t = 0.5s$)

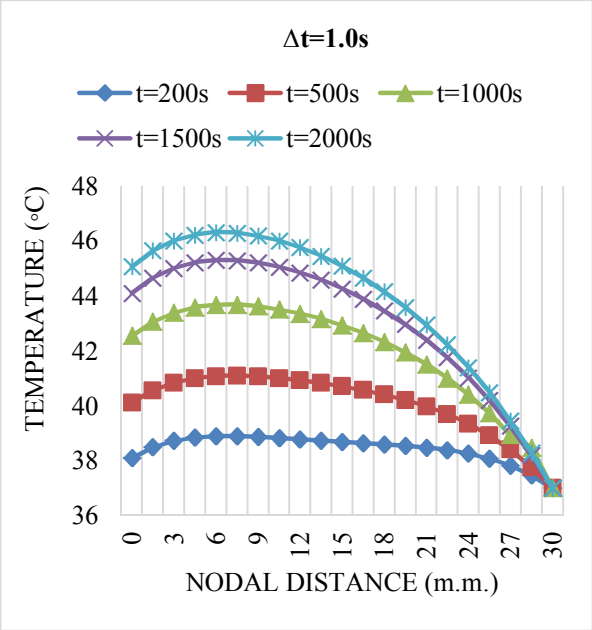

Figure-4 Temperature at different time ($\Delta t = 1.0s$)

Unsteady state results

In the unsteady state analysis different time increments are used to measure the temperature at different time. The initial temperature was 37^0C which is equal to the core temperature. The results are presented in the Figure 2, 3, and 4. These figures show that as time passes the temperature within the tissue increases and finally reached to the steady state condition. The results of these figures consider the constant spatial heating from the skin surface to the body core. There is no significant change of temperature distribution due to the change of time increment. The maximum temperature exists 46^0C at 6 mm below the skin surface.

Corresponding author: mukaddes1975@gmail.com

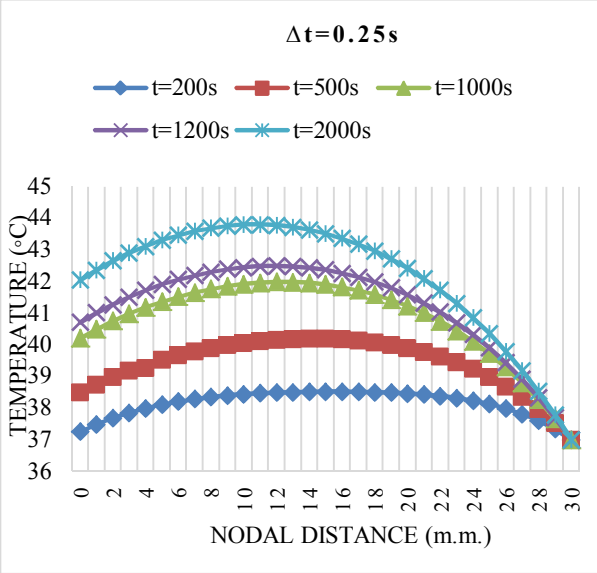

Figure-4 Temperature at different time ($\Delta t = 0.25s$)

A temperature distribution found without the spatial heating is shown in Figure-5 for the time increment ($\Delta t = 0.25s$). The comparison with the results with spatial heating shows that the position of maximum temperature is changed. The maximum temperature exists near the skin surface in case of with spatial heating and near the middle of the model in case of without spatial heating.

In the field of bio-heat transfer, finite element method can be used to design medical equipment for therapeutic applications, where operation can be time dependent or time independent. From this analysis, we have seen how temperature distribution can be changed with respect to time. The effects of time interval and different tissue properties can be analyzed using the developed system. Impacts of spatial heating have also been evaluated from this analysis. Different amount of spatial heating can give different temperature distribution. So a required temperature distribution can be synchronized by different spatial heating and different time limit.

7. Conclusion

A finite element model was developed in this work to analyze 1D steady and unsteady bio-heat transfer in biological tissue. A computer program was also developed using C language and the bio-heat problem was solved using it. Required temperature distribution can be found in human tissue for both steady and unsteady states. The FEM results coincide with analytical results for problem described in the paper. With and without spatial heating conditions are compared. The location of the maximum temperature is changed with the spatial heating. From the analysis, highest value of temperature was found at the distance of 6 m.m. from the skin (where distance from the skin to body core is 30 m.m.), which can also be varied for different conditions. Using different boundary conditions and applying different amount of heat flux one can select the suitable skin condition to maintain the acceptable tissue temperature and destroy the infected cell.

8. Future study

This work concerns with the 1D finite element analysis of bio-heat transfer equation. The coding for 2D bio-heat transfer problem is going on. The spatial heating sometimes acts on sinusoidal function which will be added in the new code. Finally a 3D bio-heat finite element system will be added to the ADVENTURE_Thermal [12] which is a module for steady and unsteady heat conduction problems using the parallel finite element method.

References

1.S. Mandal, T. Sundarajan and P. S. Ghoshdastidar, A coupled analysis of thermal and electromagnetic phenomena during hyperthermia in biological tissues. *ASME winter annual meeting,* HTD-Vol 126, pp. 59-66 (1889).

2. H. H. Pennes, Analysis of Tissue and Arterial Blood Temperatures in the Resting Human Forearm. *Journal of Applied Physiology,* Vol. 1, pp. 93-122 (1948).

3. T. Shih, Y. Ping, W. Lin and H. Kou, Analytical analysis of the Pennes bioheat transfer equation with sinosoidal heat flux condition on the skin surface, *Medical Engineering and Physics*, Vol 29, pp. 946-953, (2007).

4. W. Shen and J. Zhange, Modeling and Numerical Simulation of Bioheat Transfer and Biomechanics in Soft Tissue, *Mathematical and Computer Modeling,* Vol. 41, pp. 1251-1265 (2005).

5. F. Xu, T. J. Lu, K. A. Seffen, Biothermomechanical behavior of skin tissue, *Acta Mechanica Sinica,* Vol. 24, No. 1 pp. 1-23 (2008).

6. E. H. Ooi, W. T. Ang and E. Y. K. Ng, A boundary element model of the human eye undergoing laser thermokeratoplasty, *Computers in Biology and Medicine.* Vol. 38, pp. 727-737, (2008).

7. E. H. Ooi, W. T. Ang and E. Y. K. Ng, Bioheat transfer in the human eye: A boundary element approach, *Engineering Analysis with Boundary Elements,* Vol. 31, No. 6, pp. 494-500(2007).

8. S-C Hwang, and Lemmonier, Coupling numerical solution of bio-heat transfer equation and Maxwells equations in biological tissues during hyper-

Corresponding author: mukaddes1975@gmail.com

thermia, *Transactions on Biomedicine and Health*, Vol 2, pp. 435-443 (1998)

9. Reddy, J. N. An Introduction to the Finite Element Method, 3rd edition, McGraw Hill, Inc, (2006).

10. J. Lui and D. Zhong-Shan, Analytical study on bioheat transfer problems with spatial or transient heating on skin surface or inside biological bodies. *Journal of biomechanical engineering*, Vol-125(6), p. 638-649 (2002).

11. G. Comini, S. D. Giudice and C. Nonino, Finite Element Analysis in Heat Transfer, Taylor and Francis, USA, (1994).

11. http://adventure.sys.t.u-tokyo.ac.jp/

ICMIEE-PI-140360

Design and fabrication of a micro-class unmanned aerial vehicle (UAV) with high payload fraction

Saifur Rahman Bakaul[1], Md. Abdus Salam[2], Fairus Sakib Tanzim[3], Abdullah Al Faysal[3], Md. Shafique[3], Kh. Md. Faisal[4]

[1]Associate Professor, [2] Professor, [3]Students, [4]Lecturer, Department of Aeronautical Engineering, Military Institute of Science and Technology, Dhaka-1216, BANGLADESH.

ABSTRACT

Unmanned aerial vehicle industry is highly charismatic and constantly expanding with the growth of science and technology in the context of Bangladesh. This paper presents the design and fabrication of a micro-class UAV, capable to take maximum payload with minimum empty weight. The iterative process of design is to meet the specific requirements set by the Society of Automotive Engineers, USA for their annual international aero-design competition. The preliminary and detailed design required optimization process and trade-study, material selection, propulsion system integration, electrical system design, control system design, analysis of aerodynamics characteristics as well as determining stability and control parameters. Finally, wind tunnel tests were carried out before flight test under real flight situation to analyze the performance parameters and subsequent modification was done to turn the UAV into a desired one incorporating all necessary design requirements. The self-weight of the designed UAV was only 450 grams and it lifted another 890 grams of payload; the high payload fraction clinched 4th position out of 33 teams from different Universities of the world.

Keywords: UAV design, aerodynamics, stability and control, multi-disciplinary optimization, trade-study.

1. Introduction

Society of Automotive Engineers (SAE), USA has been organizing SAE Aero-Design Competition among the Universities of the World since 1986. Design and fabrication of the unmanned aerial vehicle (UAV) presented in this paper started with the aim of participating in SAE Aero-Design Competition 2014 with the specific objective of maximizing the payload fraction. Payload fraction is the ratio of the weight of the external load that the UAV carries to the total weight of the UAV. Maximizing the payload fraction requires blending the knowledge on aerodynamics, aero-structure, stability and control, strength of materials and multi-disciplinary optimization.

The design process was started with the conceptual design, where all the basic aspects like configuration, power-plant, wing, empennage and fuselage were designed. A trade study analysis ensured that the selected value of wing loading and power to weight ratio will lead to the maximum payload fraction. Detailed design was carried out basing on the frozen design and parts and sub-systems were fabricated. Lastly, flight tests were carried out and further modifications were incorporated before fabricating the final version of the UAV.

2. Conceptual design

Configuration was chosen on the basis of sensitivity analysis which determined how well the UAV could accomplish the task of the mission. Wing and tail configuration, propulsion system, payload location were picked from few possible options as described below.

2.1 Wing configuration

Wing configuration was chosen on the basis of empty weight, maneuverability, aerodynamics, stability, manufacturability and payload integration and it was found that conventional configuration with high wing location would be the optimum option [1]. The idea of using low-wing would not be viable as it would create problem during landing (as designed UAV will not have any landing gear). A mid-wing is quite difficult to build an UAV due to its carry-through characteristics as well as the difficulty to provide the required taper ratio. So, a high wing was the most suitable option for this UAV. In addition, a high wing will tend to give some degree of dihedral at the time of flight as it carries the overall payload in the middle and lift is generated from the wing; such dihedral increases rolling stability and works against any perturbation appearing from gust wind or any other environmental disturbance during actual flight.

2.2 Tail configuration

Among the available options of tail configuration, the option of T-tail was not considered because of its being heavier than conventional tail [1] and requirement of additional strength of the empennage. V-tail was another option as it reduces wetted area, but it gives adverse maneuverability which causes great difficulties for the controls engineer to design effectively how the control surfaces of the UAV would behave. Finally, considering system weight, stability and control, landing and take-off, drag and ease in manufacturing, conventional tail was considered as the best option for the UAV under design.

2.3 Propulsion system integration

In order to keep the system simple, a battery pack and propeller configuration was found to be the most suitable for this UAV. Considering system weight, power to weight ratio, and effect on stability and controllability, this UAV was decided to be fitted with

single tractor propulsion system. Because of being small aircraft, corkscrew effect wouldn't affect this design.

2.4 Payload location

Payload location was preferred inside the fuselage to lessen drag, ease of launch and elementary manufacturability. If the payload were positioned outside the fuselage, it would cause additional drag and if the payload were hung with sling, it would be difficult to accurately position the CG position, which is vital for stability and controllability analysis. In addition, the payload bay was designed in such a way that the location of the CG can be slightly changed as per the requirement of stability basing on the atmospheric condition and associated disturbances.

3. Preliminary design

Successive iterative procedure was adopted for important design parameters and multi-disciplinary optimization was implemented during preliminary design phase to reach to highest payload fraction. Minimizing empty weight and increasing lifting capability as well as maximum capability of carrying payload with minimum weight became the driving motive of all the design phases and sizing trade-offs.

3.1 Airfoil selection

With a view to increase the performance, 'aerodynamic twist' was introduced using two different airfoils: Eppler 214 at the root and Selig 1223 at the tip of the planform. Such combination was chosen to ensure the desired stall characteristics of the UAV. By conducting the wind tunnel test of the modified airfoil, it was seen that the combination airfoil provided optimum values of maximum lift coefficient ($C_{L,max}$), zero lift drag coefficient ($C_{D,0}$), max thickness (t_{max}/c), pitching moment coefficient (C_M), maximum value of C_L/C_D and stalling characteristics. The maximum lift coefficient for this modified airfoil came out to be 2.044.

3.2 Motor and propeller optimization

As in case of motor-driven remote-controlled aircraft, propeller pitch and diameter are related to motor power, motor power was optimized first and propeller specifications were set accordingly. On the basis of the experimental performances of three different motors, EMAX BL CF2822 was proved to be the most optimum.

3.3 Battery, Electronic Speed Controller (ESC) and Servo motor optimization

Among the components of the propulsive system, battery is the power supplier. With the increment in battery cell, power generation increases along with a significant increase in battery weight. So, an 850 mAh 3-cell (11.1V) battery was selected which provided sufficient power to drive the motor having an acceptable self-weight. Matching with the motor specifications, a 20A Electronic Speed Controller (ESC) was selected to feed the power from battery to motor.

4. Detailed design

During detailed design, the testing effort intensified and the actual structure of the aircraft was fabricated and tested. The important part was the production design to enter the full scale development.

4.1 Design features and details

Optimization was done for the wing and empennage planforms. Finally, rectangular main wing was designed with chord length, span, area and aspect ratio of 6.5 in, 38 in, 247 sq in and 5.85 respectively. On the other hand, a flat plate horizontal stabilizer with chord length of 4 in, span of 12.5 in, area of 50 sq in and aspect ratio of 3.1 were used while vertical stabilizer had height of 5.8 in, root chord of 5.8 in and tip chord of 2.3 in. Finally the length, width, height and gross weight of the complete airplane were 23.5 in, 38 in, 5.8 in and 329 g respectively.

4.2 Weight build up and structural characteristics

Component wise weights were calculated; weight build-up pie chart is shown in Fig.1. In addition to the structural materials, 33 gm weight was added due to connecting rod for wing, binding tape and the rubber band used for attaching wing with the fuselage. Reducing the empty weight was the prime motive in the entire design process. The loads acting at each prominent load bearing members were calculated and a factor of safety of 1.25 was used. The low factor of safety and exact calculation of stress ensured that material is not added unnecessarily, which will provide the capability of carrying highest payload by the designed airplane.

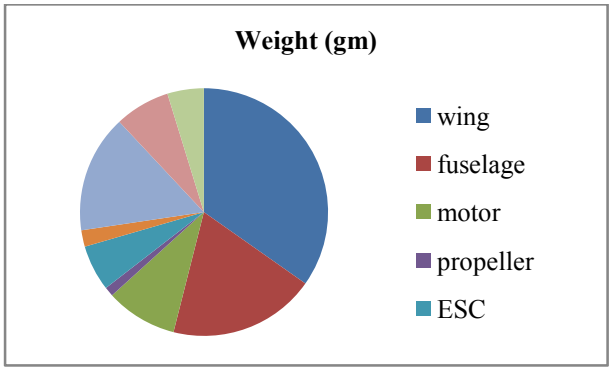

Fig.1 Weight build-up of the designed UAV.

4.3 Wing and empennage design

Aerodynamic twist was used in the wing. By using two separate airfoils, E214 at root and S1223 at the tip, the angle between the zero-lift angle of tip airfoil and the zero-lift angle of the root airfoil were different and such twisting was incorporated to reshape the lift distribution favorably. Between root and tip chord, the airfoils were meshed up while 6.5'' chord and 38'' span were used to keep the aspect ratio low as well as high lift. Theoretically this wing can carry a payload, which is 3 times the empty weight of the entire aircraft.

Conventional tail was selected in the empennage because it is easier to construct, can recover from wing drag although less effective for pitch stability at high α. However, the prime concern was to reduce the empty weight, so despite lower effectiveness at high angle of attack, conventional configuration was chosen. Flat plate was used at the empennage design which was constructed by foam sheet.

4.4 Materials used

To keep the weight low, solid foam was used in wing fabrication. To give the wing sufficient strength, it was covered with glue and later with covering paper. The covering paper was provided with heat treatment to increase strength and provide aerodynamic shape.

4.5 Electronics design and flight performance parameters

Two ailerons were controlled by two different servomotors while rudder and elevator were controlled by separate servomotor. Servo mechanism is a control system that converts a small mechanical motion into one requiring much greater power. Metal gear servos were used for greater torque and less weight factor.

5. Analysis

With all the components of the UAV, finally the wing loading, gross weight and stall speed came out to be 33.33 oz/ft^2, 1130 gm and 9.03 m/s. For further analysis, either Computational Fluid Dynamics (CFD) or Experimental Fluid Dynamics needed to be used. CFD analysis gives a computational result of the design while wind tunnel testing gives experimental results. Although, CFD analysis before the actual fabrication would be desirable, such simulation could not be carried out due to the non-availability of large computational resource. Wind tunnel testing was carried out to determine the behavior of the wing with aerodynamic twist.

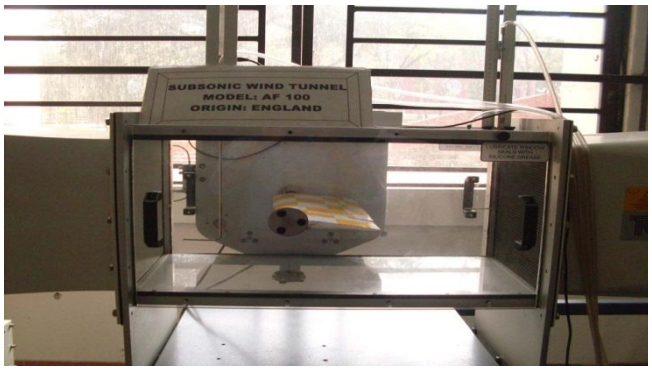

Fig.2 Experimenting the modified wing in wind tunnel.

5.1 Aerodynamic Drag Determination

Drag of UAV is calculated at Reynolds's Number of 1.5657×10^5 [5]. Component wise drag build up and UAV drag prediction is shown in Table 1.

Table 1 Data for drag build up.

Component	C_{D0}	% of total drag
Wing	0.00605	55%
Fuselage	0.00275	25%
Vertical stabilizer	0.00110	10%
Horizontal stabilizer	0.00055	6%
Motor	0.00044	4%
Total	0.0110	100%

50% of the total thrust was sufficient to produce the necessary lift for taking off without runway as it can be launched by hand. Instead of using landing gear the structure of the body was developed in such a way that it could withstand the shock it receives while landing and is able to perform necessary maneuvering which is required. To avoid the downwash effect, the concept of Aerodynamic Twist was developed such as an airfoil (selig-1223) was kept at the tip which could produce more lift while flying and then another airfoil with comparatively less lifting coefficient (Eppler-214) at the root of the wing. A bit dihedral wing was used for performance flight to make it stable and increase the weight lifting capabilities. Because of its small size, the aero elasticity effect was not that significant on the UAV, though some aero elastic effects affected the wing while performing the flight tests which caused the wings to bend 3-4 inches.

5.2 Stability analysis

The UAV was designed with the aim of positive longitudinal stability. As the stabilizer is placed aft of CG, it facilitates built in stability. The contribution of the wing was destabilizing while the contribution of the fuselage was mildly destabilizing. The tail size was calculated using tail volume coefficient method so that the desired degree of positive longitudinal stability is ensured. Using the techniques of Roskam and Etkin, stability and control derivatives were calculated, as shown in Fig. 3 while these values were confirmed through AVL.

Angle of Attack					
CLα		5.40			
CMα		-0.50			
Slide slip		Roll Rate		Yaw rate	
Cyβ	-0.30	Cyp	-0.07	Cyr	0.30
Clβ	-0.03	Clp	-0.49	Clr	+0.27
Cnβ	0.02	Cnp	0.0035	Cnp	-0.17
Pitch Rate		Aileron Deflection δa		Elevator Deflection δe	
CLq	5.75	Clsα	0.006	CLδe	0.0059
CMq	-4.5	Cnsα	0.0003	CMδe	-0.014

Fig.3 Stability derivatives

5.3 Weight and balance

Dividing the parts of aircraft with the help of Fig.4, the following Table 2 shows the weight, moment-arm and momentum of each sub-assembly. Finally the CG of the UAV was found to be located at a distance of 8.57 in from the nose [5].

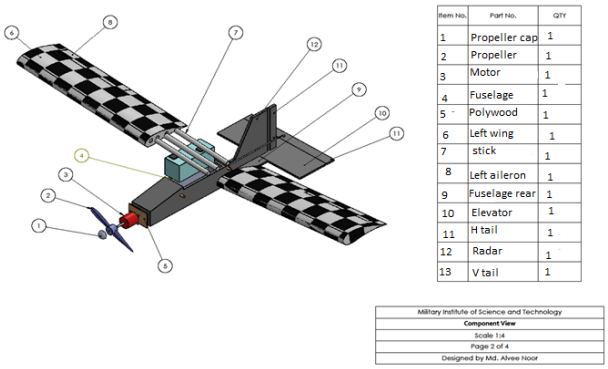

Fig.4 Calculating location of CG

Table 2 Calculation of CG location

Component	Weight(lb)	Arm length(in)	Momentum (in-lb)
Fuselage1	0.183	2.33	0.426
Fuselage2	0.068	9.75	0.663
Fuselage3	0.439	14.5	6.366
Fuselage4	0.070	19.2	1.344
Wing	0.242	8.16	1.970
V tail1	0.033	19.00	0.627
V tail2	0.066	21.25	1.403
V tail3	0.067	23.00	1.541
H tail	0.432	22.90	9.893
ESC	0.048	4.75	0.228
Receiver	0.031	10.43	0.321
Servo	0.066	12.00	0.792
Motor	0.086	1.75	0.150
Propeller	0.011	0.50	0.005
Battery	0.141	8.05	1.136
Others	1.653	2.60	4.298
Total	3.636	-	31.163

5 Testing plan

The entire UAV along with the propulsion system was tested to observe how the component works together and to determine the systems performance parameters such as thrust, torque, RPM, current, voltage at different airspeeds. Again the entire propulsion system was also tested with various types of propellers which enabled the verification of propeller optimization process. Voltage drop and the actual usable capacities were the critical performance variable in the case of battery testing. Propeller with various diameters and pitch angle were tested in a wind tunnel with the help of a constant power source and motor which helped to optimize the thrust and RPM. To check whether the material used in the UAV will be able to withstand various loads during flying or not, the bending test was conducted for the wing. The ultimate validation of the design was done through numerous flight tests.

6 Manufacturing plan and process

To conserve weight, multiple manufacturing methods were considered. Emphasis was given not only to provide a large internal area close to the CG for storing the payload and flight systems internally but also to ensure that the structure was strong and durable enough to possess dimensional accuracy over the integrated airframe. Finally, during the fabrication of the parts of the UAV, it was carefully handled in such a manner so that the whole UAV can be assembled within the time limit prescribed by SAE.

6.1 Materials selection

Careful material selection is an inescapable requirement for a good UAV as it strongly affects the design criteria of having less empty weight. Solid foam was used to construct the wing in order to get an ice shape of the airfoil as well as to gain structural strength and it can be machined easily also. Balsa wood is a very light weight wood which was used during the wing fabrication. Though it is pretty expensive, it was used for more strength as well as to keep the empty weight of the aircraft as low as possible. Foam sheet was the main material which has been used for manufacturing the UAV and these are very much ductile which allows it to absorb the shock while landing. High density foam "XPS" was used to mount the motor with the fuselage because this has the ability to sustain high vibration as well as to provide necessary strength for holding the motor. Heat was provided to fix the covering material with the wing which was used in order to cover the wing as well as to give it more strength. Fiber tape was used in order to get more strength in the joints. Thus the materials selection was done carefully so that they can provide enough strength to withstand the load imposed on it.

6.2 Subsystem manufacturing

6.2.1 Wing manufacturing

Mainly solid foam and Balsa wood were used for manufacturing the wing. First the dimensions of the wing were selected. A high lift airfoil was placed at the tip of the wing and comparatively low-lift airfoil was fixed at the root. While fabricating the wing, hotwire was used to cut the foam at the desired shape. Later on after sanding, glue was applied over the whole wing. Then the covering material was applied using some heat.

6.2.2 Fuselage manufacturing

At first a design was selected for the fuselage and gave it dimensions. Then a suitable material (Foam sheet) was selected which can meet the requirements. Different parts of the UAV were fabricated and later on assembled using adhesives. Housings were also made for each and every part of the aircraft for a stable CG point.

6.2.3 Empennage manufacturing

Firstly a suitable configuration of the empennage was selected for the UAV. Flat plate was used instead of using an airfoil shaped surface because of ease of fabrication and simplicity without affecting the performance in case of such a small UAV. A special type of adhesive (Epoxy Resin) was used for assembling the parts for better strength. This adhesive provided high strength and it has some ductility property as well.

7. Novel idea exploited in the design

The primary concern was to obtain a high payload fraction by increasing the lift per unit area as much as possible. While lift is given by

$$L = \frac{1}{2}\rho v^2 scl \quad (1)$$

where ρ (density) was considered constant due to low variation in flight altitude, S (wing area) remained constant due to design constraints and considering the aircraft to be flown at max power, the velocity was also considered constant as well, the only option available was to choose an airfoil with very high C_L with maximum optimization without compromising the stalling pattern. The two airfoils that were considered are discussed below.

7.1 Eppler 214

Eppler 214 was chosen first due to its thickness and cambered surface. The max C_L obtained by the airfoil was determined to be C_L=1.549 at an AOA of 9^0 . Any further increase in AOA caused stall to the aircraft. The associated C_D was determined to be C_D=0.0327. The weight lifted by a wing of calculated size using this airfoil was approximately 1.5 lbs.

7.2 Selig 1223

Selig 1223 was further chosen in order to increase the capability of lifting weight. It was chosen for the high C_L and cambered surface. The max C_L obtained by the airfoil was determined to be C_L=2.425 at an AOA of 8^0 . Any further increase in AOA caused stall to the aircraft. The associated C_D was determined to be C_D=0.0371. The weight lifted by a wing of calculated size using this airfoil was approximately 2 lbs.

7.3 Aerodynamic twist

Both the airfoils were integrated in the designed aircraft in order to obtain a better and optimum result. The Selig 1223 airfoil was kept at the tip and the Eppler214 was kept at the tip of the wing. The stalling of Selig 1223 takes place earlier and the stalling of Eppler214 at root took place later. Initiation of the stall from the tip causes a juddering in the tail plane and sends an indication of upcoming stall of the whole aircraft and the UAV controller can take preventive action accordingly. In addition, the novel idea of aerodynamic twist introduced in our design increased the lift coefficient and reduced the drag coefficient, which was found from the flight tests. The amount of weight lifted by the aircraft with the customized wing was approximately 3 lbs.

8. Performance in the actual competition

The designed and fabricated UAV was flown in the final competition of SAE Aero Design Competition (West) at Texas, USA from 28-30 March 2014. The UAV successfully took-off with the payload of 1.85 lbs while the empty weight of the UAV was only 0.99 lbs. Thus, the payload fraction was 1.85/(1.85+0.99) = 0.65, which was the 4th best payload fraction among the 25 teams participating from renowned Universities of the World. The details of the participating teams and payload fraction of each UAV are shown in Fig.5. Mentionable that, this is the best achievement and highest positioning by any team from Bangladesh till now in any International Aero Design Competition.

9 Conclusions

The design process was started with the conceptual design, where the ideas of every aspect of aircraft design were contemplated and evaluated including overall configuration, wing and tail configuration, fuselage type and payload storage. Hand launch system was incorporated instead of landing gears for easy take-off and reduction of empty weight as payload fraction was the main concern. From the back-of-the-napkin design, propulsion system, airfoil and wing, wing/body plan form and other structural aspects were designed and analyzed while multi-disciplinary optimization was the heart of the trade-off study. Finalizing the detailed design with every individual configuration, it was seen that the aircraft generates an ample amount of lift with the help of two different airfoils known as "Aerodynamic Twist". The propulsion system such as battery, motor, ESC and others were chosen to work with the lowest possible weight and the lightest possible combination of structure to support a strong and dynamically stable aircraft. Finally extensive flight testing in addition to comprehensive wind tunnel testing confirmed the desired performance capabilities. The ultimate output of the design was the successful flight of the UAV in the skies of USA and clinching 4th position out of 25 teams in payload fraction category, which is the best result by any Bangladeshi UAV till now.

NOMENCLATURE

R_n	Round score
P_n	Payloads
PF_n	Payload fraction
C_l	Lift coefficient
C_d	Drag coefficient
$\frac{t}{c}$	Thickness to chord ratio
$\frac{Cl}{Cd}$	Lift to drag ratio
C_{D0}	Zero lift drag co-efficient
α	Angle of attack
$C_{L\alpha}$	R/C of lift coefficient with angle of attack
$C_{M\alpha}$	R/C of pitching moment coefficient with AOA

SAE: 2014 Aero Design West (Fort Worth, TX)

Micro Class Payload Fraction

Pos.	No.	Country	School	Team Name	Best Payload Fraction
1	319	Canada	Univ of Western Ontario	Western Aero Design - Micro	0.8121
2	310	Poland	Polish Air Force Academy in Dyblin	Young Enigineers Team-ArrowPro	0.8016
3	324	Poland	Wroclaw University of Technology	JetStream	0.7634
4	315	Bangladesh	Military Inst of Science & Technology	MIST Aero Thunder Green	0.6526
5	330	India	Indian Institute of Tech - Kanpur	Team Pushpak	0.6445
6	317	India	M M Engineering University	VIVAN	0.5904
7	303	India	Vellore Institute of Technology	VIMAANAS	0.5634
8	322	India	PES School of Engineering	Avions	0.5625
9	327	United States	Louisiana State Univ	Flying Tigers	0.5328
10	328	India	PES Institute of Technology	Icarus	0.5294
11	326	Turkey	Anadolu Universitesi	Flying Anatolia	0.5080
12	314	United States	Univ of Hawaii - Manoa	UH MICRO Warriors	0.4991
13	302	Turkey	Middle East Technical Univ	Owl Tamers	0.4918
14	329	India	BMS College of Engineering	Team Mach	0.4621
15	325	India	Hindustan University	GARUDA	0.3780
16	312	India	KIIT University	KIIT AERO	0.3268
17	320	India	M.H. Saboo Siddik College of Engrg	Team Aerosouls Micro	0.0000
18	308	United States	Saint Louis Univ	Parks Micro	0.0000
19	311	India	Sona College of Technology	TEAM DANPHE	0.0000
20	331	India	SRM University - NCR Campus	ONE	0.0000
21	313	United States	Univ of Nevada - Las Vegas	Rebel Recon	0.0000
22	321	India	Fr Conceicao Rodrigues College of Engrg	Team Vaayushastra Micro Class	0.0000
23	318	India	Manipal Institute of Tech	AeroMIT	0.0000
24	305	Canada	Queen's Univ - Ontario Canada	Queen's Eh	0.0000
25	323	United States	Wright State Univ	Flyboys	0.0000

Fig.5 Final result in flying (payload fraction) at SAE Aero Design Competition, Texas, USA from 28-30 March 2014.

Cy_b R/C of side force coefficient with yaw angle

C_{lb} Rate of change of rolling moment coefficient with yaw angle

C_{nb} R/c of yawing moment coefficient with yaw angle

C_{yp} R/C of side force coefficient with roll rate

C_{lp} R/C of rolling moment coefficient with roll rate

C_{np} R/C of yawing moment coefficient with roll rate

C_{yr} R/C of side force coefficient with yaw rate

C_{lr} R/C of rolling moment coefficient with yaw rate

C_{nr} R/C of yawing moment coefficient with yaw rate

C_{lq} R/C of rolling moment coefficient with pitch rate

C_{mq} R/C of pitching moment coefficient with pitch rate

$C_{L\delta a}$ R/C of Lift coefficient with aileron deflection

$C_{M\delta a}$ R/C of Pitching Moment coefficient with aileron deflection

$C_{L\delta e}$ R/C of Lift coefficient with elevator deflection

$C_{M\delta e}$ R/C of Pitching Moment coefficient with elevator deflection

$C_{L\delta f}$ R/C of Lift coefficient with flap deflection

$C_{M\delta f}$ R/C of Pitching Moment coefficient with flap deflection

REFERENCES

[1] Daniel P. Raymer, Aircraft Design: A Conceptual Approach, 4th ed. AIAA Education Series, USA, 2006.

[2] Connor M. Shirley, Joseph A. Schetz, and Rakesh K. Kapania, Tradeoffs of Wing Weight and Lift/Drag in Design of Medium-Range Transport Aircraft, Journal of Aircraft, Vol. 51, No. 3, May–June 2014

[3] John P Fielding, Introduction to Aircraft Design, Cambridge University Press, 1999

[4] Ajoy Kumar Kundu, Aircraft Design, Cambridge Aerospace Series.

[5] John D Anderson, Aircraft Performane and Design, 10th addition.

ICMIEE-PI-140367

Operating cost reduction of HVAC system of square pharmaceuticals limited

Khairun Nahar[1], Md. Pavel Ali [1] & Sharmin Aktar [1]*
[1]Department of Industrial & Production Engineering, Rajshahi University of Engineering & Technology
Rajshahi-6204, BANGLADESH

ABSTRACT
Heating, ventilation and air-conditioning (HVAC) play an important role in ensuring the manufacture of quality pharmaceutical products. The manufacturing plant of the pharmaceutical company, Square Pharmaceuticals Ltd, in Bangladesh, had low energy efficiency in both its office buildings and production facilities. Heating, Ventilation and Air-Conditioning (HVAC) system was identified to be the major energy consumer in the plant. An HVAC specific energy management tool was utilized to monitor the energy efficiency and calculate the heat gains and cooling loads. In the office building, the HVAC operation schedule was revised, and motion detection lighting control was installed and configured to save electricity. In the Hormone Building, in Air Handling Unit (AHU) models it is suggested to include a Heat Recovery Wheel (HRW) which on average reduce almost 6°C temperature from the ambient temperature in face of the requirement to achieve minimum energy consumption thus reduce costs. By disabling the dehumidifier that results in costs savings in total, of direct electricity, steam consumption and electricity for chilled water consumption, valued of BDT 1,181,696 per year.

Keywords: HVAC, HRW, chiller, dehumidifier, boiler.

1. Introduction

A well designed HVAC system will produce quality pharmaceuticals and also provide comfortable conditions for operators. This paper focused on energy saving in any industry needs to keep proper comfortable conditions for operators. This paper focused on energy saving in an office building and a production facility, with special focus on the Heating, Ventilation and Air-Conditioning (HVAC) system.

Based on observed problems this paper will try to fulfill the following objectives-

(1) To evaluate the energy consumption performances of PF by calculating EUI of each building.
(2) To identify the causes of high energy consumption of buildings.
(3) To strategize solutions and to implement energy saving measures to minimize waste in energy consumption.

2. Literature review

ASHRAE 581-RP Project Team, 1993 [3] stated that the purpose of the HVAC system is to add or remove heat and moisture, as well as to remove undesirable air components from the facility in order to maintain the desired indoor environment. Usually, an HVAC system consists of motors, ducts, fans, controls and heat exchange units which deliver cooled or heated air to various parts of the facility. Almost all the office and manufacturing areas are air conditioned all year around, due to the high temperature and humidity and the strict requirement for pharmaceutical plants. An HVAC system functions to provide an environment in which some control factors are maintained within desired ranges. Examples of some standard parameters are-

- Dry bulb temperature of 23°C
- Relative humidity of 40%-60%.
- ASHRAE 62-1999, 2001 and 62.1 - 2004 ventilation standards.
  - CO_2 less than 1000 PPM.
  - 10 LPS outside air per person.

In order to achieve these goals, an HVAC system must have a source of cold to remove heat and a source of heat to reduce humidity. Furthermore, a distribution network is needed to deliver this air to the points of use and control the air change rate. They divide an HVAC system into two parts to discuss them separately: the HVAC primary equipment which is to produce hot and cold fluids and distribute the fluids to each AHU, and the HVAC secondary system which uses the cold and hot fluids to transfer heat with outside air in order to adjust the air temperature and humidity and distribute the air into each room.

Ending Zhang et al. (2008) [6] says, to maintain corporate competitiveness and achieve more environmentally friendly operation, energy management plays a crucial role. Data on electricity and natural gas consumption was collected, analyzed and benchmarked against industrial average. It was found that the current energy efficiency is not satisfactory. The HVAC system is the main contributor of the high energy consumption. A pharmaceutical manufacturing environment has its unique indoor air quality requirements to ensure product safety and quality, as well as the comfort of occupants.

Most of the time, the highest level of these requirements is maintained throughout the year, which may result in significant amount of waste. Developing and revising operation schedules for the HVAC system regularly, relaxing the environment standards by shutting down equipment that is not necessary and optimizing system settings would reduce wasteful usage of energy, without compromising the indoor environment standard.

*Khairun Nahar
Tel.: +88-01916800200
E-mail address: shapla05.ipe@gmail.com

In this project, an energy management spreadsheet is developed, which enables the user to effectively monitor the energy efficiency after various forms of energy consumptions are known. It also allows the energy manager to find out the heat gain and cooling load of the HVAC system.

For the office building, a better HVAC operation schedule for office building is developed and implemented which may potentially realize 16.5% energy saving in the AHU motor electricity. Motion detection lighting control was implemented in the office building, which could reduce electricity consumption.

Natasa Djuric et al. (2007) [7], growing building complexity can induce increased energy consumption in the future without tools for improving building performances. In the near future, energy savings can be obtained mainly through optimal control and early fault detection of building HVAC systems. Therefore, different commissioning tools are necessary to make buildings sustainable and energy-efficient.

An important means for the practical application of any commissioning tool in existing building is BEMS. Sometimes, however, it can be difficult to make the connection among the building geometry, the HVAC system schema, and the BEMS measurements due to the building modifications through its lifetime. There are now, however, easily available e-data related to a building. Therefore, it is necessary to estimate the validity of the data that are used for any building assessment. Contacts with the maintenance services, the system acquirement, and additional measurements can help in the data quality estimation.

Çağlar Selçuk et al. (2003) [8], Action plan was defined and hypermarket and non-food store AHUs are focused. Controls scenarios of these AHUs are deeply investigated revisions are made. Some HVAC control strategies such as optimum start-stop, night purge, night cycle are implemented. Control loops and parameters are tuned due to characteristics of the building. The idea is originated by using more functions on HVAC control system. To implement strategies on HVAC control system, energy audit was generated. This was very helpful deciding where to focus our retrofit study. Some retrofit options are implemented such as optimum start-stop and night purge. Night cycle are implemented. Control loops and parameters are tuned due to characteristics of the building. The idea is originated by using more functions on HVAC control system. To implement strategies on HVAC control system, energy audit was generated. This was very helpful deciding where to focus our retrofit study. Some retrofit options are implemented such as optimum start-stop and night purge.

Melvin W. First et al. (1998) [10], the high efficiency particulate air (HEPA) filter has become an indispensable item in the maintenance of biological safety and is also used as a means of preserving cultures from contamination originating in the surrounding air. HEPA filters originated with military requirements for protection against chemical, biological, and radiological warfare agents and to avoid emissions from nuclear weapons production facilities A thorough understanding of these filters proved to be so important that they stimulated research and development activities that established the science of air filtration on a firm theoretical basis and promoted rapid advances in materials of construction and production method.

Eric Bloom, Bob Gohn et al. 2012 [17], the smart building industry has been busy over the last few years. Advances in technology that make it easier to manage energy have considerably broadened the energy conversation, engaging not just facility managers, but also CEOs and CFOs. Although the effects of the global economic recession are still felt throughout the building and construction industries, technology vendors and integrators have continued to uncover new opportunities to improve energy efficiency in the existing building stock. The potential for energy efficiency has hardly been tapped even today. Smart buildings employ a wide range of technologies that improve efficiency and connect buildings to each other as well as to the grid using intelligent, information and communication technology (ICT)-based devices and networks. Many of the technologies required for qualifying as a smart building, such as energy efficient heating, ventilation, and air conditioning (HVAC) systems and submitters are mature.

Eric Kozubal, Ron Judkoff, and Jason Woods et al. 2012 [18], air-Conditioning operates on the same principle, but is indirect: Incoming air is in thermal contact with a moistened surface that evaporates the moisture into a separate air stream. As the evaporation cools the moistened surface, it draws heat from the incoming air without adding humidity to it. The system uses a desiccant to absorb water vapor. Because this is an exothermic process, it releases heat that can warm both the desiccant and the incoming air. However, DEVAP's liquid desiccant is also in contact with a plastic sheet that provides thermal contact between the desiccant and a stream of water, which is wicked into a flocked surface that is bonded to the plastic sheet. As outdoor air flows past, water evaporates, cooling this surface. The cooler water also draws heat from the desiccant, keeping it cool and maintaining its effectiveness. The two stages of DEVAP allow it to operate effectively in a wide range of climates without consuming high levels of water.

From the above study it can be concluded that HVAC system is the major energy consumer in the plant. The study of different researches on this area are provides the knowledge to reduce energy consumption with particular focus on AHUs, chilled water and steam usages. In this paper it is suggested that in the plant if there is an improved energy management tool that help to regularly monitor and control energy consumption which would enable the energy engineers to better understand the system behaviors and find energy management opportunities, to support the energy saving endeavor. We develop a general energy management tool to analyze energy consumption pattern and calculate cooling load of the HVAC system in both the office building and the production facilities to explore various

energy saving opportunities and chose to focus on the HVAC rescheduling and reduce energy consumption in GSB.

3. Method analysis

3.1 Direct method testing

This is also known as 'input-output method' due to the fact that it needs only the useful output (steam) and the heat input (i.e. fuel) for evaluating the efficiency. This efficiency can be evaluated using the formula:

Boiler efficiency, $\eta = \frac{heat\ output}{heat\ input} \times 100$

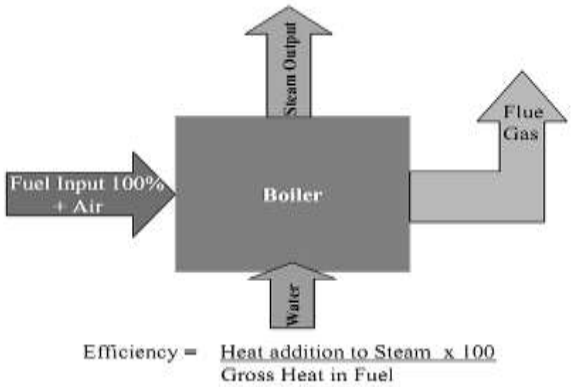

Fig.1 Boiler Efficiency

Heat Input = Gas consumption
Heat Output= Steam Generation
Input-
={(64.8×2.02×1038.45×252)÷(0.028×1000)} KCal/hr
=1223360.561 KCal/hr
Where,
Gas Used Per Hour = 64.8 ft^3
Power Factor = 2.02
1ft^3 gas consumption equal to 1038.45 BTU/ft^3
So,
1038.45 BTU/ft^3 = (1038.45 × 252)/1000 kcal
Output-
= {20.5× 8 × 4 × $(12)^2$} in^3/hr
= 94,464 in^3/hr
= {94464 × $(.0254)^3$ } m^3/hr
= 1.5479 × 1000 L^3/hr
= 1548 kg/hr
= (4286412÷4.2) Kcal/h
=1020574 Kcal/hr
Where,
Steam container height in inch = 20.5
Steam container length in inch = 8
Steam container width in inch = 4
Efficiency = (1020574 ÷ 1223602.81) × 100= 83.4%
Error= $\frac{3900-1548}{1548}$×100= 60.31%

3.2 Proposal of Energy Efficiency Increasing in Air Handling System

By air re-circulation in hormone building energy can be increased. This system is done by using Energy Recovery Wheel. Overall procedures are shown in figure 3.2 and figure 3.3.

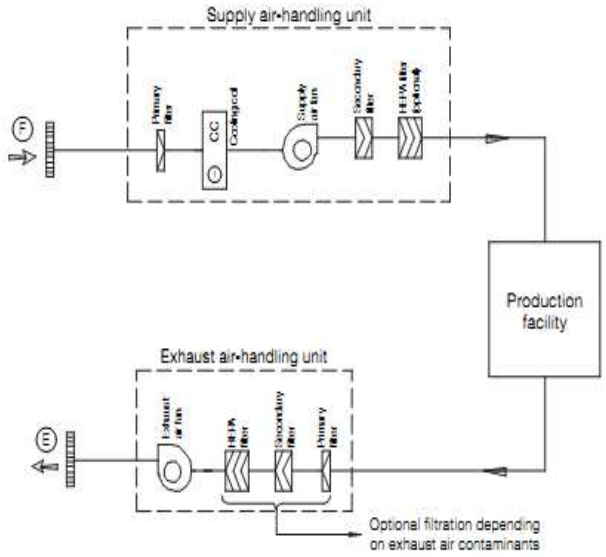

Fig.2 Full fresh air system [2]

The used air which is coming from production room contains approximately 28°C. That air again is used to cool the outside air which contains approximately 40°C. The re-circulated air will pass through a cooling coil inside of the energy recovery wheel and then the outside air pass through the contact of the cooling coil and also reduce the temperature of this air.

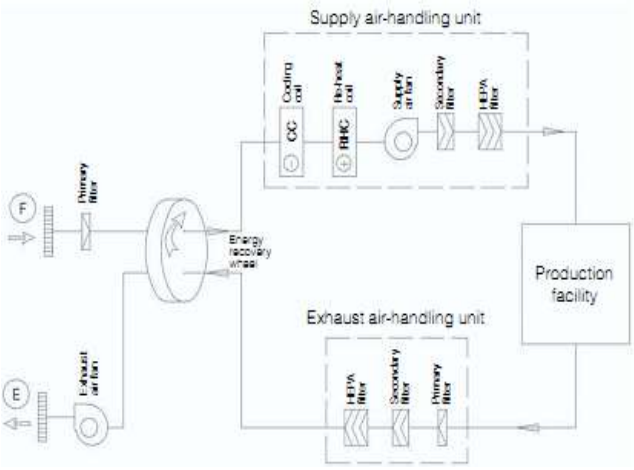

Fig.3 Full fresh-air system with energy recovery [2]

By this procedure temperature of outside air will be reduced approximately 6°C that increased the energy efficiency of Air Handling Unit.[2]

Average temperature would be = (40°C + 28°C) / 2 = 34°C

3.3 Disabling dehumidifier

3.3.1 Direct electricity savings

The rated powers of the reactivation air fan and desiccant wheel motor are noted. Assuming the power factor is 0.95 and the unit electricity cost is BDT 9.33/ kWh the electricity savings and cost savings are estimated by:

Electricity savings= rated power × power factor × duration of shutdown [8]

Cost savings = unit electricity cost × electricity savings [8]

3.3.2 Savings of steam consumption

As steam is generated by burning natural gas, the steam savings are converted to the savings in the natural gas consumption. From the site's historical data, the natural gas consumption for producing each kg of steam is found to be 0.003234 m^3. Unit cost of natural gas is assumed to be BDT 5.86/ m^3 therefore,

Natural gas savings in m^3 = steam savings in Kg × 0.003234 m^3 [8]

Cost savings = BDT 5.86/ m^3 × Natural gas savings in m^3 [8]

3.3.3 Savings of chilled water consumption

After disabling the dehumidifier, the supply air stream fully bypasses the desiccant and thus is not heated up by the desiccant rotor. This exerts less cooling load for the downstream post-cooling chilled water coil: i.e. less energy from the air is to be extracted by the chilled water to reach the same off-coil set point temperature.

The process for moist air cooling is illustrated in figure 4 under constant pressure. Air at a particular temperature and RH has a fixed specific enthalpy and humidity ratio. With known mass flow rate, temperature and RH, the difference in energy content, which must be extracted by the chilled water cooling coil, can be calculated.

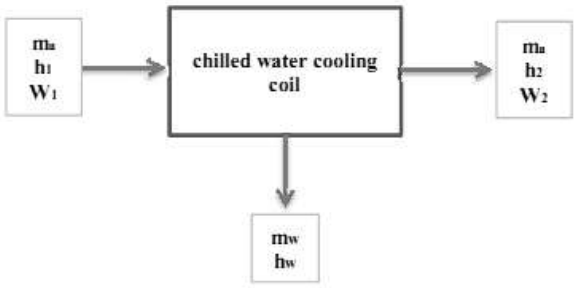

Fig.4 Air cooling

The electricity and cost savings are then obtained with the duration of shutdown and the unit cost of electricity of BDT 9.33/KWh.

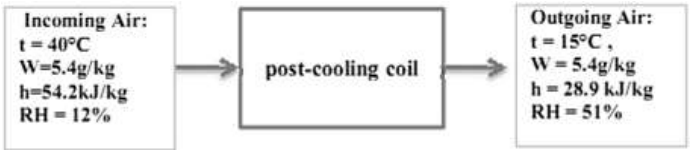

Fig.5 Before disabling dehumidifier

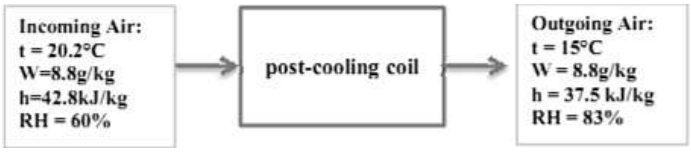

Fig.6 After disabling dehumidifier

qbefore = ma [(h1 – h2) – (W1 – W2) hw]
= (12,000 kg/hr) (54.2 – 28.9) kJ/kg
= 303600 kJ/hr
= 84.3 kW
= 24.0 RT

qafter = ma [(h1 – h2) – (W1 – W2) hw]
= (12,000 kg/hr) (42.8 – 37.5) kJ/kg
=63600 kJ/hr
=17.7 kW
=5.0 RT

Δq = 24.0 RT – 5.0 RT = 19.0 RT

With the chiller efficiency of 0.68 kW/RT, power savings is calculated:

Power savings = 0.68 kW/RT × 19.0 RT = 12.92 kW

Annual energy and cost savings is calculated:

Annual electricity savings =12.92 KW × 24 hr/day × 365 days = 113,179.2 kWh

Annual cost savings =113,179.2 kWh × BDT 9.33 /Kw
= BDT 1,055,961.9

Table 1 Overall Savings

Areas of Energy & Cost Savings	Amount	Cost in BDT
Direct Electricity Savings	27,262 kWh	BDT 254,369.7
Savings of Steam Consumption	4045.5 m^3	BDT 23,706.64
Savings of Chilled Water Consumption	113,179.2 kWh	BDT 1,055,961.94

4. Results

The existing boiler 66% energy is consumed to generate steam. By calculating the existing boiler efficiency it found that there are 60.31% errors in steam generation for smaller input cause of burner problem of the boiler.

By using HRW in AHU fresh air temperature (almost 6°C) will be reduced by contacting with exhausted air and

also this procedure reduce the pressure of filtration system.

By disabling the dehumidifier direct electricity savings will be 32371.45kWh per year which value is BDT 102,029.3 per year and Savings of Steam Consumption will be 4045.5 m^3 per year which value is BDT 23,706.64 per year and Savings electricity for Chilled Water Consumption will be 113,179.2 kWh per year which value is BDT 1,055,961.94 per year. In totally per savings would be of BDT 1,181,696 per year.

5. Conclusions and discussions

By calculating the existing boiler efficiency it found that the efficiency meets the specification of that boiler but the capacity does not match with the specification for smaller input cause of burner problem of the boiler.

By using HRW in AHU fresh air temperature will be reduced by contacting with exhausted air and also this procedure reduce the pressure of filtration system.

Dehumidifier is installed in production facility to maintain relative humidity (RH) for the RH sensitive products. But it maintains almost 55% to reduce relative humidity to the RH insensitive products also. That is really the main source of costing.

In Pharmaceuticals industry HVAC system is the main source of energy consumer. Basic elements of HVAC systems are boiler, chiller, AHU. Generally 66% energy is consumed to generate steam. By calculating the existing boiler efficiency it is found that the efficiency meets the specification of that boiler but the capacity does not match with the specification. There are 60.31% errors in steam generation for smaller input cause of burner problem of the boiler.

There is absence of HRW in AHU of hormone section in Square Pharmaceuticals Ltd. for this case fresh air always re-circulates. But using HRW fresh air temperature will be reduced by contacting with exhausted air and also this procedure reduce the pressure of filtration system.

6. Recommendations & limitations

Listed recommendations & limitations are-

ii Standardize the procedure of HV (House Vacuum), PV (Process Vacuum), and DC (Dust Collector) shutdown during non-production time.

iii Enable the motion detecting lighting control.

iv Disabled the dehumidifier in RH insensitive production area.

v Only three period data collection time due to lack of available time from the plant was granted.

vi At the time of water height measurement of boiler the parallax error may be exist.

8. References

[1] http://en.wikipedia.org/wiki/Square_Pharmaceuticals.

[2] http://www.squarepharma.com.bd/about-us.php.

[3] Barney L. Capehart, CEM Wayne C. Turner, *Guide to Energy Management, Ernest Orlando Lawrence Berkeley National Laboratory*, Fourth Edition, pp 219-256.

[4] ©World Health Organization WHO Technical Report, *Supplementary guidelines on good manufacturing practices for heating, ventilation and air-conditioning systems for non-sterile pharmaceutical dosage form*, Series, No. 961, 2 Annex 5, pp 4-46.

[5] Christina Galitsky, Sheng-chieh Chang, An ENERGY STAR® Guide for Energy, *Journal of Ernest Orlando Lawrence Berkeley National Laboratory*, pp 17-24, (2008).

[6] Ending Zhang, Improving Energy Efficiency in a Pharmaceutical Manufacturing Environment - Production Facility, *Journal of Massachusetts Institute of Technology*, pp 8-71, (2008).

[7] Natasa Djuric, Real-time supervision of building HVAC system performance, *Journal of Doctoral thesis NTNU Norwegian University of Science and Technology,Faculty of Engineering Science & Technology*, Department of Energy and Process Engineering, pp 6-9.

[8] Çağlar Selçuk, Optimization of HVAC Control Strategies By Building Management Systems Case Study, *journal of Izmir Institute of Technology Izmir*, Turkey, September, pp 29-53 (2003).

[9] A. Bhatia, HVAC Design for Pharmaceutical Facilities, *journal of continuing education and development*, Inc.9Greyridge farm court,pp 3-50.

[10] Melvin W. First, HEPA FILTERS, *Journal of the American Biological Safety Association*, 3(1) pp. 33-42 (1998).

[11] ASHRAE 581-RP Project Team, *Air-conditioning Systems Design Manual*, Second Edition (1993).

[12] Sheng-chieh Chang, Ernst Worrell, *Energy Efficiency Improvement and Cost Saving Opportunities for the Pharmaceutical Industry An ENERGY STAR® Guide for Energy.*

[13] www.beeindia.in/energy_managers_auditors/documents/.../2Ch2.

[14] R. PANNEERSELVAM, Production & Operation Management, prentice-Hall of India private limited, New Delhi-110001, 2006, pp 312-330 (second edition).

[15] Danny S. Parker, Stephen F. BarkasziJr., "*Roof solar reflectance and cooling energy use: field research resultsfrom Florida".*

[16] http://en.wikipedia.org/wiki/Roof_coating.

[17] Eric Bloom, Bob Gohn, Smart buildings: Trends to watch in 2012 and beyond (2012).

[18] Eric Kozubal, Ron Judkoff, and Jason Woods, Development and Analysis of Desiccant Enhanced Evaporative Air Conditioner Prototype (2012).

.

ICMIEE-PI-140368

Providing efficient maintenance schedule for HVAC system of square pharmaceuticals limited

Khairun Nahar[1], Sharmin Aktar[1] & Md. Pavel Ali[1]*
[1]Department of Industrial & Production Engineering, Rajshahi University of Engineering & Technology
Rajshahi-6204, BANGLADESH

ABSTRACT
Maintenance scheduling plays very important role in any industry. It is related to the production and other facility, and also crucial in increase the productivity. Maintenance Excellence is requisite to the achievement of World-Class Operations (an organization that is competitive with the best in the world). Well-planned, properly scheduled, and effectively communicated jobs accomplish more work, more efficiently, and at a lower cost. Maintenance recommendations are based on industry standards and experience in Reclamation facilities. However, equipment and situations vary greatly, and sound engineering and management judgment must be exercised when applying these recommendations. In the production building of the square pharmaceuticals use preventive maintenance but they do not use any suitable maintenance scheduling procedure. And they required and spent around 703 minutes of working hour per maintenance period in total. This paper proposed an effective maintenance sequence thus schedule by using Johnson's extension rule that could reduce the time significantly to only 274 minute per maintenance so that it is almost save 429 minute of working hour per maintenance period.

Keywords**:** sequencing, scheduling, maintenance, Johnson's algorithm, time saving.

1. Introduction

Scheduling is the allocation of start and finish time to each particular order. Therefore scheduling can bring productivity in shop floor by providing a calendar for processing a set of jobs. It is nothing but scheduling various jobs on a set of resources (machines) such that certain performance measures are optimized. Scheduling is the process of establishing the timing of the use of equipment, facilities, and human activities in an organization. Scheduling is the allocation of start and finish time to each particular order.

Based on observed problems this paper will try to fulfill the following objectives.

(1) Reduced maintenance cost.
(2) Improved quality of maintenance work by adopting the best methods and procedures and assigning the most qualified workers for the job.
(3) Minimizing the idle time of maintenance workers.

Most maintenance departments do not plan to fail, they simply fail to plan and therefore do indeed fail. The major reason behind failure to plan is that putting out today's fires is given priority over planning for tomorrow – thereby insuring that future equipment failures will require reactive response.

2. Literature review

Bureau of Reclamation 2012 [1] Maintenance recommendations are based on industry standards and experience in Reclamation facilities. However, equipment and situations vary greatly, and sound engineering and management judgment must be exercised when applying these recommendations. Other sources of information must be consulted (e.g., manufacturers recommendations, unusual operating conditions, personal experience with the equipment etc.) in conjunction with these maintenance recommendations. Equipment and situations vary greatly, and sound engineering and management judgment must be exercised when applying these recommendations. It should not be the sole source of information used in conducting maintenance activities. Other sources of information should be consulted (e.g., manufacturers recommendations, unusual operating conditions, personal experience with the equipment, etc.) for references associated with these maintenance schedules. Performing maintenance on electrical equipment can be hazardous. Electrical and mechanical energy can cause injury and death if not managed properly. All maintenance activity must be conducted in accordance with FIST 1-1, Hazardous Energy Control Program (HECP), and Reclamation Safety and Health Standards (RSHS).

Ville Mattila, Kai Virtanen, Raimo P. Hämäläinen [2] The maintenance is time-consuming and therefore needs to be scheduled adequately. The objective of scheduling is to maximize the availability of the aircraft which ensures the operational capability of the fleet. In practice, the timing of the maintenance is affected by uncertainties such as unplanned failure repairs and thus the planned and actual starting dates of the maintenance may be different. This presents an additional objective, since workforce, equipment, and spare parts are supplied for the activities according to the planned starting dates. The deviations between the planned and the actual starting dates should be minimized. A maintenance decision-maker (DM) must ultimately select one of the non-dominated Solutions for implementation. The presented approach provides an effective way to construct and update maintenance

* Khairun Nahar
Tel.: +88-01916800200
E-mail address: shapla05.ipe@gmail.com

schedules. It offers maintenance DMs considerable savings in time as well as improved schedules. We illustrate the approach by analyzing a real life scheduling case.

Lorne MacDonald [4], as a former Operations/ Maintenance Coordinator who was sick and tired of operating in a reactive fire-fighting mode, he understood potential benefits of proper maintenance scheduling - the challenge was getting everyone on the same page. Industry experts suggest that in order to move from reactive to proactive maintenance, at least 80% of the work should be planned on a weekly basis and compliance to this schedule should be at least 90%. Utilizing a team approach, monthly meetings were held involving representatives from Operations, the Operations Superintendent, an Operations/ Maintenance coordinator, Planner, Maintenance Supervisor, Maintenance Area Technician, E&I Supervisor, E&I Area Technician, Area Engineer, Process Control Technician, and Quality Control Technician. At these meetings a process was established for reviewing the PM program. PM Jobs were reviewed for suitability to the current operating conditions that existed in the plant. Many of these PMs were the original Manufacturers recommended PMs and the frequencies were reviewed to determine if they were still relevant. Could a weekly or monthly PM become a 3-month PM or a yearly PM? Could weekly visual inspections be handled by Operations when it came to equipment such as HVAC? A new maintenance manager was hired and his first decree was that planned preventive maintenance (PM) work was going to be the order of the day. When creating weekly schedules we had to schedule all due PM's first and then distribute the remaining man-hours according to priority. Communication is the key to successful maintenance scheduling – this involves everyone from the Planner, Scheduler, Maintenance Supervisor, Craftsman, Storeroom personnel, Operations Superintendent, to the Operator who is responsible to have the equipment secure and ready for maintenance. Any breakdown in this communication diminishes the probability of success.

Don Nyman. Joel Levitt 2006 [5] Maintenance organizations everywhere have the responsibility to assure optimum use of the capacity of an enterprise. Preventive/ Predictive Maintenance (PPM) is not conceived to put equipment in proper condition, but to maintain it in that condition from the time of acquisition or restoration. Proactive maintenance requires a cultural transition from a reactive to a proactive environment. Maintenance customers deserve to have their work performed on a timely basis. Therefore, backlogs must be kept within reasonable limits. Each hour of effective planning typically returns three to five hours in mechanic time or equivalent savings (measured in cost of material and production downtime). When a maintenance planning and scheduling function is being established, the first question that usually arises is where and how it fits into the organization. The first answer is that it is structured within the maintenance organization, not outside of it. Secondly, it should be organizationally independent of the specific maintenance supervisor(s) it is tasking, as well as supporting.

3. Method analysis

3.1 Selection of method

This paper works with maintenance schedule of HVAC system of Square Pharmaceuticals Limited which seems flow shop scheduling. The characteristic of flow shop scheduling are given bellow-

i. A set of multiple-operation jobs is available for processing at time zero (Each Job requires m operations and each operation requires a different machine)
ii. Set-up times for the operations are sequence independent, and are included in Processing times
iii. Job description is known in advance.
iv. m different machines are continuously available.
v. Each individual operation of jobs is processed till its completion without break.

To find out the sequence and maintenance time using JOHNSON'S EXTENTION RULE because it's require less time and more easily to calculate rather than other known scheduling methods like BRANCH AND BOUND TECHNIQUE, CDS HEURISTIC and PALMER'S HEURISTIC.

3.2 Calculation procedure of JOHNSON'S ALGORITHM

Step 1 Find the minimum among various workers (First person + Second person) and (Second person+ Third person).

Step 2a If the minimum processing time requires (First person + Second person),

Place the associated job in the first available in sequence.

Step 2b If the minimum processing time requires (Second person + third person), place the associated job in the last available in sequence.

Step 3 Remove the assigned job from consideration and return to step 1 until all positions in sequence are filled (ties may be broken randomly).

This procedure will give the working sequence of maintenance. After applying the EXTENSION OF JOHNSONS rule on CHILLER unit for calculating maintenance scheduling time. It also gives total idle time of worker.

The following tables (table 1 & table 2) are summarizing the schedule for the chiller unit.

Table 1 Applying the EXTENSION OF JOHNSONS rule on chiller unit

Sl	Task list	(first +second) person in min	(second +third) person in min
1	Check & record chilled water outlet temp	11	10
2	Check & record chilled water inlet pressure	5	7
3	Check & record chilled water outlet pressure	10	8
4	Check & fill up make up water level	10	11
5	Check & record oil temp, level pressure	8	9
6	Check compressor low & high pressure	9	7
7	Check the compressor oil	15	14
8	Check the insulation of chilled water line	15	14
9	Check & inspect the alignment of the bearing	13	15
10	Check the gland packing of pumps	19	20
11	Check the alternate running for all pumps	12	13
12	Check and inspect the control	18	16
13	Check and clean condenser	13	15
14	Check oil filter	15	16
15	Check load unload solenoid valve	7	7
16	Check the oil filter and change if needed	10	9
17	Check and inspect oil	10	10
18	Check all condenser fan	17	16
19	Check all compressor	14	16

Optimum sequence for the problem:

= 2-15-5-17-4-11-9-13-19-14-10-12-18-7-8-1-16-3-9

Table 2 Calculating Make-Span Time in minute

Job no.	Person-01		Person-02		Person-03		Idle time-02	Idle time-03
	In	Out	In	Out	In	Out		
2	0	3	3	5	5	10	3	5
15	3	7	7	10	10	14	2	0
5	7	11	11	15	15	20	1	1
17	11	15	15	21	21	25	0	1
4	15	20	21	26	26	32	0	1
11	20	25	26	33	33	39	0	1
9	25	31	33	40	40	48	0	1
13	31	38	40	46	48	57	0	0
19	38	45	46	55	57	66	0	0
14	45	53	55	62	66	75	0	0
10	53	62	62	72	75	85	0	0
12	62	72	72	80	85	93	0	0
18	72	81	81	89	93	102	1	0
2	0	3	3	5	5	10	3	5
7	81	88	89	97	102	108	0	0
8	88	95	97	105	108	114	0	0
1	95	100	105	111	114	118	0	0
16	100	105	111	116	118	122	0	0
3	105	111	116	120	122	126	0	0
6	111	116	120	124	126	129	0	0
Total idle time							7	10

4. Results

The square pharmaceutical's use total 703 minute to maintenance HVAC component but proposed sequence need to only 274 minute to maintenance so that it is almost save 429 minute of required working hours.

5. Conclusions and discussions

Time required in this system for CHILLER is 129 min. First person has no idle time, second person has 7 min idle time and third person has 10 min idle time. In square pharmaceutical total time required to complete the maintenance is 349 min. But it can do this same work as this sequence at low time and reduce the idle time. The time deviation in this system is = (349-129) = 216 min.

Similarly for AHU Unit time required to complete the maintenance is 304 min .But it can do this same work as this sequence at low time and reduce the idle time. The time deviation in this system is = (304-114) =190 min and for BOILER required Time required in this system is 31 min but if we apply this rule the time deviation in this system is = (50-31) = 19 min.

In square pharmaceutical's the production department wants the machine to be available. It is required to reduce the idle time of machine not worker. It is not desirable to hamper the production, so that to ensure that the engineering department took steps to reduce idle time of machine. Applying the method of Johnson algorithm for maintenance scheduling it could be possible to find the sequence of maintenance of HVAC machine and also insure the less idle time of the worker so that proper use of work hour. The square pharmaceutical's use total 703 minute to maintenance HVAC component but if to use those sequence it need to only 274 minute to maintenance so that it is almost save 429 minute of working hour and do proper maintenance. By reducing idle time of the worker it found the sequence of maintenance equipment of the HVAC system**.**

6. Recommendations & limitations

Listed recommendations & Limitations are-

i To solve of the scheduling problem in this paper only use the extension of JOHNSON'S rule.

ii It is a theoretical approach.

iii In this paper just find out the optimal time of scheduling but cannot apply. If we apply it should be reduce the time.

iv Other equivalent optimal policy can also be used for scheduling.

7. References

[1] Bureau of Reclamation (2012)" Maintenance Scheduling for Electrical Equipment"

[2] Ville Mattila, Kai Virtanen, Raimo P. Hämäläinen, *Maintenance Scheduling of a Fighter Aircraft Fleet with Multi-Objective Simulation-Optimization*

[3] R. PANNEERSELVAM (second edition), *Production & Operation Management*, prentice-Hall of India private limited, New Delhi-110001, 2006, pp 312-330.

[4] Lorne MacDonald, *Maintenance Scheduling 101*

[5] Don Nyman. Joel Levitt., Maintenance Planning, Scheduling & Coordination

[6] Kirkpatrick, S., Gelatt, Jr., C.D., Vecchi, M.P., *Optimization by Simulated Annealing*, Science 220(4598) (2008) 671-680

[7] Salo, A., Hämäläinen, Preference Assessment by Imprecise Ratio Statements. *Operations Research* 40(6) (1992) 1053-1061

[8] Winterfeldt, von, D., Edwards, Decision Analysis and Behavioral Research, *Cambridge University Press* (1986)

[9] *Heuristic Scheduling Systems: With Applications to Production Systems and ...Thomas Morton, David W. Pentico - Google Książki*

[10] https://www.google.com.bd/?gws_rd=cr,ssl&ei=_Xe2U7u_Ecu78gXk-4L4Dg

[11] http://www.squarepharma.com.bd/about-us.php.

[12] Barney L. Capehart, CEM Wayne C. Turner, Guide to Energy Management, *Ernest Orlando Lawrence Berkeley National Laboratory*, Fourth Edition, pp 219-256.

[13] www.beeindia.in/energy_managers_auditors/documents/.../2Ch2

[14] http://en.wikipedia.org/wiki/Roof_coating

ICMIEE-PI-140370

Safety Condition in Rural Engineering Workshop in Bangladesh

Md. Arafat Hossain[1], Mahbubur Rahman [2]*
[1,2] Department of Mechanical Engineering, Khulna University of Engineering & Technology, Khulna-9203, BANGLADESH

ABSTRACT
Safety is the condition being protected against any hazardous situation and any other type of failure, error and accidents. As a developing country our technology is growing day by day. But the man who works to develop this technology and works in different industries, factories and rural engineering workshops is deprived of their required safety. The safety issues provided for the workers are not properly maintained in Bangladesh. Almost no safety is provided for the workers in rural engineering workshop in Bangladesh and for that they are affected by physical, social, spiritual, financial, political, emotional, occupational, educational or other types or consequences of failure, damage, error, accidents, harm or any other event which could be considered non-desirable. Many accidents have already been taken place due to not providing enough safety to the workers. Therefore, safety must be provided minimizing accident hazards and risks. The workshops safety situation in Bangladesh is very severe by international standard. An overview of the prevailing accident problem characteristics and some working safety priorities that should be addressed with due urgency are briefly discussed in the paper. In this paper an attempt has been made to highlight the workers safety issues in rural engineering workshops in Bangladesh.

Keywords: Safety issues, Rural engineering workshop, Occupational Safety.

1. Introduction

A workshop is a part and parcel of any engineering section. There is no doubt that rural engineering workshops play an important role in our economic and social welfare. But safety issue is a crucial question here. Thousands of accidents and cases of illness are reported every year in rural engineering workshops. Many of these accidents are caused by ignorance, horseplay or abuse of machinery and equipment. The owners and workers both are responsible for these accidents. They take the safety issues very lightly and sometimes neglect it willingly. On the other hand child labour is a threatening issue. Illegal conditions of the environment of workplace is so murky and offensive. Otherwise the workplace is too small for an operation. In there man, machine and material stay almost in contact. Many engineering processes are potentially hazardous and these include activities such as casting, cutting, soldering, welding, etc. In addition, some processes involved the use of hazardous materials and chemicals. Furthermore, even the most basic and straightforward activities can potentially be dangerous if carried out using inappropriate tools, materials, and methods. In all cases, the correct tools and protective equipment should be used and proper training should be provided. In addition, safety warnings and notices should be prominently placed in the workplace, access to areas where hazardous processes take place should be restricted and carefully controlled so that only appropriately trained personnel can be present. In addition, the storage of hazardous materials (chemicals, radioactive substances, etc.) requires special consideration and effective access control. Successful health and safety management in small engineering workshops is about identifying the most frequent and serious risks and adopting the right precautions, taking account of time, money and resources. The information was collected in this study related to trading situation, employment and labor problems and related especially to occupational safety, health and working environment, safety measure at work, guidelines in promoting the development of safety standards at work in rural engineering workshops in Bangladesh. Various measuring methods such as reportable work injuries, hospital treated work injuries, and survey based estimates of work injuries may give different estimates of the number of work injuries.

The cases of work injuries included in this study are thus the less severe injuries, in the sense that they only include injuries causing temporary absence from work. This study aimed to provide an overview of the situation of occupational health and safety management in rural engineering workshops to gain information related to the employment situation, welfare facilities, health facilities, , accident statistics, hazardous working environments, control of hazards, occupational health and safety management, safety training and safety activities provided to workers. It can be used for the ground work for evaluating the occupational health and safety of rural engineering workshops in Bangladesh, especially the rural engineering workshops with high potential for business.

2. Method

2.1. Questionnaire development

A questionnaire was developed comprising check-box questions and open-ended questions. The questionnaire was divided into four sections that covered:

- Information about the workshop.
- Enquiry the accidents and workers condition data.
- Condition of workshops and workers.
- Occupational health and safety regulations.

The adjustment of the questionnaire was made following the comments.

* Corresponding author. Tel.: +88-01937750118
E-mail address: arafat.hossain2k10@gmail.com

2.2 Types of workshop.
The targeted workshops were small sized rural engineering workshop in Bangladesh. Which were

- Automobile service center.
- Welding shop.
- Lathe shop.
- Air cooler & refrigerator service center.
- Wood shop.
- Painting workshop.
- Fiber & glass workshop.
- Electronic device service center.
- Saw mill (cutting and processing wood).

2.3 Procedures
A cross-sectional non-experimental design was used for this study. From January 2014 to May 2014, we prepared the survey in the two districts (Jessore, Khulna) in Bangladesh. We tried to contact to the owner of different rural engineering workshop and the victim of different types of accident. Based on the type of workshops and the questionnaire that we did the survey. Finally, 80 small size rural engineering workshops were investigated for obtaining the questionnaire .All most 85% of these workshops were road side workshops.
The survey was designed to capture the common injury that occurred in rural engineering workshops as identified by safety science based on online database. Then, the survey was designed to identify the common nature of injuries, parts of body affected by injuries, causes of injuries. The survey was furnished to gather information from five major sections consisting of 35 items: (a) causes of injury (table 1); (b) nature of injuries (table 2); (c) occupational injury socio-demographic category (table 5); (d) occupational injuries in work related category (table 6); and (e) working conditions. We asked to report any injuries or experience of accident while working for the current operation.

2.4. Data analysis
Data from the questionnaire were hinted and analysis. Percentage were used.

3. Results

3.1. Accident statistics
There are many accidents and cases of injuries reported every year in the small engineering workshops. Almost two-third of all such accidents arise from the movement of people, goods and vehicles around the workshops and out of it. Of these "movement" accidents are about half involve lifting and moving goods and other half involving slips, trips and falls and hitting stationary or moving plant and equipment . "Non-movement" accidents mostly arise from the use of machinery, these account for 10 to 15% of all accidents. Electrical accidents are common and they frequently have the potential for more serious injuries. The most common occupational diseases are dermatitis, deafness, asthma and vibration white finger, and back, hand, arm, shoulder and neck problems. In any particular workshop risks which are relevant should be assessed. Those likely to be of most concern includes movement of people, goods and vehicles around the workshop, particularly manual handling, machinery safeguarding, hazardous substances, particularly metalworking fluids, degreasing solvents and dust or fume from welding, brazing, soldering, coating and painting, noise and vibration. Besides these reasons there are many other causes for accidents such as poor lighting, electrical hazards, fire hazards, poor exhaust ventilations, human carelessness etc. Unguarded and badly maintained plant and equipment are obvious causes to injuries. However most of the common causes of accidents are falls on slippery floors, poorly maintained stairways scaffoldings and obstructed passageways in overcrowded workplace.
The costs of accidents and ill health to small engineering workshops may be high. Many employees are 'key' workers whose loss through injury or ill health severely disrupts production and lowers profitability.
The overall condition and different cause for accidents in rural engineering workshops were investigated.
The accident statistics of workshops were classified by number of injured workers by different causes is shown in Table 1.

Table 1: Injuries to rural engineering workshop by accident.

Total number of injured person(investigated)	26
1.Handling and Carrying	7 (27%)
2.Falling objects	5 (19%)
3.Slipping and tripping	2(8%)
4.Machinary	10 (38%)
5.Falls from height	2 (8%)
6.Workplace transport	0 (0%)

The accident statistics of workshops were classified by nature of injury is shown in Table 2.

Table 2: Nature of injury for 26 interviewed injured wrokers.

Nture of injury	Number (%)
1. Amputation, laceration	3 (11.53%)
2.Contusion	2 (7.69%)
3.Dislocation, facture	5 (19.23%)
4. Hernia, rapture	2 (7.69%)
5.Sprain/strain,joint inflamination	9 (34.61%)
6.Scratch, abrasion	1 (3.84%)
7.Brun,multiple, miscellaneous	4 (15.38%)

The accident statistics of workshops were classified by number of injured workers in different workshop is shown inTable 3.The accident statistics of survey classified by absences of workers is shown in Table 4.

Table 3: Numbers of injuried workers in different types of rural engineering workshop by accident.

Types of workshop	Numbers of workshop	Injured workers (%)
1.Automobile service center	12	3 (11.53%)
2. welding shop	14	5 (19.23%)
3.Lathe shop	12	6 (23.07%)
4.Air conditioner & refrigeration service center	4	1 (3.84%)
5.Wood shop	10	2 (7.69%)
6.Painting shop	6	0 (0%)
7.Fiber & glass workshop	5	2 (7.69%)
8.Electronic devices service center	10	4 (15.38%)
9.Saw Mill	7	3 (11.53%)

Table 4: Accident statistics classified by absecence of workers in the workshop.

Accident case	Number (%)
1.≤1 day lost case	6 (23.07%)
2.> 1 day lost case	5 (19.23%)
3.Disability case	4 (15.38%)
4. fatal case	4 (15.38%)
5. Scikness case	7 (26.92%)

3.2. Conditions of workers & Workshops

In Bangladesh the occupational safety of rural engineering workers is not well organized. The owners are employing male workers with below 30 years of ages at the rate of 65% and the upper being 35% while the percentage of female workers is negligible. The most remarkable fact is that the percentage of child (age below than 15 years) workers in rural engineering workshop are minimum 30%. The owner of those workshop prefer them to take the opportunity of their poverty and also their wages are cheap. They are also deprived of their basic education. Their average working hour was 8.0 h/day (31%) and 48 h/week. Regarding a number of holiday/week, maximum workers had one day, two days holiday was rear. Most of the day workers had little time to lunch or breakfast. They were working from morning to till night most of the days. Most engineering workshop arranged several welfare facilities for workers namely. There was not arranged clean drinking water, suitable eating places separated from operation area, clean and good sanitation of toilet facilities, washing basins and proper resting areas inside the workshop. It is very important that the workshops provide necessary welfare facilities for workers. Occupational health and safety management was considered essential to prevent accidents and diseases in the workshops. Out of 80 rural engineering workshops studied, the workers were exposed to work by hazardous chemicals, excessive noise, working at dangerous elevation, in hot place, in confined space, low fresh air circulation, inadequate lighting quality, with excess vibration etc.

The workers are not trained enough to the proper use of tools and machines in the engineering workshops which may cause injury to the operators. Percentage of unskilled workers and illiterate worker is high. Different types of rural engineering workshops were observed and different case of accidents were investigated. Injured and non-injured people are divided into two categories firstly socio-demographic and secondly work related category. And these categories are divided into some sub-categories. So that table 4 and table 5 is related to factors of occupational injuries in different types of workshop in socio-demographic category and work related category.

Table 5: Data for factors of occupational injuries in socio-demographic category.

factors		Injured workers (total 26)	Non-injured workers (total 248)
age	< 30 years	17(65%)	108(44%)
	≥ 30 years	9(35%)	140(56%)
Material status	Unmarried	15(58%)	156(62%)
	Married	11(42%)	92(38%)
Educational level	Illiterate/basic education	20(77%)	176(71%)
	College/technical	6(23%)	72(29%)

Table 6: Data for factors of occupational injuries in work related category.

factors		Injured workers (total 26)	Non-injured workers (total 248)
Job category	Unskilled	18(69%)	104(41%)
	Skilled	8(31%)	144(59%)
Duration of work(years)	<10	16(62%)	139(57%)
	≥10	10(38%)	109(43%)
Working hours/week	>48	8(31%)	177(72%)
	≤48	18(69%)	71(28%)
Workplace supervision	No	17(65%)	150(60%)
	Yes	9(35%)	98(40%)
Machinery & maintenance	Poor	15(58%)	172(69%)
	Good	11(42%)	76(31%)
Health and safety	No	21(81%)	188(76%)
	Yes	5(19%)	60(24%)

Reviewing these two tables that the perception about the rural engineering workshop is found and which is very woeful. Some pictures are given below which shows the hazardous situation of workshops.

1 A

1 B

1 C

Fig.1 different imperfect condition in rural engineering workshop.

In figure 4 A is shown that a worker is doing gas welding without safety. His dress is lungi (one kind of Bengali dress) which is long loose. That kind of dress is too much dangerous for any kind of machining operations. In figure 4B it is viewed that a child is working in workshop. He was working there during two years.
In figure 4C it is noticed that a victim of workshop accident. He lost his one finger because of blasting the air trunk of truck.

4. Discussion

In engineering workshops accidents are unfortunately too common. They vary in degree from trivial to, in exceptional circumstances and facilities. The health and safety of people at work is covered by a variety of acts of parliament, each act containing a book of laws and regulations which govern the way in which work may be done in the workplace and the processes, operations and equipment employed to do the work. This case-control study of risk factors for injuries in rural engineering workshops recognized a number of work environment features that were connected with injury occurrence. The risk factors confirmed in multivariable regression models were high physical workload, machine-paced work or inability to take a break when tired, lack of training, absence of a lockout program, being new on the job, and being male. Overtime is considered important for workers in rural engineering workshops because they wanted to have more income. If the owners do not provide overtime work, they might move to other places causing a high turn-over rate due to low take home pay. It can be seen that workers in workshops have to work very hard, for approximately 11 h/day on average, if they do overtime jobs. The results showed that most of the enterprises did not have a suitable eating place for workers; thus workers had to bring some food for lunch or had to find a place to eat outside. The number of workshops which had a fire extinguishing training, fire drills and fire evacuation training were too low. We carried out environmental monitoring for dust, heat, noise and lighting for those workshops and found most of them complied with the law only in some parameters. Those workshops therefore still need to improve their working conditions.
Improvement of safety condition of rural engineering workshop is a multi-disciplinary task and does not occur by itself. One fundamental step should be taken by Bangladesh government and which is created an organization dedicated to initiating and coordinating safety activities for rural engineering workshop. These organizations will investigate the safety condition and give them the licenses. To ensure occupational safety and to develop the safety issues some policy should be taken which are given below.

- National Policy:
  1. Safety management should be encouraged.
  2. National occupational safety and health policy.

- Government Organizations:
  1. Establish autonomous occupational safety institute.
  2. Establish national occupational safety and health council.
- Employers Organizations:
  1. Training, awareness and motivation of employer regarding workplace safety and health.
- Labour Union:
  1. Encourage more bipartite approach.
  2. Expand union activities to all occupational sectors.
- Legislation:
  1. Update the laws and reduce inconsistencies.
  2. Increase effectiveness of the law focusing on rural engineering workshop.
  3. Encourage employment of occupational health service specialists, safety inspectors in every local zone.
  4. Introduce safety audit.
- Training organization:
  1. Develop and strengthen institutional capacity to provide education and training related to occupational safety and health.
- National Statistics:
  1. Develop active data collection system.
  2. Establish occupational diseases surveillance.
  3. Establish national and regional accident and occupational diseases database.

In Bangladesh most of the workers are illiterate. So it is very much important to give them at least primary knowledge about their work and safety measurements to be performed in their workshop.

Suitable clothing is a very important factor in an engineering workshop. Overall and protective clothing should be sufficiently loose in order to allow easy body movement but not so loose that they interfere with engineering task and activities. Maintenance and equipment must be regularly serviced and maintained by appropriately trained and experienced personnel. These not only reduce the chances of a major breakdown leading to loss of production, it lessens to chance of a major accident caused by a plant failure. Equally important is attention to such details as regularly checking the stocking and locating of First Aid Cabinets and regularly checking both the condition and location of fire extinguishers. All those check must be logged.

But before all of these recommendations the first work is to grow up the vigilance of the owners, the workers and the government. If we can ascertain the occupational safety of the workers and the safety condition of the workshop then it will help to progress our country, to improve our social value and to achieve a good international reputation.

5. Conclusion

The study shows that the importance of accident prevention is not only limited to the immediate consequences, but also that it can have a significant effect on the long term consequences in the form of early retirement for men that have had an accident at work. This paper consists of safety condition of rural engineering workshop in Bangladesh and occupational safety of workers. It was found that many rural engineering workshop are prone to accidents and casualties. Here occupational safety refers mainly to needs the workers. But the owners have no concern about their safety and their workshop environment. On the other hand they want to enjoy benefits with increased production. The occupational safety in Bangladesh is still in the developmental stage. The field of rural engineering has the potential to make the significant contributions to achieve an ideal occupational safety system by maintaining safety issues and the law. As large number of people are working in rural engineering workshop and they serve us to meet our daily needs so they should provide with sufficient safety measures. Laws should be implemented and followed strictly. If we want to improve our economy the condition of the workers must be improved and they should be facilitated by their basic needs otherwise we will lose our potentiality and our economy will be hammered. So it is very important as a developing country to pay heed to the concerns about rural engineering workshops. Thus we can improving life style of people, social values, and economical condition.

REFERENCES

[1] Valdez RS, Ramly E, Brennan PH. Industrial and Systems Engineering and Health Care: Critical Area of Research—Final Report (Prepared by Professional and Scientific Associates Under Contract No. 290-09-00027U.) AHRQ publication No. 10-0079.Rockville, MD: Agency for Health care Research and Quality. MAY 2010.

[2] Kevin Dee, Mechanical Engineering Group. Health and safety Audit. Revision of Safety Regulations and Action Pending. Mechanical Engineering Health and Safety, ME/98 HS-01, June 1998.

[3] Pornpimol Kongtip, Witaya Yoosook, Suttinun Chantanakul. Occupational health and safety management in small and medium-sized enterprises: An overview of the situation in Thailand. *Safety Science* 46 (2008) 1356–1368

[4] Champoux D., Brun J.-P. Occupational health and safety management in small size enterprises: an overview of the situation and avenues for intervention and research. *Safety Science* 41(4),(2003)), 301–318.

[5] Finn Tüchsen, Karl Bang Christensen, Helene Feveile, Johnny Dyreborg. Work injuries and disability. *Journal of Safety Research* 40 (2009) 21–24.

[6] Fernando G. Benavides, Joan Benach, Jose Miguel Martı´nez, Sira Gonza´lez. Description of fatal occupational injury rates in five selected European Union countries: Austria, Finland, France, Spain and Sweden. *Safety Science* 43 (2005) 497–50.

[7] Christina A. Holcroft, Laura Punnett. Work environment risk factors for injuries in wood processing. *Journal of Safety Research* 40 (2009) 247–255.

[8] Harns-Ringdahl, L., Jansson, T., Malmen, Y. Safety, health and environment in small process plants-results from a European survey. *Journal of Safety Science* 31 (2), 71–80, 2000

[9] Adarsh Kumar, J.K. Singh, Dinesh Mohan, Mathew Varghese. Farm hand tools injuries: A case study from northern India. *Safety Science* 46 (2008) 54-65.

[10] Hyoung-June Im, Young-Jun Kwon, Soo-Geun Kim, Yong-Kyu Kim, Young-Su Ju, Hwa-Pyung Lee. The characteristics of fatal occupational injuries in Korea's construction industry, 1997–2004. *Safety Science* 47 (2009) 1159–1162.

ICMIEE-PI-140371

Aquatic effluence triggered by tannery during beamhouse and chrome tanning operations at Hazaribagh, Bangladesh

Md. Abdul Zalil [1], *Md. Abul Hashem* [2*], *Abu Jor* [2]
[1] Department of Leather Engineering, Institute of Leather Engineering & Technology, University of Dhaka, BANGLADESH
[2] Department of Leather Engineering, Khulna University of Engineering & Technology, Khulna-9203, BANGLADESH

ABSTRACT
Real time physical and chemical parameters of discharged liquid wastes have been characterized during beamhouse and chrome tanning operations. Tanning operation converts the putrescible raw hide/skin into leather. Since raw hide/skin to make finish leather involves a series of chemical and mechanical operations and every operation produces a substantial amount of liquid and solid wastes as well as gaseous air pollutants. Result indicates that physical parameter: pH was extremely low (<2) or high (>12.0); suspended solids (SS) were 18-98 times and dissolved solids (DS) were 13-41times higher than the regulations. The biological oxygen demand (BOD) (50−2300 mg/L) and chemical oxygen demand (COD) (2696−10560 mg/L) values were high; higher the BOD and COD values have the negative effect on aquatic life. The suspended matters have the possibility to deposit on the bed of stream which causes to kill aquatic organisms; floating solids affect the stream's ability for self-purification by regeneration of oxygen from the air. Authority should take initiative to minimize the waste before discharging to the environment for cleaner leather production.

Keywords: Suspended solids, Dissolved solids, pH, Biological Oxygen Demand (BOD), Chemical Oxygen Demand (COD).

1. Introduction

Aquatic pollution is becoming great threat for the forthcoming generation including human, animals and plants. Due to industrialization, air, water and land are becoming contaminated from the discharged gaseous air pollutants, liquid and solid wastes. Tannery is one of the oldest aged industries; worldwide it is known one of the obnoxious industries due to generating solid and liquid wastes and gaseous air pollutants. Tanning operation involves the conversion of putrescible raw hide/skin to make finish leather where a series of chemical operations are required to hold several types of attributes. Each chemical treatment requires huge amount of water and after completing chemical treatment huge amount liquid waste is produced as waste water containing extremely high or low pH, suspended solids (SS), dissolved solids (DS), high chemical oxygen demand (COD) and biological oxygen demand (BOD), low level of dissolved oxygen (DO), coloring substance, sulphide, chloride, lime, heavy metals like chromium, rotten proteinaceous substances etc. for discharging. In beamhouse operation produces gaseous air pollutants such as hydrogen sulfide (H_2S), ammonia (NH_3), chlorine (Cl_2), sulfur dioxide (SO_2) etc. are immediately merged to atmospheric environment [1]. The produced gaseous air pollutants, solid and liquid waste are caused serious environmental hazards and public nuisance.

In Bangladesh 243 out of 270 tanneries are located at Hazaribagh, Dhaka [2], covering an area 25 ha [3], three sides are surrounded by the residential areas and the western side by the flood embankment. Tanneries of Bangladesh have gained a negative image in the society due to generating environmental pollution therefore facing a severe challenge to survive. On the other hand, it is one of the largest export earning sectors to strengthen the national economy for the country. The Export Promotion Bureau (EPB) reported that Bangladesh earned US$765 million from the leather sector in the fiscal year of 2011-2012. Besides, gradually demands of finished and fashionable leather products growing all over the world and the government of Bangladesh already declared as a priority sector [4].

Since the last few decades of development, Bangladesh has faced the environmental degradation of the river, Buriganga and supplementary linked rivers due to picking up the discharged green solids and liquids from the leather industries at Hazaribagh, Dhaka, Bangladesh [5]. None of the leather industries have effluent treatment plant (ETP) excluding for one modern tannery (Apex Tannery, Unit-2).

Many researchers have accounted on tannery wastes by characterization of the parameters and their impact assessment on the environment [6, 7]. Mostly samples are picked up after mixing of discharged waste liquid from the tanneries before falls to the river, Buriganga from where it is difficult to recognize the specific effluent load from the tannery in a specific operation as well as the real feature of the effluent.

In this study real time physical and chemical parameters of discharged liquid wastes have been characterized during beamhouse and chrome tanning operations. The obtained results were complied with the standard.

2. Experimental

2.1 Sample collection

All the year round production base big tannery at Hazaribagh, Dhaka was selected for sample collection. The samples were collected into polyethylene bottles without air gap just after completing chemical treatment and kept in the refrigerator at 4ºC until to complete the

* Corresponding author. Tel.: +88-01674590373
E-mail address: mamashem96@yahoo.com

experiment. In Fig. 1 shows the operational sequences for chemical treatment of beamhouse to chrome tanning.

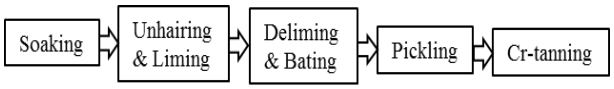

Fig. 1 Conformist beamhouse to Cr-tanning operations

3. Methodology

3.1 Determination of pH

pH of the samples was measured instantly after finished the chemical operation on that day by using pH (Orion, Model 370, USA) meter. Prior to measure the pH, meter was calibrated in three points by the standard solutions.

3.2 Determination of total solids (TS)

Total solids (TS) of the samples were determined gravimetrically as per standard methods of APHA [8]. A 10 mL liquid waste was passed through the glass fiber filter and dried at drying oven at 103 to 105°C until to obtain a constant weight.

3.3 Determination of chloride (Cl^-)

Chloride is determined by titration with $AgNO_3$ solution using ferric alum indicator. The end point is indicated by the appearance of a permanent brown red color.

3.4 Determination of Dissolved oxygen (DO)

Dissolved oxygen was measured on that day by using the DO (HQ40d, HACH, USA) meter. DO meter was calibrated before using.

3.5 Determination of BOD and COD

BOD was measured by OxiTop method. COD was determined by the titration with ammonium iron (II) sulphate $[(NH_4)_2Fe(SO_4)_2 \cdot 6H_2O]$ as ferroin indicator until color changes from the blue-green to red-brown.

3.6 Determination of Chromium (Cr)

After filtration the spent chrome liquor, total chromium was measured by the atomic absorption spectroscopy (Varian AA 240) at Dhaka University, Bangladesh.

4. Results and Discussion

4.1 pH level

The level of pH at different stages from soaking to chrome tanning is shown in Fig. 2. The pH in soaking, liming (unhairing & liming), deliming & bating, pickling and Cr-tanning was 7.7, 12.1, 7.7, 1.9 and 3.5, respectively. It seems that pH level was neutral to high alkaline (7.7−12.13) for soaking to liming. On the other hand in pickling pH (< 2) was extremely low; in Cr-tanning pH (< 4) was also acidic. The pH for liming, pickling and Cr-tanning was beyond the standard levels (pH 6–9) [9]. After completing chemical or mechanical operation liquid waste is discharged through drain and all these liquid waste is allowed to be mixed prior to fall the river, Buriganaga. The liquid waste contains sodium chloride, unused sodium sulphide, calcium hydroxide, dissolved hide/skin proteins, ammonium salts, keratin protein, etc. are causing aquatic problem.

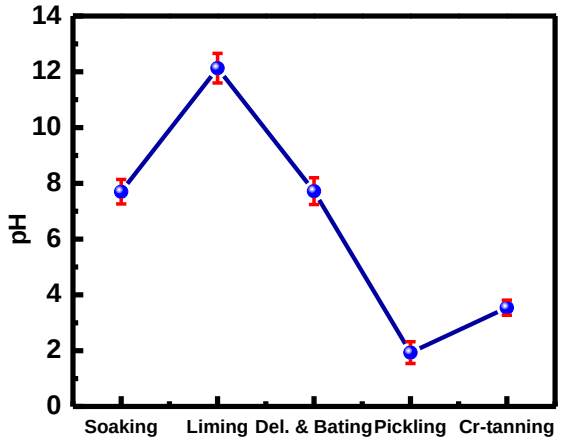

Fig. 2 pH level in beamhouse to Cr-tanning operations

4.2 Total solids (TS)

The total suspended solids (TSS), total dissolved solids (TDS) and total solids (TS) are shown in the Fig. 3. The suspended solids (SS) and dissolved solids (DS) value were so high and in some cases the level was several times higher than the standard level. Especially in soaking, liming and deliming & bating the suspended solids level was 70, 66, and 98 times higher than the standard level (Table 1), respectively.

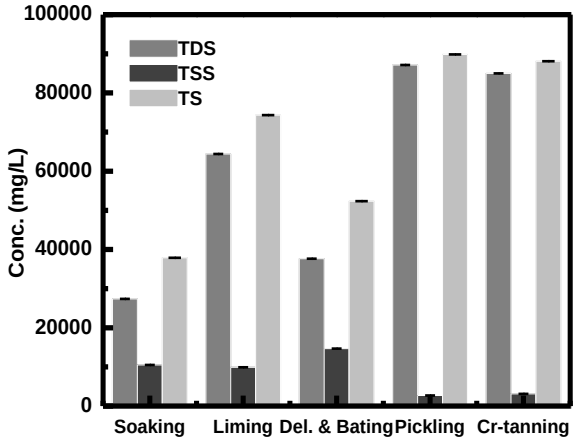

Fig. 3 The level of TSS, TDS and TS

The TDS level was 18-40 times higher the standard for beam house to Cr-tanning operations. The discharging solids substances get deposited on the bed of the stream and kill aquatic organisms of the stream bottom. The

floating solid interfere the streams ability for self-purification by re-generation of oxygen absorbing from the atmosphere. It also effects on the photosynthesis activity of the stream plankton and aquatic plants. The suspended solids (SS) are caused the turbidity which decreases the infiltration of sunlight into water thus reduces photosynthesis activity of aquatic plants.

4.3 Chloride (Cl^-) concentration

The chloride concentration in beam house and chrome tanning operation is shown in Fig. 4.

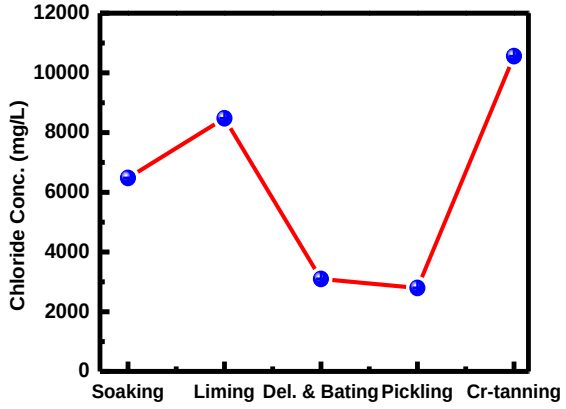

Fig. 4 Chloride levels in beamhouse and Cr-tanning

Chloride increases the electrical conductivity of the water and thus increases the corrosivity. Due to its corrosivity metal vessels of tanning react with chloride ions to form soluble salts [10] as a result increasing levels of metals in the water bodies. In some cases wastes water containing chloride is discharged through lead pipe which enhances the galvanic corrosion [11]. Finally all the metal containing waste water falls to low lying area to river, Buriganga.

4.4 Level of Dissolved Oxygen (DO)

In Fig. 5 represents the dissolved oxygen levels in the beamhouse to chrome tanning operations.

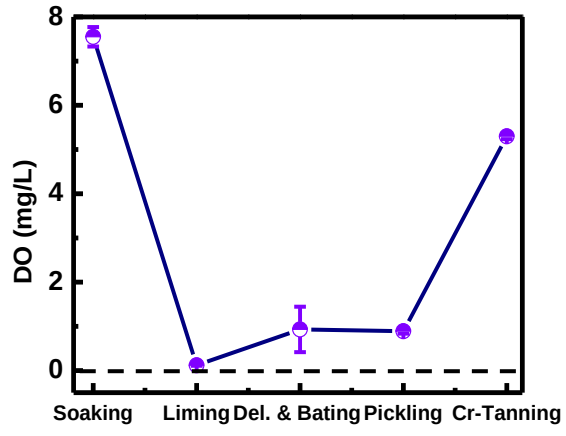

Fig. 5 DO level in beamhouse to Cr-tanning operations

DO levels were placed between 0.9 mg/L–7.6 mg/L. In the surface water DO level is 8.5 mg/L at 24ºC [12] and standard for waste from the industrial unit is 4.5–8.0 mg/L. In case of soaking and Cr-tanning DO values were between the ranges for industrial unit. The rest of operations DO values were very low; in case of liming DO was extremely low (<1). The lower DO values containing waste liquors are directly discharged to environment. Liquid waste from the various operations as well as from the different tanneries falls to the river, Buriganga which is one of the most reasons to decrease the DO level. Resulting numbers of fishes as well as aquatic plants are disappearing due to lack of DO.

4.5 Level of COD and BOD

Fig. 6 shows the BOD level in beamhouse to Cr-tanning operation. The liquid wastes are enriched with high BOD_5 except in pickling (50 mg/L). The BOD_5 level in Cr-tanning, deliming & bating, soaking and liming is (2-45) times higher than the tannery effluent standards in Bangladesh. The higher BOD_5 indicates the higher concentration of organic substances existing in the liquid wastes which consume DO. As a result, aquatic livings are getting suffocation due to lack of oxygen.

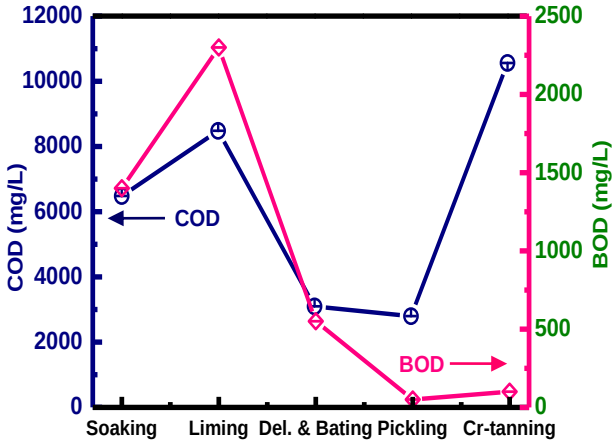

Fig. 6 BOD and COD in beamhouse to Cr-tanning operations

It is clear from the Fig. 6 that the COD values in the liquid wastes range vary from 2796−10560 mg/L. The ratio between COD: BOD of untreated tannery effluent is in the range 2:1 to 3:1 [13]. The higher the ratio between COD and BOD implies that bacteria cannot easily break down organic contaminants in the effluent or it could be said that in the biological treatment unit less organic substance will be break down. As a result, the ratio of COD and BOD has the negative effect not only in aquatic life also in the treatment technologies.

4.6 Total chromium (Cr) concentration

The concentration of total chromium (Cr) in the spent chrome liquor was 2656 mg/L. The level of chromium concentration was extremely high and it was 1328 times

higher than the industrial standard (2 mg/L) [9]. Prior to chrome tanning, during pickling stage pH is maintained at 2.5–3.0 for better chrome penetration into pelts [14] and subsequently chrome tanning the pH is raised ~4 to fix chromium with collagen [15]. In that context in pickling pH is low (< 2) thus limiting the fixation of chromium into the pelt resulting discharged as waste. The high concentration of chromium is discharged directly from the tannery without applying recover or reuse system.

During carrying the discharged spent chrome liquor through the drain; it mixes with simultaneously discharged lime liquor (pH 12.13) which produces toxic hydrogen sulphide (H_2S) gas; a fraction of chromium is precipitated as chromic hydroxide or absorbed by soil/sediment or carrying as liquid phase and falls to the low lying adjacent areas. Onset of favorable condition the adsorbed chromium could be desorbed/leached from the soil/sediment to ground water that might be a great threat in the near future of the adjacent residential area.

4.7 Effect of physiochemical parameters on aquatic life

The pH is vital for aquatic organisms and physiological process which can be activated under a relatively wide pH range 6.0−9.0 [16]. Elsewhere this pH range is stressful and potentially lethal to fish; if the pH is getting too far from optimal range even organisms may die. The extremely low pH (< 2) in pickling is contained chloride ion which could dissolve the metals from tanning vessels or from the sediment which may be taken up by the aquatic animals or plants [17]. The pH below 5.0 productivity of aquatic ecosystems is significantly reduced which successively reduces the food supply for higher organisms [18] as a result reduction the number of fish or growth rates.

Dissolved oxygen is essential for survival of aquatic livings. Low dissolved oxygen (DO) primarily results from the excessive algae growth; resulting insufficient amounts of dissolved oxygen available for fish and other aquatic lives. Deficiency of DO also occurs death of submerge plants.

The suspended substances can be altered the taste, temperature, odor and reduce the levels of DO particularly in deeper. The higher the total solids (TS) are responsible for turbidity of water which causes the photosynthesis process because turbidity impedes deep penetration of light in water [19]. The total dissolved solids (TDS) causes toxicity by increasing the salinity, changes the ionic compositions of water and toxicity of individual ions [20]. The quality of the river water, Buriganga is becoming worse due to receiving tannery liquid wastes.

4.8 Comparison data with standard

In Table 1 data was obtained from the experiment comparison with the tannery effluent standard in Bangladesh. Obtaining data exceeds the standard level which means the liquid waste is directly contaminated the receiving aquatic bodies.

Table 1 Comparison the parameters with standard

Parameters	Obtained	Standard
pH	1.9-12.1	6-9
SS	2693−10498	150
BOD_5 20°C	2796−10560	100
Sulphide (as S)	Not detected	1
T. Chromium (as Cr)	2656	2
TDS	27378−87145	2100

* The unit of the parameters is mg/L except pH

5. Conclusions

In beamhouse to chrome tanning operations substantial amount of liquid wastes are produced which contain high or extremely low pH, high TDS and TSS. The ratio of COD and BOD is also high. The spent chrome liquor contained high amount of chromium. The entire waste liquids' final reservoir is the river, Buriganga which has a great adverse impact in aquatic life. Due to deficiency of oxygen aquatic livings are becoming disappear, suspended matters obstacle to infiltrate the sunlight in the photosynthesis process. Authorities have to be minimized the liquid wastes to follow the environmental regulation before discharging to the environment. In case of spent chrome liquor it could be reuse or recover system for environmental friendly leather production.

REFERENCES

[1] H. K. Das, Chemical Toxicity and Environmental Hazards of Tanneries in Bangladesh. *Framco-Bangladesh Association of Scholars and Trainees (FBAST)*, pp 15-19, (2000).

[2] FMA. Slam, Shah Md. Reduwan Billah, Leather Industry: Environmental Pollution and Mitigation Measures, *SEHD (Society for Environment and Human Development)*, pp 2, (1998).

[3] M. Ahmed, Effect of leather tanning industries on the environmental pollution and food chain. *Bangladesh AOTS Alumni Society (BASS)*. pp 17-19, (2012).

[4] H. L. Paul, A. P. M. Antunes, A. D. Covington, P. Evans, P. S. Phillips, Bangladeshi Leather Industry: An Overview of Recent Sustainable Developments, *Journal of the Society of Leather Technologists & Chemists*, Vol. 97(1), pp 25-32, (2013).

[5] A. Zahid, K.-D. Balke, M. Q. Hassan, M. Flegr, Evaluation of aquifer environment under Hazaribagh leather processing zone of Dhaka city, *Environmental Geology*, Vol. 50, pp 495-504, (2006).

[6] K. A. Ahmed, Surface water pollution from leather industries, *Bangladesh Leather*, Vol. 11, pp 9-15, (1997).

[7] M. A. Rouf, M. S. Islam, M. Z. Haq, N. Ahmed, T. Rabeya, Characterization of effluents of leather industries in Hazaribagh area of Dhaka city, *Bangladesh Journal of Scientific and Industrial Research*, Vol. 48, pp 155-166, (2013).

[8] APHA (American Public Health Association), American Water Works Association, *Water Environment Federation*, 1999.
[9] The Environment Conservation Rules, *Ministry of Environment and Forest, Bangladesh*, pp 221-222, (1997).
[10] Sodium, chlorides, and conductivity in drinking water: a report on a WHO working group, Copenhagen, WHO Regional Office for Europe, (EURO Reports and Studies 2), (1978).
[11] R. Gregory, Galvanic corrosion of lead solder in copper pipe work. *Journal of the Institute of Water and Environmental Management*, Vo. 4(2), pp 112-118 (1990).
[12] Parameters of Water Quality-Interpretation and Standards, *Environmental Protection Agency*, Ireland, 2001.
[13] TFL Eco Guidelines, *Reduction of COD & BOD in tannery waste water*, Part 1, pp 1-20, (2008).
[14] A. D. Covington, Tanning Chemistry, RSC Publishing, UK, pp 127, (2011).
[15] F. M. Karim, Recovery and reuse of chromium, *Framco-Bangladesh Association of Scholars and Trainees (FBAST)*, pp 10-14, (2000).
[16] NAS (National Academy of Sciences), Water Quality Criteria, (1972).
[17] K. Addy, L. Green, H. Elizabeth, University of Rhode Island. Contribution #4059 of the RI Agricultural Experiment Station, URIWW-3, pp 1-4, (2004).
[18] J. S. Alabaster, R. Lloyd, Water quality criteria for freshwater fish. European Inland Fisheries Advisory Commission Report (FAO). Buttersworth, London-Boston. 297p, (1980).
[19] LN. Muoghalu, V. Omocho, Environmental Health Hazards Resulting from Awka Abattoir. *African Journal Environmental Studies*, Vol. 2, pp 72–73 (2000).
[20] P. K. Weber-Scannell, L. K. Duffy, Effects of Total Dissolved solids on Aquatic Organism: A Review of Literature and Recommendation for Salmonid Species. *American Journal of Environmental Sciences*, Vol. 3(1), pp 1–6 (2007).

ICMIEE-PI-140-378

Polyimide – Polysiloxane Nanohybrid : Synthesis and Performance

Shaikh Md. Mominul Alam

Bangladesh University of Textiles, Tejgaon, Dhaka-1208, BANGLADESH.

ABSTRACT
A series of polyimide (PI) and polysiloxane (PSX) nano-hybrids were prepared through in-situ sol-gel process of PSX to investigate the functional group and rational effect of PSX in PI-PSX hybrids. PI was prepared from 3, 3′, 4, 4′-biphenyltetracarboxylic dianhydride (BPDA), p-phenylenediamine (PDA). PSX like polydimethylsiloxane (PDMS), polymethylphenylsiloxane (PMPS) and polydiphenylsiloxane (PDPS) were prepared by the sol-gel reaction of diethoxydimethylsilane (DEDMS), diethoxymethylphenylsilane (DEMPS) and diethoxydipheylsilane (DEDPS) accordingly. PI-5%PDMS hybrid provided higher elongation at break% where as PI-5%PDPS hybrid had higher tensile modulus than pristine PI. PI-5%PDPS or PMPS hybrid became more transparent but PI-5%PDMS hybrid became opaque. Weight residue % at 800˚C, glass transition temperatures of all hybrids were higher than pristine PI.

Keywords: Polyimide, Polysiloxane, sol-gel reaction, tensile modulus, opaque.

1. Introduction

Polyimides are considered to be one of the super-engineering materials due to their excellent thermal, mechanical and dielectric properties [1] which has been applied it to a wide range of industrial fields, such as microelectronics and aerospace engineering.

Hybridization is an up-date technique to incorporate inorganic materials into polyimide for combining the advantages of organic polymer and inorganic materials [2-4].

Among inorganic materials, PSX are the most common and one of the most important organosilicon polymers used in polymer chemistry[2]. The functional group of polysioxane can play an important role on their behaviors. PDMS is widely used polysiloxane whose repeating unit is [-$SiO(CH_3)_2$-] in where two methyl groups are attached as side chain. Another form of PSX is phenyl containing siloxanes. The phenyl group is usually incorporated as PMPS [-$Si(CH_3)(C_6H_5)O$-] or a PDPS [-$Si(C_6H_5)_2O$-]. Though the main chain of PDMS, PMPS, PDPS is same (-Si-O-Si-) but due to the side functional group their properties are so different among one another (Scheme 1).

The present study is carried out to provide results useful for comparing the properties of among the hybrids produced from PI and different ratios (5, 10, 20, 50%) of PDMS, PMPS and PDPS. PDMS, PMPS, PDPS were developed into polyamic acid from alkoxysilane like DEDMS, DEMPS and DEDPS respectively through in-situ sol-gel process. The current research interest is to prepare hybrids with PI and those 3 PSX individually to observe the effect in performance of hybrids mainly thermal and mechanical aspects.

2. Experimental

2.1 Reagents

BPDA and PDA from Tokyo Kasei Kogyo Co. Ltd, Japan were purified by sublimation. N-Methyl-2-Pyrrolidone (NMP) from Osaka Chemicals, Japan was dried by distillation under reduced pressure over Sodium Hydride. DEDMS, DEDPS, DEMPS from Wako Pure Chemical, Japan were used as received. PAA was prepared from BPDA and PDA in NMP (Scheme 2) in where inherent viscosity of the PAA was 2.20 dl/g (0.5g/dl in NMP at 30˚C).

2.2 Synthesis of PI

In a three necked flask fitted with a mechanical stirrer, 2.589g (24mm) PDA 86.90ml of NMP was

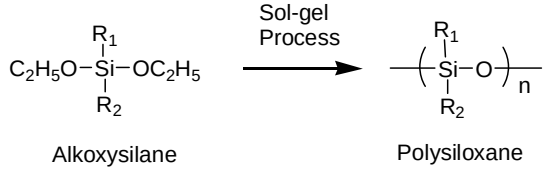

DEDMS : $R_1=R_2=CH_3$
DEMPS : $R_1=CH_3$, $R_2=Ph$
DEDPS : $R_1=R_2=Ph$

PDMS : $R_1=R_2=CH_3$
PMPS : $R_1=CH_3$, $R_2=Ph$
PDPS : $R_1=R_2=Ph$

Scheme 1. Synthesis of PSX

* Corresponding author. Tel.: +88-01713171365
E-mail address: dalim70@yahoo.com

stirred until clear solution were got under nitrogen atmosphere. 7.06g (24mm) of BPDA and rest amount of NMP were added and stirring was continued up to 12 hrs at room temperature. The solution was cast onto a glass plate and successive heating at 60˚C/16h, 100˚C/1h, 200˚C/1h, 300˚C/1h, 350˚C/15 min affording transparent film (Scheme 2).

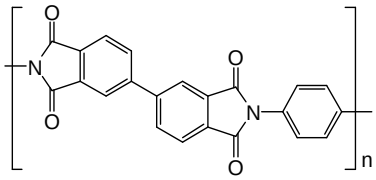

Scheme 2. Structure of PI (BPDA/PDA)

2.3 Preparation of PI-Silica-PDMS hybrids under Sol-Gel process:

The PI-PDMS hybrids were prepared the following way: Into a flask equipped with mechanical stirrer, certain amount of PAA was stirred with required amount of DEDMS about half an hour. Water (mole ratio of DEDMS and H_2O=1:2) was then added and stirred about 24 hrs. The solution was cast on glass plates, dried in vacuum oven at 60°C/16 h, 100°C/1h, 200°C/1h, and then 300°C/1h, 350°C/15 min. in an air circulating oven to obtain solid films.

PI-PMPS and PI-PDPS hybrids were prepared in the similar way by using DEMPS and DEDPS as PSX, respectively.

2.4 Measurements

IR spectra were obtained with Jasco Spectrophotometer model FT/IR-420. DSC was recorded using Rigaku Thermo Plus 2DSC8230 at a heating rate of 10˚C/min under nitrogen. TGA was performed with Rigaku Thermo Plus 2TG-DTA TG8120 at a heating rate of 5˚C/min under argon. Dynamic mechanical analysis (DMA) were conducted on ORIENTEC Automatic Dynamic Viscoelastomer Rheovibron model DDV-01FP at 35Hz at a heating rate of 4°C/min. Tensile properties were recorded with Imada Seisaku-sho Model SV-3. SEM from Hitachi S-4800 was used to check the particle size of inorganics.

2.5 IR of PI-PSX hybrids

Imidization and curing of the hybrids were checked by IR. In case of all PI- hybrids, after 350°C curing, the characteristic peak related to absorption of imide group at 1776cm-^{1} C=O symmetric stretching, 1730cm^{-1} C=O asymmetric stretching, 1365cm^{-1} C=N stretching were found which proved the hybrids are PI-hybrids. The absorption peak related to Si-O-Si were seen at 1000-1100 cm^{-1}, which also became larger after adding higher content of inorganics. The Si-OH related pick were found at 1000-1050cm^{-1}, which became smaller after arising curing temperature and proved the conversion from Si-OH to Si-O-Si. In case of PI-PMPS and PI-PDPS hybrids, the C-H stretching of phenyl group were seen at 3070cm^{-1} which proved the presence of side functional group in hybrids as well.

2.6 DSC of PI-PSX hybrids

Polymerization were confirmed by DSC. In case of all hybrids endotherm happened due to imidization of PI mainly. After 200°C curing, endotherm disappeared and polymerization may be completed. IR-spectras of the hybrids also shown the characteristics picks related to PI at 200°C curing and supported the DSC results. The amount of endotherm of pristine PI at 100°C curing is about 146.05 J/g. The amount of endotherm at 100°C curing are 78.94, 58.12, 46.2, 31.55 J/g for PI-PDMS hybrids, 126.05, 116.94, 114.58, 77.97 J/g for PI-PMPS hybrids and 142.21, 124.79, 120.18, 63.24 J/g for PI-PDPS hybrids at 5,10, 20, 50% inorganics. The amount of endotherm of PI-PSX hybrids became lower at higher contents of PSX which proved the addition of inorganics in hybrids at higher ratios. The amount of endotherm related to PI-PDPS, PI-PMPS hybrids are lower than those of PI-PDMS hybrids may be due to higher crystalline in nature of phenyl related PSX. In XRD-results, we have seen no pick in case of PI-PDMS related hybrids. But in case of XRD-results of PI-PDPS hybrids, pick related to the crystalline structure of PDPS have seen. PI-50%PMPS-hybrids also showed slight pick in XRD.

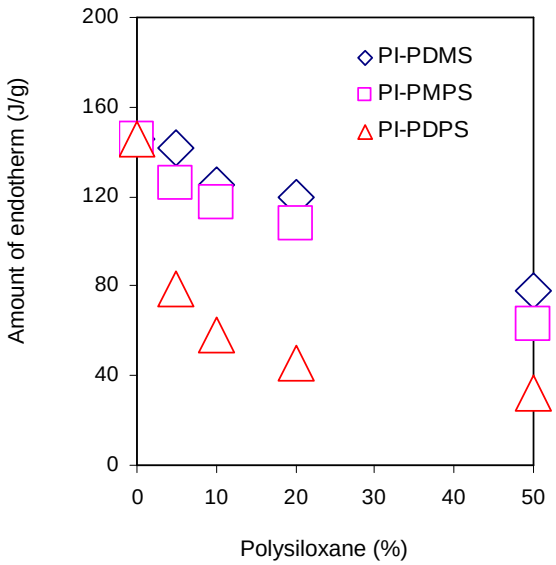

Fig 1. Amount of endotherm of PI-PSX hybrids

2.7 Transparency of PI-PSX hybrids

The transparency of the hybrids were checked by UV-spectrophotometer and results are plotted in Fig. 2. Pristine PI transparency is about 76% at 700nm wave no. The transparency reduced tremendously like 7.6, 1.4, .016, .014% after adding 5, 10, 20, 50% PDMS. But when introduced 5, 10, 20, 50% PDPS, the transparency became 82, 77, 76, 60%. The transparency

became 80, 72, 9, 0.4% after adding various ratio (5, 10, 20, 50%) of PMPS. It is well known that aromatic PI with coloration of pale yellow to deep brown strongly absorb visible light because of their aromatic conjugated structure and the intermolecular and intra molecular charge transfer complexes (CTCs) formed between and within Polymer chain. Phenyl-phenyl (PI-PDPS) interaction increase compatibility between two phases. Small PDPS and PMPS domain affect the electron state of PI and hinder to develop intermolecular CTCs and increase transparency. The higher contents of polysiloxane reduced transparency due to the aggregation of inorganics.

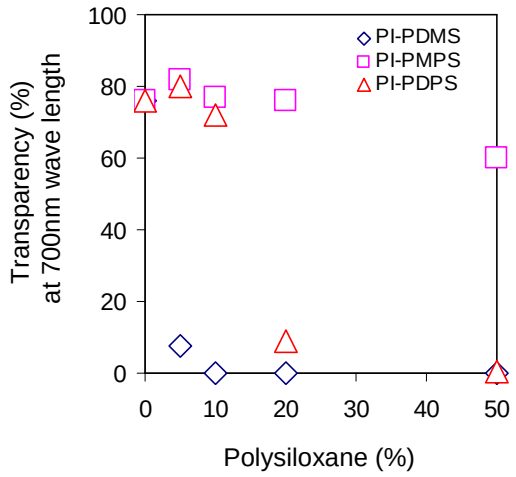

Fig 2. Transparency of PI-PSX hybrids

2.8 Morphological study

The shape and size of inorganics in various PI-hybrids were seen by SEM. SEM-images were taken both from fracture surface and etching system. In PI-PDMS hybrids, the inorganic particle size were about 30-60 nm in case of PI-5%PDMS hybrids. The particle became aggregated at high contents (10-50%). The PDPS and PMPS particles sizes were about 30-50nm at low content (5 and 10%) PSX related PI-hybrids. In case of high content of PI-PDPS (20, 50%) hybrids, the particles became aggregated but the aggregation is not as severe as PI-PMPS (20, 50%), PI-PDMS (20, 50%) hybrids. From above discussion, it can conclude that the tendency of self condensation of methyl related PSX is much more higher than phenyl-related PSX may be due to π-π interaction between PI and Phenyl functional group of PSX. High condensation rate produced bigger particle also aggregation in case of PI-PDMS related hybrids. The aggregation of PDMS and high (20, 50%) content PMPS made the hybrids opaque.

3. Properties of PI-Silica-PDMS films

3.1 Tensile properties

The mechanical properties of PI and PI-PSX hybrids were examined and the results are summarized in Fig 3. In comparison of pure PI, the PI-5%PDMS hybrid decreased the modulus and the tensile strength while the elongation at break increased upon incorporating PDMS as a flexible particle into the

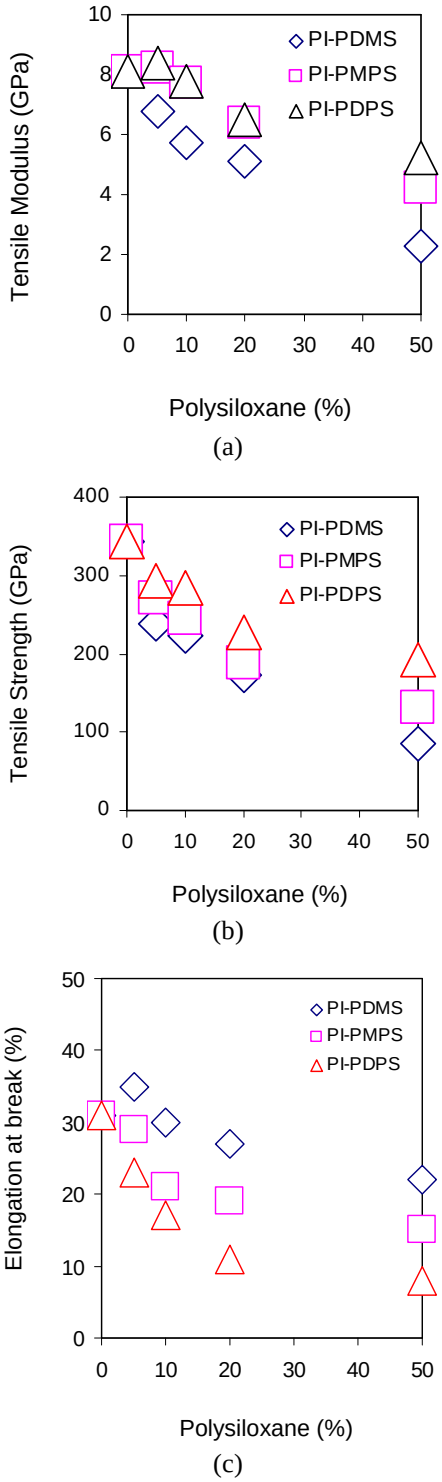

Fig 3. Effect of Polysiloxane (%) on (a)Tensile modulus (b)Tensile strength (c) Elongation at break% of PI-Polysiloxane hybrids

matrix. Due to the poor interfacial interaction between PI and PDMS particles and the incorporation of large PDMS particles with aggregation of inorganics lead to the inferior mechanical properties. In case of PI-PDPS and PI-PMPS hybrids, the modulus of PI-5 hybrids increased nicely than pristine PI due to the rigidity of side aromatic functional group and π-π interaction between PI and inorganics. Though the strength of PI-PSX hybrids were lower than pristine PI but it can be carefully observed that the hybrids related to phenolic side function groups (PI-PDPS, PI-PMPS) showed higher tensile strength due to π-π interaction than PI-PDMS hybrids. The high crystal behavior of phenolic group related PSX decreased the elongation at break% of the PI-PDPS and PI-PMPS hybrids.

3.2 Dynamic mechanical properties

DMA was done mainly to observe the glass transition temperatures of the hybrids [Fig 4]. All PI-PSX hybrids showed two T_gs---- the lower T_g is for PSX and the higher T_g is for PI. The tendency of the lower T_gs always tends to the T_g of related PSX after increasing the ratio. As example, PDMS T_g is about -120°C. The lower T_g of PI-PDMS hybrids tends to the T_g of PDMS after increasing the contents of PDMS into the hybrids. So PI-PDMS hybrids T_g decreased from -39.4°C to -68.7 after inclusion of 5 to 50% PDMS. Also PDPS T_g is about 49°C. So the lower T_g of PI-PDPS hybrids became -33.7 to 44.2°C after inclusion 5 to 50% PDPS into PI. The lower T_g of PI-PMPS hybrids showed the same phenomena.

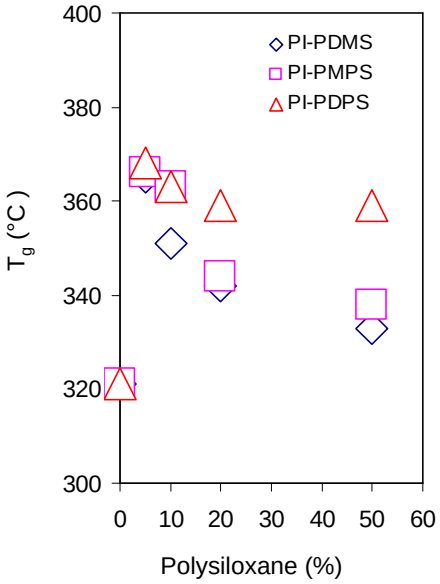

Fig 4. DMA of PI-PSX hybrids

The higher T_gs of PI-PSX hybrids are higher than the pristine PI (320°C from tanδ). This happened due to the nanometer size of inorganics which restrict the movement of PI. Also π-π interaction and H-bonding between PI and polysiloxane can provide interfacial interaction which restrict the segmental motion between phases. The loss modulus of PI-PSX hybrids decreased due to the flexibility of PSX. But Phenyl side functional group related PI-PSX hybrids showed higher modulus than PI-PDMS hybrids which proved the π-π interaction between PI, PSX phases. Even PI-5%PDPS hybrids showed higher modulus than pristine PI at 30°C.

3.3 Thermal properties

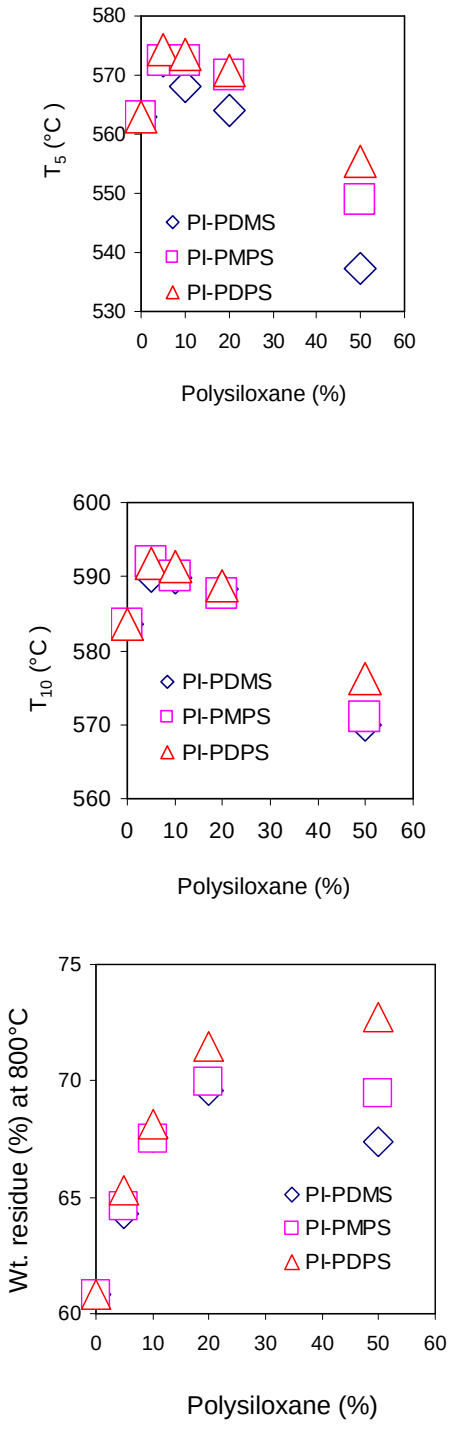

Fig 5. TGA of PI-PSX hybrids

Silicone resin possesses excellent thermal stability because of its special structure, such as high bond energy (443.7 KJ/mol) and high ionic character (about 51%) of Si-O bonds. PDMS is the most common member of the family, and many studies of its thermal properties have been reported. The incorporation of phenyl siloxane in PDMS has been shown to increase its thermal-oxidative stability. Both the onset temperature of thermal degradation and residue content of PDMS containing phenyl groups showed a neat, direct correlation between increasing phenyl content and final weight of residue. The introduction of small amount of MPS or DPS into a PDMS skeleton can increase the onset temperature from 340°C to 400°C. In case of our PI-PSX hybrids, TGA under argon was done to check the thermal stability of PI-PSX hybrids [Fig 5]. PDPS, PMPS related hybrids showed higher 5% degradation temperature (T_5), 10% degradation temperature (T_{10}) and weight residue% at 800°C than PDMS related hybrids. It also noticed that small contents of PSX increased the thermal stability of the hybrids due to the presence of PSX in to PI matrix which hinder the permeability of volatile degradation products out from the material. High contents of PSX made aggregation which degraded thermal stability of the hybrids.

4. Conclusions

PI-PSX hybrids were prepared by PI and various ratio of PSX. Side functional groups showed pronounce influence in transparency, thermal and mechanical properties of the hybrids. The ratio of PSX also can play roll effectively in performance of the hybrids. In-situ sol-gel process can provide PI-PSX hybrids successfully.

REFERENCES

1. K.L Mittal, *Polyimides: Synthesis, Characterization and Application,* Vol.1, Plenum Press, New York and London, (1984).
2. S. M. M Alam, Preparation of Polyimide-Clay Nanocomposites and Their Performance, *Journal of Scientific Research,* Vol.1(2),pp326-333(2009).
3. S. M. M Alam et al., Preparation and Properties of Polyimide-Clay Hybrids Containing In-situ Formed Polydimethylsiloxane, *J. Photopolymer Sci. and Tech*., Vol.19(2), pp293-296(2006).
4. S. M. M Alam et al., Organic-Inorganic hybrids containing polyimide, organically modified clay and in situ formed polydimethylsiloxane, *React. Funct. Polym.*, Vol.67: pp1218-1224(2007).
5. N. Furukawa et al., Surface and Morphological Characterization of Polysiloxane-Block-Polyimide, *J. Polym. Sci. A: Polym Chem.*, Vol. 35, pp2239-2251 (1997).
6. J.E. McGrath, D.L.Dunsion, S. J. Mecham, and , J.L Hedrick, Synthesis and Characterization of Segmented Polyimide-Polyorganosiloxane Copolymers, *Advances in Polymer Science,* Vol.140, pp61-105(1999)..
7. Y. Yamada, Siloxane modified polyimide for microelectronics coating applications, *High Perform. Polym.*, Vol.10, pp 69-80(1997).
8. P. Sysel, R. Hobzova, V. Sindelar, J. Brus, Preparation and characterization of cross-linked polyimide-poly(dimethylsiloxane)s, *Polymer,*Vol.42, pp10079 -10085(2001).

Energy Auditing: Necessity for Energy Management System

Mahedi Hassan, Nahid Hassan, Md. Murad Miah, Farzana Akter Sohaly, Iffat Arefa and Zahid Hasan Mahmood
Department of Applied Physics, Electronics and Communication Engineering, University of Dhaka, Dhaka 1000, BANGLADESH

E-mail:mhdiapece12@gmail.com and zhm1960@gmail.com

ABSRACT
Energy conservation could protect the present reserve of energy from the culture of wasting. In this paper energy audit has been focused to assess the state of energy usage. The methodology of energy audit is the measurement of energy performance with respect to production factor. The technical survey for the energy audit to monitor the consumption in industry, domestic area, hospital and power plant has been studied. All attempts are taken to the total energy input correlating with production for the mentioned fields. As a result of the study the areas where the energy is wastefully used and the improvements are felt, are identified and corrective measures are recommended so that the overall field efficiency could be improved. Energy sovereignty of the country could be ensured through the effective practice of energy audit which would determine the way to set increasing energy efficiency of all resources crucial with respect to both environment and economy of the country. Energy auditing is a must for the energy sovereignty of our country.

Keywords: Energy Management, Energy Auditing, Production factor, Courses on Energy Auditing

1. Introduction

For the development of a country the first important requirement that is needed is energy. To develop both socially and economically no option is getting prior without energy, but nowadays energy overview of the world is not in pleasurable condition and for Bangladesh the condition is more bad. Though quantity of natural resource is decreasing day by day, wastage of natural resource in different field is not controlled due to lake of proper management. Energy Auditing will be possible strategy in Energy management case to control such type of wasting in some field like industries, power plants, houses, different types of shops and Hospitals.

2. Definition of Energy Management

The fundamental goal of energy management is to produce goods and provide services with the least cost and least environmental effect. The term Energy Management means, the strategy of adjusting and optimizing energy, using systems and procedures so as to reduce energy requirements per unit of output while holding constant or reducing total costs of producing the output from these systems. The objective of Energy Management is to achieve and maintain optimum energy procurement and utilization throughout the organization and:

- To minimize energy costs and waste without affecting production and quality.
- To minimize environmental effects.

2.1 Purpose of Energy Management

The purposes of energy management are mentioned below:

- Improving energy efficiency and reducing energy use, thereby reducing costs
- Reduce greenhouse gas emissions and improve air quality
- Cultivating good communication on energy matters
- Developing and maintaining effective monitoring, reporting and management strategy for wise energy usage
- Finding new and better ways to increase returns from energy investments through research and development

3. Definition of Energy Audit

An energy audit is a technique for identifying energy losses, quantifying them, estimating conservation potential, evolving technological options for conservation and evaluating techno economics for the measures suggested. Assist industries in reducing their energy consumption, To promote energy-efficient technologies among industry sectors, Disseminate information on energy efficiency through training programs and workshops, To

promote transfer of energy-efficient and environmental-sound technologies to the industrial sectors in the context of climate change.

3.1 Reason of the requirement of Energy Auditing

In the case of an industry, the three top operating expenses are often found to be energy both electrical and thermal, labor, and materials.In most assessments of the manageability of the cost or potential cost savings in each of the above components, energy would invariably consider at first and thus energy management function constitutes a strategic area for cost reduction. A perfect energy audit will always help managers to understand more about the ways energy and fuel are used in their industry and help to identify those areas where waste can occur and where scope for improvement are needed. The energy audit would give a positive orientation to the energy cost reduction, preventive maintenance, and quality control programs which are vital for production and utility activities. Such an audit program will help to keep focus on variations that occur in the energy costs, availability, and reliability of supply of energy, help decide on the appropriate energy mix, identify energy conservation technologies and retrofit for energy conservation equipment. In general, the energy audit is the translation of conservation ideas and hopes into reality, by lending technically feasible solutions with economic and other organizational considerations within a specified time frame. The primary objective of the energy audit is to determine ways to reduce energy consumption per unit of product output or to lower operating costs. The energy audit provides a benchmark, or reference point, for managing and assessing energy use across the organization and provides the basis for ensuring more effective use of energy.

3.2 Types of Energy Audits

The type of energy audit to be performed depends on:

- Function and type of industry
- Depth to which a final audit is needed, and
- Potential and magnitude of cost reduction desired

Thus energy audits can be classified into the following two types:

1. Preliminary audit
2. Detailed audit

3.2.1 Preliminary Energy Audit Methodology

The preliminary energy audit uses existing or easily obtained data. It is a relatively quick exercise to:

- Determine energy consumption in the organization
- Estimate the scope for saving
- Identify the most likely and easiest areas for attention
- Identify immediate improvements and savings like low cost or no cost.
- Set a reference point
- Identify areas for more detailed study and measurement [1]

3.2.2 Detailed Energy Audit Methodology

A detailed energy audit provides a comprehensive energy project implementation plan for a facility, since it evaluates all major energy-using systems. This type of audit offers the most accurate estimate of energy savings and cost. It considers the interactive effects of all projects, accounts for the energy use of all major equipment, and includes detailed energy cost saving calculations and project cost. In a detailed audit, one of the key elements is the energy balance. This is based on an inventory of energy-using systems, assumptions of current operating conditions, and calculations of energy use. This estimated use is then compared to utility bill charges. Overall Energy Audit follows some criteria that are given below.

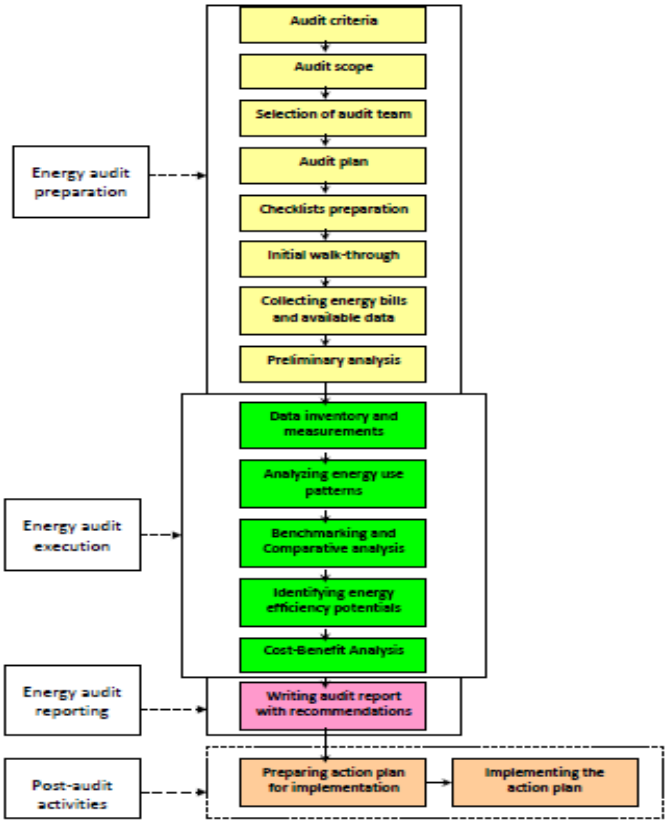

Fig.1 Detailed Energy Audit Process. [1]

4. Process of Energy Auditing in Industries

Auditing in Industries means the checking of the efficiency of the production according to the consumption of energy, this is following some steps.

• Preparation and planning
• Data collection and review
• Plant surveys and system measurements
• Observation and review of operating Practices
• Data documentation and analysis
• Reporting of the results and recommendations [3]

4.1 Understanding Industrial Operation

Developing an understanding of industrial operations is a prerequisite for the analysis of energy efficiency in an organization. In order to achieve that, we start with data on the general characteristics of the business followed by data collection on energy use, main utilities and characteristics of energy end-use requirements.

Table 1 General Characteristics of Energy Auditing.

Type of the section		
Type of the Product		
Production capacity (t/y)		
Capacity Utilization (%)		
National/Multinational		
History of the Industry		
When Established		
Growth Pattern		
Cost structure		
Raw Material (%)		
Labor (%)		
Energy (%)		
Other (%)		
External Environmental Fector		
Economics		
Board Economic Setting		
Development Trend		
Structure and Share of the market		
Objectives and Strategies		
Specific organizational objectives and strategies as defined by management		
Growth objectives over the next 5 years		
Policies and plans, main projects		

4.2 Preliminary Energy Audit

A Preliminary Energy Audit is essentially a data gathering exercise which aims to develop an understanding of how energy is used in an Industry and prepare a background for detailed energy audit implementation.

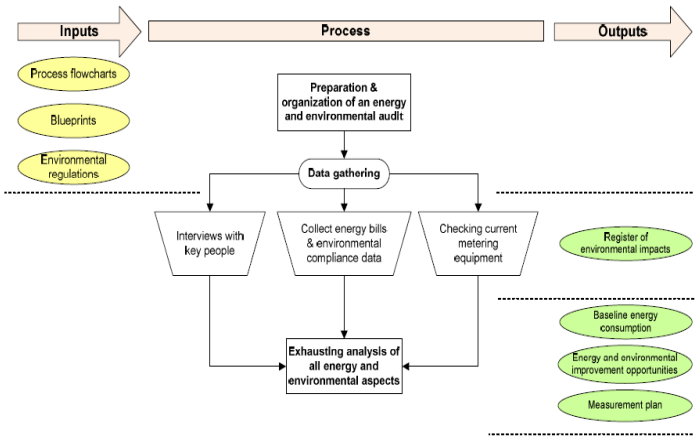

Fig.2 Preliminary Auditing Process. [2]

In an Preliminary auditing process the first requirement is to gather data from key peoples like manager and owner of the factory about the schematic design of the factory production process, production program and capacity, production of the year, using raw material, monthly and annual fuel consumption data by an interview.

Table 2 Production process of An Industry.

Production program and capacity
Production in the year
Raw materials

Short process description	
Draft scheme of the production process	
Draft scheme of the Boiler system	
Draft scheme of the Electric conversion system	
Total annual operating time [h/yr]:	
Number of shifts per working day:	
Total number of employees	
Number of employees in energy group:	
Head of group:	
Total annual cost of production:	
Total annual cost for energy and water:	

Table.3 Annual fuel consumption. [2]

Month	Deliveries [l]	Cost of delivery [ ]	Working days in a month	Consumption [l]	Cost of consumed fuel [ ]
1	*2*	*3*	*4*	*5*	*6*
I					
II					
III					
IV					
V					
VI					
VII					
VIII					
IX					
X					
XI					
XII					
Total					

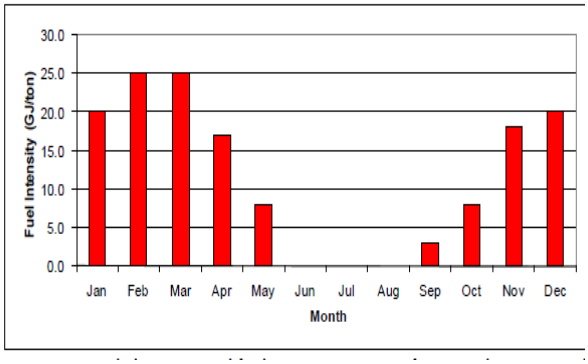

Fig.3 Bar diagram of Annual Fuel consumption reference of a Textile Mill. [3]

Table.4 Annual electricity consumption. [2]

Month	Active energy		Reactive energy		Total cost [ ]
	Consumption [kWh]	Price/unit [/kWh]	Consumption [kVArh]	Price/unit [/kVArh]	
1	*2*	*3*	*4*	*5*	*6*
I					
II					
III					
IV					
V					
VI					
VII					
VIII					
IX					
X					
XI					
XII					
Total					

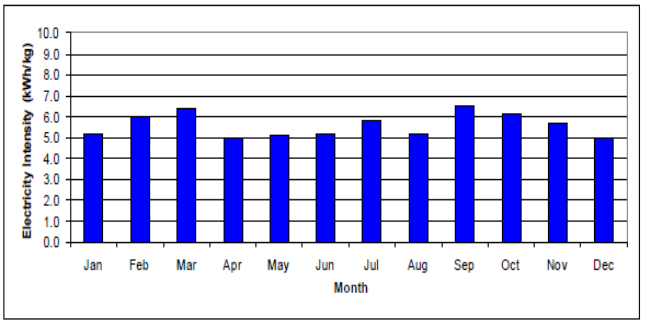

Fig.4 Bar diagram of Annual Electricity consumption reference of a Textile mill. [3]

4.4 Identification of Energy conservation opportunities

As a part of Preliminary Auditing during inspection of the plant, opportunities for energy conservation have to be identified. The following checklist should serve as a reminder as to where to look for Energy Conservation Opportunities. [2]

- Electrical system
- Air Conditioning
- Refrigeration
- Lighting
- Industrial boiler
- Steam
- Compressed Air
- Furnaces, kilns and oven

4.5 Detailed Energy Audit

A detailed energy audit aims at establishing actual energy performance of selected end-users and processes. Based on identified of energy conservation opportunities during the preliminary audit. DEA is the long term inspecting process consisting of all

types of data like production processing, equipments efficiency and performance, consumption of energy and Economic and Financial Evaluation of energy performance improvement measures includes cost-benefit analysis. The audit results have to be summarized in a report, together with an action plan containing the priorities for the implementation of performance improvement projectFig9. Detailed Energy Audit [2]

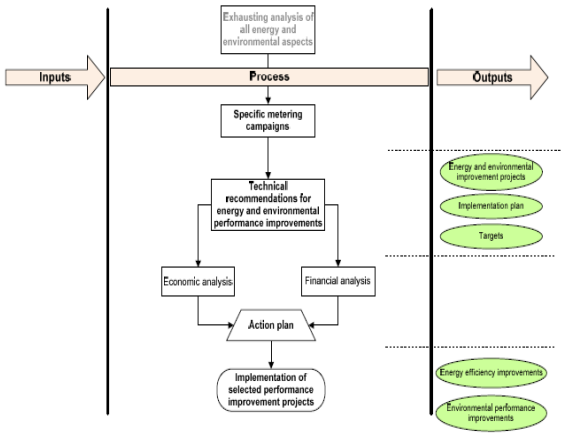

Fig.5 Process of Detail Energy Audit

4.6 Preparation and presentation of Detailed Energy Audit report and Action Plan

4.6.1. Recommended chapters for Detailed Energy Audit report

Information that must be remained in the audit report are following below:

- Executive summary
- General data on factory and processes
- Observations and comments on operational, housekeeping and maintenance practice
- Current level of production and energy consumption and energy balances
- Specifications of identified energy performance improvement measures
- Expected values of energy cost savings
- Investment analysis:
  - Economic aspects: Payback period
  - Financial aspects: Cash flow
- Quantitative target for improving energy performance
- Implementation plan for achieving the set targets
- Technical details and specifications must be attached

4.6.2. Approach to preparing an energy action plan

The order of consideration of energy conservation measures:

1. Improvement of maintenance practices
2. Improvement of operation practices
3. Improvement of equipment efficiency
4. Improvement of process efficiency

The order of priority for the implementation of energy conservation measures:

1.Introduction of systematic energy management practices including awareness, training and motivation programs

2. Improvement of energy metering, control and monitoring

3. Improved housekeeping and maintenance

4.Implementation of energy performance improvement projects with a short payback

5. Measurement of Energy Performance of a Plant of an Industry

Plant energy performance is the measure of whether a plant is now using more or less energy to manufacture its products than it did in the past, as a measure of how well the energy management program is doing. It compares the change in energy consumption from one year to another considering production output. Plant energy performance monitoring compares plant energy use from a reference year with subsequent years to determine the extent of improvement that has been made.

Production factor

The production factor is used to determine the energy that would have been required to produce this year's production output if the plant had operated in the same way as it did in the reference year. It is the ratio of production in the current year to that in the reference year.

$$\text{Production Factor} = \frac{\text{Current year's production}}{\text{Reference year's production}}$$

[1]

Reference Year Equivalent Energy Use

The reference year's energy use that would have been needed to produce the current year's production output can be called the Reference year energy use equivalent or Reference Year Equivalent for short. The reference year equivalent is obtained by multiplying the reference year energy use by the production factor that is obtained above .

Reference year equivalent = Reference year energy use X Production factor [1]

The improvement from the level of the reference year is called Energy Performance and is a measure of the plant's energy management progress. It is the reduction or increase in the current year's energy use over the reference, and is calculated by subtracting the current year's energy use from the reference year's equivalent. The result is then divided by the reference year equivalent and multiplied by 100 to obtain a ratio.

$$\text{Plant energy performance} = \frac{\text{Reference year equivalent} - \text{cunrrent year equivalent}}{\text{Reference year equivalent}} \times 100 \text{ [1]}$$

From this measurement an Auditor can get idea of energy use, consumption ,wastage and efficiency of a plant. If any result is not under satisfaction than Auditor can suggest to the Industry manager or owner to replace or change the design of the audited plant.

6. Reason of the requirement of Energy Auditing in Bangladesh

Power crisis is the main problem in Bangladesh. Though combining efficiency of all power plants are 10390 MW, productions are varied between 6000 t0 6500 MW [4]. The main background reason is the lack of maintenance and the lack of able man power for proper maintenance process. we do not generate any power from some our power plant such as Horipur EGCB power plant which is capable of generating 412MW power but the production is zero [4]. Moreover existing generating power are also wasted in industrial site as well as household by using low efficiency but high power consuming equipments. In this case energy audit can play a vital role by inspecting and measuring the efficiency of the using equipments both in industries and power plants along with household. They can give their own suggestion to the Industry owners, government in the use of the efficient equipments from their experience.In future Bangladesh will be set up 2000MW Nuclear power plant at Ruppur and 1320MW coal based power plant at Bagherhat and Moheskhali [4]. Energy Auditor will be required in such type of mega power plant for checking better production efficiency.

7. Proposal for Energy Audit program:

•During auditing process an auditor must follow the ISO-50001 Energy Management system Act [5]

• For perfect auditing an auditor must be well trained

• Universities of Bangladesh can be opened training program for the auditors and it will be either short term or long term course [5]

• For the training program following subjects like Lighting Systems, Air conditioning system, Motors and Drivers,Idea of general economics, Measurement Tools for Energy, Electric Utility & Natural Gas Bills, Heating, Electrical Distribution system savings, Heat Pumps, Ventilation, Domestic Hot Water, Water Conservation,Idea of general economics, Studies in Environment Pollution [3] [5]

7. Conclusion

Energy Auditing is a process of analyzing the energy performance of a field such industry, power plant, Home, etc. As Bangladesh is now in serious energy crisis, wastage of energy is not a good practice. In this condition, for the conservation of energy regular inspecting is a good option and for this task Energy Auditing will be shown good contribution in the conservation of energy process. It will be opened a new job option for students of Bangladesh.

REFERENCE

[1] Working Manual of Energy Auditing In Industries, Asian Publicity Organization 2008.

[2] Zoran K. Morvay and Dusan D. Gvozdenac, *Applied Industrial Energy and Environmental ManagementPart* 3, Fundament for Analysis and Calculation of Energy and Environmental Performance, John Wiley & Sons, Ltd.

[3] Ali Hasanbeigi, Lynn Price, Industrial Energy Audit Guidebook: Guidelines for Conducting and Energy Audit in Industrial Facilities, Ernest Orlando Lawrence and Barkley National Laboratory ,October 2010.

[4] Current status of the power condition from Power Develpoment board , Available at www.bpdb.gov.bd.Accessed on 16/11/2014.

[5] Zahid Hasan Mahmood ,*Accreditation: Delivering Confidence in the provision of Energy* ,keynote of Bangladesh Accreditation day 2014.

ICMIEE–PI–140380

Implementation of Disaggregation Method in Economic Lot Scheduling of a Jute Industry under Constant Demand

Subrata Talapatra [1] , *Ghazi Abu Taher* [2, *]
[1, 2] Department of Industrial Engineering and Management, Khulna University of Engineering & Technology, Khulna-9203, BANGLADESH

ABSTRACT
This paper deals with the disaggregation problem which refers to a management system for every product solely and establishes a pre-management system of economic lot scheduling. The values of Production time P_t have at the end of the aggregate plan, which is the production capacity in period t. This has to be used to be make several products. While only one product can be made at a time, demand occurs for all the products simultaneously. The available times for all the products have divided. So that, at any point in time, produce one product and build inventory while consuming it and meet the demand for the other products from the built-up inventory. Disaggregation schedule specifies the sizing and timing of production orders for specific items. The objective of any production system is to smooth the production process, enabling uniform production of item over the period.

Keywords: Disaggregation, Economic Lot Scheduling Problem (ELSP), Inventory, Multi-Product, Lot-Sizing and Scheduling, Sequence-Dependent Setups.

1. Introduction

The Economic Lot Scheduling Problem (ELSP) is the problem of finding the production sequence, production times and idle times of several products in a single facility (machine) on a repetitive basis. The demands are made without stock outs or backorders and average inventory holding. Setup costs are minimized. If a particular product or an item taken, it produces at the rate P, the demand is at the rate of D, produce for a certain period and consumes while produce. So inventory is built up at the rate of P-D. The built up inventory will consume at a certain number of period, the cycles begins again. In between the period while the inventory consumes and the next cycle begins, this item is not produced. Then produce another item. The next item start producing after the first item. There is a changeover time or setup time between the two items. The items can be produce up to the next cycle and the cycle length is T.

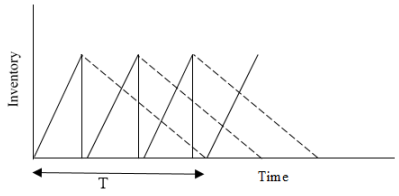

Fig.1 Total cycle time for a particular facility.

In the economic lot scheduling problem, the order of the items is not worried about which one produce first. Once the economic lot scheduling problem is solved whether the order of producing items is made, it will be the same because the cycle time is same for all products. The reason why it is not order dependent because the changeover or setup time depends only the succeeding job and does not depend on the preceding job. It is not defined as the changeover between the two successive jobs. It is defined as the changeover to the job with respect to the earlier product's job. If the changeover time is sequence dependent, which means it depends on both the current job as well as the next job to be done. Then the problem will be more complicated because sequencing them in the order that minimizes the sum of the changeover times.

In the economic lot scheduling problem, it is not assumed that changeover times in sequence dependent. So, when the changeover times are sequence independent, then the economic lot scheduling problem essentially tries to minimize the total cost which is the sum of the ordering cost and carrying cost.

Minimum Total cost (TC) = Ordering cost (OC)
+ Carrying cost (CC) ----- (1)

While the production is started in a cycle, an inventory is built up during the production and consumes it up to the next cycle. The product which is going to produce first, need no inventory to meet the demand but for the other products, need enough inventory to meet demand before the production period.

In economic lot scheduling problem, the demand (D_j)is the same for every period for each item. It means the demand is same for all periods. The presence of inventory (I_j) ensures that there is no shortage into the cycle. The sufficient inventories meet the demand for each product. The initial inventory increase the cycle length. For the long cycle the ordering cost decreases and the carrying cost increases [1].

* Corresponding author. Tel.: +88-01914883418
E-mail address: ghaziabutaher@yahoo.com

Let's assume, the cycle is long and there is no shortage of time as well as the order cost or setup cost (for manufacturing, order cost = setup cost).

Total cost = Setup cost + Carrying cost ---------- (2)

2. Literature Review

Numerous research articles have been published in order to include new approaches and extensions to this ELSP problem. Time-varying lot sizes approach which was introduced originally by Maxwell. Matthew proposed another approach which does not require strict regularity of cycle lengths. Zipkin introduced an approach in which some items may be produced repeatedly during a cycle [2]. The different runs of an item can differ in size. Gallego and Roundy extended the time-varying lot sizes approach to the ELSP which allows backorders [3]. Dobson extended his early work by allowing the setup times to be sequence dependent [4]. Gallego and Shaw showed that the ELSP is strongly NP under the time-varying lot sizes approach with or without the Zero Switch Rule (ZSR) restriction, giving theoretical justification to the development of heuristics [5]. Allen modified the ELSP to allow production rates to be decision variables [6]. He developed a graphical method to find the production rates and cycle times for a two product problem. Silver showed that production rate reduction is more profitable for under-utilized facilities [7]. Khouja provided a similar extension for systems with high utilization [8]. Gallego and Moon examined a multiple product factory that employs a cyclic schedule to minimize holding and setup costs [9]. When setup times are reduced, at the expense of setup costs, by externalizing internal setup operations, they showed that dramatic savings are possible for high utilized facilities. Gallego and Moon developed an ELSP with the assumption that setup times can be reduced by a one-time investment [10]. Moon further showed that both setup reduction and quality improvement can be achieved through investment. Khouja used genetic algorithms (GAs) for solving the ELSP which is formulated using the BP approach. Moon developed a hybrid GA based on the time-varying lot sizes approach to solve the ELSP. The stabilization period concept (during which yield rates gradually increase until they reach the target rates) to the ELSP was introduced by Moon [12].

The purposes of this research are to determine the total cycle time T, to find the value of T that optimizes the changeover cost, inventory holding cost for all the periods, to maximize the cycle length, not trying to maximize the total cost, to determine the maximum cycle length at a given inventory [13].

3. Development of Disaggregation Method

In this paper, a disaggregation of economic lot scheduling problem under constant demand and capacity of manufacturing process. For observing the disaggregation problem in manufacturing process, Khalishpur jute mill, Khulna has been visited. They are maintaining an order for their production process. They mainly produce three products such as sacking, Hessian, CBC (Carpet Baking Clothe). The daily demand and the inventory of these products remain constant. The demand and inventory is calculated in man-hours. The demand and inventory data is given in **Table 1**.

Table 1 Day to day demand and inventory data of Khalishpur Jute Mill.

Product	Sacking	Hessian	CBC
Demand	2870	1200	640
Inventory	2030	990	480
r	0.707	0825	0.75

The capacity of the industry is 4710 man-hours. Now the allocation time have to find to make the products.
The value of r represents the demand that can be met with the existing inventory. The production of product j have to start before r_j hours. The products are sorted according to increasing value of r. The order is Sacking-CBC- Hessian. The products are chosen to produce in this order. The process flow depends on the value of r. If process flows from lowest value to highest value of r.

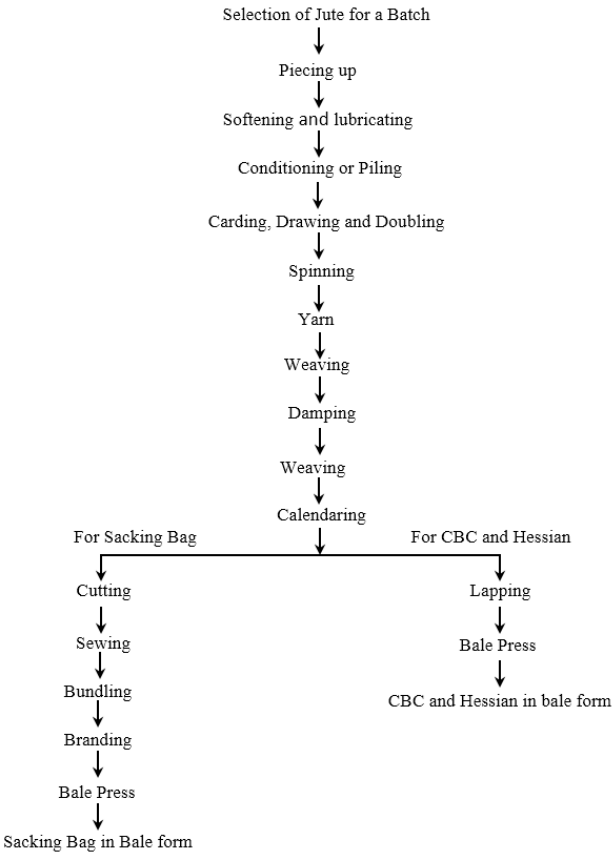

Fig.2 Process flow chart of Khalishpur Jute Mill.

Let t_j be the starting time of production of product j.

Objective function:
Minimize {Setup Cost (SC) + Inventory Cost (IC)}--(3)

The objective function is to minimize the sum of changeover costs and inventory costs. Since the total capacity is equal to the sum of monthly demands and the capacities and demands are assumed to be constant, the amount of inventory will remain same in the system at any point in time. If the inventory holding costs for all products is same, the total inventory cost will be constant.

Set up cost = Set up cost × no of set up = $C_o \times 3$
Inventory cost = Constant

Also, if inventory costs are less compared to changeover costs, the objective shifts to minimizing the number of changeovers, which is to minimize the cycle time T. The objective is to maximize T and the problem reduces to a linear programming problem.

So, Objective function: maximize T

The constraints are,
Subject to,

$$t_j \leq r_j \text{ ---------- (4)}$$

constraint for production time for Sacking,

$$(t_{CBC} - t_{Sa})\,4710 \geq T \times 2870 \text{ ---------- (5)}$$

constraint for production time for CBC,

$$(t_{He} - t_{CBC})4710 \geq T \times 640 \text{ ---------- (6)}$$

constraint for production time for Hessian,

$$(t_{Sa} + T - t_{He})4710 \geq T \times 1200 \text{ ---------- (7)}$$

constraint for production time limit for Sacking,

$$t_{Sa} \leq 0.707 \text{ ------ (8)}$$

constraint for production time limit for CBC,

$$t_{CBC} \leq 0.75 \text{ --------- (9)}$$

constraint for production time limit for Hessian,

$$t_{He} \leq 0.825 \text{ ---------- (10)}$$

Non-negativity constraints,

$$t_{Sa}, t_{CBC}, t_{He}, T \geq 0$$

Where,
t_{Sa} = Production start time for sacking
t_{He} = Production start time for Hessian
t_{CBC} = Production start time for CBC
T = Total cycle time

The first constraint ensure that the production begins before the inventory of product is exhausted. The second to forth constraints ensure that for every item, the quantity produced in a cycle is enough to meet the demand during the cycle. In constraint (5), $t_{CBC} - t_{Sa}$ represents the time in which Sacking is produced and in constraint (6), $t_{He} - t_{CBC}$ represents the time in which item CBC is produced. But in constraint (7), Sacking is produced in the second cycle at time $t_{Sa} + T$.
Each cycle involves three changeovers, one for each item and we will have 24/T cycles in a day, if the demand and inventory are in terms of man-hours/ day.

4. Algorithm

Algorithm used for solving the problem is given below:

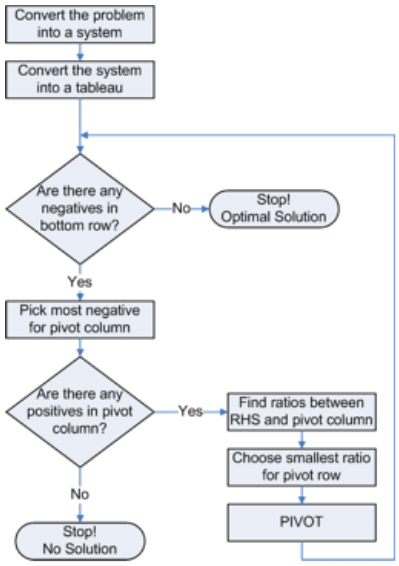

Fig.3 Algorithm of simplex method.

Here TORA software is used for solving the problem.
The optimal solution of the problem is given below,

$X_1 = t_{Sa} = 0$
$X_3 = t_{CBC} = 0.6746$
$X_2 = t_{He} = 0.8250$
$X_4 = T = 1.1071$

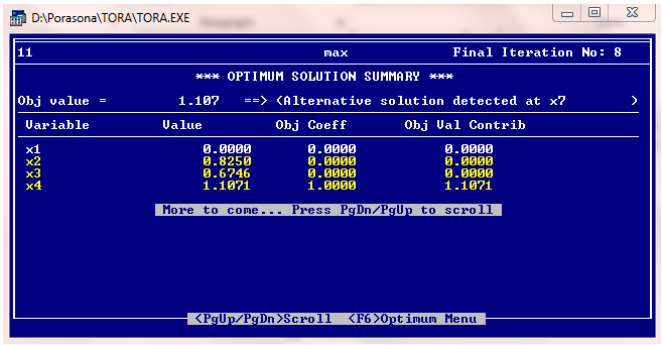

Fig.4 Optimal solution summary of linear programming by using TORA.

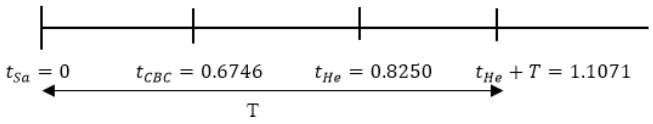

Fig.5 Cycle length.

In this solution, the total inventory in the system at any point is 3500 man-hours. The inventories of various items at the changeover times are given in **Table 2**.

Table 2 Day to day inventory position of Khalishpur Jute Mill.

Time (hours)	Sacking	CBC	Hessian	Total Inventory (man-hours)
t=0	2030	480	990	3500
t=0.6746	3272	48	181	3501
t=0.8250	2841	659	0	3499
t=1.1071	2030	480	990	3500

During the period 0 to 0.6746, Sacking is produced at the rate of 4710 man-hours. Since sacking is also consumed at the rate of 2870 man-hours, its inventory at 0.6746 is {(4710 - 2870)* 0.6746} + 2030 = 3272. CBC is consumed from inventory at the rate of 1200 man-hours. Inventory of Hessian at time = 0.6746 is, therefore, 480 – (640*0.6746) = 48.

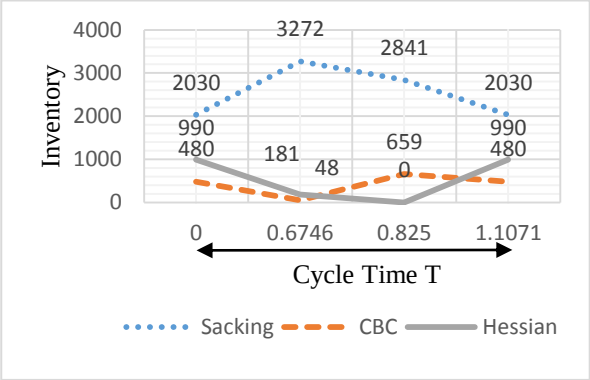

Fig.6 Graphical representation of inventory position of Khalishpur Jute Mill.

5. Increasing T by reallocating the inventory

It is assumed that there is a cycle (called a transient cycle where the inventories are distributed) and a steady state cycle when production started at the stock is zero. The production start time in the transient cycle is denoted by t'_j and the production start time in the steady state cycle is denoted by t_j. The transient and steady state cycles are shown in Fig.7.

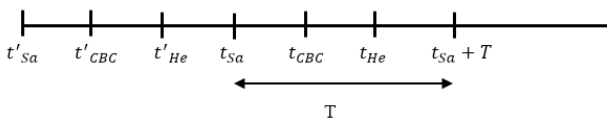

Fig.7 Transient and steady state cycle.

For next cycle $t'_{Sa}, t'_{He}, t'_{CBC}$ are the start times in the first cycle and t_{Sa}, t_{He}, t_{CBC} are in the steady state cycle.
The formulation becomes;

Objective function: Maximize T

Subject to, $t_j \le r_j$ ---------- (11)
constraint for production time for Sacking of 1st cycle,
$2030 + 4710\,(t'_{CBC} - t'_{Sa}) \ge 2870\,t_{Sa}$-------- (12)
constraint for production time for CBC of 1st cycle,
$480 + 4710\,(t'_{He} - t'_{CBC}) \ge 640\,t_{CBC}$ ---------- (13)
constraint for production time for Hessian of 1st cycle,
$990 + 4710\,(t'_{Sa} - t'_{He}) \ge 1200\,t_{He}$ -------- (14)
constraint for production time for Sacking of 2nd cycle,
$4710\,(t_{CBC} - t_{Sa}) \ge 2870\,T$ -------- (15)
constraint for production time for CBC of 2nd cycle,
$4710\,(t_{He} - t_{CBC}) \ge 640\,T$ ---------- (16)
constraint for production time for Hessian of 2nd cycle,
$4710\,(t_{Sa} + T - t_{He}) \ge 1200\,T$ -------- (17)
constraint for production time limit for
Sacking of 2nd cycle, $t'_{Sa} \le 0.707$ ---------- (18)
constraint for production time limit for
CBC of 2nd cycle, $t'_{CBC} \le 0.75$ ---------- (19)
constraint for production time limit for
Hessian of 2nd cycle, $t'_{He} \le 0.825$ ---------- (20)
Non-negativity constraints,

$$t'_j,\ t_j, T \ge 0$$

The first constraint ensures that the production in the transient cycle should start before the inventory is exhausted. Constraint (12) to (14) ensures that the production in the transient cycle plus inventory meets the demand up to the steady state production. Constraints (15) to (17) ensure that the steady state production is equal to the cycle demand.
The optimal solution to this linear programming is given below,

$X_7 = T = 2.7253$
$X_1 = t'_{Sa} = 0$
$X_2 = t'_{CBC} = 0$ [the value is very close to zero]
$X_3 = t'_{He} = 0.2199$
$X_4 = t_{Sa} = 0.7073$
$X_5 = t_{CBC} = 2.3680$
$X_6 = t_{He} = 2.7383$

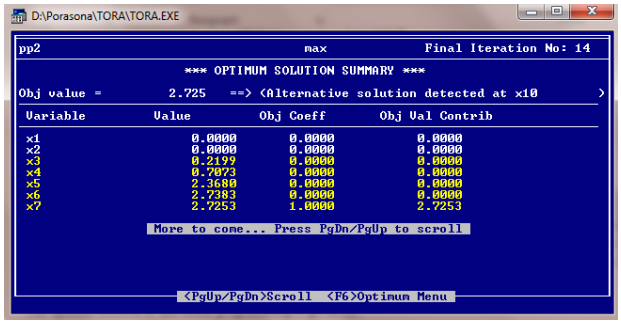

Fig.8 Optimal solution summary of linear programming by using TORA.

The next cycle starts with sacking being produced at time $= 0.7073 + 2.7253 = 3.4326$

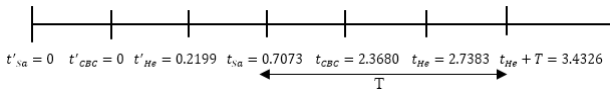

Fig.9 Total Cycle length.

The inventory position at the various time periods are shown in **Table 3**.

Table 3 Day to day inventory position of Khalishpur Jute Mill.

Time	Sacking	CBC	Hessian	Total Inventory
t = 0	2030	480	990	3500
t = 0.2199	1983	1517	0	3500
t = 0.7073	0	1035	2465	3500
t = 2.3680	3056	0	445	3501
t = 2.7383	1992	1507	0	3499
t = 3.3426	0	1035	2465	3500

The above model shows how the cycle time T can be extended by reallocating the inventory such that the products are made when the inventory becomes zero.
The graphical representation of day to day inventory position of Khalishpur Jute Mill is given below:

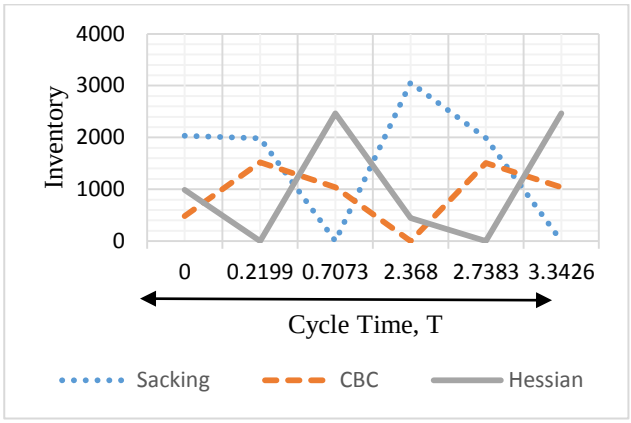

Fig.10 Graphical representation of day to day inventory position of Khalishpur Jute Mill.

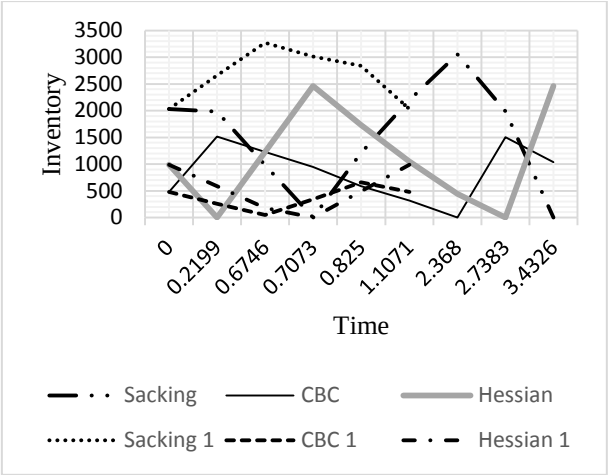

Fig.11 Graphical representation of inventory position of Khalishpur Jute Mill for different cycle time.

Result and Discussion

At the moment of steady cycle begins, sacking is produced when the inventory is zero. At the time 2.3680, when CBC start producing, the inventory is zero and so on for the hessian. But for the first model, when sacking start produced the inventory is not zero. The inventory is zero only for hessian. So, at steady state cycle the inventory is adjusted in such a manner that the values are zero which is able to increase the cycle time as long as we can. At the beginning of next cycle the inventory will be the same. From the table, the total inventory is 3500 for any period because the total demand and the total production is equal which is 4710. In the second cycle, total inventory is only redistributed among the products so that the cycle time can increase as large as possible. There are two aspects are in this problem. One is the cycle time T that depends on the total amount of inventory. If total demand is equal to the total production the cycle time depends on the total inventory. Secondly and more importantly it also depends on the way in which the existing inventory is distributed. So, the existing inventory is distributed in such a manner that the cycle time T exceeds.

Conclusion

This model help us to understand the concept of disaggregation to allocate the available time to the various products. In the second model the objective function is to maximize the cycle length that makes zero inventories at the starting point of each product whereas in the first model there is a buffer inventory at the starting point of each product. So, if the demand is purely deterministic and it does not going to change at all then one can take the risk of redistributing the inventory (like second model) in such a manner that one can achieve maximum cycle time.
The limitation of the second model is that it only works when the demand is constant and continuous. If the demand is not continuous and showing variations then there is a shortage in the cycle. To remove the shortage, a safety stock is put over the model otherwise use the

first model so that the cycle stretch solely at the last point and keep a balance of inventory of all other points. The cycle length depends both the amount of inventory and the way of distributing the inventory. If someone wants to make the cycle length smaller, he has to make the amount of inventory small. If the organizations follow the rules of zero inventories or lesser inventory, the optimization of the problem automatically leads to the smaller values of cycle time. Another dimension to it is also to seen that the tradeoff between inventory holding cost and the changeover cost. If the changeover times are smaller, then automatically more change overs are possible and also able to make more variety of product keeping the cycle time as small as possible.

NOMENCLATURE

n : no. of products or items in a cycle = 1, 2, 3… m

I_j : Inventory of each of the item on hand (man-hours), where j = 1, 2, 3… m

D_j : Demand of each of the item (man-hours), where j = 1, 2, 3… m

P_j : Production rate of the item (man-hours), where j = 1, 2, 3… m

T : Cycle length (hours)

r : ratio of inventory and demand, hours = $\frac{Inventory}{Demand}$

REFERENCES

[1] Srinivasan, G., Quantitative models in operations and supply chain management, ISBN: 978-81-203-3981-1.

[2] Zipkin PH (1991). Computing optimal lot sizes in the economic lot scheduling problem. Opns Res39:56–63.

[3] Gallego G and Roundy R (1992). The extended economic lot scheduling problem. Nav Res Log39: 729–829.

[4] Dobson G (1992). The cyclic lot scheduling problem with sequence-dependent setups.Opns Res40: 736–749.

[5] Gallego G and Shaw X (1997). Complexity of the ELSP with general cyclic schedules.IIE Trans29: 109–113.

[6] Allen SJ (1990). Production rate planning for two products sharing a single process facility: a real world case study. Prod Inv Mngt31:24–29.

[7] Silver E (1990). Deliberately slowing down output in a family production context. Int J Prod Res28:17–27.

[8] Moon I, Gallego G and Simchi-Levi D (1991). Controllable production rates in a family production context. Int J Prod Res 29: 2459–2470.

[9] Gallego G (1993). Reduced production rates in the economic lot scheduling problem.Int J Prod Res31: 1035–1046.

[10] Moon D and Christy D (1998). Determination of optimal production rates on a single facility with dependent mold lifespan. Int J Prod Econ54:29–40.

[11] Khouja M (1999). A note on deliberately slowing down output in a family production context. Int J Prod Res37: 4067–4077.

[12] Khouja M (1997). The economic lot scheduling problem under volume flexibility. Int J Prod Econ48:73–86.

[13] Gallego G and Moon I (1992). The effect of externalizing setups in the economic lot scheduling problem. Opns Res40: 614–619.

[14] Gallego G and Moon I (1995). Strategic investment to reduce setup times in the economic lot scheduling problem. Nav Res Log42: 773–790.

[15] Hwang H, Kim D and Kim Y (1993). Multiproduct economic lot size models with investment costs for setup reduction and quality improvement. Int J Prod Res31: 691–703.

[16] I Moon, BC Giri and K Choi, Pusan National University, Pusan, South Korea, "Economic lot scheduling problem with imperfect production processes and setup times", Journal of the Operational Research Society(2002) 53, 620–629. doi:10.1057/palgrave.jors.2601350.

[17] Professor Guillermo Gallego, IEOR4000: Production Management, Lecture 3, September 15, 2004.

[18] M.L. Pinedo, Planning and Scheduling in Manufacturing and Services, DOI: 10.1007/978-1-4419-0910-7_7, ©Springer Science + Business Media, LLC 2009.

ICMIEE-PI-140383

Design of a Mechanical Litter bin with Underground Waste Container

Sanjida Haque [1,*]
[1] Department of Mechanical Engineering, Khulna University of Engineering & Technology, Khulna-9203, BANGLADESH

ABSTRACT
"Underground Waste Bin", has the gravity enough to describe itself. The bin under the ground, to dispose waste not manually rather mechanically to eradicate the risk of environmental pollution as well as human diseases and infections, is Underground Waste Bin. In near about 70% of the cities in underdeveloped or developing countries, roadside open air dust bins are cast-off to control wastes. [1] People like Garbage collectors, drivers of waste collector vehicles, street children along with the health care worker, patients and the whole community either directly dealt with waste or not is in high risk. The environmental pollution including water, air and land are also in an alarming stage due to wastes. For safe and better management of waste, an underground waste collector instrument can be introduced. The main operation of this type of container is to hold wastes and can be controlled by a Hydraulic Suspension System. When the lever is pressed, the whole body of the bin can be brought above ground and burdened onto the garbage-collection vehicles by rotating it up to 90 degree. One third of this container would be above the ground to receive the waste with addition to a lid on it. This lid would automatically open with a load up to 5kg and the garbage thrown on it would be clear out into the compartment. This Mechanical Waste Bin was designed in CAD software. By implementation of this mechanism, there will be no need of using hand to collect waste thus this process will be more hygienic. This would reduce risk on human health and also diminish human effort.

Keywords: Pollution, Health hazard, Automation, Mechanical Waste container.

1. Introduction

Waste may create a serious health hazard to human beings; if it is not appropriately dispose. With the increasing global population and the rising demand for food and other essentials, there has been a significant amount of waste being generated every day. This waste is ultimately thrown into municipal waste collection centers from where it is collected by the area municipalities to be further disposition into the landfills and dumps. [7]

Wastes contain hazardous chemical such as mercury, PBDEs (flame retardant chemicals), SO_2 etc. and these toxic products are combined with a surplus of other chemicals, which eventually react and produce odor. [2] Some symptoms that odor producing chemicals may cause are dizziness, headache, watery, itchy & burning eyes and nose, depression, stress etc. Folks living near the accumulated piles of waste are at a risk of infectious diseases. [3] As the accumulated wastes produce an unpleasant odor and the decomposing waste is highly contagious in nature. An estimated 300 million people worldwide suffer from "Asthma", with 250,000 annual deaths. Among of them 11% of "Asthma" cases worldwide is responsible for workplace condition, such as exposure to dust. Also approximately 50 million people worldwide being infected every year by "Coughing" and 294,000 dying. Across the world 6% people are suffered from lung diseases because of pollution owing to waste.[4] Moreover, unattended waste lying around attracts flies, rats, and other creatures that in turn spread disease.

Generally, the harmful effects of pollution are not felt immediately, but occur after a length of time. **Diseases** that can be produced by waste are-

1. Skin and blood infections like allergy, fungal contaminations due to direct contact with waste.
2. Eye and respiratory infections resulting from exposure to infected dust, especially during landfill operations.
3. Various diseases like dengue, malaria etc. which are caused due to the bites of animals feeding on the accumulated waste.
5. Lung Cancer.
6. Developmental defects.
7. Reproduction problems.
8. Liver and kidney failure. [7-9]

Accidents can be happened during direct handling of waste materials like-

1.Bone and muscle disorders resulting from the handling of heavy containers.
2. Infecting wounds resulting from contact with sharp objects.
3. Poisoning and chemical burns resulting from contact with small amounts of hazardous chemical waste mixed with general waste.
4. Burns and other injuries resulting from occupational accidents at waste disposal sites or from methane gas explosion at landfill sites. [5, 7-10]

It is very important to ensure a safe and healthy technique for collecting and dumping waste. For an example, let's take Bangladesh as a developing country- by analyzing the data according to the World Bank, Population growth (annual %) in Bangladesh is **1.19.**

* Corresponding author. Tel.: +88-01929034987
E-mail address: haquesanjida15@yahoo.com

With this increase, there has also been an increase in the amount of wastes being produced especially in the cities.

In Bangladesh Per capita waste generation is **4.3** pounds. At this rate in a city of about **10** lakh people around **43** lakh pounds and a country of about **154.7** Million people around **70.5** corers pounds of wastes is being produced every day! [11] This huge amount of rubbish produced per day is not properly handled to dispose. In the absence of proper solid waste management, this waste lies littered on our streets, road corners and improperly disposed of in vacant land. If they are not going to accumulate in a proper way serious disaster can be occurred relating to health issues and environmental pollution.

Dustbin is the ultimate solution of this problem. But the main problem is that most of the times in developing or under developed countries, dustbins do not contain any lid. So bad odor, infectious viruses & bacteria find space to flow and mix with environment. Again, it attracts flies, rats, and other animals that in turn blow out infections. Rotting waste also provide a fertile breeding ground for flies, mosquitoes etc. Another disadvantage of normal dustbin is that, the waste scatters around it, can only be collected by direct handling. This can be very perilous to the persons who are working on this field. To avoid these problem normal dustbins can be upgraded by some modifications. Here a **Mechanical Litter bin with Underground Waste Container** can be introduced. It is mainly a mechanical system by which waste can be collected mechanically. It has a lever system to pull the bin and dump the waste to the waste collecting vehicle. It also contains a mechanical lid to block the infectious materials to blowout. Most importantly, it is user friendly and does not cost more than normal dustbins!

2. Physiology

Dustbins have only been around since the last 150 years or so. Before that waste were just disposed by burning or dumping in empty lands. But with increasing population and waste produced by them became a main concern. In **1842,** Sir Edwin Chadwick first influenced for the matter of waste clearance and disposal. [9] In **1875** the **Public Health Act** made it compulsory for each household to keep a dustbin. Normally, a large rectangular or cylindrical container is used for reserving refuse which is known as dustbin or litterbin. Early dustbins were simple in design. The temporary storage of rubbish can be traced to the 1800s; it took until the 1960s for the standardized dustbin. During this time the form of the dustbin changed significantly. Medium sized galvanized metal bins were introduced in the 1950s, and larger plastic bins were in the 1960s. [10-12] But nowadays various kinds of dustbins are introduced for different purposes which are unlike in size shape and function. Some examples are-

The Wheelie Bin which is moveable, the recycling bin where waste that can be recycled are dumped for reuse, the color coded bins that are specified by color code for specific waste and so on. But for developing countries where waste management system is insufficient there the **"Mechanical Underground Litter Bin with Waste Container"** can be introduced. It can be described in four parts. They are -

1. Automatic Lid with micro controlling system.
2. Waste reservoir for collecting waste.
3. Hydraulic Suspension system for lifting the container.
4. Rotation system for dumping the waste.

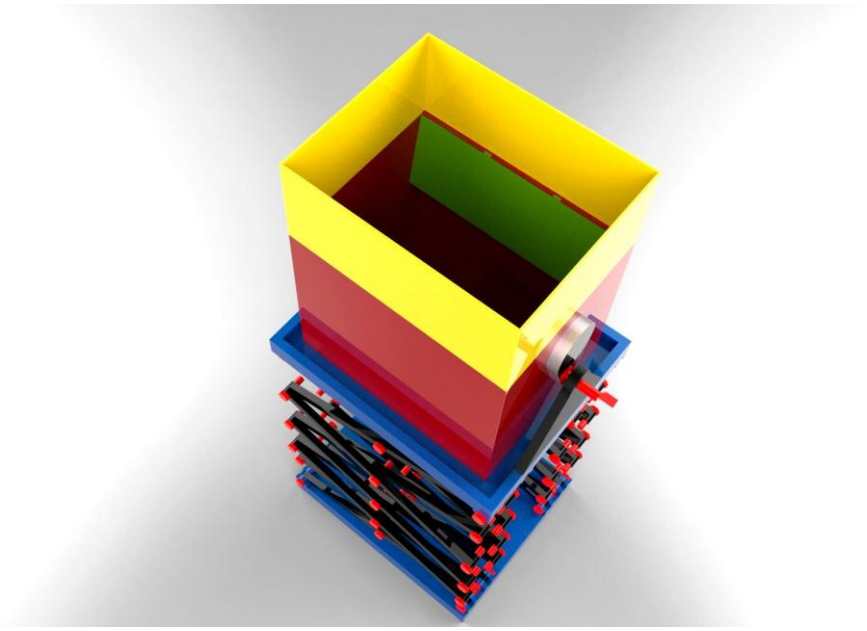

Fig.1 Mechanical Litter Bin with Underground waste Container.

3. Design Structure

Design structure of a **"Mechanical Litter bin with Underground Waste Container."** is given below-

3.1 Dimension

It is a rectangular box type construction.

Length	5 feet
Width	4 feet
Height (above ground)	2 feet
Height (below ground)	4 feet

3.2 Material

Any ferrous material can be used. But light alloy is more preferable to avoid corrosion and also it will be suitable for lifting.

3.3 Systems

Mainly three systems are used in this design.

They are -

1) Micro controlling system.
2) Hydraulic Suspension system.
3) Belt pulley system.

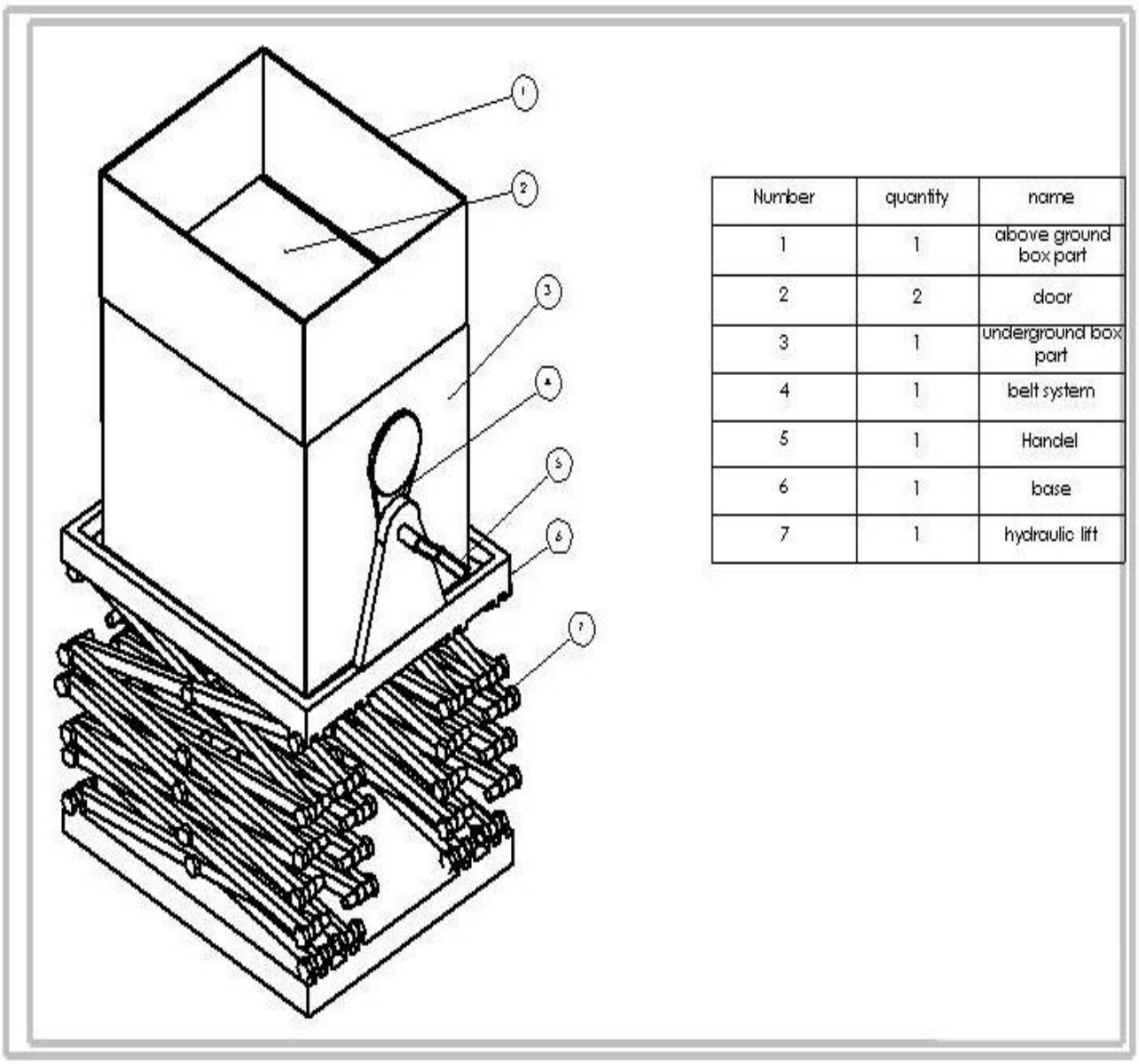

Number	quantity	name
1	1	above ground box part
2	2	door
3	1	underground box part
4	1	belt system
5	1	Handel
6	1	base
7	1	hydraulic lift

Fig.2 Dimension of Mechanical Litter Bin.

4. Design Description

It can be described part by part gradually as –

It is a rectangular box in shape. It's larger portion means 4 feet is beneath ground and smaller portion means 2 feet is above ground. The portion which is lying under ground is work as **waste container**.

Fig. 3: Mechanical litter bin.

There is a **lid** in between the upper portion and the lower portion. When the amount of garbage exceeds up to 5 kg the lid will open with a **micro controlling mechanism**. Mechanisms and equipment used in this lid are – a weight sensor, an OPAMP 741(Operational Amplifier) [17] and a motor. A weight sensor is used here so that when rubbish are dumped on the upper portion , if its weight become more than 5 kg then the lid will open up as (fig:4). Because the sensor will send signal to the OPAMP to enlarge the signal and then the OPAMP send the signal to the motor so it turns on and so the lid opens. As a result the pile of waste dumped directly into the lower part or the waste container. After dumping waste there will be no weight to sense, so the sensor will stop giving signal to the OPAMP and subsequently no signal is sensed by the motor. So, the lid will close automatically (fig: 5). The lid can be opened up manually during collection of waste. Its function is to seal up the waste container to get rid of from the unpleasant stinks. Unpleasant odor created because of hazardous chemical reaction among household wastes and other wastes collected from different places. Another function of this lid is to keep the creatures such as rats, flies, mosquitoes etc. far from the bin and thus to prevent the infectious diseases and viruses to spread. If this "**Mechanical Litter bin with Underground Waste Container"** can be introduced seemly efficient waste management and quality environment can be ensured.

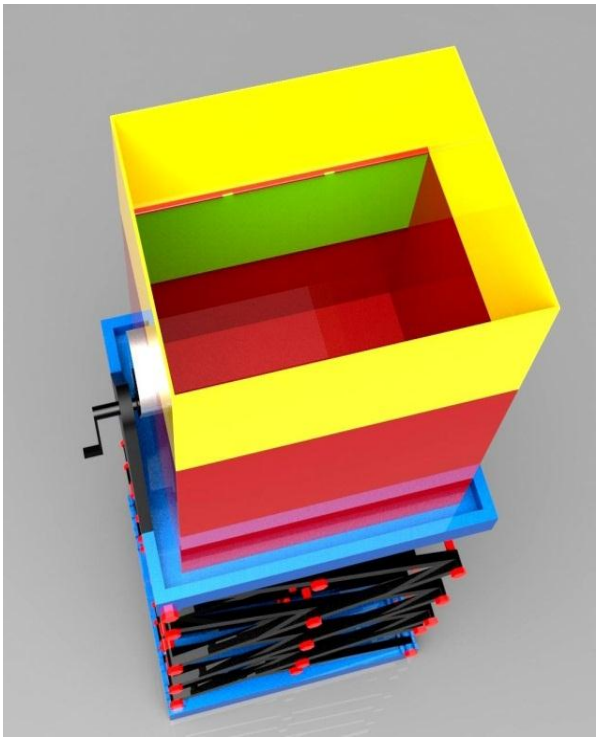

Fig. 4: Lid opens up due to weight sensor.

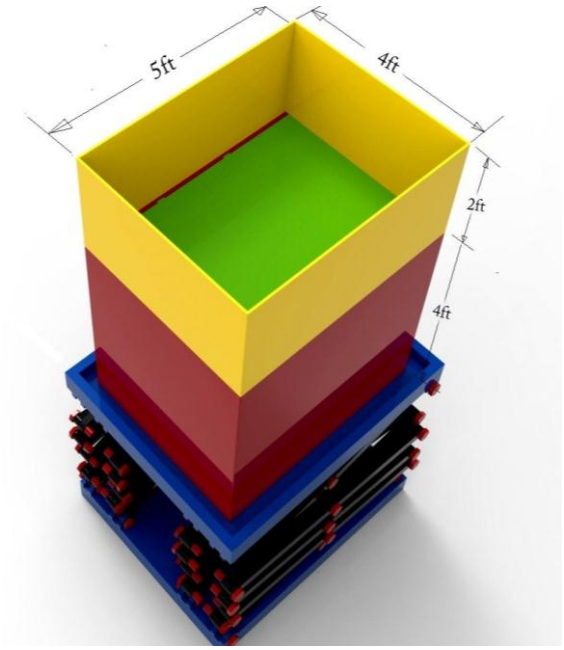

Fig. 5: Lid closed after dumping waste.

After block up the container, it can be brought up from the ground by using **Hydraulic Suspension** system (fig: 6). A hydraulic suspension system is very versatile because it puts the controller in control of the body's height via a fluid pressure system. Fluid suspension action is usually considered faster, depending on the power used to create the pressure of the hydraulics. This suspension system can be driven by using motor which can be controlled by a switch. [15-16]

Finally the total litter bin can be rotated up to 90 degree to dump the waste to the waste collecting van. To rotate the body **Belt pulley** mechanism is used (fig: 7). As the litter bin is not fixed to the platform, so by rotating the handle attached to the belt system, the total body can be rotated on its axis.

After that the litter bin can be again placed to its position. This whole process can be done without making direct contact with waste.

5. Discussion

Unmanaged waste becomes a serious environmental, economic, health and aesthetic problem around the world. As the production of waste cannot be stopped so a proper way of collecting and disposal should be introduced. In developed countries, there are many private and government institutes that collect and recycle renewable waste that comes from households, industries, restaurants, medical centers etc. But waste collection by direct handling in developing and under developed countries, causes an adverse effect on people related to this job. A **"Mechanical Litter Bin with Underground Waste Container"** can be used to serve the purpose. This is designed to collect waste without direct handling. It reduces the threat on health of the concerned people. Again at the time of collecting waste, there is a high risk of getting injured and infected by objects such as broken glass, syringes, metallic and other jagged objects. This risk can be minimized by using mechanical bin. Also because of the lid there will be no unpleasant odor. Thus environment pollution can be reduced.

6. Conclusion

After all this discussion about health hazards due to uncontrolled wastage, it can be summed up that a Mechanical Litter Bin with Underground Waste container is an ultimate option to get rid of these problems. It is suitable for reducing environment pollution, infectious diseases and human effort.

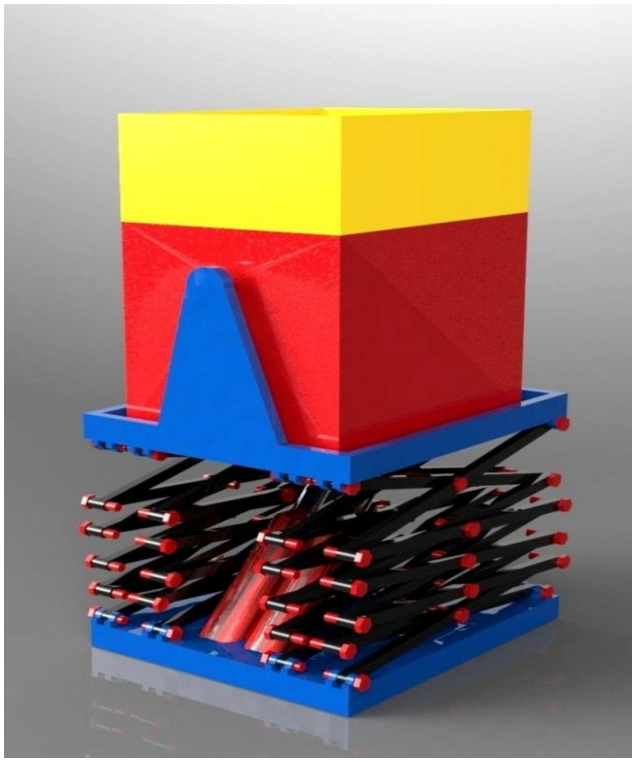

Fig. 6 Hydraulic Suspension System.

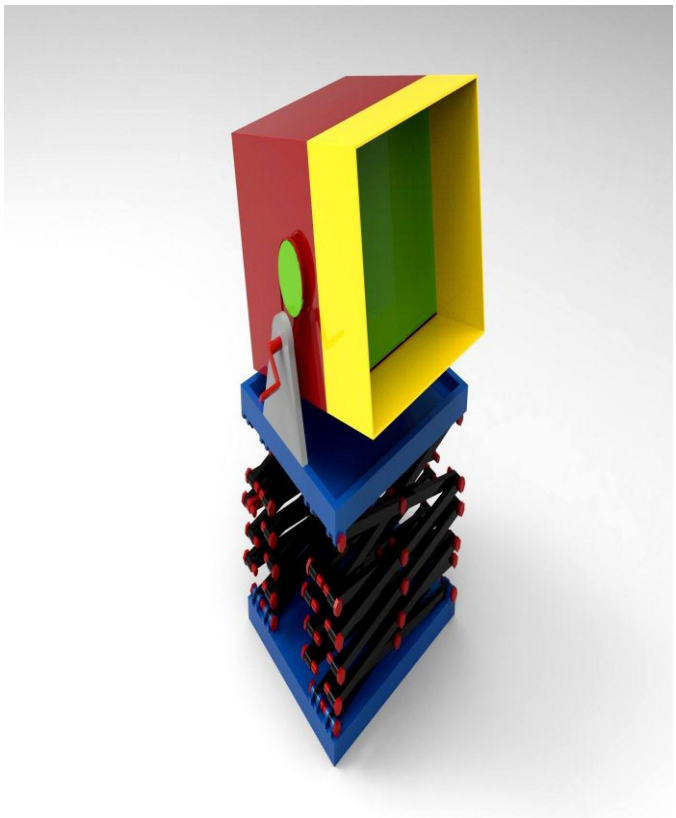

Fig.7 Rotation of Mechanical Litter Bin.

REFERENCE

[1] Lilliana Abarca Guerrero, Ger Maas ,William Hogland, Solid waste management challenges for cities in developing countries, *Waste Management,* Volume 33, Issue 1,pp 220–232,(2013).

[2] N.O. Adedipe, M.K.C. Sridhar, Joe Baker, Madhu Verma, Waste Management, Processing, and Detoxification, *Ecosystems and Human Well-being: Policy Responses*, chapter 10,(2004).

[3] Oregon Health Authority, Odor and Your Health, *Public Health Division, Office of Environmental Public Health*,(2011).

[4] Juliana Maantay, Asthma and air pollution in the Bronx: Methodological and data considerations in using GIS for environmental justice and health research, *Health & Place*, pp 32–56,(2005).

[5] Lawrence Muhwezi, Paul Kaweesa, Faisal Kiberu, I. Luke Enyenu Eyoku, Health Care Waste Management in Uganda, *International Journal of Waste Management and Technology*, Vol. 2, No. 2, (2014).

[6] Karin Lundgren, The global impact of e-waste Addressing the challenge, *ILO publications, International Lab our Organization*, (2012).

[7] Malmros P, Sigsgaard T, Occupational health problems due to garbage sorting. *Waste Management & Research 10*, pp227-234, (2001).

[8] Philip Rushbrook, Regional Advisor-Waste Management, WHO, The Health Effects from Wastes - Overplayed or Underestimated?, *IWM Annual Conference, UK*, (2001).

[9] **P. Agamuthu,** Waste Management & Research, ***University of Malaya, Kuala Lumpur, Malaysia,*** Volume 32, Issue 8, (2014).

[10] Emma Selin, Solid waste management and health effects, *UMEA University*, (2013).

[11] Md. Abdur Rakib, Md. Atiur Rahman, Most. Shamema Akter, Mohammod Ali, Md. Emadul Huda, Mohammad A. H. Bhuiyan, An Emerging City: Solid Waste Generation and Recycling Approach, *International Journal of Scientific Research in Environmental Sciences, 2(3)*, pp74-84, (2014).

[12] Rina Bao, Waste and Recycling Attitudes and Behavior of Students in Turku, *University of Turku*, (2011).

[13] Gisele de Lorena Diniz Chaves, Jorge Luiz dos Santos, Jr, Sandra Mara Santana Rocha, The challenges for solid *waste* management in accordance with Agenda 21: A Brazilian case review, *Waste Management & Research*, vol. 32, (2013).

[14] Rotich K. Henry, Municipal solid waste management challenges in developing countries, *waste management and research*, Volume 26, Issue 1, (2006).

[15] Faraz Ahmed Ansari, RajShree Taparia, Modeling, Analysis and Control of Active Suspension System using Sliding Mode Control and Disturbance Observer, *International Journal of Scientific and Research Publications*, Volume 3, Issue 1, (2013).

[16] M. M. Fateh, Seyed S. Alavi, Impedance control of an active suspension system, *Journal on Mechatronics*, vol. 19, pp. 134-140, (2009).

[17] Vaibhav Kumar, High bandwidth low power operational amplifier design and compensation techniques, G*raduate Theses and Dissertations, Iowa State University*, (2009).

ICMIEE-PI-140384

Development of a Control System and Modelling of an Automatic Window

Md.Armin Islam [1], Ishtiaq reza Emon[2], Md. Zahid Hasan[3]*

[1,3] Department of Mechanical Engineering
Khulna University of Engineering & Technology, Khulna-9203, BANGLADESH

[2] Department of Computer Science & Engineering
Khulna University of Engineering & Technology, Khulna-9203, BANGLADESH

ABSTRACT

Now a day's human comfort has become most significant conscience of engineers .The project is one step further about human comfort. The goal of this project is to close the window automatically as well as the zebra curtain too. The control system is prepared by using two motors, two sensors (one is water sensor and another is ambient light sensor), a microcontroller and some other necessary objects needed for circuit implementation. The ambient light sensor will be connected with the microcontroller which will sense the ambient light intensity. The sensor will send the result to microcontroller (which is a customized with program) and microcontroller will give necessary output to motor for controlling zebra curtain. Another is the water sensor which will work like the ambient sensor. Water sensor is set on the window and will sense the water drop on the window. Then it will send the result to microcontroller and after that the window will turn automatically off. The whole system is designed to get an autonomous control of window and zebra curtain whether the people is at home or not. The system will act according to weather condition.

Keywords: Automatic Window, Sensors, Microcontroller, Curtain controller, Control system.

1. Introduction

The project is aimed to be a widely used product to help enhancing human comfort by working with great accuracy. Many times we forget to close our window when raining and also forget to close down the curtain. Besides sometimes it feels bother to walk and close these. This system brings the solution. It automatically closes the window when it starts raining outside as well as it shuts down the curtain sensing a minimum light intensity of 300 lux outside. For example in a busy office where all the employees are too busy with their work, if an employee working at a distance from window suddenly faces rain or high sunlight outside then what will he do? He might not be intended to go to near window to close it because it may cause of interruption in his concentration of work. If this system was implemented there it could automatically close the window or curtain as necessary without having interruption during his work. The automation of window can be overdone using either sensors or a Bluetooth controlled remote device. The window will be designed to be sensitive to rain only. Its components will be so designed so that it can be easily manufactured and would be affordable to the common man. A typical house window is made of an aluminum frame. The glass used is double paned. Each frame has two window doors, both of which are sliding. A rain sensor is a device which is actuated by rainfall. For the purpose of our project we considered the use of the capacitive sensor. Capacitive sensors are preferred over resistive sensors as they are less prone to false detection of rainfall. If the resistive sensor gets contaminated by a carbon containing particle, the resistance changes and the system is triggered, whereas this is not the case with the capacitive sensors. And in case of light sensor Monolithic Silicon IC based light to voltage sensor was used. The device provides a linear voltage output that is proportional to light and covers a wide range of speed and fast response to ambient light.

2. Background

The background of this project consists with Atmel ATmega328p, Light sensor TS 12SM-LF, water sensor WS10 series, Motor Driver L293D, Motor DC (12V, Model: HN-GH12-1634T - 30:1)

2.1 Atmega328p

The Atmega-328p is a high-performance Atmel Pico Power 8-bit AVR RISC-based microcontroller. It has 32KB ISP flash memory with read-while-write capabilities, 1024B EEPROM, 2KB SRAM, 23 general purpose I/O lines. It combines 32 general purpose working registers, three flexible timer/counters with compare modes, internal and external interrupts, serial programmable USART, a byte-oriented 2-wire serial interface, SPI serial port, a 6channel 10-bit A/D, programmable watchdog timer with internal oscillator, and five software selectable power saving modes [1].

* Corresponding author. Tel.: +88-01745-602423
E-mail address: armin.aone@gmail.com

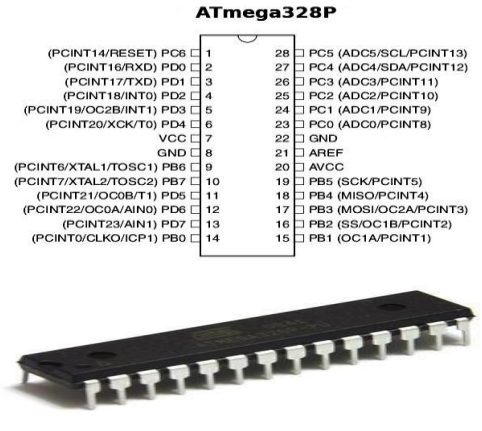

Fig.1 Atmega328p

2.2 Motor DC

Rating: (12V, Model: HN-GH12-1634T - 30:1) The rated voltage of the motor is 12 v DC and voltage operating range is 6-12 v. The rated load of this motor is 0.78Kg-cm. If the rated voltage is exceeded then damage may occur. The rotating speed at 12v DC is 200 RPM +/- 10%. But the rotating speed at Rated Load is (0.78Kg-cm) 163 RPM +/- 10%. Load current of this motor is less than 115mA but Current at Rated Load (0.78Kg-cm) is less than 285mA. The Shaft End-Play is Maximum 0.8m/m. Insulation Resistance is 10M ohm at 300vdc and Withstand Voltage is 300v DC for 1 second. The gear motor is not intended for instant reverse. The gear motor must be stopped before reversing. The gear motor does not include protection from water or dust etc [1].

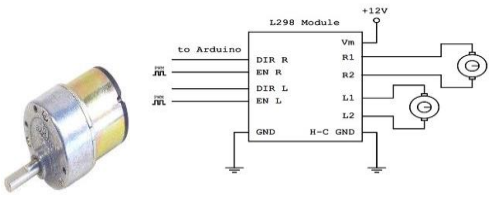

Fig.2 Motor DC

2.3 L293D Motor Driver

L293D is a typical Motor driver or Motor Driver IC which allows DC motor to drive on either direction. L293D is a 16-pin IC which can control a set of two DC motors simultaneously in any direction. The L293d can drive both small and big motors as well. L293D is a dual H-bridge motor driver integrated circuit (IC). Motor drivers act as current amplifiers. They take a low-current control signal and provide a higher-current signal. This higher current signal is used to drive the motors. For the purpose of best result here two motor driver were used.

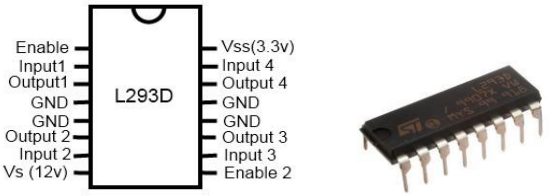

Fig.3 L293D Motor Driver

2.4 Light Sensor TS 12SM-LF

The TSL12SM-LF is a highly integrated light-to-voltage optical sensor with feedback resistor of 80 MΩ. It is cost-optimized, highly integrated light-to-voltage optical sensors each of which combining a photodiode and a Trans-Impedance amplifier (feedback resistor = 80 MΩ, 20 MΩ, and 5 MΩ, respectively) on a single monolithic integrated circuit. The photodiode active area is 0.5 mm sensors respond to light in the range of 320 nm to 1050 nm. Output voltage is linear with light intensity (irradiance) incident on the sensor over a wide dynamic range [2].

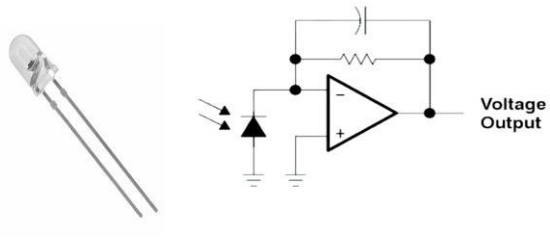

Fig.4 Light sensor

2.5 WS10 series Water Sensor

The Pall WS10 Series water sensor is used in this project. It is an ideal, low-cost, in-line, monitoring solution for measuring dissolved water content in hydraulic, lubricating and insulating fluids. It is specifically designed for use in harsh and often remote industrial environments. It can transmit readings continuously to the user's control systems as a key component in the predictive maintenance of plant and machinery. There are two separate analog 4-20 ma output signals (0-100% Saturation & -13 to 260F). It is rugged all in one modular housing and sensing probe [2].

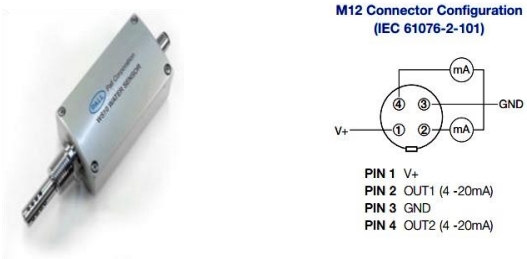

Fig.5 Water sensor

2.6 Zebra Curtain

It is also known as soft gauze rainbow curtain. It has dimming roller blinds and the double roller blinds are spaced by a small piece of a small piece of equal width fabrics and gauze woven into a textile material. It has one end fixed and the other end with the scroll action to achieve the purpose of regulating the light softer light when the gauze and gauze coincidence, to some extent reduce the direct light, the light is completely covered when the cord and cord coincide, and ultimately to block out light [3].

Fig.6 Zebra curtain

2.7 Sliding Window

In our project the window that was used for experiment had two sliding doors. We used Thai aluminum glass window for our work. The two doors can easily move through the guideway, each of which has a handle to slide it on the guideway. In experiment we worked with only one door of the window.

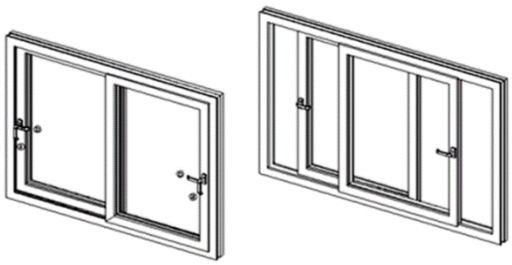

Fig.7 Sliding Window

3. Design and Implementation of Control System

The design and implementation process of whole project is given below:
First Atmega328p microcontroller was set in the project board. PORT D was taken as the input port of the microcontroller. Light sensor TS 12SM-LF was connected with the PORT D 0 pin through a switch. As well as water sensor WS10 series was connected with PORT D 1 pin through switch in the same way. Now PORT B was taken as output port. PORT B 1 pin was connected with the DC motor-1 by a motor driver (L293D) and PORT B 2 pin was connected with the DC motor-2 by a motor driver (L293D). The motor drivers (L293D) were used for output power amplification.

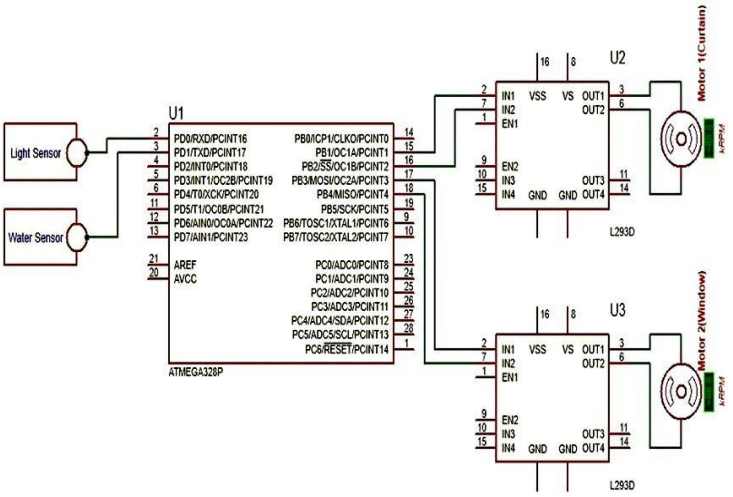

Fig.7 Circuit Diagram

DC motor-1 was connected with zebra curtain and DC motor-2 was connected with the one door of the window. When a light intensity (above 300 lux) was fallen on the curtain, the light sensor then sent it to the microcontroller pin PORT D 0 and output result was find from PORT B 1 pin which makes the motor-1 to rotate. When water drops were fallen on the curtain, the water sensor also sent the sense to the microcontroller pin PORT D 1 and output result were find from pin PORT B 2 which makes the motor-2 to rotate, thus working [4][6]. The circuit diagram and block diagram of the whole process is given below:

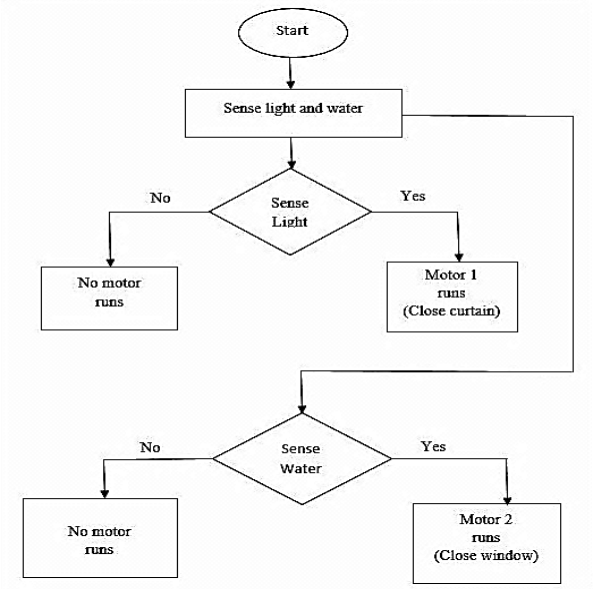

Fig.8 Flow Chart of logical expression

4. Modeling

The modeling process for the system is described below:
For modeling the process, two sensors were set up on their position, water sensor in the middle of the door of the

window and light sensor in the middle of the curtain. Then the two sensors were connected with control system at one upper corner of the window. When the light sensor sensed by light intensity, motor-1 started to rotate. One end of an strong thread was tied with the shaft of the motor and another end of the thread was tied with the handle (by turning manually the handle zebra curtain shuts down) of zebra curtain [5]. When motor-1 started to rotate itself and rolled the thread on the shaft, by rotating, the curtain came to close. From Fig.9 the process can be observed.

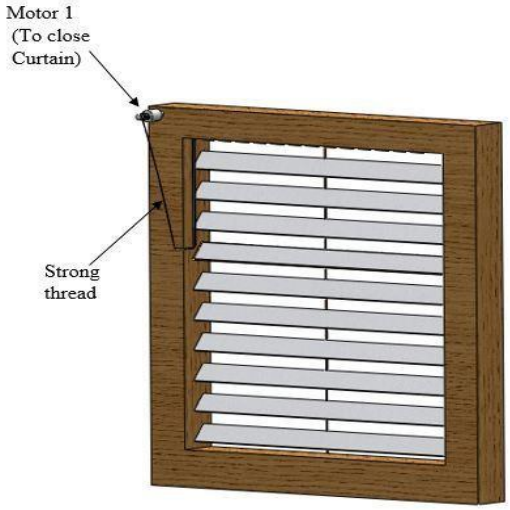

Fig.9 When motor-1 starts to rotate it rolls the thread on the shaft surface, thus closing the curtain.

In the same way, when the water sensor sensed by water drops, motor-2 started to rotate. One end of the thread was tied with the shaft of the motor and another end of the thread was tied with an extra handle which was at top position of the door. When motor-2 started to rotate and rolled the thread on the shaft it turned the door to the off position, through guide way. This process is presented at figure 10.

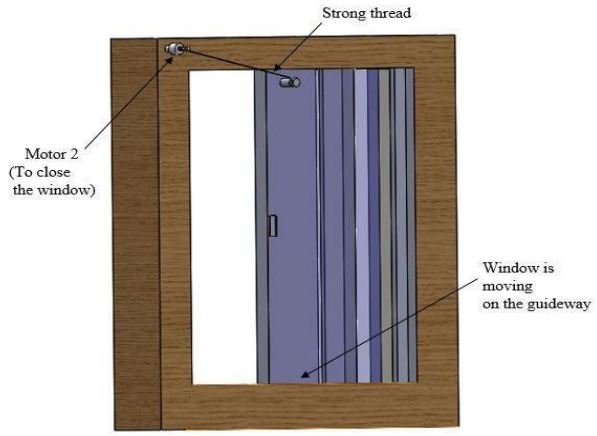

Fig.10 When motor-2 starts it rolls the thread around the body of the shaft and turns the window close.

[For convenience to understand two operations are shown in two different figures]

5. Methodology

The whole system is made to perform automatically. The light sensor is connected with the zebra curtain in the middle and the water sensor is connected with the window door in the same way. When the light sensor gets light intensity of at least 300 lux it sends the sense to microcontroller pin PORT D 0 and the microcontroller then provides the necessary output at pin PORT B 1.Then motor-1 which connected with the motor driver starts to rotate. If the light sensor does not get minimum light intensity, it will not send any sense to microcontroller pin PORT D 0 for which PORT B 1 will not give any output result and motor -1 will not rotate as a result the curtain will remain open.

In the same process the water sensor is connected with the window door. When the water sensor gets water drops on it, it sends the sense to microcontroller pin PORT D 1 and the microcontroller then provides output result at pin PORT B 2. Then motor-2 which is connected with the motor driver starts to rotate. If the light sensor does not get any water drops or fog on the window door, it will not send any sense to microcontroller pin PORT D 1 for which PORT B 2 will not give any output result and motor -2 will not rotate for which the window will not close. It will remain open. Working procedure of the system is given by a block diagram below:

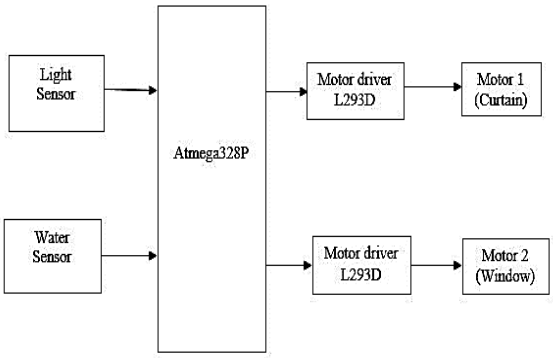

Fig.11 Block Diagram

6. Analysis of Result

The whole system was tested for few times to get the fastest and accurate result. For example, in some test few water drops were dropped on the window. When the water sensor sensed the water drops it was taking different time in different tests to close the window. In some test it took a little late to close the window because of some friction between guide way and window. In case of light sensor which was connected with the zebra curtain, several tests were made. In some tests sunlight of different intensity were drop on the curtain. Every time it was taking almost same time to shut down the curtain. The result of some tests were given in a table: (Start time of motor was observed from the control system)

Table1 Test Results

Time Required				
No of tests	Motor 1 (Curtain) To Start	Motor 2 (Window) To Start	Curtain To Close	Window To Close
Tests no 1	1 Sec	1 Sec	4 Sec	5 Sec
Tests no 2	1 Sec	2 Sec	4 Sec	5 Sec
Tests no 3	2 Sec	1 Sec	5 Sec	5 Sec
Tests no 4	1 Sec	1 Sec	3 Sec	5 Sec

7. Discussion

The test was conducted by the system in a real house room**.** It gave perfect results as expected. Though in some tests it took maximum 5 sec to response but in some test the system provided a very fast result of minimum 3 sec to perform which. Because of some existing friction between the window and the guide way it was taking a little more time to response. Here the whole system is described. This system will be very beneficial not only for office but also in domestic house. Almost all type of sliding window as well as all kind of zebra curtain can be used to set up with the control system. It is a great attempt to promote human comfort. This project can really minimize a little bit human toil to close the window while raining and to close the curtain at high light even when no one is at home. People can keep the system off if they wish.

8. Conclusion

In this project, a microcontroller based system is designed and implemented something like for enhancing human comfort. Atmel ATmega328p, Light sensor TS 12SM-LF, Motor Driver L293D and Water sensor WS10 series were utilized. The system will be really an useful one as it works with the sudden change of weather even the user is not alert about it. This system will not be a costly one to use everywhere and can really reduce a little bit human slog by doing its work automatically.

REFERENCES

[1] Yao-Chiang Kan, Hsueh-Chun Lin,Wen-Pei Sung, "Developing An Intelligent Control System Of Automatic Window Motor With Diverse Wireless Sensor Network Devices", Indian Academy Of Sciences, Sadhana Vol. 39, Part 4, August 2014, Pp. 809–818

[2] N. M.Z. Hashim, S. H. Husin, A. S. Ja'afar, N. A.A. Hamid, "Smart Wiper Control System", International Journal Of Application Or Innovation In Engineering & Management (IJAIEM), ISSN 2319-4847, Volume 2, Issue 7,July 2013

[3] Shukla Abhishek, Dwivedi Rohan, "Design and Implementation Of Vision System Aid In Windscreen Assembly", International Journal Of Computer Applications (0975 – 8887) Volume 7– No.12, (2010), Pp. 6-10.

[4] Ucar Mehmet, Ertunc Huseyin M., Turkoglu Onder, "The Design and Implementation Of Rain Sensitive Triggering System For Windshield Wiper System" IEEE, (2001), Pp 329-336.

[5] Mehran Kamyar, Takagi Sugeno, "Fuzzy Modeling for Process Control", Industrial Automation, Robotics And Artificial Intelligence (EEE8005) School Of Electrical, Electronic And Computer Engineering Newcastle University 2008.

[6] **Tis**a T.A, Nisha Z.A, Kiber A; "Design Of An Enhanced Temperature Control System For Neonatal Incubator*",* Bangladesh Journal Of Medical Physics, Vol. 5, No. 1, Bangladesh 2012

ICMIEE-PI-140386

Quantifying the contributions of different time-scales to wind speed using wavelets

Md. Mahbub Alam [a,b,], S. Rehman [c], L. M. Al-Hadhrami [c], Mohammad Russel [d], J.P. Meyer [e]*

[a]Institute for Turbulence-Noise-Vibration Interaction and Control, Shenzhen Graduate School
Harbin Institute of Technology, Shenzhen, China
[b]Key Kab of Advanced Manufacturing and Technology, Shenzhen Graduate School
Harbin Institute of Technology, Shenzhen, China
[c]Center for Engineering Research, Research Institute, King Fahd University of Petroleum and Minerals
Dhahran-31261, Saudi Arabia
[d]School of Food and Environmental Science & Technology, Dalian University of Technology, Panjin 124221, PR China
[e]Mechanical and Aeronautical Engineering Department, University of Pretoria, Pretoria, South Africa

ABSTRACT
Wind data analysis and accurate wind energy assessment are critical for proper and efficient development of wind power application and is highly site-dependent. The wind power is intermittently available due to the fluctuating nature of the wind and hence needs to be understood well. The present work exploits daily mean values of wind speed from different meteorological stations spread over the Kingdom of Saudi Arabia to understand the dynamic nature of the wind using wavelet transform and fast Fourier transform power spectrum. It is found that wind speed changes by ±0.6 to ±1.6 knots over a long period of about 10 years depending on the locations. The long-term mean wind speed of 5.6, 8.9, 6.25, 8.1, 6.0, 7.1, 6.0, 8.6 and 7.3 knots were obtained at Abha, Dhahran, Gizan, Guriat, Hail, Jeddah, Riyadh, Turaif and Yanbu, respectively.

Keywords: wind energy, wind speed, wavelet, fast Fourier transform, power spectrum.

1. Introduction

The variability of wind speed covers a wide spectrum of time-scales from seconds to several years, say, random variation at very short interval (turbulence scale), synoptic scale, seasonal variation, annual cycle variation, etc. This statistical information is required not only for a feasibility study of the wind farm to be installed but also for wind power prediction at different years/seasons/months/day as well as wind turbine control. Without analytical prediction, the statistical information on variations of past wind at different at time-scales can give us a rough idea about how the wind will behave in the near future [1-2]. Usually, most of the signals contain numerous non-stationary or transitory characteristics such as drift, trends, abrupt changes, and beginnings and ends of events. These characteristics are often the most important part of the signal and are needed to be analyzed to understand physical phenomena hidden behind the signal. Wavelet analysis allows the use of long time intervals where we want more precise low-frequency information, and shorter regions where we want high-frequency information.

To investigate the timescale structure of natural wind, the wavelet transform is employed to the time history of measured wind velocity data [3]. Ref. [4] applied the wavelet transform to the time data of roof-corner pressures with extreme local loads and obtained the PDFs on the time-dependent characteristics of the pressure transients. Based on these PDFs, a method to generate synthetic signals was developed, and time histories similar to the original roof-corner pressure data were composed. A new wind speed data generation scheme was introduced in Ref. [5], based on wavelet transform and compared this scheme with existing wind speed generation methods. Their results proved that the proposed wavelet-based method was found to be the best for wind speed data generation compared with existing methods. Wavelet transform as a time-frequency analysis to meteorological data for the region of Adrar, Algeria was exercised in Ref. [6] to investigate the power spectra behaviors of wind speed and its variations with time. The results showed significant synoptic oscillations for periods of 2 to 16 days in the cold weather. The wavelet power spectrum also revealed the presence of intra-seasonal oscillations for periods of 30 to 60 days.

When the wind has salient periodic features only over limited intervals of times, a global Fourier analysis is theoretically possible; but it may not be practical or efficient. The Fourier transform is limited because an analysis with single window cannot detect features in the signal that are either much longer or much shorter than the window size. Therefore, to have better representation of the wind spectrum for such case, we should seek a representation that is capable of following the wind spectrum as it varies with time [7]. Such representation is known by Time–Frequency Representation [8].

* Corresponding author. Tel.: +8615014047005
E-mail address: alamm28@yahoo.com; alam@hitsz.edu.cn

The signals of meteorological parameters of the Kingdom of Saudi Arabia have so much noise that their overall shape is not apparent upon visual inspection. Thus, wavelet analysis is useful in revealing signal trends, a goal that is complementary to the one of revealing a signal hidden in the noise. If the signal itself includes sharp changes, then successive approximations look less and less similar to the original signal. A repeating pattern in the wavelet coefficient plots is characteristic of a signal that looks similar on many scales.

The main objective of the present work is to understand the fluctuating nature of the wind using wavelet and fast Fourier transform power spectrum techniques which are very useful to quantify the highly fluctuating natural phenomenon. The daily mean values of wind speed time series data over a period of 1990 - 2005 at Abha, Dhahran, Gizan, Guryat, Hail, Jeddah, Riyadh, Turaif and Yanbo, all in Saudi Arabia, are analyzed.

2. Steady nature of wind speeds

Wind speed data are obtained from the nine weather stations in Saudi Arabia, showing great potential for application in verifying the current criteria used for design practices. Illuminations are shed on FFT analysis results of wind speed data. Here data analysis of daily average wind-speed time series data is done for 1990 to 2005. The data was scanned every three seconds and 10-minute average values were recorded. Finally, the daily average values were obtained using 144 10-minute average values recorded during 24 hours. The total number of daily average data points in the time series for 1990 to 2005 is 5960. The power spectra of daily average wind speed time series data at the nine locations are shown in Fig. 1. While the horizontal axis represents the frequency f (1/day = D^{-1}), the vertical axis shows energy at the frequency. Abha is a station with many hills around. As seen in Fig. 1(a) for Abha, power spectral energy mostly concentrates on a low frequency range 0.002 – 0.006 D^{-1} with a peak at f = 0.0027 D^{-1}. The peak corresponds to a period of about $T = 1/f \approx 370$ days ≈ one year, implying that wind speed variation in a year is similar to that in another at least qualitatively. One should not be confused with the 370 days; the deviation from exactly 365 days arises from the frequency resolution in the FFT analysis. The f = 0.006 D^{-1} over which energy decays corresponds to about half a year. That is the half-year repetition in wind speed also exists.

Dhahran is a coastal site 3 km inland from the Arabian Gulf. There is a small single-storey airport building in the vicinity of the meteorological station. The station is

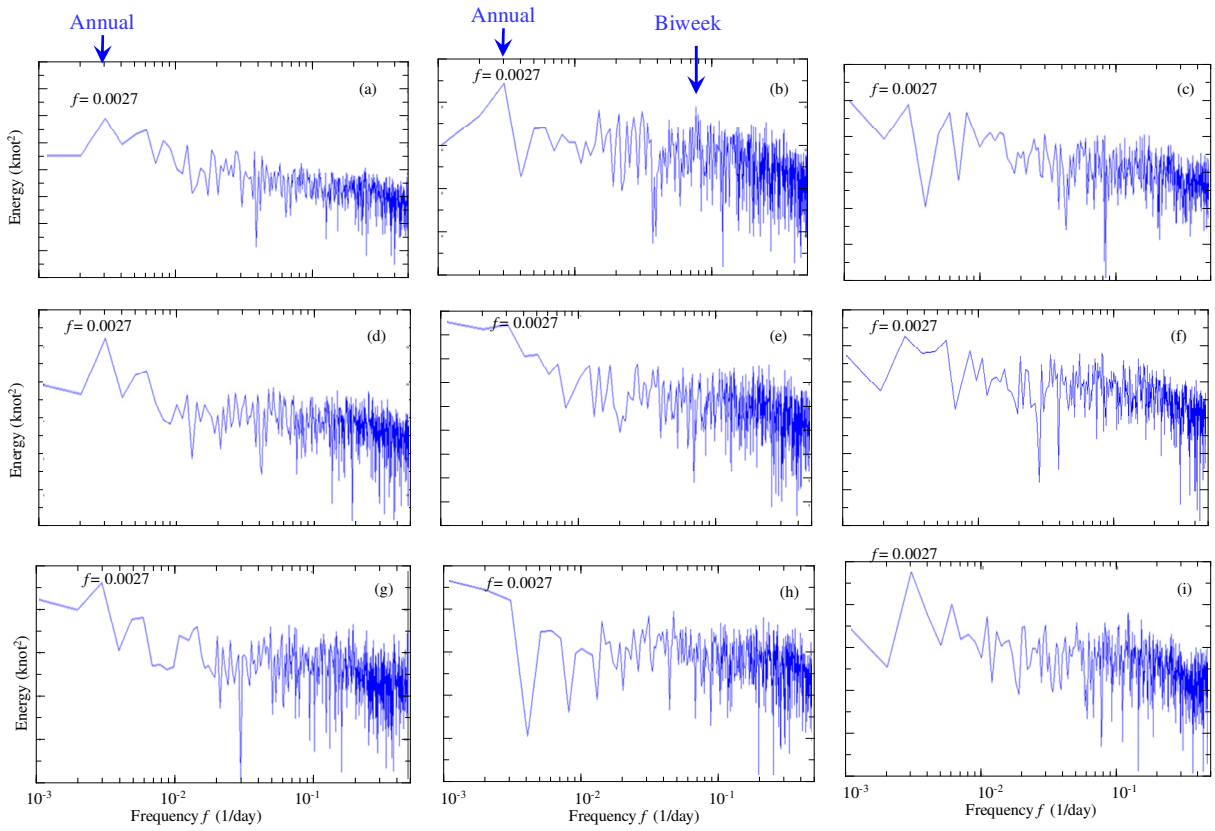

Fig. 1 FFT power spectrum of wind speed data for (a) Abha, (b) Dhahran, (c) Gizan, (d) Guryat, (e) Hail, (f) Jeddah, (g) Riyadh, (h) Turaif, and (i) Yanbo.

17 m above the mean sea level and the wind direction is mostly from the sea to the station. Here the peak corresponding to annual repetition (f = 0.0027 D^{-1}) is more clear (Fig. 1b). However, the half-year recurrence that appeared at Abha is not explicit. The high-frequency energies (f > 0.02 D^{-1}) at Dhahran (Fig. 1b) are larger than those at Abha (Fig. 1a). A small peak emerges at f = 0.074 D^{-1} at Dahran, which communicates to biweekly repetition of wind speed. The biweekly change in wind speed may be a unique feature for a coastal area as it is observed in other coastal area, namely Yanbo, which will be presented later.

Gizan is a coastal station on the west coast of Saudi Arabia, some 100 meters inland. There are one small single-storey airport building and some trees around. This station is only 5 m above the mean sea level. The Red Sea is a bit more turbulent than the Arabian Gulf on the east coast (Dhahran) and is wide open. Therefore, the annual and biweekly peaks are not as dominant as those in Abha or Dhahran (Fig. 1c). Another cause may be that the site is only 5 m above the sea level. Guryat is an inland station with high land and small hills with gentle topographical features. Since the station is high, the annual recurrence (f = 0.0027 D^{-1}) is more dominant than that at Abha and Dhahran (Fig. 1d). Hail is a highland plateau in the north central area of Saudi Arabia. As seen in Fig. 1(e), speed varies not only annually (f = 0.0027 D^{-1}) but also at further low frequencies (f < 0.0027 D^{-1}), e.g. two- and three-year repetitions which will be further clarified through wavelet analysis results later.

Jeddah station is around 10 km inland from the Red Sea. The FFT power spectrum for this station is presented in Fig. 1(f). There are many buildings around and it is situated in an urban area. The wind blows from the sea inwards and is intercepted by high-rise buildings and structures such as bridges and other industrial installations. Due to this confrontation of wind with structures, the annual maximum wind speed is smaller compared with that in Abha, Dahran, Guryat and Hail. Gizan also has similar power spectra because of wind obstructed by trees. The presence of high-rise buildings and/or trees makes the flow boundary layer wider, resulting in a smaller speed. The FFT power spectrum obtained using long-term mean wind speed data for Riyadh is shown in Fig. 1(g). Riyadh station is on the mainland and is around 450 m above the mean sea level. Riyadh is the capital of Saudi Arabia, hence it is a very developed region and surrounded by high-rise buildings, bridges and various industrial installations. The winds are prevalent from the northern and northwestern direction in this region. Since the site is quite high above sea level, the annual variation is evident.

Turaif is a small city in the northernmost part of Saudi Arabia and is a hilly inland area. The wind blows mostly from the north onto this area and accelerates due to topographical features. The power spectrum displays low-frequencies variation (f < 0.0027 D^{-1}), having similar characteristics to that at Hail. Yanbo is a coastal site on the Red Sea in the north-west of Saudi Arabia. It is an industrial area and is surrounded by a range of hills on the northern side and exposed to the sea on its western side. The station is 10 m above the mean sea level. The peak at f = 0.0027 D^{-1} is sharp, indicating the annual variation in wind speed is very regular (see Fig. 1i). A biweekly variation also exists. A scrupulous observation of all the FFT figures reveals that Abha, Dhahran, Guryat and Yanbo having a sharp peak at f = 0.0027 D^{-1} retain a more regular annual repetition of wind speed than Gizan, Hail, Jeddah, Riyad and Turaif.

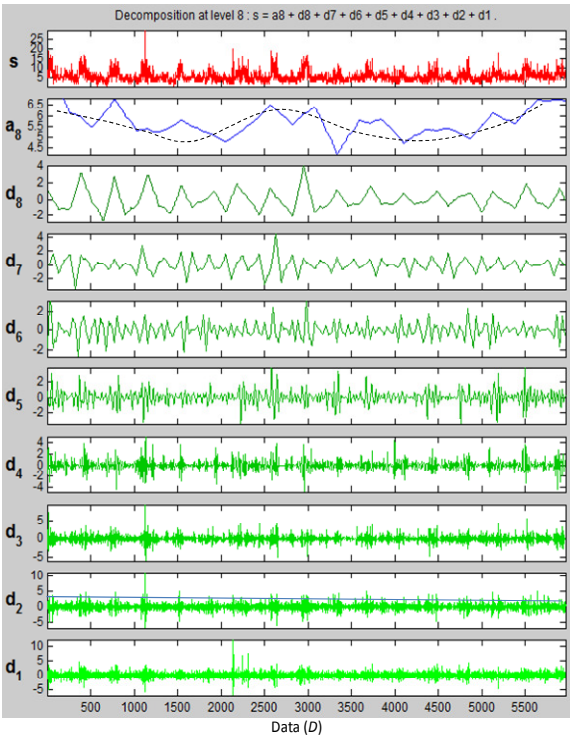

Fig. 2 Decomposition of wind speed time series data for Abha using DB8.

3. Unsteady nature of wind speeds

The daily mean values of wind speed time series data are analyzed, using Wavelet, over a period of 1990 - 2005 at the nine locations using db8. Naturally the daily mean signal captures information for a period of longer than 2 days following the Nyquist frequency criterion. The decomposition analysis results of wind speed data for Abha, Dhahran, Gizan, are shown in Figs. 2， 3 and 4, respectively, while those for Guryat, Hail, Jeddah, Riyadh, Turaif and Yanbo are not shown here. In these figures, the x-axis presents the number of days (D) of the entire data period (1990 to 2005) used in this study. Each of these figures has 10 parts. The first part 'S' represents the signal or raw data and the second part 'a_8' corresponds to the amplitude of the signal for wavelet Daubechies (db) at level 8 corresponding to a period of longer than 512 days. Note that that the dashed line in a_8 signal is not an output of the analysis,

but just a hand sketch showing the low-frequency trend. The last eight parts, i.e. d_1, d_2, d_3, d_4, d_5, d_6, d_7 and d_8 of these figures represent details of decomposed signals of the raw data at eight different levels corresponding to a period range of 2 to 4, 4 to 8, 8 to 16, 16 to 32, 32 to 64, 64 to 128, 128 to 256 and 256 to 512 days, respectively. The raw signal S in Fig. 2 (Abha) displays a sharp spike at D = 1200 and a nearly regular variation of speed. The nearly regular variation is evident in the d_8 signal with a periodicity of approximately 365 days (one year), forming a peak between June and August of each year. The minimum speed occurs sometime in December to January. The fluctuation of the speed is relatively high, -2.5 to 2.5 knots for D < 3300 (<1998) and -2 to 2 knots for D > 5000 (> 2003) and small, -1 to 1 knots for D = 3300 to 5000 corresponding to year 1998 to 2003. On an average, the fluctuation occurs from -1.7 to 1.7 knots. That is, an annual fluctuation can contribute a speed of ±1.7 knots. Further low-frequency (longer than 512 days) variation is evident in signal a_8. This signal can also be considered as the signal of yearly (exactly 256 days) average wind speed. The duration for the average is long enough. The signal, however, contains approximately two-year undulations with small amplitudes. If the two-year undulation is ignored, the mean speed indicated by the dashed line is initially about 7 knots, slowing down to 4.7 knots at D =1700 (1995), followed by augmentation to 6.5 at D = 2800 (1998). This variation constitutes a period of about 8.5 years as evidenced by the dashed line.

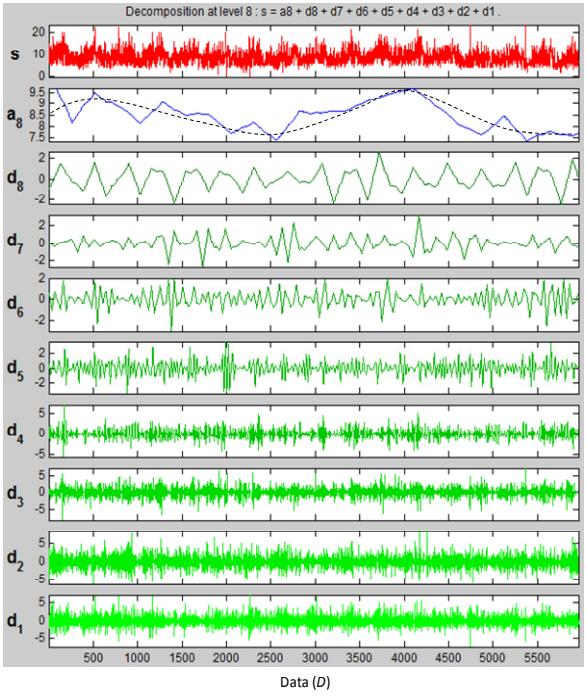

Fig. 3 Decomposition of wind speed time series data for Dhahran using DB8.

This information is very useful for a long-term wind prediction and power production. The observation also explains why a long-term wind speed trend at a location should be known to run a wind farm productively. Signals d_7 and d_6 display oscillation with a period of about a half and a quarter year, respectively. The oscillation is, however, small (±2 knots). The d_5 and d_4 signals have some large amplitude variations in the ranges of peaks in d_8 signal. The amplitude is greater in d_4 (±2.0 knots) than d_5 (±1.5 knots). The observation insinuates that the monthly variation in wind speed is stronger than the bimonthly variation and it occurs in the peak season (June to August) of wind speed. The d_3 and d_2 signals display a spike at D = 1200; the spike is nevertheless larger at d_2 than d_3. It has been mentioned that in signal S there is a spike at D = 1200 where the magnitude of speed is about 27 knots, which can now be explained with a view on d_2 signal that around D =1200 (1993) there was a persistent wind gust or storm in a period of 4 to 8 days. Similarly, another wind gust is observed in d_1 signal at D = 2200 (1996) for a shorter period of 2 to 4 days. Overall, wind speed variation is stronger for a period of one year (d_8), half a year (d_7), one month (d_4) and less than 8 days (d_1 and d_2) but weaker for a period of a quarter year (d_6), bimonthly (d_5), and bi-weekly (d_3).

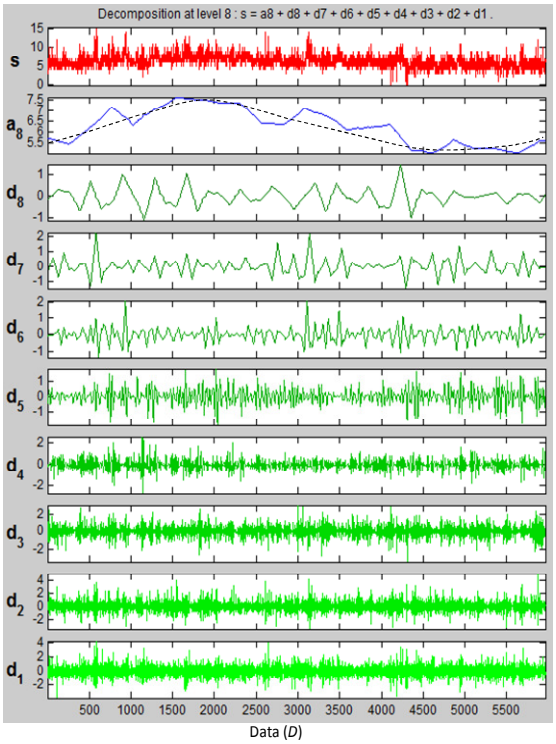

Fig. 4 Decomposition of wind speed time series data for Gizan using DB8.

The raw signal 'S' at Dhahran (Fig. 3) displays sharp spikes at D = 500, 800, 2000, 3400, 4150, 4750, 5400. Gusty winds were afoot more frequently. Here the long-term variation shown by the dashed line in a_8 represents a period of about 9 years. This long-term variation period is almost the same for both Abha and Dhahran.

Table 1. Intrinsic features of wind speed at different locations. June to August is the wind peak season.

Site	a_8			d_8	d_4	d_1
	Long-term mean speed (knots)	Long-term period (years)	Long-term fluctuation (knots)	Annual fluctuation (knots)	Monthly fluctuation, June – August (knots)	Half-weekly fluctuation (knots)
Abha	5.6	8.5	±0.9	±1.7	±2.6	±2.5
Dhahran	8.9	9	±0.6	±1.3	±2.9	±3.3
Gizan	6.25	12	±0.9	±0.7	±1.5	±1.6
Guryat	8.1	9	±0.9	±3.0	±3.0	±3.8
Hail	6.0	9	±1.5	±1.0	±2.4	±3.0
Jeddah	7.1	10.5	±0.9	±1.1	±2.4	±2.5
Riyadh	6.0	9.5	±0.65	±1.1	±2.8	±2.9
Turaif	8.6	10	±1.4	±0.9	±2.5	±3.5
Yanbo	7.3	10.5	±1.6	±1.7	±2.5	±3.0

The speed fluctuates from 8.3 to 9.5 knots (dashed line), while that for Abha oscillates from 4.7 to 6.5 knots. Therefore, the mean speed over the whole duration can be considered as 8.9 knots for Dhahran and 5.6 knots for Abha. The contribution of the long-term variation to the speed is about ±0.6 and ±0.9 knots for Dhahran and Abha, respectively. The annual variation of speed (d_8 signal) is more regular for Dhahran than for Abha, forming a peak in the months of April to June of each year. This regularity was also reflected in the power spectrum results with a peak at f = 0.0027 appearing sharper at Dhahran than at Abha. While the mean variation in amplitudes at Dhahran (d_8 signal) is about ±1.3 knots, that at Abha is about ±1.7 knots, i.e. slightly larger in the latter. The $d_7 - d_3$ signals display almost the same characteristics as those for Abha. The d_2 and d_1 signals, however, have larger amplitudes at Dhahran than Abha. The larger amplitudes at Dhahran result from the fact that Dhahran is 17 m above the sea level and very close (3 km) to the sea.

At Gizan (Fig. 4), which is located on the south-west coast of Saudi Arabia, the long-term variation period (dashed line) is slightly longer, about 12 years with a change in speed from 5.0 to 7.5 knots. The entire duration average is about 6.25 knots. The annual variation in amplitude is very small here, about ±0.7 knots (d_8 signal). Because of the small amplitude, the corresponding peak at f = 0.0027 in the FFT power spectrum was not distinguished enough (Fig. 1c). Wavelet analysis results for Guryat, Hail, Jeddah, Riyadh, Turaif and Yanbo are not shown here. Table 1 extracts important intrinsic features of wind speed analysis results in Figs. 2-4 and in the other figures not shown. The long-term (16 years) mean speed (second column), long-term period (third column) and long-term fluctuation (fourth column) are extracted from a_8 signals. On the other hand, annual fluctuation (fifth column), monthly fluctuation (sixth column) and half-weekly fluctuation in speed are obtained from d_8, d_4 and d_1 signals, respectively. Having smaller fluctuations, other data are not included in Table 1. The data in Table 1 are plotted in Figs. 5 and 6 for the sake of a better perceptibility of comparison between different locations. The long-term mean speed is a minimum of 5.6 knots at Abha (Table 1, Fig. 5). Dhahran, Guryat and Turaif undergo a higher speed of 8.9, 8.1 and 8.6 knots, respectively (Table 1, Fig. 6). It is interesting that the wind speed has a long period of about 10 (8.5 to 1.2) years (third column of Table 1) which contributes to a change in speed by ±0.6 to ±1.6 knots (fourth column) depending on the location.

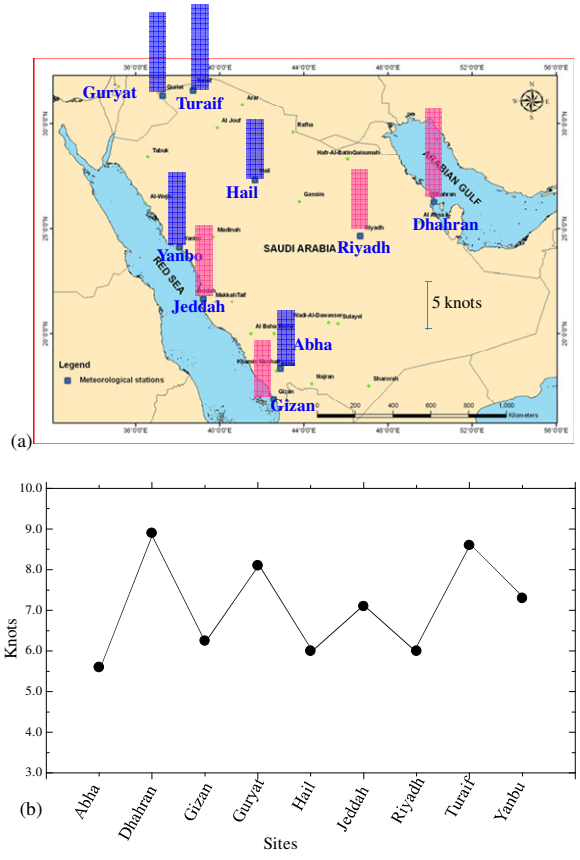

Fig. 5 Long-term (16 years) mean wind speed at different sites, shown in (a) bar diagram, and (b) Cartesian coordinate.

The long-term contribution is, however, maximum at Yanbo (±1.6 knots) and Hail (±1.5 knots). It was found in the FFT analysis results that Abha, Dhahran, Guryat and Yanbo showing a sharp peak at f = 0.0027 preserved a more regular annual repetition than Gizan,

Hail, Jeddah, Riyad and Turaif. The data in the fifth column agree with the observation in the FFT analysis results, displaying larger fluctuations (±1.3 to ±3.0 knots) at the former locations and smaller (±0.7 to ±1.1 knots) at the latter locations. The annual variation is, however, the largest (±3.0 knots) at Guryat and the smallest (±0.7 knots) at Gizan. Except for the small value (1.5 knots) at Gizan, the monthly fluctuation is less dependent on location, nestling between ±2.4 and ±3.0 knots. Among the long-term, annual, monthly and half-weekly fluctuations (Table 1 and Fig. 6), the half-weekly fluctuation is the largest at all locations, varying from ±1.6 to ±3.8 knots. This observation points to the fact that the daily fluctuation should also to be investigated. Overall, the annual, monthly, and half-weekly fluctuations are the largest at Guryat and the smallest at Gizan. The most possible cause behind the largest and smallest fluctuations at Guryat and Gizan, respectively, is that while Guryat is a high land with low and high hills, Gizan is a coastal area only 5 m above the sea level. The information in Table 1 will be very useful for short- and long-term wind forecasts, hence to distinguish idle and running periods of a wind turbine. Using wavelet transform, Chellali *et al.* [6] made a time-period analysis of wind speed data recorded at Adrar, Algeria for four years (2005 to 2009). Their analyzing period ranged from 2 to 64 days only, which is rather small compared with our range of 2 to 512 days investigated. They observed the dominant oscillation of periods between 2 and 16 days including intra-seasonal oscillations of periods between 30 and 60 days.

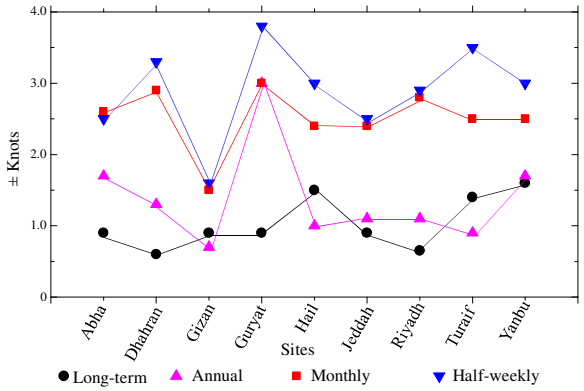

Fig. 6 Contributions of different time-scales to wind speed fluctuation.

4. Conclusions

Wavelet analysis extracted the intrinsic features of wind speed, including long-term, annual, half-yearly, quarter-yearly, monthly, biweekly, weekly and half-weekly fluctuations. The information on speed fluctuations at different periods is very useful for meteorological purposes, including wind and weather forecasting. The wind speed over Saudi Arabia has a long period of about 10 years, contributing to change in speed by ±0.6 to ±1.6 knots depending on the locations. The long-term contribution is maximum (±1.6 knots) at Yanbo and minimum (±0.6 knots) at Dhahran. The long-term mean wind speed is 5.6, 8.9, 6.25, 8.1, 6.0, 7.1, 6.0, 8.6 and 7.3 knots at Abha, Dhahran, Gizan, Guryat, Hail, Jeddah, Riyadh, Turaif and Yanbo, respectively. The annual fluctuation in wind speed is larger (±1.3 to ±3.0 knots) and more regular at Abha, Dhahran, Guryat and Yanbo, while smaller (±0.7 to ±1.1 knots) and less regular at Gizan, Hail, Jeddah, Riyad and Turaif, with the greatest (±3.0) and smallest (±0.7) at Guryat and Gizan, respectively. Among long-term, annual, half-yearly, quarter-yearly, monthly, biweekly, weekly and half-weekly fluctuations, the largest change in wind speed occurs half-weekly, by about ±1.6 to ±3.8 knots depending on location. The highland and coastal sites, Dhahran, Guryat and Yanbo, correspond to larger annual, monthly and half-weekly fluctuations of wind speed.

ACKNOWLEDGMENTS

Alam wishes to acknowledge supports given to him from the Research Grant Council of Shenzhen Governmentthrough grants JCYJ20120613145300404 and JCYJ20130402100505796.

REFERENCES

[1] O.A. Jaramillo, M.A. Borja, Winds peed analysis in La Ventosa, Mexico: a bimodal probability distribution case, *Renewable Energy*, Vol. 29, pp 1613-1630 (2004).

[2] A.P. Garcia-Marin, J. Estevez, F.J. Jimenzez-Hornero, J.L. Ayuso-Munioz, Multifractal analysis of validated wind speed time series, *Chaos, Non-Linear Science*, Vol. 23, pp 013133 (2013).

[3] T. Kitagawa, T. Nomura, A wavelet-based method to generate artificial wind fluctuation data, *Journal of Wind Engineering and Industrial Aerodynamics*, Vol. 91, pp 943–964 (2003).

[4] C.L. Pettit, N.P. Jones, R. Ghanem, Detection and simulation of roof-corner pressure transients, *Journal of Wind Engineering and Industrial Aerodynamics*, Vol. 90, pp 171–200 (2002).

[5] H. Aksoy, Z.F. Toprak, A. Aytek, N.E. Unal, Stochastic generation of hourly mean wind speed data, *Renewable Energy*, Vol. 29, pp 2111–2131 (2004).

[6] F. Chellali, A. Khellaf, A. Belouchrani, Wavelet spectral analysis of the temperature and wind speed data at Adrar, Algeria. *Renewable Energy*, Vol. 35, pp 1214–1219 (2010).

[7] M.M. Alam, M. Moriya, H. Sakamoto, Aerodynamic characteristics of two side-by-side circular cylinders and application of wavelet analysis on the switching phenomenon. *Journal of Fluids and Structures*, Vol. 18, pp. 325-346 (2003).

[8] M.M. Alam, H. Sakamoto, Investigation of Strouhal frequencies of two staggered bluff bodies and detection of multistable flow by wavelets. *Journal of Fluids and Structures*, Vol. 20, pp 425-449 (2005).

ICMIEE-PI-140390

Fluid dynamics around two tandem cylinders of different diameters

Md. MahbubAlam[1,2,], Longjun Wang[1], Xuewei Han[1] and Yu Zhou[1]*
[1]Institute for Turbulence-Noise-Vibration Interaction and Control, Shenzhen Graduate School, Harbin Institute of Technology, Shenzhen 518055, China
[2]Key Kab of Advanced Manufacturing and Technology, Shenzhen Graduate School
Harbin Institute of Technology, Shenzhen 518055, China

ABSTRACT
The paper associated with two tandem cylinders presents the upstream cylinder size (diameter d) effect on global parameters of the downstream cylinder including time-mean drag coefficient (C_D), fluctuating drag and lift coefficients (C_D' and C_L'), shedding frequencies and flow structures at the spacing ratio L/d = 1.0 ~ 8.0, where L is the distance between the center of the upstream cylinder and the forward stagnation point of the downstream cylinder. d is varied as 8, 16, 24, 32 and 40 mm, while the downstream cylinder diameter D is fixed at 40 mm, corresponding to diameter ratio d/D ranging from 0.2 to 1.0. The Reynolds number is kept constant at 4.27×10^4 based on D. C_D, C_D' and C_L' are measured using a sectional load cell, while the shedding frequency is estimated from hotwire-measured fluctuating velocity in the wake. Flow structures are obtained using smoke visualization technique. The critical L/d dividing the reattachment and coshedding flows is larger at smaller d/D. C_D, C_D' and C_L' at the critical spacing leap for d/D =1.0 - 0.4, but decline for d/D = 0.2. In the coshedding regime, the downstream-cylinder shedding frequency locks-in with the shedding frequency of the upstream cylinder for d/D = 1.0, 0.8 and 0.6, in addition to a subharmonic lock-in for d/D = 0.6 only. The lock-in however does not occur at d/D = 0.4 and 0.2, the shedding frequencies of the upstream and downstream cylinders being much higher and smaller, respectively, compared to the shedding frequency of a single cylinder. C_D in general increases with d/D. C_D' and C_L', on the other hand, generally wane and grow as d/D decreases from 1.0 to 0.6 and 0.4 to 0.2, respectively. While the former phenomenon is dominantly influenced by impaired vortices/shear-layer with the decreases in d/D, the later by increased flow velocity between the gap.

Keywords: Tandem arrangement; Flow structures; Fluid forces; Reattachment position

1. Introduction
Flow around two tandem cylinders of identical diameters is in general classified into three major regimes [1]: (i) the extended-body regime ($0.5 < L/d < 1.0$; d is the upstream cylinder diameter, and L is the distance between the center of the upstream cylinder center and the leading stagnation point of the downstream cylinder); (ii) the reattachment regime ($1.0 < L/d < 3.5$); (iii) the coshedding regime ($L/d > 3.5$). There is a transition L/d range between the reattachment and coshedding regimes, where both reattachment and coshedding flows appear intermittently, switching from one to the other. The transition L/d is called critical or bistable flow spacing. Furthermore, the reattachment regime is further divided into two [2]: alternating reattachment regime ($1.0 < L/d < 2.5$) and steady reattachment regime ($2.5 < L/d < 3.5$). At the coshedding regime, it is well established that the two cylinders shed vortices separately at the same frequency [2-5]. For a given downstream cylinder, different cross sections of the upstream cylinder with the same characteristic width result in a different frequency of vortex shedding from the upstream cylinder, and the frequency of vortex shedding from the downstream cylinder modifies accordingly to lock-in, adjusting itself to that of the upstream one [6]. On the other hand, for a given upstream cylinder size, a change in the cross section of the downstream cylinder does not influence the shedding frequency of the upstream cylinder [6].

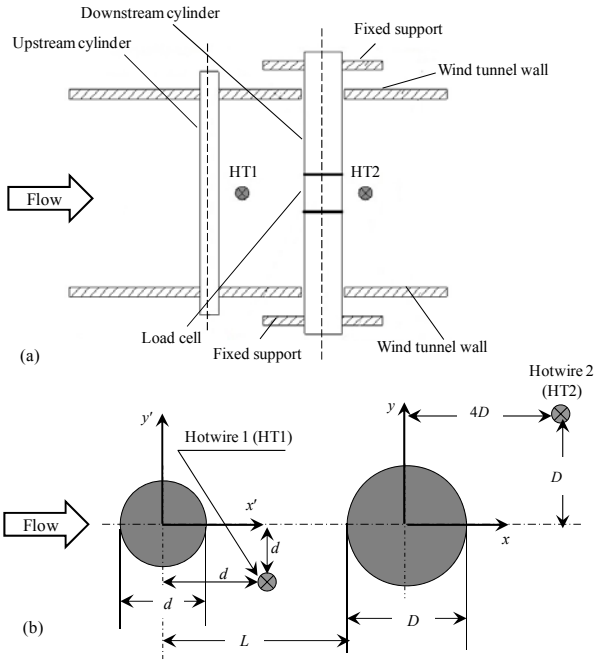

Fig. 1 (a) Experimental setup and (b) definition of symbols.

It was concluded that the hydrodynamic stability of the flow around two tandem cylinders is predominantly

* Corresponding author. Tel.: +88-01713255226
E-mail address: mdmashud@yahoo.com

controlled by the upstream cylinder, not by the downstream cylinder. Measuring time-mean drag coefficient C_D, fluctuating drag coefficient C_D', fluctuating lift coefficient C_L' and Strouhal number St on two identical cylinders at Reynolds number Re = 6.5×10^4 for L/d < 8.5, C_D, C_D', C_L' and St on the downstream cylinder are highly sensitive to L/d particularly in the reattachment regime [2]. Investigations associated with different diameter cylinders are very scarce.

The major objectives of this work are to examine (i) the effect of the upstream cylinder diameter on C_D, C_D', C_L', St and wake of the downstream cylinder at L/d = 1 - 8, covering all possible flow regimes, and (ii) how the critical L/d corresponding to transition between reattachment and coshedding flows is dependent on d/D.

2. Experimental setup

Experiments were performed in a closed-circuit wind tunnel with a 5.5 m long test section of 0.8 m × 1.0 m. The downstream cylinder diameter D (= 40 mm) was kept fixed, and the upstream cylinder diameter d was changed as d = 8, 16, 24, 32 and 40 mm, resulting in diameter ratio d/D = 0.2, 0.4, 0.6, 0.8, and 1.0, respectively. The spacing ratio L/d between the cylinders was systematically varied from 1.0 to 8.0. The freestream velocity U_∞ was 16 m/s, corresponding to Re = 4.27×10^4 based on D. This Re lies in the higher subcritical Re range where fluid forces acting on a single cylinder are comparatively insensitive to Re. The turbulence intensity of the uniform flow was 0.45%. The maximum blockage is 4% and the aspect ratio of the cylinder is 20.

Fluid forces acting on the downstream cylinder are measured using a sectional load cell (65 mm long) installed at the midsection of the cylinder (Fig. 1). Therefore, C_D, C_D', and C_L' are estimated from the load cell output. Fig.1 shows schematically the arrangement of the cylinders and definitions of coordinates (x', y') and (x, y) with the origins defined at the upstream and downstream cylinder centers, respectively. Two single tungsten hotwires, placed in the gap between the cylinders and behind the downstream cylinders, respectively, were used to measure the longitudinal velocity fluctuation u from which vortex shedding frequency was extracted using FFT. The hotwire probe holders were positioned perpendicular to the wake-center plane to minimize the disturbance to the flow.

Smoke-flow visualization technique was used to investigate the flow structure in the gap between two cylinders and behind the downstream cylinder. Pressure measurement on the periphery of the downstream cylinder also carried out, with 32 pressure taps connected to a pressure scanner.

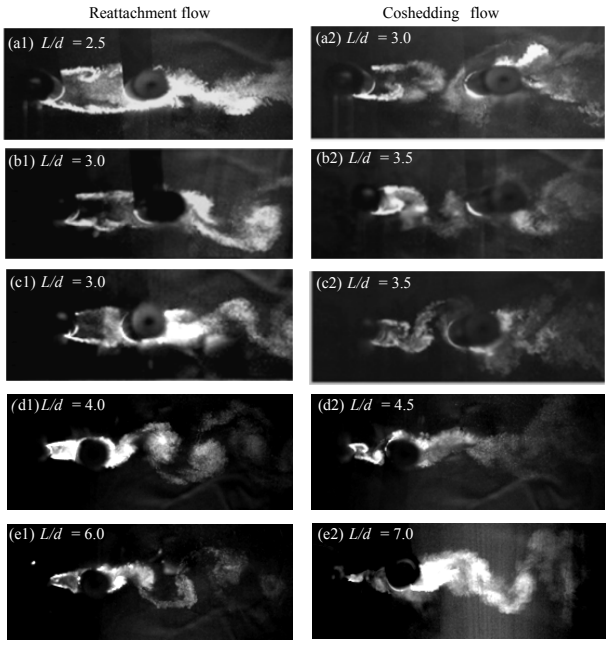

Fig. 2 Visualized flow structures at (a) d/D = 1.0, (b) d/D = 0.8, (c) d/D = 0.6, (d) d/D = 0.4, and (e) d/D = 0.2. Left- and right-column pictures represent reattachment and coshedding flows, respectively.

3. Results and discussion

3.1 Flow structures and shedding frequency

Figure 2 shows flow structures at different d/D around the two cylinders near critical L/d where the left column displays the photographs corresponding to reattachment flow and the right column to the coshedding flow. Clearly the upstream cylinder shear layers at d/D = 1.0 reattach on the downstream cylinder at L/d = 2.5 (Fig. 2a1) but roll up in the gap between the cylinders at L/d = 3.0 (Fig. 2a2). That is, the critical spacing lies between L/d = 2.5 and 3.0. Similarly that at d/D = 0.8 and 0.6 nestles between L/d = 3.0 and 3.5 (Fig. 2b-c). d/D = 0.4 and 0.2, nevertheless, correspond to the critical spacing at 4.0 < L/d < 4.5 and 6.0 < L/d < 7.0, respectively. What is interesting here is that with a decrease in d/D from 1.0 to 0.2 the upstream cylinder wake width shrinks gradually; the shrinking is larger in the coshedding regime than the reattachment regime.

The transmutation of flow with d/D and L/d could be further discussed with the aid of power spectral density functions (Fig. 3) of fluctuating velocities obtained in the gap between the cylinders (HT1) and behind the downstream cylinder (HT2). St (= f_vD/U_∞, f_v is the vortex shedding frequency) jumps from 0.141 to 0.172 between L/d = 2.5 and 3.0 for d/D = 1.0 and from 0.158 to 0.212 between L/d = 3.0 and 3.5 for d/D = 0.8. Apparently the jump is due to a drastic modification of reattachment flow to coshedding flow when L/d is increased. While the higher St at the former d/D is smaller than the St (= 0.197) of an isolated cylinder, that at the latter is higher. In the coshedding flow (i.e., $L/d \geq$ 3.0) for d/D = 1.0, albeit shedding vortices individually,

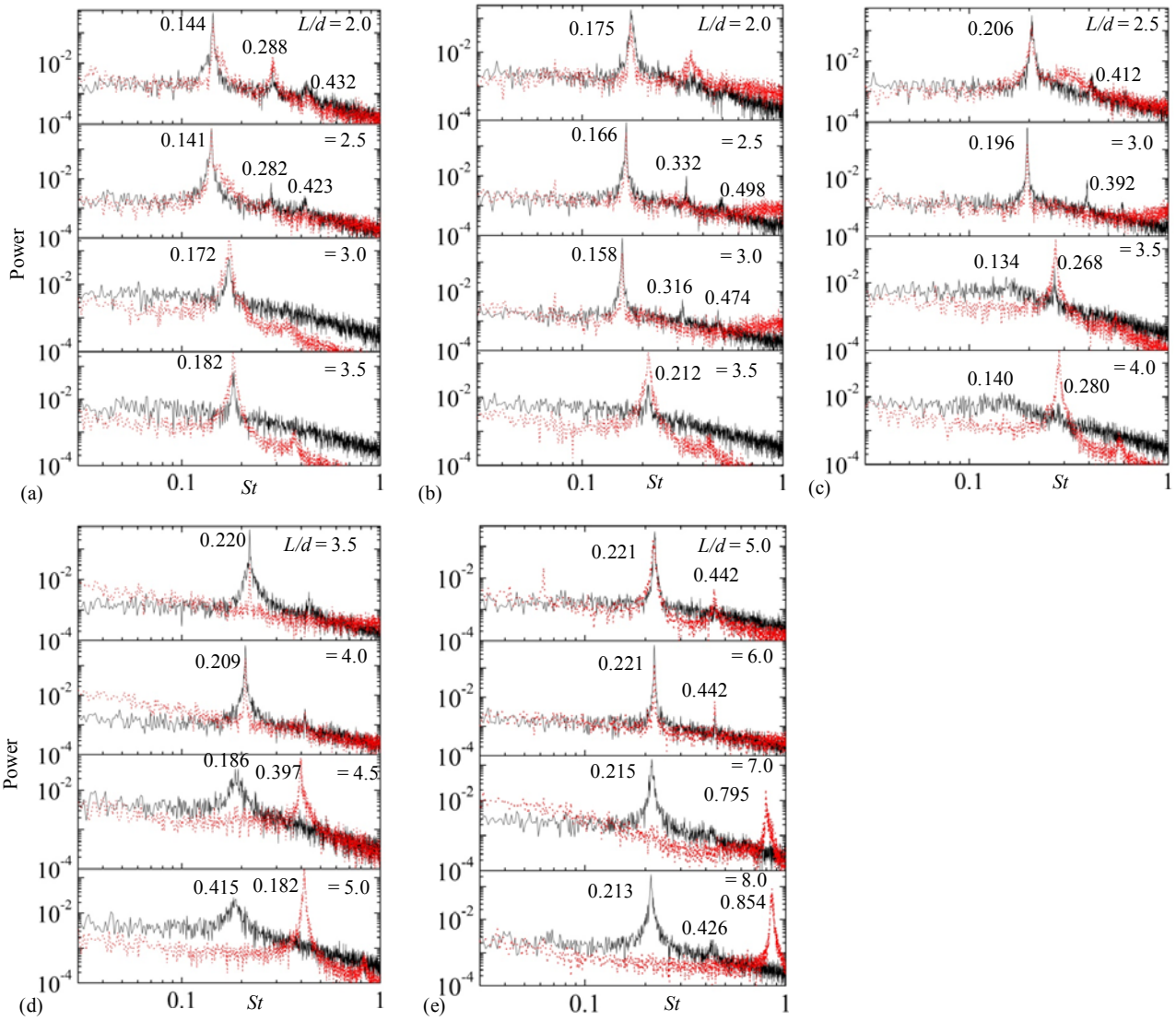

Fig. 3 The power spectral density functions of hotwire (HT1 and HT2) signals at different *d/D* and *L/d*: (a) *d/D* = 1.0, (b) *d/D* = 0.8, (c) *d/D* = 0.6, (d) *d/D* = 0.4, and (e) *d/D* = 0.2, at different *L/d*. Dotted line, HT1; solid line, HT2. The *St* is based on *D*.

the two cylinders have an identical *St*, slightly smaller than the isolated cylinder. This is an established phenomenon for the same diameter tandem cylinders that the convective vortices from the upstream cylinder trigger the shedding from the downstream cylinder, making both *St* identical [6]. On the other hand, though having different diameters at *d/D* = 0.8, the two cylinders have again identical *St*, slightly larger than the isolated cylinder. One may arise a question, why is this *St* larger? Indeed, now the upstream cylinder diameter is small, $d = 0.8D$. The shedding frequency from the upstream cylinder is thus larger, given the same approaching flow velocity. *St* based on *d* can be calculated as $0.212 \times 0.8 = 0.17$ that is almost the same as that at *d/D* = 1.0. The downstream cylinder displays two *St* (say, 0.134 and 0.268 at *L/d* = 3.5) at *d/D* = 0.6 in the coshedding regime, where the upstream cylinder *St* = 0.268, suggesting both fundamental and subharmonic locks-in. Since the higher *St* of the downstream cylinder fades away at *L/d* = 4.0, it is reasonable to assume that the fundamental lock-in perhaps weaker than the subharmonic. At *d/D* = 0.4 and 0.2, thought *St*(s) of two cylinders are identical in the reattachment regime, they are different in the coshedding regime. The fundamental *St* (upstream cylinder, downstream cylinder) = (0.268, 0.134) at *L/d* = 3.5 for *d/D* = 0.6, (0.397, 0.186) at *L/d* = 4.5 for *d/D* = 0.4, and (0.795, 0.215) at *L/d* = 7.0 for *d/D* = 0.2. Both *St* augment with *d/D*. While the augmentation of the upstream cylinder *St* with a decrease in *d/D* is due to a decrease in diameter, that of the downstream cylinder is caused by a larger flow velocity in the gap between the cylinders. When the upstream cylinder *St* = 0.268 at (*d/D*, *L/d*) = (0.6, 3.5), 0.397 at (*d/D*, *L/d*) = (0.4, 4.5), and 0.795 at (*d/D*, *L/d*) = (0.2, 7.0) are normalized by *d* instead of *D*, they becomes 0.1608, 0.159, and 0.159, respectively, comparable to those at *d/D* = 0.8 and 1.0.

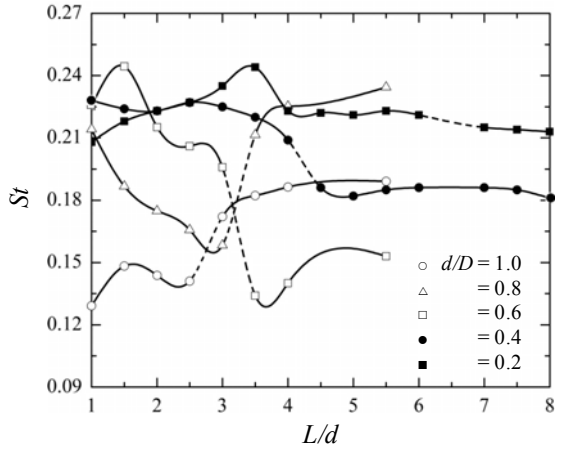

Fig. 4 Dependence of Strouhal number *St* on *L/d* and *d/D*.

shedding. Again a smaller *d/D* in general corresponds to a higher *St* between *d/D* = 0.4 and 0.2.

3.2 Pressure distributions and forces

Distributions of pressure coefficient C_p around the surface of the cylinder at various *L/d* and *d/D* are shown in Fig. 5. C_p displays a peak at θ = 20°-70° depending on *d/D* at the reattachment flow regime and at θ = 0° at the coshedding flow regime. The peak at the reattachment flow regime represents the shear layer reattachment. C_p at the whole surface in the reattachment regime (open symbols) is negative for *d/D* ≥ 0.6, even at the reattachment peak, while that for other *d/D* is positive at and near the reattachment. At a given *L/d*, C_p at the reattachment increases with a decrease in *d/D*. At the same time, the reattachment position moves toward the forward stagnation point. If it is assumed that the shear layer velocity is the same for all *d/D*, the

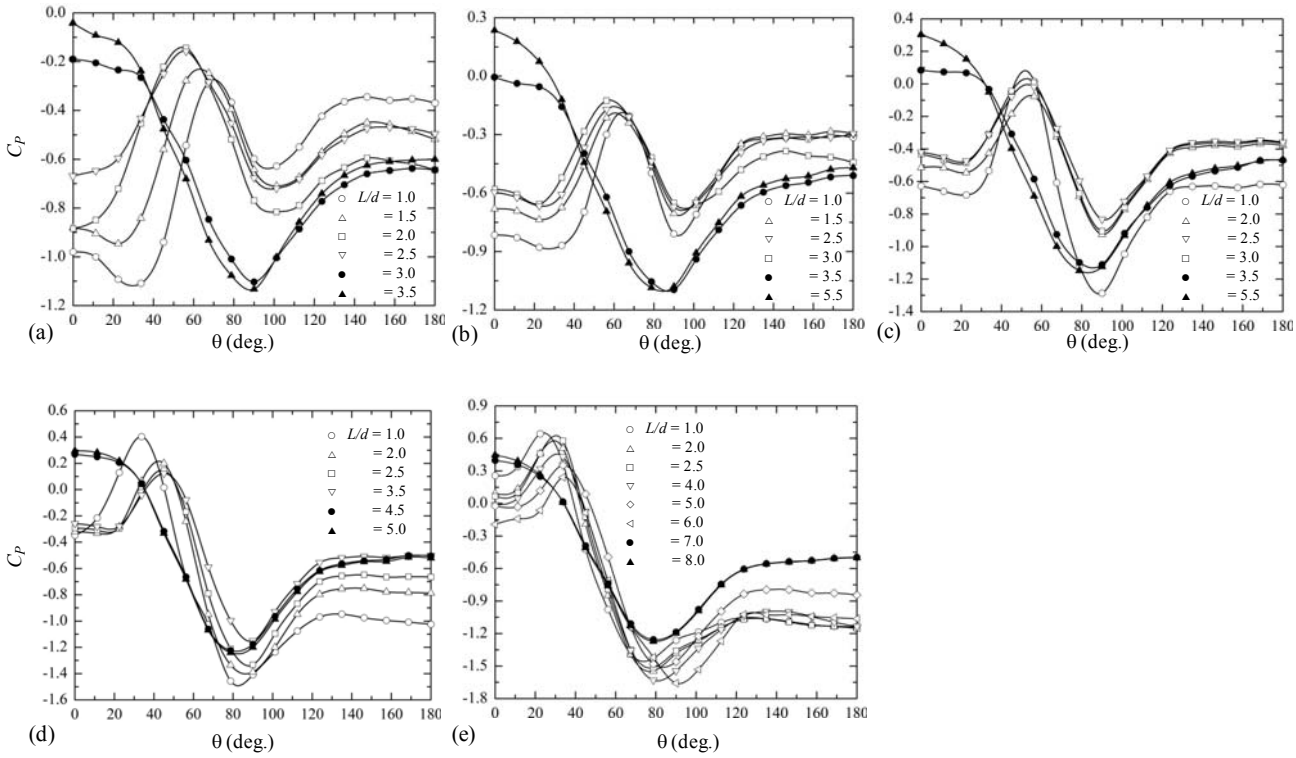

Fig. 5 Distribution of time-averaged pressure coefficient C_P along the surface of the cylinder: (a) *d/D* = 1.0, (b) *d/D* = 0.8, (c) *d/D* = 0.6, (d) *d/D* = 0.4, (e) *d/D* = 0.2.

How the *St* of the downstream cylinder is influenced by *L/d* and *d/D* is shown in Fig. 4. *St* is sensitive to *L/d* essentially in the reattachment flow regime, especially for *d/D* = 1.0, 0.8, and 0.6. *St* in the reattachment regime increases with *d/D* decreasing from 1.0 to 0.6. The change in *St* between *d/D* = 0.4 and 0.2 in the reattachment regime is relatively small. In the coshedding regime, St is greater at *d/D* = 0.8 than *d/D* = 1.0. Its explanation has been given above. But *St* at *d/D*= 0.6 is much smaller because of the lock-in of the downstream cylinder vortex shedding at the subharmonic frequency of the upstream cylinder

higher C_P may result from the shear layer reattachment at a smaller angle of incidence which accompany a shift in reattachment position toward the forward stagnation point. In the coshedding regime as well (solid symbols), a smaller *d/D* accompanies a larger C_p at the forward stagnation point, which further insinuates that the smaller the *d/D*, the larger the flow velocity in the gap between the cylinders. It is worth noting that when a reattachment flow modifies to a coshedding flow, C_P on the base of the cylinder decreases significantly for *d/D* = 1.0-0.6, declines a little for *d/D* = 0.4 and increases considerably for the other *d/D*.

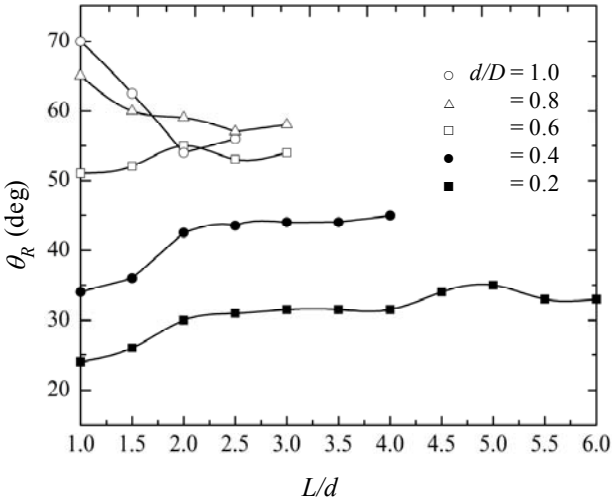

Fig. 6 Variation in reattachment position θ_R with increase in L/d.

The reattachment position θ_R obtained from the C_p distribution is shown in Fig. 6. It seems that while d/D = 1.0 - 0.6 have almost the same trend in θ_R, other d/D (= 0.4 and 0.2) have a different trend, with θ_R being smaller. There should be a dormant relationship between θ_R and forces on the cylinder [2]. C_D, C_D' and C_L' variations with L/d shown in Fig. 7 reflect that they are strong functions of L/d and d/D, especially before the critical spacing. For d/D = 1.0 and 0.8, as L/d increases from 1.0 to 2.0, θ_R precedes and C_D, C_D' and C_L' all escalate. At the same L/d range, d/D = 0.6 and 0.2 have the opposite behaviors; θ_R recedes and C_D, C_D' and C_L' all drop. A small increase in θ_R for d/D = 1.0 and 0.6 between L/d = 2.0 and 2.5 is accompanied by a small decrease in C_D, C_D' and C_L'. The correlation between θ_R and forces is, however, weak for smaller d/D (= 0.4 - 0.2). It is remarkable that at the critical spacing C_D, C_D' and C_L' all jump for d/D = 1.0 - 0.4, but drop for d/D = 0.2. The corresponding flow physics is expected to be different, but not known at this stage. C_D in general enhances with a decrease in d/D except at d/D = 1.0, L/d = 2. C_D' and C_L', on the other hand, generally decreases with d/D decreasing from 1.0 to 0.6 and increases with d/D decreasing from 0.4 to 0.2. While the former behavior is mostly influenced by vortices/shear-layer weakening with the decrease in d/D, the latter by a larger flow velocity between the gap.

A flow map showing reattachment, bistable and coshedding flows is given in Fig. 8. The critical spacing associated with possible bistable flow extends with decrease in d/D.

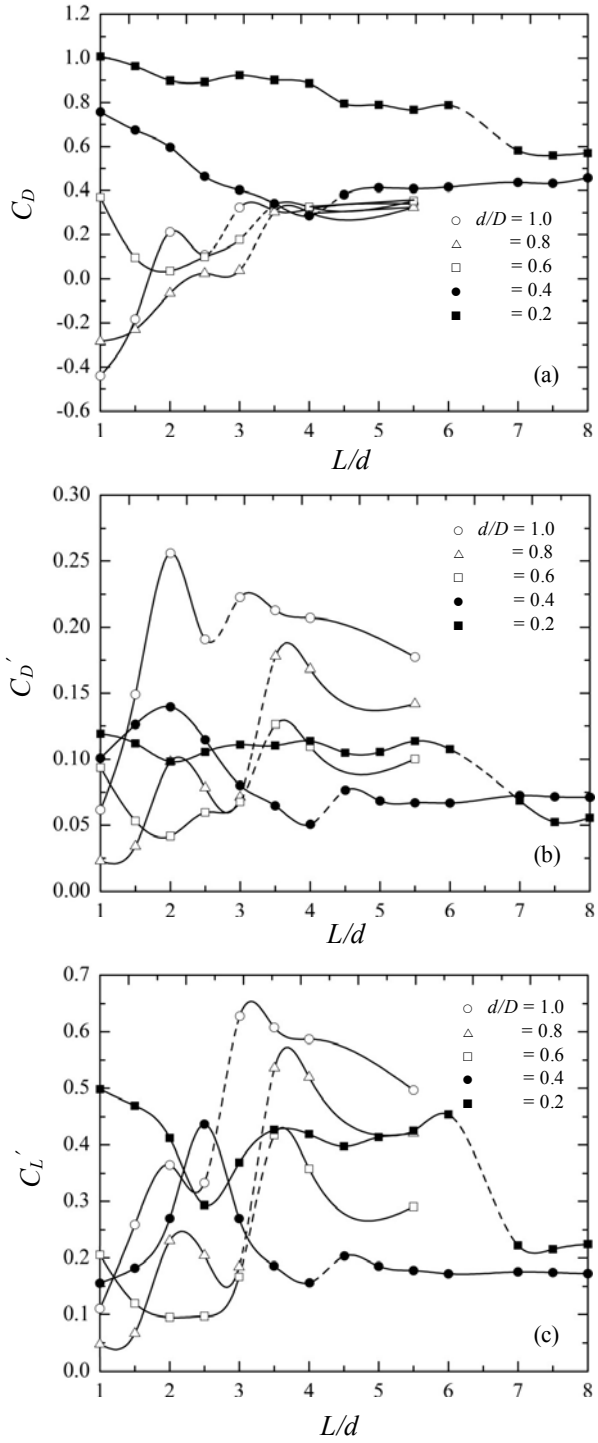

Fig. 7 Dependence on L/d of (a) C_D, (b) C_D', and (c) C_L'.

4. Conclusions

Fluid dynamics around two tandem cylinders is investigated, where the upstream cylinder size is reduced from d/D = 1.0 to 0.2. Flow structure, pressure distribution, forces and St are paid attention. The main results of this study may be summarized as follows.

1. St is identical for both cylinders in the reattachment regime regardless of d/D. In the coshedding regime, the downstream cylinder shedding frequency locks-in to the upstream cylinder for d/D = 1.0, 0.8 and 0.6.

At d/D = 0.6, a lock-in of the downstream cylinder shedding with the subharmonic of the upstream cylinder shedding is also noticed. For the other two d/D, the upstream cylinder shedding frequency is much higher than the downstream cylinder; lock-in is not observed.

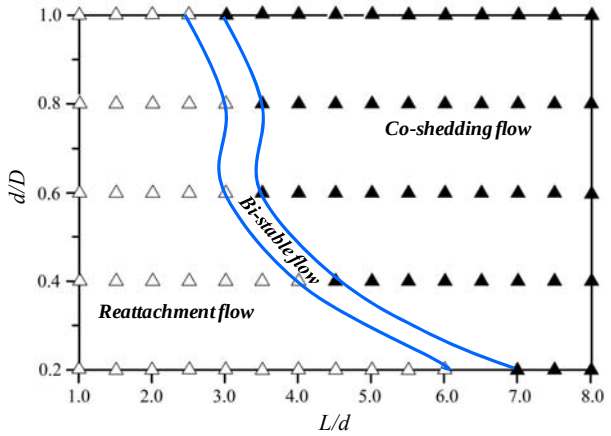

Fig. 8 Flow map in L/d - d/D plane.

2. The critical L/d dividing the reattachment and coshedding flows is larger at smaller d/D, nestling at $2.5 < L/d < 3.0$, $3.0 < L/d < 3.5$, $4.0 < L/d < 4.5$, and $6.0 < L/d < 7.0$ for d/D =1.0, 0.8-0.6, 0.4 and 0.2, respectively. At these critical spacing, while C_D, C_D' and C_L' leap for d/D =1.0 - 0.4, they fall for d/D = 0.2.
3. C_D, C_D' and C_L' of the downstream cylinder are very sensitive to L/d in the reattachment regime, being highly influenced by the shear-layer reattachment position on the downstream cylinder. C_D in general increases with d/D except at d/D = 1.0, L/d =2.0. C_D' and C_L' generally diminish and climb with d/D decreasing from 1.0 to 0.6 and 0.4 to 0.2, respectively. While the former behavior is mostly influenced by vortices/shear-layer weakening with the decrease in d/D, the latter by a larger flow velocity between the gap.

ACKNOWLEDGMENTS

Alam wishes to acknowledge supports given to him from the Research Grant Council of Shenzhen Government through grants JCYJ20120613145300404 and JCYJ20130402100505796.

NOMENCLATURE

d : upstream cylinder diameter
C_D : time-mean drag coefficient
C_D' : fluctuating drag coefficient
C_L' : fluctuating lift coefficient
L/d : spacing ratio
D : downstream cylinder diameter
d/D : diameter ratio
St : Strouhal number
Re : Reynold number
U_∞ : the coming flow velocity
u : local streamwise velocity
f_v : vortex shedding frequency
C_P : pressure coefficient
θ : azimuthal angle of pressure tap position
θ_R : shear layer reattachment position

REFERENCES

[1] M.M. Zdravkovich, The effects of interference between circular cylinders in cross flow, *Journal of Fluids and Structures*, Vol. 1, pp 239–261, (1987).
[2] M.M. Alam, M. Moriya, K. Takai, H. Sakamoto, Fluctuating fluid forces acting on two circular cylinders in a tandem arrangement at a subcritical Reynolds number, *Journal of Wind Engineering and Industrial Aerodynamics*, Vol. 91, pp 139–154, (2003).
[3] S. Ishigai, E. Nishikawa, E. Nishimura, K. Cho, Experimental study of structure of gas flow in tube banks axes normal to flow, *Bulletin of the Japan Society of Mechanical Engineering*, Vol. 15, pp 949–956, (1972).
[4] M.M. Alam, H. Sakamoto, Y. Zhou, Effect of a T-shaped plate on reduction in fluid forces acting on two tandem circular cylinders in a cross-flow, *Journal of Wind Engineering and Industrial Aerodynamics*, Vol. 94, pp 525–551, (2006).
[5] M.M. Alam, Y. Zhou, Phase lag between vortex sheddings from two tandem bluff bodies, *Journal of Fluids and Structures*, Vol. 23, pp 339–347, (2007).
[6] M.M. Alam, H. Sakamoto, Y. Zhou, Determination of flow configurations and fluid forces acting on two staggered circularcylinders of equal diameter in cross-flow, *Journal of Fluids and Structures*, Vol. 21, pp 363–394, (2005).

ICMIEE-PI-140392

Effect of Location of Cambered Spoiler on Aerodynamic Characteristics of a Car

Ahsan Ferdaus [*], *Minhaz Hossain and Khandkar Aftab Hossain*
Department of Mechanical Engineering, Khulna University of Engineering & Technology, Khulna 9203, BANGLADESH.

ABSTRACT
In the present study, the effects of locations of Cambered Spoiler on aerodynamic stability of a car are investigated numerically. A car model and a cambered spoiler are designed in CAD software. Afterwards the spoiler is placed on the rooftop and rear position of the car. The CAD data is then analyzed in CFD software. The analysis shows that spoiler in rear position develops maximum down force than rooftop and thus increases road traction and stability of the car while driving. So, for efficient performance of the vehicle, spoiler placement at rear is well suited than rooftop.

Keywords: Cambered Spoiler, down force, lift force, drag force, stability.

1. Introduction

In general, aerodynamic is simply how air flows around a car, truck or airplane. The main concerns of automotive aerodynamics are optimizing drag, improving vehicle stability and preventing unwanted lift forces [1]. Having more power under the hood leads to higher speeds for which the aerodynamic properties of the car given by the designer are not enough to offer the required down force and handling. The performance, handling, safety, and comfort of an automobile are significantly affected by its aerodynamic properties [2]. Extra parts are added to the body like spoilers, lower front and rear bumpers, air dams and many more aerodynamics aids as to direct the airflow in different way and offer greater drag reduction to the car and at the same time enhance the stability. In spite of this, many aerodynamics aids are sold in market mostly spoilers. It is an aerodynamic device that design to 'spoil' unfavorable air movement across a car body. A spoiler also can be attached to front or rear bumper as air dam. It can also be mounted at the rear of the vehicle or at the end to rooftop of the vehicle. Spoilers contributed some major aerodynamics characteristics as lift and drag. Increase of down force of the vehicle enables the manufacturer to design light weight vehicle and thus saving fuels and moreover spoilers can also be used to control stability during driving especially at cornering.

When a driver drives a car in high speed, especially at highway at speed 60 m/sec, the car has high tendency to lift over. This is possible to happen because as the higher pressure air in front of the windshield travels over the windshield; it accelerates, causing the pressure to drop. This lower pressure literally lifts on the car's roof as the air passes over it. Once the air makes its way to rear window, the flow of the air leaves a vacuum or lower pressure space that the air is not able to fill properly [3]. The flow is said to be detached and the resulting lower pressure creates lift that then acts upon the surface area of the trunk. To reduce lift that acted on the rear trunk, a spoiler can be attached on it to create more pressure. Spoiler can be mounted on both on the rooftop and rear of the vehicle. The most suitable and optimized position for spoiler is determined through this investigation.

2. Mathematical Formulation

2.1 Continuity Equation

A continuity equation in physics is an equation that describes the transport of a conserved quantity [4].

$$[(\delta u/\delta t) + (\delta u/\delta x) + (\delta u/\delta y) + (\delta u/\delta z)] = 0$$

2.2 Navier Stoke's Equation

Taking the incompressible flow assumption into account and assuming constant viscosity, the Navier Stokes equations is in the vector form [5]:

$$\overbrace{\rho\left(\underbrace{\frac{\partial \mathbf{v}}{\partial t}}_{\text{Unsteady acceleration}} + \underbrace{\mathbf{v}\cdot\nabla\mathbf{v}}_{\text{Convective acceleration}}\right)}^{\text{Inertia (per volume)}} = \overbrace{\underbrace{-\nabla p}_{\text{Pressure gradient}} + \underbrace{\mu\nabla^2\mathbf{v}}_{\text{Viscosity}}}^{\text{Divergence of stress}} + \underbrace{\mathbf{f}}_{\text{Other body forces}}$$

Note that gravity has been accounted for as a body force, and the values of g_x, g_y, g_z will depend on the orientation of gravity with respect to the chosen set of coordinates

$$\rho\left(\frac{\partial u}{\partial t} + u\frac{\partial u}{\partial x} + v\frac{\partial u}{\partial y} + w\frac{\partial u}{\partial z}\right) = -\frac{\partial p}{\partial x} + \mu\left(\frac{\partial^2 u}{\partial x^2} + \frac{\partial^2 u}{\partial y^2} + \frac{\partial^2 u}{\partial z^2}\right) + \rho g_x$$

$$\rho\left(\frac{\partial v}{\partial t} + u\frac{\partial v}{\partial x} + v\frac{\partial v}{\partial y} + w\frac{\partial v}{\partial z}\right) = -\frac{\partial p}{\partial y} + \mu\left(\frac{\partial^2 v}{\partial x^2} + \frac{\partial^2 v}{\partial y^2} + \frac{\partial^2 v}{\partial z^2}\right) + \rho g_y$$

$$\rho\left(\frac{\partial w}{\partial t} + u\frac{\partial w}{\partial x} + v\frac{\partial w}{\partial y} + w\frac{\partial w}{\partial z}\right) = -\frac{\partial p}{\partial z} + \mu\left(\frac{\partial^2 w}{\partial x^2} + \frac{\partial^2 w}{\partial y^2} + \frac{\partial^2 w}{\partial z^2}\right) + \rho g_z.$$

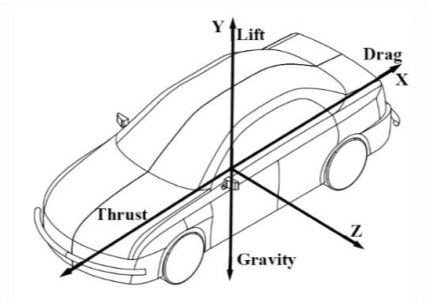

Fig.1: Forces acting on a car.

* Corresponding author. Tel.: +88-01912067928
E-mail address: ahsan.ferdaus@gmail.com

2.3 Drag Force

Aerodynamics drag force is the force which opposes the forward motion of the vehicle when the vehicle is traveling. This drag force acts externally on the body of a vehicle. Aerodynamic drag force is characterized by,

Drag force, $F_D = \frac{1}{2}\rho v^2 C_d A$

2.4 Lift Force

The aerodynamic drag force is acted horizontally to the vehicle and there is another component, directed vertically, called aerodynamic lift. It reduces the frictional forces between the tires and the road, thus changing dramatically the handling characteristics of the vehicle. This will affect the handling and stability of the vehicle. The lift force, L is quantified by the below equation

Lift force, $F_L = \frac{1}{2}\rho v^2 A C_L$

3. Generic Model Preparation

3.1 Generic Model of Vehicle

A Sedan type of car is selected, a generic model of a Sedan car is prepared with the help of CAD software.

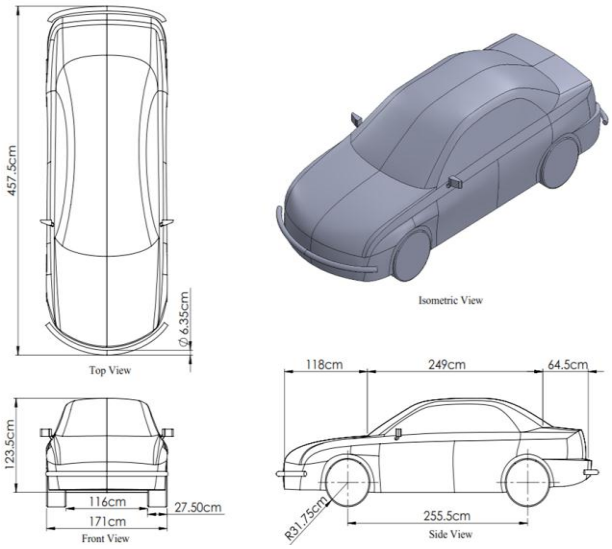

Fig.2: Generic model of the vehicle.

3.2 Generic Model of Spoiler

For the cambered shape, NREL's S821 airfoil is used.

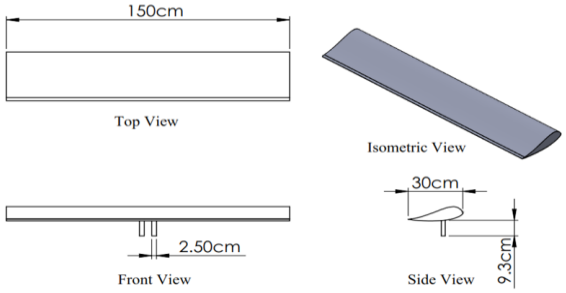

Fig. 3: Generic Model of Spoiler Assembly

The spoiler is assembled together with the car body and they are used for numerical analysis in CFD Software. These assemblies are shown in Fig. 4 below:

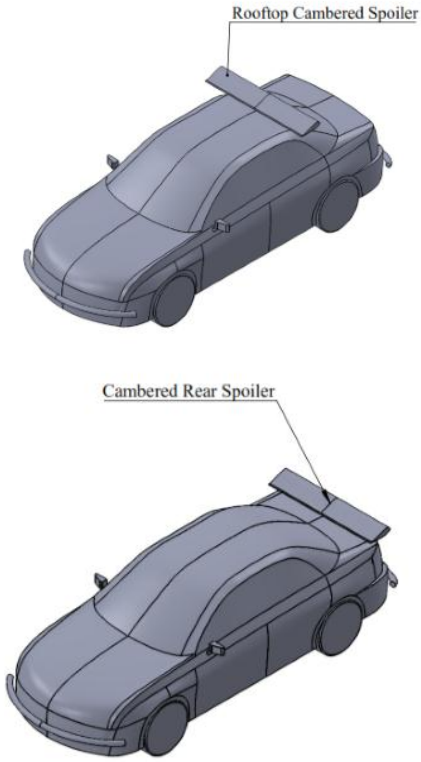

Fig.4: Car body assembly with different types of spoiler position.

3. Virtual Wind Tunnel and Vehicle Orientation

The vehicle with different spoiler positions shown above in Fig 4, have been orientated in the virtual wind tunnel one-by one to perform simulation for different conditions. A virtual air-box has been created around the 3D CAD model shown in the Fig. 5 below. More space has been left in the rear side of the vehicle model to capture the flow behavior mostly behind the vehicle [7].

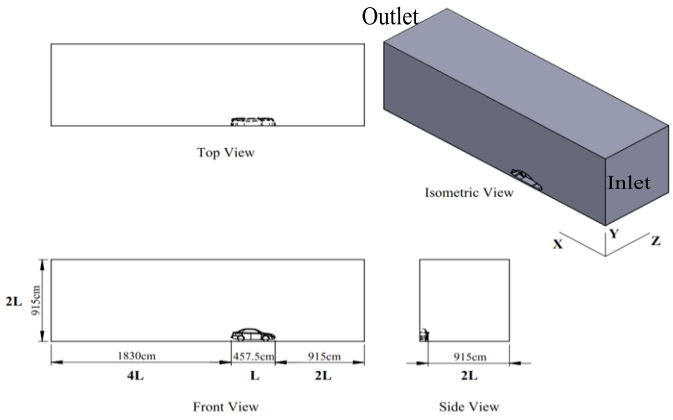

Fig.5: Virtual Wind Tunnel.

4. Mesh Generation

The triangular shape surface mesh was used due to its changing curves and bends. With the global mesh sizing setting, there is some curvature around the body. With some parameter sizing is done for getting better result [6]. To capture car surface phenomena more accurately, inflation layer is also added.

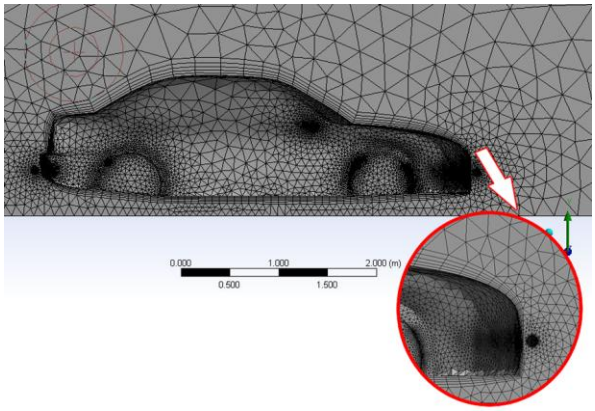

Fig.6: Mesh Generation.

This mesh is generated for the geometry with rooftop spoiler and rear spoiler.

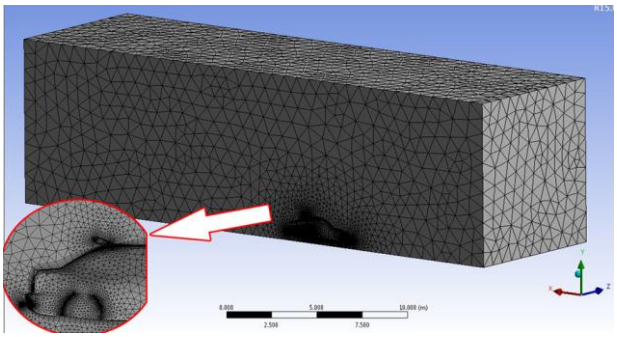

Fig.7: Vehicle with Cambered Roof Spoiler Mesh.

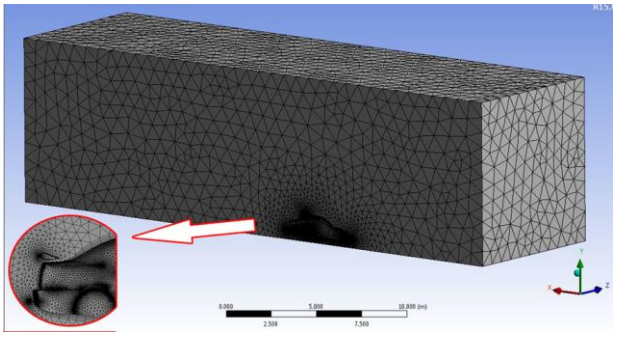

Fig.8: Vehicle with Cambered Rear Spoiler Mesh

5. Boundary Conditions

After the completion of required quality of mesh, it is transferred to the solver where respective boundary conditions are provided to solve the problem. The inlet of the wind tunnel is defined by velocity inlet and the outlet is defined by pressure outlet. The car body and road is defined as wall with no slip and surrounding boundary is defined as symmetry zone. Afterwards the solver is set according to the following conditions:

Table 1 Solver Settings

Simulation		
Turbulent Model	k-epsilon (2 eqn)	
Scheme	Coupled	
Velocity Inlet	Velocity Magnitude	15 m/sec, 30 m/sec, 45 m/sec, 60 m/sec
Pressure Outlet	Gauge pressure	0 Pascal

6. Results and Discussion

After simulation being completed, the numerical value of the coefficient of lift (C_l) and coefficient of drag (C_d) are obtained. Also result can be displayed in various contours like pressure contours, velocity contour, velocity vectors etc.

For each simulation process, first 100 iterations is carried out using First Order Upwind scheme. After that, Second Order Upwind scheme is applied. Each time, from monitoring section, Co-efficient of lift (C_l) and Co-efficient of drag (C_d) is calculated and plot is done against iteration. For some certain time, the C_l & C_d curve fluctuates in large amplitude with the increase of iteration. Then as simulation progresses, these fluctuations come to a steady state condition and that remarks the convergence of the whole simulation process.

Now, for all cases and for different speed set the obtained value of Co-efficient of lift (C_l) and Co-efficient of drag (C_d) are shown in graphical form in Fig.9 and Fig.10. And the percentage increase of C_d and C_l in all cases is given in Table 2 & 3.

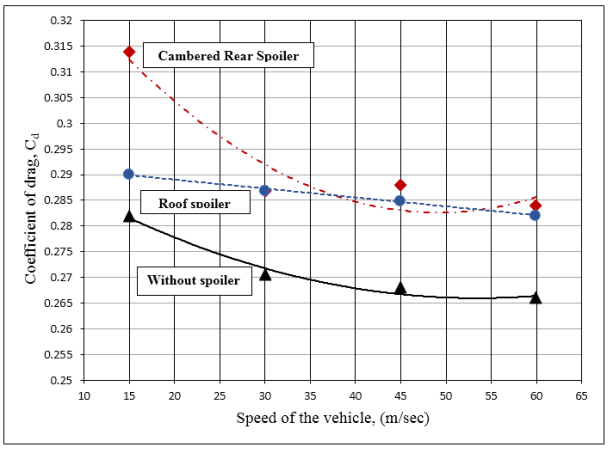

Fig.9: Variation of Coefficient of drag with Speed of the car.

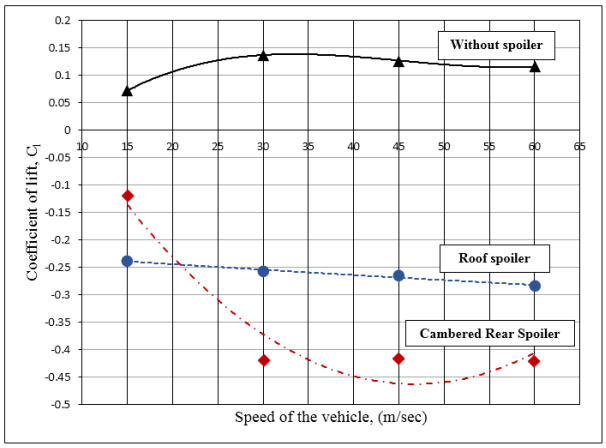

Fig.10: Variation of Coefficient of lift with Speed of the car.

Table 2: Percentage increase in Coefficient of drag for different case at different speed:

	Roof Spoiler	Cambered Spoiler
Speed (m/sec)	% increase C_d	% increase C_d
15	2.84	11.34
30	6.10	6.70
45	6.34	7.46
60	6.02	6.77

Table 3: Percentage increase in Coefficient of lift for different case at different speed:

	Roof Spoiler	Cambered Spoiler
Speed (m/sec)	% decrease C_l	% decrease C_l
15	76.72	62.63
30	65.23	75.32
45	67.68	76.61
60	70.93	78.40

Table 4: Forces acting on the vehicle at different speed:

Vehicle with Cambered Spoiler at Rear		
Speed	Down Force (N)	Drag Force (N)
15	16.83	43.68
30	232.56	159.687
45	520.76	360.53
60	936.93	632.04
Vehicle with Cambered Spoiler at Rooftop		
Speed	Down Force (N)	Drag Force (N)
15	33.10	40.35
30	143.0	159.70
45	333.0	356.77
60	630.0	627.60

Now, from the obtained data, various contours are generated and some are given bellow:

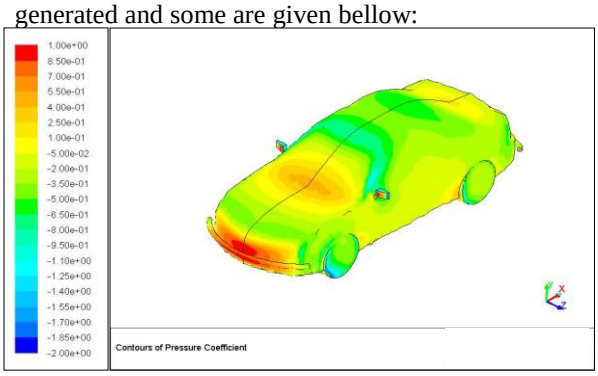

Fig.11: Pressure distribution on the car body for Vehicle model without spoiler at 45 m/sec.

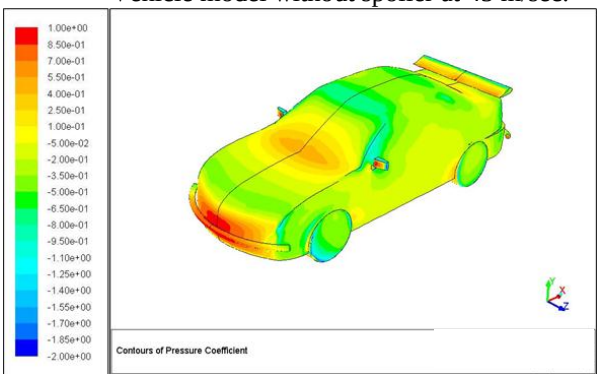

Fig.12: Pressure distribution on the car body for Vehicle model with rear spoiler at 45 m/sec.

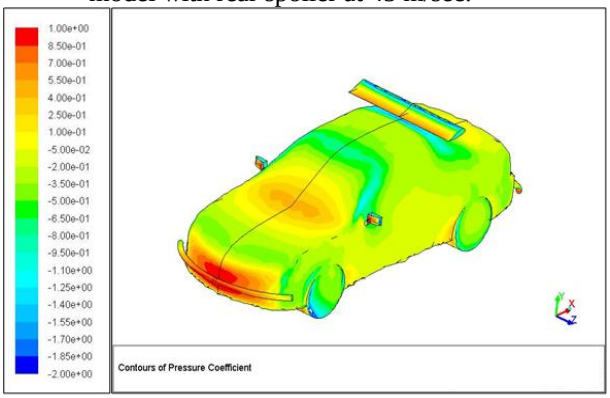

Fig.13: Pressure distribution on the car body for Vehicle model with rooftop spoiler at 45 m/sec.

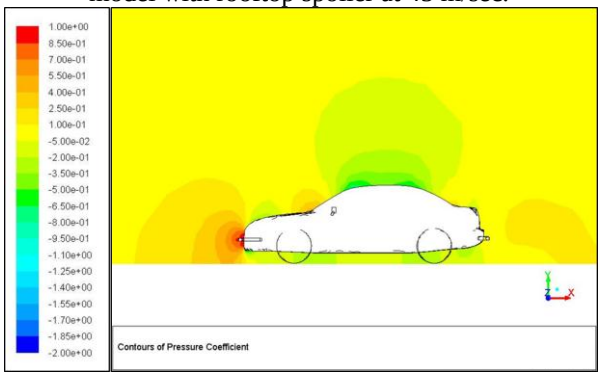

Fig.14: Pressure distribution in the symmetry plane for Vehicle model without spoiler 45 m/sec.

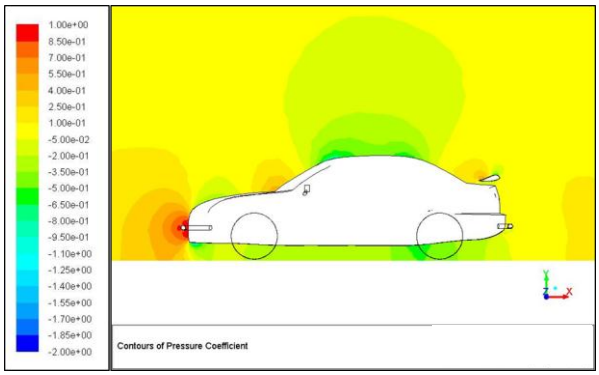

Fig.15: Pressure distribution in the symmetry plane for vehicle model with Cambered rear spoiler at 45 m/sec.

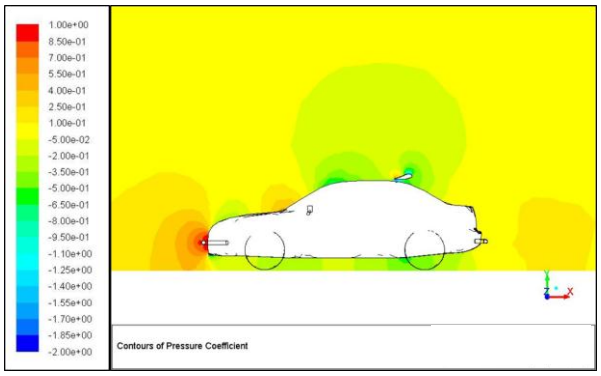

Fig.16: Pressure distribution in the symmetry plane for vehicle model with Cambered rooftop spoiler at 45 m/sec.

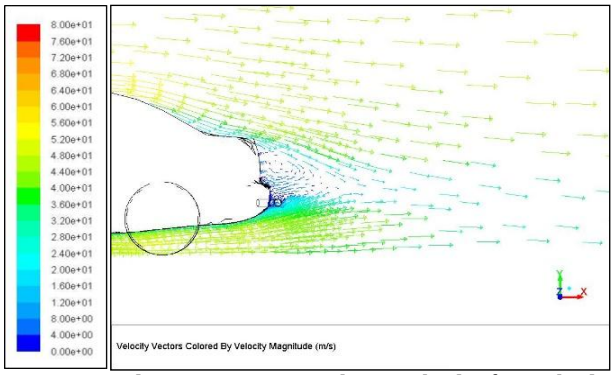

Fig.17: Velocity Vector on the car body for vehicle model without spoiler at 45 m/sec.

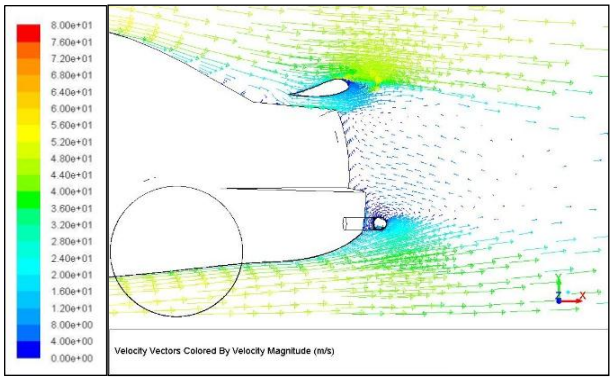

Fig.18: Velocity Vector on the car body for Vehicle model with Cambered rear spoiler at 45 m/sec.

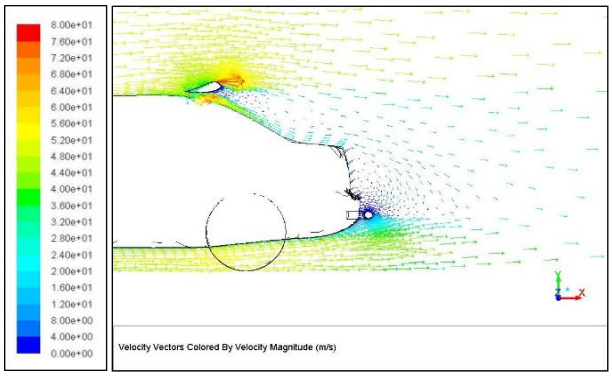

Fig.19: Velocity Vector on the car body for Vehicle model with Cambered rear spoiler at 45 m/sec.

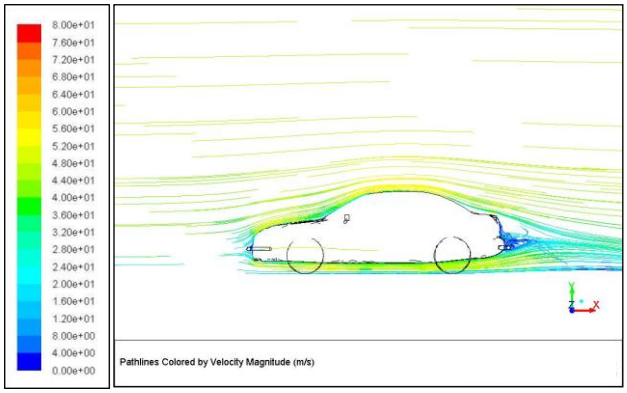

Fig.20: Streamlines of flow in the symmetry plane for vehicle model without spoiler at 45 m/sec.

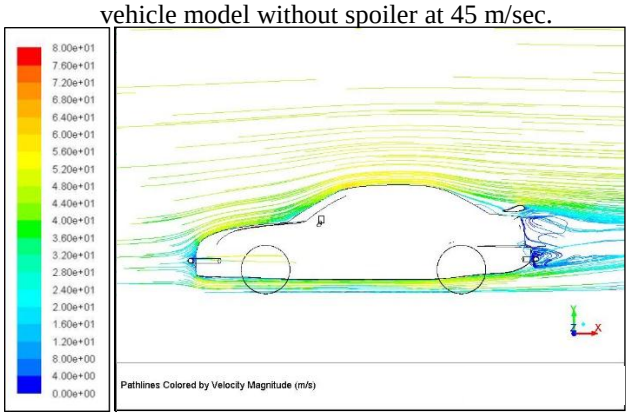

Fig.21: Streamlines of flow in the symmetry plane for vehicle model with Cambered rear spoiler at 45 m/sec.

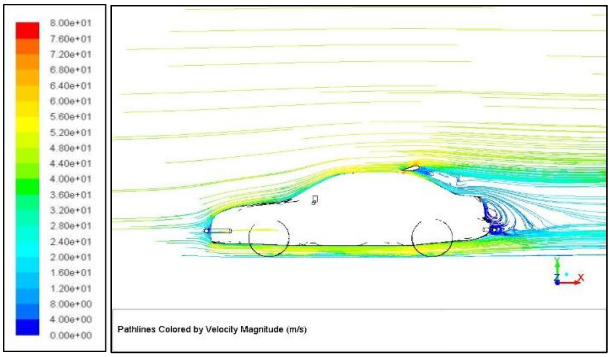

Fig.22: Streamlines of flow in the symmetry plane for vehicle model with Cambered rooftop spoiler at 45 m/sec.

From the obtained data and analysis, the following result can be produced to achieve the predetermined objectives of this investigation.

Fig. 9 shows the drag coefficient with the speed of the car and it is observed that the drag coefficient decreases with the increase of speed of the car. Again, it is observed that the drag shows higher value for the cambered spoiler at the rear location at 15 m/sec speed of the car whereas lower value at the speed of 45 m/sec. Fig.10 shows that the lift coefficient with the speed of the car and it is observed that the down force increases with the increase of speed of the car. Again, it is observed that the down force shows higher value for the cambered spoiler at the rear location at 45 m/sec speed of the car whereas lower value at the speed of 15 m/sec. From Table 4, for 45 m/sec speed, the acting drag force is about 159.0 N and lift force is 335.5 N. Now, from the analysis of rooftop spoiler and rear spoiler, it is found that for all cases, there is a significant change in down force. But, all of them have a slightly contribution to the change in drag force. But, taking into account the percentage increase in down force, the negligible increase of drag coefficient means the stability of the vehicle.

Fig. 15 shows, pressure contour at speed 45 m/sec for Cambered spoiler located at the rear of the car and Fig. 16 shows the pressure contour at same speed but located at the rooftop of the car. It is observed that the pressure increases more at the rear Cambered spoiler than at the rooftop Cambered spoiler. Fig. 17-19 shows the velocity vector at a speed 45 m/sec of the car for without spoiler, with Cambered spoiler at rooftop and rear of the car. It is observed that the two wakes developed, one behind the spoiler and other rear of the car for spoiler at rooftop. But for spoiler at rear of the car a single wake is developed at the rear of the car, which is away from the car body. Similar phenomena observed from Fig. 20-22, which show the streamlines at a speed 45 m/sec of the car.

Again, as for the consideration of the position of the spoiler on the vehicle, it is observed that the drag force for both the cases is same. But down force for Cambered rooftop spoiler is about half of the down force generated by the Cambered rear spoiler. It is observed from the Table 4 that at a speed 45 m/sec, 333N down force is produced in Cambered roof spoiler whereas Cambered rear spoiler produces about 520.76N down force. So, for better road stability and traction control, it is effective to use Cambered spoiler at the rear of the vehicle.

7. Conclusion

The above investigation shows that the location of Cambered spoiler at the rear of the car produces more down force than at the rooftop of the car. So, for the good stability of the vehicle, rear Cambered spoiler is the best choice than rooftop Cambered spoiler.

NOMENCLATURE

ρ : Density
υ : Viscosity
A : Projected area of the vehicle on the inlet surface.
F_L : Lift Force
F_D : Drag Force
C_d : Co efficient of drag
C_l : Co efficient of lift
V : Velocity of the flow

REFERENCES

[1] Chainani. A, Perera. N, "CFD Investigation of Airflow on a Model Radio Control Race Car', Proceedings of the *World Congress on Engineering* 2008, Vol II WCE 2008, July 2 - 4, 2008, London.

[2] Xu-xia Hu, Eric T.T. Wong, "A Numerical Study on Rear-spoiler of Passenger Vehicle", *World Academy of Science, Engineering and Technology*,Vol 5, No 9, Year 2011.

[3] W.Stapleford, "Aerodynamic Improvements to the Body and Cooling System of a typical Small Saloon Car", *Journal of Wind Engineering & Industrial Aerodynamics*, Vol. 9, 1981 pp. 63-75.

[4] http://en.wikipedia.org/wiki/Continuity_equation

[5] http://en.wikipedia.org/wiki/Navier%E2%80%93Stokes_equations

[6] "Lanfrit Marco, Best Practice Guidelines for Handling Automotive External Aerodynamics with FLUENT"

[7] W.Kieffer, S.Moujaes, N.Armbya; "CFD study of section characteristics of Formula Mazda race car wings".

ICMIEE-PI-140393

Thermal Performance of a New Residential House Wall System

Fayez Aldawi [1], *Firoz Alam* [2,*] , *Harun Chowdhury* [2]
[1] Department of Mechanical Engineering and Industrial Engineering, Yanbu Industrial College, Yanbu, SAUDI ARABIA
[2] School of Aerospace, Mechanical and Manufacturing Engineering, RMIT University, Melbourne, AUSTRALIA

ABSTRACT
The residential housing sector consumes a significant amount of fossil fuel energy and thereby the sector generates a large percentage of greenhouse gas emissions that contribute to global warming and climate change. At present, approximately 40% of the total household energy used is required for space heating/cooling and a substantial amount of that energy is lost through the house walls. Additionally, the floor space area and volumetric dimension of modern residential houses are increasing at a constant rate in most developed countries including Australia. This additional space also requires energy for heating and cooling. Therefore, the energy consumption for heating and cooling and greenhouse gas emissions will be increasing rapidly. A continuous upward energy consumption trend in residential housing sector worldwide will continue for years to come unless energy efficient and carbon neutral house wall systems are developed. One of the biggest challenges is to develop a smart house wall system made of thermal mass and insulation materials that can provide reduced energy needs for on-going heating and cooling with lower carbon footprint as most house wall construction materials are very energy intensive and have large carbon footprints. In order to develop a new energy smart house wall system, a study has been undertaken on thermal performance of two house wall systems (one is currently used conventional brick veneer house wall and other is an alternative house wall). The thermal performance (heat gain or loss through the wall) has been determined using computational modelling and experimental measurements. The economic analysis of both house wall systems has also been carried out. The effects of various climate conditions on these two house wall systems have also been determined. The findings indicate that the new house wall system provides better thermal efficiency than that of currently used conventional house wall.

Keywords: House wall system, thermal performance, energy efficiency, thermal mass, insulation material.

1. Introduction
The expansion of global economy and population growth has led to the expansion of cities and urbanisation. This expansion has dramatically increased not only the demand for new buildings and houses but also energy need. For example, in 2020, the energy consumption in the Australian residential house sector will be almost 467 PJ compared to 299 PJ in 1990 which means the demand will increase by over 50%. The number of residential houses is expected to be around 10 million in 2020 compared to 6 million in 1990. In most developed countries including Australia, the demand for residential buildings has been rapidly increasing due to population growth [1, 2]. More buildings and houses need more energy. Fig 1a illustrates the increasing trend for the Australian housing sector energy consumption for coming years. Additionally, the average floor space of new Australian residential houses is increasing progressively. As a result, the energy consumption is also increasing for the additional space heating and cooling. This additional energy consumption leads to higher CO_2 emissions (see Fig 1b) [3].

Each residential household consumes nearly 40% of the total energy for ongoing heating and cooling as shown in Fig. 2. Therefore, heating and cooling are considered to be an important factor for the reduction of energy consumption. Governments and regulatory authorise in many countries including Australia have formulated policies and enacted laws to improve energy efficiency in the residential housing sector [4, 5].

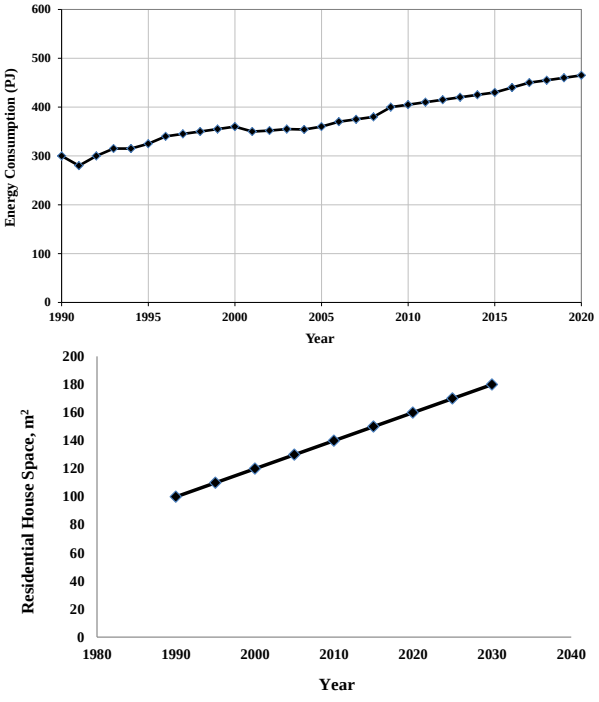

Fig.1 (a) Australian housing sector energy consumption; (b) residential house space increasing

* Corresponding author. Tel.: +61 3 9925 6103
E-mail address: firoz.alam@rmit.edu.au

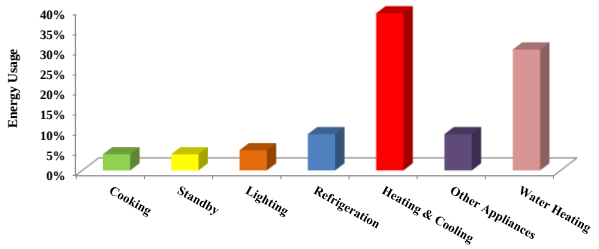

Fig.2 Australian household energy usages at residential buildings

Many researchers have investigated sustainable house construction systems using various wall materials, but scant information is available for zero carbon wall structure. The present state of knowledge is still inadequate for such a treatment because most researchers in the past have focused on energy savings in the building operation. Researchers paid little focus on energy saving by improving house construction systems using smart materials [6-10]. In this study, we have undertaken thermal performance modelling of two residential house wall systems: a conventionally used house wall system (namely brick veneer) and a non-conventional house wall system. The thermal performance modelling was conducted using commercially available software.

2. Energy load and climate zone

2.1 Energy loads for Australian localities

According to the state and territory government regulations since 2008, all the new residential houses must comply with certain minimum energy consumption measured against a star rating for ongoing heating and cooling. Australia's 69 micro climate zones have been rated with a star rating for their ongoing needs for heating and cooling. These scale ratings are called Star Energy Rating at a scale of 0 to 10. For example, to comply with 6 star energy rating, the residential house located in Melbourne metropolitan should not require more than 114 MJ/m² per year for the space heating and cooling [4]. Fig 3 illustrates the star energy rating for the required heating and cooling energy of Australian cities [4].

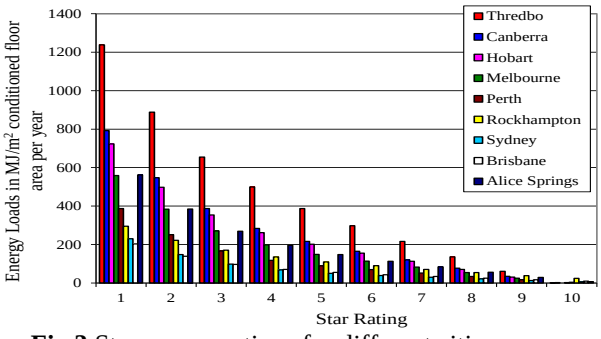

Fig.3 Star energy ratings for different cities across Australia

2.2 Australian climate zones

The climate in Australia varies significantly starting from arid, middle, tropical and subtropical zones. Australian climate zones are classified into six main climate zones based on climate conditions, metrological data and solar radiation. However, for better representation and energy consumption estimation, the entire country has been subdivided into 69 micro climate zones with a certain amount of energy required for heating and cooling. The energy requirement for the conventional and the new house wall systems were modelled for 6 major cities. These cities are Melbourne, Brisbane, Darwin, Hobart, Adelaide and Sydney. These cities experience moderate, tropical, subtropical, arid climates and humid climates (see Table 1).

Table 1 Climatic weather zones for different cities and states in Australia

City	State	Weather description
Melbourne	VIC	Mid warm to warm summer, cold winter
Brisbane	QLD	Warm humid summer
Darwin	NT	Hot humid summer
Hobart	TAS	Mid warm summer
Adelaide	SA	Warm summer, cool winter
Sydney	NSW	Warm summer, mid cool winter

2.3 Importance of thermal masses

Thermal mass of a house envelope minimizes the effect of temperature fluctuations. Generally high density materials have higher thermal masses. For example, concrete and bricks have higher thermal mass as they have higher specific density and absorb and keep heat during day or night and release it gradually in 7-8 hours. High thermal mass materials take a longer time to release the heat content once the heat source is removed. On the other hand, lightweight materials with lower specific density such as timber or weatherboard have low thermal mass requiring a shorter time to release the heat content. It takes less time (2-3 hours) to store or release heat as shown in Fig 4. Therefore, the appropriate of high thermal masses for the house wall system can provide a comfortable house environment and reduce energy required for heating and cooling. In this study, the new house wall possesses higher thermal masses than the conventional brick veneer house wall system as the new house wall system is made of insulated reinforced concrete [12]. Table 2 shows thermal properties for common building materials used in Australia.

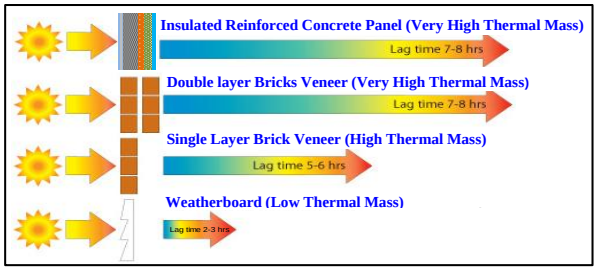

Fig.4 Heat flow through different house envelopes' thermal masses

Table 2 Building materials thermal properties

Material	Volumetric heat capacity (kJ/m³.K)	Thermal conductivity (W/m.K)
Concrete	2112	0.80
Glass	2108	0.65
Brick veneer	1484	0.80
Timber (hard)	1414	0.15
Render	900	0.25
Timber (soft)	1057	0.13
Plasterboard	924	0.25
Glass fibre batt	10.6	0.034
Polystyrene	5.5	0.035

3. Thermal performance modelling procedure

3.1 Description of simulated house

The house selected for this study is an average size residential house built in Australia. The house has three bedrooms with the total floor area and physical volume of approximately 161.33 m² and 460 m3 respectively. The house consists of living or dining area, kitchen, three bedrooms, two bathrooms, an alfresco area and a laundry. The total area of external walls, windows, floors and roof are 113 m², 32.9 m², 100.2 m² and 124.9 m² respectively. The roof slope angle is around 20º, a widely used roof inclination angle for most houses built in Australia. Windows are standard in dimensions and consist of a single glass and aluminum frame. Fig 5 illustrates a plan view of the house [13].

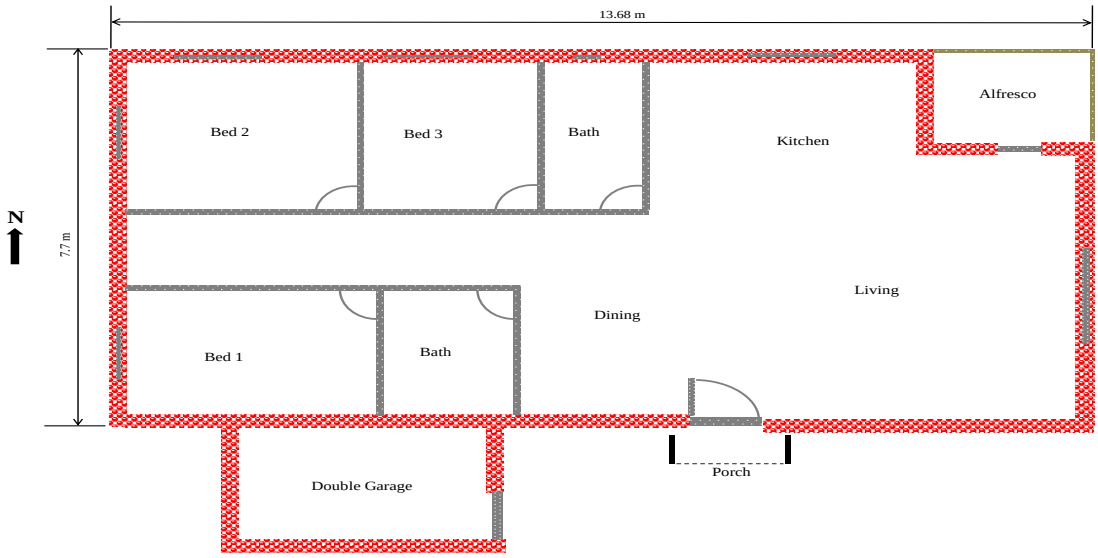

Fig.5 House plan view

The foundation of both house envelopes is the reinforced concrete and classified as "H class concrete slab". Generally there are two types of reinforced concrete foundations popularly used in Australia. The conventional variety is generally made of reinforced concrete. However, recently a waffle concrete foundation is becoming more popular due to its better insulation properties and lower construction costs [14]. This study considered the reinforced concrete foundation only. Fig 6 shows a typical reinforced concrete floor foundation used for both houses.

Fig.6 Slab on ground

3.2 Energy performance simulation software

The most commonly used thermal performance simulation software in Australian all states and territories is AccuRate software. It was developed by the Commonwealth Scientific and Industrial Research Organization (CSIRO). It is a significantly improved version of the first generation software known as the National House Energy Rating Scheme (NatHERS). It is widely used for the simulation of house energy performance. The simulation also identifies the house energy needs for ongoing heating and cooling on a scale rating of 1 to 10. The higher the star rating, the better it is for energy saving. The software has a large library of physical and thermal data for a wide range of construction materials, and weather data for different climate zones across Australia. The software contains all functions and features of heat transfer equations that are required for all 3 modes of heat transfer (conduction, convection and radiation). It also incorporates the effects of natural ventilation in the house energy rating [15]. The physical data for the non-conventional and conventional house wall systems was fed into the AccuRate software to model the thermal performance.

4. Wall system

4.1 Conventional house wall system

The brick veneer house wall system consists of 110 mm brick veneer and 40 mm air gap from outside. The 90 mm timber frame structure is filled with 2 mm insulation foil. Fibreglass insulation with thickness of 59 mm is inserted in between the external timber structure and the internal plaster board (10mm thick.) The floor foundation is made of 100 mm thick reinforced concrete. The roof structure is made of timber with terracotta/concrete tiles with an angle around 20°. Figs 7 a & b illustrates a typical exterior brick veneer house under construction in an outer Melbourne suburb.

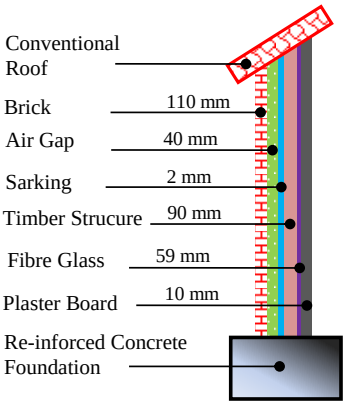

(a)

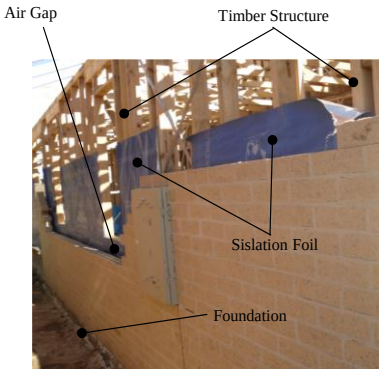

(b)

Fig.7 (a) Schematic of house wall; (b) conventional house wall systems near Melbourne

4.2 New house wall system

The new house wall system consists of 10 mm render, a layer of reinforced concrete panel with 150 mm thickness and standard 59 mm polystyrene insulation. The interior part is made of 10 mm plaster board. The physical data for the new and conventional house wall systems was fed into the AccuRate software to model the thermal performance. The schematic of the new wall system is shown in Fig 8. Table 3 provides additional details for both house wall materials and their thicknesses [13].

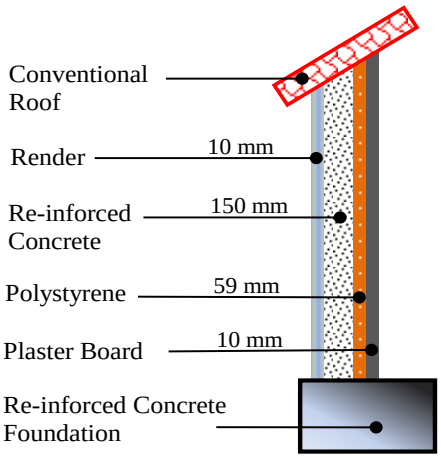

Fig.8. New house wall system

5. Thermal Performance Modelling Results

The two residential house wall systems (conventional and new wall systems) were modelled using AccuRate for 6 cities located in different climate zones. The results obtained show the thermal performances of two house wall systems. The roof structure, foundations, doors and internal walls were all kept constant for both house wall systems. The total energy requirement for the conventional and new house wall systems is shown in Fig 9. With the conventional system, Darwin has the highest total energy needs for the heating and cooling while Brisbane has the lowest energy need. Adelaide and Melbourne have similar energy requirements for the ongoing heating and cooling. Hobart's energy load is in between of other cities. On the other hand, the new house wall system used in this study needs significantly less energy for all six cities. A notably less energy (~ 30%) for the heating and cooling using the new house wall system (envelope) is required for the city of Darwin. Likewise, the heating and cooling energy reductions for other four cities were 28%, 20%, 14%, 20% and 19% (Adelaide, Melbourne, Hobart, Brisbane and Sydney) respectively. Energy required for heating and cooling, and star rating for all six cities are shown in Tables 4 and 5.

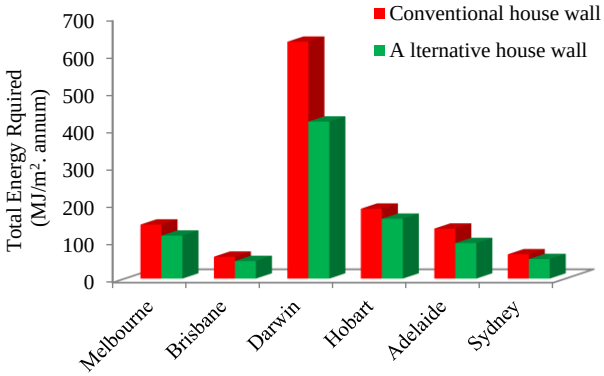

Fig.9 Total energy required for on-going heating and cooling for selected six cities

Table 3 Comparison between conventional and new house envelopes

No.	Items	Conventional house envelope	Thickness (mm)	New house envelope	Thickness (mm)
1	External Wall	Brick veneer (single)	110	Render	10
		Air gap	50	Reinforced concrete panel	150
		Insulation foil	2	Insulation polystyrene	59
		Timber structure	90	Single glass window	3
2	Internal Wall	Plaster board	10	Plaster board	10
3	Ground/Floor	Reinforced concrete slab	100	Reinforced concrete slab	100
4	Roof	Timber with concrete tiles (20°)	90+20	Timber with concrete tiles (20°)	90+20
		Insulation batts + plaster board	20+10	Insulation batts + plaster board	20+10

Table 4 Total energy required for conventional house wall system for selected Australian metropolitan cities

No.	City	State	Heating load MJ/m^2. annum	Cooling load MJ/m^2. annum	Total energy required MJ/m^2. annum	Star rating 0-10
1	Melbourne	VIC	107.2	37.3	144.5	5.1
2	Brisbane	QLD	4.3	54.3	58.6	4.7
3	Darwin	NT	0.0	633.5	633.5	2.1
4	Hobart	TAS	182.6	4.3	186.9	5.3
5	Adelaide	SA	45.3	88.4	133.7	4.8
6	Sydney	NSW	7.9	57.9	65.0	4.1

Table 5 Total energy required for new house wall system for selected Australian metropolitan cities

No.	City	State	Heating load MJ/m^2. annum	Cooling load MJ/m^2. annum	Total energy required MJ/m^2. annum	Star rating 0-10
1	Melbourne	VIC	91.1	33.3	115.0	5.7
2	Brisbane	QLD	2.5	55.0	47.0	4.8
3	Darwin	NT	0.0	423.0	420.0	4.7
4	Hobart	TAS	163	17.3	160.0	5.4
5	Adelaide	SA	37.6	62.5	95.0	5.8
6	Sydney	NSW	3.4	48.4	52.3	4.9

6. Conclusions

The paper presents a thermal performance modelling of two house wall systems (conventional and new) for six Australian cities. The study evaluated the total ongoing heating and cooling requirements using two wall systems and compared their energy performances. The following conclusions are drawn from the study:

- The new house wall system provides better thermal performance than the conventional wall systems for all six Australian cities.
- Using the new house wall system energy savings ranging from 14% to 33% various climate zones is achieved. This will reduce the greenhouse gas emission, enhance sustainable environment and energy security. However, further study is required to understand the full potential of the new house wall system.

The thermal performance of the conventional house wall system is poor as it needs more energy for ongoing heating and cooling. However, a retrofit with smart materials can improve its thermal performance.

REFERENCES

[1] F. Alam, A. Akbarzadeh, C. Dixon, T. Theos, 2010, Thermal performance of residential house envelopes, *proceedings of the International Conference on Mechanical, Industrial and Energy Engineering (ICMIEE2010)*, Paper MIE10-158, ISBN: 978-984-33-2300-2. Khulna, Bangladesh.

[2] Report on energy use in the Australian residential sector 1986-2020, 2008, Department of the Environment, Water, Heritage and the Arts, Commonwealth of Australia, Canberra.

[3] F. Alam, M. Khan, M. Rasul, 2008, Comparative study of residential household energy consumption in Australia and USA, *the International Journal of Mechanical Engineering and Materials Science*, Vol. 3 (2), pp 127-132.

[4] F. Alam, M. Rasul, W. Saman, T. Theos, M. Khan, A. Akbarzadeh, 2009, Residential house energy rating in Australia, *Central Region Engineering Conference (CREC)*, ISBN 1-921047-62-3, p 1-6, Rockhampton, Australia.

[5] A. Chowdhary, M. Rasul, M. Khan, F. Alam, 2010, Performance analysis of a novel building material

to achieve superior thermal comfort and energy efficiency in arid climate, *proceedings of the International Engineering Conference on Hot Arid Regions (IECHAR 2010)*, Al-Ahsa, Saudi Arabia.

[6] Y. Chen, A. Athienitis, K. Galal, 2010, Design and thermal performance of a BIPV/T system thermally coupled with a ventilated concrete slab in a low energy solar house: Part 1, BIPV/T system and house energy concept, Solar Energy, 84: 1892–1907.

[7] L. Zhu, R. Hurt, D. Boehm, 2010, Detailed energy saving performance analyses on thermal mass walls demonstrated in a zero energy house, *Energy and Buildings*, 41: 303–310.

[8] M. Kordjamshidi, S. King, 2009, Overcoming problems in house energy ratings in temperate climates: *A proposed new rating framework, Energy and Buildings*, 41: 125–132

[9] R. Judkoff, 2008. Increasing Building Energy Efficiency through Advances in Materials, National Renewable Energy Laboratory, *MRS Bulletin*, Vol. 33, p 449 454. USA.

[10] H. Tommerup, J. Rose, S. Svendsen, 2007, Energy-efficient house built according to the energy performance requirements introduced in Denmark, *Energy and Building*, Vol. 39, p 1123-1130.

[11] Australian climatic zones, Australian Government, Bureau of Metrology: http://www.bom.gov.au/climate/environ/travel/map.shtml, accessed April 04, 2012).

[12] K. Gregory, B. Moghtaderi, H. Sugo, A. Page, 2008, Effect of thermal mass on the thermal performance of various Australian residential constructions systems, *Energy and Buildings*, (40) 459-465.

[13] F. Aldawi, F. Alam, H. Moria, 2012, Energy Efficient House Wall System for Arid and Moderate Climatic Regions, Journal paper, accepted after peer review for *Yanbu Journal Engineering and Science* (YJES).

[14] Renovation robot, Australian house foundation, accessed on 15 April 2012, http://www.renovationrobot.com.au/foundations/housefoundations.html

[15] AccuRate Sustainability, Hearne Scientific Software Pty Ltd, technical software for professional, energy thermal performance for residential household.

ICMIEE-PI-140395

Fundamental Solution of 3D Transversely Isotropic Elastic Material

Md. Mazharul Islam[1], Mahesh Kumar Sah[1], Md. Sadekur Rahaman[1], Md. Sobur Ali[1], Md. Zahidul Islam[1]
[1] Undergraduate Student, Department of Mechanical Engineering,
Khulna University of Engineering & Technology, Khulna-9203, BANGLADESH

ABSTRACT
A transversely isotropic elastic material is one which physical properties are symmetric about an axis normal to a plane of isotropy. A large number of joints in advanced electronic devices are carried out with the application of these materials. In this paper, an expression of 3D transversely isotopic elastic material is derived. An algorithm of fundamental equation is developed to check the continuity at interface of bonded joint. The Green's function is used for the fundamental solution of three-dimensional transversely isotropic elastic material. Boundary conditions are applied at the interface of the bonded joint and continuity is checked at interface. The effect of displacements(u, v, w), normal stress$(\sigma_x, \sigma_y, \sigma_z)$, and shear stress $(\tau_{xy}, \tau_{yz}, \tau_{zx})$ with varying distance is analyzed. Finally, united solutions are provided which are suitable for all stable transversely isotropic and isotropic materials.

Keywords: Fundamental Solution, Transversely Isotropic, Bonded Joint, Green's Function

1. Introduction

Elastic material is one which can regain its shape and size after the force applied from that material. Fundamental solutions or Green's functions play an important role in both applied and theoretical studies on the mechanics of solids. Fundamental solutions can be used to construct many analytical solutions of practical problems when boundary conditions are imposed [1]. As a useful calculation approach in engineering science, the boundary element method has been greatly developed in recent years. One of the most important points in the theory of the boundary element method is the point force solution or Green's function [2]. Hu [3] obtained the fundamental solutions for an infinite transversely isotropic solid when $s_1 \neq s_2$, and Pan and Chou [4] also obtained the united solutions for an infinite transversely isotropic solid when $s_1 \neq s_2$ and $s_1 = s_2$, but with different forms of constants. M. S. Islam, H. Koguchi [5] analyzed the intensity of singular stress fields in three-dimensional transversely isotropic piezoelectric bonded joints. Elliott [6] obtained the solution for an infinite medium applied at a point force perpendicular to the plane of isotropy. Kroner [7] obtained the solution for an infinite solid applied at a point force parallel to the plane of isotropy. This paper present the simplest expression of displacement, shear stress and normal stress of 3D transversely isotropic elastic material and a united solution for transversely isotropic and isotropic material. Therefore, the purpose of this study is to check the continuity of 3D transversely isotropic elastic bi-material joints.

2.1 Basic equations

In the absence of body forces, the governing equation of three dimensional elastic materials is;

$$\sigma_{ij,j} = 0 \tag{1}$$

Where σ_{ij} is stress tensor. These equations are the elastic equilibrium equation. Constitutive relation for elastic material is expressed by Hooke's law;

$$\sigma_{ij} = c_{ijkl}\varepsilon_{kl} \tag{2}$$

Where, ε_{kl} is strain tensor, & c_{ijkl} is elastic constant for material. The elastic strain displacement in Cartesian coordinate $u_i(i = 1,2)$ are related to the strain by the following relation

$$\varepsilon_{ij} = \frac{1}{2}(u_{i,j-}u_{j,i}) \tag{3}$$

Where, $u_{i,j}$ is displacement vector. The characteristics equation of the transversely isotropic elastic material is obtained by solving the given equation.

* Corresponding author. Tel.: +88-01914007093
E-mail addresses: linconkuet2k9@gmail.com

$$C_{33}C_{44}s^4 - \left[C_{11}C_{33} + {C_{44}}^2 - (C_{13} + C_{44})^2\right]s^2 + C_{11}C_{44} = 0$$

Square root of the eigen-equation is denoted by S_1 , S_2 and S_3 is given as below,

$$S_1 = \sqrt{\frac{(\bar{C}_{13} - C_{13})(\bar{C}_{13} + C_{13} + 2C_{44})}{4C_{33}C_{44}}} + \sqrt{\frac{(\bar{C}_{13} + C_{13})(\bar{C}_{13} - C_{13} - 2C_{44})}{4C_{33}C_{44}}}$$

$$S_2 = \sqrt{\frac{(\bar{C}_{13} - C_{13})(\bar{C}_{13} + C_{13} + 2C_{44})}{4C_{33}C_{44}}} - \sqrt{\frac{(\bar{C}_{13} + C_{13})(\bar{C}_{13} - C_{13} - 2C_{44})}{4C_{33}C_{44}}}$$

$$S_3 = \sqrt{{C_{66}}/{C_{44}}} \qquad \left[\text{Where, } \bar{C}_{13} = \sqrt{C_{11}C_{33}}\right]$$

2.1 General Solutions:

The general solution for the governing equations of 3D transversely isotropic elasticity has been given by Hu.

When force acting on bonded material, the displacement equations u, v, w is given as follows at $s_1 \neq s_2$

$$u = \sum_{i=1}^{2} \frac{\partial \varphi_i}{\partial x} + \frac{\partial \varphi_3}{\partial y};\ v = \sum_{i=1}^{2} \frac{\partial \varphi_i}{\partial y} - \frac{\partial \varphi_3}{\partial x};\ w = \sum_{i=1}^{2} \alpha_i \frac{\partial \varphi_i}{\partial z_i}$$

where, $\alpha_1 = \dfrac{c_{11} - c_{44}s_1^2}{(c_{13} + c_{44})s_1}$ and $\alpha_2 = \dfrac{c_{11} - c_{44}s_2^2}{(c_{13} + c_{44})s_2}$

If φ is the displacement functions for transversely isotropic material then the normal and shear stress equation at $s_1 \neq s_2$ is given as follows;

$$\sigma_x = c_{66}\left[\sum_{i=1}^{2} k_{1i} \frac{\partial^2 \varphi_i}{\partial z_i^{\,2}} + 2\left(\sum_{i=1}^{2} \frac{\partial^2 \varphi_i}{\partial x^2} + \frac{\partial^2 \varphi_3}{\partial x \partial y}\right)\right]$$

$$\sigma_y = c_{66}\left[\sum_{i=1}^{2} k_{1i} \frac{\partial^2 \varphi_i}{\partial z_i^{\,2}} + 2\left(\sum_{i=1}^{2} \frac{\partial^2 \varphi_i}{\partial y^2} - \frac{\partial^2 \varphi_3}{\partial x \partial y}\right)\right]$$

$$\tau_{xy} = 2c_{66}\left(\sum_{i=1}^{2} \frac{\partial^2 \varphi_i}{\partial x \partial y} - \frac{\partial^2 \varphi_3}{\partial x^2} + \frac{\partial^2 \varphi_3}{\partial y^2}\right)$$

$$\tau_{zx} = \sum_{i=1}^{2} \omega_i \frac{\partial^2 \varphi_i}{\partial x \partial z_i} + \omega_3 \frac{\partial^2 \varphi_3}{\partial y \partial z_3}$$

$$\tau_{yz} = \sum_{i=1}^{2} \omega_i \frac{\partial^2 \varphi_i}{\partial y \partial z_i} - \omega_3 \frac{\partial^2 \varphi_3}{\partial x \partial z_3}$$

$$\sigma_z = c_{66} \sum_{i=1}^{2} k_{2i} \frac{\partial^2 \varphi_i}{\partial z_i^{\,2}} \qquad (4)$$

Where, $\xi_i = k_{1i}c_{66};\ \ \vartheta_i = k_{2i}c_{66};\ \ k_{3i} = (\alpha_i + s_i)/s_3^2$

$k_{2i} = (c_{33}\alpha_i s_i - c_{13})/c_{66};\ \ k_{1i} = (c_{13}\alpha_i s_i - c_{12})/c_{66}$

$\omega_i = k_{3i}c_{66}\ ;\ \ \omega_3 = c_{44}s_3$; [Where, $i = 1,2$]

3. Fundamental Solution:

At the interface of the bonded joint consisting of two transversely isotropic material is such that the property of the upper material is equal to that of the property of the lower material. Fundamental solution of transversely isotropic elastic material at the interface of the bonded joint when point force applied at a distance h above the interface in x-direction are as follows:

$$\varphi_i = \frac{D_i x}{\bar{R}_{ii} + s_i|z-h|} + \sum_{j=1}^{2} \frac{D_{ij} x}{R_{ij} + z_{ij}}$$

$$\varphi_3 = \frac{D_3 y}{\bar{R}_{33} + s_3|z-h|} + \frac{D_{33} y}{R_{33} + z_{33}}$$

$\bar{z}_{ii} = z_{ii} = s_i(z-h)\ ;\ \ z_{ij} = z_i + h_j = s_i z + s_j h$

$\bar{z}_{33} = z_{33} = s_3(z-h)$

$$\bar{R}_{ii} = \sqrt{(x^2 + y^2) + {s_i}^2(z-h)^2}$$

$$R_{ij} = \sqrt{(x^2 + y^2) + \left(z_i + h_j\right)^2}$$

$$\bar{R}_{ii}^{\ *} = \bar{R}_{ii} + s_i|z-h|;\ \ R_{ij}^{\ *} = (R_{ij} + z_{ij})$$

$$R_{33} = \sqrt{r^2 + {z_{33}}^2};\ \ \bar{R}_{33} = \sqrt{r^2 + {\bar{z}_{33}}^2}$$

$$\bar{R}_{33} = R_{33} = \sqrt{(x^2 + y^2) + s_3^2(z-h)^2}$$

$$D_1 = \frac{s_1(c_{11} - c_{44}s_2^2)T}{4\pi c_{11}c_{44}(s_1^2 - s_2^2)};\ \ D_2 = -\frac{s_2(c_{11} - c_{44}s_1^2)T}{4\pi c_{11}c_{44}(s_1^2 - s_2^2)}$$

$$D_3 = \frac{T}{4\pi c_{44}s_3};\ A_1 = -A_2 = \frac{(c_{13} + c_{44})T}{4\pi c_{33}c_{44}(s_2^2 - s_1^2)}$$

Where, φ_i & φ_3 are displacement functions and A_i, D_i, $R_{ij}, \bar{R}_{ii}, R_{33}, \bar{z}_{ii}, z_{ij}$ & z_{33} are known constants.

$$u = \sum_{i=1}^{2}\left[D_i\left(\frac{1}{\bar{R}_{ii}^{\ *}} - \frac{x^2}{\bar{R}_{ii}\bar{R}_{ii}^{\ *2}}\right) + \sum_{j=1}^{2} D_{ij}\left(\frac{1}{R_{ij}^{\ *}} - \frac{x^2}{R_{ij}R_{ij}^{\ *2}}\right)\right]$$
$$+\left[D_3\left(\frac{1}{\bar{R}_{33}^{\ *}} - \frac{y^2}{\bar{R}_{33}\bar{R}_{33}^{\ *2}}\right) + D_{33}\left(\frac{1}{R_{33}^{\ *}} - \frac{y^2}{R_{33}R_{33}^{\ *2}}\right)\right] \qquad (5)$$

$$v = -xy\left[\sum_{i=1}^{2}\left\{\frac{D_i}{\bar{R}_{ii}\bar{R}_{ii}^{\ *2}} + \sum_{j=1}^{2}\frac{D_{ij}}{R_{ij}R_{ij}^{\ *2}}\right\} - \left\{\frac{D_3}{\bar{R}_{33}\bar{R}_{33}^{\ *2}} + \frac{D_{33}}{R_{33}R_{33}^{\ *2}}\right\}\right] \qquad (6)$$

$$w = -x\sum_{i=1}^{2}\alpha_i\left[sign(z-h)\frac{D_i}{\bar{R}_{ii}\bar{R}_{ii}^{\ *}} + \sum_{j=1}^{2}\frac{D_{ij}}{R_{ij}R_{ij}^{\ *}}\right] \qquad (7)$$

$$\sigma_x = \sum_{i=1}^{2}\xi_i x\left[\left(\frac{D_i}{\bar{R}_{ii}^3} + \sum_{j=1}^{2}\frac{D_{ij}}{R_{ij}^3}\right)\right.$$
$$-2C_{66}\left\{\sum_{i=1}^{2}\left\{D_i\left(\frac{3}{\bar{R}_{ii}\bar{R}_{ii}^{\ *2}} - \frac{2x^2}{\bar{R}_{ii}^2\bar{R}_{ii}^{\ *3}} - \frac{x^2}{\bar{R}_{ii}^3\bar{R}_{ii}^{\ *2}}\right)\right.\right.$$
$$\left.+\sum_{j=1}^{2}D_{ij}\left(\frac{3}{R_{ij}R_{ij}^{\ *2}} - \frac{2x^2}{R_{ij}^2R_{ij}^{\ *3}} - \frac{x^2}{R_{ij}^3R_{ij}^{\ *2}}\right)\right\}$$
$$-D_3\left\{\left(\frac{1}{\bar{R}_{33}\bar{R}_{33}^{\ *2}} - \frac{2y^2}{\bar{R}_{33}^2\bar{R}_{33}^{\ *3}} - \frac{y^2}{\bar{R}_{33}^3\bar{R}_{33}^{\ *2}}\right)\right.$$
$$\left.\left.\left.+D_{33}\left(\frac{1}{R_{33}R_{33}^{\ *2}} - \frac{2y^2}{R_{33}^2R_{33}^{\ *3}} - \frac{y^2}{R_{33}^3R_{33}^{\ *2}}\right)\right\}\right\}\right] \qquad (8)$$

$$\sigma_y = \sum_{i=1}^{2}\xi_i y\left[\left(\frac{D_i}{\bar{R}_{ii}^3} + \sum_{j=1}^{2}\frac{D_{ij}}{R_{ij}^3}\right)\right.$$
$$-2C_{66}\left\{\sum_{i=1}^{2}\left\{D_i\left(\frac{1}{\bar{R}_{ii}\bar{R}_{ii}^{\ *2}} - \frac{2y^2}{\bar{R}_{ii}^2\bar{R}_{ii}^{\ *3}} - \frac{y^2}{\bar{R}_{ii}^3\bar{R}_{ii}^{\ *2}}\right)\right.\right.$$

$$+\sum_{j=1}^{2} D_{ij}\left(\frac{1}{R_{ij}{R_{ij}}^{*2}}-\frac{2y^2}{R_{ij}^2{R_{ij}}^{*3}}-\frac{y^2}{R_{ij}^3{R_{ij}}^{*2}}\right)\Bigg\}$$

$$-D_3\left\{\left(\frac{1}{\bar{R}_{33}{\bar{R}_{33}}^{*2}}-\frac{2y^2}{\bar{R}_{33}^2{\bar{R}_{33}}^{*3}}-\frac{y^2}{\bar{R}_{33}^3{\bar{R}_{33}}^{*2}}\right)\right.$$

$$\left.+D_{33}\left(\frac{1}{R_{33}{R_{33}}^{*2}}-\frac{2y^2}{R_{33}^2{R_{33}}^{*3}}-\frac{y^2}{R_{33}^3{R_{33}}^{*2}}\right)\right\}\Bigg\} \quad (9)$$

$$\tau_{xy}=2c_{66}y\left[\sum_{i=1}^{2}\left\{D_i\left(\frac{2x^2}{\bar{R}_{ii}^2{\bar{R}_{ii}}^{*3}}+\frac{x^2}{\bar{R}_{ii}^3{\bar{R}_{ii}}^{*2}}-\frac{1}{\bar{R}_{ii}{\bar{R}_{ii}}^{*2}}\right)\right.\right.$$

$$\left.+\sum_{j=1}^{2} D_{ij}\left(\frac{2x^2}{{R_{ij}}^2{R_{ij}}^{*3}}+\frac{x^2}{{R_{ij}}^3{R_{ij}}^{*2}}-\frac{1}{R_{ij}{R_{ij}}^{*2}}\right)\right\}$$

$$+\left\{D_3\left(\frac{4x^2}{{\bar{R}_{33}}^2{\bar{R}_{33}}^{*3}}+\frac{2x^2}{{\bar{R}_{33}}^3{\bar{R}_{33}}^{*2}}+\frac{2}{\bar{R}_{33}{\bar{R}_{33}}^{*2}}-\frac{1}{{\bar{R}_{33}}^3}\right)\right.$$

$$\left.\left.+D_{33}\left(\frac{4x^2}{{R_{33}}^2{R_{33}}^{*3}}+\frac{2x^2}{{R_{33}}^3{R_{33}}^{*2}}+\frac{1}{R_{33}{R_{33}}^{*2}}-\frac{1}{{R_{33}}^3}\right)\right\}\right] \quad (10)$$

$$\tau_{xz}=-\sum_{i=1}^{2}\omega_i\left[sign(z-h)D_i\left\{\frac{1}{\bar{R}_{ii}{\bar{R}_{ii}}^{*}}-\frac{x^2}{{\bar{R}_{ii}}^3{\bar{R}_{ii}}^{*}}\right.\right.$$

$$\left.-\frac{x^2}{{\bar{R}_{ii}}^2{\bar{R}_{ii}}^{*2}}\right\}+\sum_{j=1}^{2} D_{ij}\left\{\frac{1}{R_{ij}{R_{ij}}^{*}}-\frac{x^2}{{R_{ij}}^3{R_{ij}}^{*}}-\frac{x^2}{{R_{ij}}^2{R_{ij}}^{*2}}\right\}\Bigg]$$

$$-\omega_3\left[D_3 sign(z-h)\left\{\frac{1}{\bar{R}_{33}{\bar{R}_{33}}^{*}}-\frac{y^2}{{\bar{R}_{33}}^3{\bar{R}_{33}}^{*}}-\frac{y^2}{{\bar{R}_{33}}^2{\bar{R}_{33}}^{*2}}\right\}\right.$$

$$\left.+D_{33}\left\{\frac{1}{R_{33}{R_{33}}^{*}}-\frac{y^2}{{R_{33}}^3{R_{33}}^{*}}-\frac{y^2}{{R_{33}}^2{R_{33}}^{*2}}\right\}\right] \quad (11)$$

$$\tau_{yz}=xy\sum_{i=1}^{2}\omega_i\left[D_i sin(z-h)\left\{\frac{1}{{\bar{R}_{ii}}^3{\bar{R}_{ii}}^{*}}+\frac{1}{{\bar{R}_{ii}}^2{\bar{R}_{ii}}^{*2}}\right\}\right.$$

$$\left.+\sum_{j=1}^{2} D_{ij}\left\{\frac{1}{{R_{ij}}^3{R_{ij}}^{*}}+\frac{1}{{R_{ij}}^2{R_{ij}}^{*2}}\right\}\right]$$

$$-\omega_3 xy\left[D_3\ sin(z-h)\left\{\frac{1}{(\bar{R}_{33})^3{\bar{R}_{33}}^{*}}+\frac{1}{(\bar{R}_{33})^2{\bar{R}_{33}}^{*2}}\right\}\right.$$

$$\left.+D_{33}\left\{\frac{1}{{R_{33}}^3{R_{33}}^{*}}+\frac{1}{{R_{33}}^2{R_{33}}^{*2}}\right\}\right] \quad (12)$$

$$\sigma_z=\sum_{i=1}^{2}\vartheta_i x\left[\frac{D_i}{\bar{R}_{ii}^3}+\sum_{j=1}^{2}\frac{D_{ij}}{R_{ij}^3}\right] \quad (13)$$

Fundamental solutions of 3D transversely isotropic elastic material at the interface of the bonded joint when point force applied at a distance h above the interface in z-direction are as follows:

$$\varphi_i=A_i sign(z-h)\ln(\bar{R}_{ii}+s_i|z-h|)+\sum_{i=1}^{2}A_{ij}\,ln(R_{ij}+z_{ij})$$

$$\varphi_3=0$$

$$u=\sum_{i=1}^{2}\left[sign(z-h)\frac{A_i x}{\bar{R}_{ii}{\bar{R}_{ii}}^{*}}+\sum_{j=1}^{2}\frac{A_{ij}x}{R_{ij}{R_{ij}}^{*}}\right] \quad (14)$$

$$v=\sum_{i=1}^{2}\left[sign(z-h)\frac{A_i y}{\bar{R}_{ii}{\bar{R}_{ii}}^{*}}+\sum_{j=1}^{2}\frac{A_{ij}y}{R_{ij}{R_{ij}}^{*}}\right] \quad (15)$$

$$w=\sum_{i=1}^{2}\alpha_i\left[\frac{A_i}{\bar{R}_{ii}}+\sum_{j=1}^{2}\frac{A_{ij}}{R_{ij}}\right] \quad (16)$$

$$\tau_{xy}=2c_{66}\,xy\sum_{i=1}^{2}\left[A_i sign(z-h)\left\{\frac{1}{{\bar{R}_{ii}}^3{\bar{R}_{ii}}^{*}}+\frac{1}{{\bar{R}_{ii}}^2{\bar{R}_{ii}}^{*2}}\right\}\right.$$

$$\left.-\sum_{j=1}^{2}A_{ij}\left\{\frac{1}{{R_{ij}}^3{R_{ij}}^{*}}+\frac{1}{{R_{ij}}^2{R_{ij}}^{*2}}\right\}\right] \quad (17)$$

$$\tau_{yz}=-\omega_i y\sum_{i=1}^{2}\left[\frac{A_i}{{\bar{R}_{ii}}^3}-\sum_{j=1}^{2}\frac{A_{ij}y}{{R_{ij}}^3}\right] \quad (18)$$

$$\tau_{zx}=-\omega_i x\sum_{i=1}^{2}\left[\frac{A_i}{{\bar{R}_{ii}}^3}-\sum_{j=1}^{2}\frac{A_{ij}x}{{R_{ij}}^3}\right] \quad (19)$$

$$\sigma_x=-\xi_i\sum_{i=1}^{2}\left[\frac{A_i\bar{z}_{ii}}{{\bar{R}_{ii}}^3}+\sum_{j=1}^{2}\frac{A_{ij}z_{ij}}{{R_{ij}}^3}\right]$$

$$+2c_{66}\sum_{i=1}^{2}\left[A_i sign(z-h)\left\{\frac{1}{\bar{R}_{ii}{\bar{R}_{ii}}^{*}}-\frac{x^2}{{\bar{R}_{ii}}^2{\bar{R}_{ii}}^{*2}}-\frac{x^2}{{\bar{R}_{ii}}^3{\bar{R}_{ii}}^{*}}\right\}\right.$$

$$\left.+\sum_{j=1}^{2}A_{ij}\left\{\frac{1}{R_{ij}{R_{ij}}^{*}}-\frac{x^2}{{R_{ij}}^2{R_{ij}}^{*2}}-\frac{x^2}{{R_{ij}}^3{R_{ij}}^{*}}\right\}\right] \quad (20)$$

$$\sigma_y=-\xi_i\sum_{i=1}^{2}\left[\frac{A_i\bar{z}_{ii}}{{\bar{R}_{ii}}^3}+\sum_{j=1}^{2}\frac{A_{ij}z_{ij}}{{R_{ij}}^3}\right]$$

$$+2c_{66}\sum_{i=1}^{2}\left[A_i sign(z-h)\left\{\frac{1}{\bar{R}_{ii}{\bar{R}_{ii}}^{*}}-\frac{y^2}{{\bar{R}_{ii}}^2{\bar{R}_{ii}}^{*2}}-\frac{y^2}{{\bar{R}_{ii}}^3{\bar{R}_{ii}}^{*}}\right\}\right.$$

$$\left.+\sum_{j=1}^{2}A_{ij}\left\{\frac{1}{R_{ij}{R_{ij}}^{*}}-\frac{y^2}{{R_{ij}}^2{R_{ij}}^{*2}}-\frac{y^2}{{R_{ij}}^3{R_{ij}}^{*}}\right\}\right] \quad (21)$$

$$\sigma_z=\vartheta_i\sum_{i=1}^{2}\left[\frac{A_i\bar{z}_{ii}}{{\bar{R}_{ii}}^3}+\sum_{j=1}^{2}\frac{A_{ij}z_{ij}}{{R_{ij}}^3}\right] \quad (22)$$

Similarly, when force applied in upper material, then displacements, (u', v', w'), normal stress, $(\sigma_x', \sigma_y', \sigma_z')$, and shear stress, $(\tau_{xy}', \tau_{yz}', \tau_{xz}')$ of lower material has also been derived. Fundamental solutions of 3D transversely isotropic elastic material at the interface of the bonded joint when point force applied at a distance h below the interface have also been derived.

4. Material Properties and Boundary conditions

Transversely isotropic elastic material joint comprising of zinc as upper material and cobalt as the lower material is analyzed for this paper. Elastic constants of the material are tabulated below.

Table 1 Elastic constants of the material

Material	c_{11}	c_{12}	c_{13}	c_{33}	c_{44}	c_{66}
Zinc (GPa)	158.35	31.5	47.44	61.6	40	63.4
Cobalt (GPa)	307	165	103	358.1	75.3	71

Assume that the two-phase elastic material is perfectly bonded. Therefore the boundary conditions on the interface $(z = 0)$ are given below;

$$u = u' \qquad v = v' \qquad w = w'$$
$$\sigma_{zz} = \sigma_{zz}' \qquad \tau_{xz} = \tau_{xz}' \qquad \tau_{yz} = \tau_{yz}'$$

Where prime refers to the variables in the lower material, $z \leq 0$ and the other ones refers to those in the upper material, $z \geq 0$.

5. Model of 3D transversely isotropic elastic material

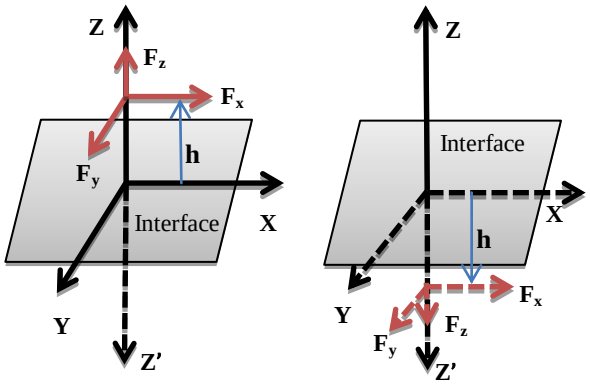

Fig.1 Model of 3D bonded joint

Numerical investigation is performed by Green's function with the application of point force at a distance h (50mm) above and below the interface in x, y & z directions. Dimension of upper and lower material is 100mm×100mm×100mm when the value of z varies from -100 mm to 100mm.

4. Result and discussion

Graphical representations of the value of displacement, shear stress and normal stress are given below for both upper and lower material. In all graphs there have a deflection at point 50mm for upper material and –50mm for lower material of the distance, z where the point force is applied. Displacements, (u, v, w) & (u', v', w'), normal stress, $(\sigma_z$ & $\sigma_z')$ and shear stress, (τ_{yz}, τ_{xz}) & (τ_{yz}', τ_{xz}') shows continuity at interface. Normal stress, (σ_x, σ_y) & (σ_x', σ_y') and shear stress, $(\tau_{xy}'$ & $\tau_{xy})$ shows discontinuity at interface of 3D transversely isotropic elastic bi-material joint.

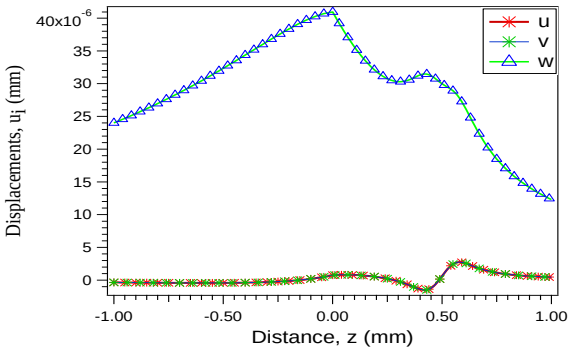

Fig.2 Distribution of displacement $(u, v$ & $w)$ against distance, z with force in z direction of upper material

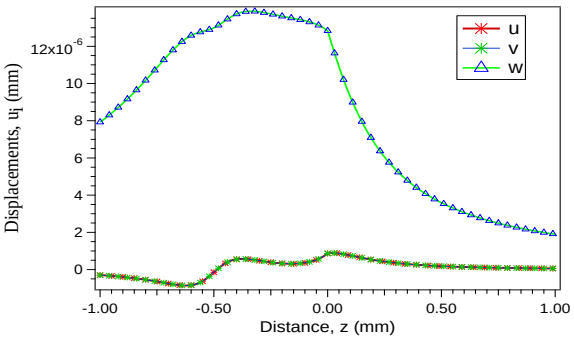

Fig.3 Distribution of displacement $(u, v$ & $w)$ against distance, z with force in z direction of lower material

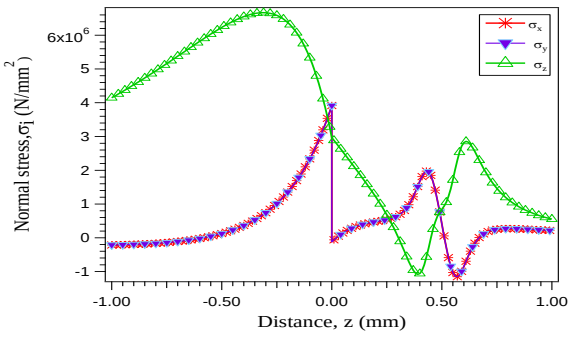

Fig.4 Distribution of normal stress (σ_x, σ_y & σ_z) against distance, z with force in z direction of upper material

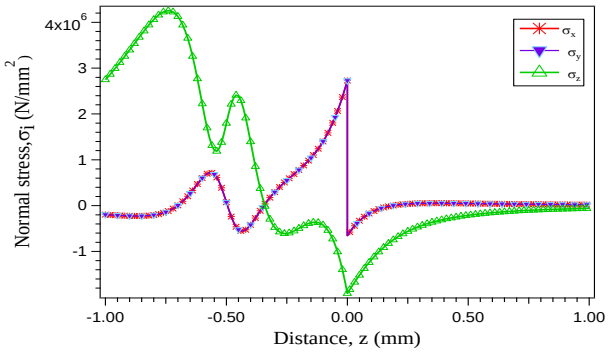

Fig.5 Distribution of normal stress (σ_x, σ_y & σ_z) against distance, z with force in z direction of lower material

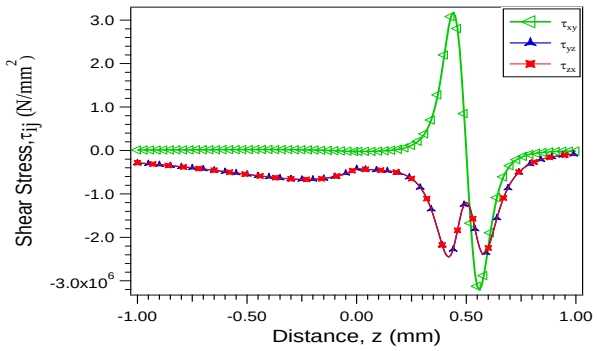

Fig.6 Distribution of Shear stress (τ_{xy}, τ_{yz} & τ_{zx}) against distance, z with force in z direction of upper material

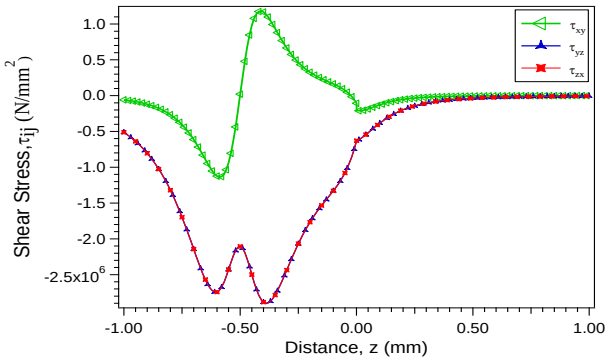

Fig.7 Distribution of Shear stress (τ_{xy}, τ_{yz} & τ_{zx}) against distance, z with force in z direction of lower material

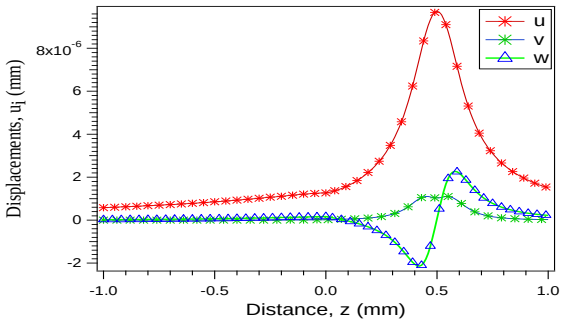

Fig.8 Distribution of displacement (u, v & w) against distance, z with force in x direction of upper material

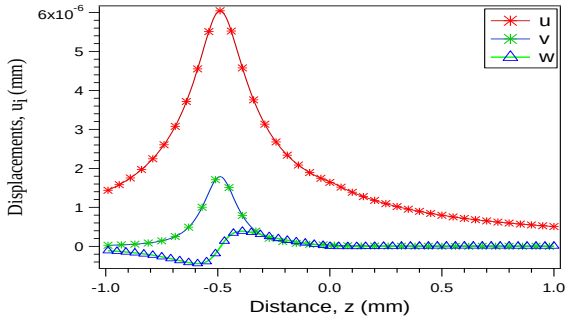

Fig.9 Distribution of displacement (u, v & w) against distance, z with force in x direction of lower material

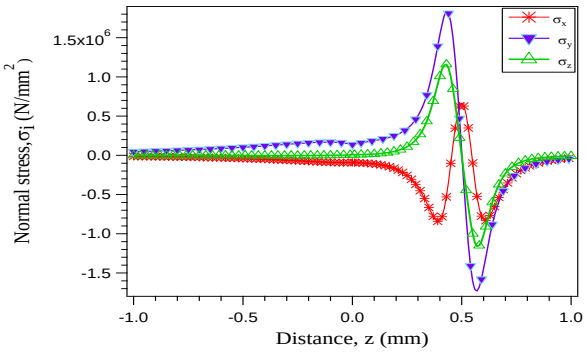

Fig.10 Distribution of normal stress (σ_x, σ_y & σ_z) against distance, z with force in x direction of upper material

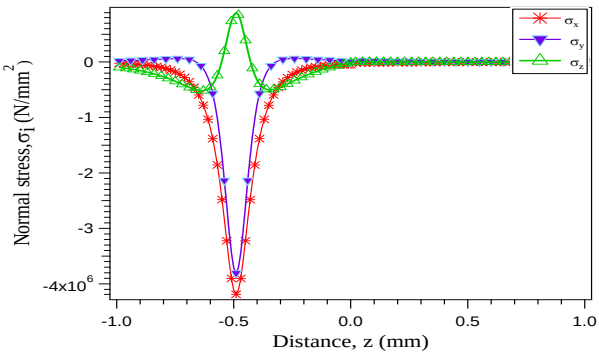

Fig.11 Distribution of normal stress (σ_x, σ_y & σ_z) against distance, z with force in x direction of lower material

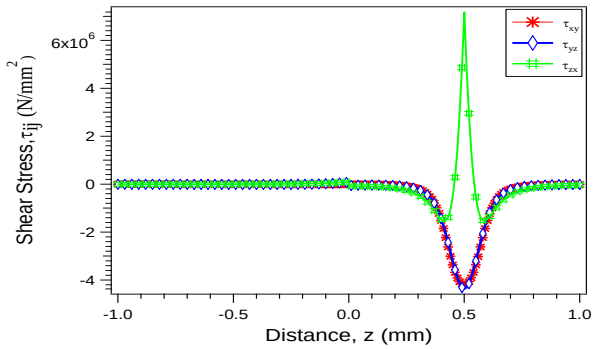

Fig.12 Distribution of Shear stress (τ_{xy}, τ_{yz} & τ_{zx}) against distance, z with force in x direction of upper material

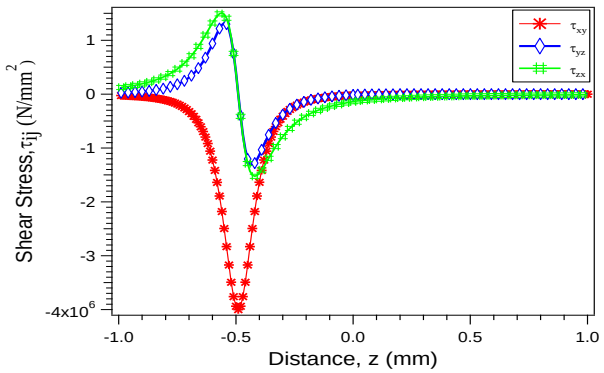

Fig.13 Distribution of Shear stress (τ_{xy}, τ_{yz} & τ_{zx}) against distance, z with force in x direction of lower material

From the graph, the distribution of stress at every point of the bonded material gives the useful information about the permissible amount of force that the material can withstand before its facture. The higher value of displacement and stress occurs at the free edge of the material joint than the inner portion of the joint. The possibility to debond and delamination at interface of the transversely isotropic elastic material joints was due to the higher stress and displacement concentration at the free edge.

5. Conclusion

In this paper, the expression of fundamental equation of 3D transversely isotropic elastic material is derived and algorithm for the fundamental solution is developed by the FORTRAN code. Finally the continuity of the fundamental equation at interface of 3D transversely isotropic elastic material is checked. This analysis clearly shows that the elastic constants and point force have great influence on the material joint.

NOMENCLATURE

u, v, w	: Elastic displacements
σ_x, σ_y, σ_z	: Normal stresses (N/mm^2)
τ_{xy} , τ_{yz}, τ_{zx}	: Shear stresses (N/mm^2)
φ_i, φ_3	: Displacement functions
A_i, D_i	: Known constants
A_{ij}, D_{ij}	: Undetermined constant
$\omega, \xi, \vartheta, \alpha, k$	: Dimensionless material parameters
T	: Point force
c_{ijkl}	: Elastic stiffness tensor
s_1, s_2, s_3	: Characteristic roots

REFERENCES

[1] Ding Haojiang, Weiqiu Chen and L. Zhang, Elasticity of Transversely Isotropic Materials, *Solid Mechanics and its Applications*, Vol. 126, pp.71-92, *(*2006).

[2] Ding Haojiang, Liangjian and Chenbou, The United Point Force Solution For Both Isotropic and Transversely Isotropic Media, Vol. 13, pp.95-102 (1997).

[3] Hu Haichang, On the equilibrium and vibration of a transversely isotropic elastic body, *Sci. Sin.*, Vol.5, pp.1-18 (1956).

[4] Y. C. Pan and T. W. Chou, Point force solution for an infinite transversely isotropic solid, *ASME J. Appl. Mech.*, Vol.43, pp.608-612 (1976).

[5] Md. Shahidul Islam and Hideo Koguchi, Analysis of Intensity of Singular Stress Fields in Three-dimensional Transversely Isotropic Piezoelectric Bonded Joints, *2nd International Conference on Mechanical, Industrial and Energy Engineering (ICMIEE 2012), Khulna, Bangladesh*, 1-2 February, (2013).

[6] H. A. Elliott, Three-dimensional stress distributions in hexagonal aeolotropic crystals, *Proc.Cambridge Philos. Soc.*, Vol.44, pp.522-533 (1948).

[7] E. Kroner, Das Fundamental Integrate der anisotropen Elastischen Differential gleichungen, *Zeitschrift fur Physik*, Vol.136, pp.402-410 (1953).

ICMIEE-PI-140397

Dielectric properties could be potential tools for investigating materials (VOCs) toxicity

Mohammad Russel[1,*], *Sun zheng xiang*,[1] *Md. Mahbub Alam* [2]

[1] School of Food and Environmental Science & Technology, Dalian University of Technology, Panjin 124221, PR China
[2] Institute for Turbulence-Noise-Vibration Interaction and Control, Shenzhen Graduate School, Harbin Institute of Technology, Shenzhen 518055, China

ABSTRACT
A new approach applied to study the VOC's toxicity LC_{50} (Lethal concentration) using dielectric properties. In this paper a simple procedure with the combination of VNA and TDR was used for measuring the dielectric properties of selected volatile organic compounds. We have tried to draw a relationship between toxicity LC_{50} and the dielectric constant (Ɛ') of selected VOC's. The interesting findings are: for alkane (Isopentane, Octane), when the dielectric constant (Ɛ') goes high, the toxicity (LC_{50}) of the compounds rises accordingly. But the relationship for alcohol (butanol, ethanol & methanol) is just reverse. That is, when the Ɛ' increases , the toxicity (LC_{50}) of the compounds becomes low. The cause might be arising from the compounds structural orientation.

Keywords: Dielectric constant, Toxicity, LC_{50}, VNA, TDR.

1. Introduction

The study of harmful interactions between chemicals and biological system is named as toxicology. All the living animals (man, other animals, and plants) in the modern world are increasingly being exposed to chemicals of an enormous variety. The current challenges of toxicology are to apply basic biochemical, chemical, pathological and physiological knowledge to an understanding of why certain substances cause the disruption in a biological system which may lead to toxic effects. Statistically we found that around 65000 chemicals are currently produced in the USA and 500-1000 new chemicals are added each year. Because of the rapid introduction of the numbers of chemicals, our environment may become progressively toxic. It is thus very important to have some knowledge of the effects they may have and to attempt to substantiate and assess these effects [1].

Modern society currently faces extreme indoor air quality problem due to exposure of votalite organic compounds (VOC's). Cave dwellers are perhaps the first to be concerned with the indoor air quality problem, when they built fires inside their caves [2]. Most of the air quality problems arise from the indoor accessories like building materials, finishing agents, floor finishing, painting, new-furniture finishing materials and so on. Since people in developed countries spend approximately 90% of their time indoors, and VOC concentrations measured indoors typically exceed those outdoors [3], it is important to understand the potential health implications of indoor exposure to specific VOCs [4-5].

The scope of chemical compound selection in indoor air quality has now evolved to consider not only traditional material function (e.g., mechanical, optical and electrical properties) and manufacturing economics but also inherent potential toxicity to humans and ecosystems. A rising challenge to the chemical engineering community is the integration of a robust toxicity indicator tool for comparing various materials within components in products.

The measurement of dielectric properties of materials at radio frequency has gained increasing importance, especially in the research fields, such as material science, microwave circuit design, absorber development or noise suppressors [6-7], biological research, etc. Dielectric measurement is important because it can provide the electrical characteristics of the materials, which were proved useful in many research and development fields.

Many techniques have been developed to measure these dielectric properties such as techniques in time domain or frequency domain with one port or two ports, etc. Every technique is limited to specific frequencies, materials and applications by its own constraint. With the advance of new technologies, the techniques can be employed with a software program that measures the group delay (τ_g), complex reflection, transmission coefficients with a vector network analyzer and converts the data into the complex dielectric property parameter.

Electromagnetic properties of any materials are in general frequency dependent. Determination complex dielectric properties of dielectric materials were practiced for many years using conventional short-open circuit method using the slotted line. Dielectric properties of materials are usually derived from measurement of reflection or transmission coefficients, using both instances [6]. Reflection/transmission methods are being popular for obtaining broadband measurement in both time domain and frequency domain system.

* Corresponding author. Tel.: +86- 0427-2631798
E-mail address: mrussel@dlut.edu.cn

In this study, we apply a new approach to (i) study the selected VOC's dielectric properties to understand their harmfulness to compare with their known LC_{50} from MSDS (materials safety data sheet) in vitro toxicological test results, and (ii) explore the relationship between toxicological ranking with their dielectric properties. We measured the dielectric constant of some known dielectric volatile organic compounds using our prototype probe. Matlab and origin pro programs have been used for calculating the complex dielectric properties including group delay and correcting the phase shift to get the S-parameters from the surface plane of the sample. De-embedding technique which compensates both phase and magnitude is used to get rid of unwanted S-parameter from device under test (DUT). Their is a complete package model to study the dielectric properties of any liquids.

Online measurements and its non-invasive are necessary to investigate the physical and chemical properties of different environmental materials such as application of VOCs and their impact and minimize the environmental pollution. The development of technology in recent years has increased the number of methods and decreased the price of monitoring tools for application in environmental analysis. A few examples of the progress were observed to study the environmental pollutants physical and chemical properties of using into electrical signals and measurements in high frequency range.

An important parameter for dielectric material (e.g., VOCs) monitoring is τ_g that directly influences the real part of the material permittivity known as dielectric constant (ε_r') of a material [8]. Indirect measurement of τ_g using its dielectric properties seems to be the right direction for the researchers. The objective of this study is to explore the relationship between materials (VOC's) toxicological ranking and dielectric properties (τ_g and ε_r'). Our research hypothesis to be convincing, our experiment is into four parts. Firstly, τ_g and ε' or ε_r' are studied for some selected VOC's, using Close-Ended Coax airline Probe with a vector network analyzer (VNA) and Time Domain Reflectometry (TDR) methods. Secondly, a comparison of τ_g obtained from the two methods for five VOCs is made. Thirdly, ε_r' is measured for some known dielectric VOCs materials and compared with the reference values at a specific frequency. Finally, the measured dielectric properties (τ_g, ε') data and their known LC_{50} values are interconnected to have a deeper understanding of their toxicological strength.

Theory

The most fundamental concept (Fig. 1) of high-frequency network analysis involves incident, reflected and transmitted waves travelling along transmission lines. It is helpful to think of travelling waves along a transmission line in terms of a light wave analogy. We can imagine incident light striking some optical component like a clear lens. Some of the light is reflected off the surface of the lens, but most of the light continues on through the lens. If the lens were made of some lossy material, then a portion of the light could be absorbed by the lens. If the lens had mirrored surfaces, then most of the light would be reflected and little or none would be transmitted through the lens. This concept is valid for RF signals as well, except that the electromagnetic energy is in the RF range instead of the optical range, and our components and circuits are electrical devices and networks instead of lenses and mirrors [9].

Network analysis is concerned with the accurate measurement of the ratios of the reflected signal to the incident signal and the transmitted signal

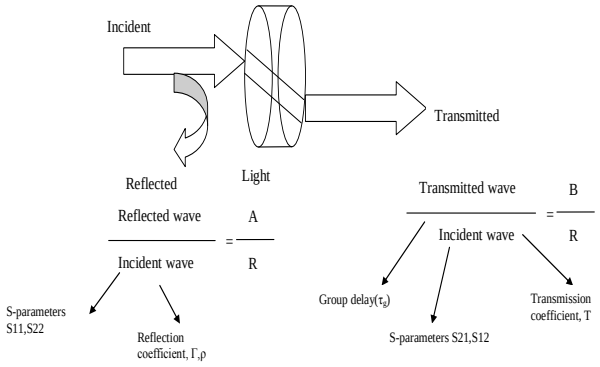

Fig. 1 Flow diagram of reflected and transmitted wave components. τ = group delay, scattering parameter S11, S21, S22 and S12. Reflected wave = A, Incident wave = R, and transmitted wave = B.

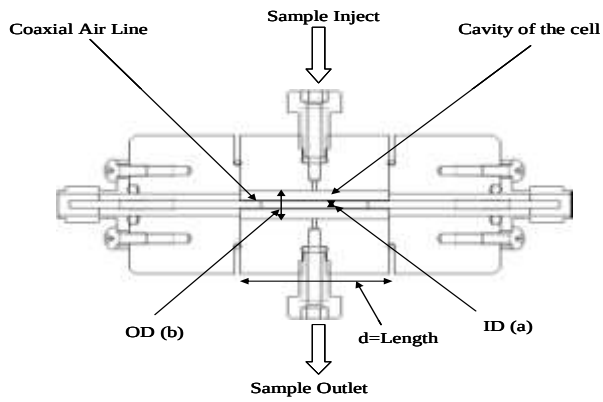

Fig. 2 Prototype probe diagram OD (b) = outer core diameter = 0.005 m and ID(a) = inner core diameter = 0.00196 m and length d = 0.02018 m.

to the incident signal. Based on fundamental concept form Fig. 1 we have measured reflected and transmission coefficients by using our proto type probe (Fig. 2). The dielectric properties of the VOCs materials can thus be studied with aid of this transmission and reflected wave data.

Measurement Approach

Group delay and dielectric constant measurement approaches using VNA and TDR

The first approach used to estimate the dielectric constant was based on the relationship between Group delay (τ_g) and real part of permittivity (ε_r') or dielectric constant. Group delay is related to the dielectric constant of the materials. For example, S21 transmission coefficient is a complex number and is expressed in terms of magnitude and phase, S21 = |S21|ejφ. The phase φ is related to the dielectric constant (ε_r'(ω)) and the sample length (L) through the phase factor β as $\varphi = -\beta L = \{-2\pi\sqrt{\varepsilon'(\omega)}/\lambda_0\}L$ where λ_0 is the wavelength in vacuum. The real part of the dielectric constant (ε_r'(ω)) is then calculated from this formula.

Group delay is (i) a measure of device phase distortion, (ii) the transit time of a signal through a device, versus frequency, and (iii) the derivative of the device's phase characteristic with respect to frequency. Mathematically, the group delay can be expressed as bellows:

Group delay = $\tau_g = -\partial\varphi/\partial f$ = -1/360*$\partial\theta/\partial f$ = time delay where θ = degree, f = ω/2π Hz

Time domain reflectometry (TDR) provides the estimation of changes in the group delay directly from measurements. The probe was then tested for the same materials using both TDR and VNA systems.

Transmission-line techniques are the simplest methods for electromagnetic characterization in wideband frequencies. They include short and open lines (one-port measurement) and transmission/reflection lines (two-port measurements). For the transmission/reflection method (TR), the measuring cell is made up of a section of coaxial airline filled with the sample to be characterized. The sample electromagnetic parameters are deduced from the scattering matrix defined between the sample planes and are usually measured with an automatic network analyzer. The Nicolson–Ross–Weir (NRW) procedure [10,11] is the most commonly used method for performing this calculation. This method has the advantage of being non-iterative and applicable to coaxial line cells.

We used TEM propagation mood for our coaxial airline probe system to measure the reflection and transmission scattering parameters S11 and S21. Then we transferred the data to our software program which is written by Matlab and Origin pro. It will correct the S11 and S21 phase shift value to get the accurate measurement scattering parameter value from the sample surface plane. Simple algorithm is used to correct the phase shift [12,13].

For S11(ω),

$\Delta\varphi 11 = 2a * 2\pi f/c$, (1)

and for S21(ω),

$\Delta\varphi 21 = (a+b) * 2\pi f/c$, (2)

where f = frequency, and c = light speed in vacuum.

The phase shift correction concept is drawn in Fig. 3.

We can the calculate permittivity and permeability using improved NWR methods [14-15] and scattering parameters of reflection and transmission S11, S21. Characteristic impedances are in unique for test materials under specified condition. As an electromagnetic sine wave within a specified frequency range is passed from ports 1 to 2 during traveling a specific length d of sample, the electromagnetic wave will produce reflection and transmission coefficient along the direction of propagation. As per Hao Zhou [14] improved and simplified technique, we can write,

From NWR method [10-11] C1 and C2 can be found

$C1 = \mu r/\varepsilon_r$ (3)

$C2 = \mu r * \varepsilon r$ (4)

The propagation coefficient

$T = \exp -j\omega\sqrt{\mu\varepsilon} * d = \exp[-j(\omega/c)\sqrt{\mu r * \varepsilon r} * d]$ (5)

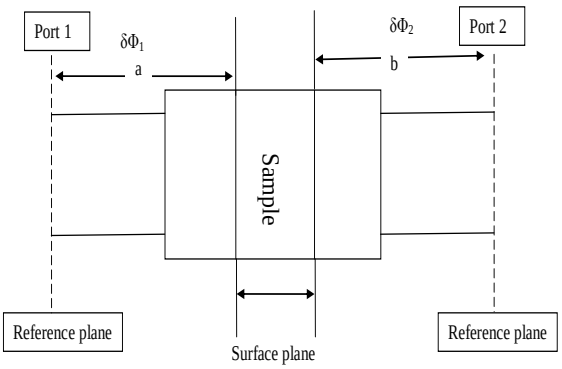

Fig. 3. Phase Rotation from reference plane to sample plane.

We can write the transmission coefficient as per Ruler formula

$T = \cos\theta - j\sin\theta$, (6)

where the period is $t = d/c\sqrt{C2}$ and θ = ω*t, ω = phase velocity, and the reflection coefficient,

$\Gamma = \sqrt{C1}-1/\sqrt{C1}+1$, (7)

so that

$S11(\omega) = (1+T2)*\Gamma/ 1-\Gamma 2* T2$, and (8)

$S21(\omega) = (1-\Gamma 2)* T/ 1-\Gamma 2*T2$. (9)

Furthermore, relative permittivity and permeability can be calculated as follows.

$\varepsilon r = m*Z$, and (10)

$\mu r = m/Z$, (11)

where Z is the characteristic impedance [16].

$m = \varphi/(k0*d)$, (12)

where k0 = ω/c=2πf/c, f is the frequency and c is the velocity of light and then

$\varphi = -j.\log(p)+2\pi n$. (13)

We can use this algorithm to calculate materials dielectric constant.

TDR principle

The time domain reflectometer is set up as shown in Fig. 4.

The step generator produces a positive going incident wave which is fed into the transmission system under test. The oscilloscopes high impedance input bridges the transmission system at its junction with the step generator. The step travels down the transmission line at the velocity of propagation of the line. If the load impedance is equal to the characteristic impedance of the line, no wave is reflected, and what will be seen on the oscilloscope is the incident voltage step recorded as the wave passes the point on the line monitored by oscilloscope.

If a mismatch exists at the load, part of the incident wave will be reflected. The reflected voltage wave will appear on the oscilloscope display algebraically added to the incident wave. The reflected wave is readily identified since it is separated in time from the incident wave. The quality of the transmission system is indicated by the ratio of this reflected wave to the incident wave origination at the source [17]. This

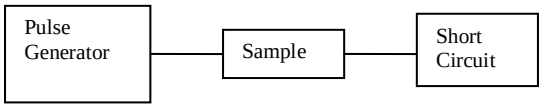

Fig. 4 TDR measurement system.

ratio is called voltage reflection coefficient (ρ) and is related to the transmission line impedance by the followingequation:

$$\rho = Er/Ei = Z_L - Z_0 / Z_L + Z_0, \quad (14)$$

where Er = reflected wave and Ei = incident wave, Z_L= load impedance Z_0 = characteristics impedance.

The time is also valuable in determining the length of the transmission system from the monitoring point to the mismatch. If D = length,

$$D = vp*T/2, \quad (15)$$

where, vp = velocity of propagation, T = total transit time of the round trip from the monitoring point to mismatch.

Calculating the group delay (Fig 5) directly from TDR system and VNA, slope of unwrap S21 phase of the materials ($\tau_g = -\partial\Phi/\partial f$). Then we can get an accurate dielectric material delay of materials from TDR subtracting the time of known materials like air value.

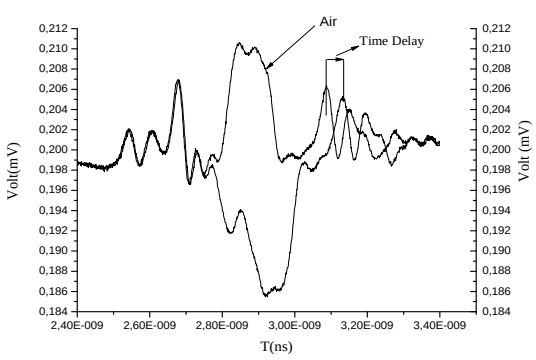

TDR

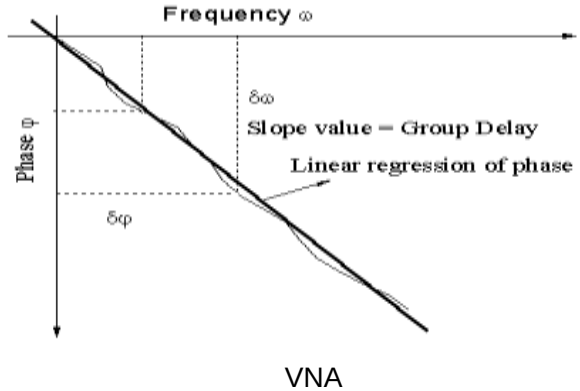

VNA

Fig 5 Time Delay measuring using TDR and VNA

Instrumentation

Matlab and origin pro softwares are combined to perform the following objectives. These are, to save the scattering reflection S11 and transmission coefficient S21 from the VNA to computer, then interlink those parameters with our Matlab and origin pro program for setting up various parameters to format the data, calculate the group delay and dielectric constant by using the derived formula and, to display and save the various graphs and results.

We used Agilent E8358A VNA, Agilent. Infiniium86100C DCA-J TDR and Matlab with origin pro 8.0 programming language were used to measure the parameters and design the software.

Measurement Results

Simulation of Close-ended coaxial airline with the dominant TEM mode is performed using the high frequency structure simulator. Measurement is performed using Agilent E8358A VNA, Agilent and infiniium86100C DCA-J TDR with appropriate calibration.

TDR measurement results

For TDR system, we directly connected our close-ended coaxial airline probe with 0.0035 m SMA connector.

During the TDR portion of testing, the sample assemblies were connected directly to the TDR sampling head while the opposite end was terminated with a 0.0035 m precision short circuit standard. This was done to ensure a well-defined and controlled termination. For the TDR time delay measurement, a sample assembly, fitted with precision short circuit termination, was connected to the TDR and the round-trip time delay value was recorded using our own origin-pro program time delay measurement algorithm. The time delay was recorded at a 205 mV level. The round trip time delay was taken as the total time required to travel the sine-wave through the coaxial airline probe from one end to the other end which is short circuited. And the time delay of materials was calculated by subtracting the air time delay from the materials time delay as shown in Fig. 5. The actual

sample assembly time delay is one half the measured round-trip time delay, as shown in Fig. 6.

VNA Measurement Results:

Simulation of coaxial line is performed with proper selection of boundaries and ports. The sample cavity is placed in the middle of the coaxial line. Coaxial line with dimensions inner radius of the outer conductor 0.005 m, outer radius of inner conductor 0.00196 m and length 0.002018 m with samples, which fit in the coaxial line with thickness of 0.00130 m, is used in both simulation and measurement to obtain values of S-paameters. De-embedding techniques are used to obtain the S-parameters of the sample which are at the center of the coaxial line, canceling the effect of unwanted regions. For the de-embedding, S-parameters were obtained from the port extension technique in VNA. Since simulation of unknown sample is not possible, measurement was performed by using some known samples like air, water, methanol, ethanol, and butanol (Fig.7).

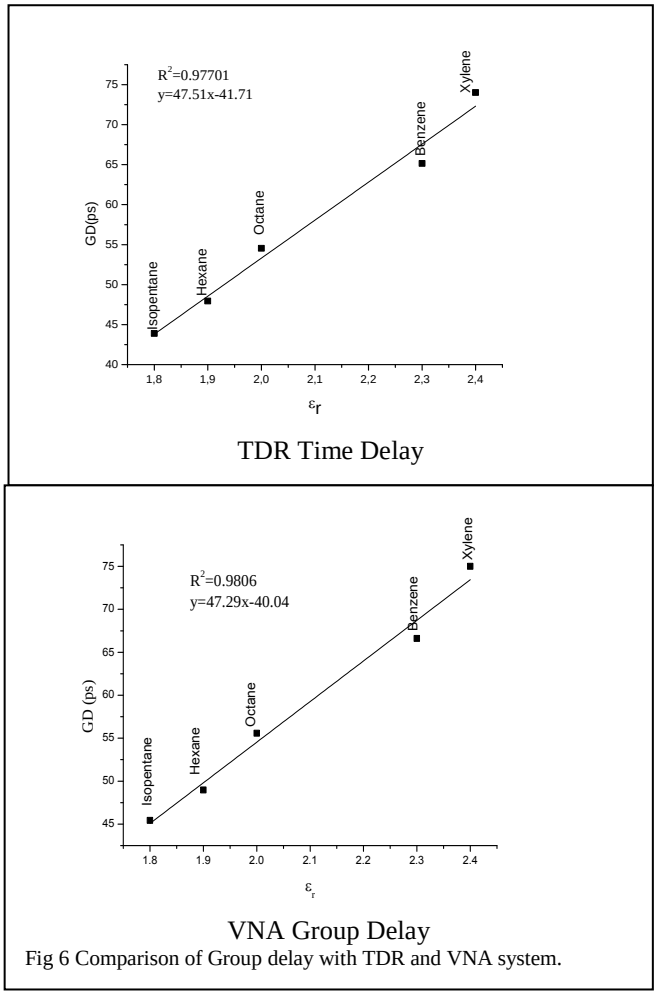

Fig 6 Comparison of Group delay with TDR and VNA system.

For our analysis, fluid samples are injected to the cavity 0.0013L (coaxial airline probe) to the dimensions of coaxial line and the results are verified at a 3×10^9 Hz frequency data with references Von hipple. The de-embedded S-parameters from simulation and measurement are analyzed, following the techniques used in Refs. [12-13,18]. The values of real part of permittivity of samples at 3×10^9 Hz frequency [19] are presented in Fig.8.

There exists an uncertainty when the length of the sample is comparable to half wavelength of the electromagnetic wave propagating through it [20]. That's why the thickness of sample was chosen relatively small, presently 0.002018 m to avoid uncertainties due to length. Also the measurement values are not consistent throughout the frequency range due to some mechanical imperfections and environmental factors such as temperature, pressure, humidity during experimentation.

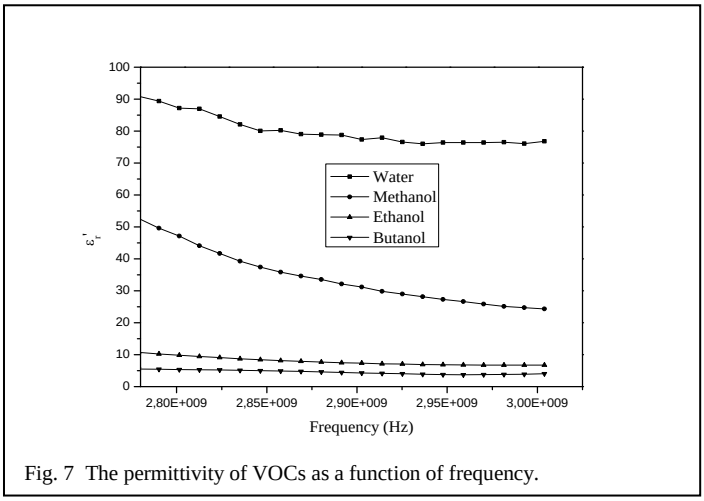

Fig. 7 The permittivity of VOCs as a function of frequency.

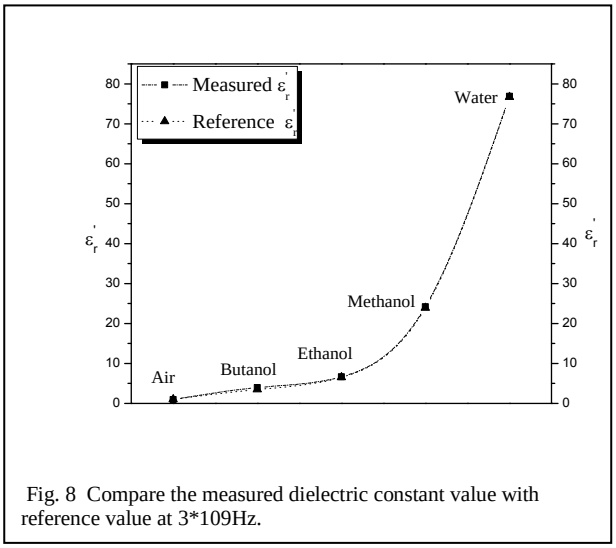

Fig. 8 Compare the measured dielectric constant value with reference value at 3*109Hz.

Relationship between toxicity LC_{50} and dielectric properties

The data show a good accordance relationship between the dielectric constant and the group delay. When the group delay number goes high, so does the permittivity of the compounds, the correlation being positive. When we come to the relationship between the toxicity and ~~the~~ dielectric constant, some exciting phenomena are observed. For alkane (Isopentane,Octane), when the dielectric constant rises, the toxicity of the compounds

follows the same. But this relationship in alcohol (butanol, ethanol & methanol) is just opposite. As the permittivity grows, the toxicity of the compounds declines (Fig. 9). Even though, they have a possible relation in common, that is the structure of their carbon chain. The more carbon in the chain the compound contains, the more toxic it is. We don't know the exact relationship between the structure and their toxicity, but we do believe they are connected each other, and this is what we will do in the next step.

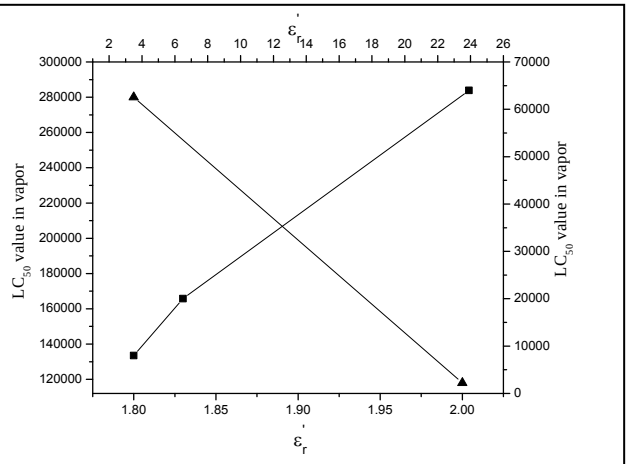

Fig. 9 Exploring the relationship between εr' and LC_{50} in vapor.

Conclusion:

The fundamental goal of this paper was to explore a relationship between dielectric properties (group delay and real part of permittivity) and toxicity strength (LC_{50}) of the materials. We found higher the group delay higher the real part of dielectric permittivity/dielectric constant (εr'). Good correlation for both time and frequency domain system measured the group delay where R^2 >0.95. So it is revealed that our probe is sensitive enough to measure dielectric constants of fluids. And it is a simple method for easily and effectively measuring the group delay and the complex permeability and permittivity of any fluids material.

When it comes to the relationship between toxicity and the dielectric constant, we also find some exciting phenomenta: for alkane (Isopentane, Octane), when the dielectric constant (ε_r') increases, the toxicity (LC_{50}) of the compounds correspondingly follows the same trend. But this relationship in the alcohol (Butanol,Ethanol & Methanol) is just opposite, an increase in the permittivity (ε_r') accompanies a decrease in the toxicity (LC_{50}) of the compounds.

The results prove that the proposed method is an effective alternative way to study the dielectric properties of fluid materials and it could be a potential tool to extract inherent information on the toxicity of the materials. Our next plan is to study the compound morphology which could possibly lead us to understand the insight into materials' toxicity.

Acknowledgment

This work was supported in part by grants from The fundamental Research Funds for the Central Universities (5002-842301& 5002-851001).

REFERENCES

[1] John Timbrell, Introduction to Toxicology,Introduction to toxicology,3rd edition,CRC press boca raton London new York Washington,D.C.,2002.

[2] J. R. BEALL AND A. G. ULSAMER, Presented as part of a Symposium on Health Aspects of Indoor Air Pollution held by the Committee on Public Health of the New York Academy of Medicine at the Academy on May 28 and 29,1981.

[3] Billionnet, C., Gay, E., Kirchner, S., Leynaert, B., Annesi-Maesano, I., 2011. Quantitative assessments of indoor air pollution and respiratory health in a populationbased sample of French dwellings. Environ. Res. 111, 425-434

[4] Klepeis, N.E., Nelson, W.C., Ott, W.R., Robinson, J.P., Tsang, A.M., Switzer, P., Behar, J.V., Hern, S.C., Engelmann, W.H., 2001. The National Human Activity Pattern Survey (NHAPS): a resource for assessing exposure to environmental pollutants. J. Expo. Anal. Environ. Epidemiol. 11, 231-252.

[5] Sabit Cakmak, Robert E. Dales, Ling Liu, Lisa Marie Kauri,Christine L. Lemieux, Christopher Hebbern, Jiping Zhu, Residential exposure to volatile organic compounds and lung function: Results from a population-based cross-sectional survey. Environmental Pollution 194 (2014) 145-151

[6] Product notes no 8510-3.Measuring dielectric constant with the HP8510 network analyzer. "The measurement of Both Permittivity and Permeability of Solid Materials".

[7] D. Popovic, C. Beasley, M. Okoniewski, J. H. Booske, "Precision Open-Ended Coaxial Probes for In Vivo and Ex Vivo Dielectric Spectroscopy of Biological Tissues at Microwave Frequencies". IEEE Trans. on Microwave Theory and Techniques,. vol. 53, no.5, pp.1713-1722 May 2005..

[8] Z. Lu, M. Lanagan, E. Manias and D. D. Macdonald, "Two-Port Transmission Line Technique for Dielectric Property Characterization of Polymer Electrolyte Membranes". J. Phys. Chem. B vol.113, pp. 13551-13559 August,2009.

[9] http://www.rfmw.org/network_analyzer_network_analyzer_basics_network_analyzer_basics.html

[10] A.M.Nicolson and G.F. Ross, "Measurement of the intrinsic properties of materials by Time-Domain Techniques".IEEE Trans. on instrumentation and measurement,Vol. IM-19,No.4,pp.377-382,November 1970.

[11] W. B.Weir, "Automatic measurement of complex dielectric constant and permeability at microwave frequencies". Proceeding of the IEEE,Vol. 62,No.1,

pp.33-36,January 1974.
[12] L.F.chen,C.K.Ong,C.P.Neo, V.V.Varadan and V.K Varadan, Microwave electronics: measurement and materials characterization, John Wiley and Sons Ltd., 2004, Ch-4,pp.185.
[13] Rohde and Schwarz application note.Measurement of dielectric material properties.RAC067-0019.
[14] H. Zhou,G. Lu,Y. Li,S. Wang and Y.Wang, "An improved method of determining permittivity and permeability by S parameters" PIERS Proceedings,Beijing,China, pp.,768-773,March 23-27, 2009.
[15] A.H. Boughriet, C. Legrand, and A. Chapoton, "Noniterative Stable Transmission/Reflection Method for Low-Loss Material Complex Permittivity Determination", IEEE Trans on Microwave Theory and Techniques, vol. 45, no. 1,pp.52-57, January, 1997.
[16] Y. Guang, J. Shan and W. Guodong, "Modified algorithm on electromagnetic parameters test", Theory and method, Vol. 26,No. 8,pp.15-17, August,2007.
[17] Hewlett Packard Time Domain Reflctrometry. Application note 62.
[18] Agilent de-embedding and embedding S-parameter networks using a vector network analyzer. Agilent Technologies,Application note 1364-1,March 2001.
[19] Dielectric materials and applications Arthur von hippel.published by Boston, London 1995.
[20] E.Ni, "A uncertainty analysis for the measurement of intrinsic properties of materials by combined transmission-reflection method." IEEE Trans. On instrumentation and measurement, Vol.41,no.4, pp.495-499,August 1992.
[21] http://pubchem.ncbi.nlm.nih.gov/
[22] http://avogadro.chem.iastate.edu/MSDS/methanol.htm
[23] http://avogadro.chem.iastate.edu/msds/1-butanol.htm
[24] http://avogadro.chem.iastate.edu/msds/ethanol.htm

ICMIEE-PI-140398

Regression Equation and Neural Network Model for Material Removal Rate and Surface Finish

Md. Ashikur Rahman Khan[1,*], *M. M. Rahman*[2], *Md. Bellal Hossain*[3], *Zayed-Us-Salehin*[1], *Muhammad Afsar Uddin*[3]
[1]Department of Information and Communication Technology, Noakhali Science and Technology University Noakhali -3814, Bangladesh
[2]Faculty of Mechanical Engineering, Universiti Malaysia Pahang, 26600 Pekan, Pahang, Malaysia
[3]Department of Computer Science & Telecommunication Engineering, Noakhali Science and Technology University, Noakhali -3814, Bangladesh

ABSTRACT
In electrical discharge machining (EDM), a complete and clear theory has not yet been established. The developed theory (physical models) yields results far from reality due to the complexity of the physics. Modelling the process is an effective way of solving the critical problem of relating the process parameters to the performance measures. Therefore, the purpose of the present work is to develop the mathematical models to predict performance characteristics of EDM on Ti-5Al-2.5Sn titanium alloy. Response surface method (RSM), and artificial neural network (ANN) were employed to develop the mathematical models. Analysis of variance (ANOVA) has been performed to verify the fit and adequacy of the developed models. The results evidence that the developed mathematical model can predict the performance characteristics of EDM successfully. The ANN model is more precise than the mathematical model. It becomes a precise tool, making the EDM process cost-effective and efficient.

Keywords: Artificial neural network, material removal rate, modelling, response surface method, surface finish.

1. Introduction

In spite of the increased utility of titanium alloys, the capability to produce parts products with high productivity and superior quality becomes challenging. It is extremely difficult to machine titanium alloys with the traditional machining process owing to their poor machinability [1]. Titanium is difficult-to-cut material can be machined effectively by a non-conventional technique, that of electrical discharge machining [1, 2, 3]. One of the most significant deficiencies of the EDM process is the high manufacturing time. In this instance, inadequate selection of machining conditions may introduce high process times. Typically, this is carried out by relying heavily on the operator's experience and conservative technological data provided by the EDM equipment manufacturers, which produce inconsistent machining performance [3, 4]. The parameter settings given by the manufacturers are only applicable to the common steel grades. Proper selection of parameters in EDM is very much essential for achieving better performance characteristics, and that is still a challenging job. Using the physical properties of the electrode materials, several attempts have been made by previous researchers to develop theoretical model. Longfellow et al. proposed an equation for wear ratio [5]. However, this equation shows a poor fit with experimental values [6, 7]. The experimental wear ratio was found 15–19 times as high as the calculated wear ratios. Dibitonto et al. presented a theoretical cathode erosion model for EDM performance measures [8]. In the model validation test, the predicted value was found to be 1.5–46 times as high as experimental values. A non-linear, transient, thermo-physical model of die-sinking EDM was developed using the finite element method (FEM) to predict the shape of the crater cavity and the material removal rate (*MRR*) [9]. The result confirmed that the analytical results over-predict the *MRR* compared with the experimental results. Their numerical model was also validated by experimental result, and the model's predicted value was 1.5–14 times as high as the experimental value. The growth of the plasma channel, energy sharing between electrodes, the process of vaporization, formation of a recast layer, plasma-flushing efficiency, and the thermal properties of the work material are a few physical phenomena that make the machining process highly complex and stochastic. It is very difficult to consider all these complex phenomena in mathematical form. Therefore, mathematical prediction of process characteristics shows wide variation compared with experimental results. On the other hand, experiment-based modelling of EDM helps to give a good understanding of the complex process [6]. Experimentalists have tried to formulate regression model for the EDM process by employing several techniques such as RSM, ANN, and so forth.

Through response surface methodology, regression model was developed to evaluate the surface quality, and material removal rate in terms of machining parameters [10; 11, 12, 13, 14]. Modelling for *MRR* was performed for EDM on silicon-infiltrated silicon carbide, aluminium-silicon carbide, metal matrix composite (MMC) copper steel (EN-8), tungsten carbide and cobalt composites, FW4 steel material [12, 13, 15, 16, 17, 18]. Study was carried out to model surface finish of aluminium-silicon carbide, F-1110, alumina-based ceramic composite, Ck60 steel, MMC, EN-8, tungsten carbide and cobalt composites, FW4

* Corresponding author. Tel.: +88-01836350710
E-mail address: ashik.nstu@yahoo.com

steel workpiece [13, 10, 11, 14, 15, 16, 17, 18]. In recent years, the ANN has been transformed into a very useful tool for modelling complex systems [19]. A neural network (NN) is able to model non-linear processes by catching the desired input and output vectors. Cybenco and Nielsen showed that such a network is capable of estimating any non-linear function with desired accuracy [20]. Mahdavinejad used artificial intelligent to distinguish the EDM pulse type [21]. Neural network models were proposed in order to assess *MRR* for HE15, 15CDV6, and M250, C40 steel, nickel-based alloy [22, 23, 24]. Neural network was employed to model surface finish of HE15, 15CDV6, and M250, nickel-based alloy, mild steel (St 37), alloyed steels and high strength low alloyed (HSLA) steels such as a microalloyed (Mic/al 1) steel [22, 24].

It is evident from the prior work that the mathematical model was developed for particular work-tool combination, and for particular electrode polarity. Moreover, it is revealed that mathematical model with titanium alloy, specifically Ti-5Al-2.5Sn, in EDM process is still lagging. In this context, an effort has been made to develop regression equation and neural network model in order to predict material removal rate and surface finish of Ti-5Al-2.5Sn titanium alloy. In outstanding, distinct electrode materials such as copper (Cu), copper-tungsten (Cu-W), and graphite (Gr), and all polarities (positive and negative) of electrode have been considered for modeling in this work. Besides, a comparison has been performed between regression equation and neural network model.

2. Mathematical modelling

Mathematical models were developed for predicting material removal rate, and surface finish mainly surface roughness (*SR*) considering first-order and second-order polynomial equation using response surface methodology. In addition, feed-forward multilayer perceptron (MLP) neural network model was set up in order to evaluate *MRR* and *SR* through artificial neural network. Henceforward, the confirmation test is performed for model validation. The peak current (I_p), pulse-on time (T_{on}), pulse-off time (T_{off}), and servo-voltage (S_v) were selected as the process variables for the present research. Positive and negative polarity of the Cu, Cu-W, and Gr electrode were considered.

2.1. Regression equation

Response surface methodology describes the correlation between responses and quantitative factors. The process parameters can be represented as [25]

$$Y = f(X_1, X_2, X_3, \ldots X_n) + \varepsilon \tag{1}$$

here, Y is the response, f is the response function, X_1, X_2, X_3, . . ., X_n are factors, and ε is the experimental error. In support of the present work, the response material removal rate and surface roughness can be written by (2) and (3) respectively.

$$MRR = f(I_p, T_{on}, T_{off}, S_v) + \varepsilon \tag{2}$$

$$SR = f(I_p, T_{on}, T_{off}, S_v) + \varepsilon \tag{3}$$

Single-order response surface mathematical models can be developed using (2) and (3):

$$MRR = A_0 + \sum_{i=1}^{4} A_i X_i + \varepsilon \tag{4}$$

$$SR = B_0 + \sum_{i=1}^{4} B_i X_i + \varepsilon \tag{5}$$

where X_i is the process variables (I_p, T_{on}, T_{off}, and S_v); the term A_0, and B_0 are the constants. The term A_i, and B_i are the single-order regression coefficient for MRR and SR, respectively. Neglecting the error (ε), equation (4) and (5) can be written as

$$MRR = A_0 + A_1 I_p + A_2 T_{on} + A_3 T_{off} + A_4 S_v \tag{6}$$

$$SR = B_0 + B_1 I_p + B_2 T_{on} + B_3 T_{off} + B_4 S_v \tag{7}$$

where the parameters A_1, A_2, A_3, and A_4 are the regression coefficients of the linear effect of the connecting factor for MRR; and B_1, B_2, B_3, and B_4 are the regression coefficients which represent the linear effect of the connecting factor for SR.

A second-order response surface model for MRR and SR consists of the following terms:

$$MRR = A_0 + \sum_{i=1}^{4} A_i X_i + \sum_{i=1}^{4} A_{ii} X_i^2 + \sum_{i,j=1, i\neq j}^{4} A_{ij} X_i X_j + \varepsilon \tag{8}$$

$$SR = B_0 + \sum_{i=1}^{4} B_i X_i + \sum_{i=1}^{4} B_{ii} X_i^2 + \sum_{i,j=1, i\neq j}^{4} B_{ij} X_i X_j + \varepsilon \tag{9}$$

where X_i are the input variables such as I_p, T_{on}, T_{off}, and S_v; X_i^2 and X_iX_j are the squares and interaction terms of the input variables, respectively; A_i, A_{ii}, and A_{ij} are the regression coefficients for *MRR*; B_i, B_{ii}, and B_{ij} are the regression coefficients for *SR*.

Therefore, the second-order polynomial models, when neglecting the experimental error, can be written as

$$\begin{aligned} MRR = {} & A_0 + A_1 I_p + A_2 T_{on} + A_3 T_{off} + A_4 S_v + A_{11} I_p^2 + \\ & A_{22} T_{on}^2 + A_{33} T_{off}^2 + A_{44} S_v^2 + A_{12} I_p T_{on} + A_{13} I_p T_{off} \\ & + A_{14} I_p S_v + A_{23} T_{on} T_{off} + A_{24} T_{on} S_v + A_{34} T_{off} S_v \end{aligned} \tag{10}$$

$$\begin{aligned} SR = {} & B_0 + B_1 I_p + B_2 T_{on} + B_3 T_{off} + B_4 S_v + B_{11} I_p^2 + \\ & B_{22} T_{on}^2 + B_{33} T_{off}^2 + B_{44} S_v^2 + B_{12} I_p T_{on} + B_{13} I_p T_{off} \\ & + B_{14} I_p S_v + B_{23} T_{on} T_{off} + B_{24} T_{on} S_v + B_{34} T_{off} S_v \end{aligned} \tag{11}$$

In the present study, both the first-order and second-order polynomial models were studied using the experimental results. The analysis of variance was carried out for first-order and second-order polynomial models to determine the adequacy of the fitted model. The model adequacy checking includes testing for significance of the regression model (mainly R^2, R^2-adjusted), testing for significance of model coefficients, and testing for lack-of-fit [10, 26].

2.2. Artificial neural network

Neural networks are able to model non-linear processes through catching the desired input and output vectors [19]. The distinct architectures of neural network are studied and eventually, MLP neural network is developed owing to its more appropriate result. The general network with four input variables and two responses is supposed to be 4-j-2 for the network with one hidden layer. In MLP neural network with one hidden layer, the net input to unit *j* in the hidden layer, and the net input to unit *o* in the output layer are expressed in (12) and (13) respectively.

$$(\text{net input})_{hidden}=\sum_{i=1}^{I} w_{i,j}x_i + b_j \tag{12}$$

$$(\text{net input})_{output}=\sum_{j=1}^{J} w_{j,o}h_j + b_o \tag{13}$$

where $w_{i,j}$ is the weight between the input neurons and hidden neurons; $w_{j,o}$ is the weight between the hidden and output neurons; x_i is the value of the input as $x_1=I_p$, $x_2=T_{on}$, $x_3=T_{off}$, and $x_4=S_v$; h_j is the value of the output for hidden nodes; b_j is the bias on the hidden nodes; and b_o is the bias on the output nodes.

The output for hidden nodes, and the output for output nodes (y_o) can be given as (14) and (15),

$$h_j=f((\text{net input})_{hidden}) \tag{14}$$

$$y_o=f((\text{net input})_{output}) \tag{15}$$

where f is the transfer function and y_o is the ANN predicted output, namely *MRR*, and *SR*. The output for hidden nodes (h_j) and the output from the output nodes (y_o) with the sigmoid function can be written as (16) and (17).

$$h_j = f((\text{net input})_{hidden})=\frac{1}{1+ e^{-\sum_{i=1}^{I} w_{i,j}x_i + b_j}} \tag{16}$$

$$y_o = f((\text{net input})_{output})=\frac{1}{1+ e^{-\sum_{j=1}^{J} w_{j,o}h_j + b_o}} \tag{17}$$

Hence, the neural network model for *MRR* and *SR* with one hidden layer can be presented as

$$y_o=\frac{1}{1+ e^{-\sum_{j=1}^{J} w_{j,o}h_j + b_o}} \tag{18}$$

Likewise, the network structure with four input variables and two responses can be defined as 4-*j*-*k*-2 for the network with two hidden layer. The values of the output for first hidden layer (h_j), and for second hidden layer (z_k) with sigmoid function can be represented as written as equation (19) and (20) respectively.

$$h_j=f((\text{net input})_{hidden1})=\frac{1}{1+ e^{-\sum_{i=1}^{I} w_{i,j}x_i + b_j}} \tag{19}$$

$$z_k=f((\text{net output})_{hidden1}) = \frac{1}{1+ e^{-\sum_{j=1}^{J} w_{j,k}h_j + b_k}} \tag{20}$$

where $w_{i,j}$ is the weight between the input neurons and first hidden neurons; $w_{j,k}$ is the weight between first hidden layer and second hidden layer; b_j is the bias on the first hidden layer; and b_k is the bias on the second hidden layer.

Thus, the neural network output ($(y_o= f(z_k))$ for *MRR* and *SR* with two hidden layer can be expressed as (21).

$$y_o = \frac{1}{1+ e^{-\sum_{k=1}^{K} w_{k,o}z_k + b_o}} \tag{21}$$

$w_{k,o}$ is the weight between the last hidden neurons and output neurons; and b_o is the bias on the output layer.

Several networks were trained with different numbers of neurons in the hidden layer. A trial-and-error approach was used to ascertain the optimal structure. It is obvious that the weight of the optimal neural network will be transformed for distinct electrode-polarity combination.

3. Results and discussions

3.1. Regression equation

The collected experimental data have been analysed using response surface. Analyses have been accomplished through first-order as well as second-order regression equations. The result obtained through ANOVA revealed that the second-order mathematical model is more adequate and significant than the first-order model. Consequently, the formulated model of material removal rate for positive Cu, negative Cu, positive Cu-W, negative Cu-W, positive Gr, and negative Gr electrode based on (10) are presented by (22), (23), (24), (25), (26) and (27) respectively. Similarly, the formulated model of surface roughness

for positive Cu, negative Cu, positive Cu-W, negative Cu-W, positive Gr, and negative Gr electrode based on (11) can be represented by (28), (29), (30), (31), (32), and (33), respectively.

The developed models are verified through confirmation test, and it is found that the average errors of the mathematical models are in the range of 3.98–4.85%, and 3.55–5.17%, for *MRR* and *SR*, respectively. Thus, it is obvious that the accuracies of the developed models are satisfactory. Correspondingly, these models can predict the responses within an agreeable error (>6%).

$$\begin{aligned} MRR = {} & 2.195 + 0.0678 I_p + 2.727\times10^{-3} T_{on} - \\ & 3.28\times10^{-3} T_{off} - 0.042 S_v + 1.424\times10^{-3} I_p^2 - \\ & 1.19\times10^{-6} T_{on}^2 + 2.01\times10^{-6} T_{off}^2 + 1.93\times10^{-4} S_v^2 \\ & + 1.15\times10^{-5} I_p T_{on} - 8.61\times10^{-5} I_p T_{off} - \\ & 4.15\times10^{-4} I_p S_v - 1.89\times10^{-6} T_{on} T_{off} - \\ & 1.73\times10^{-5} T_{on} S_v + 3.21\times10^{-5} T_{off} S_v \end{aligned} \quad (22)$$

$$\begin{aligned} MRR = {} & -0.164 + 0.086 I_p + 4.25\times10^{-3} T_{on} - 3.71\times10^{-3} T_{off} \\ & + 5.10\times10^{-4} S_v + 1.31\times10^{-3} I_p^2 - \\ & 4.54\times10^{-6} T_{on}^2 + 5.22\times10^{-6} T_{off}^2 + 2.12\times10^{-5} S_v^2 \\ & + 5.93\times10^{-5} I_p T_{on} - 1.35\times10^{-4} I_p T_{off} - \\ & 7.79\times10^{-4} I_p S_v + 2.97\times10^{-6} T_{on} T_{off} \\ & - 3.56\times10^{-5} T_{on} S_v + 2.34\times10^{-5} T_{off} S_v \end{aligned} \quad (23)$$

$$\begin{aligned} MRR = {} & 0.978 + 0.12 I_p + 4.43\times10^{-4} T_{on} - 2.55\times10^{-3} T_{off} \\ & - 0.019 S_v + 1.74\times10^{-3} I_p^2 - 1.93\times10^{-6} T_{on}^2 + \\ & 6.76\times10^{-6} T_{off}^2 + 9.76\times10^{-5} S_v^2 + 2.16\times10^{-6} I_p T_{on} \\ & - 1.13\times10^{-4} I_p T_{off} - 9.67\times10^{-4} I_p S_v - 5.53\times10^{-6} \\ & T_{on} T_{off} + 1.25\times10^{-5} T_{on} S_v + 1.43\times10^{-5} T_{off} S_v \end{aligned} \quad (24)$$

$$\begin{aligned} MRR = {} & -0.527 + 0.130 I_p + 4.02\times10^{-3} T_{on} - 4.89\times10^{-3} T_{off} \\ & + 6.63\times10^{-3} S_v + 2.48\times10^{-3} I_p^2 - 7.93\times10^{-6} T_{on}^2 \\ & - 3.55\times10^{-6} T_{off}^2 - 3.46\times10^{-5} S_v^2 + 3.52\times10^{-5} I_p T_{on} \\ & - 1.66\times10^{-4} I_p T_{off} - 1.40\times10^{-3} I_p S_v + 1.91\times10^{-6} \\ & T_{on} T_{off} - 1.49\times10^{-5} T_{on} S_v + 7.13\times10^{-5} T_{off} S_v \end{aligned} \quad (25)$$

$$\begin{aligned} MRR = {} & 1.799 + 0.0977 I_p + 1.58\times10^{-3} T_{on} - 5.9\times10^{-3} T_{off} \\ & - 0.034 S_v + 1.94\times10^{-3} I_p^2 - 5.86\times10^{-6} T_{on}^2 + \\ & 6.60\times10^{-6} T_{off}^2 + 1.71\times10^{-4} S_v^2 + 8.75\times10^{-5} \\ & I_p T_{on} - 6.63\times10^{-5} I_p T_{off} - 1.02\times10^{-3} I_p S_v + 7.55\times10^{-7} \\ & T_{on} T_{off} - 2.94\times10^{-7} T_{on} S_v + 3.69\times10^{-5} T_{off} S_v \end{aligned} \quad (26)$$

$$\begin{aligned} MRR = {} & 4.939 + 1.285 I_p + 0.0481 T_{on} - 0.059 T_{off} - \\ & 0.1271 S_v + 0.0321 I_p^2 - 8.59\times10^{-5} T_{on}^2 + \\ & 6.588\times10^{-5} T_{off}^2 + 8.95\times10^{-4} S_v^2 + \\ & 3.81\times10^{-4} I_p T_{on} - 8.90\times10^{-4} I_p T_{off} - 0.0132 \\ & I_p S_v + 3.31\times10^{-5} T_{on} T_{off} - 2.313\times10^{-4} T_{on} S_v \\ & + 3.29\times10^{-4} T_{off} S_v \end{aligned} \quad (27)$$

$$\begin{aligned} SR = {} & -2.639 + 0.806 I_p - 0.0259 T_{on} + 3.787 T_{off} \times10^{-3} + \\ & 0.0265 S_v - 1.72\times10^{-3} I_p^2 + 1.97\times10^{-5} T_{on}^2 - \\ & 4.77\times10^{-6} T_{off}^2 + 1.04\times10^{-4} S_v^2 - 2.51\times10^{-4} I_p T_{on} \\ & - 6.49\times10^{-5} I_p T_{off} - 6.25\times10^{-3} I_p S_v + 7.28\times10^{-6} \\ & T_{on} T_{off} + 2.39\times10^{-4} T_{on} S_v - 3.06\times10^{-5} T_{off} S_v \end{aligned} \quad (28)$$

$$\begin{aligned} SR = {} & -2.929 + 0.2113 I_p + 0.0329 T_{on} - 1.48\times10^{-3} T_{off} \\ & + 0.032 S_v - 7.61\times10^{-3} I_p^2 - 5.63\times10^{-5} T_{on}^2 + \\ & 8.65\times10^{-6} T_{off}^2 - 1.55\times10^{-4} S_v^2 + 2.43\times10^{-4} I_p T_{on} \\ & + 9.0\times10^{-5} I_p T_{off} + 1.29\times10^{-3} I_p S_v - 2.41\times10^{-6} T_{on} T_{off} \\ & - 7.58\times10^{-5} T_{on} S_v - 2.85\times10^{-5} T_{off} S_v \end{aligned} \quad (29)$$

$$\begin{aligned} SR = {} & 1.6685 + 0.2018 I_p + 4.72\times10^{-3} T_{on} - \\ & 9.02\times10^{-4} T_{off} - 0.0131 S_v - 2.22\times10^{-3} I_p^2 \\ & - 1.23\times10^{-5} T_{on}^2 + 1.08\times10^{-4} I_p T_{on} \end{aligned} \quad (30)$$

$$\begin{aligned} SR = {} & -8.473 + 0.263 I_p + 0.0232 T_{on} + 0.0198 T_{off} \\ & + 0.1125 S_v - 6.62\times10^{-3} I_p^2 - 6.49\times10^{-5} T_{on}^2 - \\ & 4.18\times10^{-6} T_{off}^2 - 4.89\times10^{-4} S_v^2 + 3.63\times10^{-4} \\ & I_p T_{on} - 4.60\times10^{-5} I_p T_{off} + 5.14\times10^{-4} I_p S_v \\ & - 8.49\times10^{-6} T_{on} T_{off} + 5.24\times10^{-5} T_{on} S_v - \\ & 1.57\times10^{-4} T_{off} S_v \end{aligned} \quad (31)$$

$$\begin{aligned} SR = {} & 2.7598 + 0.2287 I_p - 8.5\times10^{-3} T_{on} + 0.0225 T_{off} - \\ & 0.0537 S_v - 0.0079 I_p^2 + 1.25\times10^{-5} T_{on}^2 \\ & - 5.82\times10^{-5} T_{off}^2 + 1.35\times10^{-4} S_v^2 + 3.46\times10^{-4} I_p T_{on} \\ & - 1.27\times10^{-4} I_p T_{off} + 7.50\times10^{-4} I_p S_v \\ & - 1.45\times10^{-5} T_{on} T_{off} + 1.057\times10^{-4} T_{on} S_v \\ & - 1.39\times10^{-6} T_{off} S_v \end{aligned} \quad (32)$$

$$\begin{aligned} SR = {} & -2.938 + 0.629 I_p + 0.0215 T_{on} + 0.02447 T_{off} \\ & - 1.843\times10^{-4} S_v - 0.0132 I_p^2 - 5.244\times10^{-5} T_{on}^2 - \\ & 5.83\times10^{-5} T_{off}^2 - 3.07\times10^{-5} S_v^2 + 6.82\times10^{-4} I_p T_{on} \\ & - 3.47\times10^{-4} I_p T_{off} + 5.39\times10^{-4} I_p S_v + 3.43\times10^{-5} \\ & T_{on} T_{off} + 2.56\times10^{-5} T_{on} S_v - 3.07\times10^{-5} T_{off} S_v \end{aligned} \quad (33)$$

3.2. Neural network model

Table 1 Best Configurations of Neural Network Models.

Electr-ode	Polar-ity	Network structure	No. of hidden layers	Learn-ing rate	Mome-ntum factor	No. of training repeti-tions	Max no. of epochs
Cu	+	4-12-2	1	0.7	0.5	3	60000
	-	4-10-2	1	0.5	0.5	3	40000
Cu-W	+	4-10-2	1	0.7	0.5	3	40000
	-	4-8-5-2	2	1.0	0.7	3	30000
Gr	+	4-10-2	1	1.0	0.4	3	60000
	-	4-8-5-2	2	1.0	0.5	3	50000

A number of networks are constructed, altering the number of hidden neurons, maximum epochs, training repetition, learning step size, and momentum factor, and each of them is trained separately [23]. The best network was selected based on the accuracy of the predictions in the training and testing phase. The configurations shown in Table 1 give the best prediction for the performance measure (*MRR* and *SR*) for different electrode-polarity combination. The developed neural network models with all settings are tested and validated. It is observed that the performance measures such as MSE and r-value are within the range of 0.0175–0.0513 and 0.9693–0.9962, respectively for *MRR*. Similarly, the values of MSE and r during testing are within the range of 0.0069–0.0981, and 0.9593–0.9963, respectively for *SR*. The high r-value (1) and small MSE (approaching zero) ensure that the NN model gives the best prediction. Thus, it is evident that the MSEs obtained are within the acceptable range, and the neural network models are adequate. The average errors of the ANN models during validity test are in the range of 1.53–4.31%, and 1.92–3.34% for *MRR*, and *SR* respectively. Thus, it is obvious that the error is within the agreeable limit and the accuracy of the developed model is satisfactory. Considering all electrodes and polarities, average errors of the ANN models are 2.61%, and 2.77% for *MRR*, and *SR*, respectively. The same for the regression equations are 4.34%, and 4.17% for *MRR*, and *SR*, respectively. Thus, it seems that the accuracy of the ANN model is better than that of the RSM model.

4. Conclusion

In outstanding, this research work established the regression equation as well as neural network model in order to evaluate the responses as material removal rate and surface finish for distinct electrode-polarity combination. The second-order regression equation evidenced more fitness and adequacy. The best neural network models were set up with one hidden layer and two hidden layer that link with electrode-polarity combination. The developed models can predict the responses agreeably and effectively. In addition, the NN model is more accurate whilst compared with RSM. It constructs the EDM process cost-effective and efficient.

NOMENCLATURE

I_p : peak current, A
T_{on} : pulse-on time, µs
T_{off} : pulse-off time, µs
S_v : servo-voltage, V
ε : experimental error
X_i : process variables
$w_{i,j}$: weight between the input neurons and hidden neurons
$w_{j,o}$: weight between the hidden and output neurons
h_j : value of the output for hidden nodes
b_j : bias on the hidden nodes
b_o : bias on the output nodes

REFERENCES

1. M.M. Rahman., M.A.R. Khan, K. Kadirgama, M.M. Noor, and R.A. Bakar, Optimization of machining parameters on tool wear rate of Ti-6Al-4V through EDM using copper tungsten electrode: A statistical approach, Advance Material Research, Vol. 152–153, pp 1595–1602 (2011).
2. M.M. Rahman, M.A.R. Khan, K. Kadirgama, M.M. Noor, and R.A. Bakar, Modeling of material removal on machining of Ti-6Al-4V through EDM using copper tungsten electrode and positive polarity, International Journal of Mechanical and Materials Engineering, Vol. 1(3), pp 135–140 (2010).
3. M.A.R. Khan, M.M. Rahman, K. Kadirgama, M.A. Maleque, and R.A. Bakar, Artificial intelligence model to predict surface roughness of Ti-15-3 alloy in EDM process, World Academy of Science, Engineering and Technology, Vol. 74, pp 121–125 (2011).
4. M.A.R. Khan, M.M. Rahman, K. Kadirgama, and R.A. Bakar, Artificial neural network model for material removal rate of Ti-15-3 in electrical discharge machining. Energy Education Science and Technology— Part A: Energy Science and Research, Vol. 29(2), pp 1025–1038 (2012).
5. J. Longfellow, J.D. Wood, and R.B. Palme, The effect of electrode material properties on the wear ratio in spark machining, Journal Institute of Metals, Vol. 96(II), pp 614–617 (1968).
6. M.L. Jeswani, Dimensional analysis of tool wear in electrical discharge machining, Wear, Vol. 55, pp. 153–161 (1979).
7. P.J. Wang, and K.M. Tsai, Semi-empirical model on work removal and tool wear in electrical discharge machining, Journal of Materials Processing Technology, Vol. 114, pp 1–17 (2001).
8. D.D. DiBitonto, P.T. Eubank, M.R. Patel, and M.A. Barrufet, Theoretical models of the electrical discharge machining process–I, A simple cathode erosion model, Journal of Applied Physics, Vol. 66(9), pp 4095–4103 (1989).
9. S.N. Joshi, and S.S. Pande, Thermo-physical modeling of die-sinking EDM process, Journal of Manufacturing Processes, Vol. 12, 45–56 (2010).
10. I. Puertas, and C.J. Luis, A study on the machining

parameters optimisation of electrical discharge machining, Journal of Materials Processing Technology, Vol. 143–144, pp 521–526 (2003).
11. K.M. Patel, P.M. Pandey, and P.V. Rao, Determination of an optimum parametric combination using a surface roughness prediction model for EDM of Al2O3/SiCw/TiC ceramic composite, Materials and Manufacturing Processes, Vol. 24, pp 675–682 (2009).
12. C.J. Luis, I. Puertas, and G. Villa, Material removal rate and electrode wear study on the EDM of silicon carbide, Journal of Materials Processing Technology, Vol. 164–165, pp 889–896 (2005).
13. R. Karthikeyan, P.R.L. Narayanan, and R.S. Naagarazan, Mathematical modelling for electric discharge machining of aluminium–silicon carbide particulate composites, Journal of Materials Processing Technology, Vol. 87, pp 59–63 (1999).
14. G. Petropoulos, N.M. Vaxevanidis, and C. Pandazaras, Modeling of surface finish in electro-discharge machining based upon statistical multi-parameter analysis, Journal of Materials Processing Technology, Vol. 155–156, pp 1247–1251 (2004).
15. N.P. Hung, I.J. Yang, and K.W. Leong, Electrical discharge machining of cast metal matrix composites, Journal of Materials Processing Technology, Vol. 41, pp 229–236 (1994).
16. K.D. Chattopadhyay, S. Verma, P.S. Satsangi, and P.C. Sharma, Development of empirical model for different process parameters during rotary electrical discharge machining of copper–steel (EN-8) system, Journal of Materials Processing Technology, Vol. 209, pp 1454–1465 (2009).
17. D. Kanagarajan, R. Karthikeyan, K. Palanikumar, and J.P. Davim, Optimization of electrical discharge machining characteristics of WC/Co composites using non-dominated sorting genetic algorithm (NSGA-II), The International Journal of Advanced Manufacturing Technology, Vol. 36(11–12), pp 1124–1132 (2008).
18. M.R. Shabgard, and R.M. Shotorbani, Mathematical modeling of machining parameters in electrical discharge machining of FW4 welded steel, World Academy of Science, Engineering and Technology, Vol. 52, pp 403–409 (2009).
19. R.A. Mahdavinejad, EDM process optimisation via predicting a controller model, Archives of Computational Materials Science and Surface Engineering, Vol. 1(3), pp 161–167 (2009).
20. J.S. Donat, N. Bhat, and T.J. McAvoy, Neural net based model predictive control, International Journal of Control, Vol. 54(6), pp 1453–1468 (1991).
21. R.A. Mahdavinejad, Optimisation of electro discharge machining parameters, Journal of Achievements in Materials and Manufacturing Engineering, Vol. 27(2), pp 163–166 (2008).
22. G.K.M. Rao, G.R. Janardhana, D.H. Rao, and M.S. Rao, Development of hybrid model and optimization of metal removal rate in electric discharge machining using artificial neural networks and genetic algorithm, ARPN Journal of Engineering and Applied Sciences, Vol. 3(1), pp 19–30 (2008).
23. D. Mandal, S.K. Pal, and P. Saha, Modeling of electrical discharge machining process using back propagation neural network and multi-objective optimization using non-dominating sorting genetic algorithm-II, Journal of Materials Processing Technology, Vol. 186, pp 154–162 (2007).
24. K. Wang, H.L. Gelgele, Y. Wang, Q. Yuan, and M. Fang, A hybrid intelligent method for modelling the EDM process, International Journal of Machine Tools & Manufacture, Vol. 43, pp 995–999 (2003).
25. M.A.R. Khan, M.M. Rahman, K. Kadirgama, and A.R. Ismail, Mathematical model for wear rate of negative graphite electrode in electrical discharge machining on Ti-5A1-2.5Sn, Jurnal Teknologi, Vol. 59, pp 57–61 (2012).
26. I. Puertas, C.J. Luis, and L. Alvarez, Analysis of the influence of EDM parameters on surface quality, MRR and EW of WC–Co, Journal of Materials Processing Technology, Vol. 153–154, pp 1026–1032 (2004).

ICMIEE-PI-140399 *International Conference on Mechanical, Industrial and Energy Engineering 2014*
26-27December, 2014, Khulna, BANGLADESH

Study on Power Consumption and Social Aspects of Battery Operated Auto-rickshaw

Md.Zulkefa Rian[1]*,Dr. A. N. M. Mizanur Rahman* [2,*]

[1]UG student, Dept. of Mechanical Engineering,Khulna University of Engineering & Technology, Khulna-9203
[2] Professor, Dept. of Mechanical Engineering,Khulna University of Engineering & Technology, Khulna-9203

ABSTRACT
For short distances 3-wheelers dominateour transportation sector but several disadvantages force us for better means of transportation. Battery operatedauto-rickshaw, which are now common in transport sector, consumes a considerable amount of electricity during charging of their batteriesand thereby causes of load shading.At the same time,they reduce the unemployment problem partly. This paper found out the feasibility of battery operated auto-rickshaw as an alternative transport by analyzing power consumption, effects on national electricity supply, reduction of unemployment and socio-economic aspects of people involved with it and finally the environmental aspects of these vehicles. A questionnaire was developed and information was collected by interviewing the auto-rickshaw drivers of different areas of Khulna city. It also predicts the emission of polluting gases from different power plants. The study revealed that battery operated auto-rickshaw reduces unemployment problems to some extent, as well as improve their socio-economic condition. Average power consumption of a battery operated auto-rickshaw is about 8 - 11 kWh per day. Also, there is less emission of polluting elements provided the discharges of the batteries are performed in a systemic way. The operating cost ofbattery operated auto-rickshaw is less than that of a fuel operated 3-wheelers.So, from national point of view and considering the social impact for short distances battery operated auto-rickshaw is more suitable.

Key Words: Battery operated auto-rickshaw, Easy bike, Economic aspects, Social impacts, Air pollution.

1. Introduction

Battery operatedauto-rickshaw popularly known as 'Easy-bike' is newly added to the transportation sector of Bangladesh. It has been playing a significant role as a means of transport for short distances as well as an income generating source for unemployment people since the introduction of this. From the start, it is being used as popular transportation means especially for lower, lower-middle, even middle income people in urban areas. It involves relatively lower travel cost as well as provides much more comfort and safety. It is convenient to the users during travel compared to other public transport system. So, urban employment generation largely depends on it.

Easy-bikes are operated by rechargeable lead-acid batteries as their sourcesof power. These batteries are charged with electricity taken from the domestic or commercial lines which indirectly burdens the national grid. At present electricity seems to be a low cost power sources for these vehicles as compared to commercial fuels like petrol or diesel. The operating cost of Easy-bike seems to be low as compared to commercial fuel operated 3-wheelers. As petrol is burned in 3-wheelers engines, these vehicles also emit pollutantsas exhaust gases while Easy-bikes havealmost no pollutants.Thus, Easy-bikes can play an important role in the transportation sector. At the same time, because of significant amount of electricity is used for charging the batteries of these vehicles, so, the country is experiencing tremendous shortage of electricity. As a result load shading is very common today. These electrically charged vehicles run almost all over the cities and districts of Bangladesh. So, huge number of Easy-bikes enhanced the load shadingproblem. Bangladesh Power Development Board (BPDB) claims that these electrically charged vehicles consume approximately 4MWhrof electricity every day for charging their batteries. But there is no authentic data for this claim. At the same time since the socio-economic condition of some low income people is improving with the inclusion of these vehicles.Therefore, an exclusive comparative study is necessary to decide whether electricity will be used to recharge the batteries or not. Also, question arises whether these vehicles should continue or they should be banned is a big question.

To cope up the problem a survey was conducted in Khulna city with a questionnaire. The objectives were to find out the real consumption pattern of electricity, the socio-economic condition of the stake holders, the environmental issues and some other parameters.

2.Overview of Battery operated Auto-rickshaw and Fuel operated 3-wheelers

Batteries have advantages of being quick responsive, useful in a wide range of power levels, efficient, simple to install and easy to maintain. The Easy-bikes are built on small chassis and three small wheels. The chassis is generallymade from mild steel and the body is with GI pipes. The front face is slightly aerodynamic shape, the overall dimensionsare287×105×178 cm depending different manufactures. The space is suitable for 5passengers. A water-proofdc motor, powered by lead acid batteries, is used as source of power and the output

*Corresponding author; E-mail: drmizan84@gmail.com; Tel.: +88-01714002333

of the motor is about 1000-1250 watts. The cost of Easy-bike ranges from BDT 130,000 to 160,000 [1]. Generally, 5 batteries of 12 volts in some case 4 or 6 batteries of 12 volts of totaling 60 voltsand 140 ampsare used. Batteries need approximately 8 hours for charging at new condition but it need 10-12 hours after using 8-12 months. Each battery costs about BDT 12,000–13,000 [1]. The various models of Easy-bikes are now present in Bangladesh. The common models are: XINGE, DOWEDO, JET FIGHTER, MAINBON GROUP, GANGCHILL, XINGEBANGand JT TRICYCLE.The photographic view of two models ofEasy-bike is shown in Figure 1 and 2.

Figure 1: Model: JET FIGHTER

For short distancesfuel operated 3-wheelers arepopular transport medium in many cities of Bangladesh from seventy's and thesevehicles are run by petrol. These are 2-stroke SI engines [2]. These vehicles generally travelled a distance of 30 km to 35 km per liter of petrol. Number of passengers of these vehicles isalso five. The cost of such a vehicle is approximatelyBDT350,000. Thevarious gasesemitted from these 3-wheelers pollute the environment.

There are other disadvantages of 2-stroke SI engines. It has more fuel consumption, bad emission of harmful gases; noisy sound etc. Its engine oil is relatively expensive and thiscreates smoky emission. 2-stroke engines do not use fuel efficiently as the lubrication system is not efficient. The consumption of lubricating oil is large in a 2-stroke engine because of high operating temperature. These engines produce lot of pollution [2]. They emits significant amount of un-burnt hydrocarbons, CO_2, CO, NOx and so many harmful gases to the environment.

3.Electricity Consumption and No. of Easy-bike

About four lakh Easy-bikes are running across the country which consumes approximately4MWhr of electricity per day for charging their batteries as reported by BPDB on May 2014 [3].

The owners of the Easy-bike charge the batteries either from domestic power connections or from vendors. Sometimes the vendor's connections are illegal resulting in a loss of electricity and also create an unexpected pressure on the national grid. An Easy-bike needs on an average 8 - 11 kWh of electricity per day which is not negligible.

Figure 2: Model: XINGE BANG

The number of battery operated auto-rickshaw running all over country (including all districts and urban areas under these various divisions) as reported in the literature [3 - 5] are presented in Table 1.

Table 1: Approximate No. of Battery operated Auto-rickshaw running on divisional areas:

Name of Division	Number of Easy-bikes (Approximated on May,2014)
Dhaka	67,753
Chittagong	63,580
Khulna	60,820
Rajshahi	54,342
Sylhet	56,885
Barisal	47,740
Rangpur	43,642

Source: The New Age, 7November, 2013

4. Power Scenario of Bangladesh

In Bangladesh various types of resources are available to generate electricity. Mainly natural gas is used; but coal, furnace oil, diesel, hydropower etc. are also used to generate electricity. Table 2 and Table 3 show the present electricity generation capacities on the basis of type of fuels and type of resources respectively [6].

Table 2: Present Generation Capacity by Type of Fuel as on 2013

Sl. No.	Type of Fuel	Capacity (MW)	Total (%)
01.	Coal	200	2.34
02.	Furnace Oil	1876	21.97
03.	Natural Gas	5730	67.12
04.	Diesel	511	5.99
05.	Hydro	220	2.58
	Total	**8537**	**100**

*Corresponding author; E-mail: drmizan84@gmail.com; Tel.: +88-01714002333

Table 3:Present Generation Capacity by Type of Resources as on 2013

Sl. No.	Type of Plant	Capacity (MW)	Total (%)
01.	Hydro	220	2.58
02.	Steam Turbine	2193	25.69
03.	Gas Turbine	1295	15.17
04.	Combined Cycle	1455	17.04
05.	Reciprocating Engine	3374	39.52
	Total	**8537**	**100**

Source:http://www.bpdb.gov.bd/annual report 2013

The zone-wise production of electricity is shown in Table 4. This also shows the differences between the installed capacities and the actual generations [7].

Table 4: Summary of Present Electricity Generation of Bangladesh Zone-wise

Sl. No.	Name of Zone	Installed Capacity (MW)	Present Capacity (MW)	Actual Generation(MW)
01.	Dhaka	3894	3664	2403
02.	Chitta-gong	1207	1127	827
03.	Comilla	1392	1297	1125
04.	Mymen-singh	232	219	163
05.	Syllet	760	746	630
06.	Khulna	1609	1510	990
07.	Barisal	73	65	55
08.	Rajshai	837	819	688
09.	Rangpur	337	287	227
	Total	**10341**	**9727**	**6962**

Source: http://www.bpdb.gov.bd/total generation report May, 2014

5. Emission of CO_2 Gas from Power Plants

Although, the majority of electricity produced in Bangladesh is from natural gas but still the emission of $CO_2$and other polluting gases have been rising in the power sector due to use of different kinds of oils and coals to produce the same. The rising trends of carbon emissions in the power sector is ultimately the result of using coal and petroleum oils like diesel and furnace oil as these produce more carbon dioxide while combustion.The emissions will be even more, if coal-based power plants are introduced more in the country as coal is considered to be the dirtiest fuel for power generation. In contrast there is no emission of CO_2 in hydro-electric or nuclear power plants but their uses are still not prospective. The total electricity generation capacity in the country as on May, 2014 is around 10,341 MW against a maximum demand of over 7,500 MW and the actual generation was 6,962 MW. Of the total production approximately 67% comes from natural gas, 26% from petroleum oils while the remainder is from coal and hydro-power.

In the country there is a mix of power plants that use different energy sources such as furnace oil, HSD, coal, natural gas and hydro power. Each kWh of electricity can be produced by using different energy sources and each source is characterized by a factor that indicates the amount of CO_2 released into the atmosphere to produce each kWh electricity.CO_2 gas in the atmosphere is the main cause of global warming, which directly affects the increase of earth's temperature and affects greatly the change of climate. Table 5 shows the emission of CO_2 from various sources [8, 9].

Table 5:CO_2Emission to produce each kWh of electricity by different types of fuel

Sl. No.	Type of Fuel	CO_2 Emissionsgm/kWh
1.	Coal	800 to 1050
2.	Natural Gas	469 to 600
3.	Diesel	570 to 650
4.	Furnace Oil	640 to 765
Average Total		**592.61**

Source:http://en.wikipedia.org/Greenhouse gas/Carbon dioxide emissions/power plants;
http://www.sunearthtools.com

6.CO_2 Emission from Fuel Operated 3-wheelers

In the country the number of 3-wheelers has grown rapidly, as a result, pollution levels have been increasedwhich is a serious threat for the environment. 3-wheelers are running by petrol and the exhaust gases from these create heavy smoke which contains various harmful gases mostly CO_2 and NO_x.They also create sound pollution. The CO_2emission is approximately 153.78 gm per km distance travelled by a 3-wheeler [10]. Figure 3shows the photographic view of CO_2 emission from a fuel operated 3-wheeler.

Figure3: Photographic view of emission of various harmful gases from a 3-wheeler.

7. Survey and Collection of Data

A questionnaire has been developed to collect information from both the Easy-bike drivers and fuel operated 3-wheelers in Khulna city. In this study 200 Easy-bike drivers were interviewed.Some information were collected from the fuel operated 3-wheeler drivers and their Union office. The information regarding the

*Corresponding author; E-mail: drmizan84@gmail.com; Tel.: +88-01714002333

charging was taken from the field survey as well as in the Laboratory. Finally the data were analyzed.

All data's regarding the economic and social aspects of the stake holders were collected from Easy-bike drivers by interviewing and closely observing them. These information broadly include: (i) General and personal,(ii) Vehicular, (iii) Energy requirement and related, (iv) Economic related, (v)Overall financial, (vi) Problems, social or other related and many more. Some information was collected from internet as well as various newspapers and social media.

8. Results

Socio-economic condition

The analysis of data revealed that the socio-economic condition of the Easy-bike drivers and their families are improving day by day. More than 80% of the drivers agree with the increase in their daily income and remainder 20% disagree with this. More than 50% agree that this vehicle brought prosperity in their economic condition. Most of the drivers think that, it is a comfortable job than their previous jobs and its change their life style. Table 6 shows the average daily and monthly income of the Easy-bike drivers.

Table6: Daily and Monthly Income of Drivers

Daily Income Range BDT.	%	Monthly Income Range	%
> 500	07	> 5000	12
500-600	10	5000-6000	08
600-700	51	6000-7000	07
700-800	12	7000-8000	16
800-900	09	8000-10000	14
1000 <	11	10000 <	43

Source: Survey data from Khulna City, 2014

Electricity Consumption

Although, the consumption of electricity for charging the batteries are taken during the survey but the same were also measured in the laboratory for three vehicles for seven days.From the laboratory data it is seen that battery operated auto-rickshaw consumed on an average 8 - 11 kWh of electricity per day during charging their batteries. Table 7 shows the result of 7 days observations while the batteries were fully charged.

Cost Calculation

A Battery operated auto-rickshaw generally consumed 8 to 11 kWh of electricity during their charging. The price of 1 kWh of electricity is BDT 7.42 [12] for commercial rate at off-peak time and BDT 13.20 as on IPPs [12]. The cost for running per km distance travelled per person is calculated based on data from ten vehicles.

Fuel operated 3-wheelers are usually driven by petrol and small amount of mixture of lubricants. These vehicles generally travelled a distance of 30 to 35 km per liter of petrol. The cost for travelling per km per person is also calculated for these.

Table 7: Charging Information of Battery operated auto-rickshaw.

Day	Energy Consumption in kWhr			Remarks
	Vehi-cle-1	Vehi-cle-2	Vehi-cle-3	
1	10.27	8.86	10.05	Vehicle-1 is relatively old; Vehicle-2 is new & vehicle-3 is medium aged.
2	11.72	10.09	10.09	
3	10.05	9.41	8.40	
4	11.63	8.70	10.66	
5	10.55	9.53	10.38	
6	10.45	8.58	9.08	
7	11.78	10.04	9.84	
Avg.	**10.92**	**8.15**	**9.79**	

Cost Comparison per passenger per km

For battery operated auto-rickshaw the average cost per person per km is about BDT 0.1365and for fuel operated 3-wheelers the same per person per km is about BDT 3.74, which is thirty times higher than battery operated auto-rickshaw.

Comparison of CO_2 emission

Power plants produce 592.6412 gmof CO_2 per kWh of electricity. The amount of energy consumed by the battery operated auto-rickshaw is near about 8 to 11 kWh per charging.It can travel an average distance of 60-70 km per charging.The total amount of energy consumed per km is 0.143 kWh. So, to produce 0.143kWh, the amount of CO_2 emission from the power plant is near about 84.67 gm. The actual emission in gm/km by fuel operated 3-wheelers is about 153.78 gm. So, the emission of $CO_2$from a battery operated auto-rickshaw is less than that of a fuel operated 3-wheelers.

9. Discussion

The socio-economic condition of battery operated auto-rickshaw drivers are improving with the inclusion of this vehicle.

The battery operated auto-rickshaw is directly related to electrical power consumption of the country because it consumes electricityduring charging their batteries. The data shows that four lakhs such vehicle consumes about 4 MWhr of electricity every day.

The transportation cost of battery operated auto-rickshaw is lower than fuel operated 3-wheelers as well as no direct emission of harmful gases from battery operated auto-rickshaw.Fuel operated 3-wheelers are also noisy which causes sound pollution.

*Corresponding author; E-mail: drmizan84@gmail.com; Tel.: +88-01714002333

It is also envisioned that the power plants emits various harmful gases which causes serious pollution of environment as well as health hazard.The coal based plants are the largest contributor of these pollutants.

Proper handlingof discharges of batteries in systematic way has no adverse effect on the environment. Sometimes it creates traffic jam in a narrow road. Auto-rickshaws are being parked in the busy road as well as foot path and traffic jams are the consequence of this mismanagement. Excessive number of battery operatedauto-rickshaws is increasing this traffic jam. So, it should be controlled in right way to reduce traffic jam.

While collecting the data from the survey there was little problem to get the accurate information such as some of the drivers could not gave the answers all of the questions fully and sometimes there information was not fully correct, some data which were far away from them these data were neglected. So it seems to be difficult to find the real data.

10. Conclusion

From the analysis of the data obtained from the survey the following conclusions can be made.

- The inclusion of battery operated auto-rickshaw improves the socio-economic condition of many poor unemployed people.
- The interest of lower-middle income people on this transportation system is more in short-distance because of lower travel cost than rickshaw and 3-wheelers.
- The transportation cost of battery operated auto-rickshaw is less than fuel operated 3-wheelers.
- A battery operated auto-rickshaw seems apparently non-polluting and a very silent transport system for urban and rural areas of country.
- It is apparently cost effective vehicle as it is environment friendly vehicle.
- The fuel operated 3-wheelers emit CO_2 and other polluting gases. Indirectly this is true for battery operated auto-rickshaw as electrical power plants generate CO_2.
- To pollutants from disposal of batteries could be reduced by proper disposal of the same.
- Although, these vehicles consumes electricity from the national grid but considering the economic and social improvement of the families of battery operated auto-rickshaw, it is more advantageous than fuel operated 3-wheelers.

References

[1] A. K Auto-rickshaw, Khulna, Bangladesh.
[2] Crouse-Anglin, *Automotive Machines*, Tata McGraw-Hill publishing company limited.
[3] http://www.bpdb.gov.bd/annual report 2013
[4]The New Age, Thursday, November 7, 2013
[5] The Independent, Saturday, 25 January 2014
[6] The Daily Star, Sunday, May 18, 2014
[7] http://www.bpdb.gov.bd/annual report 2013
[8] http://en.wikipedia.org /Greenhouse gas/ Carbon dioxide emissions/ power plants
[9] http://www.sunearthtools.com /CO_2-emissions
[10] http://www.dhakatribune.com
[11] http://en.wikipedia.org/ gas power plant
[12] http://www.edfenergy.com

*Corresponding author; E-mail: drmizan84@gmail.com; Tel.: +88-01714002333

International Conference on Mechanical, Industrial and Energy Engineering 2014
26-27 December, 2014, Khulna, BANGLADESH

ICMIEE-PI-140400

Design and Construction of a Parabolic Dish Solar Cooker

Erina Baynojir Joyee[1] *and Dr. A. N. M. Mizanur Rahman*[2,*]

[1] UG student, Dept. of Mechanical Engineering, Khulna University of Engineering & Technology, Khulna-9203
[2]Professor, Dept. of Mechanical Engineering, Khulna University of Engineering & Technology, Khulna-9203

ABSTRACT:
The use of renewable energy, particularly solar energy, is increasing day by day to promote its contribution to national economy. Solar energy can be used in heating, drying, cooking and also for generating electricity. In this paper the design, construction and performance test of a parabolic dish solar (PDS) cooker is discussed. The cooker having an aperture diameter of 106 cm and focal length of 54 cm was designed, constructed and the performance was tested. Plane mirror was used as reflecting material in the cooker. The maximum temperature inside the cooking pot was found to be 97°C.As performance test rice and dal were cooked in various amounts at different days and times. Experiments showed that the temperature inside the cooker varies with the available solar radiation. The cooker could cook 300 gm rice and 100 gm dal within 40 minutes at an available radiation level of 320 -390 W/m². An economic analysis of the cooker was performed and it showed a payback of 16 months, which is realistic and very promising.

Key Words: Solar cooker, parabolic dish, concentrating cooker, design and development of cooker.

1. Introduction

Energy crisis, at present is one of the major global challenges faced by mankind. Natural energy resources such as fossil fuel, oil, natural gas etc. are depleting in nature and will exhaust in one day. So, the need for conserving conventional energy and for developing energy alternatives has led to considerable research and development work in this direction and significant progress has been made. In a developing country like Bangladesh the crisis is more serious. The use of renewable energy, particularly solar energy, is increasing day by day to promote its contribution to national economy. Solar Home System (SHS) is now becoming popular in remote areas. The development of LED lights accelerated the use of solar home system. The initiation taken by Government through Infrastructure Development Company Limited (IDCOL) and different NGO's popularize this system within the country.

Cooking is one of the major energy consumption sectors is Bangladesh where mainly non-renewable sources (i.e. firewood, natural gas, LPGetc.) are used. As these sources are limited, their conservation is very important for future use and also for our next generation. There are three different ways of remedying suchan insufficient supply of non-renewable energy sources:(i) Increasing the treeplantation program of high yielding varieties, (ii)Introducing more and more energy efficient cooking stoves, (iii) Developing indigenous alternative sources of fuelor promoting green energies i.e. solar energy, which is efficient for cooking. Solar energy can be one of the most available and enormous sources of energy in Bangladesh, where the maximum and minimum day times are 12.5 and 10 hours respectively in the year round.The solar radiation level is in the range of 4 to 6.2 kW/m^2 per day. Using concentrating solar collectors the radiation level can be enhanced by capturing them from a larger area and directing them to a relatively smaller area. In concentrating type solar cooker usually a mirror or some type of reflective material is used to concentrate the incomingsolar radiation into a small cooking area. Some absorbing materials are used to absorb solar radiation and convert it into heat [1]. There are various types of solar cooker, among them parabolic dish solar cooker is a good solution for use of solar energy for cooking purpose because of its higher temperature. Parabolic dish solar cooker has the highest efficiency in terms of the utilization of the reflector area because there is no loss due to aperture projection effects. Also, radiation losses are small because of the small area of the absorber at the focus.

In the present study a parabolic dish solar (PDS) cooker was designed and constructed whose parabolic dish was madeusing small pieces ofplane mirror for better performance. It also caused more solar radiation to be concentrated into a smaller area for obtaining more heat. The radiation losses were also small because of smaller absorber area. Further in this paper the detailed design and construction of the cooker, performance test, data analysis and economic feasibility are discussed.

2.Geometry of ParabolicDish Solar (PDS) Cooker

In the proposed PDS cooker more solar radiation can be capturedby utilizinglarger reflector area. Also,there is less loss due to aperture projection effects andheat losses

*Corresponding author; E-mail: drmizan84@gmail.com; Tel.: +88-01714002333

are small because of small absorber area which is situated at a distance from the center of the dish known as focal length.

The surface of revolution which formed by rotating a parabolic curve about its axis is called a paraboloid. Solar concentrators having a reflective surface in this shape are often called parabolic dish concentrators. Parabolic dish concentrators as shown in Fig. 1, uses a truncated portion of the surface generated by rotating the parabolic curve [2].

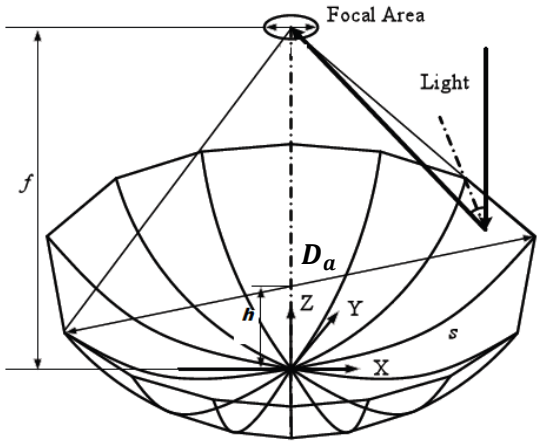

Fig. 1: Parabolic dish parameters and variables

The size of a parabolic dish is often specified in terms of linear dimension such as aperture diameter, D_a, or focal length, f. The height of the parabolic dish,h is defined as the maximum distance from the vertex to a line drawn across its aperture. In terms of focal length and aperture diameter, the height (h) of the dish is [2]:

$$h = \frac{D_a}{16f}$$

The parabolic dish aperture area,the most important parameter to solar energy designer, is simply the circular area defined by the aperture diameter D_a and is given by:

$$A_a = \frac{\pi D_a^2}{4}$$

The basic function of a parabolic dish solar cooker is to collect solar radiation over a large area and concentrate it onto a smaller area, the focal point, where the absorber containing food is located [2]. The temperature of the absorber as well as the food rises when more and more solar radiation concentrated and reflected onto the absorber and after some time the food is cooked.The incident solar radiation consists of direct and diffuse radiation. However, the majority of concentrating collectors can utilize only direct part of the radiation.

3. Design and Calculations

The heat demand of the cooker was assumed so that it could cook 400 gm rice at a time. Cooking of rice using conventional methods require5 volumes of water to one volume of rice, while cooking with a solar cooker requires two volume of water to one volume of rice[2]. In conventional methods about 25% of the water required for cooking is lost to the surrounding by evaporation whereas in solar cooking rate of evaporation is less.

Sizing of the solar cooker:

Assuming mass of water, m_w = 0.8kg, mass of rice, m_r=0.4kg with specific heat of water and rice as C_{pw} = 4.186 kJ/kg°C andC_{pr}= 1.76kJ/kg°C; the density of water as ρ = 997.01kg/m^3 at 25°C, the energy requirement for cooking rice is –

$Q = Q_r + Q_w = m_r C_{pr}(T_f - T_i) + m_w C_{pw}(T_f - T_i)$
= 0.4× $1.76(100 - 25)$+0.8× $4.186(100 - 25)$
= 303.96 kJ

So, total energy required should be, $Q \approx 304\ kJ$
Again,it is known thatQ= $\eta_{th} I_b A_a t$. Assuming, average solar intensity, I_b = 485 W/m^2 andefficiency of the solar cooker as, η_{th} = 20% and time requiredfor cooking as, t = 1hr; then –

Q= 304× $10^3 J$ = 0.20 ×485× 3600 × A_a

⇨ A_a= 0.871 $m^2 = \frac{\pi {D_a}^2}{4}$

⇨ D_a = 1.06 m = 106 cm

Concentration ratio is defined as,C = $\frac{A_a}{A_{abs}}$;
Assuming, C=10;$A_{abs} = \frac{0.871}{10}$ = 0.0871m^2

Again, the cooking pot has a cylindrical part and a flat bottom part. Assuming, 2*L_{abs} = D_{abs}. So,

$A_{abs} = \frac{\pi {D_{abs}}^2}{4} + \pi D_{abs} L_{abs} = \frac{\pi}{4} {D_{abs}}^2 + \pi D_{abs} \left(\frac{D_{abs}}{2}\right)$;

⇨ $0.0871 = \frac{\pi {D_{abs}}^2}{4} + \pi D_{abs} \frac{D_{abs}}{2}$

⇨ D_{abs} = 0.1926 m = 19.26 cm

⇨ L_{abs} = 9.63cm

Assuming thickness of cooking pot as 2mm

⇨ l_{abs} = 9.43cm, D_{abs} = 19.06 cm ,

⇨ Assuming h = 13 cm, then the focal length,

⇨ $f = \frac{{D_a}^2}{16h}$= 54 cm

4. MaterialSelection for Construction of PDS Cooker

Apart from the design and construction of parabolic dish solar cooker the materials used in its construction of different components should be carefully selected to achieve best results so that the proposed cooker can reflect more solar radiation to heat up the cooking

*Corresponding author; E-mail: drmizan84@gmail.com; Tel.: +88-01714002333

element in the cooking pot thus consumeless time and also ensure long life of the cooker.The cooking pot holder and the reflector weremounted on a structure called frame. MS flat bar was used for this. The whole frame was supported by another structure constructed from MS angle and flat bar. The frame could be rotated to direct the dish towards the sun. In this project commercially available dish could not be used because of cost and also it was not available in local market. So,the reflector was made by several pieces plane mirror by attaching them to a plastic mold. The plastic mold was supported by the MS flat bar as mentioned before.

In this cooker, absorber works as the cooking pot.Aluminum is selected as absorber material because it has high thermal conductivity, good corrosion resistance,high absorbing capability of heat and light weight. Also, it iseasily available in the local market and most importantly can be colored dark to its external surface easily.

For reflecting systems, materials of high quality and good specular reflectance properties are required. A light glass mirror of high surface quality and good specular reflectance was selected. The glass mirror of 2 mm thickness was chosen to reduce the overall weight. Glass mirror was selected over polished aluminum surface because of its reflectivity of 95% is better than that of aluminum (85%).Finally the cooking pot was painted with a mixture of black oxide and varnish. This mixture has the property to increase the absorption capability of the material on which it is coated.

5. Data Collection

After completion of the construction works, it was placed under open sky directing towards the sun. For the assurance of the fact that the reflector surface is fully directed to the sun it has to be observed that the surface of the cooking pot has enlightened by all side of its outer periphery. After every 15 minute the cooker was manually tracked for perfect focusing all the time to get the highest solar intensity at every time. Temperature of the cooking elements was recorded from the digital temperature collector with 10 minutes time interval. At the same time the solar intensity was also recorded from a solarimeter. According to the measurement water is taken into the cooking pot and when temperature of water was raised to 75º to 80ºC the rice and dal was added.

Different amount of rice and dal were used at different observations. For a fixed amount of rice and dal five observations were taken at different time of the day at different days. Total 20 observations weremade for various amounts of rice and dal. The typical results obtained are shown in Table 1 and Table 2 respectively,for (200 gm rice+50 gm dal) and (300 gm rice+50 gm dal)

Figure4.1: Photographic view of PDS Cooker

Table 1: Experimental data on 22.5.14

No. of obs	Cooking item with quantity	Watch time	Inten-sity W/m²	Energy Wh/m²	Tem p ºC
Started at: 11.40 am End at: 12.15 pm					
1	Rice = 200 gm Dal = 50 gm Water = 500 ml	11.40	376	00	29
2		11.50	387	103	82
3		12.00	394	367	97
4		12.10	401	536	97
5		12.15	370	689	97
Remarks: 200 gm rice and 50 gm dal boiled properly at 35 mins. Stagnation temperature: 97°C					

Table 2: Experimental data on 12.5.14

No. of obs	Cooking item with quantity	Watch time	Inten-sity W/m^2	Energy Wh/m^2	Temp ºC
Started at: 09.50 am End at: 10.30 am					
1	Rice= 300 gm Dal=50 gm Water=	09.50	317	00	33
2		10.00	331	114	68
3		10.10	346	278	82
4		10.20	392	385	96
5		10.30	402	584	96

*Corresponding author; E-mail: drmizan84@gmail.com; Tel.: +88-01714002333

	700 ml				
Remarks: 300 gm rice and 50 gm dal boiled properly at 40 mins. Stagnation temperature: 96°C					

6. Result & Discussion

The variation of temperature of water and cooking element inside the cooking pot with time plotted and are shown in Figure 1 to Figure 4.

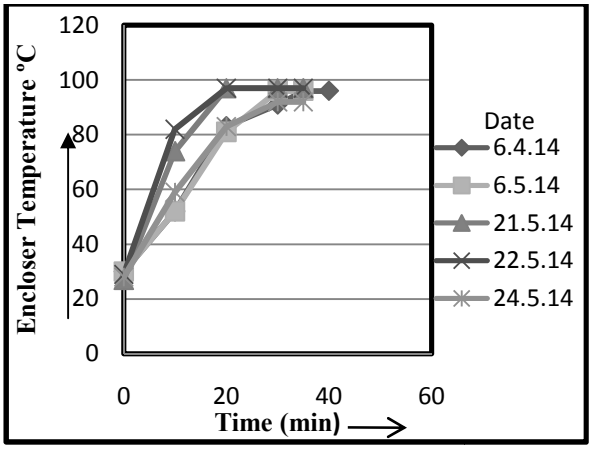

Figure 1: Temperature vs time curve for 250 gm load for different days

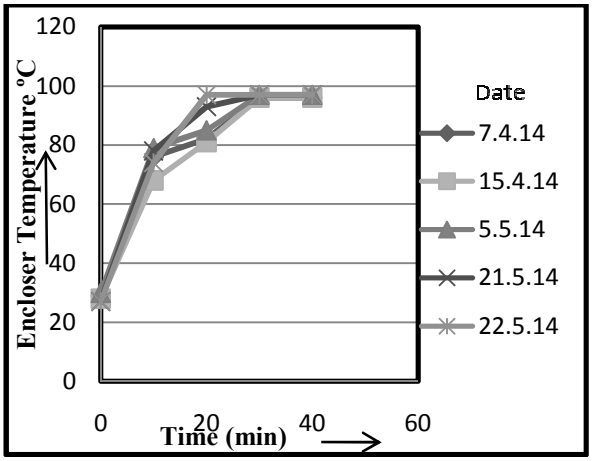

Figure2: Temperature vs time curve for 300gm load for different days

From Figures 1 to 4 it was seen that the temperature within the cooking pot increased with time. It was also seen that on different dates the increasing of temperature with time varies. It was because of the variation of intensity. The higher the radiation the higher the temperature obtained.

From Figure 1, it was seen that among all the data for 250 gm rice and dal, the highest time was taken on 6.4.14. It was because the average intensity was 301 W/m² on that day which was the lowest. The highest temperature recorded was 97° C.

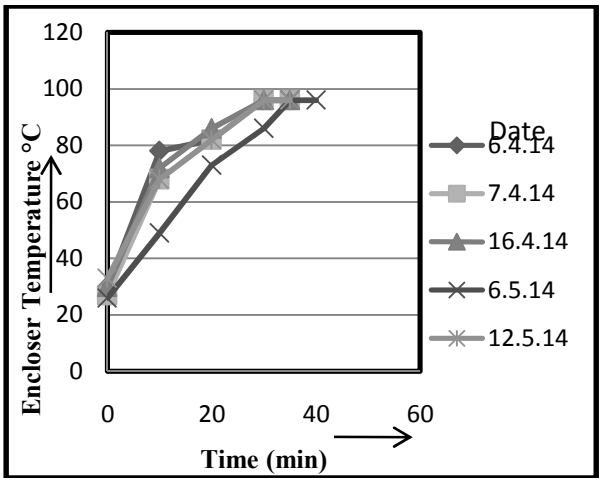

Figure3: Temperature vs time curve for 350gm load for different days

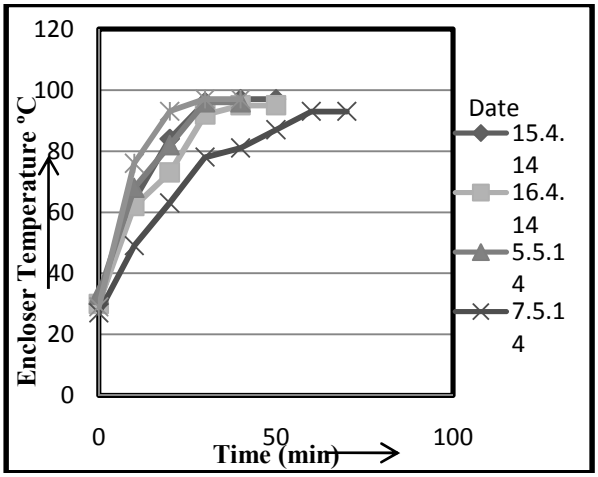

Figure4: Temperature vs time curve for 400 gm load for different days

From Figure2, it was seen that, for 300 gm rice and dal almost same time was taken for cooking on various days. But on 15.4.14 the temperature was relatively less than the other day's after 10 minutes. It was because of intensity at that time was fallen to a very low value of 285 W/m² compared to other days values. The highest temperature recorded was 97° C.

From Figure3, it was seen that all the data for 350 gm rice and dal were almost same. On 6.5.14 it was seen that the time taken for cooking was 50 minutes. It was the highest time taken among all the data for cooking 350 gm rice and dal because, it was a cloudy day. So, the

*Corresponding author; E-mail: drmizan84@gmail.com; Tel.: +88-01714002333

intensity varies randomly. The highest temperature recorded was 96° C.

From Figure4, it was seen that on 7.5.14 the time taken for cooking was about 70 minutes. It was the highest time among all the data for cooking 400 gm rice and dal because, it was a cloudy day. So, theintensity varies randomly as on 6.5.14. The highest temperature recorded was 97° C.

7. Economic Analysis

The cost analysis of the constructed solar cooker wasperformed on the basis of present market price of various materials used. The material quantity and their cost are shown in Table 1.

Table 1: Shows construction cost of the solar cooker

Materials	Quantity	Cost in Tk
Angle bar	12 kg	750
Flat bar	3 kg	175
Glass (3 mm)	2 piece(96× 42 sq. in)	1000
Glue	600 ml	140
Black oxide	20 gm	50
Hardware		50
Total cost		2165

For the economic analysis of the constructed cooker the main approaches were calculating the annual cost and calculating the life cycle cost. This is summarized in Table 2.

Table 2: Life cycle cost of the constructed cooker

Type of Cost		Annual cost Tk.	Life cycle costTk.
Fixed cost	1.Construction cost	2165	2165
Total fixed cost		2165	2165
Variable cost	1.Maintenance cost a. Paint required for cooking pot b. Washing chemical	50 80	250 400
Total variable cost		130	650
Total cost		2295	2815

Assuming the constructed solar cooker can cook about 800 gm per day and about 200 days per year [3]. From experience the cost for cooking 800 gm rice in household Chula by using wood as cooking fuel is 5 Tk. [4].

Table 3: Cost benefit comparison of parabolic dish type solar cooker

Cooker	Annual cost	Life cycle cost(5 yrs)in Tk	Remarks
Solar Cooker	563	2815	Saving by Parabolic dish type solar cooker is Tk.437 annually
Household chula	1000	5000	

From the Table 3, the cost benefit ratio [5] for 5 years is,2815/5000 =0.563.

Pay Back Analysis:

Total construction cost = 563.00 Tk.From Table 3, net saving = Tk.437.00. So, Payback period is total investment to net saving = 563/437= 1.3 yr. =16 months.

8. Conclusion

In near future solar energy will contribute a major share in energy sector. So, proactive utilization of solar power is important.Energy consumption for cooking in developing countries like Bangladesh is a major component of the total energy consumption. The parabolic dish solar cookerrepresents a potential subsidiary way of cooking upon the conventional ways. According to the design the cooker was constructed with the materials which are available in the local market. After construction it was tested with different operating conditions and the cooker can cook 300 gm rice and 100 gm dal within 40 minutes at an available radiation level of 322-390 W/m². So, the efficiency of cooking of the cooker found satisfactory. Though its construction and operational cost is low, so this type of solar cooker can be promotes in remote and rural areas.

References:

[1]http://en.wikipedia.org/wiki/Renewable_energy_policy_of_Bangladesh
[2] Ibrahim Ladan Mohammed, "Design and Development of a Parabolic Dish Solar Thermal Cooker", International Journal of Engineering Research and Applications, Vol. 3.Department of Mechanical Engineering, Kaduna Polytechnic, Kaduna, Nigeria.
[3]http://www.accuweather.com/en/bd/bangladesh-weather
[4] Md. Arifur Rahman, "Construction and Performance Test of a Box type solar cooker", Thesis report. Bachelor of Science in ME.
[5] http://financial-dictionary.thefreedictionary.com/Cost-benefit+ratio

*Corresponding author; E-mail: drmizan84@gmail.com; Tel.: +88-01714002333

ICMIEE-PI-140403

Design, Construction & Performance Test of a Rotational Digital viscometer

Md Mahbubur Rahman [1], Md *Rasedul Islam*[2], *G. M Sultan Mahmud Rana*[3], *Mihir Ranjan Halder*[4], *Md Tareq Hassan* [5], *Shamim Ahmed*[6]
[1]Department of Mechanical Engineering, Khulna University of Engineering & Technology, Khulna-9203,BANGLADESH

ABSTRACT

A coaxial cylindrical rotational viscometer is such a type in which a solid (inner) cylinder is rotated inside a hollow cylinder which contains test sample of liquid. The torque experienced by the solid cylinder due to viscous effect of the test sample is measured and hence viscosity can be calculated. The design, construction and performance of a coaxial type rotational viscometer have been performed with locally available materials in order to measure the viscosity of different liquids at different temperatures which have been presented in the paper. The inner cylinder has been made from aluminum, rotated by a dc motor and outer cylinder has been fabricated from GI sheet. A temperature controlling bath has been provided in order to maintain a constant temperature in the test sample. The bath has been constructed with GI sheet and having 1 cm insulation of glass wool. An arrangement has been made to show the temperature of sample liquid and its viscosity digitally. The test has been carried out within the temperature range 35 ^{o}C to 80 ^{o}C for water, diesel and kerosene. But there is a remarkable deviation of the measured viscosity from the actual. In order to minimize the deviation a correction coefficient '*C'* has been introduced and multiplied with the measured value. With the help of curve fitting, empirical equation of correction coefficient for water, diesel and kerosene has been determined. Finally it can be said that when multiplying the value of *C* from empirical equation with measured value, the deviation from actual viscosity has been greatly reduced. Though equation of correction coefficient for each sample has been developed using data within the range 35 ^{o}C to 80 ^{o}C, it can be applied to any temperature since trend of the best fit curve of correction coefficient vs. temperature is very close to the actual curve.

Keywords: Viscometer, Viscosity, Materials, Temperature, Correction Coefficient.

1. Introduction

The Viscometer is a device by which the viscosity of fluids is measured. Rotational viscometer is such a type where a solid shaped body named cylinder or spindle is rotated immersing in the fluid whose viscosity is to be measured. A typical rotational viscometers work on the principle that the torque required to turn an object in a fluid is a function of the viscosity of that fluid. From the measurements of rotational speed of the solid body and the required torque, the viscosity is calculated [1].

Rotational viscometer has several advantages over others. The measurement of fluid viscosity is very important in many practices such as chemistry, chemical industry, and many types of manufacturing practices. So, viscosity should be measured properly and correctly. A typical viscometer is not always preferable in some cases where values with precision and time saving measurement of fluid viscosity are important factors. Hence developments on a typical rotational viscometer are necessary. This will eliminate all sorts of possible errors in the existing viscometer like improper alignment of inner cylinder and driving motor shaft.
The interest to design a digital rotational viscometer with locally available materials that could be used in the measurement of viscosity of different fluids, due to the listed reasons below:

- *Unavailability of the instrument in the local market.*
- *High cost of the instrument for the importation.*
- *Use of local technology and skills for the construction of the device.*

The objectives of this project are:

- *To construct a digital co axial rotational viscometer*

2. Rotational Viscometer and Digitalization of its measuring system.

2.1 Dimensions

In this project, the diameter of the inner cylinder was assumed as 3 cm. Generally height is to be taken as twice the diameter [2].

So height of the inner cylinder was taken as 6 cm. So we can conclude the dimension of the inner cylinder as below.

Diameter of inner cylinder = D_i=3 cm

Md. Mahbubur Rahman. Tel.: +88-01937230054
E-mail address: mahbub.kuet.08@gmail.com

Height=h= 6 cm

Diameter of outer cylinder= D_o=6cm

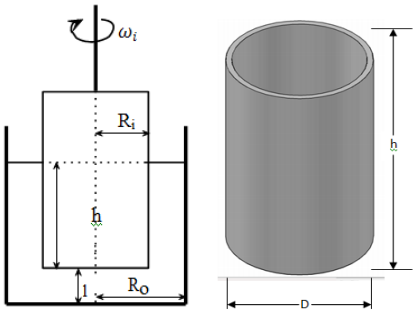

Fig.1 Basic structure of a coaxial cylinder viscometer

2.2 Material:

The material, whose heat transfer capacity is low, can be used to fabricate the temperature bath to reduce heat loss to the outside. In this project two layer GI sheet has been used and insulation has also been provided.

2.3 Insulation:

Insulation is used to reduce heat loss to the outside. In this project, an insulation of 1 cm thickness to all sides of the temperature bath has been provided. Glass Wool has been be used as insulating material since it has lower thermal conductivity and its numerical value is .04 *W/(m.K)*.

2.4 Heater:

Two heaters each having capacity of 500W, are used in control temperature bath. Each heater operates at 220-240V.

2.5 Specification of motor:

The specification of motor is listed below

Type: DC

Capacity: 25W

Operating voltage: 6-12V

Operating current: upto 2 amp

Rpm at free load: 1800

2.6 Structural view

The device of the project has been developed in that manner below.

Fig.2 Shaft Coupler

The joint had been made by a screw mechanism. The main shaft is drilled to allow the motor shaft to enter in it and then a screw is set to have rigid coupling.

Fig.3 Adjustable Motor Base

To ensure proper alignment of motor and the main shaft an adjustable motor base is provided. The motor is rigidly attached to the base and the base is movable relative to the frame.

Fig.4 Adjustable Cylinder Base

A new cylinder base was constructed for outer cylinder which is adjustable within the heating bath. By placing the outer cylinder to the appropriate position, the required co-axial alignment of the two cylinders can be set.

Fig.5 Revolution Counter Plate

2.7 Theory and Evaluation for coaxial cylinder viscometer:

When a thin film of a liquid is held between two glass plates, moving the plates relative to each other requires the application of force. The liquid layers that are directly adjacent to each the plate surfaces are held to them by forces of adhesion, and forces of cohesion act between the molecules of the liquid. On movement, a linear velocity gradient is formed within the liquid between the two plates.

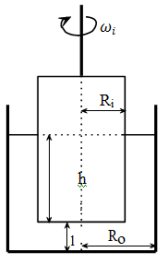

Fig6. Basic structure of a coaxial cylinder viscometer

When a fluid is held between two surfaces and a linear velocity gradient is formed within the fluid then we have according to Newton's law of viscosity from equation [3]

$$\tau = \frac{F}{A} = \mu \frac{dv}{dy}$$

where,

μ = Viscosity

τ = Shear stress

$\frac{dv}{dy}$ = velocity gradient

F = Force required to move liquid layers

A = Area of contact between the plate and the liquid

At low rotational velocity the moment of rotation or torque $T(r)$ which is exerted on a cylindrical layer of liquid with a radius r and a height h conforms to the following relationship as a result of the rotation of the inner cylinder [4]

$$T = F \times r$$
$$\Rightarrow T = \tau A \times r$$
$$\Rightarrow T = \tau(2\pi r h)r$$
$$\Rightarrow \tau = \frac{T}{2\tau h r^2} \text{ ----------(1)}$$

Combining equation (2.1) and (2.4), we have

$$\frac{dv}{dy} = \frac{T}{2\tau\mu h r^2}$$
$$\Rightarrow dv = \frac{T}{2\tau\mu h r^2}\, dy$$

Replacing $dy = -dr$ since r decreases with the increase of y where 'y' is the distance from outer cylinder

$$\Rightarrow dv = -\frac{T}{2\tau\mu h r^2}\, dr \text{ ----------(2)}$$

Considering

v_i = Velocity of inner cylinder

v_o = Velocity of outer cylinder = 0 (since it is stationary)

ω_i = Angular Velocity of inner cylinder

ω_o = Angular Velocity of outer cylinder (since it is not rotating)

R_i = Radius of inner cylinder

R_o = Radius of outer cylinder

Integrating equation (2.5) within the limit v_o to v_i and R_o to R_i

$$\int_{v_o}^{v_i} dv = \frac{T}{2\pi\mu h} \int_{R_o}^{R_i} \left(-\frac{dr}{r^2}\right)$$
$$\Rightarrow v_i - v_o = \frac{T}{2\pi\mu h}\left({}^1/_{R_i} - {}^1/_{R_o}\right)$$

Here,

v_0 = 0 since outer cylinder is stationary

$v_i = \frac{2\pi N_i}{60} \times R_i$ where N_i is rpm of inner cylinder

So we have,

$$\Rightarrow \frac{2\pi N_i}{60} \times R_i = \frac{T}{2\pi\mu h}\left({}^1/_{R_i} - {}^1/_{R_o}\right)$$
$$\Rightarrow \mu = \frac{T \times 60}{4\pi^2 N_i h}\left({}^1/_{R_i^2} - {}^1/_{R_i R_0}\right) \text{ ----------(3)}$$

This is the desired equation by which viscosity of a fluid can be measured. The equation is valid for those case in which shear is proportional to velocity gradient.

2.8 End Effects:

The main concern with the coaxial cylinder viscometer is the end effects. The equation has been derived without considering the end effects. End effects are the resistances offered by the test sample at the base and top of the inner cylinder. End effect at the top may be avoided by ensuring that the wetted height will not be higher than the height of the inner cylinder. Several scientists have been working to determine end effect. In this section, various approaches for end effect at the base will be discussed.

Couette and Hatschek modified the design to eliminate end effects by the use of guard rings [5].

Mallock suggested that the inner cylinder can have a concave base in which a bubble of air could be trapped to reduce the drag on the base. However, the difficulty of trapping the same volume of air during each measurement prevented its wide range use [6].

Lindsley and Fisher found that the end effect is negligible in the range of 1 to 150 poise, but the viscosity must be corrected when it is below 1 poise [7].

Lindsley and Fisher, and Highgate and Whorlow suggested that modification of the design may not be adequate to account for the end effects. Therefore experimental measurements and theoretical analysis were proposed by a number of researchers to correct the viscosity for end effects [8].

Kobayashi provided end corrections for several combinations of bob (inner cylinders) and cup(outer cylinder) design. For rotating bob viscometer system, the end correction appears to increase for Reynolds numbers above 10, even for low viscosity. A conical end of the inner cylinder and a wide gap between the inner and outer cylinder give a larger end correction. But wide gap between inner and outer cylinder tends to break linearity of velocity potential in the gap [9].

In this project, end effect will be compensated by carrying out experiment of different sample. Finally a correction coefficient will be provided which will take into account end effect and other instrumental error.

2.8 Digitalization of the Device

The measuring procedure is fully automatic. A microcontroller will control all the steps orderly according to the program. The input values are determined by high precision semiconductor devices (IR LED, temperature Sensor etc.) and feed to the microcontroller. To convert AC current into DC current bridge rectifier and regulator ICs are used. The motor speed is properly measured by IR LED and precisely controlled by microcontroller. To determine fluid temperature, temperature sensor is used and so microcontroller is able to switch off the heater when desired temperature is reached. The following circuit elements have been used in the project:

1) Resistor
2) Capacitor
3) Diode
4) LED
5) Regulator IC
6) Transistor
7) MOSFET
8) IR Emitter
9) IR Absorber
10) Temperature Sensor
11) PCB

2.8.1 Main Circuit Board

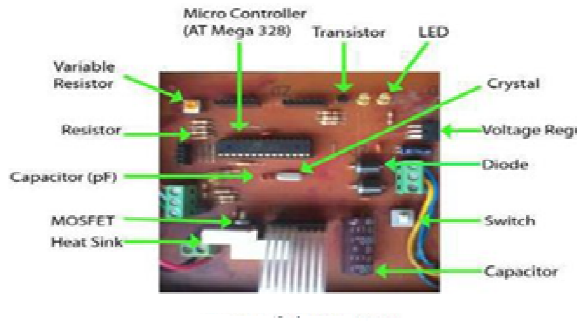

Fig7. A photograph of circuit board

2.8.2 Simulation of the project

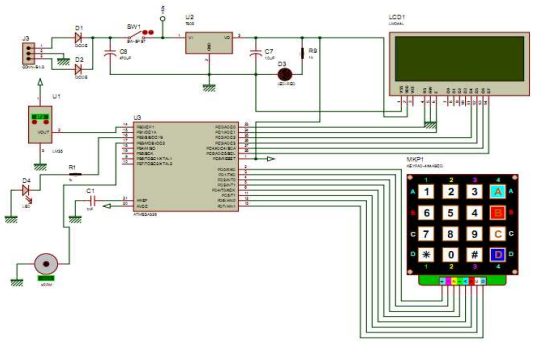

2.9 Operation

At first the device will ask for setting (PWM) Pulse Width Modulation. After setting PWM, DC motor will start rotating. The microcontroller circuit will read no load power and the motor rpm and calculate no load torque. The motor will be switched off by a button of keypad then. Sample liquid will be poured into the outer cylinder. The heater will be started . The temperature sensor will show liquid temperature. Then decision will be taken to switch off the heater. Now for the same PWM , the microcontroller will read the motor rpm, power and calculate torque at load condition. The program will calculate the difference between load torque and no load torque and finally show the viscosity of the sample liquid at that temperature.

3. Experimentation

In order to carry out the experimentation of the digital viscometer, viscosity of few samples will be measured by the viscometer. Then the measured viscosity will be compared with the actual viscosity. Finally a correction coefficient will be provided. In order to obtain the actual viscosity, measured viscosity will be multiplied by the correction coefficient.

3.1 Parameter Measured In The Test

Rpm of inner cylinder at load = N_L
Rpm of inner cylinder at no load = N_{NL}
Ampere of the DC input = I in amp
Voltage of the DC input = V in volts

3.2 Equation Used In Calculation

Power at the motor shaft,
P_m = VI in Watt---------- (4)

Ampere of the DC input = I
Voltage of the DC input = V

Torque of the motor shaft at no load,

$T_{NL} = \frac{P_m \times 60}{2\pi N_{NL}}$ in Nm---------- (5)

Torque of the motor shaft at load,

$T_L = \frac{P_m \times 60}{2\pi N_L}$ in Nm---------- (6)

Torque offered by the test sample,

$T = T_L - T_{NL}$---------- (7)

From equation (3), viscosity can be expressed as

$$\mu = \frac{T \times 60}{4\pi^2 N_i h}\left(1/R_i^2 - 1/R_i R_0\right)$$

Here,

$R_i = 1.5\ cm = .015\ m$

$R_o = 3\ cm = .030\ m$

$h = 6\ cm = .06\ m$

$N_i = N_L$

By putting this value in above equation we get,

$\mu = 45031 \times \frac{T}{N_L}$---------- (8)

3.3 Experimental Value of Viscosity

Table 1 Viscosity of water at different temperatures.

Temperature (°C)	Measured viscosity (Pa.s)	Actual Viscosity (Pa.s)
35	2.32×10^{-3}	0.723×10^{-3}
40	2.1×10^{-3}	0.656×10^{-3}
45	1.85×10^{-3}	0.599×10^{-3}
50	1.62×10^{-3}	0.549×10^{-3}
55	1.43×10^{-3}	0.506×10^{-3}
60	0.89×10^{-3}	0.469×10^{-3}
65	0.76×10^{-3}	0.436×10^{-3}
70	0.53×10^{-3}	0.406×10^{-3}
75	0.42×10^{-3}	0.380×10^{-3}
80	0.26×10^{-3}	0.357×10^{-3}

Table 2 Viscosity of kerosene at differenttemperatures.

Temperature (°C)	Measured viscosity (Pa.s)	Actual Viscosity (Pa.s)
35	6.85×10^{-3}	1.95×10^{-3}
40	6.25×10^{-3}	1.766×10^{-3}
45	6.01×10^{-3}	1.583×10^{-3}
50	5.4×10^{-3}	1.4×10^{-3}
55	5.3×10^{-3}	1.32×10^{-3}
60	4.95×10^{-3}	1.24×10^{-3}
65	4.69×10^{-3}	1.16×10^{-3}
70	4.28×10^{-3}	1.08×10^{-3}
75	3.83×10^{-3}	1×10^{-3}
80	3.45×10^{-3}	0.98×10^{-3}

4. Results

4.1 Presentation of Result

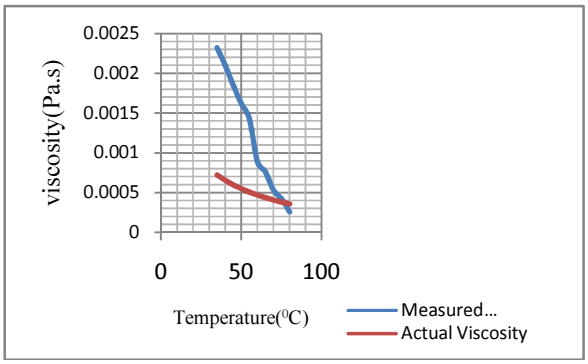

Fig8. Actual Viscosity and Measured Viscosity(Multiplying Correction coefficient) of water at different temperatures.

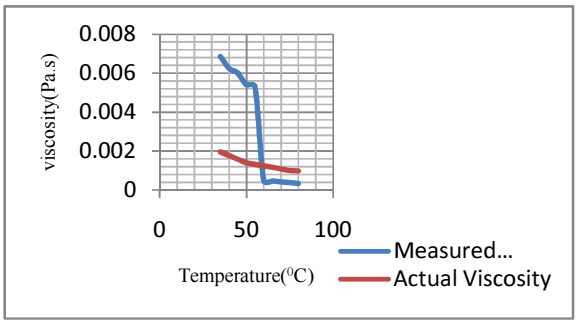

Fig9. Actual Viscosity and Measured(Multiplying Correction coefficient) of kerosene at different temperatures.

4. Discussion

The determination of viscosity of fluid was carried out on two samples at different temperatures.

The samples were water and kerosene and the tests were done in the temperature range 35-80°C.

with each at 5. intervals (i.e. 35 °C,40 °C,45 °C, 50 °C, 55 °C, 60 °C, 65 °C, 70 °C, 75 °C and 80 °C).

First, viscosity was calculated from equation (4.5). In the test, it was seen that this measured viscosity was not conformed to the actual viscosity.This can be corrected by introducing a Correction Coefficient. This is the usual practice what every viscometer manufacturer does. For every viscometer, manufacturer provides a correction coefficient. It has been observed that measured viscosity decreases with the increase of temperature which validates the properties of a liquid.

When water was taken as sample the values of Water viscosity at temperature 35. was measured 2.32×10-3 Pa.s. In comparison of the actual viscosity (0.723×10-3 Pa.s) it gives almost three times. Some other values like at 60. the measured value is doubled of actual value

which signifies that temperature has an effect on correction factor.

When kerosene was taken as sample the viscosity measured digitally varies in 3.2 to 4 times of the actual value still signifying the effect of temperature on correction factor. The actual viscosity of kerosene at 55. is 1.32×10-3 Pa.s where the digitally measured value is 5.3×10-3 Pa. s which is almost 4 times.

The correction coefficient. C.=1.8401-0.0698Θ+0.0008Θ^2 for water

C=0.4979-0.0084Θ.+0.00007Θ^2 for kerosene

were suggested for our experimented value.

5. Conclusion

A coaxial cylindrical rotational viscometer has been developed and digitalized in this project. The provision for the measurement of viscosity of liquids at different constant temperatures has been provided with the instruments. The tests are carried out for water kerosene within the temperature range from 35℃ to 80℃ and observed as follows.

- At 80℃ actual viscosity of water is 0.357×10^{-3} Pa.s where measured viscosity is 0.26×10^{-3} Pa.s So there is a deviation between the actual and measured viscosity. In order to minimize the deviation, a correction coefficient has been introduced and multiplied with the measured value. Using curve fitting, an equation for the correction coefficient has been developed in terms of temperature. The value of *C* at 80℃ is 1.3761 and multiplying with the measured value finally viscosity of water at 80℃ is 0.3577×10^{-3} Pa.s which is very close to the actual value.
- At 80℃ actual viscosity of kerosene is 0.98×10^{-3} Pa.s where measured viscosity is 3.45×10^{-3}. The value of *C* at 80℃ is 00.3579 and multiplying with the measured value finally viscosity of kerosene at 80℃ is 1.235×10^{-3} Pa.s which is very close to the actual value.
-

NOMENCLATURE

C : Correction coefficient: Helmholtz function, kJ
D_i : Diameter of the inner cylinder
D_o :Inner diameter of the outer cylinder
h : Height of the inner cylinder
I : Moment of Inertia
N_{NL} : rpm of inner cylinder at no load
N_L :rpm of inner cylinder at load
T : Torque
R_i : Radius of the inner cylinder
R_o : Inner radius of the outer cylinder
μ : Dynamic coefficient of Viscosity
τ : Shear stress
ω_i : Angular velocity of the inner cylinder

REFERENCES

[1] Naoto Izumo , " Physical Quantity Measured by a vibration viscometer", Tsukuba Center Inc. Tsukuba, Japan, October 2~3, 2006

[2] M. Couette, Études sur le frottement des liquids, Ann. Chim. (Phys), 21,433-510 (1890).

[3] P.N. Modi and S.M. Seth, Hydraulics and Fluid Mechanics including Hydraulic Machines, New editions 2005-2006.

[4] E. M. Barber , J. R. Muenger , F. J. Villforth, "High rate of shaer rotational viscometer" *Anal. Chem.*, 1955, 27 (3), pp 425–429, DOI: 10.1021/ac60099a030.

[5] E. Hatschek, The General Theory of the Viscosity of Two-phase Systems. Trans. Faraday Sco. 9, 80-93 (1913)

[6] A. Mallock, Determination of the viscosity of water, Proc. Roy. Soc. 45, 126-132 (1888).

[7] C. H. Lindsley and E. K. Fisher, End-effect in rotational viscometers, J. Appl. Phys. 18, 988-996 (1947).

[8] D. J. Highgate and R. W. Whorlow, Migration of particles in a polymer solution during cone and plate viscometry, Polym. Syst Proc. Annu. Conf. Brit. Soc. Rheol. Ed, Wetton, R. E. Macmillan, London, UK, 251-261 (1968). D. J. Highgate and R. W Whorlow, End effects and particle migration effects in concentric cylinder rheometry, Rheologica Acta, 8(2), 142-151 (1969).

[9] H. Kobayashi, T. Nashima, Y. Okamoto, and F. Kaminaga, End effect in a coaxial cylindrical viscometer, Rev. Sci. Instrum. 62(11), 2748-2750 (1991).

ICMIEE-PI-140404

DESIGN, CONSTRUCTION AND PERFORMANCE TEST OF A RAIN SENSING SHADE

Shudipto Sekhar Roy [1, *], *Tarun Chandro Karmoker* [2], *Mihir Ranjan Halder* [3]
[1, 2, 3] Department of Mechanical Engineering, Khulna University of Engineering & Technology, Khulna-9203, BANGLADESH

ABSTRACT
This paper presents a design, construction and performance test of micro-controller based rain sensing shade to protect materials from rain, which is an automatic system where water sensors are used to detect rain and send signals to the microcontroller. Then the microcontroller drives the motors to provide a shade over the required area. At the stoppage of rain the full system returns to its initial condition and again the products are open to desiccate under the sun. In this project a model of rain sensing shade is constructed with two sensors where each sensor sends a signal to the microcontroller at every 250 milliseconds. After sensing a drop of water by any sensor, the motors take 1.25 seconds to start and the shade covers 20.3 cm ×10.15 cm area within 20 seconds. The full system returns to its initial state within 20 seconds when the sensor's surfaces are dried out indicating the stoppage of rain. The performance test of the constructed unit shows a good agreement with the desired expectations. By installing this automatic system, industries can utilize their manpower somewhere else without fetching the products during rain and bringing it back to desiccate after rain. So a full time supervision over the products can be introduced by installing this automatic system.

Keywords: Rain, Water sensor, Micro-controller, Shade, Control

1. Introduction

The weather of Bangladesh is mysterious. No one can say whether it'll rain or not. So a system is necessary to develop for those industries where rain causes destruction to their materials.

Every year many industries like Jute Industries, Dyeing Factories even Laundry Businessmen need to delay their delivery dates because of this rain, which can be proved as a hazard from their business perspective. As we know that, Bangladesh is popular for jute. It is one of the principle crops of Bangladesh. A large amount of jute is cultivated here. Bangladesh is the world's largest grower of quality jute. So jute mills are extended here rapidly. Bangladesh Jute Mills Corporation (BJMC), which is a government organization and the world's biggest state owned manufacturing and exporting organization of all kinds of jute products. Also, Bogra has turned into a hot spot of red chili trading with renowned spice producers and marketers sourcing bulk of their raw materials from the place. For producing packaged red pepper, companies like Square, Acme and BD Foods now collect their chilies from as many as 12 purchase centers at Fulbari, Bogra. Over 2000 poor rural women are employed in these centers having potentials of supplying about 3000 MT red chilies. They use to make their business by desiccating their products in the sun. A sudden rain is an obvious threat to them. So a full time maintenance is needed, though doing it manually can be costly and a matter of hardship. By introducing an automatic system these obstacles can be overcome.

A rain sensing shade can be introduced in this purpose which can be operated automatically with the help of microcontroller and water sensors, where, the water sensor module is a part of the Grove system. So, it can indicate whether the sensor is dry, damp or completely immersed in water by measuring conductivity. The sensor traces have a weak pull-up resistor of 1 MΩ. The resistor will pull the sensor trace value high until a drop of water shorts the sensor trace to the grounded trace. Motors and other mechanical parts can be used as the brawny member of this system. Batteries can be used as power supply for remote places and in the case of electrical unavailability.

Modern day control engineering is a relatively new field of study that gained a significant attention during 20th century with the advancement in technology. It can deal with multi-input and multi-output (MIMO) systems. Control engineering or control systems engineering is the engineering discipline that applies control theory to design systems with desired behaviors. The practice uses sensors to measure the output performance of the device being controlled and those measurements can be used to give feedback to the input actuators that can make corrections toward desired performance. When a device is designed to perform without the need of human inputs for correction, it is called automatic control.

This project requires basic knowledge on microcontroller and electronics. Computer programing knowledge comes handy for microcontroller programing. This project also requires the knowledge of designing some mechanical components, power transmission and CAD (Computer Aided Design).

This rain sensing shade can cover required area during rain and save the dry products from being wet. So industries don't need to use their manpower to fetch the products during rain and bring it back to desiccate after rain. A considerable amount of time can be saved by minimizing the times for fetching and bringing the products back manually. A full time supervision can be introduced by installing this automatic system.

2. Design

2.1 Structure Design

Wood was used for framing the structure. For a shade capable of covering 20.3cm×10.15cm area, base of the structure was 40.6cm×20.3cm for proper observation.

* Corresponding author. Tel.: +88-01738041433
E-mail address: shudipto67@gmail.com

Design of the structure had been done by using SolidWorks platform. The mechanical drawing of the structure had been also extracted from the 3D design for guiding the construction work. Proper dimensions were included in the drawing as shown in Fig.1.

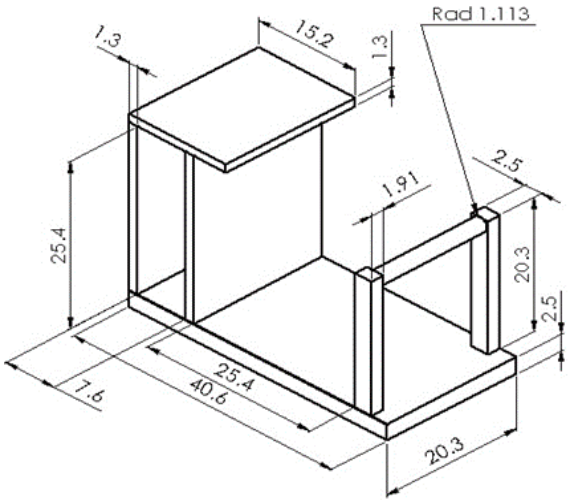

Fig.1 Mechanical Drawing of the structure
(All dimensions are in centimeters)

2.2 Microcontroller Selection

As microcontroller the Arduino Uno was used. Because it could be simply connected to a computer with a USB cable or could be powered with an AC-to-DC adapter or battery to get started. It was based on the ATmega328. It had 14 digital input/output pins, 6 analog inputs, a USB connection, a power jack, and a reset button. It contained everything necessary to support the microcontroller.

In this rain sensing shade, microcontroller was being used as the brain. It received signals from the sensors mounted on the roof and analyzed the signals to determine whether it was raining or not with the help of the code uploaded in it. After that it sent output signals according to the code.

2.3 Water Sensor Selection

Among many water sensors Grove Water Sensor was used because it could sense a single drop of water on its surface by measuring conductivity. The sensor traces had a weak pull-up resistor. The resistor would pull the sensor trace value high until a drop of water shortened the sensor trace to the grounded trace. This circuit worked with Arduino.

The structure of rain sensing shade had two seats mounted on the roof for two sensors. Sensors acted as the nerve of this system. They sent signals to the microcontroller about the environment. Each sensor sent an analog signal in every 250 milliseconds. If the weather was dry then their analog values ranged from 900 to 1100 and if the sensors sensed any water then their analog values ranged from 100 to 300.

2.4 Motor Selection

Motors were the muscles of this project. For covering an area of 20.3cm × 10.15cm within 20 seconds two motors of 2.19×10^{-6} Nm torque were needed. A gear motor of 6 volt, 250 mA and 120 rpm was available in market which was used in this model as it could give 0.12 Nm torque which was good enough for this purpose. It could also be empowered by microcontroller so the complications of power supply could be avoided.

These two gear motors were mounted on the structure of rain sensing shade. The microcontroller operated these motors according to the code uploaded in it. These motors ran efficiently at 6 volt connection.

2.5 Shade Selection

As a model of rain sensing shade was being constructed in this project rexine sheet was used as it was light in weight and could be folded easily over the shaft after serving its true purpose by resisting water to penetrate.

2.6 Selection of Shaft and Bearing

Plastic shafts were used for minimizing the weight of the motor arrangement. One end of a shaft was connected with a gear motor and the other end was attached with a bearing. Ball bearings were used in this project. This ball bearing is a type of rolling element bearing which uses balls to maintain the separation between the bearing races. The purpose of using this ball bearing was to reduce rotational friction and support radial and axial loads.

2.7 Other Accessories Selection

The followings were the accessories used for the unit:

- Cord String
- Bread Board
- Batteries
- Connectors
- Jumper Wires

3. Construction

For the construction of rain sensing shade wood was used for the structure. According to the mechanical design the structure was made. The structure provided a place for keeping the batteries, microcontroller and rest of the electrical circuit.

Motors, shafts and bearings were mounted on the structure at their certain positions. Motors and bearings were clamped with the structure by means of metal sheets.

On the opposite side of the motors there was a cylindrical support for changing the direction of the cord strings from the first motor toward the second one. That cylindrical support was engraved cylindrically at two points to allow the cord strings to pass over. The height of the cylindrical support was somewhat less than that of the first motor, so the rexine would be inclined during rain and could minimize the risk of storing rain water on it.

Fig.2 Wooden frame for the rain sensing shade

Plastic pens were used as shafts and attached with the gear motors. Plastic shaft was used for diminishing the weight of the gear arrangement. On the other side of the shaft a ball bearing was mounted over the shaft to give it a frictionless rotation and support.

Fig.3 Gear Motor, Shaft and Bearing arrangement

Rexine was used as the shade and it remained folded over the shaft when the weather was sunny. Rexine sheet was sewed with cord strings and the strings were tied with the shafts. Each shaft contained two holes for attaching the strings.

Fig.4 Rexine sewed by string cord

The power supply was a 9 volt battery to run the microcontroller and the microcontroller empowered the motors and the sensors. So the electrical circuit consisted of one 9 volt battery, one Arduino Uno Microcontroller Board, two water sensors, one bread board and several jumper wires.

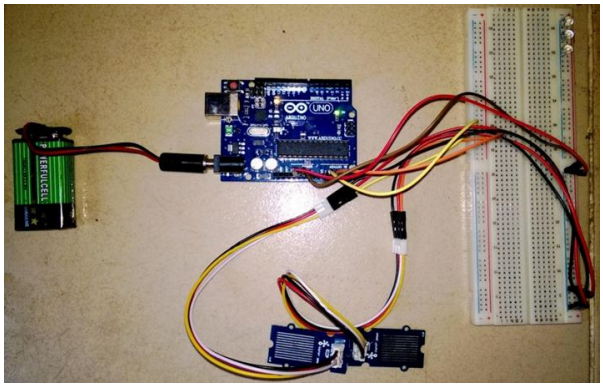

Fig.5 Electrical circuit of the model

Wires were connected to the motor poles by the process of soldering. The bread board was used for connection convenience.

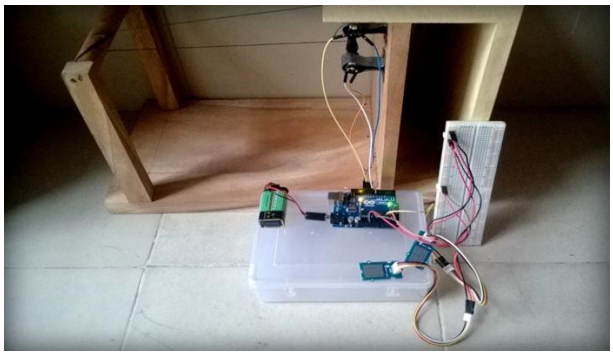

Fig.6 Model with electrical circuit

On the roof of the structure two seats were made where the sensors were mounted. The sensors were kept slightly inclined by design so that the risk of storing droplets of rain water on them could be minimized. The roof also offered rain protection to the motors, shafts, bearings and electrical circuit.
Final view of the constructed model is given below:

Fig.7 View of the constructed model when sensor's surfaces were dry

Fig.8 View of the constructed model when sensor's surfaces were wet

4. Performance Test

For testing the performance of the model two sensors were set on the roof of the model. Each sensor used to send a signal to the microcontroller at every 250 milliseconds. If the surfaces of the sensors were dry then the shade would remain folded. But when any one of the sensors would sense any water on its surface then the microcontroller would detect the water by analyzing the signals sent by the sensor and it would start the motors and the shade would be provided over the required area. After that when the sensors would sense dry surfaces on them then the microcontroller would detect the dry environment by analyzing the signals sent by the sensors and run the motors in reverse direction.

Table 1 Data for the test of performance of rain sensing shade

No. of obs.	Time for starting the motors after sensing water (sec.)	Time for covering the required area (20.3cm × 10.15cm) (sec.)	Time for starting the motors after sensing dry surfaces of sensors (sec.)	Time for returning to initial position (sec.)
01	1.25	19.3	1.25	19.2
02	1.25	19.1	1.25	18.9
03	1.25	18.9	1.25	19.4
04	1.25	19.1	1.25	19.2
05	1.25	18.8	1.25	19.1
Avg.	1.25	19.04	1.25	19.16

5. Results and Discussion

From table 1, it was observed that, after sensing a drop of water by any sensor the motors took constantly 1.25 seconds to start and the shade covered 20.3cm×10.15cm area within 19.04 seconds on average. The full system was found to return to its initial state within 19.16 seconds on average when the sensor's surfaces were dried out indicating the stoppage of rain and again the motors took constantly 1.25 seconds to start.

Here, it has been seen that times for covering the required area (20.3cm×10.15cm) are not same for all observations. Times for returning to initial position also vary. These slight variations may happen because of friction between the string cord and the cylindrical support. Although times for starting the motors after sensing water and times for starting the motors after sensing dry surfaces of sensors remain constant for all observations.

So, after testing the performance of the model it can be said that the rain sensing shade satisfies the design assumptions and this project achieves its goal successfully.

6. Conclusion

The following conclusion could be made for the project:

- A rain sensing circuit has been designed by making a suitable electrical circuit and placing the sensors in proper positions.
- A rain sensing shade has been designed and constructed according to design assumptions.
- Performance of the rain sensing shade has been tested and found to respond during rainy and sunny weather as per the design.
- After sensing a drop a water by any sensor the motors take 1.25 seconds to start and the shade covers 20.3cm×10.15cm area within 20 seconds. The full system returns to its initial state within 20 seconds when the sensor's surfaces are dried out indicating the stoppage of rain.

7. Recommendation

The following recommendations could be made for the project:

- Instead of two motors, single motor can be used by gear arrangement for shade movement.
- AC power supply can be used instead of battery.
- Pulleys can be mounted on cylindrical bar for frictionless movement of rope.
- Metallic sheet can be used as shade instead of rexine.

BIBLIOGRAPHY

1. V. M. Faires, Design of Machine Elements, Fourth Edition, The Macmillan Company
2. Herbert Schildt, C: The Complete Reference, Fourth Edition, Tata McGraw-Hill Publishing Company Limited
3. V K Puri, Digital Electronics Circuits and Systems, Tata McGraw-Hill Publishing Company Limited
4. http://en.wikipedia.org/wiki/Rain_sensor
5. http://arduino.cc/en/Main/arduinoBoardUno
6. http://textilefashionstudy.com/jute-mills-in-bangladesh-government-and-private-sector/
7. http://bangladesheconomy.wordpress.com/2009/12/02/red-chilli-business-at-fulbari-of-bogra/

ICMIEE-PI-140405

Experimental and Numerical Analysis of Fluid Flow through an Orifice Meter

Md. Tanbin Hasan Mondal [1,*] , *Md. Mostafizar Rahman* [2] , *Dr. Mihir Ranjan Halder* [3]
[1, 2, 3] Department of Mechanical Engineering, Khulna University of Engineering & Technology, Khulna-9203, BANGLADESH

ABSTRACT
An orifice meter is a differential pressure flow meter which reduces the flow area using an orifice plate. Orifice meter is a device commonly used for measuring fluid flow in industrial purposes such as metering flow in the natural gas industry. Experimental and numerical computations of pressure drop (ΔP) and coefficient of discharge (C_d) in an orifice are presented in this paper. Marker and Cell (MAC) algorithm is used for numerical computation. Standard κ-ε model is used for turbulent quantities. The numerical computations are done for the range of Reynolds number $3.3X10^4$ to $4.6X10^4$. Numerical computation is calibrated computing the fully developed length and it is found to have the fully developed length as (138x0.05) or 6.9. Numerically the coefficients of discharge are found 0.61, 0.63 and 0.64 respectively. The coefficients of discharge are also found from experimentation for the same dimensions and input parameters of numerical computation as 0.62, 0.64 and 0.65 respectively for the corresponding flows of numerical solution. In this study the experimentally obtained values of coefficient of discharge are always found higher by 1.95%, 1.56% and 1.54% respectively than that of numerical computation.

Keywords: Orifice meter, MAC algorithm, κ-ε model, Numerical model, Coefficient of discharge.

1. Introduction

An orifice meter is a differential pressure flow meter which reduces the flow area using an orifice plate [1]. The orifice plate is inserted between two flanges perpendicularly to the flow, so that the flow passes through the hole with the sharp edge of the orifice pointing to the upstream. Orifice meter is commonly used for measuring fluid flow in industrial purposes such as metering flow in the natural gas industry. The popularity of the orifice meter can be attributed primarily to its simplicity, relatively low cost and little maintenance requirements in comparison to other fluid meters. In this paper, the study of water flow through an orifice meter by both numerically and experimentally has been presented. This type of fluid flow problem can be solved by computational fluid dynamics (CFD) [2]. For this problem MAC algorithm is chosen to use. The MAC algorithm method is one of the earliest and most useful methods for solving full Navier-stokes equations [4]. It was basically developed to solve problems with free surface flows but can be applied to any incompressible fluid flow problem. The numerical computations are done for the range of Reynolds number $3.3X10^4$ to $4.6X10^4$. An experimental set up has been fabricated with a pipe diameter, 0.05 m, pipe length, 4.5 m, and an orifice diameter, 0.025 m and tested in the laboratory. The pressure drops in the orifice meter and the corresponding coefficients of discharge for flow through the orifice meter have been determined.

2. Model Details

The theoretical analysis refers to a typical orifice meter as shown in Fig.1. The entry of liquid to the orifice meter is in axial direction [5]. Conservation equations for axisymmetric flow of water through the orifice meter were solved simultaneously satisfying the respective boundary conditions by an explicit finite difference computing technique developed by Hirt and Cook following the original MAC (Marker and Cell) method due to Harlow and Welch. The steady state solution of top flow was achieved by advancing the equations in time till the temporal derivatives of all the variables fall below a pre-assigned small quantity ∂ [3]. The standard k-ε model has been adopted for the computation of turbulent flow. The space derivatives of the diffusion terms were discretized by the central differencing scheme while the advection terms were discretized by the hybrid differencing scheme based on the local peclet number Pe associated with the cell. A 66X36 variable sized adaptive grid system was considered with clustered cells near the inlet and orifice. The variations in the size of grids were made uniformly. It was checked by further refinement of the cells (with doubling and quadrupling the number of grids in both the directions) but did not show the change in velocity (both axial and tangential) components and turbulent kinetic energy by more than 2% [4].

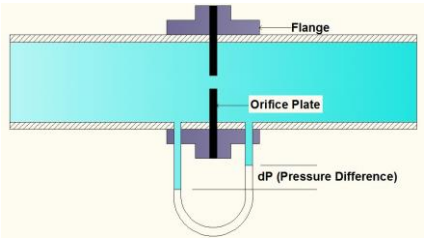

Fig.1 Schematic diagram of a short square-edged orifice inserted in a smooth run pipe

2.1 Governing Equations

The governing equation for this flow situation is simplified considering axisymmetric flow in cylindrical polar coordinate system (r, θ, z). Assuming unit angle in θ direction, the governing equations in dimensionless

* Corresponding author. Tel.: +88-01676110465
E-mail address: showrove.hasan@gmail.com

Continuity equation:

$$\frac{\partial Vr}{\partial r}+\frac{Vr}{r}+\frac{\partial Vz}{\partial z}=0$$

Momentum equation:

r- Momentum

$$\frac{\partial Vr}{\partial t}+\frac{\partial (Vr)^2}{\partial r}+\frac{\partial (VzVr)}{\partial z}+\frac{(Vr)^2\_(V\theta)^2}{r}$$
$$=\frac{\partial P1}{\partial r}+\frac{2}{Re}\frac{\partial}{\partial r}\left(\mu eff\frac{\partial Vr}{\partial r}\right)$$
$$+\frac{2}{Re}\frac{\mu eff}{r}\left(\frac{\partial Vr}{\partial r}-\frac{Vr}{r}\right)$$
$$+\frac{1}{Re}\frac{\partial}{\partial z}\{\mu eff\left(\frac{\partial Vz}{\partial r}+\frac{\partial Vr}{\partial z}\right)\}$$

z- Momentum

$$\frac{\partial Vz}{\partial t}+\frac{\partial}{\partial r}(VrVz)+\frac{\partial}{\partial z}(Vz)^2+\frac{VrVz}{r}$$
$$=-\frac{\partial P1}{\partial z}$$
$$+\frac{1}{Re}\frac{1}{r}\frac{\partial}{\partial r}\left\{r\mu eff\left(\frac{\partial Vr}{\partial r}+\frac{\partial Vr}{\partial z}\right)\right\}$$
$$+\frac{2}{Re}\frac{\partial}{\partial z}(\mu eff\frac{\partial Vz}{\partial z})$$

θ- Momentum

$$\frac{\partial V\theta}{\partial t}+\frac{\partial}{\partial r}(VrV\theta)+\frac{\partial}{\partial z}(VzV\theta)+\frac{2Vr}{r}V\theta$$
$$=\frac{1}{Re}\frac{1}{rr}\frac{\partial}{\partial r}\left\{r\mu eff\left(\frac{\partial V\theta}{\partial r}+\frac{V\theta}{r}\right)\right\}$$
$$+\frac{1}{Re}\frac{\partial}{\partial z}(\mu eff\frac{\partial V\theta}{\partial z})$$

Where, $P_1 = p+\frac{2}{3}\kappa$

$\mu eff = 1+\mu_t$

$\mu_t = \frac{C\mu Re\,\kappa^2}{\varepsilon}$

Turbulent kinetic energy equation:

$$\frac{\partial \kappa}{\partial t}+\frac{\partial}{\partial t}(Vr\ \kappa)+\frac{\partial}{\partial z}(Vz\,\kappa)+\frac{Vr\,\kappa}{r}$$
$$=\frac{1}{Re}\frac{1}{r}\frac{\partial}{\partial r}\left(r\frac{\mu_t}{\sigma_\kappa}\frac{\partial \kappa}{\partial r}\right)$$
$$+\frac{1}{Re}\frac{\partial}{\partial z}\left(\frac{\mu_t}{\sigma_\kappa}\frac{\partial \kappa}{\partial z}\right)$$
$$+\frac{1}{Re}\mu\left[2\left\{\left(\frac{\partial V_t}{\partial r}\right)^2+\left(\frac{Vr}{r}\right)^2\right.\right.$$
$$\left.+\left(\frac{\partial Vz}{\partial z}\right)^2\right\}+\left(\frac{\partial V\theta}{\partial r}-\frac{V\theta}{r}\right)^2$$
$$\left.+\left(\frac{\partial Vr}{\partial z}+\frac{\partial Vz}{\partial r}\right)^2+\left(\frac{\partial V\theta}{\partial z}\right)^2\right]$$
$$-\varepsilon$$

Turbulent kinetic energy dissipation rate equation:

$$\frac{\partial \varepsilon}{\partial t}+\frac{\partial}{\partial r}(Vr\,\varepsilon)+\frac{\partial}{\partial z}(Vz\varepsilon)+\frac{Vr\,\varepsilon}{r}$$
$$=\frac{1}{Re}\frac{1}{r}\frac{\partial}{\partial r}\left(r\frac{\mu_t}{\sigma_\varepsilon}\frac{\partial \varepsilon}{\partial r}\right)$$
$$+\frac{1}{Re}\frac{\partial}{\partial z}\left(\frac{\mu_t}{\sigma_\varepsilon}\frac{\partial \varepsilon}{\partial z}\right)$$
$$+\frac{1}{Re}C_{1\varepsilon}\frac{\varepsilon\mu_t}{\kappa}\left[2\left\{\left(\frac{\partial Vr}{\partial r}\right)^2\right.\right.$$
$$\left.+\left(\frac{Vr}{r}\right)^2+\left(\frac{\partial Vz}{\partial z}\right)^2\right\}$$
$$+\left(\frac{\partial V\theta}{\partial r}-\frac{V\theta}{r}\right)^2$$
$$\left.+\left(\frac{\partial Vr}{\partial z}+\frac{\partial Vz}{\partial r}\right)^2+\left(\frac{\partial V\theta}{\partial z}\right)^2\right]$$
$$-C_{2\varepsilon}\frac{\varepsilon^2}{\kappa}$$

2.2. Boundary conditions

The numerical solution domain for an axisymmetric pipe flow problem can be written as $0\leq r\leq R$; $0\leq z\leq L$. Which is a rectangle shown in **Fig.2**.The corresponding boundaries are also indicated in the **Fig.2**.If we rotate the rectangle 360^0 about the axis, we obtain the three dimension pipe geometry.

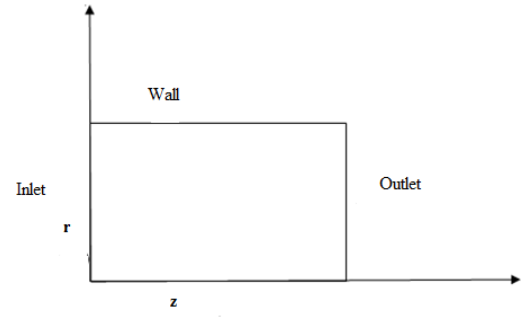

Fig.2 The problem domain and boundaries for axisymmetric pipe flow problem.

Inlet: $V_z = 1$, $V_r = 0$, $V_\theta = 0$, $\kappa = \kappa_{in}$ and $\varepsilon = \varepsilon_{in}$

Outlet: $\frac{d\phi}{dz} = 0$, Where $\phi = V_r, V_z, V_\theta, \kappa$ and ε

Wall: $V_z = V_r = V_\theta = 0$, logarithmic law of wall

Axis:

$$\frac{\partial Vz}{\partial r} = Vr = V_{\theta = 0}$$

Orifice:

When z = 80 then, from r = 0.25 to r = 0.5

$V_r = 0$ and $Vz = 0$

When r = 0.25 then, from z = 80 to z = 80.1Vr = 0

When z = 80.1 then, from r = 0.25 to r = 0.5

$V_r = 0$

3. Numerical Experimentation

The numerical code is applied to observe the flow field in a circular pipe. The fully developed length is found as 3.45. The fully developed velocity profile is found at that length in numerical computation. So, the numerical code is valid for fully developed length. The fully developed velocity profile is shown in the following figures for discharge, $Q = 0.01 m^3/s$.

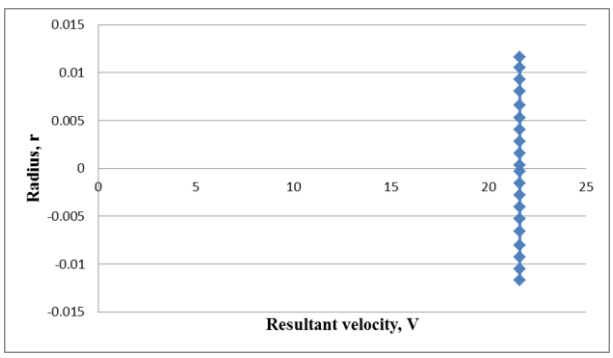

Fig.3 Velocity profile at distance z = 1.2 for Reynolds number, Re = 509296.22.

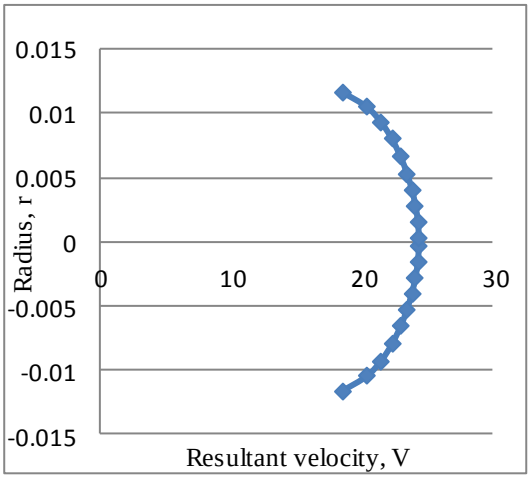

Fig.4 Velocity profile at distance z = 88.6 for Reynolds number, Re = 509296.22.

From the above figures it may be said that not all fluid particles travel at the same velocity within a pipe. The shape of the velocity curve (the velocity profile across any given section of the pipe) depends upon whether the flow is laminar or turbulent. If the flow in a pipe is laminar, the velocity distribution at a cross section will be parabolic in shape with the maximum velocity in the center being about the twice the average velocity in the pipe. In turbulent flow, a fairly flow velocity distribution exists across the section of the pipe, with the result that the entire fluid flows at a given single value. The velocity of fluid in contact with the pipe wall is essentially zero and increases the further away from the wall. By analyzing the figures it may be said that velocity profiles varies slightly in shape for turbulent pipe flow. The following figures represent the flow field in an orifice meter of a given geometry and given operating conditions.

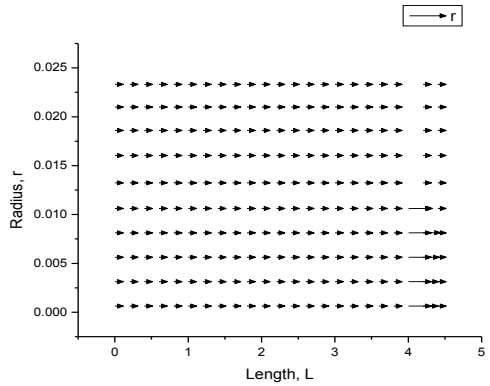

Fig.5 Velocity vector in a circular pipe with an orifice plate for Re=33104.25.

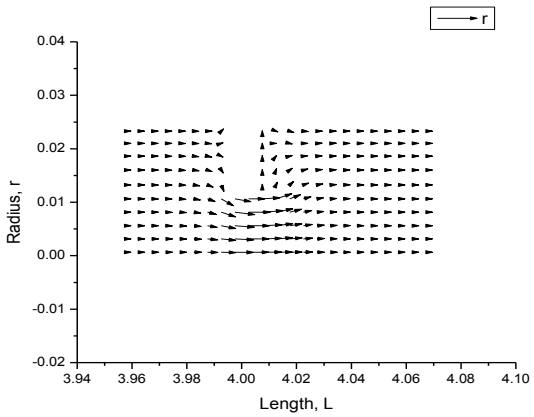

Fig.6 Velocity vector in a circular pipe for Re=33104.25 around the orifice.

Numerical Experimentation was done for the orifice meter in a circular pipe specified dimensions given in **Table 1**.

Table 1 Dimension of orifice meter, pipe and input

Serial No.	Diameter of the Pipe , D(m)	Diameter of the orifice , d(m)	Length of the pipe , L (m)	Flow rate in the pipe , Q (m^3/s)	Reynolds number , Re
1.	0.05	0.025	4.5	0.0013	33104.254
2.				0.0016	40743.698
3.				0.0018	45836.660

The numerical experimentation was done within the following range of Reynolds number $3.3X10^4 < R_e < 4.6X10^4$

Table 2 Numerical results for Q = 0.0013 m^3/sec

Discharge Q (m^3/sec)	Resultant velocity V_{res} (m/s)	Velocity at the end V_{end} (m/s)	Discharge at the end Q_{end} (m^3/s)	Theoretical Discharge Q_{th}(m^3/sec)	Pressure drop $(\Delta P)_{num}$ (Pa)	Coeff. of discharge, $(C_d)_{num}$
0.0013	0.661658	0.661658	0.00129961	0.00210	19492.27	0.61

Table 3 Numerical results for Q = 0.0016 m^3/sec

Discharge Q (m^3/sec)	Resultant velocity V_{res} (m/s)	Velocity at the end V_{end} (m/s)	Discharge at the end Q_{end} (m^3/s)	Theoretical Discharge Q_{th} (m^3/s)	Pressure drop $(\Delta P)_{num}$ (Pa)	Coefficient of discharge, $(C_d)_{num}$
0.0016	0.81469	0.81469	0.0015996	0.002536	24040.691.	0.63

Table 4 Numerical results for Q = 0.0018 m^3/sec

Discharge Q (m^3/s)	Resultant velocity V_{res} (m/s)	Velocity at the end V_{end} (m/s)	Discharge at the end Q_{end} (m^3/s)	Theoretical Discharge Q_{th} (m^3/s)	Pressure drop $(\Delta P)_{num}$ (Pa)	Coefficient of discharge, $(C_d)_{num}$
0.0018	0.91731	0.91731	0.0018	0.002918	45836.660	0.64

4. Experimental setup

A 0.5 m diameter pipe of 4.5 m long was used for the construction of orifice meter. An orifice plate with an orifice diameter 0.25 m was placed inside the 0.5 m diameter pipe. Two pressure tapping points one at 1.5 D before the orifice plate and other at 0.5 D after the orifice plate were constructed to connect with a U-tube differential manometer for the measurement of pressure head difference. Water enters the pipe and finally passes away through the orifice as shown in Fig.6. For every discharge the pressure head difference and discharge readings were recorded.

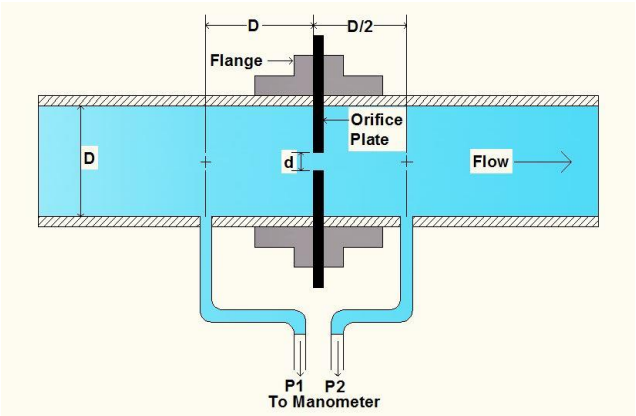

Fig.7 Experimental set up for an orifice meter

5 Experimental Data and Analysis

Table 5 Data for discharge Q = 1.3x10^{-3} m^3/sec.

Serial No.	Vol. of water Liter	Time Sec	Q_{ac} (m^3/sec)	Average Q_{ac} (m^3/sec)	Press. head h cm	Average h cm
1.	20.5	15.76	1.3x10^{-3}	1.3x10^{-3}	10.4	10.5
2.		15.70	1.3x10^{-3}		10.6	
3.		15.77	1.3x10^{-3}		10.4	
4.		15.77	1.3x10^{-3}		10.6	
5.		15.75	1.3x10^{-3}		10.5	

Table 6 Data for discharge Q = 1.6x10^{-3} m^3/sec

Serial no.	Liter	Time (sec)	Q (m^3/sec)	Average Q (m^3/sec)	Pressure head h (cm)	Average h (cm)
1.	20.5	12.81	1.6x10^{-3}	1.6x10^{-3}	15.1	15
2.		12.80	1.6x10^{-3}		15.1	
3.		12.79	1.6x10^{-3}		14.9	
4.		12.80	1.6x10^{-3}		14.9	

Table 7 Data for discharge Q = 1.8x10^{-3} m^3/sec

Serial no.	Liter	Time (sec)	Q (m^3/sec)	Average Q (m^3/sec)	Pressure head h (cm)	Average h (cm)
1.	20.5	12.81	1.8x10^{-3}	1.8x10^{-3}	18.6	18.5
2.		12.80	1.8x10^{-3}		18.5	
3.		12.79	1.8x10^{-3}		18.5	
4.		12.80	1.8x10^{-3}		18.4	
5.		12.81	1.8x10^{-3}		18.5	

5.1 Data analysis

Calculation for discharge Q = $1.3x10^{-3}$ m^3/sec

Pressure drop, $(\Delta P)_{exp} = (P_2-P_1) = h\rho g = 13998.379$ Pa

$Q_{th} = C_c A_o (2gh)^{0.5} = 2.0655x10^{-3}$ m^3/sec

Coefficient of discharge, $C_d = Q/Q_{th}$

$= (1.3x10^{-3})/ (2.0655x10^{-3})$

$= 0.6293$

Similarly, for Q = $1.6x10^{-3}$ m^3/sec and $1.8x10^{-3}$ m^3/sec C_d values become 0.64 and 0.65

6. Results & Discussion

The different values of C_d for different values of discharges in the range of $1.3x10^{-3}$ to $1.8x10^{-3}$ m^3/sec both for experimental and numerical experimentations have been placed in **Table 8**. It was found that the values of C_d increases with the increase of discharge for both cases. It was also observed that numerically calculated values were always less than experimentally obtained values. **Fig.8** shows the variation of C_d with different discharges. The C_d value was found to increase with the increase of discharge in both cases. Again, experimental values were found higher than the numerical ones.

Table 8 Comparison of experimental and numerical results

Q (m^3/ sec)	Pressure drop $(\Delta P)_{exp}$ (Pa)	Pressure drop $(\Delta P)_{num}$ (Pa)	$(C_d)_{exp}$	$(C_d)_{num}$	$(C_d)_{num}$ is less than $(C_d)_{exp}$ by
0.0013	13998.4	19492.3	0.629	0.617	1.95%
0.0016	19997.685	24040.69	0.64	0.63	1.56%
0.0018	24663.811	31823.56	0.65	0.64	1.54%

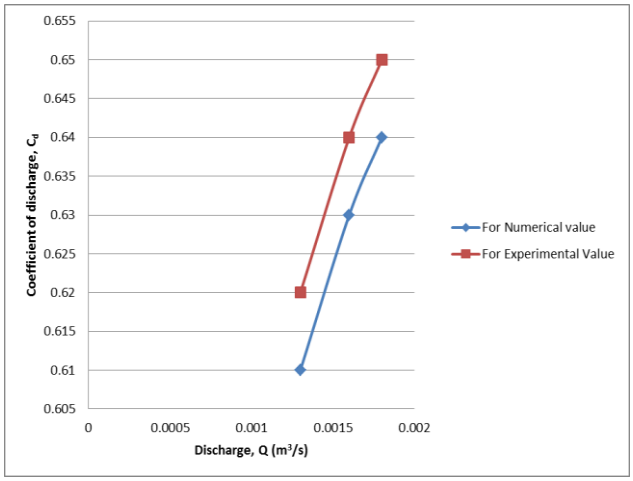

Fig.8 Relation between discharge and coefficient of discharge for numerical and experimental values

7. Conclusion

A numerical code for the computation of coefficient of discharge and pressure drop in an orifice meter through a circular pipe is written and executed by using MAC algorithm in the present work. An experimental set up is fabricated for orifice meter to get experimental values. The numerical results are compared with the experimental results. The following features have been observed

- The coefficient of discharge is found to increase with the increase of discharge or Reynolds number in both experimental and numerical studies
- The values of coefficient of discharge, C_d from experimental study are always found higher than that of in the numerical study and the maximum deviation is found 1.95%

NOMENCLATURE

V_z: Velocity in z direction, m/s
V_r: Velocity in r direction, m/s
P: Pressure drop, N/m^2
ΔP: Change in pressure, N/m^2
∂t: Time step, sec
μ: Viscosity, N.s/ m^2
Q: Actual volume flow rate, m^3/s
Q_{th}: Theoretical volume flow rate, m^3/s
A: Area of pipe, m^2
A_o: Area of orifice, m^2
ρ: Density of fluid, Kg/ m^2
D: Diameter of pipe, m
d : Diameter of orifice, m
τ_w :Wall shear stress
Re: Reynolds number
κ: Turbulent kinetic energy, J
ε: Turbulent kinetic energy dissipation rate, W/m^2
$C\mu, C_{1\varepsilon}, C_{2\varepsilon}$: Empirical constants of κ-ε equations
C_c : Coefficient of contraction
C_d : Coefficient of discharge
Subscript
r: In radial direction
z: In axial direction
Superscript
i: z directional grid
j: r directional grid
Δx: distance between two nodes in z direction
Δy: distance between two nodes in r direction

REFERENCES

[1] Dr. P.N Modi, Dr.S.M Seth, Hydraulics and Fluid Mechanics, Standard Book house, 2006

[2] H K Versteeg, W Malalasekera, An Introduction To Computational Fluid Dynamics.

[3] K Muralidhar, T Sundararajan, Computational Fluid Flow and Heat Transfer, Narosa, 2nd Edition

[4] John D. Anderson. Jr, Computational Fluid Dynamics, McGraw-Hill International Edition.

[5] Pervin, M.S.A, Halder, M.R. Numerical Modeling on Solid Cone Nozzle without a Vane Swirled, Paper 06.

ICMIEE-140406

Generation of Various Micropattern Using Microlens Projection Photolithography

Md. Nazmul Hasan[1,*], *Md. Momtazur Rahman*[2], *Md. Jahid Hasan*[3]
[1] Department of Mechanical Engineering, National Cheng Kung University, No. 1 university road, 701 Tainan, TAIWAN
[2] Department of Energy Science & Technology, University of Ulm, Helmholtzstraße 18, 89081 Ulm, GERMANY
[3] Department of Mechanical Engineering, Khulna University of Engineering & Technology, Khulna-9203, BANGLADESH

ABSTRACT
This paper discusses about review of various process for microlens array fabrication and their application in microlens projection photolithography. Microlens array fabricated by excimer laser machining used in photolithography to produce arrays of microstructures in photoresist. In this technique, the uniform UV illumination is used for exposure and by using a single mask with a single microlens array this system can produce arrays of micropattern in photoresist with a single exposure, which is very useful for mass production. Generated micropatterns can have 3D and uniform image by using a gray-scale mask. Multiple exposure with multiple mask can generate modified and combined pattern on the resist. This technique can generate microstructure with submicron resolution.

Keywords: Microlens array, photolithography, microstructure, excimer laser**.**

1. Introduction

Now a day, microlens arrays have become important optical elements that play a crucial role in advanced micro-optical devices and systems which are being used in optical data storage, digital display, optical communication and so on. Different technologies have been developed for the fabrication of microlens arrays. Some conventional methods used are listed as photoresist thermal reflow [1], photo thermal method [2], photo-polymer etching [3], micro-jet method [4], and micro-molding or hot embossing method [5]. Although the above-mentioned methods are widely used, the common problem for these methods is that the microlens surface profile is not controlled accurately as well as unexpected surface roughness. To fabricate a microlens array with better surface profile and roughness, excimer laser micromachining integrated with a planetary contour scanning method is developed [6]. But the filling factor of arrayed microlenses is limited and it cannot be used in mass production so the efficiency of this method is low. Later, the above method was upgraded into excimer laser dragging method for fabricating varieties of microstructures with arrays based on mask projection and mask/sample movement methods [7], [8]. Common excimer laser KrF (248nm) with wavelength in UV region is used for those machining. The process for material removal by excimer laser is through thermal ablation and/or photo ablation of the materials, i.e. the covalence bonding of the material is broken and vaporized by each laser pulse. The covalence bonding energy of polymer material is relatively low and it has good optical properties so it is suitable for excimer laser micromachining, and hence the photo-ablation mechanism can dominate the material removal [9], [10]. In this method less thermal effect is involved when the laser source can directly break the covalence bonding between polymer molecules, so smooth machined surface can be easily obtained [11].

A simple photolithography method has been discussed in this paper that uses arrays of microlenses to generate arrays of micropatterns with submicron resolution. Conventional lithography techniques form a single image for each exposure and require precision optical systems, expensive apparatus, chrome masks & steppers. Microlens array photolithography (MAP) can generate: (1) array of images by a single exposure because each lens forms an image of photomask. (2) simple repetitive features with minimal equipment & inexpensive masks. (3) Image can connect & overlap to generate varieties pattern. (4) patterns can have symmetries and periodicities. (5) pattern size as small as 500nm. This technique includes collimated flood illumination and masked illumination method which can produce arrays of repetitive micropatterns with shape same as mask pattern. The array of microlenses produce images of bright patterns of the mask and projects an array of size-reduced micropatterns onto the resist layer [12].

2. Experimental setup

Those experiments have been divided into two sections and some subsections:

2.1 Fabrication of plano-convex microlenses array

In the following subsection some methods have been discussed to fabricate plano-convex aspheric microlens array.

(1) Excimer laser planetary contour scanning method
Excimer laser micromachining with the planetary contour scanning method can accurately achieve pre-designed axially symmetrical 3D microstructures. This method based on the concept of machining probability and integration of both rotation and revolution of samples, and hence the machined surface profiles can be very accurate and smooth. The machining system includes a KrF (248nm) excimer laser, optical components for shaping laser beam, a 4-axis servo-

* Md. Nazmul Hasan. Tel.: +886-0979211612
E-mail address: nazmul.eng@gmail.com

controlled stage movement, and a personal computer for system control [6]. The machining pattern depends on the window opening profile in the photo-mask shown in Fig.1. Since each single laser pulse removes a certain amount of sample material form object, the machining depth depends on the laser fluence and sample material properties. To fabricate 3D microlens, sample is moved by 4-axis stage system and synchronized with laser pulse firing sequences so that laser energy distributes uniformly on object surface. The machining profile of microlens can be directly observed by zoo lens microscope. Fig.1 shows a photo-mask with a typical window-opening pattern for fabrication of single microlens and Fig.2 shows the procedure for fabricating arrays of microlens.

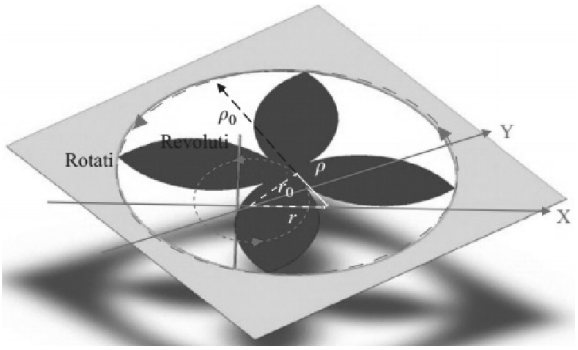

Fig. 1 Excimer laser machining of microlens using a planetary contour scanning method [6].

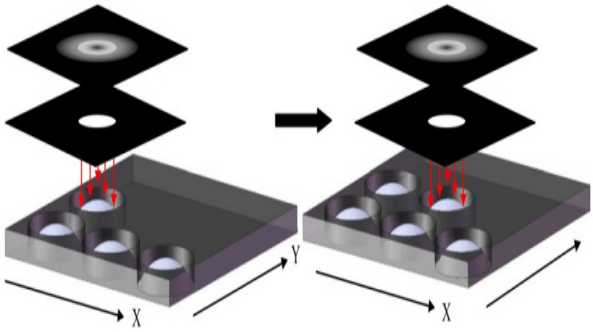

Fig. 2 The steps for fabricating an array of micro-lenses.

(2) Excimer laser dragging method

This method represents an improved excimer laser micromachining method over the planetary contour scanning method for fabricating arrayed microstructures with a predesigned surface profile. This method is developed from a conventional biaxial laser dragging method. The excimer laser with stage system used in this method is same as previous method. A contour mask, called binary photo mask with a polynomial designed pattern through which laser light is passed and the pattern is made on the object surface along with a programmed scanning path. So the overall or overlapped laser energy projected on the sample surface has a predesigned spatial distribution. If the scanning paths are just straight lines and one direction only then one can get 2D microstructure. Since contour mask contains periodic patterns so scanning from another direction perpendicular to the first line is superimposed each other to create arrayed 3D microstructures in a very straightforward way known as the excimer laser dragging method [13]. Fig. 3 shows a rectangular array of plano-convex 3D microlens obtained by a contour mask with biaxial (x-y) laser line scanning/dragging method. An array of 5×5 microlenses with aperture sizes of 100μm with pitch 100 μm and a designed aspheric profile are obtained experimentally. The machined surface profiles are closely matched to desired ones with a deviation below 1 μm and the average surface roughness around 5 nm. The optical performance of the machined microlens array for minimizing the focal spot sizes are measured which approach to optical diffraction limit [11].

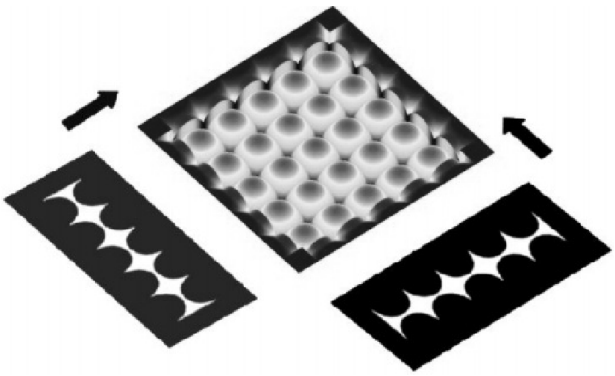

Fig. 3 Excimer laser machining with a contour mask and biaxial laser dragging method for fabricating arrayed microlens [11].

2.2 Microlens Projection Photolithography

In the following subsections, some experimental setup and methods about microlens projection photolithography have been discussed.

(1) Microlens lithography using collimated illumination

This method depends on the shapes and profiles of the microlens arrays to control the irradiance distribution of the optical micropatterns [12]. It has very simple optical setup which includes a microlens array attach with photoresist by PDMS. The thickness of PDMS maintains the focal length of microlens so that each microlens can make pattern in the image plane. Fig. 4 shows the optical setup for the microlens lithography using collimated illumination. The micropatterns produced by this technique depend on three factors: (i) lenses size, shape and profile, (ii) image distance and (iii) lens refractive index. The patterns produced by this method are uniform over the whole illuminated area. Those uniform micropatterns are generated over areas of 10 cm^2 by a single exposure using microlens array with sizes more than 1μm.

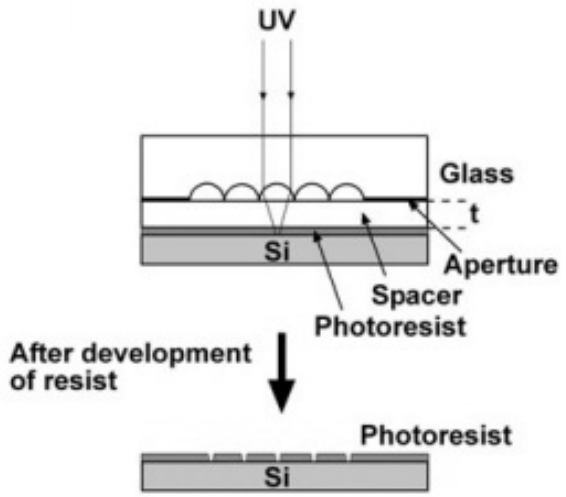

Fig. 4 Arrays of small holes in photoresist are fabricated by collimated flood illumination [12].

(2) Microlens lithography using patterned illumination
This method has simple equipment for optical setup which includes a UV illumination source, a photomask, a microlens array, PDMS for positions microlens array at a focal length distance and a photoresist. An overhead transparency projector or a UV lamp is used as a light source for the illumination system or exposure. The mask which is patterned on photoresist is first designed with CAD software and then printed onto a transparency paper using a desktop printer. An optical diffuser such as ground glass is placed in front of the projector to homogenize the illumination. The diffuser scatters the illumination from the light source and produces a uniform illumination. This illumination passes through the clear areas of the transparency mask. The microlenses receive the patterned illumination and project an array of micropatterns on the photoresist surface. Fig. 5 illustrates the optical system for microlens projection photolithography.

The transparency mask was placed on top of the Fresnel lens of the projector which acts as a condenser lens that converge the illumination onto the image plane and generates a bright illuminated area on this plane. The image plane is about 40–60 cm from the Fresnel lens, depending on projector design. The lens array and the photoresist are positioned with PDMS spacer to patterned illumination into the image plane. For a resist layer with a thickness of~400 nm, the exposure took between 10 s to 5 min. The membrane is removed from the resist after exposure, and the resist is developed in a sodium hydroxide solution. The surface topology of the photoresist is examined with a scanning electron microscope [12].

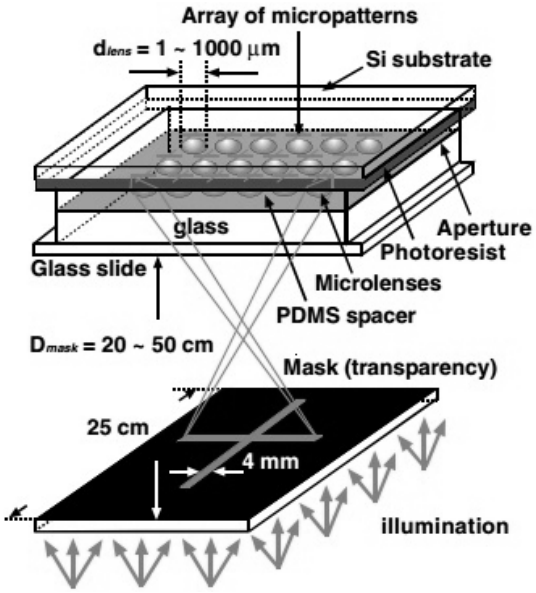

Fig. 5 Optical system for microlens projection lithography with masked illumination [12].

3. Result and discussion

3.1 Micropatterns produced by collimated flood illumination
Microlens arrays under flood illumination can generate arrays of uniform micropatterns over the entire illuminated area more than 10 cm^2 [14]. The micropatterns shown in Fig. 6 are produced with a diameter of 1.5 μm lens array.

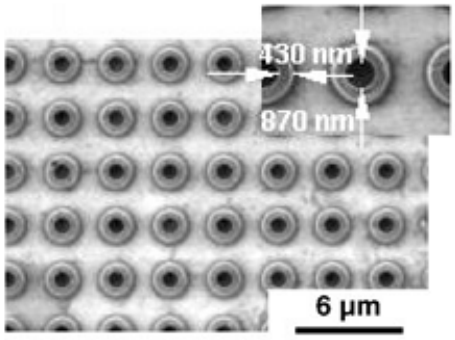

Fig. 6 An array of circular rings produced by 1.5 μm microlens array [12].

3.2 Micropattern using arrays of plano-convex microlenses
Fig. 7(a) and 7(b) illustrate two micropatterns generated by 10 μm lens array. Micron and submicron scale patterns can be achieved by arrays of plano-convex microlenses. Demagnification i.e. the size reduction of the mask on photoresist is more than 1000 [12].

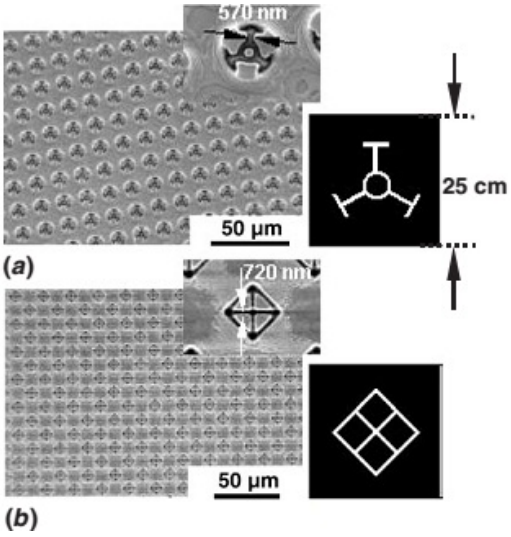

Fig. 7(a) and 7(b) SEM images of those patterns produced by an array of 10 µm plano-convex microlenses [12].

This technique can also generate arrays of complicated patterns with larger sizes of microlenses. Figures-8(a) and 8(b) show the patterns generated by square arrays of 40 µm and 100 µm lenses respectively. Fig. 8(a) shows high quality micropatterns of the logo 'VERITAS' by array of 40 µm lenses. The circuit type pattern shown in Fig. 8(b) is produced by an array of 100 µm square lenses. So this method can be applicable in the field of micro-electro mechanical systems (MEMS).

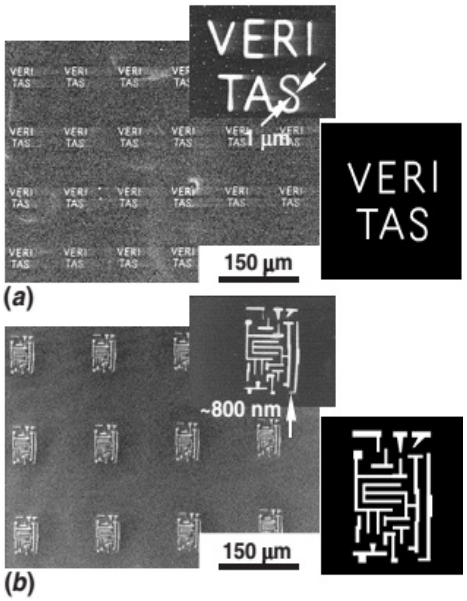

Fig. 8 SEM images of complicated patterns produced by different microlens arrays. (a) by arrays of 40 µm lenses. (b) by arrays of 100 µm lenses [12].

By this technique, generated micropatterns can be connected and rotated with horizontal axis. When the size of cross mask (l), shown in Fig. 9, is larger than a critical length lc (l>lc=10cm), the reduced micropatterns overlapped with each other to form a connected and continuous pattern [15]. Micropatterns can be rotated with high-symmetry directions at 27° and 45° and highest periodicity at 27°. Fig. 9(a) and 9(b) illustrate the separated images and connected images respectively.

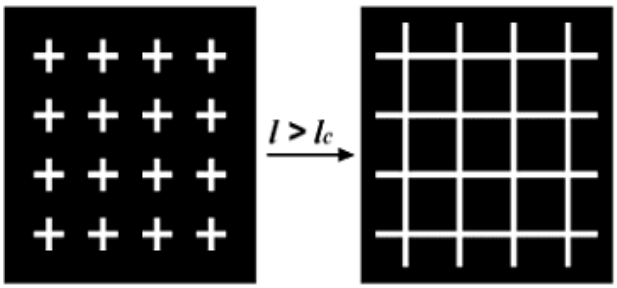

Fig. 9(a) and 9(b) separated and connected pattern produced by an array of 100µm plano-convex microlenses [15].

3.3 Micropatterns correction with gray-scale masks

Gray scale mask has two advantages over the binary mask: (i) reduce distortion of 2D micropatterns caused by diffraction and proximity effects [16]. (ii) generate 3D microstructures. The patterns with gray-scale opacity on the binary masks can be printed easily. Fig. 10(a) and 10(b) illustrate a comparison of two cross-shaped micropatterns arrays that is generated using a binary mask and gray-scale mask. The images of the cross-shaped micropatterns with binary mask is not uniform across line-width which is broadened at centre and tapered at the corner as shown in Fig. 10(a). By contrast, gray-scale mask produces an array of crosses with more uniform line-width as shown in Fig. 10(b).

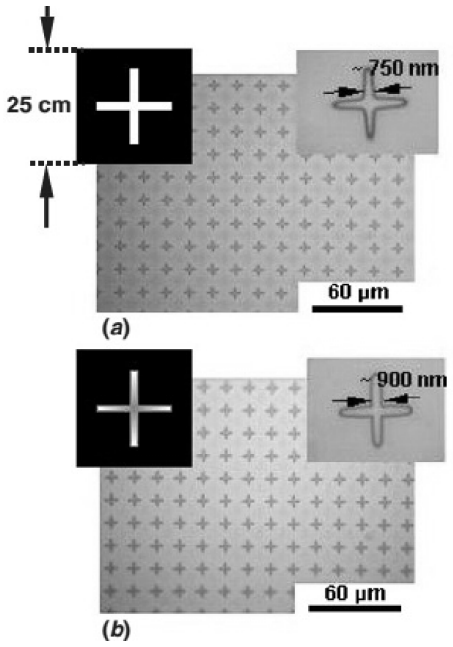

Fig. 10 SEM images of cross-shaped patterns produced by an array of 10 µm lenses. (a) using a binary mask (b) using a gray-scale mask [12].

3.4 Micropatterns using multiple exposure with multiple mask

Multiple exposures with multiple masks are used to modify microstructures as like as post processing. In this process, different mask is used for each exposure without changing the position of lens array and photoresist. The profile of developed resist shows a modified, combined pattern of all the masks. Fig. 11(a) shows an array of hexagonal microstructures produced by gray-scale mask with single exposure. Then another exposure with binary mask that has a binary pattern of a tripole, shown in Fig. 11(b), generates an array of connected microstructures using two masks with double exposures. But it has a limitation that fine modification of a microstructure can be done only at specific locations.

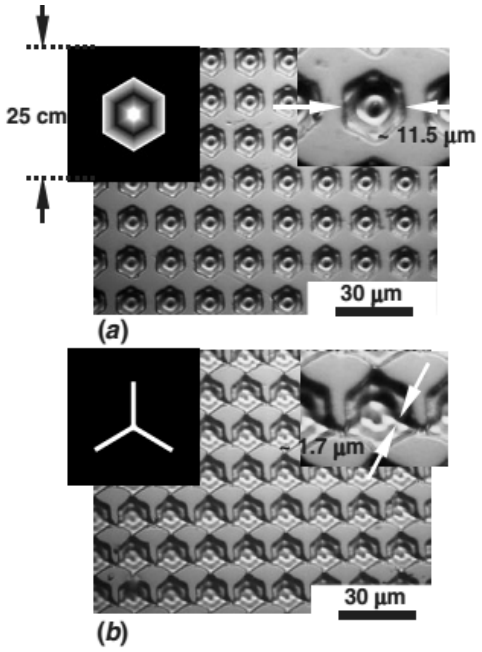

Fig. 11 SEM image of micropatterns using two exposures with two masks. (a) array of hexagonal microstructures using a gray-scale mask. (b) array of connected hexagonal microstructures generated after second exposure through a binary mask [12].

4. Conclusion

This work demonstrates that a single microlens array can produce varieties of structures by a single mask. Microlens array is fabricated by planetary contour scanning method. Since it has limitation to fabricate large microlens arrays so excimer laser dragging method is also presented which can create 100x100 lens array [11]. Various types of microlens projection photolithography techniques are also presented which have very simple optical setup, low-cost and microstructure having dimensions from 300 nm to more than 10 µm. Micropatterns fabrication with two types of illumination named as collimated flood illumination and patterned illumination is presented. In the result and discussion section, SEM image of various fabricated micropatterns such as simple, complicated and connected pattern are illustrated by various figures. Resulted micropatterns can be modified by gray scale mask and multiple exposures with multiple masks. This technique will be useful in applications of repetitive microstructures: e.g., frequency-selective surfaces, flat-panel displays, information storage devices, sensor arrays and array based bio-systems.

REFERENCES

[1] Z. D. Popovic, R. A. Sprague, G. A. Connell, Technique for monolithic fabrication of microlens arrays, *Applied Optics.* Vol. 27, pp 1281–1284, (1988).

[2] N. F. Borrelli, D. L. Morse, R. H. Bellman, W. L. Morgan, Photolytic technique for producing microlenses in photosensitive glass, *Applied Optics.* Vol. 24, pp 2520–2525, (1985).

[3] M. B. Stern, T. R. Jay, Dry etching for coherent refractive microlens array, *International Society of Optics and Photonics,* Vol. 33, pp 3547–3551, (1994).

[4] D. L. MacFarlane, V. Narayan, J. A. Tatum, W. R. Cox, T. Chen, D. J. Hayes, Microjet fabrication of microlens array, *IEEE Photonics Technology Letter*, Vol. 6, pp 1112–1114, (1994).

[5] S. Ziółkowski, I. Frese, H. Kasprzak, S. Kufner, Contactless embossing of microlenses -- a parameter study, *Optical Engineering,* Vol. 42, pp 1451–1455, (2003).

[6] C. C. Chiu, Y. C. Lee, Fabricating of aspheric micro-lens array by excimer laser micromachining, *Optical and Lasers in Engineering,* Vol. 4, pp 1232–1237, (2011).

[7] G. P. Behrmann, M. T. Duignan, Excimer laser micromachining for rapid fabrication of diffractive optical elements, *Applied Optics*, Vol. 36, pp 4666–4674, (1997).

[8] M. C. Gower, Industrial applications of laser micromachining, *Optics Express.* Vol. 7, pp 56–67, (2000).

[9] P. E. Dyer, J. Sidhu, Excimer laser ablation and thermal coupling efficiency to polymer films, *Journal of Applied Physics,* Vol. 57, pp 1420–1422, (1985).

[10] J. H. Brannon, Excimer-laser ablation and etching, *IEEE Circuits and Devices Magazine,* Vol. 6, pp 18–24, (1990).

[11] Chi-Cheng Chiu, Yung-Chun Lee, Excimer laser micromachining of aspheric microlens arrays based on optimal contour mask design and laser dragging method, *Optics express*, Vol. 20, pp 5922-5935, (2012).

[12] Wu, Ming-Hsien, George M. Whitesides, Fabrication of two-dimensional arrays of microlenses and their applications in photolithography, *Journal of micromechanics and microengineering,* Vol. 12, pp 747, (2002).

[13] H. Hocheng, K. Y. Wang, Analysis and fabrication of minifeature lamp lens by excimer laser

micromachining, *Applid Optics,* Vol. 46, pp 7184–7189, (2007).
[14] Fujita, Katsumasa, Real-time confocal two-photon fluorescence microscope using a rotating microlens array. *Optical Engineering for Sensing and Nanotechnology (ICOSN'99)*, pp 3990-393, (1999).
[15] Wu, Hongkai, Teri W. Odom, George M. Whitesides. Connectivity of features in microlens array reduction photolithography: generation of various patterns with a single photomask, *Journal of the American Chemical Society*. Vol. 124, pp 7288-7289, (2002).
[16] Robertson, P. D., F. W. Wise, A. N. Nasr, A. R. Neureuther, C. H. Ting. Proximity effects and influences of nonuniform illumination in projection lithography, *Microlithography Conferences* 1982, pp. 37-43. (1982).

ICMIEE-PI-140408

Pond Evaporation Systems for Harvesting Algae

Md. Ashikur Rahman[1], Md. Mizanur Rahman[1], Noor Ajian Mohd. Lair[1], Chi-Ming Chu[1]*
Faculty of Engineering, Universiti Malaysia Sabah (UMS), 88400 Kota Kinabalu, Sabah, Malaysia.

ABSTRACT
The production of algae is important because it is used as a source of energy and fertilizer. Algae production and quality depend on the evaporation of water. Therefore, in this paper are reviewed different types of evaporation systems to develop a suitable evaporation measurement technique for large scale algae production. The temperature at air-water interfaces; the humidity; the air-water surface area; the air temperature and the airflow rate above water surface are identified as influencing factor that control evaporation. Usually, evaporimeters, empirical equations, and analytical methods are used to determine the rate of evaporation. In the evaporimeter method, the amount of evaporation is determined from the deviation of water level and the meteorological data but the accuracy is questionable. In the empirical equations method, the equations are developed based on boundary conditions of experimental data where the accuracy is frequently uncertain. The analytical methods are often the least accurate because of their theoretical basis.

Keywords: Evaporation rate, Algae, Algae cultivation, harvesting Algae

1.0 Introduction

Since the industrial revolutions, fossil fuels, such as coal and petroleum have been the main fuel source in the world. The combustion of fossil fuels contributes to atmospheric climate change. Therefore alternative fuel sources are increasingly important. Algae can be used a resource by turning it into bio-fuel [1]. In algae cultivation and harvesting, major components of water management concern its usage, losses, and quality. Large amount of energy needed to manage the water is associated with algae cultivation systems. The total amount of water required is partially used for supporting a culture toward the target biomass productivity level and to replace water that is natural lost or evaporation lost. In part, this stems from cultivation of dilute biomass concentrations of conventional systems, such as raceway ponds as well as flat plate and tubular photo-bioreactors (PBRs), where algae cells are suspended in the liquid phase. These technologies require (a) in excess of 6000 gallons of water to cultivate 1 gallon of algae oil, (ii) a large amount of energy for pumping and circulating a dilute algae suspension as large as 385.71 MJ/kg of cultivated algae, and (iii) energy intensive dewatering and biomass concentration processes for downstream use of the biomass resulting in energy requirements of up to 82 MJ/ kg algae biomass produced [2]. Separating algae from algal biomass concentrating are known as harvesting. The algae harvesting involve recovering, dewatering and drying algae biomass. Selection of harvesting processes depends on the nature of algae. The most common harvesting methods are screening, coagulation, flocculation, sedimentation, flotation, filtration and centrifugation [3]. Evaporation is the opposite phenomenon of condensation. Condensation is a process that forms liquid from gaseous phase. In the evaporation process, liquid molecules are vaporized from a free surface of liquid and enter the gaseous phase. In this process, when a portion of molecules of the free liquid surface has received sufficient heat energy from surrounding sources, the molecules would escape from the liquid surface [4]. If the relative humidity is less than 100%, then the liquid vapor molecules is absorbed by the air. As a result, the liquid temperature will go down until the equilibrium is reached. The water budget, energy budget, mass transfer, empirical equation and evaporation pan measurement methods are used to determine evaporation rate. The energy budget includes net radiation, energy need to evaporate water, sensible heat transfer etc. that require precise measurements. The mass transfer method is based on Dalton's law; give reasonably good results in many cases of potential evaporation rates. The use of empirical formulas requires extra attention to (a) difficulties in the measurement of variables related to evaporation, (b) limitation of range for the stated accuracy in the model and (c) difficulties in comparing one empirical method with other empirical methods due to method specification model. Finally, the evaporation pan method is the easiest method to measure the evaporation from free water surface. The deviation of water level directly determine over time from a sample of open water pan of specified dimensions and sitting subject to pan coefficient. In conclusion, determining the most suitable evaporation rate measurement method will depend on the availability of data collected from experiment. It also will be depending by the influence of the accuracy of the estimated evaporation rate.

1.1 Evaporation

Evaporation is the process by which water changes from liquid to vapor state. There are two phenomena involved in the evaporation system. The first phenomenon is the change of the phase and the second phenomenon is the transfer of vapor. The change of the phase from liquid to vapor requires energy to provide the latent heat of

* Corresponding author. Tel.: +6088320000 Ext: 3135, 3060
E-mail address: chrischu@ums.edu.my or mizanur@ums.edu.my

vaporization. Solar energy is the main source of energy to recover latent heat of vaporization in the pan evaporation method [4]. The ability to transfer vapor by evaporation from a surface to the surrounding air is subject to relative humidity, wind speed, air temperature, and concentration of liquid, vapor pressure of air on water surface etc. Evaporation process is separated from three categories as evaporation from open water body; actual and Potential evapotranspiration [4]**.**

1.2 Evaporation from an Open Water Body

Evaporation from an open water body is the process where water transfer directly from reservoir's free water surface to the atmosphere. Generally, it is not possible to drive the equation for measuring the evaporation rate, using meteorological data onto. The difficulty arose out of the fact that this type of evaporation is affected by meteorological factors of solar radiation, difference in vapor pressure between water or liquid surface and the overlying air, relative humidity, air temperature, wind speed and atmospheric pressure.

1.3 Actual Evapotranspiration

Actual evapotranspiration includes the evaporation and transpiration from a land surface and its vegetation. It depends on the availability of water. Moist areas like the tropical rain forests have higher evaporation rates than arid regions. The amount of water that evaporates from the land surface depends on the amount that is contained in the soil. Transpiration is the process of water movement towards a plant, its evaporation aerial parts, such as from the leaf and stems of the plants. Plants absorb soil water through their roots. This water can be originated from deep down in the soil. Plants pump water from the soil to deliver nutrients to theirs leave. Foliage is the plant life or the plant ground cover of a region, life forms, structure spatial extent or any other specific botanicals or organic characteristics. The actual evapo-transpiration for any soil land surface depends on soil moisture status. It will be greater for a saturated soil than the unsaturated soil. The actual evapotranspiration can be determined by analysis of concurrent records of rainfall and runoff from watershed [4].

1. 4. 3 Potential Evapotranspiration

Potential evapotranspiration is defined as the evapo-transpiration that would result there is always adequate water supply available to fully vegetate the surface. The potential evapotranspiration is the simplified form of actual evapotranspiration. Estimates of potential evaporation are generally used to represent evaporative demand. Conceptually, potential evaporation represents the maximum possible evaporation rate and is the rate that would occur under given meteorological conditions from a continuously saturated surface. Notionally, the concept of potential evaporation is simple. The practical implementation of the concept is problematic and ambiguous due to the many ways that potential evaporation can be, and has been, formulated. It is the actual evapotranspiration from a soil matrix which is held the constant at field capacity for spraying the land regularly.

2. 0 Evaporation Measurement Technique

An evaporation rate is expressed as the mass or volume of liquid water evaporated per area in unit of time usually in a day. The amount of evaporation depends on temperature, humidity, solar radiation, vapor pressure and wind speed **[5].** Generally, evaporation is higher at higher temperatures and also for liquids with lower surface tension. Therefore, an evaporation rate function is combinations of meteorological variables and the liquid properties. The amount of evaporation from a liquid or water surface is estimated by evaporimeter or Evaporation pan data; empirical equation methods for estimating evaporation rate; analytical methods for estimating evaporation rate etc.

2. 1 Evaporimeter or Evaporation pan data

In evaporimeter or evaporation pan data measurement system, pans containing water is exposed to the atmosphere. The water lost through the evaporation is measured in a regular interval or sample time. The pond evaporation (E) is equal to loss of water in the pan by evaporation (E_{pan}) within a sample time duration and pan coefficient (K) [5, 6].

$$E = K \times E_{pan} \quad (1)$$

Pan evaporation is combined the effects of climate elements such as humidity, temperature, rainfall, drought dispersion, solar radiation and wind speed. Evaporation is greatest on hot windy, dry, sunny days and is greatly reduced when clouds block the sun and when air is cool, calm and humid. The evaporation pan is used to hold water during observation periods for the determination of the quantity of evaporation at a given location. It is normally installed on a wooden platform set on the ground in a grassy location and an opened area to away from trees and other wind obstruction, which may affect the natural air flow in the area. The measurement of evaporation rates for this method is conducted using many types of the pan which are Class A evaporation pan, ISI standard evaporation pan, Colorado sunken evaporation pan, USGS floating evaporation pan etc. In this method, the evaporation rate is measured by the product of parameter pan coefficient with pan evaporation from the time formerly this method eliminates objectionable boundary effects of radiation on the side walls, heat to exchange between the atmospheres and the pan itself, wind action. Pan coefficient is a constant. It is dependent on the size, shape and pan material. Table-1 shows of pan coefficients for some types of the pan.

2.2 Class A evaporation pan

Class A evaporation pan is a large standardized pan containing water that represented open water in an open atmosphere. This pan is used to estimate the evaporative

capacity of the atmosphere traditionally practiced for irrigation scheduling purpose. The pan consists of a shallow vessel according to a standard specification. Fig.1 shows the dimensions of standard class A evaporation pan [4, 8-12].

Table-1: Value of the evaporation pan coefficient [7].

SI. No	Types of pan	Average Value	Range
1	Class-A evaporation pan	0.70	0.60 – 0.80
2	ISI evaporation pan	0.80	0.65 – 1.10
3	Colorado Sunken evaporation pan	0.78	0.75 – 0.86
4	USGS Floating evaporation pan	0.80	0.70 – 0.82

It is made of galvanized iron sheets and installed on a wooden bed. The pan is filled water to a depth around 19 cm up to 20 cm. The free height of free water surface is measured with hook gauge and stilling, electronic sensor, naphthalene sensor, differential manometer, float indicators with pointer ruler etc. The difference between water level heights at two consecutive observed times are indicating the pan evaporation rate.

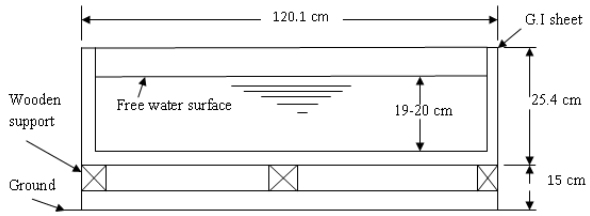

Fig. 1: Class A Evaporation Pan

2.1.3 ISI Standard Evaporation Pan

ISI standard evaporation pan is shown in Fig. 2 is a modified form of the class A evaporation pan. The pan consists of a shallow vessel made of copper sheets, tinned inside and painted outside. It is installed on a wooden grillage platform 10 cm above ground surface. The pan has small stilling well in which a fixed point gauge with Vernier scale is installed to measure the change in water level due to evaporation. The daily evaporation rate is computed from the difference between the observed water levels in the pan.

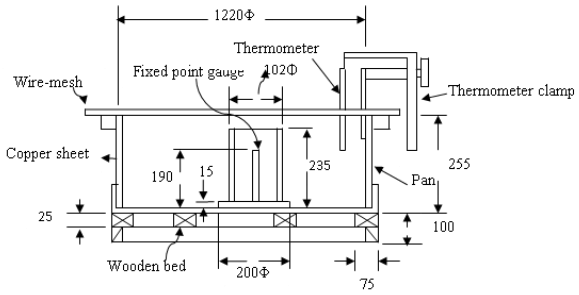

Fig. 2: ISI Evaporation Pan

2.1.4 Colorado Sunken Evaporation Pan

A Colorado sunken evaporation pan is shown in Fig 3. It is hidden into the ground such that the top level of the evaporation pan is at ground level. The pan is 92 cm squares in the plan and 46 cm in depth. It is made of unpainted galvanized iron sheets. The main disadvantage of this evaporation pan over the class A pan is the radiation and aerodynamic characteristics are closer to those of reservoir.

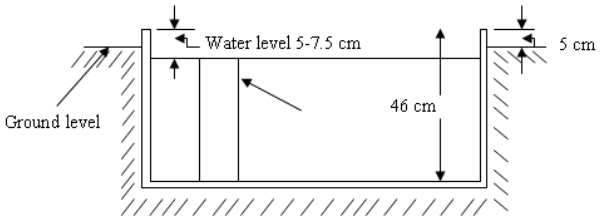

Fig. 3: Colorado Sunken Evaporation Pan

2.1.5 US Geological Survey Floating Evaporation Pan

A USGS floating evaporation pans is made according to the standard dimension of 90 cm squares in the plan and 45 cm in depth. It is supported by drum floats in the middle of a raft of size $4.25m \times 4.87m$. USGS floating evaporation pan is shown in Fig. 4. It is floating in a lake with a view to simulating the characteristic of a large body of water. The water level in the evaporation pan is kept at the same level as that of the lake. The diagonal baffles are built in the pan to reduce the wave action and wash. This type of evaporation pans is used only for geological surveys. The installation and maintenance cost are very high for this type of pan.

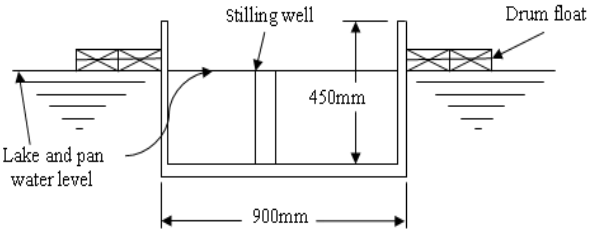

Fig. 4: Schematic diagram of USGS floating pan

2.1.6 Measurement of Water Level

The estimation of the evaporation is highly influenced by the accuracy in measuring the reduction of the water level. The water level reduction in the evaporation pan can be determined by using fixed point gauge and stilling or automatic method (Electronic sensor) or ruler scale with float pointer. The fixed point gauge consists of a pointer rod placed vertically at the center of a cylindrical well. The measuring tube has a cross sectional areas of one hundredth of the evaporation pan area. It is subdivided into 20 equal divisions each of which equal to 0.20mm of water in the pan. The water level in the evaporation pan is set at the reference point and after 24 hours, the enough water is added by the measuring tube, back to original level at the apex of fixed point gauge. The amount of water needed to bring the water back to the original level is equivalent to the amount of water

loss through evaporation. In the automatic measurement method, the recoding process can be automated by electronically measuring the rate of change of water height. An ultrasonic Doppler depth sensor housed inside a stilling well would measure the height of water in the evaporation pan. The sensor installed at about 3.5 cm above the water level in the evaporation pan. In the ruler scale and float pointer measuring instrument, the ruler scale with floating indicator are installed with evaporation pan. A pointer is moving over the ruler scale due to the reduction in the water level.

3.0 Empirical Equation to Estimate Evaporation
The empirical equations such as Dalton-based formula, Meyer's formula and Rohwer's formula are developed based on experimental data and boundary condition [13].

3.1 Dalton's Evaporation Formula
In the Dalton's Evaporation formula Evaporation rate (E) depends on the wind speed correction factor$\big(f(u)\big)$, saturate $\big(e_{pw}\big)$ and actual vapor pressure$\big(e_{pa}\big)$.

$$E = kf(u)\big(e_{pw} - e_{pa}\big) \quad (3)$$

In this the equation, the challenging issue is to determine the wind speed correction function which is a major drawback to use this equation**.**

3.2 Meyer's Evaporation Formula
This equation is a modified form of Dalton's evaporation formula to determine the lake evaporation(E_l). In this equation monthly mean wind velocity(U_9) above 9 m from ground level and a coefficient (k_m) accounting 0.36 for large deep water and 0.050 for small shallow lake are introduced.

$$E_l = k_m\big(e_{pw} - e_{pa}\big)\left(1 + \frac{U_9}{16}\right) \quad (4)$$

3.3 Rohwer's Evaporation Formula
This equation is developed to calculate evaporation of large pool or lake and is also developed form of Dalton's evaporation formula, incorporated with mean barometric pressure (P_a) and wind speed effect.

$$E_l = (1.132 - 0.00054P_a)(0.44 + 0.07U_0)\big(e_{pw} - e_{pa}\big) \quad (5)$$

4.0 Analytical Method to Estimate Evaporation
Water balance, Energy balance and combination of water and energy balance methods are used to estimate evaporation from evaporation pan.

4.1 Water Balance Method
In this method, evaporation is calculated from changes in the volume of water in evaporation pan. Therefore, the evaporation(E) depends on water in $(I)$and out (O) flow, surface seepage losses (S_l) and change in water storage (S). The main challenge in this method is measurement accuracy.

$$E = I - O - S - S_l \quad (6)$$

4.2 Energy Balance Method
In this method, the evaporation from a water body is estimated at the energy component required for evaporating water from the reservoirs. Fig. 5 shows the energy component during evaporation from pan.

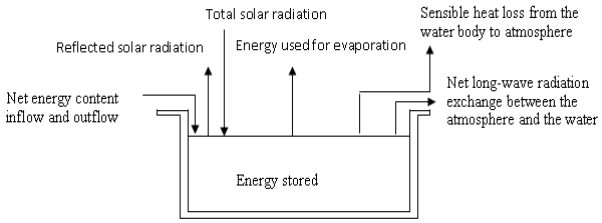

Fig. 5: Water Body Energy Balance during Evaporation

According to the energy balance method, the net radiation absorbed by water body $(Q_n)$and the net energy content of inflow and outflow elements (Q_v) is same as sum of the energy use for evaporation (Q_e), sensible heat transfer (Q_h) and amount of energy change in pan water (Q_t).

$$Q_n + Q_v = Q_h + Q_e + Q_t \quad (7)$$

Sensible heat transfer of the atmosphere is difficult to measure for the reason that the amount of air mass heat gain from water reservoirs is unknown and it is different in different location of atmosphere. If the sensible heat transfer(Q_h) to air from water is function of humidity(R) and water evaporation(Q_e). Then sensible heat, humidity and daily evaporation can be determine by using the equations

$$Q_h \approx R \times Q_e \quad (8)$$

$$R = \gamma\frac{T_w - T_a}{e_{pw} - e_{pa}} \quad (9)$$

$$E = \frac{Q_e}{\rho L_e} \quad (10)$$

Where,T_a and T_w are air and water surface temperature in ℃ and $e_{pa}$and e_{pw} are air and saturated vapor pressure; γ is the psychometric constant and L_e is the latent heat of evaporation. Therefore the energy balance can be simplified as

$$E = \frac{Q_n + Q_v - Q_t}{\rho L_e(1 + R)} \quad (11)$$

4.3 Combination method
A combined method is the modification of the energy method. Evaporation may be occurring by the aerodynamic method at what times the energy supply is not limiting, and by the energy balance method when the vapor transport is not limiting. Equation 12 is based on a combination of aerodynamic and energy balance equations [11].

$$E = \frac{mR_n + \rho c_p E_r}{L_e(\gamma + m)} \quad (12)$$

where, m is the slope of the saturation vapor pressure versus temperature curve at the air temperature in P_a/k, R_n is the net irradiance in W/m^2, and E_r is the parameter including wind speed and saturated vapor pressure deficit in $P_a m/s$. The value of m can be determined from the empirical shown in equation 13 and 14.

$$m = 0.04145e^{-0.06088T} \quad (13)$$

$$m = \left\{4098 \times \left(\frac{0.6108e^{\frac{27.27T}{T+237.3}}}{(T+237.3)^2}\right)\right\} \quad (14)$$

For long wave radiation, net long wave radiation is equal to the long wave flux coming from the atmosphere, minus the amount of reflected from the surface and the amount radiated from the surface [12]. Mathematically

$$R_n = \varepsilon_w \varepsilon_{at} \sigma {T_a}^4 - \varepsilon_w \sigma {T_s}^4 \quad (15)$$

Where, ε_w and ε_{at} are water and effective emissivity which is a function of humidity and cloud cover in sky. The average value of the effective emissivity is 0.98.

Consider the incident solar radiation outside the atmosphere on a horizontal surface. The net irradiance (R_n) is the different between incoming and reflection radiation(R_l) [14]. The amount of coming radiation on water body can be determined from the equation 16.

$$R_i = R_A(1-r)\left(a + b\frac{n}{D}\right) \quad (16)$$

Where, R_A is the total possible radiation for the period of estimation, it is function of latitude and season; r is the reflection coefficient (albedo) varies $0.05 \sim 0.12$; a is a constant depending upon the latitude $0.29\cos\phi$ where ϕ is the latitude; b is a coefficient an average value 0.5; and n/D is the fraction of possible sunshine from climatic atlas. The net back radiation flow from water surface is calculated from equation 17.

$$R_l = \sigma T^4\left(0.56 - 0.092\sqrt{e_{ap}}\right)\left(0.1 + 0.9\frac{n}{D}\right) \quad (17)$$

Where, σ is Stefan-Boltzmann constant 2.01×10^{-9} mm/day. In the equation 12, the psychrometric constant (γ) is the function of air pressure and ratio of molecular weight of air to water. So the equation 12 becomes

$$E_{mass} = \frac{mR_n + \rho c_p(1 - 0.01RH)e_w g_a}{\lambda(\gamma + m)} \quad (18)$$

5.0 Comparison of Evaporation in Different Methods

After comparing it is found that analytical methods can provide good results. They involve parameters that are difficult to assess. Empirical equations can at best give approximate values of the correct order for magnitude. In view of the above, pan measurements find wide acceptance in practice.

6.0 Effect of Concentration on Evaporation

Fick's law of diffusion states that the mass diffusion flux has an inverse relationship to the solute concentration [12]. Mathematically,

$$m_A = -\rho D_{AB} \nabla m f_A \quad (19)$$

Where, m_A is mass flux; $D_{AB}$is binary diffusion coefficient, C_A is concentration of species A and $\Delta m f_A$ is mass fraction of species A. Study showed that the rate of evaporation from sea water is about 2-3% less than from fresh water because of concentration difference [15].

6.1 Effect of Algae on Evaporation

A large amount of algae is present in the evaporation pan which increases the density of solution in the pan. According to the Fick's law, the density of the solution or liquid is higher due to solute or suspended solids, so rate of evaporation must be slower. In terms of energy consumption of a fresh water pond, the net solar energy is used for evaporating the water only. Other than in an algae cultivation pond, net solar energy is used for both the water evaporation and physiological function of algae (Osmosis and photosynthesis). Algae containing nutrients and in general, nutrient-like substances that dissolve in water tend to slightly decrease water's evaporation rate. Therefore, it can be thought that algae cultivation in the pond will reduce the evaporation rate.

7.0 Summary of Factors Affecting Evaporation

Evaporation is a function of climatic and environmental conditions and it is influenced by different factors. The factors are

- The lowest evaporation rate is found in winter season where as the highest in either monsoon or pre monsoon season.
- The evaporation rate is found slower when the solute concentration in a liquid is higher.
- The evaporation of water reduces with increasing reflectance of solar irradiance from the water surface. The change of reflectance of solar energy is required a surface modification.
- The evaporation rate is increased with increased vapor pressure deficit.
- Higher vapor pressure deficit means the lower relative humidity.
- Air temperature is one of the principal factors causing evaporation.
- The flow of less saturated air leads increased evaporation rate. A natural draft chimney above the pond can be used to artificially increase air evaporation rate.
- At higher elevations, the atmospheric pressure is less than at a lower altitude. At a lower atmospheric pressure, it is easier for a liquid to evaporate.

- The rate of evaporation increases with water temperature however, the evaporation rate might be lower at another location with the same average temperature due to a higher relative humidity. Water temperature can be controlled by using a suitable insulator on the outer surface of the evaporation pan.
- The net result is a decrease in evaporation that is more or less proportional to the decrease in temperature.
- The large surface area has more surface molecules that are able to escape easily as a result the rate of evaporation is faster than the same volume of water but has a smaller surface area.
- The building is a resistor to wind movement. The air direction and speed can be changed by the building as a result evaporation rate will be slower.

4. 1 Conclusion

Evaporation is an important factor that influences cultivation and harvesting of algae. The amount of water that must be refilled into the algae cultivation pond annually is equal to the loss by evaporation. By algae cultivation, the farmer should gain the right knowledge of the evaporation characteristic in algae culture ponds and also should estimate the amount of water to be lost through evaporation.

Dewatering algae by the natural convection method included draft enhancement of installing a wire mesh on the chimney may be a higher expectable novel technology which is to promise zero-energy input. The rate of dewatering algae for the convection dewatering will be measured by the evaporation rate. The measurement of evaporation rates entails the measurement of water volume reduction in evaporation over a period of time.

It can be predicted by using water balance, energy balance, combination energy and water balance or Penman equation. Selection of a suitable evaporation measurement method depends on the character of the water reservoir and the surrounding aerodynamic condition. The combination of mass and energy transfer balance or Penman equation will yield higher accuracy of the result but the measurements of its variables are difficult. The pan measurement method is simple to compare with other evaporation rate measurement methods. In the pan measurement method, the pan has a constant surface area; therefore the water volume reduction is only the function of water depth of the evaporation pan. The accuracy of pan evaporation results depends on the pan size and shape, pan materials and place of installations of the pan.

References

[1] Kuan-Yeow Show, Duu-Jong Lee, Jo-Shu Chang, 2013, Algal biomass dehydration. Bio-resource Technology 135, 720–729.

[2] Altan Ozkan, Kerry Kinney, Lynn Katz, Halil Berberoglu, (2012), Reduction of water and energy requirement of algae cultivation usingan algae biofilm photobioreactor, vol. 114, pp. 542-548, Bioresource Technology.

[3] John J. Milledge, Sonia Heaven, (2013), A review of the harvesting of micro-algae for biofuel Production, , vol. 12, pp. 165-178, Rev Environ Sci Biotechnol.

[4] McMahon, T.A, Peel, M.C, Lowe, L., Srikanthan, R., and McVicar, T.R., (, 2013), Estimating actual, potential, reference crop and pan evaporation using standard meteorological data: a pragmatic synthesis, vol. 17, April, pp. 1331-1363, Hydrology and Earth System Sciences.

[5] Fekih Malika, Bourabaa Abdenour and Mohamed Saighi (2013) Evaluation of two methods for estimation of evaporation from Dams water in arid and semi-arid areas in Algeria, Volume 2, January, ISSN 2319 – 4847, International Journal of Application or Innovation in Engineering & Management (IJAIEM)

[6] Ahmet Ertek, Suat Sensoy, Cenk Kucukyumuk, Ibrahim Gedik, (2006), Determination of plant-pan coefficients for field-grown eggplant (Solanum melongena L.) using class A pan evaporation values, vol. 85, May, pp. 58–66, Agricultural water management.

[7] Engineering Hydrology Book by K Subramanya, 1994.

[8] Hao LIU, Ai-wang DUAN, Fu-sheng LI, Jing-sheng SUN, Yan-cong WANG and Chi-tao SUN,(2013) Drip Irrigation Scheduling for Tomato Grown in Solar Greenhouse Based on Pan Evaporation in North China Plain, vol. 12(3), March, pp. 520-531, Journal of Integrative Agriculture.

[9] Kisi Ozgyr,(2013), Evolutionary neural networks for monthly pan evaporation modeling, vol. 498, June, pp. 36–45, Journal of Hydrology.

[10] Jacobs A.F.G., Heusinkveld B.G., Lucassen D.C., (1998), Temperature variation in a class A evaporation pan, vol. 206, pp.75-83, Journal Of Hydrology.

[11] Chu Chia-Ren, Li Ming-Hsu, Yi-Ying Chen, Kuo Yi-Hsin, (2010) A wind tunnel experiment on the evaporation rate of Class A evaporation pan, vol. 381, November, pp. 221–224, Journal of Hydrology.

[12] Lim Wee Ho, L. Roderick Michael, T. Hobbins Michael, Chin Wong Suan, D. Farquhar Graham, (2013), The energy balance of a US Class A evaporation pan, Series. 182– 183, July, pp. 314– 331 Agricultural and Forest Meteorology.

[13] J. Donohue Randall, R. McVicar Tim, L. Roderick Michael, (2010) Assessing the ability of potential evaporation formulations to capture the dynamics in evaporative demand within a changing climate, vol. 386, March, pp. 186-197,Journal of Hydrology.

[14] Khudair abass dawood, Farhan Lafta Rashid, Ahmed Hashim, (2013), Reduce Evaporation Losses From Water Reservoirs, Vol.1, No 1, December pp. 23-29, International Journal of Energy and Environmental Research

ICMIEE-PI-14-140409

DEVELOPMENT OF AN UNMANNED AERIAL VEHICLE (UAV) AND ITS REMOTE CONTROLLING SYSTEM

Md. Syed Ali Molla[1] and Md. A. Rahim[2]
[1]Professor, ME, KUET, pmsali@me.kuet.ac.bd;
[2]Mechanical Engineer, KUET, Khulna, [2] mark05078@gmail.com [2]

ABSTRACT
This investigation explores controlling of an UAV from a remote place by sending signals. The signals are sent from wireless remote keyboard. When a controller presses buttons one after another randomly or sequentially, then the signals are received in the form of analog signals and these analog signals are converted into binary form. Though a microcontroller is capable of receiving and processing both binary and analog signals (Or data), but it is not possible to recognize any remote signal by the microcontroller directly. So it is necessary to build a signal receiver to recognize them. Signal receiver can recognizes the signals that can be in any frequency and can converts the frequencies in the four digits binary number through the four output pins Q_1, Q_2, Q_3 and Q_4. Just like 0001 when the button "1" is pressed and 0010 when the button "2" is pressed and so on. In this remote controlled system, twelve possible signals can be utilized to control the operations separately. For an unmanned aerial vehicle, it is enough to control it by twelve different frequency signals. This UAV is controlled according to the signal received from remote control system which is sent to the microcontroller pins and corresponding controlling motors. This is a model investigation to run an unmanned aerial vehicle by five motors out of which three motors are for lifting, one for propulsion and the rest one for the ladder or aviation direction control. Final model test will be made with an unmanned aerial vehicle having fixed wing, flap and navigation ladder and propulsive motor with necessary self-balancing facilities.

Keywords: Unmanned aerial vehicle, remote control system, vehicle balance.

1. Introduction

The UAV is an acronym for Unmanned Aerial Vehicle, which is an aircraft with no pilot on board. UAVs can be remote controlled aircraft (e.g. flown by a pilot at a ground control station) or can fly autonomously based on pre-programmed flight plans or more complex dynamic automation systems. UAVs are currently used for a number of missions, including reconnaissance and attack roles. For the purposes of this article, and to distinguish UAVs from missiles, a UAV is defined as being capable of controlled, sustained level flight and powered by a jet or reciprocating engine. In addition, a cruise missile can be considered to be a UAV, but is treated separately on the basis that the vehicle is the weapon. The acronym UAV has been expanded in some cases to UAVS.

The FAA has adopted the acronym UAS to reflect the fact that these complex systems include ground stations and other elements besides the actual air vehicles.[1] UAV systems, despite having no onboard human pilots, require a high amount of human involvement to accomplish successful operations. A typical modern UAV system involves a launch crew (1-3 people), a mission crew (2-5) people, personnel using the imagery data captured from the UAV onboard sensors, such as forward ground troops or intelligence analysts, and possibly others, including lawyers and politicians. Furthermore, since a single UAV mission can last for over 24 hours, missions often involve one or more shift changes of the mission crew. Thus, there is a significant amount of human-human and human-vehicle interaction involved in UAV system operations. Much of this collaboration is done between geographically distributed people (e.g. the mission crew may be in the United States while the launch crew and information consumers may be in Afghanistan). Officially, the term 'Unmanned Aerial Vehicle' was changed to 'Unmanned Aircraft System' to reflect the fact that these complex systems include ground stations and other elements besides the actual air vehicles. The term UAS, however, is not widely used as the term UAV has become part of the modern lexicon. [1]

The military role of UAV is growing at unprecedented rates. In 2005, tactical and theater level UA alone, had flown over 100,000 flight hours in support of Operation ENDURING FREEDOM (OEF) and Operation IRAQI FREEDOM (OIF). Rapid advances in technology are enabling more and more capability to be placed on smaller airframes which is spurring a large increase in the number of SUAS being deployed on the battlefield. The use of SUAS in combat is so new that no formal DOD wide reporting procedures have been established to track SUAS flight hours. As the capabilities grow for all types of UAV, nations continue to subsidize their research and development leading to further advances enabling them to perform a multitude of missions. UAV no longer only perform intelligence, surveillance, and reconnaissance (ISR) missions, although this still remains their predominant type. Their roles have expanded to areas including EA, strike missions, SEAD/DEAD, network node or communications relay, CSAR and derivations of these themes. These UAV

* Corresponding author. Tel.: +88-01713255226
E-mail address: mdmashud@yahoo.com

range in cost from a few thousand dollars to tens of millions of dollars, and the aircraft used in these systems range in size from a MAV weighing less than one pound to large aircraft weighing over 40,000 pounds.

Research and development - used to further develop UAV technologies to be integrated into field deployed UAV aircraft . Civil and Commercial UAVs - UAVs specifically designed for civil and commercial applications.

In the past, UAVs were known by many different names, such as robot plane, drone, pilotless aircraft, and RPV. Later, the Federal Aviation Administration implemented a generic class name for them, UAS, to indicate that these aircraft systems also comprise a data link, control systems, ground stations, and other related support equipment. However, they are generally known as UAVs. UAVs are powered, aerial vehicles without an onboard human operator and can fly independently from pre-programmed flight plans or through a remote pilot. They are capable of carrying a lethal or nonlethal payload and come in different sizes, from the size of an insect to that of a commercial airliner. These devices have proven their effectiveness in recent warzones, such as Kosovo, Afghanistan, and Iraq.

When compared to manned aerial vehicles, UAVs are believed to provide two important benefits - they are cost effective and reduce the risk to a pilot's life. However, accident rates in today's UAVs are over 100 times than that of manned aircraft. Therefore, improved safety and reliability are still required.

The first pilotless aircrafts, called aerial torpedoes, were developed shortly after World War I and resembled modern cruise missiles. The current UAVs originate mostly from radio controlled pilotless target aircrafts built in the US and UK in the 1930s. [2]

An unmanned system is not just a vehicle. It is composed of the vehicle, communications, data links and control stations[2]. Degree programs at UVU take a systems engineering approach. Graduates will enter the unmanned career field in the areas of R&D, vehicle design, sensor development, vehicle communications and data links, sense and avoid systems, human machine interfaces, autonomous control, vehicle navigation, alternative power and operations.

The International Journal of Unmanned Systems Engineering (IJUSEng journal promotes the advancement of the applied science, technology and operation of unmanned systems through the dissemination of original research representing significant advances in the design, development, testing and operation of unmanned systems. IJUSEng provides a platform for authors and researchers for communicating their latest findings, ideas and methods at the forefront of technology in the field of unmanned systems engineering. The scope is wide, covering research, design, development, operation, safety and reliability. For more information on the journal visit. [3]

Hengyu"Robbie" Hu,conducted research investigation[4] on Autonomous Quadrotor for the 2013and reported that the quadrotor that is capable to traversing through narrow corridors of an unknown building using Simultaneous Localization and Mapping (SLAM) algorithms. While exploring, the vehicle uses image recognition program to identify the assistive Arabic signs and the flash drive ultimately, a passive Retrieval mechanism consist adhesive and magnet secures the flash drive and releases a decoy through mechanical levers. Include returning, all mission shall be completed within ten minutes limit.

The forerunner of today's UAV is reported to be the American Navy Curtiss/Sperry "flying bomb"[4]. This primitive cruise missile first flew on March 6, 1918. The Charles Kettering Aerial Torpedo, also known as the Kettering Bug, was a parallel effort backed by the American Army. Orville Wright acted as a consultant on the project. The "Bug" was a gasoline fueled propeller driven biplane which flew on a preset course for approximately 50 miles late in 1918. The guidance systems for both aircraft, composed of a gyroscope and barometer/altimeter were designed by Elmer Sperry.

The German Fiesler FI 103 V1, "Buzz Bomb" or "Doodle Bug" of 1944, was the first successful cruise missile.[5] This ram jet powered weapon traveled at speeds up to 400 mph and was able to strike London from launch sites in France. Germany also developed and used the Henschel Hs 293 and Fritz-X radio controlled glide bombs. These weapons were launched in midair from a controlling mother ship and steered to the target by radio commands made by a human operator. On Sept.9, 1943, the Italian battleship Roma was sunk by two Fritz-X bombs.

The first UAVs developed for surveillance were not utilized until the Vietnam War, where many Fire bee drones were introduced for simple reconnaissance activities. Initially, these drones were equipped with simple cameras and later fitted with communications, night photo and electronic intelligence. [5]

Some early UAVs are called drones because they are no more sophisticated than a simple radio controlled aircraft being controlled by a human pilot (sometimes called the operator) at all times. More sophisticated versions may have built-in control and/or guidance systems to perform low level human pilot duties such as speed and flight path stabilization, and simple prescript navigation functions such as waypoint following. From this perspective, most early UAVs are not autonomous at all. In fact, the field of air vehicle autonomy is a recently emerging field, whose economics is largely

driven by the military to develop battle ready technology for the war fighter. Compared to the manufacturing of UAV flight hardware, the market for autonomy technology is fairly immature and undeveloped. Because of this, autonomy has been and may continue to be the bottleneck for future UAV developments, and the overall value and rate of expansion of the future UAV market could be largely driven by advances to be made in the field of autonomy.

M. M. Syed Ali[6] conducted research work with pneumatic powered robot and firefighting system. A mobile phone was used to operate the firefighting system and the pneumatic powered robot. The firefighting system and pneumatic power robot were operated and controlled by mobile phone guided GSM Network perfectly. This was shown in national TV and ATN News channel in 2008. Later on M. M Syed Ali took an undergraduate research project on GSM Network Base Remote Control System for an Unmanned Vehicle [7]. This scheme is known as Dual Tone Multi-Frequency (DTMF), Touch-Tone or simply tone dialing. The test result showed that mobile phone guided wireless remote control system is applicable to control, surface vehicle and low height aerial vehicle wirelessly. M. M. Syed Ali et al. also conducted research works on automatic firefighting system and robot assisted firefighting system using this mobile phone guided GSM Network where it is found to work satisfactorily.[8]

2. Methodology

Here a model UAV has been constructed to control by a remote control system. To control an UAV, here a mobile phone is used to send signal by pressing button. These signals have been utilized for controlling the vehicle. A receiver is placed in the UAV to read the incoming signals from pilot and these signals are prepared to send in the micro controlling unit. When the pilot will press a button, according to the preprogrammed, the controlling unit or autopilot will lead the UAV to take off from land. Three motors are used for lifting and one for going ahead. Another motor is used for ladder or aviation direction control.

Autonomy is commonly defined as the ability to make decisions without human intervention. To that end, the goal of autonomy is to teach machines to be "smart" and act more like humans. The keen observer may associate this with the development in the field of artificial intelligence made popular in the 1980s and 1990s such as expert systems, neural networks, machine learning, natural language processing, and vision. However, the mode of technological development in the field of autonomy has mostly followed a bottom-up approach, and recent advances have been largely driven by the practitioners in the field of control science, not computer science. Similarly, autonomy has been and probably will continue to be considered an extension of the controls field. In the foreseeable future, however, the two fields will merge to a much greater degree, and practitioners and researchers from both disciplines will work together to spawn rapid technological development in the area. To some extent, the ultimate goal in the development of autonomy technology is to replace the human pilot. It remains to be seen whether future developments of autonomy technology, the perception of the technology, and most importantly, the political climate surrounding the use of such technology, will limit the development and utility of autonomy for UAV applications.

The receiver's signals can be transmitted over a radio to switch ON or switch OFF home appliances, flash lights, motors, cameras, warning systems, irrigation systems and so on. These encoded data can be stored and processed in a microcontroller to perform different tasks.

3. Design & construction of UAV body

3.1 Design of the main frame of the UAV

The designs and construction of the model UAV are shown in figure 1. MS channel (12mm X 12mm) are selected for main frame of the structure as shown below.

Fig.1 Structure of the main frame of the UAV.

3.2 Assembly of the model with motors

All the five motors are assembled on the main frame of the UAV as shown in figure1.

Fig. 2 Construction of UAV body.

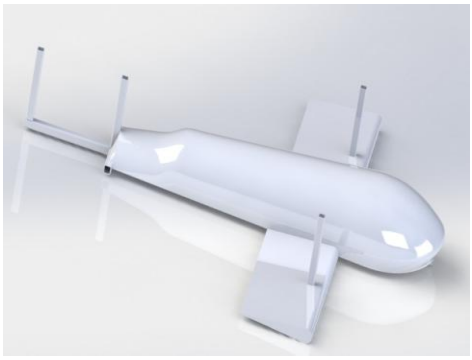

Fig. 3 Recommended model for future development.

4. Controlling system of UAV

4.1 Layout of the UAV Controlling System

The layout of the whole controlling system is shown in figure 4 below.

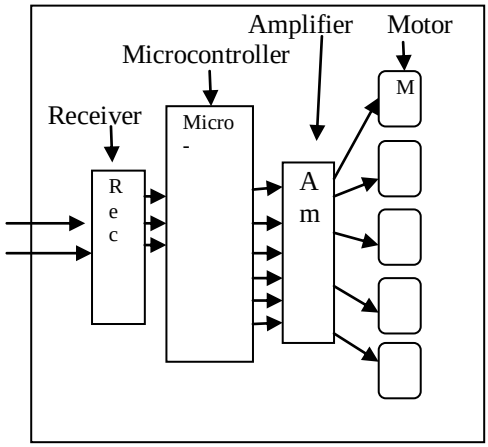

Fig. 4 Layout of signal receiver by microcontroller and transmission to power supply unit.

The design of the signal receiver unit with circuit diagram is shown in figure 5. It just contains IC chip, some diodes, resistors, capacitors and crystal.

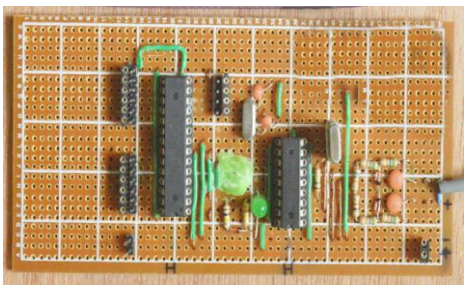

Fig.5 Combination unit of both signal receiver and microcontroller

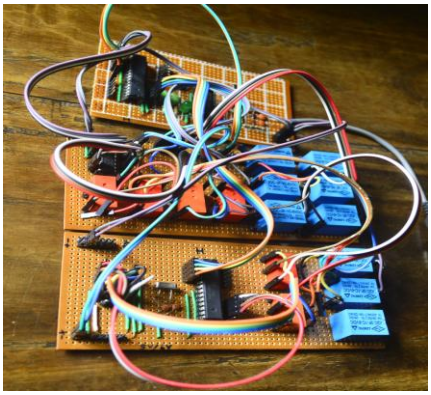

Fig. 6 Power supply system with controlling system.

4.2 Controlling of motors

In UAV the devices are controlled by controlling power supply in the respective motor. During take-off, one propulsive motor and 3 nos. lifting motors are started by a single command from ground station for generating propulsive and lift force. Again direction of the aviation control is done by changing rotational direction of the controlling motor.

Generally, brushless motors having high ampere current capacity and high speed are used in such cases. A brushless motor with 14,000-15,000 rpm and 4-5 ampere rating can lift 5-6 kilogram weight.

5. Performance test

The assembly of the controlling system and UAV body has been tested in the laboratory and it is seen that the remote control system is working properly. Thus UAV can be controlled from remote place necessary for aviation control.

The performance of the UAV is tested in the laboratory to ensure the operation of controlling system and preparation of flying. It has some sequential procedure to start and control the UAV.

a) UAV is connected with the controlling system from remote distance.
b) All the 4 motors for lifting and propulsion are operated in its design mode for low speed and high speed operation.
c) The direction of aviation control is tested by operating the 5^{th} motor in clockwise and anti-clockwise rotation.
d) Finally, UAV can be operated from remote place according to the pre-programmed loaded in microcontroller.

The tested result shows that the controlling system is working properly. Since there is no visual camera attached in the UAV body and motor powers are insufficient so the operation of motors are tested in the laboratory only.

6 . Result and discussion

The test result shows that all motors can be controlled by the remote control system successfully in the laboratory. The construction of UAV body and its controlling system are accomplished to fulfill are the requirements of aviation for an UAV. However the major objective is to develop a body and a controlling system, so that the test result can help for future development of UAV. These test results can help in

- developing controlling device
- assessment of the material required for body construction
- motor power necessary to operate the UAV.
- and assessing cost and power weight ratio of a UAV

The reduction of the weight of the UAV body reduces the power consumption and cost of the vehicle. If the motors are of desired rating are used then the UAV will able to fly. Finally, the performance of all the five motors required for flying of the UAV is found satisfactory.

7. Conclusion

In this research project, remote control system a similar to a previous study[7] is used with a different vehicle model shape for easy balancing of the UAV. The test result shows that

- the operation of the model motors can be started by this remote control system.
- the motors power installed are not sufficient to develop sufficient lift force for flying this UAV. Brass- less motors are required to be installed which could not be managed
- development of surveillance control system is also required with remote control system.
- the model needs a further development for better sensing, balancing and development of remote control system before aviation test.

NOMENCLATURE

UAV	= Unmanned aerial vehicle
UAVS	= Unmanned aircraft vehicle system
UAS	= Unmanned aircraft system
RPV	= Remotely piloted vehicle
EA	= Electronic attack
SEAD	= Suppression of enemy air defense
DEAD	= Destruction of enemy air defense
CSAR	= Combat search and rescue
MAV	= Micro air vehicle
TCS	= Tactical control system

REFERENCES

[1] F.B. Da Silva, S.D. Scott, and M.L. Cummings "Design Methodology for Unmanned Aerial Vehicle (UAV) Team Coordination

[2] http://www.uxvuniversity.com/

[3] www.ijuseng.com

[4] Hengyu"Robbie" Hu, "Autonomous Quadrotor for the 2013, International Aerial Robotics Competition "Mechanical Engineering, minor Computer Engineering 2014

[5] http://en.wikipedia.org/wiki/Kettering_Bug

[6] M.M. Syed Ali, "Mobile Phone Operated Firefighting System and Pneumatic Power Robot", *ATN News* , VISUAL DIARY , 26th January 2008 , TV C-34-0126-1554407

[7] M.M. Syed Ali, M.A., Al Mamun, and M.A. Alim, "Design and Construction of GSM Network Base Remote Control System of an Unmanned Vehicle. "*Undergraduate Thesis,* 2012-13, Department of Mechanical Engineering, KUET, Khulna 9203, Bangladesh

[8] M.M Syed Ali, M .Shafiq Sayid, M.A. Al-Mamun and Md. Muhaiminul Hassan, "Experimental study on a robot assisted automatic firefighting system using GSM & AGSM networks and other surveillance system" Proceedings of the 15th Annual Paper Meet 07-08 February 2014 Dhaka, Bangladesh, Mechanical Engineering Division The Institution of Engineers, Bangladesh.

Analyzing Distribution Networks of Supply Chain in Perspective of Bangladesh

[1]Farjana Nur, [2]N.U.I Hossain*

[1*] Department of Industrial Engineering & Management, Khulna University of Engineering & Technology, Bangladesh
[2]Department of Mechanical Engineering, Khulna University of Engineering & Technology, Bangladesh

Abstract:

Supply chain is the sequence of processes involved in the production and distribution of a commodity. And designing distribution network is one of the crux factors of supply chain management. Shortly, a distribution network is the system that a company uses to get products from the manufacturer to the retailer. A fast and reliable distribution network is essential to a successful business because customers must be able to get products and services when they want them. With a view to designing a supply chain, we need to consider how all supply chain drivers should be used together to support the competitive strategy of a company and maximize supply chain profits. This paper aims to discuss various mode of distribution networks of supply chain in perspective of Bangladesh and their recent transformation into another mode due to introduction of new business types.

***Keywords**: Distribution Network, Drop Shipping, Manufacturer, Distributor, Retailer.*

1. Introduction

There are two key factors needed to be considered to design the supply chain network. And performance of a distribution network is evaluated through these two dimensions. These two dimensions are:

1.**Customer needs that are met (Customer Service):

- Response time (Time it takes for a customer to receive an order)
- Product variety (Number of different products that are offered)
- Product availability (Probability of having a product in stock)
- Customer experience (Ease of placing and receiving orders)
- Order visibility (Ability of customers to track their orders)
- Returnability (Ease of returning unsatisfactory merchandise)

2.**Cost of meeting customer needs (supply chain cost):

- Inventory (All raw materials, WIP, and finished goods)
- Transportation (Moving inventory from point to point)
- Facility & handling (Locations where product is stored, assembled, or fabricated)
- Information (Data and analysis of all drivers in a supply chain)

Distribution network design options must therefore be compared according to their impact on customer service and the cost to provide this level of service.

Changing the distribution network design directly affects the following supply chain cost.

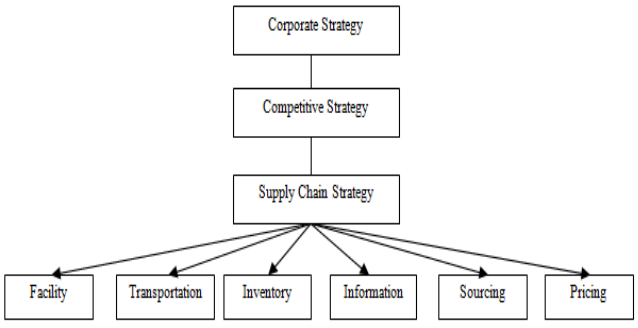

Fig 1. Factors that affect distribution network

2. Literature Review

In 1982, the term "supply chain management" was first coined by Keith Oliver . However, the concept of a supply chain in management was of

Corresponding email:farjana.mitu08@gmail.com

great importance long before, in the early 20th century, especially with the creation of the assembly line. The characteristics of this era of supply chain management include the need for large-scale changes, re-engineering, downsizing driven by cost reduction programs, and widespread attention to Japanese management practices. Then starts integration era. In this era of supply chain management studies was highlighted with the development of electronic data interchange (EDI) systems in the 1960s, and developed through the 1990s by the introduction of enterprise resource planning (ERP) systems. This era has continued to develop into the 21st century with the expansion of Internet-based collaborative systems. This era of supply chain evolution is characterized by both increasing value added and cost reductions through integration. Then in 1990s specialization era, phase1 began. In this era, companies began to focus on "core competencies" and specialization. They abandoned vertical integration, sold off non-core operations, and outsourced those functions to other companies. This changed management requirements, by extending the supply chain beyond the company walls and distributing management across specialized supply chain partnerships. After that, specialization era, phase2 began which is known as supply chain management as service. Specialization within the supply chain began in the 1980s with the inception of transportation brokerages, warehouse management, and non-asset-based carriers, and has matured beyond transportation and logistics into aspects of supply planning, collaboration, execution, and performance management.

3. Design Options For a Distribution Network:

There are two key decisions associated with designing a distribution network

- Will the product be delivered to the customer location or picked up from a preordained site?
- Will product flow through an intermediary?

Most importantly there are eleven steps are considered to align a distribution network for Competitive Advantage.

Step 1: Identify scope and current network constraints
Step 2: Determine your goals
Step 3: Gather data on the current network situation
Step 4: Cleanse and verify the data
Step 5: Select design tools
Step 6: Build baseline models
Step 8: Model potential strategic network scenarios
Step 9: Model potential strategic network scenarios
Step 10: Determine capital investment requirements
Step 11: Recommend and develop your implementation plan

4.Types Of Distribution Network:

Answers that are ratified based on those two previous key questions, there are six distinctive distribution networks are used to move products from manufacturer to consumer or end user.

Those six types of distribution networks are presented in below figure:

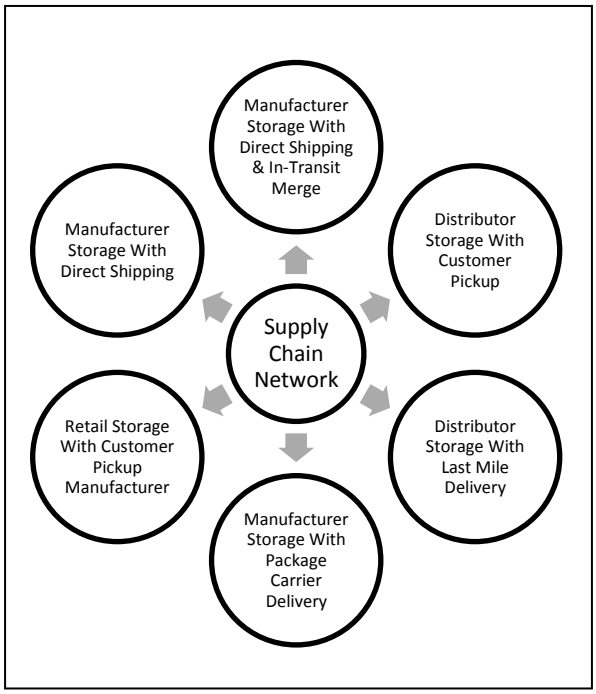

Fig 2. Types of supply chain distribution network.

Corresponding email:farjana.mitu08@gmail.com

4.1 Manufacturer Storage with Direct Shipping (Drop Shipping)

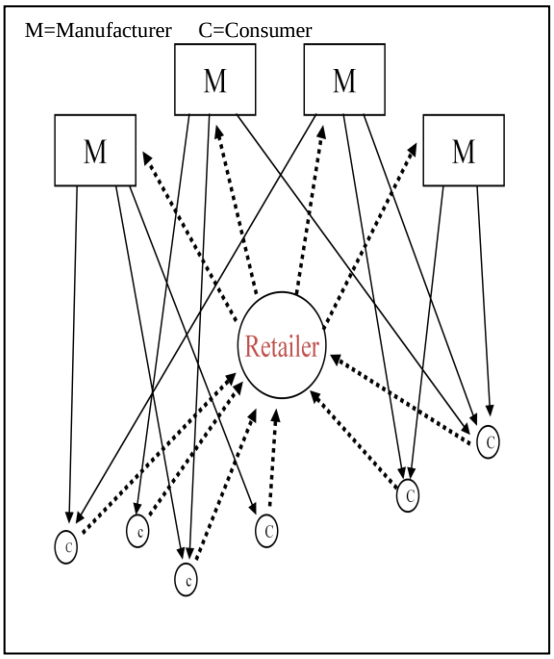

Fig 3. Manufacturer Storage with Direct Shipping

Product Flow: ⟶
Information flow:----------

Example:
-Western Marine (Large Ship/ Vessel)
-Ananda Shipyard (Large Ship/ Vessel)

Characteristics of this distribution networks are stated below:

- Products are shipped directly to the consumer from the manufacturer
- Retailer is an information collector:
  - Passes orders to the manufacturers
  - It does not hold product inventory
- Inventory is centralized at manufacturer
- Drop shipping offers the manufacturer the opportunity to postpone customization
- Effective for high value, large variety, low demand products
- High transportation cost

4.2 .Manufacturer Storage with Direct Shipping and In-Transit Merge

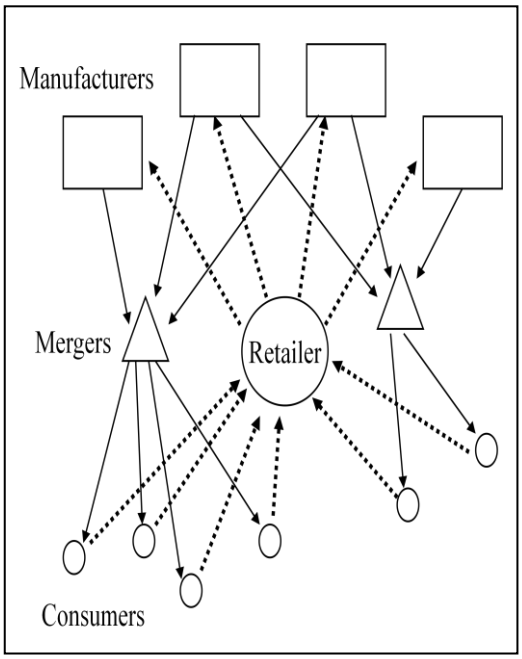

Fig 4. Manufacturer Storage with Direct Shipping and In-Transit Merge

Product Flow: ⟶
Information flow:----------

Example:
-Energypac Power Genretaion Limited. (EPGL) assemblies generator by sourcing engine and alternator from different manufacturers.
-Aftab Automobiles merge engine and various automobiles parts produced by different manufacturers to assembly Toyota & Hino Vehicles.

Characteristics of this distribution networks are stated below:

- Shipments from multiple manufactures are merged before making a single delivery to the consumer
- Shipments to Mergers are larger so economies of scale is achieved
- Mergers increase facility costs
- Response time may go up

Corresponding email:farjana.mitu08@gmail.com

4.3 . Manufacturer or Distributor Storage With Customer Pickup

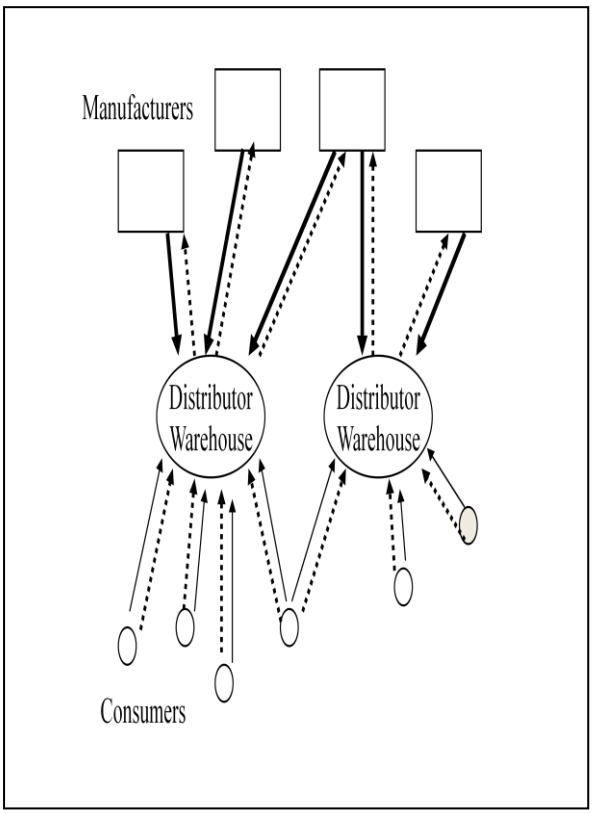

Fig 5. Manufacturer Storage with Direct Shipping

Product Flow: ⟶
Information flow:----------

Example:
-Bangla CAT (Sole distributor of Caterpillar Products in Bangladesh)
-Clarke Energy (Sole distributor of Jenbecher)
-Walton Product

Characteristics of this distribution networks :

- Customers come to pick up sites (warehouse, retailer) to get the products
  - If consumers are willing to pick up the products, let them do so. Otherwise, they would be charged for the delivery costs
- Order tracking is crucial. Consumers must be alerted when their order is ready for pick up. Once a consumer arrives at the pick up site, the products must be quickly located.
- Significant amount of information is required
- Increased handling cost

4.4 Distributor Storage with Last Mile Delivery (Home delivery)

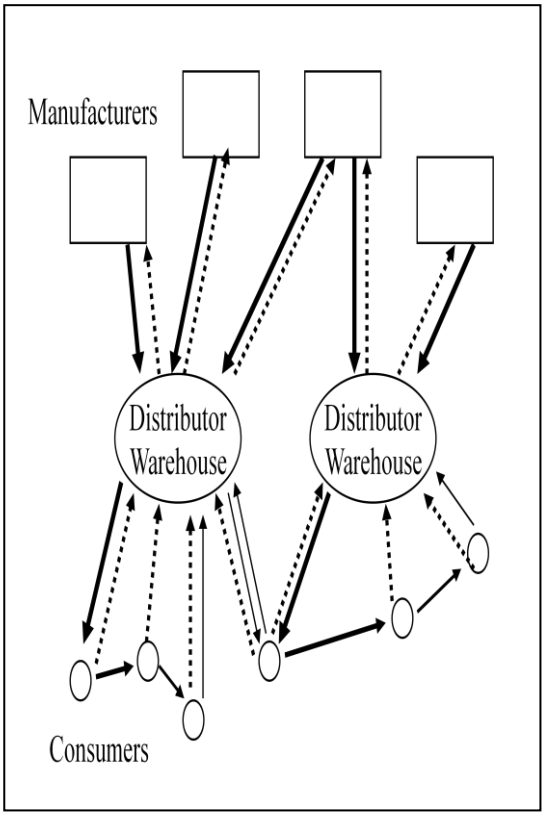

Fig 6. Distributor Storage with Last Mile Delivery

Product Flow:⟶
Information flow:----------

Example:
-Milk delivery
-Chaldal.com
-Niloy grocery home service.

Characteristics of this distribution networks :

- Warehouse delivers to customers instead of carrier
  - Warehouses are located closer to consumers
  - Transportation costs go up because warehouses are not as effective as package carriers in aggregating loads to have economies of scale
- Warehouse may need to own a trucking fleet so the physical infrastructure costs are higher.
  - Products must be flowing fast to justify the infrastructure
  - Processing cost are high

Corresponding email:farjana.mitu08@gmail.com

4.5 Distributor Storage with Carrier Delivery

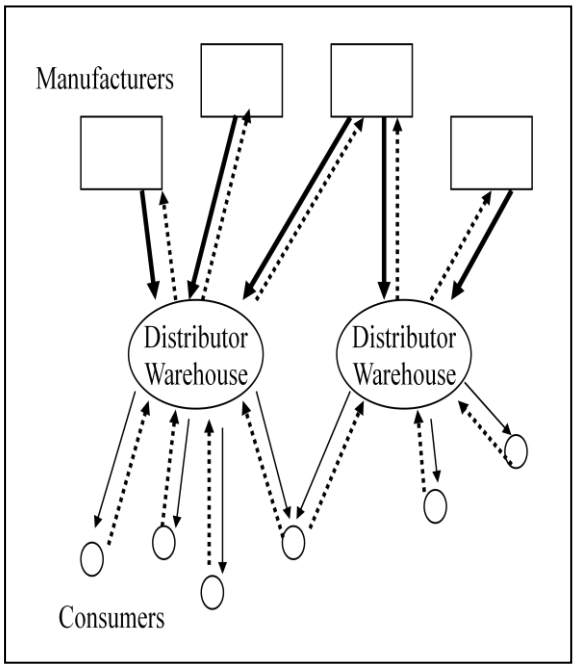

Fig 7. Manufacturer Storage with Direct Shipping

Product Flow: ⟶
Information flow:----------

Example:
-Sundorban Querier Service
-Continental Querier Service
-SA Poribahan, Querier Service

Characteristics of this distribution networks are stated below:

- Inventory is held at a warehouse which ships to customer by carriers
- With respect to direct shipping
  - Inventory aggregation is less
  - Higher inventory costs
  - Facility costs are higher
  - Less information to track
- Warehouses are physically closer to consumers which leads to
  - Faster response time
  - Lower transportation cost
- Not effective for slow moving items

4.6 Retail Storage with Customer Pickup

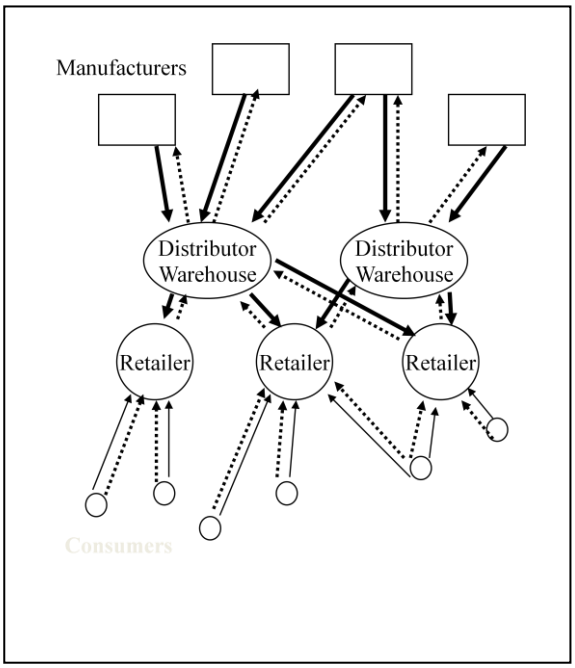

Fig 8. Manufacturer Storage with Direct Shipping

Product Flow:⟶
Information flow:----------

Example:
-Agora Retail Store (Rahimafrooz),
-Shopno Retail Store (ACI),
-Meena Bazar

Characteristics of this distribution networks are stated below:

- Customers pick up product from retailers
  - Low transportation cost
  - High facility cost
  - Relative easy returnability
  - Increased inventory cost
- No order tracking necessary
  - If the product is available at the retailer, the consumer buys. Otherwise goes to another retailer
- Effective for fast moving items

Corresponding email:farjana.mitu08@gmail.com

5.0 Comparing among distribution network in prospective of Bangladesh

Table 1. Comparison among distribution network

Criteria	Manufacturer storage with direct shipping	Manufacturer storage with direct shipping & In transit Merge	Distributor storage with carrier delivery	Distributor storage with last mile delivery	Manufacturer/Distributor storage with customer pick up	Retail storage with customer pickup
Response time	4	4	3	2	4	**1**
Product variety	**1**	**1**	2	3	**1**	4
Product availability	**1**	**1**	2	3	**1**	4
Customer experience	4	3	2	**1**	5	1-5
Order visibility	5	4	3	2	6	**1**
Return ability	5	5	4	3	2	**1**
Inventory	**1**	**1**	2	3	**1**	4
Transportation	4	3	2	5	**1**	**1**
Facility & Handling	**1**	2	3	4	5	6
Information	4	4	3	2	5	**1**

1=Strongest Performance,6=Weakest Performance

6.0 Share of various supply chain distribution network of Bangladesh

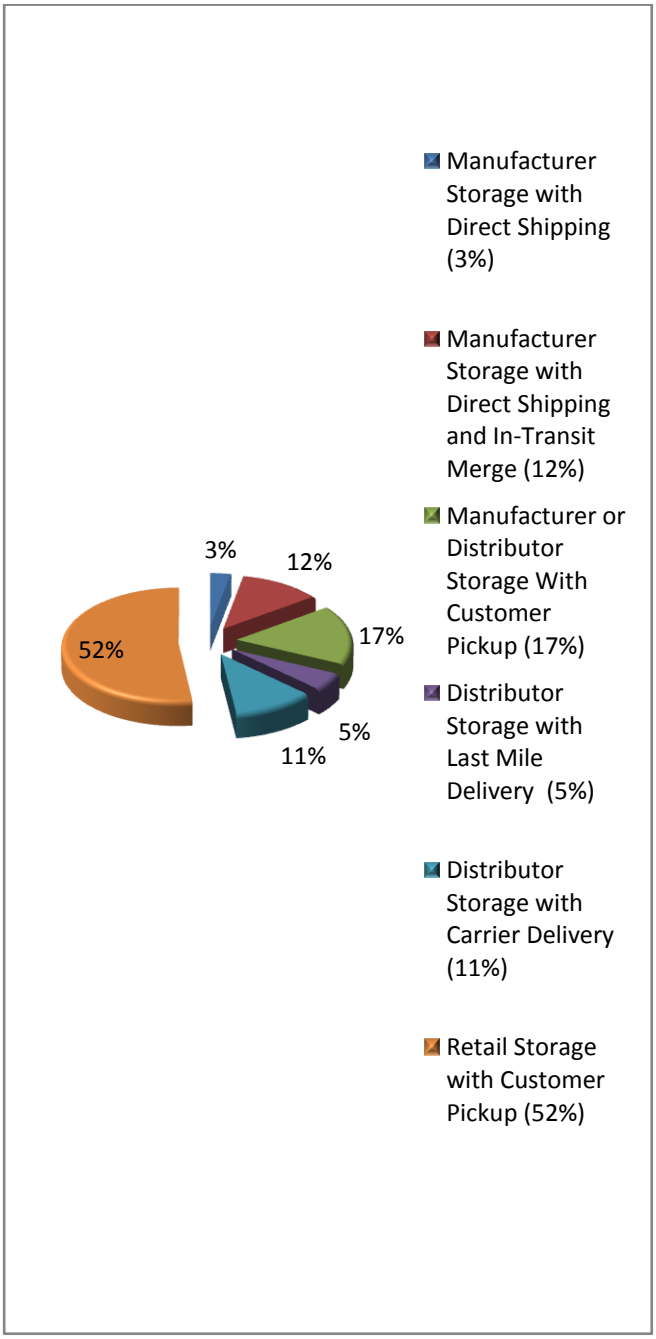

Fig 9. Contribution of various distribution network in Bangladeshi market (% wise) **.**

According to recent survey of supply chain network among various district of Bangladesh below calculative percentage can be obtained.

Corresponding email:farjana.mitu08@gmail.com

Table 2. Product characteristics & customer preference

Criteria	Manufacturer Storage with Direct Shipping	Manufacturer Storage with Direct Shipping and In-Transit Merge	Manufacturer or Distributor Storage With Customer Pickup	Distributor Storage with Last Mile Delivery	Distributor Storage with Carrier Delivery	Retail Storage with Customer Pickup
High Demand Product	-2	-1	-1	+1	0	+2
Medium Demand Product	-1	0	0	0	+1	+1
Low Demand Product	+1	0	+1	-1	+1	-1
Very Low Demand	+2	+1	+1	-2	0	-2
Many Product Sources	-1	-1	0	+1	+2	+1
High Product Value	+2	+1	+2	0	+1	-1
Quick Desired Response	-2	-2	-2	+1	-1	+2
High Product Variety	+2	0	+2	0	+1	-1
Low Customer Effort	+1	+2	-1	+2	+2	-2

+2: Very suitable;
+1: Somewhat suitable;
0: Neutral;
-1: Somewhat unsuitable;
-2: Very unsuitable

7.0 Conclusion

The purpose of this study is to identify the factors that influence supply chain distribution network and analyzing and comparing various distribution method in comparing to Bangladeshi perspective. Since many of those factors are under the control of the seller, identifying them may help sellers improve the outcome of their sales. However, in recent days in Bangladeshi business market, one supply chain network is converting into another supply chain network due to ease of end user. For an example, due to invent of more online shops recently the network of distributor customer pickup is now converting into distributor storage with last mile delivery. Therefore, it may assume from the study that customer will certainly involve themselves that network is much more convenient for them .

References

[1]. Chopra, S., & Meindl, P. (2001). Supply chain management:Strategy, planning, and operation. Upper Saddle River, NJ: Prentice-Hall.
[2] .Lummus, R., & Vokurka, R. (1999). Defining supply chain management: A historical perspective and practical guidelines. *Industrial Management & Data Systems, 99*, 11-17
[3]. Arntzen, B.C., Brown, G.G., Harrison, T.P., Trafton, L.L., 1995. Global supply chain management at digital equipment corporation. Interfaces 25, 69–93.
[4]. Keskinocak, P., & Tayur, S. (2001). Quantitative analysis for internet-enabled supply chains. Interfaces, 31(2), 70-89.
[5]. Williams, Jack F., 1981. Heuristic Techniques for Simultaneous Scheduling of Production and Distribution in Multi-Echelon Structures: Theory and Empirical Comparisons, Management Science, 27(3): 336-352.
[6] Towill, Denis R., 1996. Time Compression and Supply Chain Management - A Guided Tour, Supply Chain Management, 1(1): 15-27.

Corresponding email:farjana.mitu08@gmail.com

Multi Echelon Supply Chain Network Design Using Fuzzy TOPSIS & LINGO Software

[1*]Subrata Talapatra, [2]H.M Mohiuddin, [3]Md. Mominul Islam, [4]Farjana Nur

Department of Industrial Engineering and Management, Khulna University Of Engineering & Technology
Khulna-9203, Bangladesh

ABSTRACT

This paper aims at multi-objective optimization of single-product for three-echelon supply chain architecture consisting of suppliers, production plants, and customer zones (CZs). The key design decisions are: supplier selection, the number and location of plants in the system, the flow of raw materials from suppliers to plants, the products quantities to be shipped from plants to CZs so as to minimize the combined facility location and shipment costs subject to a requirement of meeting maximum customer demands. Here, three echelon supply chain is further divided into two sections, which is from suppliers to manufacturers (upstream) and from manufacturers to customer zones (downstream). In upstream, fuzzy TOPSIS is used to determine appropriate suppliers and in downstream, minimize the combined facility location by using LINGO software. This can be used as decision support system for facility locations, demand points allocation and monitoring material flow for three echelon supply chain network.

Keywords: *Multi Echelon, Fuzzy TOPSIS, Customer Zone, LINGO software*

1.0 Introduction

A supply chain (SC) is a network of organizations involved through upstream and downstream linkages in the different processes and activities that produce value in the form of products and services in the hand of the ultimate customer . Uncertainty in supply is caused by the variability brought about by how the supplier operates because of the faults or delays in the supplier‟s deliveries. Thats why supplier selection is the key factor for supply chain profitability. Also determining the best locations for new facilities is an important strategic challenge as environment and other social and economical factors can challenge its long run operational feasibility. Here our main objective is to establish a more efficient approach for three echelon supply chain ,select the best supplier, determine optimum facility location and establishing a more efficient approach for three echelon supply chain.

2.0 Literature Review

The early study of location theory begins in 1909 with Alfred Weber‟s work on positioning a single warehouse so as to minimize the total distance between it and several customers. After that considerable work in location theory is done by Hakimi , who work on locating switching centers in a communications network and police stations in a highway system. There are comprehensive studies performed before such as Dickson , Weber et al. , De Boer et al. and Sanayei et al. However, in this part, at first, the literature will be reviewed according to the selection criteria and then the methodologies used for supplier selection problem will be explained mainly based on a previous study performed by Ayhan . Many studies have been performed by using different criteria starting from the Dickson's 23 criteria. Cheraghi et al. updated Dickson's criteria with 13 more and stated that as the pace of market globalization quickens, the number of criteria to be considered will increase. As a brief of all criteria that have appeared in literature since 1966, quality, price, and delivery performances are suggested as the most important selection criteria . When the methodologies used for solving supplier selection problem are reviewed, it is observed that, various multi criteria decision making methods are implemented, which can be grouped into three broad categories . 1) *Value Measurement Models:* AHP and multi attribute utility theory (MAUT) are the best known method in this group. 2) *Goal, Aspiration, and Reference Models:* Goal programming and TOPSIS are the most important methods that belong to the group. 3) *Outranking Methods:* ELECTRE and PROMETHEE are two main families of methods in this group.
Among many systems to supplier selection TOPSIS, which is a widely accepted multi attribute decision making tool can be used . The concept of TOPSIS is that the most preferred alternative should not only

Corresponding Email:farjana.mitu08@gmail.com

have the shortest distance from the positive ideal solution, but should also be farthest from the negative ideal solution. Chen et al. extended the concept of TOPSIS to fuzzy environments by using fuzzy linguistic values. This fuzzy TOPSIS method fits human thinking under actual environment Fuzzy set theory has been studied extensively over last 40 years. The use of fuzzy set theory as a methodology for modeling and analyzing decision system is of particular interest to researchers in real world management due to the ability of fuzzy set theory for quantitative and qualitative model problems which involve vagueness and imprecision. Fuzzy logic starts with a concept of a fuzzy set. Fuzzy sets are an extension of classical (crisp) set theory and are used in fuzzy logic. In classical set theory the membership of elements in relation to a set is assessed in binary terms according to a crisp condition-an element either belongs to or does not belong to set. By contrast, fuzzy set theory permits the gradual assessment of the membership of elements in relation to a set; this is described with the aid of a membership function. A fuzzy set on a classical set X is defined as follows. If X is a collection of objects denoted generally by x, then a fuzzy set Ă in X is a set of ordered pairs. A fuzzy set on a classical set X is defined as follows: If X is a collection of objects denoted generically by x, then a fuzzy set Ă in X is a set of ordered pairs Ă= {(x, μa(x) x €X} (Zimmerman, Fuzzy set theory, and its application,1985). μa(x) is called membership function that quantifies the degree of membership of elements x to the fundamental set X. An element mapping to the value 0 means that the member is not included in the given set, 1 describes a fully included member. The range of the membership function is a subset of the nonnegative real numbers. The values strictly between 0 and 1 characterize the fuzzy members .

In this study, we used LINGO software to solve facility location; that is how much units will be produced at each manufacturing plant, which plants is necessary to open and which one is needed to be closed to meet the future demands.

3.0 Application results using fuzzy TOPSIS

A garment industry involved in producing shirts desires to select suitable suppliers for raw materials. A committee of five decision-makers, D1, D2, D3, D4 and D5 has been formed to select the most suitable supplier.
The computational procedure of the proposed method is summarized as follows:

Steps 1 & 2: The decision-makers use the linguistic weighting variables with triangular fuzzy numbers to assess the importance of the criteria and alternatives which is shown in Tables1 and Table2The importance weights of the criteria determined by these five decision makers are shown in Table3.
Step 3: The decision-makers use the linguistic rating variables to evaluate the ratings of alternatives with respect to each criterion. It is shown for criteria 1 in Table 4.
Step 4: Then the performance ratings of the 7 alternatives and importance weights of the criteria are used to form the normalized decision matrix(Table5).
Step 5: The weighted normalized decision matrix is constructed (table 6)
Step 6: Determination of the positive ideal solution and negative ideal solution as in Table7.
Step 7: Calculate the distance D^{*+} and D^{*-} of each reverse logistics provider from positive and negative ideal solution with respect to each criterion.
Step 8 & 9: Determine the closeness coefficient of each reverse logistics provider and rank the alternative (supplier) according to the descending order of closeness coefficient as shown in Table 8.
From Table 8**,** it is concluded that supplier1 is selected among the 7 alternatives.
Performance ratings are calculated by the following way:
For S1: (MP+MG+F+MG+F)/5= 5.4; similarly others are calculated.

Step1 & 2: (Table1, Table 2, Table 3)

Table 1. Linguistic variables for rating of each alternative

Linguistic data (Rating of each alternative)	Triangular Fuzzy number
Very poor	(0,0,1)
Poor	(0,1,3)
Medium poor	(1,3,5)
Fair	(3,5,7)
Medium good	(5,7,9)
Good	(7,9,10)
Very good	(9,10,10)

Corresponding Email:farjana.mitu08@gmail.com

Table 2. Linguistic variables for importance of each criterion

Linguistic data (For each criteria)	Triangular fuzzy number
Very low(VL)	(0,0.2,0.3)
Low(L)	(0.2,0.4,0.5)
Medium(M)	(0.4,0.6,0.8)
High(H)	(0.6,0.8,1.0)
Very high(VH)	(0.8,0.9,1.0)

Table 3. Importance weights of criteria from five decision-makers

Criteria	D1	D2	D3	D4	D5	Weight
Quality (C1)	VH	H	M	H	H	0.78
Delivery (C2)	H	H	VH	H	H	0.82
Reverse Logistic Cost (C3)	VH	H	VH	VH	H	0.86
Rejection rate inability to meet future (C4)	VH	L	H	M	M	0.65
Demand (C5)	L	M	VL	L	M	0.43

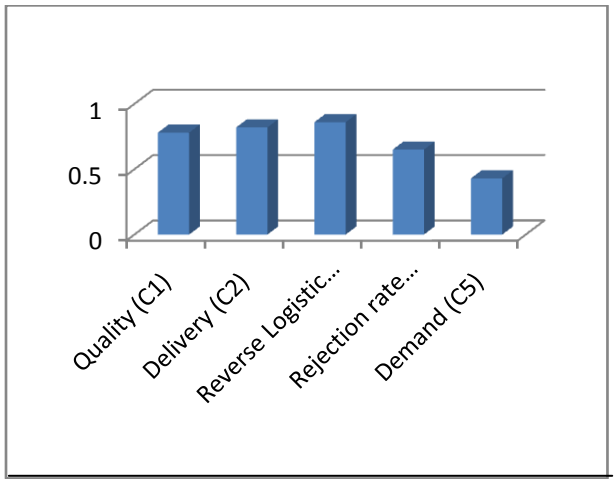

Fig1. Graphical representation of weights of criteria from five decision-makers

Step 03:

Table 4. Decision make's rating of alternatives for criteria 1

		Decision Makers					Rating
Criteria	Alternative	D1	D2	D3	D4	D5	
C1	S1	MP	MG	F	MG	F	5.4
	S2	VP	VP	P	VP	VP	0.993
	S3	MP	P	MP	MP	F	3.03
	S4	VG	MG	MG	VG	G	9.03
	S5	F	MG	G	F	F	6.16
	S6	P	P	VP	MP	MP	1.7
	S7	VG	MG	MG	VG	G	8.49

Step 04:

Table 5. Normalize matrix for S1

r_{ij}= $5.4/\sqrt{(5.4^2+.933^2+3.03^2+9.03^2+6.16^2+1.7^2+8.49^2)}$ =.3532

Normalized Decision Matrix

Alternatives	C1	C2	C3	C4	C5
S1	0.3532	0.5245	0.5204	0.5014	0.4614
S2	0.061	0.0615	0.4174	0.4368	0.4417
S3	0.1982	0.5245	0.5441	0.1132	0.2451
S4	0.5907	0.3042	0.0872	0.6033	0.4614
S5	0.4209	0.2778	0.3019	0.4128	0.4524
S6	0.1112	0.2024	0.3806	0.0506	0.0708
S7	0.5554	0.4848	0.1227	0.088	0.0068

Step 05:

Table 6. Weighted normalized matrix

For supplier 1: W_{ij} =.3532*.78 =.2755

Alternatives	C1	C2	C3	C4	C5
S1	0.2755	0.43	0.4475	0.3293	0.1999
S2	0.0475	0.0504	0.3589	0.2868	0.1913
S3	0.1545	0.43	0.4679	0.0743	0.1062
S4	0.4607	0.2494	0.0749	0.3961	0.1999
S5	0.3142	0.2277	0.2596	0.271	0.196
S6	0.0867	0.1659	0.3273	0.0332	0.0306
S7	0.4332	0.3975	0.1055	0.0577	0.0029

Corresponding Email:farjana.mitu08@gmail.com

Step 06:

Table 7. Positive and negative ideal solution

Ideal Solution	C1	C2	C3	C4	C5
V^{*+}	0.4607	0.43009	0.4679	0.3961	0.1999
V^{*-}	0.0475	0.0504	0.0749	0.0332	0.0029

Step 07:

Table 8: Distances of alternatives to positive ideal solutions, the related closeness coefficient & ranking

Alternative	Distance (D*+)	Distance (D*-)	Closeness efficient	Rank
S1	0.1979	0.6792	0.774	1
S2	0.5820	0.4248	0.4219	6
S3	0.4539	0.5677	0.5556	4
S4	0.4325	0.6171	0.5879	2
S5	0.3485	0.4801	0.5794	3
S6	0.6243	0.2816	0.3108	7
S7	0.5352	0.52036	0.4929	5

4.0 Application of LINGO software for optimum plant location

Problem description

Demands at each customer zone, monthly plant capacities, fixed costs per month of running plants, production and distribution costs per thousand units are given in table

Table 09:Input data for LINGO (scenario1)

Plant	Cost/unit shipment				Capacity of each point	Fixed cost of plant
	CZ1	CZ2	CZ3	CZ4		
P1	6	2	6	7	39	91
P2	4	9	5	3	35	70
P3	8	8	1	5	31	24
Demand at each zone	15	17	22	12		

Table10. Output data of Lingo
(Optimum location and distribution of products for scenario1)

Plant	The optional location and distribution of goods from plant distribution centres				Optional location of plants
P1	15	17	0	3	1
P2	0	0	0	0	0
P3	0	0	22	12	1
Total quality supplied	15	17	22	12	
Total demand	15	17	22	12	

Corresponding Email:farjana.mitu08@gmail.com

From this table, Objective function
$Min\Sigma^{n}_{i=1}f_i yi + \Sigma^{m}_{j=1}\Sigma^{n}_{i=1} C_{ij}X_{ij}$ =
91*1+24*1+70*0+6*15+2*17+3*7+1*22+5*12=342
Total demand, 15+17+22+12=66
Total capacity, 39+35+24 = 105; that is total demand can't exceed plant"s capacity.

Table 11. Input data for LINGO (Scenario 2)

Plant	Cost unit shipment				Capacity of each point	Fixed cost of plant
	CZ1	CZ2	CZ3	CZ4		
P1	5	4	2	3	35	80
P2	4	6	7	2	32	72
P3	6	6	2	4	34	28
Demand at each zone	18	23	14	16		

Table 12. Output data of LINGO
(Optimum location and distribution of products for scenario 2)

Plant	The optional location and distribution of goods from plant distribution centres				Optional location of plants
P1	2	23	0	0	1
P2	16	0	0	16	1
P3	0	0	14	0	1
Total quality supplied	18	23	14	16	

Input Data through LINGO Software

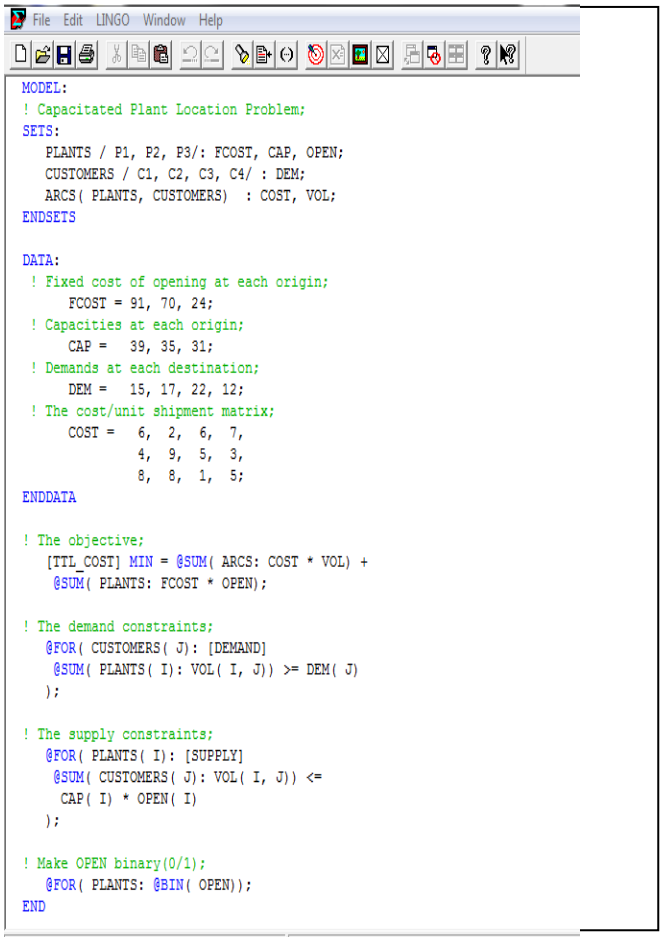

4.1 Application & Key benefit of LINGO for optimum plant location

LINGO will help to cut ones development time. It lets us formulate linear, nonlinear, integer problems quickly in a highly readable form. LINGO"s modeling language allows us to express models in a straight forward intuitive manner using summations and subscripted variables. Models are easier to build, easier to understand, and therefore easier to maintain.

**LINGO takes the time and hassle out of managing our data. It allows us to build models that pull information directly from data bases and spreadsheets.

**LINGO is available with comprehensive set of fast, built in solvers for linear, nonlinear, integer, stochastic problems.

Corresponding Email:farjana.mitu08@gmail.com

**We can build and solve models within LINGO, or we can call LINGO directly from a written application.

**LINGO provides all of the tools we need to get up and running quickly. We get the LINGO user manual, which fully describes the command and features of the program.

4.2 Output of LINGO

Table 12 shows the optimum location of plants and optimum distribution of goods to different CZs for scenario 1 solved using proposed LINGO. From the results, it is evident that it is optimal for the company to close the plants P2 while keeping the plants P1and P3 open for scenario 1. With the demand allocation shown the company incurs a total cost of 406.

5.0 Discussion

In this study, fuzzy TOPSIS is used to select appropriate supplier and LINGO is used to determine optimal facility location. Fuzzy TOPSIS is used for supplier selection because: Fuzzy logic is conceptually easy to understand. The mathematical concepts behind fuzzy TOPSIS reasoning are very simple. With any given system, it is easy to layer on more functionally without starting again from scratch. Fuzzy TOPSIS is also tolerant of imprecise data. Fuzzy TOPSIS can model nonlinear functions of arbitrary complexity. One can create a fuzzy system to match any set of input-output data. This process is made particularly easy by adaptive techniques like Adaptive Neuro-fuzzy interface systems (ANFIS) which are available in Fuzzy TOPSIS Toolbox software. Fuzzy logic can also be blended with conventional control techniques. Fuzzy TOPSIS is based on natural language. The basis for fuzzy logic is the basis for human communication. The observation underpins many of the other statements about fuzzy logic. As fuzzy logic is built on the structures of qualitative description used in everyday language, it is easy to use. The last statement is perhaps the most important one and deserves more discussion. Natural language, which is used by ordinary people on a daily basis, has been shaped by thousands of years of human history to be convenient and efficient.

On other hand, LINGO is used for optimum facility location because It is flexible, easily understood. It gives the optimum number of units to be produced at each plant or manufacturer to satisfy customer demand.

LINGO is a comprehensive tool designed to make building and solving linear, nonlinear (convex & non convex/global), quadratic, quadratically constrained, second order cone, stochastic, and integer optimization models faster, easier and more efficient. LINGO provides a completely integrated package that includes a powerful language for expressing optimization models.

It is always a tough decision for the management of a company or decision makers to determine what quantities will be produced at each plant, which plants are needed to be open and which are needed to be closed to meet final demand. Such problems can be easily managed by LINGO.

6.0 Conclusion

In this paper, an analytical model is formulated for the location and allocation of facilities from plant to customer zone supply chain network for the optimal facility location and capacity allocation decisions. Fixed location and variable material cost, production, inventory and transportation costs are considered while making strategic decisions. Two objective functions of minimizing total SC cost and maximizing fill rate are considered. LINGO is used as optimizer.

References

[1]. Krajewsld, L.J., and Ritzman, L.P., (1996) *Operations Management Strategy and Analysis*. Addison-Wesley Publishing Co., London, UK.
[2]. Ghodsypour, S.H., and O"Brien, C., (1998) "A Decision Support System for Supplier Selection Using an Integrated Analytic Hierarchy Process and Linear Programming", *International Journal of Production Economics*, Vol. 56-57(20), 199-212.
[3]. Önüt, S., Kara, S.S., and Işık, E, (2009) "Long Term Supplier Selection Using a Combined Fuzzy MCDM Approach: A Case Study for a Telecommunication Company", *Expert Systems with Applications* Vol. 36(2), 3887-3895.
[4]. Liao, C.N., and Kao, H.P., (2011) "An Integrated Fuzzy TOPSIS and MCGP Approach to Supplier Selection in Supply Chain Management", *Expert Systems with Application* Vol.38(9), 10803-10811.
[5]. Kilic, H.S., (2013) "An integrated approach for supplier selection in multi item/multi supplier "
[6].Azapagic, A., & Clift, R. (1999). The application of life cycle assessment to process".

Corresponding Email:farjana.mitu08@gmail.com

ICMIEE-PI-140412

Design and Construction of a portable air cooler

Gopesh Dey , Suvro Deb Sikder , Mohammad Ariful Islam
Department of Mechanical Engineering, Khulna University of Engineering & Technology, Khulna-9203, BANGLADESH

ABSTRACT
Human being wants to live in comfortable condition. Temperature is one of the most important factors for human comfort. When temperature of air is above the comfort limit then cooling of air is necessary. Air cooler is required to reduce the temperature of air for comfort. In this project a portable air cooler with evaporative cooling is designed and constructed. It consists of a fan, a water-wetted pad, a pump to recirculate the water and revolving wheels to move from one place to another. Room air is drawn through the water-wetted pad and is blown into the room. The cooling system slightly increases the humidity of the entering air. This type of system is very useful where the environment where temperature is high but the relative humidity is relatively low. Performance of the constructed air cooler is tested. Results showed that it can be reduced the temperature about 4℃ to 6℃.

Keywords: Evaporative air cooling, Temperature, Humidity, Human Comfort

1. Introduction

Human satisfaction is called human comfort. Human comfort is an integral part of human life. Human comfort depends on four factors. These are

- Temperature of air
- Humidity of air
- Purity of air
- Motion of air

Among the four factors, temperature and humidity of air are very essential for human comfort. We know that among six seasons, the summer portion is higher than others. So comfort cooling & dehumidification is necessary. But cooling & dehumidification is difficult to control simultaneously [1].

Portable air cooler is a mobile device which is used to cool air. There are several methods of air cooling.

Evaporative cooling is one of the most ancient and energy efficient methods because the energy consumption of energy is very low. Direct evaporative cooling adds moisture to the air. It is suitable for dry and acid climates .In wet climates; the results are not satisfactory, because of unacceptable indoor humidity. Indirect evaporative cooling, without added humidity, is less effective, costs more system [1].

Evaporative coolers are cooling devices that use the evaporation of water into the air to cool the air temperature. They are sometimes called air coolers, desert coolers or swamp coolers. Evaporative coolers use a quarter of the electricity of air conditioners and are relatively inexpensive. In addition, they do not use ozone-harming chlorofluorocarbons (CFCs) and hydro chlorofluorocarbons (HCFCs).

This study also contains:

- ❖ Design a portable air cooler.
- ❖ Construction of a portable air cooler.

2. Thermodynamics of Evaporative Cooling

When a large quantity of water is constantly circulated through a spray chamber that is insulated from surroundings, the air-water vapor mixture is passed through the spray chamber and in doing so; it evaporates some of the circulating water. The air may leave at a certain humidity ratio or in a saturated state (Fig-2.1). The increase in specific humidity is equal to the quantity of water evaporated per unit mass of dry air. As the spray chamber is insulated from surroundings, no heat transfer takes place between the spray chamber and the surroundings. Therefore, the energy required for evaporation is supplied by the air, and consequently, the DBT is lowered. After the process has been in operation for a sufficient length of time, the circulating water approaches the WBT of air [1].

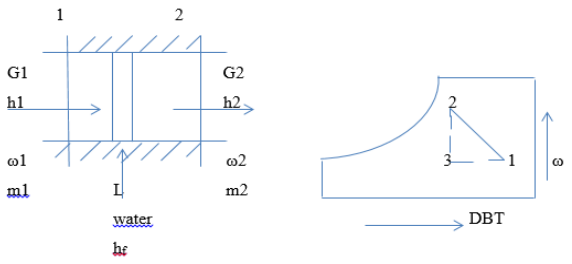

Fig 2.1 Adiabatic evaporative cooling.

* Corresponding author. Tel.: +88-01747325012
E-mail address: gopesh2k9.86@gmail.com

The energy balance and other relation may be expressed mathematically as follows:

G1 = G2 = G ……..(i)

G1ω1+L= G2ω2 ……..(ii)

L= G (ω2-ω1) ……(iii)

G1h1+L h_f= G2 h2 ……(iv)

G (h1-h2) + G (ω2-ω1) h_f= 0 ……(v)

h1 – ω1 h_f = h2 – ω2 h_f ……(vi)

The process can be shown on psychometric chart by state 1 and 2 (Fig-). From this chart

Sensible heat transfer = G (h1 – h3)

Latent heat transfer = G (h2 – h3)

3. Design of the portable air cooler:

The schematic diagram of the evaporative cooling system is shown in figure 3.1. The major components of the evaporative cooling system are:

a)Water-wetted pad

b)Supply container

c)Receiver container

d)Frame

e)An Exhaust Fan

f)Water Pump

i)Connections Pipes

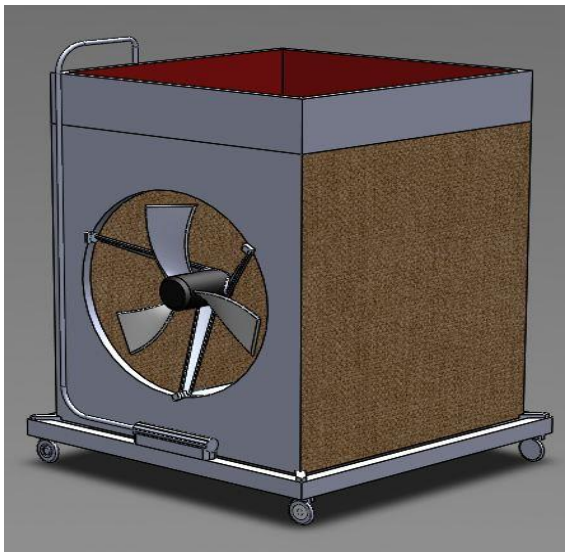

Fig- 3.1: Schematic diagram of a portable air cooler.

3.1 Selection of fan

The fan is a critical component of the portable air cooler. The cooling performance depends on fan size and speed. On the basis of this considerations the following specifications of fan was selected.

Diameter, D =10 inch= .25m

Power= 43 watt

Diameter of fan with casing, $D' = 0.3048\ m$

Velocity of air supplied by fan, V = 2.07 m/s (measured by anemometer)

Area through which air is supplied, $A = D'^2$

$= 0.3048 \times 0.3048$

$= 0.09290\ \ m^2$

3.2 Design of supply container

Considering outside condition

Let,

DBT = 33 ℃

WBT = 28 ℃

Relative humidity RH = 69%

Specific humidity at 33 degree Celsius, ω_0 = 0.0122 kg/kg dry air

Density of air at $33℃, \rho = 1.156\ \ kg/m^3$

Specific heat of air at $33℃,\ \ c_p = 1.0061\ \ kJ/kg.k$

Mass flow rate of air m_a = ρAV ……(vii)

$= 1.156 \times 0.09290 \times 2.07$

$= 0.2223\ kg/s$

Inside condition

Let DBT = 27℃

Let total amount of water reserved $= 6\ litre$

$= 6\ kg$

And backup time $= 60\ min$

Total amount of water reserved

$= (2 \times$ amount of water evaporated $) \times$ back up time

Or, amount of water evaporated $G = 6 \div 2 \div 3600$

$= 0.000833\ kg/sec$

Amount of moisture transferred $G = m_a\ (\omega_i - \omega_o)$ ……..(viii)

$or,\ 0.000833 = 0.2223. \times 3600(\omega_i - 0.0122)$

$or, \omega_i = 0.015948$ kg/kg dry air

Amount of specific humidity increased

$= 0.015948 - 0.0122$

$= 0.003748\ kg/kg\ dry\ air$

Latent heat transferred $, Q_L = m_a\ h_{fg}(\omega_i - \omega_o)$ ……(ix)

$0.2223 \times 2440 \times (0.015948 - 0.0122)$

$= 2.033$ kJ/sec

Sensible heat transferred $Q_S = m_a\ c_p(t_o - t_i)$ ……(x)

$= 1.3419$ kJ/sec

Length $= 40.64\ cm$

Width $= 40.64\ cm$

Height $= 7.62\ cm$

Total volume= $12585.26515\ cm^3$
So that it could contain 6 liter water
Water Height= $3.63\ cm$
Time required emptying the tank,

$$T = \frac{2A\sqrt{H}}{C_d\, a\sqrt{2g}}$$

……(xii)
Where,
C_d = Discharge coefficient = 0.62
T=Back up time
H = Height of the water in the tank
a = area of the orifice

$$3600 = \frac{2 \times (40.64 \times 40.64) \times \sqrt{3.63}}{0.62 \times a \times \sqrt{2 \times 981}}$$

Or, $a = 0.063657\ cm^2$

Let diameter of each hole $d = 1\ mm$
Number of hole $= n$
So,

$$n \times \frac{\pi d^2}{4} = a$$

…….(xiii)
Or, $n = 9$

3.3 Design of frame

The frame is important component of a portable cooling system. It carries supply container on top, fan in one side, and pad in three sides. So the length and width of the frame would be equal to the supply container. And the height of the frame should be such that fan can be installed at the centroid of those side of the frame.

Considering above condition the following size of the frame was designed.
Length $= 40.64\ cm$
Width $= 40.64\ cm$
Height $= 45.72cm$

3.4 Design of water reserve container

The size of the water reserve container would be such that it could contain the dropped water at the bottom of the box.
Rate of water evaporated, $G = 8.33 \times 10^{-4}$ kg/sec
Amount of water evaporated $= 8.33 \times 10^{-4} \times 3600$
$= 3\ kg$
Rest amount of water $= 6 - 3 = 3\ kg$
Rest amount of water
= amount of water absorbed
+ amount of water dropped

Let,
water dropped $= \frac{1}{2} \times rest\ amount\ of\ water$
……..(xiv)
$= 1.5\ kg$
Considering above condition the following size of the reserve container was selected.
Length $= 45.72\ cm$
Width $= 45.72\ cm$
Height $= 1.27\ cm$

3.5 Design of water wetted pad

The function of water wetted pad is to absorb as much as water for a long period. And it must have the ability to pass air easily through the pad .It should be insured that no air will flow through the pad without wetted. For considering above reason the following size of the water wetted pad surrounding three sides of the frame was selected
Length $= 3.81\ cm$
Width $= 35.56\ cm$
Height= 30.48 cm

3.6 Selection of water pump

The following specification of water pump was selected
Voltage = 12 volt
Current = 6 amp
Power = 72 watt

3.7 Cost analysis of the project:

ITEMS	COST(TK)
1) **Exhaust Fan**	950/-
2) **AC Pump**	750/-
3) **Metal sheet(5 kg)**	750/-
4) **Pipe**	50/-
5) **Power Supply**	200/-
6) **Wheels(4 pieces)**	200/-
7) **Wetted Pad**	400/-
8) **Manufacturing Cost**	1000/-
Total	4300/-

4. Result and Discussion

4.1.1 Performance Test in open room:-

The cooling system was placed in a room of size 5.4m$\times$ $1.7m \times 3.5m$ at the door. The wet bulb and dry bulb temperatures were recorded at inlet and outlet of the cooling system by sling psychometer with different temperature water.

Table -4.1: Data Sheet For open room

Date	Duration	Water Temperature (℃)	Inlet Condition		outlet Condition	
			DBT (℃)	WBT (℃)	DBT (℃)	WBT (℃)
04-06-14	10.00-11.00 AM	27	35	31	31	30.5
	11.00 AM-12.00 PM	28	34	30	31.5	29.5
05-06-14	10.00-11.00 AM	26	37	31	33.5	31.5
	11.00 AM-12.00 PM	27	36	31	33	31.5
08-06-14	10.00-11.00 AM	26	38	30	34	29.5
	11.00 AM-12.00 PM	28	39	30.5	36.5	30
09-06-14	10.00-11.00 AM	18	34	29	28	27
	11.00 AM-12.00 PM	17	33	28	28	27
10-06-14	10.00-11.00 AM	16	35	30	29	27
	11.00 AM-12.00 PM	17	34.5	30	29	27

Table 4.2 Result Sheet For open room

Date	Duration	Relative Humidity, RH (%)		Latent Heat, Q_L (kj/kg)	Sensible Heat, Q_S (kj/kg)	Sensible Heat Factor, SHF	Mass Of Water Evaporated, G (kg/s)
		Inlet	Outlet				
04-06-14	10.00 AM - 11.00 AM	79.8	96.2	0.4339	0.89336	0.67	0.000178
	11.0b0 AM - 12.00 PM	83	92.6	0.0542	0.55585	0.91	0.000022
05-06-14	10.00 AM - 11.00 AM	64.9	86.6	1.4645	0.78119	0.35	0.0006
	11.00 AM-12.00 PM	69.7	89.8	1.3560	0.67002	0.33	0.000556
08-06-14	10.00 - 11.00 AM	55.6	71.6	0.4339	0.89336	0.67	0.000178
	11.00 AM-12.00 PM	54	62.1	0.0542	0.55585	0.91	0.000022
09-06-14	10.00 - 11.00 AM	68.8	92.5	0.5966	1.34005	0.69	0.000245
	11.00 AM-12.00 PM	68.2	92.5	0.2169	1.11771	0.84	0.000089
10-06-14	10.00 - 11.00 AM	69.3	85.5	1.6814	1.34005	0.44	0.000689
	11.00 AM-12.00 PM	71.8	85.5	1.7899	1.22888	0.41	0.000734

4.1.2 Performance Test in closed room:-

The cooling system was placed in a room of size at the door. The wet bulb and dry bulb temperatures were recorded at inlet and outlet of the cooling system by using psychometer with normal and cold water.

	AM					

Table -4.3: Data Sheet for closed room with normal tap water

Date	Duration	Water Temperature (℃)	Inlet Condition		outlet Condition	
			DBT (℃)	WBT (℃)	DBT (℃)	WBT (℃)
12-06-14	10.00 - 10.20 AM	27	36	31	33	30.5
	10.20 AM - 10.30 AM		35	30.5	32.8	30
	10.30 - 10.40 AM		34.5	30	32.5	29.5
	10.40 AM- 10.50 AM		33	29.8	32	29.2
	10.50 - 11.00 AM		32	29.5	31.5	29

Table -4.4: Data Sheet for closed room with cold water

Date	Duration	Water Temperature (℃)	Inlet Condition		outlet Condition	
			DBT (℃)	WBT (℃)	DBT (℃)	WBT (℃)
15-06-14	10.00 - 10.20 AM	17	35	31	30	29
	10.20 AM - 10.30 AM		32	29.5	30.5	28.5
	10.30 - 10.40 AM		31	29	30	28
	10.40 AM- 10.50 AM		30	29.3	29.5	27.5
	10.50 - 11.00		30.5	29	29	27

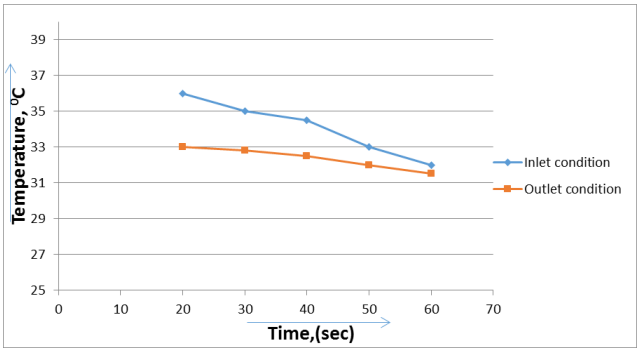

Figure-4.1: Time vs. Temperature diagram (27 ℃ Normal Tap water).

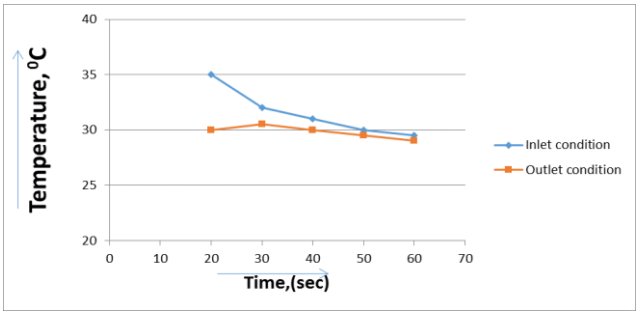

Figure-4.2: Time Vs. Temperature diagram (17 ℃ Cold water).

4.2 Discussion:

The cooling performance of portable cooling system mainly depends on the temperature and relative humidity of air and the contact surface between air and water. From Table 4.1 it was showed reduction of temperature depend on water temperature. When the temperature of water raised with ambient temperature reduction of temperature decreased. Besides with relative humidity increased with time. The constructed portable cooling system reduced the temperature of the room by an average of 4℃ with normal tap water and 6℃ with cold water from the atmosphere. This is a poor value .From fig 5.1 it was founded that after 20 minutes of installation of cooling system temperature reduced from 36 ℃ to 33℃ .And after 1 hour of installation of cooling system temperature reduction found 4.5 ℃. The difference between inlet and outlet temperature was also reduced with time because same air circulated through the system. At last difference was found about 1.5 In case of cold water temperature reduced from 35 ℃ to 30℃. And last temperature reduction found about 5 ℃ at outlet condition and difference between inlet and

outlet temperature was found about 0.5℃. The main difficulties of the constructed portable air cooler was the long distance between the fan and water wetted pad . For this reason the fan was unable to circulate the air at desired speed. Another reason may be the jute water wetted pad that would be rotten in course of time. The system was unable to provide enough cooling effect because the relative humidity of the air was already at a higher value.

6.1 Conclusion:-

The portable air cooler was designed to port from one place to another place. Some values such as inlet dry bulb, wet bulb temperature, outlet dry bulb temperature, amount of reserved water and back up time were assumed primarily to complete the design. The system made portable by attaching four revolving wheels with the corner of the frame. A water pump was installed to recirculate the water and reduce human effort. Its performance was tested in both open and closed room with normal and cold water. It followed the evaporative cooling system. It reduced the temperature about 4℃ to 6℃ for using normal tap water and cold water respectively but increased humidity 16% to 20% for normal and cold water respectively. It showed better performance in closed room but relative humidity slightly increased than open room because the room was being saturated.

The following recommendation can be made to increase the performance of portable air cooler:

1. The pump was controlled manually. It may be made automatic using water sensor. Two water sensors can be set at the highest and lowest water level in supply tank. When the water level falls below the bottom sensor a signal will turn on the motor. And when the water level rises above the upper sensor the motor will be automatically turned off.
2. As the water was evaporating continuously, few times later the bottom reservoir will be blanked. So a system of supplying make up water may be attached with bottom reservoir. And it can be controlled automatically.
3. The main disadvantage of this system is increasing humidity. Humidity can be reduced by using humidity absorbing materials such as silica jell, glycol, etc.

4. The pad was made by jute fiber which will be rotten in course of time and has low permissibility. So synthetic pad can be used to recover this difficulty.

REFERENCES

[1] Arif Hosain MD. And Mahmud Hasan MD. A thesis report on “Design, construction and testing of an evaporative cooling system” Held at KUET, Khulna on FEBRUARY, 2006.

[2] C P Arora; Refrigeration and Air Conditioning, Second Edition, Tata McGraw- Hill Publishing Company Limited; New Delhi.

[3] http://GlobalSpec.com/Evaporative Coolers Information

[4] http:// www.wikipedia.org/ Evaporative cooler

ICMIEE-PI-140413

Simulation investigation on flow characteristics for the flow over a propeller used in VTOL RC aircrafts

S. M. Mahbobur Rahman [1,*], *Mohammad Mashud*[1]
[1] Department of Mechanical Engineering,
Khulna University of Engineering & Technology, Khulna-9203, BANGLADESH

ABSTRACT
This paper illustrates the scenario of fluid flow characteristics for the flow over a propeller used in vertical takeoff and landing (VTOL) radio controlled (RC) aircrafts. Simulation investigation has been conducted through SolidWorks flow simulation using a propeller model. Whenever air flows over the propeller, due to the rotational motion a thrust force is generated which will lift the aircraft in the air. This thrust force is important in selecting the motor to be used in the aircraft model. Thrust force along with pressure, velocity, temperature distribution and velocity flow trajectory were determined numerically. These parameters imply the feasibility of using the propeller, consequently selecting the proper power source in order to get a rigid and stable flight of the aircraft.

Keywords: SolidWorks flow simulation, flow characteristics, VTOL RC aircrafts, thrust force, feasibility

1. Introduction

Propellers are the main source of propulsion in general aviation and radio controlled (RC) airplane market. As RC airplanes grow in size, the propulsion systems for these vehicles now become viable sources of propulsion for small drone aircraft which do not have the range and endurance parameters of the predator or Global Hawk systems. The ability to evaluate the performance of these propulsion systems via simulation, as well as their effects on the rest of the flight vehicle, enables the designer to choose engine/blade combinations which are more optimal for the role of the particular vehicle. Accurate simulation of the complete vehicle aerodynamics, including the contributions from propeller flow-field, can lead to robust autopilot design. With these benefits of simulation in mind, now consider the advances and industrial use of CFD over the last decade or so [1]. The flow over a propeller is one of the most challenging problems in the field of computational fluid dynamics (CFD). Due to the airflow over the propeller, thrust force and torque will generate to lift the unmanned aircraft in the air. Various numerical simulation approaches (boundary elements, panel methods, etc.) for studying propeller geometries have been used for decades, but only recently, due to the rapid advances in computer power and in the parallelization capabilities, different
CFD methods are increasingly applied to simulate the full three-dimensional viscous and turbulent flow for various propeller geometries [2-5]. In an unmanned VTOL RC aircraft the propeller generates the sufficient thrust to lift the aircraft in the air, which is the prime objective of propeller design and analysis. Through numerical simulation certain thrust forces were determined for different rotational speeds to test the feasibility either the aircraft will fly efficiently or not. The numerical simulation was done in SolidWorks flow simulation and the propeller data were taken from UIUC propeller database site [6].

2. Methodology

The validation of the simulation boundary conditions were initially followed the ASTM standard with Numerical simulation. Flow Simulation analysis was conducted using SolidWorks.

2.1 Propeller Performance and Design Fundamentals

A propeller can be considered as a number of equally spaced advancing rotating blades, kept in rotation by the torque of the engine. The combined lift and drag result in propeller thrust and torque, respectively the axial force and moment. The direct result of the rotation is an increased pressure directly behind the propeller and a decreased in front of it.

2.1.1 Propeller Performance

A propeller blade (Fig.1) is simply a rotating airfoil, similar to an airplane wing, which produces lift and drag. It has both induced upwash and downwash due to the complex helical trailing vortices that it generates. The most two important parameters of a propeller for design and analysis projects such as this are the thrust and torque it produces [7].

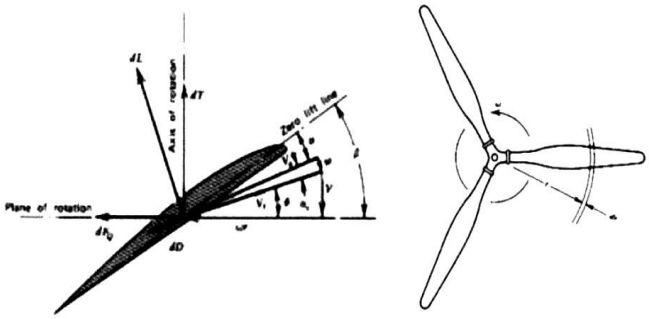

Fig.1 Depiction of a propeller blade cross section

The Thrust of a propeller depends on the volume of air (or water) accelerated per time unit, on the amount of

* Corresponding author. Tel.: +88-01736941309
E-mail address: mahboburr6@gmail.com

the acceleration, and on the density of the medium. Based on momentum considerations, it can be expressed by the following formula:

$$T = \frac{\pi}{4} \cdot D^2 \cdot \left(v + \frac{\Delta v}{2} \right) \cdot \rho \cdot \Delta v$$

	T	thrust	[N]
	D	propeller diameter	[m]
	v	velocity of incoming flow	[m/s]
where:	Δv	additional velocity, acceleration by propeller	[m/s]
	ρ	density of fluid	[kg/m³]
		(air: ρ= *1.225 kg/m³*, water: ρ = *1000 kg/m³*)	

2.1.2 Propeller Modeling and Selection

In the field of RC aerial vehicles, selection of proper propeller is an important scenario. Depending upon the required flight phenomena, appropriate propeller should be modeled and selected. For this simulation investigation 10*4.7 propeller model was selected because of its appreciable flexibility and light weight (13g approx.). 10*4.7 indicates that the propeller has a diameter of 10 in and pitch of 4.7 in per revolution. Fig.2 represents the design flow-chart for the selected propeller.

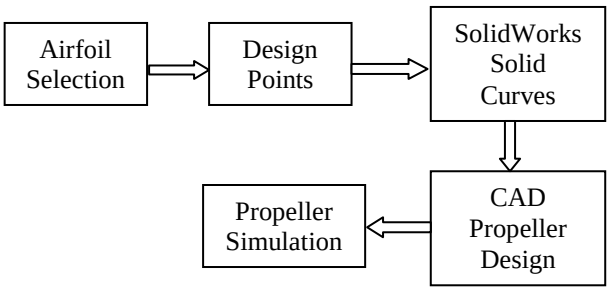

Fig.2 Propeller Design and Analysis Flow-Chart

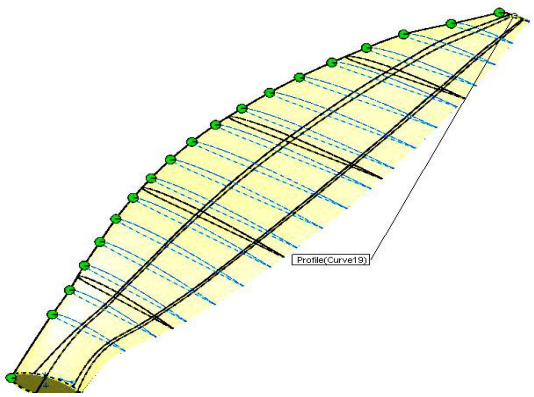

Fig.3 Sketch for loft feature in SolidWorks

Using the data from the UIUC database site [6], the points through x-y-z were generated and then by

Fig.4 Final rendered model of 10*4.7 propeller

Providing a loft feature a solid propeller model was obtained. Fig.3 and 4 illustrates the scenario of generating the solid model of the propeller through a loft feature. Fig.4 shows the rendered output of the designed model. Rendering was performed in a commercial rendering software Luxion Keyshot 4.2 (version).

2.2 Numerical Simulation

Simulation investigation was performed satisfactorily in SolidWorks Flow Simulation by setting required boundary conditions, defining the computational domain and rotating region.

2.2.1 Model Geometry

The numerical simulation was performed using a small two-bladed propeller having a diameter of 10 in and pitch of 4.7 in. Fig.4 represents the propeller geometry. Propeller model was designed using a commercial software package SolidWorks 2013.

2.2.2 Rotating Reference

After finishing modeling, the model was inserted in flow simulation by opening a new wizard from the SolidWorks flow simulation tab. For this type of design problem, a rotating reference frame is used to simulate the effect of blade turning and generating thrust.

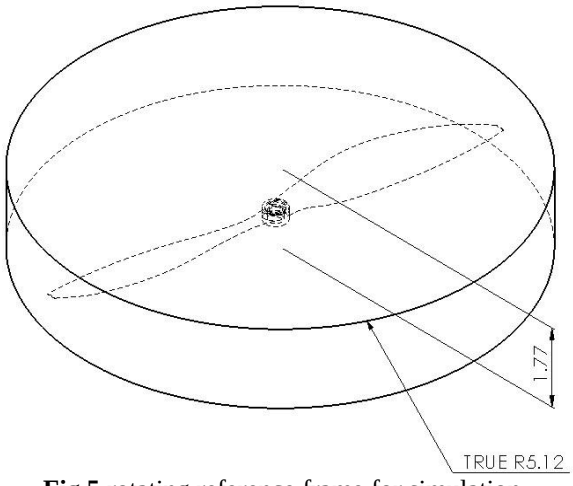

Fig.5 rotating reference frame for simulation

For this purpose a circular body should be created and the key is that the frame diameter shall be just a tiny bit larger than the blade diameter, not smaller in any case.

Axis of rotation was set about Y-axis. This illustrates that air will flow along Y-axis, when the propeller starts to rotate in order to provide a thrust force beneath. Fig.5 shows the optimum rotating frame (dimensions are in inch) used during investigation.

2.2.3 Computational Domain

The computational domain refers to a simplified form of the physical domain both in terms of geometrical representation and boundary condition imposition. For this investigation, a rectangular block surrounding the propeller acts as the computational domain.

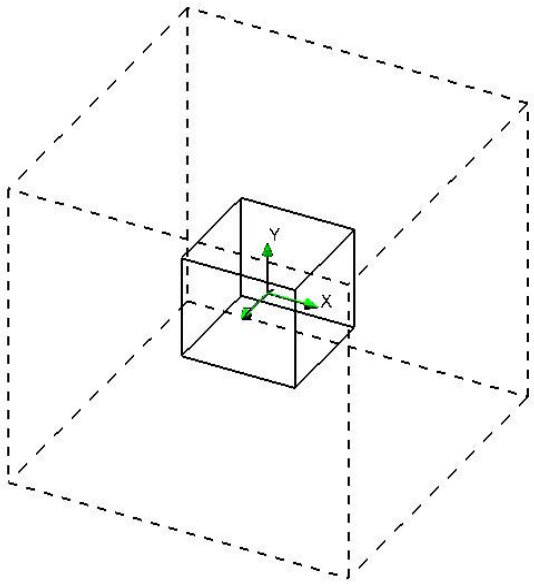

Fig.6 Simplified computational domain

Fig.6 represents the simplified computational domain, sub-domain for the propeller model in symmetrical attitude. Basically, the mathematical calculation of all fluid cells for the flow phenomena will take place in this defined domain through 3D simulation.

2.2.4 3D Mesh Generation

Effective mesh generation and update is one of the most important components of a 3D flow simulation environment capable of fast and accurate 3D computation of problems with complex geometries, including, and especially, problems with spatial computational domain changing as a function of time [8]. A 3D, solid and standard mesh generation was performed over the propeller model. Total node and element size were 15925 and 7750 respectively.

Table 1 Mesh Information

Study Name	3D Mesh
Mesh Type	Solid Mesh
Solver	Flow Simulation
Fluid Cells	2790315
Partial Cells	48527
Iterations	326
Travels	2.00126
Iterations per 1 travel	163
Refinement	326
Warnings	No Warnings
CPU time to complete mesh(hh:mm:ss)	02:06:24
Result Resolution	

Fig.7 3D meshing over the surface of propeller blades

Proper mesh generation is an important step for simulation and Fig. 7 represents the 3D meshing of the propeller model.

2.2.5 Boundary Conditions

Necessary boundary conditions were set for the simulation purpose in the defined computational domain- at inlet, inlet free stream velocity, inlet mass flow, Mach number were imposed; same had gone for the outlet. Standard pressure and temperature were maintained for a mass flow rate of 0.0001 kg/s. Boundary layer was set to turbulent and turbulent length and intensity (I_t and L_t) were set as turbulent parameters (I-L). I_t and L_t were set 0.1% and 0.0177165 in respectively.

Initiating the boundary conditions, all the data provided will help in the mathematical calculation at each fluid cells in the computational domain. For computational algorithms applied to flow simulations, discrete boundary conditions are required. Hence, in order to receive a satisfactory output from the simulation investigation, proper boundary conditions should be defined.

3. Simulation Output and Discussion

After defining all the requirements, for different rotational speeds, thrust force was measured. The rotational speed was denoted in rpm as available in motor rating. Basically, the thrust force generated by the propeller indicates the motor power to be used in the aircraft. This phenomena ease the motor selection scenario to get a rigid flight. Thrust forces for different rotational speeds were numerically as illustrated in Table 2.

Table 2 Thrust force at different speeds

Speed in rpm	Thrust Force (N)	Maximum Value (N)	Minimum Value (N)	Delta
750	.055	.055	.044	.004
1500	.222	.224	.211	.013
2250	.508	.508	.417	.031
3500	1.221	1.221	.990	.086
4500	1.531	1.518	1.476	.109

Using the propeller data from UIUC data site [6] for the selected model 10*4.7, a graph can be plotted as shown in Fig.8 that represents the relationship among propeller radius, pitch and chord length.

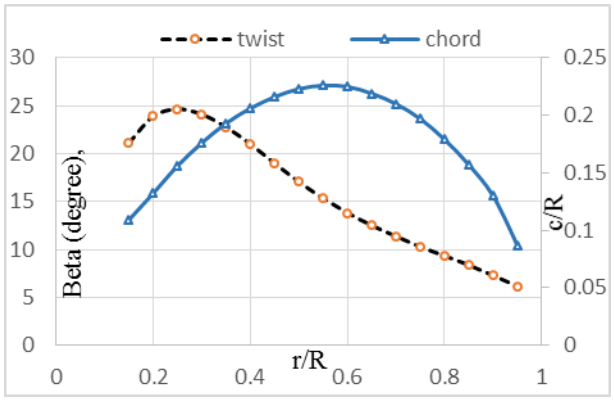

Fig.9 Graphical plot of APC slow flyer 10*4.7

Again another graph (Fig.9) using the data obtained by simulation can be plotted; thrust force (T) vs rotational speed (P).

From the graph it can be seen that, thrust force gradually increases with the rotational speed. But this increment will continue to a certain limit as propeller material has certain elastic limit. Mathematical formulation for determining the maximum rotational speed that a propeller can withstand is,

$$P = Kv * (V_{in} - V_{loss}) \quad (1)$$

Hence, maximum thrust will be obtained at maximum rotational speed.

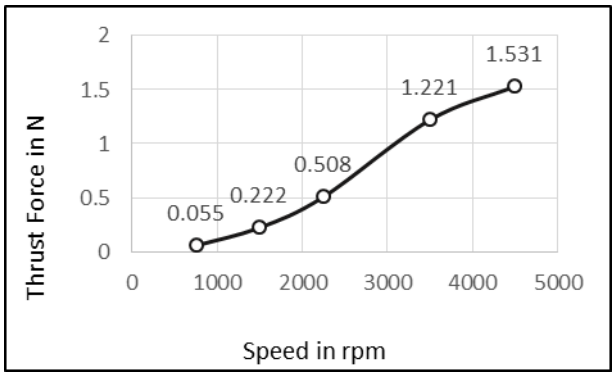

Fig.9 Thrust force at different rotational speeds

Pressure, Velocity and temperature distribution along with the velocity flow trajectory, velocity vector and velocity streamline have been represented for different rotation speeds (sample: 3500 and 4500 rpm) in the following figures by color contour. Fig.10 to Fig.14 represents the contours for speed 3500 rpm.

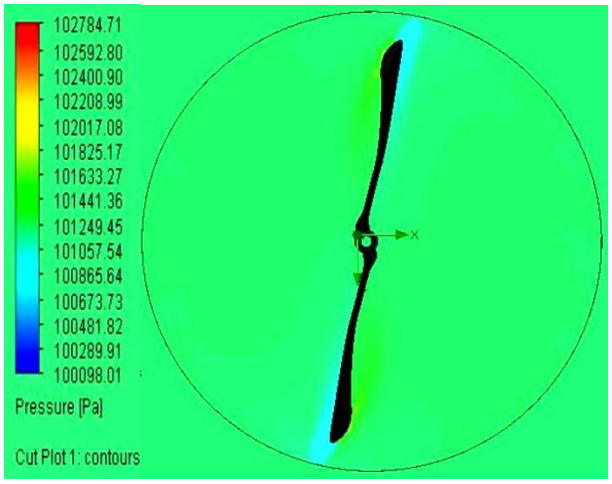

Fig.10 Pressure distribution contour

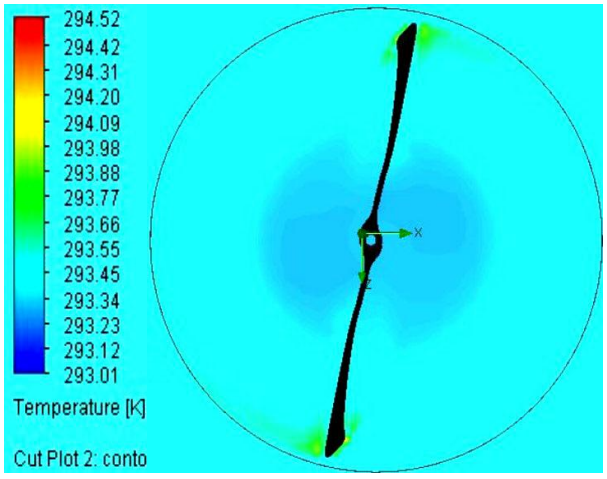

Fig.11 Temperature distribution contour

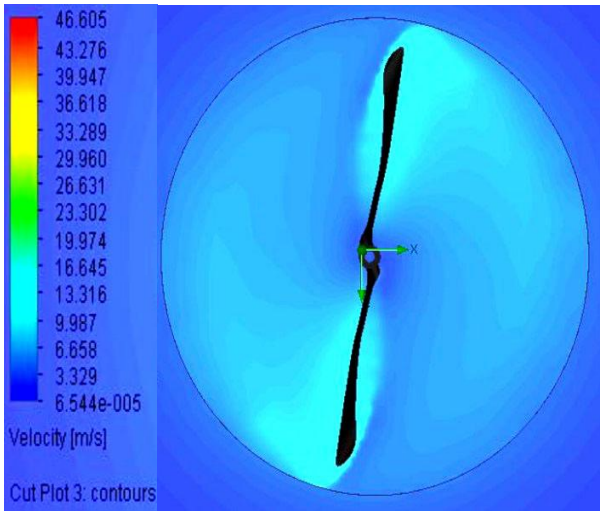

Fig.12 Velocity distribution contour

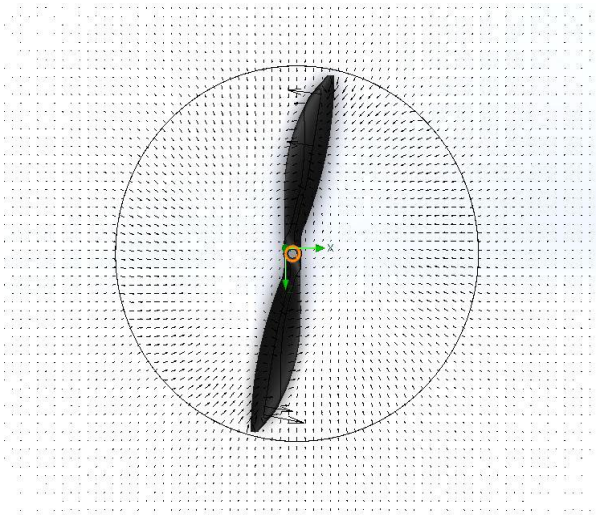

Fig.13 Velocity vector

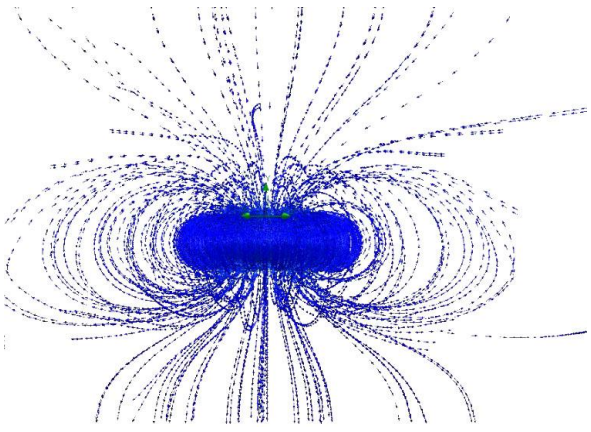

Fig.14 Velocity flow trajectory

For higher rotational speeds, it was observed that, the propeller reached to its critical situation as higher torque and thrust were generated. Fig.15 to Fig.19 represents the contours for speed 4500 rpm.

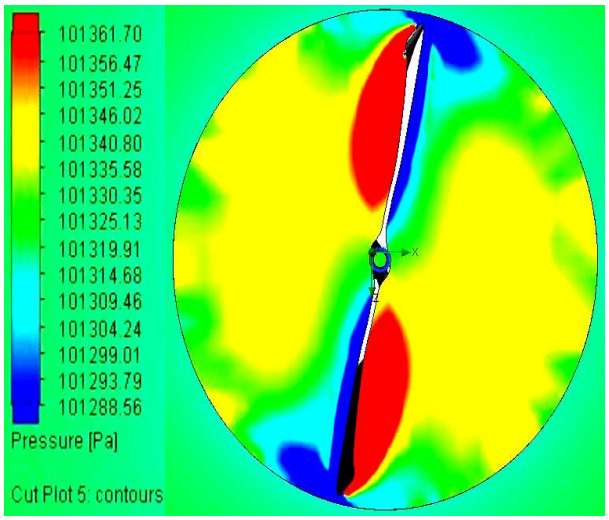

Fig.15 Pressure distribution contour

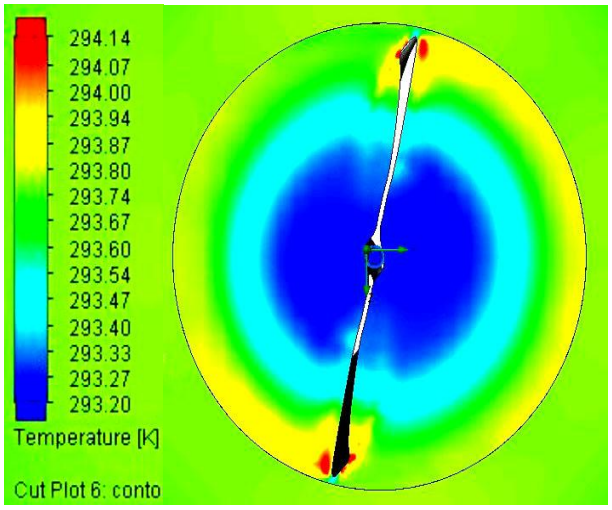

Fig.16 Temperature distribution contour

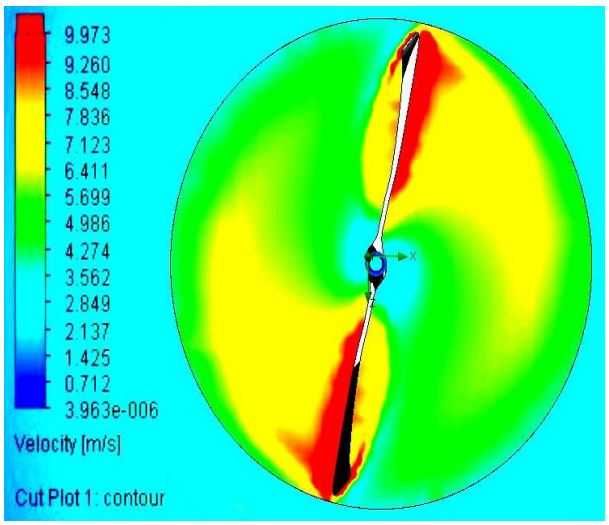

Fig.17 Velocity distribution contour

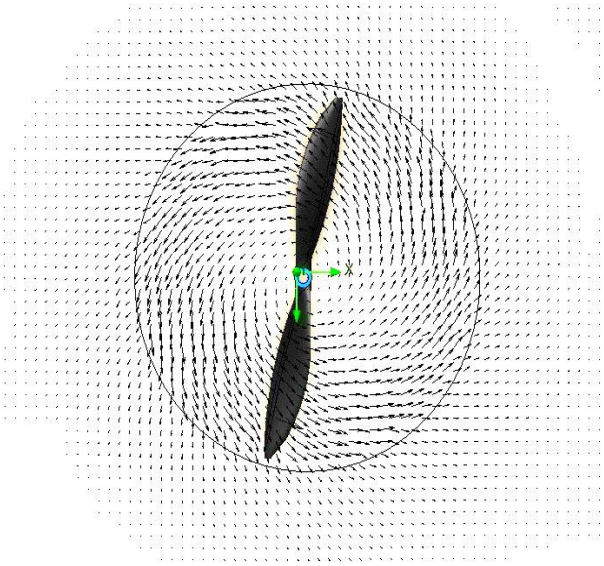

Fig.18 Velocity vector

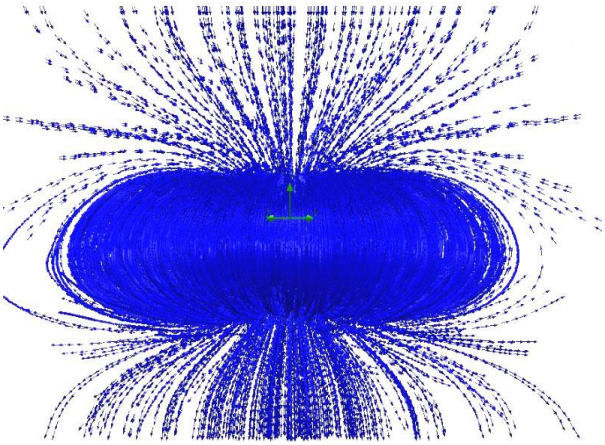

Fig.19 Velocity flow trajectory

Velocity flow trajectory shows that, due to the rotational motion, fluid (air) flows to the downward direction exerting an effective thrust force.
Simulation outputs exhibits the characteristics of the designed propeller model. It was observed that, with increasing the rotation speed, the propeller performance was satisfactorily enhanced till the critical condition. Hence, it is recommended to use the propeller in its elastic limit.

4. Conclusion and Recommendation

Propellers are considered as the main source of propulsion system in the field of radio controlled (RC) aerial vehicles. So, it is much more necessary to select the proper propeller model for the aircraft to get a satisfactory flight. Numerical simulation ease the way to expose the aerodynamics of the propeller. Here comes the main objective of this simulation investigation.
In this investigation at preliminary stage, the design fundamentals of a propeller were studied. Then, the selected model was prepared for numerical study through SolidWorks flow simulation by providing the perquisite conditions. Hence, required thrust force at different rotational speed was determined along with other propeller aerodynamics.
Design can be modified for the optimization of burrs and vibration. Variation in computational domain, grid refinement and change in boundary conditions should be considered for the improvement in mesh generation technique.

NOMENCLATURE

P : rotational speed, rpm
T : Thrust force, N
Kv : motor rating(power), kilo volt(Kv)
V_{in} : input voltage, volt

REFERENCES

[1] W. Shawn Westmoreland, Robert W. Tramel, and Jennie Barber, "Modeling Propeller Flow-Fields Using CFD", *46th AIAA Aerospace Sciences Meeting and Exhibit,* AIAA 2008-402, 7-10 January 2008, Reno, Nevada.

[2] M. Abdel Maksoud, F. Menter and H. Wuttke, "Viscous flow simulations for conventional and high-skew marine propellers", *Ship Technology Research*, 45:67-71, 1998.

[3] K. –J. Oh and S. –H. Kang, "Numerical calculation of the viscous flow around a propeller shaft configuration", *International Journal of Numerical Methods in Fluids*, 21(1):1-13, 1995.

[4] A. Sánchez-Caja, P. Rautanhiemo and T. Siikonen, "Simulation of Incompressible Viscous Flow Around a Ducted Propeller Using a RANS Equation Solver", *23rd Symposium on Naval Hydrodynamics,* Val de Reuil, France, 527-539, 2000.

[5] M. Stainer, "The Application of 'RANS' Code to Investigate Propeller Scale Effects", *22nd Symposium on Naval Hydrodynamics,* 222-238, 1999.

[6] Brandt, J.B. and Selig, M.S., "Propeller Performance Data at Low Reynolds Numbers", *49th AIAA Aerospace Sciences Meeting,* AIAA Paper 2011-1255, Orlando, FL, January 2011.

[7] Ian P. Tracy, "Propeller Design and Analysis for a Small, Autonomous UAV", *Department of Mechanical Engineering, Massachusetts Institute of Technology, 5-6,* June 2011.

[8] A. A. Johnson and T. E. Tezduyar, "Advanced mesh generation and update methods for 3D flow simulation", *Computational Mechanics 23(1999) 130-143,* © Springer-Verlag 1999.

ICMIEE-PI-140414

Automatic Control System for Lighting of a Single Door Room with Bidirectional People Counter

Md. Saddam Hossain[1], **Helal-An-Nahiyan*[1],
[1]Department of Mechanical Engineering, Khulna University of Engineering & Technology, Khulna-9203, BANGLADESH

ABSTRACT
This paper presents an automatic control system which turns ON or OFF room light based on counting how many people are present in the room. If there is no person in the room the light remains OFF and when there is any person enters in the room the system turns the room light ON. This system is a bi-directional people counter which contains a pair of ultrasonic distance sensor (HC-SR04), a microcontroller, and a relay. When somebody enters in or leaves the room, he has to cross a pair of sensors. These sensors send information to the micro-controller with the sequence he crossed the sensors. According to the sequence a pre-programmed micro-controller adds or subtracts the number of people present in the room and turns ON or OFF the relay which actually turns the room light ON or OFF.

Keywords: Automatic Control, Ultrasonic Sensor, Microcontroller, Bidirectional Counter

1. Introduction

Electricity scenario in developing countries like Bangladesh is still not up to the mark. Financial crisis and limitation of natural resources are the major constraint to establish more power plants and upgrade the situation. As a result limited capability of power stations cannot generate enough electricity according to the demand. Beside this power generation limitation, careless using of electrical appliances increases the demand much more. In our daily life, we often keep the lights and fans ON even there is nobody in the room. This happens due to negligence or subconscious mistakes to turn the lights off especially when we are in hurry. Whatever the situation is, the electricity demand rises. To avoid all such situations this paper presents an "Automatic control system for lighting of a single door room with bidirectional people counter". This system saves unnecessary consumption of electricity and ensures more comfort in busy lifestyle. The complete project is divided into two modules: first module is known as "Digital People counter" and second one is "Automatic control system for lighting". Main concept of "Digital People counter" is counting the number of persons entering in any room like seminar hall, conference room, class room, etc. This function is implemented by using a pair of ultrasonic distance sensors. No of people counted is incremented if somebody enters into the room and at the same time lights are turned ON. In reverse way, counting is decremented if somebody leaves the room. When the number of persons inside the room is zero, lights inside the room are turned OFF using a relay interface. In such way Relay does the operation of automatic control of lighting [1]. By combining all these, this research implemented a cost efficient automatic lighting system which can restrict the misuse of electricity.

2. Background

Automatic system for controlling the lighting makes our regular life more comfortable and it also saves unnecessary wastage of electrical energy. There are different types of automatic control system for lighting is available in the market. Most of them use a pair of IR transmitter and IR receivers as sensing device for detecting human entry or exit [2]. In case of using IR sensors the IR transmitter and IR receiver need to be placed in a straight line on both side of the door. Any kind of deviation in placing the IR transmitter and receiver in a straight line may cause counting error [3]. To avoid this counting error, this project uses ultrasonic sound distance sensor which is placed on one side of a door only. There is no possibility of displacement problem and it gives more accurate counting than IR sensor. Beside these, the cost of the IR based automatic lighting control system is much higher than ultrasonic sound sensor based lightning control system. The cost of automatic control system for lighting based on IR sensor from *MicroTronics Technologies* [4] is about 5200 BDT. Whereas the cost of this system based on ultrasonic sensor is about 1500 BDT. So this project is cost efficient and more reliable than the IR based automatic control system for lighting.

3. Design Consideration

The design of this project consists of two parts: first one is designing a people counter and second part is automatic control system for lighting. The people counter is designed in such manner that when anyone enters in a room, he has to pass over the sensor A and then sensor B as shown in the fig-1. When this sequence occurs the people counter counts plus one. In case of exits from the room, a person has to pass over sensor B and then sensor A as shown in fig-1. If this sequence occurs the people counter counts minus one. Thus the counter is designed. Automatic control system for lighting is designed on the basis of number of person present in the room according to the people counting

* Corresponding author. Tel.: +88-01911208438
E-mail address: nahiyan.me@gmail.com

system. When there is more than or equal to one people in the room the system turns light ON and when there is no people in the room it turns OFF light. The schematic diagram of design consideration is shown in fig-1.

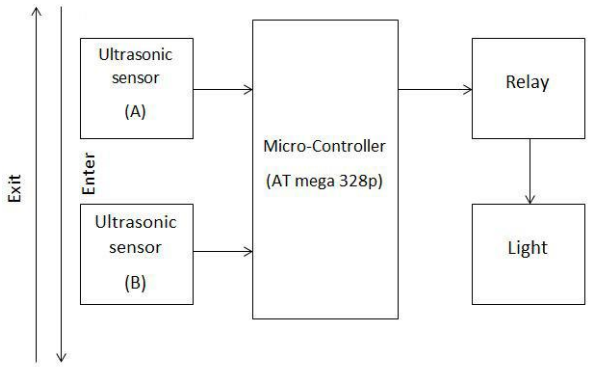

Fig.1 Schematic Diagram of Automatic Control System for lighting

4. Electrical Components

In this project a pair of HC-SR04 ultrasonic sensor, an ATmega328PU microcontroller and a 6V DC relay is used.

4.1 Ultrasonic Sensor (HC-SR04)

The HC-SR04 ultrasonic sensor uses sonar signal to determine the distance to an object like bats or dolphins do. It offers excellent non-contact range detection with high accuracy and stable readings in an easy-to-use package from 2cm to 400 cm. Its operation is not affected by sunlight or black material [5].

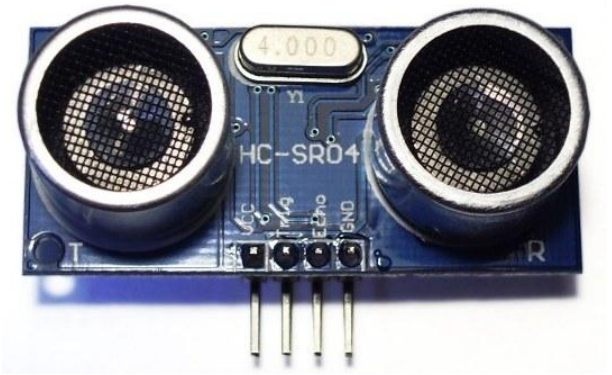

Fig.2- HC-SR04 module

4.2 ATmega328PU microcontroller

This is the CPU (central processing unit) of our system. This microcontroller have 32 Kbytes self-programmable Flash program memory, 1Kbytes EEPROM, 2 Kbytes internal SRAM, 8 bit AVR and 23 programmable I/O lines. Operating voltage of this microcontroller ranges between 4.5V-5.5V [6]. This is helpful for multifunctional automated system with low cost and low power consumption.

Fig.3- ATmega328PU microcontroller

The various functions of microcontroller are like:

- *Bidirectional Visitor counters section* – It is bidirectional because 2 sensors are used on a single door. Microcontroller does the function of Reading the digital input from two ultrasonic sound distance sensor and calculates the number of persons from them.

- *Automatic Room Light controller section* – Microcontroller turns on the Room Light when person count is greater than or equal to one. And turn off lights when count is zero. This is done by Relay. Since relay is used, an AC bulb or DC bulb can be connected as per the requirement.

4.3 6V DC Relay

Since microcontroller cannot turn on relay directly, we have used a Relay driver circuit with 6V DC relay. This circuit consists of a transistor which is used to turn on the relay through microcontroller. We have used a SPDT (Single Pole Double Throw) relay. In this project we have provided 2 pin connector as an output of Relay. One of these 2 pins is connected to the normally open terminal of the Relay which is also known as NO contact.

Fig.4- 6V DC Relay

4. Circuit Diagram

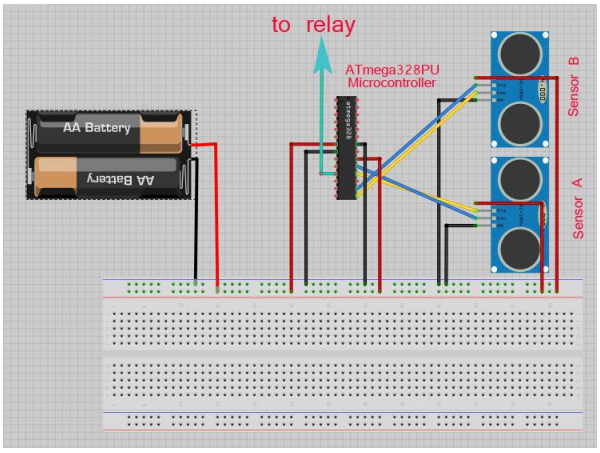

Fig.4- Circuit Diagram of Automatic control System for lighting

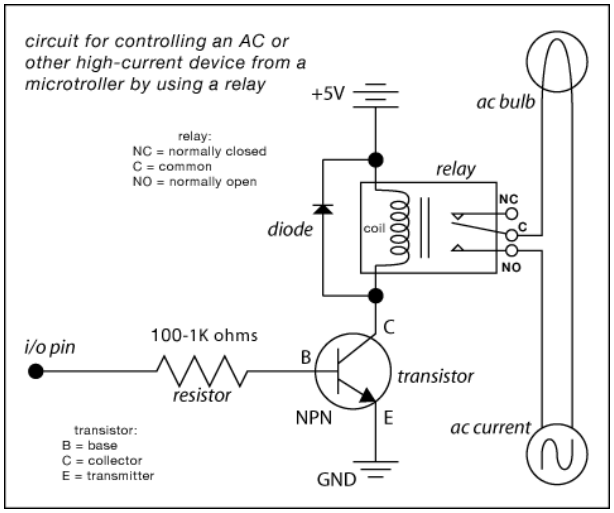

Fig.5- Relay setup

There are four pins on each ultrasonic sound distance sensor. Two of them are VCC and GND line and other two are Trig pin and Echo pin. Trig pin of sensor A is connected with the pin no 18 of ATmega328P and Echo pin is connected with pin 19. Trig pin of sensor B is connected with the pin no 16 of ATmega328P and Echo pin is connected with pin 15. The relay pin is connected with pin 11. The sensors sends signal to microcontroller when there is an obstacle placed in front of the sensor. Then microcontroller counts whether people enter in the room or exit. If there are any people in the room then microcontroller turns ON the relay which actually turns ON the light of the room. Otherwise the light in room remains turned OFF.

5. Automatic control system for lighting algorithm

The main function of automatic control system for lighting is controlled by an ATmege328PU microcontroller. When the system plugged in it starts and initialize the PWM. After initializing PWM, microcontroller checks if there is any person in front of sensor A or sensor B. If it finds any person in front of sensor A then it checks for any person present in front of sensor B. If the sensors responds within 5 second according to the sequence firstly A and then B, the microcontroller increases the number of people present in the room by one. When there is more than or equal one people present in the room, microcontroller turns the relay ON and which actually turns ON the light. After turning ON the light the microcontroller again checks there is any person in front of sensor A or sensor B. If it finds any person in front of sensor B then it checks for any person present in front of sensor A. If the sensors responds within 5 second according to the sequence firstly B and then A, the microcontroller decreases the number of people present in the room by one. When the number of people in the room is zero then the microcontroller turns OFF the relay which actually turns OFF the light. And if there is any negative value of people occurs then the microcontroller sets the value to zero because negative number of people is impossible. The microcontroller goes back to check the sensor again. All the time this process continues in a closed loop. The flow chart of the algorithm is given in fig-6.

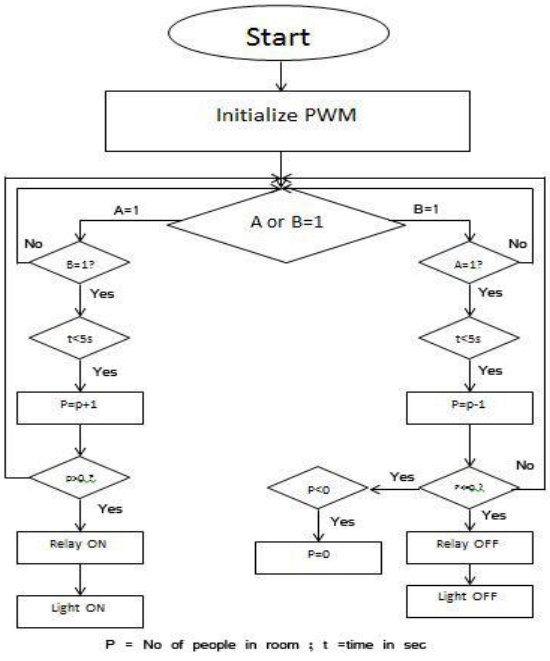

Fig.6- Flowchart of people counter and lighting system algorithm

6. Result and Discussion

The main purpose of this research is to develop an automatic control system for lighting which is cost efficient and more reliable. The cost of this project is much lower than different automatic control system for

lighting available in market. This project overcome positioning problem of IR based control system. Moreover, the system still has limitation like; it works only when one person cuts the rays of the sensor at a time hence cannot be used when two or more persons cross the door simultaneously. An additional camera sensor can solve this problem. We also have to off the switch manually when anybody is present inside the room and want to turn the light off. Above all, this project reduces the wastage of electrical energy which was the main purpose of the project. Besides the lighting control, this project can be used as counting purposes like product counting by using its counting algorithm. Therefore, we can say that this project fulfills its objectives and it can be implemented practically.

8. Conclusion

The main purpose of this project is to reduce the unnecessary wastage of electrical energy. In developing country like Bangladesh this project will be very helpful to reduce unwanted consumption of electricity and it will make life more comfortable. The cost of this project is sufficiently lower than different types of automatic control system available in market. By using the circuit and proper power supply of this project we can implement various applications such as fans, tube lights etc.

REFERENCES

[1] Y. C. Chang, T. Y. Chen, D. J. Wang, People Counting System for Getting In/Out of a Bus Based on Video Processing, *Eighth International Conference on Intelligent Systems Design and Applications(ISDA), 2008,* vol. 3, pp. 565 – 569.

[2] F. Schwartz, Performance of Narrow Field, Passive, Infra-Red Intrusion Detector, *Proceedings of The Society of Photo-Optical*, Sep. 1972, pp. 51-56

[3] Electronic management system employing radar type infrared emitter and sensor combined with counter as described in U.S. Pat. No. 4993049 A

[4] Automatic Room light Controller with Visitor Counter by *Microtronics Technologies*, 10 June, 2013

[5] Ultrasonic Sensor. "HC-SR04 datasheet". [Online]. Available: www.satistronics.com

[6] Microcontroller Atmel ATmega328PU. "Atmel ATmega328PU". [Online]. Available: http://atmel.com/.

ICMIEE-PI-140415

Production of Titania Stabilized Alumina Ceramic Cutting Tool

Md. Tanvir Faisal [1,*] *Md. Mohar Ali Bepari* [1]
[1] Department of Materials and Metallurgical Engineering, Bangladesh University of Engineering & Technology, Dhaka-1000, BANGLADESH

ABSTRACT
Cutting being an important fabrication route enables fast and easy manufacturing of different product. In this research, ceramic cutting tool samples based on Al_2O_3 with different amounts of TiO_2 (4%, 8% and 12%) additions were prepared by uniaxial pressing at about 170-180 MPa and sintering them at different temperatures (1350°C, 1400°C, 1450°C & 1500°C) for different soaking times (0 hr, 2 hr) depending upon the type of sintering schedule chosen. Initial single stage sintering data was utilized to find appropriate activation and soaking temperature for two stage sintering processes. Later two stage sintering was carried out. The sintered bodies were tested to determine the physical and mechanical properties such as density, hardness, grain size, wear and cutting property. The Scanning Electron Microscope was used to observe microstructure and co-relate it with the measured properties. And finally the major findings are reported in the conclusion section.

Keywords: Alumina, Titania, density, hardness, wear property, cutting property.

1. Introduction

The recent advancements in cutting tool technology is moving towards high speed, dry cutting processes together with focusing on increased durability and lower tool cost. The application of nano-ceramic materials with their superior physical, mechanical and chemical properties [1] has enabled to accomplish new heights in cutting tool industry. As engineering ceramics like alumina (Al_2O_3), silicon nitride (Si_3N_4), titanium carbide (TiC), titanium carbonitride (TiCN), cubic boron nitride (cBN), etc. possess high hardness, low thermal expansion, high thermal conductivity, chemical inertness, hot strength; they are undergoing increased utilization in tribological [2] applications.

Among all the ceramics Aluminum Oxide (Al_2O_3) or Alumina is readily available and cheaper than others. It possesses good hardness and wear resistance, but lacks toughness. The deficiency in toughness may cause premature failure which would render alumina unsuitable for demanding applications. In order to enhance to properties of alumina and other ceramics incorporation of small quantities of additives like ZrO_2, MgO, CaO, WC, SiO_2, TiO_2, TiC, etc. has been considered as standard practice [3,5]. Titanium Oxide (TiO_2) or Titania is a prospective additive in case of alumina. Among the other techniques application of various tool shapes, cutting angle, tool alignment, tool holder geometry, etc. have significant effects in improving cutting tool performance [4].

In the Department of Materials and Metallurgical Engineering (MME) of BUET, some attempts have already been made to develop cost-effective cutting tool inserts with titania as additive. Among them, Syed Md. Zakaria conducted research to develop cutting tools by slip casting. Later Md. Al Hossani Shuva, Abu Naser Reza and Tasneem Ara Islam made successful attempts by applying cold uniaxial pressing.

2. Experimental Procedure

2.1 Raw materials

The raw materials with following specification were used:

Table 1 Raw materials' specification

Attributes	Alpha Al_2O_3	TiO_2 (Anatase)
Purity	99.85%	99.9%
Particle size	150 nm	40nm
SSA	$10m^2/g$	$40m^2/g$
ρ	3.97 g/cc	3.89 g/cc
M_p	2045°C,	1830-1850°C
B_p	2980°C	2500-3000°C

In this current research compositions of 4% TiO_2- 96% Al_2O_3, 8% TiO_2- 92% Al_2O_3 and 12% TiO_2- 88% Al_2O_3 were used for producing cutting tool inserts.

2.2 Slurry preparation

First, appropriate amounts of Al_2O_3 and TiO_2 powders were weighed (30gm batch) and poured into an ultrasonically cleaned HDPE bottle containing zirconia balls. Two third of height of the bottle was filled with acetone as milling media. Then it was ball milled at 150 rpm form 18 hours. After that, prepared slurry was extracted using small amounts of acetone for proper cleaning purposes. The extracted slurry was kept in beaker and marked with permanent markers for easy identification.

2.3 Drying and binder addition

The slurry was dried for minimum 24 hours at 110-120°C. A stirrer was used to first crush dried cake, to add PVA binder (3-4 drops with a 2 minute interval) and then dry for another 24 hours.

* Corresponding author. Tel.: +88-01727711667
E-mail address: md.tanvir.faisal@gmail.com

2.4 Forming

Dies with 13mm internal diameter from Pike Tools was used for uniaxial compaction into cylindrical forms. The applied pressure was 2 tons (170 MPa) and holding time was 2 minutes. Formed green bodies are then dried at 110-120^{o}C for at least 24 hours.

2.5 Sintering

The green bodies were pressure-less sintered under the ambient condition using an electrically heated furnace. First, they were heated slowly (3-5^{o}C/min) to 500^{o}C and held there for 1 hour to remove binder and other volatile matter. Then they were heated to desired temperatures for different soaking times. Compacts were sintered at 1450^{o}C for 0 hour to determine activation temperature and at 1400^{o}C, 2 hour & 1450^{o}C, 2 hour to find soaking temperature. After performing preliminary steps, trail two stage sintering schedules were chosen to be 1450^{o}C, 0 hour ; 1350^{o}C, 2 hour. The final sintering cycles chosen were 1500^{o}C, 0 hour; 1350^{o}C, 2 hour & 1500^{o}C, 0 hour; 1450^{o}C, 2 hour. The cooling rate was kept within 3-5^{o}C/min.

3. Results and discussion

3.1 % Theoretical Density

In order to attain bulk density as close as possible to the theoretical density different composition, temperature and soaking time were used. The % theoretical densities of samples are given below:

Table 2 % theoretical densities of different composition

Sintering cycles	4% TiO_2- 96% Al_2O_3	8% TiO_2- 92% Al_2O_3	12% TiO_2- 88% Al_2O_3
1400^{o}C, 2 hr	90.95%	89.80%	88.49%
1450^{o}C, 0 hr	91.58%	89.32%	88.82%
1450^{o}C, 2 hr	92.1%	91.97%	87.8%
1500^{o}C, 0 hr 1350^{o}C, 2 hr	92.56%	91.29%	89.7%
1500^{o}C, 0 hr 1450^{o}C, 2 hr	93.02%	93.01%	90.21%

The following figure 1 illustrates the effect of temperature and composition on %theoretical density.

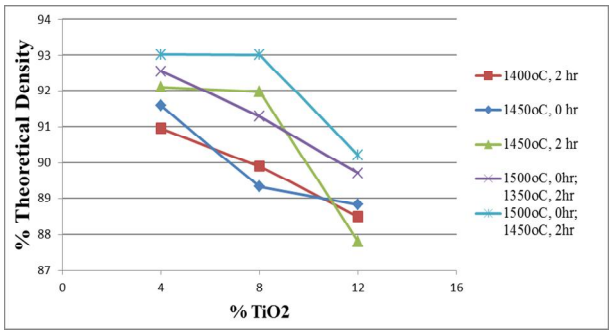

Fig.1 Variation of % theoretical density with temperature and composition.

3.2 Hardness

The hardness of the samples was measured by Vickers Micro-hardness Testing Machine using the following formula:

$$H.V = 1.854\ P * g / d^2\ \ GPa$$

Table 3 Hardness of different composition

Sintering cycles	4% TiO_2- 96% Al_2O_3	8% TiO_2- 92% Al_2O_3	12% TiO_2- 88% Al_2O_3
1400^{o}C, 2 hr	14.19 GPa	16.55 GPa	18.79 GPa
1450^{o}C, 0 hr	14.03 GPa	13.21 GPa	15.64 GPa
1450^{o}C, 2 hr	12.14 GPa	17.32 GPa	18.86 GPa
1500^{o}C, 0 hr	17.11 GPa	14.47 GPa	13.02 GPa
1350^{o}C, 2 hr			
1500^{o}C, 0 hr	19.48 GPa	23.44 GPa	---
1450^{o}C, 2 hr			

The following figure 2 illustrates the effect of temperature and composition on hardness.

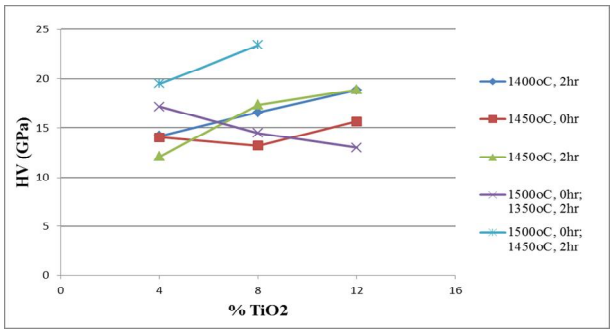

Fig.2 Variation of hardness with temperature and composition.

Addition of TiO_2 in alumina facilitates not only, reduction of the sintering temperature of alumina, but also influences its properties. It is clearly evident that, increase in the TiO_2 content increases hardness. It is because of the fact that, there are more sites of pinning the grain boundary, thus grain size is reduced and hardness is improved. We also know that density is an important factor in determining hardness. The denser the material the higher is the hardness.

3.3 Wear property

Pin – on – Disc apparatus was used to measure the wear property of the samples. The speed was 1150 rpm, dwell time was 30 minutes and applied load was 3 kg. The wear property was measured in gm/m unit. Only the final two compositions with two stage sintering were used in this case.

Table 4 Wear property of different composition (10^{-6})

Sintering cycles	4% TiO_2- 96% Al_2O_3	8% TiO_2- 92% Al_2O_3
1500^{o}C, 0 hr 1350^{o}C, 2 hr	1.41 gm/m	1.03 gm/m
1500^{o}C, 0 hr 1450^{o}C, 2 hr	0.981 gm/m	0.646 gm/m

The effect of sintering temperature and composition on wear property is illustrated in the following figure 3:

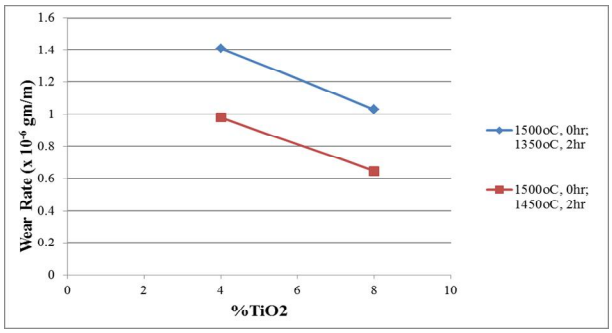

Fig.3 Variation of hardness with temperature and composition

With increase in density and hardness, wear rate decreases. This has been found throughout the project. But there were another variable such as temperature. With increase in sintering temperature it was found that, density further increased. Hardness also increased in the same manner. So the wear rate decreased.

3.4 Cutting property

The cutting specimen was mild steel (60HRC) with parameters cutting speed 465 rpm, depth of cut around 0.2 mm and cutting time of 2 minutes. After each operation, the removal of metal was measured by weighing out the chips in every cut. The tools were weighed after cutting, by the difference of initial and final weight, the tool weight loss was determined.

Table 5 Cutting property of different composition

Sintering cycles	Composition	% weight loss of insert	Weight of chips (gm)	Status
1500°C, 0hr 1350°C, 2hr	4% TiO_2-96% Al_2O_3	2.35	1.6516	Sustain
	8% TiO_2-92% Al_2O_3	4.74	3.3848	Sustain
1500°C, 0hr 1450°C, 2hr	4% TiO_2-96% Al_2O_3	2.75	3.5595	Sustain
	8% TiO_2-92% Al_2O_3	1.27	3.0515	Sustain

With increase in sintering temperature cutting property gradually improves for all composition except 8% TiO_2. The inconsistency may arise from sudden coarsening at higher temperature.

The effect of sintering temperature and composition on cutting property is illustrated in the following figure 4:

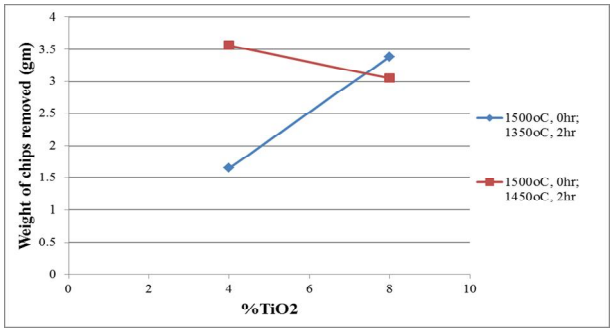

Fig. 4 Variation of cutting property with temperature and composition

3.5 Microstructural study

The SEM photographs show, bimodal type grain distribution. The microstructure mostly consists of fine grains together with some irregularly shaped large grains. It means that, the sintering temperature was high and the material was not allowed to attain homogeneity because of lack of time. In some cases, TiO_2 particles were not homogeneously distributed in the matrix meaning insufficient or inappropriate milling practice.

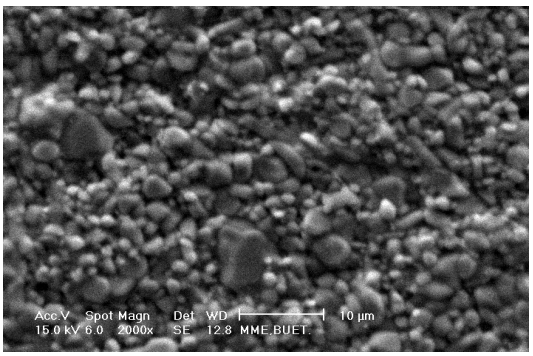

Fig. 9 SEM photograph of 4% TiO_2 -96% Al_2O_3 sample at 1500°C, 0 hr; 1350°C, 2 hr at 2000x

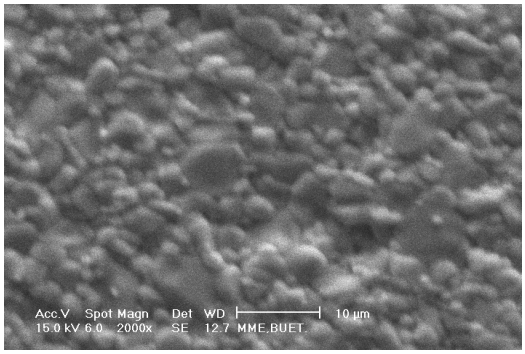

Fig. 10 SEM photograph of 8% TiO_2 -92% Al_2O_3 sample at 1500°C, 0 hr; 1350°C, 2 hr at 2000x

Conclusion

The following conclusions can be drawn from the present work:

i. The % theoretical density has gradually increased for cutting tools having composition until 12% TiO_2-88% Al_2O_3.

ii. The maximum % theoretical density of has obtained for 4% TiO_2 stabilized alumina during two stage sintering schedule of 1500^oC, 0 hr; 1450^oC, 2 hr.

iii. The hardness of 4% TiO_2 and 8 % TiO_2 stabilized alumina cutting tools increased consistently with increase in sintering temperature. Maximum hardness value was obtained for 8% TiO2 sintered at 1500^oC, 0 hr ; 1450^0C, 2 hr.

iv. As the sintering temperature and % TiO_2 increases the wear rate of cutting tools decrease. Wear rate of 4% TiO_2 stabilized alumina sintered at 1500^oC, 0 hr; 1350^0C is the lowest of all.

v. Cutting properties have also improved consistently with increasing sintering temperature and % of TiO_2.

vi. At lower temperature fine grain microstructure has been obtained and with increase in TiO_2 content relatively fine grain microstructures has been obtained even at higher temperature.

vii. Best combination of all properties has been obtained with 8% TiO_2 sintered at 14500C for 2 hours.

NOMENCLATURE

SSA : Specific surface area, m^2/g
ρ : Density, gm/cc
M_p : Melting point, ^oC
B_p : Boiling point, ^oC

REFERENCES

[1] R. Vaben, D. Stover, Processing of properties of nanophase ceramic, *J. Mater. Process. Tech.* Vol. 92, pp. 77-84 (1999)

[2] S. Jahanmir, Tribological Applications for Advanced Ceramics. *MRS Proceedings*, Vol. 140, pp. 285-291 (1988).

[3] David W. Richerson, Modern Ceramic Engineering: Properties, Processing and use in design, Part 2 in Processing of *Ceramics*. Marcel Dekker, Inc. New York, 1992.

[4] W. J. Smothers and H. J. Reynolds, Sintering and Grain Growth of Alumina, *Journal of American Ceramic Society*, Vol. 37, Issue 12 pp. 588-95 (1954).

[5] W. D. McKee, Jr., and Eugene Aleshin, Aluminum Oxide- Titanium Oxide Solid Solution, *Journal of American Ceramic Society*, Vol. 46, Issue l, pp. 54-58 (1963).

ICMIEE-PI-140416

Numerical Analysis and Comparison on Aerodynamics Characteristics of NACA-0012 & NACA-4412

G.M Hasan Shahariar [1,] *Mohammad Rashedul Hasan*[2], Mohammad Mashud[3]
[1,2,3]Department of Mechanical Engineering,
Khulna University of Engineering & Technology, Khulna-9203, BANGLADESH

ABSTRACT
The numerical analysis of the two dimensional subsonic flow over a NACA 0012 & NACA 4412 airfoil at various angles of attack which is operating at a Reynolds number of 3×10^6 is presented. A commercial computational fluid dynamic (CFD) code ANSYS FLUENT based on finite volume technique is used for the calculation of aerodynamics performance. The two dimensional model of the airfoil and the mesh is created through ANSYS Meshing which is run in Fluent for numerical iterate solution. The steady-state governing equations of Reynolds averaged Navier-Stokes is calculated for analyzing the characteristics of two-dimensional airfoils and the realizable k-epsilon model with Enhanced wall treatment is adopted for the turbulence closure. The aim of the work is to show the behavior of the airfoil at these conditions and to compare the aerodynamics characteristics between NACA 0012 & NACA 4412 such as lift co-efficient, drag co-efficient and surface pressure distribution over the airfoil surface for a specific angle of attack. Calculations were done for constant air velocity altering only the angle of attack for every airfoil model tested. This analysis can be used for the wing design and other aerodynamic modeling corresponds to these airfoil.

Keywords: *airfoil; cfd; rans; lift co-efficient; drag co-efficient; NACA 0012; NACA 4412*

1. Introduction

The rapid evolution of computational fluid dynamics (CFD) has been driven by the need for faster and more accurate methods for the calculations of flow fields around configurations of technical interest. In the past decade, CFD was the method of choice in the design of many aerospace, automotive and industrial components and processes in which fluid or gas flows play a major role. In the fluid dynamics, there are many commercial CFD packages available for modeling flow in or around objects. The computer simulations show features and details that are difficult, expensive or impossible to measure or visualize experimentally. When simulating the flow over airfoils, transition from laminar to turbulent flow plays an important role in determining the flow features and in quantifying the airfoil performance such as lift and drag. Hence, the proper modeling of transition, including both the onset and extent of transition will definitely lead to a more accurate drag prediction. [1]

For numerical simulation the first step is to construct the model of the geometry and flow domain. The body about which flow is to be analyzed requires modeling. This generally involves modeling the geometry with a CAD software package. The second step is to establish the boundary and initial conditions. Since a finite flow domain is specified, physical conditions are required on the boundaries of the flow domain. The simulation generally starts from an initial solution and uses an iterative method to reach a final flow field solution. The third step is the generation of grid i.e meshing. The flow domain is discretized into a grid. Currently all cases involve multi-block, structured grids. The grid should exhibit some minimal grid quality as defined by measures of orthogonality (especially at the boundaries), relative grid spacing (15% to 20% stretching is considered a maximum value), grid skewness, etc. The next step is to establish the simulation strategy and set up input parameters. The strategy for performing the simulation involves determining such things as the use of space-marching or time-marching, the choice of turbulence or chemistry model, and the choice of algorithms. The NACA four-digit wing sections define the profile by:

- First digit describing maximum camber as percentage of the chord.
- Second digit describing the distance of maximum camber from the airfoil leading edge in tens of percent's of the chord.
- Last two digits describing maximum thickness of the airfoil as percent of the chord.

This paper outlines the numeric procedure to analyze the NACA 0012 & NACA 4412 airfoil with a chord length of one meter and the Reynolds numbers of $3x10^6$. A two dimensional model is created to compare FLUENT's accuracy in the two dimensional analysis.

2. Computational Method

In this paper, the NACA 0012 and NACA 4412, the well documented airfoil from the 4-digit series of NACA airfoils, was utilized. The NACA 0012 airfoil is symmetrical; the 00 indicates that it has no camber. The 12 indicates that the airfoil has a 12% thickness to chord length ratio; it is 12% as thick as it is long. Reynolds number for the simulations was Re=3x106. The density of the air at the given temperature is ρ=1.225kg/m3 and the viscosity is μ=1.7894×10-5kg/ms. For this Reynolds number, the flow can be described as incompressible. The Reynolds average Navier-Stokes equations are solved using the green-gauss cell based gradient option and the IMPLICIT density-based solver is selected with a second order implicit transient

* Corresponding author. Tel.: +88-01713255226
E-mail address: hasanshahariar.kuet@gmail.com, rashedulhasan.047@gmail.com, mdmashud@yahoo.com

formulation for improved accuracy. The turbulent viscosity is computed through Realizable k-epsilon turbulence model with enhanced wall treatment. All solution variables were solved via second order upwind discretization scheme since most of the flow can be assumed to be not in line with the mesh.

2.1 Boundary conditions

The computational domain extended 15C upstream of the leading edge of the airfoil, 15C downstream of the trailing edge, and 20C above the pressure surface. Velocity inlet boundary condition was applied upstream (Inflow) with speed of (U=43.822 m/sec) and outflow boundary condition was applied downstream. An unstructured mesh arrangement with quadrilateral elements was adopted to map the flow domain in ground effect. [2] It involves inlet, outlet & wall boundary, the velocity components are calculated for each angle attack case as follows. The x-component of velocity is calculated by $x=u\cos\alpha$ and the y component of velocity is calculated by $y=y\sin\alpha$, where α is the angle of attack in degrees. Ansys recommends turbulence intensities ranging from 1% to 5% as inlet boundary conditions. In this study it is assumed that inlet velocity is less turbulent that pressure outlet. Hence, for velocity inlet boundary condition turbulence intensity is considered 1% and for pressure outlet boundary5%. In addition, Ansys also recommends turbulent viscosity ratio of 10 for better approximation of the problem [3].

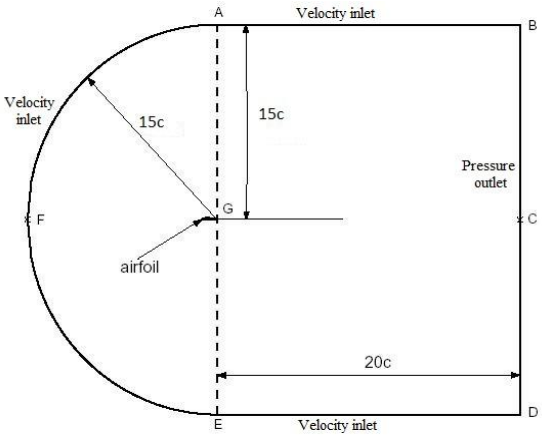

Fig 1: The dimensions and boundary conditions of the computational domain

2.2 Grid generation and Wall treatment

The grid used for simulating the NACA0012 & NACA 4412 airfoil is generated by the ANSYS Meshing is shown in Figure. The application of wall functions to modeling the near-wall region may significantly reduce both the processing and storage requirements of a numerical model, while producing an acceptable degree of accuracy.

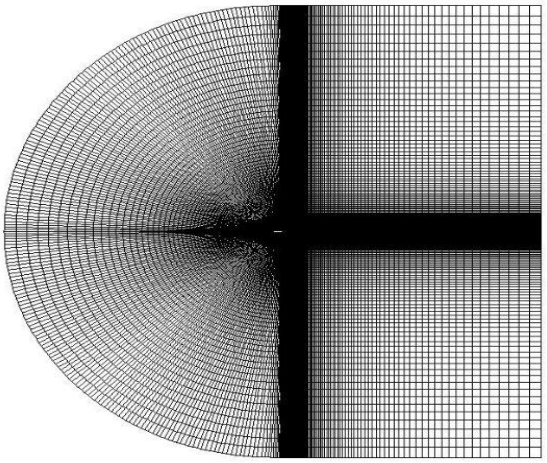

Fig 2: Mesh generation of the total structure domain

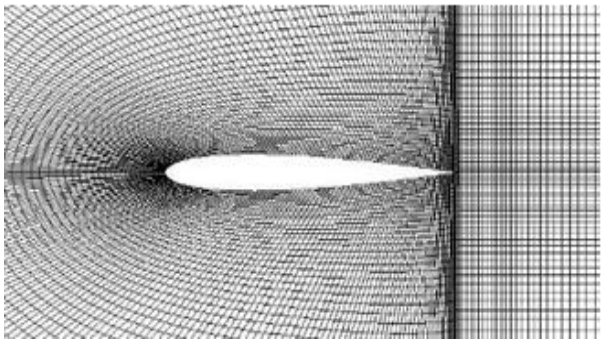

Fig 3: Mesh around NACA 0012 airfoil

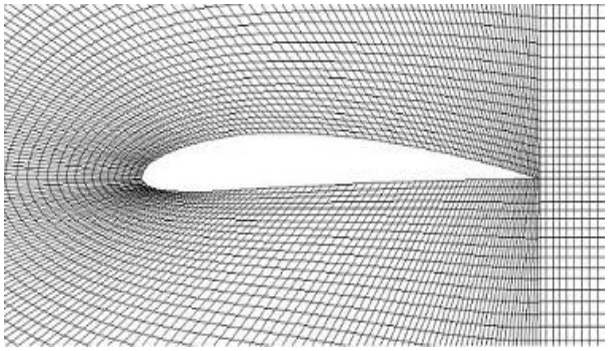

Fig 4: Mesh around NACA 0012 airfoil

To ensure sufficient boundary layer modeling, the growth rate of the inflation was set to 1.15 to give a minimum of 30 layers within the boundary layer. Beyond y+=30, the kepsilon model takes effect (due to the blending function). The non-dimensional wall parameter is defined as:

$$y^{+} = y * \frac{\sqrt{\frac{\tau_w}{\rho}}}{\mu} \qquad (1)$$

* Corresponding author. Tel.: +88-01713255226
E-mail address: hasanshahariar.kuet@gmail.com, rashedulhasan.047@gmail.com, mdmashud@yahoo.com

Here, y is the distance from the wall to the centroid of the first fluid cell, μ is the local kinematic viscosity, ρ is the air density and the subscript w denotes wall properties [4]. This study revealed that a C-type grid topology with 80000 quadrilateral cells would be sufficient to establish a grid independent solution (Figure 2). The domain height is set to approximately 20 chord lengths and the height of the first cell adjacent to the surface is set to 10-5, corresponding to a maximum y+ of approximately 0.2. A y+ of this size should be sufficient to properly resolve the inner parts of the boundary layer [5].

3.3 Grid independence study

The first step in performing a CFD simulation should be to investigate the effect of the mesh size on the solution results. Generally, a numerical solution becomes more accurate as more nodes are used, but using additional nodes also increases the required computer memory and computational time. The appropriate number of nodes can be determined by increasing the number of nodes until the mesh is sufficiently fine so that further refinement does not change the results. Figure 5 shows the effect of number of grid cells in coefficient of lift at stall angle of attack (16°). This computational model is very small compared to that of NASA's validation cases.

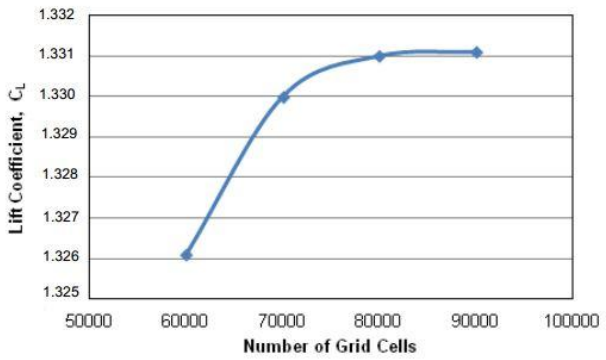

Fig 5: Variation of lift coefficient with number of grid cells [6]

3.0 Results and Discussions

After complete solution of NACA-0012 and NACA 4412 airfoil in FLUENT, resultant characteristics plot shows the effect of pressure distribution on airfoil, the training-edge pressure coefficient and pressure gradient along wall direction which suggests shock wave location and intensity. From 0 degree AoA to 16 degree AoA the lift curve is almost linear for NACA 0012. Throughout this regime no separation occurs and flow remains attached to the airfoil. At an angle of attack of roughly 15 to 16°, the flow on the upper surface of the airfoil began to separate and a condition known as stall began to develop. At stall AoA lift coefficient is reduced drastically due to intense flow separation generation. It also seen that, NACA 4412 has more lift than NACA 0012 airfoil. Also the drag co-efficient is decreases when the airfoil is camber. Figure 6 and 7 shows the variation of lift and drag co-efficient at various angle of attack. Hence it is observed that k-epsilon turbulence model with transition capabilities is predicting higher flow acceleration near the leading edge of the camber airfoil and hence relatively higher value of lift coefficient is observed. From figure 9, it is seen that the pressure distribution on upper and lower surface of NACA 4412 airfoil is more than NACA 0012 airfoil. Figures 10, 11, 12 shows the simulation outcomes of static pressure at angle of attack 8 degree with the Realizable k-epsilon turbulence model.

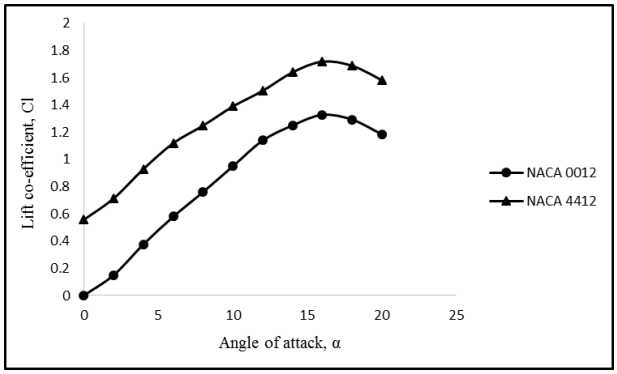

Fig 6: Lift co-efficient vs angle of attack

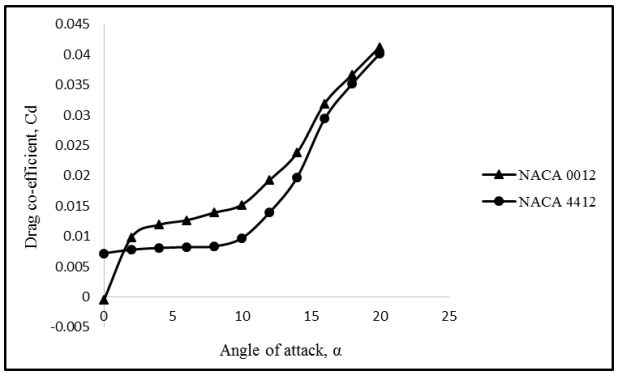

Fig 7: Drag co-efficient vs angle of attack

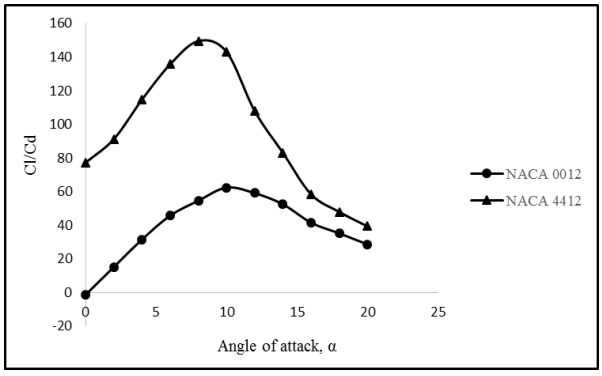

Fig 8: Lift-Drag ratio vs angle of attack

* Corresponding author. Tel.: +88-01713255226
E-mail address: hasanshahariar.kuet@gmail.com, rashedulhasan.047@gmail.com, mdmashud@yahoo.com

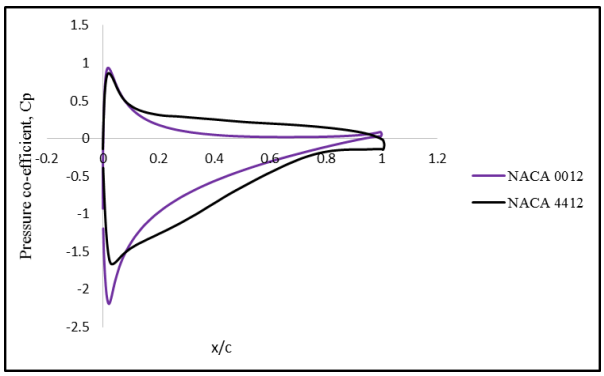

Fig 9: Pressure coefficient on the airfoil surface for 8 degree angle of attack

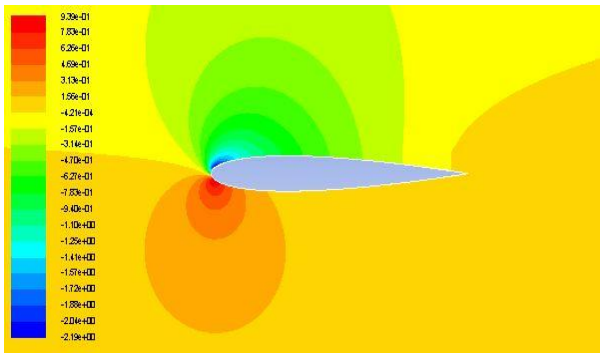

Fig 10: Contours of static pressure for 8 degree angle of attack for NACA 0012

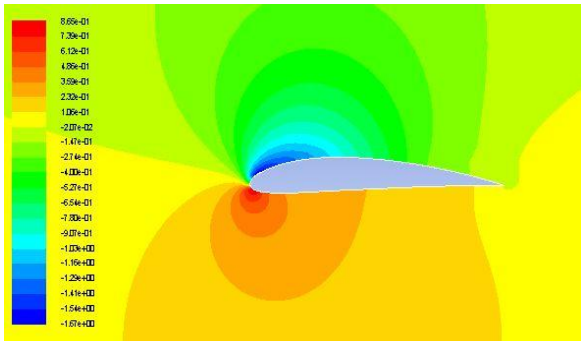

Fig 11: Contours of static pressure for 8 degree angle of attack for NACA 4412

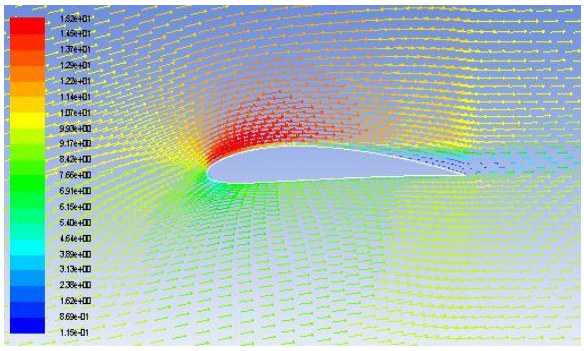

Fig 12: Velocity vectors for 8 degree angle of attack for NACA 4412

4. Conclusion

The main objective of this project is to study ANSYS FLUENT CFD software and to see the effect of aerodynamic characteristics of NACA-0012 and NACA 4412 airfoil. The flow characteristics for two-dimensional are analyzed with RANS equations and approximated by finite volume schemes with Realizable k-epsilon turbulence models. The difference in the flow characteristics of for NACA 0012 and NACA 4412 based on this study, some conclusions can be drawn as:

- Maximum lift co-efficient for NACA 0012 is 1.32803 and maximum lift co-efficient for NACA 4412 is 1.71935 at 16 degree angle of attack
- As the increase of angle of attack, drag co-efficient increases as shown in the figure
- The lift to drag ratio for NACA 0012 is 149.56 at 8 degree AOA and for NACA 4412 is 62.44 at 10 degree angle of attack

REFERENCES

[1] Ravi.H.C, Madhukeshwara.N, S.Kumarappa, "Numerical Investigation Of Flow Transition For Naca-4412 Airfoil Using Computational Fluid Dynamics", International Journal of Innovative Research in Science, Engineering and Technology, Vol. 2, Issue 7, July 2013

[2] Tousif Ahmed, Mohammad Tanjin Amin, S.M. Rafiul Islam, Shabbir Ahmed, "Computational Study of Flow Around a NACA 0012 Wing Flapped at Different Flap Angles with Varying Mach Numbers", Global Journal of Researches in Engineering, Volume XIII Issue IV Version I, Year 2013

[3] Wilcox, David C, "Turbulence Modeling for CFD", Second edition, Anaheim, DCW Industries, 1998.

[4] C.G. Speziale and R. Abid and E.C. Anderson, "Critical Evaluation of Two-Equation Models for Near-Wall Turbulence", AIAA J., Vol. 30 No. 2, pp. 324-331(1992).

[5] P. M. Gresho and R. L. Lee and R. L. Sani, "On the Time-Dependent Solution of the Incompressible Navier-Stokes Equations in Two and Three Dimensions", In Recent Advances in Numerical Methods in Fluids, Pineridge Press, Swansea, U.K (1980).

[6] Eleni, Douvi C., Tsavalos I. Athanasios, and Margaris P. Dionissios. "Evaluation of the turbulence models for the simulation of the flow over a National Advisory Committee for Aeronautics (NACA) 0012 airfoil." Journal of Mechanical Engineering Research 4.3 (2012): 100-111

* Corresponding author. Tel.: +88-01713255226
E-mail address: hasanshahariar.kuet@gmail.com, rashedulhasan.047@gmail.com, mdmashud@yahoo.com

ICMIEE-PI-140403

DETERMINING CRITICAL SUCCESS INDEX FOR TQM IMPLEMENATAION A CASE STUDY OF CABLE INDUSTRY

[1*]*Farjana Nur*, [2]*N.U.I Hossain*, [3]*Mahmud Ullah*

[1*] Department of Industrial Engineering & Management, Khulna University of Engineering & Technology, Bangladesh
[2] Department of Mechanical Engineering, Khulna University of Engineering & Technology, Bangladesh
[3] Department of Mechanical Engineering, Ahsanullah University of Science & Technology, Bangladesh

ABSTRACT

Now a day, improving quality has turn into a company-wide endeavor as the escalating globalization of trade & commerce underscore the inevitability of incessant enhancement. Total quality management (TQM), is one of the favored technique to conquer this stratum. TQM plays a vital role in improving productivity as well other developments in the arena of cable industry.This paper aims to determine critical success index for TQM implementation in Bangladesh Cable Shilpa Ltd (BCSL). With the establishment year of 1967 through joint venture of Bangladesh government & M/s Siemens Aktiengesellschaft of West Germany, Bangladesh Cable Shilpa Ltd added a new dimension in the arena of manufacturing of telecommunication cables and wires in the country. It is sited in Shiromoni industrial area, Khulna on the bank of the river Bhairab (Geographical Position: 22°54'27.86"N and 89°30'56.42"E) about 50 Kilometer north from Mongla Sea Port and 13 Kilometer north from Khulna City.

In this article, three types of research methodologies (face to face semi structured interviews, personally administrative questionnaires and observation) are followed to investigate critical success index for TQM implementation in Bangladesh Cable Shilpa Ltd, with a view to stimulating the performance and find out the main barriers to implement TQM successfully in this field.

Keywords: *Total Quality Management, Critical Success Index, Bangladesh Cable Shilpa Ltd, Benchmark*

1.0 Introduction

Total Quality Management is a management approach that originated in the 1950's and in 1970s, competition based on quality has grown in importance and has generated tremendous interest, concern, and enthusiasm & became steadily popular in early 1980's. Total Quality is a description of the culture, attitude and organization of a company that strives to provide customers with products and services that satisfy their needs. The culture requires quality in all aspects of the company's operations, with processes being done right the first time and defects and waste eradicated from operations. [1]

Therefore most organization possess an endeavor to appease their customer demand and expectation. This can only be attained through customer focus, incessant improvement and benchmarking. So,TQM is the focus on identifying root causes of quality problems and correcting them at the source, as opposed to inspecting the product after it has been made. Not only does TQM encompass the entire organization, but it stresses that quality is customer driven. TQM attempts to embed quality in every aspect of the organization. It is concerned with technical aspects of quality as well as the involvement of people in quality, such as customers, company employees, and suppliers.[2]

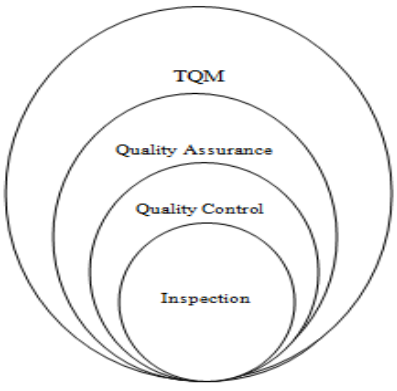

Fig1. Evolution of TQM

Corresponding Email:farjana.mitu08@gmail.com

Implementing total quality management requires broad and sweeping changes throughout a company. It also affects all other decisions within operations management. The decision to implement total quality management concepts throughout the company is strategic in nature. It sets the direction for the firm and the level of commitment. For example, some companies may choose to directly compete on quality, whereas others may just want to be as good as the competition. It is operations strategy that then dictates how all other areas of operations management will support this commitment. Also, supply chain management is affected as our commitment to quality translates into partnering with suppliers. As you can see, virtually every aspect of the operations function must change to support the commitment toward total quality management.[2]

Bangladesh economy is dominated by a diversified private sector, along with sidestate-owned enterprises. The Bangladesh textile industry is one of the largest in the world, employing 13 million people and generating over $25 billion in foreign exchange. Other major exports include medicine, software, seafood, leather goods, ceramics, electronics and ships. There are reserves of natural gas and coal, with further exploration planned in the Bay of Bengal. Agriculture holds a crucial position in the economy and employs most of the country's workforce.

However, Cables industry is one of emerging sectors contributing a significant role to develop the economy of Bangladesh. .To ensure maximum utilization of energy this industry produces cables in domestic and industrial arena.

Bangladesh Cable Shilpa Ltd produces different types of cables with Foam-skin insulation, Cellular Polyethylene and Polyvinyl Chloride insulation and PE/PVC sheathed cables for telecommunication. In addition, this company also manufactured other specifications of cables as per customer demand which is very rare.

2.0 Critical Success Index for TQM

Critical success Index(which is also known as critical success factors) is the term for an element that is necessary for an organization or project to achieve its mission. It is a critical factor or activity required for ensuring the success of a company or an organization. TQM CSFs have a positive impact on the operational performance i,e TQM firms perform better in contrast to non-TQM firms in operational performance such as improving delivery performance, reduction in production costs, increasing productivity, improving flexibility, reducing scrap and improving the quality of products. And the term key success factor can be used in four different ways:

a) as a necessary heuristic tool for managers to sharpen their thinking.

b) as a necessary ingredient in management information system.

c) as a description of the major skills and resources required to be successful in market.

d) as a unique characteristics of a company.

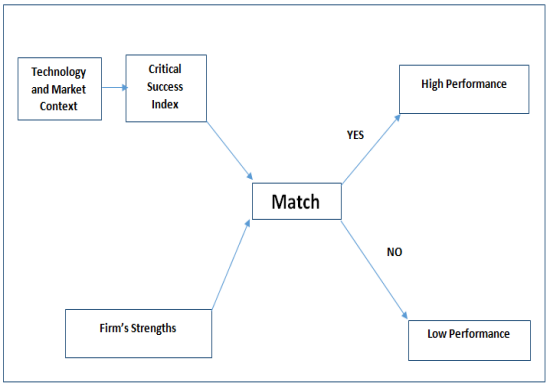

Fig 2. The shared experiences view on key success factors (From Sousa de Vasconcellos & Hambrick;1989)

3.0 Research Methodologies

In this study, three process are followed to accumulate the data; a) Face to face semi structured interview (Qualitative research methods), b) questionnaires (Quantitative research methods) and c) observation. The interview method is mainly used to support the finding while questionnaires aimed to identify critical success index of TQM implementation in BCSL and finally observation process is use to compare between these two methods.

Face to face interviews were conducted with the key persons of different departments of BCSL to find out the issues that are related to TQM implementation and recent struggle of this industry.

Questionnaires often seem a logical and easy option as a way of collecting information from people. They are actually rather difficult to design and because of the frequency of their use in all contexts. However, 55 personally administrative questionnaires were

Corresponding Email:farjana.mitu08@gmail.com

distributed among the targeted workforce of BCSL. The questionnaires includes 23 statements to identify the critical success index and possess five point likert scale (strongly disagree, disagree, impartial, agree, strongly agree). All the statements of the questionnaires are made by discussing with four TQM specialists. And SAP Lumira software & Zoho Sheet program were used to analysis the data.

Table 1. Five point likert scale

Criteria	Point
Strongly disagree	1
Disagree	2
Impartial	3
Agree	4
Strongly agree	5

Where,

3< implies overall disagreement with the statement
Average = (1+2+3+4+5)/5=3
3> implies overall agreement with the statement

Finally, observation was taken place to make compare among the aggregated data of two previous methods.

4.0 Findings of Critical Success Index

The factors of the survey can be carved up into two ways:

1. Individual level factor
2. Group level factor

4.1 Individual level factors

- Proper vision & plan (factor A)
- Dynamic leadership (factor B)
- Motivation (factor C)
- Production of diversified product (factor D)
- Education & training (empowerment) (factor E)
- Employee fulfillment (recognition & reward) (factor F)
- Improvement of tools & technique (factor G)
- Quality data report (measurement & feedback) (factor H)
- Development of human resource department (factor I)
- Customer focus & supplier management (factor J)
- Proper Government support (factor K)

4.2 Group level factors

- Strong group cohesiveness (factor L)
- Strong level of cooperation among the workforce (factor M)

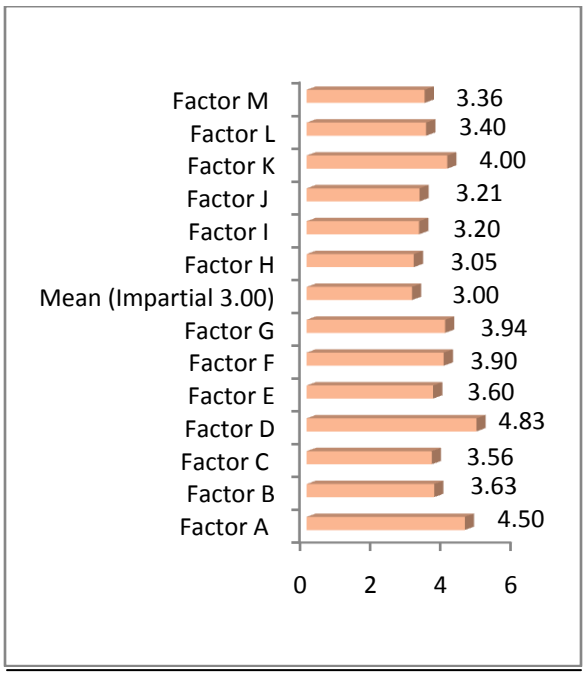

Fig 3. Critical success factor of BCSL

5.0 Hindrance to TQM implementation

The major barriers are:

- Lack of proper strategic planning & vision
- Government bureaucracy
- Rapid increase of demand of supplementary products (mobile phone)

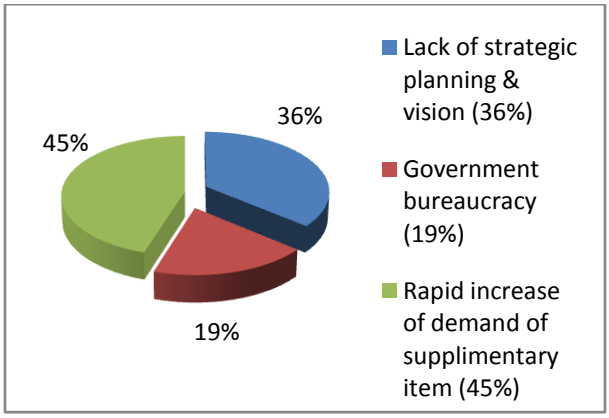

Fig 4. Major barriers to TQM implementation (% wise)

Corresponding Email:farjana.mitu08@gmail.com

It is evident from the above figure that lack of proper strategic planning and vision is the one of the barriers to TQM implementation. Therefore, a detailed long term planning and vision should be stated clearly to implement TQM tools and technique in this cable industry.

Government bureaucracy should be minimized as much as possible for the sake of proper execution of TQM tools.

Due to advent and popularity of mobile phones, now a day public often feel reluctant to use land telephones. Therefore the demand of telecommunication wires falls rapidly. So, government should take some initiatives and launch some package or program to make this popular among the mass people.

6.0 Conclusion:

As long as this is the first survey to investigate TQM execution in the field of cable industry in Bangladesh and within a short period of time 13 success factors & 3 major barriers are found to execute this issue. Therefore further detailed and well directed researches & analysis are suggested to find the factors to implement the TQM and upgrade the overall performance of the industry.

Reference

[1].UK. Department of Business Innovation and Skills,.2009
[2].Critical success factors for total quality management implementation within the libyan iron and steel company by massoud m. arshida &syed omar agil.
[3].Edward Sallis, Total Quality Management in Education, (Tidball , UK, 1993) , p.26
[4].Karuppusami, G., & Gandhinathan, R. (2006). Pareto analysis of critical success factors of total quality management: A literature review and analysis. *The TQM Magazine*, *18*(4), 372-385.
[5].Chapman, R., & Al-Khawaldeh, K. (2002). TQM and labour productivity in Jordanian industrial companies. *The TQM Magazine*, *14*(4), 248-262.
[6].Al-Khalifa, K. N., & Aspinwall, E. M. (2000). The development of total quality management in Qatar. *The TQM Magazine*, *12*(3), 194-204.
[7]. Critical success factors for TQM implementation and their impact on performance of SMEs by Salaheldin Ismail Salaheldin
[8]. Vouzas, F. K., & Gotzamani, K. D. (2005). Best practices of selected Greek organizations on their road to business excellence: the contribution of the new ISO 9000: 2000 series of standards. The TQM Magazine, 17(3), 259-266.
[9].Baidoun, S. (2004). The implementation of TQM philosophy in Palestinian organization: a proposed non-prescriptive generic framework. The TQM Magazine, 16(3), 174-185.
[10].Fotopoulos, C. B., & Psomas, E. L. (2009). The impact of "soft" and "hard" TQM elements on quality management results. International Journal of Quality & Reliability Management, 26(2), 150-163.
[11].Hokoma, R. A., Khan, M. K., & Hussain, K. (2010). The present status of quality and manufacturing management techniques and philosophies within the Libyan iron and steel industry. The TQM Journal, 22(2), 209-221.
[12].Idris, M. A., & Zairi, M. (2006). Sustaining TQM: a synthesis of literature and proposed research framework. Total Quality Management and Business Excellence, 17(9), 1245-1260.

Corresponding Email:farjana.mitu08@gmail.com

ICMIEE-PI-140413

Design and Construction of a Digital Anemometer

Niaz Ahmad[1], Hari Krishna Kumar Sah[1], Md. Saddam Hossain[1], Mohammad Ariful Islam[2]
[1] Undergraduate Student, Department of Mechanical Engineering,
Khulna University of Engineering & Technology, Khulna-9203, BANGLADESH
[2] Professor, Department of Mechanical Engineering,
Khulna University of Engineering & Technology, Khulna-9203, BANGLADESH

ABSTRACT
Anemometer is a measuring device used for measuring wind speed. Since the beginning of its invention, it has been modified several times. Many types of new generation of Anemometers are available nowadays. But these anemometers complicated and very high in price. Our objective was to develop an anemometer of simple design and construction with ease of use. In this paper, design, construction and testing of a three cup anemometer has been described. A three cup anemometer was designed as three cup anemometers are simpler and yet has less errors. Microcontroller was used to make it digitalized. It was tasted with a standard anemometer to perform necessary calibration. After calibration, it was tested again on various wind speeds and the errors were found to be 3.04% and the minimum air that it can measure is 3km/hour.

Keywords: Wind Speed, Anemometer, Digital anemometer, microcontroller, cup anemometer.

1. Introduction

An anemometer is a device used for measuring wind speed, and is a common weather station instrument. The term is derived from the Greek word ''*anemos"*, meaning wind, and is used to describe any airspeed measurement instrument used in meteorology or aerodynamics. It was first invented by Leon Battista Alberti around 1450 [1]. Anemometers are commonly used in weather recording and forecasting. It is also used in mines, tunnels and ventilation systems; in aircraft testing and other experimental work; and in aerial navigation. Sailors also use the anemometer as wind speed is a great factor on sea. Different kinds of anemometers are present now. But among all those types of anemometer, it is best to use a three cup anemometer as it has less error than a four cup anemometer, it does need to face the wind and no need to give any additional effort or parts to make sure that it faces the wind continuously as the wind from any direction will force the cups to rotate and an angular acceleration will be created.

Modern anemometers are too much costly to purchase. Objective of this project is mainly developing an anemometer with better calibration and better performance which will give instant and continuous results digitally. By using a digital anemometer, time can be consumed, data can be stored for further uses and a better understanding of weather can be gained. So, design and use of a three cup digital anemometer is very useful and cost effective in perspectives of our country.

The objectives of this project are to:

a) Design a three cup anemometer.
b) Construct a three cup anemometer.
c) Testing and improving the anemometer.

2. Literature Review

2.1 Working Procedure

When the anemometer faces the wind, concave surfaces of the cup create more resistance than it's convex surfaces and hence an unbalanced moment is produced which causes rotational motion with respect to its center axis. Under steady flow condition, the rotational speed of the anemometer is directly related to the wind speed.

One of the fan blades have tiny magnets mounted on it and each time when the arms make a single rotation, the magnet move past a magnetic detector called a reed switch. When the magnet is nearby, the reed switch closes and generates a brief pulse of electric current, before opening again when the magnet goes away. This kind of anemometer effectively makes a series of electric pulses at a rate that is proportional to the wind speed. Counting how often the pulses come in and the wind speed can be measured from that.

* Corresponding author. Tel.: +88-01677413281
E-mail address: niazahmad065@gmail.com

2.2 Magnetic Sensor

Magnetic sensors are most commonly used nowadays. When brought into a magnetic field the reeds, which are ferromagnetic will close, creating a switching function. The orientation and direction of the permanent magnet determine when and how many times the switch will open and close.

When a magnetic force is generated parallel to the reed switch, the reeds become flux carriers in the magnetic circuit. The overlapping ends of the reeds become opposite magnetic poles, which attract each other. If the magnetic force between the poles is strong enough to overcome the restoring force of the reeds, the reeds will be drawn together [1].

Figure 2.1: Magnetic Reed Switch [1]

2.3 Arduino Board

Arduino board is a microcontroller embedded control system. In general an arduino board has a microcontroller, external power supply, usb interface, reset button, power led, digital and analog pins, I2C, ICSP Header embedded on it [3].

Figure 2.4: Arduino Board (UNO)

Arduino started in 2005 as a project for students at the Interaction Design Institute Ivrea in Ivrea, Italy. At that time program students used a "BASIC Stamp" at a cost of $100, considered expensive for students. Massimo Banzi, one of the founders, taught at Ivrea [1].

A hardware thesis was contributed for a wiring design by Colombian student Hernando Barragan. After the wiring platform was complete, researchers worked to make it lighter, less expensive, and available to the open source community. The school eventually closed down, so these researchers, one of them David Cuartielles, promoted the idea [1].

There are different types of Arduino board. Such as Arduino Diecimila, Arduino Duemilanove, Arduino UNO, Arduino Leonardo, Arduino Mega, Arduino Nano, LilyPad Arduino [3].

2.3.1 Features of Arduino

- It has an ATmega328 microcontroller integrated with it.
- It's operating voltage is 5V. Recommended input voltage for Arduino is 7V to 12V. It's highest limit is 20V.
- It has 14 digital I/O pins (Of which 6 provide PWM output).
- It has 6 analog input pins
- It has a flash memory of 32 KB of which 0.5 KB is used for boot loader.
- It has a clock speed of 16 MHz
- It has SCRAM of 2 KB.
- It has EEPROM of 1 KB.

3. Design and Construction

Among the different types of anemometers that are discussed before in this report, a three cup anemometer was chosen for this project. The reasons for choosing a three cup anemometer are as followed:

- It has less error than a four cup anemometer [1].
- Its construction is simple than others.
- It does not need to manually faced to the wind or to add any other medium to do this job like vane anemometer. It can give reading from any direction of the wind.
- It is cheaper than other anemometers like Hot Wire type or Laser Doppler type anemometer.

As for the above cases, designing a three cup anemometer and making it digital is more effective.

3.1 Design Assumptions

The anemometer was designed based on the above stated design assumptions.

- The design was based on appropriate sensing of wind flow.
- Designed is assumed to work under a sufficient range of wind velocity. The range was assumed to be from 2 km/hour to 35 km / hour.
- Inertia and frictional loss is assumed to be minimum.
- Torque produced by the minimum wind force is assumed to overcome the inertia of the body.
- Full contact of air to the cups was assumed.

3.2 Construction

Construction was completed regarding the assumptions. First the mechanical part of the connection was completed, then the electrical parts were connected to the anemometer and then the code was prepared to obtain desired result.

Fig.3.1 Constructed Anemometer

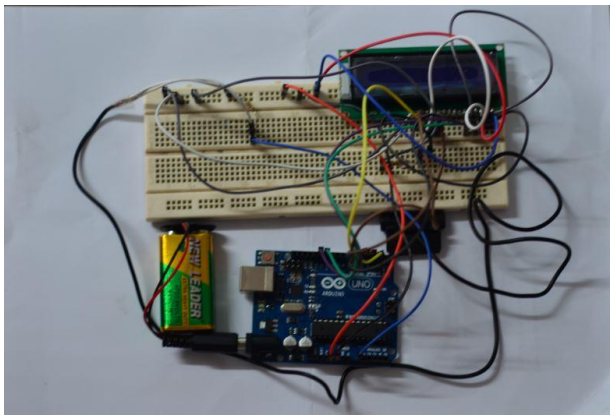

Fig.3.2 Circuit Of the calculation unit

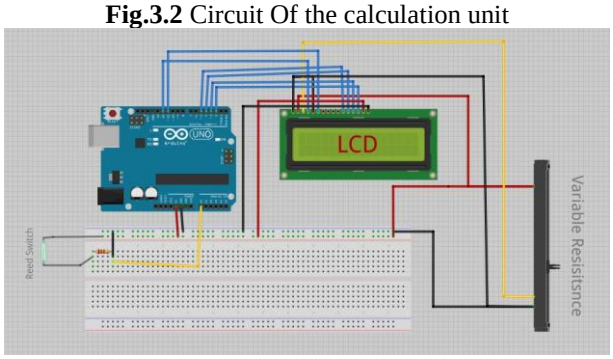

Fig.3.3 Circuit Diagram of Microcontroller Unit

3.3 Code Development

Code for the microcontroller was developed using Arduino IDE. Code for the microcontroller unit is given below:

```
#include <LiquidCrystal.h> // Including Library For LCD
// Variables to Display on LCD Screen
LiquidCrystal lcd(12, 11, 5, 4, 3, 2);
//Magnatic contact Sonsor pin diclaration
int reedPin = 0;    //analog input, but could also be digital

// Other variables to calculate speed and read time
float wheelDiameter = 37;   // THE DIA OF WHEEL IN CENTIMETER(CM)
float wheelC = 3.14 * wheelDiameter;
int circleNum = 0;
int Time=0;
float RPM=0;
float speedometer = 0;
float MPH = 0;
float KPH = 0;
float km=0;
int reedTime;
int reedTimeDelta;
boolean reedOn = false;
```

```
// Setting the pins input and output and setting the LCD
void setup(){
  // set up the LCD's number of columns and rows:
  lcd.begin(16, 2);
  // Print a message to the LCD.

  Serial.begin(9600);//Starting the serial monitor
  reedTime = millis();
}

// Main working function or main loop
void loop(){
  checkReed(); // Calling the checkReed Function
  getSpeed(); // Calling the getSpeed Function
   //RPM=km/(2*3.1416*18.5);
  //Printing Speed in Kilometer per hour
    lcd.setCursor(0, 0);
    lcd.print("KPH: ");
    lcd.setCursor(5, 0);
    lcd.print(km,2);
  //Printing no of revolution
    lcd.setCursor(0, 1);
    lcd.print("RPM:");
    lcd.setCursor(5, 1);
    lcd.print(RPM,2);
    }
// The checkReed Function
void checkReed(){
  //int Time=0;
  Time = millis()/1000;

  int r = analogRead(reedPin);
  if(r > 10 && reedOn == false){
    reedOn = true;
    reedTimeDelta = millis() - reedTime;
    reedTime = millis();
    circleNum++;


   //prints all metrics when magnet passes switch
    printAll();
  }

  else if (r < 10 && reedOn){
    reedOn = false;
  }
}

//Speed Caculation Function
void getSpeed(){
  speedometer = wheelC/reedTimeDelta;
  MPH = speedometer * 22.369;
  KPH = speedometer * 36;
  km=1.8*pow(KPH,1.063);
  RPM= 14.348*KPH;

}

// Printing the values on serial monitor Function
void printAll(){
  Serial.print("KPH: ");
  Serial.println(km, 2);
  Serial.print("MPH: ");
  Serial.println(KPH, 2);
}
```

4. Performance Test of Anemometer

To check the efficiency of the constructed anemometer, we checked its performance with a standard and calibrated anemometer on different wind speed.

Table 4.1:- Data taken from the experimental setup.

No. of Observation	Value from Standard Anemometer (KM/ Hour)	Value From Constructed Anemometer (KM/ Hour)
01	4.4	2.32
02	5.8	2.63
03	6.3	3.11
04	6.7	3.5
05	7.3	3.85
06	8.5	4.19
07	9.5	4.35
08	9.7	4.66
09	10.6	5.41
10	11.5	5.89
11	12.5	5.97
12	13.5	6.46
13	17.5	8.3
14	19.5	8.45

From the above data, a standard vs constructed graph was plotted and relation was determined.

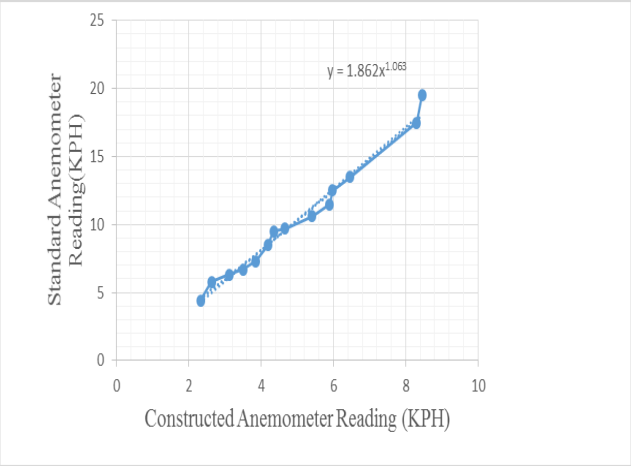

Figure 4.1: Value from standard anemometer vs Value from constructed anemometer

From the above graph, the best fit curve was drawn and the best suited curve was the power series. The Equation of the of the relation between the Actual value and the given value by the constructed anemometer is,

$$y = 1.862x^{1.063}$$

Here,
y= standard anemometer reading
x= constructed anemometer reading
After calibration, anemometer was tasted again with the actual value. Data of the test are given below:

Table 4.2: Data taken after calibration

No. of Observation	Value from Standard Anemometer (KM/ Hour)	Value From Constructed Anemometer (KM/ Hour)
01	23.2	22.85
02	18.55	18.4
03	16.90	17.4
04	14.46	14.9
05	12.55	12.7
06	11.33	11.6

From the above data, a graph of standard anemometer vs constructed anemometer was plotted:

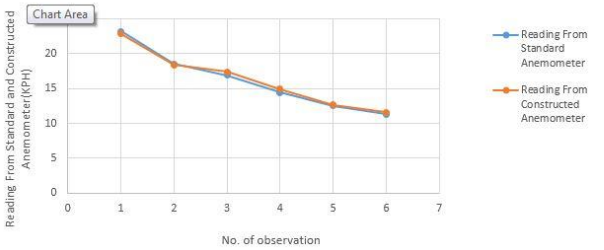

Figure 4.2: Reading from standard and constructed anemometer vs no. of observation

Above graph can be used to calculate the final error and the obtained graph showed that after calibration, the constructed Anemometer gives almost the same reading with the standard Anemometer.

From the above calculated data and graph, error was calculated by the following formula:

$$Error = \frac{SAR - CAR}{SAR} \times 100\%$$

Here,
SAR= Standard Anemometer Reading
CAR= Constructed Anemometer Reading

By using the above formula, error was calculated for each set of data and summing and by calculating the average value of errors, the average error was found to be 1.7732%(+ or -), maximum error was 3.04% and the minimum error was .8% .

6 Conclusion

An anemometer is an essential part weather forecasting. Wind speed can give certain information of weather which are necessary in the field of aviation, shipping, agricultural field and many more industrial and experimental works. On the basis of design assumption and keeping in mind the objectives of the design, a three cup digital anemometer was constructed. It was tested with other ideal instruments and further evaluation and calibration was done to lessen the error. After calibration, the anemometer was again tested and the results were compared. An average error of more or less 1.7732% was found. The maximum error was found about -3.04% and the minimum error was .8%. The anemometer does not give a reading if the wind velocity is less than about 3 KM/Hour.

Recommendation

- Better use of material which are a bit costly but will give a better result.
- Additional parts can be added to determine the wind direction also.
- Sensor can be added to the cups to determine the Humidity of the wind.
- A memory card can be added to the Arduino board in order to store the data.

REFFARANCE

[1] http://www.en.wikipedia.org
[2] http://www.explainthatstuff.com
[3] http://www.arduino.cc
[4] http://www.engineersgarage.com
[5] http://www.azosensors.com
[6] http://www.sparkfun.com

ICMIEE-PI-140419

ANALYSIS OF SUPPLY CHAIN EFFICIENCY AND SUGGESTIONS FOR IMPROVEMENT, A CASE STUDY

[1]Md. Rezaul Karim, AKM Sarower Kabir, Md. Aslam Khan, Md. Minul Ehsan And S.K.Biswas[2]
[1] Graduates of Department of Mechanical and Production Engineering, Ahsanullah University of Science & Technology, (AUST), Dhaka, Bangladesh
[2] Professor, MPE (Mechanical & Production Engineering) Dept., AUST, Dhaka, Bangladesh

ABSTRACT
The supply chain is the connected series of activities, in relation to any production or service organization, which is concerned with planning, coordinating and controlling of materials, parts and finished goods from supplier to customer. Supply chain efficiencies have been the central theme of focus in any organization in designing and implementing supply networks. In this paper, we tried to improve the efficiency of supply chain of a local furniture industry, on the basis of highest moving and lowest moving product. A number of key findings were found, like the deficiency in the logistics system, which in our opinion played an important role in supply chain analysis. Study was made by PARETO analysis, time study and demand forecasting. We found the relationship between productivity and other measures of performances by analyzing Pareto chart with other methods. Experimental verification of efficiency in terms of logistic, demand forecasting and time study were also made. Finally we came to the conclusion that the companies that manage the supply chain as a single entity and ensure the appropriate use of tools and techniques in order to meet the need of the market, will not be left behind in the fight for survival. We think the findings will be helpful to the management of the company.

Keywords: Supply Chain Management, Logistics, Pareto Analysis, Time study, Forecasting

1. Introduction[1][3],[12] and [13]

Considering the importance of supply chain in an industry, we decided to apply our theoretical knowledge of supply chain to practical problems. As a part of the case study we selected RFL Furniture Ltd at Rupganj, Narayanganj. We decided to analyze the supply chain of the RFL furniture by using various related tools with a view to solving, prioritizing problems regarding supply chain distribution centers, evaluating supply chain efficiency etc. Our main objectives were: studying and analyzing the existing supply chain scenario of 'Regal furniture (RFL) Limited' and suggesting optimum solution in terms of efficiency, conducting a time study for most moving item of RFL (Regal) furniture so that standard time of producing the items can be identified. We also tried to create a relationship between customer demand and production planning by calculating demand forecasting.

2. Problem analysis [1], [2], [3] and [11]

In the following major areas, we gave relatively more attention to analyze the supply chain of RFL furniture in particular and we especially found some problems in the following areas after initial checking and verification. Major problem areas as found by us were as follows:

- Logistics
- Storage
- Production
- Maintenance
- Customers' satisfaction

By analyzing the Pareto chart, we have observed that most significant problems have been created by logistics area which leads us to scrutinize the efficiency in terms of average logistics index. Through this analysis we suggested an improvement of efficiency. Next area was customers' voice. Customers have been complaining of not getting their product in time due to varieties of different issues which encouraged us to conduct a time study for the most moving item of RFL furniture to have a look at the difference between the standard time and total cycle time.

2.1 Calculation of Supply Chain Efficiency [10], [6] and [1]

Index for measuring supply chain efficiency is given in reference [10] and may be expressed by:

$$Al_i = PE_i\,(1\text{-}SCC_i) \qquad \ldots\ldots\ldots\ldots \qquad (1)$$

Where,
Al_i = Average logistics Index
PE_i = Performance external Index
SCC_i = Supply chain cost Index
SCC_i= Total SCC/Net Sales.

Contact Adresses: tel. : +88-01817-746070, +88-01838-261758
E-mail: skbaust@yahoo.com, skbiswas.mpe@aust.edu, skbcuet@yahoo.com

Some costs related to supply chain have been stated below which were collected from the RFL officials at the plant site:

Supply Chain Costs [7] include,

Manufacturing cost = BDT 6800 per single unit

(The basis for this was: Sales of wardrobe in BDT)

In the following calculations, basis was considered as selling of 50 units of wardrobe per month with average cost of BDT5000/ unit:

Administration Cost = 4% of sales
= 4% of (50×5000)
= BDT 10000

Warehouse Cost = 8% of sales
= 8% of (50×5000)
= BDT 20000

Distribution Cost = 4% of sales
= 4% of (50×5000)
= BDT 10000

Capital Cost = 14.5% of sales
= 14.5% of (50×5000)
= BDT 36250

Ordering Cost = 6% of sales
= 6% of (50×5000)
= BDT 15000

Therefore ***total*** Supply Chain Cost for 50 numbers of item becomes = 10000+20000+10000+36250+15000
= BDT 91250

Therefore we get: $SCC_i = 91250/(50\times5000) = 0.365$

Therefore, Al_i becomes = $PE_i(1-SCC_i)$ …… (1)
$= 0.48(1-0.365) = 0.3048$

Where, $PE_i = DP_i \times LT_i \times CS_i$ …….. (2)

Where,

DP_i = Delivery Precision Index

CS_i = Customer Satisfaction Index

LT_i = Lead Time index

Therefore PE_i becomes = $DP_i \times LT_i \times CS_i$ …… (3)
$= 0.8 \times 3 \times (8/40) = 0.48$

The basis of the values considered in the above equation was as follows:

DP_i has was taken as 0.8 because we found out from the customer that 80 delivery out of 100 reached on time, so

$DP_i = 80/100 = 0.8$

LT_i was considered as 3 days: by consulting with the authorities of the RFL about the lead time, and

CS_i value was considered by conducting a survey; we asked different questions related to their satisfaction. 8 out of 40 customer gave positive feedback about the products, so CS_i index was taken as (8/40) = 0.2

Therefore as per calculation shown in (1) above existing Supply chain efficiency becomes 30.48 %, which can be considered low compared to standard efficiency in an industry. The authors think that the company might get benefit if this can be improved.

Thus our suggestions for improving the efficiency have been mentioned in discussion & in conclusion.

2.2 Time study of wardrobe [11], [14] and [12]

Time study was done on Auto panel saw, Sliding Saw, straight edging machine, CNC machine and boring machine for making different parts of making wardrobe. We conducted time study for all of the mentioned machines. Sample calculations have been shown for only two machines

Auto Panel saw:

Time taken in each machine for making the related part of a wardrobe was mentioned. Calculation was done following the basic theory of normal time and standard time calculation:

Normal time = Total operating Time × performance rating
= 37.5 hour × 0.70
= 1575 minutes

We calculated allowance factor like that mentioned in the following [11]. And actual time was found by observing time using stop watch.

- Allowance Factor = Unavoidable delay + avoidable delay + machine allowance
= 70+25+70
= 165 minutes which is approximately 7.5 % of actual operating time.

So, Allowance Factor becomes = 7.5%
= 7.5/100 = 0.075

And thus the Standard time becomes =

Normal Time × 1/(1-Allowance factor)
= 1575× (1/1-0.075)
= 17032.70 minutes
= 28.37 hours (Approx.)

**** Consulting with the management level officials of RFL Ltd. and by observing the workers while producing the product performance rating has been taken as 70%*

b) For sliding saw:

Like that in (a) for (b) Sliding Saw similar type of calculations were mentioned below:

- Normal time = Total operating Time × performance rating
= 1374.6×0.70
= 962.22 minutes

- Allowance Factor = unavoidable delay + avoidable delay + machine allowance
  = 51+23+5
  = 79 minutes which is approximately 5.7 % of operating time

  So, Allowance Factor in this case becomes = 5.7 % = 5.7/100 = 0.057

- Therefore, standard Time for (b) becomes =

  Normal Time × (1/1-%Allowance factor)
  = 962.22×(1/1-0.057)
  = 1020.38 minutes
  = 17 hours (approx.)

Similarly primary data was also taken for straight edging machine, CNC machine and boring machine.

Total Operating Time for 5 machines as mentioned above for making ***one wardrobe*** was =

37.5+22.91+16.25+21.5+8+24.16 = 130.3 hour = 5.43 days
And thus standard time becomes= 28.37+17+13.39 +15.92 +7.96 +18.38 = 101.02 hour = 4.2 days

The Company uses 120 units to make a lot.
Therefore, total delay time for lot of 120 units becomes (Operating time - Standard time ***)***
= (5.43 – 4.2)days/lot
= 0.23 days/lot
= 0.010 day/unit
= 0.246 hours / unit
= 14.76 min/unit
Pl check the above calculation for delay/unit or per lot?

Our suggestions for improvement have been mentioned in discussion & conclusion separately.

2.3 Forecasting for the sales of wardrobe [12], [3]

With a view to improve supply chain responsiveness, the gap between demand and supply needs to be reduced, by ensuring availability of the product at optimum cost, customer satisfaction can be increased. We have applied weighted moving average method and exponential smoothing method to find out forecasted sales value of wardrobe.

(a) By weighted Moving average method

Calculation for moving average method has been given as follows:

Table 2.3 (a) for weighted moving average method

Month	Actual Sales	Forecasted value
May	9	Forecast could not be found as data for April was not known
June	25	9×0.33+9×0.67=9
July	33	9×0.33+25×0.67=19.72
August	Not known	25×0.33+33×0.67=30.36

Considering weights as:
Latest month's weight= 0.67
Other month's weight=0.33

So, using above method we found forecast for July = 19.72 and that for august = 30.36. It may be mentioned that Actual sales value from RFL for April and August could not be obtained. Hence Forecasted value of May too could not be calculated.

Mean absolute deviation (MAD) has been calculated by the following relation:
MAD = summation of respective absolute values of (actual –forecasted value) / Total no. of observations

b) By Exponential Smoothing Method

Exponential smoothing method=
New forecast F_t = previous month's forecast+ smoothing constant (Actual forecast-previous forecast)

The objective is to obtain the most accurate forecast no matter the technique used:

As we know, for industrial purpose smoothing constant α in the range of 0.2-0.7 is generally used. In the following table 2.3 (b) we have considered only three values of smoothing constant α = 0.2, 0.3 and 0.5. We found out that the value of α for which MAD is minimum is by using an alpha of 0.50. Although we ended up with the lowest MAD by using the only three values of constant = α, forecasts might be more reliable using other values of alpha and also considering other related variables.

But for this particular case of forecast of RFL α = 0.5 should be used by the RFL authorities.

Table 2.3 (b) for exponential smoothing method

Month		Forecasted sales		
	Actual sales	α = 0.2	α = 0.3	α = 0.5
May	9	9	9	9
June	25	9	9	9
July	33	26.06	26.58	27.64
August	Not known	33.53	33.79	34.32
Mean Absolute Deviation		7.65	7.47	7.12

For α = 0.5 MAD is minimum

Example of sample calculation:

(i) Forecast for July for smoothing constant α = 0.2
25+ 0.2(25-19.72) = 26.06

(ii) Example for MAD calculation for α = 0.3:
[(9-9) + (25-9) + (33-26.58)] / 3 = 7.47

(c) Exponential smoothing trend adjustment method

T_t = (1-β) × previous month's trend + β × (Present Forecast value- Previous Forecast value)
Adjusted forecast with trend = Forecast without trend + T_t.

β = 0.4 was used in this paper to reduce the impact of the trend error occurring between the actual value and forecast value as this value is usually considered as equal to 0.4 by many organizations and related authors.

The following Tables 2.3 (c) and 2.3 (d) show the calculation results only and the related graph. Sample calculation has not been shown as it is similar to that shown earlier for exponential smoothing method.

Table 2.3 (c) for exponential smoothing with trend adjustment

Month	Actual	Forecast without trend	Trend	Adjusted Forecast with trend
May	9	9	0	9
June	25	9	0	9
July	33	17	3.2	20.2
August	Could not be known.	25	5.1	30.1

Among all the methods weighted moving average method was found to give optimum result. Because among them MAD is minimum for weighted moving average method.

Table 2.3 (d) : Trend graphs for forecasting adjustment

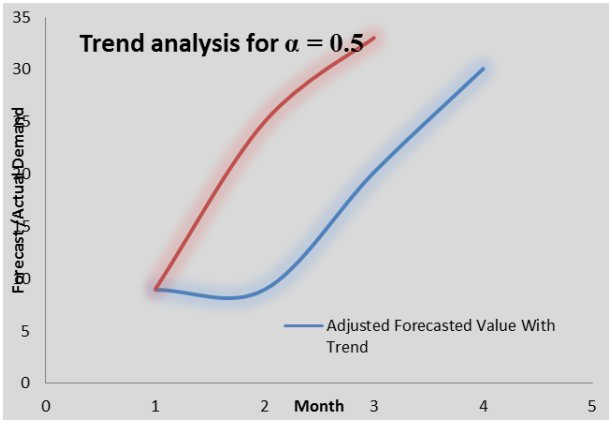

We compared the results of simple exponential forecasted values with those of trend adjusted forecasted values. But in the above figure the graph for exponential smoothing forecasting method were not shown. In the above figure the red line indicates the actual value.

3. DISCUSSION [4], [5],[8],[9]

In this study data which was taken by ourselves has been named as Primary data in the following discussion and we also used some other data provided by the company, which we call as Secondary data. In terms of data collection, secondary data was taken into consideration for sales which was applied to improve demand planning including suitable forecasting method for high moving (wardrobe) and low moving (show-case) products, smoothing constant and trend analysis,

although all sample calculations could not be shown. Time study was done using only the collected primary data by means of that we studied to find out standard time of doing operation of high moving product. Since the production schedule for show-case (low moving) was not available in the plant. Secondary data was used to measure the efficiency; later on the same was applied to determine supply chain efficiency in terms of logistics. Pareto chart, one of the basic tools of TQM has been used to identify the most significant reasons of inefficiencies. We also take into account the second most significant reasons of inefficiencies which was relevant to customers. *Our part findings and possible consequences were mentioned below***:**

Current supply chain efficiency in terms of logistics was found as not good, and this resulted in creating dissatisfaction between customers and dealers. That in turn increased overall supply chain cost.

Time study was used to determine deviation between operating time and standard time. The authors think that "Bottle Necks" in product flow processes in different machines and increments of lead time of the product (high moving), was the possible consequence of it.

Demand planning, is needed to be done to ensure actual demand forecast so that the company can satisfy customer demand otherwise profit will be cut-down by losing the customers.

Some additional findings of our work can be listed as bellow:
Due to unorganized in-process inventory, the plant is producing "bottle-necks" i.e., process is temporarily stopped for some time, in various points of product flow in the process. By reducing the amount of in-process inventory "bottle-necks" in flow process can be minimized. Proper arrangements of machine might play a vital role in eliminating bottle neck. Apart from that proper planning of material flow and daily production schedule must be done regularly, Safety measures were also found to be poor. Huge dust yielded at every machine during operation which can be considered as unhygienic for the workers as very few of them use musk and goggles. Aero-sucker might be used which in turn becomes beneficial to use for blowing dust from the production area to the outside bin. After the conversation with the workers, it was also observed that workers were found not to be much motivated to contribute in the productivity. Performance bonus, award system and granting of occasional leave along with other appropriate measures might play a vital role in motivating workers.

4. CONCLUSION [6],[4]and[3]

Supply chain starts from the procurement of raw materials to produce a particular product and ends when that product is purchased by the customer. It is a very large chain which always tries to give best efficiency with perfect responsiveness to the consumer. When we were assigned to analyze the supply chain efficiency of two particular product WAREDROBE and SHOWCASE of RFL furniture we decided to do the work by finding problems in every section of the supply chain, related with those particular products such as procurement process, transportation for procuring items, storage and quality control for both raw materials and finished goods, material handling systems for processing, distribution system for finished goods, transportation facilities for distribution, customer feedback for those products and overall production. We found overall logistics played a vital role for the supply chain efficiency. Current status of supply chain efficiency and how it can be improved has been brought to light through this research work. Dissatisfaction of customer and how it is affecting the product's penetration in the market was also found out through this work. Forecasting of customer demand would be the key for success of RFL furniture in next few years. Small but continuous improvement will be the best solution in the production planning to get the supply chain efficiency. Time study for the high moving optimum item (WAREDROBE) showed how much time should be utilized during the processing of that particular product. Proper utilization of work hour must be ensured by the company to increase the total supply chain efficiency. Safe and healthy work environment will motivate the employees for attaining the company's profitability goal. By following the best way and working hard in that technique is the key to success for the RFL furniture. We feel, if the managing authorities of RFL Company try to introduce the findings as described in this paper, we are sure the company might overcome the difficulties which is being faced now and the company might be benefited in the long run.

NOMENCLATURE

SCC	Supply Chain Cost
MRR	Material Receiving Report
LC	Letter Of Credit
DET	Double End Trimmed
JIT	Just In Time
CRM	Customer Relationship Management
CPL	Certified Professional Logistician
PLM	Product Life-Cycle Management
MRP	Material Requirement Planning
ERP	Enterprise Resource Planning
$\mathbf{SCC_i}$	Supply Chain Cost Index
$\mathbf{PE_i}$	Performance External Index
$\mathbf{AL_i}$	Average Logistic Index
CNC	Computer Numerical Control
ISO	International Standards Organizations
PR	Purchase Requisition / performance rating
$\mathbf{CS_i}$	Customer Satisfaction Index
$\mathbf{LT_i}$	Lead Time index

ACKNOWLEDGEMENT:
The authors gratefully acknowledge the contributions, suggestions, advices by RFL authorities during the study. The authors are also grateful to the AUST authorities for giving permission to work in RFL relating to final year thesis work of students.

REFERENCES

[1] Ayers, J. B. (2001). Handbook of Supply chain management, St. Lucie Press, USA, Florida.

[2] Ballou, R. H. (2004). Business logistics / Supply chain management: planning, organizing, and controlling the Supply chain (5 ed.). Pearson Prentice Hall, Upper Saddle River, N.J.

[3] Beamon, B. M. (1999). Measuring Supply chain performance. International Journal of Operations & Production Management, Vol. 19, No. 3, pp. 275-292.

[4] Bowersox, D. J. & Closs, D. J. (1996). Logistical Management – The Integrated Supply Chain Process, McGraw-Hill Companies Inc, New York.

[5] Chandra, C. and Kumar, S. (2000). Supply chain management in theory and practice: a passing fad or a fundamental change. Industrial Management Data Systems,No. 100, pp. 100-113.

[6] Chen J. (1997). Achieving maximum Supply chain efficiency. IIE Solutions, Vol. 29, pp. 30-35.

[7] Christopher, M. (1998). Logistics and Supply Chain Management: Strategies for Reducing Costs and Improving Services (2nd ed.). Pitman, London

[8] Christopher, M. & Gattorna, J. (2005). Supply chain cost management and value-based pricing. Industrial Marketing Management, Vol 34. 2, pp. 115-121

[9] Christopher, M. & Towill, D. (2000). Supply Chain migration from lean and functional to agile and customised, Supply Chain Management: An international Journal, Vol. 5, No. 4, pp. 206-213. Collin, J (2003). Selecting the right Supply Chain for a Customer in project business.
Diss. Tekniska högskolan Helsingfors. Helsingfors.

[10] Annelie Pettersson Measurements of efficiency in a Supply chain, Division of Industrial logistics, Luleå University of Technology

[11] Cooper, M. C. and L. M. Ellram (1993). Characteristics of Supply Chain Management and the Implications for Purchasing and Logistics Strategy. The International Journal of Logistics Management. Vol. 4, pp.13-24. Cooper, M.C., Lambert, D.M. & Pagh, J.D. (1997). Supply chain management: more than a new name for logistics. International Journal of Logistics Management,Vol. 8. No.1, pp.1-14.

[12] Production and operation management by J. Heizer & B. Render, Pearson Publication.

[13] Rezaul Karim, Sarower Kabir, Aslam Khan, Mainul Ehsan, " Analysis of Supply Chain Efficiency of RFL Furniture limited and provide recommendations for improvement", B.Sc. Eng. thesis submitted to the MPE Dept, AUST, in 2014.

[14] Motion and Time study by Barns

ICMIEE-PI-140420

Design and Construction of an Automatic Gas Welding System

Muhtasim Zarif Siraj , Md. Golam Kader
Department of Mechanical Engineering, Khulna University of Engineering & Technology,
Khulna - 9203, Bangladesh.

ABSTRACT
In the age of Automation, where human safety & comfort is the key concern, one of the most common sector of engineering remained unaltered and that is the Automation of gas welding, one of the most age old technology, is yet to be applied in industrial scale. Automation of welding requires the combination of electrical and mechanical system. The various parts used for automation of Oxyacetylene in-line gas welding comprise of Rack and Pinion, Bearing, Geared motor, Motor driver, Arduino board. As it is the model of actual system, the construction is made of wooden frame Two geared motors are used; one for feeding filler metal and other is for feeding the job. Both of the motors are controlled by micro-controller. The job is clamped on top of workbench and is fed in a controlled speed. The filler metal holder which is placed at 0^o with workbench along X-axis and slightly angled ($5\text{-}10^o$) with X -axis is also fed the filler rod in controlled way. The main working principle is as follows: The lighted up nozzle will be held over the job to be welded and when the metal will be heated up, filler rod will approach underneath the flame and will melt. The melted filler metal will drop on top of the heated metal and when cools down, the pieces will be joined. The output of the system is quite satisfactory which implicates the veraciousness of idea. The necessity of the system is with proper and accurate automation, the most commonly used welding technique will be safe for human health and production quality will increase.

Keywords - Automation, Rack and pinion system, Microcontroller, Motor driver, Gas Welding.

1. Introduction

The more mankind steps into the modern scientific world, the more men grasp the fruits of technology into their daily life. In the field of engineering the effect of adapting newer ways of doing work are much prominent. Welding and joining technologies are fundamental to engineering and manufacturing. Without the ability to make strong and durable connections between metals it would be impossible to produce the many different items we all rely on in our everyday lives – from the very large (buildings, pipelines, trains and bridges) to the very small (medical implants and electronic devices). Now-a-days there are numerous types of welding methods, which are used according to their purposes. But the pristine technology does not lose its interest through time. Oxyacetylene gas welding is still one of the most used gas welding process. The main reason behind that are e.g. equipment is relatively inexpensive and simple, mastering the technique requires is relatively easy to other methods, so implementing automation to this welding process would be a huge step forward.

2. Working Method

The system comprise of three parts. Methodology of accomplishing task of each system is briefly described below:

2.1 Work Bench:

Work bench is where the job is placed and clamped and it controls the welding speed. It produces reciprocating motion from the motor geared to the "Rack and Pinion" system. The speed of the motor is controlled by motor driver. A circuitry system connects the "motor driver" and "Arduino board". A program for the desired speed is uploaded to Arduino which can be powered either by AC line or USB cable connected with computer/Laptop.

2.2 Feeding Device:

The main mechanism of feeding is the use of friction. To facilitate this mechanism, the platform is made slightly angled (approx. 5^o) with horizontal. As motor is switched on and off in a controlled way, so when shaft will rotate, filler rod which already placed upon pinion, will receive feed. As double sided taped is used over the shaft, thus no slippage will occur when motor will pause.

2.3 Gas nozzle holder:

It is a platform which upholds the gas nozzle to a certain limit and facilitate fixation of nozzle at prescribed angle. It is stationary part of the system.

2.4 Block Diagram of Power Transmission

The total work flow can be summarized into two block diagram which are shown below in Fig.1. The first one is for the "Workbench" and the second one is for the "Filler metal holder".

Corresponding author. Tel: +88-01722587470
E-mail address: muhtasimzarif@gmail.com

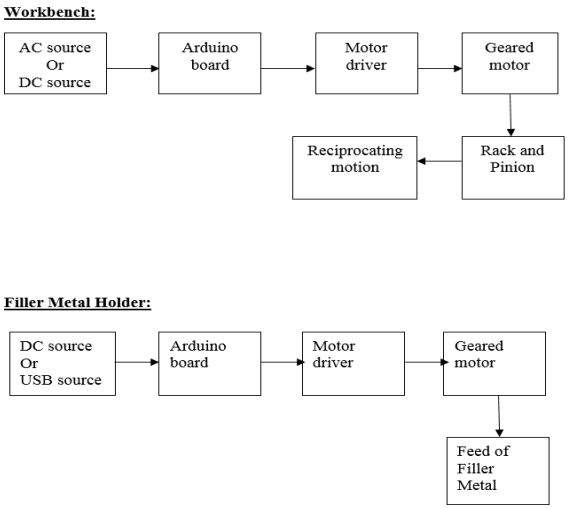

Fig. 1: Block diagram

3. Models & Solidworks Drawings:

Fig. 2: Workbench

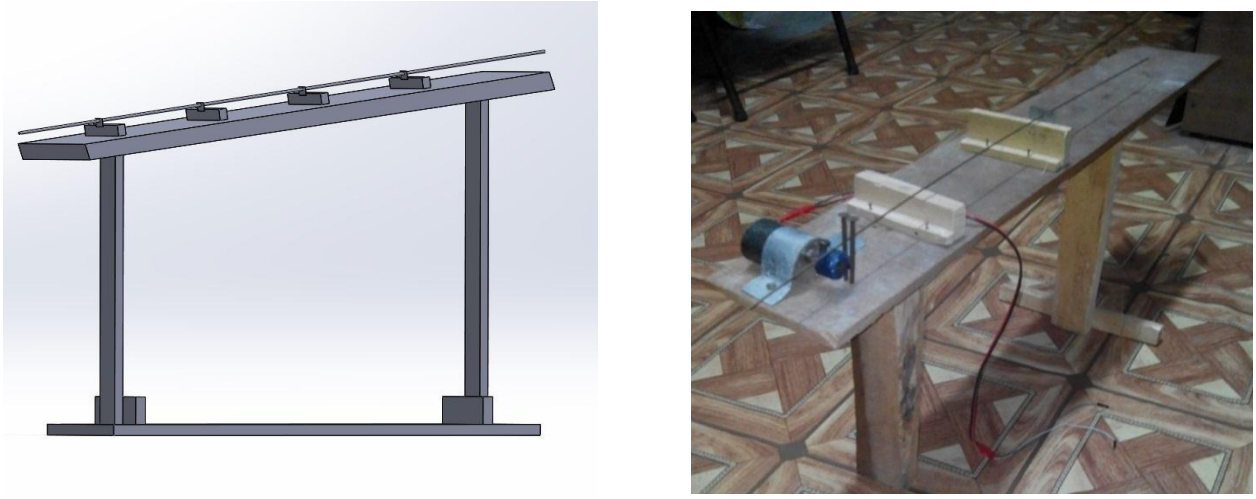

Fig. 3: Filler Metal

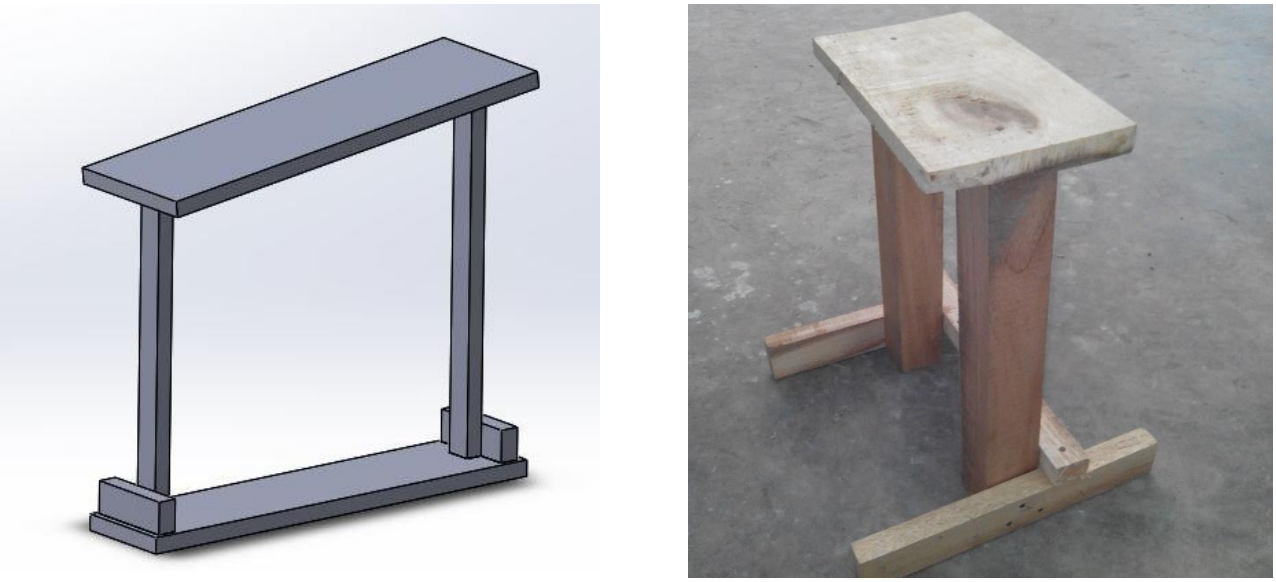

Fig. 4: Gas Nozzle

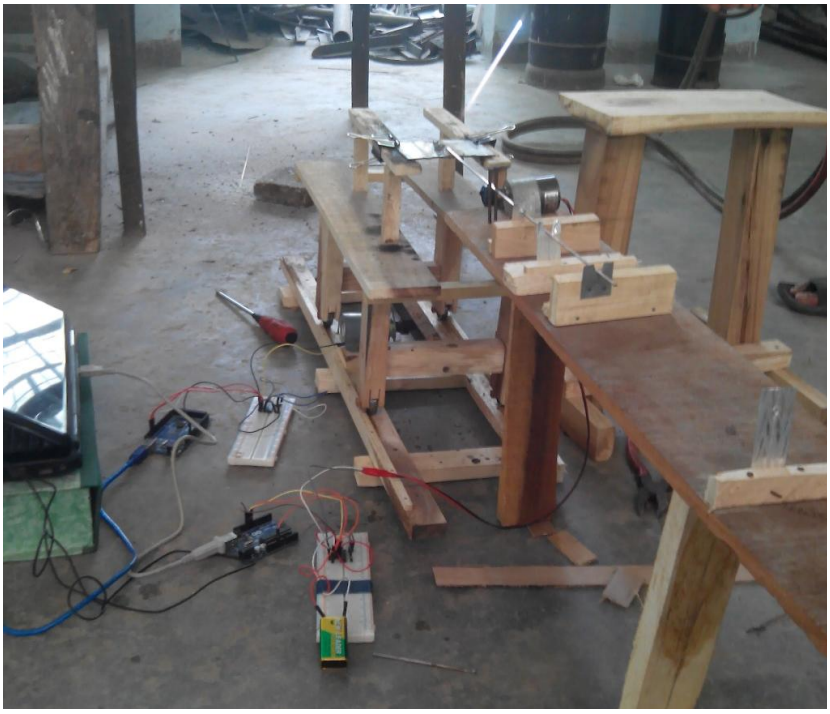

Fig. 5: The Entire System

4. Testing of System:

The workbench geared motor speed = 1.9538 mm/sec
The filler metal holder geared motor speed = 4 mm/sec
Workbench pause time = 5 sec
Workbench run time = 4 sec
Filler metal pause time = 6 sec
Filler metal run time = 2 sec
Thickness of metal = 13 gauge = 0.072 inch = 1.828 mm
Filler metal material = Brass
Tested job length = 76.2 mm
Welding Speed = 1.2 mm/sec

Fig. 6: A butt welded workpiece

5. Conclusion

The performance testing shows that, the system is quite feasible. The system proves that the idea is flawless. As there is no gauge or metering system to control the flame precisely, so various facts come into play in actual practice. The system can adequately weld two pieces of metal which satisfy the objectives of the project. The sole purpose of this project is the auto-mechanization of gas welding using the components which are being used from the very beginning. After successful completion it can be concluded that

1. All the dimensions are based on designed value.
2. Rotational speed was converted to linear motion for convenience.
3. There was no clash between teeth of Rack and Pinion.
4. Only straight line welding can be done with the model.
5. Various types of job have been tested to prove its feasibility.
6. The performance of the system is quite satisfactory for different jobs.

The modification of the system does not finished with the end of the project. The future scopes of improvement are

1. To control the flow of flame, a solenoid valve can be attached with the nozzle, which can be powered from Arduino.
2. A filler rod melting powder reservoir can be attached.
3. A frame may be created which enables different types of joints as well as Lap joint and Butt joint.
4. Modification of Filler Metal Feeding device may be done which enables holding of filler metal of different sizes and shapes.
5. Modification of filler metal feeding platform can be done which will help the vertical lift of the filler metal for proper adjustment.

REFERENCES

[1] Rao P.N., "*Manufacturing Technology – Foundry, Forming and Welding*", 2nd Edition, © 1998 Tata McGraw-Hill Publishing Company Limited, New Delhi.

[2] Doyle L.E., "*Manufacturing Processes and Materials For Engineers*", 3rd Edition, © 1985, 1969, 1961 by Prentice-Hall Inc., Englewood Cliffs, New Jersey.

[3] S.B. Chen. "*Research Evolution on Intelligent Technologies for Robotic Welding at SJTU*", Lecture Notes in Electrical Engineering, Vol. 88, RWIA'2010.

[4] Ai-min Li, "*Design of Automatic Welding Machine Based on PLC",* Intelligent Computation Technology and Automation (ICICTA), 2011 International Conference on (Volume:1), March 2011.

[5] LU Zhi-jiang. "*PLC Application in the Automatic Straight-line Welder [J]*", Occupation,2010,02(01):159.(in Chinese).

[6] Abdullah al Mamun, Roll No: 96511 and Md Moniruzzaman, Roll No: 96530, "*Construction of An Automatic Electric Arc Welding Machine*", Supervised by Mr. Md. Golam Kader, Assistant Professor, Department of Mechanical Engineering, Khulna, June 2002.

ICMIEE-PI-140422

Experimental investigation on a direct gasoline fuel injection (DGI) system with high turbulence fuel-air mixing and enhanced engine security measures

Md. Syed Ali Molla[1], Md. Shafiq Sayid[2], Md. Muhaiminul Hassan[3] & Md. Al, Mamun[3]
[1] Dept. of M. E., Khulna University of Engineering & Technology (KUET), Bangladesh
[2] Motor Walla Ltd, USA
[3] Ahsanullah University of Engineering and Technolgy
[4] M.Sc. Eng student,. BUET, Bangladesh
Email: mmsali03@yahoo.com, & pmsali@me.kuet.ac.bd , s.sayid@gmail.com, *muhaiminul7@gmail.com*

ABSTRACT

A Direct Gasoline Fuel (GDI) engine can provide fuel economy and higher engine efficiency. Harmful emissions levels can also be controlled accurately with the GDI system. These gains can be achieved by the precise control over the amount of fuel injection, proper fuel air mixing and injection timings which can be varied according to engine load and operating conditions. In addition, there are no throttling losses in some GDI engines, when compared to a conventional fuel injection system, which greatly improves efficiency, and reduces 'pumping losses' in engines without a throttle plate. The Direct Gasoline Injection (DGI) technologies have the advantages over manifold fuel injection system and port fuel injection system for maximum fuel economy, and thereby it can minimize environmental pollution at an accessible price by harnessing the DGI's inherent advantages. DGI-technologies deliver a 10~30 % improvement in fuel economy over a current other model engine, along with enhanced drivability. Though in the present model DGI system vehicles, fuel is injected at the end of compression stroke where fuel-air mixture get less opportunities of homogeneous mixing rather it burns like heterogeneous mixture like diesel engine when the tendency of formation pollution increases. Moreover high pressure injection system is required to inject gasoline fuel in compression stroke which increases the cost of fuel injection kits. But in this present research work, a different idea of direct gasoline fuel injection is used where fuel is injected in suction stroke inside the cylinder when low pressure and high turbulence prevail in air-fuel mixing. The fuel air mixture gets more opportunity of homogeneous mixing in suction and compression stroke unlike the presently used direct gasoline fuel injection system in SI engine. Thus pollution reduction potentials increases and low cost fuel injection can be used. Even TBI and PFI fuel injection kit can also be used with little or no modification. More over high coolant temperature and low oil pressure are the main causes of major failures in IC engine. This fuel injection system is designed and programmed with additional security measure to prevent engine from oil starvation and high engine coolant temperature. Thus this fuel injection system can not only reduce pollution reduction potentials and cost of fuel injection system but also it increases engine security measures.

Keywords: Direct gasoline fuel injection system (DGI), microcontroller, high turbulence, low pressure fuel injector.

1. Introduction

The construction of the carburetor is relatively simple and it has been used almost exclusively on gasoline engines in the past. However, in response to recent demands for cleaner exhaust emissions, more economical fuel consumption, and improved drivability, the carburetor now must be equipped with various compensating devices and it makes carburetor more complex. In place of carburetor, therefore, the injection system is used, assuring the proper air-fuel ratio to the cylinder by using electronic controlling devices in accordance with various driving conditions. Compared with throttle body (TBI) and port fuel injection (PFI) systems, direct gasoline injection system (DGI) is more difficult and expensive. But the payback for the added complexity is higher torque, dramatically reduced emissions and increased engine efficiency. This is possible as fuel can be injected in the exact quantity, time and location that it's demand by the engine.

Engines generate their worst emissions-just after cold-start. During warm-up of a DGI engine, a small shot of fuel is injected just before the exhaust valve opens. There's still enough heat and oxygen in the chamber for this charge to ignite, and the heat from that after burn gets the catalyst up to operating temperature just seconds after cold-start. The injectors are either open or closed, and pulsed as in a port-injection system (PFI). Since the fuel flows directly into the combustion chamber instead of impinging on the intake valve, the nozzle can be designed to form a "cloud" of fuel with a specific size and shape [1]. The DGI-technologies can deliver a 10~30 % improvement in fuel economy over a current EFI-engine, along with enhanced drivability [1]. The engine management system continually chooses among three combustion modes: ultra lean burn, stoichiometric and full power output. Each mode is characterized by the air fuel ratio. The stoichiometric air-fuel ratio for gasoline is 14.7:1 by weight (mass), but ultra lean mode can involve ratios as high as 25:1 (or even higher in some engines, for very limited periods). These mixtures are much leaner than in a

* Corresponding author. Tel.: +88-01714087350
E-mail address: mmsali03@yahoo.com : pmsali@me.kuet.ac.bd

conventional engine and reduce fuel consumption considerably [2].

The 1955 Mercedes-Benz 300SL, the first production sports car to use fuel injection, used direct injection. The Bosch fuel injectors were placed into the bores on the cylinder wall used by the spark plugs in other Mercedes-Benz six-cylinder engines (the spark plugs were relocated to the cylinder head). Later, more mainstream applications of fuel injection favored the less-expensive indirect injection methods. Toyota's D4 direct injection system first appeared on various Japanese market vehicles equipped with the SZ and NY engines [3-5]. Toyota later introduced its D4 system to European markets with the *1AZ-FSE* engine found in the 2001 Avenis [6] and US markets in 2005 with the *3GRE-FSE* engine found in the *Lexus GS 300*. Toyota's *2GR-FSE* V6 first found in the Lexus IS 350 uses a more advanced direct injection system, which combines both direct and indirect injection using two fuel injectors per cylinder, a traditional port fuel injector (low pressure) and a direct fuel injector (high pressure) in a system known as D4-S [6].

Renault introduced the 2.0 IDE (Injection Directe Essence) [7], first on the Megane. Rather than following the lean burn approach in 1999. Renault's design uses high ratios of exhaust gas recirculation to improve economy at low engine loads, with direct injection allowing the fuel to be concentrated around the spark [8]. Later gasoline direct injection engines have been tuned and marketed for their high performance as well as increased fuel efficiency. PSA Peugeot Citrogen, Hyundai, and Volvo entered into a development agreements and licensed Mitsubishi's GDI technology in 1999 [9-13]. The Mitsubishi engines were also produced in the NetCar factory and used in the 1.8 L Carisma and the GDI-powered Volvo S40/V40 models [14-15]. In 2002, the Alfa Romeo 156 with a direct-injection engine, the JTS (Jet Thrust Stoichiometric) went on sale[16] and today the technology is used on almost every Alfa Romeo engine. Infiniti produced the M56 which includes DI. Motus Motorcycles is developing, with Katech Engines, a direct-injected V4 engine named the KMV4 as the powertrain for their MST Motorcycle. In 2011 the Hyundai Snonata 2011 model l came with GDI engines, including a turbo-charged 2.0-litre that produces 274 hp. Hyundai's Theta I-4 engine family is a proprietary design, engineered in Namyang, Korea and currently in production for applications all over the world [17]

M.M. Syed Ali et al. carried out experimental investigation in on direct fuel injection system in 2010 and found that fuel injection quantity can be varied with engine speed and load [18]. M. M. Syed Ali et al. also took research investigations [19-20] on single cylinder EFI System and 4 cylinder Port Fuel Injection System where fuel could be controlled according to engine demands.

M.M. Syed Ali also investigated with a different model for a low pressure DGI System instead of existing high pressure DGI model considering several advantages. Instead of high pressure fuel injection system Low Pressure DGI System was modeled for a 4 cylinder SI engine where air fuel mixing gets high turbulence and long duration for air fuel mixing [5]. This can provide better fuel air mixing before combustion. The experimental investigation [21] showed fuel air ratio at different operating condition can be maintained to achieve high fuel economy and less pollution formation specially carbon monoxide (CO) and hydrocarbon (HC) pollutants.

2. Layout and components of a DGI system

The fuel delivery system incorporates the following components:

(i) Fuel tank, (ii) Fu el pump (iii) Fuel filter (iv) Fuel delivery pipe (rail) (v) Pulsation damper (in many engines) (vi) Fuel injectors (vii) Cold start injectors (most engines) (viii) Fuel pressure regulator etc.

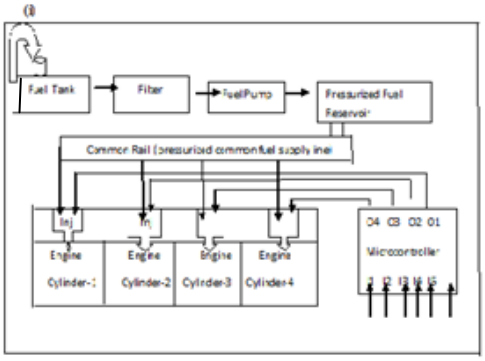

Fig. 1 Layout of the experimental setup

Usually fuel injection pressure in DGI system is nearly 40 times higher than the fuel injection pressure in EFI system. Fuel injection at low pressure is preferred considering several advantages in system. There are two types of electric fuel pump used in the EFI systems. The early conventional EFI system used an externally mounted in-line pump. These roller cells pumps incorporate an integral pressure pulse damper or silencer designed to smooth out pressure pulses and provide quiet operation. Later model engines utilize an in-tank pump integrated with the fuel sender unit. These turbine pumps operate with less discharge pulsation and run quieter than the in-line variety. In-tank pumps can be serviced by removing the fuel sender unit from the tank. In this case intake turbine pump has been selected and used.

Injector

In a direct fuel injection engine, the fuel must be injected in a short period of time and at pressures at least 40 times higher than in port fuel injection [4].

High pressure fuel injector
in the present DGI System

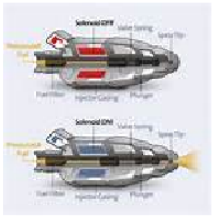

Low Pressure fuel injector
in the test model of DGI

Fig. 2 High pressure and low pressure injectors

The electric fuel pump supplies the fuel to the injectors under pressure. As soon as the injector opens, fuel sprays out. An electric solenoid in the injector opens and closes the injector.

In this investigation low pressure fuel injectors are taken considering fuel injection at low pressure inside the cylinder and availing high turbulence air-fuel mixing. This can enhance homogeneous air fuel mixture and can reduce CO and HC pollutions. More over the cost of fuel pump and injectors will be reduced considerably.

3. Design and considerations

In this present design following additional considerations are taken unlike present DGI system.

3.1 Design of new fuel injection system (LPHT-DGI) for better fuel air mixing

In the presently used DGI fuel injection system, fuel is injected at the end of compression stroke using high pressure fuel pump and injectors. Cylinder air velocity, swirl, turbulent kinetic energy increases and decreases at different crank angles [5] and follows the different fluctuating patterns as shown in Figure 3.1 to Figure 3.5 as shown below .

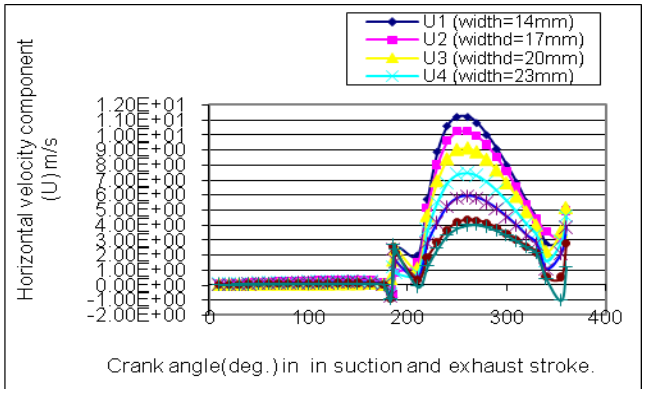

Fig. 3.1 Comparison of horizontal velocity components (U m/s) of intake air in the cylinder for different intake valve diameters in suction stroke

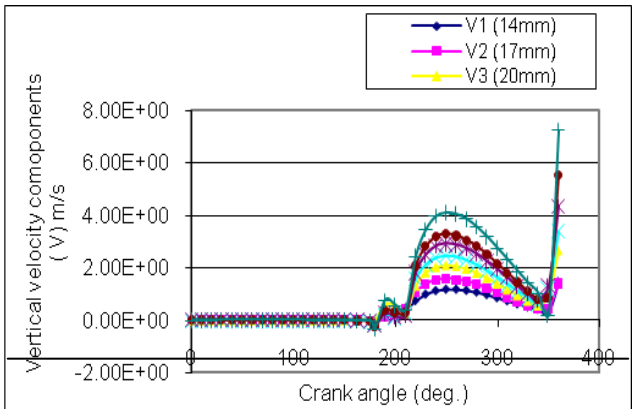

Fig. 3.2 Comparison of vertical components (V m/s) of intake air in the cylinder for different intake valve diameters in suction stroke

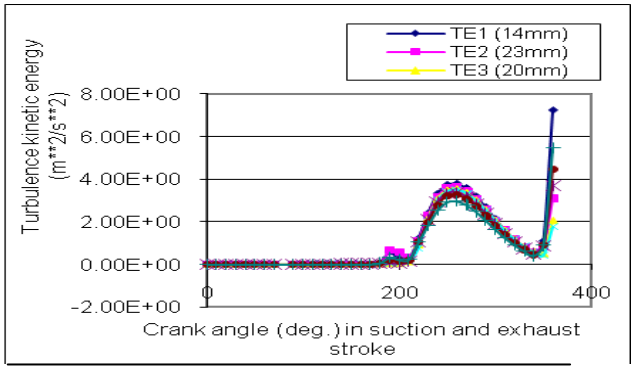

Fig. 3.3 Comparison of turbulence kinetic energy (TKE m**2/s**) of intake air for different intake valve diameters in suction stroke

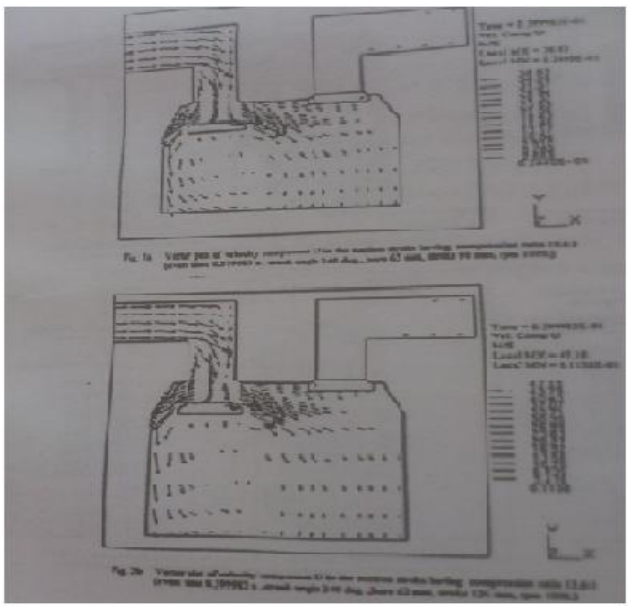

Fig. 3.4 variation of velocity component (U & V) in vector forms in different crank angle which shows velocity increases from valve opening timing.

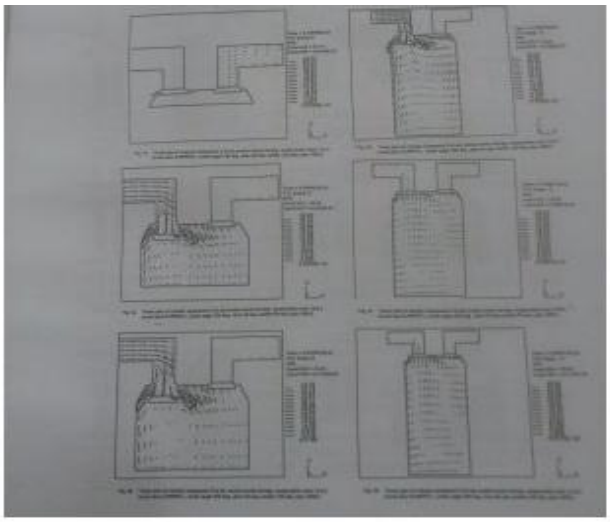

Fig. 3.4 variation of velocity component (U & V) in vector forms in different crank angle where velocity components (U&V) increases gradually from valve opening timing 180^{o} (TDC) to 270^{o} and then decreases till valve closing timing360^{o} (BDC) .

These variations of air velocity, swirl, turbulent kinetic energy does not help in air fuel mixing in the presently used DGI system. But these fluctuations help in better fuel air mixing and complete combustion in the model under investigations reducing the potential of the formation of CO, HC pollutants. But in the present DGI system, it get less time for fuel air mixing and provide heterogeneous mixture like diesel fuel injection. More over low pressure fuel injector and pump like TBI and PFI can be used. This reduces the cost of fuel injection system. Thus cost of fuel injection system, fuel economy and emission reduction potential will be improved.

3.2. Design considerations and program for microcontroller

A microcontroller has been built with an ATMega 8 IC for controlling device as depicted in figure 4. DGI system was designed for variable speed and variable load and other operating conditions of a real engine. The engine management system usually continually chooses among three combustion modes: ultra lean burn, stoichiometric, and full power output. Each mode is characterized by the air-fuel ratio. The stoichiometric air-fuel ratio for petrol (gasoline) is 14.7 to 1 by weight, but ultra lean mode can involve ratios as high as 25:1. These leaner mixtures of DGI system is much leaner than in a conventional engine, reduce fuel consumption [4].

In this design instead of three mode six modes of engine operation with specially, staring (choke circuit) idle circuit, slow speed circuit, medium speed circuit, high-speed circuit, acceleration circuit. In each running condition there is provision of extra fuel supply for high load and low load operation so that wide varying of fuel air ratio can be supplied keeping in conformity of engine operating conditions. Various types of sensors, ICs and transistors are used to sense the speed and suction pressure and engine operating conditions

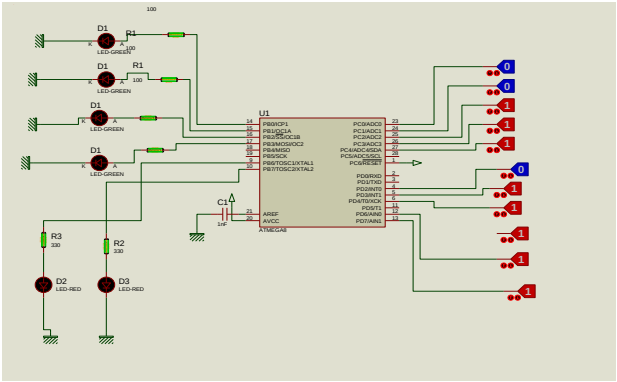

Fig. 4: Microcontroller IC and input output diagram.

An engine demand various quantity of air depending on load and speed. The intake air flow and air pressure represents the variation of load. The distributor of EFI and DGI systems have built in signaling system for engine rpm and crank angle position. Ne – signal and Ge-signal give engine rpm and crank angle position. Oxygen signal fitted in Catalytic converter give presence of oxygen in exhaust gas which in term give information to the engine that it is running with lean or rich or with optimum fuel air ratio. The program was made on the logics required for operating conditions of the engine. The air velocity and pressure in the intake manifold can determine the loading position in each mode. The Oxygen sensor gives the level of fuel air ratio.

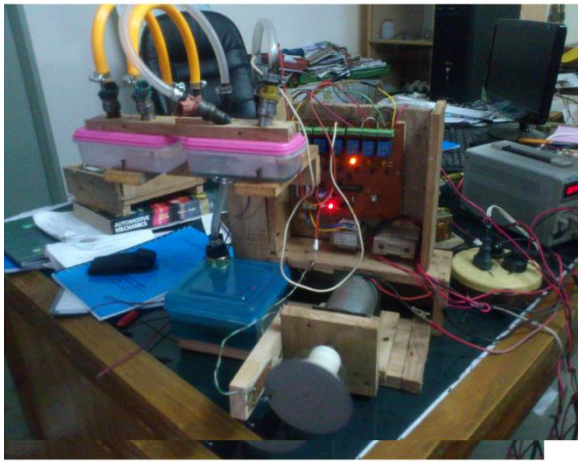

Fig. 5 Experimental setup for high turbulence DGI fuel injection system

All these parameter are set to the program to get required output signal for fuel flow injector. Before programming on a microcontroller based DGI system, the fuel air ratio required in all engine operating conditions like starting system (choke system), idle system, slow speed, medium speed, high speed system, acceleration system with variable engine load are considered accordingly the

required input are set to microcontroller. The output of microcontroller controls the injectors, where the fuel injection quantity varies depending on engine operating conditions.

4. Results & discussion

After completion of the experimental set-up (Fig. 5) of the fuel injection system, the performance of the direct gasoline fuel injection system was tested. The fuel injection quantity can be varied to any required quantity depending upon engine load and speed. Moreover the fuel injection is found to be stopped as soon as it receive signals from high coolant temperature and low oil pressure during engine operation. This will immediately stop the engine avoiding major damage of crankshaft, crankshaft bearing, piston and piston-rings etc. This module can be used in other model like EFI or Port Fuel Injection system vehicle with small modification. Carburetor vehicle with electronic distributor has the facility to give engine speed (rpm), crank angle position. In other word carburetor mounted vehicle with electronic distributor can be modified to this system where the amount of fuel to be supplied from injector to engine cylinder in all engine operation modes can be controlled by this microcontroller.

5. Conclusion

At the end**,** it may be concluded that

(i) The microcontroller based Low pressure high turbulent direct fuel injection system is found to work properly.

(ii) The model test showed that variable fuel injection quantity at different speed and load can be maintained.

(iii)There more opportunity of homogeneous air-fuel inside the cylinder during high turbulence phase in suction and compression stroke. This can help to reduce the formation of carbon monoxide (CO) and hydrocarbon (HC) pollution during combustion of fuel- air mixture..

(iv) The emission reduction potential is very high as fuel injection can be controlled depending upon the engine running condition.

(v) Fuel delivery cost of module of DGI system is nearly 1500-2000 USD in US market but this microcontroller based module will be reduced

(vi) The introduction of low pressure high turbulent direct gasoline fuel injection system will also reduce the cost of presently used high pressure direct fuel injection system.

(vii) Introduction of oil pressure signal and temperature signal can give primary signals (alarm or red light) for low engine oil pressure (P < 2 bar) and high coolant temperature (t>85^{o}C) . At the predetermined low engine oil pressure (P<1.5 bar) and coolant temperature (t>90^{o}C) control signal will stop fuel injection to avoid major engine damages. Thus it can enhanced engine security significantly

Nomenclature

CO	Carbon monoxide pollutants
DGI	Direct gasoline fuel injection
EFI	Electronic fuel injection
HC	Hydrocarbon emissions
IC	Integrated circuit
LPHT	Low pressure high turbulence
PFI	Port fuel injection
TBI	Throttle body injection

References

[1] W. H, Crouse and D, L. Anglin, "Automotive Mechanics", *10th revision/McGraw-Hill Book Company*, USA

[2] Fuel Systems at Sears® | *Sears.com*

[3] 30_39-Jfl/'Ý„v" (PDF). Retrieved 2009-07-17.

[4] www.Sears.com/Fuel-System- services

[5] M.M. Syed Ali**,** M. Sapuan Salit, M. M. H. Megat Ahmad, W. Asrar, " *Effects of intake valve diameter on suction air pressure and volumetric efficiency in a four stroke internal combustion engine"* Suranaree Journal of Science and Technology, July-Sept. 2004,Thiland

[6] "Improving the Environmental Performance of Internal Combustion Engines". *Toyota.1999-02-22.* Retrieved 2009-08-21.

[7] Crouch, Jonathan. "Renault Megane Cabriolet 1997-2003". *uk.cars.yahoo.com.* Archived from the original on 2011-07-18. Retrieved 2012-06-21.

[8] Wan, Mark (2000). "Lean Burn Engine". Autozine Technical School. Retrieved 2010-11-14.

[9] Yamaguchi, Jack (2000-02-01). "Mitsubishi's new GDI applications". *Automotive Engineering International (highbeam)*. Retrieved 2013-09-09.

[10] Beecham, Matthew (2007-12-07)."Research Analysis: a review of gasoline direct injection systems". *Just-Auto.* Retrieved 2013-09-09.

[11] "Mitsubishi Motors and PSA Peugeot Citroen Reach Agreement on GDI Engine Technical Cooperation" (Press release*). Mitsubishi Motors.* 1999-01-12. Archived from the original on 2009-01-12. Retrieved 2013-09-08.

[12] "Mitsubishi Motors Supplies Hyundai Motor Co. with GDI Technology for New V8 GDI Engine" (Press release). *Mitsubishi Motors.* 1999-04-28. Archived from the original on 2009-01-12. Retrieved 2013-09-08.

[13] Motor Business Japan. Economist Intelligence Unit. 1997. p. 128. Retrieved 2013-09-09. "Hyundai is second only to Volvo among companies borrowing the technology from Mitsubishi."

[14] Japan Quarterly 46. Asahi Shimbun. 1999. p. 22. Retrieved 2013-09-09.

[15] "Not so nuts" (98). *AutoSpeed.* 2000-09-19. Retrieved 2013-09-09.

[16] "News 2002". *italiaspeed.com.* Retrieved 2007-10-24.

[17] Abuelsamid Sam (2009-11-13). "New Hyundai 2.4-liter GDI four cylinder makes 200 hp in 2011Sonata". AOL *Inc.* Retrieved 2010-11-14.

[18] M. M. Syed Ali, Husnay Mobarok and Md. Mominul Haque " Experimental study on aprogram controlled direct gasoline fuel injection (DGI) system in SI engine for variable speed and load", *Undergraduate project thesis 2010*, Department of Mechanical Engineering , KUET, Khulna, Bangladesh.

[19] M. M. Syed Ali, Rubel Shikder, Md. Jahirul Islam, "Development of a Microcontroller based EFI System for a Single Cylinder Four SI Engine," *Undergraduate project thesis*, Department of Mechanical Engineering, Khhulna University of Engineering & Technology, Khulna-9203, Bangladesh, 2012-2013.

ICMIEE-PI-140423

Experimental investigation on developing remote controlled and robot assisted firefighting system for better security in home, industry and forest areas

Md. Syed Ali Molla[1] , Md. Shafiq Sayid[2] , Md. Muhaiminul Hassan[3] & Md. Al, Mamun[4]
[1]Department of Mechanical Engineering, Khulna University of Engineering & Technology
[2] Electrical Engineer, Mororwala Ltd, USA
[3] B.Sc. Electrical Engineering student, Ahsan Ullah University
[4] M.Sc. Eng student,. BUET, Bangladesh
Email: mmsali03@yahoo.com, & pmsali@me.kuet.ac.bd , s.sayid@gmail.com, *muhaiminul7@gmail.com*

ABSTRACT
The firefighters of developing and developed countries are equipped with modern firefighting system, still they become helpless in many cases as found in the forest fire in Australia, USA and even in Russia. Every year, fire hazards cause a lot of damages in domestic, commercial and industrial areas. Several fire hazards in commercial and garment industries in Bangladesh made the awareness and need of developing firefighting equipments so that factory, people and wealth can be protected from the devastation of fire. This research investigation shows that automatic emergency door opening system can protects the occupants in industries from burning and other fire hazards. Automatic water supply can help to extinguish and control the fire spreading in domestic, commercial and industrial areas. Improved water supply system can protect fire from one floor to another in multistoried building. Automatic and remote controlled firefighting system can also be operated from outside. Experimental investigation on an automatic firefighting system and remote control robot assisted firefighting system was made by the authors and it is found that these systems be used more efficiently in domestic, industrial and forest areas. This paper describes the usages of auto-controlled and remote controlled firefighting system with and without surveillance system and developed necessary program and microcontroller circuit to control the firefighting equipments. These investigations showed that the fire hazards can be controlled satisfactorily by auto controlled firefighting system and robot assisted remote control system with and without surveillance r system

Key words: Auto-control, remote control, mobile phone, robot assisted, firefighting system.

1. Introduction

Most of the firefighting systems are equipped with electric motor driven vehicle or IC engine driven vehicle. Battery powered patrol car of different model like Electric Patrol Car with 48V/3.7kw, CE 1, Trojan Patrol Car, Electric Car, Electric Patrol Car and Electric Vehicle are available in international markets. IC engine vehicle mounted firefighters like ISUZU *Fire truck*, Water *truck* , *Fire* engine *truck* are also available but robot assisted firefighting system are rarely found.
Robots can be used in many operations of industrial processes. Industrially developed countries are widely using robots in their industrial processes, but its application is rare in firefighting system. In the robot assisted automated firefighting system, the robot is started automatically soon after getting the signals of the initiation of fire and robotic gun can supply water in the room in all directions as per design and program in robot. Near future the application of robot will be more in firefighting equipments because of the facts that human being cannot work so efficiently and so rapidly like a robot.

Zoppi, M et al. [1-4] established an integration of mechanical and control aspects involved in the design of an innovative 3-D of parallel kinematics machine. The openness of control systems has been addressed in several ways by worldwide research projects both in the field of robot and machine tools (i.e. OROCOS OSEC/JOP, OMAC, OSACA) [1-4].
Lange, E. et al. [2-5] established a sensor based control with different types of sensors and investigated for robots with a positional interface. Sensor data are used to build a representation of the desired path.

Flordal, H et al. [3-6] developed a method for automatic generation of collision free, blocking free and work cycle time optimized supervisors for industrial robot cells has been implemented. The individual robots' tasks are specified as a set of targets that the robot should

* Corresponding author. Tel.: +88-01714087350
E-mail address: mmsali03@yahoo.com : pmsali@me.kuet.ac.bd

visit in arbitrary order. Minimum of six degree of freedom is required; three for position and three for orientation. This makes a good intuitive sense as the description of an object in space requires six parameters.

M. M. Syed Ali [7] conducted research work with pneumatic powered robot and fire fighting system. A mobile phone was used to operate the firefighting system and the pneumatic powered robot. The firefighting system and pneumatic power robot were operated and controlled by mobile phone guided GSM Network perfectly. This was shown in national TV and ATN News channel in 2008.

Later on M. M. Syed Ali et al. [8] took an undergraduate research project on GSM Network base Remote Control System for an Unmanned Vehicle. This scheme is known as Dual Tone Multi-Frequency (DTMF), Touch-Tone or simply tone dialing. The test result showed that mobile phone guided wireless remote control system is applicable to control, surface vehicle.

M. M. Syed Ali et al. [9] also took this research works on automatic robot assisted firefighting system using this mobile phone guided GSM and surveillance AGSM network. The robot assisted fire fighting system can be controlled from far remote area or from other country by 3G mobile network. It is also found that laptop surveillance system can also be used to the robot assisted firefighting system by the installation of program in and webcam with microcontroller module for operating the robot and connecting the operator and robots with surveillance system.

2. Construction and main components of the firefighting system:

The main components of firefighting systems are water supply system, controlling unit, and firefighting robot.

2.1 Water supply system:

An electric motor (220V, 0.75Hp), water tank (pot) and water supply lines and hoses have been used to construct water supply system for the building and robotic gun.

2.2 Controlling System:

2.2.1 Auto-starting system: In this auto starting system, the fire fighting system receive signals and opens the emergency gate, starts firefighting equipment, and robot at any pre-set room condition.

2.2.2 Mobile phone guided starting system: In addition to the above auto starting system, it can start the same operation of the fire fighting system by remote control system or mobile telephone using its keypad and GSM networks.

2.2.3 Firefighting Robot with remote surveillance control system: Micro-controller based firefighting robot is guided by GSM and AGSM network. It is necessary to make the circuit so that signal from the mobile phone can send signal to the input of the microcontroller. Special care should be taken in this regard as these wires are laminated and the lamination must be removed before the wires are connected to the signal decoder. The decoder receives the tone and sends the corresponding binary number to the microcontroller. According to the program in the microcontroller, the water pump motor or unmanned water vehicle will start moving.

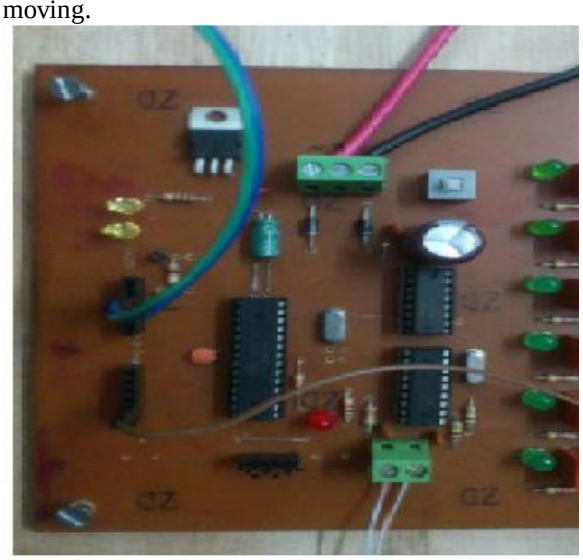

Fig. 1: Micro-controlled circuit board for input and output device.

This hardware circuit is consist of the microcontroller, decoder, ULN relay driver as shown in figure 1. The ULN relay driver is high-current Darlington transistor arrays. The ULN relay driver are supplied in 16 pin plastic DIP packages with a copper lead frame to reduce thermal resistance.

2.3 Firefighting Robot:

This robot has been contracted with the three degree of free-doom so that it can operate water gun to any stirred or place as desired. The robotic firefighting system can be started automatically. It can be operated by its own program

3. Experimental Set-up and Results:

Three experimental setups for three different models of the fire fighting equipments have been constructed and tests with the following multilayer facilities and security system.

3.1 Experimental Set-up - 1 :

Mobile Phone Guided Automatic Firefighting System: In this model test figure 2, a three storied model house has been constructed with emergency gate and

firefighting system including water pump, water tank and a microcontroller board. This firefighting system is equipped with necessary accessories. The test result shows that the following facilities can be obtained from this model test.

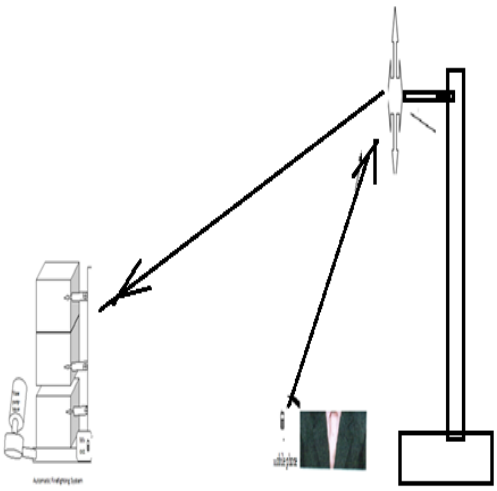

Fig. 2 Experimental set-up 1 for an automatic and remote controlled firefighting system

(i) The firefighting system is automatically started if fire occurs and it can supply water to the water hose pipe of the firing spot or floor in building so that occupants can also use and supply water to dire fire spot.

(ii) An emergency gate of the hall room or store under fire will be opened automatically so that occupants can go out of fire and are not burnt.

(iii) If emergency gate of the hall room or store under fire is not opened automatically, the emergency gate can be also be opened by remote control switch board or mobile phone keypad by the controlling officers from factory or from out of the factory or from other country or subcontinent.

(iv) Firefighting system can be started and operated by controlling officers using mobile phone keypad and GSM networks.

(v) Firefighting system is designed and developed in such a way so that water supply and cooling device will protect the fire spreading from one floor to other floor.

(vi) It can also be started manually by the operator in ground floor.

(vii) It can also be started by occupants of respective floor where fire is initiated.

(viii) If fire is initiated, two alarms will come from smoke sensor and light sensors so that occupant can take preventive measures from fire initiation.

(ix) Thus the occupants under fire will be able to get automatic water supply, automatic emergency door opening, emergency door opening by mobile phone for their own protections. Thus the firefighting system can be equipped with multi-layer security systems to protect people in homes, commercial areas, and in industries.

3.2 Experimental Set-up 2

Robot Assisted Automatic Firefighting System Controlled by Mobile Phone Guided GSM Networks: In addition to above automatic firefighting system, robot assisted firefighting system was constructed and tested to improve overall performance of the fire fighting system as shown in figure 3. The test result shows that it can provide the following additional facilities

(i) The robot assisted fire fighting system may be over-head mounted or floor mounted industries and the robot may be movable or stationary.

(ii) In the robot assisted fire fighting system, the robot is started automatically and supplies water in the room in all directions (in horizontal plane and in vertical plane with reciprocating motion) as per program in robot and designed and installed.

Fig.3.1 Experimental set-up 2 for a robot assisted firefighting system with remote controlled system

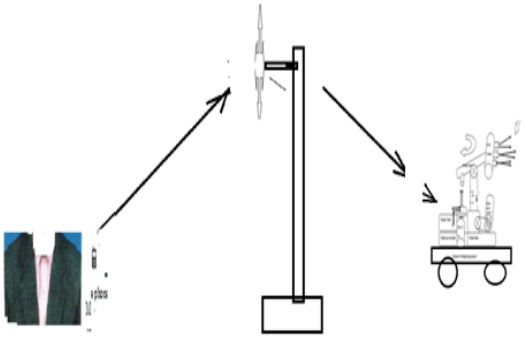

Fig.3.2 Experimental set-up 2 for a robot assisted firefighting system with remote controlled system

(iii) Robot assisted firefighting system can also be started by mobile phone and the robot can be operated in manually control mode or in auto motion by the key pad of mobile phone.
(iv) In automatic robot assisted firefighting system, the robot will supply water in designed motion without operator in horizontal plane and in vertical plane as programmed.
(v) In manual control mode, the robotic water gun can be operated and controlled by the key pad of mobile phone.
(vi) If the robot is mounted on vehicle, the vehicle motion can also be controlled by mobile phone.
(vii) For short distance, the remote control system can be operated by eye vision where no surveillance control is required. Firefighting robot can be installed on water tanker for better performances.

These robot assisted firefighting system are preferably applicable in big store of sea port, air port, in garment industries, factory, and store of factory.

3.3 Experimental Set-up 3

Robot Assisted Surveillance Firefighting System using AGSM Networks:
Some time the operator cannot enter in the store room during fire where robot can enter the room with external water spray and internal cooling system. Here remote surveillance control system can guide and operate the robot from outside. The following distinct facilities and features are available in this system as depicted in figure 4.
(i) The robot assisted fire fighting system can be controlled from remote area or from other country by 3G mobile network or by the installed surveillance control system between operator and robot module where webcam camera and microcontroller fitted with robot.

(I)
(II)

Fig. 4.1 Experimental Set-up 3 for surveillance remote controlled firefighting system for industries

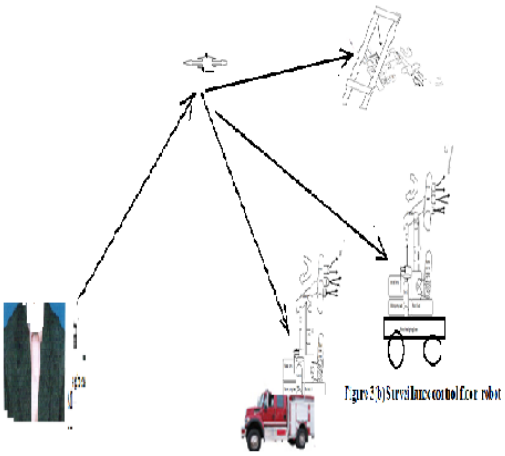

Fig. 4.2 Experimental Set-up 3 for future surveillance remote controlled firefighting system for industries and forest ares

(ii) A self cooling for self protection for robot or robotic vehicle can be added so that it can enter hot area during fire extinguishment.
(iii) Robot can be mounted in 3-wheel vehicle or 4-wheeled vehicle or on water tank which can be operated surveillance control device and mobile keypad applicable in house or store of factory and factory

4. Conclusion

In this research work, the remote control and surveillance system of firefighting robot were tested. The following conclusions may be made

(i) Automatic opening of emergency door can protects occupants from fire burning.
(ii) Automatic staring of water pump and water supply system can provide instant water supply to different floor and occupants which is helpful to control fire.
(iii) Robotic water gun can be used more effectively in controlling fire.
(iv) Both robot and auto-fire fighting can be operate remote control system using mobile phone and GSM network
(v) Surveillance system of 3G mobile or separately installed surveillance system with necessary program and module can used to control these firefighting equipments.

Reference

[1] E. Wernholt, "Multivariable frequency-domain identification of industrial robots", Division of Automatic Control; ISBN 978-91-85895-72-4 ISSN 0345-7524.

[2] Academons; "Robotics", Written in 2002; Paper #027856.

[3] L.E. Bruzzone, R.M. Molfino, M. Zoppi and G. Zurlo, "Experimental tests on the prototype of an impedance controlled three-degree-of-freedom parallel robot" Proceedings of RAAD'03, 12th International Workshop on Robotics in Alpe-Adria-Danube Region.

[4] L.E. Bruzzone, R.M. Molfino, M. Zoppi Mechatronic design of a parallel robot for high-speed, impedance-controlled manipulation" Proc. of the 11th Mediterranean Conference on Control and Automation, June 18-20, 2003,Rhodes, Greece

[5] F. Lange and G. Hirzinger, "Stability preserving sensor-based control for robots with positional interface", *IEEE International Conference on Robots and Automation (ICRA2005*), April 2005, Barcelona, Spain.

[6] H. Flordal, D. Spensieri, K. Akesson and M. Fabian, "Supervision of multiple industrial robots: optimal and collision free work cycles" Control Applications, 2004. *Proceedings of the 2004 IEEE International Conference* on; Volume 2, Issue, 2-4 Sept. 2004 Page(s): 1404 - 1409 Vol.2.

[7] M. M; Syed Ali, "Mobile phone operated firefighting system and pneumatic power robot", *ATN News, VISUAL DIARY* , 26th January 2008 , in TV C-34-0126-1554407

[8] M. M. Syed Ali, Al Mamun , and M. A. Alim, "Design and Construction of GSM Network Base Remote Control System of an Umanned Vehicle. "*Undergraduate Thesis,* 2012-13, Department of Mechanical Engineering, KUET, Khulna 9203, Bangladesh.

[9] M. M. Syed Ali, Shafiq Sayid, Al mamun, and M.M. Hassan, "Experimental study on robot assisted automatic firefighting equipment using gsm, agsm networks and surveillance system", Presented in *APM, IEB, 27-28 Dhaka*, Bangladesh, Dec, 2013.

ICMIEE-PI-140424

Fracture Properties of Graphene Oxide (GO) and GO/CNT Hybrid papers

Md. Nizam Uddin [1] *& Jang-Kyo Kim* [2]
[1] Department of Mechanical Engineering, Khulna University of Engineering and Technology (KUET), Khulna-9203, Bangladesh
[2] Department of Mechanical and Aerospace Engineering, The Hong Kong University of Science and Technology, Clear Water Bay, Kowloon, Hong Kong

Email address: engrnizam02@gmail.com

Abstract
The fracture behaviors of graphene oxide (GO) and GO/multi-walled carbon nanotube (MWCNT) hybrid papers are studied in mode-I and mode-III fracture. The effects of GO sheet size and CNT content on fracture and tearing toughness of the papers are evaluated using double-edge-notch tension (DENT) and trouser tear specimens, respectively. The tearing studies of all paper specimens under mode-III loading exhibited stick-slip tearing. The concept of Linear Elastic fracture mechanics (LEFM) is used to measure the fracture toughness of GO and bucky papers and GO/CNT hybrid papers. Large GO papers give rise to a higher energy release rate and tearing toughness than those made from small GO sheets: about 36% and 70% enhancements are shown for the large GO papers due to a more compact structure and better GO sheet alignment. Hybridization of GO papers with MWCNTs also improves these properties when up to 5 wt.% of MWCNTs is incorporated, attributed to the stronger GO interlayer bonds through pi-pi interactions with intercalated MWCNTs. Fracture surface examination indicates that cleavage failure prevails in mode-I fracture depending on the size of GO sheets: the unsorted and large GO papers fail mainly by brittle cleavage of GO sheets whereas small GO papers fail by combined brittle cleavage and minor pullout following de-bonding of GO bundles. In contrast, combination of cleavage and de-bonding failures is dominant in mode-III fracture of GO papers, regardless of GO size. CNT pullout is the dominant failure mechanism in both fracture modes of bucky papers.

Keywords: Graphene oxide paper, Fracture toughness, Energy release rate, Cleavage failure, Vacuum filtration.

1. Introduction
Since its discovery in 2004 [1], graphene - the parents of all graphitic materials has become one of the most exciting topics of research in the last few years. Graphene consists of one atom thick sp^2 bonded carbon atoms arranged in a honeycomb lattice structure, and possesses exceptionally high in-plane electronic mobility, mechanical properties and thermal/electrical conductivities [2, 3]. Among different methods for the fabrication of graphene based materials, graphene oxide (GO) synthesized from oxidation of graphite is the most versatile method [4]. GO is an atom thick sheet of graphite containing oxygenated functional groups on its basal plane and at its edges, which form a hybrid structure of sp^2 and sp^3 hybridized carbon atoms, making it dispersible in water and organic solvents [5].GO has been widely used as a building block in composites, mechanical actuators, nano-robots, energy related materials, biological and medical applications [6, 7]. In recent years, GO-based paper materials have attracted much interest because of their outstanding strength, modulus and high degree of flexibility [8]. These paper-like materials may be used as sealants, actuators, bio-compatible substrates, flexible substrates and super-capacitors with high chemical and thermal stability [9]. GO papers can be easily fabricated from aqueous GO dispersion via vacuum-assisted self-assembly to form a free standing layer-by-layer hierarchical structure.

The mechanical properties of GO papers have been extensively studied mainly in unidirectional tensile and bending modes [10, 11]. GO papers had a high strength and modulus in tension and bending due to the interlocking-tile microstructure of individual GO nano-sheets in the paper. Earlier studies indicate that these properties of GO papers outperformed other paper-like materials [12] while being similar to those of flexible graphite foils and carbon nanotube (CNT) bucky papers [11]. However, depending on a number of factors, including the precursor materials and how they are produced, the measured properties differed considerably, e.g. the tensile strength varied between 76 and 293MPa and the moduli between 6 and 42

GPa [13]. Significant efforts have been directed towards improving the mechanical properties of GO papers, mainly by intercalation of polymer layers and chemical cross-linking between the GO sheets. These techniques include intercalation of divalent ions, such as Mg^{+2} or Ca^{+2} [12], polyvinyl alcohol films [14, 15], octadecyclamine (ODA) [10], polydopamine (pDOP) [16] and the combination of pDOP and polyetherimide (PEI) [13]. The mechanical properties of GO papers have been extensively studied mostly in uni-axial tensile mode [17-19]. While very few studies have been reported on the properties of GO paper in other modes of deformation, such as in shear or tearing. The lateral dimensions of GO sheets have significant impacts in controlling the properties and application of GO papers. Large and small GO sheets, respectively, are ideally suited in a variety of applications. For example, polymer-based composites containing small GO sheets are useful for bio-sensing and drug delivery [20, 21], whereas large GO sheets with controlled sizes are preferable for optoelectronic devices [22, 23].Various methods have been proposed to control the GO size or to obtain large sizes with varied successes [24-26], including the use of less oxidation and sonication. In this study, a series of centrifugation was used to sort as-produced GO sheets into different size groups based on our previous study [23]. Like GO papers, papers made from CNTs is a viable engineering material due to their useful mechanical, electrical and thermal properties. They are used in applications, like actuators, capacitors, electrodes, field emission devices, radio frequency filters, artificial muscles and strain sensing [27, 28].CNTs were also combined with GO sheets to synthesize hybrid papers in this study. This works aims the evaluation of the fracture resistance and identifying the corresponding failure mechanisms of neat GO and hybrid papers in two different modes, including mode I fracture using the double edge notched tensile (DENT) test and mode III tearing using the trouser test. Experiments were performed to determine the fracture and tearing toughness of GO papers and GO/CNT hybrid papers. In addition, the study specially focuses on the effects of GO sheet size and CNT content on the fracture properties of these papers were specifically studied.

2. Experimental

2.1 Fabrication of GO and GO/CNT hybrid papers

GO was prepared from purified natural graphite flakes (Asbury Graphite Mills) based on modified chemical method [29, 30] and the procedure for GO synthesized is described elsewhere [23, 31]. GO paper was fabricated by flow-directed vacuum filtration of aqueous GO dispersions through a Millipore filter membrane (90 mm in diameter and 0.22 μm pore size) followed by air drying and peeling off from the filter paper. The thickness of each paper is controlled by adjusting volume of the aqueous GO dispersions. For the fracture toughness testing specimen, the thickness of the paper was about 20±0.001μm. All the specimens were dried in an oven at 60°C for seven days to achieve low moisture content before testing. To investigate the effect of GO sheet size on the fracture properties the as prepared unsorted GO solution was separated into 'small GO' and "large GO" through three-step centrifugation on a table-top centrifuge (SIGMA 2-16P) whose average areas were 1.1 and 272μm^2, respectively [32]. Raman spectroscopy (Renishaw MicroRaman/Photoluminescence System with a 633 nm He-Ne laser) and **X**-ray diffraction (XRD, X'pert Pro, PANalytical, using Cu Kα1 (λ =0.154 nm) radiation) analysis were used to evaluate the carbon structure and the interlayer distance between adjacent GO layers with different size groups. For the GO/CNT hybrid paper fabrication, the functionalized CNTs solutions were poured into GO aqueous dispersion while stirring followed by 0.5 hr ultrasonication. The GO/CNT hybrid paper was prepared by vacuum filtration of GO/CNT hybrid mixture followed by air drying and peeling from the filter paper and finally dried in a vacuum oven at 60°C. The CNT content was varied between 2.5 and 90 wt%.

2.2 Fracture toughness tests and characterization

The fracture resistance of papers was characterized both in mode I tension using the double edge notched tension (DENT) test and in mode III out-of-plane shear using the trouser tear test. The specimens were prepared according to the specifications ASTM E399 and ASTM D1938, respectively, and their dimensions are as shown in Fig. 1. For the DENT specimens, the width, *2b*, was varied between 5 and 30mm while the crack length to width ratio, *a/b*, was varied between 0.15 and 0.69. The critical stress intensity factor, K_{IC}, was calculated using the equations (1) and (2) when the external stress reached a critical value, σ_c, for crack propagation [33]:

$$K_C = \sigma_C\sqrt{\pi a}\ F\left(a/b\right) \quad (1)$$

Where $F\left(a/b\right)$ is a geometric correction factor and for a double edge notch tension specimen is given:

$$F\left(a/b\right) = 1.12 + 0.203\left(a/b\right) - 1.197\left(a/b\right)^2 + 1.93\left(a/b\right)^3 \quad (2)$$

The mode-I stress intensity factor, K_C, is related to the energy release rate, G_C, by

$$G_C = \frac{K_C{}^2}{E} \qquad (3)$$

Where E is the Young's modulus of the material for plain stress condition

For the trouser tear test specimens, two different ligament lengths of 30 and 50mm were employed while the initial crack length was fixed at 15 mm. The tearing toughness, G, was calculated by:

$$G = {}^{2F}/_{t} \qquad (4)$$

Where F is the mean force calculated by averaging the load over the entire ligament length; and t is the thickness of the specimen. Thus, the tearing toughness is the internal tearing resistance and measures the force perpendicular to the plane of the paper necessary to tear a single sheet through a specified distance after the tear has already been started. Specimens were cut to the dimensions shown in Fig. 2 and the initial cracks were made using a sharp surgical blade. The specimens were dried in an oven at 60°C for seven days to uniformly dry before testing. The DENT and trouser tear tests were conducted on a universal testing machine (Alliance RT/5) at cross-head speeds of 1 and 250 mm/min, respectively, according to the specifications. The fracture surface morphologies were examined on a scanning electron microscope (SEM, JEOL 6700F, JSM) and an optical microscope (LEICA M205C).

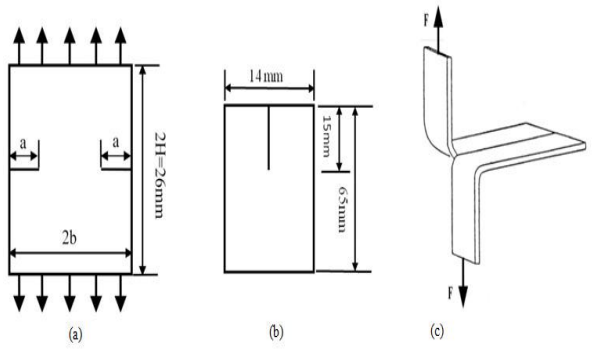

Figure 1. (a) Double edge notched tension specimen and (b) Trousers tear specimen and (c) model geometry (tearing test).

3. Results and Discussion

3.1. Materials Characteristics

Fig.2a. shows the Raman spectra of small, unsorted and large GO papers and the corresponding I_D/I_G intensity ratio. The G band (at ~1590 cm^{-1}) is Raman active for sp^2-hybridized carbon-carbon bonds in graphene [34, 35] while D band (at ~1354 cm^{-1}) is associated with the presence of defects in the graphite material such as bond-angle disorder, bond-length disorder, vacancies, edge defects, etc. [36]. The intensity ratio I_D/I_G is widely used to measure the defects quantity in graphitic materials [37].The Raman spectra shows an increase in the D/G intensity ratio from 2.02 for large GO to 2.43 for small GO, clearly indicate the increased defects quantity in small GO sheets for a given area of materials.

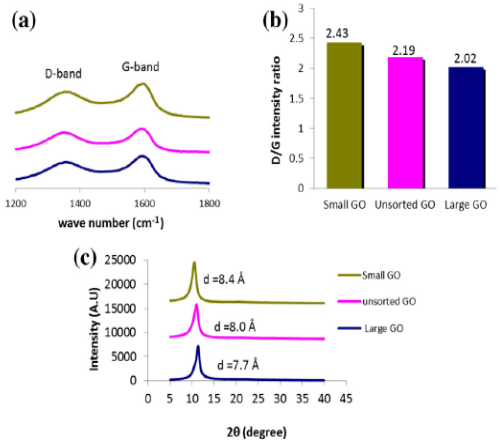

Figure 2. Raman spectra of small, unsorted and large GO papers (a) D- and G-band peaks; (b) I_D/I_G intensity ratio and (c) X-ray diffraction patterns of small, unsorted and large GO papers.

The XRD pattern (Fig.2c) of small, unsorted and large GO papers exhibits a characteristic XRD peak at 2θ = 10.53°, 11.03°, 11.35° and corresponding to a distance of, 8.4 Å, 8.0 Å and 7.7Å between the stacked GO sheets. The larger was the GO sheets, the smaller was the d-spacing. This observation is consistent with the Raman intensity ratio, where the large GO sheets contained fewer oxygenated functional groups for a given area, leading to a shorter distance between them. In other words, the large GO papers had a more compact structure and better GO sheet alignment formed during the self-assembly process than the small GO papers [32].

3.2. Fracture properties of GO papers and GO/CNT hybrid papers

The mode-I strain energy release rates, G_c, were calculated using equation (3) from the Young's moduli of GO papers determined by the dynamic mechanical analysis**.** The results on the effects of initial crack length and specimen width are shown in Fig. 3. The strain energy release rate showed a maximum value of ~0.34 kJ/m^2 for a/b in the range of 0.38 to 0.46, and decreased gradually when a/b ratio was reduced or increased. A further study on the effect of specimen width, 2b, indicates that the energy release rate leveled off when 2b reached ~10 mm for both a/b = 0.38 and 0.46.

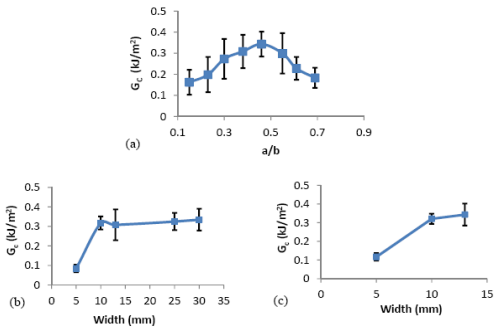

Figure.3- Energy release rates of GO papers: (a) Effect of initial crack length to specimen width, a/b, for a fixed width b = 13mm; Effect of specimen width 2b for a fixed crack length to width ratio (b) a/b = 0.38 and (c) a/b = 0.46

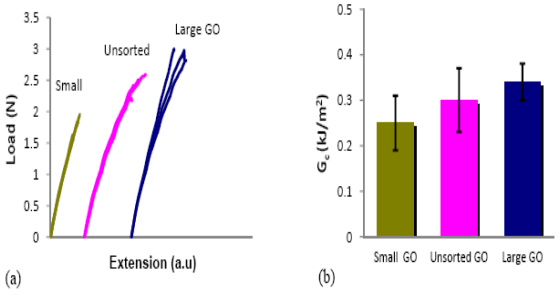

Figure. 4 (a) Load- extension curves and (b) comparison of the strain energy release rates of small GO, unsorted GO and large GO papers, crack length to width ratio a/b = 0.38, width 13mm

As prepared GO sheets were sorted as small GO and large GO sheets and the effect of GO sheets size on fracture properties were investigated. The representative load-extension curves obtained from the fracture toughness tests are shown in Fig.4 (a) and the corresponding strain energy release rates are given in Fig. 4(b). From Fig. 4(a) load increased almost linearly with extension when crack initiated until it reached the maximum where catastrophic failure occur. This indicates that fracture behavior of GO paper is like a brittle material. The energy release rates were higher in the ascending order of small, unsorted and large GO papers, with a significant 36% difference between the small and large GO sheets.

To understand the different fracture behaviors of GO papers made from different size groups, SEM images were taken from the cross-sectional fracture surfaces, as shown in Fig. 5.

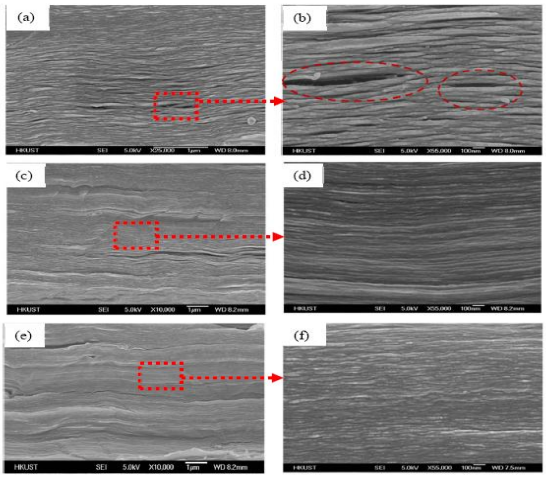

Figure 5. SEM photographs of the fracture surfaces of GO paper (a,b) unsorted GO,(c,d), large GO and (e,f) small GO

GO paper assembled in a layer-by-layer hierarchy where GO sheets are bridged on the edges (intralayer) and adjacent graphene sheets (interlayer) through *sp*2 carbon-carbon covalent bonds, hydrogen bonds, van der Waals forces [32]. When the crack propagated across to the stacked GO sheets, it generally followed a straight path without much deflection. The *sp*2 carbon-carbon covalent bonds are short-ranged and the deformation of GO sheets generally involves the localized processes of bond breaking. [38]. Therefore, all fracture surfaces presented mainly cohesive failure via brittle cleavage of GO sheets with limited GO sheet pullout. However, depending on the GO size group used, the surface morphologies presented obvious differences in term of degree of GO sheet alignment in the horizontal direction and the occurrence of de-bonding between them. It is of interest to note that the large the GO sheets, the better the alignment and the less the tendency to de-bonding. However, the elongated elliptical holes shown in Fig. 5(b) appear to be the trace of de-bonded GO sheets or bundles, consistent with the size of small GO sheets ranging from a few hundred nm to a few μm in lateral

length. In summary, it can be said that the fracture mechanisms of unsorted and large GO papers were dominated by brittle cleavage of GO sheets whereas small GO papers were failed by combined brittle cleavage and minor pullout following de-bonding of GO sheets.

Similar to GO papers, specimens made from CNT papers and the GO/CNT hybrid papers were tested at a/b = 0.38 to measure the fracture toughness. The critical stress intensity ratios, K_c, of GO/CNT hybrid papers are presented as a function of CNT content in Fig. 6(a). (Due to the lack of individual Young's modulus data, the K_c values are shown.) The stress intensity factor of the neat CNT papers was below one tenth that of the neat GO paper (K_c = 0.103 vs 1.5 MPa$\sqrt{m}$) although the strain energy release rate was only five times lower (G_c = 0.072 vs 0.34 kJ/m^2), a reflection of the difference in Young's modulus. The neat CNT papers are a mat of randomly entangled CNTs with a randomly interconnected porous structure. During the filtration process the CNTs were self-assembled by van der Waals forces. The interaction of individual CNT plays an important role in determining the mechanical properties of the bucky paper [39, 40]. When load is applied, individual CNTs began to unravel (disentangle) by tube to tube shearing from each other until a peak load is reached and following this limit, crack propagates across the sample by pullout of the CNTs. The failure mechanism involved complete pullout of the CNTs across the crack (Fig. 6(b)). The fracture toughness of GO/CNT hybrid papers showed an interesting variation with CNT content (Fig. 6(a)).

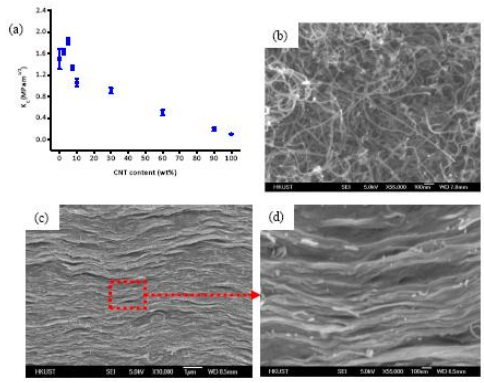

Figure. 6 (a) Fracture toughness of GO/CNT hybrid papers as a function of CNT content; fracture surface morphologies of (b) neat CNT bucky paper and (c, d) 95 wt.% GO/5 wt.% CNT hybrid paper.

It sharply increased for CNT contents up to 5 wt.% before a consistent, parabolic reduction with further increase in CNT content. A small amount of CNTs intercalated between the GO sheets positively contributed to resisting the crack opening force by strongly adhering to the GO sheets via π-π interactions which are considered stronger than the hydrogen bonds or van der Waals forces present between the GO sheets alone. This may explain the initial surge in fracture toughness by 22% with 5 wt.% CNTs. The SEM images corresponding to these papers (Fig. 6(c) and 6(d)) indicate that the fracture mechanisms were largely different from those of the neat GO papers and two distinct features can be identified. There was evidence of GO bundle pullout along with the intercalated CNTs, and as a result the fracture surface was much rougher than the neat GO papers. The bundle pullout mechanism is considered to positively contribute to the toughness of the hybrid papers through crack tip deflection. The addition of a small quantity of CNTs hindered cleavage as well as deboning of GO sheets. Another feature is that the GO sheets were stacked with a high degree of wrinkles in the form of sinusoidal waves along with uniformly intercalated CNTs. The presence of wrinkles may have helped the pullout of GO sheet bundles, which otherwise seldom occurred in well-aligned GO sheets (Figs. 5d, 5f).

However, the excessive amount of CNTs beyond 5 wt.% failed to enhance the fracture toughness because the bonds with the GO sheets were not as strong due to the agglomeration of CNTs, while inevitably increasing the total paper thickness because of the loose packing density of CNTs compared to the neat GO sheets.

3.3. Tearing properties of GO papers and GO/CNT hybrid papers

The out of plane mode-III trouser tear tests were carried out to determine the tearing toughness of papers. The effects of GO sheet size on tearing toughness are shown in Fig. 7. It shows the typical load-extension curves obtained during tear propagation of small, unsorted and large GO papers. From the load extension curves it is observed that force slowly increase to a maximum value and drops rapidly to a minimum value with corresponding variations in the rate of propagation. The crack initiate at maximum force while arrest at minimum force. This type of tearing is called stick-slip tearing. At regular intervals, the crack initiation and arrest repeats itself [41]. The stick-slip tearing has also been observed in thermoplastic elastomers [42, 43] and polyvinyl alcohol gel sheets [44]. As expected, there was a linear increase in tearing toughness with increasing paper thickness (Fig. 7(b)). The effect of GO sheet size on tearing toughness is shown in Fig. 7(c), the large GO papers presenting ~70% enhancement compared to the small GO papers. The

dependence of tearing toughness on GO size is attributed to two interrelated characteristics, namely the compactness of GO paper and the presence of defects in GO sheets. The XRD analysis clearly indicated a shorter interlayer distance between the large GO sheets, i.e. with a more compact structure, than the small sheets, while the large GO sheets contained fewer defects than small GO sheets as indicated by the Raman I_D/I_G intensity ratio (Fig. 2). In fact, the dependency of tearing toughness on GO sheet size has a significant analogy with the dependency of tearing toughness of cellulose papers on fiber length: it was shown that the tearing resistance increased with increasing fiber length, particularly when there was low bonding between the fibers [45].

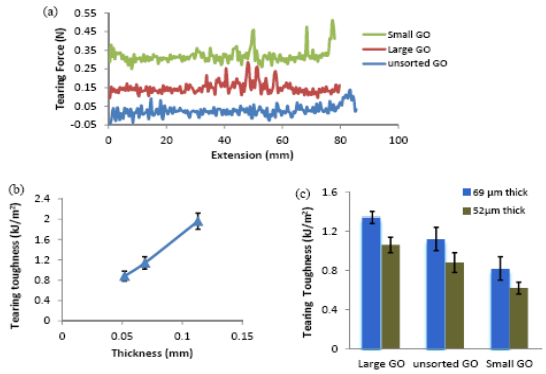

Figure 7. (a) Tearing force-extension curves of 0.052 mm thick GO papers; (b) tearing toughness of unsorted GO papers as a function of specimen thickness; and (c) tearing toughness of GO papers with different size groups.

The degree of bonding in the paper significantly affected the tearing process. In papers with a higher degree of bonding, the fibers were well anchored in the paper and the load during the tear test caused fibers to break [46]. This finding on cellulose papers is also very similar to our observation in GO papers as discussed below. The tearing process in GO papers was complex because the plane of fracture changed during the tear propagation: the fracture surface was initially oriented perpendicular to the paper face and tended to become almost 180° at the end [47], showing large, flat torn surface areas (Figs. 8(a) and 8(c)).On the microscopic scale, the torn fracture surfaces were uneven and irregular: although there were large differences in overall tearing toughness, the torn surface morphologies were in general similar for all GO papers. Essentially, fracture occurred due to the combination of two distinct failure modes, namely cohesive and adhesive failures. Because the cracks always propagate through the weakest paths, there were competitions between the tearing strength of the individual or bundle GO sheets and the force to separate between them, leading to cleavage fracture and de-bonding, respectively, once the driving force overcame each of the resistance. Judging from the lower tearing toughness of the small GO papers than the large GO papers, it is assumed that cleavage was more dominant than the de-bonding mechanism.

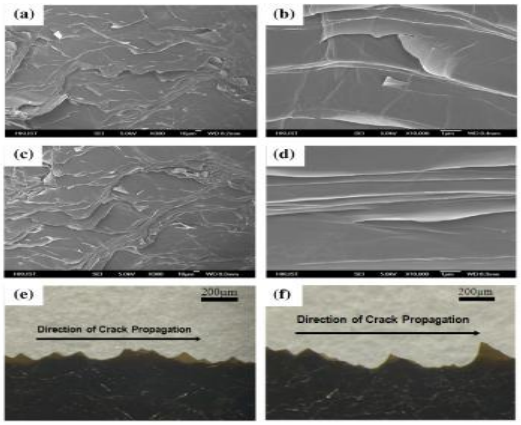

Figure 8. SEM photographs of torn surfaces of (a, b) small GO papers and (c, d) large GO papers; optical images of torn edges of (e) small and (f) large GO papers.

This hypothesis is partly confirmed by the optical images showing twisty crack paths at the edges of the papers (Figs. 8(e) and 8(f)). The torn edges presented typical of a saw tooth wave with disordered oscillation where the large GO papers exhibited generally higher amplitude peaks than the small GO papers, a reflection of inherent GO sheet size. The tearing toughness of GO/CNT hybrid papers is plotted as a function of CNT content as shown in Fig. 9(a). The tearing toughness of the neat CNT paper was only ~3.0% that of neat GO papers (0.033 vs 1.1 kJ/m^2 for 69 μm thick papers), and was even much less than half the mode I fracture toughness (0.072 kJ/m^2) of the same material.

Figure 9. (a) Tearing toughness of GO/CNT hybrid papers as a function of CNT content; typical SEM image of torn surface of GO/CNT hybrid paper with (b) 5 wt.% and (c) 10 wt.% CNTs.

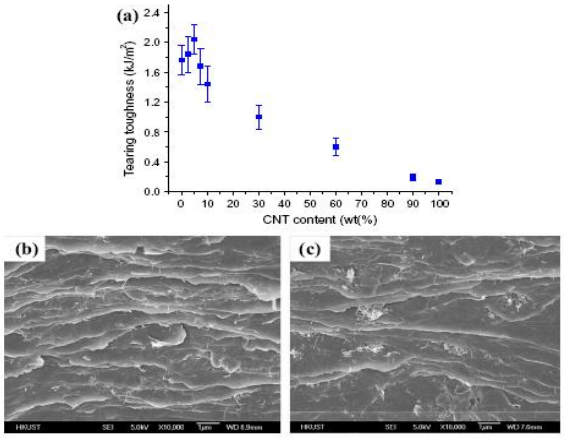

It is assumed that the highly porous structure of CNT papers was less resistance to fracture in out-of-plane shear than in uni-axial tension because the crack propagation occurred mainly by disentanglement of CNT bundles assembled by weak van der Waals forces. The torn fracture surface of the CNT papers had a much the same morphology as for the mode I fracture surface (Fig. 6(b)), indicating CNT pullout was the dominant failure mechanism in tear.

Resembling the mode I fracture toughness values (Fig. 6(a)), the hybrid papers containing a small amount of CNTs showed an ameliorating effect on tearing toughness. With 5 wt.% CNTs, the tearing toughness of the hybrid papers increased by almost 15% compared to the neat GO papers, a manifestation of strong bonds between the CNTs and GO sheets. With further addition of CNTs, the tearing toughness continued to drop, similar to mode I fracture toughness, but above the value corresponding to the neat CNT papers. The torn surface of the GO/CNT hybrid papers produced complex fracture morphologies (Figs. 9(b) and 9(c)) which significantly differ from those of the neat GO papers (Figs. 8(b) and 8(d)), all of whom were taken at a similar magnification. It is interesting to note that the hybrid papers showed generally more GO torn edges than the neat GO papers, perhaps as a result of more uniform dispersion of GO sheets aided by the presence of CNTs. The intercalated, small amount of CNTs enhanced the GO inter sheet bonds through the π-π interactions as discussed above. The CNTs were well dispersed when the CNT content was low (5 wt.%), and with increasing the CNT content (10 wt.%) they tended to be agglomerated, unable to improve the tearing toughness.

4. Conclusions

The fracture resistance of neat GO and GO/CNT hybrid papers was studied and the corresponding failure mechanisms are identified in two different modes, including mode I fracture using the double edge notched tensile (DENT) test and mode III tearing using the trouser test. The effects of GO sheet size and CNT content on the fracture properties of these papers were specifically studied. An easy and efficient centrifugation was used to sort the (as-prepared) GO sheets into two different size groups, large and small GO sheets. The following can be highlighted from the experimental study.

GO paper made from large GO sheet gives higher fracture and tearing toughness than those from small GO sheets. About 36% enhancement of strain energy release rate and 70% enhancement of tearing toughness were observed. Hybridization with CNTs also enhanced these two properties only when small amounts of CNTs were incorporated so as to maintain strong bonds with the surrounding GO sheets: the fracture toughness increased by 22% and tearing toughness by 15% after hybridization with 5 wt.% of CNT, compared to the neat GO papers. The failure mechanisms taking place during the quasi-static fracture and trouser tearing tests were identified from the microscopic examination of the fracture surfaces. Cohesive failure and combination of cohesive/adhesive failures were found in mode-I and mode-III fracture of GO papers, respectively. The torn edges exhibited typical of a saw tooth wave with disordered oscillation where the large GO papers had generally higher amplitude peaks than the small GO papers. In contrast, the GO/CNT hybrid papers failed mainly by a combination of the above mechanisms plus CNT pullout, depending on CNT content.

References

[1] K.S. Novoselov, A.K. Geim, S.V. Morozov, D. Jiang, Y. Zhang, S.V. Dubonos, V. Grigorieva, A.A. Firsov, Electric field effect in atomically thin carbon films, Science, 306, 666-669, 2004.

[2] K.S. Novoselov, A.K. Geim, S.V. Morozov, D. Jiang, M.I. Katsnelson, S.V. Dubonos, A.A. Firsov, Two dimensional gas of mass less dirac fermions in graphene, Nature, 438, 197–200, 2005.

[3] A.K. Geim, K.S. Novoselov, The rise of graphene, Nat. Mater, 6, 183-191, 2007.

[4] W.S. Hummers, R.E. Offeman, Preparation of graphitic oxide, J. Am. Chem. Soc. 80, 1339, 1958.

[5] S. Stankovich, R. Piner, S.T. Nguyen, R.S. Ruoff, Synthesis and exfoliation of isocyanate-treated graphene oxide nanoplatelets, Carbon, 44, 3342–3347, 2006.

[6] Z.D. Huang,B. Zhang, S.W. Oh, Q.B. Zheng, X.Y. Lin, N. Yousefi, J.K. Kim, Self-assembled reduced graphene oxide/carbon nanotube thin film as electrodes for supercapacitors, J Mater Chem, 22, 3591–3599, 2012.

[7] N. Yousefi, M.M. Gudarzi, Q.B. Zheng, S.H. Aboutalebi, F. Sharif, J.K. Kim, Self-alignment and high electrical conductivity of

ultralargegrapheneoxide-polyurethane nanocomposites, J. Mater. Chem. 22, 12709-12717, 2012

[8] D. Li, M.B. Muller, S. Gilje, R.B. Kaner, G.G. Wallace, Processable aqueous dispersions of graphene nanosheets, Nat.Nanotechnol, 3, 101-105, 2008.

[9] Z.D. Huang, B. Zhang, R. Liang, Q.B. Zheng, S.W. Oh, X.Y. Lin, N. Yousefi and J.K. Kim, "Effects of Reduction Process andCarbon Nanotube Content on Supercapacitive Performance of Flexible Graphene Oxide Papers"Carbon, 50, 4239-4251, 2012.

[10] A.R. Ranjbartoreh, B. Wang, X. Shen, G. Wang, Advanced mechanical properties of graphene paper, J. Appl. Phys., 109, 014306-6, 2011.

[11] D. A. Dikin, S. Stankovich, , E. J Zimney, R. D. Piner, G. H. B. Dommett, G. Evmenenko, S. T. Nguyen, R. S. Ruoff, Preparation and characterization of graphene Oxide Paper. Nature, 448, 457-460, 2007

[12] S. Park, K. S.Lee, G. Bozoklu, W. Cai, S. B. T. Nguyen, R. S. Ruoff, Graphene Oxide Papers Modified by Divalent Ions—Enhancing Mechanical Properties *via* Chemical Cross-Linking. ACS Nano, 2, 572-578, 2008.

[13] Y. Tian , Y. Cao , Y. Wang , W. Yang , and J. Feng, Realizing Ultrahigh Modulus and High Strength ofMacroscopic Graphene Oxide Papers Through Crosslinkingof Mussel-Inspired Polymers. Adv. Mater. *25*, 2980–2983, 2013

[14] O. C. Compton, S. W. Cranford, K. W. Putz, Z. An, L. C. Brinson, M. J. Buehler, S. T. Nguyen, Tuning the Mechanical Properties of Graphene Oxide Paper and Its Associated Polymer Nanocomposites by Controlling Cooperative Intersheet Hydrogen Bonding. ACS Nano, 6, 2008-2019, 2012

[15] M, Cano, U. Khan, T. Sainsbury, A. O'Neill, Z.M. Wang,I.T. McGovern, W.K. Maser, A.M. Benito, J.N. Coleman. Improving the mechanical properties of graphene oxide basedmaterials by covalent attachment of polymer chains, Carbon, 52, 363-371, 2013

[16] W.O. Lee, J.U. Lee, B.M. Jung, J.H. Byun, J.W. Yi,S.B. Lee, B.S. Kim. Simultaneous enhancement of mechanical,electrical and thermal properties of graphene oxidepaper by embedding dopamine. Carbon, 65, 296-304, 2013

[17] D.A. Dikin, S. Stankovich, E.J. Zimney, R.D, Piner, G.H.B. Dommett, G. Evmenenko, S.T. Nguyen, R.S. Ruoff, Preparation and characterization of graphene oxide paper, Nature, 448, 457-60, 2007.

[18] S. Park, K.S. Lee, G. Bozoklu, W. Cai, S.T. Nguyen, R.S. Ruoff, Graphene oxide papers modified by divalent ions-enhancing mechanical properties via chemical cross-linking, ACS Nano, 2, 572–578, 2008.

[19] A.R. Ranjbartoreh, B. Wang, X. Shen, G. Wang, Advanced mechanical properties of graphene paper, J. Appl. Phys., 109, 014306-6, 2011.

[20] X. Sun, Z. Liu, K. Welsher, J. Robinson, A. Goodwin, S. Zaric, H.J. Dai, Nano-graphene oxide for cellular imaging and drug delivery, Nano Res. 1, 203-212, 2008.

[21] Z. Liu, J.T. Robinson, X.M. Sun, H.J. Dai, Pegylatednano-graphene oxide for delivery of water insoluble cancer drugs, J. Am. Chem. Soc. 130, 10876-10877, 2008.

[22] S.J. Wang, Y. Geng, Q.B. Zheng and J.K. Kim, "Fabrication of highly conducting and transparent graphene films" Carbon 48,1815-1823, 2010

[23] Q.B. Zheng, W.H. Ip, X.Y. Lin, N. Yousefi, K.K. Yeung, J.K. Kim, Transparent conductive films consisting of ultralarge graphene sheets produced by Langmuir-Blodgett assembly, ACS Nano, 5, 6039–6051, 2011.

[24] S. Pan, I.A. Aksay, Factors controlling the size of graphene oxide sheets produced via the graphite oxide route, ACS Nano, 5, 4073-4083, 2011.

[25] X. Wang, H. Bai, G. Shi, Size fractionation of graphene oxide sheets by pH-assisted selective sedimentation, J. Am. Chem. Soc. 133, 6338-6342, 2011

[26] L. Zhang, J. Liang, Y. Huang, Y. Ma, Y. Wang, Y. Chen, Size-controlled synthesis of graphene oxide sheets on a large scale using chemical exfoliation, Carbon, 47, 3365-3380, 2009.

[27] M.M. Waje, X. Wang, W. Li, Y. Yan, Deposition of platinum nanoparticles on organic functionalized carbon nanotubes grown in situ on carbon paper for fuel cells, Nanotechnology, 16, 395-400, 2005

[28] F. Zheng, D.L. Baldwin, L.S. Fifield, N.C. Jr. Anheier, C.L. Aardahl, J.W. Grate, Single-walled carbon nanotube paper as a sorbent for organic vapor preconcentration, Anal Chem, 78, 2442–2446, 2006.

[29] Y. Geng, S.J. Wang, J.K. Kim, Preparation of graphite nanoplatelets and graphene sheets, J. Colloid Interf. Sci. 336, 592-598, 2009

[30] W.S. Hummers, R.E. Offeman, Preparation of graphitic oxide, J. Am. Chem. Soc. 80, 1339, 1958.

[31] S.H. Aboutalebi, M.M. Gudarzi, Q.B. Zheng, J.K. Kim, Spontaneous formation of liquid crystal in ultralarge graphene oxide dispersions, Adv. Funct. Mater, 21, 2978–2988, 2011

[32] X.Y. Lin, X. Shen, Q.B. Zheng, N. Yousefi, L. Ye,Y.W. Mai, J.K. Kim, Fabrication of highly-aligned, conductive, and strong graphene papers using ultralargegraphene oxide sheets, ACS Nano, 6, 10708–10719, 2012.

[33] Standard test for plane strain fracture toughness of metallic materials, ASTM E-399, American

Society for Testing and Materials, Philadelphia, PA, 1987.
[34] A. Gupta, G. Chen, P. Joshi, S. Tadigadapa, P.C. Eklund, Raman scattering from high-frequency phonons in supported n-graphene layer films, Nano Lett. 6, 2667–2673, 2006
[35] A.C. Ferrari, J.C. Meyer, V. Scardaci, C. Casiraghi, M. Lazzeri, F. Mauri, S. Piscance, D. Jiang,K.S. Novoselov, S. Roth, A.K. Geim, Raman spectrum of graphene and graphene layers, Phys. Rev. Lett. 97, 187401- 4, 2006
[36] G. Venugopal, M.H. Jung, M. Suemitsu, S.J. Kim, Fabrication of nanoscale three dimensional graphite stacked junctions by focused-ion-beam and observation of anomalous transport characteristics, Carbon, 49, 2766-2772, 2011.
[37] M.A. Pimenta, G. Dresselhaus, M.S. Dresselhaus, L.G. Cançado, A. Jorio, R. Saito, Studying disorder in graphite-based systems by Raman spectroscopy, Phys. Chem. Chem. Phys. 9, 1276-1291, 2007.
[38] Q.B. Zheng, Y. Geng, S.J. Wang, ZG Li and J.K. Kim, "Effects of functional group on the mechanical and wrinkling properties ofgraphene sheets" Carbon, 48, 4315-4322, 2010.
[39] X.F. Zhang,T.V. Sreekumar,T. LiuandS. Kumar, Properties and structure of nitric acid oxidized single wall carbon nanotube films, J. Phys. Chem. B, 108, 16435-16440, 2004.
[40] J.W. Zhang, D.Z. Jiang, H.X. Peng, F. Qin, Enhanced mechanical and electrical properties of carbon nanotube buckypaper by in situ cross-linking, Carbon, 63, 125-132, 2013
[41] D.F. Caulfield and D.E. Gunderson, Paper testing and strength characteristics, TAPPI proceedings of the 1988 paper preservation symposium: Wahsington, DC, USA. TAPPI Press: pp. 31-40, 1988.
[42] H.W. Greensmith, A.G. Thomas, Rupture of rubber -III Determination of tear properties, Rubber Chem. Technol.29 372-381, 1956.
[43] R.G. Stacer, L.C. Yanyo, F.N. Kelley, Observations on the tearing of elastomers, Rubber Chem. Technol. 58, 421-435, 1985.
[44] Y. Tanaka, H. Abe, T.Kurokawa, H. Furukawa, J.P. Gong, First Observation of Stick-Slip Instability in Tearing of Poly(vinyl alcohol) Gel Sheets, Macromolecules, 42, 5425-5426, 2009.
[45] Seth, R. S. (1996): Optimizing reinforcement pulps by fracture toughness. TappiJ., vol. 79, no 1, pp. 170-178.
[46] D.H. Page and J.M. MacLeod, Fiber strength and its impact on tearstrength. Tappi, J. vol. 75, 172-174, 1992
[47] H. Karlsson, L. Beghello, L. Nilsson, L. Stolpe. Abaca as a reinforcement fibre for softwood pulp, TAPPI J. 6, 25-32, 2007

ICMIEE-PI-140425

International Conference on Mechanical, Industrial and Energy Engineering 2014
26-27 December, 2014, Khulna, BANGLADESH

Comparison of Sliding Frictions of Different Materials Using a Digital Sliding Friction Tester

Kamrul Hasan Chowdhury, Md. Nafis Soyaib and Dr. Sobahan Mia[*]
Department of Mechanical Engineering,
Khulna University of Engineering & Technology, Khulna-9203,BANGLADESH

ABSTRACT: Friction Tester has a greater importance in the field of fundamental friction studies such as friction testing of metal surfaces, soft and hard coatings, plastics, glasses, polymers and different types of fabrics with or without lubricants. So it has been decided to construct a friction tester and measure the coefficient of friction of various materials in different conditions. In order to do that, various types of friction tester has been studied and finally it has been decided to design and construct a Digital Sliding Friction Tester. In this construction a 24 Volt dc motor was used which elevates a sliding plate. A gear mechanism was used to transfer the motion from motor to shaft. After construction performance test has been done with respect to various parameters and conditions. The obtained result from Digital Sliding Friction Tester was compared with manually calculated friction tester and standard ASTM chart. This showed a very good accuracy with a deviation of negligible amount of 1-6%. Results showed that the coefficient of friction is independent of load and is totally dependent on material and surface roughness.

Keywords: Friction, Static Friction, Coefficient of Static Friction, Friction Tester, Lubrication.

1.Introduction

Friction is the force resisting the relative motion of solid surfaces, fluid layers, and material elements sliding against each other. As a consequence of friction, the process of motion and the dynamic behavior of the whole system are influenced or disturbed and some part of the energy of motion is dissipated [1].

There are four types of friction namely. Static friction is friction between two or more solid objects that are not moving relative to each other.Static frictional forces from the interlocking of the irregularities of two surfaces will increase to prevent any relative motion up until some limit where motion occurs. It is that threshold of motion which is characterized by the coefficient of static friction. The magnitude of static friction depends upon μs (coefficient of static friction) and N (net normal reaction of the body). Kinetic friction denoted as $\mu_k$comes into play when a body just starts moving along a surface. When external applied force is sufficient to move a body along a surface then the force which opposes this motion is called as kinetic frictional force. μk is coefficient of kinetic frictional force and N is the net normal reaction on the body. The magnitude of kinetic frictional force is always less than magnitude of static frictional force. When value of applied net external force, F is more than f_k then body moves with a net acceleration and when these forces are equal then body moves with a constant velocity. Rolling frictional force is a force that slows down the motion of a rolling object [2]. Basically it is a combination of various types of frictional forces at point of contact of wheel and ground or surface. When a hard object moves along a hard surface then static and molecular friction force retards its motion. When soft object moves over a hard surface then its distortion makes it slow down. When a body moves in a fluid or in air then there exists a resistive force which slows down the motion of the body, known as fluid frictional force. A freely falling skydiver feels a drag force due to air which acts in the upward direction or in a direction opposite to skydiver's motion. The magnitude of this drag force increases with increment in the downward velocity of skydiver. At a particular point of time the value of this drag force becomes equal to the driving force and skydiver falls with a constant velocity.

*Corresponding author. Tel.: +88-01711951400
E-mail address: smia@me.kuet.ac.bd

Coefficient of friction is the ratio of the weight of an object being moved along a surface and the force that maintains contact between the object and the surface[3]. The coefficient of friction is not always the same for objects that are motionless and objects that are in motion; motionless objects often experience more friction than moving ones, requiring more force to put them in motion than to sustain them in motion. The static coefficient of friction is the coefficient of friction that applies to objects that are motionless. The kinetic or sliding coefficient of friction is the coefficient of friction that applies to objects that are in motion.

2. Design and Construction

2.1 General Components

The general components of a Digital Sliding Friction Tester are:

Base Plate: The Base Plate is the part which supports the whole foundation and the other parts of the Friction Tester are mounted on it.

Sliding Plate: Sliding plate is that part on which the test specimen is placed. It is welded with the main shaft.

Main Shaft: The main shaft is welded with the Sliding Plate. The two ends of the shaft are attached to the Base Plate. For smooth rotation of the shaft two bearings are mounted at the two ends of the shaft.

Motor: In this machine the motor is the main mechanical power source to elevate the sliding plate by rotating the main shaft. For smooth elevation of the sliding plate a motor of low rpm and high torque is used.

Gear arrangement: For transmitting the power from motor to main shaft a 2:1 spur gear arrangement is used.

Bearings: A pair of 6202 bearings is used to support the main shaft.

Electronic components: Microcontroller ATmega8, 16x2 LCD Screen, Motor Driver L298N, IR Sensor etc.

2.2 Design Details

Study of mechanics of friction dates back to the sixteenth century, after the invention of Newton's law of motion. The variation of friction depends on interfacial conditions such as geometry, relative surface motion, surface roughness of contact surfaces, type of material, lubrication etc. Among these factors material and surface roughness are two major factors which play significant role for the variation of friction. And in this observation it is high lightened to observe the variation of static friction for different material. In order to determine this observation a Digital Sliding Friction Tester has been designed. This machine is not available in our country. In foreign countries such as China and Canada analog version of this machine is used. Different type of Friction Tester has been studied on internet and learned about the analog version of this machine. Then the machine has been designed in Solid Works 2013.

A schematic diagram of the design has been shown on the Fig.1. Here, the base of the structure is constructed with 0.0625 inch thick galvanized iron sheet. The sliding plate is attached to the rotating shaft. The gear is attached at the middle of the shaft. This whole arrangement is further attached with the base with the bearings. The electric motor is used as a source of mechanical power. A pinion is attached with the motor shaft to transmit power from motor to shaft. The experiment was carried out for different materials.

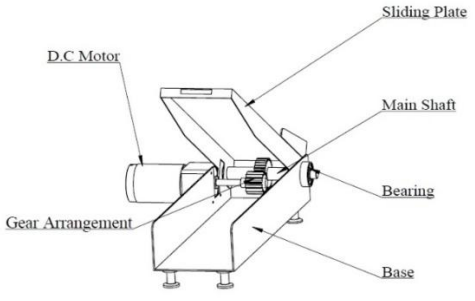

Fig.1 Aschematic diagram of Digital Sliding Friction Tester.

Fig.2 A Digital Sliding Friction Tester after construction.

3. Testing Procedure

To determine the influence of surface roughness of various materials on static coefficient of friction were carried out under both dry and wet condition. At first the testing specimen was placed on sliding plate which was in initial position (0º angle) and another specimen of same material was attached with a sliding block and placed on top of that material. Then the machine was switched on and the sliding plate started to lift at an angle with a constant velocity. For accurate results the angular velocity of the sliding plate should be maintained at a range of 0.3-0.5 rpm. A certain time later for a certain angle the weight block started to move on and the sliding plate stops at that angle immediately. Since the motor speed varies with the load, the load shouldn't exceed 5N. A photo sensor was used to facilitate that immediate action. After that the angle was taken on account and doing the whole calculation with the help of microcontroller the final result was showed on LCD screen. That was the result of static coefficient of friction for that specific material. Finally, another switch was used to bring back the sliding plate in its initial position.

4. Experimental Data

The data collected during the performance test at 70% relative humidity are as follows:

Table1: Coefficient of static friction of various materials without lubrication

M1	M2	Static Coefficient of Friction, μ_s			D (%)
		μ_{s1}	μ_{s2}	μ_{s3}[4]	
Glass	Glass	0.44	0.46	0.45	2.22
Cast Iron	Glass	0.67	0.68	0.70	4.30
Glass	Wood	0.47	0.47	0.45	4.44
GI Sheet	Glass	0.64	0.66	0.50-0.70	1.54
Plywood	Plywood	0.80	0.78	0.70-0.80	1.00
Plywood	GI Sheet	0.59	0.58	0.60	1.67
GI Sheet	Brass	0.36	0.36	0.35	2.78
Cast Iron	GI Sheet	0.63	0.64	0.65	3.08
Wood	Brass	0.65	0.62	0.60	3.33
Wood	Wood	0.48	0.48	0.50	4.00
Cast Iron	Wood	0.60	0.59	0.50-0.60	1.67
Wood	GI Sheet	0.66	0.63	0.65	1.54
Hard board	Hard Board	0.78	0.77	0.75	4.00
Hard board	GI Sheet	0.69	0.68	0.70	1.43
Brass	Glass	0.36	0.36	0.35	2.78
Plywood	Brass	0.53	0.54	0.55-0.60	3.64
Brass	Hard Board	0.58	0.60	0.50-0.60	3.33
Carton	Carton	0.68	0.68	0.70	2.86
Glass	Carton	0.70	0.72	0.75	4.00
Carton	Cast Iron	0.60	0.59	0.60	1.67
Brass	Carton	0.71	0.71	0.70	1.41
Tiles	Tiles	0.56	0.57	0.60	5.00
Brass	Tiles	0.48	0.49	0.50	4.00
Tiles	Cast Iron	0.58	0.59	0.60	3.33

5. Discussion

The main goal in this project was to investigate the influence of surface roughness of various materials on coefficient of friction. The nature of friction is to

Table2: Coefficient of static friction of various materials with lubrication

M1	M2	Static Coefficient of Friction, μ_s			D (%)
		μ_{s1}	μ_{s2}	μ_{s3}[5]	
Glass	Glass	0.21	0.22	0.2	5.00
Cast Iron	Glass	0.28	0.29	0.3	3.33
Glass	Wood	0.32	0.33	0.35	5.71
GI Sheet	Glass	0.34	0.36	0.35-0.40	2.86
GI Sheet	Brass	0.24	0.26	0.25	4.00
Cast Iron	GI Sheet	0.30	0.29	0.30	3.33
Wood	Brass	0.36	0.38	0.40	5.00
Cast Iron	Wood	0.37	0.39	0.35-0.40	2.5
Wood	GI Sheet	0.36	0.34	0.35	2.86
Hard board	GI Sheet	0.38	0.37	0.40	5.00
Brass	Glass	0.24	0.26	0.25	4.00
Brass	Hard board	0.45	0.47	0.45	4.25
Tiles	Tiles	0.33	0.32	0.35	5.71
Brass	Tiles	0.29	0.29	0.30	3.33
Tiles	Cast Iron	0.33	0.33	0.35	5.71

increase with the increase of normal force. Frictional force is independent of apparent area of contact. It has been found that by applying lubricant between the contact surfaces friction can be minimized significantly. For wet condition the friction is also reduced between the contact surfaces. For changing the angular position of the sliding plate smoothly a motor of low speed and high torque was used. The construction was made such a way so that the specimens can be loaded and unloaded easily. Since vibration has a great effect on frictional phenomena, the main basement was welded with legs. During the performance test for keeping one surface fixed clamps were used. The relative humidity of the atmosphere has a great effect on the static friction coefficient. At humid condition, for a pair of metal the water particles of the air act as lubricant at the contact surfaces. But for glass and polymers the coefficient of friction increases with the increase of relative humidity. Lubricants play a great role in reducing the friction. The co-efficient of static friction varies with different lubricants with different additives. The viscous properties of the lubricants vary with the temperature. From tables 1 and 2 it can be seen that for both with and without lubricants the digitally obtained results vary at a range of 1-6% in comparison to the standard values from ASTM chart. The magnitudes of friction coefficient are different for different sliding pairs and lubricants, therefore maintaining appropriate level of relative humidity as well as appropriate choice of sliding pair, friction may be kept to some optimum value to improve mechanical processes.

6.0 Conclusion

From the study and within the experimental setup, the following conclusions may be drawn:

The Coefficient of static friction of various materials at different conditions has been measured. From the test it can be concluded that-

I. The co-efficient of friction depends on contact surface condition of material.

II. The frictional force is independent of apparent area of contact.

III. Test result is satisfactory with 15% variation.

NOMENCLATURE

N: normal reaction force, N

F: force, N

Θ : angle, ^{o}

μ_s :coefficient of static friction.

μ_{s1} :coefficient of static friction obtained digitally.

μ_{s2} :coefficient of static friction obtained manually.

μ_{s3} :coefficient of static friction obtained from ASTM chart.

M 1: Material 1

M 2: Material 2

D : Deviation with standard chart, %

REFERRENCES

[1] R.J. Wakelin (1974), "The friction, lubrication and wear of moving parts", Vol. 4, UK, p. 221.

[2] G. Vogelpohl (1958), "Reliable bearings", Springer, Berlin.

[3] M. Fuchsel (1929), "Ober Verschlei & Berkeit the materials in dry friction", Organ Fortschr. Eisenbahnwes, p. 84, 413.

[4] Peter J. Blau (1964), "Friction Science and Technology: From Concepts to Applications", Second Edition, Taylor and Francis group, p. 25

[5] ASM Handbook (1997), "Friction, Lubrication and Wear Technology", Vol. 18, p. 112.

ICMIEE-PI-140426

International Conference on Mechanical, Industrial and Energy Engineering 2014
26-27 December, 2014, Khulna, BANGLADESH

Construction and Performance Test of a Thermal Cracking Apparatus

Md. Nizam Uddin, Md. Noman Morshed and Farhan Islam
Department of Mechanical Engineering, Khulna University of Engineering and Technology (KUET), Khulna-9203, Bangladesh
Email address: engrnizam02@gmail.com

ABSTRACT

Bio-fuel is a source of energy that human beings have been used since ancient times. Now a day's the demand of bio-fuels for energy generation purposes increase because they allow mitigation of greenhouse gases. Thermo-chemical conversions of vegetable oils have become an attractive and alternative method for the production of high grade bio-fuels. In this project, bio-fuel has obtained by thermal cracking of rice bran oil and sunflower oil. These bio-fuels have characterized by density, viscosity, gross calorific value and boiling point. The pyrolysed or cracked bio-fuels exhibit physical properties very similar to traditional fossil fuels and the bio-fuel production does not show the typical setback of transesterification methodology for producing bio-fuel. The main focus of this study is construction of a thermal cracking apparatus and characterized the cracked bio-fuels. Here the main consideration was the recovery of liquid products which are composed of higher boiling point hydrocarbons. The cracking temperature was 380ºC or 400ºC and the residence time was 1 hour or more.

Keywords: Thermal cracking, bio-fuel, pyrolysis, two neck flask.

1.0 Introduction

Vegetable oils and animal fats are prospective sources for the production of bio-fuel and hydrocarbons [1]. The world's accessible oil reservoirs are gradually depleting due to a burgeoning demand of fossil fuel. In addition, the production and consumption of fossil fuels have caused severe environmental pollution by generating carbon dioxide leading to greenhouse effects. Therefore, there is a pressing need for the development of alternative energy sources as useful fossil fuel substitutes. The search for alternatives has been stimulated by petroleum price and supply oscillations as well as by predictions of petroleum scarcity [2]. Life at the present moment is caught between two major crises because of fossil fuel depletion and environmental degradation. Bio-fuel is derived from a renewable, domestic resource, thereby relieving reliance on petroleum fuel imports. It is biodegradable and nontoxic. In comparison to petroleum-based diesel, carbon dioxide produced by combustion of bio-fuel can be recycled by photosynthesis, thereby minimizing the impact of bio-fuel combustion on the environment problem. In brief, these merits of bio-fuel make it a good alternative to petroleum-based fuel and have led to its use in many countries especially in environmentally sensitive areas. Bio-fuels are generally referred to gaseous or liquid fuels that are produced from renewable sources. A variety of liquid fuels can be produced from renewable resources and those are ethanol, methanol, bio-diesel and Fischer-Tropsch gas oil using synthesis gas obtained from biomass. Gaseous fuels such as hydrogen and methane can be produced from a number of renewable sources. Liquid bio-fuels are generally used to fuel transportation vehicles, but they are also applicable to fuel engines or fuel cells for electricity generation [3]. The application of renewable natural sources in the bio-fuels production has significantly grown over the past decade. Technologies to produce these environmentally friendly fuels based on the conversion of vegetable oils have been highlighted in the last years. One of the methods to obtain green fuels is the production of diesel like by the thermal cracking of vegetable oils. The pyrolysis process, also known as thermal cracking is based on thermo-chemical decomposition of matter in the absence of oxidants [4-5]. The products of this decomposition are: a mixture of gases (CO2, CO, H2, CH4, etc.),

heavy hydrocarbons (gas condensable pyrolysis oil) and coke (carbon fixed and inert residual). The proportions of these products depend on process parameters, namely temperature, heating rate, the residence time of the raw material in the reactor, pressure and the raw material. Also, researchers have focused on the analysis of physicochemical properties of liquid obtained at the end of the process. Wiggers et al.[6] studied the pyrolysis of waste fish oil. According to their results, it appears that the liquid product obtained after the process has a high acid index, which is about 131.1 mg KOH/g, whereas this value should be very low, so it is very difficult to be used as fuel for diesel engines. The thermal cracking methodology to obtain hydrocarbons has been applied since Second World War in China by thermo-cracking of Tung oil. A myriad of studies about thermo-cracking have been developed since Second World War [7]. Thermal cracking is a process in which hydrocarbons such as crude oil are subjected to high heat and temperature to break the molecular bond and to reduce the molecular weight of the substance being cracked. This process is used to extract usable components, known as fractions, which are released during the cracking process. It is one among several cracking methods used in the petroleum industry to process crude oil and other petroleum products for commercial use. The thermal cracking method (also known as "Shukhov cracking process") was invented by Russian engineer Vladimir Shukhov and patented in 1891 in the Russian empire, patent no. 12926, November 27, 1891. This process was modified by the American engineer William Merriam Burton and patented as U.S. patent 1,049,667 on June 8, 1908. Various improvements to thermal cracking were introduced into the 1920s by French chemist Eugène Houdry. Important variables in thermal cracking are temperature, pressure and residence time. Side reactions like condensation and polymerization reactions also occur leading to gum formation and tar-like polymerization products. Simple Thermal cracking process produces gas, naphtha, middle distillates and thermal tar from almost all variety of charge stocks from distillates to the heaviest crude and residual oils. The feed is heated to cracking temperature 350 – 400ºC and the cracked products containing gas and Full Boiling Range distillates enters the fractionators after passing through an intermediates separator vessel. The process of cracking vegetable oils or animal fatties takes place in two successive and distinct stages. The first stage, known as primary cracking, is characterized by the formation of acid species through the decomposition of triglyceride molecules which occurs through breakage of the C–O bonds within the glycoside part of the triglyceride chain. The second stage is characterized by the degradation of the acids produced in the first stage leading to the formation of hydrocarbons with properties similar to those of petroleum products. This stage is called secondary cracking [8-13]. Various catalysts have been studied to produce hydrocarbons from oils and fatties. Among the main catalysts, zeolites, metallic oxides, pillared clays, silica, alumina and the mixture of this standout [8-11]. This works aims to construct a thermal cracking apparatus for bio-fuels production and the evaluation of properties of cracked bio-fuel and compare it with commercial diesel fuel.

2.0 Experimental

2.1 Thermal cracking

The thermal cracking reactions of rice bran oil and sunflower oil were carried out at temperatures between 380 and 400°C under atmospheric pressure. There are three different systems for thermal cracking: simple cracking (SC), modified simple cracking (MC) and fractionated cracking (FC), as presented in Fig. 1. In the SC system, a 46-cm straight condenser and a thermocouple are coupled to a two-mouthed round bottomed flask which serves as the reactor.

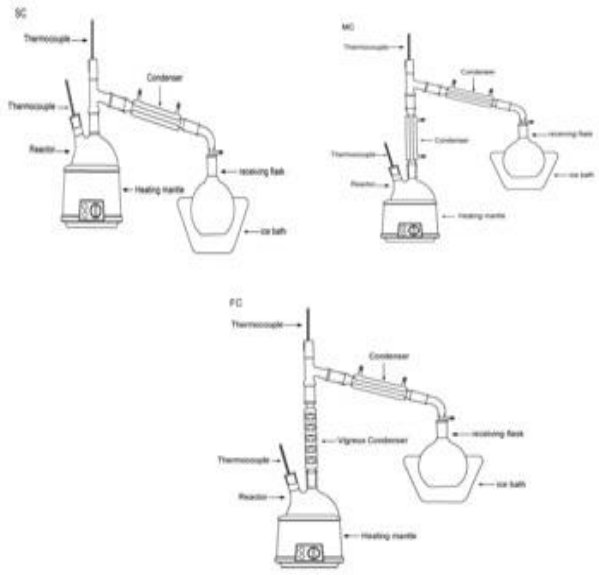

Figure 1 Different system for thermal cracking. SC- Simple cracking, MC- Modified simple cracking and FC- Fractioned cracking

The MC system differs from the SC system in the use of a 25-cm straight condenser without the passage of water which is coupled to a flask this promotes the

condensation of substances that volatilize in the course of cracking. In the FC system, the straight condenser of the MC system is replaced by a 31-cm-long Vigreux column [14].

2.1 Construction of thermal cracking apparatus

The thermal cracking apparatus consists of the four main components: Two neck flask, Electric heater, Condenser, Receiver flask. A two neck flask was used as a reactor for this study. It is made of Pyrex glass and its capacity is 500 ml. The heating of the reactor was carried out by a regulator control electric heater. It can develop up to 450ºC. One neck of the flask is connected with a thermometer via a rubber cork. Another neck is connected with one end of a V-shaped glass neck by using another cork. The other end of the V-shaped glass neck is connected with the condenser. There is a receiver flask connected behind the condenser and is kept on an ice bath. The complete set up is shown in figure 2.

Fig.2 Thermal cracking apparatus

2.2 Cracking the rice bran oil and sunflower oil

The experiment was carried out using simple system. The thermal cracking reactions of rice bran oil and sunflower oil were carried out using 150 ml of commercial rice bran oil and sunflower oil in a two neck flask, served as a reactor. The oil was taken into the reactor through the neck. Both necks were tightly sealed by high strength rubber cork so that no gas can come out during the experiment. A thermometer was connected to the reactor through the rubber cork through one neck. The thermometer was connected in such a way that it touched the oil that was kept inside the reactor before the reaction start. The water cooled condenser was used in the experiment. Other end of the condenser was connected to the receiver flask. The receiver flask was kept on an ice bath. The reactor was kept on an electric heater and then the heater was turned on. With the increase of time the temperature in the reactor was increased. The reactor was heated to the desired temperature (360-400ºC). At this temperature, the cracking reaction was taken place and the oil was started to vaporized. The vapor was passed through the v shaped neck to the condenser. Since the condenser was water cooled so that supply of water was made by a tap through pipe. The water was circulated through the outside chamber of the condenser and the vapor was passing through the inside chamber. While passing through the inside chamber vapor was condensed and the liquid product was collected in the receiver flask which was kept on the ice bath. The uncondensed gas was made to remove out from the receiver flask via a path that was kept above the receiver flask. Then the desired liquid product was collected from the receiver flask.

2.3 Measurement of calorific value of the as prepared bio-fuel

The calorific value of the as prepared bio-fuel was calculated using the following formula

$$\mathrm{Cx} + \mathrm{C_1 x_1} = (\mathrm{M} + \mathrm{W}) \times (\Delta\theta + 0.5 \times \Delta\mathrm{t} \times \mathrm{r})$$

Where

Gross calorific value, C

Fuse oil burned, x_1

Temperature difference, $\Delta\theta$

Time, Δ t

Mass of water content in the calorimeter, M

Water equivalent, W

Mass of oil, x

3.0 Results and discussion

3.1 Physical and thermal properties of as prepared bio-fuel

In this project two types of oil namely rice bran oil and sunflower oil were used as feedstock. These oils were collected from the local market. In this experiment 150 ml oil was used. The experiment was done separately for rice bran oil and sunflower oil. The experimental data obtained during thermal cracking process are shown in table-1.

Table-1 Experimental data for thermal cracking of rice bran oil and sunflower oil

Feed stock	Mother oil (ml)	Residence time (min)	Temperature (°C)	Cracked oil (ml)
Rice bran oil	150	70	380	40
Sunflower oil	150	75	400	50

The liquid product or cracked oil obtained after thermal cracking was light brown for both rice bran oil and sunflower oil. The amount of liquid product depends on feedstock properties. Cracking reaction was started when the temperature at the reactor reached the desired temperature. Since a high temperature was developed during the experiment, a lot of safety measures were taken under consideration during the cracking reaction of rice bran oil and sunflower oil. Bio-fuel was produced from rice bran oil and sunflower oil and the thermal properties were measured for both mother oil and cracked oil and compared with commercial diesel fuel. Figure-3 shows the thermal properties of rice bran oil and sunflower oil before and after thermal cracking.

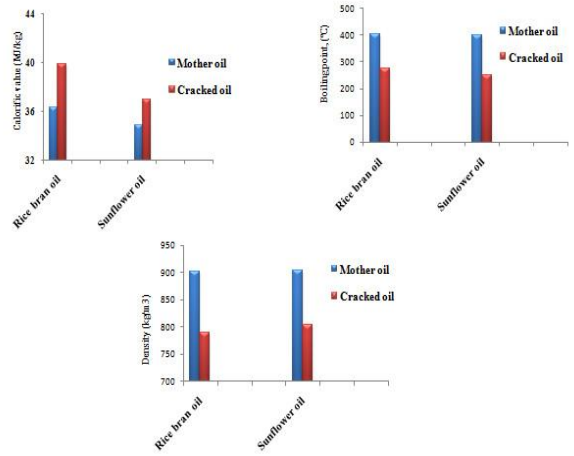

Figure 3 Thermal properties (calorific value, boiling point density) of rice bran oil & sunflower oil before and after cracking.

From fig.3 it shows that the cracked oil have higher calorific value than the as received rice bran and sunflower oil. The boiling point and density also reduced after cracking in case of two types of oil used here.

4.0 Conclusion

The present research shows that bio-gasoline could be produced from rice bran oil and sunflower using thermal cracking process The production of bio-fuels (especially bio-gasoline) from rice bran oil and sunflower oil by thermal cracking is a promising alternative. The as produced have higher calorific value than the rice bran and sunflower oil which is comparable to diesel fuel. The boiling point and density also reduced after cracking. Moreover, bio-fuel is very environment friendly because it reduces greenhouse effect on our environment by reducing carbon dioxide gas. In Bangladesh large amount of rice bran oil can be extracted from rice husk and this oil can be thermally cracked to improve their properties. So that it can use as biodiesel in various diesel like engine and it can save a huge amount of importing petroleum product from foreign countries.

References

[1] T.L Chew, S. Bhatia, Catalytic processes towards the production of biofuels in a palm oil and oil palm biomass-based biorefinery. Bioresour. Technol. 99, 2008, 7911–7922.
[2] M. Castellanelli, S.N.M. Souza, S.L. Silva, E.K. Kailer, Eng. Agric. 28 (2008) 145–153.
[3] O. Y. Kang, B. Shubash, The current status and perspectives of bio-fuel production via catalytic cracking of edible and non-edible oils, Energy 35(2010)111-119.
[4]K.D.Maher, D.C.Bressler,. Pyrolysis of triglyceride materials for the production of renewable fuels and chemicals. Bioresour Technol, 98,2007, 2351–68.
[5] L. Dandik, A. Aksoy,. Pyrolysis of used sunflower oil in the presence of sodium carbonate by using fractionating pyrolysis reactor. Fuel Process Technol, 57, 1998,:81–92.
[6] V.R.Wiggers, Jr A Wisniewski, Jr L.A.S. Madureira, A.A.C. Barros,H.F. Meier, Biofuels from waste fish oil pyrolysis: Continuous production in a pilot plant. Fuel 2009;88:2135–41.
[7] G. S.P.Alexandre, D.A.Romulo,J.W. B. Braga, P. A.Z. Suarez, Thermal diesel like analysis, Therm Anal Calorim, 110: (2012) 865–872
[8] E. Vonghia, D.G.B. Boocock, S.K. Konar, A. Leung, Energy Fuel 9 (1995) 1090–1096.
[9] K.D. Maher, D.C. Bressler, Bioresour. Technol. 98 (2007) 2351–2368.
[10] C.C. Chang, S.W. Wan, Ind. Eng. Chem. 39 (1947) 1543–1548.

[11] J.W. Alencar, P.B. Alves, A.A. Craveiro, J. Agric. Food Chem. 31 (1983) 1268–1270.
[12] R.O. Idem, S.P.R. Katikaneni, N.N. Bakhshi, Energy Fuels 10 (1996) 1150–1162.
[13] Cinara M.R. Prado, Nelson R.Antoniosi Filho, Production and characterization of bio-fuels obtained by thermal cracking and thermal catalytic cracking of vegetable oils, J. Anal. Appl. Pyrolysis 86 (2009) 338–347
[14]http://www.setlaboratories.com/therm/tabid/107/Default.aspx

Destination Mars: Frontiers in Expanding Human Presence in the Solar System

Ahsan Choudhuri, Ph.D.
Professor and Chair, Department of Mechanical Engineering
Mr. and Mrs. MacIntosh Murchison Chair II in Engineering
Director, NASA URC: Center for Space Exploration Technology Research
University of Texas at El Paso
E-mail: ahsan@utep.edu

This presentation provides an overview of the rationale and key technical challenges of the human exploration of Mars. Although the compulsion to explore Mars originates from the desire of human beings to explore, several key scientific questions provide the necessary underpinning for the Marsto be the next destination of human exploration. As a part of the inner planets of the solar system Mars has similar features such as atmosphere, polar ice cap, four seasons, and climate cycle like the planet Earth. The past and present orbiter and lander missions have revealed many interesting Earth like geological features (mountains, canyons, plateaus, and in-active volcanos) and confirmed the presence of water in the Martian atmosphere, in the subsurface, and soil. Scientific data collected through these missions indicate that Mars might have been warmer and wetter in the past. Although the surface conditions of the present-day Mars are inhospitable to terrestrial life, there is sufficient scientific evidence that around 3.5 billion years ago Mars may have had an environment conducive to the formation of lifefor over several hundred million years. Human exploration of Mars thus provides a compelling choice for understanding the origin of life on Earth, searching for life in the solar system, and developing a permanent human settlement.

From the first successful Mars fly-by mission of Mariner 4 spacecraft in 1964 to the most recent Mars Science Laboratory Rover*Curiosity* in 2012, the United States has been in the forefront of exploring the planet Mars through orbiter and robotic lander missions. The data collected from these missions have significantly improved the understanding of the geology and atmosphere of the Mars as well as advancing spacecraft technologies needed for the human spaceflight.The human spaceflight to Mars requires many technological advances as well significant budgetary and policy supportto develop complex space transportation, life-support, radiation shielding, and surface operation systems.NASA's exploration systems development effort which include the Orion Crew Exploration Vehicle (Orion CEV), Space Launch System (SLS), and Ground Systems will enable human exploration to deep space destinations including Mars.

The Center for Space Exploration Technology Research (cSETR) at the University of Texas at El Paso is a NASA University Research Center focusing on developing LO_2/LCH_4 propulsion technologies to support NASA's Mars Exploration strategies. The integrated LO_2/LCH_4 human spaceflight spacecraft architecture is based on utilizing a common fluid system (LO_2-LCH_4 for propulsion, power, and environmental control and life-support systems) scavenged from Martian atmosphere and surface using In-Situ Resource Utilization (ISRU) techniques. The LO_2/LCH_4 architecture has the potential to reduce 280 metric tons of initial launch masses to Low Earth Orbit (IMLEO) if 25 metric tons of oxygen can be produced in Mars for the Mars Ascent Vehicle (MAV). Additional IMLEO savings can also be achieved through possible production of methane using the water on Mars.

About the Speaker:Dr. Ahsan Choudhuri is a Professor and Chair of Mechanical Engineering and director and founder of the NASA funded Center for Space Exploration Technology Research at the University of Texas at El Paso, where he also holds the endowed Mr. and Mrs. MacIntosh Murchison Chair II in Engineering. Dr. Choudhuri received degrees in mechanical engineering from Khulna University of Engineering and Technology (B.S., 1992) and the University of Oklahoma (M.S., 1997, and Ph.D., 2000). Professor Choudhuri's teaching and research interests are in the area of aerospace systems and energy engineering. Dr. Choudhuri's current and previous research efforts include non-toxic cryogenic propulsion systems (NASA), fuel flexible gas turbine combustors (Department of Energy), oxy-fuel combustors (Department of Energy), materials for advanced turbines (Department of Energy), next generation green and solid propellants (Missile Defense Agency), turbopump technology for advanced liquid propellant rocket engines (Missile Defense Agency, NASA), advanced divert and attitude control systems for missile interceptors (Space and Missile defense command and Missile Defense Agency), and microgravity combustion and materials science (NASA).

AboutThe Center for Space Exploration Technology Research (cSETR):The Center for Space Exploration Technology Research (cSETR) at the University of Texas El Paso supports NASA's vision of space exploration by focusing on advanced capabilities in the areas of non-toxic and green propulsion. The cSETR vision is to establish a sustainable minority university center of excellence in advanced propulsion research through strategic partnerships and to educate a diverse future aerospace workforce. To achieve this vision and create advanced technologies and exploration capabilities for lunar, mars, solar system and beyond missions, a multidisciplinary engineering team partners with NASA centers (Johnson Space Center-lead NASA partner, Marshall Space Flight Center, Glenn Research Center, and NASA White Sands Test Facility), aerospace industries (Lockheed Martin Inc., Blue Origin, and ATK), and academic institutions (University of Maryland and Princeton University).

ICMIEE-PI-Keynote

Flow-Induced Forces and Fluid-Structure Interactions between Two Circular Cylinders

Md. Mahbub Alam [a,b,*]

[a]Institute for Turbulence-Noise-Vibration Interaction and Control, Shenzhen Graduate School
Harbin Institute of Technology, Shenzhen, China
[b]Key Kab of Advanced Manufacturing and Technology, Shenzhen Graduate School
Harbin Institute of Technology, Shenzhen, China

ABSTRACT
Flow-induced fluctuating lift (C_{Lf}) and drag (C_{Df}) forces and Strouhal numbers (St) of the downstream cylinder of two tandem cylinders are investigated experimentally for Reynolds number (Re) = 9.7×10^3 ~ 6.5×10^4. The spacing ratio L^* (= L/D) between the cylinders is varied from 1.1 to 4.5, where L is the spacing between the cylinders and D is the cylinder diameter. The results show that C_{Lf}, C_{Df} and St are highly sensitive to Re due to change in the inherent nature of the flow structure. How the flow structure is dependent on Re and L^* is presented in a flow structure map. Zdravkovich and Pridden in 1977 observed a 'kink' in time-mean drag distribution at $L^* \approx 2.5$ for Re > 3.1×10^4, but not for Re ≤ 3.1×10^4. The physics is provided here behind the presence and absence of the 'kink' that was left unexplained since then.

Keywords: fluid forces; tandem cylinders; fluid-structure interaction, flow structures, Strouhal numbers

1. Introduction

The flow over a circular cylinder is a classical case, studied extensively for over 100 years, as it contains a wide range of complex flow phenomena, despite its simple geometry. The flow displays different characteristics at different Re regimes. The most famous is the formation of the von Kármán vortex street, where counter-rotating vortices are shed from the cylinder in a periodic fashion [1]. This class of flow evolves in complexity when an additional cylinder is placed in the wake of the other [2].

Slender structures appear in groups in many engineering applications, for example, chimney stacks, tube bundles in heat exchangers, cooling of electronic equipments, high-rise buildings, overhead power-line bundles, bridge piers, stays, and chemical-reaction towers. Naturally, some structures in a group are submerged in the wake of the others. Two inline cylinders may be considered as the basic element of multiple structures, where the leeward cylinder is in the wake of the windward cylinder (Fig. 1a). The knowledge of this flow is insightful for understanding the flow around structures in groups.

The in-line configuration of two cylinders involves shear-layer and cylinder interaction that is strongly dependent on Re and L^*. The characteristics of the flow

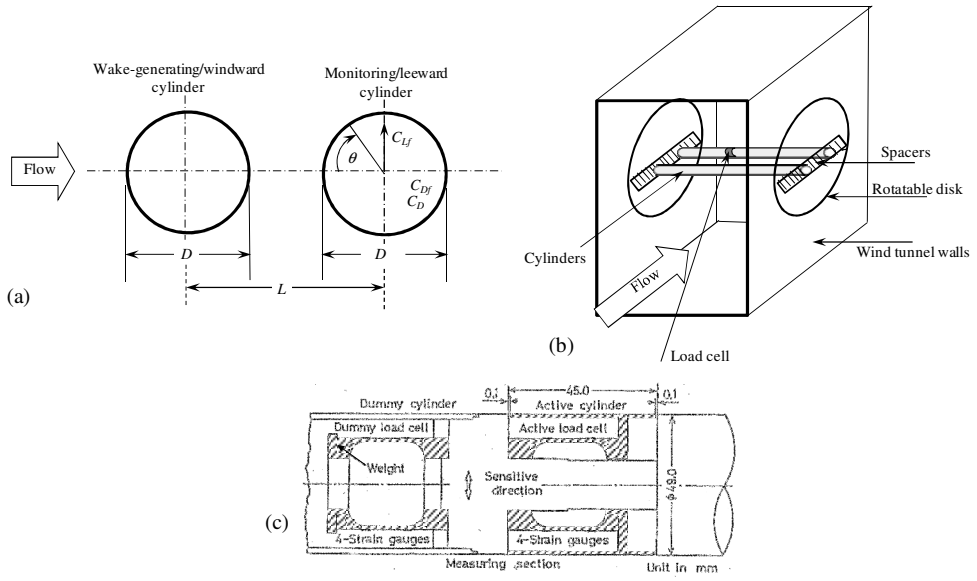

Fig. 1 (a) Notation of cylinder configuration, (b) a schematic of experimental setup, and (c) load cell details.

* Corresponding author. Tel.: +86-15014047005
E-mail address: alamm28@yahoo.com; alam@hitsz.edu.cn

around two cylinders has been extensively reviewed by [3].

Biermann and Herrnstein [4] measured time-averaged drag (C_D) on the two inline cylinders up to $L^* = 8$ (Re = 1.05×10^5). Therefore, more investigation was needed to clarify the other parameters, such as, C_{Df}, C_{Lf}, St, surface pressures, wakes, boundary layers, etc. Time-averaged pressure measurements were conducted by Zdravkovich and Pridden [5] at Re = 6×10^4 and Alam et al. [6] at Re = 6.5×10^4. The results showed that for $L^* <$ 3.5 a negative pressure on the front surface of the leeward cylinder was generated instead of a positive pressure, exceeding that on the rear surface. In case of the windward cylinder, the pressure only on rear surface was affected by the presence of the leeward cylinder.

Igarashi [7] examined the Re effects on St and pressure fluctuations for Re = 8.7×10^3 ~ 5.2×10^4, and noted that with increasing Re the pressure fluctuation on the cylinder surfaces increased and St decreased greatly between Re = 1×10^4 and 4×10^4. Zdravkovich and Pridden [5] examined the Re effect on C_D at Re = 3.1×10^4 ~ 1.2×10^5. When the two cylinders were in contact, C_D on the leeward cylinder was negative, increasing rapidly with L^*. An interruption of the increase rate occurred, forming a 'kink' at $L^* \approx 2.5$. The 'kink' was, however, absent at Re $\leq 3.1\times10^4$. The physics behind the presence and absence of the 'kink' was left unexplained, with a notation "further research is necessary to clarify this change at small Re". The literature focus in general on flow, C_D, and St for certain Re, barely giving any attention to C_{Df} and C_{Lf} in spite of the fact that the latter is of both fundamental and practical importance in fluid-structure interaction [8]. Measuring C_{Df}, C_{Lf} on two inline cylinders at Re = 6.5×10^4 for $L^* < 9$, Alam et al. [6] observed that C_{Df} and C_{Lf} on the rear cylinder are highly sensitive to L^*. Some other imperative questions left unexplained, such as, what are their dependences on Re? What is the physics behind the 'kink'? The objective of this work is to answer the above questions.

2. Experimental details

Experiments were conducted in a low-speed, closed-circuit wind tunnel with a test section of 1.20 m in height, 0.30 m in width, and 2.2 m in length (Fig. 1b). The diameter of each cylinder was 49 mm. Re based on cylinder diameter and free-stream velocity was 9.7×10^3, 1.6×10^4, 3.2×10^4, and 6.5×10^4. Surface oil-flow visualization was also conducted to get information on the shear layer reattachment and boundary layer separation. See Alam et al. [6] for details of the visualization. Flow-induced forces were measured over a small spanwise length of the leeward cylinder, using load cells (Fig. 1c). The cylinder was built in with an active ('live') section of a spanwise 45 mm ($0.92D$) length and two dummy sections. See Alam et al. [9] for details of the load cell. Definition of symbols and coordinate systems can be seen in Fig. 1(a). The position of a point on the surface of a cylinder is defined by the azimuthal angle θ, measured from the direction of free-stream flow. Experiments were performed for L^* = 1.1 ~ 4.5. Very fine-tuning of L^* ($\Delta L^* = 0.1, 0.2$) was adopted.

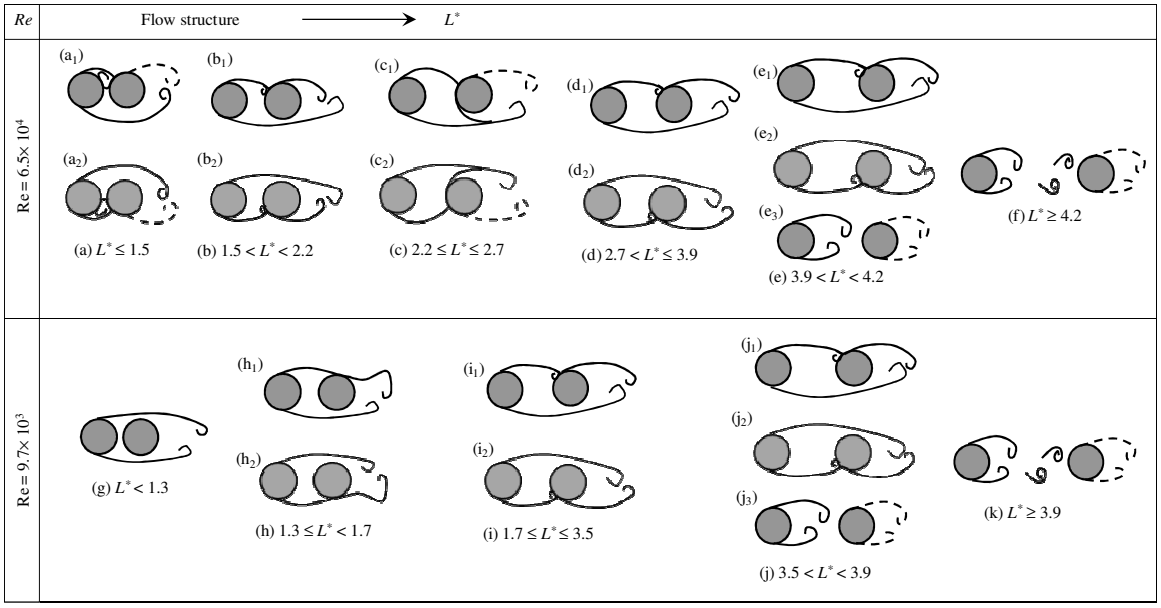

Fig. 2 Flow structures with variation in Re and L^*. (a) reverse-flow reattachment (RFR) flow, (b) front-side reattachment (FSR) flow, (c) front reattachment (FR) flow, (d) front-side reattachment (FSR) flow, (e) bi-stable (BS) flow between front-side reattachment and co-shedding flow, (f) co-shedding (CS) flow, (g) Over-shoot (OS) flow, (h) rear-side reattachment (RSR) flow, (i) front-side reattachment (FSR) flow, (j) bi-stable (BS) flow between front-side reattachment and co-shedding flows, and (k) co-shedding (CS) flow. While the solid lines represent the windward cylinder shear layers, the dashed lines stand for the leeward cylinder generated shear layers. Flow is from left to right.

3. Results and Discussion

3.1 Fluctuating forces and flow structures

Surface oil-flow visualization results are very informative, providing details of flow on the surface of the cylinder. It was found that the flow structures at Re = 6.5×10^4 and 9.7×10^3 were qualitatively similar to those at Re = 3.2×10^4 and 1.6×10^4, respectively. Therefore a sketch of flow structures based on the surface oil-flow results is presented in Fig. 2 at Re = 6.5×10^4 and 9.7×10^3 only, which will explain perspicuously the dependence of C_{Df}, C_{Lf} and St on Re and L^* in the subsequent paragraphs. Figure 3 presents C_{Df} and C_{Lf} variations with L^* and Re. C_{Df} and C_{Lf} at L^* < 3 are highly sensitive to L^* at Re = 3.2×10^4 and 6.5×10^4 but less at Re = 9.7×10^3 and 1.6×10^4. They wane with a decrease in Re, being very high at Re = 6.5×10^4.

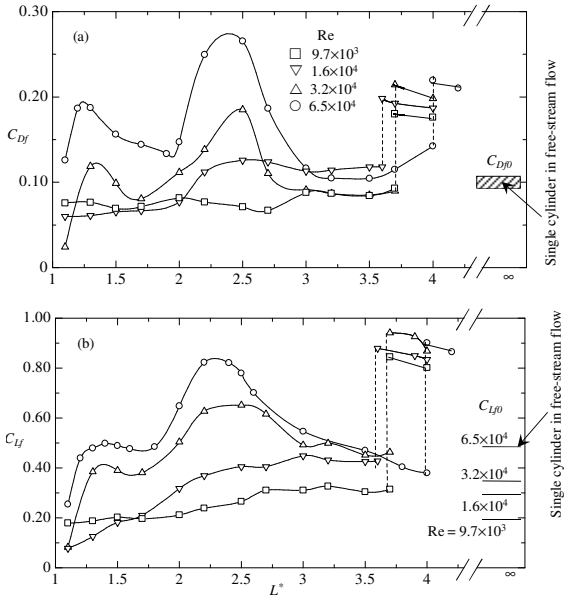

Fig. 3 Dependence of (a) C_{Df} and (b) C_{Lf} on Re and L^*.

Two peaks at L^* = 1.3 and 2.4, respectively, are formed at Re = 3.2×10^4 and 6.5×10^4 but not at Re = 9.7×10^3 and 1.6×10^4 (Fig. 3). That is, the peak at L^* = 2.4 in C_{Df} and C_{Lf} is connected to the 'kink' in C_D profile found by Zdravkovich and Pridden [5]. C_{Df} and C_{Lf} at this L^* are $2.8C_{Df0}$ and $2.0C_{Lf0}$, respectively, where the subscript '*0*' refers to a single cylinder subjected to the free-stream flow. A front-side reattachment flow is ascribed to the enhanced C_{Df} and C_{Lf} at L^* = 1.3, where the windward cylinder shear layer (solid lines) after the reattachment at θ = 66° on the leeward cylinder reverses to windward cylinder (Fig. 2a). On the other hand, at L^* = 2.4, the shear layer reattaches on the front surface at θ = 55° and goes to the other side sweeping the front surface (Fig. 2c). Here front, front-side, rear-side and rear surfaces are defined as θ = 0° ~ 60°, 60° ~ 90°, 90° ~ 120°, and 120° ~ 180°, respectively. The reattachments of the two shear layers of the windward cylinder occurred in an alternating fashion; for instance, in the first half cycle the upper shear layer (Fig 2(a_1, c_1)) reattaches and in the next half cycle the lower shear layer reattaches (Fig. $2a_2$, c_2). Beyond the critical L^* (dashed vertical lines, Fig. 3), the cylinder experiences much higher C_{Df} and C_{Lf} additionally contributed from the alternating vortices approaching from the windward cylinder (Fig. 2f, k).

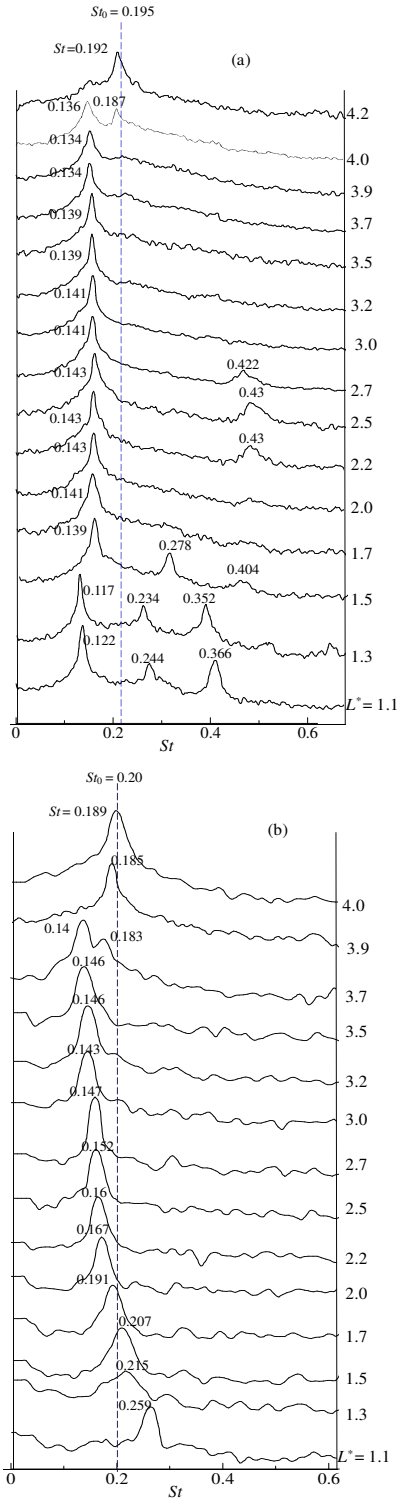

Fig. 4 Fourier power spectrum of fluctuating lift on the leeward cylinder at (a) $Re = 6.5\times10^4$ and (b) 9.7×10^3.

3.2 Strouhal numbers and spectral signatures

Fig. 4 illustrates spectral analysis results of the fluctuating lift at $Re = 6.5\times10^4$ and 9.7×10^3. Results at $Re = 3.2\times10^4$ and 1.6×10^4 were similar to $Re = 6.5\times10^4$ and 9.7×10^3, respectively, hence not presented. At $Re = 6.5\times10^4$, three St are seen for $L^* \le 1.5$ (Fig. 4a). The first St which is smaller than St_0 is connected to the vortex shedding, while the second and third St are second and third super-harmonics of the first one. Reattaching onto front-side surface of the leeward cylinder, the windward cylinder shear layer flows in the upstream direction and reattaches behind the windward cylinder forming a recirculation region between the cylinders (Fig. 2a). The entrainment from the recirculation to the shear layer weakens the shear layer velocity, resulting in a smaller St connected to the vortex shedding. The flow structures (Fig. 2a) explains why the second and third super-harmonic St exist in this L^* range.

At $1.5 < L^* < 2.2$ where only one peak is seen, the shear layer reattaching on the front-side surface goes on the same side to the downstream (Fig. 2b). On the other hand, the shear layer reattaching on front surface dives on the other side for $2.2 \le L^* \le 2.7$ (Fig. 2c) and the leeward cylinder generates a shear layer (dashed line). Therefore three shear layers interact around the leeward cylinder, producing the third superharmonic peak in the power spectra (Fig. 4a). It is interesting that when the wind cylinder shear layer after reattaching on the leeward cylinder goes into the gap between the cylinders (Figs. 2a, c), second and/or third superharmonic St appear (Fig. 4). With further increases in L^*, the shear layer again reattaches on the front-side surface and passes on the same side (Fig. 2d), which results in a single peak at $2.7 < L^* \le 3.9$ (Fig. 4a). The bistable flow occurs at $L^* = 4.0$ ($3.9 < L^* < 4.2$) corresponding to two peaks (Fig. 2e, 4a), followed by a co-shedding flow at $L^* \ge 4.2$ with a single peak (Fig. 2f, 4a). The $L^* = 4.0$ is called as the critical spacing.

At $Re = 9.7\times10^3$, St drops drastically from 0.259 to 0.215 between $L^* = 1.1$ and 1.3 (Fig. 4b). The drop is connected to a change in flow structure from an over-shoot flow (Fig. 2g) to a rear-side reattachment flow (Fig. 2h). The rear-side reattachment flow takes place at $1.3 \le L^* < 1.7$ where St is higher than St_0 and decreases slightly due to a forward advancement of the reattachment point. Further increase in L^* leads to a front-side reattachment flow for $1.7 \le L^* \le 3.5$ (Fig. 2i) where St drops from 0.191 to 0.146. The front-side reattachment flow corresponds to a St smaller than St_0. St is about 0.19 for $L^* \ge 3.9$, insinuating a co-shedding flow (Fig. 2k). Two peaks with different St values are seen at $L^* = 3.7$, indicating a bi-stable flow between the front-reattachment and co-shedding flows (Fig. 2j).

3.3 Flow structure map

C_{Df} and C_{Lf}, and St all are connected to flow structures. A flow structure map can therefore be drawn from the discussion made above and contour plots of C_{Df} and C_{Lf}, and St shown in Figs. 5, 6 and 7, respectively. A detailed flow structure map is displayed in Fig. 8. Transition in the shear layer being crucial parameter plays a role in the modification of flow structure and hence of forces and St. For a single cylinder in a free-stream, the transition length measured from the center of the cylinder decreases rapidly from $1.4D$ to $0.2D$ when Re increases from 2.0×10^3 to 6.5×10^4 [1]. This explains why the over-shot flow or rear-side reattachment flow occurs at the low Re ($= 9.7\times10^3$) but not at the higher Re ($= 6.5\times10^4$, Fig. 2). It has been shown that St is highly dependent on Re for $L^* < 2$ but not so much for $L^* > 2$. This is due to the fact that the windward cylinder shear layer transition happens around the leeward cylinder for $L^* < 2$. It shifts to the upstream with Re, so does the reattachment position. On the contrary, it occurs much upstream of the leeward cylinder for $L^* > 2$. C_{Df} and C_{Lf} vary significantly with Re even for the $L^* > 2$. Reattachment position and incidence angle of the shear layer on the cylinder are responsible for this variation. Since transition happens between the cylinders, reattachment position and angle of incidence on the cylinder vary significantly with Re.

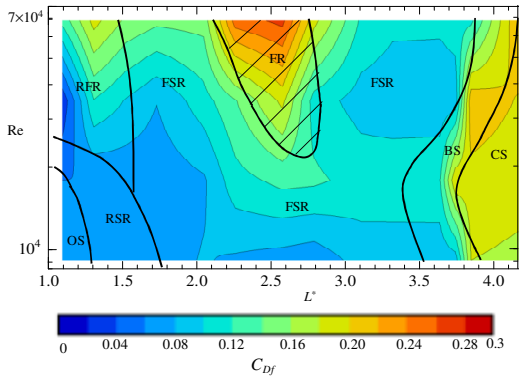

Fig. 5 Contours of fluctuating lift coefficient C_{Df} on Re - L^* plane and flow structure map. OS: Over-shoot flow; RSR: rear-side reattachment flow; FSR: front-side reattachment flow; FR: front reattachment flow; RFR: reverse-flow reattachment flow; BS: bi-stable; CS: co-shedding.

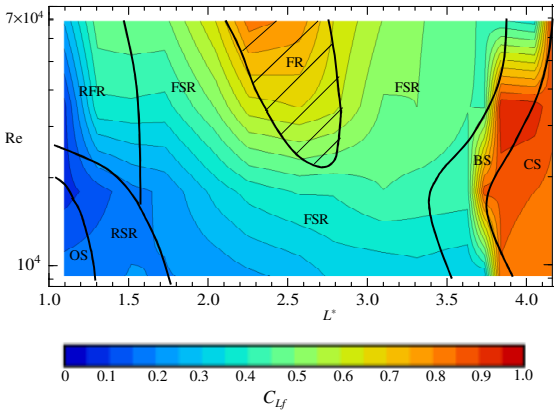

Fig. 6 Contours of fluctuating lift coefficient C_{Lf} on Re - L^* plane and flow structure map.

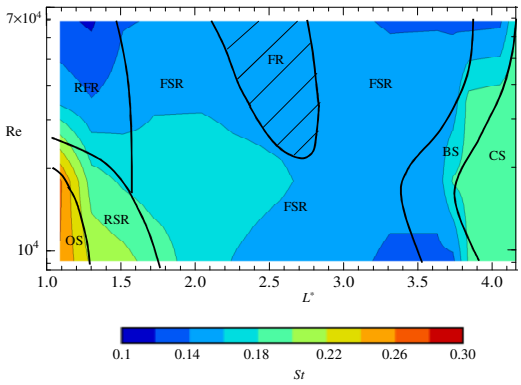

Fig. 7 Contours of Strouhal number *St* on *Re* - L^* plane.

How the flow structure changes with Re is dependent on L^* and can be explicated now. At small L^* (< 1.3), transition in the windward-cylinder shear layer occurs behind the leeward cylinder for smaller Re (<1.8×10^4), thus an over-shoot flow (OS) is possible. When Re is increased to about 2×10^4, the transition shifting upstream causes the shear layer to bow more and hence to reattach on the rear-side surface of the leeward cylinder (RSR). Further increase in Re (> 2×10^4) is accompanied by a further shift in the transition and a further bow in the shear layer. The shear layer therefore reattaches on the front-side surface, which results in a strong reverse flow reattaching on the rear surface of the windward cylinder (RFR). When L^* is increased to 1.3 ~ 1.75, the shear layer reattaches on the rear-side surface at Re < ≈1.7×10^4 (RSR). An increase in Re causes the shear layer to reattach on the front-side surface with the reverse flow reattachment (RFR, L^* < 1.6) and without the reverse flow reattachment (FSR, L^* > 1.6). At L^* = 1.75 ~ 3.5, the shear layer reattaches on the front-side surface (FSR) at Re < 2×10^4. It is interesting that when Re is increased (Re > 2×10^4), shear layer reattachment occurs on the front surface (FR) at an island like region (L^* = 1.8~2.8) marked by the hatched lines. Indeed, the 'kink' in C_D distribution and peak in C_{Df} and C_{Lf} distributions appear in this region. With further augments in L^*, bistable flow (BS) appears at L^* =3.4 ~ 4.1 depending on Re, followed by co-shedding flow.

4. Conclusions

Our findings reveal that C_{Df}, C_{Lf} and St are strong functions of Re and L^*. St diminishes, and C_{Df} and C_{Lf} augment with increasing Re. C_{Df}, C_{Lf} and spectral patterns are qualitatively similar at Re = 9.7×10^3 and 1.6×10^4, but different from those at Re = 3.2×10^4 and 6.5×10^4. With increasing L^* from 1.1 to 4.5, flow structure at Re = 9.7×10^3 changes as over-shoot (L^* < 1.3), rear-side reattachment ($1.3 \le L^* < 1.7$), front-side reattachment ($1.7 \le L^* \le 3.5$), bi-stable ($3.5 < L^* < 3.9$) and co-shedding ($L^* \ge 3.9$), while that at Re = 6.5×10^4 changes as reverse-flow reattachment ($L^* \le 1.5$), front-side reattachment ($1.5 < L^* < 2.2$), front reattachment ($2.2 \le L^* \le 2.7$), front-side reattachment ($2.7 < L^* \le 3.9$), bi-stable ($3.9 < L^* < 4.2$), and co-shedding ($L^* \ge 4.2$). The major difference in the flow structures between the two Re is that the over-shot flow and rear-side

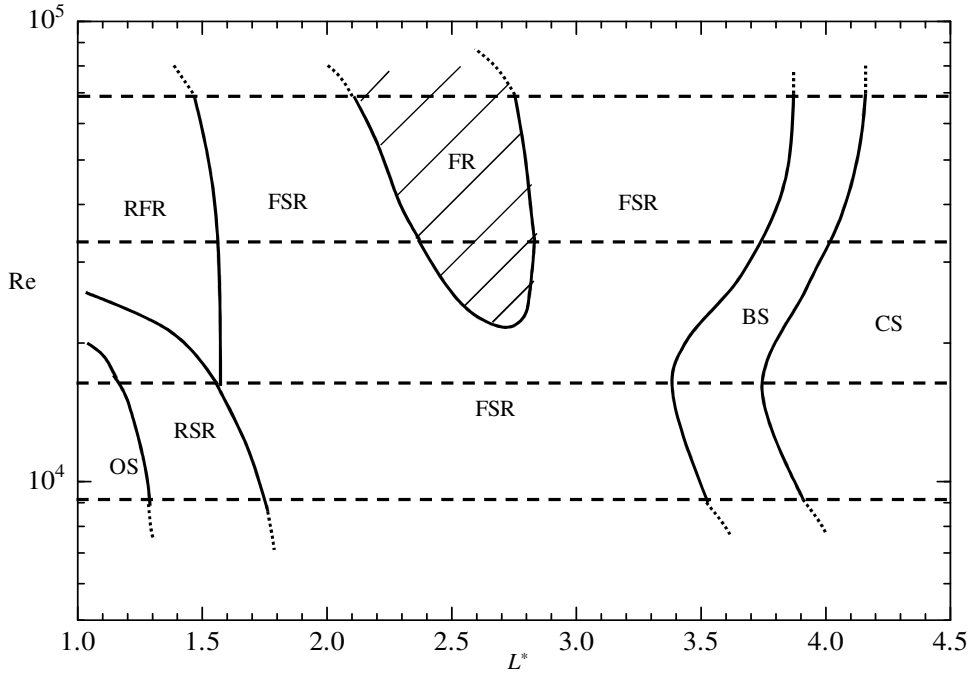

Fig. 8 Flow structure map with variation in *Re* and L^*. The hatched is the region where the kink in C_D distribution and peak in C_{Df} and C_{Lf} distributions occur. While the horizontal dashed lines represent the Re examined, the dotted lines are the predicted/extended boundaries.

reattachment flow prevail at Re = 9.7×10^3 - 1.6×10^4 and the reverse-flow reattachment flow and front reattachment flow appear only at Re = 3.2×10^4 - 6.5×10^4. Transition in the shear layer plays a major role behind the difference. The 'kink' in C_D distribution obtained in the literature or peak in C_{Df} and C_{Lf} for Re = 3.2×10^4 - 6.5×10^4 is connected to front reattachment flow (FR) where the windward cylinder shear layer reattaching on the front surface of the leeward cylinder sweeps to the other side of the cylinder.

5. Acknowledgments

Alam wishes to acknowledge supports given to him from the Research Grant Council of Shenzhen Government through grants JCYJ20120613145300404 and JCYJ20130402100505796. The author is also grateful to Professor Hiroshi Sakamoto, Kitami Institute of Technology, for his support to conduct this experiment in his laboratory.

REFERENCES

[1] M.M. Zdravkovich, Review of flow interference between two circular cylinders in various arrangements, *Journal of Fluids Engineering*, *Trans. of ASME,* Vol. 99, pp 618–633 (1977).

[2] M.M. Alam, J.P. Meyer, Global aerodynamic instability of twin cylinders in cross flow, *Journal of Fluids and Structures*, Vol. 41, pp 135-145 (2013).

[3] D. Sumner, Two circular cylinders in cross-flow: a review, *Journal of Fluids and Structures,* Vol. 26, pp 849–899 (2010).

[4] D. Biermann, Jr. Herrnstein, The interference between struts in various combinations, *National Advisory committee for Aeronautics*, Tech. Rep. 468 (1933).

[5] M.M. Zdravkovich, D.L. Pridden, Interference Between Two Circular Cylinders; Series of Unexpected Discontinuities, *Journal of Industrial Aerodynamics*, Vol. 2, pp 255-270 (1977).

[6] M.M. Alam, M., Moriya, K. Takai, H. Sakamoto, Fluctuating fluid forces acting on two circular cylinders in a tandem arrangement at a subcritical Reynolds number, *Journal of Wind Engineering and Industrial Aerodynamics*, Vol. 91, pp 139–154 (2003).

[7] T. Igarashi, Characteristics of the flow around two circular cylinders arranged in tandem (2nd Report), *Bull. of the Japan Society of Mechanical Engineers*, Vol. 27, pp 2380–2387 (1984).

[8] G.V. Papaioannou, D.K.P. Yue, M.S. Triantafyllou, G.E. Karniadakis, On the effect of spacing on the vortex-induced vibrations of two tandem cylinders, *Journal of Fluids and Structures*, Vol. 24, pp 833–854 (2008).

[9] M.M. Alam, H. Sakamoto, Y. Zhou, Determination of flow configurations and fluid forces acting on two staggered circular cylinders of equal diameter in cross-flow, *Journal of Fluids and Structures*, Vol. 21, pp 363-394 (2005).

ICMIEE-PI-Keynote

Status of Natural Fiber Composites in Bangladesh and Their Potential Applications

Mubarak A Khan[1*], Jahangir A Khan[1,2] and Jahid M M Islam[1]

[1]*Institute of Radiation and Polymer Technology, Bangladesh Atomic Energy Commission, Dhaka-1000, Bangladesh*

[2]*Department of Chemistry, Narsingdi Govt. College, Narsingdi, Bangladesh*

ABSTRACT

Composite materials which are cost-effective, environmentally friendly, light-weight and also durable are being considered for diversified applications, such as furniture, building materials, automotive industry and many more. In the recent years, the natural fiber based composites are coming forward to solve the problem associated with the synthetic fiber based composites like non-biodegradability, CO_2 production during manufacture etc. The main research of natural fiber-reinforced polymer composites is to provide a suitable compatibilizer or coupling agent between the reinforcement and the polymer matrices because the polar nature of natural fibers makes them incompatible with non-polar polymer matrices. In this paper, the present status of the natural fiber based composite materials; especially jute fiber based composites have been discussed from diversified applications and promotional view because jute fiber is the most abundantly natural fiber in Bangladesh which has high cellulose content and a low micro-fibrillar angle. Composite materials with jute fabrics have been made successfully using radiation processing technology and chemical modifications for general purpose constructions like low cost housing, sanitary accessories etc. The sample showed 147MPa tensile strength, 150MPa bending strength, 68 kJm^{-2} impact strength and more than 50 years durability. The treatments provided a synergistic effect on the mechanical performances and facilitated to develop a strong, lightweight and durable infrastructural material with an affordable cost. Many value added products like corrugated sheet, roof tiles, room insulator, shading, kitchen fittings etc. were also prepared using the same technology. Many of the products were successfully delivered to the end users where very positive feedbacks were found. The eye catching successes of field trials have caught attention of several entrepreneurs who are very interested to commercialize the products. So, this jute based composite is very promising as an alternative of commonly used construction materials in rural and urban areas of Bangladesh as well as for preparing value added products for household purposes.

Keywords: Natural fiber, Jute, Composite material, Biodegradability

*Corresponding author: Email-makhan.inst@gmail.com

1. INTRODUCTION

Jute has high cellulose content and low micro-fibril angle which are desirable properties of a fiber to be used as reinforcement in polymer matrices. Jute is one of the most common natural fibers having high tensile modulus and low elongation at break. If the low density (1.45 g/cm^3) of this fiber is taken into consideration, then its specific stiffness and strength are comparable to respective quantities of glass fiber [1, 2, 3]. In spite of these above-mentioned advantages, jute fiber – like other natural fibers – exerts some difficulties while used as reinforcement in non-polar polymer matrices. Being polar and hydrophilic in nature, jute fiber exhibits poor interfacial adhesion with hydrophobic polymer matrices. To overcome these kinds of bottlenecks, many attempts, such as physical and chemical treatments, lead to changes in the surface structure and surface energy of the fibers.Such an effort was made to prepare a composite with improved mechanical properties using radiation induced jute-urethane polymer system. The resin matrix was prepared under gamma radiation using urethane acrylate in the presence of N-vinylpyrrolidone, ethyl hexyl acrylate and trymethylol propane triacrylate. Some additives such as acetic acid, acrylamide, urea, talc, and titanium oxide were incorporated into the formulation [4]. In this context, hessian cloth (jute product) was coated with urethane pre-polymer with different formulations in the presence of plasticizers under UV radiation. Tensile properties of the composites were found to increase. It is also indicative that simulated weathering and soil degradation tests show the biodegradable nature of the prepared composites [5]. A good correlation was found between composite impact damping and yarn toughness for the jute-epoxy composites [6]. Two monomers such as 2-

* Corresponding author. Tel.: +88-01819252292

E-mail address: makhan.inst@gmail.com

hydroxy ethyl methyl acrylate (HEMA) and 2-ethyl hexyl acrylate (EHA) were successfully used as novel coupling agents for jute fabric (hessian cloth) polypropylene composite. The mechanical properties of the resulting composites increased as a result of surface treatment of the jute fabrics [7]. Polyester resin was used as matrix material for composite fabrication. The mechanical properties (tensile and bending strengths) of the surface modified jute fabrics reinforced polyester composites improved significantly [8]. The unsaturated polyester resin is quite useful for industrial and civilian world. As a low-cost, rigid, high strength-to-weight material, one can find its products in the form of mechanical parts, pipes, tanks, electronic gears, etc.They can be cured to give insoluble, infusible solid plastics through a free radical curing process. Organic peroxides are employed as free radical initiators while tertiary aromatic amines and some organic metal salts, such as cobalt naphthenate, are used as curing promoters if needed Tertiary aromatic amine and cobalt naphthenate can significantly reduce the decomposition temperature of peroxides via chemical reduction processes [9]. The objective of this research work is to prepare low cost light weight, durable, earthquake and cyclone tolerance housing materials and so on likewise products with sustainable local technology.

2. MATERIALS AND METHODS

2.1. Materials

Jute fabric was used as the reinforcing agent. The matrix polymer was a commercial unsaturated polyester resin (EPOLAC G-153ALX) containing 1.5% cobalt napthenate solution, 6% cobalt catalyst as promoter, and 36% styrene as diluent. Methyl ethyl ketone peroxide (MEKP) and wax were used as curing agent and mold releasing agent respectively. REOLOSIL fumed silica (aerosealpowder)was used as filler. A substituted aromatic tertiary amine was used as coupling agent.

2.2. Methods

2.2.1. Surface Modification

Hessian cloth was cut into rectangles (12 ×10 cm^2) and temporarily fixed in a long square sized plate (50 ×50 cm^2) where UV radiation could be given together to six equal sized rectangular samples. Then the samples were subjected to UV radiation (254–133 nm) using an irradiator (UV minicure Me-200, ISTTechnik, Germany), which delivers apower strength of 2 kW. The speed of the manicure was 4 meter/minute for each pass of the substrate under the lamp by maintaining different UV radiation intensities expressed by number of passes.

2.2.2. Composite Fabrication

Composites were fabricated using a simple hand lay-up technique. The working surfaces were treated with releasing waxes to facilitate easy removal of samples from the mold surfaces. Cobalt napthenate(catalyst) and MEKP (curing agent) were mixed thoroughly with USP at various formulations before each operation. At the beginning of fabrication, a gel coat with 2% MEKP was uniformly brushed into the finished side of the male and female parts of the mold. After 1h, when curing of gel coat was completed, each layer of the fiber was pre-impregnated with formulations made of USP. The impregnated jute samples were then placed one over another as a sandwich. This sandwich was placed into a mould. Both parts of the mold were tightened by screw-bolt and allowed 3 h for total curing (composite fabrication). The composites were cut into rectangular pieces of equal size (120×100×3mm^3) for different tests. All results are taken as the average of five samples for each testing.

2.2.3. Mechanical Tests

The tensile and bending strength of the composites were measured according to DIN 53455 and DIN 53452 standard methods by a universal testing machine (Hounsfield S Testing Series, UK) with an initial clamp separation of 20 mm and a cross-head speed of 10 mm/min. Charpy impact strength of the composite was determined by an impact tester (MT-3016) according to the DIN EN ISO 179 standard in the flat wise, unnotched mode. The test samples were conditioned at 25°C and 50% relativehumidity for several days before testing and all the tests were performed under the same conditions.The result of each test is taken as the average value of five samples

3. RESULTS AND DISCUSSION

The effect of jute content (%wt) on the mechanical properties of the resulting composites is studied here and shown in Figures 1 and 2. It was found shows poor mechanical properties due to poor fiber population and low load transfer capacity to one another. levels of fiber content (such as 20%), the composite As a result, stress gets accumulated atcertain points of the composites and highly localized strains occur in the matrix. At intermediate levels of loading (30%), the population of the fibers is just right for maximum orientation and the fibers actively participate in stress transfer. So, the mechanical properties of the composite reaches maximum. At high levels (suchas 40%) of jute content, the non homogeneous fiber matrix adhesion becomes prominent which leads to agglomeration among the fibers and stress transfer gets blocked [10]. As a result, the mechanical properties of the composite again decreased. The composite of the optimized jute content (30%w/w) showed 205% increase in tensile strength (TS), 141% in tensile modulus (TM), 226% in bending strength (BS) and 195% in bending modulus (BM) than that of the resin based composite.

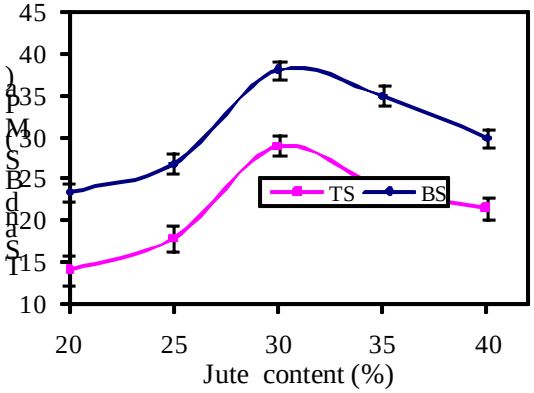

Figure 1: Effect of jute content on tensile and bending strength of composite

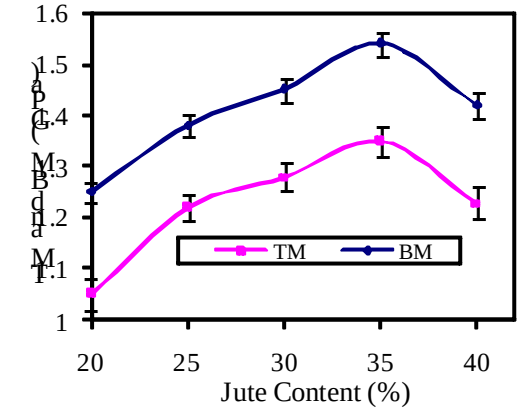

Figure 2: Effect of jute content on tensile and bending modulus of composites

The effect of UV radiation on the mechanical properties of jute based composites was investigated and presented in Figures 3 and 4. Jute content in the UV treated composite is maintained at about 30%. The UV intensities of different passes (200-400 pass) were exposed to jute surfaces.1 UV pass indicates 1 metre of UV exposure in the machine. It was found that UV intensity of 200 pass showed the highest mechanical properties. Mechanical properties, such as tensile and bending properties increase up to 200 pass, which gives 68% increase in TS, 78% in TM, 58% in BS, and 57% in BM relative to untreated jute-based composites. The TS, BS, TM and BM of the control composite were found 29.45 MPa, 38.35 MPa, 1.35 GPa and 2.54 GPa respectively. The increase of mechanical properties of the composite with increasing UV radiation may be due to the intercross-linking between the neighboring cellulose molecules, which results in the strength of jute fabrics. It is observed from Figures 3 and 4 that mechanical properties of the composite increase with UV pretreatment up to a certain limit and then decrease due to the two opposing phenomena, namely, photo cross-linking and photo degradation that take place simultaneously under UV radiation. At lower doses, free radicals are stabilized by a combination reaction and, as a result, photo cross-linking occurs. The higher the number of active sites generated on the polymeric substrate, the greater the grafting efficiency. But at higher radiation, the main chain may be broken-down and polymer may degrade into fragments and, as a result, mechanical properties were found to decrease after certain UV doses. An intense radiation results in a loss of strengths and a reduced degree of polymerization is observed [10].

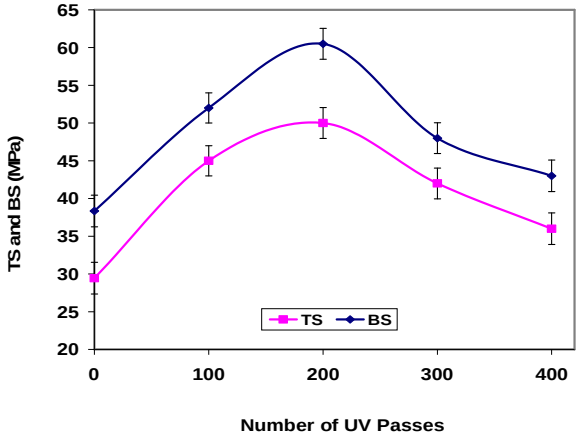

Figure 3: Effect of UV radiation on tensile and bending strength of jute-based composites

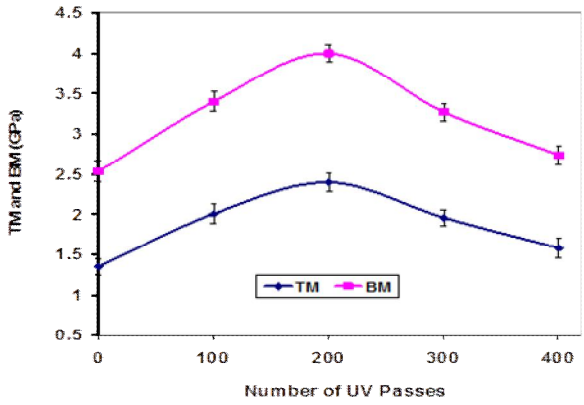

Figure 4: Effect of UV radiation on tensile and bending modulus of jute-based composites

Jute fabrics were further treated with a coupling agent (0.1 to 2.0 %) at the stage of pre-impregnating the fibers with USP resin to show its effect on to the composites. Figs 5 and 6 show the effect of coupling agent on the properties of the composites. The coupling agent with a concentration of 1.0 % performed the best of mechanical properties. It is also indicative that coupling agent treated composite showed much better mechanical properties than that of the control composite. It was found that 1.0% coupling agent treated composite showed 90, 74.7, 77.77 and 57.48% higher TS, BS, TM and BM values than that of the control composite.

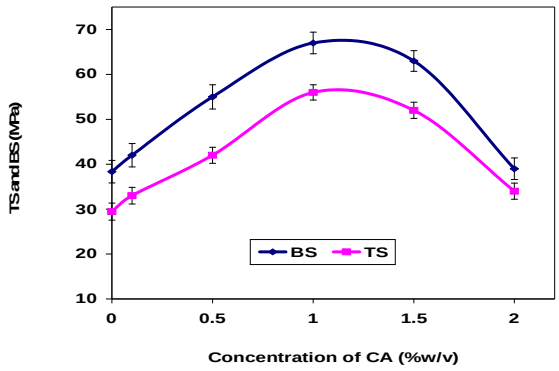

Figure 5: Effect of coupling agent on tensile and bending strength of composites

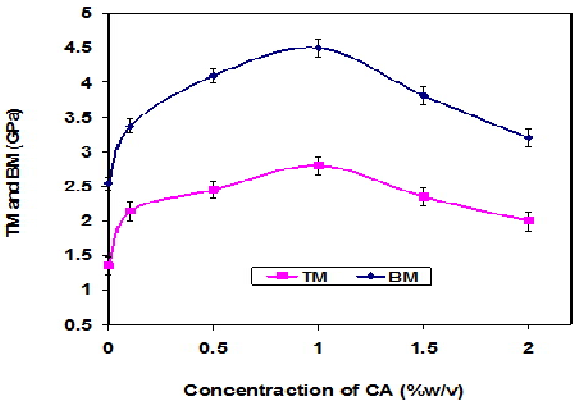

Figure 6: Effect of coupling agent on tensile and bending modulus of composites

4. Aging properties of Composite (JUTIN)

4.1. Thermal aging

Table 2.The effect of thermal aging on tensile strength of JUTIN

Sample	Room temp.	Tensile strength (MPa) 15 days			
		OºC	4ºC	50ºC	70ºC
Jutin	96	116±2.0	99.8±1.9	93±1.82	78±1.8

The JUTIN was subjected to undergo different temperature treatments at 15 days time periods to investigate the effect of thermal aging on tensile strength of JUTIN. It was found that the strength of composite increases with the decrease of temperature. The TS decreased to about 19.0 % and 3.0 % at aging temperature of 70ºC and 50ºC respectively. Whereas, in case of 4ºC and 0ºC, TS increased about 4.0% and 21.0% respectively.

4.2. Water aging

There is very negligible amount of water uptake (<1%) within 3 months. There is no change in mechanical properties within 3 months.

4.3. Normal weathering aging

The mechanical properties increased up to 7-10% within 6 months and remain unchanged up to 12 months.

5.4. Accelerated weathering aging

To study the weathering effect on the mechanical properties of Jutin, the samples of jutin were exposed under simulated weathering tester from Q-panel Co. (model QUV, USA). The weathering testing was performed in alternating cycles of sunshine over 4h (65º±2ºC) and condensation for 2h (45º±2ºC). This aging test was carried out for 600 h.Owing to this test the losses of mechanical properties more or less zero up to 300 hours and about 10% up to 600 h.

5. CONCLUSION

The tensile strength of the prepared composites composite is 150 MPa, bending strength is 147 MPa and impact strength is 68 kJm^{-2} and It will be stable up to 50 years. This jute-based polymer composite shows extra-ordinary features which are very promising to make jute based polymer composite as a effective alternative of metallic or plastic materials. It is rust proof, saline resistant, lightweight, heat resistant, sound proof, environmental friendly, Very low thermal expansion, and damaged area can be sealed very easily. In contrast, lightweight jute made composite boards fixed on steel frames with bolts & nuts are more flexible allowing lateral movements of the structures. They absorb and reduce seismic energy. The usage of natural fiber (jute) based products in post disaster management of rehabilitation & rebuilding, would become cost competitive compared to other building materials. Thus, all the properties of composite claim its position as an ideal building material.

REFERENCES

[1] Soumitra Biswas, Atul Mittal & G Srikanth, Gujarat Earthquake - Composite Materials towards Re-building & Rehabilitation

[2] Bogoeva-Gaceva G., Avella M., Malinconico M., Buzarovska A., Grozdanov A., Gentile G. and Errico M.E. (2007). Natural fiber eco-composites.*Polymer Composite*;28: 98-107.

[3] Joshi S.V., Drzal L.T., MohantyA.K.andArora S. (2004). Are natural fiber composites environmentally superior to glass fiber reinforced composites? *Composites:Part A*; 35: 371-376.

[4] Khan M.A., Ali K.M. I., Balo S.K. and Ahmad, M.U. (1998). Effect of additives reinforcement of radiation induced jute urethane polymer composites. *Journal of Applied Polymer Science*; 67:79-85.

[5] Khan M.A., Uddin M.K. and Ali K.M.I. (1997). Degradable jute plastic composite.*Polymer Degradation and Stability*; 55:1-7.

[6] Gassan J. and Bledzki A. K. (1999). Possibilities for improving the mechanical properties of jute/epoxy composites by alkali treatment of fibers.*Composites Science and Technology*; 59:1303-1309.

[7] Khan M.A., Hinrichsen G. and Drzal L.T. (2001). Influence of novel coupling agents on mechanical properties of jute reinforced polypropylene composites. *Journal of Materials Science Letters*; 20:1711-1713.

[8] Mohanty A.K, Khan M.A. and Hinrichsen G. (2000). Influence of chemical surface modification on the properties of biodegradable jute fabrics-polyester amide composites. *Composites:Part A*; 31:143-150.

[9] Khan M.A., Ganster J. and Fink H. P. (2004). Natural and man-made cellulose fiber reinforced hybrid polypropylene composites.5th Global Wood and Natural Fiber Composites symposium, in Kassel, Germany, April 27-28.

[10] KuangW. and Richardson, A. (2007).A New Amine Promoter for Low-temperature Cure of MEKP Initiated Unsaturated Polyester Resin Systems. *Composites Research Journal;* 1(4): 9-13.

[11] Abdullah-Al-Kafi, Abedin M. Z, Beg M. D. H, Pickering K. L and Khan M. A (2006). Study on the Mechanical Properties of Jute/Glass Fiber-reinforced UnsaturatedRadiation Polyester Hybrid Composites: Effect of Surface Modification by Ultraviolet Radiation. *Journal of Reinforced Plastics and Composites*; 25: 575-588.

[12] Khan, M. A. and Hasan, M. M. (2004). Surface Modification of Natural Fibers by Photo-grafting and Photo-curing, In: Mital, K. L. (ed.), Polymer Surface Modification: Relevance to Adhesion, VSP, Vol. 3, pp. 263–283.